WOODHEAD PUBLISHING SERIES IN ENERGY

Trends in Oil and Gas Corrosion Research and Technologies

Production and Transmission

Edited by A. M. El-Sherik

WP
WOODHEAD PUBLISHING

Related titles

Corrosion Control in the Oil and Gas Industry
(ISBN 978-0-12-397022-0)

The Fundamentals of Corrosion and Scaling for Petroleum and Environmental Engineers
(ISBN 978-1-933762-30-2)

Corrosion Control for Offshore Structures
(ISBN 978-0-12-404615-3)

Woodhead Publishing Series in Energy

Trends in Oil and Gas Corrosion Research and Technologies

Production and Transmission

Edited by

A. M. El-Sherik

Woodhead Publishing is an imprint of Elsevier
The Officers' Mess Business Centre, Royston Road, Duxford, CB22 4QH, United Kingdom
50 Hampshire Street, 5th Floor, Cambridge, MA 02139, United States
The Boulevard, Langford Lane, Kidlington, OX5 1GB, United Kingdom

Notices
Knowledge and best practice in this field are constantly changing. As new research and experience broaden our understanding, changes in research methods, professional practices, or medical treatment may become necessary.

Practitioners and researchers must always rely on their own experience and knowledge in evaluating and using any information, methods, compounds, or experiments described herein. In using such information or methods they should be mindful of their own safety and the safety of others, including parties for whom they have a professional responsibility.

To the fullest extent of the law, neither the Publisher nor the authors, contributors, or editors, assume any liability for any injury and/or damage to persons or property as a matter of products liability, negligence or otherwise, or from any use or operation of any methods, products, instructions, or ideas contained in the material herein.

Library of Congress Cataloging-in-Publication Data
A catalog record for this book is available from the Library of Congress

British Library Cataloguing-in-Publication Data
A catalogue record for this book is available from the British Library

ISBN: 978-0-08-101105-8 (print)
ISBN: 978-0-08-101219-2 (online)

Publisher: Joe Hayton
Acquisition Editor: Katie Hammon
Editorial Project Manager: Kattie Washington
Production Project Manager: Poulouse Joseph
Designer: Christian J. Bilbow

Typeset by TNQ Books and Journals

Biographies

Mohsen Achour holds a PhD in Chemical Engineering and Materials from Oklahoma State University (USA). He had held a professor position of chemical engineering at the University of Carthage in Tunisia for 11 years before joining ConocoPhillips in 2006 as a corrosion specialist. Mohsen has published more than 75 papers and patents in transport phenomena and corrosion and supervised more than 20 MS and PhD students. He served as an SPE Distinguished Lecturer and was a recipient of the NACE International Technical Achievement Award.

Gusai H. Aithan is working as a corrosion engineer in Consulting Services Department at Saudi Aramco. He received his bachelor degree in mechanical engineering from King Fahad University of Petroleum & Minerals (KFUPM) and master's degree from University of Tulsa. Gusai is certified with a number of professional certifications in the field of corrosion, inspection, and mechanical integrity.

John Beavers is a corporate vice president and a senior principal engineer in DNV GL's Pipeline Services Department, North American Oil and Gas. He has directed and contributed to numerous research and engineering programs on corrosion and cracking behavior of underground pipelines. The programs have been directed toward assisting pipeline operators in developing data to enhance their integrity management programs.

Anil Bhardwaj is presently working as a general manager, Head Materials & Corrosion Section at Institute of Engineering & Ocean Technology of Oil & Natural Gas Corporation Limited, India. He has 34 years of experience in upstream oil and gas industry. He has published 100 papers and three patents. He also has published four books: *Internal Corrosion of Pipelines, Dos and Don'ts: Corrosion Inhibitors, Corrosion Failure Case Studies, and Learning from Failures*.

Jim Britton has worked in the offshore corrosion field since 1973. He was educated in the UK and began his offshore career in the North Sea in the 1970s. He formed Deepwater Corrosion Services in 1986; the company now has five international offices in key offshore locations. Jim has published dozens of technical papers on offshore corrosion-related issues. He holds several patents for technology associated with asset integrity management. Since 2000, he has focused his company on life extension of aging brownfield offshore infrastructure.

Bruce Brown, PhD ChE, is the associate director of operations at the Institute for Corrosion and Multiphase Technology (ICMT) at Ohio University and project leader for their largest industry cooperative research program, the Corrosion Center Joint Industry Project (CC JIP). He has authored and coauthored numerous publications, including the 2016 NACE International Best Paper Award for "Atomic Force Microscopy Study of the Adsorption of Surfactant Corrosion Inhibitor Films," CORROSION, March 2014.

Tom Bubenik has 38 years of experience related to onshore and offshore pipeline integrity. He is a senior principal engineer in DNV GL's Pipeline Services Department, North American Oil and Gas. He is responsible for projects related to pipeline integrity management, in-line inspection, crack management, regulatory compliance, and risk management. He is a recognized authority on pipeline integrity and pipeline inspection technologies.

Todd Byrnes is a senior and coatings engineer with 22 years of experience in materials and surface engineering where he worked with onboard and outboard coatings for naval submarines; inspection and formulation of Li-ion battery electrode coatings; coating specifications and application techniques for onshore and offshore hydrocarbon pipelines. Todd has obtained his MSc., in materials engineering from Monash University, Melbourne, Australia, and he holds NACE International Protective Coating Specialist and Coating Inspection Program (CIP) level III certificate.

Cameron Campbell is a senior principal scientist with Kemira Chemical Co. Cameron has extensive field and laboratory experience and has consulted for many years in microbially influenced corrosion, petroleum microbiology, chemical optimization, and optimized monitoring programs in the oil and gas industry. Cameron is a lead instructor for the NACE International, both the basic and advanced Internal Corrosion of Pipeline course. She has written over 30 publications and has had numerous speaking engagements regarding petroleum microbiology.

Weixing Chen is currently a professor in the Department of Chemical and Materials Engineering at the University of Alberta, Edmonton. Dr. Chen pursues research activities in the microstructure−property relationship of metallic materials, the fabrication and application of coatings for corrosion prevention and carbon based electrode materials for batteries and supercapacitors.

Renato M. De Paula is currently the microbiology RD&E group leader at Nalco Champion, an Ecolab Company. Renato earned his BS degree in chemistry, MS in biochemistry, and PhD in biotechnology. He currently oversees a number of innovation and technical support projects, including development of new monitoring tools for microbial detection in oilfields and chemistries for mitigation of microbial corrosion and reservoir souring. He is an active member of NACE International and the scientific committee of ISMOS (International Symposium on Applied Microbiology and Molecular Biology in Oil Systems).

Sébastien Didierjean received his PhD in 2004. The main topic of his research was environmental ageing of Carbon Fiber Reinforced Plastics. He continued his research with a postdoc at Stanford University and worked for 4 years at the research center of AIRBUS group. In 2011, he began working as a research engineer for Flowtite Technology on projects dealing with Nondestructive Testing, numerical simulation and accelerated testing for composite pipes.

Richard Eckert has conducted pipeline corrosion/failure investigations and forensic corrosion engineering for over 33 years. His recent focus is internal corrosion management in oil and gas production, gathering, transmission and storage. He is a recognized expert in the field of microbiologically influenced corrosion (MIC), having published numerous symposium and peer-reviewed papers and two books on internal corrosion. Mr. Eckert is a certified NACE International Internal Corrosion Specialist, and currently serves on the NACE International Board of Directors. Eckert graduated with a BS in Engineering Metallurgy from Western Michigan University.

Khlefa A. Esaklul, PhD, P.E. Corrosion and Materials Advisor—Occidental Oil and Gas Corporation with over 30 years' experience in failure analysis, corrosion management, materials selection, inspection, fitness for service, development, promotion, and application of technologies that enhance asset integrity in oil and gas operation onshore and offshore. He has more than 25 publications.

Ludger Grunwald is currently the director of regulatory affairs biocides, Europe, Middle East, Asia (EMEA) at Ecolab. He has a degree in food chemistry (PhD) and has worked in the area of European Biocide Regulation for more than a decade. Ludger is a member of the European Biocide Product Forum Management Committee of European Chemical Industry Council, Brussels.

Paula Guraieb is vice president at Tomson Technologies. She oversees technical aspects for various research projects related to scale, corrosion, enhanced oil recovery, high pressure high temperature production, and unconventional production and has over 9 years of experience in the oil and gas industry. She holds a chemical engineer bachelor's degree and worked for ExxonMobil before obtaining her environmental engineering master's degree from Rice University in Houston, TX.

Shokrollah Hassani, PhD in Mechanical Engineering, from the University of Tulsa, BSc and MSc in Materials and Corrosion from Iran. Eight years' experience of corrosion research and engineering in oil/gas industry, coauthor of two book chapters, author/coauthor of 11 peer-reviewed journal papers. Worked as a postdoc at Oklahoma University and Corrosion Center at Ohio University. Currently working for BP America Upstream Engineering Center as corrosion engineer.

Sandra Hernandez has 23+ years' experience in corrosion and materials engineering. She started her career in 1990 as a corrosion engineer for the Research Center of Petróleos de Venezuela, S.A. (PDVSA). She joined British Petroleum (BP) in 2004 and worked on research, technology development, and support to O&G Operations. Since 2012, she has worked for Chevron Energy Technology Company as a senior corrosion/materials engineer. She is considered a subject matter expert in corrosion and erosion modeling.

Richard Hill has over 30 years of experience in the oil and gas industry. For the last 20 years has held senior management positions in engineering, equipment and services. Extensive experience in the international business arena. Has coauthored over 75 technical articles covering the performance of oilfield equipment and pipeline materials and market conditions influencing the manufacturing and service sectors. He is also a technical hardware specialist, including trees, controls, connectors, valves, flanges, fittings, and umbilicals.

Erin Iski received her PhD from Tufts University in 2011 under the supervision of professor Charlie Sykes. In 2013, she joined the faculty at the University of Tulsa where she specializes in electrochemical scanning tunneling microscopy to examine the effect of electrochemical reactions on the surfaces of metals.

Högni Jónsson has a degree in structural engineering. For the last 25 years he has been working on research and development of fiber reinforced plastics, mainly for use in pressure vessels and pipes. He is the manager of Product Development and Support for the Amiantit Group, the world's leading supplier of GRP pipe systems and technologies.

Victor Keasler is currently the Director of RD&E at Nalco Champion, an Ecolab Company. He has degrees in Microbiology (B.S.) and Molecular Virology and Microbiology (PhD) and has worked in the area of Petroleum Microbiology for nearly a decade. Victor has published extensively in the areas of biocide development as well as biocide usage and monitoring.

Michael Keller is an Associate Professor of Mechanical Engineering at the University of Tulsa and co-principal investigator of the Erosion/Corrosion Research Center (E/CRC). Michael Keller's research focuses primarily on the characterization and manufacturing of novel multi-functional composite materials. He is particularly interested in the development and characterization of materials with autonomic functionality, such as self-healing composites.

Aria Kahyarian has received his BSc degree in 2011 from Sharif University of Technology, Tehran, Iran. He is currently pursuing his PhD in Ohio University at the institute for corrosion and multiphase flow technology. His research focuses on the mechanisms and mathematical modeling of the aqueous metallic corrosion enhance by the presence of weak acids.

Roger King has over 40 years' experience of corrosion in the oil and gas industry. Dr. King is an independent consultant. Since 1989, he specializes in materials selection for upstream processing facilities and pipelines and its prevention by chemical inhibition, monitoring, microbiological corrosion, and the design of cathodic protection systems for pipelines, flowlines, structures, and seabed installations. He has published 100 papers on corrosion issues and is coauthor, with Andrew Palmer, of the reference book Subsea Pipeline Engineering.

Gerry Koch is senior principal engineer at DNV GL (USA). He has worked on corrosion and materials related issues in a wide range of industries, from the electric power to aircraft to oil and gas industries. Dr. Koch was the principal author of the 2002 US Cost of Corrosion Study and was the project manager of the recently completed (2015) NACE International Measures of Prevention, Application, and Economics of Corrosion Technologies (IMPACT) study. He was awarded the 2007 NACE Presidential Award, and is a NACE Fellow.

Jon Kvarekvål is a specialist group manager at the materials and corrosion department at IFE, Norway. He holds an MSc in chemistry from the University of Oslo, 1992. His professional experience includes initiation and management of international joint industry research projects and proprietary projects on internal corrosion, as well as personnel and business development. Jon has authored/coauthored around 50 publications on CO_2/H_2S corrosion in oil and gas production.

Jim Mason is a nonmetallic materials consultant with over 30 years of experience in research developing applications for plastic materials with extensive experience with engineering plastics for piping, pipeline liners, and composite structures used in oil and gas, and chemical process industries. He has over 20 technical publications and dozens of international conference presentations.

Jeremy Moloney is a Corporate Scientist at Nalco Champion where he oversees the key chemical and nonchemical corrosion control innovation and prospecting projects. He holds a PhD in Materials Science from the University of Cambridge, UK, and an MBA from the University of Lancaster, UK. Jeremy previously worked at Baker Hughes developing corrosion inhibitors and new testing and evaluation techniques. Jeremy is a chartered chemist and a chartered scientist with a number of patents and publications, one of which was received the 2012 NACE International A.B Campbell Award and 2012 NACE CORROSION Best Paper Award.

Mohammed Moniee is a science specialist at Saudi Aramco's R&D Center and has 20 years of professional and field experience in microbial corrosion, bactericides, biofouling, and bioprocessing. Mohammed holds a B.S. degree in Chemistry from the University of Toledo, USA, in 1997 and gained an MSc degree in project management (Oil & Gas Specialty) from the Liverpool University, UK, in 2012. He has authored and coauthored numerous journal and international conference publications in his areas of expertise.

Ali Moosavi has a PhD in corrosion engineering from Manchester University and over 35 years' experience in the corrosion field in various managerial and consultancy roles in ADCO (Abu Dhabi), CAPCIS (Manchester), and SGS (Aberdeen). He was also the adjunct professor of corrosion at UAE University. Dr. Moosavi was awarded the NACE International Technical Achievement Award in 2014. He is currently a project manager for DNVGL.

Faisal M. Mutahar works as a corrosion engineer with Saudi Aramco since 1999. He obtained a degree of philosophy in mechanical engineering from the University of Tulsa in 2012. He is specialized in upstream corrosion with several publications in prediction and modeling of CO_2 corrosion and erosion−corrosion.

Anass Nassef is a PhD candidate in mechanical engineering at the University of Tulsa. His PhD research area is erosion−corrosion mitigation through chemicals and protective corrosion products. He received his BS degree in materials and metallurgical engineering from the University of Tripoli (Tripoli, Libya) and his MSc degree in mechanical engineering from the University of Tulsa (Tulsa, OK, USA). Author/coauthor of three research papers published in the field of erosion−corrosion.

Srdjan Nesic is a Russ Professor of chemical engineering at the department of chemical and biomolecular engineering at Ohio University in Athens, OH, USA. Since 2002, he also serves as the director of the Institute for Corrosion and Multiphase Flow Technology at the same university, which is one of the largest research institutions of the kind. Dr. Nesic has published extensively in the field of corrosion, including more than 10 articles in books, some of which are reference sections in the best known corrosion handbooks such as Uhlig's Corrosion Handbook and Shriers's corrosion. Dr. Nesic has extensively consulted on corrosion issues for the oil and gas industry, covering a variety of projects.

Glen Nilsen is currently a senior regulatory specialist at Nalco Champion, an Ecolab Company. He has a bachelor of science in molecular biology and biochemistry and has worked in the field of petroleum microbiology for 13 years. Glen has extensive experience in petroleum microbiology and has held various roles in technical support and development, strategic marketing, and regulatory affairs.

Nihal Obeyesekere is a global integrity manager, innovation, oil services with Clariant Oil and Mining Services. Dr. Obeyesekere is a world-recognized expert in the area of Integrity in the oil and energy business. He has been a member of NACE International, SPE, and American Chemical Society (ACS), in good standing for years. During his time in NACE, he has held positions of leadership in various committees, and has been active in organizing, chairing and participating in technical symposia, which led him to be nominated and received the NACE's Distinguished Service Award for the year 2017.

Sankara Papavinasam, PhD, FNACE, FASTM consults with more than 50 oil and gas companies worldwide, developing solutions, and insights to control internal corrosion and external corrosion. He has written the book, *Corrosion Control in the Oil and Gas Industry* and has appeared as subject matter expert before National Academy of Sciences committee, USA, and Canadian Parliament Senate committee, Canada.

Dimitris Pantelis is professor and director of the Shipbuilding Technology Laboratory in the School of Naval Architecture and Marine Engineering (Division of Marine Structures) of the National Technical University of Athens (Greece). He is author or coauthor of three textbooks, one patent, more than 160 scientific papers in international journals and conferences, and nine monographs. His research work has 800 citations and his h-index is equal to 14.

Aquiles Perez has 7 years working experience on oil and gas projects in the area of equipment material selection. He has a PhD in mechanical engineering with a background in electrochemistry, materials, corrosion analysis, fracture mechanics, and asset integrity. He has been responsible for the material selection and corrosion analysis of several offshore and onshore projects. Technical hardware specialist including, pipe mill evaluation, trees, pipelines, connectors, valves, flanges, and fittings.

Sunder Ramachandran is a technology advisor for Baker Hughes Chemicals & Industrial Services. He is involved in developing corrosion inhibitors to prevent corrosion of low alloy carbon steels in oil field environments. Dr. Ramachandran has over 60 publications and 14 US Patents. Dr. Ramachandran served as the Technology Coordinator of the S Committee (Corrosion Science and Technology Committee) of NACE International from 2011 to 2013.

Kenneth P. Roberts is a professor of chemistry and biochemistry at the University of Tulsa and co-principal investigator of the Erosion/Corrosion Research Center (E/CRC). Dr. Roberts specializes in developing analytical methods to measure material properties. Dr. Roberts obtained his PhD in analytical chemistry in 2001 from Iowa State University.

Abdul Shaban received a BSc degree in Ch. Eng. from UCLA, USA, in 1981, MSc in Ch. Eng. from BUTE, Budapest, in 1992, and C. Sc. degree (candidate) in Ch. Science from the HAS, Budapest, in 1989. Since 1999, he has been a fellow at the Institute of Materials and Environmental Chemistry, Research Centre for Natural Sciences, Hungarian Academy of Sciences, and currently is working as Sr. research-fellow. His current research interests include electrochemistry, corrosion, and its inhibition.

Siamack Shirazi is the director of the Erosion/Corrosion Research Center (E/CRC) at The University of Tulsa. Professor Shirazi has over 500 publications, technical and invited presentations from which over 250 publications and conference presentations related to erosion−corrosion. He received NACE International Technical Achievement Award and is the fellow of NACE and American Society of Mechanical Engineers (ASME).

Marc Singer is an assistant professor in the chemical and biomolecular engineering department at Ohio University. He joined the Institute for Corrosion and Multiphase Technology research group in 2002 for which he is currently an associate director. Marc Singer's research interests include H_2S/CO_2 corrosion of mild steel, with specialties in top of the line corrosion, material science and corrosion inhibition.

Matthew Taylor is a corrosion engineer with a PhD in materials science and engineering from The Pennsylvania State University and Institut National des Sciences Appliquées (INSA) de Lyon. Dr. Taylor applies corrosion science to offshore infrastructure world-wide, developing technologies and custom solutions to overcome a variety of challenging corrosion issues. He has contributed to a diverse set of publications concerning various aspects of corrosion.

Judit Telegdi is an emeritus professor in chemistry. She is currently full professor at the Óbuda University, Budapest. She has been active in research work on several fields: enzyme kinetic, corrosion research (especially microbiology influenced corrosion), nanolayer preparation and characterization (Langmuir—Blodgett, self-assembled molecular layers). Her DSc dissertation was based on the combination of all those topics with the surface visualization using Atomic Force Microscopy (AFM) technique.

Robin Tems is the principal consultant, Hollybeach Corrosion Management. Previously, he worked for Saudi Aramco's Consulting Services Department where he held the positions of Body Leader—Materials Engineering and Corrosion Control, Senior Engineering Consultant, Supervisor—Corrosion Technology Unit, and Downstream Corrosion Team Leader. Dr. Tems also worked for Mobil Research and Development Corporation in Dallas, Texas, and Stavanger, Norway. His expertise covers both upstream and downstream corrosion. He is a Chartered Engineer, Chartered Scientist, and an International Professional Engineer.

Timothy J Tidwell is currently a principal microbiologist with NALCO Champion, an Ecolab company. He earned his BSc in microbiology from Texas A&M University in 2010. Before joining Ecolab in 2011, he worked on numerous projects as a research associate in the department of infectious diseases at the University of Texas Medical School in Houston, Texas.

László Trif obtained his BSc degree in chemistry from the Babes-Bolyai University, faculty of chemistry and chemical engineering, Cluj-Napoca, Romania, in 2004. Since 2004, he has been working as a research fellow, in the field of colloid chemistry and instrumental analysis, at the Chemical Research Center, Hungarian Academy of Sciences, which since 2012 became the Research Centre for Natural Sciences of the Hungarian Academy of Sciences.

Theodora Tsiourva is a research and teaching assistant in the Shipbuilding Technology Laboratory in the School of Naval Architecture and Marine Engineering of the National Technical University of Athens. She holds a Diploma in Chemical Engineering and her PhD focused on corrosion of weldments. She is a coauthor in more than 20 papers in journals and in conferences and 55 citations. She has also participated in projects mainly on corrosion-related subjects.

Qiwei Wang is a science specialist at Saudi Aramco R&D Center. He has 25 years of experience on scale management, water treatment, and oilfield production chemistry. Prior to joining Saudi Aramco, he worked for Nalco Champion as R&D coordinator on flow management and senior specialist on scale mitigation. He has over 90 publications and nine US patent applications. Qiwei holds a PhD from Texas A&M University.

Neil Wilds has a BSc, in applied chemistry. He has extensive experience in maintenance and fast cure coatings and high temperature coatings and corrosion under insulation (CUI) technologies before moving to a more customer focused role in the later years of 29 years' service. He has been an active member of NACE International helping to develop guidelines and standards. Now working as a product manager for Sherwin Williams looking at corporate specifications and technology transfers.

Xiangyang Zhu has over 25 years of experience in teaching, R&D, and technical services in academia, research institutes, and energy industries. He is a pioneer in introducing modern molecular microbiology technologies into oil and gas industry. Dr. Zhu has authored and coauthored more than 40 publications in peer-reviewed scientific journals and international conferences in the applications of conventional and molecular microbiology in various industries. He holds three U.S. patents.

Preface

The current global cost of corrosion is estimated to be US$2.5 trillion, which is equivalent to 3.4% of 2013 global Gross Domestic Product (GDP). By using available corrosion control practices, it is estimated that savings between 15% and 35% (US$375 and $875 billion) of the cost of corrosion could be realized annually on a global basis. These costs typically do not include savings due to safety or environmental consequences. Despite these figures, some still believe that corrosion is "an old" science and there is no further need for new research and technology development. Significant gaps still exist in our understanding of corrosion mechanisms of the different types of corrosion and therefore gaps in their mitigation and control. There is also a lack of standardized laboratory test methods, inspection and monitoring technologies, and lack of reliable modeling and prediction tools. This is especially true for the most insidious types of corrosion namely sour corrosion, pitting corrosion, under deposit corrosion, corrosion under insulation, stress corrosion cracking, microbiology-influenced corrosion, and hydrogen damage just to name a few.

The intended objective of this book was to collect and make available, in one reference book, knowledge gaps, and new developments in corrosion research and technologies for the oil and gas production and transmission sectors. In addition to academia, the main intended audience of this book are the oil & gas industry and its satellite industries such as service providers, technology and materials developers, chemical suppliers, and research centers. The ultimate goal is to ensure efficient and effective knowledge management by gathering, in one book, current knowledge and knowledge gaps as well as recent developments and trends in corrosion research and technologies. The content and scope of this book fills an existing gap in the literature.

This book, containing 34 chapters, is divided into the following six parts:

Part I: Corrosion in the Oil & Gas Upstream and Midstream: Introduction
Part II: Corrosion in Oil & Gas Production & Transmission: Current Knowledge & Challenges
Part III: Corrosion Mechanisms: Current Knowledge, Gaps & Future Research
Part IV: Advancements in Testing and Monitoring Technologies
Part V: Advancements in Corrosion Mitigation
Part VI: Advancements in Modeling and Prediction

The book's six parts are set in a logical order such that the first three parts discuss current industry knowledge of corrosion in the oil & gas production and transmission sectors and present corrosion gaps and challenges that still face the industry in these

sectors. The intended objective of these first three parts is to set the stage for the latter three parts dealing with various aspects of advancements in corrosion technologies.

The breadth and depth of coverage will help make the book useful to corrosion and materials engineers, scientists, technicians, and students from a wide range of disciplines. References to other books, journals, and standards that readers can consult for further information are listed at the end of each chapter.

The 60 authors who have contributed to the 34 chapters come from different sectors, oil & gas producers and operators, materials and chemicals suppliers, consulting companies, government, and academia and from 30 organizations spanning 10 countries. This diversity brings a variety of perspectives to and further enriches the different topics of this book.

I would like to convey my gratitude and thanks to all authors for contributing chapters in their areas of expertise. Also I would like to acknowledge the contribution of reviewers who, in anonymity, reviewed the draft chapters and provided their comments, suggestions, and recommendations to the authors to ensure high quality content.

If this book helps in its quest in gathering, in one volume, current knowledge and knowledge gaps as well as recent developments and trends in corrosion research and technologies, then the efforts of the entire team of contributors who worked tirelessly in preparing it will have been rewarded.

A.M. El-Sherik
Dhahran, Saudi Arabia
June 2017

Contents

PART I

Corrosion in the oil and gas upstream and mid-stream: introduction

Cost of corrosion

1

Gerhardus Koch
DNV GL USA, Dublin, OH, United States

1.1 Introduction

In 2002, the US Federal Highway Administration (FHWA) released a breakthrough study on costs associated with metallic corrosion in a wide range of industries [1]. Results of the study showed that the total annual estimated direct cost of corrosion in the US was US$276 billion—equivalent to 3.1% of the US gross domestic product (GDP). Along with detailed cost analyses, the FHWA study broadly included preventive corrosion control strategies. Although this benchmark study is still widely used and has been updated in terms of total annual estimated direct cost of corrosion in the United States utilizing inflation, no attempt has been made to extend the study to a more in-depth look at the effects of corrosion as related to overall corrosion management practices. In 2016, NACE International released the International Measures of Prevention, Application, and Economic of Corrosion Technologies (IMPACT) study, an initiative to examine the role of corrosion management in establishing industry best practices [2].

The current global cost of corrosion is estimated to be US$2.5 trillion, which is equivalent to 3.4% of the global GDP (2013). By using available corrosion control practices, it is estimated that savings of between 15% and 35% of the cost of corrosion could be realized, i.e., between US$375 and $875 billion annually on a global basis. These costs typically do not include individual safety or environmental consequences. Through near misses, incidents, forced shutdowns (outages), accidents, etc., several industries have come to realize that lack of corrosion management can be very costly and that, through proper corrosion management, significant cost savings can be achieved over the lifetime of an asset. To achieve the full extent of these savings, corrosion management and its integration into an organization's management system must be accomplished by implementing a Corrosion Management System.

1.2 Methodologies to calculate the cost of corrosion

Since the 1950s, several countries considered the economic consequences of corrosion. Studies conducted during this time indicated that the cost of corrosion to society was significant. The different approaches used to arrive at this cost included:

- The Uhlig method [3], which defines corrosion cost as the total expenditure by manufacturing industries and corrosion−protection measures.

Trends in Oil and Gas Corrosion Research and Technologies. http://dx.doi.org/10.1016/B978-0-08-101105-8.00001-2

- The Hoar method [4], which estimates corrosion costs for individual industrial sectors, taking into account both direct corrosion cost and spending on countermeasures. In addition to operational costs, the cost of capital can also be included.
- The input–output (IO) economic model, used in the 1970s Battelle study [5], which uses domestic commercial interactions among industries.
- The direct–indirect cost model developed in the 2002 US FHWA study [1].

1.2.1 Uhlig method

The Uhlig method [3] defines corrosion cost as the total expenditure by manufacturing industries and corrosion-protection measures.

The 1949 study, "The Cost of Corrosion in the United States" by H.H. Uhlig, was the earliest effort to estimate the US national cost of corrosion. The study attempted to measure the costs of corroding structures to both the owner/operator (direct cost) and to others (indirect cost). The total cost of corrosion to owners/operators was estimated by summing the cost estimates for corrosion prevention products and services used in the entire US economy, such as coatings, inhibitors, corrosion-resistant materials, and cathodic protection (CP), and multiplied these totals by their respective prices. Three items were selected as examples to estimate the cost of corrosion to private consumers–users, i.e., domestic water heater replacement, automobile internal combustion engine repairs, and replacement of automobile mufflers. Adding up both the direct and indirect costs, the annual cost of corrosion to the Unites States was estimated to be $5.5 billion or 2.1% of the 1949 gross national product (GNP).

1.2.2 Hoar method

The Hoar method [4] estimates corrosion costs for individual industrial sectors, taking into account both direct corrosion cost and spending on countermeasures. In addition to operational costs, the cost of capital can also be included.

The Hoar method determined the cost of corrosion for various industry sectors of the economy. The cost of corrosion for each industry sector was subsequently added together to arrive at an estimate of total cost of corrosion for the whole UK economy. The industry sectors included building and construction, food, general engineering, government departments and agencies, marine, metal refining, and semifabrication, oil and chemical, power, transport, and water. Information was gathered by interviewing corrosion experts who worked in companies and agencies and by surveys on expenditures for corrosion protection practices. Corrosion experts estimated corrosion costs and the potential savings based on their experiences with major economic sectors.

1.2.3 Input–output model

The input–output economic model, used in the 1970s Battelle study [5] uses domestic commercial interactions among industries. In this model, the GDP is calculated under the assumption of three universes:

- (Universe I) Actual world with corrosion.
- (Universe II) Imaginary world with no corrosion.

- (Universe III) Ideal world with inhibited corrosion.
  The GDP for each universe is calculated, and then the corrosion cost and avoidable corrosion cost are calculated by
- Corrosion cost = GDP (Universe II)−GDP (Universe I).
- Avoidable corrosion cost = GDP (Universe III)−GDP (Universe I).

1.2.4 Direct−indirect cost model

In this model [1], the total cost of corrosion is divided into the two main categories of direct and indirect costs. Direct costs are defined as the costs that are directly incurred by the owner of a facility, plant, or structure. Indirect costs are defined as those costs that are incurred by others, such as public, and are not directly felt by the owner or operator. The direct cost of corrosion includes the annual expenditures spent on maintenance and repairs, plus corrosion control techniques such as coatings, linings, chemical treatment, CP, corrosion resistant alloys, and nonmetallic materials. Inspection and testing costs are also part of the cost of corrosion. Indirect costs result from planned or unplanned plant shutdown, excess capacity, redundant equipment, loss of product, loss of equipment efficiency due to corrosion, contamination of product, and overdesign. Indirect costs due to "lost or deferred production" can reach many times the cost of replacing or repairing corroded equipment but are often difficult to estimate. Methodologies used in cost of corrosion surveys have varied significantly.

In order to determine accurate corrosion costs, it is important to include indirect cost in the analysis of alternatives. The cash flow must include all expenditures by the owner and all expenditures to others, such as the costs of delays, service interruption, or environmental damage. The design with the lowest annualized cost is then the design with the lowest cost of providing the service to the entire society. If, on the other hand, only direct costs are included, the design with the lowest cost to the owner may not be the one with the lowest cost to society.

1.3 Review of published studies

Since 1949, several national cost of corrosion studies have been conducted. The early studies focused on direct costs and failed to account for indirect costs. The early studies also tended to survey only corrosion control providers (e.g., coatings suppliers, chemical suppliers, etc.) and therefore did not include the significant costs of corrosion management in end-user companies. The later studies started to incorporate indirect costs, which resulted in much higher estimates of the total cost than previously estimated.

The following paragraphs describe some of major national studies on the cost of corrosion:

1.3.1 United States (1949): the Uhlig report

The 1949 study, "The Cost of Corrosion in the United States" led by H.H. Uhlig [3] was the earliest effort to estimate the costs of corrosion. The annual cost of corrosion to

the United States was estimated to be US$5.5 billion or equivalent to 2.1% of the 1949 GNP. Assuming a GDP of US$220 billion for 1949, the cost of corrosion is equivalent to 2.5% of the GDP. This study measured the total costs by summing up the cost for (1) the owner/operator and (2) the users of corroding components. The cost for the owners/operators was estimated by summing up cost estimates for corrosion prevention products and services used in the entire US economy (for example, coatings, inhibitors, corrosion-resistant metals, and CP). The cost for private consumers—users was evaluated as costs due to select services (domestic water heater replacement, automobile internal combustion engine repairs, and replacement of automobile mufflers). An advantage of the method is that the cost data are more readily available for well-defined products and services. The disadvantage is that several costs can be left out including other operational costs and costs of capital due to corrosion of assets.

1.3.2 West Germany (1969)

West Germany conducted a study of corrosion costs at the end of the 1960s [6]. The total cost of corrosion was estimated to be 19 billion Deutschmarks (DM) (US$6 - billion) for the period of 1968—1969. Of this cost, 4.3 billion DM (US$1.5 billion) was estimated to be avoidable. This gave a total cost of corrosion equivalent to approximately 3% of the West German GNP for 1969 (equivalent to 2.8% of estimated GDP) (US$215 billion in 1970) and avoidable costs were estimated to be 25% of total corrosion costs. There was no detailed information separating the corrosion cost into economic sectors.

1.3.3 United Kingdom (1970): the Hoar report

In March 1966, the UK Committee on Corrosion Protection was established by the UK Minister of Technology under the chairmanship of T.P. Hoar [4]. In 1970, the committee issued its report entitled “Report of the Committee on Corrosion and Protection”. The committee summarized its findings as follows: “We conservatively estimate the cost of corrosion as £1,365 million per annum, which represents 3.5% of the gross national product of 1970. We believe that a saving of approximately £310 million per annum could be achieved with better use of current knowledge and techniques.” This represented savings of approximately 23% of the total national corrosion costs.

1.3.4 Japan (1974)

Japan conducted a survey of the cost of corrosion to its economy in 1977 through the Committee on Corrosion and Protection [7]. The committee was chaired by G. Okamoto and was organized by the Japan Society of Corrosion Engineering and the Japan Association of Corrosion Control. Support for the study came from the Ministry of International Trade and Industry. The survey determined that the annual cost of corrosion to Japan was approximately 2.5 trillion yen (US$9.2 billion) in 1974. Estimating Japan’s GDP at US$472 billion for 1974, the cost of corrosion was the equivalent of 2.0% of Japan’s 1974 GDP.

1.3.5 United States (1975): the Battelle-NBS report

In response to a Congressional Directive, the National Bureau of Standards (NBS), now the National Institute of Standards and Technology (NIST) studied the cost of metallic corrosion in the United States using Battelle Columbus Laboratories (Battelle) to perform the analysis [5]. The Battelle-NBS study was the first to combine the knowledge of corrosion and economics experts to determine the economic impact of corrosion on the US economy. The study used a version of the Battelle National IO Model to estimate the total corrosion cost. This model quantitatively identified corrosion-related changes in the resources (i.e., materials, labor, and energy), changes in capital equipment and facilities and changes in the replacement lives of capital items for entire sectors of the economy. The IO model is able to account for both the direct effects of corrosion on individual industry sectors and the interactions among the various sectors.

The final results of the Battelle-NBS study for the base year of 1975 were (1) the total US cost of metallic corrosion per year was estimated to be US$70 billion, which is equivalent to 4.5% of the GDP in 1975 (US$1549 billion) and (2) 14% or US$10 billion was estimated to be avoidable by the use of the most economically effective, presently available corrosion technology.

1.3.6 Australia (1982)

In 1982, the Commonwealth Department of Science and Technology commissioned a study to determine the feasibility of the establishment in Australia of a National Center for Corrosion Prevention and Control. The feasibility study included a determination of the annual cost of corrosion to Australia. The results were presented in a 1983 report entitled "Corrosion in Australia—The Report of the Australian National Centre for Corrosion Prevention and Control Feasibility Study" [8].

The study concluded that the annual cost of corrosion to the Australian economy was AUD2 billion at 1982 prices[1], approximately 1.5% of Australia's GNP in 1982 (equivalent to 1.0% of the GDP; estimated at AUD196 billion). The report indicated that improved technology transfer and implementation could potentially recover a large portion of the corrosion costs. Furthermore, it was noted that the value of the savings to the Australian community from improved corrosion control would make a worthwhile contribution to the nation's economy.

1.3.7 Kuwait (1978/1992)

In 1992, Kuwait conducted an economic assessment of the total cost of corrosion to its economy using a modified version of the Battelle-NBS IO model [9]. The base year study (1987) gave a total cost of corrosion estimated at US$1 billion (1987 dollars), equivalent to 5.2% of Kuwait's 1987 GDP. Avoidable corrosion costs were estimated at US$180 million or 18% of the total cost.

[1] In 1982, 1 AUD = 1.128 USD.

On the sector level, the estimates for total cost of corrosion in the oil sectors (crude petroleum and petroleum refining) were US$60 million in 1987. The avoidable cost in these sectors was estimated to be US$10 million. The commercial services sector, the government, and the social and household services sectors were responsible for the largest share (70%) of the total cost of corrosion.

It is noteworthy that the corrosion control cost assessment in the refining sector predated major disasters at the Mina Al-Ahmadi Refinery in June 2000 and two fires at the Al-Shueiba Refinery since January 2000. The Mina Al-Ahmadi fire resulted in six dead and over 50% of the 480,000 bbl refinery destroyed. Both options to demolish the refinery and to attempt repair were evaluated. A ballpark estimate of the cost to rebuild a refinery such as the Mina Al-Ahmadi Refinery was estimated to be on the order of US$4 billion (2000). The fire occurred due to a vapor cloud explosion caused by a corrosion leak in a 10-in. condensate line. No specific information was made available on the causes of leaks and fires at the Shuaiba refinery that resulted in two deaths. In the upstream sector, a fire at the Raudatin gathering center in February 2002 shut down one-third of the nation's oil production and resulted in 4 fatalities and 17 were injured. The cause of this fire was attributed to an explosion of a vapor cloud that resulted for a corrosion lead in the facility piping.

1.3.8 Japan (1997)

In 1999, 25 years had passed since the prior 1974 study and the industrial structure in Japan had changed. Correspondingly, the Committee on the Cost of Corrosion in Japan was organized in 1999 jointly by the Japan Society of Corrosion Engineering and the Japan Association of Corrosion Control to update the cost of corrosion [10]. The project was funded by the National Research Institute for Metals as part of the Ultra-Steels (STX-21) Project.

Cost of corrosion in 1997 was estimated by the Uhlig method and the Hoar method. In addition to the above estimation, a preliminary analysis by the IO method was performed to estimate the total cost of corrosion including the direct and indirect costs. The overall corrosion-related costs estimated by the Uhlig and Hoar methods were 3938 billion yen (JPY)[2] and 5258 billion JPY, respectively, which were equivalent to 0.77% and 1.02% of the 1997 GNP [converting to GDP (560,993 billion JPY in 1997), the cost of corrosion is equivalent to 0.70 and 0.94 respectively]. The total cost including the direct and indirect costs, which were estimated by the IO analysis, was equivalent to 1.88% of the 1997 GNP (1.73% of GDP). The value for the IO economic model for 1997 is similar to the 1974 cost of corrosion, i.e., equivalent to 1.8% of the GDP.

The GNP and GDP analyses gave similar values for the percent cost of corrosion (especially when considering the conversions used to estimate the GDP) and because the Hoar method provided a division by sectors, the Hoar method values were used in the global cost of corrosion analysis.

[2] In 1997, 1 JPY = 18.41 USD.

1.3.9 United States (1998): the FHWA report

In 1998, the US Congress approved an amendment to the Transportation Equity Act for the 21st century to conduct a cost of corrosion study [1]. This study was funded through the FHWA and performed by CC Technologies, Inc. (now part of DNV GL) partnering with NACE International. This project used a combination of the Uhlig and Hoar methods with the inclusion of significant expert knowledge input.

The total direct cost of corrosion was estimated at US$276 billion per year, which is 3.1% of the 1998 US GDP. This cost was determined by analyzing 26 industrial sectors in which corrosion is known to exist and extrapolating the results for a nationwide estimate. The sectors were divided among five major categories: infrastructure, utilities, transportation, production and manufacturing, and government. The indirect cost of corrosion was conservatively estimated to be equal to the direct cost (i.e., total direct cost plus indirect cost is 6% of the GDP). Social cost (lost time and productivity of the general public due to delays and business interruption caused by corrosion and corrosion control activities) was the primary indirect cost considered. It was found that the sectors of drinking water and sewer systems (US$36 billion), motor vehicles (US$23.4 billion), and defense (US$20 billion) had the largest direct corrosion impact. A total of US$121 billion per year was spent on corrosion control methods and services.

1.3.10 United States (1998): Electric Power Research Institute

The Electric Power Research Institute (EPRI) initiated a study of the cost of corrosion in the electric power industry concurrent with the FHWA national study [11]. EPRI estimated the cost of corrosion in the electric power industry to be US$17.3 billion or 0.20% of US GNP, which compares with 0.24% found by the Battelle-NBS study. The FHWA study estimated US$6.9 billion for the same sector. EPRI report 1004662 claims these differences are due to ignoring indirect costs in the FHWA study.

1.3.11 Saudi Arabia (2006)

Although no national study was conducted in Saudi Arabia, its national oil company Saudi Aramco initiated a study in 2003 to define the cost of corrosion throughout its core operations with the objective of focusing plant, engineering, and research investment in corrosion control to the areas that had the largest economic impact on corporate performance [12]. The study concluded that Saudi Aramco corrosion costs were in line with industry experience. The identified cost of corrosion in the company's existing operations was approximately US$900 million per year (2003). Of this amount, approximately 25% or US$225 million was estimated to be avoidable by the use of improved corrosion technology and management.

For its five domestic refineries, 36% of maintenance budget was due to corrosion. For gas sweetening plants, it was found that 25% of the maintenance budget was committed to corrosion control. For gas fractionation plants, 17% of the maintenance budget was due to corrosion. For production operations onshore, corrosion is responsible for 28% of maintenance costs. Offshore, corrosion accounted for 60%–70% of

maintenance costs. For plants or systems that were capacity limited, the biggest single corrosion cost impact on the total cost of operations is deferred production. The total cost of corrosion including deferred production costs for gas fractionation plants was estimated to be five times the direct corrosion maintenance costs. The total cost of corrosion including deferred production costs for refineries ranged up to three times the direct costs. In a gas sweetening plant, indirect costs including deferred production costs were found to be 50 times the direct cost of corrosion for the specific case reported.

1.3.12 Australia (2010)

The Australian Corrosion Association in conjunction with industry experts performed a project to (1) examine, identify, and estimate corrosion failure costs attributable to industry practices, industry skilling and regulatory frameworks, and (2) estimate potential corrosion failure cost reductions by implementing avoidable/preventable strategies within the water transportation, processing, and sewage industry in Australia [13].

The study included water loss from pipeline leakage, water loss from pipeline failures, intangible costs associated with water and sewer pipe failures and replacements, water pipeline corrosion repairs, sewer pipeline corrosion repairs, sewage treatment costs due to infiltration, capital cost for water and sewer pipeline replacements, maintenance and repair water treatment plants, maintenance and repair of other assets (tanks, pump stations etc.), and maintenance and repair sewage treatment plants.

1.3.13 India (2011–2012)

In a study led by R. Bhaskaran at Lovely Professional University, Phagwara, Punjab, India and N.S. Rengaswamy at Central Electrochemical Research Institute, Karaikudi, India, the cost of corrosion was estimated using the NBS IO economic model for 2011–2012 [14].

The India study gave one of the most detailed sector breakdowns to date of any of the national costs of corrosion. The direct cost of corrosion for India was US$26.1 - billion or 2.4% of the India GDP. The avoidable cost of corrosion was US$9.3 billion or 35% of the direct cost of corrosion. The indirect cost of corrosion was US$39.8 billion or 3.6% of India GDP. Several of the indirect corrosion costs for the India study (IO model) were classified as direct costs in the 1998 US study (Hoar method). These include loss of product, loss of efficiency, and production loss; only social costs were classified as indirect costs in the US study. If only the social costs are classified as indirect costs, the direct cost of corrosion in India is 4.5%.

1.3.14 United States (2016): IMPACT study

NACE International initiated the International Measures of Prevention, Application, and Economics of Corrosion Technologies (IMPACT) study to examine the current role of corrosion management in industry and government and to establish best

practices [2]. This study used national corrosion costs available at the time of the study to estimate the global cost of corrosion. The global cost of corrosion was estimated to be US$2.5 trillion, which is equivalent to 3.4% of the global GDP (2013). By using available corrosion control practices, it was estimated that savings of between 15% and 35% of the cost of corrosion could be realized; i.e., between US$375 and $875 billion annually on a global basis. In addition, these costs typically do not include the consequential costs, such costs to individual safety, environmental consequences, lost revenue, product replacement, replacement cost, and effect on reputation.

The most significant conclusion of the IMPACT study was that in order to reduce what continues to be an astoundingly high cost of corrosion, a change in how corrosion decisions are made is required. Although important to continue investment in corrosion control technology, it is required that this technology is put into an organizational management system context, thereby requiring that justifying corrosion control actions are justified by business impact. It was further concluded that the community that would require the greatest adaptation to this change is the corrosion community. Hence, the corrosion professionals must become conversant in the language of management systems and adopt financial and risk tools that are used by those that make financial decisions. Ultimately, making organizational or industry-wide impact requires commitment to this common way of working by all levels in organizations.

1.3.15 China (2016)

The China Institute of Oceanology, Chinese Academy of Sciences is completing a national cost of corrosion survey, which is being led by Baorong Hou (Academician of Chinese Academy of Engineering) [15].

Organized by the Chinese Academy of Engineering, the study was supported by over 30 Chinese academicians and hundreds of experts from Chinese Society for Corrosion and Protection and many other related organizations.

The survey includes corrosion costs based on data from 2013 to 2014 and analyzed using Hoar's and Uhlig's methods. The study further addresses corrosion prevention strategies in five industry segments, i.e., infrastructure, transportation, energy, water, and manufacturing covering over 30 industries. These include

- highway bridges, ports and terminals, constructions, airports,
- oil and gas industries (i.e., exploration and production, storage, and distribution, refining),
- coal industries, thermal electrical utilities, renewable power utilities (i.e., hydropower, nuclear power, wind power, and solar power),
- ships, motor vehicles, aircrafts, railcars, and railroads,
- offshore platforms, subsea pipelines, marine cultivation,
- desalination of sea water, drinking water, and sewer systems,
- pulp and paper, chemical and pharmaceutical industries,
- mining,
- electronics and home appliances, telecommunication, medical equipment, food processing,
- agriculture,
- historical artifacts.

1.4 Current estimate of global cost of corrosion

The global cost of corrosion is estimated to be US$2.5 trillion, which is equivalent to 3.4% of the global GDP of 2013 [14]. By using available corrosion control practices, it is estimated that savings of between 15% and 35% of the cost of corrosion could be realized, i.e., between US$375 and $875 billion annually on a global basis. These costs typically do not include individual safety or environmental consequences. Through near misses, incidents, forced shutdowns (outages), accidents, etc., several industries have come to realize that lack of corrosion management can be very costly and that through proper corrosion management, significant cost savings can be achieved over the lifetime of an asset. To achieve the full extent of these savings, corrosion management and its integration into an organization's management system must be accomplished by implementing a corrosion management system (CMS).

Because various geographic regions differ in the proportion of different economic sectors in their economy, to relate the above cost of corrosion studies to a global cost of corrosion, a relationship between economic sectors and corrosion costs is needed. Moreover, the GDP of the economic sectors by country must be known to permit the use of the "percent cost of corrosion by economic sector" within the extrapolation to global corrosion costs. For instance, those studies that provide only a total IO model cost of corrosion for the whole country do not permit a global cost of corrosion based on an economic sector analysis.

Considering the data in the available studies, the economic sectors used in this analysis were (1) agriculture, (2) industry, and (3) services. For each of these sectors, (1) the cost of corrosion was estimated by summing the costs of the appropriate subsectors for a given study and (2) the GDP for every nation globally divided into these sectors was available from the World Bank data [15].

The studies that were included in the IMPACT cost of corrosion study [2] were India 2011−12, United States 1998, Japan 1997, Kuwait 1987, and United Kingdom 1970. Each of these studies provided data that could be divided into the three economic sectors discussed above.

The economic breakdown for the five countries used in this analysis is shown in Fig. 1.1. The United States, United Kingdom, and Japan, with advanced industrial and service economies, are very similar; whereas India, with a significant agricultural economy, and Kuwait, with a significant oil industry, has different profiles. In order to address the economic sectors for different parts of the world, the global economy was divided into economic regions with similar economies (according to World Bank). These were United States, India, European Region, Arab World (as defined by the World Bank), China, Russia, Japan, Four Asian Tigers + Macau, and Rest of the World.

1.5 Corrosion management financial tools

Corrosion management includes all activities, through the lifetime of the structure, that are performed to prevent corrosion, repair its damage, and replace the structure, such as

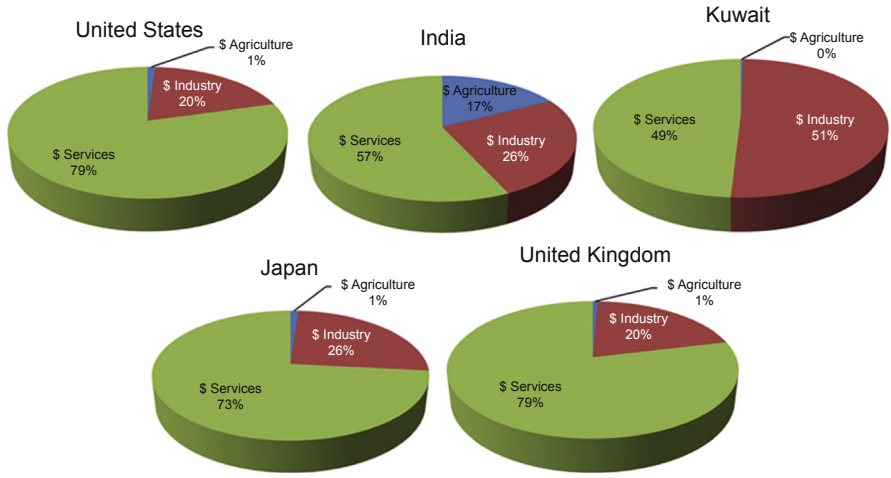

Figure 1.1 Economic sectors for the five countries used in the Global Cost of Corrosion Study.

maintenance, inspection, repair, and removal. These activities are performed at different times during the lifetime of the structure. Some maintenance is a regular activity, characterized by annual cost. Inspections are scheduled as periodic activities, and repair is done as warranted. Rehabilitation may be done once or twice during the lifetime of the structure, and the cost is usually high. Applying different corrosion management methods may positively affect the lifetime of a structure of a particular design without increasing the cost.

In order to meet the corrosion management objectives, tools or methodologies are available to calculate the cost of corrosion over part of an equipment's or asset's lifetime or over the entire life cycle. Return on investment (ROI) is a primary performance measure used to evaluate the efficiency of an investment (or project) or to compare the efficiency of a number of different investments. ROI measures the amount of return (profit or cost savings) on an investment relative to the investment's cost. An ROI calculation is used along with other approaches to develop a business case for a given investment proposal. ROI is calculated by simply dividing the return or cost savings (projected or achieved) on an investment divided by the cost of the investment. The complex part of ROI is determining the cost savings and investment costs. To compare investment proposals, ROI must either be annualized or the time over which the ROI is achieved is stated.

For example, the IMPACT study has suggested that as much as 30% of the corrosion costs can be saved by implementing state-of-the-art corrosion control technologies [14]. If the cost of this implementation is 10% of the savings, the following ROI is realized over the applicable time frame. If your annual corrosion costs are US$10,000 and state-of-the-art corrosion control is implemented, projected annual savings would be US$3000 at an annual cost of US$300. The cost of a given project may be

- An annual cost (chemical treatment)
- A one-time cost with a specified life expectancy (coatings)
- A one-time capital investment with an annual cost to maintain (CP)

Each of these can be converted to an annual cost or a cost over a lifetime based on the corrosion control method. ROI can be calculated over a defined life or on an annual basis. In the example, the savings (avoided cost) is $3000 and the investment is $300, giving an ROI of 10. This is sometimes expressed as a ratio; e.g., 10:1. An ROI of less than 1.0 is often expressed as a percentage. The key is to include all costs in the calculation of investment:

- Capital cost
- Installation cost
- Maintenance cost
- Abandonment/decommissioning costs (if applicable)

Include all savings in the avoided costs:

- Capital savings (extended life of an asset)
- Maintenance savings (fewer shutdowns or longer time between outages)
- Decreased inspections if applicable
- Increase in reliability (lower risk of failure)
- Decreased risk of environmental accidents
- Decreased risk of personal injury
- Decreased shareholder or public confidence

Some of the savings may be difficult to monetize, such as decreased risk of environmental accidents, decreased risk of personal injury, lower risk of failure (possibly related to environmental risk and safety), and a cost associated with poor public relations. The details of how to handle these can be different for different industries and applications. One way to deal with these is a risk-based approach and to analyze the risk benefit of a specific project (how much will the performance of a project decrease the risk picture for the organization).

Life cycle costing (LCC) provides a well-established financial tool to use some form of ROI or cost benefit to evaluate and differentiate between different approaches.

The LCC approach determines the cost of corrosion [16,17] of assets by examining:

- Capital cost (CAPEX)
- Operating and maintenance cost (OPEX)
- Indirect cost caused by equipment failure
- Residual value
- Lost use of asset (i.e., opportunity cost)
- Any other indirect cost, such as damage to people, environment, and structures as a result of failure

The LCC approach makes it possible to compare alternatives by quantifying a long-term outlook and determining the ROI. LCC analysis in corrosion management can be used to assess various corrosion management alternatives. Because the analysis is a cost minimization methodology, it is a good method to compare the cost of different options for corrosion management. It determines the annualized equivalent value [from the present discounted value (PDV)] of each option and compares these with the lowest cost option. Because in this analysis it is assumed that all options meet the same service requirement, the lowest cost option is therefore the most cost effective

option to achieve the service requirement. Although LCC is an appropriate method to compare the costs of different options, it simplifies the benefit side by only considering the benefits of the specified service level.

For example, if the required service level is a four-lane bridge that is designed to last for 60 years, the benefit of the bridge will be very different for one serving 5000 cars per day than for one serving 50,000 cars per day. An analysis of the former case would probably conclude that a two-lane bridge would have been sufficient, whereas an analysis of the latter case would conclude that a six-lane bridge would have been required.

Structures and facilities are built to serve a desired function. Because there is more than one way to achieve the requirement of the structure, LCC can be used to compare the cost of different options that satisfy the service requirement:

- Costing of project alternatives cannot be based on their first estimate costs. For example, an uncoated carbon steel pipeline (first option) costs less at construction than a coated carbon steel pipeline (second option); however, the latter option lasts longer. Therefore, for the correct comparison, the construction cost must be annualized over the entire lifetime of the pipeline. A comparison of the two options is, therefore, based on the annualized value (AV) of each.
- It is further incorrect to simply sum up all corrosion related costs that occur during the lifetime of the structure. Continuing the above example, assume that both options have rehabilitation scheduled at two-thirds of their lifetime (year 13 for the unprotected pipeline and year 27 for the protected pipeline). For simplicity, assume that the rehabilitation costs are the same for both options. In the case of simply adding up all costs, the bare carbon steel pipe may look better because its initial cost was lower. However, when the different costs are expressed in an annualized form, rehabilitation of the coated pipe will result in lower costs.

The different concepts that are incorporated in an LCC approach are discussed in the following sections.

1.5.1 Current cost of corrosion

The current cost of corrosion is defined as the sum of the corrosion related cost of design and construction or manufacturing, the cost of corrosion related maintenance, repair, and rehabilitation, and the cost of depreciation or replacement of structures that have become unusable as a result of corrosion. The current cost of corrosion is the difference between the approach where no consideration is given to corrosion and corrosion control and the current approach. It is calculated by LCC analysis and characterized by the AV.

Measurement of the current cost of corrosion is carried out in the following steps:

- Determine the cash flow of corrosion
- Describe corrosion control practices (materials, actions, and schedule), determine the elements of corrosion cost, and assign cost to all materials and activities that are corrosion related
- Calculate PDV of cash flow
- Calculate the AV for the PDV

These steps are discussed in more detail in the following sections.

1.5.2 Cash flow

After the corrosion management practices are analyzed, the direct and indirect elements of the corrosion costs are identified. The corrosion cash flow of a structure includes all costs, direct and indirect, that are incurred due to corrosion throughout the entire life cycle of the structure.

1.5.3 Corrosion control practices

1.5.3.1 Determine current practice

The current practices to control corrosion vary greatly between the different industries and government organizations. Even within an industry or government organization, there are different approaches to design, maintenance, and depreciation of similar facilities or structures.

1.5.3.2 Elements of corrosion control practices

As discussed previously, corrosion cost is divided into direct and indirect costs. The direct costs are defined as the costs of the following elements:

- Amount of additional or more expensive material used to prevent corrosion damage multiplied by the (additional) unit price of the material.
- Number of labor hours attributed to corrosion management activities multiplied by the hourly wage.
- Cost of the equipment required as a result of corrosion related activities. In case of leasing the equipment, the number of hours leased multiplied by the hourly lease price.
- Loss of revenue due to lower supply of a good. For example, consider the case of a leaking liquids pipeline. When as a result of the leak the pipe needs to be shut off for repair, the revenue loss due to this interruption in service is accounted for as a cost of corrosion. If the market is such that other companies in the industry at the same cost can satisfy the demand, then the revenue loss of one company is the additional revenue gain of another, a transfer within the industry, therefore, not counted as corrosion cost.
- Cost of loss of reliability. Repeated interruption in the supply of a good or a service could lower the reliability of the service to such a level that consumers select an alternative and possibly a more expensive service. For example, if repeated interruption in the supply of natural gas forces consumers to rely on electricity for heating, then the cost of this revenue loss is accounted for as a cost of corrosion for the oil sector, but it is a gain for the electricity sector. If consumers choose other petroleum products as their new energy source for heating, then the cost would be transferred within the oil sector from natural gas to petroleum; therefore, it would not be accounted for as a cost of corrosion for the oil sector.

As previously defined, indirect costs are incurred by others than the owner or operator. Examples of indirect costs are

- The loss of trust in the reliability of product or service delivery by the company
- Increased costs for consumers of the product (lower product supply on the market result in higher cost to consumers)
- Lost tax revenues

- Effect on local economy (loss of jobs)
- Effect on the natural environment by pollution
- Effect on reputation

Once a monetary value is assigned to these items, they are included into the cash flow of the corrosion management and treated the same way as all other costs.

1.5.4 Present discount value of cash flow

Structures are designed to serve their function for a required period of time, which is referred to as the design service life. More than one option can be utilized to satisfy service level for the required service time. These options, that already satisfy the service requirement, have different lengths of life, depending on, among other things, design and overall management. Once the cash flow for the whole lifetime is determined, the value of each option for the entire life cycle can be determined. One cash flow cycle (a complete life cycle) of a structure is as follows:

- Year zero
  Direct cost is the total initial investment of constructing a new structure or facility. If there is an old structure, its removal cost is not included. User cost is associated with the construction of a new structure. If there is an old structure, user cost associated with its removal is not included.
- During service
  Direct cost includes all costs associated with maintenance, repair, and rehabilitation. User cost can be generated by worsening conditions of the structure that reduces the level of service by temporary being out of service of the structure during any maintenance, repair, or rehabilitation.
- Last year
  Direct cost includes all cost of structure removal. If the old structure is replaced with a new one, the cost of the new structure is not included. User cost is associated with the removal of the structure. After the removal of the old structure, a new life cycle begins.

All materials and activities that are corrosion related during the lifetime of the structure must be identified, quantified, and valuated. Direct costs of the corrosion management activities, or cost to the owner or operator, include material, labor, and equipment costs. When determining their costs, all related activities need to be accounted for. For example, if a corrosion-related maintenance activity on a bridge deck requires traffic maintenance, its cost needs to be included. The price of labor, material, and equipment is assumed to be the same for all design and all corrosion management alternatives.

The corrosion management schedule of the structure determines the direct cost cash flow. In the following sections, the calculation of the present value (PV) the cash flow entries is presented.

The *initial investment* occurs in the "present"; therefore, no discounting is necessary.

Annual maintenance is assumed to be constant throughout the life cycle of the structure. This is the present discounted annual value, PDV{AM}, and is calculated back to the present as follows:

$$\mathrm{PDV}\{\mathrm{AM}\} = \mathrm{AM} \times \left[1 - (1 + \mathrm{i})^{-\mathrm{N}}\right]/\mathrm{I},$$

where AM is the cost of annual maintenance (US$ per year); N is the length of the structures service life in years; i is the interest rate.

For the calculation of the PV of activities that grow annually at a constant rate (g), a modified interest rate needs to be calculated by the following formula:

$$i_0 = (i - g)/(1 + g) \text{ and } i > g,$$

where i_0 is the modified interest rate; i is the interest rate; g is the constant annual growth rate.

If the first payment (P_1) occurs in year 1, the PV of a cash flow that grows annually at a constant rate over n years is calculated by the following formula:

$$PV\{P\} = [P_1/(1 + g)] \times \left[1 - (1 + i_0)^{-n}\right]/i_0$$

PV{P} is the present value of a cash flow series that starts at P_1 in year 1 and grows at a constant rate g for n years when interest rates are i, which are equivalent to the PV of an annuity of $[P_1/(1 + g)]$ for n years when interest rates are i_0, where i_0 is given by the equation above.

The first payment for repair activities, however, usually does not occur in year 1, but, rather, in year t; therefore, the above formula calculates a value at year (t−1) that is equivalent of the cash flow series of repair through n years. This value needs to be calculated back to year zero of the life cycle to determine the PDV of the repair:

$$PDV\{P\} = PV\{P\} \times (1 + i)^{-(t-1)}$$

The PV of one-time costs, such as one-time repairs (R), rehabilitation (RH), or removal of an old structure (ROS) is calculated as follows:

$$PDV\{R\} = R \times (1 + i)^{-tR}$$

$$PDV\{R\} = RH \times (1 + i)^{-tRH}$$

$$PDV\{ROS\} = ROS \times (1 + i)^{-tROS},$$

where R is the cost of the repair; RH is the cost of the rehabilitation; ROS is the cost of removing the old structure; T is the year in which the cost is acquired.

The PV of alternatives is calculated as the sum of the PV of its cash flow:

$$PV = I + PV\{AM, P, R, RH, ROS\}$$

1.5.5 Annual value of cash flow

In calculating the lifetime cost of alternative corrosion management approaches, the irregular cash flow of the whole lifetime is transformed into an annuity (a constant

annual value paid every year) for the same lifetime. The AV of the alternative approach is calculated from the PV by the use of the following formula:

$$\mathrm{AV} = \mathrm{PV} \times \mathrm{i} \big/ \left[1 - (1 + \mathrm{i})^{-\mathrm{N}}\right],$$

where, N is the service life of the structure.

The annuity of the initial investment (I) made in year zero is determined such that its PDV is equal to the PDV of its annuity:

$$\sum_{\mathrm{n}=1}^{\mathrm{N}} \left[\mathrm{A}\{\mathrm{I}\} \big/ (1 + \mathrm{r})^{\mathrm{N}}\right] = \mathrm{PDV}\{\mathrm{I}\} = \mathrm{PDV}[\mathrm{A}\{\mathrm{I}\}],$$

where A{I} is the AV of the capital investment; A{CM} is the AV of all corrosion management costs; R is the annual discount rate; N is the service year, n = 1… N; N is the entire service life; PDV{I} is the PDV of the initial investment; PDV[A{I}] is the PDV of annuity of the initial investment.

The actual corrosion management costs throughout the "n" years of the structure's service life will fluctuate. The fluctuating cash flow is replaced with an equivalent uniform cash flow of its annuity. The annuity of the corrosion management yearly cash flow is determined such that the PDV of the original cash flow is equal to the PDV of the annuity:

$$\sum_{\mathrm{n}=1}^{\mathrm{N}} \left[\mathrm{A}\{\mathrm{CM}\} \big/ (1 + \mathrm{r})^{\mathrm{N}}\right] = \mathrm{PDV}[\mathrm{A}\{\mathrm{CM}\}] = \mathrm{PDV}\{\mathrm{CM}\},$$

where PDV{CM} is the PDV of the original cash flow of corrosion management; PDV [A{CM}] is the PDV of the uniform cash flow or annuity.

The annuity of the original cash flow is then

$$\mathrm{A} = \mathrm{A}\{\mathrm{I}\} + \mathrm{A}\{\mathrm{CM}\}$$

This annuity or "annualized cost" is a constant annual value paid every year whose PDV is equal to the PDV of the irregular cash flow for the whole lifetime of the structure.

In summary, the current cost of corrosion is the sum of the amount spent preventing corrosion at the design and construction phase, the amount spent on maintenance, repair, and rehabilitation to control and correct corrosion (cost of corrosion management), and the amount spent on removing and replacing structures that become unusable due to corrosion (depreciation or cost of replacement).

Measuring the current cost of corrosion requires the following steps:

- Determine the cash flow of corrosion.
  Describe corrosion management practice (materials, actions, and schedule), determine the elements of corrosion cost, and assign cost to all materials and activities that are corrosion related.
- Calculate present discounted value (PDV) of cash flow.
- Calculate AV for the PDV.

1.5.6 Past trends of corrosion management costs and benefits

The current cost of corrosion is merely one point in time that is the result of past trends and developments. If the history of corrosion management practices can be determined, current practices can be placed in perspective. By examining the past, the following questions may be answered:

- Have material options and their costs changed?
- Have corrosion management practices and their costs changed?
- What is the effect of different materials and corrosion management practices on the lifetime of a structure?
- Has the number of failures due to corrosion (incidents, injuries, fatalities, and property damage) changed?
- Has the cost of failures caused by corrosion changed (cost of environmental cleanup, litigation)?

1.6 Cost saving through improvement of corrosion management

Within a specific industry sector there is a range of current practices in dealing with corrosion, from old technology to state-of-the-art. The cost and results of each of these practices are different. Although one of the practices achieves the most for its cost, i.e., it is the most cost effective, others could be improved to be more cost effective. An important question is whether improvement of currently used practices could indeed lower the current cost of corrosion. As better ways are developed to protect against corrosion, the potential for saving will increase.

The goal of corrosion management is to achieve the desired level of service at the least cost, including user costs. Finding the corrosion management program that has the greatest net benefits, including user costs, to society requires an understanding and careful analysis of all the direct and indirect costs involved. Cost benefits could be demonstrated by changing optimal corrosion management and more corrosion resistant materials.

Because of the complexity of corrosion control and corrosion management issues, there is usually insufficient information available to identify the design maintenance option with the lowest annual cost, including user costs. However, the results of the surveys and associated interviews for the various industry segments during the 2016 IMPACT study [2] have indicated a wide range of corrosion management practices, suggesting that one of these practices could more optimal than the others.

Managing the threat of corrosion requires consideration of both the likelihood and consequence of corrosion events. The consequence, or impact, of corrosion is defined here as the potential or actual monetary loss associated with the safety, environment, or asset integrity. This value is typically quantifiable when considering lost revenue, cost of repairs, and clean-up costs, as applicable. Other aspects of corrosion impact include deterioration of an asset to the point where it is no longer fit for its intended purpose (e.g., lost future production).

In general, corrosion threats should be mitigated to a point where the expenditure of resources is balanced against the benefits gained. One outcome of this is that a financial analysis might conclude that a technically sound corrosion mitigation action is unjustified. To determine whether a corrosion management investment is appropriate, it can be compared to the potential corrosion consequence through a return on investment (ROI) analysis. ROI is the benefit (or return) of an investment divided by its cost. For corrosion investment, the costs may include inspection and other maintenance costs and the benefit of ROI is not always measured in financial gains, but in the avoidance of safety or integrity costs. Some risks are hard to monetize including reputation and societal costs. The ROI for corrosion management can be linked to the risk-management concept of as-low-as-reasonably-practicable.

It must be noted that there are uncertainties in quantifying both the likelihood and consequences of corrosion. These uncertainties include both data and models (models can include analytical expressions, numerical models, and expert opinions/mental models). Therefore, additional mitigation measures (also sometimes referred to as defense in depth) are often taken beyond the calculated ROI.

One way to visualize the benefit of combining corrosion technology-specific activities with management system elements is through a two-by-two matrix shown in Fig. 1.2. With poor corrosion technology and a weak management system, corrosion is neither controlled nor managed (i.e., it is unsafe). With sound corrosion technology, corrosion is controlled but not optimized (i.e., it is expensive). A mature management system without sound corrosion technology cannot be effective (i.e., it is unsound). Combining a mature management system with sound corrosion technology is ideal in that it results in an effective and efficient management of a degradable asset.

Investing in corrosion control activities such as inspections and maintenance may not prevent all corrosion events because the likelihood of failure is rarely zero. Additionally, the consequences of corrosion events, when they occur, may be compounded due to system-related issues such as lack of training, not following procedures,

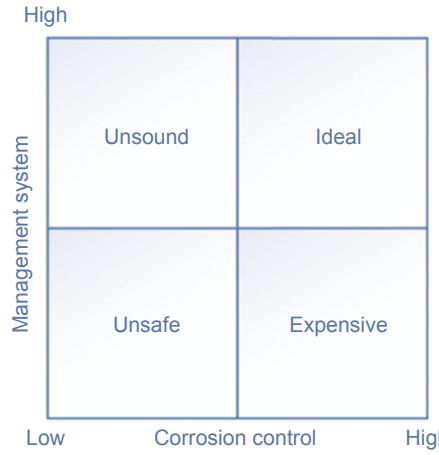

Figure 1.2 A two-by-two matrix illustrating the benefit of combining sound corrosion technology with a mature management system.

inadequate emergency response, etc. Therefore, investing in a CMS to frame the corrosion activities with the system elements necessary for planning, execution, and continual improvement should be considered as part of the ROI.

1.7 Incorporating corrosion management into corporate management systems

Realizing the maximum benefit in reducing corrosion costs (both direct and consequential) requires more than technology: it requires integration of corrosion decisions and practices within an organization's management system. This is enabled by integrating a CMS within system elements that range from corrosion-specific procedures and practices up through organizational policy and strategy; i.e., all levels of the management system pyramid (Fig. 1.3). This figure is central to illustrating the incorporation of corrosion management into corporate management systems. It is essential that traditional corrosion management procedures and practices (lower levels of the pyramid) be explained to policy setters and decision makers (higher levels of the pyramid) in the form and terminologies of organizational policies. Simply stated, the corrosion practices need to be translated into the language of the broader organization. The organization as a whole must commit to ownership of the CMS and its processes. This means buy-in at all levels within an organization.

The framework for a CMS is based on a series of central elements that ensure the effectiveness, consistency and communication of corrosion management processes. The corrosion management must be implemented in a consistent and holistic manner in all stages of asset integrity management. The following sections highlight the elements necessary for the development and implementation of a CMS, referring to the elements shown in Fig. 1.3.

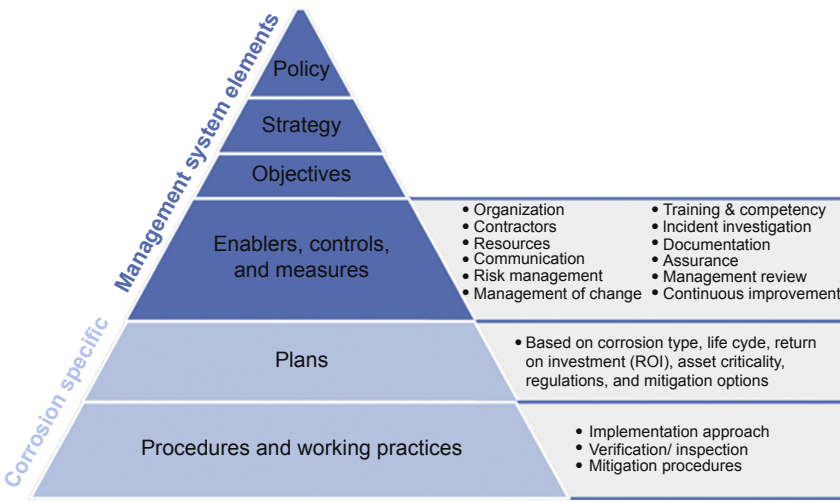

Figure 1.3 The corrosion management system pyramid.

1.7.1 Corrosion management policy, strategy, and objectives

A corrosion management policy includes the principles and requirements used to manage the threat of corrosion over the life cycle of assets. The policy must be in line with the organization's mission and values as shown in the organization's strategic plan. The policy lays the foundation for the corrosion management strategy or long-term plan for managing corrosion for an organization's assets by way of specific and measurable objectives.

During the development of the corrosion management policy, strategy, and objectives, the internal and external context, or environments in which the organization seeks to achieve its objectives, must be considered. Examples of external context include the regulatory environment and the organization's perceived reputation, wherease examples of internal context include an organization's culture as well as internal standards and business models.

Although corrosion management policy, strategy, and objectives may be contained in stand-alone documents, they are ideally grouped with the policies, strategies, and objectives that are used to manage other threats to an organization's assets.

1.7.2 Enablers, controls, and measures

1.7.2.1 Organization

An optimized CMS requires defined and documented roles and responsibilities with respect to corrosion management throughout the organization. The defined roles and responsibilities should include personnel involved in the development, implementation, review, and continual improvement of the CMS, as well as personnel performing corrosion assessments and determining and prioritizing corrosion prevention and mitigation activities. Often, the roles and responsibilities are communicated internally through the use of organizational charts. Additionally, any applicable external personnel, such as contractors or consultants, should be included in the organizational charts.

1.7.2.2 Contractors, suppliers, and vendors

When utilizing contractor services, the organization is responsible for verifying that the contractor services meet or exceed the requirements of the CMS. Additionally, the contractor(s) should be held responsible for meeting or exceeding the requirements of the CMS as defined by the organization. The same considerations should be applied to the qualification of any subcontractors used by the contractor.

1.7.2.3 Resources

The organization should commit to determining and providing the resources required for developing, implementing, and continually improving the CMS. Resources include staffing, infrastructure, and equipment, such as inspection tools or repair equipment. Staffing requirements may be met by providing a combination of organization staff

and contracted personnel; however, the organization must commit to ownership of the CMS and its processes. Allocation of appropriate resources to deliver programs, which are consistent with the CMS, must be ensured. This is accomplished by allocating proper budgets, setting achievable staffing levels, and developing and implementing training programs to ensure the right amount and the right competence levels of staffing.

1.7.2.4 Communication

The organization must create processes to establish and maintain internal and external communication processes associated with corrosion management. These processes include identification of the stakeholders and information that require communication. Channels should exist to allow communication to flow from management to project/field personnel and vice versa.

1.7.2.5 Internal communication

Internal communication processes facilitate awareness of the CMS and corrosion processes throughout the organization, including awareness and understanding of the CMS policy, objectives, plans, processes, and procedures. Communication links management, employees, and other internal stakeholders and allows employees to give feedback and provide possible solutions to issues. It is of particular importance to open up and maintain internal communication between all levels in the organization, as well as across the organization between different group and departments because this is one of the key means to incorporate corrosion management into an organization's management systems.

Key internal communication processes include communication of the following:

- Roles, authorities, and responsibilities
- Best practices
- Learning opportunities from ongoing activities, near-misses, and incidents, both internal and external

1.7.2.6 External communication

External communication processes facilitate awareness, understanding, and acceptance of the CMS by contractors and other external stakeholders. As with internal communication, these processes include identification of the stakeholders and information that require communication. Additionally, the organization should make visible points of contact and exchange information regarding corrosion management with external stakeholders. This may include members of the public, regulators, industry organizations, emergency responders, and law enforcement. Adequate training in communication to external stakeholders is essential.

For contracted personnel, achieving buy-in of the CMS is crucial to the overall management of corrosion for an organization's assets and asset systems. This is why clear communication of the CMS, expectations of the contractor, and responsibilities of the contractor within the CMS framework are essential.

Key external communication processes include communication of the following:

- The CMS activities and processes to be conducted or reviewed by the external organization, including scope, boundaries, and applicable standards and procedures.
- Roles, authorities, and responsibilities
- Best practices
- Learning opportunities from ongoing activities, near-misses, and incidents
- Management of change (MOC), including key contacts and elevation plans for technical and nontechnical inquiries
- Approval processes for subcontracting or other contractual changes

1.7.2.7 Risk management

The risk management process coordinates activities to direct and control an organization with regard to risk. In the case of a CMS, the organization needs to establish, implement, and maintain documented processes and procedures for the ongoing identification and assessment of corrosion risks, as well as the identification and implementation of necessary control measures throughout the life cycle of the assets or asset systems.

A risk management approach is well suited to corrosion management where the final plan must include specific tasks and actions required to optimize costs, risks, and performance for assets and asset systems having a wide range of safety, environmental criticality, and business importance.

The ISO 31000 [18] standard provides a useful reference in terms of the components and basic requirements for a consistent approach to risk management, but in general terms the organization's methodology for risk management need to be

- Proportional to the level of risk under consideration.
- Defined with respect to its scope, nature, and timing to ensure it is proactive rather than reactive.
- Included where appropriate, the assessment of how risk can change over time and service life.
- Provided with the classification of risks and identification of those risks that are to be avoided, eliminated, or controlled by asset management.
- Consistent with the organization's operating experience and the capabilities of mitigation measures employed.
- Provided with the monitoring of required actions to ensure that both the effectiveness and timeliness of their implementation.
- Provided with the classification of risks and identification of those risks that are to be avoided, eliminated, or controlled by asset management.
- Consistent with the organization's operating experience and the capabilities of mitigation measures employed.

In terms of corrosion as a specific threat to the asset integrity or lifetime, the planning process described in Fig. 1.4 is a crucial step conducted by corrosion experts to establish the probability of credible corrosion-related events and the various options for mitigation to achieve the integrity or lifetime objectives of that specific asset.

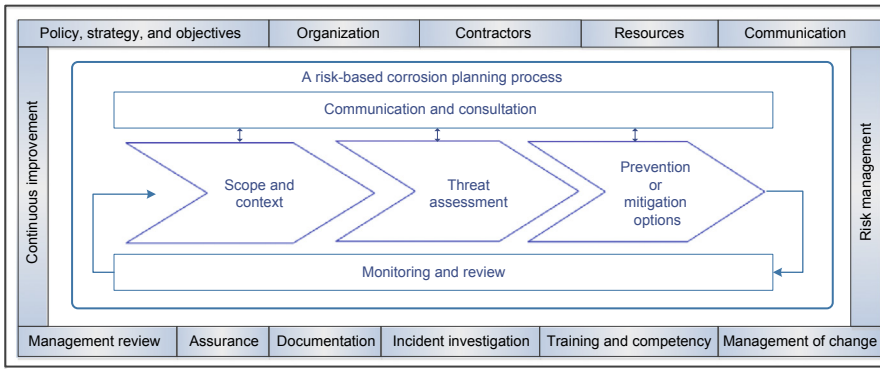

Figure 1.4 Corrosion management system framework.
Based on ISO 31000, Risk Management—Principles and Guidelines.

Fig. 1.4 shows how corrosion management fits into the framework of an overall management system through the standard management system elements. The figure shows the risk-based corrosion planning process, similar to ISO 31000 [18], which incorporates threat assessment and prevention or mitigation options. This type of analysis, which fits into the lower two segments of the management triangle in Fig. 1.3, requires an in-depth technical knowledge of the existing or potential corrosion mechanisms and the available options for mitigation. The process can also serve as input to a complete risk-based decision process that includes associated consequences and context. However, other types of corrosion planning processes may also be utilized depending on the type of industry, regulatory compliance, the required reliability, and ROI considerations.

To complete the "risk picture", the credible consequences of a failure or event as a result of this corrosion mechanism need to be determined. The type or context of the consequence will vary according to the asset type and criticality, but consideration should be given to safety, environment, reputation, and business loss. Applicable regulations or organization procedures may also require a "reverse" risk management process, whereby the consequence criticality of a specific asset is determined first and then the corrosion threat analysis is only conducted for those assets with unacceptably high consequences.

Similar risk pictures will normally be established for other types of threats and then decisions about future investment and plans for asset management will be made based on the (risk) classification of a specific threat. ISO 31010—*Risk Assessment Techniques*, which is a supporting standard to ISO 31000, provides guidance on the selection and applications of systematic techniques for risk assessment [19].

1.7.2.8 Management of change

The MOC process is used to control, evaluate, and verify technical and nontechnical changes to the corrosion management processes, the CMS, assets, or asset systems. Each MOC request must be reviewed by appropriate subject matter experts to evaluate

the effect of each proposed change or suite of changes based on the significance of the change, the need, technical basis, and expert evaluation of the risk associated with the change. Utilizing this information, authorization to proceed with the change should be determined.

It is critical that the MOC process is effectively documented and communicated to all impacted parties throughout the organization.

1.7.2.9 Training and competency

The organization is responsible for ensuring and documenting that personnel whose roles fall within the scope of the CMS have an appropriate level of competence in terms of education, training, knowledge, and experience. Training and competency requirements are applicable to both the organization's staff and contractor personnel.

The organization should develop a process for training personnel on the organization-specific CMS processes and procedures. Additionally, competency evaluations for personnel, such as certifications, internal, or external written or oral examinations, demonstrations of competence, previous job experience, or on-the-job evaluations, should be defined, implemented, and documented. It is important to consider the needs for retraining and evaluations, as well as the difference between training requirements for new and experienced personnel.

1.7.2.10 Lessons learned

Learning from both internal and external events is critical to the continuous improvement of a management system. Formal and consistent processes, such as incident and "near miss" investigations, are used to verify that a continuous improvement loop is in place to learn from events. In this context, "incident" is used to describe an undesirable event that affects the CMS, corrosion process, safety and environment, asset, or asset systems. "Near miss" is used to describe an event that could potentially have affected these.

Examples of incidents include unintentional failure of an asset due to corrosion or failure to follow a defined CMS process or procedure. The goal of an incident investigation is to identify necessary improvements to the CMS, corrosion processes, or procedures. These improvements must be evaluated using the MOC process, communicated throughout the organization, and reviewed by management for effectiveness.

1.7.2.11 Documentation

An organization is responsible for assembling, managing, and maintaining the documentation and records required to support and continually improve the CMS. The term "document" refers to plans or instructions for what actions will be performed; examples include the CMS policy, strategy, objectives, plans, procedures, and inspection forms. Alternately, a "record" refers to proof of compliance with a document's requirements at a specific time. Examples of records include training records, corrosion inspection reports, and meeting minutes. A needs analysis may be performed to determine which records and documents should be retained, both for regulatory or legislative reasons, as well as to conform to an organization's requirements.

1.7.2.12 Assurance

The corrosion management plans (CMPs) and work processes need to be audited periodically to ensure that they are being followed and adhered to and that they remain effective and consistent with the CMS strategy and objectives. The audits can be performed by either the organization's own staff or using a third-party consultant. The audit reports can serve as major input to the management review and continuous improvement process.

1.7.2.13 Management review

A management review is an important aspect of a management system that demonstrates commitment from the organization for implementing, reviewing, and continually improving the management system and associated processes and documents. Management reviews are carried out at the optimized frequency determined by the organization to promote the continuing effectiveness of the CMS, examine current issues, and assess opportunities for improvement.

Typical information inputs for management reviews include:

- Findings from nonconformances, incidents, and failures, both internal and external
- Status of preventive and corrective actions
- Follow-up actions from previous management reviews
- Changes in the organization's operational environment that could affect the CMS including the requirements for additional or revised resources or changes to applicable regulations or standards
- Audit results, both internal and external
- Overall performance in terms of key performance indicators
- Opportunities for improvement

Typical outputs of the management reviews include

- Changes to policy, strategy, or objectives associated with the CMS
- Reallocation or supplementing of resources
- Changing organizational details, including staffing or responsibility updates
- Corrective and preventative measures
- Changes to the CMS processes, procedures, or documents

A process should be implemented to track the completion of any required actions determined during the management review.

1.7.2.14 Continuous improvement

In addition to formal processes that affect continuous improvement, including incident investigations and management reviews, informal opportunities, such as employee concerns and impromptu feedback, should be utilized in an appropriate manner to improve the CMS as well as the corrosion processes and procedures. Continuous improvement can be used to evaluate both the effectiveness of the CMS and its continued relevance to the organization's goals and objectives. Improvements may take the form of changes to the overall policy, strategy, or objectives, or the individual elements of the CMS and their associated processes and procedures.

1.8 Strategies for successful corrosion management

The maximum savings from the impact of corrosion can only be realized by the incorporation of sound corrosion management practices throughout an organization. The organization as a whole must commit to ownership of the CMS systems and processes. Hence, the adoption of a CMS into an organization's management system requires buy-in from top and bottom.

Buy-in into a CMS can be defined as the acceptance of and commitment to a specific concept or course of action that optimizes corrosion management. The ultimate goal of buy-in may be different for the chief executive officer than for the operation's staff as is illustrated in Table 1.1.

The adoption of a CMS into an organization's management system requires buy-in at both the top and bottom of the organization. The technical manager (corrosion/integrity/risk/maintenance manager, part of middle management) is the likely promoter of the need for a CMS. However, without buy-in at the top, initiatives have little chance of getting off the ground. Buy-in by senior management is necessary to gain approval to move forward and garner resources. To ensure that the message is effective, organizations require a business case that includes a clear statement of the problem, outlines its impact on the organization, lists the required resources, and includes the outcome in terms of cost reductions, increased productivity, improved quality, and/or decrease in risk (environmental, safety, business interruption, public relations, etc.).

Buy-in from front-line employees is necessary to create a shared understanding of the change and to ensure compliance. Individuals may understand the change, but take a wait-and-see stance until they see how it will affect them personally. Thus, in order to facilitate business case communication between corrosion professionals and senior management leading to integration of a CMS throughout an organization's management system, the following steps are necessary.

- The corrosion professional should broaden his/her competence with respect to business tools to include financial decision making, risk assessment, and management systems. Use of financial and risk assessment tools should be a normal and expected activity for evaluating corrosion control expenditures. Whenever relevant and possible, financial tools, such as LCC, should be considered.

Table 1.1 Different purposes for buy-in

Target audience	Purposes
Senior management	Gain approval to make the change
	Garner sponsorship and resources
Middle management	Speed up adoption
	Identify change agents to lead by example
Front-line employees	Develop a common understanding of the change
	Ensure widespread adoption and compliance

- Communication between those inside and outside of the corrosion profession should be in the language of the external decision maker (e.g., operations or business manager) or stakeholder (e.g., regulatory, policy, or public) with the goal of business improvement.
- Organizations should develop, integrate, and implement corrosion management elements into their overall management system.

References

[1] G. Koch, M. Brongers, N. Thompson, P. Virmani, J. Payer, Corrosion Cost and Preventive Strategies in the United States, FHWA-RD-01-156, March 2002.
[2] G. Koch, J. Varney, N. Thompson, O. Moghissi, M. Gould, J. Payer, International Measures of Prevention, Application, and Economics of Corrosion Technologies Study, NACE International, 2016. http://www.impact.nace.org.
[3] H.H. Uhlig, The cost of corrosion to the United States, Chemical Engineering News 27 (1949) 2764 or Corrosion 6 (1950) 29.
[4] Chairman T.P. Hoar, Report of the Committee on Corrosion and Protection − A Survey of Corrosion Protection in the United Kingdom, 1971.
[5] J.H. Payer, W.K. Boyd, D.G. Lippold, W.H. Fisher, NBS-Battelle Cost of Corrosion Study ($70 billion!), Part 1−7, Materials Performance (May−November 1980).
[6] D. Behrens, British Corrosion Journal 10 (3) (1967) 122.
[7] Chairman G. Okamoto, Report of the Committee on Corrosion and Protection − A Survey of the Cost of Corrosion to Japan, Japan Society of Corrosion Engineering and Japan Association of Corrosion Control, 1977.
[8] B.W. Cherry, B.S. Skerry, Corrosion in Australia − The Report of the Australian National Centre for Corrosion Prevention and Control Feasibility Study, 1983.
[9] F. Al-Kharafi, A. Al-Hashem, F. Martrouk, Economic Effects of Metallic Corrosion in the State of Kuwait, Final Report No. 4761, KISR Publications, December 1995.
[10] Survey of Corrosion Cost in Japan, Committee on Cost of Corrosion in Japan, 1997.
[11] B.C. Syrett, J.A. Gorman, M.L. Arey, G.H. Koch, G.A. Jacobsen, Cost of corrosion in the electric power industry, Materials Performance (March 2002).
[12] R. Tems, A.M. Al Zahrani, Cost of corrosion in oil production and refining, Saudi Aramco Journal of Technology (2006). Summer.
[13] The Australian Corrosion Association Inc. Corrosion Challenge Project, November 2010.
[14] An analysis of the updated cost of corrosion in India, Materials Performance 53 (8) (2015) 56−65.
[15] B. Hou, et al., China National Cost of Corrosion Study, The China Institute of Oceanology, Chinese Academy of Sciences, 2017.
[16] D.G. Woodward, Life cycle costing − theory, information, acquisition and application, International Journal of Project Management 15 (6) (1997) 335−344.
[17] P.S. Jackman, Life Cycle Costing in the Oil and Gas Industry—A Guideline, European Federation of Corrosion (EFC32), 2003.
[18] ISO 31000, Risk Management—Principles and Guidelines.
[19] ISO 31010, Risk Assessment Techniques.

Further reading

[1] The World Fact Book, GDP—Composition, by Sector of Origin (%). https://www.cia.gov/library/publications/the-world-factbook/fields/2012.html.

Petroleum fluids properties and production schemes: effect on corrosion

2

Anil Bhardwaj
Institute of Engineering and Ocean Technology, ONGC, Panvel, India

2.1 Introduction

Corrosion occurs in hydrocarbon production and transmission systems only in the presence of water and corrosion causing agents. Whether corrosion will occur or not and the extent of corrosion will depend upon corrosive components present in produced gas and other constituents of fluids produced from wells as well as chemical composition of produced fluids and variations in their composition.

The hydrocarbons are produced from underground reservoirs as crude oil, gas, and condensate. Water is invariably produced along with hydrocarbons, which may accompany from the onset of production or it may start at a later stage. This depends upon thickness of the hydrocarbon pay zone and hydrocarbon/water contact.

For example, well "C" in Fig. 2.1, which is near to oil/water contact, will be the first to start producing water with oil and will be the source of water that can initiate corrosion process, of course depending upon several other factors that are discussed in this chapter. By the same token, well "A" will be the last to produce water.

The composition of gas produced from a well will depend on whether it occurs as nonassociated free, gas-cap over crude oil or solution gas, as shown in Figs. 2.2a–c, respectively.

Free gas is lean gas (Fig. 2.2a), predominantly methane; gas produced from gas cap (Fig. 2.2b) has methane along with ethane, and solution gas (Fig. 2.2c) has a lower proportion of methane and relatively higher proportions of ethane, propane, and higher components.

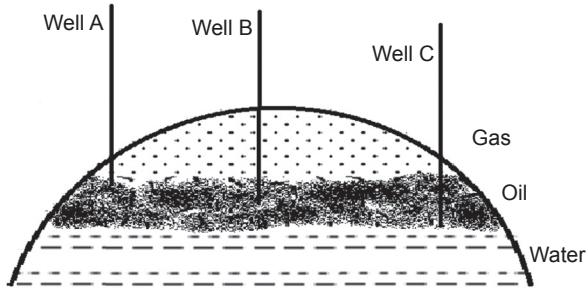

Figure 2.1 Oil, water, and gas in a reservoir.

Trends in Oil and Gas Corrosion Research and Technologies. http://dx.doi.org/10.1016/B978-0-08-101105-8.00002-4

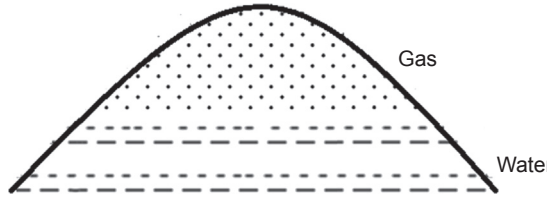

Figure 2.2a Nonassociated gas reservoir.

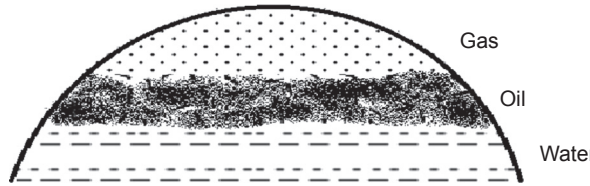

Figure 2.2b Free gas-cap reservoir.

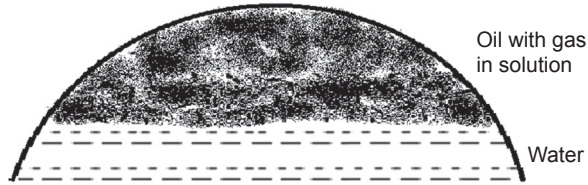

Figure 2.2c Dissolved gas reservoir.

2.1.1 Composition of produced fluids

In addition to water, there are other nonhydrocarbon components that are produced along with oil and gas. The nonhydrocarbon gases that are produced are carbon dioxide, hydrogen sulfide, nitrogen, helium, hydrogen, etc. The nonhydrocarbon constituents of oil have nitrogen, oxygen, sulfur, and metals like vanadium (V), nickel (Ni); sometimes also iron (Fe), aluminium (Al), sodium(Na), potassium (K), calcium (Ca), and copper (Cu).

Oil is a mixture of various hydrocarbons and organic molecules with heteroatoms. Metallic components are also present in oil to the extent of ppm levels only. Leaving aside metallic constituents, oil can be categorized as saturates, aromatics, and heteroatom compounds. Saturates include normal alkanes, branched alkanes, and cycloalkanes. A few examples are

Normal alkanes	Branched alkanes	Cyclo alkanes
Heptane (C_7H_{16})	Iso-heptane	Cyclo heptane (C_7H_{14})
Octane (C_8H_{18})	Iso-octane	Cyclo octane (C_8H_{16})
Nonane (C_9H_{20})	Iso-nonane	Cyclo nonane (C_9H_{18})
Decane ($C_{10}H_{22}$)	Iso-decane	Cyclo decane ($C_{10}H_{20}$)

Aromatics can be benzene, alkyl derivatives of benzene, multifused rings of benzene such as naphthalene, phenanthrene, etc. Heteroatom compounds can be sulfur-containing compounds such as thiols (mercaptans), thioethers, thiophenes; nitrogen-containing compounds such as pyridines, pyrroles; oxygen-containing heterocompounds such as carboxylic acids, volatile fatty acids (VFAs), naphthenic acids (NA), phenols; oxygen and nitrogen-containing compounds such as amides, etc. [1]. Crude oils generally contain no alkenes. Alkenes (olefins) are unsaturated hydrocarbons. Alkenes are formed in oil refining units and are contained in gasoline (to 25 vol%) and kerosene (to 5 vol%).

Crude oil can also be characterized on the basis of saturate, aromatic, resin and asphaltene (SARA) analysis. This method divides crude oil components according to their polarity. The saturate fraction consists of nonpolar material including linear, branched, and cyclic saturated hydrocarbons (paraffins). Aromatics, which contain one or more aromatic rings, are more polarizable. Resins and asphaltenes are polar constituents, the distinction between the two is that asphaltenes are insoluble in an excess of heptane (or pentane), whereas resins are miscible with heptane (or pentane).

Crude oils are also classified according to their specific gravity. Light crude oil has a low density and American Petroleum Institute (API) gravity between 25° and 45°. Heavy crude oil has API gravity between 10° and 25°, it does not flow easily at room temperature and has high viscosity. Generally, it is rich in aromatics and sulfur. Bitumen is a highly viscous form of heavy crude and has API gravity less than 10°.

Crude oil is also defined as sweet if it contains less than 0.5 wt% sulfur. It can be in the form of hydrogen sulfide and also as bonded to carbon atoms.

There can be wide variations in compositions of crude oil and gas that are produced from different reservoirs as illustrated in Tables 2.1 and 2.2.

2.1.2 Production and surface transportation of hydrocarbons

Oil and gas are produced from underground reservoirs in the earth by drilling a hole up to the target depth. The hole is stabilized by placing steel tubes (called casing) in a telescopic design. Drilling is carried out using drilling fluids or drilling muds to remove the rock cuttings and keep the hole stabilized. Once target depth is attained, the well completion process starts to get oil and gas production from the well. First of all, the drilling fluid is replaced by a fluid called “completion fluid”. Various tests are conducted to measure and record reservoir parameters. This fluid is then left in the annular region of a well between tubing and casing above a packer. Typical well diagram is shown in Fig. 2.3.

Schematics of in-field layout, from wells to processing installations in onshore as well as offshore, are depicted in Figs. 2.4–2.6.

Well fluids, including gas, oil, and water, flow from well bore to well head. Natural gas, dissolved in oil due to pressure of the reservoir, separates out when pressure reduces as oil traverses from well bore to surface. These fluids are transported from well head platform to process platform, in case of offshore fields and from wells to processing installation in onshore.

Table 2.1 Range of gas compositions produced from different reservoirs

Components	Unit	Field				
		A	B	C	D	E
Nitrogen	mol%	0.0397	11.8	3.5221	51	0.6
Carbon dioxide	mol%	9.2231	6.79	6.4866	20.4	2.45
Hydrogen sulfide	ppm	100	39,000	400	100	0
Methane	mol%	84.7388	73.8	75.22	47.21	90.43
Ethane	mol%	4.1379	–	7.4357	0.09	4.00
Propane	mol%	0.9102	–	4.6057	0.1	1.39
Iso butane	mol%	0.3153	–	00.9094	0.09	0.19
n Butane	mol%	0.2444	–	1.1342	0.02	0.39
Neo pentane	mol%	0.0084	–	–	0	–
Iso pentane	mol%	0.1600	–	00.2848	0	0.09
n Pentane	mol%	0.0767	–	0.0814	0	0.11

Table 2.2 Range of crude oil compositions produced from different reservoirs

Parameter	Oil						
	A	B	C	D	E	F	G
Density, 15°C (60°F)	0.8706	0.8817	0.9090	0.904	0.8848	0.96	0.83
API gravity, 15°C (60°F)	30.96	28.9	24.08	24.94	28.33	16	38
Pour point (°C)	36	27	42	36	36	9	30
Wax content, mass%	18.4	14.5	29	16.14	12.19	4.86	14.1
Saturates, mass%	54.68	56.81	53.24	73.06	74.47	–	–
Aromatics, mass%	34.7	36.89	36.78	19.75	20.35	–	–
Resin, mass%	9.88	6.15	3.27	7.07	5.12	9	19.7
Asphaltene, mass%	0.56	0.15	6.33	0.12	0.06	11.88	3.5
Resin/asphaltene ratio	17.64	41	0.52	58.5	85.3	0.76	5.63

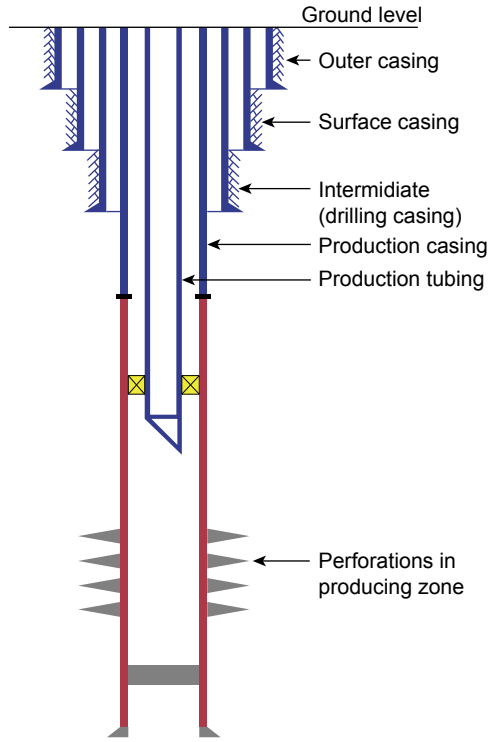

Figure 2.3 Schematic of well design.

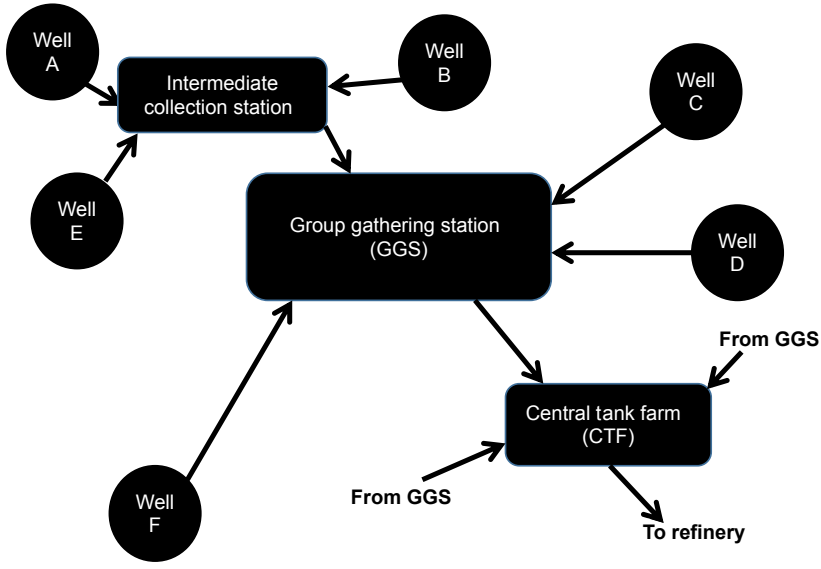

Figure 2.4 Transportation of fluids from onshore wells to processing station, Scenario 1.

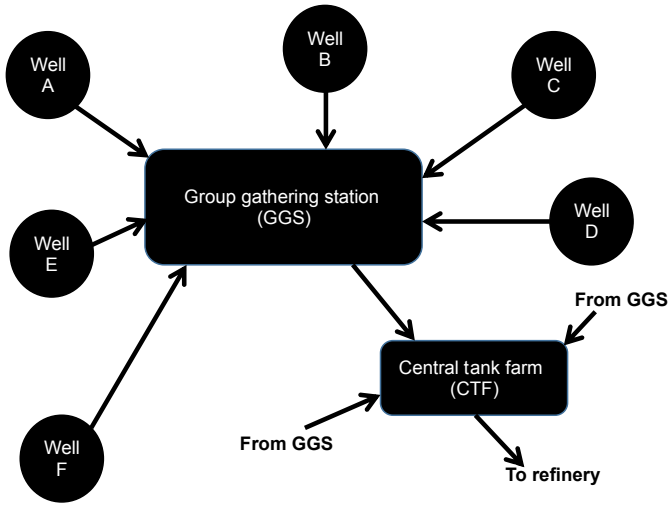

Figure 2.5 Transportation of fluids from onshore wells to processing station, Scenario 2.

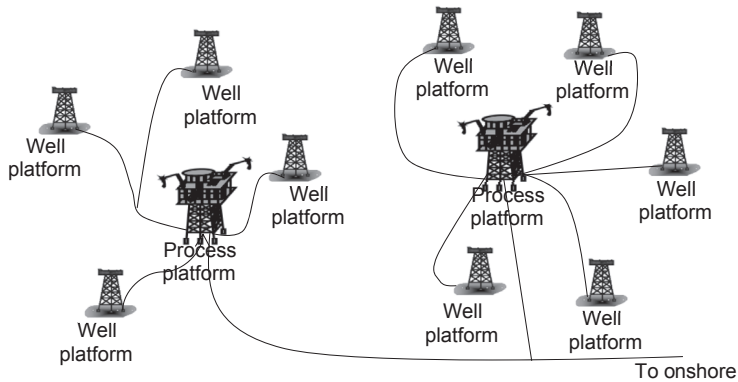

Figure 2.6 Transportation of fluids from offshore wells to processing station [2].

The separation of gas, oil, and water takes place at the processing platform in offshore and collection/processing installation in onshore. A generalized view of process, onshore as well as offshore, is shown in Fig. 2.7. There can be several variants in this process scheme, which will depend upon the nature of fluids produced and requirements.

The pipelines in upstream oil and gas industry can be grouped under three categories:

1. Short distance lines that collect unprocessed fluids (gas, oil and water) from wells and deliver them to processing installation/platform. These pipelines, generally, range from 4 to 12 inches in diameter, pipelines up to 18 inches are also prevalent. They are defined as gathering lines or well fluid lines/flow lines.
2. Collector lines move oil and gas from one processing installation or platform to the trunk pipelines or to another installation. They are generally bigger than gathering lines, but smaller than trunk lines.

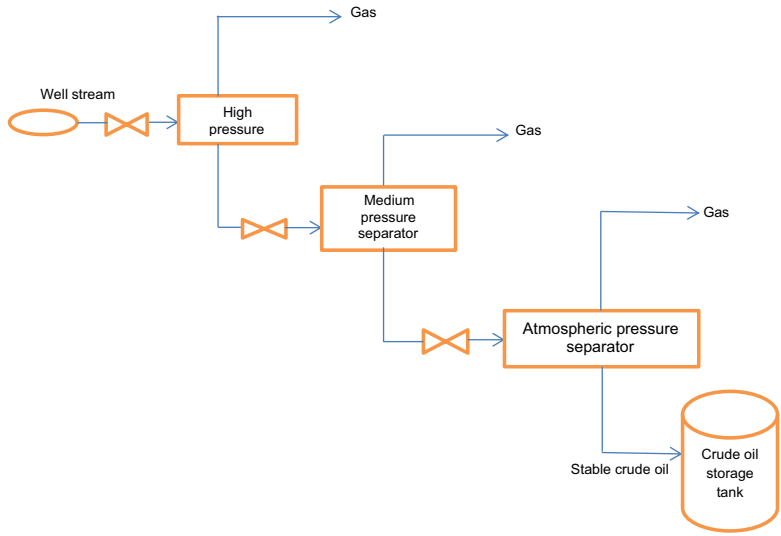

Figure 2.7 General schematics of oil and gas processing installation.

3. Trunk lines transport oil and gas to refineries within a country or across international boundaries. They are also designated as transmission lines and can be up to 56 inches in diameter.

2.2 Corrosion in oil and gas production

The corrosion process can start as the fluids start flowing from well bore through the tubing to surface. Corrosion can also occur in well head facilities, in well fluid pipelines, and separators where gas, oil, and water are separated and effluent/produced water lines. Corrosion can also occur in collector and transmission lines.

The corrosion causing agents that can be present along with crude oil and gas are

- Water
- Corrosion causing gases
  - Carbon dioxide
  - Hydrogen sulfide
  - Oxygen
- Corrosion causing bacteria, like sulfate-reducing bacteria

Oxygen, which also causes corrosion, is not produced along with hydrocarbons from underground reservoirs. But it has been reported to be present in natural gas transmission lines, leading to the issue of black powder [3,4].

Crude oil or natural gas or carbon dioxide or hydrogen sulfide or oxygen—none of them is corrosive in dry state. Corrosion of steel begins in the presence of an electrolyte, i.e., water and carbon dioxide or hydrogen sulfide or oxygen.

Corrosion control measures such as material selection, coating, lining, corrosion inhibition, biocides, pigging, etc., are taken to avert corrosion at each stage.

2.2.1 Water chemistry and corrosion

Chemistry of water further has influence on corrosion process. The ionic composition of water can vary to a great extent. A few examples are shown in Table 2.3.

The presence of chloride and bicarbonate ions in water can have significant influence on corrosion process. Chloride ions tend to increase pitting corrosion and the tendency of pitting corrosion increases with increase in chloride concentrations. Bicarbonate ions act as buffer ions and tend to reduce corrosion rate by enhancing pH of the system. Results of calculations from NOROK M506 [5] software, shown in Table 2.4, demonstrate the influence of variation in bicarbonate and chloride concentration in water on corrosion rate.

Table 2.3 Example of variations in water composition produced from several hydrocarbon reservoirs

Parameters	Unit	Water source						
		A	B	C	D	E	F	G
Carbonate	mg/L	Nil	Nil	Nil	165.5	Nil	Nil	Nil
Bicarbonate	mg/L	549	297	488	2167	3677	1460	61
Chloride	mg/L	18,460	42,095	19,525	3480	4016	8399	142
Sulfate	mg/L	683	75	132	18	10	541	80
Calcium	mg/L	461	–	1136	24	36	140	20
Magnesium	mg/L	134	–	94	19.5	24	12	6

Table 2.4 Effect of variation in corrosion rate with salinity and bicarbonate concentration carbon dioxide: 2%, temperature: 50°C (122°F), line pressure: 30 kg/cm^2, diameter: 10 cm, liquid flow rate: 500 m^3/day, gas flow rate: 100 m^3/day

Bicarbonate (mg/L)	Salinity 2000 mg/L	Salinity 20,000 mg/L	Salinity 40,000 mg/L
	Corrosion rate (mm/year)	Corrosion rate (mm/year)	Corrosion rate, (mm/year)
0	9.7	9.9	9.9
100	4.4	4.8	5.3
500	1.9	2.2	2.5
1000	1.4	1.4	1.7
2000	0.98	0.98	0.98

Table 2.5 Water chemistry dependent corrosion rates. Experimental conditions: static, no CO_2, atmospheric temperature and pressure, open system in presence of air, and dissolved oxygen

Parameter	Treated effluent water	Technical water
Average corrosion rate after exposure of 2 days, mpy	3.89	4.79
Average corrosion rate after exposure of 7 days, mpy	2.36	3.17
pH	7.74	6.83
Salinity, mg/L	14,437	1982
Bicarbonate, mg/L	2013	345

Corrosion rates are reduced by 10 times and 4.5 times as bicarbonate concentration increases from 0 to 2000 mg/L and 100 mg/L to 2000 mg/L at 2000 mg/L salinity. The effect of salinity is more pronounced at intermediate bicarbonate concentrations of 100 and 500 mg/L.

In an experiment, API 5LX 56 carbon steel coupons were exposed to two different waters in the presence of dissolved oxygen. The two waters had different chemistries. The corrosion rates, after exposure of 2 and 7 days, in the two waters, were different as illustrated in Table 2.5. The effluent water, with high concentration of buffering bicarbonate ion and high pH is less corrosive than technical water in spite of higher salinity.

Brine chemistry can influence corrosion of carbon steel in crude oil−brine system in different ways [6−9]:

1. By influencing partitioning of surfactants from crude oil phase to aqueous phase. Generally, increase in salinity reduces this tendency.
2. The ionization of acidic, basic and amphoteric constituents of crude oil is influenced by pH and some of them may become more surface active at a certain pH. Acidic pH generally stabilizes water-in-oil emulsion, whereas basic pH increases stability of oil-in-water emulsion. The in situ pH of brines produced from reservoirs is generally less than seven and will tend to support water-in-oil emulsion, of course, depending on water content.

2.2.2 Nature of oil and corrosion

The nature of oil can have a significant effect on corrosion in a multiphase flow pipeline. The paraffins in light paraffinic oils may tend to separate out during flow in the pipeline as temperature falls along downstream. If the wax deposits as uniform layer

along the length of the pipeline, it may provide protection against internal corrosion. But this is too an idealistic assumption. Thus it is hard to rely on paraffins present in the crude oil to provide assured protection. Water may also get stagnated in pockets under the wax when it is soft. This environment can provide habitat for bacteria and lead to microbiologically influenced corrosion (MIC) or underdeposit corrosion (UDC). Thus, wax segregation and deposition in the pipeline will have a deleterious effect under these circumstances.

The resins and aphaltenes present in oil are natural emulsifier and promote formation of strong water-in-crude oil emulsion. In such an event, the water present in the multiphase will not come in contact with pipeline internal surface and pipeline will be protected against internal corrosion. These constituents of oil can support even high percentage of water and keep the water in emulsified form. On the other hand, light paraffinic crude oils do not form strong emulsions and even water content as low as 20 vol% will form a separate layer. Therefore, the multiphase pipelines carrying light crude oils will be more vulnerable to internal corrosion.

Riekeis et al. [10] observed that the fraction *n*-C_{15} to *n*-C_{23} of condensate had the most inhibitive effect, with alkylated carbazoles (polycyclic compound with a pyrrole ring fused between two benzene rings) having high probability of this inhibitive behavior. Paraffin and asphaltenes present in crude oils have been found to act as natural corrosion inhibitors, reducing the corrosion rate of carbon steel by over 90%, under static conditions [11]. However, localized corrosion was observed when paraffin layer was present at the steel surface, probably temperature made such film weaker. Asphaltenes layers seem to be more protective than the paraffin ones, maybe due to the polar nature of asphaltenes, which form stronger bonds with the steel surface.

The studies by Mendez et al. [12] demonstrated that different components of crude oil, viz. SARA showed some degree of inhibition, however, the aromatic compounds (including sulfur-containing aromatics) present in the resin fraction of the crude oil had the highest effect in controlling the corrosion. Ajmera et al. [13] observed that asphaltenes provided corrosion inhibition, especially when used as solution in toluene. They observed that in the presence of asphaltenes, the wettability of the steel surface depended on the wetting sequence. The surfaces prewetted with water tended to stay hydrophilic, whereas surfaces prewetted with oil tended to remain hydrophobic.

2.2.3 Factors influencing corrosivity of oil

All compounds contained in crude oil are not corrosive and aggressive to metals and alloys. Low molecular weight organic acids (formic and acetic) are more corrosive than high molecular weight organic acids, some of them and their derivatives are corrosion inhibitors. NA contained in some crude oils represent high corrosive concern for oil refineries.

The proposed chemical formula of NA is R(CH2)nCOOH, where R is one or more cyclopentane rings and n is more than 12. They are usually concentrated in high boiling distillate fractions and can corrode inner surfaces of distillation columns at ~230−360°C (445−680°F). NA that pass from crudes into petroleum products are not corrosive at ambient temperatures ~20°C (68°F) of their storage and transportation.

Additional organic acids can appear in refined products as a result of decomposition of peroxides and hydroperoxides, which can be formed due to oxidation of refined products by entrapped oxygen during their storage, distribution, and use. A wide range of nitrogen compounds are present in various crude oils, such as pyridines, quinolines, alkylquinolines, benzoquinolines, acridines, pyrroles, indoles, carbazoles, benzo carbazoles, pyrroles, and amides. Some of the nitrogen compounds and their derivatives are known to provide corrosion inhibition. Organic N-containing compounds break down at high temperature and form ammonia (NH_3), which is a corrosion inhibitor of carbon steel but aggressive to zinc, copper, and their alloys [14].

VFAs are water-soluble short-chain carboxylic acids containing one to five carbon atoms per molecule, including carbon atom of carboxylic group. These are organic acids such as formic acid (HCOOH), acetic acid (CH_3COOH), propionic acid (C_2H_5COOH), butanoic acid (C_3H_7COOH), and valeric acid (C_4H_9COOH). However, the single-carbon carboxylic acid, formic (HCOOH), is not generally found in natural, unpolluted waters [15]. Other acids have high vapor pressure. These acids are completely miscible with water. The dissociation constant (K_a) value for the last three acids is in the same range and of the order of 10^{-5}, whereas dissociation constant of formic acid is around 10 times higher (1.77×10^{-4}) than acetic acid (1.75×10^{-5}). Most of the studies involving VFA, use acetic acid as the representative acid because dissociation constant of other acids is in the same range as that of acetic acid and equivalent concentrations of undissociated acetic and formic acid lead to a similar corrosion rate [16].

Concentrations of VFA in a typical produced water analysis by chromatography were as follows: acetic acid, 362 mg/L; propionic acid, 37.88 mg/L; and butyric acid, 8.05 mg/L.

The various studies on corrosion due to VFA have reported [17–21]:

- Increased cathodic reaction
- Slightly inhibited anodic reaction
- Prevention of protective film of iron carbonate and increase in time required to form protective iron carbonate film, when corrosion studies are carried out in presence of carbon dioxide
- Increase in corrosion rate due to lowering of pH

The presence of both acetate and propionate ions influences the alkalinity as measured by standard water analysis and as a result inflated bicarbonate value is reported [22,23]. The acetate concentration measured with ion chromatography is more reliable.

VFAs, acetic and propionic, which are water soluble, significantly influence corrosion rates and corrosion rate of API 5L X65 has been reported to stabilize at around 5 mm/year (200 mpy) in the presence of 80% brine, 20% oil, 500 ppm acetic acid, and 1 bar (14.5 psi) CO_2 [24].

Dissolution of ingredients from crude oils may alter the corrosiveness of the aqueous phase. The corrosivity of crude oil containing water can be determined by a combination of three properties: the type of emulsion formed between oil and water, the wettability of the steel surface, and the corrosivity of water phase in the presence of oil [25].

Corrosion rates of brine equilibrated with different crude oils have been reported to decrease. The extent of reduction in corrosion rate varies with nature of crude oil. The corrosion rates determined in pure brine will be generally in excess of actual corrosion rates of brine, which has equilibrated with crude oil in field conditions [26].

ASTM G205 further provides a guideline for classifying crude oils into four categories based on the effect of the oil on the corrosivity of water: corrosive hydrocarbons, neutral hydrocarbons, inhibitive hydrocarbons, and preventative hydrocarbons [27]. Corrosiveness of the aqueous phase in the presence of oil can be determined by methods described in test Method NACE TM0172 [28].

An oil-wet surface is not susceptible to corrosion because of higher electrical resistance. Wettability can be characterized by measuring the contact angle or the conductivity (spreading method). In the contact angle method, the tendency of water to displace hydrocarbon from steel is measured directly by observing the behavior of the three-phase system. The contact angle is determined by the surface tensions (surface free energies) of the three phases. A hydrocarbon−steel interface will be replaced by a water−steel interface if this action will result in an energy decrease of the system. To determine whether the surface is oil wet, mixed wet, or water wet, the angle at the oil−water−solid intersection is measured.

In the spreading method of determining wettability, the resistance between steel pins is measured. If a conducting phase (for example, water) covers (wets) the distance between the pins, conductivity between them will be high. On the other hand, if a nonconducting phase (for example, oil) covers (wets) the distance between the pins, the conductivity between them will be low.

Collier et al. [29] studied corrosivity of 11 conventional and bitumen derived crude oils with density varying from 783 to 977 kg/m^3 and all of the tested crude oils were found to inhibit the corrosivity of brine by 88%−99%, with no correlation with density. The rotating cage test method was used in these studies, with medium comprising of oil/brine ratio of 25:75.

de Waard et al. [30] found a correlation between API gravity, emulsion stability, and water wetting of steel on the basis of two sets of field data on tubing corrosion, that heavier oils are more protective than lighter ones. Heavier oils provide more wetting of steel than the lighter oils. Studies by Badmos et al. [31] also revealed that higher density oil with lower hydrogen content provides better oil wetting of steel surface and hence provides increased corrosion inhibition. Several other studies also concluded that heavy crude oils, which are rich in surface active and heteroatom provide better corrosion resistance [32−35].

It has been reported, though qualitatively, that light oils give low protection against corrosion compared to heavy oils. This relative protection is dependent on water cut as well. But gas condensate does not provide any significant protection even at very low water cut. Hydrocarbon chemistry plays a role in this process, high molecular weight oils, rich in surface active agents can better entrain water in water-in-oil emulsion and thus provide protection.

Crude oil grades have not been observed to differ in their corrosivity, but there are measurable variations in certain corrosion-related properties of crude oil, such as wettability and emulsion-forming tendency [36]. This influence of crude oil on

corrosion of steel will depend upon its ability to stabilize water-in-oil emulsion, and thus retain the water, which in turn is affected by other variables also, such as temperature, flow regime, velocity, and chloride content. Finally, the conductivity of the water-in-emulsion so formed will guide the corrosion behavior. The studies carried out by Turris et al. [37] with crude oil of API 25 (density = 902 kg/m^3) observed inhibitive effect of crude oil and the inversion of water-in-oil emulsion (noncorrosive) to oil-in-water emulsion (corrosive) occurred at 50 vol% water.

The water-soluble constituents in crude oil are heteroatom compounds, having atoms like nitrogen, sulfur, and oxygen, in addition to carbon and hydrogen-containing organic compounds. These include compounds like pyridines, indoles, benzofurans, phenols, amines, organic acids, thiols, ketones, and aldehydes. All are organic compounds that are water soluble and surface active to varying degrees [38,39].

2.2.4 Water/oil ratio and corrosion

Crude oils wet the pipeline internal wall surface to varying degrees. This provides protection against corrosion. Condensate produced with gas provides considerably lower wetting and in pure gas wells no such wetting is available. Thus, vulnerability to corrosion of the pipelines carrying corrosive gases and oil along with water varies as: crude oil < gas with condensate < pure gas. Further, the flow behavior in oil and gas wells is different. The flow velocities in gas pipelines and wells are higher than in oil wells. Therefore, the likelihood of erosion–corrosion in gas pipelines and wells is higher than in crude oil wells and pipelines. Most oil transmission pipelines are in laminar flow because of oversizing and energy conservations requirements. This results in water settling in the pipeline.

The amount of water present in the fluids flowing through the pipelines determines probability of water wetting of the metal surface. Water wetting increases with increase in water content, thus increasing the probability of corrosion in the pipeline system. Further, the salinity of water is determined by the fact whether it is condensed water or formation water, the latter generally has much higher salinity.

When water and oil are coproduced, different situations may arise:

1. They do not form an emulsion and stay separated. In such a case, oil–water dispersion can result if velocity is high and the two will flow as segregated phases if velocity is low with denser water forming the lower phase. The latter situation will augment probability of corrosion along bottom quadrant of the pipeline.
2. They form water-in-oil emulsion. In such a situation, inner surface of the pipeline will be wet with crude oil and shall be protected against corrosion. Moreover, water-in-oil emulsion has low conductivity and will be less corrosive.
3. They form oil-in-water emulsion. Such emulsions are normally produced when oil proportion is very low or some special chemicals are present that can invert water-in-oil emulsion to oil-in-water emulsion even at a higher proportion of oil. But this situation is not encountered under natural flow conditions of a reservoir. Therefore, formation of oil-in-water emulsion is limited to only former condition or they exist in produced water. Such emulsions have high conductivity and are more corrosive compared to water-in-oil emulsions.

Papavinasam et al. [40] experimentally determined the effect of wettability on pit growth rate. Electrochemical noise data, exchange current densities of potentiodynamic polarization plots, and the surface layer thickness measurement using scanning electron microscope was utilized by them to measure the pit growth rate. The wettability was varied from water wet to mixed wet to oil wet, while maintaining all other factors constant. The pit growth rate varied from 60 to 10 to 5 mpy, respectively.

Craig [41] has defined the corrosion behavior of steels due to crude/water ratios in three different regions where different mechanisms are present:

- Region I, where the mixture is an emulsion of water in crude oil and the water is present only in very small proportions, dispersed in the crude phase. Corrosion rates are minimal in such a case.
- When the emulsion is not stable, the water drops initially dispersed in the crude begin to coalesce and tend to wet the metal surface, increasing the corrosion rate behavior that defines region II.
- In region III, water is the continuous phase and the crude is in dispersed phase. Depending on the characteristic of the crude, solid particles, and agitation, a stable emulsion of crude oil in water can be formed. However, in this region, the mechanism that predominates on corrosion is not conductivity instead it is a continuous layer of water on the metal and the transport of corrosion agents towards it.

Castillo et al. [42] in their studies in a stirred autoclave, under the experimental conditions of 80°C (176°F) and 4.9 bar (71 psi) of CO_2 partial pressure, observed that crude oil rich in paraffins, resins, and aromatics provided better protection against corrosion of the L 80 carbon steel. From 100 vol% brine, the corrosion rate decreased rapidly by adding only small quantities of crude. Then, the corrosion rate increased up to a maximum at 5% of crude oil in case of the crude oil richer in these components, where it decreased again and stabilized to lower values. Although the corrosion rate increased up to a maximum at 20% of crude oil in case of the crude oil leaner in these components, where it decreased again and stabilized to lower values. The protection of steel was assigned to organic compounds in crude oil and water phase. Autoclave studies by different workers have shown that at lower water cuts (up to 45 vol%) carbon steel corrosion is minimized, with any type of crude oil. At higher water cuts, corrosiveness depends on the crude oil [43].

Laboratory experimental studies were carried in a high temperature high pressure autoclave at 72°C (162°F) and 0.33 bar (4.7 psi) CO_2 partial pressure. The experiments were conducted for 6 h duration. The aqueous medium was produced water from an oil field. The corrosion rate reduced from 88.89 mpy in 100% produced water to 19.38 mpy in the presence of 20 ppm of a commercial corrosion inhibitor and to 9.34 mpy in the presence of 80:20 produced water:crude oil from the field, along with 20 ppm of commercial corrosion inhibitor. Thus, the presence of crude oil in the medium played a significant role in bringing down corrosion rate.

Carew et al. [44] studied corrosion behavior of API L80 carbon steel with varying proportions of crude oil and observed that up to 20 vol% water, corrosion was uniform and pitting occurred at higher water proportions in the stirred system containing CO_2 and H_2S.

The corrosion rates in carbon dioxide partial pressure of 7.9 bar (114.5 psi), liquid velocity 1 m/s, and 0%, 20%, and 60% oil fraction (for two different oils similar to condensate and light oil) have been reported to decrease rapidly for oil fraction above 60% [45]. This was established to be primarily due to the fact that for oil fraction up to 60%, the bottom of the pipe was in contact with the water and that resulted in the high corrosion rates.

The water content in oil transport pipelines is generally specified ~1 vol% with the premise that it will not segregate during flow from oil processing installation to receiving end. Because of this microbial and electrochemical corrosion problems can be avoided. But this limit of 1% is not sacrosanct. If flow velocity is more than 1 m/s, this water can be entrained even in light crude oil. But if this velocity is less than 1 m/s, even 1% water may segregate and cause corrosion along bottom of the pipeline. However, if oil density is relatively higher, ca, more than 900 kg/m^3, water content even 2% or higher can be easily entrained. Therefore, to minimize the probability of corrosion along bottom quadrant of pipeline, permissible limit of water content in oil in the transport pipeline will depend upon oil density as well as flow velocity. Further, as the oil production in a field declines due to aging, flow velocity in the pipeline will reduce and therefore, water content requirement will have to be revised. Here, the situation becomes complex because aging fields produce more water and treatment facilities are not able to handle increased amount of water. As a result, the operator is hard pressed to maintain low water content in the dispatch oil.

Efird also studied the influence of amount of brine in a crude oil on carbon steel corrosion [46]. Different crude oils were seen to behave in entirely different manner:

- Crude oil A: Abrupt increase in corrosion rate started at ~5% produced water cut
- Crude oil B: Abrupt increase in corrosion rate started at ~20% produced water cut
- Crude oil C: There was no sharp change in corrosion rate even up to 30% produced water cut

Simple rules-of-thumb such as water-to-oil ratio exceeding 30% have been applied to delineate between a noncorrosive from corrosive system. Yet, it is known, from substantial experience in the oil industry, that water/oil systems are quite complex and that corrosion in one oil field may occur with as little as 1% water in oil; although in others, the water cut may exceed 50% before measurable corrosion occurs.

Conductivity of the solution can give a qualitative estimate of the corrosiveness of a solution because corrosion rates generally increase with increasing solution conductivity. Although the corrosion current is the sum of all reaction steps in the system, if one of those steps has a conductivity significantly less than the others, it will be rate controlling. Thus, for low-conductivity solutions, the corrosion rate can be assumed to be primarily a function of solution conductivity. To relate conductivity to corrosion tendency, it has been suggested that a conductivity of at least 10^{-7} S/cm for organic liquids is necessary to produce corrosion [47].

When water comes in contact with oil, the following sequence of events can happen that will lead to different corrosion scenarios [33]: (1) small quantities of water are solubilized in oil which may or may not affect conductivity and hence corrosion, (2) water-in-oil emulsion will form once solubility limit of water is exceeded and stability and extent up to which water will get emulsified, depends upon nature of oil as well

physical conditions such as, temperature and mixing forces; and (3) further increase in water content will eventually lead to separation of free water. In this situation, role of wettability becomes significant.

Corrosion rate break test has been described by Efird [46] that can be used to determine if steel can be used and to specify the produced water level where chemical treatment must be initiated and the recommended chemical treatment. It has been defined as the sudden increase in the corrosion rate between two produced water levels. The corrosion tests are conducted at 10% by volume produced water increments starting with 100% crude oil until a high corrosion rate is obtained. Corrosion inhibitors are then evaluated at a produced water content 5%−10% above the corrosion rate break level.

2.2.5 Sediments in crude oil

Oil flowing from a reservoir contains not only water, but also some solids along with paraffins, asphaltenes, and resins. These collectively are defined as bottom sediments and can settle in storage tanks and pipelines, along with water. Therefore, the term BS&W (basic sediments and water) is used to define quality of oil for transportation purpose.

The presence of sediment and water makes crude oil corrosive. Crude oil transmission lines have a limit of BS&W. The crude oil flow velocities in the lines are generally sufficient to prevent settling of water. But sometimes settling of sediments can occur even when BS&W is less than 0.5%. Solubility of water in crude oil is very low, ca. of the order of 50−100 ppm only and water droplets that are dispersed in oil phase generally have size less than 10 μm. The droplet size will increase due to the coalescence over a period of time. The sludge containing hydrocarbons, sand, clay, corrosion products, salt, water, and bacteria when settled at the bottom can cause UDC. The sludge so separated can be analyzed while it is collected during pigging. Solids, water, and oil content of the sludge are determined by Dean and Stark method. It is generally tested for solubility in organic solvents, water and acids. Energy dispersive spectroscopy (EDS) is also carried out for elemental analysis, especially iron that provides an idea about the extent of corrosion. Microbiological analysis can provide information on the presence of microbes that can influence corrosion. Sand in the sludge can be quantified by mineralogical analysis.

The sludge collected from pipelines during pigging can show a wide range of variation. In one oil-transporting pipeline, which is pigged quarterly, chloroform extractable organic matter varied from 89.65% to 99.2% over a period of 3 years.

EDS provides elemental composition of corrosion debris collected from a pipeline or tank. The relative amounts of elements detected are categorized as major, minor, or trace. The elements that are detected by EDS may include C, Fe, and O as major, Ca, S, Cl, and Si as minor, with traces of Na, K, and Al. Ba and Sr may also be detected in the scale if barium and strontium sulfate are present, which form scale due to their low solubility. Deposits in pipelines can consist of iron oxide, iron carbonate, iron sulfide, sand, clay, and mud. X-ray diffraction (XRD) analysis of the deposits can be used to get direct compositional phase analysis. Wet chemical analysis of deposits can be

used on-site to obtain information about corrosion processes occurring in the pipeline, such as CO_2 corrosion, H_2S corrosion. But the results of wet chemical analysis have to be interpreted with care because carbonate present in different forms other than $FeCO_3$, such as $CaCO_3$ in scale, will also effervesce and only makinawite form of iron sulfide actively reacts with hydrochloric acid while other forms of iron sulfides are less reactive to the extent that no H_2S may be evolved during spot acid test [48].

2.2.6 Influence of flow velocity

If an oil pipeline is idle for long time, the water entrained/emulsified in crude oil can settle at the bottom of the pipeline. The settled water will accumulate in low points and will stay there until it is moved by high flow or pigging. This settled water causes corrosion in those low spots [49].

Laboratory experiments by Wicks and Fraser [35] have shown that there is a critical velocity for a given diameter of a pipeline below which water will not be entrained in flowing oil. The following factors influence the formation and size of water droplets:

- the specific gravities of oil and water
- the crude oil/water interfacial tension
- the crude oil viscosity
- the pipeline diameter
- the velocity of flowing fluids

The liquid velocity necessary to entrain free water increases with an increase in

- pipeline inside diameter
- crude oil viscosity
- crude oil density
- an increase in crude/water interfacial tension

The entrainment velocity will also increase with decrease in temperature, which results in increase in crude oil viscosity, crude oil/water interface tension, and crude oil density.

Therefore, it is always desirable to maintain a crude oil flow velocity such that water phase remains in the entrained state and it re-entrains settled water from the pipe bottom. de Waard et al. [50] developed an empirical factor multiplier to be used in their corrosion prediction correlation based solely on the water cut and the liquid velocity, i.e., steel surface will oil wet when

- water cut $\leq 30\%$ and
- liquid velocity ≥ 1 m/s

Pots and Kapusta [51] modified this empirical assumption, on the basis of field measurements of the water distribution and water wetting in a number of oil pipelines and extensive laboratory data, as

- water cut $\leq 40\%$
- liquid velocity ≥ 1.5 m/s

Under these conditions, corrosion is not expected to occur. But, the other factors mentioned by Wicks and Fraser [35] will also influence corrosion probability.

Cai et al. [52] developed a model that predicts that the critical velocity for a light crude oil increases significantly with water cut and pipeline diameter and slightly with oil surface tension, but decreases with oil density and viscosity. For a low density oil (density = 820 kg/m^3, viscosity = 2 cp, oil/water interfacial tension = 0.029 N/m), critical velocity approached 1.5 m/s with water cut as low as $\sim$10%.

In the presence of gas along with water and oil, different flow regimes such as stratified, slug, and annular, can occur that affect preferential water or oil wetting of pipeline steel in different ways.

2.2.7 Role of interfacial phenomena

The amount of water that can be retained as water-in-oil emulsion, before the water separates out depends also on crude oil/water interfacial tension, $\gamma_{\text{oil-water}}$. Low API gravity crude oils have low $\gamma_{\text{oil-water}}$ and hence lower API gravity (higher density) crude oils are expected to form a more stable water-in-emulsion. Furthermore, when three interfacial tension values are considered with respect to oil, water, and steel, the variants are oil/water interfacial tension ($\gamma_{\text{water-oil}}$), oil/steel interfacial tension ($\gamma_{\text{oil-steel}}$), and water/steel ($\gamma_{\text{water-steel}}$) and the three are related as

$$(\gamma_{\text{oil-water}}) = (\gamma_{\text{oil-steel}}) - (\gamma_{\text{water-steel}})$$

Assuming that interfacial tension between steel and water is constant (or there is not much variation), lower oil/water interfacial tension implies lower oil/steel interfacial tension. This results in enhanced wetting of the steel by the oil, thereby reducing the rate of corrosion. Thus, it is expected that high-density crude oils, which generally have low oil/water interfacial tension, will wet steel surface and protect it against corrosion. These crude oils also facilitate formation of water-in-crude oil emulsion upto high water content, which has crude oil as external phase and thus provide protection against corrosion.

Condensates and low density crude oils (high API gravity) are not rich in natural surfactants, therefore, will have high oil/water interfacial tension and hence high oil/steel interfacial tension, and will not significantly wet steel surface. They also do not form stable water-in-oil emulsion even in the presence of low water content (even $\leq$ 10%). Thus, they are not able to provide protection against corrosion. The only way corrosion can be low in such systems if velocity is high enough to entrain water.

In a study by Bhardwaj and Hartland [53], aphaltenes were removed from crude oil by solvent precipitation and resins by silica gel adsorption. The resultant crude oil fraction that was devoid of both asphaltenes and resins could not form a stable emulsion. The crude oil formed stable water-in-emulsion and asphaltenes as well as resins supported a stable water-in-oil emulsion. The studies by Villalba and Bello [54] concluded that an increase in the resin content of crude oil enhanced corrosion protection of steel.

2.2.8 Microbiologically influenced corrosion

This type of corrosion is encountered in many of the oil fields after water injection, which is used to improve oil recovery. Sulfate-reducing bacteria (SRB) are the most dominant microbes that are responsible for majority of this type of corrosion failures under anaerobic environment. The most conducive temperature for these bacteria is, generally, around 40°C (104°F), though SRB that can survive higher temperatures have also been reported. In the metabolic process of SRB, sulfate is reduced to sulfide and hydrogen that is produced by cathodic reaction is also consumed. The net reaction is

$$SO_4^{2-} + H_2 = H_2S + H_2O$$

The overall corrosion process is accelerated due to (1) increase in cathodic reaction rate caused by cathodic depolarization and (2) increase in anodic reaction rate due to H_2S.

2.3 Summary

The corrosion of carbon steel in upstream oil and gas production and transmission lines will depend upon factors that relate to chemistry of crude oil, water, and gas as well as proportions of various components, interfacial phenomenon, temperature, and flow characteristics. These factors have been grouped in Table 2.6.

Table 2.6 Summary of factors influencing corrosion of carbon steel

Factors	Details
Crude oil chemistry	• Asphaltenes, resins, wax • Natural corrosion inhibitors • Natural surfactants of crude oil
Crude oil physical parameters	• Density • Viscosity
Gas	• Corrosive components: CO_2, H_2S • Partial pressures of corrosive components
Water chemistry	• pH and ionic composition
Physical parameters of water	• Density • Water content in liquid • Water droplet size distribution
Interfacial properties	• Crude oil/water interfacial tension • Metal surface wetting behavior
Pipeline	• Diameter • Bathymetry
Flow	• Velocity • Pattern • Wall shear forces

There can be a number of combinations of these parameters and there exist a large number of possibilities that these parameters can interact, which can affect wetting of steel and hence influence corrosion rate.

References

[1] J.G. Speight, The Chemistry and Technology of Petroleum, fourth ed., CRC Press, 2007.
[2] A. Bhardwaj, B. Raj, Internal Corrosion of Pipelines, Narosa Publications, 2015, p. 1.7.
[3] N. Sridhar, D.S. Dunn, A.M. Anderko, M.M. Lencka, H.U. Schutt, Effects of water and gas compositions on the internal corrosion of gas pipelines-modeling and experimental studies, Corrosion 57 (3) (2001) 221−235.
[4] F.F. Lyle, Carbon Dioxide/Hydrogen Sulfide Corrosion under Wet Low-Flow Gas Pipeline Conditions in the Presence of Bicarbonate, Chloride and Oxygen, PRCI Final Report PR-15-9313, 1997.
[5] CO_2 Corrosion Rate Calculation Model, NORSOK M 506.
[6] S. Kokal, Crude-oil emulsions: a state-of-the-art review, in: SPE Annual Technical Conference, 2002. Paper 77497.
[7] J.D. McLean, P.K. Kilpatrick, Effects of asphaltene solvency on stability of water-in-crude-oil emulsions, Journal of Colloid and Interface Science 189 (1997) 242−253.
[8] S.H. Standal, A.M. Blokhus, J. Haavik, A. Skauge, T. Barth, Partition coefficients and interfacial activity for polar components in oil/water model systems, Journal of Colloid and Interface Science 212 (1999) 33−41.
[9] H. Fang, L. Zhang, L. Luo, S. Zhao, J. An, Z. Xu, J. Yu, A. Ottova, H. Ti Tien, A study of thin liquid films as related to the stability of crude oil emulsions, Journal of Colloid and Interface Science 238 (2001) 177−182.
[10] L.M. Riekeis, R.V. Seetharam, R.M. Krishnamurthy, C.F. Kroen, J.L. Pacheco, R.H. Hausler, N. Kaczorowski, V.A.W. Semerad, Management of corrosion in the Arun field, Corrosion 53 (1) (January 1997) 72−81.
[11] J.L. Morales, J.J. Perdomo, M. Ramirez, A. Viloria, Effect of crude oil contaminants on the internal corrosion in gas pipelines, in: CORROSION 2000, 2000. Paper No. 40.
[12] C. Mendez, S. Duplat, S. Hernandez, J. Vera, On the mechanism of corrosion inhibition by crude oils, in: CORROSION 2001, NACE, 2001. Paper No. 1044.
[13] P. Ajmera, W. Robbins, S. Richter, S. Nesic, The role of asphaltenes in inhibiting corrosion and altering the wettability of the steel surface, in: CORROSION 2010, 2010. Paper No. 10329.
[14] A. Groysman, Corrosion in systems for storage and transportation of petroleum products and biofuels, in: CORROSION 2015, 2015. Paper 5455.
[15] G.B. Farquhar, A review and update of the role of volatile fatty acids (VFA's) in seawater injection systems, in: CORROSION 98, March 22−27, 1998, San Diego Ca, NACE International, 1998.
[16] R.T. Morrison, R.N. Boyd, Organic Chemistry, sixth ed., Prentice Hall of India Private Limited, 2000, pp. 715−735.
[17] V. Fajardo, C. Canto, B. Brown, S. Nesic, Effect of organic acids in CO_2 corrosion, in: CORROSION 2007, NACE, Houston, Texas, 2007. Paper No. 07319.
[18] J. Amri, E. Gulbrandsen, Effect of acetic acid on propagation and stifling of localized attacks in CO_2 corrosion of carbon steel, in: CORROSION 2009, NACE, Houston, Texas, 2009. Paper No. 9284.

[19] J.L. Crolet, N. Thevenot, A. Dugstad, Role of free acetic acid on the CO_2 corrosion of steels, in: CORROSION 1999, NACE, Houston, Texas, 1999. Paper No. 466.
[20] J.L. Crolet, M. Bonis, Why so low free acetic acid thresholds in sweet corrosion at low PCO_2, in: CORROSION 2005, 2005. Paper No. 272, Houton, Texas.
[21] O.A. Nafday, S. Nesic, Iron carbonate film formation and CO_2 corrosion in the presence of acetic acid, in: CORROSION 2005, NACE, Houston, Texas, 2005. Paper No. 05295.
[22] B. Hedges, L. McVeigh, The role of acetate in CO_2 corrosion: the double whammy, Paper No. 21, in: CORROSION/99, NACE International, Houston, Texas, 1999.
[23] J.D. Garber, R.S. Perkins, V.R. Jangama, R.R. Alapati, Calculations of downhole pH and delta pH in the presence of CO_2 and organic acids, Paper No. 176, in: CORROSION/96, NACE International, Houston, Texas, 1996.
[24] M.W. Joosten, J. Kolts, J.W. Hembree, Organic acid corrosion in oil and gas production, in: CORROSION 2002, 2002. Paper 02294.
[25] A. Groysman, Corrosion for Everybody, Springer, Dordrecht, 2010, p. 368.
[26] K. Daniel Efird, The range and variability of crude oil effects on steel corrosion in sweet and sour production, in: CORROSION 2015 Conference & Expo, 2015. Paper 5635.
[27] ASTM G205.
[28] Test Method NACE TM0172.
[29] J. Collier, S. Papavinasam, J. Li, C. Shi, P. Liu, M. Podlesny, Comparison of corrosivity of crude oils using rotating cage method, in: NACE 2012 Northern Area Eastern Conference, Toronto, Canada October 2831, 2012, Presented at the Symposium on Crude Oil Corrosivity Paper Number: 2012 − 06, 2012.
[30] C. de Waard, L.M. Smith, B.D. Craig, The influence of crude oils on well tubing corrosion rates, in: CORROSION 2003, 2003. Paper 03629.
[31] A.Y. Badmos, H.A. Ajimotokan, E.O. Emmanuel, Corrosion in petroleum pipelines, New York Science Journal 2 (5) (2009).
[32] U. Lotz, L. van Bodegom, C. Ouwehand, The Effect of Type of Oil or Gas Condensate on Carbonic Acid Gas Corrosion, NACE Corrosion 90, Las Vegas, Paper 41.
[33] B. Craig, Predicting the corrosivity of water-oil solutions as a means to estimate corrosiveness, Corrosion 54 (8) (1998) 657.
[34] C. Mendez, S. Duplat, S. Hernandez, J. Vera, On the Mechanism of Corrosion Inhibition by Crude Oils, NACE, 2001. Paper 1030.
[35] M. Wicks, J.P. Frazer, Entrainment of water by flowing oil, Materials Performance (May 1975) 6−12.
[36] Managing corrosion of pipelines that transport crude oils, Pipeline and Gas Journal 240 (3) (March 2013).
[37] A. De Turris, M. de Romero, S. Papavinasam, R. Lastra, Effect of SRB, CO_2, crude oil and chemical treatment on the corrosivity of synthetic produced water, in: CORROSION 2013, 2013. Paper 2213.
[38] H.H. Hasiba, F.W. Jessen, Film forming compounds from crude oils, interfacial films and paraffin deposition, Journal of Canadian Petroleum Technology 7 (1) (January−March 1968) 1−12.
[39] J.S. Smart, Wettability—A Major Factor in Oil and Gas System Corrosion, in: CORROSION/93, NACE International, New Orleans, March 1993. Paper 93070.
[40] S. Papavinasam, A. Doiron, R.W. Revie, Model to predict internal pitting corrosion of oil and gas pipelines, Corrosion 66 (3) (March 2010) 035006-1−035006-11.
[41] B. Craig, Corrosion in oil/water systems, Materials Performance (August 1996) 61.
[42] M. Castillo, H. Rincon, S. Duplat, J. Vera, E. Baron, Protective properties of crude oils in CO_2 and H_2S Corrosion, in: CORROSION 2000, NACE, 2000. Paper No. 00005.

[43] U. Lotz, L. Van Bogdegom, C. Ouwehand, The effect of type of oil or gas condensate on carbonic acid corrosion, in: CORROSION 90, 1990. Paper No. 46, Las Vegas, Nevada.
[44] J.A. Carew, A. AI-Sayegh, A. AI-Hashem, The effect of water-cut on the corrosion behaviour of L80 carbon steel under downhole conditions, in: CORROSION 2000, 2000. Paper 00061.
[45] W.P. Jepson, The effect of flow characteristics on sweet corrosion in high-pressure, three-phase, oil/water/gas horizontal pipelines, in: Prevention of Pipeline Corrosion Conference, Houston, Texas, October 17−20, 1994, 1994.
[46] K.D. Efird, Preventive corrosion engineering in crude oil production, in: 23rd Annual OTC, Houston, Texas, May 6−9, 1991, 1991.
[47] J. Demo, Factors affecting corrosion in organic systems, Paper no. 175, in: CORROSION/91, NACE, Houston, TX, 1991.
[48] A.M. Sherik, Black powder in gas transmission pipelines, in: W. Reive (Ed.), Oil & Gas Pipelines: Integrity & Safety Handbook, Published by Wiley, 2015, pp. 423−436 (Chapter 29).
[49] J.O. Hinze, AIChE Journal 1 (1955) 289.
[50] C. de Waard, U. Lotz, Prediction of CO_2 corrosion of carbon steel, Paper 69, in: CORROSION 93, 1993.
[51] B.F.M. Pots, S.D. Kapusta, Prediction of corrosion rates of the main corrosion mechanisms in upstream applications, in: CORROSION 2005, 2005. Paper 05550.
[52] J. Cai, S. Nesic, C. de Waard, Modeling of water-wetting in oil-water pipe flow, in: CORROSION 2004 Conference, 2004. Paper No. 04663.
[53] A. Bhardwaj, S. Hartland, A new mechanism for stability of water in crude oil emulsions, in: Presented at Symposium on Surfactants in Solution, June 10−15, 1992, Varna, Bulgaria, 1992.
[54] R. Villalba, K. Bello, Crude oil effect on corrosive potential at Pirital-Santa Barbara oilfield North district in Venezuela, in: CORROSION 2006, 2006. Paper No. 06379.

Corrosion management

3

Sankara Papavinasam
CorrMagnet Consulting Inc., Ottawa, ON, Canada

3.1 Introduction

Between the sources of the hydrocarbons and the locations of their use as fuels, there is a vast network of oil and gas industry infrastructures. The oil and gas industry includes production, transmission, storage, refining, and distribution sectors. Failure in any of these units not only affects its operation but also negatively impacts the downstream sectors, i.e., oil and gas industry infrastructures are continuum. For example, failure in a production sector may affect the transmission pipeline and refinery sectors downstream.

Integrity management ensures that all assets and pipelines perform effectively and efficiently for the entire duration of their designed life. Integrity management may also be known as asset integrity management (AIM) and pipeline integrity management (PIM) when applied to asset and pipelines, respectively. Implementation of integrity-management process requires evaluation of all risks. One of the risks to oil and gas infrastructures is corrosion. Therefore, reducing corrosion risk is a key component of integrity management.

The annual cost of corrosion in the US oil and gas industry is over $27 billion [1], leading some to estimate the global annual cost of corrosion of oil and gas industry as exceeding $60 billion [2]. For companies with oil or gas infrastructure the need to reduce corrosion-related costs is pressing. The oil and gas industry is striving to reach "zero failure" because of corrosion. Meeting that target requires integration of several activities—carried out at different stages, including conceptual, design, construction, commission, operation, repair, and maintenance.

Effective leadership and appropriate management tools should be in place to coordinate and integrate activities carried out at different stages. These activities may be carried out by the following persons:

- Designers of oil and gas infrastructure
- Engineers responsible for oil and gas equipment and infrastructure
- Educators and trainers of the workforce
- Construction and maintenance supervisors working in ditches, plants, and on rigs
- Consultants who advise, develop, and implement corrosion control strategies and plans
- Officials who inspect equipment and infrastructure and regulate the industry
- R&D performers who develop new knowledge and insights

This chapter discusses some commonly used management tools including 5-M methodology, Risk-Based Inspection (RBI), and direct assessment (DA) to control

Trends in Oil and Gas Corrosion Research and Technologies. http://dx.doi.org/10.1016/B978-0-08-101105-8.00003-6

corrosion in the oil and gas industry. It also describes the concept of "integrity operating windows (IOWs)" and highlights the need for considering IOWs in the corrosion control.

3.2 5-M methodology

Corrosion is a natural phenomenon, and it can neither be avoided nor be prevented. However, with appropriate strategies and tools, it can be controlled so that the wall thickness of the material used exceeds the wall thickness loss due to corrosion over the design service life of the equipment. The keys to effective and economical corrosion control are the following:

- Better assessment of corrosion risks
- Selection of cost-effective methods to mitigate corrosion
- Quantitative measurement, estimation, and monitoring of corrosion rates and/or inspection of remaining wall thickness at regular intervals
- Treatments of oil and gas infrastructures as continuum so that changes to one segment's corrosion management program do not affect that of other downstream segments
- Integration of the top-down and bottom-up approaches
- Better understanding of the bases for corrosion control practices and standards

The 5-M methodology integrates all the aforementioned key activities.

3.2.1 Elements of 5-M methodology

The 5-M methodology consists of five individual elements including modeling, mitigation, monitoring, maintenance, and management:

1. The primary function of modeling is to predict if a given material is susceptible to a particular type of corrosion (corrosion damage mechanisms (CDM)) in a given environment and to estimate the rate at which the material would corrode in that given environment.
2. The objective of mitigation is to develop mitigation strategies if modeling predicts that the corrosion rate is high, i.e., that at this corrosion rate the minimum thickness of the material used as corrosion allowance is inadequate.
3. The objective of monitoring is to ensure that the pipeline is performing in the way the model predicts and that the mitigation strategies are adequate.
4. All these strategies would fail if good maintenance strategies were not developed and implemented.
5. Corrosion management integrates corrosion control strategies (modeling, mitigation, monitoring, and maintenance) with overall integrity management.

The following paragraphs describe the characteristics of these five elements, starting with corrosion management. In an ideal situation, the elements of corrosion management are established first, and other elements are developed and implemented based

on it. However, the 5-M methodology may be developed and implemented starting with any of the 5 M's.

3.2.1.1 Management

Corporate management implements top-down approach (risk avoidance, goal based, financial oriented) to minimize the risk from corrosion. On the other hand, corrosion professionals estimate risk in bottom-up approach (field experience, fact based, technical oriented). Corrosion management provides vital and seamless link between top-down corporate management approach and bottom-up corrosion professional approach. In a way, the corrosion management is a combination of art and science to balance financial and technical requirements.

Corrosion management is thus a systematic, proactive, continuous, ongoing, technically sound, and financially viable process of ensuring that the people, infrastructure, and environment are safe from corrosion. The activities of corrosion management include the following:

- Evaluation and quantification of corrosion risks during design, construction, operation, shutdown, and abandonment stages, and identification of factors causing, influencing, and accelerating these corrosion risks (Section 3.2.1.2: Modeling)
- Establishment and implementation of organizational structure, resources, responsibilities, best practices, procedures, and processes to mitigate (Section 3.2.1.3: Mitigation) and monitor (Section 3.2.1.4: Monitoring) corrosion risks
- Maintenance and dissemination of corporate strategies, regulatory requirements, finance, information affecting corrosion, and records of corrosion control activities (Section 3.2.1.5: Maintenance)
- Review the success of implementation of corrosion control strategies and identify opportunities for further correction and improvement

3.2.1.2 Modeling

Primary function of modeling is to predict if a given material is susceptible to a particular type of corrosion (CDM) in a given environment and to estimate the rate at which the material would corrode in that given environment. This prediction may be based on laboratory experiments and/or based on field experience. Modeling helps the corrosion professionals to establish corrosion allowance (i.e., material wall thickness) and decide if additional corrosion mitigation strategies are required.

The models that have been developed to predict corrosion can be classified broadly into corrosion science, electrochemical science, and corrosion engineering models.

The corrosion science approach to developing models that predict the corrosion of oil and gas infrastructures involves the following steps:

- The factors influencing corrosion are assumed.
- Laboratory experiments are carried out to determine the extent of the influence of these parameters on corrosion rates.
- A theoretical explanation (based on corrosion kinetics and/or thermodynamics) is developed.
- The influences of various parameters are integrated.

Most corrosion mechanisms follow electrochemical principles. Therefore electrochemical principles are used in model corrosion. The electrochemical science—based models typically consider corrosion process as occurring in three stages:

1. Formation or characterization of passive or surface layers on the metal surface
2. Initiation of pits/defects at localized regions on the metal surface where passive or surface layers break down
3. Pit or defect propagation and eventual penetration of the metal wall

Since electrochemical reactions are involved in all three stages, each phase of pitting corrosion can be modeled using electrochemical principles.

A corrosion engineer typically determines the risk due to corrosion from field operating conditions, including system pressure, temperature, water, oil, gas, and solid compositions, and flow velocity.

The ability of models to predict the corrosion can be summarized by assessing the answers to the following six key questions:

1. Does internal corrosion pose a significant risk?
2. If so, when during operation is a failure likely to occur?
3. Where in the pipeline or infrastructure is the failure likely to occur?
4. What is the failure mechanism (CDM) likely to be?
5. Which operating parameters should be monitored to accurately predict the failure?
6. How can the predictions be validated and utilized in a user-friendly manner?

None of the three approaches alone covers all elements of corrosion, but each one of them has a few advantages on certain aspects of corrosion. Table 3.1 compares the three model approaches in terms of their ability to characterize corrosion.

3.2.1.3 Mitigation

Mitigation strategies are required if model-predicted corrosion rate is high, i.e., at this corrosion rate the minimum thickness of material used as corrosion allowance is inadequate.

Table 3.1 Comparison of corrosion science, electrochemical science, and corrosion engineering models to predict corrosion of oil and gas infrastructures

Question	Corrosion science	Electrochemical science	Corrosion engineering
If	Yes	Yes	No
When	Yes	Yes	No
Where	No	Yes	Yes
What	No	Yes	Yes
Which	No	No	Yes
How	No	No	Yes

Time-tested and proven methodologies to control internal corrosion include cleaning (pigs), corrosion inhibitors, and biocides, and internal liners and to control external corrosion are coatings and cathodic protection.

3.2.1.4 Monitoring

The objective of monitoring is to ensure that the infrastructure is performing in the way the model predicts and that the mitigation strategies are adequate.

Corrosion monitoring may occur in three stages:

- In the laboratory at the design stage to evaluate the suitability of a given material in the anticipated environment. (This activity is normally carried out in the "modeling" step).
- In the field, during operation, the infrastructure is monitored to determine the actual corrosion rate and to optimize pigging frequency, corrosion inhibitor dosage, and inhibitor application frequency.
- In the field, during operation, the infrastructure is inspected to ensure that the material is continued to be safe under the field operating environment, i.e., to ensure that the corrosion allowance thickness has not exceeded.

3.2.1.5 Maintenance

All strategies (selection of appropriate materials that can withstand corrosion in a given environment, development of appropriate model to predict the behavior of the system, implementation of mitigation strategies to control corrosion, and monitoring of the system to ensure that the corrosion of the system is under control) would fail if good maintenance strategies were not developed and implemented. A comprehensive and effective program requires maintenance of five interdependent entities:

- Equipment: the equipment is the piece of apparatus or infrastructure that should be kept in a good working condition.
- Workforce: the people are the workforce that develops, deploys, and performs necessary activities.
- Data: the historical operational data that provide guidelines on the past history and information for future action.
- Communication: strategies that disseminate appropriate information among varies groups within the company and outside the company.
- Associated activities: activities that provide support to the company or industry.

3.2.2 Implementation of 5-M methodology

All five elements must be implemented to effectively control corrosion in the oil and gas industry. To facilitate the implementation of the 5-M methodology, establishment of key performance indicators (KPIs) is required. Industry surveys and failure analysis have identified 50 KPIs (Table 3.2). Detailed descriptions and implications of all 50 KPIs are available elsewhere [3].

The next subsections briefly describe the 50 KPIs.

3.2.2.1 Management—context of corrosion control

Not all units are equal from a corrosion perspective. Corrosion in a unit may be tolerated, whereas corrosion in other unit may not be tolerated. For example, corrosion

Table 3.2 Key performance indicators (KPIs) for effective and economical implementation of corrosion control strategies

5 M elements	KPI identification	Number of KPIs
Management (context of corrosion)	1, 2, 3, 4, 5	5
Model (internal corrosion)	**6, 7, 8, 9, 10, 11,** 12, **14, 15,** 39, 40	11
Mitigation (internal corrosion)	16, 17, 18, 19	4
Monitoring (internal corrosion)	24, 25, 26, 27, **32,** 33, **35, 36**	8
Model (external corrosion)	**6, 7, 8, 9, 10, 11,** 13, **14, 15,** 41, 42	11
Mitigation (external corrosion)	20, 21, 22, 23	4
Monitoring (external corrosion)	28, 29, 30, 31, **32,** 34, **35, 36**	8
Maintenance	37, 38, 43, 44, 45, 46, 47, 48	8
Management (continuous improvement)	49, 50	2
		50[a]

[a]11 KPIs are common for both internal and external corrosion and are indicated in bold letters.

control in a sweet production pipeline operating in a remote area may not be as important as that of a sour production operating in a populated area. Therefore it is important for management to establish the "context of corrosion control." The context of corrosion control is established using five (5) KPIs. Table 3.3 describes these KPIs and the stages of implementation.

Table 3.3 Characteristics of key performance indicators (KPIs) to establish the context of corrosion control

KPI number	KPI description	Stages of implementation
1	Segmentation of the infrastructure: the infrastructure should be segmented and each segment should have uniform corrosion characteristics	Conceptual
2	Corrosion risks: all types of corrosion risks including cracking should be included	Conceptual
3	Location of the infrastructure: location determines the consequence of corrosion failure	Conceptual
4	Overall corrosion risk: risk (KPI 2) times consequence (KPI 3)	Conceptual
5	Life of the infrastructure	Conceptual

3.2.2.2 Model—internal corrosion

Model is a road map or a guideline to indicate what will be the material loss over time due to internal corrosion. Nine (9) KPIs are used to predict internal corrosion (Table 3.4).

Table 3.4 Characteristics of key performance indicators (KPIs) to model internal corrosion

KPI number	KPI description	Stages of implementation
6	Materials of construction	Design
7	Corrosion allowance: wall thickness allowed to account for corrosion	Design
8	Main operating conditions: temperature, pressure, chemical and physical conditions, and flow	Design
9	Potential upset conditions in the upstream sector affecting this sector	Design
10	Potential upset conditions in this sector affecting downstream sector	Design
11	Mechanisms of corrosion: risk (KPI 2) should be based on top two or three internal corrosion mechanisms	Design
12	Maximum corrosion rate: corrosion rate of the material in the operating conditions (KPI 8) in the absence of any mitigation strategies	Design
14	Installation of proper accessories during construction: e.g., inhibitor port	Construction
15	Commissioning: e.g., removal of hydrotested water	Commission
39	Internal corrosion rate after maintenance activities should be less than or equal to maximum corrosion rate (KPI 12)	Operation
40	Percentage difference between mitigated internal corrosion rate or corrosion rate from monitoring or inspection technique (whichever is decided in KPI 27) and corrosion rate before maintenance activities	Operation

3.2.2.3 Mitigation—internal corrosion

If model indicates that the wall lost due to corrosion would exceed the corrosion allowance within the design life of the infrastructure, then strategies should be taken to mitigate corrosion. Four (4) KPIs are used to implement mitigation strategies (Table 3.5).

Table 3.5 Characteristics of key performance indicators (KPIs) to mitigate internal corrosion

KPI number	KPI description	Stages of implementation
16	Mitigation to control internal corrosion: mitigation is necessary if the corrosion allowance is lower than corrosion rate (KPI 27 in Table 3.6) times life of infrastructure (KPI 5)	Operation
17	Mitigation strategies to control internal corrosion: time tested and proven internal corrosion strategies are cleaning, corrosion inhibitors, biocides, and internal coatings	Operation
18	Mitigated internal corrosion rate, target, i.e., the corrosion rate after the implementation of mitigation strategies	Operation
19	Percentage time efficiency of internal corrosion mitigation strategy: the mitigation strategies should be effective 100% of time. Otherwise, corrosion rate will proportionately increase from that established in KPI 18 to that anticipated in KPI 12	Operation

3.2.2.4 Monitoring—internal corrosion

Eight (8) KPIs are used to monitor internal corrosion (Table 3.6).

3.2.2.5 Model—external corrosion

Model is a road map or a guideline to indicate what will be material loss over time due to external corrosion. Eleven (11) KPIs are used to predict external corrosion (Table 3.7).

3.2.2.6 Mitigation—external corrosion

If model indicates that the wall lost due to corrosion would exceed the corrosion allowance within the design life of the infrastructure, then strategies should be taken to mitigate corrosion. Four (4) KPIs are used to implement mitigation strategies to control external corrosion (Table 3.8).

3.2.2.7 Monitoring—external corrosion

Eight (8) KPIs are used to monitor external corrosion (Table 3.9).

3.2.2.8 Maintenance

A comprehensive and effective maintenance program requires implementation of five interdependent entities equipment, workforce, data, communication, and associated activities. Eight (8) KPIs are used to monitor external corrosion (Table 3.10).

Table 3.6 Characteristics of key performance indicators (KPIs) to monitor internal corrosion

KPI number	KPI description	Stages of implementation
24	Internal corrosion monitoring techniques: the techniques should be able to monitor the type of corrosion (or CDM) anticipated (See KPI 11)	Operation
25	Number of probes per square area to monitor internal corrosion: there should at least be one probe per segment (KPI 1)	Operation
26	Internal corrosion rate, from monitoring technique	Operation
27	Percentage difference between mitigated internal corrosion rate and corrosion rate from monitoring technique	Operation
32	Frequency of inspection	Operation
33	Percentage difference between mitigated internal corrosion rate or corrosion rate from monitoring techniques and corrosion rate from inspection technique	Operation
35	Measurement data availability: certain data are routinely measured, and they can provide indirect information on corrosion (e.g., pH)	Operation
36	Validity and utilization of measured data; the validity of the measured parameters (KPI 35) should be ascertained before using them	Operation

Table 3.7 Characteristics of key performance indicators (KPIs) to model external corrosion

KPI number	KPI description	Stages of implementation
6	Materials of construction	Design
7	Corrosion allowance: wall thickness allowed to account for both internal and external corrosion	Design
8	Main operating conditions: temperature, pressure, and external environment	Design
9	Potential upset conditions in the upstream sector affecting this sector: normally increase of temperature	Design
10	Potential upset conditions in this sector affecting downstream sector: normally increase of temperature	Design

Continued

Table 3.7 Continued

KPI number	KPI description	Stages of implementation
11	Mechanisms of corrosion: risk (KPI 2) should be based on top two or three external corrosion mechanisms	Design
13	Maximum corrosion rate: corrosion rate of the material in the operating conditions (KPI 8) in the absence of any mitigation strategies	Design
14	Installation of proper accessories during construction: e.g., cathodic protection current measurement ports	Construction
15	Commissioning: e.g., accidental damage to external coating	Commission
41	External corrosion rate after maintenance activities should be less than or equal to maximum corrosion rate (KPI 13)	Operation
42	Percentage difference between mitigated external corrosion rate or corrosion rate from monitoring or inspection technique (whichever is decided in KPI 31) and corrosion rate before maintenance activities	Operation

Table 3.8 Characteristics of key performance indicators (KPIs) to mitigate external corrosion

KPI number	KPI description	Stages of implementation
20	Mitigation to control external corrosion: mitigation is necessary if the corrosion allowance is lower than corrosion rate (KPI 27) times life of infrastructure (KPI 5)	Operation
21	Mitigation strategies to control external corrosion: time-tested and proven external corrosion strategies are coatings and cathodic protection	Operation
22	Mitigated external corrosion rate, target, i.e., the corrosion rate after the implementation of mitigation strategies	Operation
23	Percentage time efficiency of external corrosion mitigation strategy: the mitigation strategies should be effective 100% of time. Otherwise, corrosion rate will increase from that established in KPI 22 to that anticipated in KPI 13	Operation

Table 3.9 Characteristics of key performance indicators (KPIs) to monitor external corrosion

KPI number	KPI description	Stages of implementation
28	External corrosion monitoring techniques: the techniques should be able to monitor the type of corrosion anticipated (See KPI 11)	Operation
29	Number of probes per square area to monitor external corrosion: there should at least be one probe per segment (KPI 1)	Operation
30	External corrosion rate from monitoring technique	Operation
31	Percentage difference between mitigated external corrosion rate and corrosion rate from monitoring technique	Operation
32	Frequency of inspection	Operation
34	Percentage difference between mitigated external corrosion rate or corrosion rate from monitoring techniques and corrosion rate from inspection technique	Operation
35	Measurement data availability: certain data are routinely measured, and they can provide indirect information on external corrosion (e.g., soil type, soil pH)	Operation
36	Validity and utilization of measured data: the validity of the measured parameters (KPI 35) should be ascertained before using them	Operation

Table 3.10 Characteristics of key performance indicators (KPIs) for maintenance

KPI number	KPI description	Stages of implementation
37	Procedures for establishing the maintenance schedule: if corrosion or other damage mechanism has deteriorated section of an infrastructure, it should be repaired or replaced	Operation
38	Maintenance activities should be coordinated in consideration with other operational issues/requirements	Operation
43	Workforce—capacity, education, and training: industry guidelines for workforce capacity, education, and training not currently available	Operation
44	Workforce—experience, knowledge, and quality; quality of work depends on the workers experience, knowledge, and ability	Operation

Continued

Table 3.10 Continued

KPI number	KPI description	Stages of implementation
45	Data management—data to database: certain regulations require collection and storage of data for the entire duration of operation	Operation
46	Data management—data from database: data from the database should be made easily available to control corrosion	Operation
47	Internal communication strategy: all relevant information should be available for concerned personnel	Operation
48	External communication strategy: corrosion professionals may be obligated to provide information—after a corrosion incident has occurred	Operation

Table 3.11 Characteristics of key performance indicators (KPIs) for continuous improvement

KPI number	KPI description	Stages of implementation
49	Corrosion management review: frequency of review should be as high as reasonably possible	Operation
50	As the corrosion-management practice improves, the frequency of failure or incidence due to corrosion will decrease	Operation

3.2.2.9 Management (continuous improvement)

Management should continuously review the success of corrosion control. Two (2) KPIs are used to identify opportunities for continuous improvement (Table 3.11).

3.2.3 Scoring key performance indicators

Status of implementation of each KPI can be indicated either by color indicators or scores or by both (Table 3.12). By summing individual KPI scores, "overall scoring" can be determined. Assuming that for all KPIs the maximum score is 5, the "maximum overall score" possible is 250. Based on the "overall score" and "maximum overall score", percentage scores for "corrosion" and "corrosion control" are calculated. For example, if the "overall score" for an asset is 50, then "percentage corrosion control score" is 80 and "percentage corrosion score" is 20.

Table 3.12 Scoring key performance indicators (KPIs)

KPI	KPI color indicator	KPI score[a]
Not relevant[a]	Blue	0
Accounted for adequately	Green	0–2
Accounted for inadequately	Yellow	2–4
Not adequately accounted for	Red	4–5

[a]If a KPI is not used, it is not included for calculating the overall score.

3.2.4 Case histories

The applicability of 50 KPIs in implementing effective corrosion control has been evaluated in several oil and gas infrastructures including oil and gas production pipelines, steam-assisted gravitational drainage oil sands production system, risers, oil transmission pipelines, gas transmission pipelines, above-ground storage tanks, and product pipelines. Detailed information of the case studies ise presented elsewhere. Salient features of five (5) case studies are presented in the following paragraphs.

3.2.4.1 Riser [4]

The risers are important constituents of the off-shore oil and gas industry. They transport oil, gas, and water produced from the seafloor to production and drilling facilities and injection fluids from production and drilling facilities to seafloor. The risers analyzed in these case studies were operating in a production platform in Gulf of Mexico. They were all constructed from carbon steel, but their characteristics (diameter and length) and operating conditions (fluids, temperature, pressure, and flow velocities) vary considerably.

Fig. 3.1 presents the status of implementation of the 50 KPIs in these risers. Because of the environmentally sensitive nature of the location of the risers, the consequence of failures is high. Therefore the overall corrosion risk (probability x consequence) score is high (KPI 4). But many corrosion control strategies (corrosion control score: 64%) have been placed so reduce the probability of corrosion to low.

3.2.4.2 Oil production pipeline [5]

The 323.9 mm (12 in.) diameter, 305 km (189 mile) carbon steel pipeline was operating at a maximum allowable operating pressure (MAOP) of 99 bar (1350 psi). It was transporting light, high-sulfur-content (>0.5 wt%) crude oil from the production sector. The nominal wall thickness was 4.78 mm (188 mil) and for the section of pipeline crossing the river the wall thickness was increased to 7.92 mm (312 mil). The external surface of the pipe was protected with coal tar coating. The section of the pipeline crossing the river was coated with polyethylene tape and was further protected with concrete weight coating.

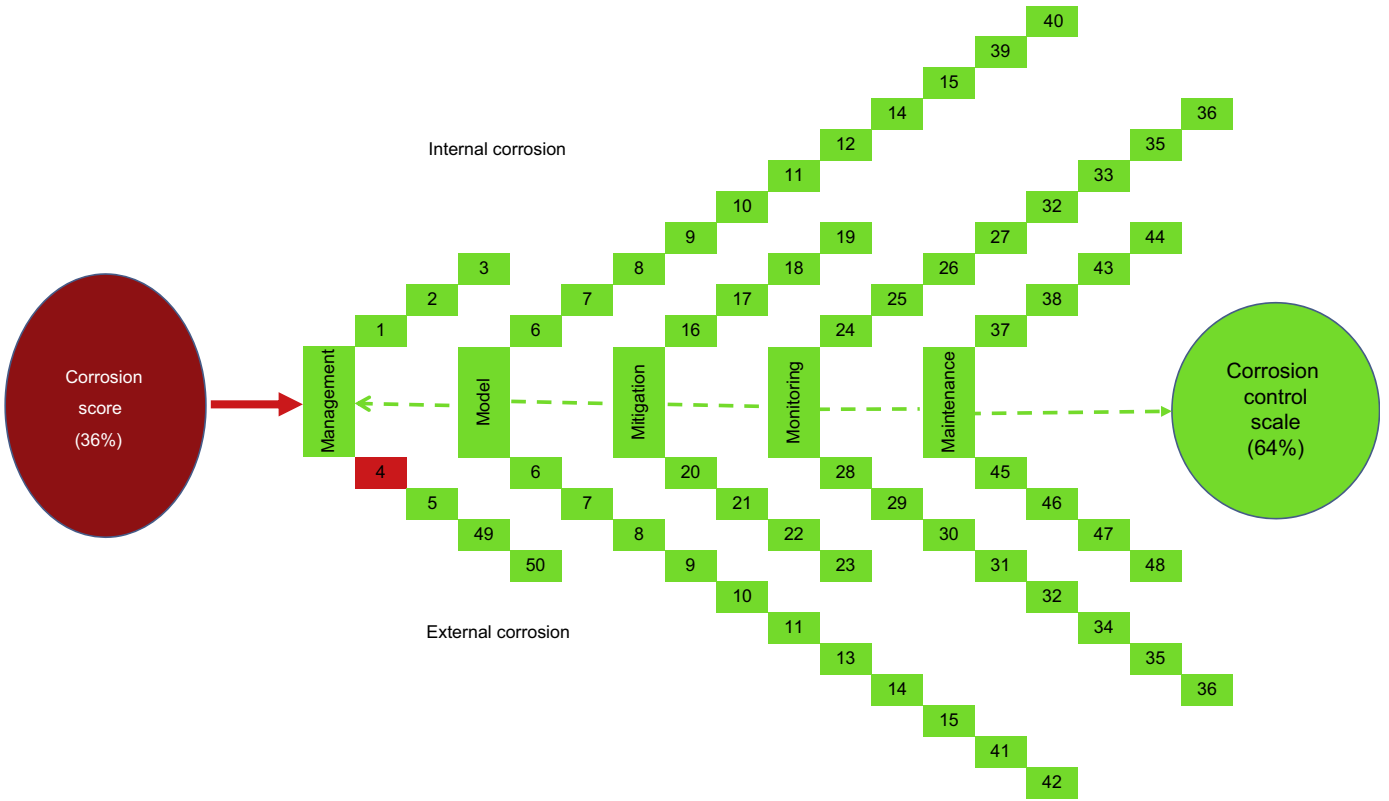

Figure 3.1 Status of implementation of the 50 key performance indicators in the riser.

Fig. 3.2 presents the status of implementation of the 50 KPIs in this pipeline:

- Green bar indicates that the KPI was implemented appropriately (good). Thirty-three KPIs with respect to corrosion control were implemented appropriately;
- Yellow bar indicates that the KPI was implemented inadequately (fair). Ten KPIs with respect to corrosion control were implemented inadequately; and
- Red bar indicates that the KPI was implemented poorly (poor). Seven KPIs with respect to corrosion control were implemented poorly.

Analysis indicated that the KPIs to control corrosion (corrosion control score: 61%) were appropriately implemented. Consequently the pipeline did not fail from corrosion (though it had failed due to noncorrosion—related event) during the review period.

3.2.4.3 Oil transmission pipeline [6]

The pipeline under study was constructed in 1975 and placed into service in 1976 to transport Western Canadian condensate, sweet and sour crude oil from Sarnia to Montreal. The minimal wall thickness of the carbon steel pipeline was 6.35 mm.

Fig. 3.3 presents the status of implementation of the 50 KPIs in this pipeline. Overall the pipeline is in safe and reliable operating conditions from the perspective of corrosion. Additional management oversight will further increase the integrity of the pipeline.

3.2.4.4 Oil and gas transmission pipeline network [7]

In this case study, the concept of 50 KPIs was applied to overall corrosion control strategies in a large company with approximately 5592 miles of oil pipelines and 2346 miles of gas pipelines. These pipelines were transporting various types of oil and gas at different pressures, temperatures, and flow velocities. The diameter of the pipelines varied between 4 and 36 in. Most of these pipelines are buried underground at depths between 3 and 6 ft, and some of them are above ground.

Fig. 3.4 presents the status of implementation of the 50 KPIs in this pipeline. Many of the KPIs are not implemented or not adequately applied. However, no corrosion failure has occurred during this review period, indicating the intrinsic noncorrosive nature of oil and gas. But continued operation, without improving control strategies, will result in failure due to corrosion.

3.2.4.5 Gas transmission pipeline [8]

The gas transmission pipeline used in this case study receives dry natural gas from another transmission line and transports it to several factories and distribution centers all along its path. This 30-year old pipeline is 6 in. in diameter, 80 km in length, and has a nominal wall thickness of 5.56 mm. It operates at 60 bars (870 psi) of pressure and at 25°C (77°F).

Fig. 3.5 presents the status of implementation of the 50 KPIs in this pipeline. Many of the KPIs are not implemented or not adequately applied. However, no corrosion failure has occurred over 20 years of operation, indicating intrinsic noncorrosive nature of natural gas. But continued operation, without improving control strategies, will result in failure due to corrosion.

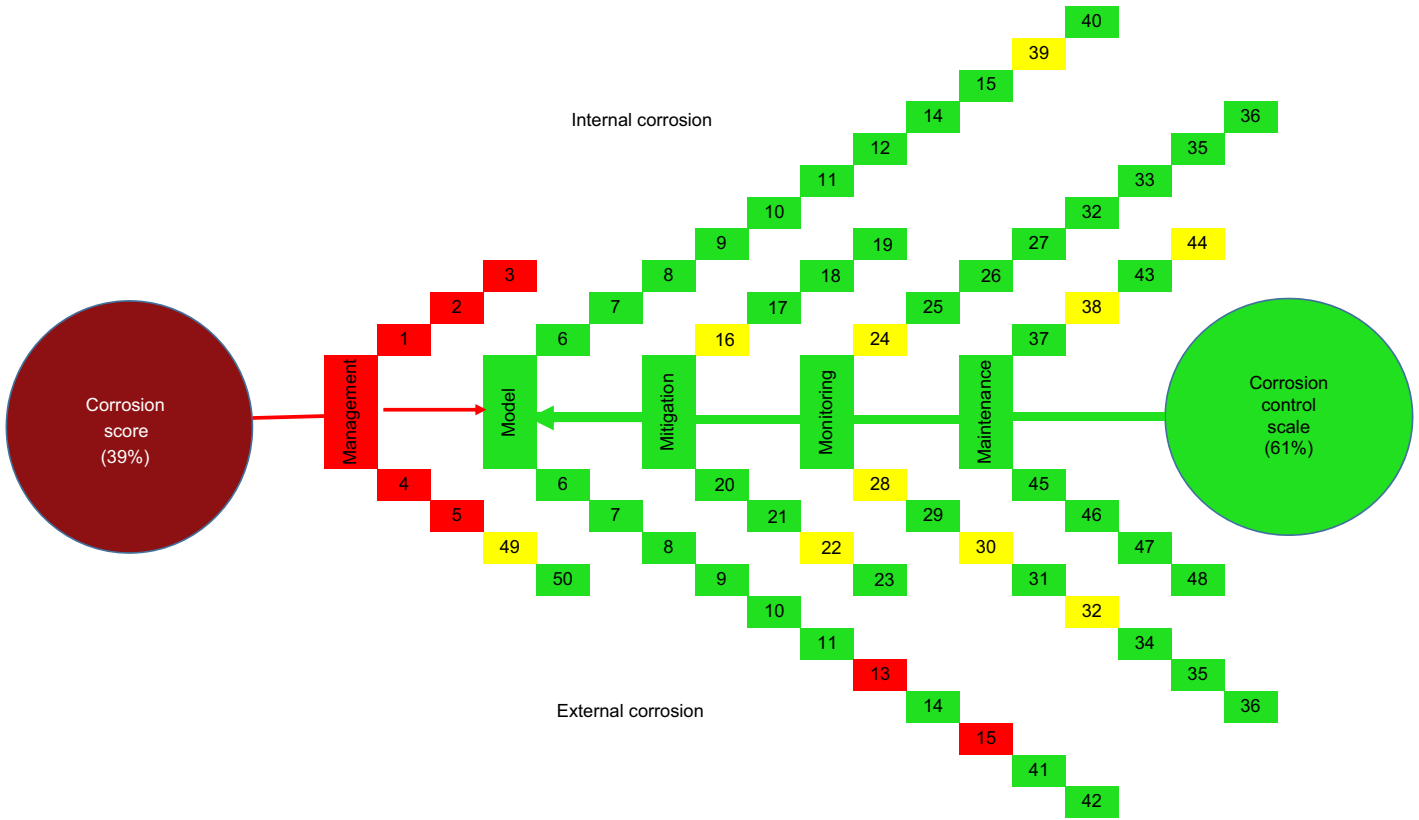

Figure 3.2 Status of implementation of the 50 key performance indicators in oil production pipeline.

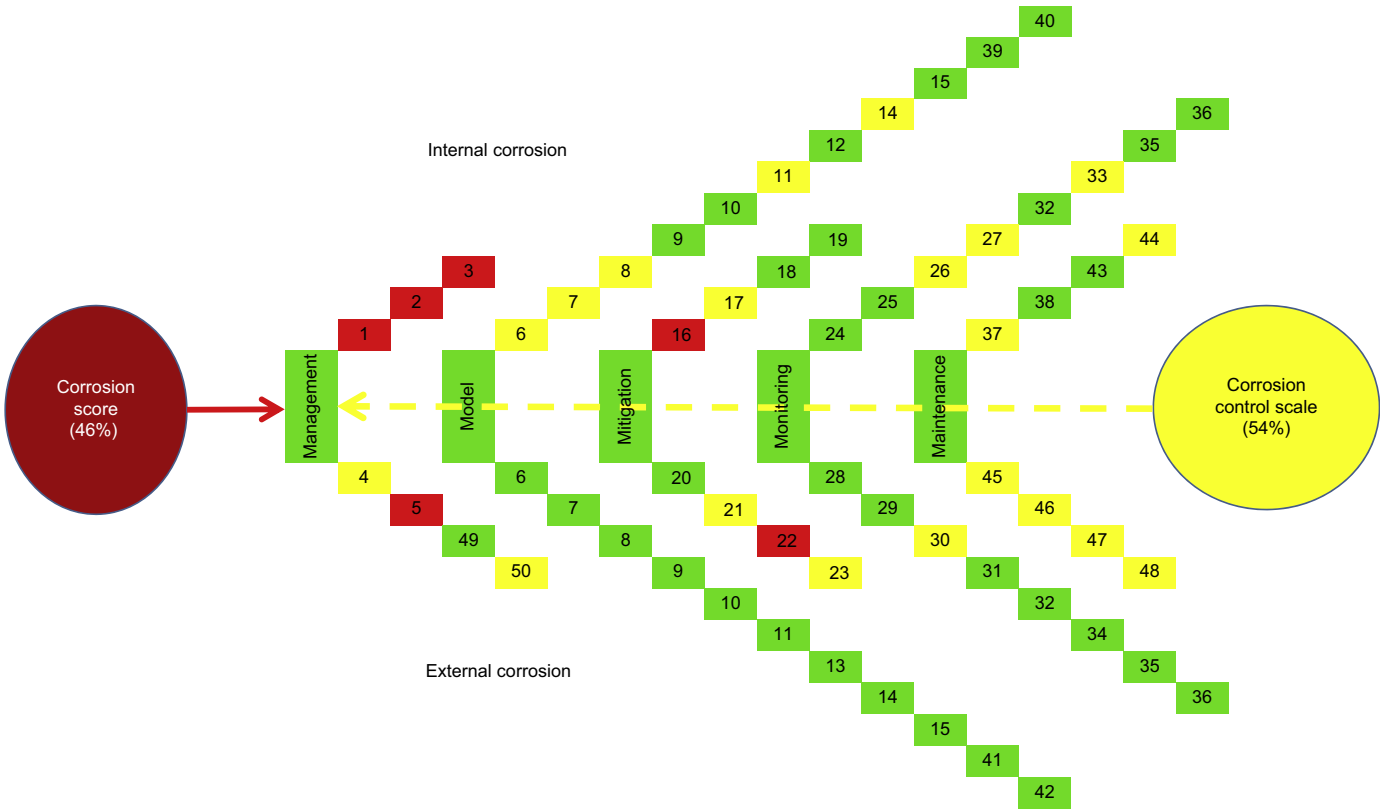

Figure 3.3 Status of implementation of the 50 key performance indicators in oil transmission pipeline.

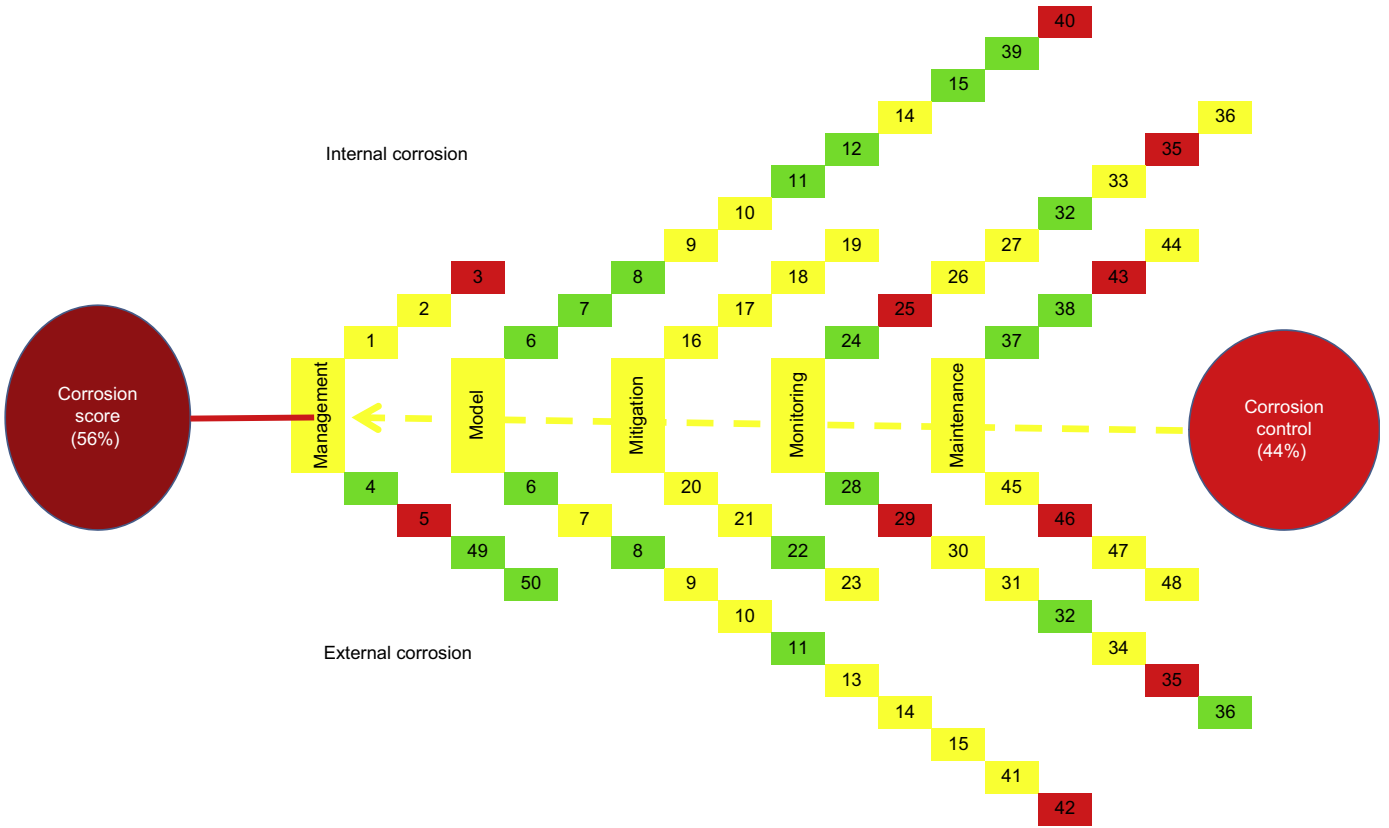

Figure 3.4 Status of implementation of the 50 key performance indicators in oil and gas transmission pipeline.

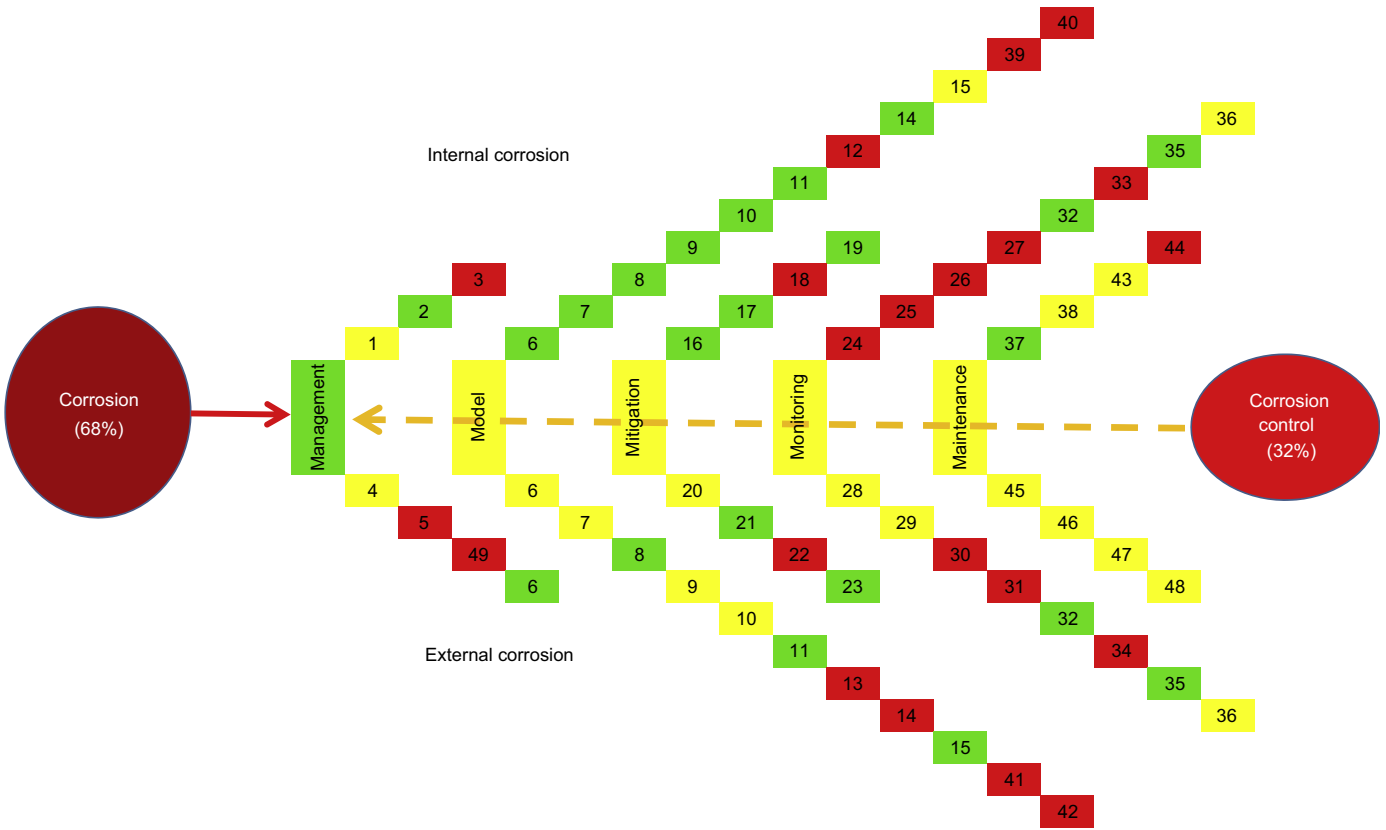

Figure 3.5 Status of implementation of the 50 key performance indicators in gas transmission pipeline.

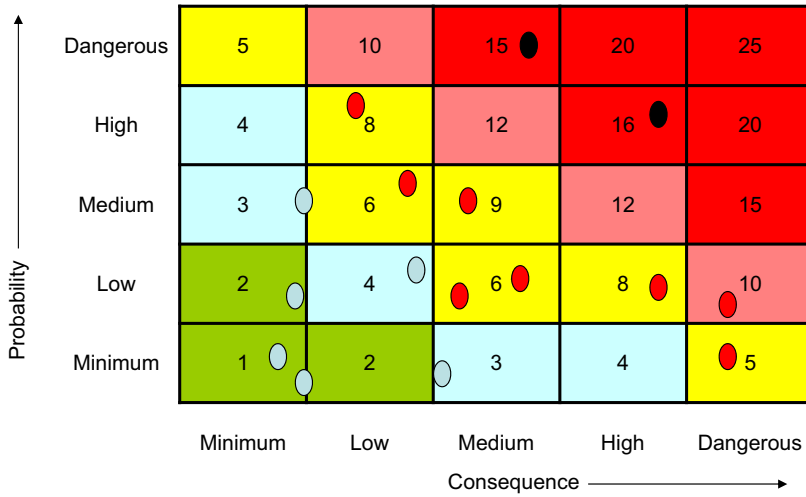

Figure 3.6 Quantification of risk.

3.3 Risk-based inspection

RBI is a process of understanding both the probability of risk and consequence of it. This process identifies all risks including that from corrosion, causes and enhancers of risk, and stage of the asset (commissioning, operation, or beyond designed duration). The product of risk and consequence is scored using a matrix system, and the overall risk score is established (Fig. 3.6). Based on the risk score, inspection schedule and frequency are prioritized, and cost-effective solutions to reduce risk (e.g., repair or replace) are established.

The RBI process significantly decreases the number of locations to be inspected, i.e., inspection is performed only on the equipment in the high-risk category, and no inspection is performed in the low-risk category. This process thus significantly reduces the cost of corrosion control without increasing the risk.

The RBI process is primarily carried out for equipment and piping in the refinery but can also be used for any oil and gas assets [9,10].

3.4 Direct assessment

In a way, the principle of direct assessment (DA) process is similar to that of RBI process. In both processes, the areas of highest risk are identified and attention (mostly inspection) is focused on areas of higher risk. The DA process is primarily developed for oil and gas pipelines that cannot be internally inspected using inline inspection technology.

The DA process can be used to evaluate internal corrosion, external corrosion, and external stress corrosion cracking [11−16]. All DA processes have four steps:

1. Preassessment: in this step all relevant, historic, essential, and current data are collected to determine the feasibility of carrying out the DA process. If the data are not sufficient then the DA process cannot be carried out.
2. Indirect inspection: in this step the data collected are used to predict the overall severity of different segments of the pipeline. This step also includes segmentation of the pipeline according to its operating and surface profile conditions. Based on the analysis, locations of pipelines susceptible to corrosion are identified.
3. Direct inspection: in this step the locations predicted to be having higher corrosion risk (in step 2) are nondestructively inspected.
4. Postassessment: in this step, all data collected and analysis carried out in steps 1 through 3 are used to prioritize mitigation, maintenance, or repair strategies. In this step the time for next inspection is also established.

3.5 Integrity operating windows or boundary of operation

All the management best practices of this chapter are developed and implemented assuming that the asset is operated within certain boundary-operating conditions. However, during operation the asset may exceed these operating boundaries. Such operational "short-term" excursions will increase the overall risk. Such operational excursions must be accounted for in establishing the overall risk. For this purpose the concept of "integrity operating windows (IOW)" has been developed (Fig. 3.7) [17]. In the IOW, five zones of operations are established:

- Safe zone
- Standard high
- Critical high
- Standard low
- Critical low

Obviously the asset should be operated within the safe zone and when the operational excursions happen, management control must be placed to bring the asset back to the safe zone. Furthermore, the extent and duration of the excursion should be considered, and the overall risk should be reevaluated.

It is further noted that in the 5-M methodology that the concept of IOWs is accounted for through KPIs 9 and 10.

3.6 Corrosion control document

The management approaches to control corrosion in an asset must be explicitly written and disseminated to all concerned persons within the company, organization, and industry. Such document may be known by several names. Some common names include Corrosion Control Document (CCD), Corrosion Manual (CM), and Corrosion

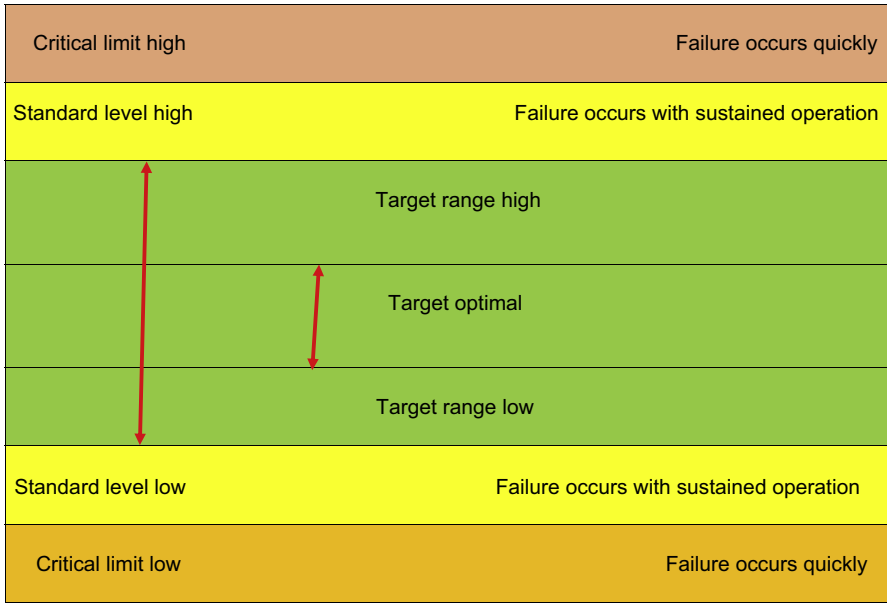

Figure 3.7 Integrity operating window (based on API 584) [17].

Control Best Practices (CCBP). Some common information available in corrosion control documents includes the following:

- Description of the asset
- Material of construction
- Operating conditions including start up, normal operation, and shutdown conditions
- Corrosion circuits (or regions and subregions of corrosion) within an asset
- Corrosion damage mechanisms (or types of corrosion) or probable failure modes in each corrosion circuit or subregion
- Mitigation and monitoring strategies
- Responsible persons/teams (e.g., operations, inspection, maintenance)
- Applicability of IOWs (or operational excursions)
- Other information affecting corrosion

3.7 Current status and future development

Regulatory, public, environmentalists, and media attention on oil and gas industry is at a higher level. It is not only important to keep the risk due to corrosion at a low level but also important to demonstrate that the risk is kept at low level. Toward that objective the importance of corrosion management is increasingly being recognized. Table 3.13 provides an overall comparison of currently available management tools.

It is anticipated and necessary that the oil and gas industry continues to use management tools and progressively improves them. Innovative and modern

Table 3.13 Comparison of different corrosion-management approaches

Characteristics	5-M methodology	Risk-based inspection	Direct assessment
Stages of implementation	Ideally at the conceptual/design stage. But can be implemented at any stages, i.e., operation, management of change, and shutdown	Ideally at the conceptual/design stage. But can be implemented at any stages, i.e., operation, management of change and shutdown	Developed specifically for pipelines to assess corrosion during operation
Features	Integrates model, mitigation, monitoring, maintenance, and managements aspects	Focuses on identifying areas/ locations for inspection	Focuses on identifying areas/ locations susceptible for corrosion
Strengths	Inclusive and systematic in integrating scientific, engineering, and management. Flexible so that implementation of it can be started with what is possible under a given operating and can be progressively improved	Identification of locations for increased inspection and hence helps to optimize cost	Can be applicable when no other corrosion control tools (e.g., pigging, inline inspection) are available
Weaknesses	Relatively a new management tool though more and more companies and standards organization have started using it	Does not address mitigation aspects. Relays too much on inspection in high-risk areas. The concept of double checking by inspecting in a known low-risk area is not considered	Cannot be used if reliable data are not available and relays heavily on historical field data, which may not be possible to obtain in all infrastructures
Applicability	All oil and gas infrastructures	All oil and gas infrastructures	Applicable only to oil and gas pipelines
Virtue	Provides five layers of protection against corrosion	Inspection prioritization tool	Assessment tool

technologies to disseminate knowledge (e.g., online training course) of these tools are available and are being used. The use of modern technologies in implementing management tools will continue to grow.

References

[1] G.H. Koch, M.P.H. Brongers, N.G. Thompson, Y.P. Virmani, J.H. Payer, Corrosion Cost and Preventive Strategies in the United States, US Department of Transportation, Federal Highway Administration, Research, Development, and Technology, Turner-Fairbank Highway Research Center, March 2002, 6300, Georgetown Pike, McLean, VA, 22101−2296, FHWA-RD-01-156.
[2] NACE IMPACT, "International Measures of Prevention, Application, and Economics of Corrosion Technologies" Study, NACE International, March 2016. Houston TX.
[3] S. Papavinasam, Corrosion Control in the Oil and Gas Industry, 1020 pages, Gulf Professional Publication, October 2013 (Imprint of Elsevier), ISBN: 978-0-1239-7022-0.
[4] A. Chandra, Corrosion Control of Risers, STEM-Corrosion, CMT 2015-08, December 2015, www.CorrMagnet.com/technical.
[5] S. Rao, Implementing Pipeline Integrity Management Using KPIs, STEM-Corrosion, CMT 2015-04, July 2015, www.CorrMagnet.com/technical.
[6] N. Ebrahimi, Implementation of 50 Key Performance Indicators (KPIs) in Corrosion Control of an Oil Transmission Pipeline, STEM-Corrosion, CMT 2015-06, December 2015, www.CorrMagnet.com/technical.
[7] E.N.R. Galvis, Analysis and Evaluation of 50 Key Performance Indicators from Transmission Pipelines, STEM-Corrosion, CMT 2015-05, December 2015, www.CorrMagnet.com/technical.
[8] M.J. Gutierrez, Case Study: Key Performance Indicators Implementation in Gas Transmission Pipeline, STEM-Corrosion, CMT 2015-07, December 2015, www.CorrMagnet.com/technical.
[9] American Petroleum Institute (API) 580, Risk Based Inspection.
[10] American Petroleum Institute (API) 581, Risk Based Inspection Technology.
[11] NACE Standard Practice, SP0206, Internal Corrosion Direct Assessment Methodology for Pipelines Carrying Normally Dry Natural Gas (DG-ICDA) (Houston, TX: NACE), 2016.
[12] NACE Standard Practice, SP0204, Stress-Corrosion Cracking (SCC) Direct Assessment Methodology (Houston, TX: NACE).
[13] NACE Standard Practice, SP0208, Internal Corrosion Direct Assessment for Liquid Petroleum Pipelines (Houston, TX: NACE), 2007.
[14] NACE Standard Practice, SP0110, Wet Gas Internal Corrosion Direct Assessment Methodology for Pipelines (Houston, TX: NACE).
[15] NACE TG 426 Standard Practice, Multiphase Flow Internal Corrosion Direct Assessment (MP-ICDA) Methodology for Pipelines (Houston, TX: NACE), 2016.
[16] NACE Standard Practice, SP0502, Pipeline External Corrosion Direct Assessment Methodology (Houston, TX: NACE).
[17] American Petroleum Institute (API) RP 584, Integrity Operating Window.

PART II

Corrosion in oil and gas production and transmission: current knowledge and challenges

Downhole corrosion

4

Robin D. Tems
Hollybeach Corrosion Management, Denver, CO, United States

4.1 Corrosion management of the downhole environment

Corrosion management of downhole completions for producing wells is complex and dynamic. The conditions in downhole completions will change during the life of the well, whereas process plant normally has carefully defined operating conditions and cycles. Pressures and temperatures will change over the operating life as the formation depletes; wells that originally produce condensate water may start producing formation water, water cuts increase, scaling, or other downhole deposits such as sulfur or asphaltenes may occur. Production well conditions are not static, and due account of this must be taken in the estimation of likely corrosion rates and the appropriate mitigation methods. Fig. 4.1 presents an example of changing corrosion rates in upstream operations [1].

For existing fields, the best predictor of corrosion behavior is a detailed analysis of existing well data, failure rates, failure analysis, corrosion monitoring data, and various tubing examination methods, with due regard for the position of wells within the geologic structure and developing encroachment of formation water. For new fields, corrosion management design decisions are nearly always dependent upon samples collected during the drilling and well test process, and these are inevitably contaminated with drilling and completion fluids.

The primary corrosion control decision in the design of a new downhole completion is the mechanical design of the well so that required material strength levels can be matched to potential damage mechanisms and possible corrosion control options. To meet low- to medium-strength requirements, carbon steel tubulars are often the lower CAPEX first choice and are usually available on short notice. API Specification 5CT (ISO 11960) provides the required details for these materials. Where higher strength tubing strings are required, corrosion-resistant alloys are usually selected, but these are high CAPEX items and are likely to have very long lead times for delivery. API Specification 5CRA (ISO 13680) provides the required details for these materials. The availability of compatible downhole hardware such as packers, polished bore receptacles (PBRs), subsurface safety valves, and tubing hangers can be challenging as well, because different product forms such as solid bar may be necessary to machine the complex geometries of downhole "jewelry." Nonmetallic components, elastomers, seals, etcetera may also be present in "jewelry," and must also be carefully selected for the well environments.

In addition to compatibility between the production tubing and the production environment, consideration must be given to other fluids that may be encountered. Brine or

Trends in Oil and Gas Corrosion Research and Technologies. http://dx.doi.org/10.1016/B978-0-08-101105-8.00004-8

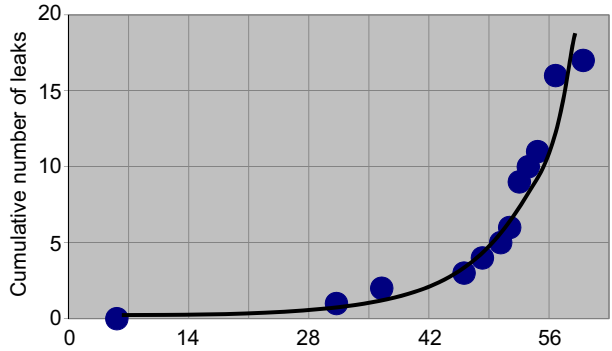

Figure 4.1 Development of trunkline corrosion leaks in an upstream field.
Adapted from R.D. Tems, Managing the Cost of Corrosion, Eurocorr 2009, Nice, France, 2009.

oil-based packer fluids may be used in the tubing casing annulus, and seal leaks can result in corrosive gases dissolving into the packer fluid. Wells may require acidizing or other workover fluids, and these must be shown to be compatible with exposed metallic components. Deeper, high-pressure wells usually require heavy brine packer fluids as opposed to hydrocarbon-based packer fluids, and corrosion control of this casing-tubing annulus becomes more complex. Both new and existing completions may require remedial work such as "acidizing" to remove downhole deposits and also to facilitate production increases. Depending on the exact problem being addressed, acidizing chemicals may include hydrochloric acid, hydrofluoric acid, acetic acid, formic acid, chelating agents, or other specialty products.

For older fields, increasing water cuts result in increasing corrosion, although the break-point for the onset of corrosion depends on the properties of the liquid hydrocarbon phase and its ability to oil wet the surface, plus consideration of any naturally inhibitive components within the hydrocarbon. Efird [2,3] published an early notable paper on this. Wells that previously experienced little or no corrosion develop corrosion problems as the wells age. In addition to increased water production, well temperature profiles can change, again resulting in an increase in corrosion. The implementation of secondary or tertiary recovery techniques can significantly alter the producing environment. Sweet wells may sour, carbon dioxide partial pressures may change, oxygen contamination may occur, and scaling may occur. The implementation of secondary or tertiary production regimes may also involve the use of gas lift equipment downhole, electric submersible pumps, or mechanical pumps with sucker rod strings.

4.2 Principle corrosive agents in production fluids

The primary corrosive gases experienced in production are carbon dioxide and hydrogen sulfide. Extensive research has been performed concerning each of these damage mechanisms, although much of the work is targeted toward pipelines rather than downhole per se. Additional challenges include oxygen/air contamination and

sulfate-reducing bacteria (SRB). Oxygen may be introduced by systems such as, but not limited to, corrosion inhibitor injection, workover fluids, sulfur solvents, and in surface pipelines by hydrate prevention fluids. SRB may be introduced during the drilling process itself or during the injection and subsequent production of water or other fluids. Lignosulfonate drilling muds are commonly associated with SRB contamination and, in some notable cases, have resulted in the souring and microbial contamination of an entire producing field.

Carbon dioxide results in localized corrosion attack of carbon steels that can be accentuated by flow enhanced phenomena. Fig. 4.2 presents an example of classic Mesa corrosion from a US flow line. The morphology of the attack is affected by factors including the flow regime, the partial pressure of carbon dioxide, the presence of other gases such as hydrogen sulfide, and the composition of the water produced from the well, which may be either condensed water or produced formation water. The presence of organic acids in the production fluids greatly enhances the corrosion rate [4]. Fig. 4.3 presents an example of flow enhanced corrosion from a gas well completed with L-80 carbon steel.

Historically, simple rules of thumb were used to determine corrosivity of CO_2 systems. Systems with over 30 psi partial pressure of CO_2 were considered corrosive when the water/liquid hydrocarbon ratio exceeded 25% [5]. In the range from 3 to 30 psi partial pressure CO_2, wells were considered possibly corrosive. With the development of Prudhoe Bay, these classical models were found to be inadequate with corrosion causing downhole failures in wells with only trace amounts of water [6].

Because of the inadequacy of rules of thumb, multiple models have been developed to calculate the predicted corrosion rates in wells and various surface equipment including pipelines. These models are developed either based on laboratory experimentation of varying degrees of sophistication, theoretical analyses, or empirical

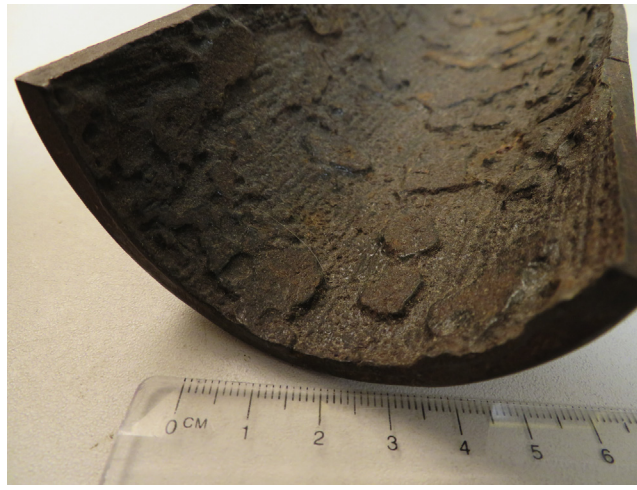

Figure 4.2 Mesa corrosion of flow line.

Figure 4.3 Flow enhanced corrosion, L-80 carbon steel, gas condensate well.

practical experience. The models may focus on one specific damage mechanism, such as general metal wastage due to carbon dioxide corrosion or maybe multifaceted. The first model developed from experimental data was by DeWard and Milliams [7], which was then developed [8,9] further, finally being refined into Shell's HydroCorr program. Other models are based on practical experience such as Total's Lipucor and the University of Southwestern Louisiana model. The models may be retained as in-house company propriety programs may be available for purchase or lease on the commercial market, depending upon the particular program. These programs have been the subject of various reviews [10,11]. The NACE International Technical Report, "Prediction of Internal Corrosion in Oilfield Systems from System Conditions," reviews many of these programs [12]. The challenge of these programs most commonly lies in finding sufficiently detailed and reliable input data to populate the requirements of the model. Accurate detailed formation water analyses are difficult to obtain, and water samples are frequently contaminated with drilling fluids, workover fluids, etcetera. Gas analyses can be affected by the metallurgy of the sampling vessel, and bottom hole sample collection is strongly recommended.

The presence of hydrogen sulfide in addition to carbon dioxide in the produced fluids changes the corrosion phenomenon experienced. The various corrosion reactions provide the possibility to form several different corrosion product films, and these films have varying degrees of protectiveness, depending upon the exact formation conditions. According to Kermani [13] et al., there are three corrosion domains for mixed

carbon dioxide/hydrogen sulfide systems, which can be represented by the ratios of their partial pressures in the system:

$CO_2/H_2S < 20$	Iron sulfide is the main corrosion product
$20 < CO_2/H_2S < 500$	Mixed regime with both iron sulfide and iron carbonate corrosion products
$CO_2/H_2S > 500$	CO_2 corrosion dominates with iron carbonate as the main corrosion product

Prediction equations can be reasonably established for the higher concentration CO_2 systems, based on the extensive research performed over the last few decades. Hydrogen sulfide–dominated systems present more of a challenge. The complexity of corrosion product formation in sour systems has been investigated by Smith [14] and updated by his rigorous reviews of the subject in 2015 [15,16]. Smith argues that there is little scientific basis for the predominance of CO_2 corrosion above a CO_2/H_2S ratio of 500 in common oil and gas production environments and states that small variations in thermodynamic data would cause the ratio to alter by orders of magnitude [17].

There are multiple iron sulfide corrosion product films including, most notably, mackinawite and pyrrhotite. Mackinawite is usually not very protective whereas pyrrhotite often imparts some protection. The kinetics of mackinawite formation are rapid so that it may form preferentially in a mixed H_2S/CO_2 system even when iron carbonate would thermodynamically be expected. Mackinawite formation is favored by lower temperatures (broadly, less than 90°C, or 194°F) and lower concentrations of H_2S. The rate of corrosion is dependent upon flow regime, solution chemistry, and pH. Pyrrhotite is usually found at higher temperatures and higher concentrations of H_2S and under such conditions can be found to impart considerable corrosion protection due to film stability. Several workers have noted examples of wells with pyrrhotite scale that have experienced little measurable corrosion after even decades of exposure. However, damage to the protective film results in rapid pitting. At very high H_2S concentrations and temperatures, pyrite is formed as shown in Fig. 4.4.

Iron sulfide films are never present as one pure substance and are usually composed of several different crystallographic forms and so the discussion above indicates the predominant phase rather than the only phase. Failure of the iron sulfide film can result in highly localized pitting as has been reported by workers including Choi [18]. Velocity, chlorides, and the presence of precipitated elemental sulfur result in damage of each type of sulfide film with resulting rapid localized corrosion.

Many of the corrosion calculation models make broad assumptions in regards to the severity of corrosion in mixed CO_2/H_2S systems, and this subject has been reviewed in detail in NACE technical report [18]. Kvarekval et al. [19] found that under conditions expected to produce more mackinawite, the presence of H_2S at a H_2S/CO_2 ratio of 0.1 resulted in increased general wastage by a factor of 3–5 times. The mackinawite was not protective. At somewhat higher temperatures, higher H_2S partial pressures and an

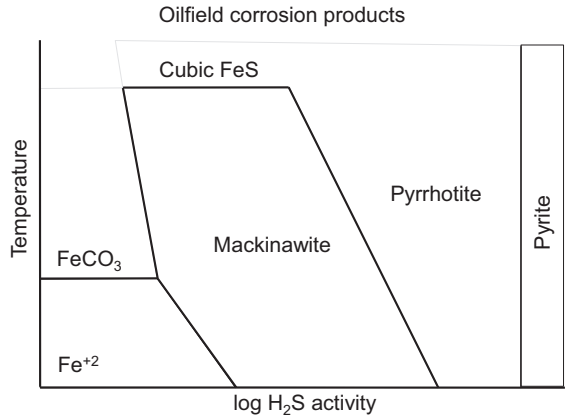

Figure 4.4 Schematic stability zones for various iron sulfides [17].

H_2S/CO_2 ratio of 0.53, a more adherent sulfide film was produced, general wastage rates were approximately the same as in the CO_2 baseline experiments, and pitting penetration rates were 10 times higher. Place [20] in his classic paper on the Thomasville deep sour gas developments reported uninhibited pitting rates of 300 mpy with 28−46 mol% H_2, although sulfur could have also contributed to this penetration rate.

4.3 API RP14E

API Standard RP14E has often been applied to downhole production. The standard has been used to define limits for production rates and prevent erosion or flow-enhanced corrosion. The origins of the standard are obscure, and it has been suggested that these may have arisen from acoustic limits on plant piping. Work continues on validating and developing more meaningful equations through the University of Tulsa research consortium that has produced multiple papers [21]. Generally, for carbon steel systems, an empirical constant, "c-factor," of 100 is assumed in the standard's equations; however, with corrosion-resistant alloy (CRA) completions, higher numbers from 150 to 200 have been used. Success has been observed in specific fields when a much higher c-factor has been used even for carbon steel with the practical result that the flow rate increased, the temperature profile of the well was altered, and water condensation occurred outside of the tubing string, thereby minimizing corrosion.

4.4 Environmental cracking

Uncontrollable downhole failures due to sulfide stress cracking (SSC) of higher strength carbon steel and alloy steel tubing and equipment are a major safety risk in well streams producing more than 0.3 kPa (0.05 psi) partial pressure H_2S. SSC failures

often occur rapidly with little prior warning. The failures are brittle with no attendant plastic deformation. Following some serious Canadian and west Texas failures, NACE International Materials Requirement MR0175 was developed, based on field experience and laboratory testing. It was adopted into law by various bodies such as the Texas Railroad Commission. The subject has been one of considerable research, the origins of which are reported in the NACE compilation on the subject [22]. More recent work has focused on improvements in steel chemistry and microstructure to develop higher strength materials with resistance to SSC.

The NACE Materials Requirement was merged with ISO 15156 in 2003 and is composed of three parts: 1—General Principles for Selection of Cracking-Resistant Materials, 2—Carbon and Low-alloy steels, and 3—Cracking Resistant CRA's and Other Alloys. SSC of carbon and low alloy steels is dependent upon microstructure, strength, hardness, temperature, and exact system conditions. Typically, SSC of carbon steels is worse at temperatures in the region of 60°C (140°F) and decreases with increasing temperature, so that hard, high-strength materials such as Q125 may be used successfully at higher temperatures above 107°C (225°F). Higher strength materials are more susceptible to SSC, so that a commonly used grade is L-80 carbon steel, as this is safe for use under all conditions. Approved materials normally have restricted harnesses with a Rockwell hardness level of HRC 22 being the maximum.

For carbon steels, the standard defines four exposure regions with partial pressure of H_2S and pH of the aqueous environment as the key measurements, and these are shown in Fig. 4.5 [23]. Region zero presents no risk of SSC whereas the requirements for the other regions, 1, 2, and 3, are defined in the text of the standard. The standard allows for approval of specific materials under specific field conditions provided that laboratory

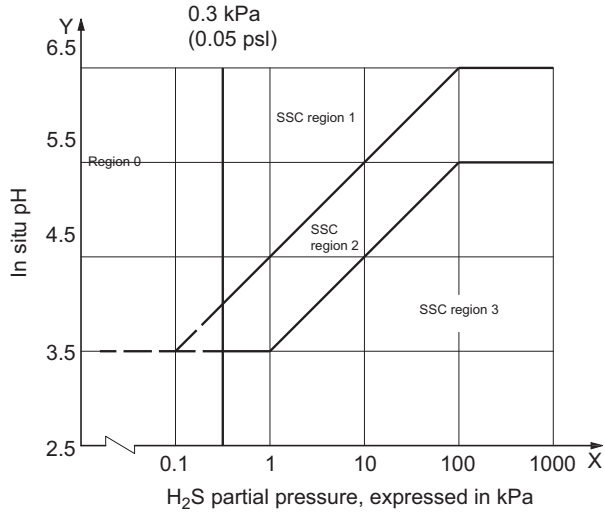

Figure 4.5 Sulfide stress cracking regimes for carbon steel.

tests can demonstrate the safety of the intended application. Various workers are seeking to approve a 125°ksi yield strength material for specific conditions. The challenge with this approach is that exact conditions cannot always be predicted. Well workover fluids may cool the tubing temperature, moving the conditions into a more severe cracking regime. Acidizing treatments of the formation may change the pH for months to come, driving the environment into a more aggressive cracking regime.

Small alloying additions to carbon steel generate materials with improved general corrosion resistance but often poorer resistance to SSC environments. One such material is the martensitic stainless steel, 13 chrome. Caution must be used in employing this material in sour environments, and the maximum exposure is limited to an H_2S partial pressure of 1.5 psi [23].

In severe corrosive environments where higher strength materials are needed to get to the bottom of the hole, CRAs are often used for tubing, liners, and critical exposed materials. Alloys such as the nickel-based alloy, Hastelloy C276, nickel-chromium−cobalt−based alloy, MP35N, and Titanium alloys may be used for the most severe environments, whereas at the other end of the cost spectrum are materials such as 22 Cr duplex stainless steel. These materials are addressed in Part 3 of ISO 15156.

For CRAs, the failures considered by the standard are SSC, stress corrosion cracking (SCC), and galvanically coupled hydrogen stress cracking (GHSC). While SSC and GHSC occur at lower temperatures, the chloride-based SCC is a higher temperature failure; therefore, testing must be performed over a much wider range of environmental conditions. Pitting is also of interest with these materials that are normally immune to general corrosion. As with carbon steels, consideration must be given to all fluids that may be injected, used in, or produced from the well. CRAs are particularly prone to damage by acidizing chemicals.

CRA tubing strings must be matched with compatible well "jewelry." These items are commonly fabricated from bar stock as opposed to tubing material, and different chemistries are required to obtain through-bar properties. Materials such as Inconel 625 and Inconel 718 are commonly used for more aggressive wells but must also be extensively tested for all the failure modes of concern.

Sulfur depositing from the produced fluids on the metal surface is extremely detrimental to the cracking performance of both carbon steels and alloys. It may also contribute to downhole or surface equipment plugging along with asphaltenes, diamantanes, and related products.

4.5 Corrosion inhibition

Although carbon steel is commonly subject to corrosion wastage once the well stream produces sufficient water, the lifetime of carbon steel tubulars can be successfully extended through the use of corrosion inhibitors, particularly in applications up to 150°C (302°F). Applications above that temperature are possible but require extra diligence in design and operation. The European Federation of Corrosion monograph on inhibition includes discussion of downhole applications [24]. The UK Health and

Safety Executive review [25] provides excellent guidance on inhibitor system management and control including key performance indicators (KPIs), but is focused on pipeline operations rather than downhole applications. Corrosion inhibitor efficiency has also been the subject of papers by Crossland et al. [26,27], and these papers are useful references despite the focus on pipeline applications.

Corrosion inhibitors can be applied in producing wells downhole by several different methods, each of which has advantages and disadvantages. The keys to a successful corrosion inhibitor program are focused selection of products, careful design and maintenance of the inhibitor injection system, diligence in correct application of the inhibitor, continual corrosion and process monitoring, and regular planned analysis and reporting of inhibitor system performance and of system exceptions. KPIs must be established for the system and reported on a regular basis.

Continuous corrosion inhibitor injection can be achieved in several ways. If the well is completed with an open annulus and no packer or PBR, corrosion inhibitor in a suitable carrier fluid can be injected through the annular space to provide protection for the tubing [27]. Areas below the end of the tubing will not be protected. Depending on the formation and details of the completion, various operators may choose to ignore the lower portions of the well or if the decision is taken early in the drilling and completion process—a CRA liner may be installed at the bottom of the well. The corrosion inhibitor package must be selected based not only on its ability to prevent corrosion but also on the ability of the corrosion inhibitor to remain in the liquid state before and after injection under the pressures and temperatures at the injection point.

Other methods of continuous inhibition include completion of a well with a dual string or completion with an injection mandrel in the tubing string and delivery of the inhibitor through the annulus, the use of capillary or "spaghetti" tubing to deliver inhibitor and inject through a mandrel, or the use of the gas-lift system (if one is installed) to inject the inhibitor. Each of these techniques has advantages and disadvantages, and detailed attention must be made in the selection of an appropriate product through laboratory evaluation. Specific properties will be required for each particular application method. For example, injection through a small diameter (spaghetti) tube will require the highest purity inhibitor solution with no solids or potential for solid formation, carefully defined viscosity, and excellent heat stability. Injection through umbilicals to subsea wellheads will require careful evaluation of the performance of the product during the extended low-temperature transmission.

Continuous inhibitor treatment can also be achieved through weighted inhibitors or time release inhibitors which may be solid or liquid and applied through the wellhead. The heavy weight products fall to the bottom of the well and are produced back with the production fluids.

Batch treatment of corrosion inhibitor provides a periodic coating of the tubing walls, which must be repeated frequently. An inhibitor slug is displaced down the well by dead crude, diesel, or nitrogen. Retreatment periods are typically between several months to a few weeks, depending upon the well production. For older wells with limited formation pressure it is important not to liquid load the well and essentially kill it. The use of low-quality nitrogen from a generator can result in the injection of oxygen downhole, which would greatly accentuate corrosion damage.

Squeeze is the process by which an inhibitor solution is forced back into the formation and allowed to feedback slowly over several months, providing effectively a one-time batch treatment followed by continuous replenishment from the inhibitor squeezed back into the reservoir. It is generally assumed that one-third of the inhibitor squeeze is permanently lost to the formation, one-third of the inhibitor is produced back immediately, and one-third remains to feedback slowly as a continuous treatment. Displacement of the inhibitor into the formation may be by nitrogen, diesel, or other appropriate fluid. As is the case of tubing displacement, it is possible to kill the well by liquid loading. It is also possible to cause damage to the formation, and therefore formation core tests with all the fluids involved are essential.

All corrosion inhibitor systems must be carefully evaluated before use. The properties of the corrosion inhibitors must be evaluated in their neat state and in any diluted condition, because of the use of additional solvent or carrier fluid. Finally, corrosion inhibitors must be evaluated at their planned treatment rate. Concentrated corrosion inhibitors can themselves be corrosive. Temperatures and pressures experienced downhole may affect the performance of the product.

Oil and gas field corrosion inhibitors are normally organic surface active compounds usually containing a nitrogen group, although also possibly based on sulfur or phosphorus chemistries. Amines, imidazolines, and quaternary ammonium salts are among the many types of chemical applied to these applications. Commercial products are blends of one or more active ingredients, solvent, surfactants, and other components as needed. Products may be specially formulated for extreme cold or heat stability to account for ambient conditions at the storage and application locations in addition to being formulated for the specific corrosion damage mechanism and well temperature and pressure extremes. Inhibitors may be oil soluble, oil soluble−water dispersible, or water soluble. The solubility affects the ability of the inhibitor to remain in solution, to move to the required location, and the inhibitor's effectiveness at remaining on the surface. The solubility also affects the test protocols that can be selected to evaluate the product, because some test methods are inevitably biased toward one type of product solubility over another. Electrochemical tests in mostly aqueous environments usually favor water-soluble products unless the test is carefully designed.

The corrosion inhibitor must be compatible with the materials of construction of the injection system. This includes pump material and any nonmetallic components. The inhibitor must be compatible with other treatment chemicals that it may encounter downhole or when produced back on the surface [28]. This includes, but is not limited to, biocides, scale inhibitors, sulfur solvents, and hydrate preventives. The corrosion inhibitor must not cause problems in downstream processing, whether that involves the formation of emulsions or foams in separation equipment or impacts catalysts or processes within the refinery. The corrosion inhibitor must be compatible with water disposal requirements, as water is separated out in processing, be that offshore or onshore. Environmental regulations may limit the use of more water-soluble products that tend to travel with the water stream. The inhibitor package must meet fire and safety requirements. Usually, a minimum flash point requirement is mandated for offshore applications. Particularly toxic or carcinogenic compounds may also be restricted, depending on local codes.

NACE International Publication 31215 [29] lists multiple laboratory tests for evaluating both the physical properties and corrosion inhibition performance of corrosion inhibitors. It also provides additional information for regulations concerning disposal in sensitive areas such as the North Sea. In addition to the methods listed, it is critical to provide analytical techniques to serve as a baseline for future quality control evaluations of delivered chemicals. Advanced infrared spectroscopy is often used for this purpose, and other analytical techniques may also be helpful.

Evaluation of corrosion-inhibiting properties can be achieved through a variety of test methods. Each test method has advantages and disadvantages, and it is necessary to be fully aware of each of these before entering into a test program. Tests performed at essentially ambient or slightly elevated pressures using atmospheric rotating cylinder electrodes, coupons, or atmospheric pressure rotating cages are easy to achieve but are unlikely to adequately model downhole conditions. Use of autoclaves with static or rotating cage coupon arrangements can be much more useful because it is possible to simulate downhole temperature and pressures with active gas components. The inclusion of a hydrocarbon phase is also beneficial. Significant changes can occur in test solution chemistry especially during extended tests with limited liquid inventories. Some test designs attempt to compensate for this with pH adjustment or other methods. The use of pressurized flowloops is perhaps the ultimate test protocol, but the number of facilities that can perform these tests is extremely limited, and the tests are expensive to perform.

Challenges abound in maintaining the integrity of test environments. Use of commercial gases rather than high-purity gases can introduce oxygen. Environments with small partial pressures of H_2S are hard to sample accurately in the field because H_2S can react with sample containers. These same environments are hard to maintain in the laboratory because in fixed inventory tests, H_2S can be consumed. Test environment pH's frequently change, and solutions may become contaminated with iron corrosion products. These challenges are compounded with the fact that stable iron sulfide films may take many days to grow, so that longer term tests with precorroded samples are preferred but difficult to achieve. The environment selected for a test and the method of applying corrosion inhibitor within the test is also worthy of due consideration.

Once an inhibitor is approved for field application, it is essential to establish a quality assurance protocol to ensure that the correct product is being delivered to the site location and that it is being injected at the design rate. Retained samples of delivered product should be taken and securely stored. A regular reporting schedule must be established, and discrepancies from the injection plan flagged for follow-up action. Depending on the operating company philosophy, these operations may be completed by service company personnel or the operating company staff.

Field monitoring of corrosion inhibition performance is essential. Perhaps the most reliable measure is tubing−casing annulus pressure measurement which will indicate communication through the tubing. This can be due to corrosion penetration or a mechanical issue. However, in either case this is an "after-the-fact" measurement rather than a proactive measurement. Downhole corrosion coupons or probes are offered by corrosion-monitoring companies, but these require wireline access to retrieve and usually special fittings downhole. Furthermore, because corrosion may vary at different depths in the well, downhole monitoring is best achieved by multiple

locations up the string, which increases the cost and complexity of downhole monitoring. Alternatively, downhole calipers that may be mechanical finger calipers or electromagnetic calipers can be run to establish corrosion rates of inhibited wells at regular intervals. These calipers have been known to enhance corrosion themselves by removing corrosion product and providing a fresh metal surface, so corrosion inhibition programs may need to be increased after such downhole measurements. Fig. 4.6 presents an example of caliper enhanced corrosion.

Surface monitoring of well stream production is possible. Such monitoring will indicate changes to the system and establish trends but may well not be directly correlated with downhole conditions. Corrosion coupons mounted some distance downstream of the choke will provide pitting and general corrosion data over months. High-sensitivity electrical resistance probes located in the same location will provide system changes after a few hours. Produced water samples can be collected at convenient locations and iron compounds determined. Residual inhibitor analyses have proved useful for some, but certainly not all, systems.

Smith and Pakalapati [30] presented field experience with various inhibitor programs from the Big Escambia Field collected over 30 years. These experiences illustrate many of the practical challenges described above.

4.6 Comparison of costs for downhole corrosion prevention methods

While the CAPEX of a carbon steel tubing string is lower than that of a CRA string, ongoing maintenance costs from the operation of corrosion inhibitor programs can be a significant factor in operating costs (OPEX). Well interventions usually require

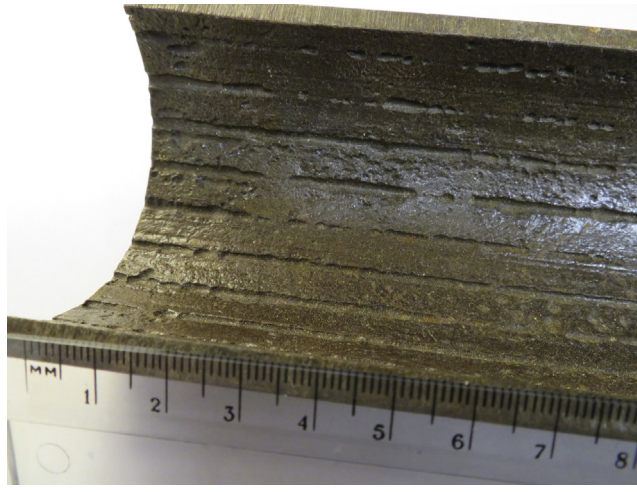

Figure 4.6 Caliper-caused downhole tubing damage.

stopping production with the associated lost revenue. Displacement fluids such as nitrogen can be costly. Inhibitors themselves are specialty products and priced accordingly. Manpower to maintain injection systems, perform monitoring tasks, and report program updates is not insignificant if well performed. Over many years, therefore, the higher initial CAPEX choice of CRA tubing strings may become more attractive. Tems [31] and Al-Zahrani reported on various examples of upstream inhibition corrosion costs.

4.7 Downhole internal coatings and nonmetallic materials

Downhole internal plastic coatings are used in production systems. A survey of one oil and gas production company found about one quarter of tubing products to be internally coated. There are varying views on the efficiency of corrosion protection that they provide. Frequently, they have not been deemed sufficient on their own to prevent corrosion completely but do give assurance that carbon steel wells will not fail from massive wastage corrosion attack. Downhole coatings have been subject to damage especially in relation to tubing connections and therefore subject to localized attack at areas of coating damage. They do provide some assurance that the tubing will not be parted by corrosion but can be retrieved more easily for workovers. In production environments, coatings are sometimes used in combination with inhibitor treatments to provide a "belt and braces (suspenders)" approach. NACE documents call for care in handling downhole-coated products with the aim of preventing mechanical damage. A recent paper by Lauer [32] discusses improvements in formulations to provide improved performance.

In addition to internal plastic coatings, other coating materials such as cementitious coatings have been used. Internal coatings are used more commonly in injection environments, and indeed the performance requirements of injection wells are more moderate. Fiberglass products have been used for downhole tubing and sucker rods, although the mechanical properties of fiberglass materials tend to degrade with time.

4.8 Control of external corrosion

Although this chapter has focused on internal corrosion problems, some acknowledgment must be given to external corrosion challenges, which can arise because of incomplete cement jobs and corrosive aquifers. External coating of casing is specified by some companies who believe it beneficial in reducing the total surface area that is subject to corrosion damage. Clearly the drilling and completion practices will result in damage to the external coating. However, when combined with external cathodic protection (CP), the use of coating allows more effective coverage by the CP system.

4.9 Conclusions

Downhole production presents a plethora of production scenarios, from high-pressure, high-temperature deep sour gas wells to fairly shallow oil pumping wells and wells under enhanced oil recovery, from offshore wells on unmanned platforms in deep water to land-based wells that are easily accessible. Each of these scenarios presents its own unique set of problems with questions to be addressed. Ultimately, research is dominated by economics—what questions must we answer to produce these wells with the greatest economic return but still maintain the required assurance of safety and environmental protection? What do we need to know to show due diligence as an operator or service provider and also to meet the requirements of local and international standards? Deep sour production often presents the most dramatic challenges as we try to optimize the window between required strength, downhole environments and treatments, cracking resistance, cost, and delivery. Yet, at the other end of the spectrum, there are older secondary or tertiary fields with large numbers of wells where optimization of corrosion control can present the balance between profitable production or loss.

We must ask, "do we know enough about our wells?" Often a failure is repaired without spending adequate money to investigate the problem. There is a need for better field data. Full failure analyses of tubing strings is often beneficial, showing distribution of corrosion attack within a string, analyzing corrosion product films and damage morphology. Improved remote sensing and monitoring of corrosion rates, chemical injection systems, and residuals are essential with low-maintenance, low-cost monitoring systems integrated into the process management system; good data are required for decision-making. Reliable, low-cost, remote monitoring systems are essential at both ends of the production spectrum—unmanned offshore platforms, subsea completions, and multiwell onshore operations.

Good field data are necessary to allow validation and improvement of corrosion models. Also required in the further development of corrosion models is better understanding of the effects of H_2S in the H_2S/CO_2 mixed corrosion system. It is only through better understanding of these corrosion processes that we can design better laboratory tests for the evaluation and development of corrosion control methods such as corrosion inhibition.

Corrosion inhibitors are an area where we must not be complacent and must continue to push the boundaries of high-temperature and high-pressure applications and improved delivery systems. Developments in corrosion inhibitors will also be necessary for the modified environments produced by enhanced oil recovery. Tagging of inhibitors is a technology that enhances system monitoring and control and has found its first applications in offshore gas fields.

Nonmetallics represent another opportunity for future research. Potential applications include improved elastomers, improved coating systems, improved lining systems, and solid tubing systems.

References

[1] R.D. Tems, G.R. Lobley, N. Al-Bannai, S. Al-Zubail, Managing the Cost of Corrosion. Eurocorr 2009, Nice, France, 2009.

[2] K.D. Efird, R.J. Jasinski, Effect of Crude Oil on Corrosion of Steel in Crude Oil/Brine Production, Corrosion 45 (February 1989) 165−171.

[3] K.D. Efird, J.L. Smith, N. Davis, S. Blevins, The Crude Oil Effect on Steel Corrosion: Wettability Preference and Brine Chemistry. NACE Annual Corrosion Conference, Corrosion 2004, Paper 04366, NACE International, Houston, Texas, 2004.

[4] J.L. Crolet, M.R. Bonis, Why So Low Free Acetic Acid Thresholds in Sweet Corrosion at Low P_{CO2}. NACE Annual Corrosion Conference, Corrosion 2005, Paper 05272, NACE International, Houston, Texas, 2005.

[5] P.E. Townshend, G.T. Colegate, T.L. van Waart, Carbon Dioxide Corrosion at Low Partial Pressure in Major Submarine Gas Pipelines. SPE European Spring Meeting, Paper 3741, Amsterdam, 1972.

[6] H.G. Byars, J.M. Galbraith, An Integrated Corrosion Control and Monitoring Program for Prudhoe Bay Alaska. NACE Annual Corrosion Conference, Corrosion'83, Paper 50, National Association of Corrosion Engineers, Houston, Texas, 1983.

[7] C. de Waard, D.E. Milliams, Prediction of Carbonic Acid in Natural Gas Pipelines. First International Conference on Internal and External Protection of Pipes, University of Durham, England, 1975.

[8] C. de Waard, U. Lotz, D.E. Milliams, Predictive Model for CO_2 Corrosion Engineering. NACE Annual Corrosion Conference, Corrosion'91, Paper 91577, NACE International, Houston, Texas, 1991.

[9] C. de Waard, U. Lotz, A. Dugstad, Influence of Liquid Flow Velocity on CO_2 Corrosion—A Semi-Empirical Model. NACE Annual Corrosion Conference, Corrosion'95, Paper 95128, NACE International, Houston, Texas, 1995.

[10] R. Nyborg, Guidelines for Prediction of CO_2 Corrosion in Oil and Gas Production Systems, Institute for Energy Technology, Kjeller, Norway, 2003.

[11] Selection of Pipeline Flow and Internal Corrosion Models, NACE Publication 21410, NACE International, Houston, Texas, 2015.

[12] Prediction of Environmental Aggressiveness in Oilfield Systems from System Conditions, Technical Report, NACE TG 076, NACE International, Houston, Texas, 2017, to be published.

[13] B. Kermani, J. Martin, K. Esaklul. NACE Annual Corrosion Conference, Paper 06121, NACE International, Houston, Texas, 2006.

[14] S.N. Smith, J.L. Pacheco, Prediction of Corrosion in Slightly Sour Environments. NACE Annual Corrosion Conference, Paper 02241, NACE International, Houston, Texas, 2002.

[15] S.N. Smith, M.W. Joosten, Corrosion of Carbon Steel by H_2S in CO_2 Containing Oilfield Environments − 10 Year Update. NACE Annual Corrosion Conference, Corrosion'15, Paper 5484, NACE International, Houston, Texas, 2015.

[16] S.N. Smith, Current Understanding of Corrosion Mechanisms Due to H_2S in Oil and Gas Production Environments. NACE Annual Corrosion Conference, Corrosion'15, Paper 5485, NACE International, Houston, Texas, 2015.

[17] S.N. Smith, The Carbon Dioxide/Hydrogen Sulfide Ratio—Use and Relevance, Materials Performance 54 (May 2015) 64−67.

[18] H.J. Choi, H.A. Al-Ajwad, Flow Dependency of Sweet and Sour Corrosion of Carbon Steel Downhole Production Tubing in Khuff-Gas Wells. Corrosion'08, Paper 8638, NACE International, Houston, Texas, 2008.
[19] J. Kvarekal, G. Svenningsen, R.D. Tems, V. Casanova, Top-of-Line Corrosion in Sour Environments. 15th Middle East Corrosion Conference, Bahrain, 2014, Bahrain Society of Engineers and NACE International, 2014.
[20] M.C. Place, Corrosion Control – Deep Sour Gas Production. SPE8310, Dallas, Texas, 1979.
[21] J.R. Shadley, S.A. Shiraz, E. Dayalan, E.F. Rybicki, Prediction of Erosion-Corrosion Penetration Rate in a Carbon Dioxide Environment With Sand, Corrosion 54 (1998) 972–978.
[22] R.N. Tuttle, R.D. Kane (Eds.), H_2S Corrosion in Oil and Gas Production: A Compilation of Classic Papers, NACE International, Houston, Texas, 1981.
[23] ISO 15156, International Standards Organization.
[24] J.W. Palmer, W. Hedges, J.L. Dawson (Eds.), The Use of Corrosion Inhibitors in Oil and Gas Production, European Federation of Corrosion Publication 39, Maney Publishing, London, 2004.
[25] J. Hobbs, Reliable Corrosion Inhibition in the Oil and Gas Industry, Research Report 1023, Health and Safety Executive, UK, 2014.
[26] A. Crossland, R. Woollam, J. Palmer, G. John, S. Turgoose, J. Vera, Corrosion Inhibitor Efficiency Limits and Key Factors. NACE Annual Corrosion Conference, Paper 11062, NACE International, Houston, Texas, 2011.
[27] A. Crossland, J. Vera, A. Fox, S. Webster, G. Hickey, Developing a High Reliability Approach to Corrosion Inhibitor Injection Systems. NACE Annual Corrosion Conference, Paper 10324, NACE International, Houston, Texas, 2010.
[28] M. Rithauddeen, S. Al-Adel, R.D. Tems, Study for Offshore Mideast Field Shows Inhibitor and Sulfur Solvent Compatible, Oil and Gas Journal (October 6, 2014) 88–97.
[29] NACE Technical Committee Report 31215, Laboratory Evaluation of Corrosion Inhibitors Used in the Oil and Gas Industry, NACE International, Houston, Texas, 2014.
[30] S.N. Smith, R.S. Pakalapati, Thirty Years of Downhole Corrosion Experience at Big Escambia Creek: Corrosion Mechanisms and Inhibition. NACE Annual Corrosion Conference, Corrosion 2004, Paper 04744, NACE International, Houston, Texas, 2004.
[31] R.D. Tems, A.M. Al-Zahrani, Cost of Corrosion in Oil Production and Refining, Saudi Aramco Journal of Technology (Summer 2006) 2–14.
[32] R.S. Lauer, New Advancements in the Abrasion Resistance of Internal Plastic Coatings. NACE Annual Corrosion Conference, Corrosion 2013, Paper 2208, NACE International, Houston, Texas, 2013.

Corrosion in onshore production and transmission sectors—current knowledge and challenges

5

Ali N. Moosavi
DNVGL, Kuwait

5.1 Introduction

In 1983, I was studying for my PhD at The Corrosion and Protection Center in University of Manchester Institute of Science and Technology in the United Kingdom. The head of the center was Professor Graham Wood, Britain's first Professor of Corrosion, and an internationally recognized expert on high temperature oxidation. That year he was also receiving the UR Evans Award, one of the highest awards in the field of corrosion. Fittingly, the award was in the shape of a sword, made of stainless steel. I was one of the many people present at the award ceremony. The reason that this occasion has been etched so firmly in my memory is because of a few words in Professor Wood's acceptance speech. He said something to this effect: "I believe all the important discoveries about corrosion have already been made and all the future findings will be no more than a footnote in the science of corrosion." These words astounded me. Here I was, studying for a PhD in the subject and hoping to find some new, exciting hereto unknown discoveries about corrosion and I was being told that the most I could hope for was finding a few minor facts about this subject.

Fast forward to 2016. I had just finished writing a book for the major onshore oil and gas exploration company that I had been working for the past 21 years. The book was a selection of corrosion related failure investigations that I had carried out during my years with the company, including the causes of the failures and lessons learned from them. Going over the book, what struck me was the similarity of the causes of these failures and also the lessons learned from them. Also this, in these failures, spanning 21 years, there was nothing in either the causes or the preventive measures that had not already been known for many years before. Then the words of Professor Wood flashed before me and I finally understood that he was perfectly right. We have more than enough knowledge to prevent, or at least minimize, corrosion. What we need to do is to concentrate on what I call the three C's: competency, cost, and care.

If those involved in design and operation lack the sufficient competency for their job, then no amount of manuals and books would make any difference in significantly lowering the risk of corrosion. Also, if we do not incorporate the concept of life cycle cost at the design stage, instead of capital cost, then we may not be spending what it

Trends in Oil and Gas Corrosion Research and Technologies. http://dx.doi.org/10.1016/B978-0-08-101105-8.00005-X

takes to control corrosion; which will in the long run cost us much more. Last, but by no means the least, devoting sufficient care in both design and operation of facilities to ensure that all the relevant standards, manuals, and lessons learned have been reviewed and taken into account, is the best and most cost-effective means of corrosion control.

This chapter is based upon my own practical experience of working as a corrosion and materials specialist in the oil and gas industry. It concerns corrosion processes that are most prevalent in onshore operations and the most tried-and-tested methods of controlling them. A guide to materials selection is also included and the most prevalent methods of corrosion monitoring and inspection are also discussed.

5.1.1 Onshore atmospheric corrosion

Although it is generally true that the onshore environment is more benign and less corrosive than offshore, there are cases where special care and attention is needed. Plants and structures located in coastal locations will be prone to salt spray and will require extra attention for protection of external surfaces.

Pipelines laid on the desert floor can be quickly covered by sand and, if not externally coated, can suffer from corrosion by the water produced by humidity or rain and entrapped by the sand. Even the use of "sleepers" may not overcome this problem. Any structures near chemical plants may be subject to corrosive fumes or sprays.

5.1.2 Onshore underground corrosion

Buried pipelines are generally coated and many will also be supplemented with cathodic protection (CP). There are instances where, due to the possibility of microbiologically influenced corrosion (MIC), special attention is required. One such location is the so-called "Sabkha" regions in the desert. These are places where the underground soil is entrenched in highly saline water. These locations are extremely corrosive as they not only cause chloride-induced corrosion but also act as fertile ground for MIC causing organisms such as sulfate-reducing bacteria (SRB). Pipelines exposed wholly or partly to such soil require both a high-performance coating and CP.

5.1.3 Onshore oil pipelines—internal corrosion

Internal corrosion of these pipelines represent the most common mode of corrosion in the onshore oil industry. That is corrosion (usually localized) along the 6 o'clock position (i.e., bottom of the pipeline) as can be seen in Fig. 5.1.

This corrosion is caused by stagnant liquids containing corrosive substances. Oil itself acts like a corrosion inhibitor by forming a fairly protective viscous film on the metal surface. Therefore, corrosion only ensues when oil contains water. There have been many discussions about how much water it takes to change the surface of the metallic pipeline from "oil wet" to "water wet". The figure of 30 vol% water cut seems to be the most common one, although in stagnant situations, water cuts much lower than this can cause corrosion. The change in corrosion dynamics when changing from oil wet to water wet is huge and can change the pipeline surface environment

Figure 5.1 A leak caused by localized corrosion at the bottom (6 o'clock position) of an onshore oil flowline.

from noncorrosive to highly corrosive. The best way of preventing this type of corrosion is to prevent the formation of stagnancy in the pipeline.

The three most common reasons for formation of stagnant liquids in pipelines are as follows.

5.1.3.1 Dead legs

The occurrence of dead legs can normally be prevented at the design stage. Though in some cases, this may not be preventable due to the topography of the terrain and the pipeline route profile, in most cases dead legs can be eliminated at the design stage by carefully removing any pipeline angles of 90° or less.

5.1.3.2 Shut downs

During shut downs, if the pipeline was being inhibited, then the corrosion inhibitor may become ineffective. To avoid corrosion during shut downs, proper mothballing is required, ideally using cleaning pigs to remove debris and pools of stagnant liquid where corrosion cells can form.

5.1.3.3 Low flow rate

This is another design-related issue. During pipeline design, usually a lot of attention is focused to ensure that the pipeline diameter is not too small, which could result in erosion corrosion. However, by the same token, if the pipeline diameter is too large, then stagnation and corrosion can take place. One of the most common reasons for selecting a too large a pipeline diameter during design is basing the design on maximum future production and flow rather than the present and short-term production. Another reason is standardizing. It certainly helps during purchasing to have one size diameter pipeline as a large volume of one size pipeline should work out more economically than two medium size orders for different diameter pipelines. This, however, could prove to be false economy if widespread corrosion takes place resulting in production shut downs, pipe repairs, and replacements.

5.1.4 Onshore gas pipelines—internal corrosion

With gas pipelines, especially those carrying sour gas, the primary concern is environmental cracking. This issue is amply covered elsewhere in this book. Suffice to say that by ensuring that the pipeline is manufactured in conformance with ISO 15156/NACE MR0175, and controlling the steel chemistry, we can prevent sulfide stress cracking (SSC) and hydrogen-induced cracking (HIC). Stress corrosion cracking (SCC) can also be prevented by taking care to ensure that the pipeline material/operating environment is not prone to SCC.

If the gas is completely dry, then corrosion will not be an issue. The key word here is "completely". There have been many cases where "completely dry" has been interpreted as having very little water. This unfortunate interpretation has led to many corrosion incidents. It may be tempting to say that we should always assume that the gas contains some water, when we are selecting the material for the pipeline. This, however, could have a very significant financial impact. Although for dry gas, standard carbon steel pipe would be fine, wet gas may require exotic and expensive alloys, depending on the gas composition. Therefore, it is essential, at the design stage, to ascertain whether the gas is going to be dry.

The internal corrosion process can be both uniform and localized. Most common causes of uniform corrosion are as follows:

1. Erosion by either the flow velocity exceeding the permitted erosional velocity or by particles such as sand being present in the pipelines, thus removing the inherent protective scales of steel or organic and inorganic films formed by corrosion inhibitors and scaling, respectively.
2. Attack by carbonic acid being produced by any CO_2 in the pipeline reacting with water.

Localized corrosion tends to be more common and its most frequently seen causes are

1. Stagnation of liquid as described earlier.
2. Microbiologically influenced corrosion (MIC), where internal conditions in the pipeline are apt for the growth of corrosion-inducing bacteria, such as SRB; this generally means low or no flow, presence of bacteria and nutrients for their growth, and sediments or other deposits harnessing the bacteria.

5.1.5 Onshore multiphase pipelines—internal corrosion

In order for corrosion to ensue, one of the phases must be water. After that, the nature and relative amount of each phase determine the degree of corrosivity. One of the subjects that has been widely studied is the influence of the CO_2/H_2S ratio in a gas mixture on the corrosivity of the mixed gas.

For many years, a popular assumption used by corrosion engineers when dealing with corrosion in a mixed CO_2/H_2S environment has been the following:

- For CO_2/H_2S ratio <20, the corrosion is fully governed by H_2S. For carbon steels, the primary corrosion product is a nonstoichiometric iron sulfide (Fe_xS_y), with varying protective properties depending on its crystallographic structure.
- For high CO_2/H_2S ratios (normally >500 but depends on environmental variables), the corrosion rate is fully governed by CO_2. The primary corrosion product is iron carbonate ($FeCO_3$). For intermediate ratios, the corrosion regime is complex and difficult to anticipate.

However, more recent work [1] has indicated that in mixed CO_2/H_2S systems, H_2S plays a much larger role than assumed before and even a few ppm of H_2S can significantly slow down the corrosion process.

5.2 Control of pipeline corrosion

There are always two options for controlling or minimizing corrosion: (1) materials selection and (2) corrosion control. If a material is going to operate in an environment where it is likely to suffer from corrosion attack, we can either change the material to a more corrosion resistant one or use a corrosion control measure. By "corrosion control" we mean changing the corrosive environment immediately surrounding the material to a noncorrosive, or at least a less-corrosive one or shielding the material from the corrosive environment. The deciding factor for what type of selection usually is based on practicality, cost, and safety.

Some years ago, a common strategy was to Do Nothing. If a leak did not present major safety concerns and could be immediately located and fixed, or when the cost of the protection/control options was not far from replacing sections, or even the whole line, then this strategy was adopted. However, now with the focus on environment, and the heavy fines imposed on the oil companies in many countries for any oil leaks, Do Nothing is no longer a common option.

The process of pipeline corrosion control is usually achieved by a combination of two or more of these methods: control, monitoring, inspection, and assessment. The combination of these measures can be termed corrosion management.

5.2.1 Materials selection

The overwhelming majority of pipelines worldwide, be it for oil, gas, or water, are constructed from carbon steel. It is a material that is readily available, relatively cheap, with good mechanical properties, excellent weldability, and whose corrosion resistance can be enhanced by a number of ways such as coating, lining, cladding, CP, and chemical inhibition. There is also a vast amount of information and track record on its use. It is very important, and sometimes critical, to involve corrosion engineers in any new project from the early stages of the design and engineering process. Their early involvement could prevent failures down the line due to corrosion related deficiencies in design and materials selection.

When selecting the pipeline material, we need to have as much information as possible about its operating environment and other relevant factors as explained below. It should also be noted that many of these environmental conditions may change through the course of the design life of structures and equipment and their impact on the corrosion process may change accordingly. Therefore, it is good practice to check the original design data used for material selection with the actual data from operating conditions from time to time.

- *Water Content*—Without water there is no corrosion; therefore, the presence and amount of water are of critical importance. This is especially important in oil pipelines. Oil is not only

noncorrosive but also provides a degree of corrosion inhibition by forming a viscous film on the metal surface. Experience over the years has shown that with little or no water, the metal surface remains "oil-wet" and corrosion is kept to a minimum. However, increasing water content changes the metal surface environment from "oil-wet" to "water-wet" leading to a sharp rise in the corrosion rate. There is no agreed figure for the level of water required to bring about this change. A popular postulation is that at around 30 vol% water, the change from oil-wet to water-wet takes place. It is not just important to know the water content in the pipeline but, just as importantly, when the high water level is reached. This information can then be evaluated alongside the expected design life to reach to the best techno-economic selection.

- *Gases*—The gases whose presence and levels have a major influence on material selection are oxygen, hydrogen (produced by the cathodic reaction), carbon dioxide, and hydrogen sulfide. Oxygen greatly accelerates the corrosion process and has to be kept out of the pipeline. Carbon dioxide reacts with water to produce carbonic acid, resulting in acidic pH and subsequent rise in corrosion. The main danger with both hydrogen sulfide and hydrogen is environmental cracking: HIC, SSC, and stress oriented hydrogen induced cracking (SOHIC). With hydrogen sulfide, there is also a health and safety risk as it is a highly toxic gas, fatal even at very low levels, and therefore its uncontrolled release to atmosphere must be prevented at all costs, especially in populated places. However, H_2S can also be beneficial by forming a protective iron sulfide film on the metal surface.
- *Pressure and Temperature*—Increasing the operating pressure, increases the partial pressure of gases, making them more soluble and able to cause corrosion. Increasing the temperature in most cases increases the rate of corrosion reaction. Also, it is very important to know the minimum operating temperature as it may necessitate the requirement of materials resistant to cracking in very low temperatures, such as a low temperature steel.
- *Flow Rate*—Both the maximum and minimum flow rates have an important bearing on corrosion. With the maximum flow rate, if it exceeds the erosional velocity, then significant erosion corrosion can take place. On the other hand, very low levels of flow rate can cause stagnation and build-up of liquids and solids, leading to underdeposit corrosion and MIC.
- *pH*—The three constituents that most affect the pH are CO_2 and H_2S (lowering the pH) and bicarbonates (increasing the pH).
- *Design Life*—This can have a significant effect on the cost aspect of material selection, when using the life cycle cost analysis. For the same environment, a short design life may allow the use of carbon steel with no further corrosion control, whereas a long design life may require a number of corrosion control measures, or even a higher grade material.

A 5-point step for material selection, shown later in the Downhole Corrosion section, can more or less be equally applied here. It is becoming increasingly commonplace to use the software that predict corrosion rates and select the most appropriate material for the operating environment and design life of the pipeline or other equipment. Of course, such software are very convenient and, as they become ever more user friendly, very popular with corrosion engineers. These, however, are still far from perfect and should always be backed up with field and lab data.

Nonmetallic materials are finding increasing usage as pipeline material, either as lining material (Fig. 5.2) or as a stand-alone material. However, when considering non-metallics as pipeline material, environmental factors such as maximum pressure and temperature must be carefully considered. For nonmetallic pipelines being laid on the desert, soil and sand movements must also be considered. Such environmental factors can have an adverse impact on the material (Fig. 5.3).

Figure 5.2 Insertion of high density polyethylene internal liner onto a carbon steel pipeline.

Figure 5.3 Upheaval of a reinforced thermoplastic pipeline laid in the desert.

5.2.2 Corrosion control

Corrosion can be defined as the deterioration of a material by reaction with its environment. Therefore, for controlling corrosion in a corrosive environment we have to either change the material or the environment. Selection of which option will depend on many factors, among them: safety, practicality, cost, track record, design life, etc.

With regards to material change, there are two main options. One is to change from metallic to nonmetallic. Examples of nonmetallic pipelines include glass-reinforced epoxy (GRE), high-density polyethylene (HDPE), and polyvinyl chloride (PVC). The change can be in two ways: changing the pipe as a whole or inserting a nonmetallic pipe into a metallic pipe. The latter option has gained popularity in recent times as it offers the advantages of combining the strength of metal with the corrosion resistance of nonmetal and being able to do this in situ as a rehabilitation option.

The other material change option is to upgrade to a higher, more corrosion resistant alloy (CRA). Again, as in the nonmetallic case, this can be achieved in two ways. Either have a pipeline made of solid CRA or, as it is more common, clad the steel pipeline with typically 2−3 mm of a CRA. It should be noted that both the CRA cladding and the internally fit nonmetallic pipe only offer protection from internal corrosion.

The main environmental change options for internal corrosion protection include chemical inhibition, dewatering pigging, and coating or lining. Though the main chemical used for corrosion control is corrosion inhibitors, quite often this is added in combination with other chemicals such as oxygen scavengers and biocides. Selection of chemicals will depend on the specific environment of the pipeline.

As the main culprit in corrosion is water, simple removal of water by dewatering pigging using foam pigs, can be very effective. It needs, however, to be performed on a regular basis. It also prevents stagnant water build-up and thus prevent localized corrosion.

Internal coatings or linings are also utilized in some pipelines, particularly those carrying oil. The most common coating used for internal protection is epoxy, either in liquid form or as fusion-bonded epoxy.

As regards to external corrosion protection, the choices are mainly dictated by the environment. Pipes laid on the desert floor, for example, can be placed on stands (called sleepers) to raise the pipes above the ground to a height where they will be reasonably immune to being covered by sand. The "sleepers" should preferably be made of concrete or nonmetals. If this measure is taken, no further external protection may be necessary. Otherwise for external protection of buried lines normally a combination of coating and cathodic protection is recommended.

When selecting a coating, one of the critical factors is the operating and design (upset) temperatures. For example, a coating that is suitable for oil pipelines with a design temperature of 85°C (185°F) may not be correct for gas pipelines with a design temperature of 110°C (230°F). Although CP design is fairly standard for pipelines and any problems can usually be fixed with straightforward adjustment of current and potential, a coating problem can lead to kilometers of coating breakdown on buried pipelines. Such problems can lead to total replacement of pipelines as it may be less costly to do this than try to rehabilitate failed coatings in situ.

5.2.3 Corrosion monitoring

Corrosion monitoring can be classified in a number of ways. One classification is historical versus current. Corrosion coupons provide historical data. They cannot provide accurate corrosion rates or the specific start time of the onset of corrosion within their exposure time, which typically is 6 months to a year. Corrosion probes, on the other hand, provide continuous measurements; their readings will tell us the time the corrosion started, when it reached its highest rate, and the rate of corrosion. Another type of classification is intrusive versus nonintrusive. Both corrosion coupons and probes are intrusive types, in direct contact with the liquid measuring the corrosivity of the liquid. Nonintrusive types, such as hydrogen probes or special belts and mats, are placed on the external side of the pipeline.

Nonintrusive monitoring instruments are particularly useful for pipelines carrying sour oil and gas. One reason is from health and safety viewpoint where installing and retrieving intrusive coupons and probes is always accompanied by a risk of exposure of personnel and environment to the deadly H_2S gas. Another reason is that in sour systems many online intrusive probes malfunction due to build-up of iron sulfide film on the probe circuit causing it to short out and provide erroneous data.

For nonintrusive internal corrosion monitoring of above-ground pipelines, hydrogen probes, mounted on the external surface of pipelines, have also been used. Because hydrogen is produced in the cathodic reaction of the corrosion process, its monitoring can provide an indication of internal corrosion activity. More importantly, it can provide a warning about potential of hydrogen induced cracking. However, hydrogen probes have not had a high degree of reliability for various reasons (leakage of gas from outside, incorrect location of the probe, etc.) and their use has become limited.

Ultrasonic-based instruments, such as the Field Signature Method, have been used with some success. However, the two main drawbacks of these techniques are their high cost and, more importantly, the criticality of placing the instrument in a representative location, as each unit only covers a small area on either side of it.

With all monitoring instruments, in particular nonintrusive types, as they tend to be very expensive, it is critical to select the correct location for placing the instruments. A monitoring instrument at an unrepresentative location can provide erroneous data that could be widely exaggerating or totally missing any ongoing corrosion.

It should also be noted that one of the primary purposes of corrosion monitoring is to both assess the effectiveness of chemical inhibition and fine tune the chemical dosage rate.

5.2.4 Inspection

Inspection is the cornerstone of any corrosion control program. It is the oldest and, in many ways, the most important and widely practiced form of corrosion control. Regular inspection can prevent unexpected failures. Even the most basic form of inspection, which is simple visual inspection by walking up and down the pipelines, can be more beneficial than it seems.

A popular and reliable form of inspection is to use ultrasonic thickness gages. However, when we are dealing with many kilometers of pipeline and limited resources, it is essential to adopt risk-based inspection (RBI). This form of inspection ensures that the critical lines are inspected when necessary and the inspection budget is used wisely. There are software available, which analyze all the data related to pipelines and determine the inspection interval for each line.

The most effective and trusted method of pipeline inspection is by in-line inspection (ILI), commonly known as intelligent pigging. A “Pig” is launched from one end of the pipeline and collected at the other end. Intelligent pigs are equipped with electronic sensors that “feel” the full circumference of the pipeline while traveling through it and record any deformities such as metal losses. One of the main advantages of this technique is that the exact location of a deformity can be identified, thus saving

time and energy and improving the safety factor. A combination of RBI and ILI provides the best form of pipeline inspection.

For a pipeline to be inspected by ILI, the line has to be "piggable", i.e., it must be fitted with pig launcher and receiver. Even for lines that are not piggable, there are techniques for carrying out ILI in them.

In case of buried lines, where CP and coating have been applied, inspection techniques for verification of the stability and performance of these corrosion control measures are used. For CP, Close Interval Potential Survey (CIPS) is the most common technique while Direct Current Voltage Gradient (DCVG) provides information both on the stability of CP and performance of the coating.

5.2.5 Corrosion assessment

There are two methods of corrosion assessment: Internal Corrosion Direct Assessment (ICDA) and External Corrosion Direct Assessment (ECDA). In these techniques, all the inspection and monitoring data, and any other relevant data for the pipelines, are analyzed and locations of high corrosion risk in the pipelines are identified. Obviously, the success and accuracy of these techniques depend on the quality and quantity of the data provided for analysis. A list of the common methods of corrosion control, monitoring, and inspection is provided in Table 5.1.

Table 5.1 Some of the common methods of corrosion control, monitoring and inspection

	Internal	External
Corrosion Control	Material Selection Chemical Inhibition Coating/lining HDPE liners Cladding Dewatering Pigging	Material Selection Coating Cathodic Protection
Corrosion Monitoring	Weight-Loss Coupons Electrochemical Probes Hydrogen Probes	Tomography Thermography Field Signature Method Ultrasonic Thickness Gauge
Inspection	In-Line Inspection	Visual CIPS DCVG
Corrosion Assessment	Internal Corrosion Direct Assessment	External Corrosion Direct Assessment

5.3 Tanks and vessels

5.3.1 Storage and other tanks

This group includes oil storage tanks, Flow Suction Tanks (FST), oil skimmer tanks and others not subjected to high internal pressures.

The external corrosion protection of these tanks can be divided into two sections: Bottom of the tank and the rest of the tank. The most critical section is the bottom of the tank which is vulnerable to corrosion by ground water. There are basically two common methods used for protection of this section. The more effective way is to apply impressed current cathodic protection (ICCP). The other method is to isolate the bottom from ground by a layer of nonmetallic insulation or coating. For the rest of the tank external, coating is sufficient.

For internal protection of the tanks, coating—sometimes in conjunction with sacrificial anodes—is used. In the case of oil skimmer tanks, where sediments can pile up quickly at the tank base, regular cleaning is necessary to avoid MIC.

5.3.2 Pressure vessels

Oil, gas, and multiphase separators often require an extra level of protection. These separators often include corrosive gases such as CO_2 and H_2S. The high internal pressure in these vessels translates into high partial pressures of these gases. Therefore, very special high quality coatings, capable of withstanding high temperatures and depressurizations, are required. For gas separators it is often recommended to use full CRA cladding.

For external protection of these vessels, the same principles used for tanks can be used.

5.3.3 Minor but important items

A seemingly minor, but quite important items, are nuts and bolts used for fastening structural elements. Often when walking in plants these stand out due to the rust gathered on them. Not only this makes for poor aesthetics but, more importantly, it can cause difficulties in loosening and fastening these nuts and bolts and lead to their regular replacement. A particular common mistake is to use carbon steel nuts and bolts on stainless steel features or use uncoated nuts and bolts on coated structures. A simple way to avoid these problems is to use fluoropolymer coated nuts and bolts which have proven lasting qualities.

5.4 Downhole corrosion

Corrosion of downhole casings and tubings is potentially a bigger problem than topside corrosion. It is more difficult to monitor and inspect and the costs of any failure can dwarf that of say, pipeline corrosion. Any unplanned work over due to corrosion will have a very significant loss, not to mention its impact on production. Although there have been a number of electrochemical systems designed for monitoring of downhole corrosion, as of yet there are no proven systems which can be used in any type of well, especially oil and gas wells. The only tried and tested method for

Figure 5.4 An almost totally corroded tubing pulled out of a well.

downhole monitoring and inspection remains the caliper surveys in which the caliper is lowered into the well where it "feels" the internal surfaces of casing and tubing around it and transmit data into a data logger. Any damage or metal loss due to corrosion is recorded so that rehabilitation actions can be performed.

5.4.1 Downhole material selection

Material selection for downhole casing and tubing is more critical and important than topside pipelines as the consequences of even small corrosion pits, if they result in penetration and "communication" between the internal and external environments, can have very significant financial impact.

There are some wells for which material selection is relatively straightforward, such as L-80 carbon steel for oil wells with low water cuts and very low levels of CO_2 or 13% Chrome stainless steel for sweet wells with high levels of CO_2 and long design life. However, some others, for example, oil and gas wells with varying and changing levels of water cut, CO_2 and H_2S, require very careful material selection. In such cases, the concept of life cycle cost (LCC) analysis is very important and must be adhered to. Lack of proper material selection can lead to early and wholesale failure. Fig. 5.4 shows an example of a completely corroded tubing retrieved from a well.

The more data and information the corrosion engineer has at his/her disposal, the more accurate the material selection can become, resulting in fit-for-purpose materials. For downhole material selection, most of this data is supplied by reservoir and petroleum engineers. The corrosion engineer should provide the reservoir and petroleum engineers with templated tables, such as Tables 5.2 and 5.3, to be filled as much as possible.

5.4.2 Downhole corrosion control

The majority of the corrosion control options that can be used topside can also be used downhole. Chemical inhibition, applied as continuous, batch or squeeze treatment, is a

Table 5.2 Template table for environmental data for materials selection

Environment condition	Value
Well type (oil producer/water injector/etc.)	
Depth (ft)	
Tubing size (in)	
Oil production (bopd)	
Gas production (mmscfd)	
Gas injection rate (mmscf)	
Bottom hole pressure (psi)	
Water hole pressure static (psi)	
Water hole pressure flow (psi)	
Bubble pt (psi)	
Water hole temperature (°F)	
Bottom hole temperature (°F)	
Gas−oil ratio (scft/bbl)	
H_2S (ppm)	
CO_2 (mol%)	
Cl (ppm)	
HCO_3 (ppm)	
Water cut (vol%)	
Design life (years)	
Inhibition available?	

widely-used method for downhole corrosion. CP has been used to protect the casings. Coatings have also been used for the top and surface casings. The use of nonmetallics, such as GRE, has also advanced, especially in water disposal or water injection wells. The usage is either in the form of solid nonmetallic components or as coating or lining.

For proper material selection, the following steps should be taken, in this order:

1. Study of the history of materials used in similar environments, starting with wells belonging to the company for which the material, is being selected. Of special importance are any corrosion logs carried out?
2. Consult the company's material selection and corrosion control standards.
3. Consult the relevant international standards.

Table 5.3 Template table for water data for materials selection

Properties of flashed water			**Value**		
Relative density at 60/60°F					
Resistivity (ohm-m)					
Kinematic viscosity (cST)					
pH					
Chemical Composition					
Total dissolved solids (mg/L)					
Total suspended solids (mg/L)					
	mg/L	mg/L		mg/L	mg/L
Sodium			Chloride		
Calcium			Bicarbonate		
Magnesium			Sulfate		
Iron (total)			Carbonate		
Barium			Hydroxide		
Acetate (Dionex)			Formate (Dionex)		
Propionate (Dionex)			Butyrate (Dinex)		

4. Carry out desk top corrosion rate prediction and material evaluation analysis using one or more of the available software for this purpose.
5. Carry out LCC to select the most techno-economically suitable material.

5.5 Conclusions

The most common forms of corrosion that occur in the onshore oil and gas industry are well understood by the corrosion engineers. However, corrosion-related problems occur from time to time because of a variety of reasons. These include

- Negligence in design, for example, oversizing, or undersizing pipelines, not removing dead legs, and wrong material selection. Some of these may be due to not involving the corrosion specialists from the early stages of design.
- Changes in operating conditions through the design life of structures.
- Not studying the history of materials performance in the company, or other companies with similar operating conditions and learning lessons from the past.

By keeping things simple, learning lessons, good communication, continuous updating of company's standards, and following up to ensure that the recommended actions have been carried out, it is possible to greatly limit corrosion-induced damages and make major cost savings.

5.6 Corrosion challenges in onshore sectors

Notwithstanding the points raised in the introduction to this chapter, there are still many challenges facing the onshore oil and gas industry. These include

1. Corrosion under insulation (CUI) (inspection and monitoring, inhibition, modeling, and predicting the location of the CUI, high temperature coatings)
2. Under deposit corrosion (inhibition, modeling, and prediction)
3. Top of line corrosion (inhibition, modeling, and prediction)
4. Improved standard test methods for qualification and selection of inhibitors
5. Reliable nonintrusive corrosion monitoring probes and intrusive probes for sour systems, with the possible use of fiber optics
6. Downhole corrosion monitoring
7. Coatings for high temperature pipelines
8. Accurate and affordable ILI techniques for flowlines not equipped with pigging facilities
9. Accurate prediction of corrosion in multiphase environments (sweet and sour)
10. Faster and reliable techniques for leak detection

Reference

[1] S. Nesic, S. Wang, H. Fang, W. Sun, J.K.-L. Lee, A new updated model of CO_2/H_2S corrosion in multiphase flow, in: NACE International CORROSION/2008. Paper 08535, 2008.

PART III

Corrosion mechanisms: current knowledge, gaps and future research

Sour corrosion

6

Jon Kvarekvål[1] *and Jeremy Moloney*[2]
[1]Institute for Energy Technology (IFE), Kjeller, Norway; [2]Nalco Champion, an Ecolab Company, Sugar Land, TX, United States

6.1 Introduction

Sour corrosion is a customary term for aqueous corrosion in the presence of hydrogen sulfide (H_2S) at a level high enough to significantly affect the corrosion behavior and corrosion products compared with otherwise the same conditions without H_2S. The term was first used to describe corrosion in Louisiana wells in the 1940s. It is typically used for general and localized corrosion of carbon and low-alloy steels, but some parts of the industry also include hydrogen embrittlement and sulfide stress cracking in the definition.

The number of sour oil and gas fields located in regions with low production cost per barrel is on the rise. Sour oil and gas production and transport always imply a risk of material damage and shutdowns due to CO_2/H_2S corrosion and especially localized corrosion attacks. Development of these fields necessitates development of better, and more economical, corrosion control methods to prevent environmental hazards and production upsets caused by leaks and ruptures. In this chapter the frontiers and gaps of current research and knowledge on sour corrosion are addressed.

Sour corrosion may take place on all upstream and downstream steel components exposed to H_2S, such as well tubing, flowlines, transport pipelines, and processing equipment. Fig. 6.1 illustrates a cross section of an example of a multiphase wet gas pipeline with the different liquid and gaseous phases indicated. All water-wet internal surfaces are prone to various types of sour corrosion attack, either by corrosive produced water/brine in the bottom of the line or condensed water in the upper sector of the line (top-of-line corrosion, TLC). Under-deposit corrosion may cause localized attacks on areas where solid particle settling and deposit build-up take place. Deposits containing iron sulfide (FeS) particles may be exceptionally corrosive because of the electrical conductivity of FeS.

Field experience shows that iron sulfide films formed on carbon steel during sour oil and gas production and transmission can be very protective for long periods of time, but there are also many reports of corrosion failures. The magnitude of the corrosion attacks can often be related to the nature of the corrosion films.

In long sour gas pipelines, for which carbon steel is the only economically viable material candidate, corrosion inhibitors are widely used to mitigate general and localized corrosion. The inhibitor dose rates required for sour systems are often 10−100 times higher than typical dose rates for sweet systems (CO_2 only), possibly due to the increased cathodic reactant present and/or because of inhibitor consumption by

Trends in Oil and Gas Corrosion Research and Technologies. http://dx.doi.org/10.1016/B978-0-08-101105-8.00006-1

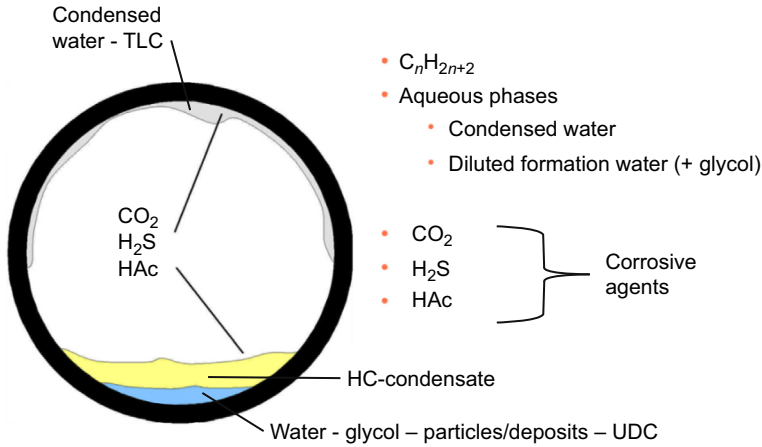

Figure 6.1 Schematic illustration of a cross section of a typical multiphase wet gas pipeline. *TLC*, top-of-line corrosion; *UDC*, under-deposit corrosion.

adsorption on iron sulfide particles. This means that inhibitor treatment in sour conditions has a greater impact on both environment and economy compared with sweet conditions. The pH stabilization technique has been considered as an alternative corrosion control method in gas/condensate pipelines.

The mechanisms behind localized CO_2/H_2S corrosion are not fully explained, with unanswered questions regarding the effect of FeS corrosion film breakdown, contribution of galvanic effects from electronically conductive FeS films to pit growth, and the effect of steel microstructure on localized corrosion. This chapter provides a discussion on the mechanisms of different types of localized H_2S/CO_2 corrosion attacks, based on observations from laboratory experiments and the field.

6.2 Sour corrosion rates and electrochemistry

6.2.1 Electrochemical reactions

Sour corrosion takes place through a series of complex chemical and electrochemical reaction mechanisms, as described in many of the publications referred to in this chapter. The predominant simplified net reaction, however, is the oxidation of iron (0) to iron (II) and reduction of protons to elemental hydrogen. From an adsorbed state on the cathodic surface (steel or iron sulfide), the hydrogen may either form H_2 gas or be absorbed in the metal. The latter may cause hydrogen embrittlement and increase the susceptibility of cracking (HIC, SSC). The fraction of hydrogen absorbed in the metal depends on i.a. (inter alia) the microstructure (ferritic/austenitic, defect types and concentration), permeability of the metal and effect of iron sulfide surface layers.

$$Fe + H_2S \rightarrow FeS + 2H_{ad}$$

Measurements and calculations of sour corrosion rates on bare steel surfaces are limited by the presence of iron sulfide layers growth and would, under most circumstances, have little relevance for sour corrosion of oil and gas field installations. The effect of iron sulfide layers on the electrochemical behavior has been reported by Shoesmith [1] amongst others, who found both anodic and cathodic Tafel slopes on FeS-covered iron to be higher than 240 mV at pH 4, which was ascribed to heavy polarization of both anodic and cathodic reactions because of a protective mackinawite ($Fe_{1+x}S$) layer on the iron surface.

6.2.1.1 Anodic reactions—iron dissolution

The anodic dissolution of iron in H_2S-containing solution has been studied by several workers [1–4]. All of them have identified bisulfide ions (HS^-) as a complexing agent in the initial stage of the dissolution mechanism, followed by two electron transfer steps—one of which is rate determining for the overall anodic reaction—to produce an $FeSH^+$ complex. Further reactions with the $FeSH^+$ complex lead to formation of iron sulfide corrosion films (typically $Fe_{1+x}S$, mackinawite) or aqueous Fe^{2+} ions. Anodic Tafel gradients in the range of 40–80 mV/decade were reported for bare steel surfaces in acidic H_2S solutions (pH > 3), whereas much steeper gradients were observed in the presence of iron sulfide layers.

6.2.1.2 Cathodic reactions—hydrogen reduction

Hydrogen evolution is the prevailing cathodic charge transfer reaction during anodic dissolution of iron in CO_2/H_2S solutions. In addition to H^+ ions, other species such as H_2CO_3, H_2S, HCO_3^-, and HS^- are also electron acceptor candidates. Dissolved H_2S may contribute to the cathodic reaction rate through mechanisms analogous to the direct reduction of carbonic acid. Experimental evidence and mechanisms of direct H_2S reduction in acidic solutions (pH < 3) were published by Naumann and Carius as early as 1959 [5], well before the theory of direct reduction of carbonic acid, and has later been confirmed by other workers [6,7]. Cathodic Tafel slopes between 110 and 120 mV/decade have been recorded on bare iron and steel surfaces in H_2S solutions with pH less than 5 [4,8,9]; however, steeper slopes may be observed in the presence of protective iron sulfide layers [1]. The cathodic reaction rates have been found to be proportional to the H^+ and H_2S concentrations. On areas with high corrosion rates, mass transport limitations of the cathodic reaction rates may apply.

Cathodic reactions may also take place on the surfaces of iron sulfide layers and deposits in electrical contact with the steel surface. With porous layers and deposits the cathodic area of the iron sulfide may be much larger than the area of the adjacent steel surface, causing a significant galvanic corrosion attack. The electrochemical properties of various iron sulfides have been studied by Tjelta et al. [10].

6.2.2 The effect of FeS layers on the corrosion rate

Dense corrosion product layers act as a barrier for mass transport and can significantly reduce the corrosion rates. The natural corrosion protection offered by such iron sulfide

layers is sometimes so good that it alone is sufficient for operating purposes. On the other hand, porous iron sulfide layers are not only less protective than dense layers but may also increase the corrosion rates if the iron sulfide exhibits significant electrical conductivity and galvanic cells between the steel and the iron sulfide are established.

When the general corrosion rate is controlled by protective corrosion product layers the charge transfer current−potential response may be linear (Ohmic) rather than exponential (Faradaic, Butler−Volmer). The rate-controlling ionic and electronic properties of iron sulfide films were first described by Hausler et al. [11]. It is likely that these properties vary with the stoichiometry and crystallinity of the iron sulfide. Solid-state diffusion through iron sulfide corrosion films may determine the corrosion and film growth rate in accordance with Wagner's oxidation rate law for high-temperature gas phase corrosion. This theory is also applicable for iron sulfide formation [12]. The theory predicts a parabolic relationship for metal loss (m) with formation of protective films as a function of time (t):

$$m^2 \propto t \Rightarrow m \propto t^{0.5}$$

Accordingly, the instantaneous corrosion rate (CR) as a function of time is inversely proportional to the square root of time (t):

$$CR(t) \propto t^{-½}$$

The relationship above has been reported to apply for short-term aqueous H_2S corrosion behavior [13]. In a gravimetric corrosion study, it was found that iron sulfide layers (and corresponding metal loss) exhibited parabolic growth rates for a period after immersion at pH 4−5 in NaCl solutions saturated with H_2S and CO_2/H_2S mixtures at 1 bar total pressure [14]. Fig. 6.2 shows data obtained over a period of 10 days. After a few days of exposure the layers were observed to crack and partially detach from the coupon surfaces, and this was also reflected in the subsequent measurements.

The identity of the diffusing species controlling the corrosion rate may be different for various types of iron sulfides. It is generally agreed that sulfide diffusion is slower than iron ion diffusion, whereas lattice diffusion of H_2S does not occur at room temperature. On the other hand, given that the FeS film is electronically conductive, cathodic reduction of H_2S, as well as H^+ and H_2CO_3, can proceed on the film surface. This means that the corrosion rate is controlled by either Fe^{2+} diffusion or electronic conductivity of FeS films. Hausler et al. [11] suggested that outward diffusion of Fe^{2+} ions was likely to be rate determining for both n-type and p-type iron monosulfides, i.e., FeS_{1-x} and FeS_{1+x}, respectively. It was also concluded that the diffusion model approach was too simplistic for complex cases of H_2S corrosion, because observations showed that the parabolic rate law did not apply for longer exposures, or that the rate constants changed with time. These observations could be related to breakdown of the films or coformation of sulfur-deficient and sulfur-rich iron sulfides in "sandwich" film structures.

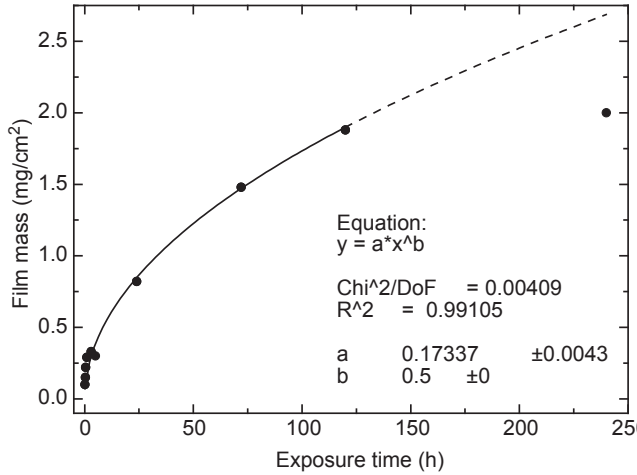

Figure 6.2 Film mass increase as a function of exposure time. Data points are averages of two measurements. The continuous line represents the best fit for a square root function up to 120 h [14].

6.3 Sour corrosion products and surface layers

Corrosion of steel and iron in aqueous H_2S−containing solutions almost always leads to precipitation of iron sulfides, which exist in a variety of subspecies with different crystallinity, lattice structure, stoichiometry, and physical properties. To predict and understand the impact of H_2S on CO_2 corrosion, it is important to anticipate the type of iron sulfides formed at given conditions.

Metal sulfides in general are more covalent than the corresponding oxides. This reduces the formal charge on the metal site which favors metal−metal bonding (S is less electronegative than O). The covalent nature of iron sulfides facilitates nonstoichiometric polymorphs. Sulfides can form layered structures because of the large polarizability of the anions.

Crystal structures, solubility constants, and electronic properties for the various types of iron sulfides found in literature [15−17] are given in Table 6.1. Pyrrhotite has the lowest solubility of the iron sulfides with approximate 1:1 stoichiometry, but it does not appear to be the initial corrosion product on iron in CO_2/H_2S solutions. The reaction rate of mackinawite (and amorphous FeS) formation is rapid, and further transformation into pyrrhotite seems to be a slow process at temperatures less than about 100°C (212°F).

The stability of iron sulfides with respect to pH and electrode potential at 25°C (77°F) and 0.01 bar (0.145 psi) H_2S has been suggested in various Pourbaix diagrams for the Fe−S−H_2O system [18]. The stability region for mackinawite is relatively large and covers the range of pH values and corrosion potentials usually encountered in anoxic CO_2/H_2S solutions.

Table 6.1 Properties of the various iron sulfides

Name	Formula	Lattice structure	Conductor type	Solubility (25°C)
Amorphous FeS	$Fe(HS)_2$, FeS_x	Nanocrystalline		$1.4 \cdot 10^{-17}$, $K_{sp} = a_{Fe^{2+}} a_{S^{2-}}$
Mackinawite	$Fe_{1+x}S$, $x = 0.005-0.025$	Tetragonal	Metal	$2.9 \cdot 10^{-18}$, $K_{sp} = a_{Fe^{2+}} a_{S^{2-}}$
Cubic FeS	FeS	Cubic	*p*-type metal	
Troilite	FeS	Hexagonal	Metal	$6.2 \cdot 10^{-17}$, $K_{sp} = a_{Fe^{2+}} a_{S^{2-}}$
Pyrrhotite	$Fe_{1-x}S$	Hexagonal	*p*-type metal	$2.7 \cdot 10^{-19}$, $K_{sp} = a_{Fe^{2+}} a_{S^{2-}}$
	Fe_7S_8	Monoclinic		
Smythite	Fe_9S_{11}, Fe_7S_8	Hexagonal		
Greigite	Fe_3S_4	Cubic	Half-metal	$3.0 \cdot 10^{-55}$, $K_{sp} = a^3_{Fe^{2+}} a^4_{S^{2-}}$
Marcasite	FeS_2	Orthorhombic	Semiconductor	$5.6 \cdot 10^{-31}$, $K_{sp} = a_{Fe^{2+}} a^2_{S^{2-}}$
Pyrite	FeS_2	Cubic	Semiconductor	$5.0 \cdot 10^{-31}$, $K_{sp} = a_{Fe^{2+}} a^2_{S^{2-}}$

6.3.1 Amorphous iron sulfide

Amorphous FeS films are difficult to characterize with respect to structure and oxidation states, because crystallinity is observed only at a nanoscopic level. Rickard [19] identified amorphous iron sulfide as a short-lived, black precipitate with the formula $Fe(HS)_2$, which acts as a basis compound for formation of other iron sulfides. It has later been claimed that amorphous iron sulfide is actually nanocrystalline mackinawite [20].

6.3.2 Mackinawite (FeS_{1-x})

Mackinawite is a sulfur-deficient iron sulfide with a tetragonal crystal structure and a specific gravity of 4.26 g/cm^3. It is frequently detected as a primary H_2S corrosion product in wet H_2S environments at temperatures up to 140−160°C [1,3,21], at which it decomposes to form other iron sulfides, mainly troilite or pyrrhotite. Mackinawite has metal-type electronic conductivity and depolarizes the hydrogen evolution reaction (HER), making it an excellent substrate for cathodic reduction of protons, carbonic acid, acetic acid, and hydrogen sulfide.

Mackinawite formation on iron in aqueous H_2S solutions is described as a solid-state reaction taking place directly on the iron surface [22]:

$$(1+x)\mathrm{Fe} + \mathrm{H_2S} \rightarrow x\mathrm{Fe_O^{\cdot\cdot}} + (2x)\theta + \mathrm{FeS} + \mathrm{H_2}$$

The resulting sulfide contains iron interstitials ($Fe_O^{\cdot\cdot}$) and excess electrons (θ) in a tetragonal FeS lattice, which may explain its metallic conductor properties. With the possibility of electron transport through the corrosion film, the HER may proceed on the mackinawite/solution interface, whereas the total reaction rate is controlled by diffusion of Fe^{2+} ions through the corrosion film. However, a highly porous film with a large effective area could cause a diffusion-controlled cathodic process. The mackinawite base layer is observed to be thin and tarnishlike.

It was later found that iron sulfides, including mackinawite, are formed from an amorphous iron sulfide intermediate, $Fe(HS)_2$ [19]. Nucleation of mackinawite by polymerization of amorphous iron sulfide was suggested to proceed as follows:

$$n\mathrm{Fe(HS)_2} \rightarrow (\mathrm{FeS})_n \cdot \mathrm{H_2S} + (n-1)\mathrm{H_2S}$$

According to the above, H_2S molecules are included in the produced mackinawite. Through hydrogen bonding, these could possibly act as “binders” between nanocrystals, thus enhancing the thermodynamic stability (or providing a kinetic barrier against transformation into other sulfides) and the mechanical strength of the compound.

Research on mackinawite suggests that mackinawite is a stoichiometric monosulfide, i.e., not containing excess iron, and that the nonstoichiometry previously reported is due to erroneous analysis methods [23]. However, this does not explain the Fe-rich nonstoichiometric iron sulfide layers, observed in EDS analyses [5]. Many of these layers have also been identified as mackinawite by XRD. If mackinawite is, in fact, stoichiometric FeS, the existence of Fe-rich/sulfur-deficient iron sulfides is ruled out.

Electrical conductivity values for mackinawite are not available, but the mineral has been considered to be metallic based on its short FeFe distance (2.60 Å), which is close to that of elemental iron (2.48 Å for α-iron) [24]. Sour corrosion products on steel specimens, determined by XRD to be mainly mackinawite, were recently characterized by infrared absorption. It was concluded that the iron sulfide was electrically conductive ("metallic or semimetallic") and that the band gap had to be less than 0.03 eV [25]. The limited availability of data for mackinawite is probably due to the fact that it is metastable and oxidizes easily if exposed to air. Ref. [16] also claims that mackinawite is a good conductor. It should be mentioned that the layered structure results in conductivity mainly in the in-plane direction, cf. graphite.

6.3.3 Troilite (FeS)

Troilite, also referred to as "stoichiometric FeS," has a hexagonal lattice with few vacancies. In nature, troilite is found only in meteor debris. Because of low concentration of defects in the troilite crystal lattice, troilite is probably less conductive and does not enhance cathodic activity to the same extent than mackinawite. The troilite structure is closely related to the NiAs-structure. Despite the low abundance of troilite in nature [26], it has been reported as a possible product of sour corrosion.

6.3.4 Pyrrhotite ($Fe_{1-x}S$)

The term pyrrhotite was previously used collectively on what is now divided into troilite, monoclinic pyrrhotite, and hexagonal pyrrhotite. Pyrrhotite is a good conductor, whereas troilite has a somewhat higher resistivity. Nevertheless, both pyrrhotite and troilite can be considered as low-mobility metals [27].

Monoclinic pyrrhotite has a NiAs crystal structure, in which each ferrous ion is surrounded by six sulfide ions in an octahedron. Pyrrhotite may form spontaneously during corrosion or with mackinawite as a precursor.

The Fe_7S_8 variation of pyrrhotite is an ordered (two-dimensional) superstructure based on troilite, with alternating filled and deficient metal layers. Octahedral sites are vacant in the deficient layers, and the stacking sequence can be represented as $SFe_{1.0}SFe_{0.75}SFe_{1.0}SFe_{0.75}S$. Also, more complex superstructures such as Fe_9S_{10} and $Fe_{11}S_{12}$ exist. In the work of Smith and Miller [28] pyrrhotite is stated to be a *p*-type semiconductor.

6.3.5 Smythite (Fe_7S_8—Fe_3S_4) and greigite (Fe_3S_4)

Mackinawite, a typical initial sour corrosion product, may react with carbonic acid to form smythite and siderite. Although greigite is not a typical anaerobic CO_2/H_2S corrosion product, it could form through decomposition of smythite at elevated temperatures. Despite its thermodynamic stability, smythite is rarely observed, which is explained by a slow nucleation rate compared with other iron sulfides [29].

Also for greigite, there is limited data on conductivity available in the literature. As for mackinawite, greigite is metastable and prone to oxidation when exposed to air. Greigite has been claimed to be highly conducting [16], half-metallic [30], and semimetallic, but more experimental data are required to determine the electronic structure [31]. Nevertheless, conductivity measurements on synthetic samples indicate a resistivity in the range of 10^{-1}–10^{-3} Ω cm [32].

6.3.6 Pyrite and marcasite (FeS_2)

Pyrite has a cubic structure resembling that of NaCl, in which the S–S bonds of the S_2^{2-} ions are oriented transversely to the crystal lattice axes. The stoichiometric variation of pyrite crystals is reported to be small, and it can be either sulfur or iron deficient. Marcasite has an orthorhombic structure with various degrees of sulfur deficiency.

Pyrite and marcasite have frequently been identified as corrosion products on steel exposed to H_2S, both in laboratories and industrial process installations. FeS_2 formation in aqueous H_2S-containing solutions requires mildly oxidizing conditions, e.g., the presence of sulfur, polysulfides, or small amounts of oxygen. O_2 may react with H_2S to form elemental sulfur (S_8) and polysulfides (S_z^{2-}).

Pyrite is a diamagnetic semiconductor. Here Fe^{2+} is in the low spin so that (in the intrinsic case) all the t_{2g} orbitals are filled, whereas the e_g orbitals are empty. However, the short Fe–Fe distance produces overlap between e_g orbitals so that a band is produced. Dopants, deviations from stoichiometry, or thermal excitation across the 0.9-eV band gap would therefore render pyrite a semiconductor [16].

6.3.7 Types of iron sulfides formed during sour corrosion

It has been reported that the predominant corrosion product on iron with a CO_2 + 13% H_2S gas mixture is mackinawite [21]. Pyrite and troilite were also detected. These experiments were carried out at 24°C (75°F), 1 atm bar (14.5 psi) total pressure and pH values between 3.1 and 11.0. At pH between 6.5 and 8.8 the corrosion films consisted of mackinawite only. These films had poor corrosion protection properties as compared with films containing pyrite and troilite. In the pH range of maximum mackinawite yield bisulfide (HS^-) ions prevail and were thus regarded as unfavorable reactants with respect to protective iron sulfide formation. The best corrosion protection was offered by sulfide films formed at pH 3.2 and 11.0, half of which was mackinawite and the remainder troilite and pyrite or marcasite.

According to Shoesmith [1] the corrosion product from aqueous H_2S corrosion at room temperature consists of three phases; mackinawite, cubic iron sulfide, and troilite. Initially mackinawite is formed, which, by cracking, causes high local corrosion rates and precipitation of cubic iron sulfide and troilite. Thermodynamically, troilite is the most favorable of these compounds. However, because of low nucleation rate at room temperature, only small amounts of troilite are formed. At higher temperatures (>50°C (>122°F)) the nucleation rate increases because of higher corrosion rates

and supersaturation of Fe^{2+} ions. Thus, troilite is the main constituent of corrosion films formed at temperatures of 75°C (167°F) and higher.

Tasseva et al. [33] reported a variation of the sequence above, in which mackinawite is the primary corrosion product on steel in aqueous H_2S environments at temperatures between 25 and 40°C (77 and 104°F). However, in this case the secondary corrosion products consisted of greigite and pyrite, indicating the presence of polysulfide or elemental sulfur species in the aqueous phase.

Rhodes [34] found that the main corrosion product at 1 bar (14.5 psi) H_2S and 90°C (194°F) was pyrrhotite, $FeS_{1.15}$. In his experiments, which were carried out with 1 M NaCl brines, an aqueous $FeCl_2$ layer was formed between the steel surface and the corrosion film. The $FeCl_2$ layer maintained the anodic reaction rate and thus the corrosion rate. Similarly, Milliams and Kroese [35] found that high concentrations of chloride ions prevented the buildup of protective iron sulfide films at 25°C (77°F).

In solutions with pH less than 5, H_2S partial pressures up to 20 bar (290 psi) and temperatures between 80 and 180°C (176°F and 356°F) mackinawite transformed into higher sulfides according to the following sequence [36]: *Mackinawite → cubic FeS → troilite → pyrrhotite → pyrite*. At room temperature and atmospheric H_2S partial pressure, the transformation sequence seems to end with the formation of troilite [1]. Each step of transformation is initiated by dissolution of existing iron sulfides. Subsequently, the modified iron sulfide is precipitated on the metal surface or on top of the present corrosion film. Thus, several modifications of iron sulfide have been observed to coexist.

Smith and coworkers have reviewed and analyzed a large number of publications on the occurrence, stability, and sequence of formation of the various iron sulfides [37–40]. They concluded that mackinawite and pyrrhotite are the prevailing corrosion products under sour conditions, and conceptual phase diagrams were constructed to illustrate the transition between the two polymorphs. Other types of iron sulfides, such as the chloride-intolerant stoichiometric cubic iron sulfide, were found to be less stable. Furthermore, the complex and unpredictable nucleation of troilite, often in coexistence with pyrrhotite, was discussed. It was argued that troilite, for all practical purposes, can be regarded as a low-temperature, stoichiometric form of pyrrhotite. Areas for further studies of the role of iron sulfides in sour corrosion were identified, with emphasis on rupture of protective mackinawite films and transition/stability regions of the different iron sulfides with respect to temperature, H_2S, pH, and time conditions. It was pointed out that the challenge of developing reproducible procedures for generating the desired iron sulfide films is now easier to meet because of new knowledge on thermodynamic stability and experimental/analytical methods.

Ning and coworkers developed a thermodynamic model to predict corrosion products for an $H_2S–H_2O–Fe$ system with focus on the conditions typical for oil and gas production [41–43]. Pourbaix diagrams generated by the model were experimentally validated by XRD analysis of corrosion products. For example, with around 0.1 bar (1.45 psi) H_2S and a few days of exposure, mackinawite and pyrrhotite were detected as corrosion products at 25°C (77°F), whereas mackinawite, pyrrhotite, and pyrite were found at 80°C (176°F).

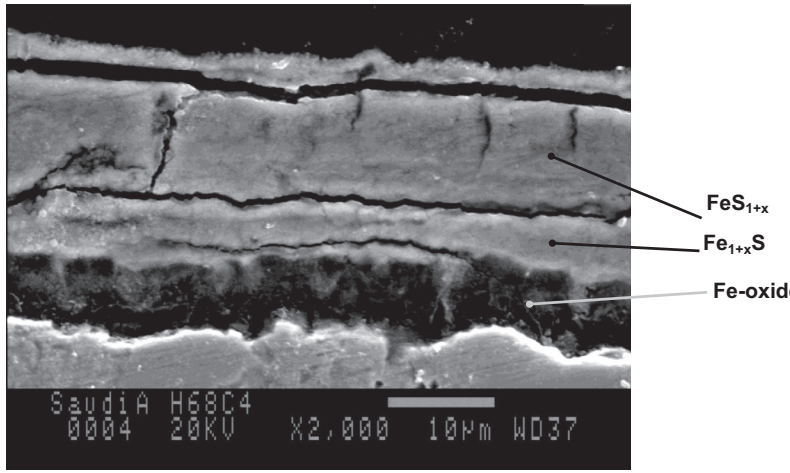

Figure 6.3 SEM picture of multilayer iron sulfide corrosion product film [22].

Coexistence of different iron sulfides in corrosion product layers is sometimes observed as multilayer or "sandwich" structures. An example of such a layered structure is shown in Fig. 6.3, consisting of three layers with different chemical composition [22]. The inner layer (next to the steel surface) consisted mostly of iron and oxygen with some sulfur, probably magnetite or iron carbonate with a little iron sulfide. This inner layer appeared quite porous. A layer of sulfur-deficient FeS, probably mackinawite, could be identified on top of the iron oxide layer. The top layers of the corrosion films consisted of sulfur-rich FeS, probably pyrrhotite with various degrees of nonstoichiometry. There were distinct boundaries between the sulfur-deficient and sulfur-rich iron sulfides, indicating marked structural differences between the two iron sulfide types. As previously described, mackinawite has a tetragonal crystal structure, whereas pyrrhotite crystals can be hexagonal or monoclinic.

6.4 Sour corrosion morphology

Corrosion attacks caused by the various sour corrosion mechanisms have different characteristics when it comes to surface appearance and morphology. Everything from smooth uniformly corroded surfaces to severe pitting attacks has been observed both in the field and laboratory studies. Corrosion morphology definitions frequently used in literature include the following:

- *Uniform/general corrosion*—Corrosion that proceeds at about the same rate over a metal surface.
- *Localized corrosion*—Corrosion at discrete sites, for example, pitting, crevice corrosion, and stress corrosion cracking.
- *Pitting corrosion*—The localized corrosion of a metal surface, confined to a point or a small area, that takes the form of cavities.

- *Crevice corrosion*—Localized corrosion of a metal surface at, or immediately adjacent to, an area that is shielded from full exposure to the environment because of close proximity between the metal and the surface of another material.
- *Galvanic corrosion*—Accelerated corrosion of a metal because of an electrical contact with a more noble metal or a nonmetallic conductor in a corrosive electrolyte.

6.4.1 Pitting attacks

Localized corrosion may be triggered by inherent features of the FeS corrosion layer growth. A number of important papers on H_2S corrosion and iron sulfides have reported unprovoked cracking and/or spalling of iron sulfide layers during the corrosion process. Pound et al. [3] found cracking and spalling of FeS corrosion films in an electrochemical study under typical baseline conditions (0.05 mol/L H_2S, pH 5.8, low chloride). Wikjord et al. [36] and Shoesmith et al. [1] published key papers on formation of different iron sulfides under basic sour conditions. They do not report localized corrosion explicitly although the discussions and conclusions suggest that it may have occurred ("local high iron dissolution rates" and similar phrases). Tewari et al. [44] published an important paper on iron sulfide film growth rate, kinetics, and mechanisms under baseline conditions (1 atm H_2S, different temps). Early cracking of mackinawite layers was reported to take place after only 6–8 h exposure.

Leaks and ruptures caused by internal sour corrosion in tubing and pipelines are often caused by large, wide pits and pit clusters. Some cases of leaks in gas well tubing caused by wide pits have been reported by Choi et al. [45]. The average local corrosion rates were up to 10 mm/year in the middle of the pits. The pits were surrounded by uniformly corroded areas that apparently had been well protected by condensed hydrocarbons or corrosion product films. Isomorphic pitting attacks have been observed in sour corrosion experiments with small diameter pipes (15 mm) tested in flow loops (Fig. 6.4) [46]. Although the environmental parameters (e.g., temperature, pH and CO_2/H_2S partial pressures) and history are different, the similarities between the field and lab pits indicate the presence of a common pitting mechanism [46].

Groups of smaller pits can merge into larger and wider attacks as they grow [47]. Fig. 6.5 shows two cases of pit clusters formed under different sour conditions. Photo 6.5a shows an attack on an X65 steel coupon exposed in a corrosion inhibitor test. The pit cluster was the only localized attack formed in the test, and other X65 coupons exposed simultaneously in the same test were well inhibited. All coupon surfaces were inspected for impurities before exposure, and examination of the microstructure did not reveal anything that could explain the gathering of pits on this particular spot. It can so far only be ascribed to the random nature of localized corrosion. The photo in Fig. 6.5(b) shows a pit cluster formed in a long-term sour pH stabilization experiment. In addition to the large cluster the coupon was covered with numerous smaller pits and clusters.

6.4.2 Edge and crevice attacks

Edge and crevice corrosion are often observed in corrosion tests as an artifact of the test geometry, but this does not mean that the results are irrelevant to the industry.

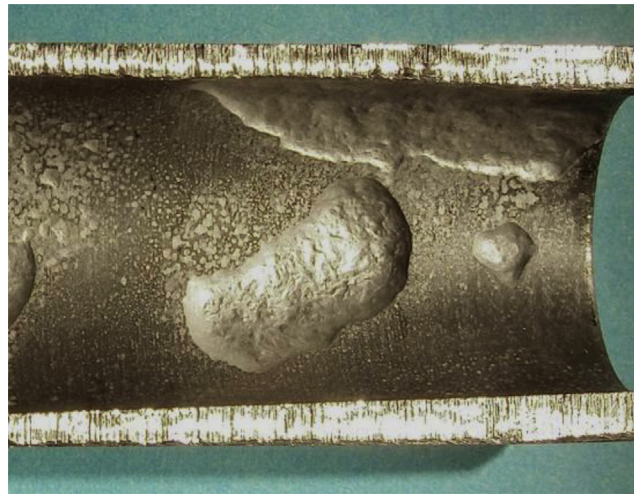

Figure 6.4 Wide pits formed in a sour pH stabilization experiment with 0.5 bar H_2S, 5 bar CO_2, 5000 ppm Cl^-, pH ~7, 60°C, and 1 m/s flow rate [46].

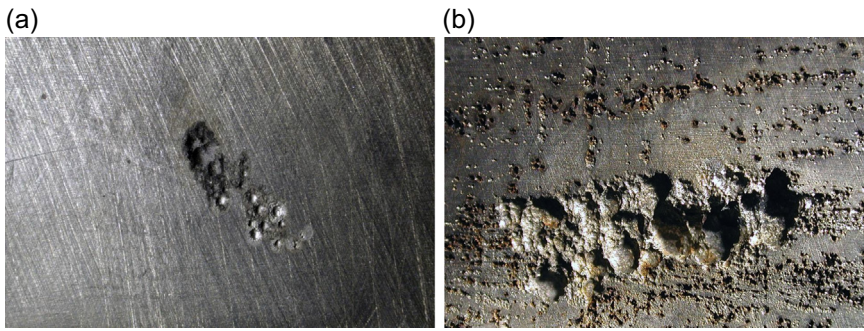

Figure 6.5 Pit clusters on X65 steel coupons exposed in sour corrosion control experiments with (a) corrosion inhibition and (b) pH stabilization [47].

Crevices can also be found in field installations, and the ability of a corrosion control method to mitigate edge corrosion in the lab can be an indicator of its robustness in field service.

Fig. 6.6 shows an X65 steel coupon that developed severe edge corrosion in a sour pH stabilization experiment with 25 days duration [47]. The middle of the coupon had suffered no localized attacks and very little uniform corrosion. Almost all of the weight loss was related to the edge corrosion. This type of edge attacks were explained as an effect of the experimental setup and are hardly representative for conditions in a smooth pipeline. The main reason seems to be a galvanic effect caused by highly saline test solutions and electronically conductive iron sulfides precipitated on the specimen holders, possibly enhanced by flow disturbances caused by asymmetric test geometry.

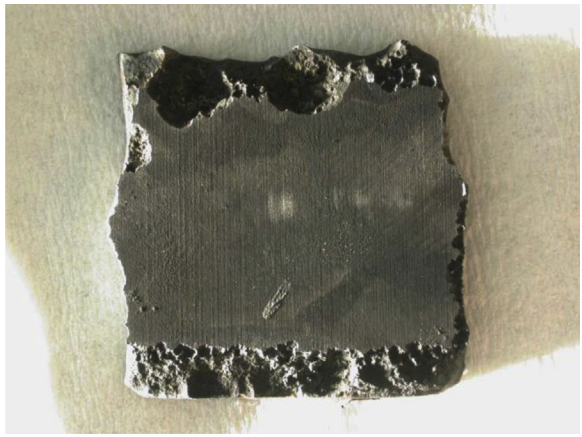

Figure 6.6 Severe edge corrosion on an X65 steel coupon (dimensions 25 mm× 25 mm× 3 mm) exposed in a sour pH stabilization experiment [47].

6.5 Environmental factors affecting sour corrosion

Sour corrosion rates and morphology are dependent on typical operating conditions such as temperature, H_2S and CO_2 partial pressures, pH, concentrations of dissolved salts, flow velocity and regime, and chemical treatment. A brief description of various effects as reported in literature is given in this section.

6.5.1 Effect of temperature

Variations in temperature affects all the physiochemical processes of corrosion, such as chemical and charge transfer reaction rates, solubilities, and surface layer formation. Thus, the overall temperature effect is difficult to predict. Examples of temperature trends for highly sour conditions are given in Fig. 6.7, where average weight loss corrosion rates are plotted against temperature [48]. Results obtained with synthetic formation water, with a temperature range of 10−120°C (50−248°F), and condensed water conditions with temperatures 25−120°C (77−248°F) are shown. The lowest corrosion rates are observed at 90−100°C (194−212°F), indicating that the most protective FeS layers were formed at these temperatures.

6.5.2 Effect of H_2S partial pressure

The partial pressure and corresponding aqueous concentration of H_2S affect the activities of oxidants (H^+ and molecular H_2S) and precipitating anions (sulfide/bisulfide). Thus, a change in the H_2S partial pressure has opposing effects with respect to corrosivity.

An experimental study of sour downhole conditions [22] was run with high temperature of 120°C (248°F) and wall shear stress (135 Pa, 10 m/s) at H_2S levels from 1.4 to

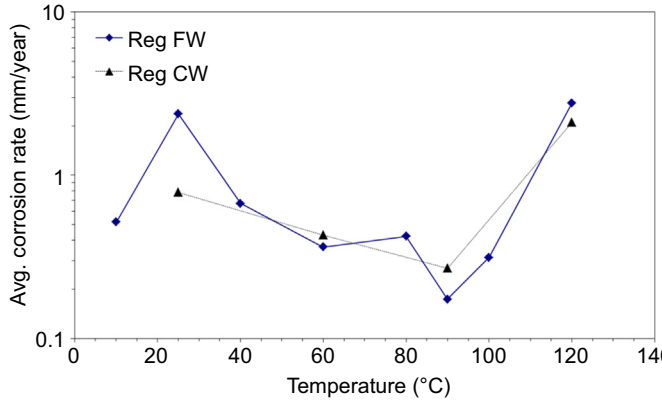

Figure 6.7 Average corrosion rates plotted against temperature. 10 bar H_2S, 10 bar CO_2. *FW*, formation water (100 g/L NaCl, 150 ppm bicarbonate); *CW*, Condensed water (0.1 g/L NaCl) [48].

4.2 bar (20−61 psi). Some shallow pitting was found at the lowest H_2S/CO_2 ratio of 0.2 (1.4 bar/20 psi H_2S, 6.9 bar/100 psi CO_2), whereas no localized corrosion was observed at the higher H_2S partial pressures. In a flow loop study of sour corrosion under flowline conditions [49], pitting with depths up to 100 μm after 3 weeks exposure was observed with 10 bar (145 psi) H_2S, whereas in a corresponding test with 30 bar (435 psi) H_2S the corrosion attack left a surface with high surface roughness without discrete/isolated pits.

Fig. 6.8 shows H_2S partial pressure trends in the range 1−17 bar (14.5−248 psi) for autoclave experiments performed at 25°C (77°F) with 100 g/L NaCl and 150 ppm

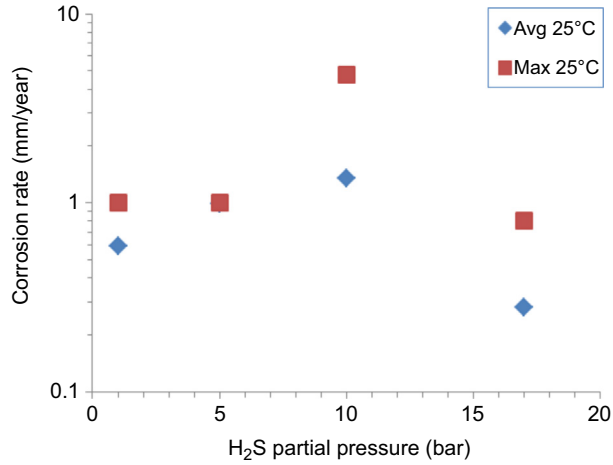

Figure 6.8 Average weight loss maximum pitting corrosion rates versus H_2S. 100 g/L NaCl, 150 ppm HCO_3^- [48].

bicarbonate [48]. The CO_2 partial pressure was also varied, which adds some uncertainty. The exposure time for these experiments was 2−3 weeks. At 25°C (77°F) and high-salinity conditions, both average and maximum pitting rates reached maximum values, 1.35 and 4.8 mm/year, respectively, with 10 bar (141 psi) H_2S. Interestingly, the lowest average and pitting rates were measured with 17 bar (248 psi) H_2S.

6.5.3 Flow velocity/wall shear stress

Flow and convective forces affects the conditions on a corroding surface in several ways, e.g., through removal of (cracked) surface layers and influence on mass transport limitations. Even stagnant and low flow velocities may increase the corrosivity, by facilitating deposition of solids and accumulation of water. In a field corrosion survey by Bonis [50,51], it was concluded that low flow or stagnant conditions were characteristic of the most corrosive cases.

Results from high-temperature sour corrosion tests in autoclaves with rotating coupons (3 m/s tangential velocity) were published by Dougherty [52] in 1988. In a 20% NaCl solution saturated with a 10% H_2S, 4% CO_2, and 86% methane gas mixture at 310 bar (4500 psi), no localized corrosion and corrosion rates less than 1 mm/year were seen at temperatures of 150°C (302°F) and below. At 204°C (400°F), however, localized corrosion (erosion−corrosion) took place at a rate of almost 10 mm/year. On nonrotating coupons the corrosion rate was around 3 mm/year at this temperature, and no localized corrosion occurred. In another sour corrosion study with rotating coupons by Papavinasam et al. [53], the probability of pit initiation was reported to increase with increasing flow rate, temperature, and chloride concentration, whereas increases in CO_2 and H_2S partial pressures and alkalinity decreased pitting susceptibility.

6.5.4 Dissolved salts/salinity

High salinity/chloride levels are necessary for severe sulfur corrosion and other types of localized attacks (e.g., galvanic corrosion) to occur. Li et al. [54] reported pitting corrosion in solutions with 5 wt% NaCl and higher (15 and 20 wt%). The test conditions were 3.5 bar (51 psi) CO_2, 3.5 bar (51 psi) H_2S, and 60°C (140°F). Attack depths up to 180 μm were detected after 2 weeks exposure (20 wt% NaCl). No localized corrosion was found in experiments with 0.5−1 wt% NaCl under otherwise similar conditions, but the weight loss corrosion rates were higher than with 5−20 wt% NaCl.

6.5.5 Alkalinity/pH

Increasing the alkalinity and correspondingly the pH of a sour aqueous environment decreases the concentration of oxidants (H^+) and increases the concentration of precipitating anions (sulfide/bisulfide). These effects typically decrease the corrosion rate, but experiments have shown that increased pH may also cause localized corrosion. Research on the effect of H_2S on pH stabilization (addition of alkaline chemicals to

mitigate corrosion) has been published in a number of NACE papers [55–58]. In these studies, increased risk of localized corrosion due to glycol and added alkaline chemicals was observed at H_2S levels higher than 0.1 bar (1.45 psi). Large, severe local attacks were experienced in strongly buffered glycol solutions (pH 7), especially in loop tests with disturbed flow patterns (flow obstacles). It was concluded that pH stabilization of sour glycol systems could, in fact, be worse than with no anticorrosion treatment at all. The presence of glycol without added alkalinity (pH ~5) still produced pitting attacks, but these were less severe than at higher pH. Likewise, pitting was also observed in strongly buffered sour solutions without glycol, making it clear that glycol and alkalinity can act as pitting triggers on their own. No localized corrosion took place in corresponding baseline tests without glycol or pH buffering.

6.5.6 Organic acids

The presence of organic carboxylic acids (e.g., formic, acetic and propionic acid) contributes to the total level of oxidants in the system. In addition, organic acids may trigger pitting mechanisms that are not yet explained.

Flow loop results reported by Singer et al. [59,60] showed that a combination of H_2S (0.004–0.13 bar) and acetic acid (1000 ppm in the aqueous phase) gave significantly higher corrosion rates than H_2S alone and minor pitting attacks. They also observed cracking of the corrosion film at the higher H_2S partial pressures, and internal stress in the films was suggested as an explanation. Sun et al. [61] also found that organic acids increased the pitting rates in tests at 50°C with 1–3 bar H_2S and 2.5–4.5 bar CO_2. However, all recorded pitting rates in this study were below 1 mm/year and decreased with increasing test duration.

In SSC tests of X70 and X80 steels with 10%–100% H_2S at ambient pressure [62], the presence of 0.5% acetic acid was found to cause pitting corrosion, making the SSC results difficult to interpret. For each pit, it had to be determined whether the pit had terminal crack features (fail) or not (pass).

6.5.7 Gas hydrate inhibitors

Alcohols such as monoethylene glycol (MEG) and methanol are frequently used as thermodynamic gas hydrate inhibitors in subsea gas transport pipelines. Such hydrate inhibitors are added in large concentrations, making them a part of the solvent system. The effect on sour corrosion is complex and not fully explained. Glycols, for example, have been found not only to decrease general (weight loss) corrosion rates but also increase the risk of localized corrosion [62].

It has been shown that extensive pitting took place in experiments with ~1 bar H_2S, glycol (50% MEG), and low/moderate alkalinity (pH 5.5) [56]. Different carbon steels were tested, and comparison revealed that the pitting morphology and frequency depended on steel microstructure. After these tests most of the work was focused on lower H_2S levels (20 mbar), which gave moderate/minor pitting in buffered glycolic solutions (pH <6.5). Breakdown of protective iron sulfide corrosion product layers (blistering/delamination/cracking) was observed on several test coupons but could

not be directly tied to pit formation. On the other hand, it was demonstrated that pit initiation/growth was enhanced by suspended FeS particles.

The effect of methanol, with different concentrations of oxygen, on sour corrosion was investigated by Park et al. [63]. It was found that pitting occurred with 75% or more MeOH, regardless of oxygen content (both aerobic/anaerobic). Greigite was formed in methanol solutions, which was thought to be looser and less protective than mackinawite and other iron monosulfides formed without methanol.

6.6 Effects of elemental sulfur, polysulfides, and oxygen

Elemental sulfur, combined with other factors, appears to be the most severe type of localized corrosion encountered in oil and gas production. However, its appearance is limited to sulfur-bearing gas wells with little condensate production and sour systems with oxygen ingress.

In 1990 Günter Schmitt published a comprehensive review paper on sulfur chemistry and corrosion [64]. A comprehensive description of the chemistry of the $S-H_2O$ system was given, with several reaction paths relevant to sulfur corrosion. Furthermore, pioneer work on sulfur corrosion was summarized and reviewed, including evaluation and details on different proposed mechanisms. Early studies on basic sulfur corrosion were carried out by Farrer et al. [65], who also patented sulfur as an etchant for iron and steel. However, the first mechanistic study of sulfur corrosion was reported by MacDonald et al., in 1978 [66]. An electrochemical mechanism for oxidation of iron by sulfur was proposed, with the net overall reaction being

$$x\mathrm{Fe} + \mathrm{S}_y \cdot \mathrm{S}^{2-} + 2\mathrm{H}^+ \rightarrow x\mathrm{FeS} + \mathrm{H_2S} + \mathrm{S}_{y-x}$$

Physical contact between the sulfur particles (insulators) and the metal or a conductive film is necessary for charge transfer to take place. The mechanism suggests that the oxidizing species is a sulfur−sulfide complex formed by chemisorption of sulfide ions on the surface of a particle of elemental sulfur, and that lowering the pH increases the corrosion rate. Indications were also found that the iron sulfides formed in the reaction act as autocatalysts, probably acting as cathodes with large surface areas as observed in experiments with FeS deposits. Direct contact between sulfur particles and the metal surface was said to be essential for the reaction to occur. This mechanism is regarded as the most plausible for explaining the very high local penetration rates sometimes observed in sulfur-containing systems.

A second mechanism published by Schaschl et al. [67] suggests that the elemental sulfur contained within dissolved polysulfides act as oxidants. However, contact/noncontact experiments with elemental sulfur have shown that direct contact between solid (or liquid) sulfur and the metal is necessary for significant corrosion, and that the contribution from polysulfide corrosion is negligible as long as the temperature is lower than 120°C (248°F). Elemental sulfur reacts with H_2S to form polysulfides (sulfanes) at temperatures above 120°C (248°F) and H_2S partial pressures higher

than 1 bar (14.5 psi). The reaction is catalyzed by amines, an effect which is utilized in sour gas wells to prevent sulfur deposition. At elevated temperatures (typically 150°C or 302°F) disproportionation of sulfur takes place at a considerable rate in aqueous environments, forming H_2S, polysulfides, and sulfuric or polythionic acids. Sulfur disproportionation also takes place in alkaline media at room temperature; however, the reaction rates are low and insignificant. The most abundant polysulfide species are S_4^{2-} and S_5^{2-}. The polysulfide sulfur chains contain one high-energy bond, which easily reacts with Fe(II) to marcasite, FeS_2.

$$\frac{z-1}{8}S_8 + S^{2-} \rightarrow S_z^{2-}$$

$$Fe^{2+} + S_z^{2-} \rightarrow FeS_2 + S_{z-2}^{2-}$$

At temperatures over 120°C (248°F), polysulfide corrosion may still be insignificant, because molten elemental sulfur may form a separate liquid phase with a high contact area against the metal.

A third mechanism suggests that sulfur corrosion can be attributed to the reaction products formed by disproportionation of elemental sulfur; H_2S and sulfuric acid [68,69]:

$$4S + 4H_2O \rightarrow 3H_2S + H_2SO_4$$

Although it was recognized that this reaction produces enough H_2S to form detectable amounts of iron sulfide (in practice a sulfur-bearing environment already contains substantial amounts of H_2S), the experimental evidence presented was not regarded sufficient to prove that this mechanism is predominant or even significant. For example, there was direct contact between the elemental sulfur and the metal in the experiments, but this fact was not considered in the author's discussion.

The effect of dissolved salts and H_2S on sulfur corrosion was also discussed in Schmitt's paper [64]. A systematic electrochemical study of the effect of chlorides on sulfur corrosion was initiated after rupture of a sour gas line with triethylene glycol-containing water, elemental sulfur, and NaCl [70]. It was found that the dissolved salts providing counter ions allow certain corrosion reactions to proceed at a high rate. Also, the anodic reaction in high-chloride solutions (around 1 M NaCl) involved the formation of iron−chloro complexes, which were found to increase the solubility of corroded iron. The H_2S partial pressure was not found to have a very significant effect even at elevated H_2S partial pressures.

Rhodes [34] reported on corrosion tests carried out in autoclaves at 1 bar (14.5 psi) H_2S in 1 M NaCl solution at a temperature of 90°C (194°F). A barnacle type of localized corrosion (pits under extensive FeS buildups) was observed. A corrosion/pitting mechanism is proposed based on the experiments, in which the presence of an aqueous $FeCl_2$ layer of approximately 5 μm thickness between the metal and iron sulfide layer (up to 7.5 mm thick) enables the anodic reaction on metal to be sustained by cathodically active iron sulfides. The assumed presence of certain polysulfides (H_2S_2, HS_2^-)

in H_2S/NaCl solutions is suggested as a cause for pit initiation and growth. Considering Schmitt's review, significant amount of polysulfides are not formed at this temperature, and unless significant O_2 ingress has occurred, the attacks are caused by normal H_2S corrosion. The exposure time is not given, but considering the thick iron sulfide layers observed these appear to be long-term experiments.

Hausler [71] reported from a sour corrosion study that provided fundamental insight on the rate-determining effect of FeS film formation through parabolic film growth, giving a predictable decrease in corrosion rate with time. It was found that ingress of very small amounts of O_2 (16 ppb in water) linearized mass loss versus time, giving a constant corrosion rate. More than 40 ppb O_2 (1000 ppm in gas) led to localized corrosion/pitting that kept growing and was not counteracted by removing the O_2 source. Some inhibitors were effective against these pits. Also, the corrosion rates were found to increase with flow in 1/6th power, which is not explainable by fluid mass transfer and is probably related to film mass transfer. Spalling of FeS film (without O_2) was observed and explained by volumetric stress (the Piling−Bedworth effect) caused by surface layer growth or transformation of mackinawite to other iron sulfides with different density. The specific gravity is 4.7 and 7.8 g/cm^3 for FeS and Fe, respectively.

Schutt and Rhodes [72] found that H_2S and O_2 synergistically increased corrosion rates in neutral aqueous solutions, possibly a result of oxidation of sulfide to elemental sulfur. Corrosion rates up to 15 mm/year (600 mpy) were measured in solutions with 1 mM H_2S and 8 ppm O_2 and pH 7. The pH was adjusted by additions of ammonia (NH_3).

Gregg et al. [73,74] have published two papers on field experience, laboratory studies, and corrosion inhibition policies in very sour gas pipelines with elemental sulfur. Some of the experimental data were previously published by Dougherty et al. [75]. It was suggested that pitting corrosion problems in the pipelines investigated are caused by one or more of the following parameters: high−chloride-formation water, low H_2S/CO_2 ratios, and methanol and sulfur. The combination of accumulated high-Cl^- water and elemental sulfur in low spots (hilly terrain) is found to be most aggressive. Field corrosion test coupons were mounted in a test well and exposed to uninhibited conditions. General corrosion rates on these coupons were 0.05−0.86 mm/year, whereas pitting corrosion rates were in the range of 2−9 mm/year. The pitting corrosion rates were typically more than 10 times higher than the general corrosion rates. The laboratory experiments were carried out in autoclaves. Addition of elemental sulfur to sour brines was found to increase pitting rates, both in the form of dispersions in brine and deposits on the metal surface. However, deposited sulfur gave much higher pitting rates than dispersed sulfur. The presence of dispersed iron sulfides or polysulfides together with sulfur further enhanced the pitting attacks. With elemental sulfur as the only addition to the sour brine the maximum pitting rate was over 10 mm/year. Addition of polysulfide and sulfur gave pitting rates of more than 15 mm/year, whereas sulfur and iron sulfides gave around 40 mm/year. Polysulfides alone did not cause any pitting at all except just an increase in general corrosion rates compared with sour brines alone. Inhibitor tests with elemental sulfur showed that most inhibitor products did not offer complete protection against pitting. The presence of hydrocarbons improved the inhibitor performance at high temperatures.

A paper by Smith and Craig [76] contains a summary and review of previous work on elemental sulfur corrosion. Two sulfur corrosion mechanisms are discussed; the direct contact mechanism and the polysulfide reduction mechanism. The discussion is in favor of direct contact mechanisms, because severe corrosion is only reported with solid sulfur present. This is supported by Pourbaix diagrams showing instability of polysulfides in favor of solid S at acidic-neutral pH.

Bonis et al. [50] have published an extensive review paper discussing several possible triggers of serious corrosion attacks in the field, such as H_2S and CO_2 levels, chloride level, flow velocity, sulfur, deposition of solids, and inhibitor efficiency. Elemental sulfur was seen as the worst threat of the factors mentioned, especially at high chloride levels, with tubing/pipeline lifetimes (penetration times) as low as 3−12 months. All the field cases with elemental sulfur received the highest/worst corrosion classification ("very high"). On the positive side, sulfur corrosion is thought to be a problem only in "condensate dry" systems, because direct contact between sulfur and metal is required and condensate/oil dissolves and removes the sulfur.

Horner et al. [77] presented results from laboratory experiments carried out in autoclaves at 50°C (122°F) with 3.5 bar (51 psi) H_2S and 3.5 bar (51 psi) CO_2. With insufficient batch inhibitor treatment an "average pitting rate" of 1.4 mm/year was observed after 26 days, increasing to 1.8 mm/year after 62 days. Addition of iron sulfides and sulfur to the system gave increased pitting rates at higher flow (rotating cylinder electrode rotation speed), e.g., at 2000 rpm the pitting rate increased by a factor of 4 (2.2 mm/year to 10 mm/year) compared to sour brine without any particles. This corrosion behavior was attributed to elemental sulfur reacting with the iron sulfide surface layer and possible erosion from free solids (FeS).

The redox properties of electroactive species in alkaline bisulfide solutions related to H_2S scrubbing was discussed in a paper by Miller et al. [78]. It was found, through theory and experimental studies, that the corrosion potential in H_2S-loaded amine solutions attained the redox potential for the sulfur/bisulfide redox couple:

$$S + H_2O + 2e^- \leftrightarrow HS^- + OH^-$$

The standard redox potential for the sulfur/bisulfide redox couple is −478 mV versus NHE. Through electrochemical techniques, it was shown that electrochemical oxidation of bisulfide to elemental sulfur on the steel surface actually took place in this environment. A similar situation may apply for corrosion in sour solutions with high alkalinity, e.g., when pH stabilization is applied. Calculations based on the Nernst equation show that the sulfur/bisulfide redox potential is about $-0.48\ V_{Ag/AgCl}$ in a solution with 1 mol/L bisulfide and pH 7, which is ca 0.1 V higher than typical corrosion potentials in this solution. However, the redox potential calculation is based on thermodynamic data for pure water, and it is likely that this potential will vary with the brine.

In a paper by Fang et al. [79], possible disproportionation of elemental sulfur to H_2S and sulfuric acid was investigated in addition to sulfur corrosion of steel in the absence of H_2S. It was not found that significant disproportionation took place in the temperature region investigated (up to 80°C). On the other hand, it was demonstrated that

sulfur corrosion could take place in the absence of H_2S. Small pits (15 μm) were formed under sulfur deposits after 1−5 days.

In a study on the effect of oxygen on sour corrosion, Song et al. [80,81] demonstrated that not only elemental sulfur is formed when H_2S and O_2 react but also oxysulfur ions of the type $S_xO_y^{2-}$, such as sulfite, thiosulfate, and sulfate. These reaction products in their acid form are all stronger acids than H_2S and were found to increase the corrosion rates and also cause localized corrosion in H_2S solutions that otherwise gave mostly uniform corrosion. The findings are in contrast to the prevailing assumption that elemental sulfur is the only significant reaction product in H_2S systems with oxygen ingress.

6.7 The effect of steel microstructure

Carbon steels are typically heat treated to attain desired properties of hardness, ductility, and strength. The resulting microstructure may also affect the corrosion resistance of the steel, but the corrosion resistance of carbon steel without mitigation (e.g., coatings or inhibition) is so low that the microstructure effect is often disregarded. Sour service-certified steels are designed to minimize sulfide- and hydrogen-related cracking susceptibility and are not significantly more resistant to general corrosion than regular carbon steels. However, the lower sulfur content of HIC-resistant steels may reduce pitting corrosion because pits often initiate around surface-emergent metal sulfide inclusions.

The microstructure of the steel should be considered when analyzing pitting initiation and growth.

Microstructural elements reported to affect localized corrosion behavior are metal sulfide inclusions (Ca, Mg, Mn sulfides), the pearlite structure (preferential iron dissolution on pearlite phase), microalloying metals (e.g., Cu), and weld zones (e.g., preferential attack of the heat affected zone (HAZ)).

Sour corrosion experiments with different steel types exposed simultaneously sometimes produce results affected by microstructure. Fig. 6.9 shows the surface appearance and microstructure of two steel coupons (X65 and 0.5%Cr pipeline steels) exposed to identical conditions in a sour pH stabilization flow loop experiment [56]. The 0.5%Cr steel contained more chromium and less manganese than the X65 steel (see Table 6.2). The exposure time was 27 days. Pitting corrosion occurred on both coupons, but the appearance and morphology of the pits are markedly different. The X65 coupon surface is covered with more than 100 narrow pits, many of which are grouped in pit clusters. About half of the pits are located very close to the edges of the coupon and may be classified as edge attacks and possibly experimental artifacts. The pit frequency was much lower on the 0.5%Cr coupon surface, which contained 16 larger wide pits randomly distributed on the surface. The maximum pit depths were about 200 μm on the X65 coupon and 350 μm on the 0.5%Cr coupon. For both coupons very modest uniform corrosion attacks had taken place on the surface areas surrounding the pits.

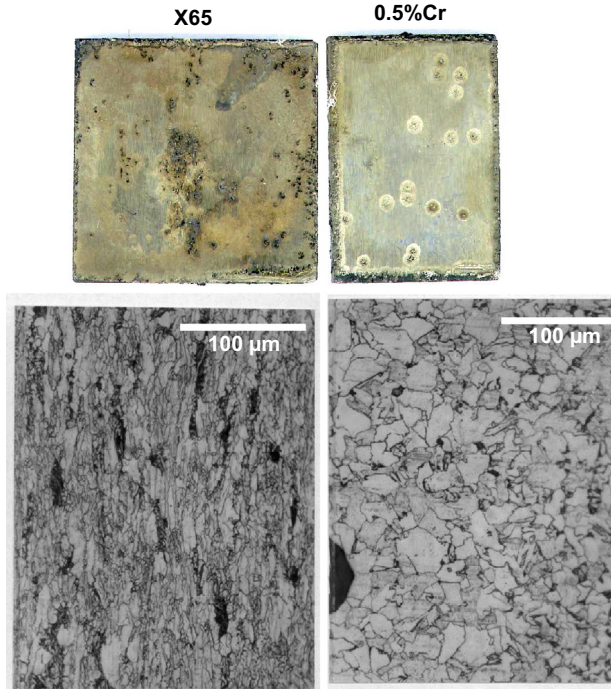

Figure 6.9 Surface appearance and microstructure of an X65 steel coupon (left, 25 mm × 25 mm) and a 0.5Cr steel coupon (right, 25 mm × 15 mm) exposed in a sour corrosion test. Test conditions: 1.3 bar H_2S, 0.6 bar CO_2, pH 5.5−6.5, 1 g/L NaCl, 50% MEG, 3 m/s [56].

Table 6.2 Elemental analysis of the X65 and 0.5%Cr steels

Steel	C	Si	Mn	S	P	Cr	Ni	V	Mo	Cu	Al
X-65	0.057	0.22	1.56	0.002	0.013	0.05	0.04	0.04	0.02	0.01	0.041
Cr0.5	0.072	0.17	0.89	0.002	0.014	0.6	0.02	0.02	0.01	0.01	0.038

The differences in pitting morphology on the steels in Fig. 6.9 may be explained by the differences in microstructure. The X65 steel has a deformed microstructure, probably because of rolling without subsequent recrystallization (cold rolling or rapid quenching), with oblong grains and large pearlite eyes. The 0.5%Cr steel, on the other hand, has a ferritic-Widmanstätten structure with larger grains, where the ferrite phase clearly predominates. The grains in the 0.5%Cr steel are more uniform and less deformed than in the X65 steel. The ferrite grain size in the 0.5%Cr steel varies from around 5 µm to 20−30 µm, whereas most of the X65 grains are less than

5 μm wide. The large pearlitic areas and small deformed grains may explain the higher number of pits formed on the X65 coupon, as compared to the 0.5%Cr coupon.

In a study by Hausler et al. [82] related to corrosivity in the Arun field, localized corrosion was found to be very sensitive to microalloying elements, especially Cu. Magnetite formation catalyzed by small amounts of Cu led to protection of L80 type steel above 150°C (302°F) in CO_2/H_2S-producing tubing (slightly sour), but substantial localized corrosion (3−30 mm/year) was seen below this temperature.

Smith and Miller [28] have reviewed several sources suggesting that metal sulfide inclusions, especially manganese sulfide, in the steel microstructure act as pit initiators. Wranglén [83] pointed out that the sulfur solubility in steel is low, which means that most of the sulfur is likely to be present as sulfide inclusions. Upon solidification of a steel melt mixed (Fe, Mn)S inclusions form, but slow cooling and heat treatment changes these into pure MnS. Rapid cooling, however, leaves some FeS, which is regarded as worse with respect to localized corrosion. Zav'yalov [84] reported results from a study (non-sour) of the effect of different inclusions in Russian steels, in which (Ca, Mg, Mn)S was found to have the most detrimental effect. The inclusion induced localized corrosion and increased weight loss by a factor of 2 to 2.5 times. Mechanisms for pit initiation at MnS inclusions were proposed by Wranglén and also by Baker et al. [85].

Sephton et al. [86] reported that a redistribution of "active sulfur" (e.g., MnS inclusions) in the steel took place in the fusion line area of carbon steel weldments, and that the highest concentrations of active sulfides corresponded with areas of increased corrosion attack.

Huang et al. [87] suggested that localized corrosion initiation in sour solutions could take place through preferential corrosion and breakdown of pearlite regions. Tang et al. [88] found that the corrosion rate of SAE-1020 carbon steel at 90°C (194°F) increased with increasing H_2S concentrations from 60 to 400 mg/L, because of a strong accelerating effect on the cathodic hydrogen evolution. Severe localized corrosion was observed, which was attributed to cementite being stripped off from the grain boundary in accordance with Huang's proposed mechanism.

Lucio-Garcia et al. [89] studied the H_2S corrosion resistance of a C−Mn pipeline steel with three different microstructures (martensite, ferrite, and ferrite + bainite) using electrochemical techniques with a 3% wt. NaCl solution at 50°C (122°F). While electrochemical noise measurements indicated that all three steels were susceptible to localized corrosion, it was also found that the steel with martensitic microstructure had corrosion rates up to two orders of magnitude higher than those for steels with ferritic + bainitic or ferritic microstructures.

Blistering of steel and iron in H_2S solutions was reported by several early papers [21,90−92]. This type of damage was caused by hydrogen entry and pressure buildup in voids in the metal matrix. Blistering does not appear to be a problem with modern tubing and pipeline steels, but one case of cracking of an X46 crude oil pipeline was reported by Azevedo [93]. The cracking was found to be caused by formation and linking of H_2 blisters rather than hydrogen embrittlement of the steel. Zhang et al. [94] observed blistering and HIC on X60 steel at high H_2S partial pressures (10−20 bar), and also localized corrosion at 20 bar H_2S. X52 steel behaved similarly,

but no blistering/HIC was observed for this steel grade. Notably, the weight loss corrosion rates increased by a factor of 4, from around 0.5 to 2 mm/year, when the H_2S partial pressure was increased from 15 bar (218 psi) to 20 bar (290 psi). The marked increase was probably caused by the onset of localized corrosion.

6.8 Summary of localized corrosion triggers

From the literature and as can be seen in this chapter, numerous parameters have been studied, both in the laboratory and in the field, and found to play a role in initiating or triggering localized corrosion in sour environments. In an attempt to pull together and summarize these in one place, many of these localized corrosion triggers are detailed in Table 6.3 along with evidence given from the references in this chapter and their proposed possible mechanisms. In some cases more than one mechanism has been suggested for a specific trigger in Table 6.3 where multiple processes have been proposed in the literature for that specific parameter. It is understood that this is not an exhaustive list in which other initiators may need to be added and the postulated mechanisms verified, refined, or disproved, especially as further research is conducted in this area. In order to collate these various factors, the triggers have been classified into the following categories:

- Direct chemical triggers (DCTs): They include chemicals in the environment that, through direct interaction on or with the metal surface, result in increased localized corrosion. Cathodic reactants, carbon dioxide, hydrogen sulfide, oxygen, organic acids, and elemental sulfur are some examples of this group.
- Indirect chemical triggers (ICTs): They comprise species in the fluids that play indirect roles in instigating or enhancing localized corrosion. Some indirect triggers may incorporate salinity, sour corrosion products, polysulfides or oilfield chemical products such as buffering agents, corrosion inhibitors, and thermodynamic hydrate inhibitors such as methanol and glycol.
- Mechanical/physical triggers (M/PTs): They contain factors that cause a mechanical impact or external stress (rather than the intrinsic or internal stresses present within the metal itself), which may include flow-induced localized corrosion, erosion−corrosion, scratching from pigging procedures, or anything that may cause corrosion film/product layer breakdown.
- Metallurgical triggers (MTs): They incorporate potential pitting initiators within the metal and microstructure. Microalloying components, pearlite structure, metal sulfide inclusions, and blistering are exemplars of this category.

Although it is appreciated that there can be concentrated sour attacks initiated by microbial activity producing hydrogen sulfide, microbiological activity involving this form of localized corrosion has been omitted from consideration in this table because this is covered in detail elsewhere in this book [see Chapter 8 for microbiologically induced corrosion (MIC)]. Likewise, it is recognized that there can be significant hydrogen sulfide−induced stress-related localized breakdown or cracking but because the attacks involving sulfide stress cracking are thoroughly covered in Chapter 11, these factors have again been excluded from Table 6.3.

Table 6.3 Localized corrosion triggers

Trigger	Trigger category	Evidence	References	Possible mechanisms
Hydrogen sulfide partial pressure	DCT	Laboratory: pitting at very high hydrogen sulfide levels 20 bar (290 psi).	[22,48,49]	Increased activity and availability of oxidants.
Oxygen ingress/contamination	DCT	Field: attacks/failures due to oxygen ingress in sour gas–gathering systems. Laboratory: caused pitting and prevented further protection from surface layers.	[71,72,80,81]	Oxidant—direct reaction with steel or oxidation of sulfide species to elemental sulfur or $S_xO_y^{2-}$.
Organic acids	DCT	Pitting in TLC and NACE TM0177 tests.	[59–62]	Oxidant (direct reduction of acid).
Elemental sulfur and polysulfides	DCT	Field: pipeline and tubing failures up to 60 mm/year. Laboratory: up to 350 mm/year short term (mixed with sand). Enhanced by i.a. chlorides, iron sulfides, polysulfides.	[50,51,64–70,73–79]	Oxidant—direct reaction with steel through contact mechanism. Disproportionation into H_2SO_4 and H_2S.
Salinity (chlorides)	ICT	High chloride level necessary for severe sulfur corrosion and other types of pitting.	[54]	Iron–chloro complex formation. Dissolved iron chloride layer between metal and iron sulfide layer. Galvanic (increased conductivity).

Table 6.3 Continued

Trigger	Trigger category	Evidence	References	Possible mechanisms
Iron sulfide deposits	ICT	Field: iron sulfide under-deposit corrosion in sour water injection lines. Laboratory: pitting and increased weight loss caused by iron sulfides.	[10,28,37,38,50,51]	Galvanic corrosion with conductive iron sulfides acting as cathodes.
Alkalinity	ICT	Pitting and spalling cracking of iron sulfide layers.	[55–58]	Galvanic (partial passivation). Volumetric ratio stress/film breakdown (almost 100% of corroded iron captured in film, hence high Pilling–Bedworth ratio).
Methanol	ICT	Field: reported as pit initiator. Laboratory: pitting at high methanol concentrations.	[63]	Possible oxygen contamination. Unknown if additional methanol reactions are involved.
Glycol	ICT	Up to 5 mm/year pitting rate. Pitting effect varies with i.a. flow, alkalinity.	[56,62]	Breakdown of iron sulfide films, Galvanic corrosion (partial passivation).
Low/stagnant flow	DCT/ICT	Field: low/no flow characteristic for most corrosive cases in a recent field corrosion survey.	[50,51]	Probably secondary effects, e.g., allowing for deposition of solids and accumulation of water.

Continued

Table 6.3 Continued

Trigger	Trigger category	Evidence	References	Possible mechanisms
High flow velocity/wall shear stress	M/PT	Field: up to 10 mm/year in gas wells. Laboratory: pitting (minor/moderate) at wall shear stress above 0.0005 bar (0.00725 psi). Erosion−corrosion at higher temperatures.	[50−53]	Erosion−corrosion. Increased mass transport. Mechanical removal of (cracked) surface layers.
Volumetric ratio stress	M/PT	Many cases of unprovoked cracking and spalling of iron sulfide films.	[11−14]	Stress build-up due to rapid iron sulfide precipitation and differences in specific gravity between Fe and FeS.
Microalloying components/ metals	MT	Various effects of i.a. Cu on localized and general corrosion.	[56,82]	Cu_2S protective at high temperatures but not at low temperatures.
Pearlite structure	MT	Preferential iron dissolution on pearlite phase. Pit morphology varies with steel microstructure.	[87,88]	Pearlite breakdown mechanism proposed.
Metal sulfide inclusions	MT	Increased localized and weight loss corrosion on steels with (Ca, Mg, Mn)S.	[28,83−85]	Possible galvanic corrosion.
Blistering	MT	Blisters resulting in rupture and cracking of steel.	[21,90−94]	Hydrogen entry and pressure build-up in voids in the metal matrix.

DCT, direct chemical trigger; *ICT*, indirect chemical trigger; *M/PT*, mechanical/physical trigger; *MT*, metallurgical trigger.

6.9 Gaps in current research and areas for future study

Sour corrosion has been a problem for the oil and gas industry for more than half a century, and substantial research has been invested to understand the corrosion mechanisms and improve corrosion control. Still unresolved issues, especially regarding the understanding and control of pitting corrosion, remain. Determination of parameters and conditions controlling the initiation, propagation, and arrest of pitting attacks is therefore a topic of ongoing and future research.

The roles and properties of different iron sulfides formed in the sour corrosion process also need to be further studied. Of particular interest is the stoichiometry and electrical conductivity of mackinawite and possible detrimental breakdown mechanisms of protective iron sulfide layers.

For the industry it is important to not only control localized corrosion but also ensure that uniform corrosion rates are kept within the limits given by the corrosion allowance. Depending on the various operators' corrosion mitigation strategies, further work may be required to determine operating windows/envelopes, indicating conditions where the baseline corrosion rates are acceptable or not.

Modeling and prediction of sour corrosion, especially localized corrosion are important in the design stage of facilities. A number of commercial and in-house models are capable of estimating general sour corrosion rates based on theoretical and empirical effects of protective iron sulfide layers, but, because of lack of knowledge on pitting mechanisms, no reliable models of sour localized corrosion have yet been developed. The risk of pitting may still be predicted by statistical and empirical methods for which gathering and compilation of reliable corrosion data from the field and laboratory work are of high importance. Continued efforts on identification and quantification of critical parameters for localized corrosion, as well as building sour corrosion databases for verification and reference, are necessary for providing the industry with adequate corrosion prediction models.

The gap between field experience and laboratory data is very difficult—if at all possible—to overcome, a fact that is acknowledged by most sour corrosion specialists and scientists. However, it is still possible to reduce discrepancies and provide more reliable laboratory results through improvement of corrosion test protocols for materials selection, inhibitor qualification, and corrosion mechanism studies. Electrochemical measurements, surface analysis methods, and test equipment can be further developed to reduce errors and artifacts in sour corrosion studies.

Although there have been significant advancements in corrosion inhibitor technologies over the last decade, the dose rates required for sour systems are still often approximately one to nearly two orders of magnitude greater than that under sweet conditions. The mitigation of localized corrosion, in regions of deposited sulfur corrosion, solely by the application of corrosion inhibitor options in the absence of accompanying sulfur solvent or dispersant is limited as are environmentally acceptable products (as per the North Sea regulations) for sour systems. Oftentimes the corrosion mitigation within these confines is made even more difficult in the presence of other oilfield chemicals such as hydrate inhibitors, scale inhibitors, and biocides, for example, in which compatibility issues with the corrosion inhibitor also needs contemplating.

Focused research and chemical development in these areas would certainly benefit the industry and in turn provide more cost-effective solutions to protect assets operating under these aggressive conditions.

The pH stabilization technique—corrosion protection of gas pipelines by addition of alkaline chemicals to increase pH (typically up to a value of 6.5−8) and thereby enhance formation of protective corrosion product layers—has been successfully applied in many sweet gas pipelines. Under sour conditions, however, research so far has indicated that pH stabilization is mostly ineffective or even detrimental. Iron sulfides are less soluble than iron carbonates and may form protective layers at lower pH values (∼4−5). More research is required on how to stabilize and exploit the natural protection from iron sulfide layers as an alternative to corrosion inhibition, e.g., by investigating whether minor additions of alkalinity can reduce general and localized corrosion to meet typical industry acceptance criteria.

Acknowledgments

Jon Kvarekvål and Jeremy Moloney wish to thank Chief Scientist Arne Dugstad and Dr. Morten Tjelta at IFE for their valuable contributions.

References

[1] D.W. Shoesmith, P. Taylor, M.G. Bailey, D.G. Owen, The formation of ferrous monosulfide polymorphs during the corrosion of iron by aqueous hydrogen sulfide at 21°C, Journal of Electrochemical Society 127 (5) (1980) 1007−1015.

[2] Z.A. Iofa, V.V. Batrakov, Cho-Ngok-Ba, Influence of anion adsorption on the action of inhibitors on the acid corrosion of iron and cobalt, Electrochimica Acta 9 (12) (1964) 1645−1653.

[3] B.G. Pound, G.A. Wright, R.M. Sharp, The anodic behaviour of iron in hydrogen sulfide solutions, Corrosion 45 (5) (1989) 386−392.

[4] X.L. Cheng, H.Y. Ma, J.P. Zhang, X. Chen, S.H. Chen, H.Q. Yang, Corrosion of iron in acid solutions with hydrogen sulfide, Corrosion 54 (5) (1998) 369−376.

[5] F.K. Naumann, W. Carius, Die Bedeutung der Korrosionsvorgänge in wässrigen Schwefelwasserstoff − Lösungen für die Bruchbildung an Stählen, Archiv für das Eisenhüttenwesen 30 (5) (1959) 1−10.

[6] D. Morris, L. Sampaleanu, D. Veysey, The corrosion of steel by aqueous solutions of hydrogen sulfide, Journal of Electrochemical Society 27 (6) (1980).

[7] Y. Zheng, B. Brown, S. Nesic, Electrochemical study and modeling of H_2S corrosion of mild steel, in: CORROSION/2013, NACE International, Houston, TX, 2013. Paper no. 2406.

[8] A. Kawashima, K. Hashimoto, S. Shimodaira, Hydrogen electrode reaction and hydrogen embrittlement of mild steel in hydrogen sulfide solutions, Corrosion 32 (8) (1976).

[9] P. Bolmer, Polarization of iron in H_2S-NaHS buffers, Corrosion 21 (3) (1965).

[10] M. Tjelta, J. Kvarekvål, Electrochemistry of iron sulfide and its galvanic coupling to carbon steel in sour aqueous solutions, in: CORROSION/2016, NACE International, Houston, TX, 2015. Paper no. 7478.

[11] R.H. Hausler, L.A. Goeller, R.P. Zimmerman, R.H. Rosenwald, Contribution to the "Filming amine" theory: an interpretation of experimental results, Corrosion 28 (1) (1972).
[12] P. Kofstad, High Temperature Corrosion, Elsevier Applied Science Publishers Ltd., 1988, p. 13.
[13] R.H. Hausler, Contribution to the understanding of H_2S corrosion, in: CORROSION/2004, NACE International, Houston, TX, 2004. Paper no. 04732.
[14] G. Svenningsen, A. Palencsar, J. Kvarekvål, Investigation of iron sulfide surface layer growth in aqueous H_2S/CO_2 environments, in: CORROSION/2009, NACE International, Houston, TX, 2009. Paper no. 09359.
[15] L.F. Power, H.A. Fine, The iron − sulfur system. Part 1: the structures and physical properties of the compounds of the low-temperature phase fields, Minerals Science and Engineering 8 (2) (1976) 106−128.
[16] C.I. Pearce, R.A.D. Pattrick, D.J. Vaughan, Electrical and magnetic properties of sulfides, Reviews in Mineralogy and Geochemistry 61 (1) (2006) 127−180.
[17] W. Davison, The solubility of iron sulphides in synthetic and natural waters at ambient temperature, Aquatic Science 53 (4) (1991) 309−329.
[18] A. Pourbaix, M. Amalhay, A.K. Singh, Contribution to the mechanisms of localised corrosion of C-steel and 13% Cr steel in H_2S environment, in: EUROCORR '97, 1997.
[19] D.T. Rickard, Kinetics of FeS precipitation: Part 1. Competing reaction mechanisms, Geochimica et Cosmochimica Acta 59 (21) (1995) 4367−4379.
[20] H.Y. Jeong, J.H. Lee, K.F. Hayes, Characterization of synthetic nanocrystalline mackinawite: crystal structure, particle size, and specific surface area, Geochimica et Cosmochimica acta 72 (2) (2008) 493−505.
[21] J.B. Sardisco, R.E. Pitts, Corrosion of iron in an H_2S-CO_2-H_2O system. Mechanism of sulfide film formation and kinetics of corrosion reaction, Corrosion 21 (1965) 245−253.
[22] J. Kvarekvål, R. Nyborg, H. Choi, Formation of multilayer iron sulfide films during high temperature CO_2/H_2S corrosion of carbon steel, in: CORROSION/2003, NACE International, Houston, TX, 2003. Paper no. 03339.
[23] D. Rickard, A. Griffith, A. Oldroyd, I.B. Butler, E. Lopez-Capel, D.A.C. Manning, D.C. Apperley, The composition of nanoparticulate mackinawite, tetragonal iron(II) monosulfide, Chemical Geology 235 (3−4) (2006) 286−298.
[24] K.D. Kwon, K. Refson, S. Bone, R. Qiao, W.-l. Yang, Z. Liu, G. Sposito, Magnetic ordering in tetragonal FeS: evidence for strong itinerant spin fluctuations, Physical Review B 83 (6) (2011) 064402.
[25] G. Genchev, K. Cox, A. Sarfraz, Sour corrosion − investigation of anodic iron sulfide layer growth in H_2S saturated saline solutions, in: EuroCorr 2014, 2014. Paper no. 7233.
[26] S. Wells, D. Alfe, L. Blanchard, J. Brodholt, M. Calleja, R. Catlow, D. Price, R. Tyler, K. Wright, Ab-initio simulations of magnetic iron sulphides, Molecular Simulation 31 (5) (2005) 379−384.
[27] R.T. Shuey, Semiconducting Ore Minerals, Elsevier, 1975, p. 290.
[28] J.S. Smith, J.D.A. Miller, Nature of sulfides and their corrosive effect on ferrous metals − a review, British Corrosion Journal 10 (3) (1975) 136−143.
[29] R.E. Krupp, Phase relations and phase transformations between the low-temperature iron sulfides mackinawite, greigite, and smythite, European Journal of Mineralogy 6 (1994) 265−278.
[30] A. Roldan, D. Santos-Carballal, N.H. de Leeuw, A comparative DFT study of the mechanical and electronic properties of greigite Fe_3S_4 and magnetite Fe_3O_4, The Journal of Chemical Physics 138 (20) (2013).
[31] A.P. Roberts, L. Chang, C.J. Rowan, C.-S. Horng, F. Florindo, Magnetic properties of sedimentary greigite (Fe_3S_4): an update, Reviews of Geophysics 49 (1) (2011) RG1002.

[32] J.M.D. Coey, M.R. Spender, A.H. Morrish, The magnetic structure of the spinel Fe_3S_4, Solid State Communications 8 (20) (1970) 1605−1608.
[33] V. Tasseva, A. Akala, T. Peev, S. Nikolov, Korrosionsprozesse in Separatorabwässern der atmosphärischen Erdöldestillation, Werkstoffe und Korrosion 40 (1989) 719−723.
[34] P.R. Rhodes, Corrosion Mechanism of Carbon Steel in Aqueous H2S Solution, Abstract No. 107, Extended Abstracts, The Electrochemical Society, 1976.
[35] D.E. Milliams, C.J. Kroese, Aqueous corrosion of steel by H_2S and H_2S/CO_2 mixtures, in: Third International Conference on the Internal and External Protection of Pipes, 1979. Paper no. H1.
[36] A.G. Wikjord, T.E. Rummery, F.E. Doern, D.G. Owen, Corrosion and deposition during the exposure of carbon steel to hydrogen sulphide-water solutions, Corrosion Science 20 (1980) 651−671.
[37] S.N. Smith, M.W. Joosten, Corrosion of carbon steel by H_2S in CO_2 containing oilfield environments, in: CORROSION/2006, NACE International, Houston, TX, 2006. Paper no. 06115.
[38] S.N. Smith, B. Brown, W. Sun, Corrosion at higher H_2S concentrations and moderate temperatures, in: CORROSION/2011, NACE International, Houston, TX, 2011. Paper no. 11081.
[39] S.N. Smith, M.W. Joosten, Corrosion of carbon steel by H_2S in CO_2 containing oilfield environments − 10 year update, in: NACE CORROSION 2015, NACE International, 2015.
[40] S.N. Smith, Current understanding of corrosion mechanisms due to H_2S in oil and gas production environments, in: NACE CORROSION 2015, NACE International, 2015.
[41] J. Ning, Y. Zheng, B. Brown, D. Young, S. Nešic, A thermodynamic model for the prediction of mild steel corrosion products in an aqueous hydrogen sulfide environment, Corrosion 71 (2015) 8.
[42] J. Ning, Y. Zheng, B. Brown, D. Young, S. Nesic, Construction and verification of Pourbaix diagrams for hydrogen sulfide corrosion of mild steel, in: NACE CORROSION 2015, NACE International, 2015.
[43] J. Ning, Y. Zheng, D. Young, B. Brown, S. Nešić, Thermodynamic study of hydrogen sulfide corrosion of mild steel, Corrosion 70 (4) (2014) 375−389.
[44] P. Tewari, A. Campbell, Dissolution of iron during the initial corrosion of carbon steel in aqueous H_2S solution, Canadian Journal of Chemistry 57 (1979) 188−196.
[45] H.J. Choi, N.S. A.-B, F.I. Al-Beheiri, D.K. Warnken, Field corrosion assessment of L80 carbon steel downhole production tubing in Khuff gas wells, in: CORROSION/2006, NACE International, Houston, TX, 2006. Paper no. 06653.
[46] J. Kvarekvål, Corrosion layer breakdown and localized corrosion in CO_2/H_2S environments, in: CORROSION/2012, NACE International, Houston, TX, 2012. Paper no. C2012−0001537.
[47] J. Kvarekvål, Morphology of localised corrosion attacks in sour environments, in: CORROSION/2007, NACE International, Houston, TX, 2007. Paper no. 07659.
[48] J. Kvarekvål, G. Svenningsen, Effect of high H_2S partial pressures on localized corrosion of carbon steel, in: CORROSION/2015, NACE International, Houston, TX, 2015. Paper no. 5720.
[49] J. Kvarekvål, A. Dugstad, I.H. Omar, Y. Gunaltun, H_2S corrosion of carbon steel under simulated Kashagan field conditions, in: CORROSION/2005, NACE International, Houston, TX, 2005. Paper no. 05300.
[50] M.R. Bonis, R. MacDonald, M. Girgis, K. Goerz, Weight loss corrosion with H_2S: using past operations for designing future facilities, in: CORROSION/2006, NACE International, Houston, TX, 2006. Paper no. 06122.

[51] M. Bonis, R. MacDonald, $H_2S + CO_2$ corrosion: additional learnings from field experience, in: CORROSION/2015, NACE International, Houston, TX, 2015. Paper no. 5718.
[52] J. Dougherty, Factors effecting H_2S and H_2S/CO_2 attack on carbon steels under deep hot well corrosion, in: CORROSION/88, NACE International, Houston, TX, 1988. Paper no. 190.
[53] S. Papavinasam, A. Doiron, R.W. Revie, Effects of surface layers on the initiation of internal pitting corrosion in oil and gas pipelines, Corrosion 65 (10) (2009) 663−673.
[54] C. Li, S. Ling, F. Cao, J. Pacheco, S. Desai, Effect of sodium chloride concentration on carbon steel sour corrosion, in: CORROSION/2013, NACE International, Houston, TX, 2013. Paper no. 2468.
[55] J. Kvarekvål, A. Dugstad, Pitting corrosion mechanisms on carbon steel in sour glycol/water mixtures, in: CORROSION/2004, NACE International, Houston, TX, 2004. Paper no. 04737.
[56] J. Kvarekvål, A. Dugstad, Pitting corrosion in CO_2/H_2S containing glycol solutions under flowing conditions, in: CORROSION/2005, NACE International, Houston, TX, 2005. Paper no. 0563.
[57] J. Kvarekvål, A. Dugstad, Corrosion mitigation with pH stabilization in slightly sour gas/condensate pipelines, in: CORROSION/2006, NACE International, Houston, TX, 2006. Paper no. 06646.
[58] J. Kvarekvål, A. Dugstad, M. Seiersten, Localized corrosion on carbon steel in sour glycolic solutions, in: CORROSION/2010, NACE International, Houston, TX, 2010. Paper no. 10277.
[59] M. Singer, B. Brown, A. Camacho, S. Nesic, Combined effect of CO_2, H_2S and acetic acid on bottom of the line corrosion, in: CORROSION/2007, NACE International, Houston, TX, 2007. Paper no. 07661.
[60] M. Singer, B. Brown, A. Camacho, S. Nesic, Combined effect of carbon dioxide, hydrogen sulfide, and acetic acid on bottom-of-the-line corrosion, Corrosion 67 (2011) 1.
[61] H. Sun, D. Blumer, J. Davis, Pit propagation of carbon steel in sour conditions, in: CORROSION/2010, NACE International, Houston, TX, 2010. Paper no. 10282.
[62] G.M. Omweg, G.S. Frankel, W.A. Bruce, J.E. Ramirez, G. Koch, Performance of welded high-strength low-alloy steels in sour environments, Corrosion 59 (7) (2003) 640−653.
[63] N.G. Park, L. Morello, J.E. Wong, S.A. Maksoud, The effect of oxygenated methanol on corrosion of carbon steel in sour wet gas environment, in: CORROSION/2007, NACE International, Houston, TX, 2007. Paper no. 07663.
[64] G. Schmitt, Present Day Knowledge of the Effect of Elemental Sulfur on Corrosion in Sour Gas Systems, NACE International, Houston, TX, 1990.
[65] T.W. Farrer, F. Wormwell, Corrosion of iron and steel by aqueous suspensions of sulfur, Chemistry and Industry 106 (1953).
[66] D.D. MacDonald, B. Roberts, J.B. Hyne, The corrosion of carbon steel by wet elemental sulphur, Corrosion Science 18 (5) (1978) 411−425.
[67] E. Schaschl, Elemental sulfur as a corrodent in deaerated, neutral aqueous solutions, Materials Performance 19 (7) (1980) 9.
[68] S.B. Maldonado, P.J. Boden, The mechanism of corrosion of mild steel by elemental sulfur/water suspensions, in: 8th International Congress Metallic Corrososion, 1981. Paper no. 338.
[69] S.B. Maldonado-Zagal, P.J. Boden, Hydrolysis of elemental sulfur in water and its effect on the corrosion of mild steel, British Corrosion Journal 17 (1982) 117.
[70] W. Kijster, H. Schlerkmann, G. Schmitt, W. Schwenk, D. Steinmetz, Corrosion reactions of elemental sulfur and plain carbon steel in aqueous media, Werkstoffe und Korrosion 35 (1984) 556.

[71] R.H. Hausler, Contribution to the understanding of H_2S corrosion, Corrosion (2004) 25.
[72] H.U. Schutt, P.R. Rhodes, Corrosion in an aqueous hydrogen sulfide, ammonia, and oxygen system, Corrosion 52 (1996) 12.
[73] M.R. Gregg, J. Lerbscher, Inhibitor developments providing mitigating benefits against pitting corrosion to carbon steel constructed assets used to process wet sulfur contaminated sour gas production, in: CORROSION/2005, NACE International, Houston, TX, 2005. Paper no. 05627.
[74] M.R. Gregg, J. Slofrstra, D. Thill, W. Sudds, Corrosion experiences inhibition practices managing wet sour salty gas pipeline environments contaminated with elemental sulfur deposits, in: CORROSION/2003, NACE International, Houston, TX, 2003. Paper no. 03174.
[75] J.A. Dougherty, Corrosion inhibition of wet, sour gas lines carrying elemental sulfur, in: CORROSION/92, NACE International, Houston, TX, 1992. Paper no. 12.
[76] L. Smith, B. Craig, Practical corrosion control measures for elemental sulfur containing environments, in: CORROSION/2005, NACE International, Houston, TX, 2005. Paper no. 05646.
[77] S. Horner, M. Girgis, K. Goerz, A laboratory evaluation of the variables that affect the application of batch corrosion inhibitors in sour gas environment − phase II, in: CORROSION/2005, NACE International, Houston, TX, 2005. Paper no. 05639.
[78] D.L. Miller, K.D. Efird, N. Davis, A. Ali, J. Ward, Corrosion rate measurements in the presence of hydrogen sulfide: electrochemical activity of solution species, in: CORROSION/2008, NACE International, Houston, TX, 2008. Paper no. 08414.
[79] H. Fang, D. Young, S. Nesic, Corrosion of mild steel in the presence of elemental sulfur, in: CORROSION/2008, NACE International, Houston, TX, 2008. Paper no. 08637.
[80] Y. Song, A. Palencsar, G. Svenningsen, J. Kvarekvål, T. Hemmingsen, Effect of O_2 and temperature on sour corrosion, in: CORROSION/2011, NACE International, Houston, TX, 2011. Paper no. 11077.
[81] Y. Song, A. Palencsár, G. Svenningsen, J. Kvarekvål, T. Hemmingsen, Effect of O_2 and temperature on sour corrosion, Corrosion 68 (7) (2012) 662−671.
[82] R.H. Hausler, D.W. Stegman, D. Tjandroso, Laboratory studies on flow induced localized corrosion in CO_2/H_2S environments, II. Parametric study on the effect of H_2S, condensate, metallurgy, and flowrate, in: CORROSION/90, NACE International, Houston, TX, 1990. Paper no. 6.
[83] G. Wranglén, Review article on the influence of sulfide inclusions on the corrodibility of Fe and steel, Corrosion Science 9 (1969) 585−602.
[84] V.V. Zav'yalov, Corrosion of oil-field pipelines, Protection of Metals 39 (3) (2003) 274−277.
[85] M.A. Baker, J.E. Castle, The initiation of pitting corrosion at MnS inclusions, Corrosion Science 34 (4) (1993) 667−682.
[86] M. Sephton, P.C. Pistorius, Localized corrosion of carbon steel weldments, Corrosion 56 (12) (2000).
[87] H. Huang, W. Tsai, W. Lee, Corrosion morphology of A516 carbon steel in H_2S solution, Scripta Metallurgica et Materialia 31 (7) (1994).
[88] Y.S. Junwen Tang, J. Guo, T. Zhang, G. Meng, F. Wang, The effect of H_2S concentration on the corrosion behavior of carbon steel at 90°C, Corrosion Science 52 (2010) 2050−2058.
[89] M.A. Lucio-Garcia, J.G. Gonzalez-Rodriguez, M. Casales, L. Martinez, J.G. Chacon-Nava, M.A. Neri-Flores, A. Martinez-Villafañe, Effect of heat treatment on H_2S corrosion of a micro-alloyed C−Mn steel, Corrosion Science 51 (2009) 2380−2386.

[90] F.H. Meyer, O.L. Riggs, R.L. McGlasson, J.D. Sudbury, Corrosion products of mild steel in hydrogen sulfide environments, Corrosion 14 (1958) 69−75.
[91] E.C. Greco, W.B. Wright, Corrosion of iron in an H_2S-CO_2-H_2O system, Corrosion 18 (1962) 119−124.
[92] W.H. Thomason, Formation rates of protective iron sulfide films on mild steel in H2S saturated brine as a function of temperature, in: CORROSION/78, NACE International, Houston, TX, 1978. Paper no. 41.
[93] C.R.F. Azevedo, Failure analysis of a crude oil pipeline, Engineering Failure Analysis 14 (2007) 978−994.
[94] L. Zhang, J. Yang, J. Sun, M. Lu, Effect of pressure on wet H_2S/CO_2 corrosion of pipeline steel, in: CORROSION/2009, NACE International, Houston, TX, 2009. Paper no. 09565.

CO_2 corrosion of mild steel

7

Aria Kahyarian[1], *Mohsen Achour*[2] *and Srdjan Nesic*[1]
[1]Ohio University, Athens, OH, United States; [2]ConocoPhillips, Bartlesville, OK, United States

7.1 Introduction

Produced oil and gas are always accompanied by some water and varying amounts of carbon dioxide and in some cases hydrogen sulfide and organic acids. All of these may affect the integrity of mild steel. This has been known for over 100 years, yet internal corrosion of pipelines and other facilities made from mild steel still represents a challenge for the oil and gas industry. Although many corrosion-resistant alloys are able to withstand this type of corrosion, it is a matter of economics: mild steel is still the most cost-effective construction material. The price of failure due to internal corrosion is enormous, both in terms of direct costs, such as repair/replacement costs and lost production, and indirect costs, such as environmental cost and impact on the downstream industries.

The following text summarizes the current degree of understanding of CO_2 corrosion of mild steel exposed to aqueous environments. Much has been understood about the basic mechanisms, enabling construction of mechanistic prediction models, but many challenges remain, particularly when it comes to effects of corrosion product layers, multiphase flow, additional species, hydrocarbon composition, inhibition, etc. The following sections start out with describing the basic physicochemical phenomena underlying CO_2 corrosion and gradually move to more complicated situations, culminating with the list of multifaceted real-life challenges seen in the field.

7.2 Water chemistry in CO_2 corrosion

Carbon dioxide (CO_2) is a stable, inert, and noncorrosive gas. However, upon dissolution in water and a subsequent hydration reaction, a more reactive chemical species, carbonic acid (H_2CO_3), is formed. This reaction is followed by dissociation reactions to form bicarbonate $\left(HCO_3^-\right)$ ion, carbonate $\left(CO_3^{2-}\right)$ ion, and hydrogen (H^+) ion, resulting in an acidic and corrosive solution. The reactions associated with these chemical equilibria and their corresponding mathematical relationship are listed in Table 7.1.

The chemical equilibria and water chemistry associated with dissolved CO_2 and its carbonate derivatives have been extensively studied [1–9]. The first step, CO_2 dissolution, is described via Eq. (7.i), where K_{CO_2} is the proportionality constant and can be expressed as Henry's constant for the simplest case of ideal gas and ideal solution. The nonideal behavior of the gas phase, represented by fugacity coefficient, and the liquid

Trends in Oil and Gas Corrosion Research and Technologies. http://dx.doi.org/10.1016/B978-0-08-101105-8.00007-3

Table 7.1 Chemical reactions of acidic water/CO_2 equilibria

Reaction	Equilibrium equation	
$CO_{2(g)} \leftrightharpoons CO_{2(aq)}$	$K_{CO_2} = \frac{\left[CO_{2(aq)}\right]}{pCO_{2(g)}}$	(7.i)
$CO_{2(aq)} + H_2O_{(l)} \leftrightharpoons H_2CO_{3(aq)}$	$K_{hyd} = \frac{[H_2CO_3]}{\left[CO_{2(aq)}\right]}$	(7.ii)
$H_2CO_{3(aq)} \leftrightharpoons HCO^-_{3(aq)} + H^+_{(aq)}$	$K_{ca} = \frac{\left[HCO_3^-\right][H^+]}{[H_2CO_3]}$	(7.iii)
$HCO^-_{3(aq)} \leftrightharpoons CO^{2-}_{3(aq)} + H^+_{(aq)}$	$K_{bi} = \frac{\left[CO_3^{2-}\right][H^+]}{\left[HCO_3^-\right]}$	(7.iv)
$H_2O_{(l)} \leftrightharpoons OH^-_{(aq)} + H^+_{(aq)}$	$K_w = [OH^-][H^+]$	(7.v)

phase, represented by activity coefficients, can be incorporated into the proportionality constant following the extended Rault's law.

The product of CO_2 hydration (reaction 7.ii), carbonic acid (H_2CO_3), is a diprotic weak acid. The term *weak acid* refers to the fact that this species is only partially dissociated in an aqueous solution. With the first dissociation constant of $pK_{ca} \approx 3.6$ (reaction 7.iii) and the second dissociation constant of $pK_{bi} \approx 10.33$ (reaction 7.iv), the carbonic acid dissociation reaction can be considered as the main source of acidity (H^+) in the solution. Although water can also be categorized as a weak acid, with $pK_a \approx 14$, it has no significant effect when compared with H_2CO_3 and HCO_3^-.

The chemical equilibria shown in Table 7.1 represent a simple case of CO_2 dissolution in pure water, such as what is observed in condensed water formed in wet gas pipelines. However, a more complex water chemistry is found in formation water, where significant amounts of various ions such as Cl^-, Na^+, Ca^+, SO_4^{2-}, organic acid (such as acetic acid, formic acid, and propionic acid), as well as hydrogen sulfide can be present [10,11]. These species can significantly alter the speciation of CO_2 equilibria by changing the acidity and ionic strength of the solution.

A more comprehensive discussion on the chemical speciation of CO_2/water system is provided in Chapter 34.

7.3 Electrochemistry of CO_2 corrosion

The aqueous CO_2 corrosion of mild steel, as seen in oil and gas industry, is by nature an electrochemical system. The spontaneous iron dissolution, causing the deterioration of the metallic structure, is an electrochemical oxidation process. On the other hand, the cathodic hydrogen evolution reaction provides the required electron sink for the iron dissolution to progress. In the CO_2 corrosion context, the hydrogen evolution reaction is a family of cathodic reactions with all having molecular hydrogen as their

Table 7.2 Electrochemical reactions associated with aqueous acidic CO_2 corrosion of mild steel

Electrochemical reaction	Dominant reaction type	
$H^+_{(aq)} + e^- \leftrightharpoons \frac{1}{2}H_{2(g)}$	Cathodic	(7.vi)
$H_2O_{(l)} + e^- \leftrightharpoons OH^-_{(aq)} + \frac{1}{2}H_{2(g)}$	Cathodic	(7.vii)
$H_2CO_{3(aq)} + e^- \leftrightharpoons HCO^-_{3(aq)} + \frac{1}{2}H_{2(g)}$	Cathodic	(7.viii)
$HCO^-_{3(aq)} + e^- \leftrightharpoons CO^{2-}_{3(aq)} + \frac{1}{2}H_{2(g)}$	Cathodic	(7.xi)
$Fe^{2+}_{(aq)} + 2e^- \leftrightharpoons Fe_{(s)}$	Anodic	(7.x)

product. That includes the reduction of H^+, H_2CO_3, HCO_3^-, and H_2O, as shown in Table 7.2. Considering the chemical equilibrium of the water/CO_2 system, it can be shown that all these reactions are thermodynamically identical. This means that they have the same reversible potential (based on Nernst equation), if the concentrations of the involved chemical species are defined by the equilibrium speciation. Hence, the main difference resides in reaction kinetics. The same would also hold true for other weak acids, such as acetic acid and hydrogen sulfide.

Table 7.2 summarizes the commonly accepted electrochemical reactions associated with aqueous CO_2 corrosion of mild steel. Reactions (7.vi)–(7.ix) are the hydrogen evolution reactions in a water/CO_2 solution. Reactions (7.vi) and (7.vii) are the hydrogen ion and water reduction reactions, respectively. Reaction (7.viii) is the reduction of carbonic acid (H_2CO_3), and reaction (7.ix) is the reduction of bicarbonate ion, which is believed to be significant at near-neutral and alkaline pH values because of the high bicarbonate ion concentration [12–15].

7.3.1 Anodic reactions

The iron oxidation as the dominant anodic reaction is a key element in acidic corrosion of mild steel. The mechanism of iron oxidation reaction in acidic media has been the subject of numerous studies over the last half a century [16–27] and has been proved difficult to explain. In this section, the mechanism of acidic iron dissolution is briefly discussed to provide the necessary context relevant to CO_2 corrosion; a thorough review of the existing literature can be found elsewhere [26,28].

El Miligy et al. [19] showed that the iron dissolution in mildly acidic environments occurs in four different states, depending on the electrode potential. The authors categorized these as *active dissolution*, *transition*, *prepassivation*, and *passive*, as demonstrated in Fig. 7.1. Each range was shown to have a different electrochemical behavior, characterized by different apparent Tafel slopes and reaction orders. The two local current maxima, observed in transition and prepassivation ranges, were showed to be also pH dependent. This suggests that the mechanism of iron dissolution at corrosion potential could depend on the solution pH and other environmental conditions.

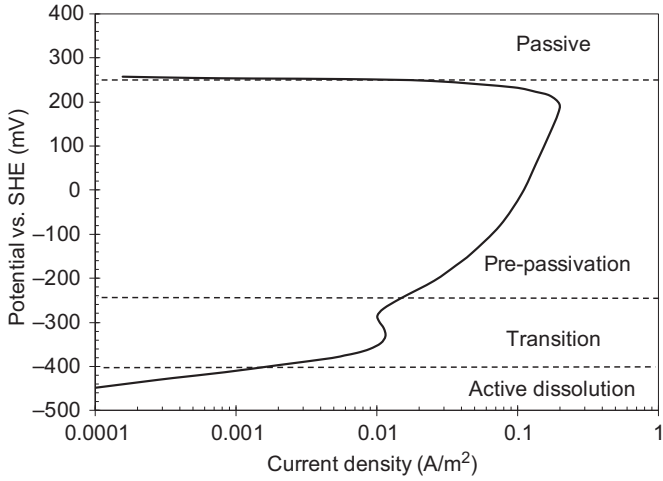

Figure 7.1 Anodic polarization curve of iron in 0.5 M Na_2SO_4 solution at pH 5 and 298K, with the scan rate of 6.6 mV/s and rotating disk electrode at 69 rps. *SHE,* standard hydrogen electrode.
Adapted from A.A. El Miligy, D. Geana, W.J. Lorenz, A theoretical treatment of the kinetics of iron dissolution and passivation, Electrochimica Acta 20 (1975) 273−281.

For the case of CO_2 corrosion, at pH values less than 5, the experimental results suggest that the corrosion is occurring at the active dissolution range [29,30]. At pH values more than 5, the corrosion potential gradually shifts towards the transition range, and eventually reaches the prepassivation range at near neutral pH values [20].

The complex behavior depicted in Fig. 7.1 is an indication of a reaction mechanism with multiple intermediate species and rate-determining steps. In the literature, there are two main mechanisms proposed for iron dissolution in acidic solutions: the "catalytic mechanism" and the "consecutive mechanism." These two mechanisms are associated with two distinct electrochemical behaviors observed specifically in the active dissolution range. The catalytic mechanism, first proposed by Heusler et al. [31], is based on the experimental Tafel slope of 30 mV and second-order dependence on hydroxide (OH^-) ion concentration. On the other hand, the consecutive mechanism proposed by Bockris et al. [24] was formulated to explain the observed Tafel slope of 40 mV and a first-order dependence on (OH^-) ion concentration. These two significantly different reaction kinetics are believed to be caused by the surface activity of the iron electrode [17], i.e., the dissolution of cold-worked iron electrodes with high internal stress occurs with a 30 mV Tafel slope, whereas a 40 mV Tafel slope was observed for dissolution of recrystallized iron [17,25,27,28]. The catalytic mechanism is described as reactions (7.xi)−(7.xiv) [28].

$$Fe + H_2O \rightleftharpoons (FeOH)_{ads} + H^+ + e^- \tag{7.xi}$$

$$Fe + (FeOH)_{ads} \rightleftharpoons [Fe(FeOH)] \tag{7.xii}$$

$$[Fe(FeOH)] + OH^- \rightarrow FeOH^+ + (FeOH)_{ads} + 2e^- \quad (7.xiii)$$

$$FeOH^+ + H^+ \rightleftharpoons Fe^{2+} + H_2O \quad (7.xiv)$$

This mechanism suggests that the $(FeOH)_{ads}$ on the so-called kink sites acts as a catalyst in the iron dissolution reaction. Although this mechanism has been criticized because of the two-electron transfer step (reaction 7.xiii) [25], it has been supported by atomistic scale discussions and electrochemical impedance measurements [21,22,27].

The consecutive mechanism [24] shares the same initial and final step with the "catalytic mechanism," as shown in reactions (7.xv)–(7.xvii). However, in this mechanism, $(FeOH)_{ads}$ is directly oxidized through a one-electron transfer elementary step (reaction 7.xvi).

$$Fe + H_2O \rightleftharpoons (FeOH)_{ads} + H^+ + e^- \quad (7.xv)$$

$$(FeOH)_{ads} \rightarrow Fe[OH]^+ + e^- \quad (7.xvi)$$

$$FeOH^+ + H^+ \rightleftharpoons Fe^{2+} + H_2O \quad (7.xvii)$$

The anodic polarization curves obtained for mild steel dissolution in CO_2-saturated environments have frequently been reported to have a 40 mV Tafel slope and a first-order dependence on hydroxide ion concentration [13,15,29,30,32], in accordance with the "consecutive mechanism" proposed by Bockris et al. [24]. Hence, this mechanism and its corresponding kinetic relationship have been commonly used to describe the anodic currents in CO_2 corrosion of mild steel [29,30,33–36]. On the other hand, although a few studies report a rather significant effect of CO_2 and other carbonate species on the acidic iron dissolution reaction [13,20], in-depth analysis on the extent of these possible effects is rarely available in the literature. In a study by Nešić et al. [20], the anodic polarization curves were used to discuss the effect of CO_2 in a short potential range ($\sim$100 mV) above the corrosion potential. The experiments were performed in perchlorate solutions, in the pH range of 2–6 and pCO_2 from 0 to 1 bar. In that study, the authors reported the Tafel slope of 30 mV and second-order dependence on OH^- ion concentration for pH values less than 4 (corresponding to the "catalytic mechanism"). In the pH range of 4–6, the reported Tafel slopes were gradually increasing, whereas the dependence on OH^- ion concentration was diminishing. Ultimately, at pH $\sim$ 6, a Tafel slope of 120 mV with zero dependence on OH^- ion concentration was reported. The results showed that the presence of CO_2 does not affect the observed Tafel slopes, whereas the exchange current densities were linearly proportional to pCO_2 over the studied pH range. The authors formulated the following mechanism to describe the effect of CO_2 on iron dissolution.

$$Fe + CO_2 \rightleftharpoons FeCO_{2ads} \quad (7.xviii)$$

$$FeCO_{2ads} + H_2O \rightleftharpoons (FeCO_2)OH_{ads} + H^+ + e^- \quad (7.xix)$$

$$(FeCO_2)OH_{ads} \rightleftharpoons (FeCO_2)OH^+_{ads} + e^- \quad (7.xx)$$

$$(FeCO_2)OH^+_{ads} + H_2O \rightleftharpoons (FeCO_2)(OH)_{2ads} + H^+ \quad (7.xxi)$$

$$(FeCO_2)(OH)_{2ads} \rightleftharpoons (FeCO_2)(OH)_2 \quad (7.xxii)$$

$$(FeCO_2)(OH)_2 + 2H^+ \rightleftharpoons Fe^{2+} + CO_2 + 2H_2O \quad (7.xxiii)$$

Although this complex mechanism was not supported with sufficient experimental evidence, the proposed steps resemble the so-called branching mechanism proposed by Drazic et al. [25]. Here the authors suggest a direct CO_2 adsorption onto the iron surface forming the surface species $(FeCO_2)_{ads}$, which acts as an active site for OH adsorption.

7.3.2 Cathodic reactions

The mechanism of hydrogen evolution reaction from H^+ ions on various metals has been extensively studied [37–44]. This reaction is commonly believed to consist of three elementary steps as shown in reactions (7.xxiv)–(7.xxvi) [45]. Reaction (7.xxiv), commonly referred to as the Volmer step, is the electrochemical adsorption and reduction of H^+ ions from the solution. This reaction is succeeded by a desorption step, either the electrochemical desorption reaction (7.xxv) (Heyrovsky step) or the chemical desorption reaction (Tafel step). Other alternative elementary steps such as the so-called surface diffusion step or the ones involving molecular hydrogen ion $\left(H_2{}^+\right)$ have also been proposed in the literature [46,47]. The kinetic parameters of the overall reaction, apparent Tafel slope and reaction order, are defined by the rate-determining step and have been shown to be influenced by numerous parameters such as the electrode material [38,48–50], surface crystal structure [50,51], pH [52,53], overpotential [49,53], adsorbed species, and trace impurities [43,50,54,55]. This suggests a significant variation of the reaction mechanism, and therefore, the apparent kinetic parameters, with rather slight changes in the surface properties and/or the environmental conditions.

$$H^+ + e^- \rightleftharpoons H_{ads} \quad (7.xxiv)$$

$$H_{ads} + H^+ + e^- \rightleftharpoons H_2 \quad (7.xxv)$$

$$H_{ads} + H_{ads} \rightleftharpoons H_2 \quad (7.xxvi)$$

The H^+ reduction reaction on an iron surface is commonly assumed to be limited by the rate of the Volmer step (reaction 7.xxvii) [20,56–60], as suggested in the studies by Bockris and coworkers [38,42,43,61]. This rate-determining step is associated with

a theoretical Tafel slope of $2 \times 2.303RT/F$ and the reaction order of 1 versus H^+ concentration [62]. Although these theoretical values have been confirmed in a number of studies [63–65], some deviations are also reported in the literature [23,66]. On the other hand, the verification of this mechanism at mildly acidic and near-neutral environments, which are more relevant to the CO_2 corrosion conditions, is lacking because of the interference from the iron dissolution reaction.

The mechanism of hydrogen evolution from weak acids has been described based on an analogy with that of the hydrogen ion reduction. Using a generic formulation, the elementary steps are shown in reactions (7.xxvii)–(7.xxix), where HA denotes any weak acid, such as H_2CO_3, HCO_3^-, H_2O, and H_2S, or any of the weak carboxylic acids, such as acetic acid [14,57,67–69].

$$HA + e^- \rightleftharpoons H_{ad} + A^- \tag{7.xxvii}$$

$$H_{ad} + HA + e^- \rightleftharpoons H_2 + A^- \tag{7.xxviii}$$

$$H_{ad} + H_{ad} \rightleftharpoons H_2 \tag{7.xxix}$$

For hydrogen evolution from water, assuming the Volmer step (reaction 7.xxvii) to be rate determining, a theoretical Tafel slope of $2 \times 2.303RT/F$ is expected with no pH dependence of the reaction rate. It has frequently been demonstrated that the solution pH does not affect the rate of water reduction in the acidic and near-neutral pH range; however, the reported Tafel slopes are significantly deviating from the theoretically expected value of $2 \times 2.303RT/F$ [15,16,30,64,66].

The mechanistic details of the hydrogen evolution reaction from other weak acids such as H_2CO_3 and HCO_3^- are rarely discussed in the literature. In the few studies addressing this subject [13,70], the proposed mechanisms are based on the same elementary steps as discussed above. However, systematic investigations on this subject are still lacking, probably because of the experimentation challenges resulting from the interference by H^+ and H_2O reduction reactions. On the other hand, considering the exchange current density expressions, commonly used in the literature for describing the rate of these reactions [12,71,72], it is generally assumed that the rate of all hydrogen-evolving reactions involved in CO_2 corrosion is limited by the Volmer step (reaction 7.xxvii).

7.3.3 Charge transfer rate calculations

The charge transfer rates are often expressed in terms of the Tafel or the Butler–Volmer relationships, using two main parameters, exchange current density and overpotential. The application of these relationships to CO_2 corrosion and the theoretical derivation of their associated parameters were discussed in more detail elsewhere [73]. Both the Tafel and the Butler–Volmer are well-known fundamental equations used to model the kinetics of reversible electrochemical reaction. However, in CO_2 corrosion, the reversibility of the electrochemical reactions is not the focus. Here, the dominating anodic reaction is iron dissolution, and the hydrogen-evolving

reactions are the dominant cathodic reactions. The reverse reactions, iron deposition and hydrogen oxidation, are commonly assumed to be negligible, for the typical conditions in CO_2 corrosion.

The application of the Butler–Volmer relationship to describe the rate of electrochemical reaction relevant to CO_2 corrosion results in overly complicated mathematical expressions and, in some cases, inconsistencies at a basic level. For example, the reversible potential of the hydrogen evolution reactions is a function of pH_2, as described by the Nernst equation. In the literature, it is commonly assumed that $pH_2 = 1$ bar [29,71,74], which is never the case in typical laboratory or field conditions for the case of CO_2 corrosion. Invariably, dissolved H_2 is present only in minute and often indiscernible concentrations, as a product of cathodic reactions. To properly define a reversible potential, one needs to assume a constant, arbitrary value for pH_2. Such unnecessary complications can be avoided by simply expressing the rates, only based on the dominant half reactions. For example, the rate of cathodic half of generic reaction (7.xxx) can be expressed as Eq. (7.1).

$$O + ne^- \rightarrow R \tag{7.xxx}$$

$$i = nFk_0\left(C_O^s\right)^p e^{\left(\frac{-\alpha nF\left(E_{app}-E_0\right)}{RT}\right)} \tag{7.1}$$

where, k_0 is the apparent reaction rate constant, C_O^s is the concentration of the reactant at the metal surface, p is the apparent reaction order, E_0 is the standard potential, E_{app} is the applied potential, and other parameters have their common electrochemical meaning. Using this approach, simple current potential relationships for the electrochemical reactions associated with CO_2 corrosion can be formulated, as summarized in Table 7.3.

The values of the reaction rate constants for the reactions listed in Table 7.3 can be recalculated from the existing literature. Considering the Tafel equation (Eq. 7.2) along with Eq. (7.1), the relationship between exchange current density and reaction rate constant is shown in Eq. (7.3).

$$i = i_0 10^{\left(\frac{E_{app}-E_{rev}}{-b}\right)} \tag{7.2}$$

$$k_0 = \frac{i_0 10^{\left(\frac{-E_{rev}}{-b}\right)}}{nF\left(C_{O,ref}^b\right)^p e^{\left(\frac{-\alpha nF\left(-E_0\right)}{RT_{ref}}\right)}} \tag{7.3}$$

The reaction rate constant and other relevant electrochemical parameters required for charge transfer rate calculations are listed in Table 7.4.

Table 7.3 **Current potential relationships for the reactions listed in Table 7.2**

Electrochemical reaction	Mathematical relationship for half reaction[a]
Reaction (7.vi)	$i_{c,\mathrm{H^+}} = -n_{\mathrm{H^+}} F k_{0\mathrm{H^+}} C^s_{\mathrm{H^+}} \mathrm{e}^{\left(\frac{-\alpha_{\mathrm{H^+}} n_{\mathrm{H^+}} F\left(E_{\mathrm{app}} - E_{0\mathrm{H^+}}\right)}{RT}\right)}$
Reaction (7.vii)	$i_{c,\mathrm{H_2O}} = -n_{\mathrm{H_2O}} F k_{0\mathrm{H_2O}} \mathrm{e}^{\left(\frac{-\alpha_{\mathrm{H_2O}} n_{\mathrm{H_2O}} F\left(E_{\mathrm{app}} - E_{0\mathrm{H_2O}}\right)}{RT}\right)}$
Reaction (7.viii)	$i_{c,\mathrm{H_2CO_3}} = -n_{\mathrm{H_2CO_3}} F k_{0\mathrm{H_2CO_3}} C^s_{\mathrm{H_2CO_3}} \mathrm{e}^{\left(\frac{-\alpha_{\mathrm{H_2CO_3}} n_{\mathrm{H_2CO_3}} F\left(E_{\mathrm{app}} - E_{0\mathrm{H_2CO_3}}\right)}{RT}\right)}$
Reaction (7.ix)	$i_{c,\mathrm{HCO_3^-}} = -n_{\mathrm{HCO_3^-}} F k_{0\mathrm{HCO_3^-}} C^s_{\mathrm{HCO_3^-}} \mathrm{e}^{\left(\frac{-\alpha_{\mathrm{HCO_3^-}} n_{\mathrm{HCO_3^-}} F\left(E_{\mathrm{app}} - E_{0\mathrm{HCO_3^-}}\right)}{RT}\right)}$
Reaction (7.x)	$i_{a,\mathrm{Fe}} = n_{\mathrm{Fe}} F k_{0\mathrm{Fe}} C^s_{\mathrm{OH^-}} \mathrm{e}^{\left(\frac{(2-\alpha_{\mathrm{Fe}}) F\left(E_{\mathrm{app}} - E_{0\mathrm{Fe}}\right)}{RT}\right)}$

[a] i_c and i_a denote the current density calculations for cathodic half reactions and anodic half reactions, respectively.

Table 7.4 **Electrochemical parameters for the relationships in Table 7.3, where** $k_{0j} = k_{0j,\mathrm{ref}} \mathrm{e}^{\left(-\frac{\Delta H_j}{R}\left(\frac{1}{T} - \frac{1}{T_{j,\mathrm{ref}}}\right)\right)}$

	n_j	α_j	$E_{0,j}$ vs. SHE (V)	$k_{0j,\mathrm{ref}}$	ΔH_j (kJ/mol)	$T_{j,\mathrm{ref}}$ (K)
$j = \mathrm{Fe}$	2	0.5[a]	−0.447[b]	$1.59 \times 10^5 \left(\frac{\mathrm{mol}}{\mathrm{s \cdot m^2 \cdot M}}\right)^a$	37.5[a]	298.15[a]
$j = \mathrm{H^+}$	1	0.5[a]	0.000	$5.18 \times 10^{-5} \left(\frac{\mathrm{mol}}{\mathrm{s \cdot m^2 \cdot M}}\right)^a$	30[a]	298.15[a]
$j = \mathrm{H_2O}$	1	0.5[c]	−0.8277[b]	$2.70 \times 10^{-5} \left(\frac{\mathrm{mol}}{\mathrm{s \cdot m^2}}\right)^c$	30[c]	293.15[c]
$j = \mathrm{H_2CO_3}$	1	0.5[a]	−0.381[f]	$3.71 \times 10^{-2} \left(\frac{\mathrm{mol}}{\mathrm{s \cdot m^2 \cdot M}}\right)^a$	50[a]	293.15[a]
$j = \mathrm{HCO_3^-}$	1	0.5[d]	−0.615[f]	$7.37 \times 10^{-5} \left(\frac{\mathrm{mol}}{\mathrm{s \cdot m^2 \cdot M}}\right)^d$	50[e]	298.15[e]

Parameters obtained or recalculated from *a*, Nordsveen et al. [71]; *b*, CRC Handbook [75]; *c*, Zheng et al. [56]; *d*, Gray et al. [15]; *e*, Han et al. [12]; *f*, Linter and Burstein [76].

7.3.4 Effect of homogeneous reactions

As discussed earlier, it appears so far that the heterogeneous electrochemical reactions at the metal surface govern the rate of the CO_2 corrosion. However, because these electrochemical reactions are heterogeneous surface processes, the rate of these reactions is defined by the concentration of the reactants at the metal surface (see Table 7.2), which is the reaction site, and can be very different from those in the bulk solution. In particular, the concentration of the so-called corrosive species (reactants of the cathodic reactions) at the metal surface may deplete if they are consumed at a faster rate than they are replenished. Ultimately, if the rate of consumption by the electrochemical reactions is sufficiently high, the process of supplying the reactants to the metal surface becomes the rate-determining step, and the so-called limiting current condition is reached. In CO_2 corrosion, the limiting current is determined by two main processes, the homogeneous chemical reactions occurring in the solution adjacent to the metal surface and mass transfer from the the bulk solution.

The effect of homogeneous chemical reactions in the water/CO_2 system on the rate of electrochemical reactions is probably the most important aspect of CO_2 corrosion that differentiates the uniform CO_2 corrosion from the corrosion induced by strong acids (e.g., HCl or H_2SO_4) or other weak acids, such as H_2S and organic acids. There are two major effects associated with homogeneous chemical reactions in CO_2 corrosion:

1. The more significant effect is related to dissolved CO_2 gas. Only ~0.2% of dissolved CO_2 molecules are hydrated to from H_2CO_3 according to the hydration equilibrium (reaction 7.ii). This means that there is a large reservoir (buffer) of dissolved CO_2 present in the solution to replenish the H_2CO_3 concentration as it is consumed by dissociation and/or reduction at the steel surface. Therefore, in addition to mass transfer of H_2CO_3 from the bulk solution, the limiting currents are increased as a result of this hydration reaction, occurring in the solution adjacent to the metal surface.
2. The second effect is associated with H_2CO_3 and its generic buffering ability as a weak acid. Considering the H_2CO_3 dissociation reaction (reaction 7.iii), the concentration of H^+ at the metal surface is buffered when the equilibrium shifts toward the right-hand side (i.e., consumption of H^+ by the reduction reaction). Although this does not influence the limiting current directly, it is of significance when discussing the mechanisms of charge transfer controlled corrosion at high CO_2 partial pressures.

The exact mechanism of the cathodic reactions involved in CO_2 corrosion, i.e., the sequence of electrochemical and chemical reactions, is a rather complex matter, in the sense that it involves a number of electroactive species that are interrelated through homogeneous chemical reactions. The arguments about the significance and the order of chemical and electrochemical reactions can be found in the literature dating back to 1970s. De Waard and Milliams, in their well-known study on prediction of CO_2 corrosion rates [77], proposed a catalytic mechanism shown in reactions (7.xxxi) and (7.xxxii). The authors suggest that carbonic acid reduction (reaction 7.xxxi) is the predominant cathodic reaction. This reaction is succeeded by the association of the produced HCO_3^- and the H^+ present in the solution, to replenish the carbonic acid concentration through a homogeneous chemical reaction (reaction 7.xxxii).

$$H_2CO_{3(aq)} + e^- \rightarrow HCO^-_{3(aq)} + \frac{1}{2}H_{2(g)} \quad (7.xxxi)$$

$$HCO^-_{3(aq)} + H^+_{(aq)} \leftrightharpoons H_2CO_{3(aq)} \quad (7.xxxii)$$

In 1977, Schmitt and Rothmann studied the effect of flow velocity and CO_2 partial pressure on the cathodic limiting current densities [78]. The authors suggested that the observed limiting currents in a CO_2-saturated acidic solution is composed of a mass transfer component associated with H^+ and H_2CO_3 and a chemical reaction component associated with a surface hydration of adsorbed CO_2. Hence, it was hypothesized that the cathodic currents result from reduction of both H^+ and H_2CO_3, where the H^+ is supplied only through mass transfer from the bulk solution, whereas H_2CO_3 is supplied both by mass transfer from bulk and by hydration of CO_2 at the metal surface [78].

Later in 1983, Więckowski et al. studied the CO_2 adsorption on electrodeposited iron electrodes using radiotracer method [68]. The authors reported no detectable adsorption of CO_2 on the metal surface. Considering these findings, Gray et al. in 1989, suggested that the CO_2 adsorption step in Schmitt and Rothmann's mechanism [78] is unnecessary for explaining the observed limiting currents [30]. Instead, the hydration reaction was considered a homogeneous reaction occurring in the solution near the metal surface. Using their proposed mechanism, the authors developed a mathematical model with iron dissolution as the anodic reaction and H^+, H_2CO_3, and water reduction as the cathodic reactions. In their model, the surface concentration of H^+ was defined by mass transfer from the bulk, whereas for H_2CO_3, the surface concentration was defined by simultaneous consideration of the mass transfer and the preceding hydration reaction [30]. This study was further extended toward higher pH values in 1990 [15]. In the latter study, Gray et al. suggest that the reduction of HCO_3^- ions also becomes significant at pH 6 and higher. In both studies, the experimental polarization curves were compared with the results from the model showing reasonable agreement, which further supported their proposed mechanism. The mechanism proposed by Gray et al. in these two studies [15,30] has become the most commonly accepted mechanism of CO_2 corrosion ever since, and has been used in numerous related studies.

The introduction of more comprehensive mathematical models in 1990s and early 2000s provided more insight into the influence of homogeneous reactions [71,72,79,80]. The key element in these models is the comprehensive consideration of the homogeneous chemical reactions at the vicinity of the electrode surface. The study by Turgoose et al. in 1992 was the first attempt to introduce one such model for the case of CO_2 corrosion [80]. Despite numerous simplifications and in some cases dubious assumptions, the authors were able to demonstrate the feasibility of this modeling approach. Considering the mass transfer limiting currents, the authors suggest that the previously proposed mechanisms by De Waard and Milliams [77,81] and Więkowski et al. [70] are only limited interpretations of numerous possibilities resulting from the complex CO_2 water chemistry in the vicinity of the metal surface. In particular, the authors suggested that the bicarbonate direct reduction is not necessarily required to explain the increased limiting currents in near-neutral CO_2-saturated

solutions [80]. This approach was improved in the study by Pots [79], who developed a model for the calculation of limiting currents observed in CO_2-saturated acidic solutions. The author reported similar results as Turgoose et al. [80], suggesting that the limiting currents can be adequately explained even if H_2CO_3 was not considered an electroactive species [79]. As explained by the author, that is due to the local concentration of chemical species at the metal surface that may deviate significantly from the equilibrium at the bulk solution. Therefore, the homogeneous H_2CO_3 dissociation near the metal surface, followed by electrochemical reduction of the produced H^+ ions, provides a parallel reaction pathway that is kinetically fast enough to result in the observed limiting currents [79].

In a series of studies, Nešić et al. further improved this modeling approach by incorporating detailed water chemistry and charge transfer rate calculations [71,72,82–84]. The significance of the homogeneous chemical reactions in the solution near the metal surface was also emphasized by Nešić et al. [72]. The authors confirmed Pots' observation [79] that the limiting currents in CO_2-saturated acidic solutions could be fully explained without requiring H_2CO_3 to be electrochemically active. However, the authors also noted that the predicted corrosion rates were in better quantitative agreement with the experimental data when direct reduction of H_2CO_3 was included in the model, but this mechanistic aspect was not further discussed [71,72].

It is important to notice that the more recent mechanistic arguments based on thorough consideration of the homogeneous chemical reactions are of significance, because they undermine the foundation of the commonly accepted mechanism, which is mainly based on the behavior of limiting current densities (e.g., the study of Schmitt and Rothmann [78] and Gray et al. [30,85]). Note that the initially proposed mechanisms by Schmitt and Rothmann [78] and Gray et al. [30,85] do not consider the possibility of preceding dissociation of carbonic acid for H^+ reduction reaction.

In 2008, Remita et al. set out to investigate the significance of H_2CO_3 reduction reaction in CO_2-saturated acidic solutions [58]. The authors developed a mathematical model similar to that of Nešić et al. [72] and formed a quantitative discussion by comparing the simulated polarization curves with experimental results. It was shown that the cathodic currents in CO_2-saturated solution at pH 4 can be reasonably explained through H^+ reduction reaction alone [58]. The authors claimed that H_2CO_3 reduction is therefore insignificant in CO_2 corrosion. However, considering the limited experimental range (pH 4 and 1 bar CO_2), where the cathodic currents are mostly under mass transfer influence (as shown in the data reported by Nešić et al. [29]), and the concentration of H_2CO_3 is low (less than 10^{-4}), it is unrealistic to generalize the observations reported in this study [58]. Note that, as discussed in earlier studies, the limiting currents are identical whether H_2CO_3 was considered electroactive or not.

This reaction sequence (i.e., H_2CO_3 dissociation followed by H^+ reduction) is now known in the literature as the "buffering effect" mechanism. It needs to be clearly distinguished from the "direct reduction" mechanism described earlier. Such mechanistic discussions are not particular for CO_2 corrosion, as similar arguments have been put forward for various weak acids, such as acetic acid and hydrogen sulfide [56,57,86,87]. Considering a generic weak acid, HA (e.g., H_2CO_3, HCO_3^-, H_2S, HAc),

its direct reduction can be expressed as reaction (7.xxxiii). As a weak acid that is only partially dissociated in the solution, HA is also involved in homogeneous chemical equilibrium described as reaction (7.xxxiv). In addition, in acidic solutions, the H^+ reduction reaction occurs as shown in reaction (7.xxxv).

$$HA + e^- \rightarrow \frac{1}{2}H_2 + A^- \tag{7.xxxiii}$$

$$HA \rightleftharpoons H^+ + A^- \tag{7.xxxiv}$$

$$H^+ + e^- \rightarrow \frac{1}{2}H_2 \tag{7.xxxv}$$

The "direct reduction" mechanism suggests that HA reduction (reaction 7.xxxiii) is significant; therefore the cathodic currents in acidic solutions are the result of two electrochemical reactions, HA reduction and H^+ reduction. On the other hand, the "buffering effect" mechanism suggests that, reaction (7.xxxiii), the reduction of HA, is insignificant as compared to reaction (7.xxxv), the reduction of H^+. Therefore, the dominant cathodic reaction in acidic solutions is H^+ reduction, while HA buffers the concentration of H^+ ions at the surface through the homogeneous reaction (7.xxxiv).

These two mechanisms may be qualitatively distinguished by studying the behavior of charge transfer controlled cathodic currents [57,86]. If the concentration of the common reactant between the two possible mechanisms (H^+) is kept constant, each mechanism shows a distinct behavior as the concentration of the weak acid is increased (Fig. 7.2) [86]. For the case of the "buffering effect" mechanism, no significant change in charge transfer controlled currents is expected, because the weak acid is not electrochemically active. On the other hand, for the "direct reduction" mechanism the charge transfer controlled cathodic currents are increased as the concentration of the reactant (the weak acid) is increased. Note that the magnitudes of the limiting current in both mechanisms are identical. In addition, as shown in Fig. 7.2(a), in certain conditions a secondary limiting current wave may also be observed in the case of "direct reduction" mechanism.

Examples for both mechanisms at play are available from experimentation, as shown in Fig. 7.3. In Fig. 7.3(a) it is demonstrated that H_2S follows the direct reduction mechanism with a clear secondary limiting current observed at moderate and high H_2S concentrations [56]. On the other hand, the buffering effect mechanism was shown to be the dominant reaction pathway in the case of acetic acid reduction (Fig. 7.3(b)), where no significant change in charge transfer controlled currents were observed with acetic acid (HAc) concentrations up to 500 mass ppm [86].

Considering the possibilities of the "direct reduction" and "buffering effect" mechanisms, Tran et al. focused on the study of the H_2CO_3 reduction reaction [88]. The authors noted that, even at higher CO_2 partial pressures the pure charge transfer controlled cathodic currents are not clearly observed on an X65 mild steel surface and that this hypothetical behavior cannot be easily verified. Therefore, the stainless

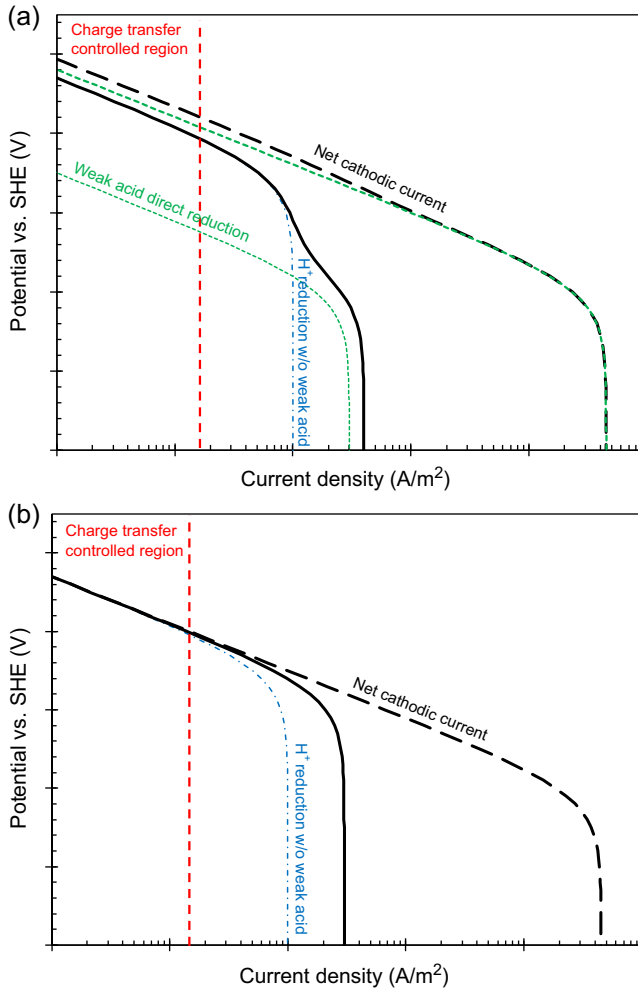

Figure 7.2 Hypothetical cathodic steady state voltammograms at a constant pH and two different concentrations of a weak acid (*solid black line* < *dashed black line*). *Black lines*: net current, *dotted-dashed blue lines*: H^+ reduction without weak acid present, and *dashed green lines*: weak acid direct reduction. (a) Direct reduction mechanism and (b) buffering effect mechanism. *SHE,* standard hydrogen electrode.

steel electrodes, being a nobler substrate, was used to eliminate the interference by the anodic iron dissolution reaction. By comparing the steady-state voltammograms for pH 4 and pH 5 at 1 and 10 bar CO_2 partial pressures, the authors reported a behavior resembling that shown in Fig. 7.2(b) and hence concluded that the cathodic currents in CO_2-saturated solutions follow the "buffering effect" mechanism [88]. However, considering the effect of alloying compounds of stainless steel (~20 wt% Cr and 10 wt% Ni) and their corresponding passive films, on the electroactivity of the metal

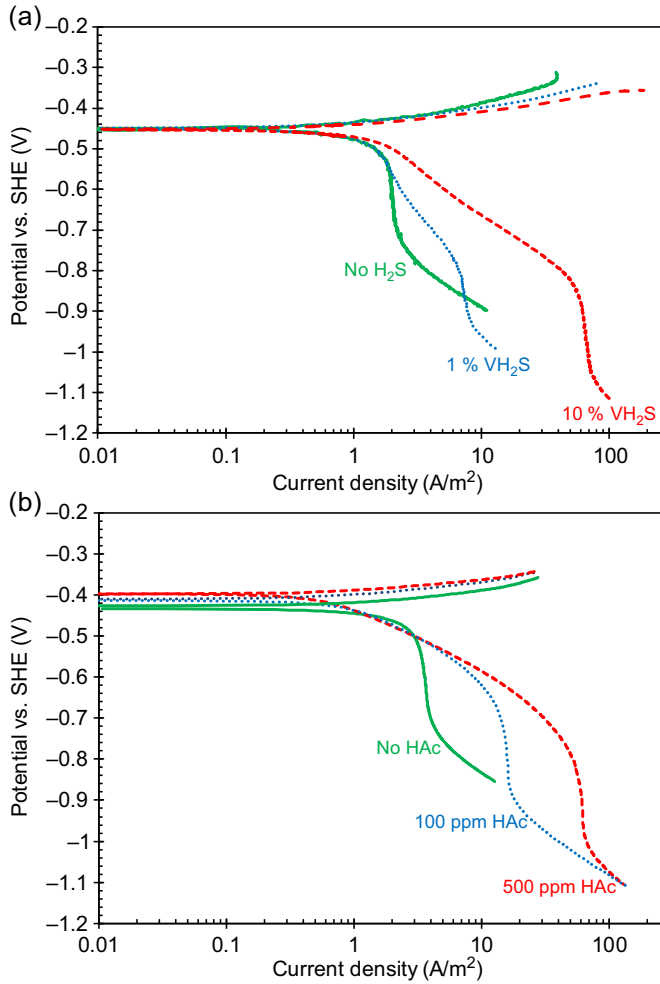

Figure 7.3 Polarization behavior of X65-API mild steel at pH 4 and 30°C (86°F). (a) H_2S system with total pressure = 1 bar (14.5 psi), 1000 rpm rotating cylinder electrode and various pH_2S expressed in volume percent. (b) Acetic acid (HAc) system at 2000 rpm rotating disk electrode and various total HAc concentrations expressed in mass fraction. *SHE,* standard hydrogen electrode.
(a) Data taken from Y. Zheng, B. Brown, S. Nešic, Electrochemical study and modeling of H_2S corrosion of mild steel, Corrosion 70 (2014) 351−365. (b) Data taken from A. Kahyarian, B. Brown, S. Nesic, Mechanism of cathodic reactions in acetic acid corrosion of iron and mild steel, Corrosion 72 (2016) 1539−1546.

surface, the observed mechanism for cathodic currents cannot be applied to mild steel without further verifications.

The discussion in this section shows a continuous development in understanding the fundamental mechanism of cathodic reactions involved in CO_2 corrosion over the years. Despite that, there are still various important aspects that remain

controversial and require further investigations. The effect of CO_2 and carbonated species on the mechanism of iron dissolution reaction, the electrochemical mechanism of hydrogen evolution reactions, and the significance of direct H_2CO_3 and HCO_3^- reduction are among the subjects that require further elucidation.

7.3.5 Effect of mass transfer

In CO_2 corrosion, in addition to the homogeneous chemical reactions as discussed in Section 7.3.4, the mass transfer from the bulk solution is another process replenishing the concentration of the corrosive species at the metal surface as they are consumed in the corrosion process. The importance of mass transfer is acknowledged in many studies [89–92]. For example, Fig. 7.4 demonstrates the effect of fluid velocity on the observed corrosion rates at 1 bar (14.5 psi) CO_2 and various pH values. The increase of corrosion rate by increasing the fluid velocity suggests that corrosion currents are under mass transfer influence at this specific conditions. However, the effect of the fluid velocity on the corrosion rate may decrease, if the solution is highly buffered (e.g., high CO_2 partial pressure ($P_{CO_2} > 10$ bar(145 psi)) [93], or in the presence of organic acids [67]). In such conditions the limiting current is significantly increased by the high rate of the chemical reactions and the corrosion rate is controlled by the rate of electrochemical reactions, which are not influence by the mass transfer rate.

The mass transfer in a corroding system consists of a molecular diffusion component, induced by the concentration gradient of the chemical species; an electromigration component, as the result of ionic movement in the presence of an electric field; and a convective flow component due to the movement of the bulk solution. The flux of each chemical species (i) involved in the corrosion process may therefore be expressed through the well-known Nernst–Planck equation:

$$N_i = -D_i \nabla C_i - z_i u_i F C_i \nabla \phi + v C_i \tag{7.4}$$

The term "vC_i" represents the convective flow toward the metal surface. In turbulent flow regime, commonly observed in transmission pipelines, turbulent mixing dominates the bulk movement of the fluid and can be characterized in terms of eddy diffusivity and lumped in with the molecular diffusion term.

Considering the typical conditions of CO_2 corrosion, Eq. (7.4) can be simplified by assuming the electromigration term is negligible. This assumption is valid in free corroding, nonpolarized systems with sufficient ionic strength, where the potential gradient inside the solution ($\nabla\phi$) is small. In its simplest form, the flux of chemical species can be described by the mass transfer coefficient (k_m) as shown in Eq. (7.5), where the mass transfer coefficient can be expressed in terms of the dimensionless Sherwood number (Sh) in Eq. (7.6).

$$N_i = k_m\left(C^b - C^s\right) \tag{7.5}$$

$$k_m = \frac{ShD}{L} \tag{7.6}$$

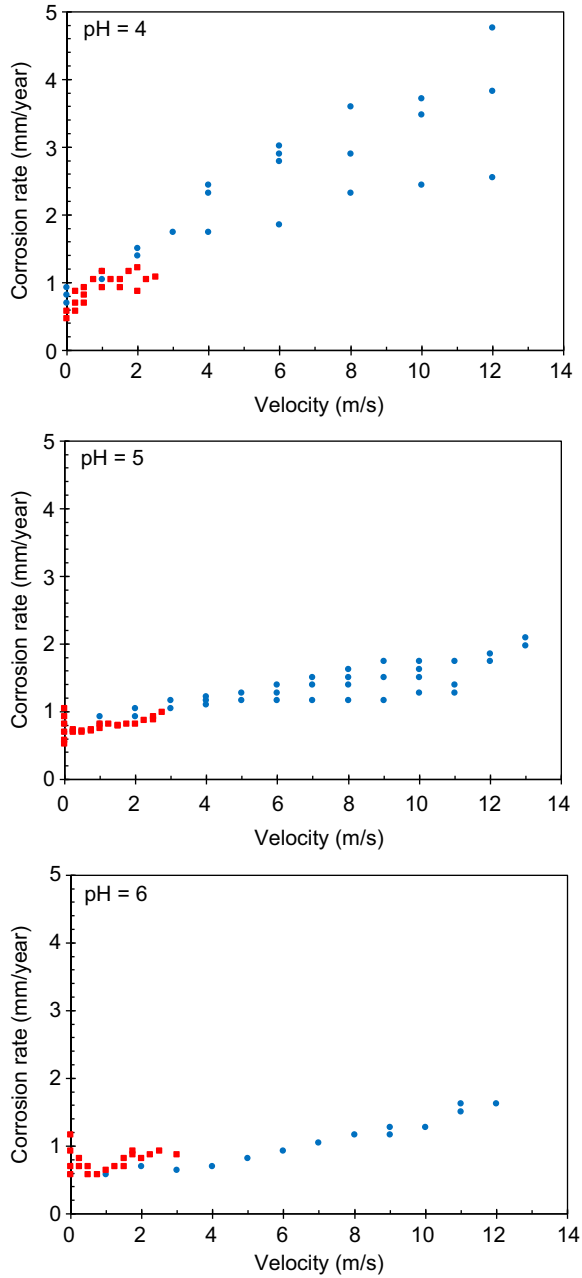

Figure 7.4 Effect of flow velocity on corrosion rate at 1 bar (14.5 psi) CO_2, 20°C (68°F), 1 wt% NaCl, and different pH values. *Blue circles*: pipe flow (15 mm ID), *red squares*: rotating cylinder (10 mm OD).
Data taken from S. Nesic, G.T. Solvi, J. Enerhaug, Comparison of the rotating cylinder and pipe flow tests for flow-sensitive carbon dioxide corrosion, Corrosion 51 (1995) 773−787.

The mass transfer coefficients for various flow regimes and geometries have been extensively studied. For the turbulent flow around a rotating cylinder electrode, the correlation of Eisenberg et al. [94] or other similar correlations can be used [95]. The mass transfer correlation in fully developed turbulent flow through smooth, straight pipes was defined by Berger and Hau [96]. For other conditions such as multiphase flow and flow around U-bends and elbows, similar correlations can also be readily found in the literature [97−101].

For an electrochemical reaction at steady state, the rate at which the electroactive species are transferred toward/away from the surface is equal to the rate of the charge transfer reaction at the surface. Therefore, the current density can also be expressed in terms of mass transfer via Eq. (7.7).

$$i = nFk_{m(C^b - C^s)} \tag{7.7}$$

In Eq. (7.7) C^b and C^s are the concentrations of the electroactive species in the bulk solution and at the metal surface, respectively. The value of C^s appearing in Eq. (7.7) and the current/potential relationships of Table 7.3 are generally unknown. However, for a first-order electrochemical reaction it can be shown that:

$$\frac{1}{i} = \frac{1}{i_{ct}} + \frac{1}{i_{\text{lim}}} \tag{7.8}$$

The i_{ct} term in Eq. (7.8) is the charge transfer controlled current, when the electrochemical reaction is proceeding without any mass transfer resistance, and it can be calculated as discussed in Section 7.3.3 knowing that $C^s = C^b$. The i_{lim} is the mass transfer limiting current that is defined by Eq. (7.7) when $C^s = 0$.

For an electrochemical reaction preceding a chemical reaction, such as H_2CO_3 reduction that follows the CO_2 hydration reaction, the limiting current is a combination of mass transfer and the chemical reaction and is obtained by simultaneous consideration of both processes. A composite limiting current calculation for H_2CO_3 reduction on a rotating disk electrode was implemented in the model developed by Gray et al. [15,30], and it is described in detail elsewhere [102]. Similar theoretical calculations for turbulent flow regimes of rotating cylinder electrode and straight pipe flow were developed and implemented by Nešić et al. [103,104]. The mathematical expression developed by Nešić et al. is shown in Eq. (7.9) [103]. In a sense, this equation is the chemical reaction limiting current multiplied by a correction factor (the $\coth(\delta_d/\delta_r)$ term) to account for the effect of turbulent mixing.

$$i_{\text{lim},H_2CO_3} = n_{H_2CO_3} F C^b_{H_2CO_3} \left(D k_{b,\text{hyd}}\right)^{1/2} \coth \frac{\delta_d}{\delta_r} \tag{7.9}$$

$$\delta_d = D/k_m \tag{7.10}$$

$$\delta_r = \left(D/k_{b,\text{hyd}}\right)^{1/2} \tag{7.11}$$

The CO_2 corrosion of mild steel is also often accompanied by the formation of a corrosion product layer. The deposited corrosion product on the steel surface can be characterized as a solid porous layer that acts as an additional mass transfer barrier. In this case, the limiting current appearing in Eq. (7.8) can be calculated using a composite mass transfer coefficient to account both for the flow effect and the resistance caused by the corrosion product layer. This composite mass transfer coefficient follows Eq. (7.12), where k_m is the mass transfer coefficient due to the flow, as shown in Eq. (7.5), and k_d is the mass transfer coefficient inside the porous layer.

$$\frac{1}{k_{\text{comp.}}} = \frac{1}{k_m} + \frac{1}{k_d} \tag{7.12}$$

The mass transfer coefficient inside the corrosion product layer, k_d, can be quantified as diffusion through a porous medium:

$$k_d = \frac{\varepsilon \tau D}{\delta_l} \tag{7.13}$$

In Eq. (7.13), the ε and τ terms are porosity and tortuosity of the corrosion product layer, respectively, D is the diffusion coefficient, and δ_l is the corrosion product layer thickness. In addition to decreasing the mass transfer of the corrosive species to the surface, the solid corrosion product layers impede corrosion also by covering/blocking the steel surface at locations where they are attached, making them unavailable for electrochemical reactions (see Fig. 7.5). A more detailed description of the corrosion product layers is given in the following chapter.

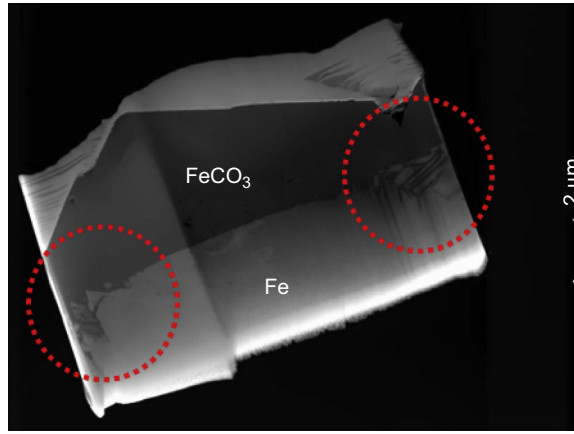

Figure 7.5 A transmission electron microscope image of mild steel surface with iron carbonate corrosion product layer. Little corrosion is seen at locations where iron carbonate is attached to the steel surface with most of the attack happening in the highlighted area between iron carbonate grains.
Adapted from Jiabin Han, Galvanic Mechanism of Localized Corrosion for Mild Steel in Carbon Dioxide Environments (Doctoral dissertation), Ohio University, 2009.

7.4 Corrosion product layers

In CO_2 corrosion, one almost always encounters formation of corrosion product layers. These will typically be made up of one or more of the following compounds:

- iron carbide (cementite)
- iron carbonate (siderite)
- iron oxide (magnetite)

7.4.1 Iron carbide (Fe_3C)

Iron carbide (Fe_3C) is often labeled as the uncorroded portion of the steel. It is primarily associated with mild steels having a high carbon content and a ferritic-pearlitic microstructure. During corrosion of such steel, the ferrite phase dissolves and a porous iron carbide network is exposed (see Fig. 7.6). Given that iron carbide is an electronic conductor, this porous network serves as an additional cathodic surface for reduction of corrosive species, which would lead to an increase in the corrosion rate. On the other

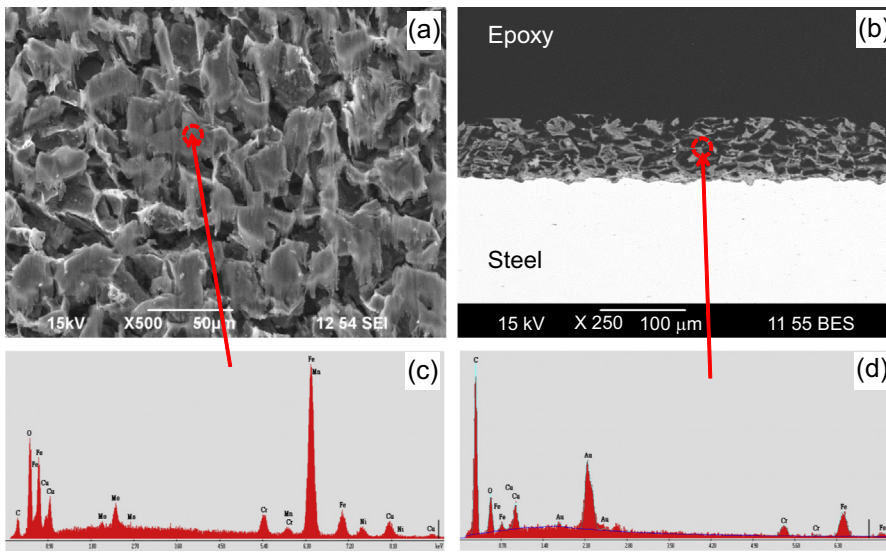

Figure 7.6 A cross-section of a mild steel specimen after 41 h of exposure in a 3 wt% NaCl aqueous solution, 80°C (176°F), pH 6, $pCO_2 = 1$ bar (14.5 psi). Scanning electron microscopy images of the (a) top view showing the iron carbide network, (b) cross-section view, and (c) and (d) the respective energy dispersive spectroscopy spectrum [105].

hand, it also presents an additional diffusion barrier, making it harder for the corrosive species to reach the steel surface, which would lead to a slight decrease in the corrosion rate. The porous iron carbide network also makes it harder for the ferrous ions to diffuse away into the bulk solution, enhancing their buildup at the steel surface. With other conditions being favorable (e.g., elevated temperature) this may lead to precipitation of protective iron carbonate within the pores of the iron carbide corrosion product layer (discussed later), dramatically decreasing the corrosion rate (see Fig. 7.7). Finally, the porous iron carbide corrosion product layer can also impede organic corrosion inhibitors from adsorbing on the underlying steel surface, although how and why this happens is not properly understood. Owing to this multitude of opposing effects, the overall influence of iron carbide corrosion product layers on CO_2 corrosion of mild steel is often simply ignored; however, research is underway to further qualify and quantify these effects.

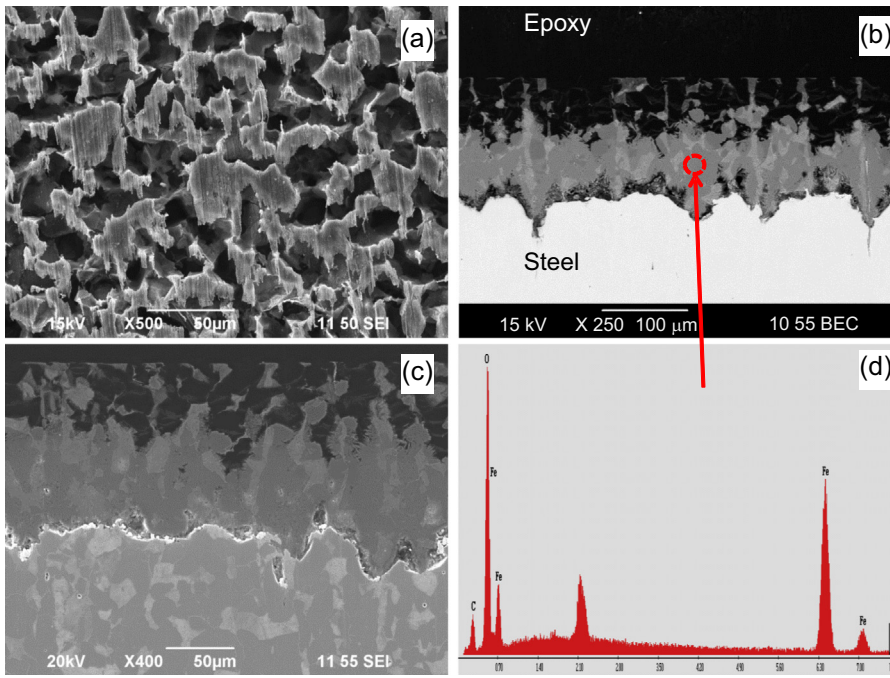

Figure 7.7 A cross-section of a mild steel specimen after 90 h of exposure in a 3 wt% NaCl aqueous solution, 80°C (176°F), pH 6, $pCO_2 = 1$ bar (14.5psi). Scanning electron microscopy images of the (a) top view showing the iron carbide network, (b) cross-section view, and (c) and (d) the respective energy dispersive spectroscopy spectrum. The steel surface cross-section (c) was etched with 2% Nital [105].

7.4.2 Iron carbonate ($FeCO_3$)

When the buildup of ferrous ions in the CO_2 aqueous solution exceeds the solubility of iron carbonate, it will precipitate according to reaction (7.xxxvi).

$$Fe^{2+} + CO_3{}^{2-} \rightarrow FeCO_3 \tag{7.xxxvi}$$

As discussed earlier, a porous iron carbonate corrosion product layer formed on the steel surface can slow down the corrosion process by presenting a diffusion barrier for the species involved in the corrosion process and by covering/blocking a portion of the steel surface and protecting it from corrosion.

Iron carbonate corrosion product layer morphology and its protectiveness strongly depend on the precipitation rate. The other important factor is corrosion of the underlying steel surface, which continuously "undermines" the iron carbonate layer. As voids are being created by corrosion, they are filled by the ongoing precipitation, with the final morphology and ultimately its protectiveness hanging in the balance. When the rate of precipitation largely exceeds the rate of undermining by corrosion, a dense well-attached and protective layer forms, sometimes very thin ($\sim$1−10 μm) but still protective (see Fig. 7.8). Vice versa, when the corrosion process undermines the newly formed scale faster than precipitation can fill in the voids, a porous and unprotective layer forms, which can sometimes be very thick ($\sim$10 m−100 μm) and still be unprotective. Therefore, it is not the thickness and overall appearance of the iron carbonate layer that are best indicators of its protectiveness, rather it is the density and particularly the degree of attachment to the steel surface that are dominant.

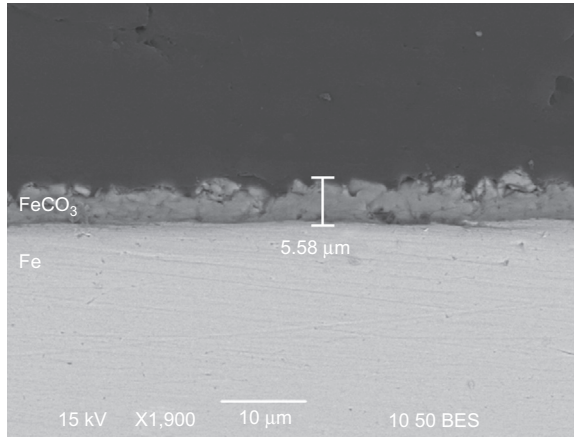

Figure 7.8 Scanning electron microscopy images of a cross-section of a mild steel specimen after 72 h of exposure in a 3 wt% NaCl aqueous solution, 80°C (176°F), pH 6.6, $pCO_2 = 0.5$ bar (7.25 psi), showing a thin and protective iron carbonate corrosion product layer.

Many factors affect the formation of iron carbonate corrosion product layers. The most important one is water chemistry, and the concept of supersaturation, which is defined as:

$$S_{FeCO_3} = \frac{C_{Fe^{2+}} C_{CO_3^{2-}}}{K_{sp}} \tag{7.14}$$

where K_{sp} is the iron carbonate dissolution equilibrium constant [106]. Owing to the relatively slow kinetics of iron carbonate precipitation, supersaturation with respect to iron carbonate has to be greatly exceeded (by a factor of 10−100) to form a protective iron carbonate layer. This usually happens at high pH, which is a key precondition for protective iron carbonate layer formation (pH > 6). It should be pointed out that this refers to the pH at the steel surface where precipitation happens, which is always higher than pH in the bulk, often by a whole pH unit or even two, particularly in the presence of other types of diffusion barriers such as iron carbide layers described earlier. Temperature is another very important factor. At room temperature, the process of iron carbonate precipitation is very slow and unprotective layers invariably form, even at very high supersaturation values. Conversely, at higher temperatures [T > 60°C (140°F)] precipitation proceeds rapidly enough to yield dense, well-attached, and very protective surface layers, even at low supersaturation.

7.4.3 Iron oxide (Fe_3O_4)

At even higher temperatures [T > 100°C (212°F)] iron oxide (magnetite) will form in CO_2 aqueous solutions. When thermodynamic conditions are favorable for the formation of magnetite (high pH and high temperature), it appears rapidly, forming a very

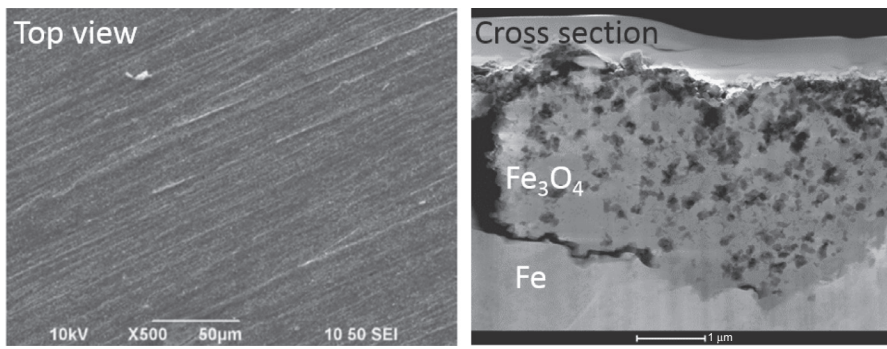

Figure 7.9 Scanning electron microscopy image of the top surface and transmission electron microscopy image of the cross-section of steel surface exposed for 4 days at 200°C (392°F), pCO_2 = 1 bar (14.5 psi) at 25°C (77°F), 1 wt% NaCl.
Reproduced with permission from Tanaporn Tanupabrungsun, Thermodynamics and Kinetics of Carbon Dioxide Corrosion of Mild Steel at Elevated Temperatures (Doctoral dissertation), Ohio University, 2013.

thin (~1 μm) and very protective layer, tightly adhering to the steel surface (see Fig. 7.9). When a magnetite layer forms, the corrosion rates typically decrease by one order of magnitude or more. Actually, there are indications that some magnetite forms even at temperatures lower than 100°C (212°F) and is often very hard to detect as it appears in small quantities in cavities and pores of the iron carbonate corrosion product layer, contributing to overall protectiveness.

Other salts can precipitate to form even more complex surface layers that may affect the corrosion rate. The most important are iron sulfides, which form in H_2S-containing aqueous solutions, covered elsewhere in this monograph. Scales containing calcium carbonate, barium sulfate etc., may form in environments containing formation water, also affecting the protectiveness of surface layers [107]. A more complete analysis of scaling and factors that affect it is beyond the scope of the present review.

7.5 Additional aqueous species

The CO_2 corrosion is often complicated by the presence of additional aqueous species. Most important examples are:

- Organic acids
- Hydrogen sulfide
- Chlorides

7.5.1 Organic acids

The first reports on the effect of organic acid in CO_2 corrosion of mild steel appeared in the 1940s, where it was shown that even concentrations as low as 300 ppm can cause severe corrosion of pipeline steel [108]. A number of low-molecular-weight, water-soluble, organic/carboxylic acids are found in oil-field brines, such as formic acid (HCOOH) and propionic acid (CH_3CH_2COOH); however, acetic acid (CH_3COOH or shortly HAc) is by far the most prevalent organic acid causing corrosion problems for mild steel. In 1983, Crolet and Bonis reported that the presence of HAc in the brine increased the corrosion rate of mild steel significantly [109]. Subsequently, carbon dioxide corrosion in the presence of acetic acid has been the subject of numerous studies. These include laboratory investigations in model systems using electrochemical methods, such as cyclic voltammetry [110,111], potentiodynamic sweeps [86,112,113], electrochemical impedance spectroscopy [114,115], as well as corrosion experiments using field brines [109,116,117]. The detrimental effect of acetic acid was primarily seen at high temperatures (>50°C) and in the lower pH range (pH 3.5−5.0). Similar to carbonic acid, HAc is also a weak, partially dissociated acid, according to reaction (7.xxxvii).

$$HAc_{(aq)} \rightleftharpoons H_{(aq)}^{+} + Ac_{(aq)}^{-} \tag{7.xxxvii}$$

The pH determines the distribution of the acetic species in the solution, as shown in Table 7.5 for a typical pH range of oil-field brines. Clearly, at pH 4, corresponding to a pure water/CO_2 system seen, for example, in condensed water, most of the acetic

Table 7.5 Acetic acid species distribution at various pH values at 80°C (176°F)

pH	[HAc]/mol%	[Ac^-]/mol%
4	88	12
5	42	58
6	6.8	93.2
6.6	1.8	98.2

species are in the form of undissociated acid. The opposite is true at pH 6.6, typical for heavily buffered brines, where most of the acetic species are in the form of acetate ion.

Similar to the case of carbonic acid corrosion, the mechanism of acetic acid corrosion has been intensely debated in the last 2 decades. Although many studies suggest that the increased corrosion rates in the presence of acetic acid is due to its direct reduction at the metal surface [32,111,115,118–121], others suggest that acetic acid corrosion follows the buffering effect mechanism [57,67,122,123]. It has now been established that the buffering effect is dominant [57,86] and that the most influential factor is the concentration of the undissociated ("free") acetic acid and not the acetate ion. Therefore, one can appreciate that the organic acids are a major corrosion concern primarily at lower pH values [114,124]. The overall corrosion reaction due to acetic acid can be written as reaction (7.xxxviii).

$$Fe_{(s)} + 2HAc_{(aq)} \rightarrow Fe_{(aq)}{}^{2+} + 2Ac_{(aq)}{}^{-} + H_{2(aq)} \quad \text{(7.xxxviii)}$$

Another aspect of the acetic acid effect is related to how it affects protective corrosion product layers typically found on the steel surface exposed to aqueous CO_2 solutions. Iron acetate is very soluble and is not found as a solid deposit on the steel surface in the pH range of interest in the oil and gas industry. However, iron carbonate, which is often present, can be protective as described earlier. There seems to be an interaction where acetic acid leads to destabilization of protective iron carbonate layers that may result in localized attack, although the mechanism is not known clearly [122,125–127]. This is the subject of some ongoing investigations.

7.5.2 Hydrogen sulfide

Corrosion of mild steel in the presence of aqueous hydrogen sulfide (H_2S) has also been extensively investigated in the last few decades [56,59,60,74,87]. Aqueous H_2S is another weak acid that affects the speciation and is directly involved with the electrochemical reactions at the steel surface. It was confirmed that hydrogen sulfide follows the direct reduction mechanism (see Section 7.3.4) [56,59,60]. A number of different solid iron sulfides can form as corrosion product layers, some of which are protective. This topic is covered in a separate chapter in the present monograph and will not be discussed here any further.

7.5.3 Chlorides

A very common species found in oil-field brines is the aqueous chloride (Cl^-) anion, which can be present anywhere from a fraction of a percent to over 10% by weight. Chlorides are generally considered to be detrimental in CO_2 corrosion of mild steel and are often lumped in with aqueous CO_2, organic acids, and H_2S, even if they are neither acidic species nor electroactive. Many of the arguments about the detrimental effect of chlorides are either purely circumstantial or are blindly transposed from systems involving stainless steel corroding in aerated solutions, which is clearly inadequate. Actually, it was shown that uniform CO_2 corrosion rate of mild steel significantly decreases with an increase of chloride concentration (above a few wt%) [128,129]. This is due to a retardation of homogenous physicochemical processes underlying corrosion, such as diffusion and chemical reactions, occurring in nonideal solutions loaded with chlorides.

On the other hand, the presence of chlorides increases electrical conductivity of the solution, and in the case of nonideal solutions, it increases the solubility of solid corrosion products. This has been thought to be the reason for failure of protective iron carbonate corrosion product layers and localized corrosion in brines with high chloride concentrations. However, it is still not clear if this effect is specific to chlorides or is a generic effect caused by nonideality and high conductivity of the electrolyte.

7.6 Multiphase flow effects

In the field, CO_2 corrosion almost always happens in flowing solutions and often in the context of multiphase flow. Multiphase flow can be defined as the concurrent flow of substances having two or more *phases*. A *phase* refers to a state of a substance, such as gas, liquid, or solid. The term *multiphase flow* is used also to refer to the concurrent flow of two or more substances that are of the same phase but do not mix and are either present as continuous or dispersed in the other [130]. In pipes, a variety of multiphase flow patterns may arise [131]. These flow patterns are often represented as bounded areas in a two-dimensional graph, termed a *flow pattern map* or *flow regime map*. An example of a flow pattern map is given in Fig. 7.10. The boundaries on the map are the transition lines, which are a function of flow rates, fluid physical properties, and pipe orientation [132].

Theoretically, there are two main ways that flow may affect CO_2 corrosion of mild steel: through *mass transfer* or via *mechanical means*. Turbulent flow enhances mass transport of species to and away from the steel surface by affecting transport through the boundary layer as described in Section 7.3.5. It has been argued that mass transfer often plays a relatively small role, as the CO_2 corrosion rate is often controlled by charge transfer or is limited by a slow chemical CO_2 hydration step, or is controlled by a protective corrosion product layer, as mentioned in Section 7.3. On the other hand, intense flow could theoretically lead to mechanical damage of protective iron carbonate corrosion product layers or inhibitor films. Both these mechanisms are aggravated by flow disturbances, such as valves, constrictions, expansions, and bends,

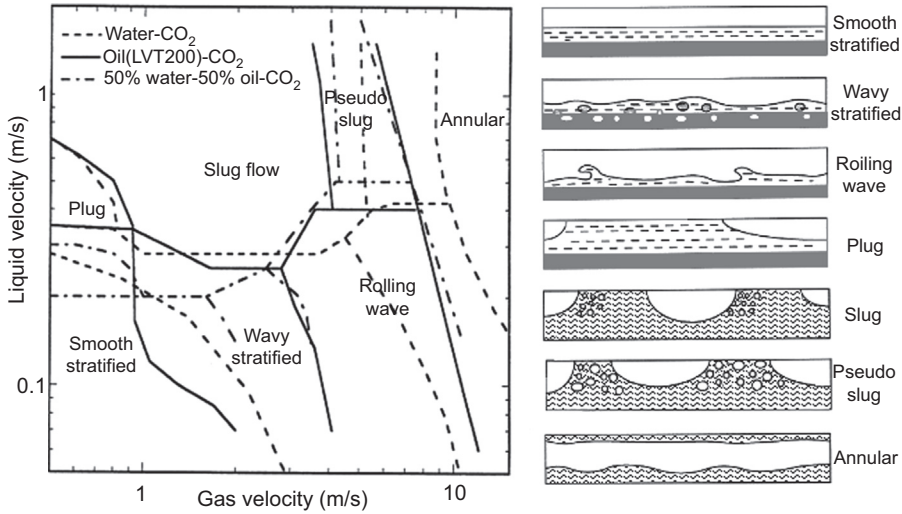

Figure 7.10 Three-phase flow patterns and flow pattern map. Transitions for two-phase flow were included in the map for comparison.
Reprint with permission from K. Kee, A Study of Flow Patterns and Surface Wetting in Gas-Oil-Water Flow (Doctoral dissertation), Ohio University, 2014.

where a local increase of near-wall turbulence is seen. The same is true for some multiphase flow regimes, which are commonplace in the field.

When it comes to the mechanical effects of flow on corrosion, the wall shear stress (WSS) has often been used as the relevant parameter to characterize this interaction. The operating hypothesis was that at some sufficiently high WSS the hydrodynamic forces at the corroding steel surface may lead to mechanical damage of the protective corrosion product layers or inhibitor films.

In single-phase liquid flow, the WSS can be readily calculated and is typically of the order of 1−10 Pa. In horizontal two-phase gas−liquid flow, laboratory investigations at atmospheric conditions have shown that the maximum WSS is of the order of 100 Pa, obtained in the slug flow regime [133]. Using mathematical modeling, it is estimated that the highest practical wall shear stress that could be expected in multiphase flow seen in the field is of the order of 1000 Pa [133]. These values are several orders of magnitude lower than the reported adhesion strength of inhibitor films or protective iron carbonate layers, which are of the order of 10^6 Pa or even higher [133−136]. This suggests that mechanical removal of protective films or layers solely by mechanical forces (WSS) typically seen in the field is very unlikely. The only exception are some very specific multiphase flow conditions that lead to cavitation or droplet impingement, when very large short-lived hydrodynamic stress fluctuations at the pipe wall are seen that can damage the protective inhibitor films and corrosion product layers, leading to localized attack. Even in those cases, using excess corrosion inhibition makes it possible to overcome the problem [137].

Another very important feature of multiphase flow is related to the so-called water wetting. Internal corrosion in pipelines occurs only if the water phase wets the internal

steel surface, a condition termed *water wetting*. When oil is in contact with the internal pipe surface, a scenario called *oil wetting*, corrosion cannot occur. The multiphase flow factors that lead to one or the other scenario are primarily water cut (amount of water), flow regime, and pipe orientation [138,139]. These factors influence the physical distribution of fluids across the pipe cross-section and across the length of the pipeline. Another factor that affects water wetting is wettability (ability to wet a surface), which is a function of the state of the steel surface and the chemical compositions of the aqueous and hydrocarbon phases. Stable water wetting is most often encountered in horizontal oil−water and oil−water−gas multiphase flow. At a low flow rate, the water flows separately as a continuous phase at the bottom of the line and can lead to corrosion. As the flow rate increases, and the main flow gains sufficient turbulence, this leads to gradual water entrainment and a transition to oil wetting, decreasing the likelihood of corrosion. However, even at high flow rates, when most of the water is entrained, it is possible to have water accumulate at low spots in the line, leading to corrosion.

The presence of solids, such as produced sand, and other inorganic and organic solid matter further complicates the effects of multiphase flow on corrosion. At high flow rates, the entrained solids may impinge on the internal pipe wall and lead to mechanical removal of any protective layer and, in extreme cases, the erosion of the underlying steel itself. This effect is particularly pronounced at flow disturbances, such as tees, valves, bends, constrictions, and expansions, and in intermittent flow patterns, such as slug and churn flow [140,141]. At the other end of the spectrum, at very low flow rates, settling of solids may occur, leading to so-called under-deposit corrosion [142,143]. Under-deposit corrosion becomes an issue when corrosion inhibitors are unable to penetrate through the solids and cannot protect the surface covered by the porous layer of solids, or when this layer leads to initiation of microbiologically induced corrosion.

Dewing corrosion often termed *top-of-line-corrosion* (TLC) occurs in wet gas pipelines, when there is a significant temperature difference between the transported fluids and the outside environment. When the gas/liquid flow is stratified, saturated water vapor condenses and forms water droplets on the side and the top of the internal walls of the pipeline. These quickly become saturated with acid gases (CO_2, H_2S, organic acids), leading to corrosion [144−146]. There is no simple mitigation method available, especially considering that the use of standard corrosion inhibitors is not feasible as they are typically liquids that do not readily evaporate and cannot reach the affected portions of the pipeline. This type of attack is very dependent on the rate of water condensation, temperature, and solubility of corrosion products. A key aspect of understanding the mechanism is the interaction between water condensation, corrosion, evolution of the chemistry in the condensed water, and formation of the corrosion product layers (usually iron carbonate) [147,148].

7.7 Effect of crude oil

In some cases the crude oil contains compounds that adsorb onto the steel surface either during oil wetting periods or by first partitioning into the water phase [139,149,150]. The most common surface active organic compounds found in crude

oil that have surfactant properties are those containing oxygen, sulfur, and nitrogen in their molecular structure. Furthermore, both asphaltenes and waxes have shown some beneficial inhibitive effects on corrosion [151]. Our present understanding of these phenomena is at best qualitative, making it virtually impossible to make any reliable predictions. When it comes to the effects of wetting, as described earlier, various crude oils have widely varying capacities to entrain water. Typically it takes much higher flow rates for light oils to entrain water ($v > 1.5$ m/s) because of their lower density and viscosity. Some heavier oils are able to do the same at velocities as low as 0.5 m/s. However, the chemical composition of crude oils, particularly the content of surface active substances, is just as important for wettability as are their physical properties.

7.8 Localized corrosion

There are many causes of localized CO_2 corrosion. In general, localized corrosion will occur at locations where important factors affecting corrosion (listed later in the discussion) are significantly different from elsewhere on the surface of the same structure. Such locations may therefore become local anodes with a higher local rate of iron dissolution, with respect to the rest of the structure surface. Localization of corrosion covers a broad range of length scales. In some cases, localized corrosion amounts to having a section of a pipeline measured in meters corroding much faster than the rest of the pipeline measured in kilometers (see Fig. 7.11(a)). This could happen, for example, as a result of water accumulation at a low spot in a line. On the other end of the spectrum, we can have very small pits, measured in millimeters, propagating much faster than the large surface area around it, measured in meters, that remains unaffected by corrosion. An example would be microbiological attack shown in Fig. 7.11(b), or one could have a pit micrometers in size, with millimeters of the metal surface around it not corroding at all (see Fig. 7.11(c)).

Factors that can lead to localized corrosion of mild steel in CO_2 solutions may be flow related, chemical, metallurgical, or biological. Each of these four main categories can be further refined, as follows:

- Flow-related causes of localized CO_2 corrosion
  - Mechanical (momentum transfer related)
    - Water settling and water wetting
    - Solids settling and under-deposit attack
    - Droplet impingement
    - Solids impingement and erosion
  - Thermal (heat transfer related)
    - Water condensation in wet gas flow
    - Cavitation
  - Mixing (mass transfer related)
    - Transport of corrosive species to the metal surface
    - Transport of corrosion products away from metal surface

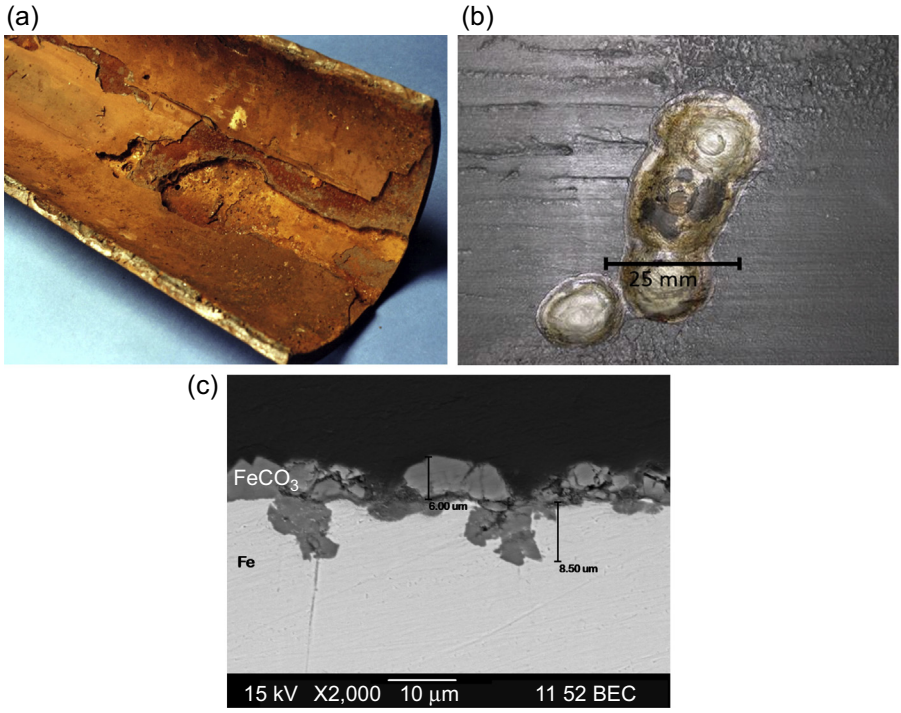

Figure 7.11 Localized corrosion at different scales. (a) Section of a pipeline exhibiting severe localized corrosion due to solids and bacteria growth at the groove. (b) Top surface of a pipeline section exhibiting a pit due to microbiologically induced corrosion attack. (c) A cross-section of mild steel surface showing failure of an iron carbonate protective corrosion product layer and localized attack due to the presence of acetic acid.

- Chemical-related causes of localized CO_2 corrosion
  - Poor or partial inhibition
  - Change of pH
  - High chlorides and/or ionic strength
  - Organic acids
  - Oxygen
  - H_2S and elemental sulfur
- Metallurgical
  - Inclusions
  - Welds
  - Iron carbide
- Biological
  - Sulfur-reducing bacteria
  - Acid-producing bacteria

In many cases, the various effects are intertwined and cannot be readily separated. For example, flow may affect the rate of chemical processes via mass transfer, leading to a rapid dissolution of a protective corrosion product layer, or a chemical change can

be at the root of biologically induced localized corrosion by acid-producing bacteria, and so on. Clearly, there are many factors whose variation across the metal surface may lead to localized corrosion, including some that may not be covered by the aforementioned list. A comprehensive explanation of all these exceeds the scope of the present review. However, in most cases the final effect amounts to local failure of a protective layer, whether a corrosion product layer or an inhibitor film. In some situations, this is aggravated by a galvanic effect that may result in localized corrosion rates exceeding the bare steel corrosion rate [152].

7.9 Inhibition of CO_2 corrosion

Mild steel corrosion can be significantly reduced by the addition of corrosion inhibitors. These inhibitors are defined as chemicals that retard corrosion when added to an environment in small concentrations [153]. Typical organic corrosion inhibitors are cationic surfactant compounds with an amphiphilic molecular structure. They are often referred to as film forming as they form very thin protective films by adsorbing at steel surfaces [154–156]. The amphiphilic inhibitor molecules consist of a polar head group and a nonpolar hydrocarbon tail. Polar head groups are often based on nitrogen-containing groups, such as amines, amides, quaternary ammonium, or imidazoline-based salts, as well as functional groups containing oxygen, phosphorus, and/or sulfur atoms. The length of a hydrocarbon tail, which is attached to a polar group, varies between 12 and 18 carbon atoms [155]. Fig. 7.12 shows some common corrosion inhibitor molecules, with thioglycolic acid included, as it is commonly added to inhibitor "packages" (complex formulations containing a wide range of compounds used in field applications).

Corrosion inhibitor molecules, being surfactant compounds, form molecular aggregates in a bulk solution when they exceed the solubility limit. The concentration at which the molecules begin to aggregate is termed the *critical micelle concentration* (CMC) [157,158]. At or above the CMC, the inhibitor molecules will form ordered molecular structures as well as adsorbed surfactant monolayers or bilayers on metal surfaces. At hydrophilic surfaces, more than one layer of surfactant molecules can form. As a result, corrosion inhibitors are more effective at concentrations above CMC than soluble inhibitor systems below the CMC [159].

The function of the polar head groups is to provide bonding between inhibitor molecules and the steel surface. This can be achieved by chemisorption, whereby polar

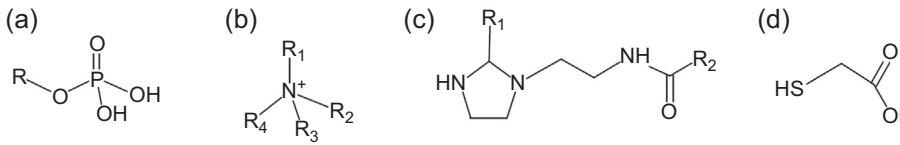

Figure 7.12 Examples of common organic corrosion inhibitors: (a) phosphate esters, (b) quaternary ammonium salts, (c) amidoethylimidazolines, and (d) thioglycolic acid.
Reprint with permission from Marian Babic, Role of Interfacial Chemistry on Wettability and Carbon Dioxide Corrosion of Mild Steels (Doctoral dissertation), Ohio University, 2017.

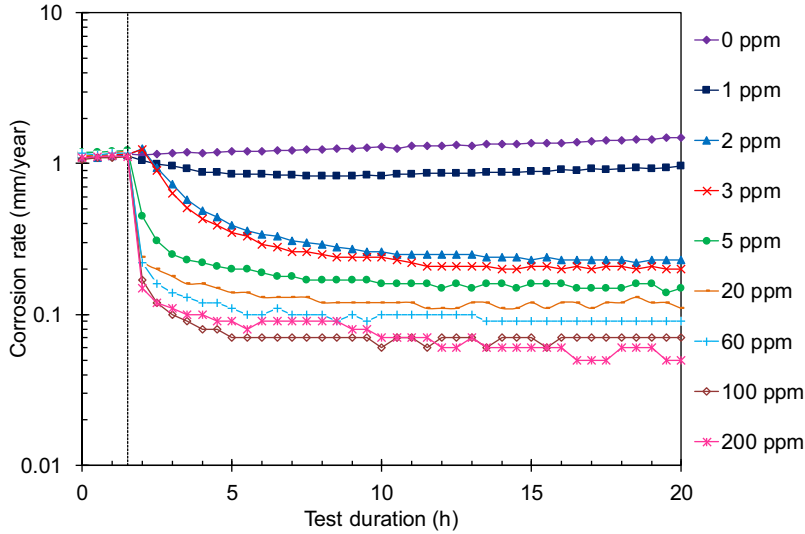

Figure 7.13 Corrosion rates obtained by linear polarization resistance measurements for different concentrations of fatty amine corrosion inhibitor. The *vertical dotted line* indicates when the inhibitor was introduced to the solution.
Data taken from C. Li, S. Richter, S. Nešić, How do inhibitors mitigate corrosion in oil-water two-phase flow beyond lowering the corrosion rate? Corrosion 70 (2014) 958−967.

groups develop intramolecular bonds at and with the surface, or by physisorption whereby they are bound to the surface by intermolecular forces [156]. Hydrophobic tails, which are facing the aqueous phase, provide a diffusion barrier for corrosive species because of steric repulsion of the hydrophobic tails [160]. Fig. 7.13 shows the measured corrosion rate as a function of inhibitor concentrations for one fatty amino surfactant-based corrosion inhibitor [161]. As can be seen from Fig. 7.13, the inhibition efficiency enhances with an increase of the inhibitor concentration.

The use of corrosion inhibitors is often considered as the most cost-effective solution for corrosion control in wells, pipelines, and production facilities carrying sweet or mildly sour wet hydrocarbons. The integrity of such structures heavily relies on the effectiveness of the corrosion inhibition program in place. Corrosion inhibition is not selected in the same way for different methods of production. Similarly, good corrosion control will vary with different fluid compositions, environmental conditions, production rates, and different flow regimes.

Gregg and Ramachandran highlighted the many different approaches for developing the proper chemistry of inhibitors for subsea applications [162]. Likewise, Cassidy provided ideas for design of inhibitors for acid corrosion mitigation [163]. One of the focus areas in corrosion inhibitor development technology is in providing environmentally safe chemicals that perform well at elevated temperatures. Inhibitor partitioning between the aqueous and hydrocarbon phases and compatibility with the other injected chemicals are additional issues that need to be considered. Interaction of inhibitors with corrosion product layers and scales, particularly various forms of iron sulfide, remains a poorly understood phenomenon.

7.10 Some field experiences and key challenges

Generally, the failure to control CO_2 corrosion in the field is often not due to the lack of understanding of corrosion, it is rather due to a failure to predict its extent and to design and implement the appropriate mitigation program. Depending on the CO_2 content, temperature, and pH, using corrosion-resistant alloys to control CO_2 corrosion is first assessed with respect to cost-effectiveness. If the cost is prohibitive, the option of using mild steel and inhibition is typically adopted. The following are some pointers indicating various types of field assets exposed to corrosion, the range of operating parameters where corrosion issues are found, and challenges to control CO_2 corrosion in the field.

Assets subject to CO_2 corrosion:

- Downhole tubing strings in gas and oil wells (e.g., rod pump wells, electrical submersible pump wells, gas lift wells)
- Casing strings exposed to production by design or due to communication through the annulus
- Wellhead equipment
- Flow lines
- Facilities (e.g., compressors, pumps, tanks, separators, valves)
- Transfer lines and piping
- Wet gas pipelines
- Oil export pipelines

Typical operating parameters:

- CO_2 content: 0.2−40 mol% in the gas phase
- Temperature: 16°C (60°F)−163°C (325°F)
- pH range: 3.5−6.5
- Flow regimes: slug, annular mist, stratified
- Flow rates: liquid velocities: 0.5−5 m/s, gas velocities: 5−20 m/s

Some of the key challenges are grouped in the following as *mechanism and prediction*, *inhibition*, and *monitoring/inspection*.

- Mechanism and prediction:
  - There is a lack of prediction models for CO_2 pitting corrosion; laboratory testing is not always possible and might not properly simulate the actual field conditions.
  - Prediction of CO_2 corrosion with traces of H_2S present in the production system is unreliable.
  - Synergy between CO_2 corrosion and erosion in rod pump wells.
  - Integrity of iron carbonate corrosion product layers and their effect on the corrosion rate.
- Inhibition:
  - Inhibitor effectiveness in high-temperature high-pressure environments: lack of clear limits of temperature and CO_2 content for effective inhibition.
  - Inhibitor ability to suppress pitting, to control preferential weld corrosion, and to perform in the presence of solids.
  - Inhibitor partitioning into the water phase.
  - Inhibitor transport in pipelines, in particular in wet gas pipelines, to manage TLC.
  - Application of corrosion inhibitors for downhole treatments.

- Prediction of corrosion inhibitor persistency for batch applications.
- Environment friendly "green" chemistries with acceptable effectiveness and cost.

- Monitoring/inspection:
  - Interpretation of caliper survey pitting data for wells.
  - Interpretation of ILI (in Line Inspection) magnetic flux leakage and ultrasonic testing survey data for pipelines.
  - Monitoring of corrosion inhibitor residuals.
  - Prediction of critical corrosion locations for monitoring program design.

References

[1] W. Stumm, J.J. Morgan, Aquatic Chemistry: Chemical Equilibria and Rates in Natural Waters, 1995.
[2] R.E. Zeebe, D. Wolf-Gladrow (Eds.), CO_2 in Seawater: Equilibrium, Kinetics, Isotopes, Elsevier, 2001.
[3] J.N. Butler, Carbon Dioxide Equilibria and Their Applications, CRC Press, 1991.
[4] Z. Duan, R. Sun, An improved model calculating CO_2 solubility in pure water and aqueous NaCl solutions from 273 to 533 K and from 0 to 2000 bar, Chemical Geology 193 (2003) 257−271.
[5] Z. Duan, D. Li, Coupled phase and aqueous species equilibrium of the $H_2O-CO_2-NaCl-CaCO_3$ system from 0 to 250°C, 1 to 1000 bar with NaCl concentrations up to saturation of halite, Geochimica et Cosmochimica Acta 72 (2008) 5128−5145.
[6] Z. Duan, R. Sun, C. Zhu, I.-M. Chou, An improved model for the calculation of CO_2 solubility in aqueous solutions containing Na^+, K^+, Ca^{2+}, Mg^{2+}, Cl^-, and SO_4^{2-}, Marine Chemistry 98 (2006) 131−139.
[7] D. Li, Z. Duan, The speciation equilibrium coupling with phase equilibrium in the H_2O-CO_2-NaCl system from 0 to 250°C, from 0 to 1000 bar, and from 0 to 5 molality of NaCl, Chemical Geology 244 (2007) 730−751.
[8] D.A. Palmer, R. Van Eldik, The chemistry of metal carbonate and carbon dioxide complexes, Chemical Reviews 83 (1983) 651−731.
[9] R.F. Weiss, Carbon dioxide in water and sea water: the solubility of a non-ideal gas, Marine Chemistry 2 (1974) 203−215.
[10] T. Barth, Organic acids and inorganic ions in waters from petroleum reservoirs, Norwegian continental shelf: a multivariate statistical analysis and comparison with American reservoir formation waters, Applied Geochemistry 6 (1991) 1−15.
[11] T.I.R. Utvik, Chemical characterization of produced water from four offshore oil production platforms in the North Sea, Chemosphere 39 (1999) 2593−2606.
[12] J. Han, J. Zhang, J.W. Carey, Effect of bicarbonate on corrosion of carbon steel in CO_2 saturated brines, International Journal of Greenhouse Gas Control 5 (2011) 1680−1683.
[13] G.I. Ogundele, W.E. White, Some observations on corrosion of carbon steel in aqueous environments containing carbon dioxide, Corrosion 42 (1986) 71−78.
[14] G.I. Ogundele, W.E. White, Observations on the influences of dissolved hydrocarbon gases and variable water chemistries on corrosion of an API-L80 steel, Corrosion 43 (1987) 665−673.
[15] L.G.S. Gray, B.G. Anderson, M.J. Danysh, P.R. Tremaine, Effect of pH and temperature on the mechanism of carbon steel corrosion by aqueous carbon dioxide, in: CORROSION 90, Paper No. 40.

[16] J.O. Bockris, D. Drazic, The kinetics of deposition and dissolution of iron: effect of alloying impurities, Electrochimica Acta 7 (1962) 293−313.
[17] F. Hibert, Y. Miyoshi, G. Eichkorn, W.J. Lorenz, Correlations between the kinetics of electrolytic dissolution and deposition of iron, Journal of the Electrochemical Society 118 (1971) 1919−1926.
[18] A. Atkinson, A. Marshall, Anodic dissolution of iron in acidic chloride solutions, Corrosion Science 18 (1978) 427−439.
[19] A.A. El Miligy, D. Geana, W.J. Lorenz, A theoretical treatment of the kinetics of iron dissolution and passivation, Electrochimica Acta 20 (1975) 273−281.
[20] S. Nešić, N. Thevenot, J.L. Crolet, D. Drazic, Electrochemical properties of iron dissolution in the presence of CO_2-basics revisited, in: CORROSION 1996, Paper No. 03.
[21] M. Keddam, O.R. Mattos, H. Takenout, Reaction model for iron dissolution studied by electrode impedance. I. Experimental results and reaction model, Journal of the Electrochemical Society 128 (1981) 257−266.
[22] M. Keddam, O.R. Mattos, H. Takenout, Reaction model for iron dissolution studied by electrode impedance. II. Determination of the reaction model, Journal of the Electrochemical Society 128 (1981) 266−274.
[23] L. Felloni, The effect of pH on the electrochemical behaviour of iron in hydrochloric acid, Corrosion Science 8 (1968) 133−148.
[24] J.O. Bockris, D. Drazic, A.R. Despic, The electrode kinetics of the deposition and dissolution of iron, Electrochimica Acta 4 (1961) 325−361.
[25] D. Drazic, Iron and its electrochemistry in an active state, Modern Aspects of Electrochemistry 19 (1989) 62−192.
[26] D.M. Dražić, C.S. Hao, The anodic dissolution process on active iron in alkaline solutions, Electrochimica Acta 27 (1982) 1409−1415.
[27] W.J. Lorenz, G. Staikov, W. Schindler, W. Wiesbeck, The role of low-dimensional systems in electrochemical phase formation and dissolution processes, Journal of the Electrochemical Society 149 (2002) K47−K59.
[28] M. Keddam, Anodic dissolution, in: Corros. Mech. Theory Pract, third ed., CRC Press, 2011, pp. 149−215.
[29] S. Nešić, J. Postlethwaite, S. Olsen, An electrochemical model for prediction of corrosion of mild steel in aqueous carbon dioxide solutions, Corrosion 52 (1996) 280−294.
[30] L.G.S. Gray, B.G. Anderson, M.J. Danysh, P.R. Tremaine, Mechanisms of carbon steel corrosion in brines containing dissolved carbon dioxide at pH 4, in: CORROSION 1989, Paper No. 464.
[31] K.E. Heusler, Encyclopedia of Electrochemistry of the Elements, vol. 9, Marcel Dekker, New York, 1982.
[32] K.S. George, S. Nešic, Investigation of carbon dioxide corrosion of mild steel in the presence of acetic acid-part 1: basic mechanisms, Corrosion (2007) 178−186.
[33] F.M. Song, A comprehensive model for predicting CO_2 corrosion rate in oil and gas production and transportation systems, Electrochimica Acta 55 (2010) 689−700.
[34] F.M. Song, D.W. Kirk, J.W. Graydon, D.E. Cormack, CO_2 corrosion of bare steel under an aqueous boundary layer with oxygen, Journal of the Electrochemical Society 149 (2002) B479−B486.
[35] A. Anderko, R.D. Young, Simulation of CO_2/H_2S corrosion using thermodynamic and electrochemical models, in: CORROSION 1999, Paper No. 31.
[36] J. Han, J.W. Carey, J. Zhang, A coupled electrochemical-geochemical model of corrosion for mild steel in high-pressure CO_2-saline environments, International Journal of Greenhouse Gas Control 5 (2011) 777−787.

[37] J.K. Nørskov, T. Bligaard, a. Logadottir, J.R. Kitchin, J.G. Chen, S. Pandelov, et al., Trends in the exchange current for hydrogen evolution, Journal of the Electrochemical Society 152 (2005) J23.
[38] J.O. Bockris, D.F.A. Koch, Comparative rates of the electrolytic evolution of hydrogen and deuterium on iron, tungsten and platinum, The Journal of Physical Chemistry 65 (1961) 1941−1948.
[39] Y. Xu, The hydrogen evolution reaction on single crystal gold electrode, International Journal of Hydrogen Energy 34 (2009) 77−83.
[40] M.A.V. Devanathan, Z. Stachurski, The mechanism of hydrogen evolution on iron in acid solutions by determination of permeation rates, Journal of the Electrochemical Society 111 (1964) 619−623.
[41] J.O. Bockris, E.C. Potter, The mechanism of the cathodic hydrogen evolution reaction, Journal of the Electrochemical Society 99 (1952) 169.
[42] N. Pentland, J.O. Bockris, E. Sheldon, Hydrogen evolution reaction on copper, gold, molybdenum, palladium, rhodium, and iron, Journal of the Electrochemical Society 104 (1957) 182.
[43] J.O. Bockris, J. McBreen, L. Nanis, The hydrogen evolution kinetics and hydrogen entry into a-iron, Journal of the Electrochemical Society 112 (1965) 1025−1031.
[44] A. Lasia, A. Rami, Kinetics of hydrogen evolution on nickel electrodes, Journal of Electroanalytical Chemistry and Interfacial Electrochemistry 294 (1990) 123−141.
[45] B.E. Conway, B.V. Tilak, Interfacial processes involving electrocatalytic evolution and oxidation of H_2, and the role of chemisorbed H, Electrochimica Acta 47 (2002) 3571−3594.
[46] K. Juodkazis, J. Juodkazyte, B. Šebeka, S. Juodkazis, Reversible hydrogen evolution and oxidation on Pt electrode mediated by molecular ion, Applied Surface Science 290 (2014) 13−17.
[47] K. Juodkazis, J. Juodkazyt, A. Grigucevičien, S. Juodkazis, Hydrogen species within the metals: role of molecular hydrogen ion H_2^+, Applied Surface Science 258 (2011) 743−747.
[48] N.T. Thomas, K. Nobe, Kinetics of the hydrogen evolution reaction on titanium, Journal of the Electrochemical Society 117 (1970) 622.
[49] S. Schuldiner, Kinetics of hydrogen evolution at zero hydrogen partial pressure, Journal of the Electrochemical Society 108 (1961) 384.
[50] J.O. Bockris, I.A. Ammar, A.K.M.S. Huq, The mechanism of the hydrogen evolution reaction on platinum silver and tungsten surfaces in acid solutions, The Journal of Physical Chemistry 61 (1957) 879−886.
[51] G.J. Brug, M. Sluyters-Rehbach, J.H. Sluyters, A. Hemelin, The kinetics of the reduction of protons at polycrystalline and monocrystalline gold electrodes, Journal of Electroanalytical Chemistry 181 (1984) 245−266.
[52] W. Sheng, H.A. Gasteiger, Y. Shao-Horn, Hydrogen oxidation and evolution reaction kinetics on platinum: acid vs alkaline electrolytes, Journal of the Electrochemical Society 157 (2010) B1529−B1536.
[53] S. Schuldiner, Hydrogen overvoltage on bright platinum II. pH and salt effects in acid, neutral, and alkaline solutions, Journal of the Electrochemical Society 101 (1954) 426−432.
[54] S.Y. Qian, B.E. Conway, G. Jerkiewicz, Kinetic rationalization of catalyst poison effects on cathodic H sorption into metals: relation of enhancement and inhibition to H coverage, Journal of the Chemical Society, Faraday Transactions 94 (1998) 2945−2954.

[55] S.Y. Qian, B.E. Conway, G. Jerkiewicz, Electrochemical sorption of H into Fe and mild-steel: kinetic conditions for enhancement or inhibition by adsorbed HS^-, Physical Chemistry Chemical Physics 1 (1999) 2805−2813.
[56] Y. Zheng, B. Brown, S. Nešic, Electrochemical study and modeling of H_2S corrosion of mild steel, Corrosion 70 (2014) 351−365.
[57] T. Tran, B. Brown, S. Nešic, Investigation of the electrochemical mechanisms for acetic acid corrosion of mild steel, Corrosion 70 (2014) 223−229.
[58] E. Remita, B. Tribollet, E. Sutter, V. Vivier, F. Ropital, J. Kittel, Hydrogen evolution in aqueous solutions containing dissolved CO_2: quantitative contribution of the buffering effect, Corrosion Science 50 (2008) 1433−1440.
[59] B. Tribollet, J. Kittel, A. Meroufel, F. Ropital, F. Grosjean, E.M.M. Sutter, Corrosion mechanisms in aqueous solutions containing dissolved H_2S. Part 2: model of the cathodic reactions on a 316L stainless steel rotating disc electrode, Electrochimica Acta 124 (2014) 46−51.
[60] J. Kittel, F. Ropital, F. Grosjean, E.M.M. Sutter, B. Tribollet, Corrosion mechanisms in aqueous solutions containing dissolved H_2S. Part 1: characterisation of H_2S reduction on a 316L rotating disc electrode, Corrosion Science 66 (2013) 324−329.
[61] P. Delahay (Ed.), Advances in Electrochemistry and Electrochemical Engineering: Volume 7 Electrochemistry, Interscience, 1970.
[62] B.E. Conway, M. Salomon, Electrochemical reaction orders: applications to the hydrogen- and oxygen-evolution reactions, Electrochimica Acta 9 (1964) 1599−1615.
[63] R.J. Chin, K. Nobe, Electrodissolution kinetics of iron in chloride solutions III. Acidic solutions, Journal of the Electrochemical Society 119 (1972) 1457−1461.
[64] T. Hurlen, Electrochemical behaviour of iron, Acta Chemica Scandinavica 14 (1960) 1533−1554.
[65] E. McCafferty, N. Hackerman, Kinetics of iron corrosion in concentrated acid chloride solutions, Journal of the Electrochemical Society 119 (1972) 999−1009.
[66] M. Stern, The electrochemical behavior, including hydrogen overvoltage, of iron in acid environments, Journal of the Electrochemical Society 102 (1955) 609−616.
[67] J. Amri, E. Gulbrandsen, R.P. Nogueira, Role of acetic acid in CO_2 top of the line corrosion of carbon steel, in: CORROSION 2011, Paper No. 329.
[68] A. Więckowski, E. Ghali, M. Szklarczyk, J. Sobkowski, The behaviour of iron electrode in CO_2^- saturated neutral electrolyte—II. Radiotracer study and corrosion considerations, Electrochimica Acta 28 (1983) 1627−1633.
[69] B. Mishra, S. Al-Hassan, D.L. Olson, M.M. Salama, Development of a predictive model for activation-controlled corrosion of steel in solutions containing carbon dioxide, Corrosion 53 (1997) 852−859.
[70] A. Więckowski, E. Ghali, M. Szklarczyk, J. Sobkowski, The behaviour of iron electrode in CO_2^- saturated neutral electrolyte—I. Electrochemical study, Electrochimica Acta 28 (1983) 1619−1626.
[71] M. Nordsveen, S. Nešić, R. Nyborg, A. Stangeland, A mechanistic model for carbon dioxide corrosion of mild steel in the presence of protective iron carbonate films − part 1: theory and verification, Corrosion 59 (2003) 443−456.
[72] S. Nešić, M. Nordsveen, R. Nyborg, A. Stangeland, A mechanistic model for CO_2 corrosion with protective iron carbonate films, in: CORROSION 2001, Paper No. 040.
[73] A. Kahyarian, M. Singer, S. Nesic, Modeling of uniform CO_2 corrosion of mild steel in gas transportation systems: a review, Journal of Natural Gas Science and Engineering 29 (2016) 530−549.

[74] Y. Zheng, J. Ning, B. Brown, S. Nesic, Electrochemical model of mild steel corrosion in a mixed H_2S/CO_2 aqueous environment, Corrosion 2014 (71) (2014) 316.
[75] W.M. Haynes, CRC Handbook of Chemistry and Physics, 2009.
[76] B.R. Linter, G.T. Burstein, Reactions of pipeline steels in carbon dioxide solutions, Corrosion Science 41 (1999) 117−139.
[77] C. De Waard, D.E. Milliams, Carbonic acid corrosion of steel, Corrosion 31 (1975) 177−181.
[78] G. Schmitt, B. Rothmann, Studies on the corrosion mechanism of unalloyed steel in oxygen-free carbon dioxide solutions part I. Kinetics of the liberation of hydrogen, Werkstoffe Und Korrosion 28 (1977) 816.
[79] B.F.M. Pots, Mechanistic models for the prediction of CO_2 corrosion rates under multiphase flow conditions, in: CORROSION 1995, Paper No. 137.
[80] S. Turgoose, R.A. Cottis, K. Lawson, Modeling of electrode processes and surface chemistry in carbon dioxide containing solutions, in: Comput. Model. Corros. ASTM STP 1154, 1992, pp. 67−81.
[81] C. de Waard, D.E. Milliams, Prediction of carbonic acid corrosion in natural gas pipelines, in: Intern. Extern. Prot. Pipes, 1975. F1-1−F1-8.
[82] S. Nešić, J. Lee, V. Ruzic, A mechanistic model of iron carbonate film growth and the effect on CO_2 corrosion of mild steel, in: CORROSION 2002, Paper No. 237.
[83] S. Nešić, M. Nordsveen, R. Nyborg, A. Stangeland, A mechanistic model for carbon dioxide corrosion of mild steel in the presence of protective iron carbonate films—Part 2: a numerical experiment, Corrosion 59 (2003) 489−497.
[84] S. Nešic, K. Lee, A mechanistic model for carbon dioxide corrosion of mild steel in the presence of protective iron carbonate films - Part 3: film growth model, Corrosion (2003) 616−628.
[85] T.J. Gray, R.B. Rozelle, M.L. Soeder, Catalytic investigations using galvanostatic techniques, Nature 202 (1964) 181−182.
[86] A. Kahyarian, B. Brown, S. Nesic, Mechanism of cathodic reactions in acetic acid corrosion of iron and mild steel, Corrosion 72 (2016) 1539−1546.
[87] S.N. Esmaeely, B. Brown, S. Nesic, Verification of an electrochemical model for aqueous corrosion of mild steel for H_2S partial pressures up to 0.1 Mpa, Corrosion 73 (2017) 144−154.
[88] T. Tran, B. Brown, S. Nešić, Corrosion of mild steel in an aqueous CO_2 environment − basic electrochemical mechanisms revisited, in: CORROSION 2015, Paper No. 671.
[89] C. de Waard, U. Lotz, A. Dugstad, Influence of liquid flow velocity on CO_2 corrosion: a semi-empirical model, in: CORROSION 95, Paper No. 128.
[90] U. Lotz, Velocity effects in flow induced corrosion, in: CORROSION 1990, Paper No. 27.
[91] A. Dugstad, L. Lunde, K. Videm, Parametric study of CO_2 corrosion of carbon steel, in: CORROSION 1994, Paper No. 14.
[92] S. Nesic, G.T. Solvi, J. Enerhaug, Comparison of the rotating cylinder and pipe flow tests for flow-sensitive carbon dioxide corrosion, Corrosion 51 (1995) 773−787.
[93] A. Mohammmed Nor, M.F. Suhor, M.F. Mohamed, M. Singer, S. Nešić, Corrosion of carbon steel in high CO_2 environment: flow effect, in: CORROSION 2011, Paper No. 242.
[94] M. Eisenberg, C.W. Tobias, C.R. Wilke, Ionic mass transfer and concentration polarization at rotating electrodes, Journal of the Electrochemical Society 101 (1954) 306−320.
[95] D.C. Silverman, Practical corrosion prediction using electrochemical techniques, in: Uhlig's Corros. Handb., John Wiley & Sons, Inc., 2011, pp. 1129−1166.

[96] F.P. Berger, K.-F.F.-L. Hau, Mass transfer in turbulent pipe flow measured by the electrochemical method, International Journal of Heat and Mass Transfer 20 (1977) 1185−1194.
[97] M.W.E. Coney, Erosion-Corrosion: The Calculation of Mass-Transfer Coefficients, 1981.
[98] B. Poulson, Measuring and modelling mass transfer at bends in annular two phase flow, Chemical Engineering Science 46 (1991) 1069−1082.
[99] J. Wang, S.A. Shirazi, J.R. Shadley, E.F. Rybicki, E. Dayalan, A correlation for mass transfer coefficients in elbows, in: CORROSION 1998, Paper No. 42.
[100] J. Wang, S.A. Shirazi, A CFD based correlation for mass transfer coefficient in elbows, International Journal of Heat and Mass Transfer 44 (2001) 1817−1822.
[101] E.L. Cussler, Diffusion: Mass Transfer in Fluid Systems, Cambridge University Press, 1997.
[102] A.J. Bard, L.R. Faulkner, Electrochemical Methods : Fundamentals and Applications, John Wiley & Sons, INC., 2001.
[103] S. Nešić, J. Postlethwaite, N. Thevenot, Superposition of diffusion and chemical reaction controlled limiting current - application to CO_2 corrosion, Journal of Corrosion Science and Engineering 1 (1995) 1−14.
[104] S. Nešić, H. Li, J. Huang, D. Sormaz, An open source mechanistic model for CO_2/H_2S corrosion of carbon steel, in: CORROSION 2009, Paper No. 09572.
[105] F. Farelas, B. Brown, S. Nesic, Iron carbide and its influence on the formation of protective iron carbonate in CO_2 corrosion of mild steel, in: CORROSION 2013, Paper No. 2291.
[106] W. Sun, S. Nešić, R.C. Woollam, The effect of temperature and ionic strength on iron carbonate ($FeCO_3$) solubility limit, Corrosion Science 51 (2009) 1273−1276.
[107] S.N. Esmaeely, D. Young, B. Brown, S. Nesic, Effect of incorporation of calcium into iron carbonate protective layers in CO_2 corrosion of mild steel, Corrosion 73 (2016) 238−246.
[108] P. Menaul, Causative agents of corrosion in distillate field, Oil and Gas Journal 43 (1944) 80−81.
[109] J.L. Crolet, M.R. Bonis, The role of acetate ions in CO_2 corrosion, in: CORROSION 1983, Paper No. 160.
[110] Y. Garsany, D. Pletcher, B. Hedges, Speciation and electrochemistry of brines containing acetate ion and carbon dioxide, Journal of Electroanalytical Chemistry 538−539 (2002) 285−297.
[111] Y. Sun, K. George, S. Nesic, S. Nešić, The effect of Cl^- and acetic acid on localized CO_2 corrosion in wet gas flow, Corrosion 2003 (2003) 1−28.
[112] J.-L. Crolet, N. Thevenot, A. Dugstad, Role of free acetic acid on the CO_2 corrosion of steels, in: CORROSION 1999, Paper No. 24.
[113] K. George, S. Nešić, C. de Waard, Electrochemical investigation and modeling of carbon dioxide corrosion of carbon steel in the presence of acetic acid, in: CORROSION 2004, Paper No. 379.
[114] K. George, S. Wang, S. Nesic, C. de Waard, Modeling of CO_2 corrosion of mild steel at high pressures of CO_2 in the presence of acetic acid, in: CORROSION 2004, Paper No. 04623.
[115] Y. Garsany, D. Pletcher, B. Hedges, The role of acetate in CO_2 corrosion of carbon steel: has the chemistry been forgotten? in: CORROSION 2002, Paper No. 273.
[116] B. Hedges, L. Mcveigh, The role of acetate in CO_2 corrosion: the double whammy, in: CORROSION 1999, Paper No. 21.

[117] M.W. Joosten, J. Kolts, J.W. Hembree, P. City, M. Achour, Organic acid corrosion in oil and gas production, in: CORROSION 2002, Paper No. 294.
[118] V. Fajardo, C. Canto, B. Brown, S. Nešić, Effects of organic acids in CO_2 corrosion, in: CORROSION 2007, Paper No. 319.
[119] E. Gulbrandsen, K. Bilkova, Solution chemistry effects on corrosion of carbon steels in presence of CO_2 and acetic acid, in: CORROSION 2006, Paper No. 364.
[120] M. Matos, C. Canhoto, M.F. Bento, M.D. Geraldo, Simultaneous evaluation of the dissociated and undissociated acid concentrations by square wave voltammetry using microelectrodes, Journal of Electroanalytical Chemistry 647 (2010) 144−149.
[121] P.C. Okafor, B. Brown, S. Nešić, CO_2 corrosion of carbon steel in the presence of acetic acid at higher temperatures, Journal of Applied Electrochemistry 39 (2009) 873−877.
[122] J. Amri, E. Gulbrandsen, R.P. Nogueira, Pit growth and stifling on carbon steel in CO_2-containing media in the presence of HAc, Electrochimica Acta 54 (2009) 7338−7344.
[123] T. Hurlen, S. Gunvaldsen, F. Blaker, Effects of buffers on hydrogen evolution at iron electrodes, Electrochimica Acta 29 (1984) 1163−1164.
[124] K.S. George, Electrochemical Investigation of Carbon Dioxide Corrosion of Mild Steel in the Presence of Acetic Acid (Doctoral dissertation), Ohio University, 2003.
[125] J. Amri, E. Gulbrandsen, R.P. Nogueira, Propagation and arrest of localized attacks in carbon dioxide corrosion of carbon steel in the presence of acetic acid, Corrosion 66 (2010) 035001/1−035001/7.
[126] J. Amri, E. Gulbrandsen, R.P. Nogueira, Numerical simulation of a single corrosion pit in CO_2 and acetic acid environments, Corrosion Science 52 (2010) 1728−1737.
[127] J. Amri, E. Gulbrandsen, R.P. Nogueira, The effect of acetic acid on the pit propagation in CO_2 corrosion of carbon steel, Electrochemistry Communications 10 (2008) 200−203.
[128] H. Fang, B. Brown, S. Nesic, High salt concentration effects on CO_2 corrosion and H_2S corrosion, in: CORROSION 2010, Paper No. 10276.
[129] H. Fang, Low Temperature and High Salt Concentration Effects on General CO_2 Corrosion for Carbon Steel (M.S. thesis), Ohio University, 2006.
[130] G.B. Wallis, One-Dimensional Two-Phase Flow, McGraw-Hill, New York, 1969.
[131] O. Shoham, Mechanistic Modeling of Gas-Liquid Two-Phase Flow in Pipes, Society of Petroleum Engineers, Richardson, TX, 2006.
[132] Y. Taitel, N. Lee, A.E. Dukler, Transient gas-liquid flow in horizontal pipes: modeling the flow pattern transitions, AIChE Journal 24 (1978) 920−934.
[133] W. Li, B.F.M. Pots, B. Brown, K.E. Kee, S. Nesic, A direct measurement of wall shear stress in multiphase flow − is it an important parameter in CO_2 corrosion of carbon steel pipelines? Corrosion Science 110 (2016) 35−45.
[134] Y. Yang, B. Brown, S. Nesic, M.E. Gennaro, B. Molinas, Mechanical strength and removal of a protective iron carbonate layer formed on mild steel in CO_2 corrosion, in: CORROSION 2010, Paper No. 10383.
[135] Y. Xiong, B. Brown, B. Kinsella, S. Nešic, A. Pailleret, Atomic force microscopy study of the adsorption of surfactant corrosion inhibitor films, Corrosion 70 (2014) 247−260.
[136] Y. Yang, Removal Mechanisms of Protective Iron Carbonate Layer in Flowing Solutions (Doctoral dissertation), Ohio University, 2012.
[137] W. Li, Mechanical Effects of Flow on CO_2 Corrosion Inhibition of Carbon Steel Pipelines (Doctoral dissertation), Ohio University, 2016.
[138] K.E. Kee, S. Richter, M. Babic, S. Nešić, Experimental study of oil-water flow patterns in a large diameter flow loop-the effect on water wetting and corrosion, Corrosion 72 (2016) 569−582.

[139] J. Cai, C. Li, X. Tang, F. Ayello, S. Richter, S. Nesic, Experimental study of water wetting in oil-water two phase flow-horizontal flow of model oil, Chemical Engineering Science 73 (2012) 334−344.
[140] J. Addis, B. Brown, S. Nesic, Multiphase Technology, Erosion-corrosion in disturbed liquid/particle flow, in: CORROSION 2008, Paper No. 08572.
[141] J.F. Addis, Erosion-Corrosion in Disturbed Liquid/Particle Flow (M.S. thesis), Ohio University, 2008.
[142] J. Huang, B. Brown, X. Jiang, B. Kinsella, S. Nesic, Internal CO_2 corrosion of mild steel pipelines under inert solid deposits, in: CORROSION 2010, Paper No. 10379.
[143] J. Huang, B. Brown, Y.-S. Choi, S. Nešić, Prediction of uniform CO_2 corrosion of mild steel under inert solid deposits, in: CORROSION 2011, Paper No. 11260.
[144] M. Singer, D. Hinkson, Z. Zhang, H. Wang, S. Nesic, CO_2 top-of-the-line corrosion in presence of acetic acid : a parametric study, Corrosion 69 (2013) 719−735.
[145] A.S. Ruhl, A. Kranzmann, Corrosion behavior of various steels in a continuous flow of carbon dioxide containing impurities, International Journal of Greenhouse Gas Control 9 (2012) 85−90.
[146] A.S. Ruhl, A. Kranzmann, Investigation of corrosive effects of sulphur dioxide, oxygen and water vapour on pipeline steels, International Journal of Greenhouse Gas Control 13 (2013) 9−16.
[147] B.F.M. Pots, E.L.J.a. Hendriksen, CO_2 corrosion under scaling conditions − the special case of top-of-line corrosion in wet gas pipelines, in: CORROSION 2000, Paper No. 031.
[148] R. Nyborg, A. Dugstad, Top of line corrosion and water condensation rates in wet gas pipelines, in: CORROSION 2007, Paper No. 555.
[149] F. Ayello, W. Robbins, S. Richter, S. Nešić, Model compound study of the mitigative effect of crude oil on pipeline corrosion, Corrosion 69 (2013) 286−296.
[150] F. Ayello, Crude Oil Chemistry Effects on Corrosion Inhibition and Phase Wetting in Oil-Water Flow (Doctoral dissertation), Ohio University, 2010.
[151] P. Ajmera, W. Robbins, S. Richter, S. Nesic, Role of asphaltenes in inhibiting corrosion and altering the wettability of the steel surface, Corrosion 67 (2011) 1−11.
[152] J. Han, B.N. Brown, S. Nešić, Investigation of the galvanic mechanism for localized carbon dioxide corrosion propagation using the artificial pit technique, Corrosion 66 (2010), 950031-1−950031-12.
[153] J.M. West, Basic Corrosion and Oxidation, Halsted Press, 1980.
[154] M. Fingar, J. Jackson, Application of corrosion inhibitors for steels in acidic media for the oil and gas industry: a review, Corrosion Science 86 (2014) 17−41.
[155] J.W. Palmer, W. Hedges, J.L. Dawson, Use of Corrosion Inhibitors in Oil and Gas Production: (EFC 39), Maney Publishing, 2004.
[156] M.A. Kelland, Production Chemicals for the Oil and Gas Industry, Secon edit, CRC Press, 2014.
[157] C. Canto, Effect of Wall Shear Stress on Corrosion Inhibitor Film Christian Canto (Doctoral dissertation), Ohio Universaity, 2010.
[158] L.G. Qiu, A.J. Xie, Y.H. Shen, The adsorption and corrosion inhibition of some cationic gemini surfactants on carbon steel surface in hydrochloric acid, Corrosion Science 47 (2005) 273−278.
[159] V. Jovancicevic, S. Ramachandran, P. Prince, Inhibition of CO_2 corrosion of mild steel by imidazolines and their precursors, Corrosion 55 (1999) 449−455.

[160] M.E. Palomar, C.O. Olivares-Xometl, N.V. Likhanova, J.B. Pérez-Navarrete, Imidazolium, pyridinium and dimethyl-ethylbenzyl ammonium derived compounds as mixed corrosion inhibitors in acidic medium, Journal of Surfactants and Detergents 14 (2011) 211−220.
[161] C. Li, S. Richter, S. Nešić, How do inhibitors mitigate corrosion in oil-water two-phase flow beyond lowering the corrosion rate? Corrosion 70 (2014) 958−967.
[162] M.R. Gregg, S. Ramachandran, Review of corrosion inhibitor developments and testing for offshore oil and gas production systems, in: CORROSION 2004, Paper No. 04422.
[163] J.M. Cassidy, Design and investigation of a north sea acid corrosion inhibition system, in: CORROSION 2006, Paper No. 482.

Microbiologically influenced corrosion (MIC)

8

Judit Telegdi [1,2], *Abdul Shaban* [1] *and Laszlo Trif* [1]
[1]Hungarian Academy of Sciences, Budapest, Hungary; [2]Óbuda University, Budapest, Hungary

8.1 Introduction

Microbiologically influenced corrosion (MIC) has received increasing attention by engineers and scientists from different fields (materials and corrosion scientists and engineers, biologists, and microbiologists). MIC refers to the possibility that microorganisms are involved in the deterioration of metallic (and nonmetallic) materials. Microbial corrosion is a significant problem affecting the oil and gas and other industries. It degrades the integrity, safety, and reliability of pipeline operations and other systems. However, the mere presence of given classes of microbes associated with MIC does not indicate that MIC is occurring. Nor does showing that the presence of a given type of microorganisms establishes a cause-and-effect relationship between the bacteria and metal dissolution. For MIC to occur, water presence, even at very low amounts, is necessary [1–4].

The last decade revealed that not only the sulfate-reducing bacteria (SRB) are responsible for MIC but also several other microbes, e.g., the acid producers, iron oxidizers, and general aerobic bacteria [1]. MIC is rarely associated with one single mechanism or one single species of microorganisms. In addition to SRB many microorganisms occurring in natural environments are also considered corrosion-causing microbes, including methanogens, sulfur-oxidizing bacteria (SOB), acid-producing bacteria (APB), iron-oxidizing bacteria (IOB), iron-reducing bacteria (IRB), and manganese-oxidizing bacteria (MOB). Each of these physiological groups of microorganisms may contain hundreds of individual species. Each group of bacteria or an individual species of bacteria alone can influence metal corrosion; however, severe MIC in a natural environment is always caused by microbial communities containing many different types of microbes.

For better understanding of MIC and its threats on pipelines and other structures, it is essential to learn more about how microbes influence metallic corrosion, to identify their presence and existence, and to monitor their destructive activities. MIC is not a new type of corrosion, but it involves microorganisms that, by their presence and active, aggressive metabolites and exopolymeric substances (EPS) (produced by microorganisms and composed mainly of polysaccharides) degrade materials, especially metals. The metabolic products (e.g., sulfide, organic acids) alter the interface chemistry resulting in increased corrosion rate and, together with the EPS, on the metal surface cause pH and dissolved oxygen gradients that lead first to localized (pitting and crevice) corrosion, which if remains unmitigated, will lead to metal wall perforations [4–6].

Trends in Oil and Gas Corrosion Research and Technologies. http://dx.doi.org/10.1016/B978-0-08-101105-8.00008-5

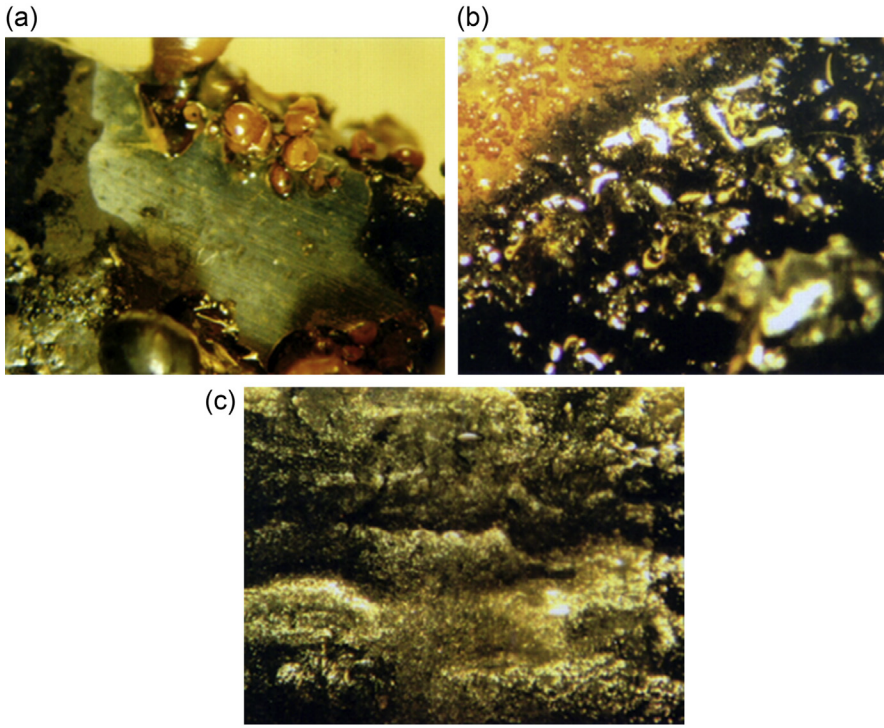

Figure 8.1 Photos of carbon steel surfaces modified in 3 months by microorganisms of mixed population. (a) Tubercles caused by aerobic iron oxidizer microbes; (b) shiny, blackish biofilm produced by anaerobic *Desulfovibrios*; (c) significantly roughened metal surface beneath the blackish deposition. (Magnification: 10×.)

Hydrocarbons are an excellent carbon source for a wide variety of microbes in all three forms of life (bacteria, archaea, and eucarya) that are responsible for MIC. Some microorganisms that produce hydrogen sulfide (H_2S) as a byproduct can cause severe problems in the gas and petroleum industry [7].

In all cases to confirm MIC, it is essential to document the presence of corrosion-relevant microorganisms. Fig. 8.1(a–c) shows images of carbon steel coupon surfaces modified in 3 months by microorganisms of mixed population. Fig. 8.1(a) shows tubercles on the metal surface deteriorated by aerobic iron-oxidizing microbes; on Fig. 8.1(b), a shiny, blackish biofilm produced by anaerobic *Desulfovibrios* is observable; and Fig. 8.1(c) shows the metal surface beneath the blackish biofilm roughened by the presence of microbial activity.

8.2 Microorganisms present in the oil and gas

Microorganisms are present everywhere (soil, water and air) and can grow and reproduce at very rapid rates. Some microorganisms that are present in the oil and gas fields

can cause problems, directly or indirectly, that can lead to significant economic losses and operational failures for the oil and gas industry [8,9].

A great deal of research was devoted to study the effects of sulfide production by microbes in oil and gas fields. Sulfide production by these microbes can cause many problems such as reservoir souring (due to H_2S), reservoir plugging (due to poorly soluble products), reduced product quality, and metallic corrosion [9,10].

Some microorganisms possess extreme tolerance to severe environments such as low (acidic) and high (alkaline) pH values, as well as low and high pressure and temperature ranges [11]. They can not only withstand such harsh circumstances but also generate some conditions to create aggressive environments, which will promote direct or indirect effect on metal deterioration.

As early as 1920s, microbiologists isolated SRB in oil environments [12]. There are several dozens of bacteria that cause MIC on carbon and stainless steels, copper, and aluminum alloys (tanks, pipelines, flanged joints) in humid or aqueous environments.

8.2.1 Microorganisms associated with microbiologically influenced corrosion

The role of microorganisms in the deterioration and failure of materials can be classified into biofouling, biodeterioration, and biocorrosion. Chemolithotrophic bacteria attain their energy from the oxidation of noncarbon compounds (inorganic) i.e., from the stored energy in chemical compounds, which is utilized by oxidation process. Sulfur, ammonium ion (NH^{4+}), and ferrous iron (Fe^{2+}) are just some examples of inorganic compounds that are utilized by these types of bacteria [13]. Chemolithotrophic bacteria that are associated with MIC in the oil and gas industry are summarized in the next sections.

8.2.1.1 Methanogens

Oil reservoir methanogenic microorganisms metabolize H_2, CO_2, acetate, methylamines etc. with production of methane [13].

8.2.1.2 Sulfate-reducing bacteria

These bacteria were the first microorganisms recovered from oil fields [14]. Microorganisms belonging to this group have four subgroups: proteobacteria (*Desulfovibrionales*, *Desulfobacterales*, *Syntrophobacterales*), firmicutes, thermodesulfobacteria, and archea.

Seawaters, which contain sulfate ions, are widely used in enhanced oil recovery operations. SRB are anaerobes that obtain their growth energy by oxidizing organic compounds or molecular hydrogen (H_2) while reducing sulfate $\left(SO_4^{2-}\right)$ to hydrogen sulfide (H_2S) [15]. In other words, SRB in an anaerobic respiration, use sulfate instead of oxygen, and oxidize organic substances to organic acids and CO_2, by the reduction of sulfate to sulfide [15]. The presence of H_2S causes serious problems by reacting with metal (mainly iron) ions and producing ferrous sulfides (FeS), which are poorly

soluble and, together with slime, cause dark-colored sludge that hinders oil flow [16]. In the oil and gas industry, carbon steels are the bulk material of choice, and the presence of black by-products (FeS) on the metal surface coupled with positive analysis of SRB microbes in the corrosion product is a strong indication of MIC due to SRB.

Many species of SRB from different parts of the world have been identified. They might slightly differ in their morphology (appearance) or in the energy source for their metabolism [17]. Some SRB bacteria can use both elemental sulfur and sulfate as electron acceptors. Common SRB include the genera *Desulfovibrionales*, *Desulfosporosinus*, *Desulfotomaculum*, *Syntrophobacterales*, *Desulfosporomusa*, and *Desulfobacterales* [16,17]. *Thermodesulfovibrio* sulfate-reducing species are also found as a member of the *Nitrospirae phylum*. At elevated temperatures, there exist two phyla of *thermophilic* SRB: *Thermodesulfobacteria* and *Thermodesulfobium*. Three genera of archaea *Archaeoglobus*, *Thermocladium,* and *Caldivirga*, which can reduce sulfate, are found in oil deposits [18].

As mentioned earlier, the damaging activities of SRB are of alarming concern to many industrial operations, specifically oil and gas industries that are seriously affected by the sulfide produced by SRB. Biogenic sulfide production causes health and safety complications, environmental hazards, and huge economic losses due to corrosion of equipment and reservoir souring.

SRB influence on the corrosion of steels can be elucidated mainly by two scenarios [11,19]:

- Chemical MIC (CMIC) of iron by hydrogen sulfide from microbial sulfate reduction occurs with “natural” organic substrates;
- SRB corrode iron by direct utilization of the metal itself. This always occurs via direct electron uptake and in only a limited number of recently discovered SRB strains. Until now, such electrical MIC (EMIC) is assumed to be widespread and of considerable technical relevance.

CMIC and EMIC are the likely primary processes that drive iron corrosion in sulfate-containing anoxic environments.

The major cause responsible for biocorrosion is attributed to SRB ability to perform dissimilatory reduction of sulfur compounds, such as sulfate, sulfite, and thiosulfate into sulfides. Some species from the *Desulfovibrio* genus (*Desulfovibrio desulfuricans*, as an example) can utilize nitrate as alternative respiratory substrate [20].

The formation of massive biofilms on metal surfaces further promotes corrosion of oil and gas pipelines [21]. Fig 8.2 presents atomic force microscopy (AFM) images of *D. desulfuricans* cells, where Fig. 8.2(a) shows several microbes scattered on the metal surface, and Fig. 8.2(b) shows the inner structure of the cell membrane visualized at nanometer scale.

8.2.1.3 Iron- and manganese-oxidizing bacteria

Iron bacteria may be described as a group of aerobic bacteria, which can metabolize by utilizing the oxidation of ferrous and/or manganous ions. The colored deposits of these microorganisms are due to the products of ferric (brown) and/or manganese (pink) salts

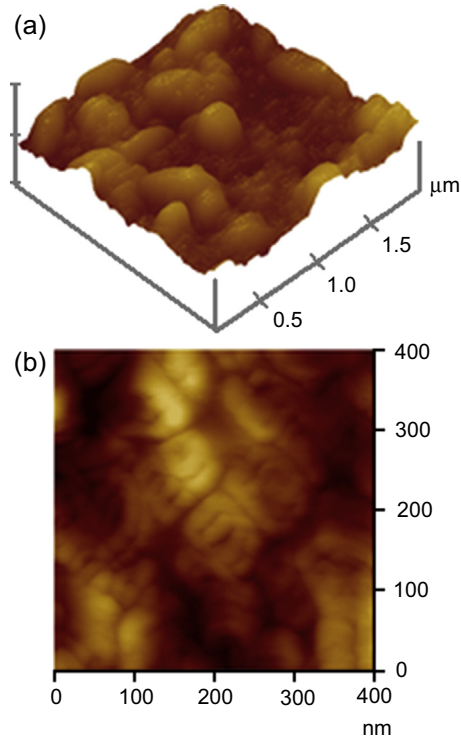

Figure 8.2 Atomic force microscopy images on *Desulfovibrio desulfuricans* cells; (a) several microbes scattered on iron surface; (b) details of cell membrane morphology visualized at nanometer scale.

(usually hydroxides). It has been speculated that the biofilms of iron- and manganese-oxidizing bacteria have a direct effect on the chemistry of the passive films of metals by attachment and deposit metal oxides on the surfaces. These oxides tend to shift the corrosion potential of the passive metals in the noble direction, causing an increase in corrosion potential, which may initiate localized forms of corrosion of passive metals [22].

IOB, such as *Gallionella*, *Sphaerotilus*, *Leptothrix*, and *Crenothrix*, which are often identified by their distinctive morphologies, such as the extracellular twisted ribbon-like stalks formed by *Gallionella ferruginea*, oxidize the ferrous iron (Fe^{2+}, a soluble form) to ferric iron (Fe^{3+}, an insoluble iron compound e.g., $Fe(OH)_3$) [22]. The iron and manganese bacteria, by oxidizing ferrous to ferric ion form, thus produce extremely aggressive ferric chlorides (very low local pH value: pH $\cong$ 1), which causes pits on surfaces of both carbon steel and austenitic stainless steel in particular [23].

8.2.1.4 Iron-reducing bacteria

Their importance is overshadowed by the IOB although they also play significant role in MIC. In cases when IRB are together with SRB, carbon steel metal samples will be

more severely damaged than in abiotic environments [24,25]. Several types of microorganisms (bacteria), including those from the genera *Pseudomonas* and *Shewanella*, have the ability to reduce manganese and/or iron oxides, which also influence corrosion reactions [3].

8.2.1.5 Pseudomonas aeruginosa

This Gram-negative bacterium is widely scattered in the environment and also plays an important role in the initiation of MIC in oil and gas industry. The biofilm formation by *Pseudomonas aeruginosa* was revealed to go through several stages: In stage I, planktonic bacteria initiate attachment to an abiotic surface formed from mainly organic components of the environment; this adhesion becomes irreversible in stage II, stage III corresponds to microcolony development, and stage IV corresponds to biofilm maturation and growth of the three-dimensional community. Finally, dispersion occurs in stage V and planktonic bacteria that are released from the biofilm to colonize other sites [3].

8.2.1.6 Sulfur-oxidizing bacteria

SOB are aerobes that gain energy by oxidation of the reduced sulfur compound [e.g., hydrogen sulfide (H_2S)] into elemental sulfur (S^0) by partial oxidation, or sulfate (SO_4^{2-}), which in water forms sulfuric acid (H_2SO_4), as well as into thiosulfate ions [26]. *Beggiatoa* and *Paracoccus* are two classical examples of SOB.

Aerobic sulfur-oxidizing prokaryotes belong to genera such as *Acidianus*, *Acidithiobacillus*, *Aquaspirillum*, *Aquifex*, *Bacillus*, *Beggiatoa*, *Methylobacterium*, *Paracoccus*, *Pseudomonas*, *Starkeya*, *Sulfolobus*, *Thermithiobacillus*, *Thiobacillus*, *Thiothrix* and *Xanthobacter* [27].

The most investigated genera of SOB (*Thiobacillus*, *Sulfolobus*, *Thermothrix*, *Beggiatoa*, and *Thiothrix* [28]), for the biological oxidation of sulfides are chemolithotrophic types. *Thiobacillus ferrooxidans*, an acidophile, (active in the pH range of 1.0−2.5) and also a thermophile [prefer temperatures of 45−50°C (113−122°F)] oxidize iron- and sulfur-containing minerals [29]. SOB also causes the biodeterioration of concrete sewers, which takes place when microorganisms living in biofilm formed on unsubmerged sections of concrete excrete sulfuric acid, which is deleterious to the concrete [28].

8.2.1.7 Slime-former bacteria

The slime formers can exist in the presence or absence of oxygen and produce a variety of extracellular mats of high-density slime that will cover partly of fully solid surfaces. Their primary unfavorable effects are the protection of anaerobes (like SRB) and aerobes (iron/manganese/sulfur oxidizers) and the removal of metal ions derived from the metal surface, and furthermore, massive pore plugging occurs inside pipelines [30]. As the formation of biofilm/biomass matures, aerobic bacteria consume oxygen, producing metabolic by-products that are nutrient for anaerobes, and these processes create real anaerobic environments underneath the biofilm.

8.2.1.8 Acid-producing bacteria

One of the most corrosive metabolites generated by microbes is acids as by-products of APB that can produce organic (acetic and butyric acids) and inorganic acids (e.g., sulfuric acid) as well as nutrients for other species (e.g., fatty acids that are used by SRB). Basically, the APB could be regarded as creating conditions for increased aggressive activities by the SRB, consuming the fatty acids produced by the APB.

The APB have now been documented as a possible major cause of corrosion, mainly because of their fermentative activities that will cause the local pH, mainly in the biofilms, to drop into the acidic range [31].

Inorganic acids, produced by microbes, are nitric acid (HNO_3), sulfurous acid (H_2SO_3), sulfuric acid (H_2SO_4), nitrous acid (HNO_2) and carbonic acid (H_2CO_3).

Sulfurous acid and sulfuric acid are mainly released by bacteria of the genera *Thiobacillus*. Other bacteria, such as *Thiothrix* and *Beggiatoa* spp., as well as some fungi (e.g., *Aureobasidium pullulans*), also produce these acids [16,32].

The focal problem in sulfuric and nitric acid corrosion is the fact that the resultant salts are water soluble and, therefore, a formation of a protective corrosion product layer is not probable. Moreover, because of the decrease in pH, protective deposits formed on the surface, e.g., calcium carbonate can easily dissolve into the liquid [31].

AFM images of a corroded iron surface (Fig. 8.3(a) and (b)) clearly show the fingerprints of the acid producer *Thiomonas intermedia* cells, and the sectional analysis proves the depth of pits on the coupon surface etched by the acid metabolites (more than 370 nm in 1 day!).

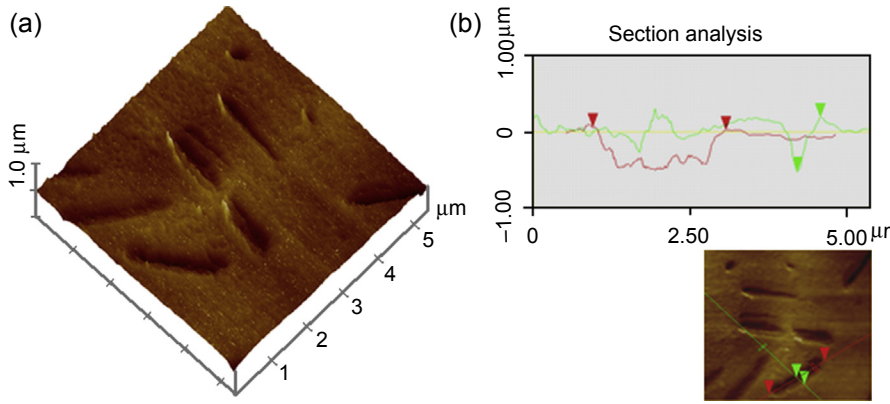

Figure 8.3 Atomic force microscopy images of iron surface after 1-day-long immersion in broth inoculated with *Thiomonas intermedia*. (a) Two-dimensional topographic image, which shows the fingerprints of microorganisms within the biofilm; (b) sectional analysis of pit depth formed on the coupon surface.

8.3 Classification of microorganisms

Taxonomy, the science of classifying organisms, consists of classifying new or existing organisms.

Microorganisms are generally classified as prokaryotes or eukaryotes. A prokaryote cell has no nucleus and it multiplies by fission. On the other hand, the eukaryote organism contains true nuclei and its division is by mitosis. All organisms are composed of eukaryotic cells, except bacteria. There are examples of eukaryotic microorganisms, including fungi, algae, and protozoa, that can take part in MIC, and prokaryotic microorganisms include the bacteria and blue-green bacteria, which are the permanent participants in MIC.

Microorganisms can also be classified according to three types of characterization: morphology, physiology, and, genetic [32].

8.3.1 Classification based on oxygen demand

Oxygen utilization by bacteria suggests the mechanism used by them, to fulfill their energy requirements. On the basis of oxygen demands, bacteria can be classified into the following different categories [32]:

- *Obligate anaerobes*: They are harmed by the presence of oxygen hindering their growth.
- *Aerotolerant organisms*: They cannot use oxygen for growth, but can tolerate its presence.
- *Facultative anaerobes*: That can grow without oxygen but use oxygen if it is present.
- *Obligate aerobes*: They need oxygen to grow; in cellular respiration these microorganisms use oxygen for oxidation of substrates such as sugars and fats when energy is generated.
- *Facultative aerobes*: They use oxygen but also have anaerobic methods of energy production.
- *Microaerophiles*: Oxygen is required for energy production, but under atmospheric oxygen they are destroyed.
- *Aerotolerantes*: They do not use oxygen directly, but the presence of oxygen does not harm them.

8.3.2 Classification of microorganisms based on energy and carbon requirement

- *Chemotrophs* (*respiration*): They respire molecular oxygen as a terminal electron acceptor (aerobic respiration); in addition, they use nitrate (anaerobic respiration). An example of this group is methane producers.
- *Chemotrophs* (*fermentation*): The energy is derived from phosphorylation.
- *Chemolithoautotrophs* obtain energy though oxidation of inorganic compounds and from CO_2 (sulfur and IOB, nitrifying bacteria).
- *Phototrophs*: They gain energy by photophosphorylation; there are both oxygen-evolving species and non−oxygen-evolving species.
- *Carbon*: The most important component in all living things.
- *Heterotrophs*: They assimilate organic compounds for their carbon needs.
- *Autotrophs*: They utilize carbon dioxide.
- *Chemoheterotrophs*, *also chemoorganotrophs*: Generally the organotrophs use variety of organic compounds as both carbon and energy source; a common sugar they use is glucose; and adenosine triphosphate (ATP) is generated by either substrate-level or oxidative phosphorylation.

- *Chemoautotrophs*, *also chemolithotrophs*: They are lithotrophs; the ATP is generated by oxidative phosphorylation;
- *Myxotrophs*: They are "chemolithotrophic heterotrophs" using carbon dioxide;
- *Photoheterotrophs and photoautotrophs*: They utilize light as energy source and CO_2 as carbon source.

8.3.3 Classification of microorganisms according to taxonomic hierarchy

Taxonomy classifies new and existing organisms. The hierarchy is the following: *domain—kingdom—phylum—class—order—family—genus—species—strains*.

The most widely employed methods for classifying microbes are the following:

1. morphological characteristics,
2. differential staining,
3. biochemical testing, DNA fingerprinting of DNA base composition, and;
4. polymerase chain reaction and DNA chips [33,34].

8.4 Biofilms: why do microbes like to live in biofilms?

Traditional understanding of MIC involves the formation of biofilm that provides a niche for corrosive microbes to grow and proliferate.

Microorganisms live either in planktonic or sessile form. From the point of view of corrosion, the planktonic microorganisms are less dangerous than those that are embedded in thinner or thicker deposits. In aqueous environments, microbes adhere to solid surfaces and prefer to exist in sessile form (better and safer living conditions), and they form biofilms, where metal degradation takes place underneath.

The microbial cell walls—the planktonic ones too!—are surrounded by EPS that consist mainly of polysaccharides, but peptides, nucleotides, and other components are also represented in them. It has a sticky nature, which allows the adhesion of microorganisms to solids.

The accumulation of microorganisms on metals results in biofilms that create different microenvironments. The thin films alter the solid surface properties (e.g., wettability, electrostatic charge), which lead to colonization of microbes. The biofilm is not necessarily uniform in time and place as well as in pH, and in dissolved chemicals and oxygen concentration [35].

The first step in biofilm formation is the development of a conditional layer on a solid surface, which consists of organic compounds and inorganic ions from the liquid environment. The accumulation of microorganisms starts with reversible and later irreversible adhesion of microbes, which is enhanced by the EPS layer (that covers the cells and is a part of the conditional film). In time, more and more microbes adhere to the layer. In a shorter (several minutes) or longer (some hours) time, further adhesion, as well as EPS production and microbial growth, results in a thick, gelatinous biofilm that mainly consists of water, organisms of different species, and other components from the environment. We should keep in mind that the biofilm is a dynamic system with transport processes and chemical reactions within the biofilm; there

is a gradient of pH value, ions, and microbes. The number of anaerobic cells will increase nearer to the solid surface. In contrast, the aerobes have higher cell number near the upper part of the biofilm. The main metabolite of the anaerobes is the H_2S formed from sulfate ions. This can form an insoluble black precipitate with the Fe^{2+} ion. This is the time when corrosion pit formation initiates by the activity of the anaerobes and the presence of FeS. The other important reaction is the oxidation of sulfide ions to sulfate ones.

Biofilm formation involves the participation of different types of microorganisms. Thus, their coherent coexistence is essential for their survival [36].

One should keep in mind that the biofilm not only protects the cells from the external environment and lets them live under safe conditions but beneath the nanolayer it also starts the deterioration of metals, and in the course of time pitting corrosion grows, which if left unmitigated, can lead to pinhole and leaks.

The tendency of microorganisms to adhere to solid surfaces can be evaluated by different approaches, such as interaction energy, thermodynamics, DLVO (Derjagin, Landau, Verwey, Overbeek), and extended DLVO theory. These methods are based on long-range and short-range interaction forces between bacteria and surfaces, by surface energy approach and the physical and chemical interactions between the solid surface, and the biofilm should be taken into consideration too [37–44]. A schematic diagram of the biofilm development, illustrated by AFM images taken at different time intervals, is shown in Fig. 8.4.

Factors that affect the biofilm development and play important role in its formation are the following:

1. Surface properties: roughness, polarization, oxide coverage, chemical composition such as pH, medium concentration, organic and inorganic strength; all these factors have significant impact on bacterial attachment and biofilm development.

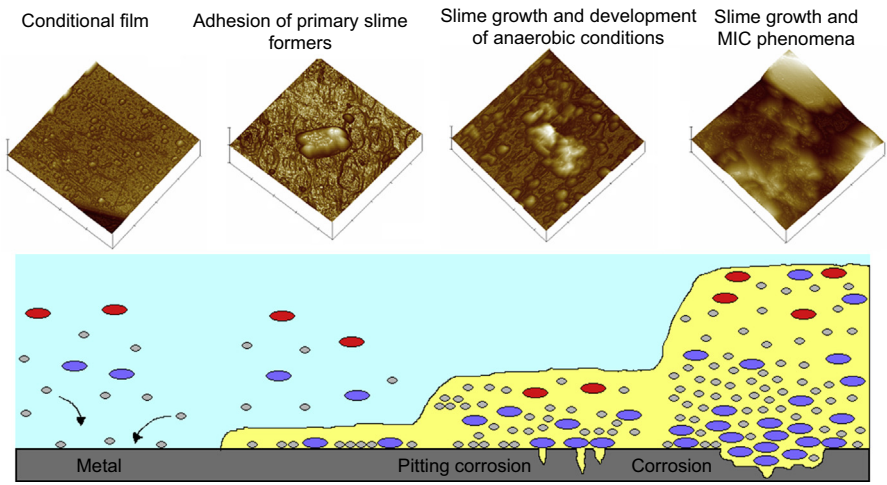

Figure 8.4 Biofilm step-by-step formation as illustrated by atomic force microscopy images.

2. Bacterial medium characteristics: the microbial cells—with some exceptions—are negatively charged at neutral pH. The attachment of some corrosion-relevant bacteria (*Desulfovibrio desulfuricans, Desulfovibrio singaporenus, Pseudomonas*) to iron alloy surfaces shows the highest adhesion forces at pH values that are close to the isoelectric points of bacteria are zero potential.

Biofouling is a progression of the biofilm formation. Once microorganisms form a thick gelatinous layer, macroorganisms that are present in the media (e.g., mussels, alga, barnacles) can accumulate on the top of the layer and, together with other inorganic insoluble chemicals (precipitates of corrosion products), form a massive, well-adhered biodeposit that also can plug pipes, decrease the heat exchange, and the debase the economic function/efficacy [45] as can be seen in Fig. 8.5(a).

8.5 Microbiologically influenced corrosion mechanisms

The role of microorganisms in metal corrosion is known since the first part of the 20th century. Since then, hundreds of publications appeared that are dedicated to understanding what happens when microorganisms are present and how can we explain the mechanisms of the metal deterioration.

Several mechanisms responsible for MIC have been proposed because of its complexity [46]. Some suggested MIC mechanisms will be explained in more details in the following sections.

8.5.1 Cathodic depolarization by hydrogenase

A depolarization of the cathodes through oxidation of the hydrogen evolved on the cathode is summarized as follows [47]:

Anodic reaction	$4Fe \rightarrow 4Fe^{2+} + 8e^{-}$
Water dissociation	$8H_2O \rightarrow 8H^{+} + 8OH^{-}$
Cathodic reaction	$8H^{+} + 8e^{-} \rightarrow 4H_2$
Hydrogen oxidation	$SO_4^{2-} + 4H_2 \rightarrow H_2S + 2H_2O + 2OH^{-}$
Precipitation	$Fe^{2+} + H_2S \rightarrow FeS + 2H^{+}$
Precipitation	$3Fe^{2+} + 6OH^{-} \rightarrow 3Fe(OH)_2$
The overall reaction	$4Fe + SO_4^{2-} + 4H_2O \rightarrow FeS + 3Fe(OH)_2 + 2OH^{-}$

This theory is also valid for other metals such as aluminum alloys [48]. Problems arose when it turned out that there were some *Desulfovibrios* (like the hydrogenase-negative *Desulfotomaculum orientis*), which cannot depolarize the cathode, whereas the hydrogenase-positive *Desulfovibrio desulfuricans* could [49]. Da Silva and his coworkers formulated a new mechanism of cathodic depolarization [50]. Other researchers demonstrated the effect of FeS in the cathodic depolarization [51–53].

Bryant et al. described another important observation that the corrosion rate depends largely on the total activity of hydrogenase within the biofilm, rather on the bacterial population size [51]. In spite of numerous publications, several important factors were not considered in the classical depolarization theory, such as the following [52]:

1. effect of sulfide, bisulfide, and hydrogen sulfide produced from the sulfate reduction in the anodic reactions;
2. effect of hydrogen sulfide on the cathodic reaction;
3. effect of elemental sulfur from the biotic or abiotic oxidation of sulfur;
4. fluctuation in the environmental conditions between anaerobic and aerobic conditions; and
5. production of other corrosive metabolites.

8.5.2 King and Miller mechanism

This mechanism theory, proposed by King and Miller in 1971, states that the iron sulfide produced by the SRB and the iron pipe material produced a galvanic cell, caused by localized corrosion, that also contributed to the rate of corrosion [53]. The proposed mechanism theory indicated that depolarization was caused by the iron sulfide rather than the SRB. Hydrogen would be adsorbed onto FeS rather than Fe, and electrons transferred to the FeS would depolarize the atomic hydrogen into molecular hydrogen, therefore allowing the SRB to use it via hydrogenase. Thus, by linking the Fe/FeS electrochemical reaction as the main mechanism for SRB corrosion, King and Miller evaded the issue of hydrogenase's ineffectiveness with regard to atomic hydrogen. In addition to avoiding the issue with hydrogenase, the main reaction in this mechanism is the electrochemical reaction, which operates at equal ratio for Fe and FeS. In the King and Miller mechanism, the role of SRB was primarily to enable the regeneration of FeS, rather than the cathodic reaction itself.

8.5.3 The anodic depolarization mechanism

The anodic depolarization mechanism was first mentioned in 1981 [54]. The results of extensive investigations are as the follows:

Anodic reaction	$4Fe \rightarrow 4Fe^{2+} + 8e^{-}$
Water dissociation	$8H_2O \rightarrow 8H^{+} + 8OH^{-}$
Cathodic reaction	$8H^{+} + 8e^{-} \rightarrow 4H_2$
Anodic depolarization	$3Fe^{2+} + 6OH^{-} \rightarrow 3Fe(OH)_2$
Hydrogen oxidation	$SO_4^{2-} + 4H_2 \rightarrow H_2S + 2H_2O + 2OH^{-}$
Dissociation of hydrogen sulfide	$H_2S \rightarrow S^{2-} + 2H^{+}$
Anodic depolarization	$Fe^{2+} + S^{2-} \rightarrow FeS$
The overall reaction	$4Fe + SO_4^{2-} + 4H_2O \rightarrow FeS + 3Fe(OH)_2 + 2OH^{-}$

According to these reactions, the corrosion of iron goes through electron generation in metal dissolution reaction, and the H^+ ions are formed in dissociation of water. After formation of H_2 (the name of this step is "cathodic polarization") the H_2 forms a layer and protects the metal surface. The main corrosion product is $Fe(OH)_2$. Then the sulfate-reducer bacteria convert the SO_4^{2-} to H_2S and after its reaction with iron ions, the formation of FeS depolarizes the anode.

8.5.4 Other mechanisms

There are some other proposed mechanisms. One of them based on sulfide describes the importance of the biomineralization in MIC [55]. The so-called three-stage mechanism elaborated by Romero [56], proposes a three-step reaction, which determines the metal deterioration.

Recently appeared the biocatalytic cathodic sulfate reduction (BCSR) theory, which is based on bioenergetics [57]. This theory explains through the activity of sulfate-reducer bacteria (which is the most dangerous one from the point of view of MIC) why and when they attack metals. The theory states that an SRB biofilm on a steel surface needs energy for its growth or maintenance. When there is a lack of electron donors (e.g., a lack of organic carbon due to diffusional limitation), the sessile cells at the bottom of an SRB biofilm will switch to elemental iron as an alternate electron donor for the oxidation of sulfate in its energy production. On the other hand, these cells may use the elemental iron simply because they are abundantly available nearby. The following equations can be used to explain the bioelectrochemistry in BCSR. In the SRB attack against carbon steel, in the anodic reaction, iron is oxidized, which releases electrons, while the cathodic reaction is sulfate reduction utilizing these electrons.

Anode	$4Fe \rightarrow 4Fe^{2+} + 8e^-$ (iron dissolution)
Cathode	$SO_4^{2-} + 8H^+ + 8e^- \rightarrow HS^- + OH^- + 3H_2O$ (BCSR)

Cathodic reaction shows the half reaction of sulfate reduction catalyzed by the biofilm.

Generally, the rate of anodic and cathodic reactions is equivalent and determines the overall MIC rate.

8.6 Consequences of MIC in the gas and oil industry

8.6.1 Degradation and deterioration

In previous parts of the chapter, the most important criterion and appearance of the MIC were discussed. Now we shall see how this type of corrosion appears in the oil and gas industry.

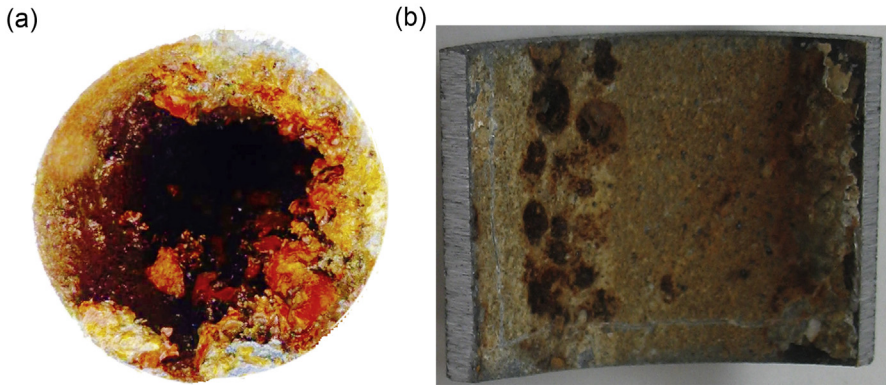

Figure 8.5 Internal corrosion of a pipeline caused by microbiologically influenced corrosion. (a) Internal clogging of pipeline, (b) local attacks on the inner surface of a pipeline.

MIC is a well-known and an ongoing problem in oil and gas production and transmission sectors. Fig. 8.5(a) and (b) show typical damage caused by MIC in pipelines.

When speaking about bacterial activity in oil, diesel, and naphtha, it refers to the microbial degradation of oil and its products as well as to the MIC in pipelines (up- and downstream pipes, fill-pipe sump, transporting pipelines), tankers, etc. In the degradation, five hydrocarbon-degrading bacteria are involved; they represent strains of two classified species. The degradation of petroleum products is important because hydrocarbons act as an excellent food source for a wide variety of microorganisms [58–60]. The biodegradation and corrosion studies revealed that these *Bacilli* degrade the $(CH_2{-}CH_2)_n$ to $(R{-}CH_3)$ in oil and diesel and are capable to oxidize ferrous/manganese into oxides. Microbial activity leads to unacceptable level of turbidity, corrosion of pipeline, and souring of stored products. The corrosion-relevant microorganisms are the same that were discussed in Section 8.2 of this chapter. Their activity is influenced by the presence of nutrient and the proper temperature.

Table 8.1 summarizes the problems that could arise because of MIC in oil and gas production, transportation and storage conditions.

Crude, gas, and water injection pipelines are subjected to different types of corrosion, one of which is MIC that results from accelerated deterioration triggered by different microbial activities existing in hydrocarbon systems. The effect of fluid flow on MIC of pipeline steel is confirmed because MIC has been detected not only in static fluid systems but also in flow systems. The structure and material properties of biofilms were influenced by the fluid flow and had a significant effect on MIC corrosion rates of metals such as carbon steels [61].

In most existing wells, oil flow contains fluctuating quantity of water, which is crucial to the microbial existence. Oil flow rates affect the biofilm adherence to the surface. For SRB, moderate flow rates (0.1–0.5 m/s) have been shown to change

Table 8.1 List of damages in the oil and gas industries, and the associated microorganisms

Damages	Microorganisms associated
Sludge accumulation	Several, different microorganisms
Clogging of pipes	Polymer-producing bacteria, fungi
Microbiologically influenced corrosion in storage tanks	Anaerobe microorganisms, fungi
Suspended solids in the oil	Several microorganisms
Biodegradation of hydrocarbons	Anaerobic microorganisms, fungi
Injectors biofouling	Aerobic bacteria, fungi
Sulfur accumulation	Sulfate-reducing bacteria
Breakage of engine parts	Degradation of lubricant

SRB biofilm morphology, increase biofilm rigidity, and produce shear stress. At sufficiently high flow rates ($\geq$3.5 m/s), SRB adhesion and biofilm growth are inhibited [61]. Studies conducted by British Petroleum indicated that at flow velocities higher than 5 m/s, microbes cannot adhere to the pipeline inner wall. On the other hand, if some microorganisms were attached to the metal surface, high turbulent flows boost the transport of nutrients for microbes and remove the metabolic products, thus enhancing the multiplication and exopolymeric substance production. All these conditions augment the biofilm thickness under which corrosion reactions are initiated. When the biofilm is already dense, a very fast stream can wash down the upper part of the film.

In the presence of oxygen the most corrosive anaerobic microbes (the sulfate reducers) do not show active life, but we have to remember that they live together in a community of aerobic microorganisms and there exist synergistic interactions among each other, i.e., oxygen consumption enhances the aerobic microbial life and makes the environment favorable for the anaerobic microorganisms. In crude pipelines, MIC is conventionally attributed to three species of bacteria, namely SRB and total general bacteria [among them are several others, direct (acid producers) and indirect (methanogen) corrosion relevant microorganisms], which are influenced by the fluid flow conditions. Pipelines transporting brackish subsurface water are subject to frequent corrosion, failures (partly electrochemical, chemical, and microbial types) despite the addition of oxygen scavengers (sodium bisulfite).

Microbial activity in *oil reservoirs* is well known. The low-molecular weight components are hydrolyzed by methanogenic consortia to methane and CO_2, while

transforming light oil to heavy oil and to bitumen. The presence of sulfate in injection water assists SRB to produce sulfide. Addition of nitrate encourages competition by stimulating nitrate-reducing bacteria with concomitant reduction in activity of SRB. Removing biogenic sulfide is important, because it contributes to pitting corrosion and the result is a pipeline failure.

Experience has shown that effective management of the MIC threat is, for operators, often more elusive and problematic than the control of other internal corrosion threats. The mitigation of the MIC in the oil and gas industry needs well-trained specialists, such as corrosion engineers, oilfield microbiologists, and scientists, to strengthen the ability to identify and manage microbial problems in all oilfield facilities.

8.7 Knowledge gaps and future research trends

This section looks closer on ways to account for knowledge gaps in the field of MIC detection, evaluation, monitoring, and control.

MIC is a nonlinear process with respect to time. Before recognizable corrosion due to MIC becomes apparent, there is an initial period in which microbial populations undergo changes and the chemical and physical properties of the metal surface alter considerably. The nonlinearity of MIC presents a substantial problem for the corrosion engineers trying to forecast the operational life of structures. Although the basics of MIC processes (as previously discussed) are quite understood, various knowledge gaps remain.

There exist several gaps between research and applications in the oil and gas fields. The following sections capture some of these gaps.

8.7.1 Knowledge and acquaintance deficiency

In many cases, MIC is referred to as "catchall" process because of its complex association with corrosion processes where other corrosion mechanisms were discarded. Furthermore, a clear understanding of the initiation and mechanism of MIC does not exist because fundamental research of MIC lags behind applied research, which is only aimed at diagnosing or solving a particular problem. A common misunderstanding among managers is that biofilms should be completely eliminated, an unmanageable and, arguably, pointless request. To enlighten and change this kind of thinking from biofilm removal to improved biofilm formation control, it is indispensable to better appreciate the complex abiotic and biotic interface interactions taking place between the metal surface and the liquid phase (mainly water). In addition, the majority of MIC subject matter experts (including microbiologists, chemists, inspectors, regulators, metallurgists) belong to diverse scientific communities, with little interaction. Data sharing from those outside the MIC research community, which may include potential crossover qualification strategies from biofilm researchers, is infrequent.

The efforts to further shrink the gap between research and applications in the oil and gas industry can be classified into the areas listed under the following topics.

8.7.2 Sampling procedures and evaluation methodologies

Generally, sampling procedures gather information on operating parameters, corrosion rates, and microbiological conditions over an identified time period so that any tendencies in the outcome results can be identified and interpreted. Because of normal statistical variations related to field-collected samples and subsequent microbiological testing, more reliable data can be obtained from performing tests on samples collected over a range of time other than single time sample collection. For instance, samples of bulk fluids from pipelines are often collected to detect and quantify levels of planktonic (dynamic) microbes. To ensure that test results are relevant to MIC, data from bulk fluids should be interrelated with other pipeline data, including liquid composition, operational conditions, sessile (attached) microbes' counts, and corrosion data.

Recent improvements in investigative methodologies (analytical, microbiological, electrochemical, and microscopy techniques) and instrumentation have made MIC evaluations, both at the laboratory and field locations, more reliable. Using microsensors to perform local chemical analysis within the biofilm is one of the most exciting advances in instrumentation.

Other noteworthy research tools for the study of biofilm structure are the following:

- Fiber-optic microprobe (optrode) for locating the biofilm−bulk water interface,
- Scanning vibrating electrode microprobe, where a highly capacitance-sensitive microelectrode scans over a metal surface (pipeline) exposed to an electrolyte and detects potential differences between anodic and cathodic sites. Current density in pitting areas is recorded, and thus cathodic and anodic areas are mapped. The current density maps can be overlapped with images of the surface attained through the microscope.

Modern instruments such as confocal laser scanning microscopy, environmental scanning electron microscope, quartz crystal microbalance with dissipation mode, and AFM allow nondestructive real-time monitoring of biofilms.

Studies of microbial species present in oil and gas pipelines have conventionally depended on the use of samples attained from pipelines to grow bacterial cultures in the laboratory. Laboratory results cannot accurately simulate the actual environments and operating conditions in assets such as pumps, pipelines, fittings, reservoirs. Therefore lab culture−dependent approaches misjudge the biocomplexity of microbial communities in biofilms. To overcome the shortcomings of the lab culture−dependent techniques, many culture-independent molecular microbiology techniques (see Chapter 22 of this book) have been developed in the past decades and introduced to oil and gas industry.

8.7.2.1 Microbiology: existence versus influence

A major knowledge gap is, knowing "which kind of microbe is causing corrosion?" One of the objectives is to assess what is there and what they might be doing. It is worth mentioning that the activity of the microbes present within the biological system is more significant than its mere presence, i.e., just knowing "the microbial inhabitants" is not enough to understand the role of microbes in the biofilm.

One crucial knowledge gap is the dynamics of microbial activity throughout the corrosion process. Until recently, techniques to identify and quantify microbial populations on corroding surfaces are mainly based on traditional techniques. Recent developments of microprobe analysis techniques will allow the chemical makeup of the corroding surface to be investigated. Fluorescence in-situ hybridization technique allows direct quantification of specific types of bacteria in microbial populations without the need to culture the cells in growth media. Enzymatic techniques provide opportunities to establish proper models to simulate microbial influenced corrosion and evaluate the behavior of metallic materials in liquids.

The utilization of special tools to identify microbes, particularly non−cultivation-based molecular tools, such as quantitative real-time polymerase chain reaction and high-throughput 16S/18S ribosomal DNA sequencing, is considered to be an important advancement in understanding the roles of different microbes associated with MIC (see Chapter 22 of this book). These non−cultivation-based molecular tools offer the potential to:

- identify dominant bacteria in a given biological environment regardless of the limitations of standard counting procedures;
- determine the fraction of MIC-causing bacteria in the entire microbe's population;
- pinpoint bacteria that are vulnerable or resilient to antimicrobial biocides;
- assess the variations in the overall microbes population caused either by the use of inhibitors (biocides) or nutrient alterations; and
- accomplish more reliable sampling methods that are not affected by time or transport concerns.

8.7.2.2 Detection and monitoring

Detection and monitoring methods are the most crucial tools in the field of MIC. Diagnosing MIC requires a wide range of field and laboratory analyses that may take time to complete. In addition, there is a strong tendency to require other mechanisms of corrosion to be disproved before MIC is diagnosed and mitigated, which lengthens the process.

Detection methods are mainly focused on the application and implementation of biological methods by making use of the features of the MIC-related bacteria. Monitoring programs for MIC have focused mainly on the assessment of planktonic populations in water samples and general corrosion by using corrosion coupons or online probes such as linear polarization resistance or electrical resistance probes. However, there exist disadvantages and doubts surrounding this kind of monitoring procedures, such as that the planktonic populations do not accurately reflect the types and numbers of organisms living in biofilms and affecting biodeterioration complications.

Additionally, the susceptibility of planktonic microorganisms to antimicrobial additives significantly differs from that of sessile organisms within the biofilm, mainly because of the protective action of their EPS.

Monitoring methods must provide information on well-established biofilms. The detection and monitoring data could be used to support development of procedures that would allow for improved prediction and modeling, because much of the industries use different approaches for collection of MIC-relevant data.

8.7.2.3 Procedures and standardization

Practical procedures and standards, such as standard corrosion test coupons and MIC-relevant standard microbial communities, are desired. These procedures and standards could be employed to achieve reliable and comparable cross-laboratories investigations. Data from such investigations can then be utilized in common databases that assist in understanding of what differentiates MIC from other forms of corrosion. It is also important to implement the results in appropriate testing standards and specifications.

8.7.2.4 Modeling and prediction

There are classes of microbes that are known to have a substantial influence (e.g., APB, SRB) on metals and materials in the oil and gas systems, but the relationship between these microbes and other microorganisms in a mixed or contaminated system is poorly understood. That is why modeling is needed to identify the role microbes play in MIC. Understanding the metabolic procedures that rule the development and persistence of microbes in oil and gas environments and/or in contact with infrastructure materials will permit the development of effective qualification tactics through the control of microbes' metabolism mechanism or inhibiting the MIC-causing agents.

Mathematical models can positively influence predicting the impact and necessity for biocide deployment as a method to limit MIC. Models need to exhibit mechanical and chemical interactions between diverse microbes present in complex biofilms formed on metals. These interactions have been problematic and difficult to measure and assess.

8.7.2.5 Future research significances

MIC researchers can perform an active role in materials, methods, procedures, and standards advancement and improvement in the direction of comprehensive understanding and recognition of MIC mechanisms. The research priorities can be listed as follows:

- *Material–microbe interaction*. To focus and identify changes microbes make on metals and their alloys.
- *Intermicrobes' interactions*. To investigate and determine which of the microbes present in the biofilm are active, mixed complex systems with multiple microbes should be examined to learn how these microbes can interact with each other.
- *Development of standards*. Standard test methods are required to guarantee that cases and accounts of MIC are being classified correctly. Collection of field samples should be of top importance for standards' development.

In the future, to overcome the difficulties caused by MIC, specialists from different fields need to work together to develop effective strategies against microbial degradation such as MIC.

8.8 Conclusions

The main types of bacteria associated with MIC in oil and gas industry are sulfate reducers (SRB), iron reducers (IRB), and iron and manganese oxidizers (IOB, MOB). Among the anaerobes the SRB with the subgroup *Desulfovibrios* are the most dangerous, but the aerobic *Pseudomonas*, which is one of the aerobic slime-forming bacteria, also cause severe corrosion of steel structures. Other microbes, i.e., acid producers, also deteriorate metals surfaces with fast metal dissolution. The planktonic cells are less dangerous than the sessile microbes embedded in biofilms.

The excretion of exopolymeric substances, which "glue" microbes onto solid surfaces, facilitates the biofilm formation. Bacterial surface and medium characteristics play important role in the microbial transfer rate, adhesion, and resulting biofilm size. A mature biofilm, which is a matrix of water, microorganisms, and organic and inorganic matter, provides an environment for anaerobes and for their metabolism near the solid surface. Such conditions favor the growth of SRB. These microorganisms produce sulfide ions from sulfate ions, which react with iron or other metal ions, forming insoluble metal sulfide. Localized corrosion starts underneath biofilms by establishing corrosion cells with very low-levels or negligible oxygen contents and low local pH values. These conditions favor the growth of SRB.

On the other hand, aerobic microorganisms (not only slime formers but also others such as acid producers) are far from the solid surface, i.e., near the top of the biofilm. Those microbes, by consuming the sulfide ions (metabolites of anaerobes), produce sulfuric acid and sulfate ions and evolve hydrogen. This postulated mechanism relates to the outer surface of vessels and structures. The environment within a pipeline is quite different. The biofilm and the aggressive metabolites alter the electrochemical reactions, change the pH values, and induce reactions at the cathodes and anodes. All these reactions that are enhanced by the presence of microorganisms increase the deterioration of crude- and gas-handling facilities through MIC.

Typical characteristic of MIC is a shiny, blackish surface and round pits scattered all over the solid surface, which in time cause the perforation of the metal. MIC is mainly prevalent underneath biofilms; the probability of biofouling is proportional to the risk of MIC. The mechanisms of MIC based on bacteria−metal reactions facilitated by microorganism also form an important part of the chapter.

After understanding the phenomenon and importance of MIC, it is important to learn as much as possible about the potential for MIC attack and circumstances/conditions (metals, microbial communities, pH, and temperature) that could lead to such attack. The first is to have a profound look at the local injury. For example, a slime or blackish shiny layer covering the metal surface could indicate MIC attack. The next step is proper pigging of the pipeline and sampling for identification of microorganisms in the collected organic-, inorganic- and biodeposits. When unambiguous is the presence of corrosion relevant microorganisms, the diagnosis is MIC, which often goes hand-in-hand with other types of corrosion and, additionally, with scaling. To decrease the influence of corrosion-relevant microorganisms, it needs the active collaboration of specialists from different fields (metallurgists, engineers, microbiologists) as only this cooperative activity will bear fruit in the future.

References

[1] A.R. Al-Shamari, A.W. Al-Mithin, S. Prakash, M. Islam, A.J. Biedermann, A. Methew, Some empirical observation about bacteria proliferation and corrosion damage morphology in Kuwait oilfield waters, in: NACE CORROSION 2013, 2013. Paper No. 2748.

[2] B.J. Little, J.S. Lee, Microbiologically influenced corrosion: an update, International Materials Reviews 59 (7) (2014) 384−393.

[3] M. Urquidi-Macdonald, A. Tewari, H.L.F. Ayala, A Neuro-Fuzzy knowledge-based model for the risk assessment of microbiologically influenced corrosion in crude oil pipelines, Corrosion 70 (11) (2014) 1157−1166.

[4] B.J. Little, J.S. Lee, Microbiologically Influenced Corrosion, Wiley Series in Corrosion, John Wiley & Sons, Inc., Hoboken, New Jersey, 2007.

[5] R. Bhola, S.M. Bhola, B. Mishra, D.L. Olson, Microbiologically influenced corrosion and its mitigation: a review, Material, Science Research India 7 (2) (2010) 407−412.

[6] R. Javaherdashtri, Microbiologically Influenced Corrosion: An Engineering Insight, Springer, London, 2008.

[7] T. Siddique, T. Penner, J. Klassen, C. Nesbo, J.M. Foght, Microbial communities involved in methane production from hydrocarbons in oil sands tailings, Environmental Science and Technology 46 (17) (2012) 9802−9810.

[8] C.G. Struchtemeyer, J.P. Davis, M.S. Elshahed, Influence of the drilling mud formulation process on the bacterial communities in thermogenic natural gas wells of the Barnett Shale, Applied and Environmental Microbiology 77 (14) (2011) 4744−4753.

[9] M. Kermani, D. Harrop, The impact of corrosion on oil and gas industry, SPE Production and Facilities 11 (03) (1996). SPE-29784−PA.

[10] N. Youssef, M. Elshahed, M. McInerney, Microbial processes in oil fields: culprits, problems, and opportunities, Advances in Applied Microbiology 66 (2009) 141−251.

[11] D. Enning, J. Garrelfs, Corrosion of iron by sulfate-reducing bacteria: new views of an old problem, Applied and Environmental Microbiology 80 (4) (2014) 1226−1236.

[12] M. Bethencourt, F. Botana, M. Cano, Biocorrosion of carbon steel alloys by an hydrogenotrophic sulfate-reducing bacterium, *Desulfovibrio capillatus* isolated from a Mexican oil field separator, Corrosion Science 48 (2006) 2417−2431.

[13] J.P. Euzéby, List of bacterial names with standing in nomenclature, a folder available on the internet, International Journal of Systematic Bacteriology 47 (1997) 590−592.

[14] E.S. Bastin, F.E. Greer, C.A. Merritt, G. Moulton, The presence of sulfate-reducing bacteria in oil field waters, Science 63 (1926) 21−24.

[15] B.J. Little, P. Wagner, F. Mansfeld, An overview of microbiologically influenced corrosion, Electrochimica Acta 37 (12) (1992) 2185−2194.

[16] E. Valencia-Cantero, J.J. Peña-Cabriales, Effects of iron-reducing bacteria on carbon steel corrosion induced by thermophilic sulfate-reducing consortia, Journal of Microbiology and Biotechnology 24 (2) (2014) 280−286.

[17] G. Muyzer, A.J. Stams, The ecology and biotechnology of sulphate-reducing bacteria, Nature Reviews Microbiology 6 (2008) 441−454.

[18] W. Allan Hamilton, Sulphate-reducing bacteria and the offshore oil industry, Trends in Biotechnology 1 (2) (1983) 36−40.

[19] S. Kebbouche-Gana, M.L. Gana, Biocorrosion of carbon steel by a nitrate-utilizing consortium of sulfate-reducing bacteria obtained from an Algerian oil field, Annals of Microbiology 62 (1) (2012) 203−210.

[20] C. Hubert, M. Nemati, G. Jenneman, G. Voordouw, Corrosion risk associated with microbial souring control using nitrate or nitrite, Applied Microbiology and Biotechnology 68 (2) (2005) 272−282.
[21] I. Neria-González, E.T. Wang, F.R. Rez, J.M. Romero, C.H. Rodriguez, Characterization of bacterial community associated to biofilms of corroded oil pipelines from the southeast of Mexico, Anaerobe 12 (3) (2006) 122−133.
[22] C.S. Chan, S.C. Fakra, D. Emerson, E.J. Fleming, K.J. Edwards, Lithographic iron-oxidizing bacteria produce organic stalks to control mineral growth: implications for biosignature formation, The ISME Journal 5 (2011) 717−727.
[23] R. Winston Revie (Ed.), Uhlig's Corrosion Handbook, third ed., John Wiley & Sons Inc., 2011.
[24] I. Beech, Corrosion of technical materials in the presence of biofilms − current understanding and state-of-the art methods of study, International Biodeterioration and Biodegradation 53 (3) (2004) 177−183.
[25] H. Mansouri, S.A. Alavi, A study of microbial influenced corrosion in oil and gas industry, Conference Paper, in: The 1st International Conference of Oil, Gas, Petrochemicals and Power Plants, 2012, pp. 15−27. Teheran.
[26] B. Huber, B. Herzog, J.E. Drewes, K. Koch, E. Müller, Characterization of sulfur oxidizing bacteria related to biogenic sulfuric acid corrosion in sludge digesters, BMC Microbiology 16 (153) (2016) 1−11.
[27] G.C. Friedrich, D. Rother, F. Bardischewsky, A. Quentmeier, J. Fischer, Oxidation of reduced inorganic sulfur compounds by bacteria: emergence of a common mechanism? Applied and Environmental Microbiology 67 (7) (2001) 2873−2882.
[28] D. Pokorna, J. Zabranska, Sulfur-oxidizing bacteria in environmental technology, Biotechnology Advances 33 (6 Pt 2) (2015) 1246−1259.
[29] M. Pósfai, R.E. Dunin-Borkowski, Sulfides in biosystems, Reviews in Mineralogy and Geochemistry 61 (2006) 679−714.
[30] M. Magot, Indigenous microbial communities in oil fields, in: B. Ollivier, M. Magot (Eds.), Petroleum Microbiology, ASM Press, Washington, DC, 2005, pp. 21−33.
[31] B.J. Little, F.B. Mansfeld, P.J. Arps, J.C. Earthman, Microbiologically influenced corrosion, in: Encyclopedia of Electrochemistry, Wiley-VCH Verlag GmbH & Co., 2007.
[32] ASM International, Corrosion in the petrochemical industry, in: V. Burt (Ed.), Essential Research, second ed., ASM International, 2015, p. 426.
[33] Boundless Microbiology, 2016. Retrieved from: https://www.boundless.com/microbiology/textbooks/boundless-microbiology-textbook/introduction-to-microbiology-1/microbes-and-the-world-19/classification-of-microorganisms-208-1908/.
[34] R. Eckert, T.L. Skovhus, Using molecular microbiological methods to investigate MIC in the oil and gas industry, Materials Performance 50 (8) (2011) 50−54.
[35] G. Leer, G.D. Lewis (Eds.), Microbial Biofilms: Current Research and Applications, Caister Academic Press, New Zealand, 2012.
[36] S.W. Borenstein, Microbiologically influenced corrosion handbook, in: Woodhead Publishing Series in Metals and Surface Engineering, Woodhead Publishing, Cambridge, UK, 1994.
[37] J. Telegdi, Microbiologically influenced corrosion (Chapter 6), in: K. Demadis (Ed.), Water Treatment Processes, Nova Science Publisher, 2012, pp. 145−167.
[38] J. Telegdi, T. Szabó, F. Al-Taher, É. Pfeifer, E. Kuzmann, A. Vértes, Coatings against corrosion and microbial adhesion, Materials and Corrosion 61 (12) (2010) 1001−1007.
[39] J. Telegdi, L. Románszki, F. Al-Taher, E. Pfeifer, E. Kálmán, Nanolayers against microbial adhesion, in: NACE International Corrosion, 2009. Paper No. 3987.

[40] G. Diósi, J. Telegdi, G. Farkas, L.G. Gazsó, E. Bokori, Corrosion influenced by biofilms during wet nuclear waste storage, International Biodeterioration and Biodegradation 51 (2) (2003) 151−156.
[41] P. Gumpel, N. Arlt, J. Telegdi, D. Schiller, O. Moose, Microbiological influence on the electrochemical potential of stainless steel, Materials and Corrosion − Werkstoff und Korrosion 57 (2006) 715−723.
[42] J. Telegdi, A. Shaban, J. Beczner, Z. Keresztes, E. Kálmán, Biofilm formation controlled by quartz crystal nanobalance, Materials Science Forum 289−292 (1998) 77−82.
[43] B. El Gammudi, I. El Musrati, A. Bourgheya, A. El Tawil, Microscopic study of bacterial attachment on AISI 304 and AISI 316 stainless steel, Surfaces International Journal of Integrative Biology 4 (2) (2008) 72−77.
[44] B. Mishra, Corrosion characterization of advanced steels for use in the oil & gas industry, International Journal of Metallurgical Engineering 2 (2) (2013) 221−229.
[45] J. Telegdi, L. Trif, L. Románszki, Smart antibiofouling composite coatings for naval applications (Chapter 9), in: M.F. Montemor (Ed.), Smart Composite Coatings and Membranes: Transport, Structural, Environmental and Energy Applications, Woodhead Publishing, 2016, pp. 123−155.
[46] S. Kakooei, M. Che Ismail, B. Ariwahjoedi, Mechanisms of microbiologiacally influenced corrosion. A review, World Applied Sciences Journal 17 (4) (2012) 524−531.
[47] C.A. Von Wolzogen Kühr, L.S. Van der Vlugt, Graphitization of cast iron as an electrochemical process in anaerobic soil, Water 18 (16) (1934) 147−165.
[48] W.P. Iverson, Direct evidence for the cathodic depolarization theory of bacterial corrosion, Science 151 (3713) (1966) 986.
[49] H. Cypionka, W. Dilling, Intracellular localization of the hydrogenase in *Desulfotomaculum orientis*, FEMS Microbiology Letters 36 (2−3) (1986) 257−260.
[50] S.D. Silva, R. Basséguy, A. Berger, The role of hydrogenases in the anaerobic microbiologically influenced corrosion of steels, Bioelectrochemistry 56 (1−2) (2002) 77−79.
[51] R.D. Bryant, W. Jansen, J. Boivin, E.J. Laishley, J.W. Costerton, Effect of hydrogenase and mixed sulfate-reducing bacterial populations on the corrosion of steel, Applied and Environmental Microbiology 57 (10) (1991) 2804−2809.
[52] P. Marcus, Corrosion mechanism in theory and practice, in: P. Marcus (Ed.), Corrosion Technology Series, third ed., CRC Press, 2011.
[53] R.A. King, J.D.A. Miller, Corrosion by sulfate reducing bacteria, Nature 233 (1971) 491−492.
[54] C. Obuekwe, D. Westlake, J. Plambeck, Corrosion of mild steel in cultures of ferric iron reducing bacterium isolated from crude oil: II. Mechanism of anodic depolarization, Corrosion 3711 (1981) 632−637.
[55] B. Little, P. Wagner, K. Hart, R. Ray, D. Lavoie, K. Nealson, C. Aguilar, The role of biomineralization of microbiologically influenced corrosion, Biodegradation 9 (1) (1998) 1−10.
[56] M. de Romero, The mechanism of SRB action In MIC based on sulfide corrosion and iron sulfide corrosion products, in: Corrosion/2005, NACE international, Houston, TX, (2005), 2005. No. 05481.
[57] T. Gu, D. Xu, Why are some microbes corrosive and some not?, in: CORROSION'2013, Orlando, FL, March (2013), 2013, pp. 17−21. Paper No. C2013-0002336.
[58] A. Rajasekar, S. Ponmariappan, S. Maruthamuthu, N. Palaniswamy, Bacterial degradation and corrosion of naphta in transporting pipeline, Current Microbiology 55 (5) (2007) 374−381.

[59] F. Bruecker, B.C. Santos, P.D. Quadros, Fuel biodegradation and molecular characterization of microbial biofilms in stored diesel/biodiesel blend B10 and the effect of biocide, International Biodeterioration and Biodegradation 95 (2014) 346−355.
[60] S. Mohanan, A. Rajasekar, N. Muthukumar, et al., The role of fungi on diesel degradation, and their influence on corrosion of API 5LX, Corrosion Prevention and Control 52 (4) (2005) 123−130.
[61] J. Wen, T. Gu, S. Nesic, Investigation of the Effect of Fluid Flow on SRB Biofilm, in: Corrosion/2007, NACE International, Houston, TX, (2007), 2007. Paper No. 07516.

Pitting corrosion

9

Nihal U. Obeyesekere
Clariant Oil and Mining Services, The Woodlands, TX, United States

9.1 Introduction

Localized corrosion is defined as the type of corrosion in which there is an intense attack at localized sites on the metal surface. These localized sites corrode faster than the rest of the metal surface. Such a phenomenon arises due to the breaking down of the protection of the metal surface at the local site with respect to overall metal surface. The chemical environment of the local area could remove protection layers such as oxides or metal salt films. Hence, these failures can be due to (1) crystal imperfection of the metal at the local site, (2) inclusions in the metal, or (3) local breakdown of the inhibitor film (in the case of chemical treatment). Once the corrosion protection layer breaks down locally, corrosion is possible in these areas [1,2].

Localized corrosion is classified into two types: crevice corrosion and pitting corrosion.

Crevice corrosion is defined as corrosion occurring in confined areas of the metal surface, where the access to the environment is restricted. These confined areas are called crevices. For example, crevices can be created under gaskets or seals and spaces covered by deposits. Under the crevice, metal ions produced from the anodic reaction are restricted to be transported outside the region. This would increase the metal ion concentration under the restricted area, promoting the hydrolysis reaction between the metal ions and water and thus lowering the local pH. This occurrence would lead to severe corrosion underneath the crevice [3,4].

Pitting corrosion is caused by local dissolution of the metal surface. This leads to the formation of deep localized pits in passivated metals exposed to aqueous media with dissolved salts [5,6]. It is the localized accelerated dissolution of metal that occurs as a result of the breakdown of the passive protective film on the metal surface. The dissolved salt anions such as chloride, thiosulfate, and bromide anions can interfere with the formation of the protective film leading to pitting corrosion [7−10]. These anions such as chloride anions (see Section 9.6) originate from strong acids and can induce pitting corrosion. Migration of chloride ions into the pit would increase $FeCl_2$ concentration and hence lowering the pH. Pitting corrosion is defined by a localized attack on an otherwise passive metal surface. For example, stainless steel forms an oxide layer on the metal surface, which greatly reduces corrosion. However, the tenacity of the metal oxide layer is weakened by the insertion of chloride into the metal oxide film attached on the metal surface. The metal chloride complex formed can be much more soluble in aggressive aqueous environments. This would lead to holidays or vacancies in the metal oxide matrix. This would expose bare metal surface to aggressive aqueous

Trends in Oil and Gas Corrosion Research and Technologies. http://dx.doi.org/10.1016/B978-0-08-101105-8.00009-7

environment leading to pitting corrosion [11]. This type of corrosion occurs on alloys that are protected by passivating oxide layers, such as stainless steels in environments that contain aggressive anion species such as chloride anions [12,13].

On the contrary, the metal in an environment with lesser protective passive films does not necessarily produce pitting corrosion. For example, metals or alloys in an aggressive low pH, high CO_2 environment, produce iron carbonate as the passive film and yield more general corrosion, whereas an aggressive sour environment that produces FeS as the passive film would yield more pitting corrosion. This is due to higher solubility of iron carbonate in aqueous solutions compared with FeS and would produce a less tenacious protective film, which in turn, would cause more general corrosion. Iron sulfides are generally less soluble in aqueous media and can make more protective and tenacious films. Iron sulfide polymorphs, which are dictated by the chemical environment, lead to various kinds of films. Some iron sulfide forms are more protective than others. However, these FeS films can break due to various reasons and expose the bare metal to aggressive aqueous medium inducing pitting corrosion [14]. Pitting initiation, propagation, nucleation, the role of the pit cover, and pitting under sweet or sour conditions are discussed in detail in the following sections.

9.2 Environmental effects in pit formation

The pit formation is highly influenced by the environment around it. The chemical environment surrounding the pit plays a greater role in pit formation and propagation. Anions such as chlorides, bromides, and thiosulfates can produce stable aggressive pits. In oil field applications, the most common anionic species is the chloride ion. Chlorides bind to cations enhancing their solubility in aqueous media. This may breakdown the passivated layer. Chloride ions are relatively small and have high diffusivity. They can go to anodic sites from the bulk solution with relative ease.

Inside and around the pit, the pH can drop because of the hydrolysis of cations as shown in reactions (9.i)–(9.iii).

$$M \rightarrow M^{+2} + 2e^{-}(\text{Anode}) \tag{9.i}$$

$$M^{+2} + 2H_2O \rightarrow M(OH)^{+} + H^{+} \tag{9.ii}$$

$$M(OH)^{+} + H_2O \rightarrow M(OH)_2 + H^{+} \tag{9.iii}$$

A considerable understanding of the pitting phenomenon has been recently developed. However, an in-depth understanding of many steps is still missing. Fundamental studies usually have focused on one or more steps of the pitting process:

1. Characteristics of the passive film, the initial formation of the passive film and its breakdown, the formation of metastable pits (initial pits formed, which grow to the micron scale and then repassivate).
2. The formation and propagation of larger and stable pits.

It should be noted that, whereas localized dissolution following the breakdown of an otherwise protective passive film is the most common and technologically important type of pitting corrosion, pits can form under other conditions as well. For instance, pitting can occur during active dissolution if certain regions of the sample are more susceptible and dissolve more than the rest of the surface.

9.3 Electrochemical methods used to determine pitting potential

It is possible to utilize electrochemical methods to understand pitting corrosion. Stable pits can be formed at potentials higher than the pitting potential (E_{pit}). The pits then grow at potentials higher than the repassivation potential (E_r). The repassivation potential is lower than the pitting potential. Table 9.1 presents the symbols that define various types of pitting potentials and their definitions.

Pitting potential (E_{pit}) is defined in several ways. The E_{pit} is defined as the potential below which pits do not nucleate and above which stable pits can survive and grow (see Fig. 9.1). E_{pit} is also defined as the applied potential necessary to maintain a salt film in a small open pit [15,16]. At E_{pit} and higher potentials, metastable pits can become stable pits. The other definition is that above E_{pit}, the passive film is locally unstable and repassivation is not possible. At the vicinity and just below E_{pit} metastable pits can grow [17]. The repassivation potential E_r is defined as the potential below which neither stable nor metastable pits can grow and above which, metastable pits can form and nucleated pits can grow.

9.3.1 Evaluation of anodic polarization curves

The defects on the surface of the metal can produce a potential drop, which can lead to pit propagation. This phenomenon can be experimentally investigated by polarizing

Table 9.1 Symbols that define various types of pitting potentials

Symbol	Name
E_b	Breakdown potential, breakthrough potential
E_c	Critical potential
E_i	Initiation potential
E_z	Potential of pit precursor
E_{np}	Nucleation potential
E_p or E_{pit}	Pitting potential
E_{rp} or E_r	Repassivation potential

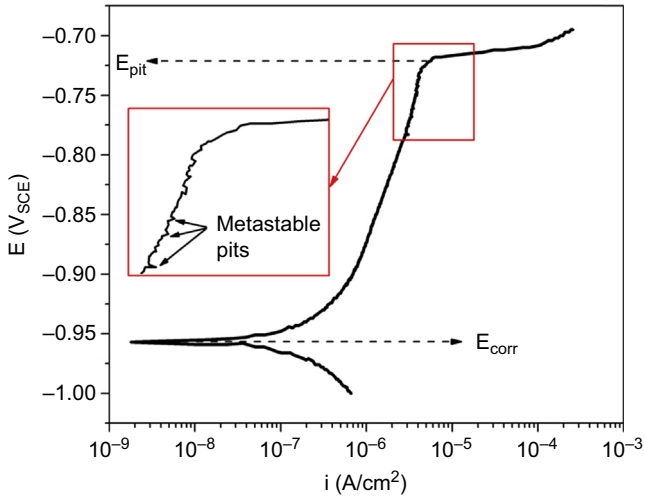

Figure 9.1 Schematic polarization curve for a metal that can undergo pitting where pitting is initiated at the breakdown potential (E_b).

the metal surface against a reference potential, using a potentiostat. An anodic polarization would lead to increasing anodic current densities (see Fig. 9.1).

Repassivation potential can be determined by measuring the polarization curve in the reverse direction, from positive to negative potential (Fig. 9.2). In the normal curve, the anodic current density starts to increase and then slows down as passivation takes place. When the potential increases further, the current density remains constant (passive region) and then it increases again as it enters the trans-passivation region. Loss of the passive film at these higher potentials is an inherent characteristic of the metals and alloys. If pitting is initiated, a sudden increase of the current density can be observed. The potential at which pitting is initiated is known as the pitting potential and denoted as E_{pit}. Earlier, it was considered the lowest potential at which pits can initiate but later observations of short-lived pitting events led to a different conclusion. The current spikes indicate pits forming but not as permanent pits. These are now commonly known as metastable pits [18].

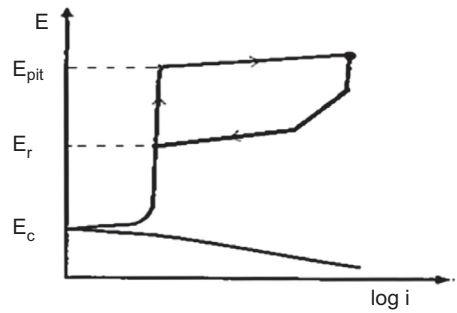

Figure 9.2 Evans polarization curves indicating current burst at potentials higher than E_{pit}.

Frequently, instabilities of current density are observed when the potential is approaching the pitting potential. The current fluctuates at this region due to initiation and repassivation of sites for pits prior to pit propagation (see Fig. 9.1). This may be due to repassivation of metastable pits. Given identical material and conditions (temperature, pressure, and salt concentration), the frequency of metastable pit formation depends on the surface conditions. Smooth and highly polished surfaces tend to produce less metastable pits and have a higher pitting potential [19].

Large metastable pits are associated with rougher surfaces. Perhaps this is due to gouging out of inclusions that support pit initiation.

There are two major influences that can help pit initiation: First, as the potential increases, the current density in the preexisting flaws in the film increases. This is until the local IR (surface potential) is exceeded and would produce active corrosion in the bottom of the flaw. Second, some anions such as chlorides are known to lower E_{pit}. The increasing anodic potential can attract more anions to the surface of the metal as it becomes more positive. This would create pitting by dissolution of metal at the site, thus inducing a pitting environment.

9.3.2 Repassivation potential measurements

Repassivation potential (E_r) is determined by the polarization curve in the reverse direction. After reaching the upper current limit, the potential is reversed and changes direction from positive to negative. As the potential decreases, the surface has the chance to repassivate. This makes the current diminish. When the current crosses the previously measured low passive current, the repassivation potential is determined (Fig. 9.2).

At the primary passivation potential, the surface starts to passivate and the current is reversed. The current at this potential (primary passivation potential or E_{pp}) is denoted as the critical anode current density (I_{crit}). I_{crit} is the current density for film formation to supply the metallic ions to be incorporated into the film. Both of these parameters should be exceeded for stable film formation. At this point, the metal surface is covered with a protective film. With increasing potential, current decreases but stops at I_{pass} due to complete formation of the protective film. The potential increase no longer affects the current because of the passivation film on the metal surface and current is a constant in this region and known as the passive region. The current does not change with increasing potential at this region. At the beginning of the transpassive region, the high potential starts to destroy the passive film. Thus increasing the current and hence the corrosion (Fig. 9.3).

9.3.3 Pit depth

When the metal starts to dissolve locally for any reason, the local chemical environment tends to change. An individual pit can happen because of the loss of the passive layer. The passive layer may be a metal oxide layer, metal salt layer, or a corrosion inhibitor film. The initial pit that forms can go back to a dormant state (repassivate) and may not become active again.

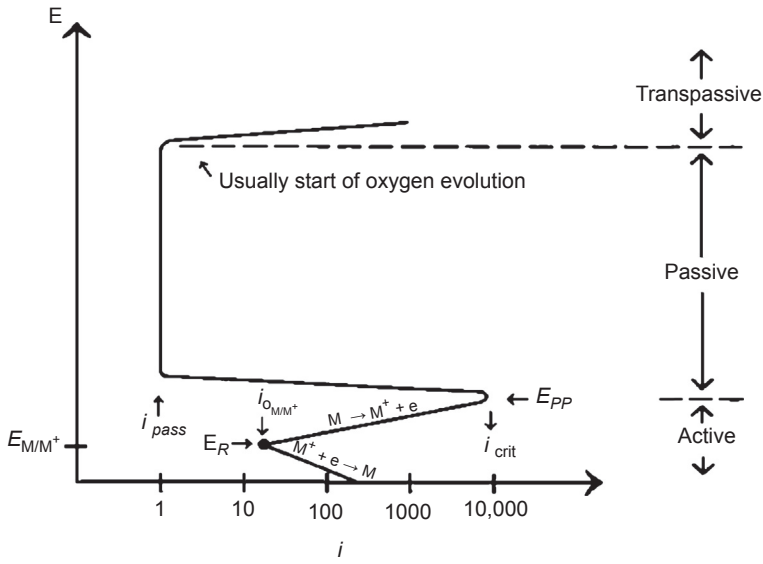

Figure 9.3 Typical anodic dissolution behavior of an active—passive metal. E_{PP} is the primary passivation potential, and i_{crit} is the critical anodic current density, and i_{pass} is the passive current density [20].

However, when repassivation does not take place for any reason, then the pit can start to grow. The metal ion that forms would create an extremely high acidic environment, thus increasing the local rate and pit depth. The types of pits formed in this manner are depicted in Fig. 9.4.

Should pitting occur, a complex mechanism for metal dissolution indicates a localized attack that may involve metal penetration in its surface. Furthermore, pitting depth can be defined by the following empirical equation (9.1):

$$D = \lambda t^n \tag{9.1}$$

where t = time, D = pit depth, and λ and n are constants.

Measured pit depth is generally a better indicator than the measured mass loss, in determining a localized corrosion attack. Pit depth measurements can be accomplished by several methods. They include metallographic examinations and microscopic measurements. In the microscopic method, a powerful microscope is focused on the top and on the bottom of the pit. The measured difference is used to calculate the pit depth.

Through the use of a high-powered digital microscope, many different characteristics of the pit can be observed. The revolver zoom lens allows a wide zoom range and field of view from 8 mm down to 0.12 mm. The triple objective turret provides magnification up to 2500×. Autocalibration of the lens is integrated and recognizes the objective lens positions as well as the zoom level. All calibration information is stored and displayed, ensuring proper equipment operation and accuracy.

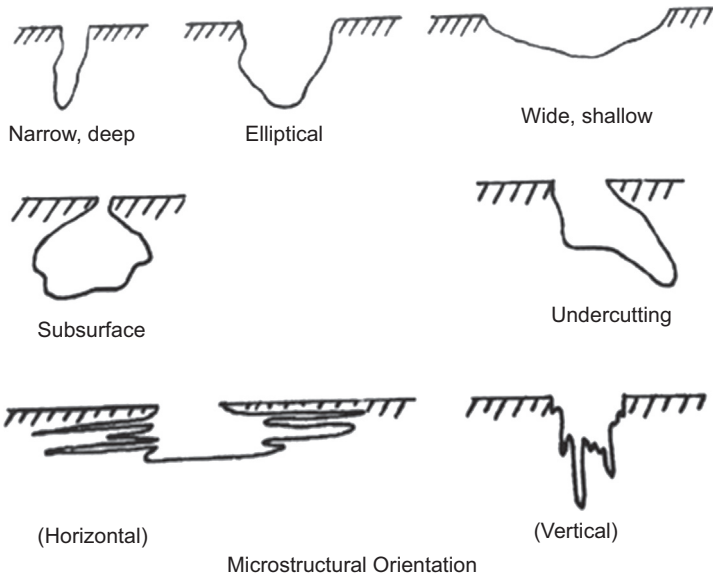

Figure 9.4 Typical shapes of pits [21].

The lens also possesses a dual illumination mechanism, which provides both coaxial and ring lighting. Ring lighting is a form of light that provides uniform illumination and reduces shadowing due to the proximity between the light source and sample. Coaxial lighting is then used to view the subject and produce a bright image. Coaxial lighting utilizes a half-mirror to reflect half of the light from the source and transmits the rest to the lens. Through the use of the dual illumination mechanism, the user can choose between one of the two light sources, or use both to capture different images of one object (Fig. 9.5).

The metal coupons are placed on the stage directly under the lens. The microscope acts as a digital camera, which outputs the images to a monitor. The coupon is not directly observed through an eyepiece (Fig. 9.6). This makes the analysis easier on the user. The motorized stage provides the user with the ability to methodically scan an object thoroughly. The microscope is able to capture two-dimensional measurements in real-time, such as length, area, angle, diameter, and surface area of the coupon.

The microscope is also able to create three-dimensional (3D) images and 3D profiles. The integrated stepping motor travels through and scans set image planes, and within a few seconds these planes are stacked to accurately create a 3D image along with a 3D profile.

The pit observed on the metal coupon in Fig. 9.6 is converted to a 3D image and 3D profile observed in Fig. 9.7. From this 3D model image and profile, it is possible to measure the pit depth accurately.

The repeatability of pit depth measurements for a single pit is given in Table 9.2. This indicates that as the magnification is increased from 65 to 370×, the average

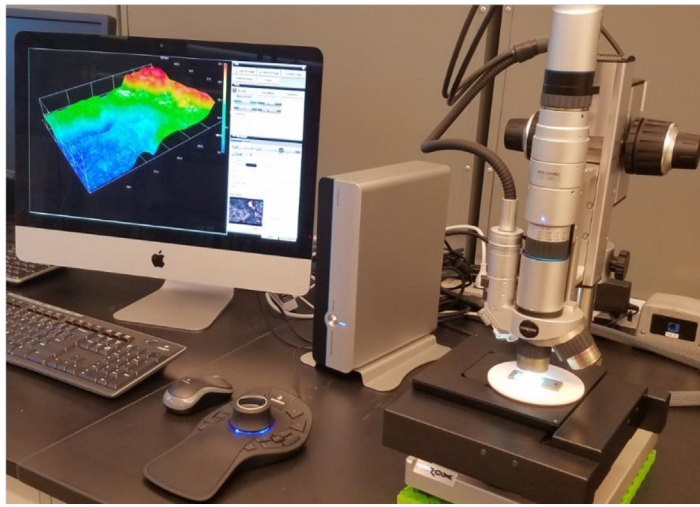

Figure 9.5 High-powered digital microscope to analyze pit depth, pit volume, pit frequency, and area of the pit. The microscope is capable of magnifying up to 2500×.
Printed with permission from Clariant Oil Services.

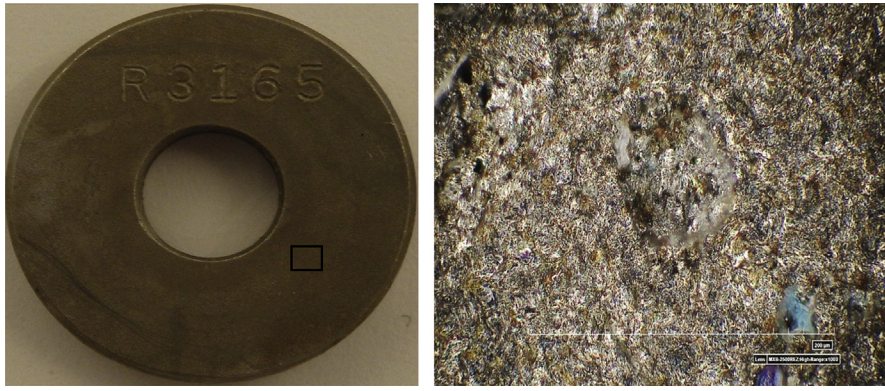

Figure 9.6 A round coupon subjected to a corrosive environment. The area of analysis is given in the *black square* (left). Photo of analyzed pit at 1000× (right).

pit depth decreased from 0.17 to 0.151 mm. Also, notice that the accuracy and repeatability of the measurement of the pit depth improved with higher magnifications.

Another method to determine pit depth is X-ray radiography. It is an easy method to quantify pitting corrosion both in terms of pit depths and percentage of effected areas. This is a nondestructive testing (NDT) technique and used to monitor and detect severe corrosion attack on metal surfaces. An X-ray beam penetrates the surface of the metal and creates a variable intensity of the transmitted beam. In the resulting X-ray photograph, the low intensity beam would cause a dark image, whereas the high intensity would give a brighter image (Fig. 9.8).

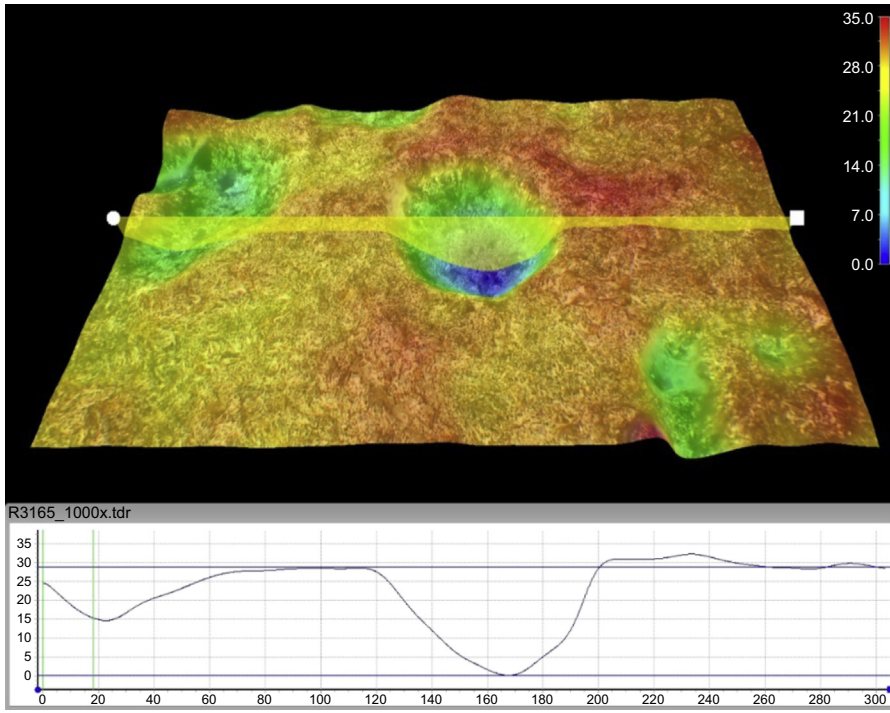

Figure 9.7 Three-dimensional profile of coupon R3165 pitting at 1000× (top photo). The pit depth was 28.6 μm (lower photo).
Printed with permission from Clariant Oil Services.

9.3.4 *Critical pitting temperature and critical crevice temperature*

Temperature increase is considered one of the main reasons for localized attack on metals and alloys. Increase in temperature causes the E_{pit} to decrease and lead to corrosion damage. The increasing temperature causes higher current transients and promotes the conversion of metastable pits into stable growing pits. The critical pitting temperature (CPT) or critical crevice temperature (CCT) is defined as the lowest temperature at which the metal surface starts to pit. Below this temperature, the steel does not suffer pitting, when exposed to any aggressive chloride solution (such as $FeCl_3$) or subjected to a constant anodic potential in a corrosive environment. An experiment at a constant anodic potential can be conducted to determine the CPT by increasing test temperature until a large pitting current occurs. The other method that can be used to determine the CPT of an alloy is by determining the temperature at which the potential is needed to produce a current density of 10 μA/cm^2 [24].

Pitting corrosion can be evaluated and ranked using the CPT in accordance to the ASTM Standard G48-03 [25]. This is the test method for pitting and crevice corrosion of stainless steels and alloys by use of $FeCl_3$. The CPT is the minimum temperature (°C)

Table 9.2 Pit depth measurements and magnification (standard guide for examination and evaluation of pitting corrosion [22])

Magnification	Pit depth (mm)
65	0.183
	0.159
	0.179
	0.174 avg
132	0.159
	0.160
	0.155
	0.159
	0.159 avg
200	0.149
	0.157
	0.150
	0.153
	0.152 avg
370	0.151
	0.151
	0.152
	0.151 avg

required to produce pitting corrosion and it is usually higher than the CCT. The standard test methods given in this document can be used to determine the effects of alloying, additives, heat treatment, surface finishes, and crevice corrosion resistance [25].

CPT can also be a function of surface roughness. A schematic of the corrosion testing equipment designed for CPT measurements is depicted in Fig. 9.9 [26]. Moayed et al. concluded that the surface roughness decreases the CPT. The authors used a potentiostatic technique and studied various surface roughnesses of 904L stainless steel in 1 M NaCl solution. These experiments revealed that the highest polished surface, at 3 μm finish, yielded a CPT of 56°C (122°F), whereas a rough surface finished at 60 grit yielded a CPT of 45°C (113°F) [27].

Eghbali et al. used a potentiodynamic measurement to determine CPT [26]. The electrochemical cell employed in this work is given in Fig. 9.9. Three electrode

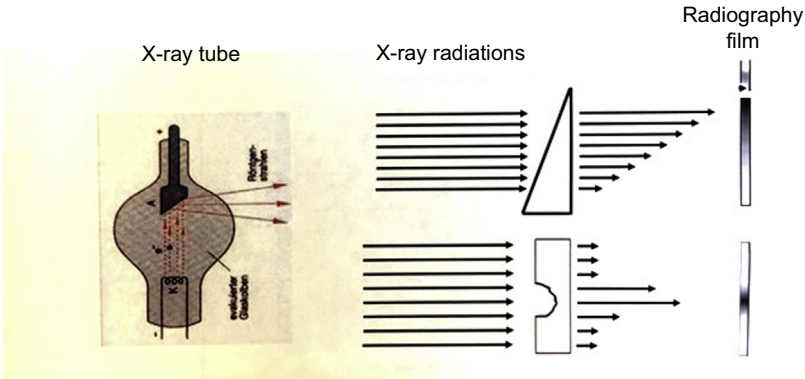

Figure 9.8 Photograph of X-ray radiography of a corroded metal [23].

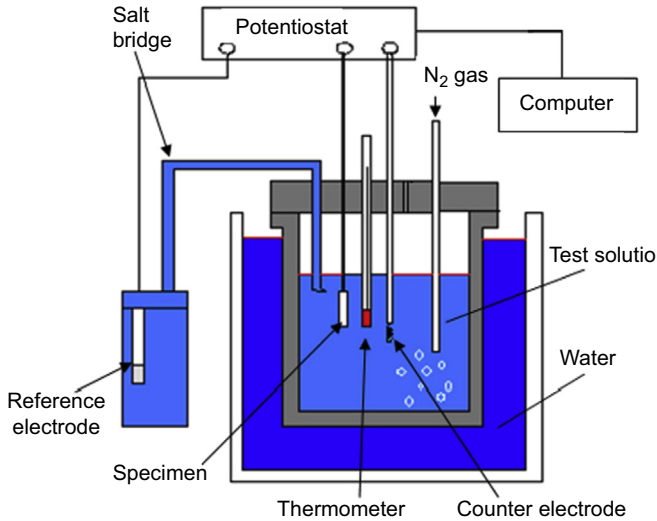

Figure 9.9 Schematic of the electrochemical cell used for corrosion testing [26].

systems (platinum was used as the counterelectrode, and saturated calomel connected through a salt bridge was used as the reference) with specimens with 600 grit surface finish were used. The study was done by varying the potential and measuring current density at a particular temperature.

Fig. 9.10(a–d) depicts the polarization curves at 0.1M NaCl solution with varying concentration of molybdate inhibitor and varying temperatures.

It was observed that the presence of the inhibitor influenced the pitting potential of alloy DSS 2205. The authors concluded that the addition of molybdate solution containing 0.1 M NaCl improves the CPT of this alloy. These experiments indicate that in the presence of 0.01 M molybdate (see Fig. 9.10(c)), the CPT of the alloy increased by 10°C (50°F). When the concentration of the inhibitor was increased to 0.1 M, the authors did not see any evidence of pitting up to 85°C (185°F).

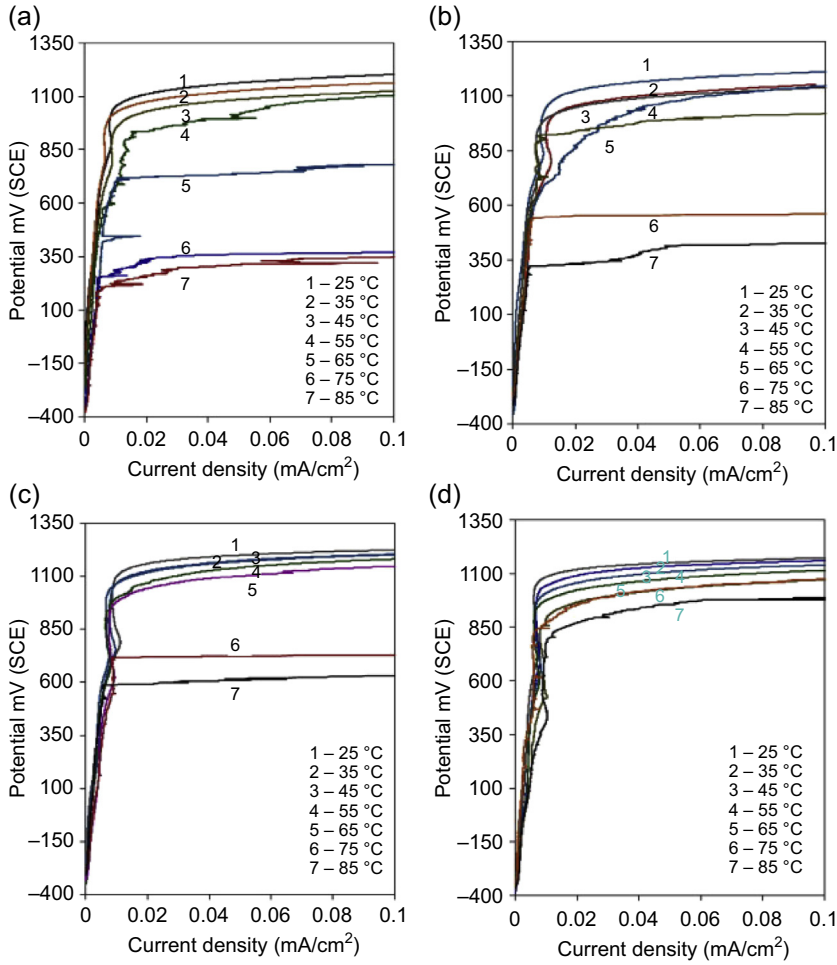

Figure 9.10 Potentiodynamic polarization curves of DSS 2205 metal with different types of brines. (a) 0.1 M NaCl with 0.00001 M MoO_4^-, (b) 0.001 M, (c) 0.01 M, (d) 0.1 M [26].

Fig. 9.11 depicts the evaluation of CPT of potentiostatic measurements at a transpassive potential of 750 mV against SCE. The temperature was increased at a rate of 0.6°C/min. The CPT increased with increasing inhibitor concentration. It is interesting to note that at lower inhibitor concentrations (0.0001 M, 0.001−0.01 M molybdate), the CPT increase was relatively low with the temperature increments of 0.5°C (33°F), 2.5°C (37°F), and 12°C (54°F), respectively. However, they did not see a CPT value after screening up to 86°C (187°F) at the inhibitor concentration of 0.1 M.

These experiments indicate that CPT can be increased by using a suitable corrosion inhibitor. The inhibitor concentration and CPT do not seem to have a linear relationship.

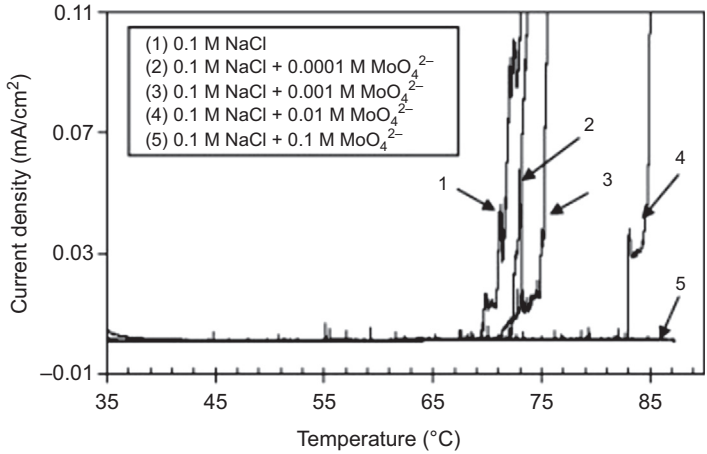

Figure 9.11 Current density versus temperature to measure critical pitting temperature at 0.6°C/min temperature. DSS 2205 metallurgy was used with several concentrations of the inhibitor [26].

9.4 Kinetics of pit growth

The rate of pit growth depends on several factors: the metal composition, ohmic potential drop inside the pit, and the electrolyte composition inside, as well as outside the pit. It is also important to consider the physical and chemical properties of the passive film that usually covers the mouth of the pit. The passive film's porosity, tenacity, elasticity, and the pit bottom potential can also play a major role in pit kinetics. Pit growth is a function of any of these factors, as well as a function of the metallurgy of the specimen. The pH of the bulk solution and the pH inside a pit can be very different. Inside a pit, the pH can be as low as zero [28]. Even metal chloride salt (e.g., iron chloride) can be found inside the pit.

9.4.1 Pit growth in a bulk specimen as a function of time

Kinetics studies of pit growth and potentiostatically were performed by Engell et al. [29]. They showed that when time (t) is measured from the beginning of the pit to the propagation stage, the total current (I) is given by the following Eq. (9.2):

$$I = k \cdot t^{b} \tag{9.2}$$

In the above Eq. (9.2), k is a constant that depends on the chloride ion concentration. The value of b can be between 0.3 and 3 and is dependent on several different factors and they are morphology of the pit, chloride ion concentration, crystal orientation, and temperature [29a,b]. Pit kinetics can be influenced by two factors: (1) the diffusion of the salt film present inside the pit towards the outside of the pit and (2)

this salt film dissolution rate, which is controlled by an ohm-like law [30]. For pit growth under diffusion control, the applied potential may not have any effect. Although for ohmic control pit growth, its current density will depend on the applied potential.

The value of b (Eq. 9.2) can be between 0.3 and 3, depending on the morphology of the pit, chloride anion concentration, temperature, and metal crystal orientation [31−33]. Pit kinetics and growth will not necessarily increase linearly with time ($b = 1$ in Eq. 9.2). Herbsleb et al. [33] measured the rate of pit growth in mild steel as a function of chloride ion concentration and applied potential in a sulfuric acid solution. They found that the pit count and the mean pit radii increased linearly with time. However, at higher pit densities the linearity deviated. The authors believed that corrosion byproduct has an activating influence on the remaining metal surface. This leads to a more rapid rather than linear ($b > 1$) relationship for mild steel [33]. The pits were mainly hemispherical and the increase of the dissolution current was independent of the potential, purity of the specimen (in this case mild steel), and sulfate iron concentration. However, the current density in the pits was dependent on the chloride ion concentration [32,34,35].

9.4.2 Initiation stages of pit growth

The initiation stages of the pit growth at the very beginning of the formation of the pit (10^{-3} to 10^{-1} s after pit nucleation) produce a very high current. Strehblow et al. conducted experiments using nickel and iron leading to the conclusion that pit growth starts with the adsorption of chloride ions on to the bare metal. This is followed by the ionization of the complexes [36]. Popov et al. [37] established different stages of pit growth. The authors considered different stages of the pit formation depending on the processes that take place inside the pit. The stages are adsorption, charge transfer, dissolution of complexes formed on the metal surface, diffusion, migration, and convection. They differentiated the different stages of pit growth.

9.5 Criteria for pit growth

9.5.1 Critical pit stability

When the conditions are correct, pits start to grow. However, many nucleated pits do not grow into stable pits. It is not known why some pits survive and others do not. Inside a growing pit, pH can be very low with salt films at its bottom. The mouth of the pit is usually covered by a layer of a passive film along with corrosion byproducts and sometimes complexes with corrosion inhibitor products. Above a critical concentration of ions in the pit electrolyte, a pit can start to grow independently. Below this critical concentration, repassivation tends to occur. This repassivation is independent of the pit radius or repassivation potential [38].

Galvie [39] suggested that for pit stability, a critical acidification is necessary inside the pit. The author postulated that metal ions hydrolyzed inside the micropits and that

pit growth is a function of active dissolution in the pit environment. As indicated in reactions (9.i)−(9.iii) (see Section 9.2), hydrogen ions produced inside the pit due to hydrolysis and a corresponding high concentration of chloride ion would migrate from the bulk solution. It was suggested that for a stable pit, pH should be sufficiently low to keep maintain the pit activity and grow [39].

The stability of pits can be increased by anions such as chlorides, but decreased in the presence sulfates [40]. The authors indicated that the presence of sulfate causes the distribution of available pit sites to be shifted to a higher potential. This implies that the pit nucleation is inhibited. It was also shown that the sulfate ions acted as an inhibitor for pit propagation in metastable and stable states. It is possible that the solubility of the decreased metal salt may have reduced pit propagation current densities.

Isaac suggested that dissolution kinetics depends on the concentration of chloride ions in contact with dissolving surfaces [41]. However, he found that the stability of the pits due to chloride ion concentration also depends on the type of the metal or alloy. The dissolution kinetics was found to depend on the chloride ion concentration in contact with the dissolving surface. For stainless steel and nickel alloys, the pits repassivated at high chloride content, whereas, with iron and nickel, the pits remained stable (active) as the chloride content decreased.

9.5.2 Role of pit cover

Pit cover is an important factor in pit growth. The cover found at the pit mouth consists of some passive film, metal, and sometimes corrosion byproducts [42,43]. The pit cover plays an important role in stabilizing the pit growth [5,44,45]. The development of a single corrosion pit thus occurs in three consecutive kinetic steps:

1. Nucleation
2. Metastable propagation
3. Stable propagation

The metal surface is initially passive prior to pitting. The growth of a corrosion pit occurs because of the weakening and breaking of the passive film surrounding the pit nucleation site. The bulk of the cover is at the initial pit nucleation site. The weakened or the damaged pit cover would allow diffusion of metal ions out of the pit to the bulk electrolyte. As the pit starts to grow larger beneath the pit cover, the pit cover would become weaker. Pit growth is controlled by diffusion of metal ions through the flowed pit cover to the bulk solution. Therefore, ions such as iron ions from the inside of the pit can transport to outside through this permeable cover. When the diffusion rate is accelerated, the pit growth rate is increased as well [46].

The stabilization of a pit can depend on the pit cover chemical composition, porosity, and strength. For example, a strong nonporous pit cover can support the pit stability. Although a weak and porous passive film can hinder the pit's ability to grow. This is also true for metastable pits. The metastable pits with a strong passive film can survive to become stable and active pits.

Pitting stages are usually described through the nucleation of pits, their growth, and repassivation. These processes are usually sequential. The formation of metal chlorides

can hinder this process [47]. The access of aggressive anions (e.g., chloride anions) at the surface of the metal can cause the passive film to break down. This happens by interacting the anion with metal oxide passive film and bonding to metal oxide layer and replacing metal oxide bond with a metal halide bond. Successive partial breakdown of the film pit cover leads to current increases. These current increases take place because of the dissolution of iron to iron ions under the pit cover. Once the cover breaks down, repassivation occurs and the current stops. A complete breakdown of the passive film at the metastable stage, leads to the dilution of the pit, and the pit will repassivate. If the cover ruptures totally before the pit can grow to a larger enough size to support itself, the corrosive fluid within the pit is highly diluted and the pit repassivates leading to the death of the pit.

The pit cover plays an important role to help pits to grow from the nucleation stage. The physical chemistry of the pit cover is important and should allow the metal ions to migrate out while not being porous enough to allow bulk solutions to come through it and dilutes the inner electrolyte of the growing pit. If the pit cover is totally ruptured, then the highly acidic electrolyte inside gets diluted and the pit dies. Conversely, if the pit is deep enough, this dilution effect would not be a factor.

9.5.3 Concentrations of halide hydrogen ions in pit growth

Halide anions and especially chloride ions are essential for pit growth. The chloride anions can compete for the metal in the metal oxide complexes, weakening and thinning the oxide layer. Finally breaking it locally as the chloride metal bond weakens the tenacity of the film. This in turn would start the pit initiation and nucleation. The chloride ion content is found to be very high inside the pit and can be up to 12 N. This study [42] was conducted on 18Cr 12Ni 2Mo 1Ti austenitic stainless steel, immersed in a vertical position in 0.5 N NaCl along with 0.1 N H_2SO_4. The experiment was conducted at 20°C (68°F) and polarized to 860 mV (NHE). The chloride concentration inside the pit increased to a maximum and then decreased with time. It was observed that the higher the accumulation of chlorides inside the pit, the slower their growth. The authors [42] concluded that the low pH of the solution within the pit is the consequence of the high chloride ions contents accumulating inside the pits.

Once again, the high chloride content associated with low pH was demonstrated by Hong et al. [48]. The high acidity inside the pits is associated with its high chloride content [42].

When the metal starts to dissolve, cations form and are trapped inside the pit. Anions (chlorides) migrate inside the pit to keep electroneutrality. The pit cover prevents the cations from escaping to the bulk solution. Thus, chloride ion concentration increases inside the pit highly. It is shown that high chloride ion concentration increases the hydrogen ion concentration inside the pit [49]. The chloride ion increase is offset by hydrogen ion increase to keep the pit in charge neutrality. The concentration of the chloride ions, however, depends on the pit size, temperature, the concentration of cations (such as H_3O^+ and Fe^{++}), and the pit cover.

9.5.4 Gas evolution in pits

Gas evolution at higher temperatures from pits was observed by Forchhammer and Engell on stainless steel [50a]. The gas was identified as hydrogen by mass spectroscopy. This hydrogen gas evolution was seen in pits for iron, steel, and other type of alloys such as aluminum, zirconium, and titanium. The evolution of hydrogen from pits may indicate that the pit is active and a chemical reaction is taking place inside the pit.

9.6 Effect of electrolyte composition in pitting corrosion

9.6.1 Pitting in halide solutions

The effect of anions is important for any given metal but this effect can differ from one type of metal to another. The correlations of the pitting potential (E_{pit}) and the concentration of the aggressive anion (E_{pit}) for halides in general are in the following order:

$$F^- < Cl^- < Br^- < I^-$$

The ability of different anions to adsorb to metal surface or metal oxide surface is different. The radius of halide ion increase and Gibbs-free energy of adsorption (ΔG) decrease is in the same order from fluoride to iodide. This indicates that the adsorption of iodide ion with a ΔG −13.1 kcal/mol is more favorable to adsorb on to a metal surface than the fluoride ion with a ΔG 8.9 kcal/mol. However, a different response of Cl^-, Br^-, and I^- in pitting with these anions is observed. More strongly adsorbed anions seem to be less aggressive. The pitting potential of chloride is less than iodide. Virtanen et al. [50b] observed a major influence on the repassivation behavior of chloride and bromide anions. These ions seem to have different responses for the initiation of pitting corrosion on steel. The authors observed a greater number of microtransients, greater than 10 s in the presence of chloride but such longer transients were absent in bromide solution.

The pitting potential generally increases from chloride to iodide in the halide series. This is not universally true. For tantalum (Ta) and titanium (Ti), the lower potentials were found in iodide rather than in the bromide solutions.

Titanium yielded the following sequence:

$$I^- < Br^- < Cl^-$$

It has been shown that in general, increasing halide ion concentration decreases the pitting potential (E_{pit}) thus making the material more susceptible for pitting corrosion [44].

The concept of critical pitting potential at which passive metals and alloys become susceptible to pitting in the presence of halide ions was thoroughly reviewed [51,52].

Roy et al. [53] tested several materials and found that in the case of alloy C-22, increasing NaCl concentrations from 1 to 5 wt% resulted in a shift in critical pitting potential (E_{pit}) to a more active value in acidic brines. The authors also noted that when the brine concentration increased above 5−7 wt% of NaCl, E_{pit} was shifted to more noble values. One of the metals subjected to these concentration changes (Ti Grade-12) was independent of the Cl^- ion concentration changes.

The acidity of the brine solution plays a role in the pitting corrosion as well. The authors [53] found that E_{pit} for several alloys at 10wt% NaCl brine, shifted to more noble values when the pH was changed from acidic to neutral. This phenomenon was explained by the acceleration of the cathodic reaction due to high concentrations of hydrogen ions in acidic solutions.

9.6.2 Pitting in electrolytes containing sulfur

Pitting corrosion in the presence of sulfur species depends on the type of metallurgy.

The sulfur species studied were sulfate $\left(SO_4^{2-}\right)$ with +6 valence for sulfur, sulfite $\left(SO_3^{2-}\right)$ +4 valance, tetrathionate $S_4O_6^{2-}$ with +2.5 valance, thiosulfate $S_2O_3^{2-}$ with +2 valance, and sulfide S^{2-} with −2 valance.

Effects of these sulfur species in electrolyte solutions depend on the sulfur valance, pH, alloy composition, and heat treatment. Fang and Staehle studied the polarization curves for alloys 600 and 800 (UNS N06600, and N08800) in various sulfur species at 60°C (140°F) and 95°C (203°F). They reported that the stability of the passive film decreases with the decrease of sulfur valance. The examination of the surfaces after polarization over the potential range indicated that the intergranular corrosion occurred mainly in solutions of sulfate $\left(SO_4^{2-}\right)$, sulfite $\left(SO_3^{2-}\right)$, tetrathionate $\left(S_4O_6^{2-}\right)$, and thiosulfate $\left(S_2O_3^{2-}\right)$, whereas S^{2-} or HS^- produced pitting. They also reported the increase of $\left(S_2O_3^{2-}\right)$ concentration at pH 6 and 95°C (203°F) accelerated the anodic dissolution [9]. However, the pH variation from 3.5 to 8 did not change anodic current for thiosulfate at a constant concentration.

The role of the chloride in thiosulfate solution is not clear. Newman et al. [54] reported that for AISI 316L, thiosulfate pitting did not occur unless the chloride concentration was fairly high and more than 10^{-2} M, and unless the molar concentration of chloride exceeded that of thiosulfate. However, there are reports of the occurrence of pitting corrosion in thiosulfate solutions without the presence of chloride ions [10].

Thiosulfates dissolved in aqueous solutions are known to be detrimental to corrosion resistance of alloys such as stainless steel [55].

Duret-Thual et al. [56] used XPS technique to study the role of thiosulfate in pitting corrosion in the presence of chlorides. The authors used several grades of Fe−17Cr alloys, with different amount of sulfur contents. They concluded that the addition of thiosulfate in the presence of chlorides (30 ppm thiosulfate in 0.02 M of NaCl) yielded a detrimental effect, increasing pitting corrosion. The detrimental effects on pitting resistance increased with increased sulfur content in the alloy.

XPS results indicated that the thiosulfates are reduced on the metallic surface, whereas they do not interact strongly with the passive film surface. The authors

concluded that sulfide islands are formed at the bare alloy surface, preventing repassivation. The sites on the bare metal with sulfide inclusions were the preferred site for further thiosulfate reduction and increasing pitting [56].

Newman et al. [7] studied the effects of various types of sulfur species for type 304 stainless steel in mildly acidic or neutral solutions with 0.5 M. These tests were conducted with potentiodynamic measurements. The concentration of sulfur species was changed from 0 to 2 M solutions. The authors reported an increase in pitting when thiosulfate concentration was increased from 0.01 to 0.02 M. However, when the concentration of thiosulfate was increased above 0.5 M, pitting was inhibited. KSCN showed a similar but lesser effect, while in the presence of sodium sulfide (H_2S in acidic solutions and HS^- at neutral pH). They observed a reduction of the pitting potential. Addition of sodium tetrathionate ($Na_2S_4O_6$) up to 0.05 M increased the pitting potential.

Sulfates in electrolyte solutions along with NaCl show an inhibitory effect. Ernest et al. [57] reported that adding sodium sulfate to 1 M solution of NaCl resulted in lowering pitting corrosion. The authors found that adding 0.1 M of sodium sulfate to a solution of 1 M NaCl produced a cover with finer holes. This would make cation transfer slower toward the bulk solution, making pitting corrosion rate slower.

Pistrous et al. [58] studied the effect of the addition of dilute sulfate into sodium chloride solutions. The study focused on metastable and stable pitting on 304 stainless steel. They observed that the sulfate causes the distribution of available pit sites to be shifted to higher potential. This implies that the pit initiation is inhibited. The pit propagation is inhibited by sulfate ions and this is true for both metastable and stable pits.

9.7 Surface roughness in corrosion

There are several reports on surface roughness related to pitting corrosion. In laboratory testing, coupons are usually prepared to 600 grit mirror polished or finer finish. The surface preparation is a very important aspect as the roughness of the test specimens may have a marked influence of the outcome of the test results. This is especially true in pitting corrosion but is universally true for general corrosion as well. Electrochemical and/or mechanochemical behavior of a surface is complicated and involves various chemical and physical and mechanical factors. The effect of the surface finish of the test material is very significant for the outcome of the test and should not be neglected. Its influence on corrosion rates, general corrosion, as well as localized corrosion is highly apparent. There are very systematic studies published in the current literature of this effect for carbon steel under carbonic acid attack. One such study concluded that CO_2 corrosion increased with increasing surface roughness [19]. Yet, previous studies did probe into mild corrosion conditions (room temperature, 1 atm of pressure). Given that the formation of a tenacious iron carbonate scale can protect the surface, it is important to perform these studies at tougher conditions.

The pitting corrosion rate can increase with increasing surface roughness [59]. This was attributed to a reduced amount of metastable pitting sites in a smoother finished

surface compared with a rougher surface. The experiments were conducted on a 304 (UNS S30400) stainless steel surface with sodium chloride as the electrolyte. However, if the surface is smoother, once a metastable pit formed, it has a better chance to achieve stable pit growth.

Sasaki et al. [60] studied the relationship of surface roughness and pitting potential using 304L stainless steel in 0.6 M sodium chloride solution. The pitting potential increased with increasing grit number. The pitting potential was lower for rougher surfaces than the smother surfaces. For example, a change from 4000 grit finished surface to 180 grit finished surface resulted in a decrease in E_{pit} of 0.44 V. They also observed that the pitting potential is linearly related to the reciprocal of the grit number. The pitting potential E_{pit}, which is the minimum potential at which stable pits are observed to propagate, is lower for rougher surfaces than for smoother surfaces. This phenomenon is in agreement with the diffusion control pitting corrosion mechanism.

The same reasoning can be applied to erosion corrosion, where impingement by sand particles (for example) can weaken the protective metal oxide barrier and replace the barrier with weaker chloride−metal bond. In this situation, the rupture of the oxide film causes a fast anodic reaction of the metal. This would allow easy nucleation and metastable pit formation. The metastable pits can transfer to stable growing pits. The damaged metal surface (because of impingent) can make a less open pit cover allowing the pit to become stable.

Contrarily to the results presented by Asma et al. [19], Yepez et al. had found the opposite behavior for general corrosion in certain conditions [61]. In this work, Yepez et al. [61] present evidence that general corrosion rate and pitting corrosion rate can behave somewhat differently. The tests were conducted using rotating cylinder autoclave (RCA) with flat CS 1080 coupons and under an oxygen-free environment under CO_2 pressure. The tests were run with 3.5wt% NaCl dissolved in water. In several cases, the corrosion rate increased as the surface roughness decreased. This, however, may have occurred because that rougher surface can corrode faster, and therefore, can produce a higher amount of the protective iron carbonate layer. Additional experiments were conducted using RCA with liquid volume to metal surface ratio of 9 (condition A) and liquid volume to metal ratio of 15 (condition B). It is known that the area of the metal surface to volume of the liquid does affect measured corrosion rate as the corrosion byproducts have more chance to dissolve or disperse in higher volume of liquid. A lower metal surface/liquid ratio presents an artificially low corrosion rate as more corrosion product can deposit on the metal surface forming a barrier to corrosion (stopping diffusion of the cations to bulk solution). Fig. 9.12 depicts results of general corrosion rate against surface finish (grit #). With increasing grit, general corrosion rate increased. Each test was conducted three times and averages were used in the graph. The test temperature was 65°C (149°F).

This test was performed using a low metal surface to liquid ratio (Method A). Though the authors expected to see better but probably better artificial protection, the trending of the corrosion rate was similar and both increased with increasing surface smoothness. Yepez et al. [61] looked into pitting corrosion but the results were inconclusive.

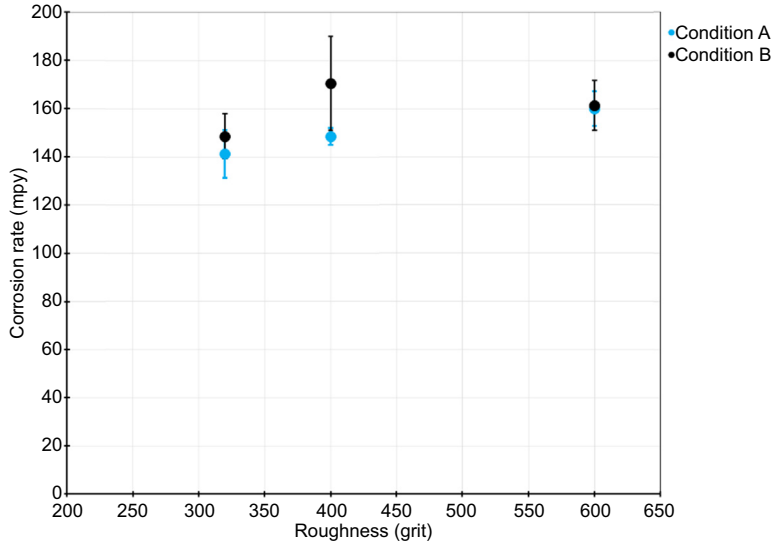

Figure 9.12 Rotating cylinder autoclave results show that both pit depth and general corrosion rate increase with increasing surface roughness.
O. Yepez, N. Obeyesekere, T. Ariyaratna, Clariant Oil Services, The Woodlands, TX, 2016, Unpublished data.

Fig. 9.13 depicts the RCA test result at different temperatures. The corrosion rates are higher at higher temperatures as expected but the corrosion rate increased as the surface smoothness increased.

Fig. 9.14 depicts the corrosion rates from RCA testing at 66°C (151°F) with 4.5 bar (65 psi) CO_2 with 3.5wt% NaCl solution. The condition B gave somewhat lower corrosion rates as the surface smoothness increased. This was attributed to the dilution of iron carbonate in the metal/volume system. The corrosion rates (pitting rates as well) are higher at higher roughness but the corrosion byproducts do not act as barrier for diffusion here as the byproducts may disperse better in the bulk solution.

9.8 Pitting corrosion behavior in sour systems

Pitting corrosion behavior in sour systems has been studied extensively for carbon steel but not yet fully understood [62,63]. The sour systems (systems containing H_2S, or a mixture of H_2S and CO_2) are prone to pitting much more readily than the sweet (CO_2 only) systems. The sweet systems tend to promote higher general corrosion, whereas H_2S containing systems tend to promote more pitting corrosion with lower general corrosion provided that all other system conditions are equal. The sour systems tend to form tenacious iron sulfide films that would influence corrosion mechanism. The general corrosion rates in the presence of CO_2, a mixture of CO_2/H_2S, and only with H_2S were studied by Pessu et al. [62]. The tests were

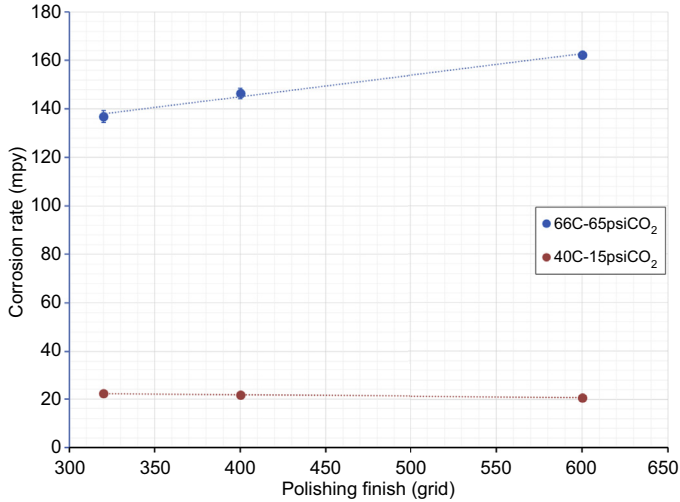

Figure 9.13 Rotating cylinder autoclave results with two different temperatures. The test was conducted with Method A. The *red dots* are corrosion rates versus surface finish at 40°C (104°F) and *blue dots* denote 66°C (151°F).

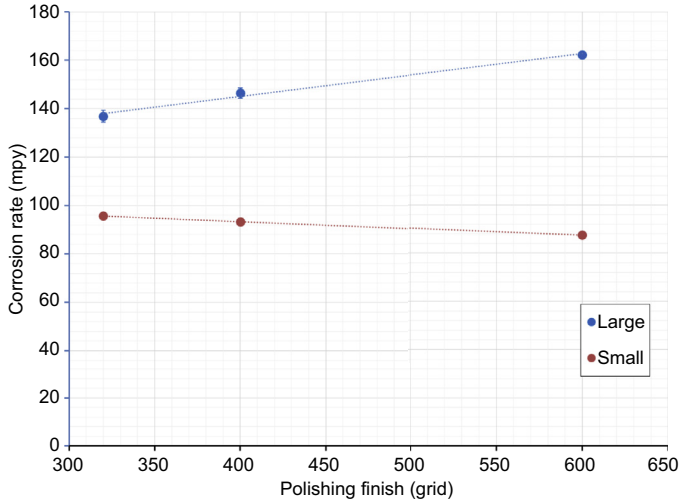

Figure 9.14 Corrosion rates versus surface finish at two different metal surface/volume ratio. Condition A versus B, 66°C (151°F), 4.5 bar (65 psi) CO_2.

conducted on X-65 (UNS K0314) material surfaces at three different temperatures. The testing temperatures were 30°C (86°F), 50°C (122°F), and 80°C (176°F). The authors concluded that the general corrosion rates were higher in pure CO_2 (saturated for 12 h with CO_2 before conducting the experiments in 3.5wt% NaCl brine). The dissolved oxygen levels were kept below 10 ppb. The sour tests were conducted

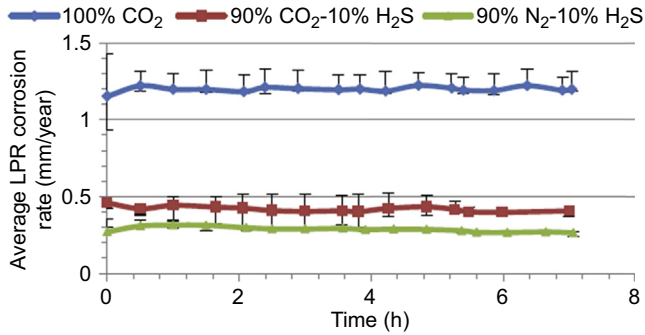

Figure 9.15 Corrosion rate of X-65 carbon steel in 3.5 wt% NaCl solution saturated with gas streams of different composition at 30°C (86°F) [62].

by deaeration with nitrogen followed by bubbling with H_2S containing gas mixtures for 30 min.

The general corrosion rates were measured using linear polarization resistance (LPR) bubble cell method. The reference electrode was Ag/AgCl and the counterelectrode was platinum. General corrosion was measured at 30°C (86°F), 50°C (122°F), and 80°C (176°F) for all three types of gases. The corrosion rate was almost three times higher at 30°C (86°F) in pure CO_2 than in CO_2/H_2S system (Fig. 9.15). The corrosion rate diminution at any given time was higher between pure CO_2 and CO_2/H_2S. However, at higher temperatures (80°C, 176°F), the difference between corrosion rates of sweet and sour systems seem to widen with time (see Fig. 9.16). There is a drastic effect on general corrosion between sweet and sour corrosion in these tests.

The authors also compared pitting corrosion behavior between sweet and sour conditions by comparing maximum pit depth (Fig. 9.17(a) and average pit depth (Fig. 9.17(b)). The average pit depth is the average of the 10 deepest pits [62]. Both maximum pit depth and average pit depth increased with increasing temperature up to 50°C (122°F) and then seems to decrease slightly at 80°C (176°F) as illustrated in Fig. 9.17.

The authors concluded that the pits initiate faster in sour than in sweet environments. The pit depths were higher in sour environments for all temperatures (30−50°C, 86−122°F) than sweet. Both pitting and general corrosion rates were reduced at higher temperatures (at 80°C, 176°F). This is an indication that iron sulfide plays a significant role in reducing general corrosion.

9.8.1 Pitting and iron sulfide polymorphism

Studying pitting corrosion in sour environment in laboratory or field environment is generally difficult. Either in laboratory or field experiments, with synthetic fluids in H_2S and CO_2 environments or with side streams pitting, it is not observed in a short period of time. In both these cases, for pitting corrosion to occur, it is necessary to

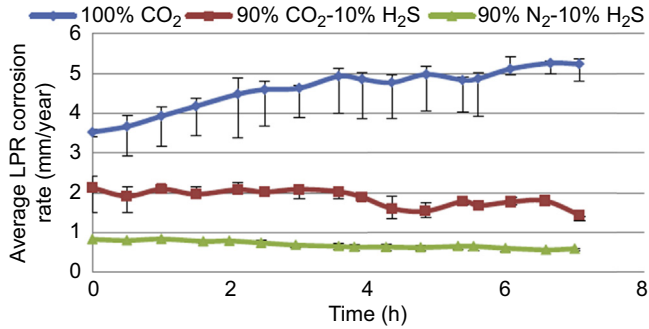

Figure 9.16 Corrosion rate of X-65 (UNS K03014) carbon steel in 3.5 wt% NaCl solution saturated with gas streams of different composition at 80°C (176°F) [62].

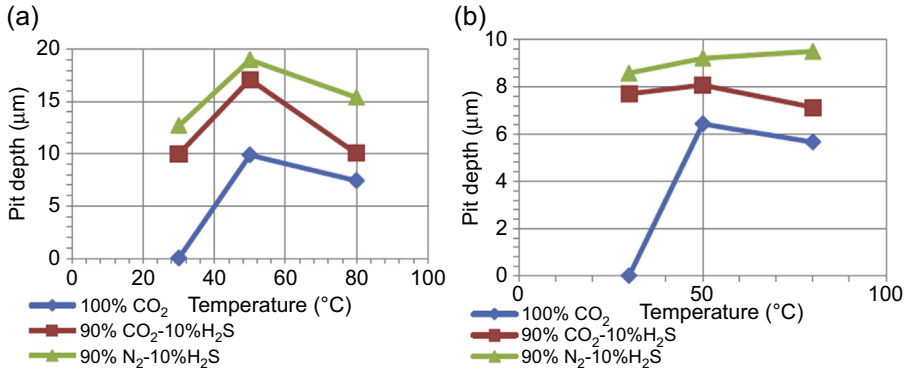

Figure 9.17 (a) Maximum pit depth (relative to corroded surface) and (b) average pit depth (relative to corroded surface) on X-65 (UNS K03014) carbon steel surface exposed to corrosion system under 100 mol% CO_2, 10 mol% H_2S−90 mol% CO_2, and 10 mol% H_2S−90 mol% N_2 gas atmosphere as a function of temperature [62].

run these tests for longer periods of time. In laboratory testing, it is not unusual to run the test for 7 days or several weeks.

Systems containing CO_2 or mixtures of H_2S and CO_2 produce films of corrosion products. Thus, in sweet systems, the major corrosion product is iron carbonate and, in sour systems, the products are different iron sulfides. In sour systems, these products are much more complex as sulfides exist as polymorphs and sour systems can produce elemental sulfur and polysulfides. These iron sulfide corrosion products can precipitate on the steel surface and inhibit corrosion. This is by covering the surface and not letting corrosive fluids to come into contact with steels surfaces.

Because the solubility of iron carbonate in brines is higher than iron sulfides, the tenacity of iron carbonate films, formed on the surface, is much less than iron sulfides. Iron carbonate, therefore, does not offer a good protection, leading to higher general corrosion under similar conditions. The localized corrosion, however, follows the opposite trend. The sour systems would produce lower general corrosion but higher pitting corrosion [63–65]. This phenomenon is defined by the protectiveness of the corrosion film and can be separated into three areas. First is the area without a corrosion film. This area, generally, suffers very high general corrosion and will not have any localized corrosion. Depending on system conditions, some sweet systems and flow induced corrosion can be in this category. The second area is fully covered with a protective film and this would produce low uniform corrosion and localized attack. The authors defined the third area as the "grey zone", low or high uniform corrosion with localized corrosion [66]. The majority of oil and gas sour systems falls into this area where partially protective films can produce pitting corrosion via galvanic and uniform corrosion.

An early work studied and reported several iron sulfide polymorphs with respect to their sulfur content and corrosivity [67]. The researchers synthesized and characterized these sulfides. The authors concluded that the corrosiveness and sulfur content in five different iron sulfides are linked. The sulfur-rich species seems to be more corrosive for mild steel than sulfur-deficient iron sulfide species (Table 9.3).

The mechanism of H_2S induced corrosion may be via direct reduction of H_2S at the cathodic site [68]. Therefore, it is logical to assume that the crystalline structure of the iron sulfide may influence the corrosivity. The pitting corrosion may depend on the type of iron sulfide forms on the metal surface. Usually, the type of iron sulfide formed under low pressure and low temperature is mackinawite, which later can transform into other species. Park et al. [69] studied film formation of iron sulfide species using RCA equipment at 50°C (122°F) and with 3447 kPa (500 psi) of H_2S partial pressure and with 6891 kPa (1000 psi) of total pressure balance with nitrogen. They

Table 9.3 Corrosivity of iron sulfide polymorphs and the sulfur content

Iron sulfide type/formula	Corrosion per mol sulfide (mg Fe/mmol)	Sulfur mol%	Comment
Pyrite/FeS_2	61.53	67	
Smythite/Fe_3S_4	19.51	57	
Greigite/Fe_3S_4	12.53	57	
Mackinawite/$Fe_{1+x}S$	10.08	c.50	The formula is controversial. Some believe it is FeS.
Pyrrotite/$Fe_{1-x}S$	6.39	c.50	

analyzed the iron sulfide film formed at various time intervals. They found that at the early stage of the testing, amorphous FeS was the main product, which changed to Mackinawite within 7 days. Mackinawite and cubic iron sulfide, along with iron oxide, were the products after 14 days. It seems, at least in laboratory conditions that iron sulfides converted from one form to a thermodynamically more stable form with time. Temperature and pressure can accelerate this process.

It was established that the general corrosion decreases with increasing H_2S concentration. However, pitting corrosion is not as direct as general corrosion. Pitting corrosion may depend on several factors in sour services. The iron sulfide polymorphs formed indeed have a strong effect on pitting corrosion. This is along with other system conditions such as temperature, pressure, presence or absence of organic acid, and presence of elemental sulfur. Pitting attack is attributed to galvanic corrosion, where the holidays among the sulfide layers can induce this type of corrosion [70,71]. However, it is not clear which type of polymorphous iron sulfide would yield the highest corrosion rate. Jon Kvarekval et al. [70] claimed that pyrrhotite was the most influencing iron sulfide in creating pitting corrosion in mild steal. However, there are some indications from other groups in Ohio University [70b] and Clariant [61] that pyrite is more effective in initiating pitting corrosion.

9.8.2 Pitting in the presence of sulfide and poly sulfides

To prevent corrosion, sweet systems that contain very little or no H_2S can be treated easily by using corrosion inhibitors. However, mitigating corrosion in systems with high levels H_2S and CO_2 is difficult. This is because these systems can produce elemental sulfur and polysulfides. These chemicals tend to cause localized and pitting corrosion rather than general corrosion.

In order to design corrosion inhibitors effectively, one needs to understand the different conditions that control the flow in flowlines, the conditions that cause corrosion and various environmental and safety restrictions for chemical usage in different parts of the world.

Corrosion occurs when sulfur particles directly contact the metal surface and exhibit the same principal characteristics as H_2S induced corrosion. A crevice-corrosion-like attack is observed [72]. However, when elemental sulfur is in contact with H_2S, various hydrogen polysulfide species of general formula H_2S_{x+1} ($x \geq 1$) are formed. These polysulfide species are considered to be stable, only when sulfur and H_2S come into direct contact, i.e., in the proximity of sulfur particles [73]. The most prominent mechanism is where the hydrogen polysulfides form the oxidant cathodic part of the corrosion reaction. It is believed that the transfer of sulfide ions to the iron sulfide surface occurs via polysulfide species, and the following reaction scheme is proposed for the accelerated corrosion process:

$$H_2S + S_x \rightarrow H_2S_{x+1} \tag{9.iv}$$

$$xFe \rightarrow xFe^{2+} + 2xe^{-1} \text{ (anodic)} \tag{9.v}$$

$$H_2S_{x+1} + 2xe^- \rightarrow H_2S + xS^{2-}_{(ad)} (\text{cathodic}) \quad (9.vi)$$

$$xFe^{2+} + xS^{2-}_{(ad)} \rightarrow xFeS \quad (9.vii)$$

Adding reactions (9.v) through (9.vii), the overall reaction for accelerated corrosion becomes

$$xFe + H_2S_{x+1} \rightarrow xFeS + H_2S \quad (9.viii)$$

The H_2S generated in reaction (9.vi) further combines with more elemental sulfur to generate more polysulfide species, in accordance with reaction (9.iv).

The production of sour gas in oil fields increases corrosion in flowlines [74,75].

The mechanism of corrosion in an aqueous solution containing CO_2 is quite different from the mechanism of corrosion in sour gas systems. In sour gas reservoirs, elemental sulfur, polysulfides, water, and CO_2 exist with hydrogen sulfide. Elemental sulfur thus can be carried out with hydrogen sulfide by dissolving in H_2S or by chemically binding to hydrogen sulfide gas as H_2S_x. Elemental sulfur dissolved in sour gas can be released (deposited) as elemental sulfur by changes in temperature and pressure. When elemental sulfur deposits in flowlines, these lines become plugged, and in the presence of water, rapid localized corrosion attacks occur. The controlling deposition of elemental sulfur is thus as important as the corrosion mitigation in flow lines. Elemental sulfur exists as a stable crown below 95°C (203°F). Above 114°C (237°F) cyclooctasulfur (S_8) polymerizes to yield zigzag chains with S−S bonds. The bond length is 0.24 nm.

In sour gases, the solubility of sulfur increases with increasing temperature and pressure and it is proportionately greater as the amount of alkanes and concentration of hydrogen sulfide increases in the system. A low hydrogen sulfide content in sour gases (less than 5 mol%) results in less elemental sulfur plugging, which can be controlled easily [76]. Elemental sulfur reacts with H_2S in sour gas systems and forms polysulfides at high temperatures (see reaction 9.iv). It is believed that the formation of polysulfides has a greater significance at higher levels of hydrogen sulfide in sour gases, which proves to be the dominant mechanism by which elemental sulfur is transported in high sour gas fluids.

On reaction (9.iv) above, higher temperatures, pressures, along with the partial pressures from hydrogen sulfide could drive the chemical equilibrium to the right. Once the pressure is released and fluids are cooled, the equilibrium will shift to the left, releasing elemental sulfur into the flow lines [77].

It is accordingly important to control the formation and deposition of elemental sulfur inflow lines, especially in view of the need to control corrosion on iron surfaces.

9.8.3 Effects of sulfur particle size on corrosion

Elemental sulfur increases the corrosivity of aqueous H_2S environments. When drops of sulfur are in direct contact with the metal in a system with sulfur/water/hydrogen

sulfide, the corrosion proceeds from the periphery of the sulfur drop toward the center. The size of the sulfur drop affects the corrosion of the metal surface. A large drop may lead to localized corrosion near the regions close to the sulfur drop, whereas small drops will attack the metal surface uniformly [77].

9.8.4 Mechanism of corrosion of mild steel by sulfur/water suspensions

Boden and Maldonando [78,79] claimed that the acidity generated in wet sulfur causes higher corrosion at ambient temperatures. They observed a decrease of pH to 1.8 when a suspension of sulfur was stirred in distilled water at ambient temperature. Rapid corrosion of mild steel is caused by the continuous replacement of hydrogen ions as they are consumed by the cathodic reaction. Boden and Maldonando attributed this effect to a disproportionate reaction that produces hydrogen sulfide and sulfuric acid as shown below.

$$S_{8(s)} + 8H_2O_{(l)} \rightarrow 6H_2S_{(as)} + 2H_2SO_{4(aq)} \tag{9.ix}$$

The acids thus produced introduce acid corrosion in the system, which escalates as iron sulfides are formed. The presence of H_2S can lead to elemental sulfur polysulfides as shown in reactions (9.x) and (9.xi).

$$H_2S + S_x \leftrightarrow H_2S_{x+1} \tag{9.x}$$

$$(x-1)Fe + S_{y-1}\cdot S^{2-} + 2H^+ \rightarrow (x-1)FeS + H_2S + S_{y-x} \tag{9.xi}$$

It has been established that the presence of elemental sulfur would lead to pitting corrosion as shown in reaction (9.ix). A sulfur drop on a steel surface would induce highly corrosive sulfuric acid in the presence of water (reaction 9.ix). This would lead to severe pitting corrosion under the sulfur droplet.

Elemental sulfur has been shown to accelerate corrosion of carbon steel in sour environments where significant amounts of H_2S are already present. Such accelerated attack predominates in the vicinity of sulfur particles that are in contact with the surface of the steel leading to predominately pitting corrosion [74].

9.9 Future research on pitting corrosion

The surface roughness is important for corrosion and pit initiation. This is an important area but least studied. Surface roughness and corrosivity may not be as directly linked as published in the current literature. Most publications indicate that there is a direct proportionality between these two factors. Studies at Clariant laboratories in Woodlands, TX, indicate that there is a correlation between surface roughness and corrosivity but this depends on many factors, among them are temperature and metallurgy. More investigations on the mechanisms, initiation, and nucleation of pit formation

are necessary. The role of pit cover should be investigated further. The correlation between the roughness of the surface and pit cover should be further investigated as well. Although the mechanism of the stable pit growth seems to be clear, the breakdown of the passive film and the production of stable pits is not very clear. The passive oxide film and the breakdown of this film due to anions should be investigated further.

Another area of ambiguity is the pitting corrosion mechanisms in the area of sour corrosion. There are several proposed mechanisms in the literature but none of them are convincing as the experimentations that led to the conclusions were not conducted universally. In other words, we do not believe all scenarios were considered before coming to conclusions by various researchers.

In the area of the role of iron sulfide polymorphs, the data in literature is conflicting. There is a correlation with the amount of sulfur in iron sulfide and corrosion. In that case, the most corrosive iron sulfide polymorph should be pyrite (and still it is). Pyrite with higher sulfur content may induce galvanic corrosion readily when it comes into contact with steel and suitable electrolyte. However, a higher corrosion activity has been assigned to pyrrhotite, which is deficient in sulfur compared with pyrite. Therefore, there are conflicting evidence in literature and the role of iron sulfide polymorphs should be investigated further.

Another question is the corrosion activity between various iron sulfide polymorphs and the metallurgy. The stoichiometry of iron sulfide is also important. In the literature, the stoichiometry of mackinawite is unclear. It is necessary to investigate further the stoichiometry of makinawite, which is sometimes presented as FeS and sometimes as sulfur-deficient FeS_{1-x}.

There are a substantial amount of technical papers published in the literature on corrosion inhibitors but there are not very many papers dealing with the mechanism of corrosion inhibition. This is especially true of inhibitors for pitting corrosion. In acidic solutions, the inhibitors mitigate corrosion by inhibiting the anode reaction, cathode reaction, and sometimes both. The mechanism of mitigating it is the least understood perhaps because the researchers consider inhibitor development as intellectual property and rarely want to share all the findings with the public. Further research should be focused on chemical species that inhibit exclusively pit initiation and pit development as this would lead to pitting corrosion.

Corrosion inhibitors are generally blends of several components and mixtures of solvents. The inhibitors generally are system specific and may not perform well in two different systems. There is a gap in corrosion inhibitor development for corrosion inhibitors that are good for very high temperatures (above 177°C, 350°F) and further research is required for corrosion inhibitors that are effective at high temperatures and pressures. This is especially true for water-soluble corrosion inhibitors where most water-soluble chemical species decompose at high temperatures in water. Furthermore, research into the development of new raw materials that are effective for HT/HP is necessary.

Pitting corrosion usually decreases when the general corrosion is reduced. However, the mechanism for mitigation of pitting corrosion by specific chemical species is not yet clear. Pitting corrosion is a two-step process with pit initiation followed by pit growth. Therefore, the species that can inhibit pit initiation can inhibit pitting corrosion.

Second, if chemical inhibitor species can inhibit the development of already nucleated pit, then this inhibitor can mitigate pitting corrosion. The third type of chemical inhibitors should be able to passivate the bare metal surface after the film is broken down. Therefore, further research is required to understand mitigation of pitting corrosion exclusively by chemical species compared with mitigation of general corrosion. The mitigation of general corrosion may happen because of the formation of a tenacious film over the entire metal surface. Therefore, a chemical that is effective for general corrosion may not necessarily be effective for pitting corrosion.

Inhibitor development for very sour systems is another area that needs attention. Further research is necessary in this area. Usually, general corrosion is very low in very high sour systems and sometimes lower than 4 mpy (0.1 mm/year), which tends to give producers a false sense of security. These systems fail not because of general corrosion but due to pitting corrosion. These systems produce protective iron sulfide scale, which can act as tenacious films on the metal surface. This would prevent acidic water coming into contact with the metal surface reducing general corrosion. However, this film can break down and the gaps can introduce water to the bare metal. Iron sulfide is conductive and can be cathodic and can induce galvanic corrosion, which can lead to pitting. Further research is necessary to develop corrosion inhibitors that can exclusively bind to cathodic iron sulfide. This would lead to repassivation of the gap created by the broken-down of the iron sulfide film. Further research is necessary to identify chemistries that can exclusively bind to active iron sulfide scale found at the gap of the FeS film. Another important question is the polymorphs of iron sulfide formed due to sour corrosion and the inhibitor development for each type of iron sulfide species. For example, is a chemical species that binds tightly to makinawite and makes a tenacious film in the gap between bare metal would it do the same thing for pyrite?

Another highly unexplored area is the development of corrosion inhibitors to mitigate pitting corrosion in sour system with elemental sulfur. The pitting corrosion in these systems is very high and currently there are no effective solutions to control very heavy pitting. Further research is necessary to develop new corrosion inhibitors to mitigate pitting corrosion in the systems with elementals sulfur.

Another gap in research activity is in the area of corrosion modeling for pitting. Most of the current models are developed for CO_2 corrosion [80–97]. Also most of the present models are based on Waard–Milliams semiempirical model [81,82]. Only a few of these models can handle elevated temperatures and pressures. Most of the current published literature cover models developed for sweet systems and the most part for flowlines. There are few models for downhole applications and even less for sour systems. There are very few prediction models that address the pitting corrosion. There is a need for a prediction model to be developed for sweet systems using activities and fugacities (non-Newtonian) to use in high temperature and pressure.

However, the most important gap is the corrosion prediction for pitting corrosion in sour systems. There are not very many good downhole models for sour pitting corrosion. This is a gap in this area, and this is especially true for HP/HT downhole pitting corrosion in the presence of high levels of H_2S.

References

[1] R.W. Staehle, B.F. Brown, J. Kruger, A. Agarwal (Eds.), Localized Corrosion, NACE-3, NACE, Houston, TX, 1974.
[2] H. Isaacs, U. Bertocci, J. Kruger, S. Smialowska (Eds.), Advances in Localized Corrosion, NACE-9, NACE, Houston, TX, 1990.
[3] N.J. Laycock, J. Stewart, R.C. Newman, Corrosion Science 39 (1997) 1791−1809.
[4] A. Turnbull (Ed.), Corrosion Chemistry within Pits, Crevices, and Cracks, HMSO Books, London, 1987.
[5] Z. Szklarska-Smialowska, Pitting Corrosion of Metals, NACE, Houston, TX, 1986, p. 347.
[6] Critical factors in localized corrosion, PV 92-9, in: G.S. Frankel, R.C. Newman (Eds.), The Electrochemical Society Proceedings Series, Pennington, NJ, 1992.
[7] R.C. Newman, H.S. Issac, B. Alman, Corrosion 38 (1982) 261.
[8] R.C. Newman, Corrosion 41 (1985) 450.
[9] Z. Fang, R.W. Staehle, Corrosion 55 (1999) 355.
[10] D. Tromans, L. Fedrerick, Corrosion 40 (1988) 633.
[11] G.S. Frankel, Journal of the Electrochemical Society 145 (6) (1998).
[12] H.H. Uhilig, Journal of the Electrochemical Society 97 (1950) 215C.
[13] T.H. Hoar, Corrosion Science 5 (1965) 279.
[14] S.N. Smith, in: CORROSION/2015, Paper No. 5484, Houston, TX, 2015.
[15] N.J. Laycock, R.C. Newman, Corrosion Science 39 (1997) 1771.
[16] N.J. Laycock, R.C. Newman, Corrosion Science 40 (1998) 887.
[17] R.B. Inturi, Z. Szklarska-Simalowska, Corrosion Science 34 (1993) 705.
[18] L. Stockert, F. Hunkeler, H. Boehni, Corrosion 41 (1985) 686.
[19] R.B.A. Nor Asma, P.A. Yuli, C.I. Moktar, Journal of Applied Sciences 11 (11) (2011) 2053−2057.
[20] M.G. Fontana, N.D. Greene, Corrosion Engineering, McGraw-Hill, New York, 1978, p. 321.
[21] S. Papavinasam, Corrosion Control in the Oil Gas Industry, Elsevier, 2013.
[22] G-46-94, ASTM Standards, (2005).
[23] M. Ghahari, et al., Corrosion Science 100 (2015) 23−35.
[24] R.J. Brigham, E.W. Tazar, Corrosion 29 (1973) 33.
[25] ASTM: G48-03, Methods for Pitting and Crevice Corrosion of Stainless Steels and Alloys by Use of $FeCl_3$.
[26] F. Eghbali, M.H. Moayed, A. Davoodi, N. Ebrahimi, Corrosion Science 53 (2011) 513−522.
[27] M.H. Moayed, N.J. Laycock, R.C. Newman, Corrosion Science 45 (2003) 1203−1216.
[28] P. Ernst, R.C. Newman, Corrosion Science 44 (2002) 927−941.
[29] (a) H.J. Engell, N.D. Stolica, Zeitschrift für Physikalische Chemie 20 (1959) 113; (b) H.H. Strehblow, B. Titze, Corrosion Science (1977) 795.
[30] F. Hunkener, H. Boehni, Werkstoff und Korrosion 34 (1983) 593.
[31] Hunkenener, Z. Szlarska-Smialowska, J. Mankowski, Corrosion Science 11 (1971) p. 209.
[32] N. Bui, F. Dabosi, Metaux Corrosion Industries 585 (May 1954) 133.
[33] Herbsleb, H.J. Engell, Werkstoff und Korrosion 17 (1966) 365.
[34] J. Tousek, Corrosion Science 12 (1972) 1.
[35] P. Forchhammer, H.J. Engell, Werkstoff und Korrosion 20 (1961) 1.
[36] H.H. Strehblow, J. Wenners, Zeitschrift für Physikalische Chemie (Neue Folge) 98 (1975) 199.

[37] Y.U. Popov, et al., Electrochemical kinetics in pitting: model of surface processes, Elektrokhimiya 14 (10) (1978) 1601−1604.
[38] Y. Hisamatsu, Study of pitting corrosion of stainless steels in chloride solution, in: R. Staehle, H. Okada (Eds.), Passivity and Breakdown of Iron and Iron Base Alloys, NACE, Houston, TX, 1976, p. 99.
[39] J.R. Galvie, Journal of the Electrochemical Society 123 (1976) 123.
[40] P.C. Pistorius, G.T. Burstein, Corrosion Science 33 (1992) 1885−1897.
[41] H.S. Isaac, Corrosion Science 29 (1989) 313−323.
[42] J. Mankowski, Z. Szklarska-Smialowska, Corrosion Science (1975) 493−501.
[43] G.S. Frankel, L. Stockert, F. Hunkeler, H. Boehni, Corrosion 43 (1987).
[44] M.F. Abd Rabboh, P.J. Boden, in: R. Staehle, B. Brown, J. Kruger, A. Agrawal (Eds.), Localized Corrosion, NACE-3, NACE, Houston, TX, 1974.
[45] H. Gohr, E. Kalsch, Corrosion Science 9 (1969) 329.
[46] G.T. Burstein, S.P. Vines, Journal of the Electrochemical Society 148 (2001) B 504−B 516.
[47] P.C. Pistorius, G.T. Burstein, Philosophical Transactions of the Royal Society A 341 (1992).
[48] T. Hong, G.W. Walter, M. Nagumo, Corrosion Science 38 (1996) 1525.
[49] T. Suzuki, M. Yamabe, Y. Kitmura, Corrosion 29 (1973) 18.
[50] (a) P. Forchhammer, H.J. Engell, Werkstoff und Korrosion 20 (1969) 1;
(b) S. Virtanen, Y. Kobayashi, H. Boehni, Electrochemical Society Proceedings 99−42 (2001) 665.
[51] H.P. Leckie, H.H. Uhlig, Journal of the Electrochemical Society 113 (1966) 1262−1267.
[52] J.M. Kolotykin, Corrosion 19 (1963) 261t−268t.
[53] A.K. Roy, D.L. Fleming, S.R. Gordon, 190th Electrochemical Meeting, San Antonio, TX, 1996.
[54] R.C. Newman, W.P. Wong, H. Ezuber, A. Garner, Corrosion 45 (1989) 282.
[55] P. Marcus, E. Protopopoff, Corrosion Science 39 (9) (1997) 1741−1752.
[56] C. Duret-Thual, D. Costa, W.P. Yang, P. Marcus, Corrosion Science 9 (1997) 913−933.
[57] P. Ernest, R.C. Newman, Corrosion Science 44 (2004) 927−941.
[58] P.C. Pistrous, O. Ernest, Corrosion Science 33 (1992) 1885−1897.
[59] G.T. Burstein, P.C. Pistorius, Corrosion 51 (1995) 380−385.
[60] K. Sasaki, G.T. Burstein, Corrosion Science 38 (1996) 2111−2120.
[61] O. Yepez, N. Obeyesekere, T. Ariyaratna, Clariant Oil Services, The Woodlands, TX, 2016, Unpublished data.
[62] F. Pessu, R. Baker, A. Neville, in: CORROSION/2014, Paper No. 4214, Houston, TX, 2014.
[63] B. Brown, S. Nesic, in: CORROSION/2012, Paper No. 1559, Houston, TX, 2012.
[64] F. Persu, Y. Hua, R. Barker, A. Neville, in: CORROSION/2016, Paper No. 7643, Houston, TX, 2016.
[65] B. Brown, D. Young, S. Nesic, in: 17th International Corrosion Congress, Paper No. 2704, Las Vegas, NV, 6−10 October 2008, 2008.
[66] Y. Sun (Ph.D. dissertation), Ohio University, 2003.
[67] R.A. King, J.D.A. Miller, J.S. Smith, British Corrosion Journal 8 (1973) 137−141.
[68] Y. Zheng, B. Brown, S. Nesic, in: CORROSION/2009, Paper No. 2406, Houston, TX, 2009.
[69] N. Park, L. Morello, G. Abraham, in: CORROSION/2009, Paper No. 9362, Houston, TX, 2009.

[70] (a) M. Tjelta, J. Kvarekval, in: CORROSION/2016, Paper No. 7478, Houston, TX: NACE, 2016;
(b) Y. Zheng, B. Brown, D. Young, S. Nesic, in: CORROSION/2016, Paper No. 7502, Houston, TX, 2016, p. 78.
[71] S. Nešić, S. Wang, H. Fang, W. Sun, J.K. Lee, in: CORROSION/2016, Paper No. 8535, Houston, TX: NACE, 2016.
[72] H. Fang, D. Young, S. Nesic, in: CORROSION/2008, Paper No. 08637, Houston, TX: NACE, 2008.
[73] J.B. Hyne, Production challenges in developing sour gas reservoirs, Chemical Engineering World XXIV (3) (March 1989) 87.
[74] D. Abayarathna, A. Naraghi, N. Obeyesekere, in: CORROSION/2003, Paper No. 03340, Houston,TX: NACE, 2003.
[75] L. Chen, N. Obeyesekere, J. Wylde, in: CORROSION/2014, Paper No. 3828, Houston, TX: NACE, 2014.
[76] D.D. MacDonald, B. Roberts, J.B. Hyne, Corrosion Science 18 (1978) 411.
[77] G. Schmitt, Corrosion 47 (1991) 285.
[78] S.B. Maldonaldo-Zagal, P.J. Boden, Mechanism of corrosion of mild steel by elemental sulfur/water suspensions, in: Proc. 8th Intern. Congr. Metal. Corros., 1, 1981, p. 338.
[79] S.B. Maldonado-Zagal, P.J. Boden, British Corrosion Journal 17 (1982) 116−120.
[80] R. Nyborg, CO_2 corrosion models for oil and gas production systems, in: CORROSION/2010, Paper No. 10371, Houston, TX: NACE, 2010.
[81] C. de Waard, D.E. Milliams, Carbonic acid corrosion of steel, Corrosion 31 (5) (May 1975) 177−181.
[82] C. de Waard, U. Lotz, D.E. Milliams, Predictive model for CO_2 corrosion engineering in wet natural gas pipelines, Corrosion 47 (12) (December 1991) 976−985.
[83] C. de Waard, U. Lotz, A. Dugstad, Influence of liquid flow velocity on CO_2 corrosion: a semi-empirical model, in: CORROSION/1995, Paper No. 128, Houston, TX: NACE, 1995.
[84] L. Smith, C. de Waard, Corrosion prediction and materials selection for oil and gas production environments, in: CORROSION/2005, Paper No. 05648, Houston, TX: NACE, 2005.
[85] V. Rusic, M. Veidt, S. Nesic, Protective iron carbonate films − part 2: chemical removal by dissolution in single-phase aqueous flow, Corrosion 62 (7) (July 2006) 598−611.
[86] V. Rusic, M. Veidt, S. Nesic, Protective iron carbonate films − part 3: simultaneous chemo-mechanical removal in single-phase aqueous flow, Corrosion 63 (8) (August 2007) 758−769.
[87] NORSOK Standard M-506 Rev2, CO_2 Corrosion Rate Calculation Model, NORSOK, Lysaker, Norway, June 2005.
[88] A. Hasan, C. Kabir, M. Sayarpour, Simplified two-phase flow modeling in wellbores, Journal of Petroleum Science and Engineering 72 (May 2010) 42−49.
[89] D. Peng, D. Robinson, A new two-constant equation of state, Industrial and Engineering Chemistry Fundamentals 15 (1) (February 1976) 59−64.
[90] P. Dranchuk, J. Abou-Kassem, Calculation of Z factors for natural gases using equations of state, Journal of Canadian Petroleum Technology 14 (3) (July 1975).
[91] Z. Duan, R. Sun, An improved model calculating CO_2 solubility in pure water and aqueous NaCl solutions from 273 to 533 K and from 0 to 2000 bar, Chemical Geology 193 (3−4) (February 2003) 257−271.
[92] Z. Duan, R. Sun, R. Liu, C. Zhu, Accurate thermodynamic model for the calculation of H_2S solubility in pure water and brines, Energy and Fuels 21 (4) (July 2007) 2056−2065.

[93] K. Pitzer, Thermodynamics of electrolytes. I. Theoretical basis and general equations, The Journal of Physical Chemistry 77 (2) (January 1973) 268−277.
[94] K. Pitzer, G. Mayorga, Thermodynamics of electrolytes. II. Activity and osmotic coefficients for strong electrolytes with one or both ions univalent, The Journal of Physical Chemistry 77 (19) (September 1973) 2300−2308.
[95] S. Nesic, H. Li, D. Sormaz, J. Huang, A free open source mechanistic model for prediction of mild steel corrosion, in: 17th International Corrosion Conference, Paper No. 2659, Houston, TX: NACE, 2009.
[96] M. Nordsveen, S. Nesic, R. Nyborg, A. Stangeland, A mechanistic model for carbon dioxide corrosion of mild steel in the presence of protective iron carbonate films − part 1: theory and verification, Corrosion 51 (5) (May 2003) 443−456.
[97] K. Addis, N. Obeyesekere, J. Wylde, Development of a corrosion model for downhole applications, in: NACE/2016, NACE, Houston, TX, 2016.

Corrosion of weldments

10

Dimitris I. Pantelis and Theodora E. Tsiourva
National Technical University of Athens, Athens, Greece

10.1 Overview of current understanding in weld corrosion

Welding is the most common method for joining different metallic components where the majority of welding in oil and gas industry accounts for the welding of pipelines. Oil and gas pipelines are constructed by welding together individual pipe joints. Although other types of joints are employed such as threaded couplings and mechanical connectors, welding is the most common method. The same welding processes can be used for both onshore and offshore oil and gas construction. Manual welding is most often used for welding procedures; however, automated welding procedures are also employed for onshore and offshore. Welding techniques such as gas metal arc welding (GMAW), submerged arc welding (SAW), shielded metal arc welding (SMAW), and electric resistance welding (ERW) are most often employed in oil and gas. Interested readers can find extensive literature on these techniques [1−3].

Corrosion is an inevitable issue in the petroleum industry due to the complex service environments and operating conditions that include the simultaneous actions of high pressures and temperatures, water with dissolved slats and gases (particularly CO_2 and H_2S), entrained sands, corrosion-influencing microbes, and complex multiphase flow regimes.

The study of weldments' corrosion has attracted attention and has been thoroughly investigated in the last several decades. Even though weldments of oil and gas structures are accomplished following well-established standard procedures, methods, and codes and are consequently approved to be void of weld defects, corrosion failures in weldments still occur. Weldments experience different forms of corrosion in the service environments of oil and gas. These corrosion attacks are strongly related to the distinct features of weldments such as microstructure, chemical composition, and residual stresses.

Fusion welding techniques, due to the thermal cycles that are imposed on the base metal or parent material (PM), lead to the creation of metallurgical transformations across the weld metal (WM) and heat affected zone (HAZ) areas. The distinct microstructures formed, depend mainly on the cooling rates and the peak temperatures in each region, thus the corrosion behavior can be quite different for each area of the weldment. Metallurgical metastable phases, like bainite and martensite, exhibit higher hardness and corrosion susceptibility due to the presence of increased lattice defects and residual stresses. In contrast, well defined heat treatment procedures can relief

Trends in Oil and Gas Corrosion Research and Technologies. http://dx.doi.org/10.1016/B978-0-08-101105-8.00010-3

the residual stresses in the lattice, form stable metallurgical phases, like ferrite and perlite and results dense corrosion products, thus inhibiting the corrosion susceptibility of the weldments. Moreover, dense, nonporous, strongly adhering corrosion products formed on weldments, can mitigate corrosion. Experiments that simulated welding thermal cycles resulted in loose porous and defective corrosion products allowing for the corrosion to progress.

Apart from the microstructure, weldment defects such as excess WM, undercut, overlap, excessive penetration, and incomplete filled groove can affect the corrosion behavior of welded mechanical components. These weld defects provide sites of stress concentration, pitting, or crevice corrosion or can even interrupt fluid flow leading to impingement corrosion.

The residual stresses in welded structures have proved to be of significant importance for the corrosion behavior of weldments. Therefore, welding residual stresses must be controlled to ensure the integrity of the structures. Several failures in carbon steel pipelines have been attributed to residual stresses. Extensive knowledge on weldment microstructure and defects can be found in literature [1−3].

The most important parameters which determine the corrosion behavior of weldments, include

- Welding practice and sequence and also choice of filler metal, which determine the metallurgical and chemical composition variations in the parent metal, HAZ, and WM. These variations favor initiation of galvanic corrosion.
- Moisture contamination that leads to hydrogen-induced cracking (HIC) of the weldment. Hydrogen entrapment in weldments can result from improperly baked or stored electrodes, moisture in the flux, or the presence of moisture and other impurities on the components to be welded.
- Oxide films and scales. The texture and the adhesion of the corrosion products formed on the weldments can affect the corrosion development. Dense, nonporous corrosion products, strongly adhering to the metal substrate, can reduce corrosion progress.
- Weld defects (e.g., incomplete weld penetration or fusion, porosity, cracks, surface flaws) act as preferential sites for local corrosion attack).
- High stresses (applied or residual) that lead to stress corrosion cracking (SCC).
- Final surface finish.

Hence, the aforementioned parameters imposed on the base metal by the welding procedure can potentially lead to galvanic corrosion and environmentally assisted cracking (EAC) of the weldments.

Galvanic corrosion, owing to the different corrosion susceptibilities of the distinct weldment microstructures (WM, HAZ, and PMs), appears as preferential corrosion either on the WM or on the HAZ.

Weldments can be susceptible to SCC under particular environmental conditions. The cracking results from the combined synergistic interaction of a corrosive environment, a susceptible microstructure, and tensile stresses. Welds often suffer from residual stresses to a level approaching the yield strength of the parent metal. Therefore, the heterogeneous microstructure of the weldment, the residual stresses, and the exposure to a corrosive environment make the weldment prone to SCC.

10.2 Forms and mechanisms of weldments' corrosion in oil and gas industry

Corrosion of weldments is strongly related to the microstructure and residual stresses formed during the welding procedure and the aggressive operating conditions. The most important corrosion forms, include galvanic corrosion, related to the microstructure of the zones formed, and EAC that appears mainly as SCC and HIC.

In the following paragraphs, these corrosion forms encountered in oil and gas industry are discussed thoroughly.

10.2.1 Galvanic corrosion

Filler metals employed in the majority of the welding techniques, along with the phase transformations induced by the thermal cycles during welding, lead to the formation of distinct areas with varying susceptibilities to corrosion. The varying susceptibilities to corrosion are due to differences in the electrochemical potential across the different zones of the weld. The resultant corrosion is usually considered as galvanic corrosion or preferential WM corrosion or preferential HAZ corrosion, according to which area is more active. If the WM and HAZ are anodic to the PM, then localized metal loss can take place in these regions. This phenomenon is accentuated by the small surface areas of the WM and HAZs compared to the large area of the parent pipe material (i.e., small anodic to large cathodic areas). In contrast, if the WM formed is more noble to the PM, then it will remain cathodic and this can be expected to reduce galvanic corrosion of the WM. Then the anodic dissolution will be spread over the large parent metal area reducing the corrosion rate.

Despite the continuing research on galvanic corrosion and its mitigation methods, preferential corrosion still occurs and failures are encountered either on the WM or on the HAZ.

10.2.2 Preferential WM corrosion

The preferential weld metal corrosion (PWC) refers to the anodic, active, behavior of the WM and depends on the chemical composition of the filler metal employed for the weld. The corrosion rate of the WM seems to be influenced by the Ni and Cr contents of the filler metal and is less affected by base metal steel composition, although steels with Cu, Ni, and Cr additions lead to nobler parent steels, hence accelerating WM attack. Matching weld consumables, with the same composition as the parent metal, have been shown to give the best resistance to PWC, whereas both 1 wt% Ni and 1 wt% Si additions are detrimental.

10.2.2.1 Case studies

Preferential corrosion attack in the weld area, leading to premature leaking, was observed in electric resistance welded (ERW) of carbon and low alloy steel pipes exposed to neutral salt-containing waters [4]. The selective and localized corrosion

prefers to occur in the weld, especially close to the fusion line. ERW seams in the presence of a corrosive environment are susceptible to preferential attack at the bond line. Because of alloying element mismatch that exists between the parent metal and the weld resulting from the ERW process, the weld generally becomes less resistant to corrosion due to the small decrease of alloying elements. The susceptibility of ERW pipe to grooving corrosion was recognized to be related to the chemical composition (particularly sulfur content) of the pipe and to the use of a postweld heat treatment. For ERW pipes made from plain carbon steels with high sulfur content of more than 0.012 wt%, grooving corrosion has contributed to nonmetallic manganese sulfide (MnS) inclusions. MnS inclusions lead to S-enriched region as a result of the rapid heating and cooling in ERW process. When electric resistance-welded carbon steel pipe was exposed to aggressive waters, grooves caused by the redistribution of sulfide inclusions along the weld line were formed in the weld. The material at the bond line is anodic to the surrounding material and the result is a V-shaped groove with the apex of the V centered on the bond line. This type of corrosion is often called as "grooving corrosion." The postweld heat treatment with higher temperature can reduce the small change in chemical compositions through the diffusion process and can thus improve the resistance to grooving corrosion [4].

A recent study by Sayed [5] of the failure of a 24″ pipeline carrying oil revealed that the failure, in the form of longitudinal crack at the 6 O'clock position (Fig. 10.1), was originated from weld defected sites, initiated by grooving corrosion, propagated by inertia at the normal designed pressure condition, and stopped when stress relief is attained.

Failure of the pipeline segment was directly related to poor quality ERW process because incomplete penetration, unmelted zones, and lack of fusion close to the pipe inner surface were present on extended regions along the seam weld line, as illustrated in Fig. 10.2 [5].

Chemical inhibition, which is employed for the mitigation of preferential weld corrosion in pipeline systems containing CO_2, has been studied by Alawadhi et al. [6]. The authors examined the performance of typical oil field CO_2 corrosion inhibitors in 3.5 wt% NaCl saturated with CO_2. A novel rotating cylinder electrode (RCE) apparatus was used to evaluate the effect of flow on the inhibition for the WM,

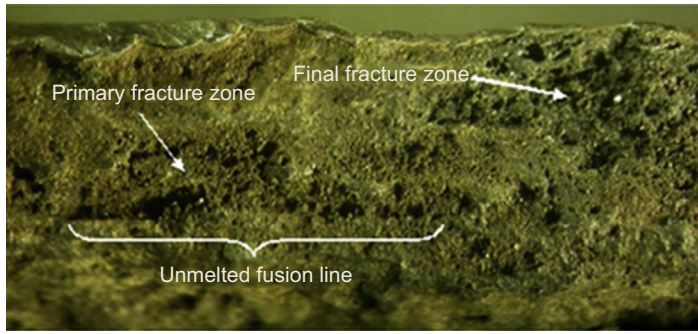

Figure 10.1 Microimage for grooving of the seam weld line just before rupture [5].

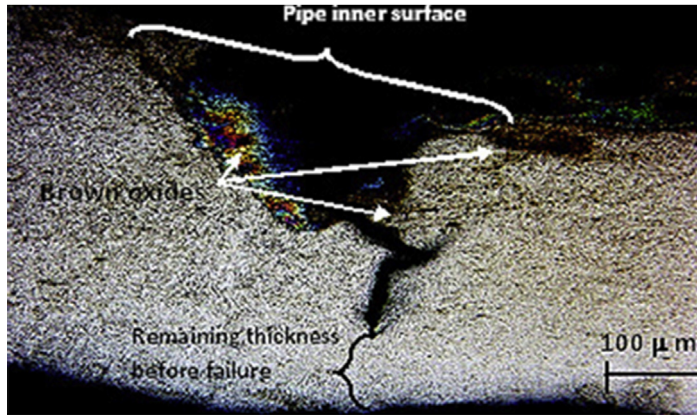

Figure 10.2 Stereoscopic image of the fractured face [5].

HAZ, and PM. For this, the galvanic currents flowing between the weld regions were recorded using parallel zero-resistance ammeters, and the self-corrosion rates of the couples were obtained by linear polarization resistance (LPR) measurements. The authors reported that under uninhibited conditions, the WM was cathodic to the PM and HAZ, whereas the addition of an oilfield corrosion inhibitor caused a current reversal at high flow rates and inhibitor film was removed preferentially from the WM so that it became strongly anodic. Moreover, under high shear stress conditions, removal of the inhibitor film took place on all weld regions and a second current reversal occurred, making the WM again the most noble area. They concluded that preferential weld corrosion is caused by unstable conditions in which the inhibitor film is selectively disrupted on the WM but remains effective on the other weld regions, and the total corrosion rates could be considered in terms of their separate galvanic and self-corrosion components [6].

10.2.3 Preferential HAZ corrosion

In some oil and gas production environments, preferential weldment corrosion may lead to enhanced HAZ attack. In the late 1980s, studies of the problems associated with preferential weldment corrosion in sweet oil and gas production systems were performed. In some cases, the HAZ was attacked, whereas in other cases, the WM was preferentially corroded. Where enhanced HAZ corrosion was observed, the composition was more influential than the microstructure; however, hardened transformed microstructures suffered increased corrosion. Postweld heat treatment at 590°C (1100°F) for stress relief proved beneficial in reducing HAZ attack [7].

Preferential HAZ corrosion in seawater was reported in the 1960s and attributed to the presence of low-temperature transformation products such as martensite, lower bainite, or retained austenite. Therefore, steel compositions favoring increased hardenability (e.g., increase in manganese content) may lead to increased localized corrosion but microalloyed steels are not susceptible [7].

It is highlighted that, as for the autogenous seam weld in ERW/HFI pipe, the difference in corrosion potential for the separate regions (parent steel, HAZ, and WM) may be only a few tens of millivolts, but due to the small surface area ratio of anode to cathode, the attack, in conductive solutions, on the anodic WM or HAZ may be very high. Also, corrosion of the parent steel will continue, and if this rate is unacceptable, mitigation methods are required for the base metal in addition to consideration of ways to control the enhanced localized attack at the weldments. Generally, such WM attack has occurred in high-conductivity media, and the measures described to ensure the WM is cathodic (more noble) relative to the parent metal have been successful. However, this may not be successful in different environmental conditions.

In HAZ, because there is no difference in composition, it is the wide range of microstructures formed that causes preferential HAZ corrosion. Corrosion susceptibility of HAZ is considered highly dependent on the thermal cycles experienced by the metal [8]. Close to the fusion boundary, the HAZ transformation to austenite on heating will be followed on cooling by transformation to either a ferrite−pearlite microstructure or bainite, or martensite or a mixture of all three, depending on material composition, peak temperature, and cooling rate. Farther from the weld, the material will be exposed to a lower peak temperature, so only partial austenization occurs, and those areas heated below the ferrite-to-austenite transformation temperature (Ac1) will not be significantly affected, other than by some carbide coarsening and tempering [1−3]. Studying the weldments microstructure in HAZ revealed that the coarsening of ferrite Widmastätten in the HAZ increased the corrosion resistance of carbon steel in acidic solutions containing NaCl [9].

Tramline corrosion is a term applied to preferential HAZ corrosion concentrated at the fusion boundaries and has been observed in acidic aqueous environments such as acid mine waters. There is clearly a microstructural dependence and studies on HAZs show corrosion to be appreciably more severe when the material composition, and welding parameters are such that hardened structures are formed. It has been known for many years that hardened steels may corrode more rapidly in acid conditions than fully tempered material, apparently because local microcathodes on the hardened surface stimulate the cathodic hydrogen evolution reaction [1].

10.2.3.1 Case studies

Tsiourva et al. [10] studied the corrosion behavior of AH36 steel welds in order to evaluate the influence of preferential corrosion of welded AH36 steel on the structural reliability of ship structures, employing electrochemical methods on the distinct areas of the weldment: WM, HAZ, and the parent metal. The HAZ with bainite microstructure exhibited the highest hardness values as can be seen in Fig. 10.3.

Based on electrochemical experiments, the obtained polarization curves (see for example Tafel extrapolated curves), it was concluded that HAZ is the most susceptible to corrosion, exhibiting the highest values of current density, as presented in Table 10.1 and Fig. 10.4. The WM is the most resistant to corrosion of the three distinct zones [10]. However, microhardness measurements are not sufficient to predict corrosion susceptibility; for example, the parent metal exhibits higher corrosion rates than the

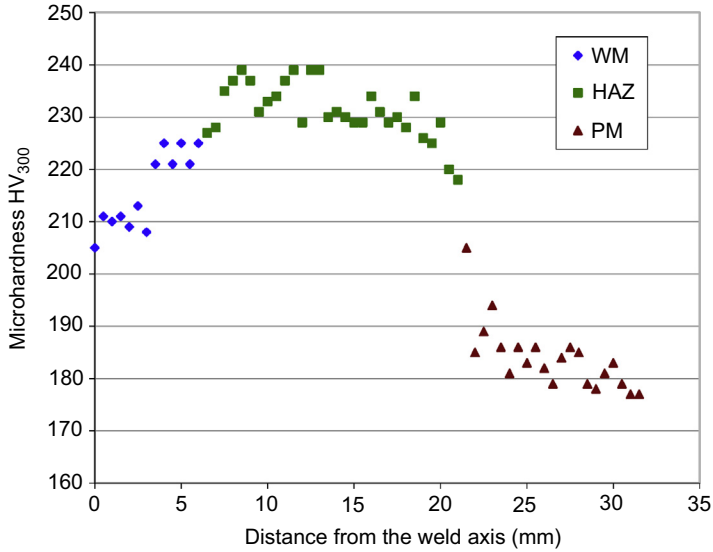

Figure 10.3 Microhardness profile of the weld [10].

WM, despite its lower microhardness values, a fact attributed to the high residual stresses present due to work hardening.

Pereda et al. [11] reported that the thermal cycles experienced by the HAZ of super martensitic welds in chloride-containing solutions do not have a significant effect on the pitting potential. Moreover, the study of API X-80 pipeline steel proved that bainite favored higher passive current densities in alkaline solutions, whereas the presence of

Table 10.1 Corrosion parameters for the distinct zones in welded AH36 steel [10]

	PM	WM	HAZ
Linear polarization			
E_{corr} (mV)	−659.4	−666.9	−640.7
I_{corr} (μA)	28.19	17.17	35.28
Corr rate (mpy)	25.65	15.63	32.10
Tafel extrapolation			
E_{corr} (mV)	−724.9	−715.2	−712.2
I_{corr} (μA)	14.41	8.75	19.94
Corr rate (mpy)	13.11	7.96	18.14

HAZ, heat affected zone; *PM*, parent metal; *WM*, weld metal.

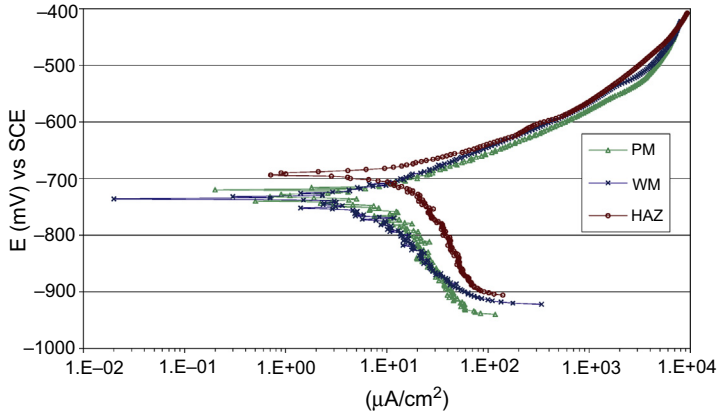

Figure 10.4 Tafel plots for parent metal, weld metal (WM), and heat affected zone (HAZ) of welded AH36 steel [10].

M−A phases in the microstructure extended the passive region to higher potentials in alkaline solutions [12].

Despite these variations, in the majority of applications, there is little influence on the corrosion performance, and preferential HAZ corrosion is relatively rare. Where preferential HAZ attack has been reported, it is more common in carbon and carbon−manganese steels than in higher-alloy grades [7].

10.2.4 Environmentally assisted cracking

Although EAC is more common in the refining and power-generation industries where components frequently operate in aggressive environments, pipeline steels also experience it. EAC or degradation can take many forms, ranging from local thinning caused by global corrosion attack, to SCC and hydrogen damage. The form of cracking or degradation depends on a number of factors, including the material, chemical composition, and microstructure, WM and HAZ properties (including hardness), weld geometry, level of welding residual stresses, operating conditions, and environment.

Corrosion of carbon and low-alloy steels by aqueous H_2S solutions (or sour waters) can result in one or more types EAC. These forms of EAC are related primarily to the damage caused by hydrogen that results from the sulfide corrosion process in aqueous media. They include loss of ductility on slow application of strain (hydrogen embrittlement), formation and propagation of hydrogen-filled blisters or voids in the material (hydrogen blistering or HIC), and spontaneous cracking of high-strength or high-hardness steels (hydrogen embrittlement cracking, also known more familiarly as sulfide stress cracking, or SSC, when involving environments that include exposure to H_2S).

10.2.5 Stress-corrosion cracking

Weldments can be susceptible to SCC under particular environmental conditions. The cracking results from the combined synergistic interaction of a corrosive environment,

a susceptible microstructure, and tensile stresses. Welds often suffer from residual stresses, to a level approaching the yield strength of the parent metal. Therefore, the heterogeneous microstructure of the weldment, the residual stresses, and the exposure in corrosive environment make the weldment prone to SCC.

Stress-corrosion cracks usually start from corrosion pits and proceeds transgranular or intergranular through the metal. Cracking is often characterized by crack branching and usually has a delay time prior to crack initiation, whereas corrosion products are often found along the fracture.

Welding parameters influence the amount and distribution of residual stresses because the extent of the stressed region and the amount of distortion are directly proportional to the size of the weld deposit; this deposit is directly related to the heat input. Welding thermal cycles are often much localized, resulting in strains that can cause distortions and residual stresses. These residual stresses can be important in the initiation and propagation of SCC.

Postweld heat treatment redistributes the localized load and reduces the residual tensile stresses and decreases susceptibility to SCC.

10.2.5.1 Case studies

Monoethanolamine (MEA) is an absorbent used to remove acid gases containing H_2S and CO_2 in oil refining operations. Failures in several refineries have shown that cracks can be parallel or perpendicular to welds, depending on the orientation of principal tensile stresses. Equipment containing MEA at any temperature and for any acid gas concentration is being postweld heat treated in order for the stresses to be relieved. Inspection programs showed that leaks were widespread and were found in vessels aged from 2 to 25 years. However, there were no reports of cracking in vessels that had been postweld stress relieved. In addition, it was found that all concentrations of MEA were involved and that MEA solutions were usually at relatively low temperatures (below 55°C or 130°F). Equipment found to suffer from cracking included tanks, absorbers, carbon-treated drums, skimming drums, and piping [7].

Contreras et al. [13] studied the susceptibility of welded X52 and X70 steels to SCC in H_2S saturated environment using strain rate test. Failure due to SCC was observed mainly in the HAZ. The authors concluded that ductile failure occurred in the air tests. In contrast, brittle type failure took place in the H_2S saturated corrosive environment as evidenced by the degradation of the mechanical properties of the material. The results of slow strain rate tests are presented in Table 10.2. Fig. 10.5 presents the relative stress versus elongation behavior. The authors further stated that the permeability of hydrogen in X52 weld is higher than in X70 weld. This suggests that HAZ of X52 grade pipes may be more susceptible to SCC in corrosive environments than those of X70. X70 pipeline has also been shown not to form stable oxides on the surface in near neutral pH solution [13].

10.2.6 Hydrogen-induced or cold cracking

HIC or cold cracking is one of the most important issues in weldments, mainly in carbon and high-strength low alloy steels. This phenomenon is also referred as delayed cracking.

Table 10.2 Summary of slow strain rate test results [13]

Steel	Environment	UTS (MPa)	EL (mm)	RA (%)	RRA
X-52	Air	391	2.03	55.6	N/A
	NACE + H_2S at 25°C (77°F)	249	1.42	13.8	0.248
	NACE + H_2S at 50°C (122°F)	233	1.88	7.25	0.130
X-70	Air	462	2.64	50.98	N/A
	NACE + H_2S at 25°C (77°F)	213	1.21	6.91	0.135
	NACE + H_2S at 50°C (122°F)	355	2.03	4.38	0.085

EL, elongation; *N/A*, not applied; *RA*, reduction area; *RRA*, ratio reduction area; *UTS*, ultimate tensile strength.

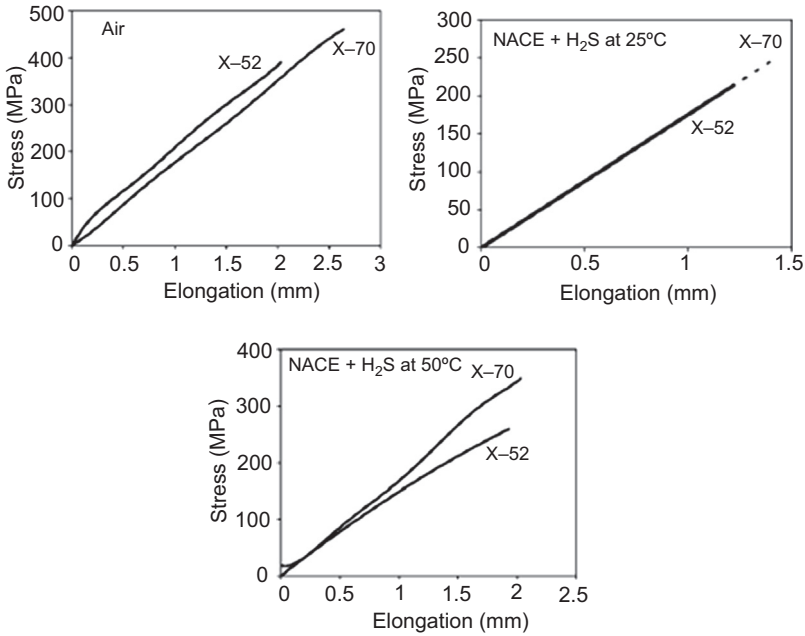

Figure 10.5 Stress versus elongation behavior under different conditions used [13].

Hydrogen coming from moisture in certain weld consumables or during nonoptimal field welding conditions can become dissolved in the liquid WM. This dissolved hydrogen can cause cracking during solidification, as well as embrittlement of the weld, due to the different dissolution in the different phases. The dissolution of hydrogen in liquid iron obeys Sievert's law. The solubility of hydrogen in iron as a function of temperature is illustrated in Fig. 10.6 [1].

Dissolved hydrogen in the material as a result of exposure wet H_2S service environments can also affect weldability and the subsequent performance of repair welds.

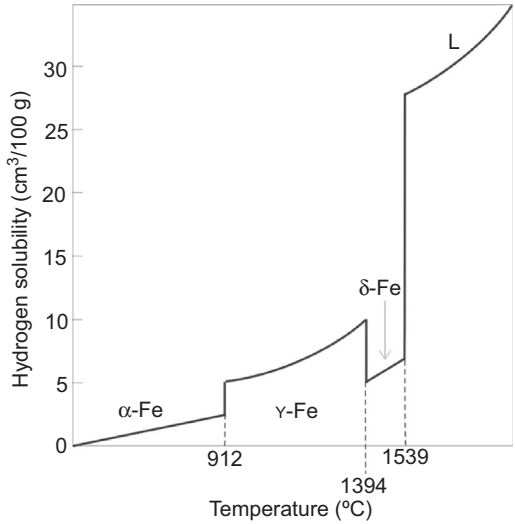

Figure 10.6 Solubility of hydrogen in iron at $P_{H2} = 1$ atm [1].

HIC is a phenomenon associated with welds in hardenable carbon and low-alloy steels and results from the combined actions of the following parameters:

- Susceptible ("brittle") microstructure
- Hydrogen presence in the WM
- Tensile stresses in the weld area
- Temperature range, from −100 to 200°C (−150 to 390°F)

Absorbed atomic hydrogen that has diffused into the material can also recombine to form molecular hydrogen (H_2) at internal defects, inclusions, and pores. Sites for recombination are commonly observed to be weak internal interfaces, such as those at MnS inclusions or microstructural laminations. Ferrite−pearlite banding and related inclusions can also produce locally weak interfaces in the material that can result in small hydrogen-filled blisters being produced [7,14]. Because hydrogen molecules are much larger than atomic hydrogen, once the hydrogen recombines to form hydrogen gas (H_2), it cannot readily diffuse out of these sites. This results in a buildup of pressure inside these blisters, which drives their growth, and eventually results in propagation and linkage of hydrogen-filled blister cracks in the material, commonly known as HIC [7,14].

Cracking may occur several hours, days, or weeks after the weld has cooled; consequently, the term delayed cracking is also used. According to the location, they are observed on a weldment; cracks are often described as toe cracking, root cracking, or underbead cracking as presented in Fig. 10.7. WM cracks may be longitudinal or transverse. Longitudinal cracks start due to stress concentrations at the root of the weld. Transverse cracking starts at hydrogen-containing defects subject to longitudinal stresses. WM cracks do not always extend to the surface. In a submerged arc WM made with damp fluxes, a unique crack morphology known as chevron cracking can occur.

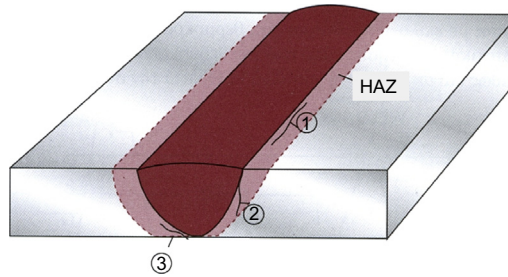

Figure 10.7 Weld metal cracks in heat affected zone (HAZ) due to hydrogen-induced cracking: (1) underbead cracking, (2) toe cracking, (3) root cracking.

HIC has been observed primarily in the parent metal and HAZ. Cracks in the HAZ are most often longitudinal. Underbead cracks lie more or less parallel to the fusion line. They do not normally extend to the surface and may, therefore, be difficult to detect. Underbead cracks will form at relatively low stress levels in martensite, when high levels of hydrogen are present. Toe cracks and root cracks start in areas of high stress concentrations. Cracking may, therefore, occur in less susceptible microstructures or at relatively low hydrogen levels. This type of cracking is often delayed while the necessary hydrogen diffuses to the area. Transverse cracking in the HAZ is less common. It will occur in high-carbon martensite under conditions of high longitudinal stresses.

HIC has been detected in both high- and low-strength steels, even under nonstressed conditions. This phenomenon usually is of concern in lower-strength plate steels—less than 550 MPa (80 ksi) and low hardness (<HRC 22) used in rolled and longitudinally seam welded or ERW pipe or plate steels used in the manufacturing of refinery vessels and tanks [7].

In low-strength steels when exposed to a hydrogen-containing environment, due to its rapid cooling and solidification, WM forms a structure of dendrites containing inclusions in the form of fine globules. In WM, up to a maximum hardness of 280 HV, do not present HIC. Exceptions are observed when highly alloyed electrodes were being used, if the WMs were made more hardenable by dilution of carbon from the parent metal, or in certain submerged arc welds, where the use of excessive arc voltage and active fluxes results in high manganese and/or silicon pickup from the flux.

10.2.6.1 Case studies

Chatzidouros et al. [15] studied the effect of hydrogen-containing environment on cracks, located in the base metal and the HAZ of X52 and X70 weldments. The authors employed the three-point bending fracture toughness method in a continuously hydrogen charged solution of NS4. They reported that X70 base metal exhibited a reduction in ductility in comparison to the tests in air, whereas HAZ exhibited only a slight reduction. The ferritic and mixed bainitic−pearlitic banded base metal of X70 proved more susceptible to hydrogen embrittlement than the banded ferritic and mixed bainitic−pearlitic−ferritic of the HAZ metal as presented in Fig. 10.8.

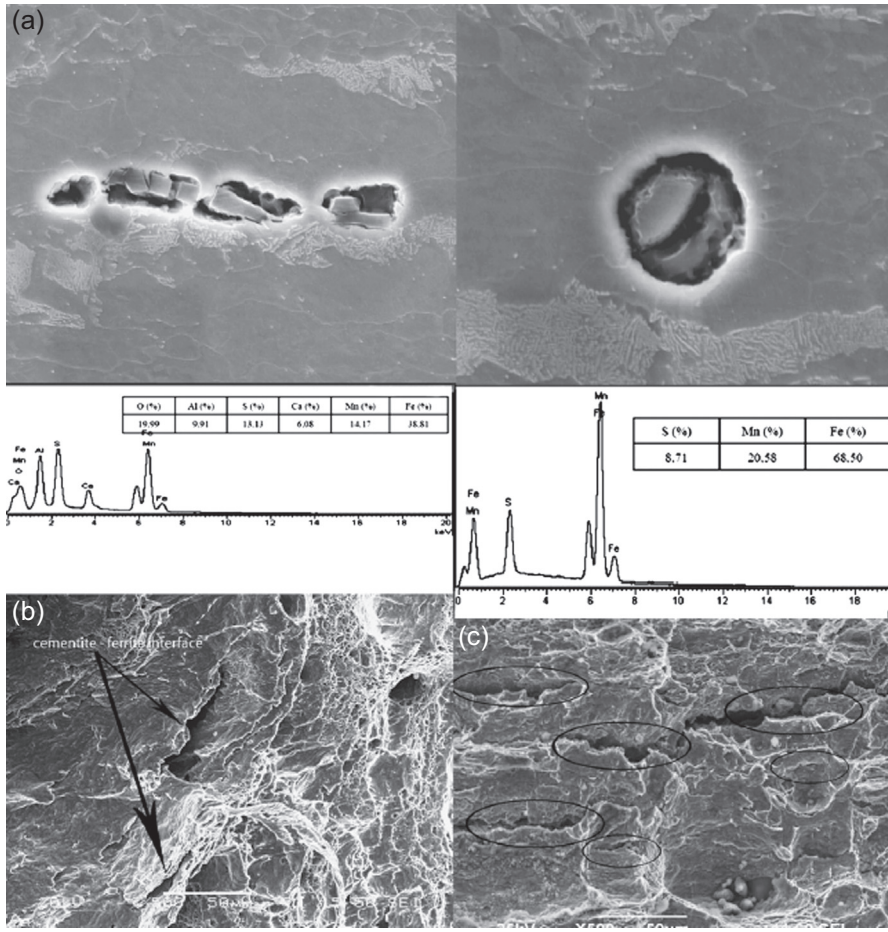

Figure 10.8 (a) MnS and Al_2O_3 inclusions existing along the bands in the X70 base and heat affected zone (HAZ) metal, (b) and (c) microcracks for X70 base metal and for the case of applied current density of 1 mA/cm^2 [15].

The continuous interface between the ferrite and the banded mixed bainite−pearlite of the X70 base metal was supersaturated with hydrogen aided by the existence of inclusions parallel and along the bands. Hydrogen dragging by moving dislocations is a possible mechanism for the accumulation of hydrogen in these interfaces, which in turn facilitate microcracking. Similar results for X52 steel proved that the base metal exhibits a reduction in ductility while this reduction is lower for the HAZ. The continuous interface between the ferrite and banded pearlite of the X52 base metal leads to hydrogen trapping of these interfaces, as hydrogen is forced to follow the ferrite band as it diffuses. Aided by the large deformation gradient between the ferrite and pearlite bands, these interfaces are supersaturated and the deformation gradient is further augmented as it is portrayed in the fracture mode that is arranged in bands.

Beidokhti et al. [16] experimentally tested the impact of manganese content (1.4 and 2.0 wt%) of X70 pipe on HIC and SSC of submerged arc welded test pieces. The authors found that the weldments with 2.0 wt% manganese content were more susceptible due to the higher hardness of the weldments.

Azevedo [17] reported stress-oriented hydrogen-induced cracking (SOHIC) failure in welded API 5L X46 steel crude oil pipeline. Parent metal and HAZ exhibited cracking (blistering) of the sulfide/matrix interface. Microfractographic examination indicated ductile fracture mechanism, implying that atomic hydrogen association rather than hydrogen embrittlement was the active mechanism during the cracking of the pipeline, as we can see in Fig. 10.9. The main cracking nucleated in the internal

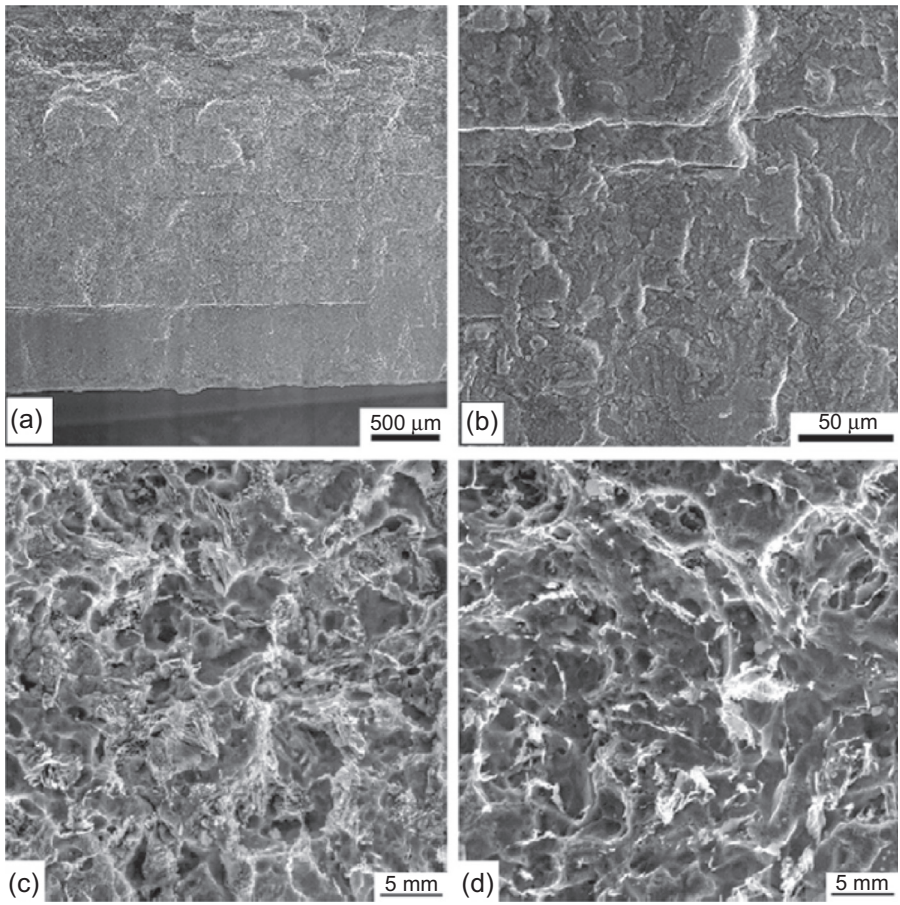

Figure 10.9 Microphotographic examination: (a) general view showing plane (bottom and central area) and rough (top area) regions and presence of parallel secondary cracks; (b) detail showing parallel secondary cracks; (c) detail inside the heat affected zone (HAZ) (plane surface) region showing predominance of ductile type fracture; (d) detail inside the base metal (rough surface) region showing predominance of ductile type fracture [17].

surface of the tube, at the boundary between the HAZ and the WM, propagating in a stable mode along the radial and longitudinal directions. The nucleation of cracking was attributed to welding defects and corrosion pits and did not seem to depend on the welding microstructure, growing perpendicular to both the internal surface and main tensile stresses. Crack propagation was, however, microstructure sensitive, with a more intense branching occurring inside the base metal rather than the HAZ region.

10.2.6.2 Prevention

For cold cracks to occur in steels, three principal factors must be present: atomic hydrogen, HAZ, or portion of the WM that is susceptible to hydrogen embrittlement and a high-tensile stress resulting from restraint. Controlling one or more of these factors may reduce the occurrence of cold cracking. Control of this cracking requires the use of low-hydrogen electrodes, high preheat, sufficient interpass temperature, and greater penetration through the use of higher currents and larger electrodes. The susceptibility of the microstructure to cold cracking relates to the solubility of hydrogen and the possibility of supersaturation.

The major preventative measures to avoid cold cracking include the following actions:

- Preheat, including maintenance of proper interpass temperature
- Heat input control
- Postweld heat treatment
- Bead tempering
- Use of low-hydrogen processes and consumables
- Use of alternate filler materials (e.g., austenitic electrodes)

One of the serious problems with HIC is the difficulty in detecting the presence of a crack. The delayed nature of some of the cracks makes the detection difficult and demands that inspection should not be carried out too soon, especially in welds that will have external stresses applied when put in service.

Moreover, some of the cracks do not extend to the surface, thus they are not detectable by visual inspection methods (liquid penetration or magnetic particle inspection). Radiography may not trace these fine cracks, and ultrasonic inspection needs well-experienced operators. Consequently, the problematic detection of this cracking mode and the increased possibility of these cracks to lead to in-service failures makes the adoption of precaution measures mandatory [7].

10.2.7 Hydrogen induced disbonding

Hydrogen-induced disbonding (HID) of stainless steel clad or weld overlaid steel plates has been observed in hydro-processing equipment [7]. This form of attack usually results in the formation of blisters at or near the bond/fusion line between the steel and the stainless alloys. HID occurs with increasing frequency at high hydrogen

pressures and service temperatures and with increased rapid cooling as a result of process changes and shutdown, start-up cycles [7].

10.2.8 Sulfide stress cracking

SSC was first identified in the production of sour crude oils when high-strength steels used for well-head and downhole equipment cracked readily after contact with produced water that contained H_2S. SSC was not experienced by refineries and petrochemical plants until the introduction of high-pressure processes that required high-strength bolting and other high-strength components in gas compressors. With the increased use of SAW for pressure vessel construction, it was found that weld deposits significantly harder and stronger than the base metal could be produced. This led to transverse cracking in weld deposits with hardness greater than 200 HB [7].

High-strength steel pipes used in drilling and completion of oil and gas wells may exhibit delayed SSC failures in environments containing H_2S. These failures result mainly from the embrittlement due to hydrogen absorption into the steel in these environments. H_2S poisons the hydrogen recombination cathodic corrosion reaction, thus favoring atomic hydrogen absorption into the material.

10.2.8.1 Susceptibility

The susceptibility to SSC increases with increasing hydrogen sulfide concentration or partial pressure and decreases with increasing pH. SSC decreases in corrosive environment with pH 8 and below 101 Pa (0.001 atm) partial pressure of hydrogen sulfide. According to literature, the cracking tendency is most pronounced at ambient temperature and decreases with increasing temperature [7].

For a given strength level, tempered martensitic steels have better resistance to SSC than normalized-and-tempered steels, which in turn are more resistant than normalized steels. Untempered martensite demonstrates poor resistance to SSC. It is generally agreed that a uniform microstructure of fully tempered martensite is desirable for SSC resistance.

The effect of alloying elements on SSC resistance of carbon and low alloy steels is controversial, except for one element. Nickel is detrimental to SSC resistance. Steels containing more than 1 wt% Ni are not recommended for service in sour environments. The susceptibility of weldments to SSC appears to be greater than that of the parent metal. The high hardness and residual stresses resulting from welding are believed to increase the susceptibility. It should be noted that SSC occurred in weldments having hardness lower than HRC 22. A maximum hardness of 248 HV should be maintained for carbon steel parent materials and regions of carbon steel weldments that are in direct contact with sour service environments [18].

Susceptibility to SSC is a function of a number of variables, two of the more important ones are strength or hardness of the steel and the level of tensile stresses. SSC is normally associated with high-strength steels and alloys—yield strength greater than 550 MPa (80 ksi)—and with high-hardness (>HRC 22) structures in weld HAZs.

Nonpostweld heat treated weldments are particularly problematic because they often contain both high HAZ hardness and high residual tensile stresses that can initiate SSC and promote crack propagation. Resistance to SSC is usually improved through the use of PWHT and through the use of lower carbon-equivalent plate steels and quenched and tempered wrought steels [7].

There is also a direct relationship between H_2S concentration and the allowable maximum hardness value of the HAZ, on one hand, and cracking threshold stress on the other. Typically, the allowable maximum hardness value decreases by 30 HB, and the allowable threshold stress decreases by 50% for a tenfold increase in H_2S concentration.

The oil and gas industry has increasing needs for the use of high-strength low-alloy (HSLA) steels such as API 5L X70 and X80. Due to their higher tensile strengths, these grades can handle higher operating pressures with thinner wall thicknesses that translates to cost savings, especially in long distance transmission pipelines. Transported crude and gas, however, are becoming increasingly sour (higher H_2S concentrations). The performance of pipeline girth welds used to connect pipe segments in the field is of interest for many scientists. Multipass circumferential girth welds cause tempering in underlying hard HAZ regions, leaving the hardest HAZ regions in the final untempered cap passes. On the pipeline exterior, welds are exposed to lower hydrogen concentrations than weld regions in contact with the sour environment in the inner pipe surface. SSC is an HE mechanism, so higher hardness values (exceeding HRC 22) should be tolerable in hard weld cap regions, which are exposed to relatively low hydrogen concentrations. In fact, it has been shown that hard external weld regions exceeding 300 HV (248 HV = HRC 22) were resistant to SSC in a stressed pipe filled with the National Association of Corrosion Engineers (NACE) test solution [18].

10.2.8.2 Cases studies

The susceptibility to SSC of welded X70 and X80 line pipe steel was studied by Omweg et al. [18] under conditions of varying applied stresses, H_2S concentrations, and peak weld hardness. They concluded that a maximum hardness of 248 HV should be maintained for carbon steel parent metals and regions of carbon steel weldments that are in direct contact with sour service environments. Comparing the steel grades, the low-carbon ($\sim$0.03 wt% C) X80 steel was found to be more resistant to SSC in the as-welded condition and tolerated much higher absolute tensile stresses than the as-welded X70 steel.

Natividad et al. [19] tested indirect electric arc (IEA) welding, to form narrow HAZ, which has proved to be more susceptible to hydrogen embrittlement. Weldments produced by IAE presented the highest resistance to SSC at 25°C (77°F), comparing to SAW and metal inert gas (MIG). This behavior was attributed to the columnar, fine-grained, homogeneous microstructure, formed with IEA process and a narrow HAZ. Moreover, specimens obtained by IAE process present better SSC compared to SAW and MIG processes. They also attributed the higher atomic hydrogen permeation flux caused by IEA to the ferrite phase of the base metal.

10.2.8.3 Prevention

The most effective way of preventing SSC is to ensure that the steel is in the proper metallurgical condition. This usually means that weld hardness is limited to HRC 22. Because hard zones can also form in the HAZs of welds and shell plates from hot forming, the same hardness limitation should be applied in these areas.

Postweld heat treatment of fabricated equipment will greatly reduce the occurrence of SSC. The effect is twofold: first, there is the tempering effect of heating to 620°C (1150°F) on most hard microstructures (the possible exception being highly microalloyed steels), and second, the residual stresses from welding are reduced. The residual tensile stresses typically represent a much larger effect on the equipment than the internal pressure or other mechanical stresses.

Equipment exposed to wet H_2S service environments often need to be baked prior to weld repairs to reduce or remove the accumulated hydrogen that can lower weldability. In some severe cases, this can result in cracks being formed as a result of high-temperature hydrogen attack.

10.3 Currents trends and needs in weld corrosion research

In 2010, International Energy Outlook reported that an increase of up to 40% is expected for the world gas consumption over the 2007 to 2035 period. This increase in demand means that a greater supply of resources is required over long distances that typically exist between the reservoirs and consumers [20].

Pipelines are the key method of transportation through which high flow rates of hydrocarbons can be provided. In order to transport a greater volume of resources through pipelines, higher operating pressures are required, while in the same time the industry aims at decreasing pipeline construction and operating costs. Approximately, 20% of the entire pipeline construction costs is due to welding, coating, and subsequent maintenance [21]. Thus, increasing the welding efficiency without losing the performance in the welded joints is of great importance.

The key areas of research are presented and briefly discussed in the next sections.

10.3.1 Development of new steels

Carbon steels like API 5L X52, X65, X70, which have been extensively studied and employed in oil and gas industry, are insufficient to meet the future needs of oil and gas industry. Steel development has focused on improving strength and mechanical properties without reducing toughness and weldability of the steels through thermomechanical treatments and alloying procedures. High strength low alloy (HSLA) steels, like X80, X100, and X120 grades, were developed to overcome such difficulties during the last decade. However, corrosion of weldments in these grades has not been studied thoroughly, limiting their widespread adoption. HSLA steels contain very low

amounts of carbon (0.05−0.10 wt%), as well as total level of microalloying elements, less than 1 wt%. HSLA steels usually contain Mn up to 2 wt%. Alloying elements such as Nb, B, V, Ti, and Mo are typically used for microalloying and the strengthening mechanisms are usually precipitation hardening and grain refinement. Corrosion behavior of weldments of API X80 pipeline steels has been studied [20]. The authors concluded that the corrosion rate of API X-80 pipeline steel is largely dependent on pH and oxidizing power of the electrolyte.

With increasing use of CO_2-enhanced oil recovery technique and the exploration of deep oil and gas reserves containing higher CO_2, CO_2 corrosion of downhole tubular steels has become more severe and is a big concern to scientists and engineers [4]. Low Cr steel, containing up to 5 wt% Cr, is a new type of steel developed for use in CO_2 environments [22]. Several papers have confirmed the good corrosion resistance of this type of steel in CO_2-containing or CO_2-saturated environments, along with its good strength and plasticity [23]. Kermani et al. [22] showed that low Cr steels, containing up to 3 wt% Cr, steel is less than 1.5 times more expensive than conventional grades (5CT C90 and X70) of carbon steel and exhibited 3−10 times better corrosion resistance in CO_2 environment.

Welding of these steels is necessary for the application of 3Cr low alloy, although it has proved to be difficult due to poor matching of the commercial wires for these low Cr steels. Several efforts for the welding of these steels have been reported, been inefficient, and unable to meet the requirements of a high-efficiency field operation or not meeting the requirements of the relevant standards [22].

Hence, it is evidenced that the corrosion behavior of the newly developed HSLA grades like X100, X120 have raised attention by the scientists. Significant efforts to investigate the role of these steels' microstructure on the corrosion behavior have been attempted. However, only few researchers have investigated the corrosion behavior of the weldments, in particular, in the operating corrosive environments of oil and gas industry.

10.3.2 Welding techniques

The most commonly applied welding techniques in oil and gas industry include SAW, GMAW, and SMAW. The progress in understanding the effect of weldments' microstructure on the corrosion failures and corrosion susceptibility led scientists to pursue new welding techniques or new welding consumables. Some scientists are trying new welding wires, whereas others apply new welding techniques like indirect electric arc welding to narrow the HAZ, which is prone to corrosion.

Yet the aforementioned efforts are limited and more welding techniques and parameters could be considered and investigated. For instance, solid-state welding techniques like radial friction welding that involves rotation and radial compression of a solid beveled ring into a V-preparation provided by the pipe ends. The pipe ends are butted together and clamped securely to stop them rotating or moving apart. A mandrel is located in the bore, at the weld location, to prevent collapse of the pipe ends and penetration of upset metal formed during the weld sequence.

10.3.3 Experimental techniques

Electrochemical techniques, namely alternating current (AC) and direct current (DC) applied potentials, are widely applied for the study of the corrosion behavior of weldments. Electrochemical impedance spectroscopy is considered as an indispensable technique for the investigation of the corrosion phenomenon.

Several scientists have adopted novel techniques like RCE produced from the different regions of the weld to study the effects of hydrodynamic conditions or jet impingement apparatus to study flow-induced corrosion [6,24]. Others have applied microelectrochemical capillary to concentrate the study in the distinct zones of the weld. Besides, some scientists have adapted electrochemical cell on hydraulic servo fatigue testing to investigate the coupling effect of stress and corrosion [4].

The aforementioned studies are promising because they include the particular characteristics of the weldments, nevertheless there are still many newly developed experimental techniques that can be exploited for the study of the corrosion of the weldments. Microelectrochemical cells can be applied in the distinct weld zones and if coupled with optical methods could provide valuable information on the corrosion of microstructure. In addition, mechanical tests coupled with electrochemical techniques could provide credible information on the behavior of weldments under the coupling effect of stress and corrosion.

10.3.4 Modeling tools progress

Corrosion phenomenon in oil and gas industry has presented significant progress over the past few decades. The influence of the many important electrochemical, chemical, hydrodynamic, and metallurgical parameters has been uncovered. Various mathematical modeling approaches have been applied to enhance the knowledge on corrosion: mechanistic modeling, semiempirical models, and empirical models [25–28].

However, research on modeling of corrosion of weldments, is yet to be developed, taking into account the complexity of the parameters influencing corrosion of weldments in particular. Significant efforts in recent studies have employed computational fluid dynamics to investigate the corrosion kinetics in CO_2-saturated fluid flow and to develop a semiempirical model to predict the corrosion rate of steels in CO_2-saturated fluid flow [29].

Exploiting the existing knowledge in weldments microstructure, corrosion kinetics in severe operating conditions, and employing modern software tools, corrosion could be predicted, contributing to the reduction of maintenance and repair costs.

The interdisciplinary approach of complicated issues like corrosion of weldments, the employment of new material, the application of new welding techniques and parameters, the adoption of new experimental techniques and modeling tools could result in the enhanced understanding of corrosion of weldments and achieve the reduction of maintenance and repair costs.

References

[1] D.I. Pantelis, V.J. Papazoglou, Welding Science and Technology, second ed., National Technical University of Athens, 2014 (in Greek).

[2] K. Easterling, Introduction to the Physical Metallurgy of Welding, second ed., Butterworth-Heinemann, Oxford, UK, 1992.

[3] S. Kou, Welding Metallurgy, John Wiley & Sons, 1987.

[4] J. Zhu, L. Xu, Z. Feng, G.S. Frankel, M. Lu, W. Chang, Galvanic corrosion of a welded joint in 3Cr low alloy pipeline steel, Corrosion Science 111 (2016) 391−403.

[5] M.H. El Sayed, Grooving corrosion of seam welded oil pipelines, Case Studies in Engineering Failure Analysis 2 (2014) 84−90.

[6] K. Alawadhi, M.J. Robinson, Preferential weld corrosion of X65 pipeline steel in flowing brines containing carbon dioxide, Corrosion Engineering, Science and Technology 46 (4) (2011) 319−329.

[7] J. Davis, Corrosion of Weldments, ASM International, 2006.

[8] A. Saarinen, K. Onnela, A method for testing the corrodibility of heat-affected zone in steels, Corrosion Science 10 (1970) 809−815.

[9] H.-H. Hang, W.-T. Tsai, J.-T. Lee, The influences of microstructure and composition on the electrochemical behavior of a 516 steel weldment, Corrosion Science 36 (1994) 1027−1038.

[10] D. Tsiourva, L.I. Dimaratos, D.I. Pantelis, V.J. Papazoglou, Corrosion behavior of shipbuilding high strength steel welds employing electrochemical methods, in: Proceedings of the 11th International Maritime Association of the Meditarranean Congress - IMAM - Maritime Transportation and Exploitation of Ocean and Coastal Resources, Lisbon (Portugal), 26−30 September 2005, Taylor & Francis, London, 2005, pp. 543−548.

[11] M.D. Pereda, C.A. Gervasi, C.L. Llorente, P.D. Bilmes, Microelectrochemical corrosion study of super martensitic welds in chloride −containing media, Corrosion Science 53 (2011) 3934−3941.

[12] S. Bordbar, M. Alizadeh, S. Hojjat Hashemi, Effects of microstructure alteration on corrosion behavior of welded joint in API X70 pipeline steel, Materials and Design 45 (2013) 597−604.

[13] A. Contreras, A. Albiter, M. Salazar, R. Perez, Slow strain rate corrosion and fracture characteristics of X-52 and X-70 pipeline steels, Materials Science and Engineering A 407 (2005) 45−52.

[14] C.-M. Lee, S. Bond, P. Woollin, Preferential weld corrosion: effects of weldments microstructure and composition, in: CORROSION 2005, Houston, Texas: NACE International, 2005. Paper 05277.

[15] E. Chatzidouros, V.J. Papazoglou, T.E. Tsiourva, D.I. Pantelis, Hydrogen effect on fracture toughness of pipeline steel welds, with in situ hydrogen charging, International Journal of Hydrogen Energy 36 (2011) 12626−12643.

[16] B. Beidokhti, A. Dolati, A.H. Koukabi, Effects of alloying elements and microstructure on the susceptibility of the welded HSLA steel to hydrogen-induced cracking and sulfide stress cracking, Materials Science and Engineering A 507 (2009) 167−173.

[17] C.R.F. Azevedo, Failure analysis of a crude oil pipeline, Engineering Failure Analysis 14 (2007) 978−994.

[18] G.M. Omweg, G.S. Frankel, W.A. Bruce, J.E. Ramirez, G. Koch, Performance of welded high-strength low-alloy steels in sour environments, Corrosion 59 (7) (2003) 640−653.

[19] C. Natividad, M. Salazar, M.A. Espinosa-Medina, R. Pérez, A comparative study of the SSC resistance of a novel welding process IEA with SAW and MIG, Materials Characterization 58 (2007) 786−793.

[20] F. Mohammadi, F.F. Eliyan, A. Alfantazi, Corrosion of simulated weld HAZ of API X-80 pipeline steel, Corrosion Science 63 (2012) 323−333.
[21] C. Zhang, Y.F. Cheng, Corrosion of welded X100 pipeline steel in a near-neutral pH solution, Journal of Materials Engineering Performance 19 (2010) 834−840.
[22] M.B. Kermani, M. Dougan, J.C. Gonzales, C. Linne, R. Cochrane, Development of low carbon Cr-Mo steels with exceptional corrosion resistance for oilfield applications, in: CORROSION/2001, NACE International, Houston, TX, 2001. Paper No. 065.
[23] A. Pfennig, A. Kranzman, Effect of CO_2 and pressure on the stability of steels with different amounts of chromium in saline water, Corrosion Science 65 (2012) 441−452.
[24] G.T. Burstein, K. Sasaki, Detecting electrochemical transients generated by erosion − corrosion, Electrochimica Acta 46 (2001) 3675−3683.
[25] S. Nesic, Key issues related to modeling of internal corrosion of oil and gas pipelines − a review, Corrosion Science 49 (2007) 4308−4338.
[26] Y.M. Zhang, T.K. Tan, Z.M. Xiao, W.G. Zhang, M.Z. Ariffin, Failure assessment on offshore girth welded pipelines due to corrosion defects, Fatigue and Fracture Engineering Materials and Structures 39 (2016) 453−466.
[27] Y. Shuo, Y. Hongqi, L. Gang, H. Yi, W. Lidong, Approach for fatigue damage assessment of welded structure considering coupling effect between stress and corrosion, International Journal of Fatigue 88 (2016) 88−95.
[28] S. Hertelé, A. Cosham, P. Roovers, Structural integrity of corroded girth welds in vintage steel pipelines, Engineering Structures 124 (2016) 429−441.
[29] Q. Li, H. Hu, Y.F. Cheng, Corrosion of pipelines in CO_2-saturated oil-water emulsion flow studied by electrochemical measurements and computational fluid dynamics modeling, Journal of Petroleum Science and Engineering 147 (2016) 408−415.

Further reading

[1] C.W. Du, X.G. Li, P. Liang, Z.Y. Liu, G.F. Jia, Y.F. Cheng, Effects of microstructure on corrosion of X70 pipe steel in an alkaline soil, Journal of Materials Engineering and Performance 18 (2) (2009) 216−220.
[2] F.F. Eliyan, A. Alfantazi, Corrosion of the Heat-Affected Zones (HAZs) of API-X100 pipeline steel in dilute bicarbonate solutions at 90°C: an electrochemical evaluation, Corrosion Science 74 (2013) 297−307.
[3] M. Shirinzadeh-Dastgiri, J. Mohammadi, Y. Behnamian, A. Eghlimi, A. Mostafaei, Metallurgical investigations and corrosion behavior of failed weld joint in AISI1518 low carbon steel pipeline, Engineering Failure Analysis 53 (2015) 78−96.
[4] Q. Qiao, G. Cheng, W. Wua, Y. Li, H. Huang, Z. Wei, Failure analysis of corrosion at an inhomogeneous welded joint in a natural gas gathering pipeline considering the combined action of multiple factors, Engineering Failure Analysis 64 (2016) 126−143.
[5] M. Law, H. Prask, V. Luzin, T. Gnaeupel-Herold, Residual stress measurements in coil, linepipe and girth welded pipe, Materials Science Engineering, A 437 (2006) 60−63.
[6] C.C. Silva, J.P. Farias, Non uniformity of residual stress profiles in butt-welded pipes in manual arc welding, Journal of Materials Processing Technology 199 (2008) 452−455.
[7] T. Muraki, K. Nose, H. Asahi, Development of 3% chromium linepipe steel, in: CORROSION/2003, NACE International, Houston, TX, 2003. Paper No. 117.

Sulfide stress cracking

11

Roger A. King
International Corrosion Services Ltd., Manchester, Great Britain

11.1 Background

Sulfide stress cracking (SSC) was first identified and the mechanism outlined in the 1940s after several failures of oil and gas systems in Texas and Canada; the initial priority was related to wellhead and pipeline valves. Industrial committees to pool data and information were established in Canada and in the United States by the National Association of Corrosion Engineers (NACE). The first conference on the topic was held in 1952 and the first document released in 1966. This document was revised and issued in 1975 as the industry standard for wellhead valves as NACE MR-0175 [1].

The scope of the document was widened in 1978 when cracking occurred in other oilfield and refinery equipment, and, in 1990 and onward, the document began to include recommendations to avoid cracking of corrosion resistant alloys (CRAs). NACE MR-0175 did not address all the factors known to be relevant, and hydrogen-induced cracking (HIC) was not considered. European studies on the effect of water composition and pH resulted in these parameters being addressed in European Federation of Corrosion (EFC) document-16 [2], published in 1995.

A major change occurred in 2003 when the different requirements for refineries and upstream production were recognized and a document specific to refineries was released, NACE MR-0103 [3]. Many materials, acceptable for refinery service, were restricted for use in upstream production where high concentrations of chlorides occur. A useful comparison of NACE MR-0175 and MR-0103 is given by Bush [4]. In the same year, NACE MR-0175 and EFC-16 were combined to create ISO 15156 [5]. The ISO document also includes requirements for resistance to HIC and stress-orientated hydrogen-induced cracking (SOHIC).

The ISO and NACE documents are now integrated and interchangeable. In some countries, the combined title, ISO 15156/NACE MR-0175, is used because the NACE document is mandated by the National Law, whereas the ISO document may not be so recognized.

11.2 NACE MR-0175

Many pipelines, and associated equipment, were built before the evolution of NACE MR-0175 into ISO 15156/NACE MR0175. It is important to note that such assets should be resistant to SSC but may not be resistant to HIC. In some respects, the

Trends in Oil and Gas Corrosion Research and Technologies. http://dx.doi.org/10.1016/B978-0-08-101105-8.00011-5

NACE document was easier to use than the ISO document. In part, this resulted from the use of common names for alloys and steels, whereas the ISO document references generic alloys, e.g., clustering stainless steels into types 3a or 3b and solid solution nickel alloys into types 4a to 4e depending on their composition.

A distinction is made between gas systems and multiphase (oil) systems. However, there is no clear definition given to aid distinction between these two basic systems. A typical definition of a gas system is one with a gas−oil ratio (GOR) above 5000, whereas the US Energy Information Administration uses a GOR of 6000 [6]. Other approaches ignore the NACE definitions and use actual values of hydrogen sulfide; for example, one Middle East operator defines a system as sour service if the concentration of hydrogen sulfide in the associated water equals or exceeds 2 ppm. The domains of sour service are represented in the NACE document as two plots; for convenience and comparison here, both gas and multiphase systems are shown in one plot, as illustrated in Fig. 11.1.

The NACE document, as noted previously, covered sour service definitions in both upstream and refinery operations. For pipelines that operate at pressures considerably above 448 kPa (65 psia), sour service and cracking is defined as when the partial pressure of hydrogen sulfide equals or exceeds 0.345 kPa (0.05 psia).

One question often raises concerns about dry gas pipelines. Without water, there will be no corrosion and consequently no risk of SSC. Although this is correct, the industry consensus is that the pipeline should be fabricated with material resistant to SSC. A failure to completely dry the pipeline after hydrotest or any upset in service that allowed water into the pipeline could result in cracking. The operator would be obliged to inspect the pipeline to ensure that cracking had not occurred. Cracks can only be reliably identified using ultrasonic inspection tools that require the pipeline to be filled with liquid, or the in-line inspection (ILI) tool would be sent through the pipeline in a

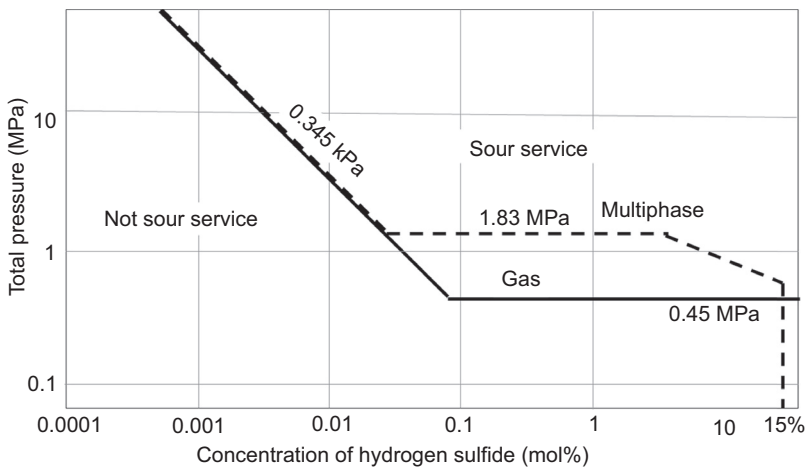

Figure 11.1 Domain of sour service according to National Association of Corrosion Engineers (NACE) MR-0175 [1].

slug of liquid. Both these options would be costly and have a significant impact on production. Electromagnetic acoustic transducer (EMAT) tools may be suitable but are less likely to identify initial cracking, which would be shallow. EMAT effectiveness in detecting a crack is directly proportional to the depth of the crack [7–9].

Other issues raised relate to the definition of the pressure of the system. Pressure used for the calculation of the partial pressure of hydrogen sulfide may be design pressure, maximum allowable operating pressure (MAOP), or maximum operating pressure. Most material selection engineers will use MAOP, though some operators prefer the use of the more conservative design pressure.

11.3 ISO 15156

The ISO document is divided into three parts: Part 1 covers the general principles for the evaluation of the resistance of materials to cracking; Part 2 the limitations and use of carbon and low alloy steels and cast irons; Part 3 the limitations of CRAs and other alloys. The ISO document also covers HIC and SOHIC. HIC is discussed in Chapter 13. SOHIC is, in brief, a combination of HIC and SSC and is discussed in more detail later.

For carbon steel pipeline material, the most significant change is the use of a combination of pH and partial pressure of hydrogen sulfide to identify the region or zone in which the material will be used. Altogether four regions are specified. A schematic of the standard plot is given as Fig. 11.2. The material requirements for resistance to cracking for each of the four domains increase as the severity increases from 0 to 3. Domain 0 would be considered to present a minimal threat of SSC but caution is

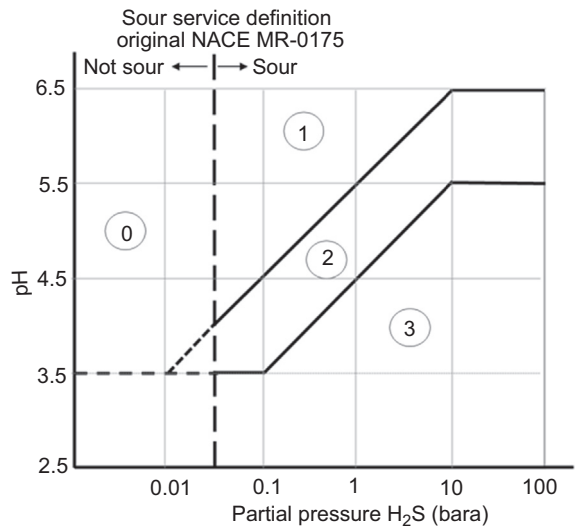

Figure 11.2 Sulfide stress cracking domains for carbon steel pipelines [5].

necessary as high strength steels (defined as 985 MPa or 143 ksi) can fail by embrittlement even with trace H_2S. Flexible pipelines fabricated with high strength steel wires that have been cold worked during pipe fabrication [>600 MPa or 87 ksi specified minimum yield strength (SMYS)] would also be at risk from hydrogen sulfide migration into the flexible wiring matrix.

The ISO methodology requires an estimate of the pH of the water that will be present. For gas pipelines, where the water will be condensed water, it is reasonable to calculate the pH based on the operating temperature and pressure and the concentration of carbon dioxide. Some corrosion prediction models modify the pH to account for the presence of hydrogen sulfide but the basis for this is not fully established. As can be seen in Fig. 11.3, there is limited dissociation of H_2S at the typical pH of water in gas and oil pipelines. For multiphase systems where the formation water may be present containing a range of dissolved salts, including bicarbonate, it is necessary to obtain an analysis of the water; representative samples of formation water may not be readily available from the early drill stem tests.

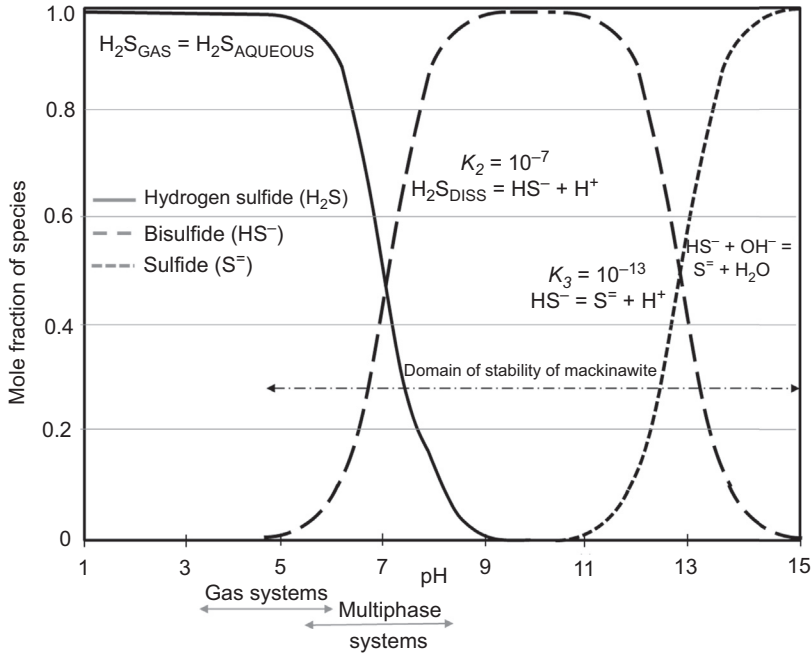

Figure 11.3 Effect of pH on dissociation of hydrogen sulfide.

Gas pipelines are at most risk because the water that condenses will, most likely, be free of salts and the pH will be unbuffered, resulting in strongly acidic conditions. The partial pressure of carbon dioxide dominates in setting the pH of the water and the form of sulfide will reflect this pH, see Fig. 11.3. The ratios of CO_2/H_2S that are used to define carbonic acid corrosion and sour corrosion (500 and 20, respectively, discussed below) show that there is little advantage in using ISO 15156 compared to the original NACE MR-0175, as can be seen in Fig. 11.4.

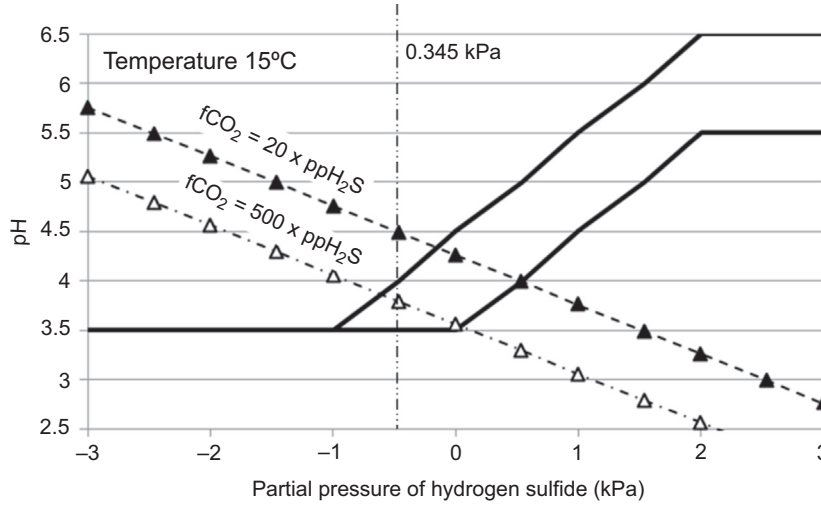

Figure 11.4 CO_2/H_2S ratios related to pH and cracking.

11.4 Sour corrosion

The terms sour corrosion and sour service are often considered equivalent but this is not always the case. Before discussing the mechanism of SSC, the distinctions between sour corrosion and sour service are presented. Sour corrosion is discussed in Chapter 6 of this book.

Sour fluids are most likely to occur in reservoirs from the Triassic, Brent, and Devonian periods, whereas reservoirs formed during the Tertiary, Upper or Lower Cretaceous, and Jurassic are less likely to be sour [10]. However, sweet reservoirs may become sour as a result of the growth and activity of sulfate-reducing bacteria in the reservoir; the SRBs are introduced in the injection water and reservoirs injected with seawater are at higher risk because of the high sulfate concentrations in the seawater. Experience in the North Sea indicated gas from sweet wells souring to several thousand milligrams per liter hydrogen sulfide [11].

Sweet service corrosion rates are modified by the presence of hydrogen sulfide. At zero and low concentrations of hydrogen sulfide, the corrosion rate is the carbonic acid corrosion rate moderated by the formation of iron carbonate, the dominant corrosion product, on the steel surface. Carbonic acid corrosion prediction models are considered valid when the ratio of the partial pressure of carbon dioxide to hydrogen sulfide is above 500, though there is limited evidence to support this ratio. The origin of the 500 ratio is discussed by Smith [12] where he noted that the ratio was extremely sensitive to the free energies used for the calculations: the ratio could vary from 420 to above 7000 and was sensitive to temperature. For example, an increase from 25°C (77°F) to 100°C (212°F) results in a decrease in the ratio by ~50%. Unpublished work by Thornhill [13] showed E-pH diagrams for the CO_2−H_2S system indicated that the corrosion product films on steel changed from carbonate to sulfide at a

concentration of hydrogen sulfide of ~100 ppm in the water phase. Other factors, including the concentration of chloride, temperature, and water pH, are also relevant to the balance and protectiveness of the iron carbonate and sulfide films.

With hydrogen sulfide present, there is often a higher incidence of pitting corrosion. At low concentrations of hydrogen sulfide, this occurs because of the formation of iron sulfide islands (mainly as mackinawite and possibly some smythite) within the porous iron carbonate film. Both mackinawite and smythite have a positive potential (i.e., more cathodic) with respect to steel and establish galvanic cells resulting in pitting corrosion. Ferrous iron released by corrosion may react with hydrogen sulfide to form nonadherent mackinawite resulting in additional corrosion at the location of the initial pit. These may be nanoparticles (or framboids) of mackinawite [14,15], which present a very large cathodic surface area.

As the concentration of hydrogen sulfide increases, the corrosion product film transfers from an iron carbonate film to a mackinawite film. Sour corrosion is considered to be dominant when the ratio of carbon dioxide to hydrogen sulfide falls below ~20 [12]. Mackinawite films grow very rapidly when there is a sufficient concentration of hydrogen sulfide. A thin intact film is formed on the steel surface by the direct reaction of the hydrogen sulfide with the steel surface, rather than by a precipitation mechanism; the reaction postulated by Sun [16] is the following:

$$Fe_{(s)} + H_2S_{(aq)} = FeS_{(s)} + H_2$$

where (s) denotes a solid and (aq) a dissolved aqueous species. By contrast, iron carbonate and iron sulfide films may be formed by precipitation:

Iron carbonate film formation	**Iron sulfide film formation**
$Fe_{(s)} = Fe^{2+}_{(aq)} + \text{electrons}$	$Fe_{(s)} = Fe^{2+}_{(aq)} + \text{electrons}$
$Fe^{2+}_{(aq)} + CO^{2-}_{3(aq)} = FeCO_{3(s)}$	$Fe^{2+}_{(aq)} + S^{2-}_{(aq)} = FeS_s$

The initial mackinawite film is protective and reduces the carbonic acid corrosion rate by an order of magnitude. The protectiveness of the iron sulfide film formed is partly related to the method of formation and also changes over time, becoming denser and more crystalline. The Sun model was extended, with some questions as to the exact mechanism of formation of the initial sulfide film, to explain the formation, overtime, of a thicker, porous iron sulfide film overlying this initial film [17]. This outer film is formed by hydrogen sulfide diffusing through the mackinawite film from the bulk solution to the steel surface where it reacts beneath the initial film resulting in undermining and detachment of the initial film and its exfoliation to form the outer, fractured, and porous mackinawite layer as shown in Fig. 11.5 [16,17]. There will also be some migration of ferrous ions from the surface where the mackinawite film is absent resulting in the precipitation of mackinawite within the porous film and at the outer surface of this film. The total iron in the sulfide film is lower by

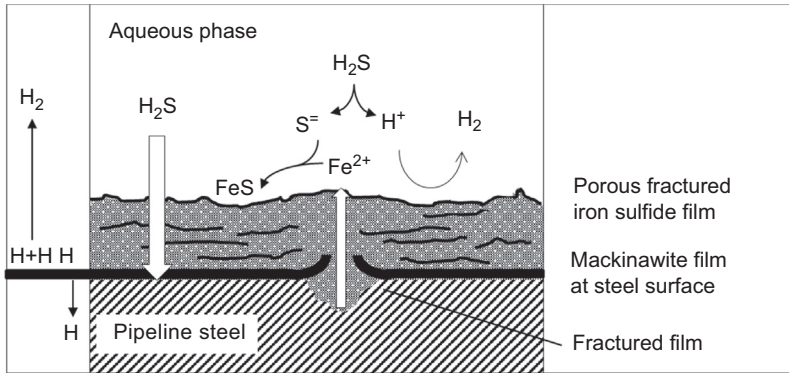

Figure 11.5 Formation of iron sulfide films.

30−60 wt% than the iron lost by corrosion, indicating that iron sulfide, or iron in some other form, migrates away from the corroding area [16].

Localized corrosion of steel occurs at areas where the continuous sulfide film breaks down, either because of mechanical damage or the instability of the film in the presence of a high concentration of chlorides. Additionally, the mackinawite film may, over time, convert from mackinawite and smythite to alternative sulfides and the volume change, caused by a change in crystal structure, will result in the fracture of the sulfide film and exposure of steel, usually at grain boundaries. Exposure of steel then results in localized corrosion. The iron sulfides and the interactions between them are illustrated in Fig. 11.6 [18].

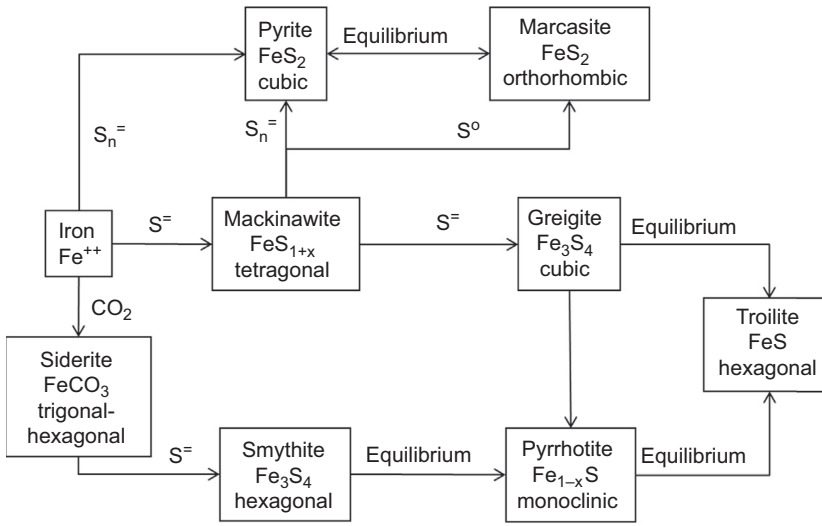

Figure 11.6 Interaction of the iron sulfides.

Table 11.1 Corrosion by iron sulfides [18]

Sulfide species	Formula	Sulfur %	Corrosion g iron per mol of sulfide	Corrosion g iron per mol of sulfur
Pyrite	FeS_2	52.5	61.53	123.06
Greigite	Fe_3S_4	42.4	12.53	50.12
Smythite	Fe_3S_4	42.4	19.51	78.04
Mackinawite[a]	$FeS_{(1-x)}$	35	10.08	10.08
Pyrrhotite	$Fe_{(1-x)}S$	36	6.39	6.39

[a]Recent research suggests that mackinawite may be stoichiometric.

Where a nonadherent mackinawite film is present in electrical contact with the steel surface, the cathodic reaction is hydrogen evolution on the cathodic mackinawite and the bulk of the acidity of the water phase results from dissociation of carbonic acid. The cathodic reaction occurs in steps: discharge of hydrogen ions to form atomic hydrogen, followed by a combination of atomic hydrogen to form molecular hydrogen. Each iron sulfide causes a characteristic amount of corrosion when in intimate contact with a steel surface; the rates are given in Table 11.1 [18]. Once this quota of corrosion has occurred, the iron sulfides appear to become dormant. It is conjectured that this dormancy results from hydrogen bonding with the sulfide. Activity of the sulfide could be blocked by it being cocooned by ferrous hydroxide or another corrosion product, but this appears unlikely. Exposure of a dormant sulfide to vacuum and gentle heat results in the sulfide regaining activity but only mackinawite and smythite recover significant corrosiveness; the percentage recovery of each species of sulfide is shown in Table 11.2 [18].

The protectiveness of the mackinawite film depends to an extent on the balance between mackinawite formation and the rate of corrosion. At small areas of bare steel surrounded by a large cathodic area of iron sulfide, the corrosion rate may be too high for the reformation of a mackinawite film and continued corrosion will occur resulting

Table 11.2 Regeneration of iron sulfides [18]

Sulfide species	1st corrosion mg per mE sulfide	2nd corrosion mg per mE of sulfide	Corrosion ratio 2nd:1st (%)
Pyrite	491.9	116.9	24
Smythite	143.9	93.3	65
Mackinawite	58.8	55.5	94
Copper sulfide	404.3	72.8	18
Nickel sulfide	296.0	58.1	20

in the formation of a pit filled with amorphous iron sulfides, as illustrated in Fig. 11.5. In stable operating conditions, it would be expected that the risk of corrosion would decline over time as mackinawite and smythite convert to pyrrhotite and troilite because the hydrogen bonding on these sulfides is less reversible. However, a change in process conditions may trigger the formation of new mackinawite resulting in renewed corrosion.

11.5 Sour service

The term "sour service" relates to the cracking of steel and does not imply sour corrosion per se. In many cases, the concentration of hydrogen sulfide is too low for the corrosion to be considered sour corrosion. Sour service occurs when there is sufficient mackinawite present on the steel surface to raise the level of atomic hydrogen permeation into the steel to a critical value. The direct reaction of hydrogen sulfide with the surface beneath the initial mackinawite film ensures a continued creation of fresh, active mackinawite and a continued production of atomic hydrogen.

The critical value of atomic hydrogen permeation to cause cracking is related, in part, to the metallurgical properties of the steel and the level of stress (both residual and applied). The threat of cracking is also increased by the presence of deep pits and the consequent increase in localized stress at the pit tip. Values are not available to quantify these effects but a schematic of the overall consequences of an increase in hydrogen sulfide is shown in Fig. 11.7.

The effect of an increase in the concentration of hydrogen sulfide is complicated as it is related to the relative coverage of the surface with sulfide film, which will result in an increase in atomic hydrogen permeation, but the overall rate of formation of atomic hydrogen will be reduced as the general corrosion rate is decreased because of the thickening of the sulfide films, which will reduce the rate of diffusion of hydrogen sulfide.

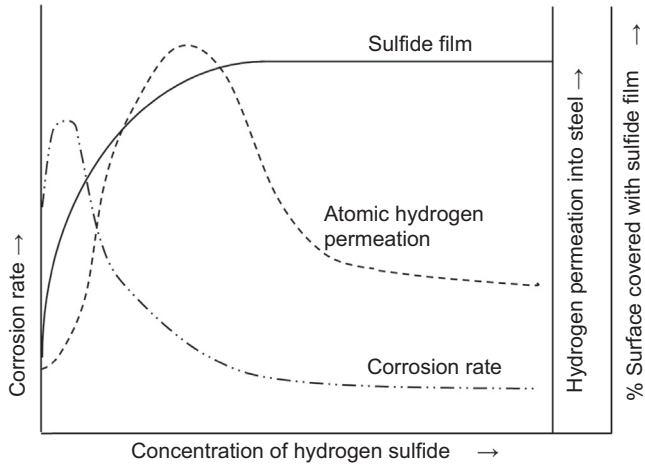

Figure 11.7 Variations in corrosion and hydrogen permeation.

The continuous generation of new mackinawite at the steel surface allows continued bonding of atomic hydrogen subsequent to the corrosion reaction, ensures a high surface concentration of atomic hydrogen, and continued migration of hydrogen into the steel.

11.6 Mechanism of SSC

Originally, the mechanism was thought to be a form of stress corrosion cracking in which the causative agent was corrosion. Though corrosion is relevant it is not volumetric metal loss that determines ultimate failure. Both the initiation and propagation of cracks are induced by the environment. Cracks initiate at weak points on the surface, often at crevices or pits, and follow an intergranular path in high-strength steels and a transgranular path and, in some cases, a mixed path in lower strength steels [19]. In both cases, the cracks propagate at 90° to the applied stress as illustrated in Fig. 11.8. In lower strength steels, the transgranular cracks may grow because of anodic dissolution at the crack tip, often termed active path corrosion. Intergranular cracks result because of embrittlement of the high strength steel by absorption of atomic hydrogen into the steel and a reduction in cohesion between grains. Major factors related to cracking include the severity of the environment (pH, partial pressure of hydrogen sulfide, chloride concentration), service temperature, composition of the material, degree of cold work, and the level of applied and residual stress. Surface condition also appears to be relevant. SSC in pipeline steels is normally intergranular.

The cracking proceeds in a series of stages. A hard area or the area around the tip of a pit has grown sufficiently deep for the stress at the tip to work harden the material, absorbing hydrogen and resulting in embrittlement. The material cracks when it is subjected to a stress high enough to cause the fracture of the embrittled material. The crack is arrested once it enters the ductile material but, over time, hydrogen charging occurs at the extended crack tip and the cycle is repeated. Eventually, the extended crack will fail by mechanical tearing. A schematic illustrates this, Fig. 11.9.

In the anaerobic environment of a pipeline, the controlling cathodic reaction is hydrogen ion discharge. Acidity in the water phase arises from dissociation of carbonic acid and the presence of short chain carboxylic acids, e.g., formic and acetic acid.

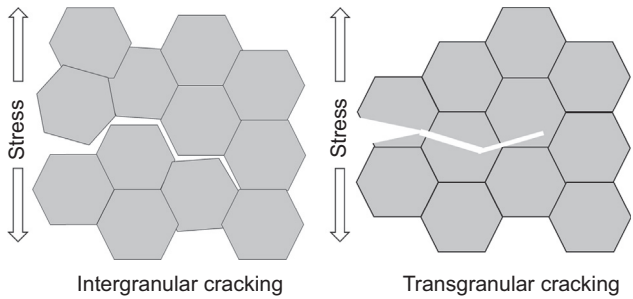

Figure 11.8 Cracking morphology.

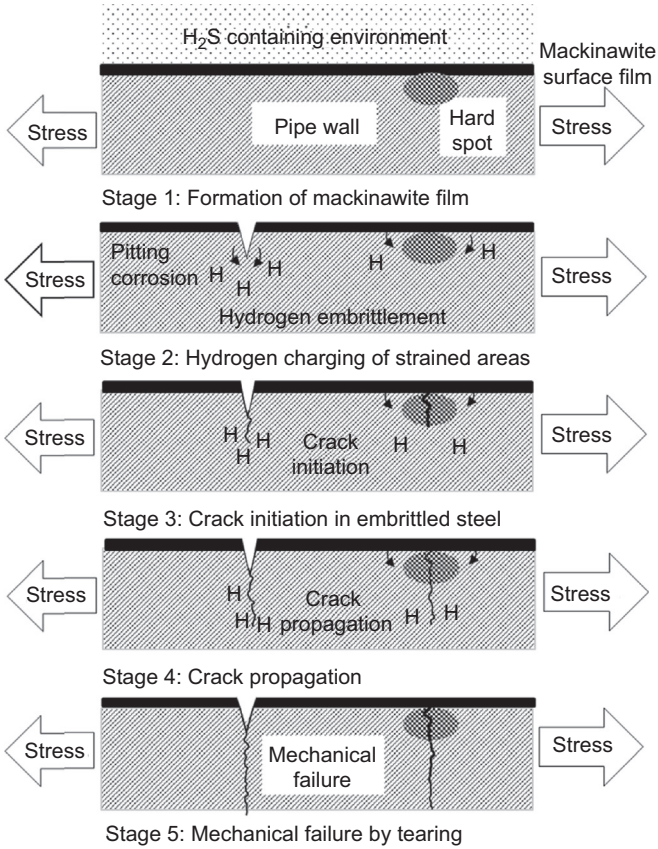

Figure 11.9 Stages in failure by sulfide stress cracking.

Depending on temperature and water composition, the pH of the water can be reduced to ~ 3.

Atomic hydrogen being a small uncharged entity can permeate through steel. The rate of permeation is partly determined by an analog of Sievert's Law [20], which relates the hydrogen in the steel lattice at the surface to the hydrogen concentration on the surface. Initial hydrogen permeation shows an increasing uptake as traps and other sinks for hydrogen are filled followed by a decline to a steady-state flux. In sweet systems, it is estimated that about 1%−3% of the atomic hydrogen generated by cathodic corrosion reactions passes through the pipe wall to the outer surface where it will combine to form molecular hydrogen; permeation rates range from 10^{-2} to 10^{-5} mm^2/s depending on temperature [21]. When a mackinawite film is present, atomic hydrogen, reversibly bonded to the mackinawite, enables a higher concentration of atomic hydrogen to permeate into the steel resulting in a similar effect as acid pickling [22]. Estimates vary but around 10%−20% of the atomic hydrogen generated on the inner surface by corrosion reactions will diffuse through the steel. SSC can result because of the higher flux of atomic hydrogen.

An alternative view is that hydrosulfide ion (HS^-) hinders the combination of atomic hydrogen to form molecular hydrogen; the term poisoning is often used to describe this effect [19]. Other compounds, e.g., arsenic, also reduce hydrogen combination. Whatever causative mechanism prevents hydrogen combination, the higher availability of atomic hydrogen results in a higher rate of permeation of hydrogen into the steel, which may result in SSC.

The hydrogen accumulating within the steel is the difference between the volume of hydrogen entering the steel and the volume of hydrogen that has passed through. When steel is stressed, there is a distortion of the atomic lattice as the steel accommodates the strain and this results in a reduction in the rate of diffusion of the atomic hydrogen; hydrogen accumulates temporarily at the stressed areas. The hydrogen atoms may be envisaged as pedestrians crossing a road: they may do this quickly when there is no traffic but progress is impeded when the road is filled with stationary traffic and the pedestrians must weave around the cars. An increase in stress can be considered as a higher number of cars to circumvent.

Steel cannot absorb much hydrogen (a few ppm), not because the interstitial spaces in the iron body centered cubic lattice are small but because the interstitials are close together; the mobility of atomic hydrogen is high. Interstitial hydrogen is located where the iron atoms form tetrahedral site (~70% of sites) or octahedral sites (~30% of possible sites), see Fig. 11.10 [23]. Carbon and nitrogen tend to occupy the octahedral interstitial sites even though these are smaller than the tetragonal sites [23], and as the carbon content in steel increases, there would be a reduction in the mobility of hydrogen because of the reduction in available interstitial sites.

Other areas where hydrogen can reside are traps; traps may be reversible or irreversible. Many traps result from dislocations in the atomic lattice resulting from cold work. Cold work increases the dislocation density and vacancy concentrations in the steel and the increased number of these increases the amount of hydrogen that is absorbed. Dislocations may form line defects in the lattice that can accumulate a chain of hydrogen atoms. If corrosion ceases, then the source of atomic hydrogen also ceases and most of the hydrogen within the steel in the reversible traps will dissipate in a few days.

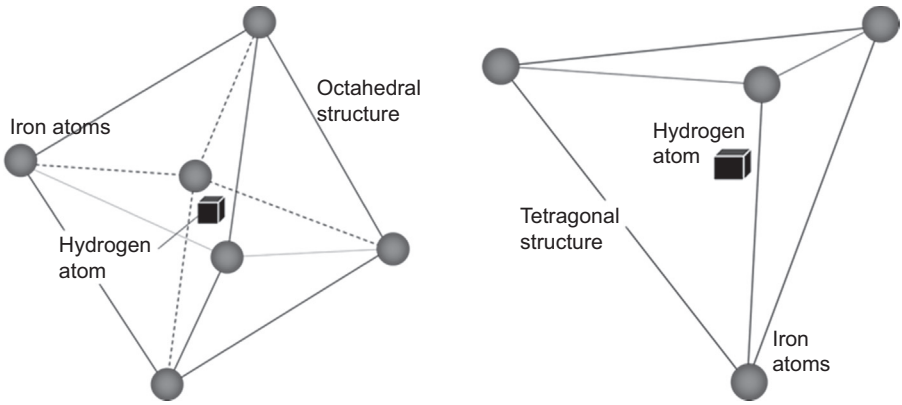

Figure 11.10 Iron atom configurations for interstitial hydrogen absorption.

However, some traps only release hydrogen when the steel is heated to high temperature (~650°C or 1202°F) and hydrogen may persist in the steel for other reasons: an absorbed hydrogen atom may become a substitutional component rather than an interstitial; two adjacent hydrogen atoms may combine to form molecular hydrogen and, in this case, a much higher stress would be required to move the dislocation. Other permanent traps are microvoids and inclusions of sulfides and phosphides where the atomic hydrogen will convert to molecular hydrogen. To reduce voids, pipeline steels are always "killed" steels, a procedure that reduces the number, and size, of voids that act as irreversible traps within the steel. Whatever the mechanism holding the atomic hydrogen in the atomic lattice, the effect is a loss of ductility in proportion to the absorbed volume.

If corrosion ceases, the production of atomic hydrogen will cease and most of the hydrogen will diffuse out of the steel, perhaps 90% over a few days. Once the bulk of hydrogen has diffused out of the steel, the steel will regain ductility and will yield normally when subject to stress. There are several working pipelines that are known to have suffered HIC but the liberal use of corrosion inhibitor has prevented the transition of blistering to stepwise cracking.

The volume of hydrogen needed to cause embrittlement is very small. Corrosion in sour service is not the only source of hydrogen; some hydrogen may be present in the steel from casting, welding, or corrosion during storage and transport and, during operation, by overprotection by the cathodic protection system. Good practice during casting and plate forming, welding (avoidance of moisture in welding rods), preheat, and postheat treatment of welds reduces the volume of residual hydrogen.

Once cracks are initiated in embrittled steel, the pipeline may fail at stresses well below the yield strength. Cracks initiate at the area of lowest strength and in most cases this is at grain boundaries where the crystalline planes are mismatched and where hydrogen will be concentrated. Deep pits introduce stress irregularities that accumulate the hydrogen resulting in embrittlement. Intergranular cracking is characteristic of failures by embrittlement. The exact mechanism of embrittlement is not clear. It is possible that hydrogen accumulation prevents movement of iron atoms along slip planes preventing plastic flow, brittle hydrides may be formed, accumulation of molecular hydrogen in voids increases local stress, and accumulation of hydrogen reduces cohesion between steel grains. A comprehensive discussion of these mechanisms is given by Cwiek [24].

As the strength of a steel increases the difference between yield and tensile strength decreases. It is common practice for submarine pipelines to ensure a sufficient difference between yield strength and tensile strength to accommodate the residual stresses imposed by S-lay installation, thereby reducing the risk that a pipeline would fail. This safety factor has been reduced, e.g., DNV OS-F101 [25], because modern computation allows sufficiently accurate estimation of the imposed installation stresses. The difference between yield and tensile strength remains, however, important for sour service. As the strength of a steel increases, less hydrogen is required for embrittlement.

Once initiated cracks propagate by cleavage along grain boundaries. In some cases, one major crack will arise from a colony of cracks when the propagation of the major crack results in a local reduction in the stress imposed on the minor cracks. When the

crack tip moves outside the embrittled zone, the steel can yield and the crack is arrested. Over time, the steel around the crack tip becomes embrittled and the crack extends further until it enters ductile material and is again arrested. As the crack length increases, the rate of crack propagation increases because the stresses at the crack tip increase and less hydrogen is required to embrittle the steel. Eventually, the material fails by ductile tearing when the crack length approaches the wall thickness.

11.7 Environmental factors

SSC only occurs when water is present. The threat of SSC increases with increasing partial pressure of hydrogen sulfide and acidity. It would be expected, however, that the threat of cracking will become constant once a certain concentration of hydrogen sulfide is exceeded, as indicated in Fig. 11.4. The acidity of the water is determined by the partial pressure of carbon dioxide through the short chain carboxylic acids, e.g., formic, acetic, propionic, will have an effect. A high salinity may result in a higher occurrence of and rate of pitting corrosion, resulting in the initiation of more cracks.

The original NACE MR-0175 did not take account of pH. The criterion for threat of SSC was related to the partial pressure of hydrogen sulfide. ISO 15156/NACE MR-0175 does take account of system pH but one issue that often arises when selecting materials of construction for a new reservoir is the lack of information on the water composition and consequent uncertainty about the pH at operational pressures and temperatures in multiphase systems.

Temperature is an important parameter. Standard tests on downhole tubing showed that the risk of SSC is highest at room temperature and then declines as temperature increases from ~25 to 200°C (77−390°F) as can be seen in Fig. 11.11 [26]. This effect is the balance between the generation of hydrogen, by corrosion, and diffusion of hydrogen through the steel. The temperature also alters the nature of the sulfide formed, which may have some effect on hydrogen migration into the steel, and consequently on the likelihood of cracking as illustrated in Fig. 11.12.

NACE MR-0175 (2003) Table D2 took account of the effect of temperature for selection of tubular goods, classifying acceptable materials at >66°C (150°F), >79°C (174°F), and >107°C (225°F). At low temperature, the rate of corrosion is reduced and less hydrogen is generated. At high temperatures, the rate of diffusion of hydrogen is higher resulting in a higher rate of permeation of atomic hydrogen through the pipe wall.

Hardness, as a proxy for strength, is the most convenient metallurgical property to measure. NACE arrived at the criterion for hardness based on the scrutiny of extensive data. For carbon steels, the limitation on hardness to avoid SSC is Rockwell hardness C (HRC) 22, equivalent to Vickers hardness number, 248 VHN. This hardness criterion is empirical. Pargeter, discussing the work by Gouche [27], highlighted that the tolerable hardness of the heat-affected zones appeared linked to the concentration of hydrogen sulfide in solution. At saturation, about 3000 ppm, the tolerable hardness was 240 VHN and at 10 ppm the tolerable hardness was 350 VHN. This raises the option that testing materials under simulated conditions may allow relaxation of the HRC 22 criterion; a useful approach for continued use of a sweet service pipeline exposed to mild sour service because of reservoir souring.

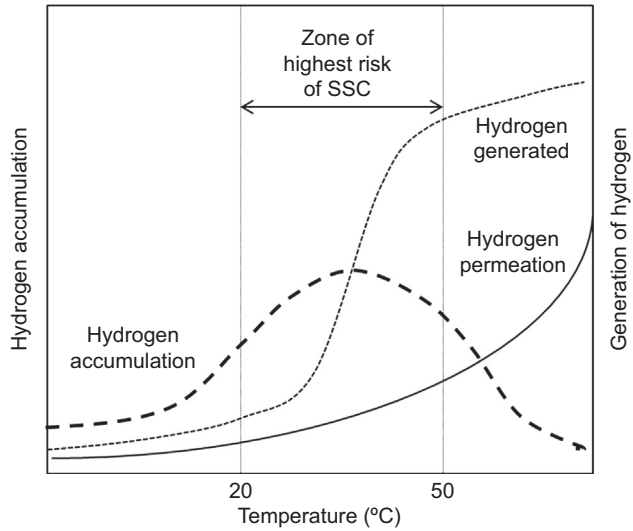

Figure 11.11 Time to failure by sulfide stress cracking related to temperature.

Although hardness is a useful guide to avoidance of SSC, steels with hardness below 22 HRC may still crack depending on the operating conditions, corrosiveness of the environment, and the applied stress [28]. In part, this susceptibility to SSC is related to microstructure and SSC may be prevented by imposing a limit on strength to eliminate crack-sensitive microstructures, e.g., inadequately tempered martensite

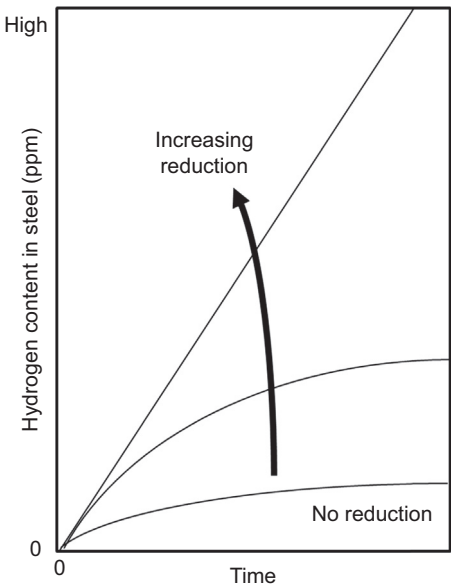

Figure 11.12 Effect of cold work on hydrogen uptake of steel in a strong acid solution.

and bainite. Avoidance of sensitive microstructure is, in part, connected to the carbon equivalent. Carbon equivalent combined with wall thickness, which determines the rate of cooling after welding, is the key factor in the formation of martensite and bainite. Additionally, some elements in steel that are not included in the carbon equivalent may also have some influence; for example, boron is included in the percentage crack measurement (PCM) formula and titanium, as a microalloying agent, may form brittle hydrides.

Girth welds present a particular risk because of the complex microstructures in the heat-affected zone resulting from the multiple welding passes. In the girth welds, some microstructures occur as local brittle zones usually composed of martensite−austenite components with hardness values of 400−600 VHN. Residual stresses are also higher adjacent to welds. Though longitudinal welds present some risk they are simpler in structure and are formed under highly controlled conditions and are subject to extensive testing.

11.8 Avoiding SSC in carbon steels

SSC is avoided by ensuring that the strength of the parent pipe and the welds is limited. For practical reasons, strength is measured indirectly using hardness that provides a suitable nondestructive method for evaluating the production welds. The hardness is restricted to HRC 22 based on the Rockwell C test procedure using 150 kg loading [1]. ISO 15156 [5] refers to the Vickers (10 kg load) hardness scale and rounds the hardness to VHN 250. Vickers has some advantages over Rockwell because the smaller impact area of the probe allows more detailed hardness profiles to be obtained across welds or through thickness. Brinell hardness is also used (3000 kg load) though less often in the present day. The equivalent Brinell hardness would be 237 BHN.

The American Gas Association (AGA) sponsored The Welding Institute (TWI) to study hardness limits relaxation in pipelines in terms of the effect of weld geometry in API 5L X52 pipe and concluded that, under certain circumstances, the hardness in the cap pass of girth welds could be relaxed to 300 VHN for pipes thicker than 10 mm (0.4 in.) [28]. TWI concluded that easing hardness limits for external pipeline girth welds would lower costs associated with qualifying weld procedures and that the increase in permissible hardness would allow the application of high-productivity mechanized metal inert gas pipe-welding systems.

Welding presents the highest likelihood of creating hard zones or spots in the pipeline material. The weld procedures for longitudinal welds and girth need to be qualified to ensure that the steel in the welds and heat-affected zones are not affected. The weld qualification is done in accordance with the requirements of ISO 15614 [29] using actual production material or a steel of the same grade and with the maximum carbon equivalent of material to be used. Welding variables are recorded during the test weld and hardness testing is mandatory. ISO 15156 details the hardness traverses that should be made for the various weld profiles. Repair weld procedures should also be qualified. Useful information on compliance to ISO 15156 during welding is given elsewhere [28].

To reduce the possibility of producing hard heat-affected zones, the carbon equivalent should be below 0.43 (International Formula, CE). For steels with a carbon content below 0.18 wt%, it is normal to use the PCM formula or specify the CE. For higher grade steels that are microalloyed, the combined vanadium and niobium content is also restricted to a maximum of 0.015 wt%. Some newer steels fabricated at higher temperatures than conventional controlled rolled plate may specify higher niobium though this requires a reduction in the manganese and carbon content.

The weld procedure qualification should be done on actual pipe material. For onshore pipelines that may be fabricated with design factors ranging from 0.5 to 0.72 several qualification tests will be needed because wall thickness is considered an essential variable and affects the cooling rate and the consequent risk of formation of martensite.

The welding procedure specifications to be used in production of longitudinal pipe or field girth welds should have parameters that match those of the qualification test piece, i.e., the welds should not differ more than −10% and +25% of the test piece and heat input, preheat and interpass temperatures should be the same, or higher, than the test piece, and welding should be restricted to the same specification and grade of steel with the same or lower carbon equivalents. This may require separate weld qualifications for bends, wyes, and tees in the pipeline as these items are often fabricated with higher carbon contents than line pipe.

If postweld heat treatment (PWHT) is used, the PWHT temperature should be as high as possible as this will provide the maximum tempering of any hard spots. Some codes allow PWHT temperatures of 550°C (1022°F) but such low temperatures may not give the required reduction in hardness and there will be a slight reduction in strength.

Though hardness is the primary criterion, pipeline steel may become sensitive to cracking if it undergoes cold work either deliberate, e.g., field bending, or because of an impact or dent (10% of failures in oil and gas pipelines were delayed failures [30]). Cold work results in an increase in internal vacancies and dislocation density and the hydrogen content of a steel would be expected to increase with increasing cold work. Zhang and Adey [30] also noted that the absorption of hydrogen into steel resulted in an increase in failure frequency (failures/1000 km year) from 10^{-7} to 10^{-1}. Pipe will be made susceptible to SSC if cold work increases the hardness above the NACE criterion but there are indications that plastic strain, insufficient to case significant hardening, may also increase the possibility of SSC. Tests on API 5L X65 pipe for installation subsea by reel ship showed increased susceptibility to SSC after straining to simulate reeling and unreeling [31]. Any pipeline deformed greater than 5% in a single event should undergo a thermal stress relief heat treatment to restore its SSC resistance [32].

The information to date indicates that plastic deformation of less than 5% outside diameter (OD) strain should not alter the materials resistance to SSC. According to American Society of Mechanical Engineers (ASME) B31.8 [33] and ASME B31.4 [34], the allowable strain at dents is 6%. However, this guideline should be treated with caution; line pipe that has a hardness close to VHN 250 may be less tolerant to strain than line pipe with a lower hardness. It is recognized that welds are more susceptible to the effect of strain and consequently dents at welds require close attention [35]. ASME B31.8 allows 2% OD strain and ASME B31.4 does not permit any.

Field bending of pipe increases local hardness and will also have the effect of increasing the volume of hydrogen absorbed into the steel, see Fig. 11.12, as a result of the increased strain and cold work [36]. The degree of cold bending allowed is restricted but there are grey areas. ASME B31.8 clause B841.23 [33] gives guidance on cold bending of pipe but essentially this requires that cold formed material for sour service should meet the NACE criterion. NACE permits 5% fiber deformation but European industry practice for pipe cold bending is 3% strain for higher strength pipe and this value is recommended as the maximum field bend forming in the absence of adequate material or test information. In all cases, it will be necessary to check that the hardness of cold worked material does not exceed the sour service criterion. Deliberate or accidental wrinkles in bends must be excluded. It is clear that vintage pipelines that have wrinkly bends (not uncommon before 1955 [37]) would not tolerate operation in sour service, although vintage pipelines present many other service issues. Hot bends may be required for acute bends to meet sour service requirements.

11.9 Corrosion resistant alloys

CRAs may also be susceptible to SSC, but in most cases both chloride ions and an elevated temperature are necessary conditions. Most CRA materials used for the fabrication of pipelines rely on chromium (and molybdenum) to provide corrosion resistance. The nickel content confers little corrosion resistance in comparison but it is essential to regain the mechanical properties lost by the addition of chromium and to enable the alloy to be welded.

Chromium is the key element forming a continuous chromium oxide layer on the surface. The role of molybdenum is to improve resistance of the chromium oxide layer to damage by chloride. The chromium oxide protective, passive layer is damaged by chloride and, as temperature increases, the chromium oxide becomes more sensitive to chloride. As corrosiveness of the fluids increases (largely related to the concentration of carbon dioxide, temperature and hydrogen sulfide), the chromium content must be increased, with a consequent increase in nickel content.

The cracking mechanism is stress corrosion cracking rather than a result of embrittlement. The generally accepted mechanism is that, at the crack tip, the imposed stress fractures any passive film formed and if the rate of corrosion exceeds the rate at which the passive film can reform, the crack will propagate. The behavior of several alloys listed in Table 11.3 illustrates the combined effect of chloride, temperature, and partial pressure of hydrogen sulfide on cracking susceptibility.

11.10 Stress-orientated hydrogen-induced cracking

SOHIC is discussed in Chapter 13 but is mentioned briefly here because the phenomenon involves SSC. HIC also involves SSC when the initial blistering converts to stepwise cracking.

Table 11.3 Resistance of the pipeline corrosion resistant alloys to sulfide stress cracking

Material	Temperature	Chloride concentration	Hydrogen sulfide partial pressure
Stainless steel 316/316L	<60°C (140°F) if exposed to a chloride-containing environment	Any	<15 psia
		50 mg/L	<50 psia
Martensitic stainless steel 12Cr	Any, pH > 3.5	Any	<1.5 psia
Duplex stainless steel 22Cr	<100°C (212°F) if exposed to a chloride-containing environment	Any	<1.5 psia
	<120°C (248°F) if exposed to a chloride-containing environment with integral external coating		
	<232°C (450°F)		
Super duplex stainless steel 25Cr	<110°C (230°F) if exposed to a chloride-containing environment	Any	<3 psia
	<130°C (266°F) if exposed to a chloride-containing environment and with integral external coating		
	<232°C (450°F)		
Alloy 825	Any	Any	Any
Alloy 625	Any	Any	Any

At least nine pipelines, over the past 20 years, are believed to have failed by the SOHIC mechanism. The cracking has generally been found adjacent to welds though not always. A failure was discovered in seamless pipe and residual stress is thought to have initiated the cracking. SOHIC appears as a combination of SSC and HIC with a vertical array of alternate planar HIC blisters linked by sulfide stress cracks and with the array normal to the maximum stress; early descriptions of SOHIC refer to ladder cracking. This form of cracking was initially described as type I, whereas cracking related to hardness (classic SSC) was classified as type II. There was a proposition that this form of cracking was limited to HIC-resistant steels. More recently, work funded by the Materials Properties Council in the USA indicated that HIC-resistant steel may indeed be more susceptible to SOHIC than conventional steels [38]. However, operational surveys suggest that HIC-resistant steels with a crack length ratio (CLR) value less than 15%, in accord with NACE TM-0284 [39], were resistant to SOHIC, and to date no steel with a low CLR value has experienced SOHIC.

The cracking mechanism is unclear. One hypothesis is that SOHIC occurs in pipe material strengthened by microalloying and, if this is the case, SOHIC would be more likely to occur in higher strength steels, API 5L X65 and above. Other cases, however, suggest that all steels may be susceptible. If the mechanism is related to microalloying, the postulate is that during welding the thermal gradients cause the microalloying elements to diffuse so that the distribution of these elements (niobium, vanadium, and titanium) is unevenly distributed through the wall thickness. A "banded" structure is formed where the bands with low microalloy content are lower strength. Imposition of tensile stresses results in ductile tearing of material in the softer bands; these retain hydrogen resulting in the formation of blisters. The expanding blister work hardens the adjacent higher strength bands, which may then crack by conventional SSC, linking the blisters to form the ladder array.

11.11 Testing for resistance to SSC and SOHIC

Testing for SSC has been standardized in NACE TM-0177 [40]. The most common test methods are tensile testing with either constant or increasing load, bend tests, and fracture mechanics testing. Constant strain tests are common because they are relatively simple and cheap. The bend test is a constant strain test, where the applied stress decreases as the crack grows. The four-point loading provides a relatively large area of uniform longitudinal stress on the deflected surface, the process wetted surface of the specimen, between the inner supports. The stress decreases to zero from the inner supports to the outer supports. Tests are carried out for 30 days.

Until recently there was no reliable small scale method of testing for SOHIC; full ring tests were considered the most reliable test method. Work by Lino [41] showed that a lower internal pressure was required in the presence of an externally applied load and that if the applied load was high enough, cracks were linked along a 45° shear plane. To achieve the required triaxial stress, the test procedure applies torsion to a sample of the pipeline material as a 2% and 5% twist combined with 4-point bend loading to 50% SMYS.

11.12 Inspection for SSC

Because of the multiple factors that combine to cause SSC, it is difficult to select areas for examination with any certainty of success of identifying cracks. A simplistic approach is to determine where water may collect within a pipeline and target these areas for inspection. The most reliable method is to do an inline inspection using an inline crack detection tool. Magnetic flux leakage (MFL) tools have been adapted to detect cracks by applying a circumferential signal, orientating the magnetic field around the pipe circumference, rather than axially along the pipeline. The MFL ILI tools are suitable for all pipelines provided the wall thickness can be fully magnetized [42].

Ultrasonic tools have also been developed to identify cracks. These are not restricted by wall thickness but require a couplant and will only work in liquid-filled pipelines though there has been successful use of ultrasonic pigs passed through a pipeline in a liquid slug. EMAT tools have been developed to identify cracking and can be used in all pipelines [8]. There has been some development of remote-field eddy current and velocity-induced eddy current techniques to detect and size cracks but these techniques are slow compared to EMAT and they have not been developed yet for operating pipelines.

Validation of cracking is achieved using ultrasonic inspection. Angled probes, phased array and time of flight diffraction, are suitable methods. Automatic systems clearly have advantage in speed and coverage compared to manual inspection.

11.13 Knowledge gaps and research trends

Research gaps fall into two groups: theoretical understanding and engineering information. The theoretic gaps include the understanding of the mechanism of intergranular cracking; how hydrogen migrates through steel and the effect of strain, metallurgy, and heat treatments; the role of chloride in cracking; what is an acceptable level of cold work and is heat treatment (normalized or quench and tempered) relevant; duplex stainless steels work harden and the effect of this on duplex resistance to SSC needs definition.

Initiation of cracking is presently premised on the presence of hard spots (>22 HRC) but the effect of fatigue and/or the presence of deep pits is not considered. Given an aging global pipeline network, there is a need to identify other causative operating and corrosion effects that might initiate SSC.

Flexible pipelines and steel reinforced thermoplastic pipeline are very useful and increasingly utilized items in pipeline networks. The permeation of hydrogen sulfide through the plastic containment sheath is far higher than that of other gases in hydrocarbon fluids. Intermediate layers have been developed to limit hydrogen sulfide permeation but more information is needed to ensure safe operation of flexibles fabricated with high strength steel reinforcements.

Engineering needs are more basic though probably not simpler: better definition of limitations in using approved materials and the need to increase the range of approved,

novel materials. Two important clarifications required are the definition of the pressure to be used in assessment of the critical partial pressure of hydrogen sulfide and the requirement for SSC-resistant materials in dry service gas pipelines.

Other information of use would be the level of stress below which SSC does not occur in a susceptible pipeline steel. There are many aging sweet-service multiphase pipelines that operate at low pressure; can these be operated if souring of the reservoir occurs? Inhibitors have been developed that reduce corrosion and migration of hydrogen into the steel. What level of corrosion, and consequent hydrogen generation, is acceptable to sufficiently delay cracking to give time to arrange an inline inspection?

Practical methods are available to prevent SSC and HIC but this is not yet the case for SOHIC. PWHT has been proposed as a palliative but there is no clear evidence that this is reliably effective.

Complications arise when materials are deleted from ISO 15156/NACE MR-0175. The components fabricated from these materials that are already in use are considered compliant but cannot be removed and reused elsewhere. One for one replacement of pipeline items can also be prejudiced.

As in most engineering systems, it is the "little things" that can cause expensive problems in pipeline operation. An industry-wide philosophy for bolting, gaskets, flange facing, valve, and pump components needs attention.

Several materials that would be useful for valve components need to have their limitations determined, one example, is the acceptance, rejection, then reacceptance of 17−4 pH. Low alloy steels containing more than 1 wt% nickel have useful low temperature ductility (e.g., high-pressure flare lines) but are prohibited for use based on research over 40 years old; it is time to reevaluate these materials. NACE MR-0103 allows the use of some materials that are not included in NACE MR-0175.

References

[1] NACE MR-0175, Sulfide Stress Cracking Resistant Metallic Materials for Oilfield Equipment, NACE International, Houston, Tx.
[2] EFC-16, Guidelines on Materials Requirements for Carbon and Low Alloy Steels for H_2S-Containing Environments in Oil and Gas Production, 1998.
[3] NACE MR-0103, ISO 17945/NACE MR0103, Petroleum, Petrochemical and Natural Gas Industries − Metallic Materials Resistant to Sulfide Stress Cracking in Corrosive Petroleum Refining Environments, 2015.
[4] D. Bush, J. Brown, K. Lewis, An overview of NACE international standard MR-0103 and comparison with MR-0175 (Paper 04649), in: CORROSION 2004, NACE International, 2004.
[5] ISO 15156, Petroleum and Natural Gas Industries - Materials for Use in H_2S-Containing Environments in Oil and Gas Production - Parts 1−3, International Standards Organisation.
[6] US Energy Information Administration, eia.gov/pub/oil_gas/petrosystem/us_table.html.
[7] T. Beuker, H. Lindner, S. Brockhaus, Review of Advanced In-Line Inspection Solutions for Gas Pipelines, Rosen, November, 2010.

[8] T. Fore, S. Klein, C. Yoxall, S. Cone, Validation of EMAT ILI for management of stress corrosion cracking in natural gas pipelines, in: 10th International Pipeline Conference Volume 2: Pipeline Integrity Management, Calgary, Alberta, Canada, September−October, 2014, 2014.
[9] EMAT-Based Inspection of Natural Gas Pipelines for Stress Corrosion Cracks, V.K. Varma, R.W. Tucker Jr., A.P. Albright, Oak Ridge Nat. Lab., Tn.
[10] C. Holtam, Structural Integrity Assessment of C-Mn Pipeline Steels Exposed to Sour Environments, Centre for Innovative and Collaborative Engineering (CICE) Loughborough University, 2010.
[11] I. Vance, D.R. Thrasher, in: B. Ollivier, M. Magot (Eds.), "Petroleum Microbiology", Chapter 7: Reservoir Souring: Mechanisms and Prevention, Am. Soc. Microbiology, 2005.
[12] S.N. Smith, Discussion of the history and relevance of the CO_2/H_2S ratio (Paper 11065), in: CORROSION 2011, NACE International 2011, 2011.
[13] R.S. Thornhill, 1980 (Unpublished work on E-pH diagrams).
[14] D. Rickard, The origin of framboids, Lithos 3 (1970) 269−293.
[15] H.Y. Jeong, J.H. Lee, H.F. Hayes, Characterisation of synthetic nanocrystalline mackinawite: crystal structure, particle size and specific surface area, Geochimica et Cosmochimica Acta 72 (2) (2008) 493−505.
[16] W. Sun, S. Nesic, A mechanistic model of H_2S corrosion of mild steel (Paper 07655), in: CORROSION 2007, NACE International 2007, 2007.
[17] Y. Zheng, J. Ning, B. Brown, D. Young, S. Nesic, Mechanistic study of the effect of iron sulfide layers on hydrogen sulfide corrosion of carbon steel (Paper 5933), in: CORROSION 2015, NACE International 2015, 2015.
[18] R.A. King, J.D.A. Miller, J.S. Smith, Corrosion of mild steel by iron sulfides, British Corrosion Journal 8 (5) (1973) 137−141.
[19] R.D. Kane, M.S. Cayard, Roles of H_2S in the behaviour of engineering alloys: a review of literature and experience (Paper 274), in: CORROSION 1998, NACE International, 1998.
[20] H.G. Nelson, J.E. Stein, Gas-Phase Hydrogen Permeation Through Alpha Iron, 4130 Steel and 304 Stainless Steel from Less than 100°C to Near 600°C (NASA Technical Note TN-D7265), 1973.
[21] T. Boellinghaus, H. Hoffmeister, A. Dangeleit, A scatterband for hydrogen diffusion coefficients in micro-alloyed and low-carbon structure steels, Welding of the World 35 (2) (1995) 83−96 (Doc. IIW-1250).
[22] Hydrogen Embrittlement of Metals: A Primer for the Failure Analyst, M.R. Louthan, U.S. Dept. Energy, Contract number DE-AC09−96SR18500.
[23] Iron and Its Interstitial Solid Solutions, R. W. K. Honeycombe, H. K. D. H. Bhadeshia, Engineering Pro, Books 24/7.
[24] J. Cwiek, Hydrogen degradation of high strength steels, Journal Achievements in Materials and Manufacturing Engineering 27 (2) (2009) 193−212.
[25] DNV OS-F101, Submarine Pipeline Systems, Det Norsk Veritas, Høvik, Norway.
[26] H.E. Townsend Jr., Hydrogen Sulfide Stress Corrosion Cracking of High Strength Steel Wire, Corrosion 28 (1) (1972) 39−45.
[27] R.J. Pargeter, A review of the concept of mildly sour environments, in: Paper IPC-98−170, 2nd Int. Pipeline Conf., (IPC'98), Calgary, Alberta, Canada, June 1998, 1998.
[28] TWI Job Knowledge 119: Complying with NACE Hardness Requirements.
[29] ISO 15614, Specification and Qualification of Welding Procedures for Metallic Materials − Welding Procedure Test, International Standards Organization.
[30] L. Zhang, R.A. Adey, Prediction of third party damage failure frequency for pipelines transporting mixtures of natural gas and hydrogen (Paper 155), in: Int. Conf. Hydrogen Safety, Corsica, 2009, 2009.

[31] F.F. Noecker, G. Pickens, G. Wilken, G. Dunn, D. Lillig, H. Woo Jin, R. Ayer, Test method to evaluate the effect of reeling on sour service performance of C-Mn steel linepipe and girth welds, in: Proc. 19th Int. Offshore and Polar Eng. Conf., Osaka, Japan, June 2009, 2009.
[32] EFC-16, European Federation of Corrosion, 2002.
[33] ASME B31.8, Gas Transmission and Distribution Piping Systems, American Society of Mechanical Engineers, New York, NY.
[34] ASME B31.4, Pipeline Transportation Systems for Liquids and Slurries, American Society of Mechanical Engineers, New York, NY.
[35] P.A. Shenton, The Effect of Strain on the Susceptibility of Pipeline Girth Welds to Sulfide Stress Cracking (Paper 05117, NACE), NACE international 2005, 2005.
[36] T. Sourmail, A review of the effect of cold-work on resistance to sulphide stress cracking (Paper 07104), in: CORROSION 2006, NACE International, 2006.
[37] (F-2002−50435), Integrity Characteristics of Vintage Pipelines, INGAA Foundation, Battelle Memorial institute, 2005.
[38] Minutes of Meeting, EFC Working Party No. 13, Corrosion in Oil and Gas Production, Eurocor, Budapest, October 2003.
[39] NACE TM-0284, Evaluation of Pipeline and Pressure Vessel Steels for Resistance to Hydrogen-Induced Cracking, NACE International, Houston, Tx.
[40] NACE TM-0177, Laboratory Testing of Metals for Resistance to Sulfide Stress Cracking and Stress Corrosion Cracking in H_2S Environments, NACE International, Houston, Tx.
[41] M. Lino, The extension of hydrogen blister crack array in linepipe steels, Metallurgical Transactions 9 (1978) 1581−1590.
[42] Stress Corrosion Cracking, Recommended Practices, second ed., Canadian Energy Pipeline Association, 2007.

Stress corrosion cracking

12

John Beavers and Thomas A. Bubenik
DNV GL USA, Dublin, OH, United States

12.1 Introduction

Stress corrosion cracking (SCC) of buried pipelines has been a known threat for over 50 years. The first recognized underground pipeline failure due to SCC occurred in 1965 in Natchitoches, Louisiana. A 24-inch (609.6-mm) diameter natural gas pipeline ruptured, resulting in 17 fatalities. The subsequent failure investigation determined the rupture initiated at a colony of cracks on the outside surface of the pipeline.

The failure triggered an intensive investigation to understand SCC, with an objective of preventing future failures. It also influenced the decision of the United States Federal government to regulate pipeline safety, beginning in 1970. The natural gas pipeline industry funded research on SCC through the Pipeline Research Committee of the American Gas Association (now referred to as the Pipeline Research Council International [PRCI]). Most of this early research was conducted under Project NG-18 [1,2] at Battelle Memorial Institute in Columbus, Ohio.

The SCC associated with the Natchitoches failure was intergranular in nature and is referred to as high pH or classical SCC. A later identified form of SCC, near-neutral pH SCC, is primarily transgranular, as discussed elsewhere in this chapter. Both forms of cracking are associated with colonies that may contain several to thousands of cracks, as shown in Fig. 12.1. The cracks are normally axial in orientation and link up to form long shallow flaws having aspect ratios greater than 10.

In some cases, external SCC may be at orientations other than axial, depending on the nature of the stresses in the pipeline. In general, the cracks are perpendicular to the maximum combined tensile stress, which can include the hoop stress from internal pressure, axial stresses, residual stresses from pipe manufacturing and construction (e.g., field bends), and stresses from in-service damage. Near-neutral pH SCC is more likely to be associated with local stress concentrators than is high pH SCC. In some cases, growth and interlinking of the SCC produce leaks or ruptures of the pipelines at normal operating pressures.

12.2 High pH SCC

12.2.1 Characteristics

The growth of high pH SCC in buried pipelines is due to a film rupture and anodic dissolution mechanism. A passivating film forms on the external surface of the pipe

Trends in Oil and Gas Corrosion Research and Technologies. http://dx.doi.org/10.1016/B978-0-08-101105-8.00012-7

Figure 12.1 Typical stress corrosion cracking colony.

as a result of the environment created by cathodic protection. When the film ruptures, bare metal surface is exposed, allowing anodic dissolution to occur at the grain boundaries while repassivation attempts to recreate (repair) the passivating film. If anodic dissolution occurs more quickly than repassivation, the crack grows between the grains of the steel.

Repassivation is a function of the local environment, cathodic protection level, and metallurgy of the steel. In addition, high pH SCC growth depends on the mechanical response of the pipe steel, which is a function of external loading (stress), the strength of the pipe steel, and the local (crack) geometry. Whether a crack becomes dormant (passivation occurs more quickly than dissolution) or remains active (dissolution occurs more quickly than passivation) depends on a delicate balance between the local external environment and the crack tip loading.

High pH SCC has occurred in pipe with a variety of diameters (6−34 inch), wall thicknesses (0.181−0.5 inch), seam weld types (double submerged arc weld, flash weld, electric resistance weld, and seamless), grades, and manufacturers. No conclusions have been drawn from the chemical composition of the pipe steels that have experienced high pH SCC. Cracking has been found in line pipe steels with a range of typical compositions [3].

The development of the high pH environment necessary for SCC requires cathodic protection more negative than −850 mV (copper/copper sulfate electrode), at least part of the time. As a result, high pH SCC is not usually associated with external corrosion of the pipe surface. Also, the cracks are primarily intergranular, and there is little evidence of corrosion of the crack faces.

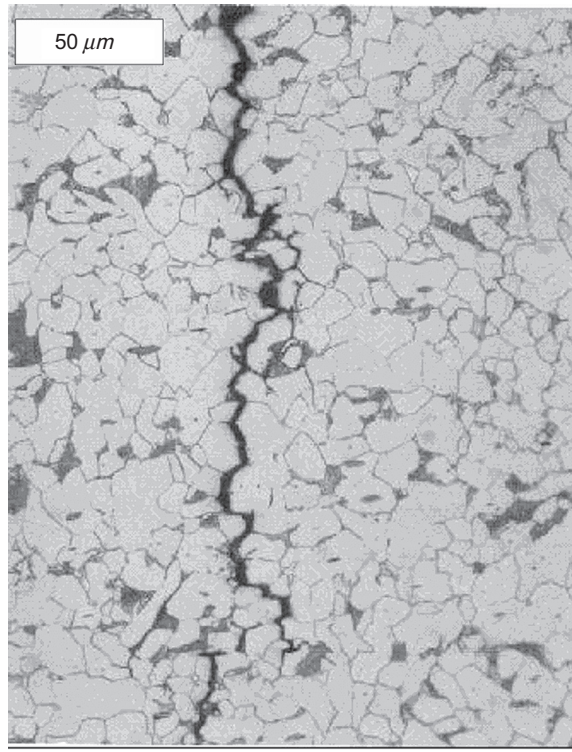

Figure 12.2 Typical high pH stress corrosion cracking morphology.

A transverse cross-section of a coupon containing high pH SCC is shown in Fig. 12.2. This particular crack is relatively straight and shows little branching. In other cases, the cracking may be more branched and angled with respect to the pipe surface. Orientation differences are thought to be related to the through thickness stress distribution in the pipe.

Research on high pH SCC has examined how metallurgical, environmental, and stress-related factors affect the cracking behavior, with a goal of identifying methods to mitigate cracking on transmission pipelines. Research has not identified any obvious metallurgical factors that can be used to mitigate high pH SCC or enhance integrity management programs. Consequently, the remainder of this chapter primarily focuses on environmental and stress-related factors.

12.2.2 High pH SCC cracking environment

In the early field investigations of high pH SCC, small quantities of liquids were found beneath disbonded coatings near the SCC colonies. The primary components of these liquids were carbonate and bicarbonate ions, along with traces of nitrates. The pH of these solutions ranged from 9.6 to 12.3. In some cases, sodium bicarbonate crystals were also found.

It was speculated that the carbonate−bicarbonate solution developed at the pipe surface as a result of the cathodic protection system and the presence of carbon dioxide in the soil (from the decay of organic matter). The reduction reactions produce hydroxide, which then reacts with the carbon dioxide to produce carbonate and bicarbonate ions. Essentially, the cracking electrolyte is a buffered solution of carbonate and bicarbonate ions. The pH and concentration depend on a number of factors, including the cathodic protection current and the available concentration of carbon dioxide. Chlorides are also commonly found in high pH SCC electrolytes.

At the time of the early discoveries, nitrates and hydroxide ions were known to cause SCC of carbon steels, but there was no evidence that carbonate or bicarbonate ions could form a potent cracking environment. Subsequent research, performed as part of Battelle's Project NG-18, demonstrated that a concentrated equinormal solution containing sodium carbonate and sodium bicarbonate was a potent intergranular cracking agent for ferritic steel. The cracking occurred over a narrow potential range, and the severity of cracking increased markedly with increasing temperature. The association of the SCC with the polarization behavior was related to the passivation behavior of the steel.

Several hundred targeted field investigations were performed in Canada in the 1980s and 1990s. These involved both high pH and near-neutral pH-SCC-susceptible sites. Analyses of soil extracts from these sites revealed that the occurrence of high pH SCC statistically correlated with the concentration of the soluble cations (sodium and potassium ions) and the concentration ratio of soluble to insoluble cations (calcium and magnesium ions) in the soils [4]. This explains how a soluble cation must be present to maintain carbonate and bicarbonate ions in solution.

12.2.2.1 Electrochemical potential and temperature

The potential range for high pH SCC lies between the native potential of steel with no cathodic protection, which is typically more positive than −650 mV (copper/copper sulfate electrode), and adequate cathodic protection, which is typically more negative than −850 mV (copper/copper sulfate electrode). Early field investigations identified temperature as an important factor in high pH SCC. Temperature can affect the SCC growth kinetics, the potential range for active cracking, deterioration of the coating, the concentration of the environment in contact with the pipe, and the moisture content of the soil near the pipeline.

The potential range for high pH SCC decreases with decreasing temperature, as does the crack velocity. At temperatures below 38−43°C (100−110°F), the potential range is narrow and the crack velocity is slow but not zero. A common susceptibility criterion of 38°C (100°F) is based on these findings.

High pH SCC typically occurs beneath disbonded coatings, and the potential beneath the coating can be significantly different than that measured at a holiday in the coating or at ground level. Accordingly, although pipe-to-soil potential data are commonly used to identify pipeline segments at risk of SCC or to select dig sites for investigation, the correlation between SCC and pipe-to-soil potentials measured in the field typically has not been very good.

For the high pH environment to develop, significant current flow to the pipe surface is required to generate the elevated pH environment needed to absorb the carbon dioxide. A high pH environment (above a pH of 9) and adequate cathodic protection typically require cathodic protection potentials more negative than −850 mV off potential (copper/copper sulfate electrode). On the other hand, the cracking range lies between the native potential of most pipelines and adequate protection (−850 mV copper/copper sulfate electrode off potential). An explanation for this apparent paradox is that the environment and potential varies on a seasonal basis and high pH SCC only occurs during periods of the year where both a potent environment and inadequate cathodic protection are simultaneously present.

The limited temperature, pH, and potential range over which high pH SCC occurs provides a possible explanation for the infrequent occurrence of high pH SCC on most pipelines. The pH and potential dependencies suggest that seasonal fluctuations are important in the cracking process [5].

12.2.2.2 Coating and surface condition

High pH SCC is most commonly associated with coal tar pipelines, but it has also been found on uncoated pipe as well as asphalt, tape, wax, and, in an isolated instance, a fusion bond epoxy coated pipelines (unpublished research by Beavers). There are roughly four to five times as many high pH SCC failures on coal tar pipelines than on tape coated lines. The one verified case of high pH SCC on a thin-film fusion bond epoxy pipeline occurred at a rock dent where the coating was damaged; the rock provided the shielding necessary for cracking. A common industry guideline is that all coatings other than fusion bond epoxy should be considered susceptible to high pH SCC.

Coating-related factors that play a role in SCC behavior include resistance to disbondment, cathodic protection current shielding behavior, and surface preparation [6,7]. Disbondment resistance affects all forms of external corrosion: an intact coating that prevents contact of the groundwater/electrolyte with the steel surface will mitigate external corrosion and SCC.

All coatings are capable of shielding cathodic protection current but how they disbond and the inherent properties of the coating can affect how they shield and the resulting potentials in the disbonded regions. The surface preparation varies depending on the coating type and can impact subsequent SCC behavior. Coal tar, asphalt, and tape coatings are commonly applied in the ditch over wire brushed, mill scaled surfaces, whereas fusion bond epoxy (FBE) coatings require a near white grit blasted surface finish for proper adhesion.

Several researchers have examined the effects of grit blasting of pipe steel surfaces on SCC behavior [6–9]. Grit blasting was found to have a number of beneficial effects:

- Generally improves resistance of the coatings to disbonding as a result of the anchor pattern created
- Removes mill scale, which results in an ability for cathodic protection to more readily move the pipe-to-soil potential out of the critical potential range for cracking

- Introduces a deformed layer, which distorts the intergranular path for cracking
- Introduces compressive stresses or strains in the surface layer

One surprising result of the laboratory and field studies was that a light brush blasted surface was actually more susceptible to SCC than a mill scaled, wire brushed surface and that a near white surface finish was required for adequate SCC resistance [6,7].

The excellent SCC resistance of pipelines with fusion bond epoxy coatings can be attributed to several factors. These coatings have good disbonding resistance, and when disbondment does occur, cathodic protection can flow to the pipe surface to provide protection. Within blisters, the coating holds the electrolyte at the pipe surface, allowing for the development of benign high pH solutions. Finally, the near-white grit-blasted surface has high compressive stresses or strains and a beneficial absence of mill scale.

12.2.2.3 Stress

As previously indicated, the majority of high pH stress corrosion cracks are oriented in the axial direction because the hoop stress from the internal pressure is typically the dominant loading. Historically, most of the high pH SCC occurred on the bottom half of the pipelines at locations where there was no evidence that secondary stresses, such as from dents, played a role [3]. The higher frequency of high pH SCC immediately downstream of the compressor or pump stations has been associated, in part, with the higher stresses at this location.

Laboratory studies demonstrated that high pH stress corrosion cracks initiated above an applied stress referred to as the threshold stress and that the surface condition affected the threshold stress. Pitting corrosion, by creating stress concentrators, lowered the threshold stress while grit blasting generally increased it. The cyclic pressures associated with the operation of a typical gas pipeline were found to lower the threshold stresses for high pH SCC initiation [10,11].

Recently, the number of reported failures of gas transmission pipelines as a function of operating stress has been evaluated; see Table 12.1 [12]. For larger diameter pipelines, nearly all failures occurred at a stress level greater than or equal to 60% of the specified minimum yield stress (SMYS). For smaller diameter pipelines, it was more common to see failures at lower stress levels. An earlier study showed incidents at hoop stresses from 25% to 72% SMYS, with 70% occurring at greater than 60% SMYS [13].

A common industry guideline is that pipelines operating over 60% SMYS should be considered more susceptible to high pH SCC. Although this guideline is frequently used, Table 12.1 shows that cracking and failures can occur at lower stress levels, especially for smaller diameter pipelines.

12.2.3 Impact of distance to compressor or pump station

The majority of high pH SCC failures have occurred within 10–20 miles (16–32 km) of a compressor or pump station, where temperatures and stress are higher. This is the

Table 12.1 Number of reported high pH SCC failures of gas transmission pipelines as a function of operating stress [12]

% SMYS	Service failures		Hydrotest failures	
	<12″ diameter	≥12″ diameter	<12″ diameter	≥12″ diameter
<30	0	0	0	0
30–40	2	0	0	1
40–50	3	0	10	0
50–60	3	0	0	1
60–70	0	9	0	37
>70	4	33	0	250

basis for industry criteria that say the first 20 miles (32 km) downstream of a station should be considered more susceptible to high pH SCC. Nonetheless, there have been failures beyond 20 miles (16 km).

The proximity to compressor discharge stations for high pH SCC in gas pipelines was quantified, as shown in Table 12.2 [12]. A total of 89% of the service failures and 95% of the hydrostatic test failures occurred within 20 miles (32 km) of a station, but some failures occurred beyond 20 miles (32 km) on both coal tar enamel and tape coated pipelines.

Table 12.2 High pH SCC failures as a function of proximity to compressor discharge stations [12]

Distance (miles)	Service failures		Hydrotest failures	
	Coal tar enamel	Tape	Coal tar enamel	Tape
0–5	19	8	107	3
5–10	10	2	88	7
10–20	10	1	17	29
20–30	2	1	3	6
30–40	0	1	0	3
40–50	1	0	0	0
>50	1	0	2	1

12.2.4 Impact of pipeline age

A number of researchers have investigated the relationship between pipeline age and high pH SCC. The earliest age for a reported failure is 6 years on a tape-coated line (18 years for a line coated with coal tar), but most occur between 20 and 30 years of installation [12]. A common industry guideline is that lines more than 10 years old should be considered more susceptible to high pH SCC. High pH SCC has led to hydrotest failures at ages greater than 50 years.

The rate of in-service failures due to high pH SCC is around 1.5 occurrences per year for the US transmission pipeline system over the past 40 years [12]. This rate has remained relatively constant as the pipe system has aged. So, there is no strong evidence that SCC failure rates increase with increasing age, which could indicate that pipeline companies are effectively mitigating existing high pH SCC.

Very few instances of hydrotest or in-service failures have been reported in pipe that was installed after 1960. This behavior may relate to the fact that the surface preparation of the pipe and the types of coatings used have changed significantly since the original SCC failures occurred.

12.2.5 High pH SCC summary

The mechanism by which high pH SCC occurs is film rupture and anodic dissolution. The carbonate−bicarbonate electrolyte necessary for high pH SCC forms under disbonded coatings when cathodic protection is at or near "adequate" levels, which are commonly taken as more negative than −850 mV (copper/copper sulfate electrode). Cracking then occurs when the pipe-to-soil potential increases (becomes more positive) into the range needed for cracking, which is more positive than −850 mV (copper/copper sulfate electrode). Seasonal variations play an important role in affecting the pipe-to-soil potentials, allowing cracks to actively grow and become dormant as cathodic protection effectiveness changes during the year.

Common industry guidelines [14] are that high pH SCC failures are most likely on pipe that is

- Within 20 miles (38 km) of a compressor or pump station,
- Over 10 years old,
- At temperatures above 38−43°C (100−110°F),
- Coated with coal tar or tape, and
- Operating at stresses above 60% SMYS.

There are exceptions to each of these guidelines, especially for smaller diameter pipe. Most notably, failures have occurred well beyond 20 miles (38 km) of a station and at stresses as low as 25% SMYS.

12.3 Near neutral pH SCC

12.3.1 Characteristics

Near-neutral pH SCC occurs by a different mechanism than high pH SCC. In high pH SCC, cracking occurs by film rupture/anodic dissolution. In near-neutral pH

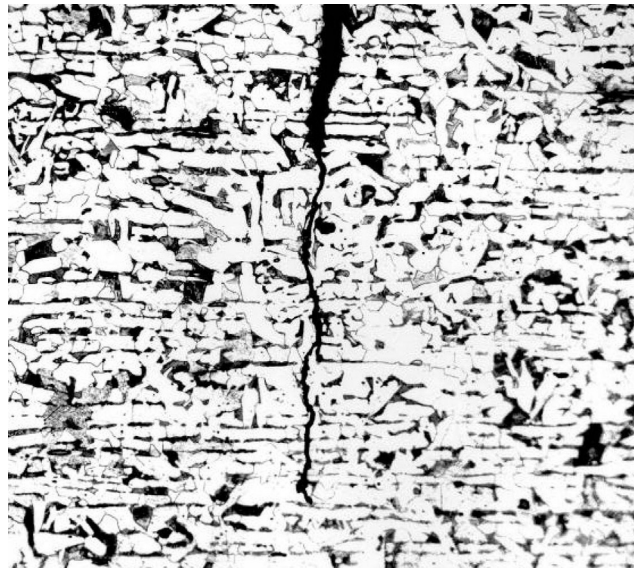

Figure 12.3 Typical near neutral pH stress corrosion cracking morphology.

SCC, corrosion and hydrogen embrittlement are thought to play important dominant roles.

Near-neutral pH SCC was first recognized in 1986 when TransCanada Pipelines initiated field and laboratory programs in response to three in-service failures on one of their gas transmission pipelines [15–17]. The SCC had some similarities to that associated with previous failures, such as the presence of axial colonies of cracks and the association of the colonies with disbonded coatings, but it quickly became apparent that the failures were the result of a new form of SCC.

The TransCanada cracks were wider and primarily transgranular (although some intergranular cracking was reported) with little branching, as shown in Fig. 12.3. They were associated with electrolytes with pH values of 7.5 or less. Two of the failures, on tape coated sections of the line, initiated at the toe of the longitudinal seam weld, which indicates that stress raisers may play a more prominent role in this form of SCC than in the case of high pH SCC.

12.3.2 Near-neutral pH SCC cracking environment

The electrolytes found beneath disbonded coatings were analyzed and found to be very dilute solutions of bicarbonate ions and carbonic acid with lower values of pH than the electrolytes associated with high pH SCC. In these studies, concentrated high pH electrolytes were discovered at some locations on the TransCanada System, but there was no near-neutral pH SCC associated with these electrolytes.

TransCanada expanded its field work to include over 600 pH analyses of undercoating electrolytes on both polyethylene tape and asphalt coated segments of the pipeline. Results conclusively demonstrated that, regardless of coating type, the SCC was associated with near-neutral pH environments. The near-neutral pH values, along with

some corrosion of the external surface of the pipe, are consistent with the pipe surface not receiving adequate cathodic protection.

The carbon dioxide concentration in the soil and the groundwater pH varied seasonally by a wide range with the highest carbon dioxide concentrations and lowest pH values in the winter months. A statistical analysis of soil and electrolyte data from sites along the TransCanada pipeline revealed that the soluble cation concentration and pH of the electrolytes were higher for non-SCC sites than for SCC sites.

On the other hand, there were no obvious trends with respect to the soluble cation concentrations of the soils at these locations. This behavior indicates that cathodic protection was affecting both the pH and the soluble cation concentration within the disbonded regions, and in so doing, affecting the cracking behavior. In subsequent laboratory tests, it was also found that the presence of carbon dioxide also promoted lower ductility in slow strain rate tests of pipe steels.

12.3.2.1 Electrochemical potential and temperature

Early field investigations focused on the first valve sections downstream of compressor stations based on the temperature dependence of high pH SCC, but it soon became apparent that the cracking did not follow the same temperature trends. Instead, the cracking behavior was relatively independent of temperature. The lack of a temperature effect is reflected in the absence of a temperature criterion for defining near-neutral pH SCC susceptible segments [14]. (Elevated temperature can accelerate coating degradation, thereby indirectly affecting where near-neutral pH SCC occurs.)

Near-neutral pH SCC occurs where cathodic protection does not penetrate the coating to reach the steel surface. The potential range for near-neutral pH SCC is more negative (slightly cathodic) than the native potential of steel with no cathodic protection: between about −670 and −790 mV (copper/copper-sulfate electrode). The potential range is not temperature dependent.

12.3.2.2 Coating

Two of the three initial SCC service failures on the TransCanada system occurred on polyethylene tape coated sections and one occurred on an asphalt coated section [14]. In the subsequent field studies, the vast majority of SCC colonies on the affected TransCanada pipeline occurred in the tape coated sections [15]. In a total of 440 excavations on the pipeline, SCC was detected at 69% of the sites with tape coating (173 of 250 sites and 1720 SCC colonies) versus only 14% of the sites with asphalt coating (27 of 189 sites and 171 colonies). Often, the tape coated sites with near-neutral pH SCC were poorly or very poorly drained, whereas asphalt coated sites were in extremely dry terrains with inadequate cathodic protection.

The results of PRCI research on coatings and SCC have demonstrated why polyethylene tape coatings are so closely tied to near-neutral pH SCC [6,7]. The research addressed the three major coating-related factors affecting SCC: resistance of a coating to disbondment, the ability to pass cathodic protection current and thereby protect the

disbonded region, and the surface preparation of the line pipe steel prior to coating application.

Polyethylene tape coatings fall short in all three areas: they have poor disbonding resistance, they shield cathodic protection current and the typical surface preparation for polyethylene tape coatings (wire brushing) renders the pipeline very susceptible to SCC. On pipelines with double submerged arc welded long seams, tape coatings can form a tent at the toe of the weld such that the region readily fills with groundwater. Furthermore, polyolefin coatings such as polyethylene tape are also very permeable to carbon dioxide, such that any carbon dioxide in the soil will readily diffuse through the coating to the disbonded region at the pipe surface.

Common industry guidelines consider coatings other than fusion bond epoxy to be susceptible to near-neutral pH SCC [14].

12.3.2.3 Stress

The three SCC service failures reported by TransCanada occurred in Class 1 locations (in Canada, the class locations as a percent of SMYS are as follows: Class 1−80%, Class 2−72%, Class 3−56%, and Class 4−44%, where the maximum allowable operating pressure corresponded to a hoop stress of 78% SMYS. In a subsequent hydrostatic test program, there were 16 failures, all of which were in Class 1 locations. Nine of the failures were attributed to SCC and occurred in tape coated sections, six were attributed to pitting corrosion and one was attributed to mechanical damage. Interestingly, SCC was associated with five of the six pitting failures, but did not contribute to the failures. In the hydrostatic retest program, three additional SCC failures were also in Class 1 locations.

The National Energy Board of Canada conducted an inquiry of SCC on Canadian Oil and Gas Pipelines in the mid-1990s [18]. The cracking experienced in Canada that was the subject of the investigation was almost exclusively transgranular and was therefore the near-neutral pH form of SCC. At that time, 22 service failures had been reported, industry wide, of which 16 (73%) were associated with axially oriented cracks, indicating that the hoop stresses controlled the failures. At the time of the failures, the hoop stresses varied between 46% and 77% of SMYS, which is similar to the range seen with high pH SCC.

TransCanada's field investigations were consistent with the service failure experience cited above; no significant cracking was detected in Class 2 or 3 locations (significant cracking is defined as cracks having a depth greater than 10% of the wall thickness and a length greater than 75% of the length of a 50% through wall crack that would fail at 110% of SMYS [19]). Similarly, none of the other Canadian Energy Pipeline Association (CEPA) member companies reported significant SCC in Class 2 or 3 locations [19]. On the TransCanada line, the extent and severity of cracking (both the number of colonies and the maximum crack depth in the colonies) increased with increasing stress level in Class 1 locations, as shown in Figs. 12.4 and 12.5. Based in part on these findings, a common industry guideline [14] states that pipelines operating at stress levels above 60% SMYS should be considered more susceptible to near-neutral pH SCC.

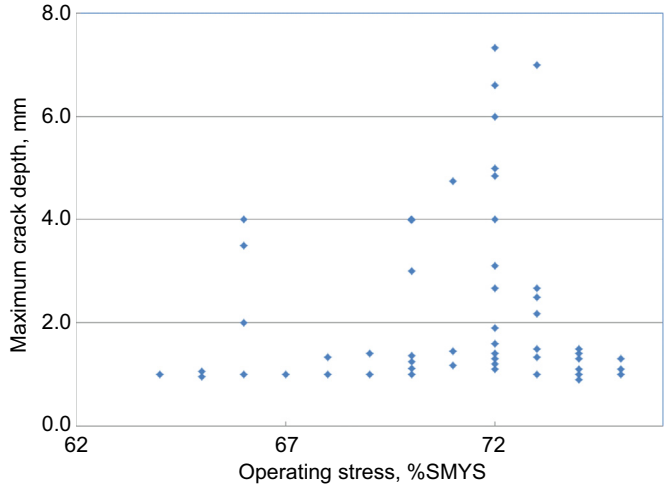

Figure 12.4 Maximum crack depth of significant stress corrosion cracking as a function of %SYMS.

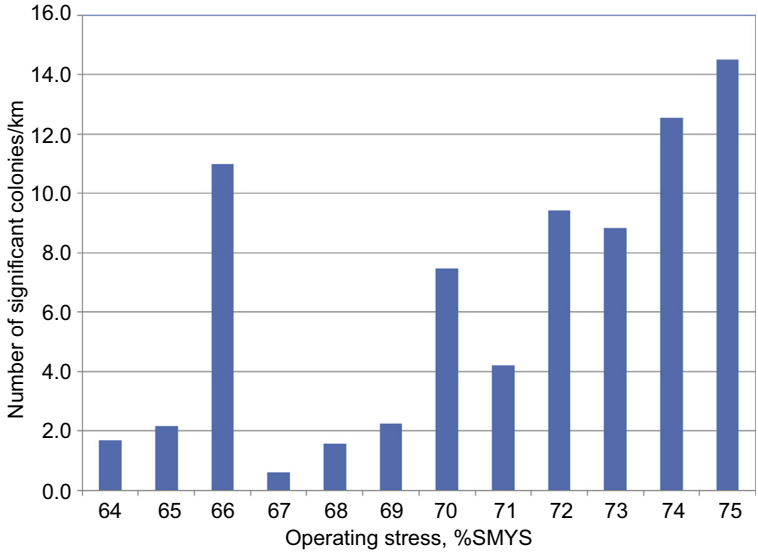

Figure 12.5 Number of significant stress corrosion cracking colonies per Km as a function of % specified minimum yield stress.

However, in nearly all of the near-neutral pH SCC failures, other factors increased the local stress levels at the failure origins. These factors included corrosion, gouges, or the geometry of the toe of the long seam welds. The association of cracking with stress concentrations is quite different from that reported for high pH SCC, where the cracking typically occurs on the bottom of the pipe away from obvious stress

concentrators. A stress concentration encourages hydrogen to accumulate, leading to embrittlement and contributing to near-neutral pH SCC.

Available field data indicate that cyclic pressure fluctuations are also important and, perhaps, more so than in the case of high pH SCC. Crack growth tests of precracked samples tested at high R ratios (ratio of minimum to maximum pressure or stress) and low frequencies, which are conditions that simulate natural gas pipeline operation, exhibit decreasing crack growth rates with time (evidence of dormancy) [20]. Specimens tested at higher frequencies and lower R ratios, which are conditions more similar to liquid petroleum pipeline operation, exhibit increasing crack growth rates with time.

Strain rate effects on near-neutral pH SCC have been established, and crack growth rates have been related to crack tip strain and displacement rates [21]. As seen in Fig. 12.6 (crack growth rate vs. ΔK), the slope of the growth rate curve is slightly more than 1, versus around 3 for corrosion fatigue. This creates a situation where SCC will dominate for small cracks and/or low cyclic loads and fatigue or corrosion fatigue will dominate for large cracks or high cyclic loads.

Chen [22] has made significant advances in understanding the role of variable amplitude loading (from variable pressure fluctuations) on near-neutral pH SCC crack growth behavior. In comparison with constant amplitude loading, underload cycles, which are typically found immediately downstream of pump or compressor stations, will accelerate crack growth, whereas overload cycles, which are found further downstream, will retard crack growth.

CEPA funded a research program to determine whether there was a correlation between initiation of near-neutral pH SCC and metallurgical factors [23]. Fourteen pipe sections that contained colonies of near-neutral pH stress corrosion cracks were

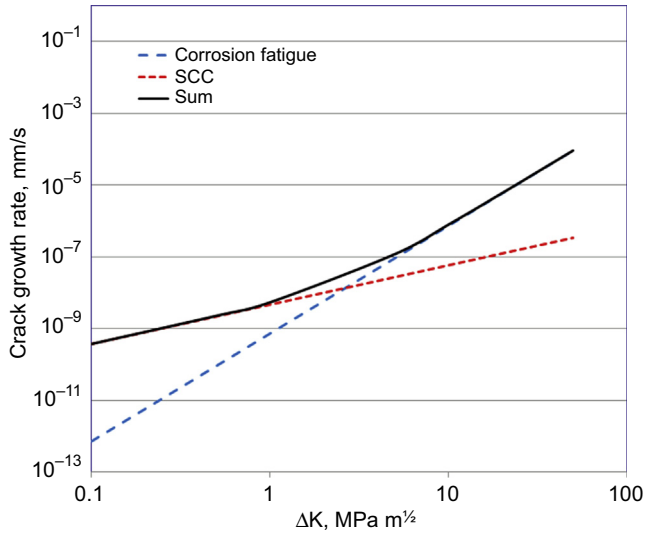

Figure 12.6 Crack growth rate as a function of stress intensity factor range.

investigated. A range of installation dates, from the 1950s to the 1970s, diameters, and grades were examined. Factors that were evaluated included the chemical composition, inclusion properties, cyclic stress strain behavior, residual stress, surface roughness, microhardness, and local galvanic behavior. A strong correlation was found between the residual tensile stress and the presence of the SCC colonies. There also was a statistically significant correlation between microhardness and the occurrence of SCC. However, no statistically significant correlation was found between the other parameters evaluated and the occurrence of near-neutral pH SCC.

As with high pH SCC, near-neutral pH SCC has occurred on pipe covering a range of diameters, wall thicknesses, grades, and seam weld types. Unlike high pH SCC, the seam welds appear to be more prone to cracking, over and above the stress concentrator associated with some weld geometries, such as double submerged arc welds. The seam welds in 1950s vintage direct current electric resistance welded pipe were reported to have lower resistance to SCC than the base metal [18]. The coarse grain heat affected zone of double submerged arc welds exhibited 30% higher crack growth rates than that of the base metal in cyclic load tests of compact tension specimens in NS4 groundwater [24].

12.3.3 Impact of distance to compressor or pump station

As with high pH SCC, most near-neutral pH SCC in-service failures have occurred within 10−20 miles (16−32 km) of a station, especially for tape coated pipelines. There have been failures beyond 20 miles (16 km), and most of these have occurred on asphalt-coated lines. Fessler reported similar results for in-service and hydrotest failures of gas pipelines [12]. Two-thirds of the failures on tape-coated lines were within 20 miles of a compressor station, but the failures on asphalt-coated lines were distributed along the entire pipeline length. Table 12.3 summarizes the in-service failure data. Based in part on failures occurring along the length of a pipeline, there is no industry criterion related to distance to compressor or pump station [14].

12.3.4 Impact of pipeline age

A number of researchers have investigated the relationship between pipeline age and the likelihood of near-neutral pH SCC. The earliest age for a reported in-service failure by near-neutral pH SCC is 12 years on a tape-coated line (compared to 22 years for a line coated with asphalt, and 35 years for a line that was wax coated) [12]. The oldest age exceeds 70 years. Table 12.4 shows recently analyzed data for in-service and hydrostatic test failures [12]. Based in part on results like these, a common industry guideline [14] states that lines more than 10 years old should be considered susceptible.

Very few instances of hydrotest or in-service failures have been reported in pipe that was installed after 1980. This behavior may relate to the fact that the surface preparation of the pipe and the types of coatings used have changed significantly since the original SCC failures occurred.

Table 12.3 Near-neutral pH SCC failures as a function of proximity to compressor or pump station [14]

Distance (miles)	Coating type		
	Tape wrapped	Asphalt	Wax
0–5	2	1	0
5–10	2	0	1
10–20	1	3	0
20–30	1	0	0
30–40	0	1	0
40–50	0	0	0
>50	0	5	0

12.3.5 Near-neutral pH SCC summary

The mechanism by which near-neutral pH SCC occurs is thought to be a form of hydrogen embrittlement/localized corrosion. The bicarbonate/carbonic acid electrolyte necessary for near-neutral pH SCC forms under disbonded coatings when cathodic protection is shielded, resulting in potentials near the open circuit potentials. Cracking occurs when the pipe-to-soil potential falls into the susceptible range for cracking, which is between −670 and −790 mV (copper/copper sulfate electrode). The reduction reaction from corrosion is thought to generate hydrogen, which is absorbed into the metal.

Common industry guidelines [14] are that near-neutral pH SCC failures are most likely on the pipe that is

- Over 10 years old
- Coated with tape or asphalt
- Operating at stresses above 60% SMYS

There are exceptions to each of these guidelines. Most notably, failures have occurred at stress levels well below 60% SMYS.

12.4 Discussion

There are three common techniques used for the management of the integrity of pipelines subject to SCC and other time-dependent threats: hydrostatic testing, in-line inspection, and direct assessment. Directly following the initial SCC failures of gas transmission pipelines in the 1960s, hydrostatic testing was the primary tool used to confirm the integrity of the affected pipelines and prevent additional failures. The pipelines were pressure tested significantly higher than the operating pressure to remove any near critical flaws.

Table 12.4 Near-neutral pH SCC failures as a function of age [14]

Pipe age, years	Number of in-service and hydrostatic test failures							
	Tape-wrapped		Asphalt		Wax		Coal tar	
	In-service	Hydrotest	In-service	Hydrotest	In-service	Hydrotest	In-service	Hydrotest
0–10	0	0	0	0	0	0	0	0
10–20	4	4	1[a]	0	0	0	0	0
20–30	3	6	3	1	0	0	0	0
30–40	0	4	5	21	1	0	0	1
40–50	0	0	2	15	0	0	0	0
>50	0	0	0	0	0	0	0	0

[a]Occurred at a region of mechanical damage.

12.4.1 Hydrostatic testing

Most hydrostatic pressure test programs used to manage SCC rely on "spike" testing. In spike testing, the pipeline is initially pressurized to a very high pressure for a short period of time, after which the pressure is reduced and held for a longer period. The spike (high) pressure is intended to fail any critical cracks, whereas the lower (hold) pressure is used for leak detection.

Pressure testing has been effective in minimizing service failures, but it has a number of limitations:

- Very few, if any, SCC flaws are removed and the pipeline must be taken out of service for testing;
- Each pressurization subjects the pipe to very high hoop stresses, which can contribute to stable crack tearing and/or fatigue;
- Pressure reversals are also possible, where the failure pressure after a hydrostatic test is lower than the maximum test pressure.

Because of these limitations, there has been a significant interest in the development of alternatives to hydrostatic testing. One alternative is the use of in-line inspection to manage time-dependent threats on operating pipelines. There is a long history of using magnetic flux leakage (MFL) and, to a lesser extent, ultrasonic tools to address internal and external corrosion threats on transmission pipelines.

12.4.2 In-line inspection

In-line inspection systems designed to find and size cracks were first introduced in the 1980s by British Gas with the advent of the elastic wave system. Later attempts have been based primarily on ultrasonic shear wave or circumferential MFL technologies. All of the early attempts suffered from both poor detection and sizing problems. The inspection tools have continued to evolve and improve.

Ultrasonic shear-wave tools generally work best with cracks that are good reflectors. That is, they work best on cracks that are planar, relatively smooth, unbranched, and somewhat open (very tight cracks can allow part of the ultrasonic wave to pass by the crack without reflection). Circumferential MFL tools work best where there is a volumetric separation between the crack faces. Theoretically, both technologies should perform better on near-neutral pH SCC than on high pH SCC because near-neutral pH SCC is a better reflector with a relatively wide opening between the crack faces.

Ultrasonic shear-wave tools (including electromagnetic acoustic transducer or electromagnetic acoustic transducer (EMAT) tools) are more commonly used for SCC than circumferential MFL tools. There is a growing consensus that new generations of ultrasonic tools will eventually eliminate the need for hydrostatic testing (or any of the elements of SCC Direct Assessment [SCCDA]). Unfortunately, the experience with crack detection tools has not yet reached this level. As a result, there have been in-service failures of pipelines that had been inspected using the tools (e.g., the Marshall Michigan failure, which was inspected with a shear-wave tool [25]). Some of the current tools are very good at finding crack-like features (sometimes detecting thousands of features), but they suffer at depth sizing accuracy. These capabilities are improving.

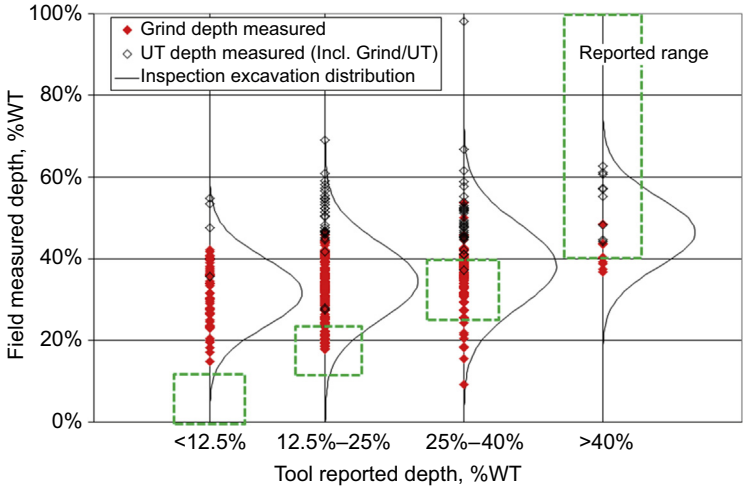

Figure 12.7 Measured versus reported crack depths.
Data courtesy of Suncor Ltd.

Depths are often binned into several categories, e.g., <12.5% of wall thickness, 12.5%−25% of wall thickness, 25%−40% of wall thickness, and >40% of wall thickness. Fig. 12.7 compares depths reported by an in-line inspection using ultrasonic shear waves with field measured depths. Both inspections were conducted in the past 6 years. There is poor agreement between the two.

Recently, EMAT in-line inspection tools have shown promise with SCC and at least one pipeline company has proposed using an EMAT inspection in lieu of hydrotesting. EMAT tools are reportedly less sensitive to shallow cracking than ultrasonic shear wave tools. Consequently, they report fewer crack-like features. The probably of detection for SCC that could threaten the integrity of a pipeline is the subject of a number of studies and test programs.

12.4.3 SCC direct assessment

There has also been interest in SCCDA. The first recommended practice for SCCDA was issued in 2004 (NACE Standard RP0204-2004 [26]). SCCDA is a four-step process intended to assist pipeline companies in assessing the extent of SCC on buried pipelines and thus contribute to their efforts to improve safety by reducing the impact of external SCC on pipeline integrity. A primary limitation of SCCDA is that not finding SCC at excavated locations does not ensure that the pipeline does not have SCC elsewhere.

The first step in the SCCDA process (preassessment) involves collecting existing information on the pipeline to assess the likelihood the pipeline is susceptible to SCC. In the case of high pH SCC, the initial selection of the most susceptible segments is usually based on the five factors discussed earlier. In the case of near-neutral

pH SCC, the selection is based three factors (excluding operating temperature and distance to upstream station).

SCCDA is not necessarily a suitable replacement for hydrostatic testing or in-line inspection in all instances. The preassessment phase of SCCDA may indicate that a particular pipeline segment is not likely to be susceptible to SCC and, therefore, other threats are of a more immediate concern. An example would be a newer pipeline with an FBE coating. On the other hand, in-line inspection, hydrostatic testing, or even pipe replacement may be warranted if extensive, severe SCC is found.

12.5 Future trends

The detection and sizing capabilities of crack detection in-line inspection tools will undoubtedly improve but there may still be a need for elements of SCCDA, developed through applied research, to prioritize pipeline segments for inspection. Depending on the pace of improvements in the precision and accuracy of in-line inspection systems, there may continue to be a necessity, for the near future, to use elements of SCCDA to help identify which features are most likely to be SCC threats. Hydrotesting is also likely to continue to be needed, especially for lines with extensive and severe cracking.

References

[1] J.M. Sutcliffe, R.R. Fessler, W.K. Boyd, R.N. Parkins, Stress corrosion cracking of carbon steel in carbonate solutions, Corrosion 28 (8) (August 1972).
[2] R.N. Parkins, Environmental aspects of stress corrosion cracking in low strength ferritic steels, in: NACE-5 (Stress Corrosion Cracking and Hydrogen Embrittlement of Iron Base Alloys), Unieux-Firminy, France, June 12−16, 1973, 1973.
[3] R.L. Wenk, Field investigation of stress corrosion cracking, in: 5th Symposium on Line Pipe Research, American Gas Association, November 1974. Catalog No. L30174.
[4] J.A. Beavers, R.G. Worthingham, The influence of soil chemistry on SCC of underground pipelines, Paper No. IPC 02−27146, in: International Pipeline Conference (IPC 2002), Calgary, Alberta, September 2002, ASME International, New York, 2002.
[5] J.A. Beavers, B.A. Harle, Mechanisms of high pH and near neutral pH SCC of underground pipelines, in: International Pipeline Conference (IPC 1996), Calgary, Alberta, September 1996, vol. 1, ASME, New York, 1996, p. 555.
[6] J.A. Beavers, N.G. Thompson, K.E.W. Coulson, Effect of surface preparation and coatings on SCC susceptibility of line pipe: phase 1 − laboratories studies, in: Corrosion/93, NACE International, Houston TX, 1993. Paper No. 93597.
[7] J.A. Beavers, N.G. Thompson, K.E.W. Coulson, Effect of surface preparation and coatings on SCC susceptibility of line pipe: phase 2 − field studies, in: Proceedings of the 12th International Conference on Offshore Mechanics and Arctic Engineering, June 1993, ASME International, New York, NY, 1993, p. 226.
[8] T.J. Barlo, R.R. Fessler, Shot peening, grit blasting make pipe steel more resistant to stress corrosion cracking, Oil and Gas Journal (November 1981) 80.
[9] G.H. Koch, T.J. Barlo, W.E. Berry, Effect of grit blasting on the stress corrosion cracking behavior of line pipe steel, Materials Performance 23 (10) (1984) 20.

[10] R.R. Fessler, T.J. Barlo, Threshold Stress Determination Using Tapered Specimens and Cyclic Stresses, Environmental Sensitive Fracture: Evaluation and Comparison of Test Methods, ASTM International, West Conshohocken, PA, 1984, p. 368.
[11] J.A. Beavers, W.E. Berry, R.N. Parkins, Standard test procedure for stress corrosion cracking threshold stress determination, Materials Performance 25 (6) (June 1986) 9.
[12] R.R. Fessler, A.D. Batte, M. Hereth, Integrity Management of Stress Corrosion Cracking in Gas Pipeline High Consequence Areas, ASME STP-PT-011, ASME Standards Technology, LLC, New York, NY, October 31, 2008.
[13] R.J. Eiber, B.N. Leis, Protocol to Identify Potential Areas of High PH Stress Corrosion Cracking, Paper presented at 11th PRCI/EPRG Joint Technical Meeting on Pipeline Research, Arlington, VA, May 1997.
[14] Managing System Integrity of Gas Pipelines, ASME Code for Pressure Piping, B31 Supplement to ASME B31.8, American Society of Mechanical Engineers, New York, NY, October 31, 2016.
[15] J.T. Justice, J.D. Mackenzie, Progress in the Control of Stress Corrosion in a 914 MM O. D. Gas Transmission Pipeline, 7th Biennial Joint Meeting on Line Pipe Research, NG-18/EPRG, 1988.
[16] B.S. Delanty, J. O'Beirne, Low pH stress corrosion cracking, in: 18th World Gas Conference, IGU/C6-91, Berlin, July 8−11, 1991, International Gas Union, Paris France, 1991.
[17] B.S. Delanty, J. O'Beirne, Major field study compares pipeline SCC with coatings, Oil and Gas Journal 90 (24) (1992) 39.
[18] Report of the Inquiry, Stress Corrosion Cracking on Canadian Oil and Gas Pipelines, National Energy Board of Canada, November 1996. MH-2−95.
[19] Stress Corrosion Cracking Recommended Practices, first ed., Canadian Energy Pipeline Association (CEPA), 1997.
[20] J.A. Beavers, C.E. Jaske, Near neutral pH SCC in pipelines: effects of pressure fluctuations on crack propagation, in: Corrosion/98, NACE International, 1998. Paper No. 98257.
[21] J.A. Beavers, C.J. Maier, C.E. Jaske, R. Worthingham, Methodology for ranking SCC susceptibility of pipeline segments based on the pressure cycle history, in: Corrosion 2007 Conference & EXPO, Nashville, TN, March 2007, NACE, 2007. Paper Number 07128.
[22] W. Chen, An overview of near-neutral pH SCC in pipelines and mitigation strategies for its initiation and growth, Corrosion 72 (7) (July 2016). NACE International.
[23] J.A. Beavers, J.T. Johnson, R. L Sutherby, Materials factors influencing the initiation of near neutral pH SCC on underground pipelines, in: International Pipeline Conference (IPC 2000), Calgary, Alberta, October 2000, ASME International, New York, 2000, p. 979.
[24] J.A. Beavers, C.L. Durr, S.S. Shademan, Mechanistic studies of near neutral pH SCC on underground pipelines, in: Proceedings of the International Symposium on Materials for Resource Recover and Transport, 37th Annual Conference of Metallurgist of CIM, Canadian Institute of Mining, Montreal, QC, 1998, p. 51.
[25] NTSB/PAR-12/01, PB2012−916501, Pipeline Accident Report, Enbridge Incorporated, Hazardous Liquid Pipeline Rupture and Release, Marshall, Michigan, July 25, 2010, National Transportation Safety Board, Washington DC, July 10, 2012.
[26] Stress Corrosion Cracking (SCC) Direct Assessment, NACE Standard Recommended Practice RP 0204-2004, Item # 21104.

Hydrogen damage

13

Khlefa A. Esaklul
Occidental Oil and Gas Corporation, Houston, TX, United States

13.1 Introduction

Despite decades of research and development with numerous publications, hydrogen damage and embrittlement in its various forms continue to play a major impact on the selection of materials and the integrity of existing assets in the energy industry, specifically the oil and gas and petrochemical industries. These challenges are stemming from the natural evolution of hydrogen as a by-product of corrosion electrochemical reaction of the environment (e.g., produced and processed fluids), external environment (e.g., cathodic protection), or trapped in the metal during manufacturing and fabrication (e.g., steel making, welding, pickling, and electroplating).

In the energy industry as a whole, corrosion is commonly occurring as a result of the presence of water, the deleterious gases (H_2S and CO_2), and ingress of oxygen and is enhanced by increased conductivity because of the presence of ionic species in the produced fluids or naturally occurring in the environment such as seawater and variation in the soil conditions. As oil fields mature and new fields are being developed from deeper reservoirs the severity of corrosion and hence the potential for hydrogen presence increases because of the increase in water production, levels of the deleterious gases, increase in pressure and temperature, or exacerbation of corrosion via contamination of the fluids through addition of other gases (steam and CO_2) used for enhanced oil recovery, ingress of oxygen, or presence of bacteria. Similarly as different corrosion-resistant alloys (CRAs) are being used in these applications, the risk of galvanic corrosion and the interaction with cathodic protection increases, resulting in ingress of hydrogen into these materials increasing the risk of hydrogen embrittlement (HE).

The basic reactions in corrosion that lead or contribute to HE are

$$\text{Anodic reaction} \quad M \rightarrow M^{++} + 2e^{-}$$

$$\text{Cathodic reaction} \quad 2H^{+} + 2e \rightarrow H + H \rightarrow H_2$$

The hydrogen atoms generated at the cathodic site can either combine to form hydrogen gas and bubble out, or if the recombination is inhibited or does not proceed, a high flux of hydrogen atoms can generate at the metal surface, adsorb and diffuse into the metal. Once the hydrogen enters the metal it can diffuse through the metal or get entrapped at microstructural features and hydrogen-trapping sites. Once hydrogen is present in the metal it can manifest its effect in many forms, depending on the type of metal or alloy, strength level, microstructure, and process condition as depicted in Fig. 13.1.

Trends in Oil and Gas Corrosion Research and Technologies. http://dx.doi.org/10.1016/B978-0-08-101105-8.00013-9

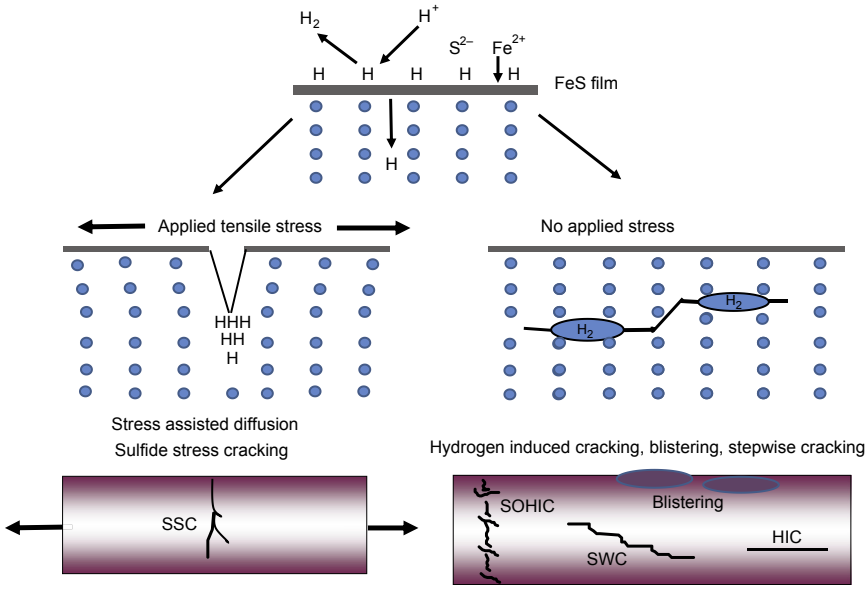

Figure 13.1 Various forms of hydrogen damage in materials.

Hydrogen effect on materials had been identified as early as 1864 [1] in the form of reduction in the physical and mechanical properties to a degree that could result in catastrophic failures. The effect has been seen in one or more of three main forms: (1) internal cracks, pores, or blisters resulting from pressure buildup due to entrapment from the melt or hydrogen diffusion into the metal, (2) hydrogen-assisted cracking (HAC) encompassing various forms of cracking and, and (3) formation of brittle metal hydrides. The latter is commonly seen in the exothermic absorbers groups such as Ti, Zr, V, Nb, and Ta [2,3]. HAC is a most widely observed damage in steels and CRAs that are in use in the energy industry [3,4]. The term HE has been used to describe the effect of hydrogen on materials regardless if the effect results in embrittlement or other forms of change in properties or damage.

The complexity of the hydrogen effects is a result of the high chemical reactivity of hydrogen, its ability to appear in different forms (atomic, molecular, and ionic), and similarity of some of its properties to those of metals. The recognized damages that can occur are as follows:

- HE or loss in ductility
- HAC
- Hydrogen-induced blistering
- Hydrogen-induced cracking
- Sulfide stress cracking (SSC)
- Stress corrosion cracking (SCC) and corrosion fatigue
- Metal hydride formation
- Hydrogen attack at high temperature

The hydrogen damage processes are generally controlled by one of these mechanisms despite the source of hydrogen:

- Internal hydrogen pressure
- Lattice decohesion
- Hydrogen-enhanced plasticity or dislocation interaction
- Hydride formation

In oil and gas production the most critical effect results from the presence of H_2S, which inhibits the hydrogen recombination reaction favoring hydrogen diffusion into the metal. This effect has limited the use of materials (e.g., high strength steels) and contributed to the increase in development cost because more sour service resistant materials are required.

13.2 Types of hydrogen damage

The term hydrogen damage or HE encompasses wide range of the deleterious effects that have been associated with hydrogen on materials. These effects occur in both hydrogen sources, aqueous and gaseous environments, and vary from one material to another, the strength level, microstructure and level of impurities or undesirable phases. Although there is agreement that hydrogen does not affect elastic properties of materials, it is recognized that hydrogen affects mechanical properties of both low- and high-strength materials, and the effect can be characterized by loss in ductility, reduction in strength, reduction in fracture toughness, and enhanced crack growth. Several theories have been proposed to account for these effects, and although there are large degrees of commonality in these models, there still no theories or models that can predict the behavior of materials when exposed to hydrogen. There is consensus among researchers that hydrogen effects depend on wide range of factors among them exposure time, type of environment, temperature, pressure, stress level and state, properties of material, microstructure, hydrogen concentration, surface conditions, diffusion rates, etc., indicating that hydrogen effects are complex and remain elusive despite decades of research that this topic has been studied.

The effect of hydrogen, in general, is proportional to the hydrogen concentration in the metal, which in turn is dependent on hydrogen pressure, hydrogen flux, exposure time, and severity of corrosion in systems that experienced corrosion. The dependence on concentration makes the effect semireversible that if the hydrogen source is removed the damage discontinues.

In steels, HE has been observed at all strength levels and the effect ranges from loss in ductility to reduction in fracture toughness and enhanced static and dynamic crack growth [4–13]. In other alloys the dominant effects are reduction in toughness, enhanced crack growth, and major loss in ductility in alloys that form hydrides [2,14]. Brinbaum [2] reported that hydrogen enhances dislocation motion and plasticity, which results in reduction in flow stress and local cracking where hydrogen is concentrated. Similarly hydrogen can segregate into grain boundaries and reduces the cohesion forces resulting in intergranular fracture. In high-strength materials, there is consensus that the hydrogen effect is a result of enhanced decohesion [4]. Both effects can coexist and mixed fracture modes can occur within the same material. Enhanced ductile microvoid coalescence,

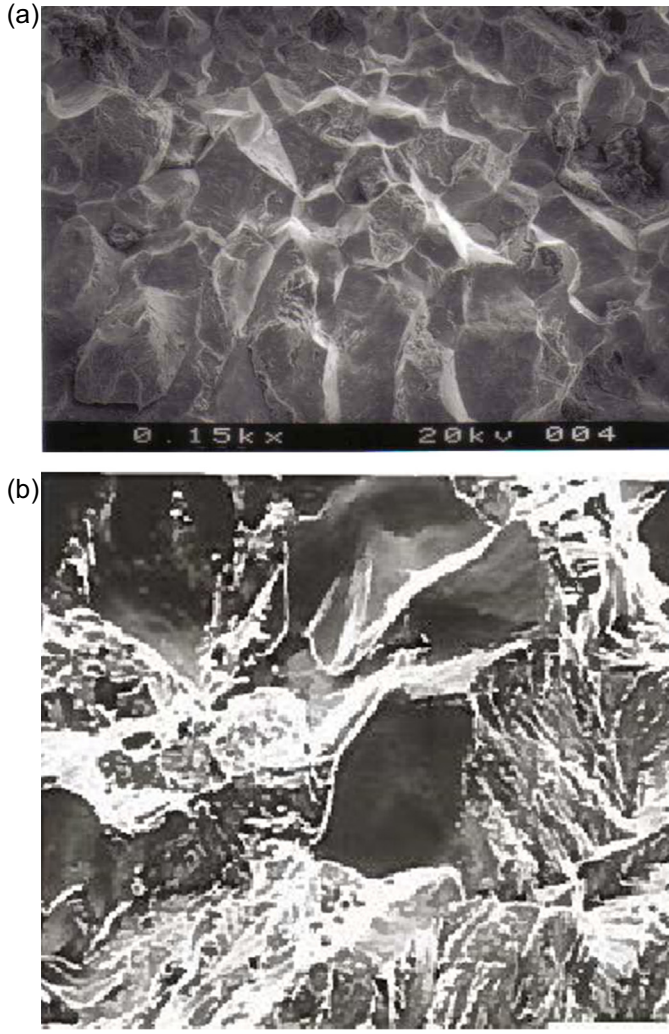

Figure 13.2 Typical failure modes of hydrogen embrittlement in steels. (a) Intergranular fracture in high strength AISI 4340 and (b) mixed fracture mode in low-strength microalloyed steel.

cleavage, and intergranular fracture have been reported [1,15]. While intergranular fracture is characteristic of HE in high-strength materials e.g., steels, in low- and medium-strength materials, hydrogen can produce mixed modes of fracture in steel as depicted in Fig. 13.2.

Today HE in its various forms has been explained by four theories: (1) internal hydrogen pressure, (2) lattice decohesion, (3) hydrogen enhanced plasticity or dislocation interaction, and (4) hydride formation. These mechanisms provide some understanding of the effect of hydrogen on the various materials in use in the oil and gas industry.

Hydrogen damage in oil and gas production can occur as a result of hydrogen entrapped in the metal during manufacturing and fabrication, being generated by corrosion, corrosion exacerbated by presence of H_2S, galvanic corrosion, and hydrogen generated by cathodic protection. Aqueous corrosion generates hydrogen in the cathodic reaction, which can diffuse into the metal. Similarly the same occurs in the presence of H_2S, which accelerates hydrogen diffusion into the metal because of inhibition of the hydrogen atom recombination reaction (recombination poisoning). In the case of galvanic corrosion, hydrogen is generated at the more noble metal. In systems that are cathodically protected, hydrogen is generated at the protected metal. The effect of hydrogen that diffuses into or preexists in the metal can vary depending on the material and strength level. In low-strength materials the effect may manifest itself in reduction in ductility or blistering, whereas in high-strength steel it reduces ductility, reduces toughness, and enhances static and dynamic cracking [4−13]. These effects are more dominant in steels, whereas in CRAs the effects are mainly, reduction in ductility, reduction in toughness, and enhanced environmental assisted cracking [2,4,14].

The following sections briefly discuss hydrogen damage exhibited by various alloys most commonly used in oil and gas.

13.2.1 Steels

Hydrogen damage in steels strongly depends on the strength level with high-strength steels being more susceptible to hydrogen effect than low strength. The types of damage that are known to occur in steel are as follows:

- HE or hydrogen stress cracking (HSC)
- hydrogen-induced cracking (HIC)
- HAC
- stress oriented hydrogen-induced cracking (SOHIC) and soft zone cracking (SZC)
- stepwise cracking (SWC)
- blistering
- high-temperature hydrogen damage

Generally, low-strength steels with less than 550 MPa (80 ksi) yield strength are less susceptible to HE compared with higher strength steels and are affected at much higher hydrogen concentrations [15]. In low strength steels, hydrogen has resulted in blistering, fissuring, delamination, void growth, and cracking. In low-strength steels such as the ones used for pressure vessels, piping, pipelines, low-strength fasteners, and structural steels for offshore platforms the effect of hydrogen is seen as reduction in tensile ductility and lower fracture toughness. Robinson and Stoltz [8] reported a reduction of fracture toughness (K_{IC}) of A516 and A106 C-Mn steel of 25%−30% at 6.9 MPa (1000 psi) and 55% at 34.5 MPa (5000 psi) gaseous hydrogen. Christenson et al. [16] reported that line pipe steel strength was not effected by hydrogen but experienced drop in ductility (reduction in area) ranging from 50% to 80%, and the fracture mode changed from microvoid coalescence to quasi cleavage. Fatigue properties have also been affected by hydrogen with increase in fatigue crack growth rate and reduction in fatigue threshold [9,17].

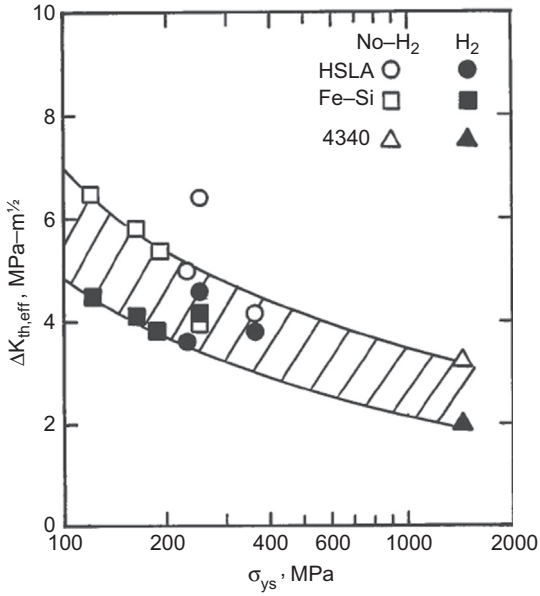

Figure 13.3 Effect of internal hydrogen on effective fatigue threshold for steels at range of strengths [21].

In high-strength steels the effect is very significant with degradation occurring at few parts per million of hydrogen. The susceptibility to HE and SCC increases with strength and hydrogen concentration. Oriani and Josephic [18] reported that for high-strength steel, hydrogen reduces the fracture toughness by 75% in 1 atm of hydrogen gas. Similarly, Gangloff [4] concluded that hydrogen can degrade the threshold stress intensity to as low as 5%–25% of the plane strain fracture toughness of high-strength alloys.

Steels with 827 MPa (120 ksi) or lower yield strengths are generally resistant to SCC and HE [19,20] in aqueous environments. Above 827 MPa (120 ksi) yield strength, K_{IEAC} decreases with the increase in yield strength with a typical threshold stress intensity value of 55–88 MPa$\sqrt{m}$ (50–80 ksi.$\sqrt{in}$) for 1000 MPa (145 ksi) yield strength quenched and tempered steels with typical fracture toughness (K_{IC}) of 220 MPa$\sqrt{m}$ (200 ksi.$\sqrt{in}$) [19,20] again reflecting the severe effect of HAC. Fatigue crack growth is enhanced and fatigue crack threshold is also reduced significantly by hydrogen in low- and high-strength steels, with internally charged samples experiencing more severe effect than in gaseous hydrogen [21,22]. Fig. 13.3 depicts the effect of internal hydrogen on fatigue threshold. The effect on threshold excluding crack closure, i.e., effective reduction due to hydrogen was in the range of 40% for high-strength steel [21].

13.2.2 Stainless steels

The effect of hydrogen on stainless steels is mainly limited to stress cracking. Solution-annealed austenitic stainless steels are considered relatively immune to hydrogen-induced stress cracking mainly as a result of their low strength and the austenitic structure that limits the hydrogen diffusion rate. Martensitic [23], duplex [24], and

precipitation-hardened stainless steels [25] are susceptible to HE and hydrogen-induced stress cracking. Rhodes [26,27] provides a summary of the environmental assisted cracking for the various type of stainless steel and CRAs in use in oil and gas production. Although the emphasis of the review was on downhole materials the same can be applied for pipelines and process facilities applications. The analyses showed that hydrogen has significant effect on duplex, martensitic, and precipitation-hardened stainless steels and less for austenitic stainless steels. Ferritic stainless steels are subject to HE in the same way as alloy steels but have limited applications because they have low strength. The effect in these alloys is complicated by the fact that it initiates by breakdown of the passive film leading to pitting corrosion and hydrogen absorption.

13.2.3 Other corrosion-resistant alloys

Nickel, titanium, copper, and cobalt-based alloys are considered more resistant to HE but not totally immune. The effect is mainly exhibited as enhanced HAC and reduction in fracture toughness. The resistance depends on the type of alloy, composition, heat treatment, strength condition; cold work versus precipitation or age hardening, and stress level. Similar to stainless steels the effect is determined by the source of hydrogen and the breakdown of the passive film that could lead to pitting and hydrogen absorption [26–29]. The material and environmental conditions under which hydrogen may effect performance of these alloys to large degree are known and can be avoided. As an example, alloys UNS N07718 and UNS N07716 are susceptible to HE when deleterious phases are present and in heat treatment conditions favored by aerospace applications [29]. Similarly, in certain grades of titanium alloys, HE is known to occur when coupled with less noble metal e.g., steel such in the case of heat exchangers if proper design is not followed.

13.3 Factors that contribute to hydrogen embrittlement and hydrogen-assisted cracking

HE and HAC are affected by environmental, operational, and metallurgical factors, with metallurgical factors being the primary elements that can be modified to improve or attain resistance to HAC.

13.3.1 Environmental factors

Hydrogen flux, as determined by severity of the environment and adsorption characteristics, plays a major role in determining the susceptibility of the material to HE and HAC. The hydrogen atoms adsorbing onto the metal or crack surfaces determine the degree of the effect in spite of the source of hydrogen, gaseous or aqueous. Factors that contribute to generation of atomic hydrogen such as lower pH, higher temperature, and cathodic poisons that inhibit hydrogen recombination will enhance the hydrogen absorption and increase the rate of HAC. The severity of HIC increases with deceasing pH and is known to depend on the alloying elements in the steel [30–32]. In plain carbon steels it can occur when the pH < 5.8 whereas in Cu-bearing steels it occurs at pH < 4.0 [31].

Similarly, hydrogen permeation decreases with the increase in pH and diminishes at pH of 7.5 but increases again at higher pH where HIC has been observed in alkaline media [31]. In addition, organic acids, chlorides, and elemental sulfur present in oil- and gas-produced fluids will increase the intensity of corrosion of steel, pitting of CRAs, and enhancement rate of HAC. Conversely, factors that reduce hydrogen generation and penetration such as increase in pH or accelerate hydrogen recombination will result in reduced rate of HAC. In the case of CRAs, the environmental factors include temperature, pH, halide ion concentration, oxygen, elemental sulfur, other oxidants, pitting tendency, and possible galvanic effect. The impact of these parameters on the resistance of CRA materials are related to the pitting resistance of the material because pitting has been proven to be the precursor to HAC and SCC. This dependence is reflected in how these materials are effected by H_2S and in the way in which the CRAs are dependent on multiple factors that cannot be generalized and require qualification of each material group with specific test requirements, strength limits (expressed as hardness), manufacturing process, heat treatment, and handling as specifically listed in NACE MR 0175/ISO 15156—Part 3 [33].

13.3.2 Effect of corrosion

Because the primary contributing source of hydrogen is corrosion reactions, corrosion has the biggest effect on HE. Practically all factors that contribute to acceleration of corrosion enhance hydrogen uptake and increase the susceptibility of materials to HE. These factors range from pH, presence of acid gases (e.g., CO_2, H_2S, SO_2, Cl_2, etc.), partial pressure of acid gases, conductivity of the corrosive media, electrochemical potential, presence of organic acids, and alkalinity. The higher the corrosion rates, the higher the hydrogen flux generated from the hydrogen dissociation reaction that occurs, adsorbs at metal surface, and diffuses into the metal [34]. In addition to the environmental conditions, metallurgical conditions that contribute to enhancing corrosion rates will have similar effect on HE. For HIC, the effect of corrosion rate may not be the same because there is evidence that even slight levels of corrosion can lead to HIC in cases where minor corrosion such as crude oil lines was detected. Although it appears that there is a critical corrosion rate below which HIC does not occur, short-term high corrosion rate during hydrotesting or swapping of hydrotest water with sour-produced fluids could lead to HIC [35].

13.3.3 Effect of H_2S

Hydrogen sulfide is present naturally in some oil and gas formations or could generate as a result of contamination of the reservoirs with sulfate-reducing bacteria (SRB) typically when water injection is used for enhanced oil recovery. H_2S contributes to hydrogen damage in two ways; first in being an acid gas that lowers the pH and intensifies corrosion, and the second the sulfide ions inhibit the recombination of hydrogen atoms promoting hydrogen atom absorption into the metal. This phenomenon, which is known as cathodic poisoning, results in high flux of hydrogen atoms that adsorb on the metal surfaces and diffuse into the metal [30]. The diffused hydrogen atoms tend to accumulate around nonmetallic particles, interfaces, and grain boundaries, leading to the various

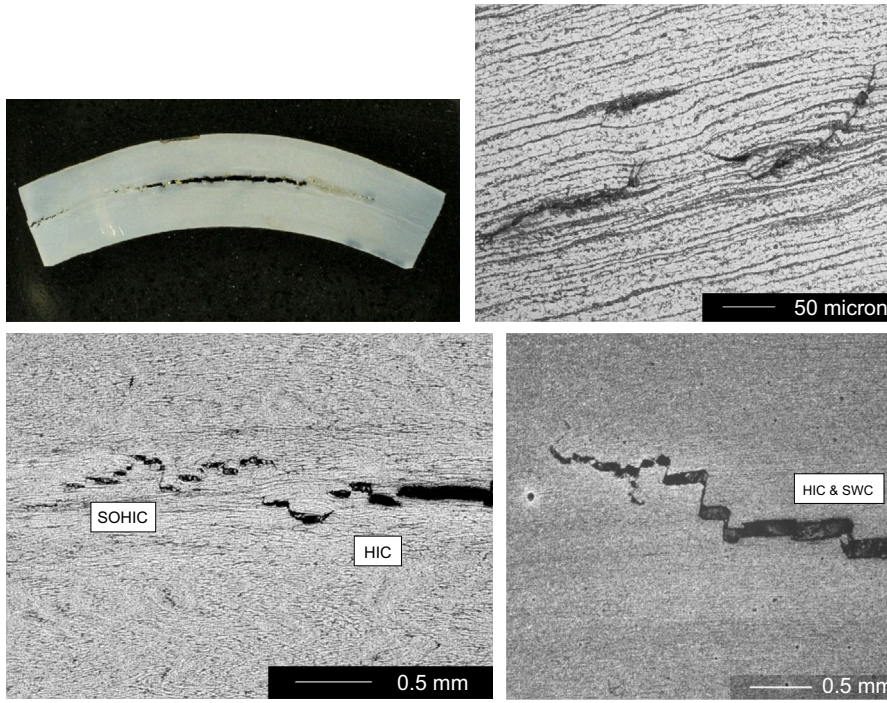

Figure 13.4 Hydrogen damage in steels showing hydrogen-induced cracking (HIC), stress oriented hydrogen-induced cracking (SOHIC), and stepwise cracking (SWC) in J-55 electric resistance welded tubing.

forms of hydrogen damage listed in previous sections and depicted in Fig. 13.1. In the cases of low-strength steels commonly used for piping, pressure vessels and pipelines in the oil and gas industry, hydrogen atoms accumulate around nonmetallic inclusions such as MnS, oxides, and oxysulfides and combine to form H_2 molecule [31]. Because H_2 molecule cannot diffuse further because of its size, it remains at these trapping sites and results in pressure buildup in the interface between the inclusion and the metal matrix. This pressure reaches very high levels leading to blistering, HIC, SWC, cracking around the inclusions and crack propagation into the metal matrix. Fig. 13.4 depicts these damages. Similarly the high flux of hydrogen atoms accelerates the diffusion of hydrogen atoms to the regions of triaxial stresses that exist internally such as at grain boundaries or the surface at stress concentrations. This leads to embrittlement and SSC in areas of tensile stresses, either applied or residual. The effect of H_2S has been shown to be an intensifier of hydrogen flux that the same damage can occur if the same level of hydrogen permeation is produced with and without H_2S as shown in Fig. 13.5 [32].

SSC and associated H_2S cracking have been one of the most studied areas since 1950 because of their wide impact on oil and gas production, refining, and transportation, an effort that led to the development of guidelines, materials requirements, and testing methodology. NACE MR 0175/ISO 15156 Part 1, 2, and 3 and NACE MR 0103/ISO 17945

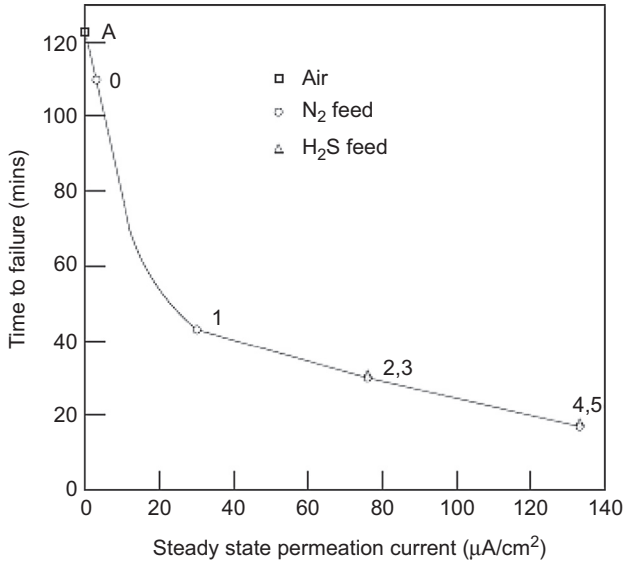

Figure 13.5 Effect of H_2S on hydrogen embrittlement of steel from ref. [32] showing the same effect when the permeation rate is equal (2 and 3) and (4 and 5) in the presence and absence of H_2S, respectively.

provide guidelines on acceptable materials, limitation on environment, and hardness for steels and nonferrous alloys [33,36]. NACE TM 0177, NACE TM 0198, NACE TM 0284, and EFC 16 provide guidelines on standards for evaluating the various H_2S effect on materials [37–40].

Table 13.1 summarizes the effect of hydrogen on materials that can occur in aqueous H_2S environment, the materials that are susceptible to damage, and the conditions that can promote it [30]. The effect is most severe at ambient temperature and decreases with increase and decrease in temperature. The decrease in severity of H_2S effect at lower temperatures has been attributed to decrease in hydrogen production and lower diffusion rate of hydrogen atoms. At higher temperatures the diffusion rates increase because of increase in thermal energy, which results in less hydrogen being trapped in the metal [30]. The latter effect is very significant, which renders SSC susceptible steels at ambient conditions to be SSC resistant at higher temperature, e.g., nonsour grades high-strength steel downhole tubulars as shown in Table 13.2 [33].

H_2S corrosion also results in the formation of iron sulfide corrosion product, which can be present in various forms depending on the temperature. The FeS is fast forming and adherent that when stable, it is an effective barrier to corrosion but because of the conductive nature of FeS a breakdown of the protective scale can lead to accelerated corrosion rates in tens of millimeters per year. Among the elements that impact the stability of the FeS protective layer are chlorides and organic acids. These effects continue to undermine reliance on FeS film as a way to reduce corrosion despite the success in the use of carbon steel downhole tubulars in the production of sour gas fields in Canada, France, and Germany without the use of corrosion inhibition.

Table 13.1 Types of hydrogen effects

Type of hydrogen damage	Hydrogen	Environment	Stress state	Strength level	Temperature	Nonmetallic impurities
Sulfide stress cracking	Atomic form	Low corrosivity	Tensile stress	High strength >500 MPa	Max risk 15−30°C (59−86°F)	Affects
Hydrogen embrittlement	Atomic form	Low corrosivity	Tensile stress	High strength >1000 MPa	Increases with temperature	Affects
Hydrogen-induced cracking	Molecular	High corrosivity	No applied stress	Low strength < 500 MPa	Max risk 20−30°C (68−86°F) Low risk <5°C (41°F) and >60°C (140°F)	Significantly affects
Stress-oriented hydrogen-induced cracking	Atomic form	High corrosivity	No applied stress	Low strength < 500 MPa	Max risk 20−30°C (68−86°F) Low risk <5°C (41°F) and >60°C (140°F)	Affects
Hydrogen blistering	Molecular	High corrosivity	No applied stress	Low strength < 500 MPa	Max risk 20−30°C (68−86°F) Low risk <5°C (41°F) and >60°C (140°F)	Significantly affects
Stress corrosion cracking	Atomic form	High corrosivity	Tensile stress	High strength	Increases with temperature	Affects
Metal hydrides	Atomic form	Low corrosivity	No applied stress	All levels	Increases with temperature	Unknown

Based on Table 24.1 of reference R.D. Kane, Sulfide stress cracking, in: R.W. Revie (Ed.), Oil and Gas Pipelines: Integrity and Safety Handbook, first ed., John Wiley & Sons, Inc., 2015, pp. 343−352 (Chapter 24).

Table 13.2 Effect of temperature on sulfide stress cracking susceptibility of steel

For all temperatures	For ≥ 65°C (150°F)	For ≥ 80°C (175°F)	For ≥ 107°C (225°F)
ISO 11960[a] grades: H40 J55 K55 M65 L80 type 1 C90 type 1 T95 type 1	ISO 11960[a] grades: N80 type Q C95	ISO 11960[a] grades: N80 P110	ISO 11960[a] grade: Q125[b]
Proprietary grades as described in A.2.2.3.3	Proprietary Q&T grades with 760 MPa (110 ksi) or less maximum yield strength. Casings and tubulars made of Cr-Mo low-alloy steels as described in A.2.2.3.2.	Proprietary Q&T grades with 965 MPa (140 ksi) or less maximum yield strength	

Temperatures given are minimum allowable service temperatures with respect to sulfide stress cracking. Low temperature toughness (impact resistance) is not considered, equipment users shall determine requirements separately.

[a]For the purposes of this provision, API 5CT is equivalent to ISO 11960:2001.

[b]Types 1 and 2 based on Q&T, Cr-Mo chemistry to 1036 MPa (150 ksi) maximum yield strength. C-Mn steels are not acceptable.

13.3.4 Effect of cathodic protection

Cathodic protection by sacrificial anodes and impressed current systems coupled with organic coatings are the primary means of protection against external corrosion in immersion conditions, particularly in offshore environments. HE is known to occur in cathodically protected structures as a result of hydrogen evolution at metal surface whenever the potential becomes more negative than the equilibrium potential for hydrogen evolution typically—800 mV versus Ag/Ag-AgCl in seawater [41]. The severity of HE increases, the more the potential drops below the −800 mV. Both sacrificial anodes and impressed currents generally produce much lower potential either inherent to the sacrificial anode material used or through lack of control of the impressed current output. This effect has been experienced in steels, martensitic stainless steels, duplex stainless steels, and nickel alloys. It started with reported failures in the 1980s of K-Monel 500 riser clamp bolts [42], HE of UNS N 05500 nonmagnetic drill collar, and cracking of high-strength steel legs of jack-up rigs [43]. Failures extended to subsea high-strength steel bolts, martensitic stainless steel, and duplex pipelines [41] as the use of CRA materials expanded particularly in deepwater applications where high-strength and corrosion-resistant materials were needed.

To avoid the risk of HE historically the strength and welding of the material are controlled. For example, alloy steel fasteners were limited to ASTM A320 L7M [44] and ASTM A193 B7M [45] grades with a maximum hardness of 22 HRC (Rockwell C hardness) (235 HB), i.e., the specified limit for sour service applications per MR 0175/ISO 15156 [33]. Because in the absence of cathodic protection, high-strength steels are typically more resistant to environmental assisted cracking (EAC) up to 124 MPa (180 ksi) tensile strength (∼40 HRC) [46,47], for cathodically protected components, it was recognized that limiting subsea fasteners to the sour service requirements is overly conservative and have shown that subsea fasteners exposed to cathodic protection can be used to a maximum hardness of 34 HRC (313 HB) per ISO/DIS 13628-1 recommended practice and API 17D [48−51]. Esaklul and Martin [52] showed that high-strength steels fasteners with hardness > 34−35 HRC are susceptible to EAC, and UNS 0718 and UNS 07725 are immune to EAC in the presence of cathodic protection at overprotection levels.

Several failures of martensitic and duplex stainless steels due to HE generated by cathodic protection have been reported [41,53−58]. Failures have occurred at high stressed areas such as fillet weld toes, flowline hub connector, girth welds, and anode pad welds. The failures were due to HAC and occurred at areas of high stress concentration and residual stresses where the localized stresses exceeded the actual yield strength. To avoid such failures control of plastic strain to below 0.5% and cathodic protection potential more negative than about −850 mV, SCE have been recommended. When control of cathodic protection (CP) potential is not possible, components should be designed with displacement and stress control [55,59]. Cracking also has been associated with unfavorable microstructure; large grains, presence of intermetallic phases; and high ferrite content in welds [57,59]. The effect is the same in duplex and superduplex stainless grades [59]. It appears that there is no detrimental CP effect in soil of either over or under protection, and there are no reported failures of either duplex or supermartensitic buried pipelines [60].

The effect of CP on pipeline steels has been studied since the late 1970s with no evidence of significant effect. Hinton and Procter [61] showed that there is no effect at potential of −800 mV, reduction in tensile ductility of X-65 steel when the CP potential is less than −800 mV, but fatigue crack growth increased at the −800 mV level, indicating a difference in hydrogen interaction at the crack tip than in the bulk. Similar results were obtained by Cabrini et al. [62] for steels with yield strength in the range of 400−600 MPa (58−87 ksi), and the best resistance to HE was observed in the steel with the tempered martensitic fine microstructure. Cabrini et al. [63] reported that steels with tensile strength in the range of 530−860 MPa (77−125 ksi) are not susceptible to HE by cathodic protection under static load up to the yield strength even at very negative CP potential. However, HE occurred when samples were subject to continuous or slow straining. They also observed that quench and tempered martensite with fine precipitate offered better resistance to HE than banded microstructure with the coarse-grained banded structure showing the highest susceptibility. Elboujdaini and Revie [64] reported loss in ductility in X-70, X-80, X-100, and X-120 steels when subject to cathodic protection, with X-100 and X-120 showing the highest susceptibility. Schoneich [65] also reported that CP overprotection will lead to HE in steels with yield strength $>$ 550 MPa (80 ksi), X80, or higher and/or a hardened steel surface such as the ones caused by third-party damage combined with pressure fluctuations. The paper concluded that to avoid HIC, cathodic overprotection should be controlled to >-1200 mV in buried pipelines that are subject to more than 1 pressure cycle per day.

Robinson et al. [66] studied the effect of increase in CP that is typically applied when SRB presence is suspected in high-strength low-alloy steel in use for offshore structures and confirmed that crack growth rates are enhanced and the threshold decreased with increase in hydrogen absorption that occurs with increase in the level of CP. Presence of SRB resulted in an increase in crack growth rate and reduction in K_{th} but did not change the failure mechanism. The effect of SRB in enhancing hydrogen absorption is believed to be a consequence of the generated H_2S and its inherent effect as cathodic poison.

Mitigation of CP-induced HE can be attained by control of the CP polarization level, which also limits the current, hence limiting the amount of hydrogen generated at the metal surface. Reduction of the polarization level from −1000 mV Ag/AgCl to −800 mV could reduce the current by a factor of 100 [48,68]. It is suggested that low potential cathodic protection can be reached by low potential sacrificial anodes or by diode control [51,67]. Al-0.1% Ga and Al-0.5% Cu type of anode chemistry produce lower potential than typical chemistries in use for sacrificial anodes. These options may not be effective because they may not provide sufficient protection and will require effective isolation from other structures [51,67,68].

In titanium alloys, HE can occur as a result of CP or galvanic coupling with pure titanium, ASTM Grades 1 and 4 are more sensitive to hydride formation, and alloyed ASTM Grades 5, 7, and 12 do not appear to be susceptible to hydride formation even at negative potential as low as −1400 mV SCE [69]. Schumerth and Demers [70] reported on several cases of titanium and ferritic stainless steel condenser tube failure due to HE. They attributed the failures to improper design and/or improper control and use of CP system. They also recommended the potential not to exceed −800 mV

SCE for ferritic stainless steel, −900 to −1000 mV SCE for titanium, magnesium anodes should be avoided owing to their high negative potential, and anodes should be placed at minimum 30 in. away from the tubesheet.

13.3.5 Effect of alloying elements and microstructure

Demand for higher strength and toughness to meet the need of the vast expansion of oil and gas production into deeper wells and remote offshore deepwater fields has also increased the need for higher strength materials that are more SSC and HAC resistant. Because strength and mechanical properties are determined by the alloy composition and microstructure, both SSC and HAC equally depend on chemical composition of the material, processing, and strengthening conditions including heat treatment and final microstructure. Development of such materials has evolved over time from the development of the various grades of SSC-resistant downhole tubulars grades such as L-80, T-90, T-95 and proprietary grades such as C-110 and higher strength pipeline grades such as API 5L X-70, X-80 and X-100. Similarly, higher strength CRAs to meet the HAC resistance have been developed to maximize the SSC resistance with optimum alloying content.

In steels the alloying elements are typically added to increase toughness and ductility and control the type and shape of the second-phase precipitates and inclusions to reduce the effect of hydrogen. In low-alloy steels that are commonly used in oil and gas and petrochemical operations, the alloying elements that are typically present are C, Mn, Si, Cr, Ni, Mo, Cu, Al, Nb, V, Ti, Pb, S, P, and possibly rare earth metals (Ce, La, Y). Although the alloying elements contribute to the hardenability and precipitation of carbide particles, they have minor mixed effect on HAC. The elements that have the most effect on HAC are C, Mn, Al, S, and P [15].

Increase in carbon content decreases the resistance to HE, and the effect depends on the heat treatment and microstructure. In general, increase in carbon leads to an increase in corrosion, which enhances the hydrogen entry into the steel.

The effect of Mn is dependent on C, S, and P levels but in general is detrimental to HAC because of the formation of MnS inclusions, and at higher than 1.0% it has the tendency to segregate in the ingot and produce hard zones within the ferritic−pearlitic microstructure.

The increase in S is known to be detrimental to HAC because of its strong tendency to segregate into grain boundaries and formation of sulfide particles. Sulfides can form and elongate during hot rolling and become hydrogen traps within the steel matrix. Control of the shape of and the level of sulfide inclusions is necessary to improve the HAC resistance. Phosphorus is similar to S in terms of segregation to grain boundaries and segregates along with Mn to form hard bands that are more susceptible to HAC.

The effect of microstructure on HAC is much more important than the chemical composition, mainly because of its effect on trapping of hydrogen. Coarse microstructures such as coarse pearlite and second-phase particles tend to have the highest trapping efficiency followed by bainite and the least is martensite [15]. In steels, it is recognized that quenched and tempered microstructures with low dislocation density and fine distribution of spherical carbides produce the highest resistance to SSC. The presence

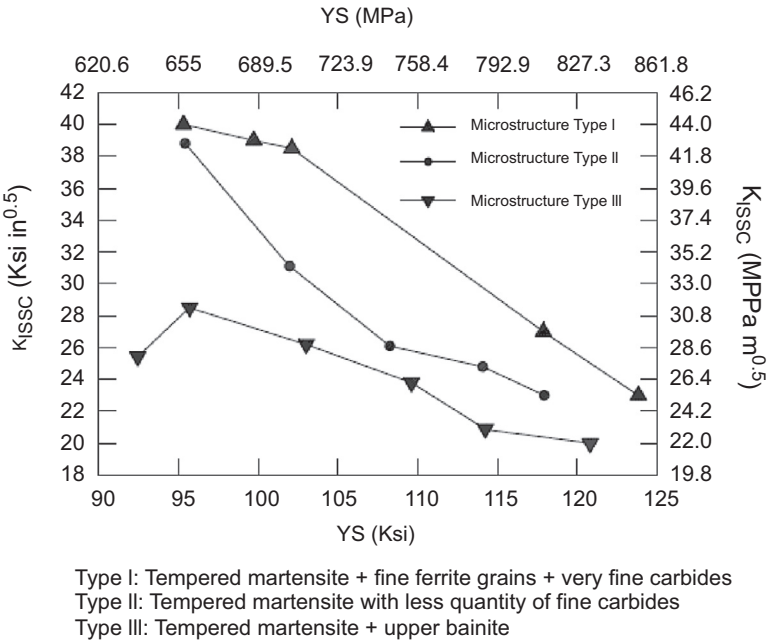

Figure 13.6 Effect of steel microstructure on sulfide stress cracking resistance [71]. Reproduced with permission from Springer.

of upper bainite results in a drastic drop in SSC resistance as can be seen in Fig. 13.6 [71]. Steel chemistry, microalloying additions, controlled rolling, and heat treatment such as double quench and temper have been optimized to obtain homogeneous fine grain quenched and tempered martensitic microstructure with high strength and improved resistance to SSC. The additions of the microalloying elements increase the strength, suppress austenite grain growth, and refine the carbide size that decreases the dislocation density and hydrogen traps. Control of S and P contents and addition of Ca minimize sites for hydrogen accumulation [27]. Omura et al. [72] showed that optimization of steel chemistry, microstructure, and processing can result in fully resistant SSC tubulars 95 and 110 ksi yield strength grades. Control of the inclusion shape is critical to the SSC resistance of all sour service grades. Presence of MnS inclusion stringers had led to failures of L-80 grades casing and tubing, which are considered fully resistant to SSC [27].

In pipelines, the most critical damage mechanism is HIC, which is purely controlled by steel chemistry and microstructure. SOHIC and SZC are rare forms of cracking that occur in low-strength steels and to a large degree effected by the same parameters as HIC. HIC is more prevalent in longitudinal welded pipe that is made of rolled plate where the chemical composition and the manufacturing process of the skelp (flat rolled plate) used to make welded pipe results in banding and encourages the formation of the inhomogeneities responsible for trapping of diffusing hydrogen atoms. HIC is known to occur at low H_2S concentration as low as few parts per million if other corrosive conditions exist and at all strength levels. The severity of HIC increases with drop

in pH but can occur even with minor corrosion if sufficient hydrogen is generated. HIC highest effect has been observed in the laboratory at ambient temperature 25°C (77°F) with failures that have been reported in pipelines that operate at 17°C (63°F)−85°C (185°F). In addition, HIC damage does not require pressure or stress [35,73]. Testing for HIC is done at ambient conditions with no applied stress [40,64]. The most critical factor in HIC is the microstructure, which is determined by the steel chemical composition, steel making, processing, and heat treatment. Formation of nonmetallic inclusions, inhomogeneities, and secondary phases will trap hydrogen and lead to HIC. Any elements, or process cycle, that contribute to the formation of these constituents will contribute to HIC. Among the most detrimental inclusions are MnS, which appear in two forms: Type I and Type II, with Type II being the most detrimental. Type-II MnS are the "pancake" type, which form mostly in Al−Si fully killed steels as a result of elongation of the soft MnS inclusions along the rolling direction during hot working of the plate or skelp. They can form at any depth in the plate thickness oriented 90 degree to the hydrogen diffusion path. Their presence blocks the hydrogen atoms diffusion through the steel and become a trap for hydrogen accumulation, leading to blistering and cracking. Type-I MnS inclusions form in Si-semikilled steels and solidify before the rest of the steel in the form globular shape particles that do not easily deform during the hot working operation. These inclusions have much less tendency to trap hydrogen [35,73]. The effect is also dependent on the rolling temperature where the optimum hot rolling temperature for steel that contain Type-II MnS inclusions is 1000°C (1832°F) likely as a result of the close deformability of MnS inclusions to the steel i.e., inhibits elongation and flattening of the MnS inclusions [74]. The author had experienced failure of new pipe that met API 5L Annex H chemical requirements manufactured in 2015 to pass the HIC test (NACE TM 0284 Method A), highlighting the criticality of both the steel chemistry as well as the hot rolling process. The HIC cracks appeared to initiate at carbide precipitates at grain boundaries and were likely a result of hot rolling of the skelp below 900°C (1652°F). Fig. 13.7 depicts the observed HIC cracks.

The second group of inclusions are aluminum oxide, silicates, iron oxide, and slag, which could result from the presence of excess aluminum in Al-killed steel, lack of proper degassing, and cropping of the ingot. These inclusions tend to be brittle and would crack during hot working operations, resulting in voids that serve as hydrogen traps. Similar effect could result if clustering of strengthening particles occur such as niobium carbonitrides or rare-earth inclusions such as CeS [35,73]. Formation or agglomeration of second-phase particles during any step in the processing of the steel plate can lead to increase in HIC susceptibility as seen in X-70 steel when heat treatment during rolling resulted in the formation of Fe_3C at the fine grain acicular ferrite grain boundaries, increasing the level of hydrogen traps [74].

Another microstructural inhomogeneity that can lead to HIC is anomalous microstructure, microthin layers of very hard material that form in the pearlite bands parallel to the rolling direction of the plate, which develops during the plate cooling. These layers are rich in Mn, P, and C to a lesser degree, which result in high level of segregation of these elements and formation of martensite/bainite upon cooling, leading to local hard zones. Hardness values of 272 VPN (25 g) to 400 VPN (50 g load) were reported for these bands

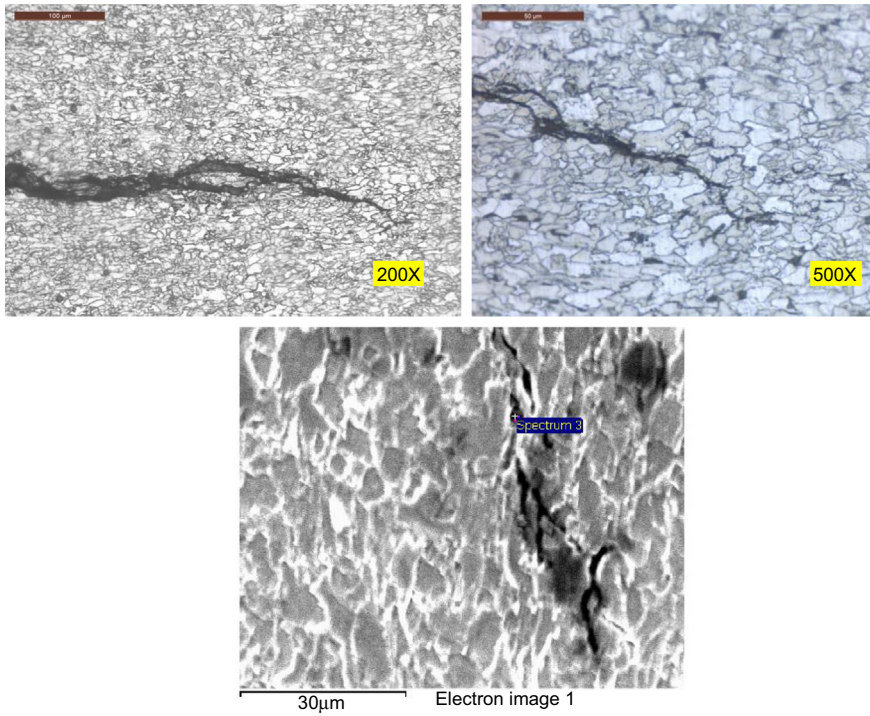

Figure 13.7 Hydrogen-induced cracking cracks in API 5L X60 steel that resulted from testing using Method A solution.

[74]. These hard bands will likely crack as a result of SSC but because the failure occurs in low-strength steels, they are included as HIC mechanism. The anomalous microstructures are common in electric resistance welded pipe and downhole tubulars because of the local heating in the weld zone and the flow bands that curve toward the ID and OD of the pipe. Their orientation along the flow bands render them to be oriented near 90 degree to the rolling direction, and when they crack, they link and could become through thickness path [73] as shown in Fig. 13.8.

Selection of steel chemistry and process conditions controls the level, size, and shape of the nonmetallic inclusions and center segregation that determines the resistance to HIC. Sulfur, being the most critical element where if controlled to low levels and Ca treatment, is utilized to prevent the formation of elongated MnS and maintain the inclusions in spherical shape, HIC resistance steel can be produced. Today, steels can be produced by controlled rolling and accelerated cooling to produce fine bainitic microstructure to meet the most stringent requirements of HIC resistance [31].

The resistance of CRAs to HAC depends greatly on the alloy chemistry, melting practices, processing, heat treatment, strength, microstructure, and final finished condition of the material. Because most of the CRAs gain their strength through either cold work, heat treatment (precipitation hardening and/or aging), the resultant microstructure, size, and distribution of strengthening particles and/or phases play a major role on how they

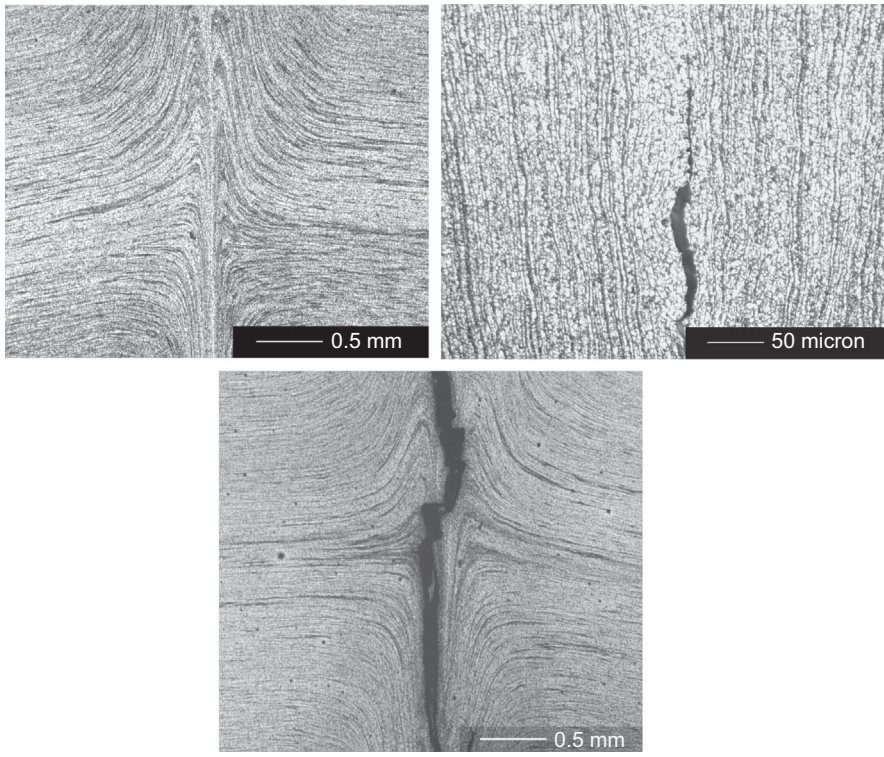

Figure 13.8 Cracking in flow bands in electric resistance welded pipe in J-55.

interact with diffusible hydrogen and if these phases or particles act as trap sites. The key factors in reducing the risk for HAC is control of the microstructure through minimizing or eliminating of untempered martensite, deleterious phases, and control of precipitate size and distribution. In martensitic stainless steel the key issue is control of untempered martensite through control of the heat treatment process or use of double tempering to transform all untempered martensite. In addition, the degree of cleanliness and control of carbides also contribute to the resistance to HAC [26,27]. For duplex stainless steel, the issue is control of the microstructure in terms of the austenite and ferrite phases, austenite spacing [58] and control of cold work process to avoid the transformation and formation of deleterious phases such as sigma phase [26]. In precipitation-hardened stainless steel the primary controlling factors are the size and distribution of the precipitate and the absence of deleterious phases such as Ý, sigma, and delta. In nickel alloys grain boundaries precipitation play a major role in the HAC resistance of high-strength nickel alloys with HAC K_{th} to decrease significantly with increase in grain boundary precipitation [75]. HAC failures have been experienced in alloys with high concentration of grain boundary precipitates [29,76]. Similarly the resistance improves with grain boundary cleanliness and control of deleterious phases such as delta, which requires control of chemistry e.g., Nb content, homogeneity of the microstructure, solution annealing, and precipitation-hardening procedures such as the

case for UNS N07718. This can be attained through refinement and control of the alloying elements that contribute to the formation of the deleterious phases, melting/refining and forging ratio, solution annealing to be above the solidus temperature for delta phase, allowing sufficient time for Nb and Ni that make up the delta phase to go back into solution, and controlling time and temperature to prevent precipitation of deleterious levels of delta phase during precipitation hardening [77]. Jebaraj et al. [78] also showed how metallurgical conditions effecting HE of UNS N07718 depend on hydrogen uptake, diffusion, trapping, and permeation, indicating that irreversible traps in cold-worked and preci pitation-hardened conditions contribute to the alloy-increased HAC resistance in these conditions. Foroni and Malara [28] showed that resistance to HE for precipitation-hardened Ni alloys depends on the chemical composition, grain size, and precipitation at grain boundaries. They observed that UNS N07718—140 ksi MYS, UNS N09935—110 ksi MYS, and UNS 09925—110 ksi MYS have the least susceptibility to HE, whereas N07718—120 ksi still has low susceptibility but more than N07718—140 ksi MYS. Their results also showed that both N07716—120 and N07716—140 ksi were highly susceptible to HE, and the results of N07716 are consistent with what was observed by Kemion et al. [76].

For cold-worked CRAs, the HAC susceptibility is also dependent on the microstructure and precipitation of second-phase particles. In addition, cold-worked high Ni alloys experience increased susceptibility to HAC because of low temperature aging (LTA), which has been attributed to A_2B-type long-range ordering [26]. Increased susceptibility had been observed at temperature as low as 150°C and most severe at 500°C aging temperature.

13.4 Summary

Hydrogen as small atom has the ability to diffuse into metals and effect material properties. The effect on materials is well established with significant impact on the mechanical properties of steels and CRAs. The most notable effects are reduction in ductility, fracture toughness, and increase in static and dynamic crack growth rates. The effects are evident in both low- and high-strength steels and CRAs. These effects are exacerbated in the presence of H_2S because it inhibits the recombination reaction and intensifies the hydrogen absorption into the metal. The theories that have been proposed to explain the HE phenomena still fall short in providing a full view of the parameters that control materials behavior in the presence of hydrogen and how the materials composition and microstructure play a role in controlling the susceptibility of materials to HE. The vast research has enabled engineers to understand the various effects of hydrogen and how to manage these effects through control of environment, selection of materials, processing, and fabrication. The evolution of standards and guidelines that cover materials limitation in cases such as materials in H_2S service or subject to cathodic protection has contributed to the reduction of risk of failure due to HE, SSC, and HIC but have not eliminated the risk because failures continue to occur. The oil and gas industry has experienced major costly failures that the root cause could not be easily identified such as the case of Kashagan pipeline SSC failures. Other cases

such as failing to pass HIC tests of HIC-resistant pipeline steel reveal that the effect of the manufacturing processes is not fully recognized. Similarly, failures of high-strength steel fasteners in subsea applications reveal that the effect of sacrificial coating and cathodic protection on fasteners is still controversial. These examples demonstrate that the effect of HE, in its various forms, remains a challenge to researchers and practitioners, and the opportunity for developing more cost effective materials that are immune to HE and SSC still exists.

13.5 Knowledge gaps and research trends

Continuing research into the elusive causes of HE and development of better understanding and models that can help explain the behavior of materials in the presence of hydrogen-inducing environments is vitally important to the development and continuous improvement of materials resistance to HE. New mechanisms such as the ones proposed by Neeraj and Srinivasan [79] of the impact of microstructure and type of hydrogen traps that can be present in any material is well established, but considerable discrepancies still exist with regard to which constituent of the microstructure plays the major role in increasing or decreasing the susceptibility and at what stress level. It appears that most of the data generated in the past that defined the operating envelop of the materials in use in oil and gas industry have been based on the assumption that materials will not experience loads near or at the specified minimum yield strength; however, experience showed that there are circumstances where the stresses have intentionally or unintentionally exceeded the yield strength and may have led to failures. Defining the true resistance of materials, particularly CRAs, to HE remains a challenge, and if the material has resistance beyond the yield strength, is this sufficient to classify materials as fully resistant to HE. Also, the effect of microstructure can be elusive because there are no common specifications that control the acceptable microstructure to the degree that distinguish the HE resistance of materials that fall within the requirements of chemical composition and heat treatment such as degree of carbides in Ni alloys e.g., UNS N07716, UNS N07718—120 ksi versus UNS N07718—140 ksi, or the degree of banding in steels that can be allowed for HIC resistance. Current standards do not, and in many cases cannot, control these factors to a level that ensures full resistance to HE. Debate is still on going on what is the acceptable test for qualification of materials and method of introducing hydrogen into the metal, length of test, and effect of baking treatment [76,80]. There are still gaps that need to be addressed. They are as follows:

- What is the maximum acceptable stress level both under normal and upset or unusual events that a material should withstand in HE-inducing environment
- What level of ductility reduction that can be accepted and still consider a material resistant to HE
- What tests are acceptable to demonstrate resistance to HE, particularly for CRAs, and how to reconcile discrepancies between tests [80]
- Impact of metallic coatings on HE of fasteners
- Acceptable barrier coatings to prevent hydrogen ingress into metals

- Common models that can predict the HE and HAC of materials
- Role of irreversible traps on resistance of materials to HE
- Synergistic effect of pitting parameters (pH, Cl^-, and pH_2S) on SSC of CRAs to determine the threshold limits of materials and develop more cost-effective materials for harsh applications [81]
- Impact of adsorbed hydrogen on stability of protective films and its synergistic effect in combination with Cl^- and pH [81]
- Verification testing of CRAs that have been grandfathered into SSC standards with no traceable test data or field experience to confirm their true resistance to SSC
- Understanding of the factors that contribute to forming of microhard spots that appears to have led to major SSC failures in high-quality pipeline steel
- Inspection technologies for detection of incipient HIC and SWC
- Acceptance criteria for degree of banding in steel plate used for manufacturing of pressure vessels and welded pipe used in sour service applications.
- Acceptable testing methods and duration for moderate- and low-sour service conditions (API 5L Committee WG 4232 Moderate Sour Service standards new initiatives).

References

[1] S.P. Lynch, Understanding mechanism of hydrogen embrittlement and stress corrosion cracking, in: Paper No. 07493, NACE Corrosion Conference, 2007.
[2] H.K. Birnbaum, Mechanisms of hydrogen related fracture of metals, in: N.R. Moody, A.W. Thompson (Eds.), Hydrogen Effects on Materials Behavior, 1990, pp. 639−658. TMS.
[3] B. Craig, Hydrogen Damage, ASM Handbook Volume 13A, Materials Park, Ohio, pp. 367−380.
[4] R.P. Gangloff, Hydrogen assisted cracking of high strength alloys, Comprehensive Structural Integrity, I. Milne, R.O. Ritchie, B. Karihaloo (Editors-in-Chief), vol. 6, Elsevier Science, New York, NY, 2003.
[5] P. Bastien, P. Azou, Effect of hydrogen on the deformation and fracture of iron and steel in simple tension, in: C.D. Beacham (Ed.), Hydrogen Damage, ASM International, Metals Park, Ohio, 1977, pp. 76−93.
[6] M.R. Louthan Jr., G.R. Caskey Jr., J.A. Donovan, Hydrogen embrittlement of metals, in: C.D. Beacham (Ed.), Hydrogen Damage, ASM International, Metals Park, Ohio, 1977, pp. 289−300.
[7] S.P. Lynch, N.E. Ryan, Mechanism of hydrogen embrittlement − crack growth in a low alloy ultra-high-strength steel under cyclic and sustained stresses in gaseous hydrogen, in: C.D. Beacham (Ed.), Hydrogen Damage, ASM International, Metals Park, Ohio, 1977, pp. 369−376.
[8] S.L. Robinson, R.E. Stoltz, Toughness losses and fracture behavior of low strength carbon-manganese steels in hydrogen, I.M. Bernstein, A.W. Thompson (Eds.), Hydrogen Effects in Metals, Conference Proceedings the Metallurgical Society of AIME, pp. 987−995.
[9] H.F. Wachob, H.G. Nelson, Influence of microstructure on the fatigue crack growth of A516 in hydrogen, in: I.M. Bernstein, A.W. Thompson (Eds.), Hydrogen Effects in Metals, Conference Proceedings the Metallurgical Society of AIME, 1980, pp. 703−710.
[10] H. Cialone, R.J. Asaro, Hydrogen effects in the fracture of spheroidzed plain carbon steel, I.M. Bernstein, A.W. Thompson (Eds.), Hydrogen Effects in Metals, Conference Proceedings the Metallurgical Society of AIME, pp. 767−774.

[11] T. Inoue, K. Yamamoto, M. Nagumo, Hydrogen embrittlement of steels with intergranular fracture mode, I.M. Bernstein, A.W. Thompson (Eds.), Hydrogen Effects in Metals, Conference Proceedings the Metallurgical Society of AIME, pp. 777–784.
[12] B. Craig, G. Krauss, The resistance of highly tempered 4130 steels to hydrogen stress cracking, I.M. Bernstein, A.W. Thompson (Eds.), Hydrogen Effects in Metals, Conference Proceedings the Metallurgical Society of AIME, pp. 795–802.
[13] B.J. Shaw, E.W. Johnson, An evaluation of hydrogen embrittlement in Cr-Mo pressure vessel steels, I.M. Bernstein, A.W. Thompson (Eds.), Hydrogen Effects in Metals, Conference Proceedings the Metallurgical Society of AIME, pp. 691–700.
[14] W.W. Gerberich, N.R. Moody, C.L. Jensen, C. Hayman, K. Jatavallabhula, Hydrogen in X/B and all B titanium system: analysis of microstructure and temperature interaction on cracking, I.M. Bernstein, A.W. Thompson (Eds.), Hydrogen Effects in Metals, Conference Proceedings the Metallurgical Society of AIME, pp. 731–743.
[15] E. Lunarska, Hydrogen-induced degradation of low-carbon steel, in: R.A. Oraini, J.P. Hirth, M. Smialowski (Eds.), Hydrogen Degradation of Ferrous Alloys, Noyes Publication, 1985, pp. 712–736.
[16] D.J. Christenson, I.M. Bernstein, A.W. Thompson, E.J. Danielson, E.M. Elices, F. Gutierrez-Solana, Hydrogen compatibility of a line pipe steel, I.M. Bernstein, A.W. Thompson (Eds.), Hydrogen Effects in Metals, Conference Proceedings the Metallurgical Society of AIME, pp. 997–1004.
[17] K.A. Esaklul, A.G. Wright, W.W. Gerberich, An assessment of internal hydrogen vs. closure effects on near-threshold fatigue crack propagation, in: Fatigue Crack Growth Threshold Concepts, 1983, pp. 299–326. Philadelphia, PA, USA.
[18] R.A. Oraini, P.H. Josephic, Equilibrium aspects of hydrogen-induced cracking of steels, Acta Metallurgica 22 (1974) 1065–1074.
[19] Atlas of Stress Corrosion Cracking Data, ASM International, 1984.
[20] J.H. Bickford, An Introduction to the Design and Behavior of Bolted Joints, second ed., Marcel Deckker, Inc., 1990, p. 560.
[21] K.A. Esaklul, The Effect of Internal Hydrogen on Near-threshold Fatigue Crack Propagation in Iron Base Systems (Ph.D. thesis), University of Minnesota, December 1983.
[22] T. Livne, X. Chen, W.W. Gerberich, Temperature effects on hydrogen assisted crack growth in internally charged AISI 4340 steel, Scripta Metallugica 20 (1986) 659–662.
[23] Y. Chung, K.R. Pytlewski, D.M. McGarry, Hydrogen embrittlement cracking of 16Cr-5Ni martensitic stainless steel in seawater, in: Paper No. 01229, NACE Corrosion Conference, 2001.
[24] W. Zheng, D. Hardie, Effect of structural orientation on the susceptibility of commercial duplex stainless steel to hydrogen embrittlement, Corrosion 47 (10) (1991) 792–799.
[25] G. Emygdio, A. Zeemann, Failures of 17-4 PH steel parts in non sour environments, in: Paper No. 4298, NACE Corrosion Conference, 2014.
[26] P.R. Rhodes, Environment-assisted cracking of corrosion resistant alloys in oil and gas production environments: a Review, Corrosion 57 (11) (2004) 923–966. NACE International.
[27] P.R. Rhodes, L.A. Skogsberg, R.N. Tuttle, Pushing the limits of metals in corrosive oil and gas well environments, Corrosion 63 (1) (2007). NACE International.
[28] L. Foroni, C. Malara, Hydrogen embrittlement susceptibility of precipitation hardened Ni-alloys, in: Paper No. 3948, NACE Corrosion Conference, 2014.
[29] P. Nice, G. Rorvik, R. Strong, J.H. Olsen, W.M. Bailey, T.G. Mobberley, Hydrogen embrittlement failure of precipitation hardened nickel alloy subsurface safety valve component installed in a North Sea seawater injection well, in: Paper No. 3892, NACE Corrosion Conference, 2014.

[30] R.D. Kane, Sulfide stress cracking, in: R.W. Revie (Ed.), Oil and Gas Pipelines: Integrity and Safety Handbook, first ed., John Wiley & Sons, Inc., 2015, pp. 343−352 (Chapter 24).
[31] N. Ishikawa, Design of steels for large diameter sour service pipelines, in: R.W. Revie (Ed.), Oil and Gas Pipelines: Integrity and Safety Handbook, first ed., John Wiley & Sons, Inc., 2015, pp. 225−231 (Chapter 17).
[32] B.J. Berkowitz, F.H. Henbaum, The role of hydrogen in sulfide stress cracking of low alloy steel, Corrosion 40 (5) (1984) 240−245.
[33] International Standard NACE MR0175/ISO15156 − Petroleum and Natural Gas Industries − Materials for Use in H2S-Containing Environments in Oil and Gas Production Parts 1, 2 and 3, 2015.
[34] M. Elboujdaini, Hydrogen induced cracking and sulfide stress cracking (Chapter 12), in: R. Winston Revie (Ed.), Uhlig's Corrosion Handbook, second ed., John Wiely & Sons, 2000.
[35] E.M. Moore Jr., Hydrogen-induced damage in sour, wet crude pipelines, Journal of Petroleum Technology, Society of Petroleum Engineers of AIME (April 1984) 613−619.
[36] International Standard NACE MR0103/ISO 17945 − Petroleum, Petrochemical and Natural Gas Industries − Metallic Materials Resistant to Sulfide Stress Cracking in Corrosive Petroleum Refining Environments, first ed., 2015.
[37] ANSI/NACE Standard TM0284-2016, Standard Test Method Evaluation of Pipeline and Pressure Vessel Steels for Resistance to Hydrogen-Induced Cracking.
[38] ANSI/NACE TM0177-2016, Standard Test Method Laboratory Testing of Metals for Resistance to Sulfide Stress Cracking and Stress Corrosion Cracking in H2S Environments.
[39] NACE TM 0198−2016, Slow Strain rate test method for Screening Corrosion-Resistant Alloys for Stress Corrosion Cracking in Sour Oilfield Service.
[40] European Federation of Corrosion Publication No. 16, Guidelines on Materials Requirements for carbon and Low Alloy Steels for H2S-Containing Environments in Oil and gas Production, second ed., Maney Publishing.
[41] D. Fairhurst, Offshore cathodic protection. What we have learnt, JCSE 4 (2001).
[42] K.D. Efird, Failure of Monel Ni-Cu-Al alloy K-500 bolts in seawater, Materials Performance 24 (1985) 87.
[43] K.C. Bendall, Alloys for offshore applications − duplex and super duplex stainless steels, cupronickel and corrosion mechanisms, Materials World 2 (4) (1994) 192−194.
[44] ASTM A 320/A 320M Standard Specification for Alloy-Steel and Stainless Steel Bolting Materials for Low-Temperature Service.
[45] ASTM A193/A193M Standard Specification for Alloy-Steel and Stainless Steel Bolting Materials for High Temperature or High Pressure Service and Other Special Purpose Applications.
[46] T.S. Nelson, E.E. Humphries, Evaluation of Stress Corrosion Cracking Resistance of Several High Strength Low Alloy Steels, NASA TM-78276, Marshall Space Flight Center Alabama, May 1980.
[47] S. Brahimi, Fundamentals of Hydrogen Embrittlement in Steel Fasteners, IBECA Technologies Corp., Montreal Canada, July 2014.
[48] Publication No. 194, Guidelines for Materials Selection and Corrosion Control for Subsea Oil and Gas Production Equipment, The Engineering Equipment and Materials Users Association, London, UK, 1999.
[49] ISO 13628−1:2005, Petroleum and natural gas industries − Design and operation of subsea production systems − Part 1: General requirements and recommendations, p. 45.
[50] API 17D, Specification for Subsea Wellhead and Christmas Tree Equipment, American Petroleum Institute, Washington D.C., 1996.

[51] Bolting and Fastener Application in the Offshore and Process Industry State of the Art, DNV Report No. 2002-3301, Det Norske Veritas.
[52] K.A. Esaklul, J.W. Martin, High strength fastners for subsea applications, in: Paper No. 04151, NACE Corrosion Conference, 2004.
[53] S. Olksen, L. Borvik, G. Rorvik, E. Aune, Risk of hydrogen embrittlement from cathodic protection on super martensitic stainless steel, in: Paper No. 01091, NACE Corrosion Conference, 2001.
[54] P. Woollin, W. Murphy, Hydrogen embrittlement stress corrosion cracking of super duplex stainless steel, in: Paper No. 01018, NACE Corrosion Conference, 2001.
[55] S.M. Hesjevik, S. Olsen, G. Rorvik, Hydrogen embrittlement from cathodic protection on supermartensitic stainless steels-case history, in: Paper No. 04545, NACE Corrosion Conference, 2004.
[56] S. Olsen, S.M. Hesjevik, Hydrogen embrittlement from CP on super Martensitic stainless steels-recommendations for new qualification methods, in: Paper No. 04546, NACE Corrosion Conference, 2004.
[57] T. Cassagne, F. Busschaert, A review of hydrogen embrittlement of duplex stainless steels, in: Paper No. 05098, NACE Corrosion Conference, 2005.
[58] S. Ronneteg, A. Juhlin, U. Kivisakk, Hydrogen embrittlement of duplex stainless steels testing of different product forms at low temperature, in: Paper No. 07498, NACE Corrosion Conference, 2007.
[59] P. Woollin, A. Gregori, Avoiding hydrogen embrittlement stress cracking of ferric austenitic stainless steels under cathodic protection, in: Proceeding of OMAE 2004: 23rd International Conference on Offshore Mechanics and Artic Engineering Vancouver, Canada 20-25 June 2004, 2004.
[60] T. Al Nabhani, N. Al Behalni, B. Johnson, Effect of over and under protection CP system on buried duplex stainless steel in soil environment, in: Paper No. 5453, NACE Corrosion Conference, 2015.
[61] B.R.W. Hinton, R.P.M. Procter, The effect of cathodic protection and over protection on the tensile ductility and corrosion fatigue behavior of X-65 Pipeline steel, in: I.M. Bernstein, A.W. Thompson (Eds.), Hydrogen Effects in Metals, Conference Proceedings the Metallurgical Society of AIME, 1980, pp. 1005−1014.
[62] M. Cabrini, S. Lorenzi, P. Marcassoli, T. Pastore, Hydrogen Diffusion and EAC of Pipeline Steels Under Cathodic Protection, EFC 16.
[63] M. Cabrini, S. Lorenzi, P. Marcassoli, T. Pastore, Hydrogen Embrittlement Behavior of HSLA Steels Under Cathodic Protection, Website source.
[64] M. Elboujdaini, W. Revie, Winston, susceptibility to hydrogen embrittlement Under cathodic protection of high-strength pipeline steels, 61-CP-09, in: 14th Middle East Corrosion Conference, 2012.
[65] H. Schoneich, Consideration on the risk of hydrogen embrittlement of pipeline steel due to cathodic overprotection, in: Pipeline Technology Conference, 2015.
[66] M.J. Robinson, P.J. Kilgallon, Hydrogen embrittlement of cathodically protected high-strength, low alloy steels exposed to sulfate-reducing bacteria, Corrosion 50 (8) (1994) 626−635.
[67] Q. Lu, P. Woollin, S. Paul, M.F. Gittos, M.D.F. Harvey, The influence of thermally sprayed aluminum coatings in controlling the hydrogen embrittlement of welded super duplex and supermartensitic stainless steels, in: Paper No. 3958, NACE Corrosion Conference, 2014.
[68] M.M. Javadi, Effect of zinc and aluminum thermal spray coatings on hydrogen embrittlement in marine industry, in: E. Lugscheider (Ed.), International Thermal Spray Conference & Exhibition, 2008, pp. 1471−1475.

[69] L. Lazzari, M. Ormellese, M. Pedeferri, CP test on hydrogen embrittlement of titanium alloys in seawater, in: Paper No 06290, NACE Corrosion Conference, 2006.
[70] D.J. Schumerth, T. Demers, Hydrogen embrittlement in titanium and superferretic stainless steel steam condenser tubing, in: Paper No. 2078, NACE Corrosion Conference, 2013.
[71] T.E. Perez, Corrosion in the oil and gas industry: an increasing challenge for materials, Journal of Metals 65 (2013) 1033.
[72] T. Omura, K. Kobayashi, A. Souma, T. Ohe, H. Amaya, M. Ueda, Environment cracking susceptibility of low alloy steel OCTG in high H2S partial pressure conditions, in: Paper No. 2308, NACE Corrosion Conference, 2013.
[73] M. Hay, Hydrogen-induced cracking in low strength steel, in: ADCO Seminar, January 2004.
[74] D.K. Han, H.G. Jung, K.Y. Kim, S.J. Kim, Effect of heat treatment on hydrogen diffusion and hydrogen induced cracking behavior of process pipe steel in sour environment, in: Proceeding of the 23rd International Offshore and Polar Engineering Conference, Anchorage, Alaska June 30-July 5, 2013, Page 30−36, 2013.
[75] S. Kemion, J.H. Magee, K.A. Heck, T.N. Weley, Effect of microstructure and processing on the hydrogen embrittlement of Ni-base superalloys, in: Paper No. 6053, NACE Corrosion Conference, 2015.
[76] D. Masouri, Hydrogen embrittlement of nickel base alloy UNS No. 7750 in sour gas environment, in: Paper No. 03133, NACE Corrosion Conference, 2003.
[77] S.A. McCoy, S.K. Mannan, C.S. Tassen, D. Maitra, J.R. Crum, Investigation of the effects of hydrogen on high strength precipitation hardened nickel alloys for O&G service, in: Paper No. 5911, NACE Conference, 2015.
[78] J.J.M. Jebaraj, D.J. Morrison, I.I. Suni, Metallurgical effects on the diffusion of hydrogen through alloy 718, in: Paper No. 4165, NACE, Corrosion, 2014.
[79] T. Neeraj, R. Srinivasan, Hydrogen embrittlement of steels: vacancy induced damage and nano-voiding mechanisms, Corrosion 73 (2017).
[80] D. Dennies, Proposed theory for the hydrogen embrittlement resistance of martensitic precipitation age-hardening stainless steel such as custom 455, Journal of Failure Analysis and Prevention ©ASM International (2013), http://dx.doi.org/10.1007/s11668-013-9684-3.
[81] S. Thomas, G. Sundararajan, P.D. White, N. Birbilis, The effect of absorbed hydrogen on the corrosion of steels; review, discussion and implications, Corrosion 73 (2017).

Erosion–corrosion

14

Sandra Hernandez [1], *Shokrollah Hassani* [2] *and Anass Salem Nassef* [3]
[1]Chevron ETC Facilities Engineering, Houston, TX, United States; [2]BP America, Houston, TX, United States; [3]University of Tulsa, Tulsa, OK, United States

14.1 Introduction

Erosion can be defined in a variety of ways; it is essentially the wastage of material due to the mechanical removal of material by flowing environments. Such wastage is more extreme when solids are present in the environment. Erosion–corrosion occurs in environments that have the potential to be both erosive (mechanical component) and corrosive (electrochemical component). The erosion and corrosion can either be independent, in which case the total wastage is the sum of the wastage produced by each mechanism in isolation, or synergistic, in which case the total wastage is greater than the sum of the independent processes of erosion and corrosion.

One useful way of defining the participation of the main components and their interactions in the total erosion–corrosion process is shown in Eq. (14.1) [1]:

$$\begin{aligned}\text{Erosion} - \text{corrosion rate} = {} & \text{Erosion rate} + \text{corrosion rate} \\ & + \text{effect of erosion on the corrosion rate} \\ & + \text{effect of corrosion on the erosion rate}\end{aligned} \tag{14.1}$$

In upstream operations, the erodent is usually sand or any other solid particle that is produced along with the production fluids. The most prevalent corrosion mechanisms are those associated with the presence of CO_2 and H_2S gas dissolved in the water produced.

In many cases, the effect of corrosion on erosion rate term in the equation above is small compared to the rates of the other components and can be neglected. The effect of erosion on corrosion, however, can be very substantial, for example, when a protective corrosion product layer is stripped away by solids erosion. Because the synergistic effect can be significantly larger than the erosion or corrosion component, erosion–corrosion research is mainly focused on systems with a significant interaction.

The three main erosion–corrosion processes in oil and gas production are as follows:

1. Erosion–corrosion in a system with a protective scale (usually carbon steels [CS]): $FeCO_3$ (iron carbonate) and FeS (iron sulfide) are the primary corrosion products of carbon/low alloy steel in production environments containing CO_2 and H_2S. $FeCO_3$ scale is generally less adherent and protective compared to FeS. However, $FeCO_3$ is more stable above 180–200°F (82–93°C).

Trends in Oil and Gas Corrosion Research and Technologies. http://dx.doi.org/10.1016/B978-0-08-101105-8.00014-0

2. Erosion–corrosion in a system with a passive scale [corrosion-resistant alloys (CRAs)]: when flow rates or particle concentrations are high, the removal of a passive film in some CS and CRAs can overcome the ability of the passive layer to reform.
3. Erosion–corrosion in a system with chemical corrosion inhibition: High velocities and particle concentration can induce damage to the protective corrosion inhibitor film, thus inducing erosion–corrosion.

Erosion–corrosion deterioration of CRAs in the presence of sand is a major issue in oil and gas production. The combined effect of erosion and corrosion can decrease the efficiency of corrosion mitigation systems, such as iron–carbonate scale formation on CS surface, passive layers on CRA, or chemical inhibition, thereby causing pitting and severe corrosion damage. Oil and gas are being produced from deeper wells in not easily reachable regions, in which highly corrosive and erosive environments are expected; these wells can have high temperatures, high pressures, and high sand production rates [2]. Typical problems of erosion–corrosion in oil and gas production occur in all downhole components including tubing, pumps, downhole screens, and subsurface safety valves. Erosion–corrosion also occurs in systems used to contain, transport, and process erosive mineral slurries, and in petroleum refinery equipment, thermal wells, which contain pumps, pipe elbows, nozzles, valve seats, and guides, which experience varying degrees of high-temperature erosion and corrosion [3].

14.1.1 Morphology/appearance of damage

14.1.1.1 Erosion

- Erosion follows flow patterns where high velocity, turbulence, or particulates are accelerating metal loss.
- Metal loss is confined to an impingement zone.
- Clean failure appearance, no corrosion products or deposits.

14.1.1.2 Erosion–corrosion

- Metal loss is confined to an impingement zone
- The protective film of the metal is intact in all areas adjacent to the damaged area
- The area where the failure occurs is usually clean, with no corrosion products or deposits

14.1.1.3 Failure modes

- Erosion and erosion–corrosion damage will most likely result in a pin-hole sized leak. Although larger sized leaks or a rupture cannot be completely ruled out, these are unlikely.

14.1.1.4 Susceptible materials

- Carbon steels
- Low alloy steels ($1^1/_4$ Cr–$^1/_2$ Mo, $2^1/_4$ Cr–1Mo, 5Cr, 9Cr steels, i.e., with chromium content less than 12%)
- CRAs (e.g., 13Cr, super 13Cr, 22Cr)

14.2 Erosion–corrosion mechanisms

Erosion–corrosion encompasses a wide range of flow-induced corrosion processes [4]. Erosive fluids can damage corrosion protective films and remove small pieces of the substrate material as well, leading to a significant increase in penetration rate. For example, CS pipe carrying water is usually protected by an oxide film and corrosion rates are typically <1 mm/year (or 40 mpy). The removal of the film by erosion causes corrosion rates of the order of 10 mm/year (400 mpy) in addition to any erosion of the underlying metal [5]. The damage to the protective film is believed to be due to the fluid-induced or solid-induced mechanical forces or flow-enhanced dissolution [6,7]. This combined action of erosion and corrosion is known as erosion–corrosion. Mechanical forces by which erosion–corrosion takes place can be summarized as follows [8]:

1. Turbulent flow, fluctuating shear stress, and pressure impacts
2. Impact of suspended liquid droplets in high-speed gas flow
3. Impact of suspended gas bubbles in liquid flow
4. The violent collapse of vapor bubbles, cavitation
5. The impact of suspended solid particles

The five mechanical force sources mentioned earlier can be found in oil and gas production. However, most of the erosion–corrosion encountered in oil and gas industry is caused predominately by the impact of suspended solid particles on piping and tubing bends, choke valves, manifolds, etc.

To understand the mechanisms and the parameters involved in erosion–corrosion, it is important to differentiate between erosion, corrosion, and erosion–corrosion. Erosion–corrosion results from the interaction between electrochemical (corrosion) and mechanical (erosion) processes. Many studies emphasize that the complexity of erosion–corrosion arises due to synergism between erosion and corrosion. This synergistic effect of erosion–corrosion results in significantly higher metal loss rates than the combined effects of erosion and corrosion acting separately.

In this chapter, erosion–corrosion refers to the combined effects of erosion and corrosion processes that take place when sand particles entrained in a flowing medium impact a protective corrosion product, i.e., iron carbonate scale, inhibitor, or oxide layer, which lead to either partial or complete removal of the protective layer, consequently corrosion takes place at higher rates.

14.2.1 Carbon steel

The mechanisms of erosion–corrosion for CS materials can be explained by understanding the interaction that takes place between erosion and corrosion, which can produce a synergistic effect. Synergism of erosion–corrosion results in higher metal loss rates than the sum of the independent erosion and corrosion mechanisms. The synergistic effect of erosion–corrosion has been described in different ways. In oil and gas production environment, the synergism between erosion and corrosion has been described by many authors as enhancement of corrosion by erosion and/or enhancement of erosion by corrosion [6–14]. In this chapter, erosion–corrosion

mechanisms for CS are described for two conditions, which have different degrees of synergism. These conditions are scale-forming and non−scale-forming conditions. The mechanisms for each condition are described in the following paragraphs.

14.2.1.1 Scale-forming mechanism

In CO_2 corrosion, iron carbonate ($FeCO_3$) scale can precipitate on a steel surface as a result of corrosion under certain environmental conditions of temperature, pH, flow velocity, and concentration of species, such as ferrous (Fe^{2+}) and carbonate $\left(CO_3{}^{2-}\right)$ ions. Iron carbonate scale is a protective corrosion product and can reduce corrosion rates to lower values if it completely covers the steel surface. However, the presence of sand particles in the flowing media can remove the protective scale through sand erosion, allowing corrosion rates to return to the high corrosion values of the bare metal. Under scale-forming conditions, there is a tendency for scale to precipitate as well as be removed by sand erosion, thereby, significant synergism occurs between erosion and corrosion. Fig. 14.1 shows a schematic illustration of the erosion−corrosion mechanism under scale-forming conditions.

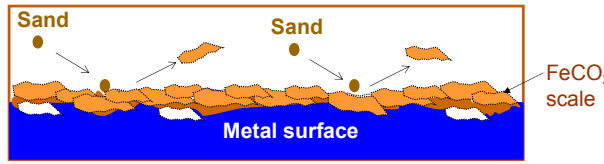

Figure 14.1 Erosion−corrosion mechanism of carbon steel material under scale-forming conditions [16].

Three broad regimes have been defined in solid particle erosion−corrosion: (1) substrate dominated, (2) scale modified, and (3) scale dominated. Which of these three regimes governs an erosion−corrosion process depends on the particle dynamics (impact energy or angle), particle loading, and scale formation rate. The substrate-dominated regime applies when the metal loss rate is controlled by erosion of the substrate. The scale-modified regime applies when there is a strong interaction between the erodent and the formation of surface scales. The scale-dominated regime applies when the particle impacts result in localized fracture and chipping of the scale, i.e., removal of scale by erosion [9]. The mechanism of the removal of the scale can take place under both brittle and ductile erosion mechanisms, depending upon the characteristics of the scale and the particles [10].

Shadley et al. [11,12] studied the mechanisms of erosion−corrosion under scale-forming conditions and identified three erosion−corrosion regimes. This study has been conducted on a CS elbow geometry using a flow loop that circulates a CO_2 saturated brine solution and sand at different flow velocities. At low-flow velocities, a protective iron carbonate scale was found to cover all the internal surface of the elbow and metal loss rates were low. For high-flow velocities, the presence of sand particles in the fluid prevented the protective scale from adhering to any elbow surface and metal loss rates were high. For intermediate flow velocities, impingement of sand particles prevented the protective scale from adhering to the elbow at impingement points while allowing

it to adhere to the rest of the elbow surface. Pitting corrosion was developed at the impingement points that have not been covered by the corrosion product scale, and penetration rates were extremely high. Flow velocities separating the three erosion–corrosion behaviors were called "threshold velocities" [11,12].

14.2.1.2 Non–scale-forming mechanism

As mentioned in the previous section, the sweet corrosion of CS at certain environmental conditions promotes the precipitation of iron carbonate scale on the steel surface. However, environmental conditions of low pH, low temperature, and low iron ion content can prevent iron carbonate scale from forming on the steel surface, and consequently result in non–scale-forming conditions. In this case, erosion–corrosion of the base metal takes place. The extent of synergy in non–scale-forming conditions is not as significant as in the previously mentioned scale-forming conditions [13]. Fig. 14.2 shows a schematic illustration of the erosion–corrosion mechanism under non–scale-forming conditions.

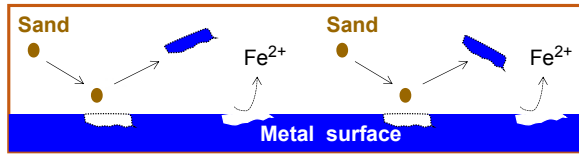

Figure 14.2 Erosion–corrosion mechanism of carbon steel material under non-scale-forming conditions [16].

An erosion–corrosion study has been conducted to investigate the interaction between corrosion and erosion processes and to quantify the synergism under non–scale-forming environmental flow conditions [14]. Tests were performed on low CS material with silica sand as the erodent particles. It has been observed that erosion enhances corrosion and corrosion enhances erosion; however, the erosion enhancement, due to corrosion, is more significant under non–scale-forming conditions. Furthermore, the corrosion rate is almost doubled in the wake of sand erosion.

Synergism in non–scale-forming conditions has been explained by the change of surface roughness [15–17]. Increasing surface roughness through erosion accelerates the corrosion by increasing the surface area exposed to corrosion. Corrosion rates can also increase by increasing the surface roughness of steel because the electron density in the indentations of the surface is higher and corrosion rates increase with increasing electron density [15–17]. Corrosion may also intensify the erosion rate through creating a favorable surface roughness for erosive action [16].

Hassani et al. [16,17] divided erosion–corrosion processes under non–scale-forming conditions into erosion part of erosion–corrosion and corrosion part of erosion–corrosion. The erosion part of erosion–corrosion is further divided into pure erosion and erosion affected by corrosion. Likewise, the corrosion part of erosion–corrosion is also divided into pure corrosion and corrosion affected by erosion. Hassani et al. [16,17] also investigated the surface morphology of a low CS subjected to sand erosion under three different conditions including pure erosion, erosion–corrosion without iron carbonate scale, and erosion–corrosion with iron carbonate scale. The pure erosion

condition reveals the change in the surface morphology by deforming the base metal and creating craters, which provides a good example of the pure erosion mechanism of ductile materials. Erosion–corrosion, without scale formation, showed a stronger effect on the surface morphology of the CS. Surface degradation by corrosion makes the metal surface more susceptible to sand erosion and more craters were found on the surface because corrosion increased the surface roughness. Corrosion increases the surface roughness by accelerated corrosion rates at grain boundaries and impurities on the surface. Fewer craters and surface deformations were observed in the presence of iron carbonate scale. Iron carbonate scale exhibits erosion behavior of brittle materials [14,15].

A flow loop study indicated that the synergistic effect of erosion and corrosion of CS in a high NaCl concentration solution under non–scale-forming conditions is negligible [15]. The measured erosion–corrosion was equal to the sum of the pure erosion and pure corrosion components. Under scale-forming condition or in the presence of corrosion inhibitor, synergistic effect of erosion and corrosion is more important.

Flow loop investigations also indicated no synergism of erosion and corrosion in the presence of imidazoline-based water soluble oil dispersible inhibitor [16,17]. In CO_2 saturated brine solution with no oil, the inhibitor was found to be very effective in reducing the corrosion contribution to the erosion–corrosion, but not as effective as for similar conditions without sand. Sand erosion has been reported to decrease the inhibitor efficiency by partially removing the inhibitor film from the surface and also, to a lesser extent, by the adsorption of inhibitor on the sand particles [16]. On the other hand, in a CO_2 saturated solution with 60% oil, the inhibitor was found to be more effective in minimizing the corrosion part of erosion–corrosion than for the same system without sand [18]. Such improvement in inhibitor efficiency was likely the result of immediate removal of iron carbide by action of the sand. Iron carbide has been found for the inhibited corrosion system with no sand. The authors found that the iron carbide (Fe_3C) left by the corrosion process impairs inhibitor performance by not allowing enough inhibitor to reach the steel surface below it [18]. In both oil and nonoil systems, inhibited erosion–corrosion rates can be obtained by adding the inhibited corrosion part of inhibited erosion–corrosion to the pure erosion rate.

14.2.2 Corrosion-resistant alloys

CRAs rely on oxide layers to gain excellent corrosion resistance properties. These oxide layers are corrosion products, protective in nature, and known as passive films. Passive films may be formed naturally by reacting with their environment or as a result of some intentional pretreatment process to enhance the protectiveness properties of films by modifying the nature of existing films. Aluminum and its alloys are good examples for the former case in which passive oxide film instantly forms on the metallic surface when it is exposed to the atmospheric oxygen. The latter case can be well explained by stainless steel alloy in which alloying elements such as chromium and nickel are added to the steel to form a passive oxide film on the steel surface. Passive films form a kinetic barrier that isolates the metal surface from the surrounding corrosive media, thus controlling the rate of the reaction [19].

Under some severe environmental conditions, it can be more economical in the long term to use CRAs instead of commonly used CS, which often demands costly chemical treatments. The use of CRAs has recently been increased in oil and gas industry. In CO_2 environments, 13Cr alloys and its modified types are the most widely used CRAs because of its excellent CO_2 corrosion resistance and low cost compared with other more expensive CRAs such as duplex stainless steel [20,21].

As mentioned earlier, addition of alloying elements to CS such as nickel, chromium, and molybdenum can improve corrosion resistance and reduce corrosion rates to much lower values for such materials. Any factor that produces partial or complete removal of the protective passive film can lead to partial or complete breakdown of the passive film and the corrosion rate can be significantly increased. Different degradation mechanisms can result in such breakdown of the passivity namely electrochemical reduction or oxidation, undermining by attack on the underlying metal at film imperfections or the mechanical disruption. The breakdown of the passive film due to flows containing solid particles like sand falls into the latter classification [19]. The stimulation of corrosion due to the breakdown of the passive film by particles entrained flow is generally referred to as erosion−corrosion [22]. Erosion−corrosion of CRAs can be defined as the accelerated deterioration of a metal because of erosion contribution in combination with corrosion, where the corrosion is initiated by the destruction or the breakdown of passive layers as a result of erosion. The interaction between erosion and corrosion (the synergistic effect) takes place and the produced material loss is greater than the additive effect of the mechanisms acting separately. Generally, the total erosion−corrosion penetration rate is estimated through four terms; pure corrosion, pure erosion, the effect of erosion on corrosion, and the effect of corrosion on erosion, where the sum of the two latter terms accounts for the synergism involved in the process. Determining whether there is a dominant term is not straight forward. This will probably depend on both the material and the environment under study [23].

Based on Lotz and Heitz [22] study, in a pure wear situation, whether erosion takes place through the breakdown of the passive layer or erosion of the base material itself, the final erosion rates would not be significantly affected. However, under corrosive conditions, damage in the surface layer and a competition between layer removals versus layer self-healing may signify huge differences in final weight losses [22].

Birchenough et al. [24] experimentally characterized erosion−corrosion of 13Cr CRA, with the objective of exploring the interactions between erosion due to sand particles and corrosion due to carbon dioxide and water/brine in a flowing two-phase system. It was found that the surface passive film that protects the 13Cr alloy material from corrosion can be removed by sand erosion. Once sand particles remove the protective passive film, a high corrosion rate could be sustained even if the sand particles are settled afterward. It was also claimed that once this protective passive layer was removed by sand erosion, the 13Cr steel alloy material would not repassivate in oxygen-free conditions.

An erosion−corrosion study of 13Cr steel alloy was conducted using weight loss technique in a flow loop with a constricted pipe test section [24]. Formation of water with sand particles at different sizes and concentration were used in this investigation. It was reported that erosion−corrosion rates increased approximately with the square

of the flow rate and linearly with sand concentration. Under CO_2 corrosion conditions, changes of the particle parameters (size, concentration) were found to be much more significant than environmental parameters (chloride content, temperature).

D. He and coworkers [25] studied the erosion–corrosion behaviors of four stainless steel materials including 1Cr13 (ferritic), 316L (UNS S31603) (austenitic), 0Cr14Ni5Mo (martensitic), and CD-4MCu ($\alpha + \gamma$ duplex) using a rotating cylinder electrolyzer apparatus. Tests were carried out in two kinds of dual-phase slurry including 3.5% NaCl + 30% Al_2O_3, and 0.5N H_2SO_4 + 3.5% NaCl + 30% Al_2O_3 at different fluid velocities. The steel's surface morphologies, variation of surface microhardness, and the hardness gradient of cross-sections were characterized after the exposure to the erosive–corrosive media. In 3.5% NaCl + 30% Al_2O_3 dual-phase slurry, it was claimed that the erosion–corrosion performance of the tested steel alloys follows the sequence D-4MCu, 1Cr13, 0Cr14Ni5Mo, and 316L SS from the most to the least resistant alloy, respectively. In 3.5% NaCl + 0.5N H_2SO_4 + 30% Al_2O_3 dual-phase slurry, CD-4MCu was reported to have superior erosion–corrosion resistance, as did 316L SS at a low velocity, but the former performed better after a long working time at a high velocity. The sequence of erosion–corrosion resistance for the tested steel alloys under this condition was CD-4MCu, 316L SS, 0Cr14Ni5Mo, and 1Cr13 from the most to the least resistant alloy, respectively. It was also argued that the high erosion–corrosion resistance of the $\alpha + \gamma$ duplex-phase stainless steel may be obtained from its high-corrosion resistance and high-work-hardening capability [25].

Flow loop tests for 13Cr steel alloy were performed under single and multiphase flow conditions [23,26–28]. Several electrochemical and conventional weight loss techniques have been adopted to explore the erosion–corrosion mechanisms that take place when the 13Cr steel is exposed to a CO_2 corrosion environment containing sand particles. Such measurement techniques include weight loss [26], thickness loss [27], linear polarization resistance [23], potentiodynamic sweeps [23], high-resolution electrical resistance (ER) probes [28], and electrochemical emission spectroscopy (EES) a modified electrochemical noise technique [29]. In general, for high erosivity conditions in both single and multiphase flow conditions, synergistic effect between erosion and corrosion took place. The reported erosion–corrosion rates of 13Cr steel were higher than the sum of the rates of pure corrosion with no sand and erosion tested separately. The erosivity obtained at high sand rate was sufficient to damage the passive oxide film leading to higher corrosion rate. Under low sand rate, the erosion–corrosion rate of 13Cr steel was much lower. The penetration rate for erosion and erosion–corrosion were almost the same. The small corrosion part of erosion–corrosion indicates that no significant synergism occurs and the passive oxide film of the 13Cr steel was healing about as fast as it was being eroded away by the impinging sand particles. In most cases, there is likely to be a competition between removal of the protective film by mechanical erosion and the protective film healing. If the removal rate of the passive film is greater than the formation rate of the passive film, then an accelerated corrosion process may take place [28]. Similar erosion–corrosion mechanisms were observed for other CRAs used in oil and gas industry, namely, super 13Cr (S13Cr) steel and duplex stainless steel (22Cr) [29].

The synergism of erosion–corrosion for martensitic stainless steel of grade UNS S42000 has been investigated under high velocity multiphase conditions [30]. Pure

erosion, pure corrosion, and erosion–corrosion experiments were conducted in a combination of a gas flow loop and a jet impingement flow loop at three different impact velocities between 10 and 60 m/s. The NaCl and solid-particle contents of the solution were 2.7 wt% and 2.7 g/L sand of size below 150 μm, respectively. Electrochemical techniques along with stereomicroscopy, scanning electron microscopy, and atomic force microscope were utilized in quantifying synergy effects as function of impact velocity. The martensitic stainless steel S42000 showed a significant interaction between erosion and corrosion under the test conditions at 10 m/s. However, at very high-flow velocity of 59 m/s, the erosion part of erosion–corrosion was the dominating mechanism, thereby no synergism was reported [31]. At 10 m/s flow velocity, it was claimed that the synergy is dominated by corrosion-enhanced erosion and the erosion–corrosion mechanism is mainly governed by erosion. It was also alleged that erosion delayed the corrosion by avoiding the formation of pits in aggressive electrolytes by impacting sand particles [31].

14.3 Erosion–corrosion risk assessment/modeling

A corrosion risk assessment allows the identification of threats and their potential consequences to be identified. As a primary outcome, the risks can be ranked and plans can be made to prioritize resourcing for their effective avoidance or mitigation.

Perhaps the most important element to perform a corrosion risk assessment is to collect relevant data for the system to be evaluated. At the design stage, a basis of design (BOD) should be developed and finalized prior to conducting a corrosion risk assessment. An incomplete or inaccurate data set will result in either over design and unnecessarily increasing capital investment or under design, potentially resulting in poor reliability and/or safety and environmental incidents.

The purpose of the BOD is to identify the governing condition(s) for materials selection and risk evaluation. Governing conditions are those most likely to result in the maximum susceptibility to corrosion, erosion, or environmental cracking. Condition changes through the life of the system and anticipated operating scenarios, such as water injection or souring, all require consideration.

Once in operation, the operating and environmental conditions need to be considered. The main objective of a corrosion risk assessment during operation is to rank equipment in relation to their corrosion risk and guide the inspection and corrosion management activities.

The corrosion risk is normally expressed as the product of the likelihood of corrosion-related failure and the consequences of such failure,

$$\text{Risk} = \text{Likelihood} \times \text{Consequence} \tag{14.2}$$

where the likelihood of failure is estimated based upon the types of corrosion damage expected to occur on a component and the consequence of failure is measured against safety, health, environmental, and operational impacts, which would result should a loss of containment occur.

A corrosion risk assessment can be performed at two levels:

- A high-level "system" assessment that group together components, which are constructed from the same materials and are subjected to the same process and operating conditions.
- A more detailed assessment, which looks at the vulnerability of specific components.

As an example, the risk assessment for a group of pipelines is carried out at the circuit level. In this case, a corrosion circuit is a group of pipelines that are likely to be affected by the same corrosion mechanisms at comparable rates, locations, and frequencies. Corrosion circuits are defined as lines within a system that share common parameters, such as the material of construction, fluid type and velocity, operating pressures and temperatures, presence of cladding, linings, or coatings, etc.

For pressure-containing equipment (PCE), the risk assessment will be carried out at the equipment item level.

Some of the process units and equipment that can be affected by erosion–corrosion include the following:

- Downhole sand screens
- Wellhead chokes
- Wellhead valves
- Subsurface safety valves
- Production manifolds
- Flowlines
- Production separators inlet piping
- Fittings
- Bends
- Flow restrictions (orifices)

A corrosion study is undertaken for each corrosion circuit and/or PCE to determine all potential failure mechanisms and the likelihood of that corrosion mechanism occurring. It is important to review the design (BOD) and process data to determine what damage mechanisms will be active. Materials and process flow diagrams should be reviewed for each circuit, keeping both normal operation and potential process excursions in mind. A mixture of corrosion subject matter expert guidance, practical experience, and engineering judgment should be used to guide the development of corrosion circuits. Circuits should be carefully controlled to a manageable size.

To assess the risk to erosion–corrosion, the following data are required for each circuit or PCE:

Erosion	Corrosion
• Flow velocity • Sand/solid concentration • Sand/solids characterization (shape, size) • Flow regime • Density, viscosity of each phase at operating conditions (oil, gas, water) • Geometry • Diameter	• Temperature • Pressure • CO_2 and H_2S partial pressure in the gas phase • Water cut • Water composition • pH • Material of construction

If the material of construction is CS, then the first step is to investigate if the conditions are prone to the formation of a protective iron carbonate scale. Process conditions for likely protective iron carbonate scale formation are pH > 5, temperature >150°F (66°C), plus a significant concentration of Fe^{2+} ions [1]. Several models have been developed that can predict iron carbonate and scale precipitation rates [31−33]; however, the degree of protectiveness of the scale is hard to predict.

Iron sulfide scales can also be protective but at much higher temperatures; however, in production operations there is usually a combination or competition between iron sulfide and iron carbonate film formation. A simplified model (for slightly sour systems) has been proposed by Smith [35] that suggests that at about 77°F (25°C), iron sulfide would form if the ratio of partial pressure of $CO_2/H_2S < 500$, whereas iron carbonate will form if the ratio is higher than 500 [34]. A second model extends such prediction to higher temperatures and partial pressures of the gases:

$$K_{(FeS/FeCO_3)} = C \times \frac{a_{CO_2}}{a_{H_2S}} \tag{14.3}$$

where K is the equilibrium constant defining the boundary between carbonate and sulfide film, C is a complex temperature correction factor, and a is the activity or partial pressure of the respective gases.

This relationship shows that steel corrodes at lower temperatures in CO_2 environments despite the H_2S content. At elevated temperatures, $FeCO_3$ forms and with increasing activity of H_2S, various sulfide films manifest in the order of mackinawite, pyrrhotite, and pyrite [35].

Although extensive research has been dedicated to understand film formation and corrosion rates under mixed CO_2/H_2S regimes, not much research has been performed on the erosion−corrosion of mixed scales.

Alloys such as stainless steels in the 300 or 400 series have a significantly harder and more adherent surface film than the one existing on CS in carbon dioxide or hydrogen sulfide service. This could change the observed mechanism of erosion/corrosion to one more consistent with erosion in noncorrosive systems [36], depending on the operating conditions.

Erosion and erosion−corrosion models (see Chapter 31) can be used to determine erosion and corrosion−erosion rates and assess the corrosion risk and time to failure at the design stages. The best models are those that take into consideration the material, the exact size, and geometrical shape of the pipework components in combination with sand particle size and fluid properties such as density and viscosity as these all will influence the actual erosion and erosion−corrosion potential per amount of sand.

The erosional velocity criteria from API RP 14E [37], even if it does not account for many of the factors influencing erosion, are still used to establish velocity limits to avoid excessive wall loss due to erosion−corrosion, varying the empirical constant to account for different materials or presence of solids. It can also be used as a first level assessment of the erosion−corrosion risk if a complete set of data is unavailable.

DNVGL Recommended Practice O501 [38] can also be used for ranking of the erosion (not erosion−corrosion) potential for pipework with reference to calculated bulk flow velocities, considering that the flow velocity determines the order of

magnitude for erosion. The class of erosive service for pipework provides a simple indication of whether a system is susceptible to erosion.

Once in operation, actual wall loss measurements can be collected by the inspection program for the areas at risk and can be used to compare and substitute the theoretical rates obtained by modeling. In the operational phases, the primary intent of a corrosion risk assessment is to guide and improve the inspection and corrosion monitoring activities.

14.4 Monitoring

In terms of sand control, most oil and gas companies have implemented a sand management strategy aiming at improving well productivity and reserve recovery, whereas sand production is controlled to a safe level. As an example, Statoil together with DNV have implemented an acceptable sand rate (ASR) strategy to assess the acceptable sand production rate from each well to optimize production [39]. This requires strict monitoring and control throughout the sand value chain to ensure the integrity of the system while optimizing production. Monitoring of erosion–corrosion requires the combination of monitoring tools for both mechanisms.

This could include a combination of

- Continuous sand monitoring
- Continuous monitoring of erosion, corrosion, or erosion–corrosion
- Nondestructive examination (NDE)

Continuous sand monitoring: Acoustic sand detectors (ASDs) are nonintrusive sand detectors that work on the principle of detecting the sound created by sand particles as they impact the inner pipe wall. The noise generated is an increasing function of both velocity and the amount of sand in the process fluids. The challenge for the ASDs is to filter out noise from mechanical sources and the flow per se and tune in to the sound from sand. The optimal location for an ASD is after a 90° bend where the monitor will pick the energy from particles impacting the inside of the pipe wall. Proper installation and calibration of these systems are critical.

There are several technology challenges related to sand monitoring systems including calibration and accuracy. There is not a good guidance or model available for determining the accuracy of the ASDs. For example, how much sand is produced when an acoustic sand detector shows no signal? What is the minimum amount of sand detectable using ASDs for different type of fluids (density, viscosity, number of phases, etc.), flow velocity, and flow regime?

The output from an ASD is a raw value containing information about the total acoustic energy level of a system, which is given by background noise and sand noise. For this reason, calibration methods are required to refine these raw values and convert them into sand signals. Each ASD supplier has developed their own calibration techniques and high variability can be observed between different sensors because of this reason. In addition, proper calibration requires updates (recalibration) as production profile change.

The accuracy of ASD is very dependent on the calibration factors being used, but it is also dependent on the flow regimes and sand particle sizes. The Erosion−Corrosion Center at the University of Tulsa has performed extensive research in this area. A broad range of operating conditions have been investigated with acoustic sand detectors at Tulsa University Sand Management Projects (TUSMP) to determine the effectiveness of sand monitoring in multiphase flow. Experiments have been performed with acoustic monitors while varying superficial gas and liquid velocity, sand size, and flow orientation [40].

One of the objectives has been to find the variation in threshold sand rates in different flow regimes and orientations for a different pipe diameter using sensors like ClampOn's DSP-06 monitor in 4- and 2-in. multiphase flow loops with 150 μm sand. Fig. 14.3 is an example of the threshold sand rate results obtained [41]. The data obtained to date indicate that there is a significant difference in the threshold sand rates for the horizontal orientation obtained in 2- and 4-in. pipes for similar operating conditions with the thresholds rates being larger in the larger pipe. Another factor that produces a noticeable change in the threshold sand rates is the flow orientation. It has been noted that the threshold sand rates decrease when the flow is in a vertical orientation; this has been observed in both 2- and 4-in. piping systems.

TUSMP is expanding this work by performing similar studies with Pulsar and Roxar, two of the most commonly used acoustic sand monitors in addition to ClampOn's. These three monitors will be run simultaneously to compare results.

In summary, ASD monitoring techniques have their own limitations in terms of detecting sand around elbows because they may not be installed in the right location of erosion. In this case, computational fluid dynamics simulation is helpful in detecting the right location for the installation of the probes. However, change in the flow conditions may change the location of maximum erosion as well.

Continuous monitoring of erosion, corrosion, or erosion−corrosion: A combination of corrosion and erosion probes constitutes another method for erosion−corrosion

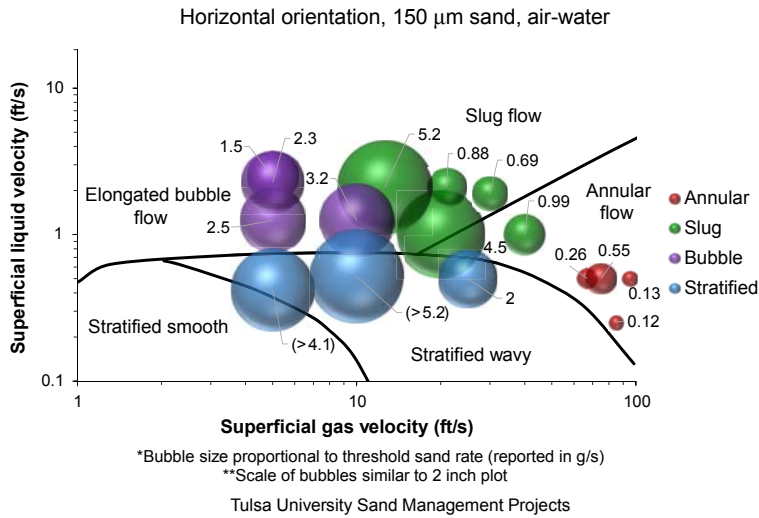

Figure 14.3 Threshold sand rate results obtained in a 4″ flowloop in horizontal orientation [41].

monitoring. Intrusive erosion monitoring probes work on the principle of detecting the actual damage caused to the metallic elements in the sensor when these are impacted by abrasive sand particles. The metal exposed in these probes is such that it is not susceptible to corrosion in the producing environment, e.g., Inconel 625. The sensor contains metal and reference elements; the metal element is exposed to the process and allowed to erode while the reference is shielded and remains unchanged. As the metal erodes, the conductive cross-sectional area is reduced thus increasing its ER with respect to the reference. The metal loss is monitored by recording the ER of each of the measuring elements on a regular basis. These probes can be flushed-mounted or intrusive; however, flushed mounted probes generally show much lower erosion rates compared to intrusive ones. Corrosion probes are based on the same principle; however, the exposed metal is chosen to closely resemble the material of the component to be monitored.

The main disadvantage of ER probes is that these can detect erosion only for a small surface area and only for limited locations in the pipe. Therefore, they may miss the right location of erosion. The response of the erosion probes is dependent both on the location and flow conditions. In a comparative study, the probes in the vertical downward section generally recorded higher erosion than those in the vertical upward section, which is expected due to the effect of gravity on the sand particles [38]. Also, the accumulated metal loss for erosion intrusive sensors is proportional to the sand particle size and this effect is more significant as the gas velocity increases.

Nondestructive examination: Ultrasonic thickness (UT) probes are normally used to measure material loss in eroding pipework. The primary limitation of this technique is that it only checks a limited section of the pipe. Other limitations of conventional UT are temperature, scanning angle, and lack of automation for probe positioning. Advanced nondestructive techniques, such as phased array (PAUT) and long-range UT technology (LRUT) have been used by some operators for better assessment of erosion−corrosion. LRUT is used to identify trouble spots while the PAUT is used to obtain a more automated scanning of already detected damaged areas [42]. The PAUT concept is based on the use of transducers made up of individual elements that can each be driven independently. These probes are connected to specially adapted drive units enabling independent, simultaneous emission, and reception from each channel. Long-range UT employs mechanical stress waves that propagate along a structure while guided by its boundaries, thus allowing long extensions and even inaccessible sections of pipe to be inspected.

Newer technologies for erosion−corrosion monitoring make use of ultrasonic-guided waves to monitor changes in wall thickness over an extended area using only a limited number of transducers. The transducers are permanently installed at predetermined external locations without the need for any mechanical movement once installed. This adds to the reliability of the instrument as recalibration is not needed; however, because it is permanently installed, the location needs to be carefully selected. Examples of these instruments are the corrosion−erosion monitor from ClampOn [43], and the Ring Pair Corrosion Monitor Spool developed by Teledyne CORMON [44].

Also, there are instruments that can be retrofitted and as such moved and used in several locations, such as Sensorlink [45] UltraMonit. This system collects real-time ultrasonic data to monitor wall thickness 360° around a pipe diameter to predict corrosion and erosion rates in pipelines. The system consists of an instrumented band that

can be installed both onshore and off-shore. These bands contain a customizable number of ultrasonic transducer arrays, which can be placed in multiple patterns around the circumference of the pipe. Furthermore, sensor bands can be fitted with inclinometers to measure orientation (and change in orientation) to help define preferential corrosion around the circumference of the pipe. Sensorlink has developed UT signal processing techniques to increase accuracy and sensitivity to changes in wall thicknesses to $\leq$0.2 and $\leq$0.01 mm, respectively. To achieve this high resolution, this technology must take measurements over several days to weeks and cannot measure wall thicknesses over any length of pipe outside contact with the transducer arrays.

NDE techniques will provide material thickness at the covered locations; however, these will not be able to differentiate between the phenomena of erosion, corrosion, and erosion−corrosion. Technology gaps exist as all of these techniques have their limits of application in terms of temperatures, pressures, pipeline outer diameter, etc. Moreover, the use of these monitoring techniques subsea is highly dependent on the sensor life, robustness of the equipment, and ability to communicate wireless or transmit the data to the host.

14.5 Mitigation

Erosion−corrosion is a common challenge in oil and gas industry. It could cause the loss of primary containment, failure, and deferral. Erosion−corrosion threat is a combination of erosion and corrosion threats and their synergistic effects.

Sometimes the erosion−corrosion threat can be mitigated by using erosion barriers. For example, if the likelihood of corrosion threat in a system is small because of iron carbonate scale formation but unexpected sand production happens and causes damage in protective scale, controlling sand production will be the appropriate barrier. In this case, erosion mitigation could help to mitigate erosion−corrosion synergy. However, there are some cases in which both erosion and corrosion barriers are required to mitigate the erosion−corrosion threat. For example, if both corrosion and erosion threat likelihoods are high then both threats need to be mitigated separately to mitigate erosion−corrosion.

Different erosion and corrosion barriers are used in the oil and gas industry, Fig. 14.4 describes these. There are several factors affecting the selection of the best barriers. Material in contact with fluid is one of the key factors for selecting the right barrier for erosion−corrosion mitigation. This section is focused on erosion−corrosion mitigation for following scenarios: iron carbonate scale formation, iron sulfide scale formation, chemical inhibition for CS, and passive film formation for CRAs. The chart below summarizes different scenarios.

14.5.1 Carbon steels

CS are commonly used because of their good properties in comparison with CRAs but are more sensitive to general corrosion for oil and gas applications. Iron carbonate and iron sulfide scale formation and also chemical inhibition help reduce the corrosion

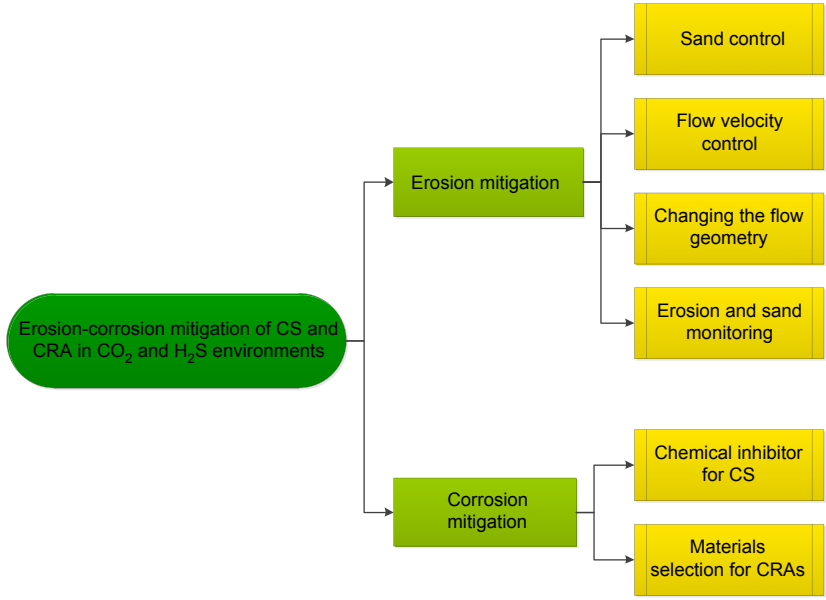

Figure 14.4 Erosion–corrosion mitigation for carbon steel (CS) and corrosion resistance alloys (CRAs) in CO_2 and H_2S environment.

rates for CS. However, a small amount of sand erosion could cause damage in the iron carbonate/sulfide scale or protective inhibitor film and consequently create synergistic erosion–corrosion effect. For example, corrosion inhibitor is used to reduce the corrosion rate. In this case, if well starts producing sand, then erosion could happen. In this case, even if models predict low erosion rate or CRA ER erosion monitoring probes show low erosion rate but sand erosion could cause mechanical removal of corrosion inhibitor film and cause synergistic erosion–corrosion for CS piping, flowline, jumper, riser, etc. A discussion of the erosion and corrosion mitigation strategies for CS materials in CO_2 and H_2S environment of oil and gas production follows.

14.5.1.1 Erosion mitigation

Sand control is one of the most well-known techniques for mitigating sand erosion. The use of sand screens downhole can be very effective for controlling sand and subsequently erosion. However, it is important to mention that the damage of sand screens can also happen because of erosion, abrasion, or corrosion. Corrosion-resistant materials are used for sand screens but corrosion damage to the sand screen could also happen during acid treatment of the well if corrosion assessment is not done correctly and right barriers are not in place. In addition, sand screens are able to control the larger sand particles but usually particles smaller than 50 μm can go through them. It is important to mention that sands smaller than 50 μm can also cause erosion and erosion–corrosion if sand concentration or flow velocity are high enough. Using sand filters could also help to remove the sand topsides.

There are several gaps related to sand control using sand screens. Prediction of remaining life of the sand screens is very important. Currently, there is very limited information available for erosion or abrasion modeling of sand screens mainly because of the complexity of the sand screens geometry.

Flow velocity control is also used for mitigating the erosion and erosion−corrosion. Controlling flow velocity could affect both erosion and corrosion parts of the erosion−corrosion [46]. However, this approach could be very expensive because during operation, reducing the flow rate means production deferrals. Flow velocity control as an erosion−corrosion mitigation approach should be applied in the design stage of the projects. Changing the size of the piping and equipment during operation could be very expensive too.

A technology gap for the erosion−corrosion mitigation using flow velocity control is erosion modeling. Erosion modeling is required to predict the operating flow velocity and if erosion modeling is not accurate enough, underprediction of erosion rate could cause leaks and overprediction could cause deferrals. Erosion rate predictions for two-phase (gas−liquid) flow, small particles, and complex geometries are some of the main challenges.

Change of flow geometry could be also used to mitigate erosion−corrosion. Geometry mainly affects the erosion part of the erosion−corrosion. There are several geometry considerations for erosion control. More details are available in the University of Tulsa, Erosion/Corrosion Research Center (E/CRC) erosion model user manual [47], ISO 13703 [48], EEMUA 194 [49], DNV RP O501 [37], API 17A [50], API 17B [51], and HSE UK Report 115 [52].

Erosion rate and sand monitoring could also be considered for erosion failure or damage mitigation by generating an alarm for controlling the production rate. In this case, monitoring tools help to mitigate the erosion−corrosion by alarming unacceptable sand production and erosion or even by automatic shutdown of the system.

14.5.1.2 Corrosion mitigation

Corrosion mitigation under erosion−corrosion conditions would be more challenging because scale formation would be very sensitive to sand erosion. E/CRC has done some work on evaluating the erosion performance of iron carbonate scale [45]. For the chemically inhibited systems, increasing the inhibitor concentration could be used to reduce the corrosivity of the system and compensate for the reduction of inhibitor efficiency by sand erosion. Sand erosion can reduce the inhibitor efficiency by the mechanical removal of inhibitor film. Sand can also adsorb inhibitor and reduce the effective inhibitor concentration in the system.

There are several technology gaps for corrosion mitigation under erosion−corrosion scenarios of CS materials. The minimum amount of sand erosion that could cause synergistic effect between erosion and corrosion in a chemically inhibited system is unknown. Different inhibitors may behave differently but it would be important to know what the erosion limit is for generic types of corrosion inhibitors used in oil and gas applications. There is also limited information available on modeling inhibitor dosage change required for a system with a specific amount of erosion.

14.5.2 Corrosion-resistant alloys

Erosion mitigation for CRA would be similar to CS. However, corrosion mitigation would be different. Materials selection is the key option for erosion–corrosion mitigation of CRAs. Some of the CRAs are susceptible to synergistic erosion–corrosion. Research at the University of Tulsa, Erosion/Corrosion Research Center (E/CRC), has shown that 13Cr is more susceptible to synergistic erosion–corrosion in comparison with higher Cr content CRAs [23].

14.6 Management

The management of erosion–corrosion requires a combination of all the elements described in previous chapters, and should include, as a minimum:

- Modeling and reduction of production rates as required
- Design to minimize flow velocities and avoid sudden changes in flow direction or direct impingement (e.g., at elbows, constrictions, and valves).
- Sand control (e.g., downhole sand screens and gravel packs)
- Measurement of sand production
- Corrosion monitoring, erosion monitoring
- Wall thickness measurements

As indicated in Fig. 14.5, the frequent review of all mitigation, monitoring, and inspection data is necessary for proper management of the mechanism. Also, key

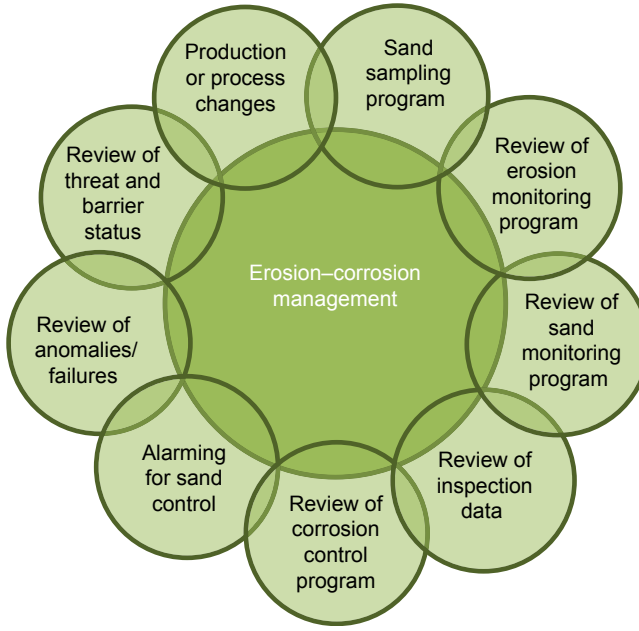

Figure 14.5 Outline of the erosion–corrosion management assessment process.

performance indicators should be established to ensure that erosion−corrosion rates are under acceptable limits and if not these actions are taken to correct the anomalies.

14.7 Conclusions

Erosion−corrosion is a complex mechanism that can affect both CS and CRAs in production environments. The current trend in Oil and Gas is to maximize the productivity of the fields while maintaining integrity of the production systems at the lowest cost. Production environments are becoming harsher in terms of temperatures and pressures, and more remote areas are been developed, which demands the development of unmanned facilities and remote and robust monitoring, possibly using online modeling to correlate inspection data. In terms of erosion−corrosion, this requires better modeling tools to predict critical velocities and assess the risk, close review, and follow-up of all monitoring and mitigation strategies.

In general, erosion−corrosion comprises a competition between the removal of a protective film (in the case of carbon and low alloy steels) or passive films (in the case of stainless steels) and the rate of formation (or repassivation) of the film. If the removal rate of the film is greater than its formation (or repassivation) rate, then an accelerated corrosion process will take place. If erosivity conditions are severe enough, base metal can also be removed by the mechanical erosion component. A mechanistic model of this competition needs to account for many factors such as film characteristics, the concentration and distribution of sand, the flow pattern, fluid flow velocities, geometry, and environmental factors.

14.8 Knowledge gaps and future research trends

This review has shown that mechanisms of erosion−corrosion in CS and CRAs are better understood in sweet environments (CO_2) but not so much in sour (H_2S) environments. Corrosion modeling capabilities are limited to CO_2 environments and limited as the corrosion mechanism is highly dependent on the specific material to be used.

The effect of corrosion inhibitors in erosion−corrosion is also an active area of research. A corrosion inhibitor can be effective in reducing the corrosion contribution to the erosion−corrosion, but not as effective as for similar conditions without sand. Sand erosion has been reported to decrease the inhibitor efficiency by partially removing the inhibitor film from the surface and also, to a lesser extent, by the adsorption of inhibitor on the sand particles. For corrosion inhibitors, it is the combination of kinetics and the adsorption mechanism under multiphase flow conditions that will make them effective in controlling erosion−corrosion. The minimum amount of sand erosion that could cause the synergistic effect between erosion and corrosion in a chemically inhibited system is unknown. Different inhibitors may behave differently but it would be important to know what the erosion limit is for generic types of corrosion inhibitors used in oil and gas applications. There is also limited information

available on modeling inhibitor dosage change required for a system with a specific amount of erosion.

In terms of field management, the current trend to avoid erosion−corrosion is to maintain velocities under certain thresholds and/or control sand production to an ASR. These thresholds are usually defined based on modeling, if erosion modeling is not accurate enough, underprediction of erosion rate could cause leaks and overprediction could cause deferrals. Erosion rate predictions for two-phase (gas−liquid) flow, small particles, and complex geometries are some of the main challenges.

The need to control sand rates, on the other hand, has led to continuous research and advances in sand and erosion−corrosion monitoring technologies. However, there are still technology challenges related to calibration and accuracy of sand monitoring tools, especially under multiphase flow regimes and small sand sizes.

References

[1] S. Shirazi, B. McLaury, J. Shadley, K.P. Roberts, E.F. Rybicki, H.E. Rincon, S. Hassani, F.M. Al-Mutahar, G.H. Al-Aithan, Erosion−Corrosion in Oil and Gas Pipelines. Oil and Gas Pipelines: Integrity and Safety Handbook, first ed., John Wiley & Sons Inc., 2015, p. 399.

[2] K. Tummala, Effect of sand production on chemical inhibition of CO_2 corrosion of carbon steel for iron carbonate scale forming conditions at high flow rates, in: Mechanical Engineering, University of Tulsa, Tulsa, 2009.

[3] R.J.K. Wood, Erosion−corrosion interactions and their effect on marine and offshore materials, Wear 261 (9) (2006) 1012−1023.

[4] B. Lu, Erosion−corrosion in oil and gas production, Research and Reviews in Materials Science and Chemistry. ISSN: 2319-6920 2 (1) (2013) 19−60. Jyoti Academic Press, http://jyotiacademicpress.net.

[5] J. Postlethwaite, M.H. Dobbin, K. Bergevin, The role of oxygen mass transfer in the erosion−corrosion of slurry pipelines, Corrosion 42 (9) (September 1986) 514−521.

[6] G.T. Burstein, K. Sasaki, Electrochim Acta 46 (2001) 3675−3683.

[7] B. Poulson, Corrosion Science 23 (4) (1983) 391−430.

[8] J. Postlethwaite, S. Nesic, Erosion−corrosion in single and multiphase flow, in: W. Revie (Ed.), Uhlig's Handbook, second ed., John Wiley & Sons, Inc., 2000, pp. 249−272.

[9] D.J. Stephenson, J.R. Nicholls, Modeling erosive wear, Corrosion Science 35 (5−8) (1993) 1015−1026.

[10] A.V. Levy, Erosion and Erosion−Corrosion of Metals Corrosion, 1995, p. 51.

[11] J.R. Shadley, S.A. Shirazi, E. Dayalan, E.F. Rybicki, Prediction of erosion−corrosion penetration rate in a carbon dioxide environment with sand, Corrosion 54 (1998).

[12] J.R. Shadley, et al., Velocity guidelines for preventing pitting of carbon steel piping when the flowing medium contains CO_2 and sand, in: CORROSION 1996, NACE International, Houston, TX, 1996.

[13] F. Al-Mutahar, Erosion−corrosion for carbon steel in sweet production with sand: modeling and experiments, in: Mechanical Engineering, University of Tulsa, Tulsa, 2012.

[14] R. Malka, S. Nešić, D.A. Gulino, Erosion corrosion and synergistic effects in disturbed liquid-particle flow, in: CORROSION 2006, NACE International, 2006.

[15] S. Hassani, K. Roberts, S. Shirazi, J. Shadley, E. Rybicki, C. Joia, Flow loop study of chloride concentration effect on erosion, corrosion and erosion−corrosion of carbon steel in CO_2 saturated systems, in: CORROSION 2011, Houston, TX, 2011.
[16] S. Hassani, K. Roberts, S. Shirazi, J. Shadley, E. Rybicki, C. Joia, Characterization and prediction of chemical inhibition performance for erosion−corrosion conditions in sweet oil and gas production, in: CORROSION 2012, NACE International, Salt Lake City, UT, 2012.
[17] S. Hassani, K. Roberts, S. Shirazi, J. Shadley, E. Rybicki, C. Joia, Flow loop Study of chloride concentration effect on erosion, corrosion and erosion−corrosion of carbon Steel in CO_2 saturated systems, in: CORROSION 2012, Salt Lake City, UT, NACE International, 2012.
[18] A. Nassef, M. Keller, K. Roberts, E. Iski, E. Rybicki, S. Shirazi, Erosion−corrosion of low carbon steel inhibition in oil-brine-sand flow, in: CORROSION 2016, NACE International, Vancouver, Canada, 2016.
[19] H.E. Rincon, Testing and prediction of erosion−corrosion for corrosion resistant alloys used in the oil and gas production industry, in: Mechanical Engineering, University of Tulsa, Tulsa, 2006.
[20] J.D. Combes, J.G. Kerr, L.J. Klein, 13Cr Tubulars Solve Corrosion Problems in Tuscaloosa Trend, Petroleum Engineer International, March 1983.
[21] M.S. Cayard, R.D. Kane, Serviceability of 13Cr tubulars in oil and gas production environments, in: CORROSION/98, Paper No. 112 (Houston, TX, USA, NACE International), 1998.
[22] U. Lotz, E. Heitz, Flow-dependeant corrosion. I. Current understanding of the mechanisnsm involved, Werkstoffe und Korrosion 34 (1983) 454−461.
[23] H.E. Rincon, J.R. Shadley, E.F. Rybicki, Erosion−corrosion phenomena of 13Cr at low sand rate levels, in: CORROSION 2005, NACE International, Houston, TX, 2005.
[24] T. Kohley, E. Heitz, Particle containing formation water for the study of erosion corrosion, ASTM STP 970, in: The Use of Environments for Corrosion Testing, American Society for Testing and Material, Philadelphia, 1988, pp. 235−245.
[25] D. He, X. Jiang, S. Li, H. Guan, Erosion and erosion−corrosion behaviors of several stainless steels in dual-phase fluid, Corrosion 58 (3) (2002) 276−282.
[26] H.E. Rincon, J. Chen, J.R. Shadley, Erosion−corrosion phenomena of 13Cr alloy in flows containing sand particles, in: CORROSION 2002, NACE International, Houston, TX, 2002.
[27] J. Chen, J.R. Shadley, H.E. Rincon, E.F. Rybicki, Effects of temperature on erosion−corrosion of 13Cr, in: CORROSION 2003, NACE International, San Diego, California, 2003.
[28] J. Chen, J.R. Shadley, E.F. Rybicki, Activation/repassivation behavior of 13Cr in CO_2 and sand environments using a modified electrochemical noise technique, in: CORRROSION 2002, NACE International, Houston, TX, 2002.
[29] H.E. Rincon, J.R. Shadley, K.P. Roberts, E.F. Rybicki, Erosion−corrosion of corrosion resistant alloys used in the oil and gas industry, in: CORROSION 2008, NACE International, New Orleans, Louisiana, 2008.
[30] G. Mori, T. Vogl, J. Haberl, W. Havlik, T. Schöberl, Erosion corrosion and synergistic effects under high velocity multiphase conditions, in: CORROSION 2010, NACE International, San Antonio, TX, 2010.
[31] Scale prediction software ScaleSoftPitzer (SSP), Brine Chemistry Consortium Joint Industrial Project at Rice University.

[32] M. Johnson, M.B. Thomson, Ferrous carbonate precipitation kinetics and its impact on CO_2 corrosion, in: Proceedings of CORROSION/1991, NACE International, Houston, TX, Paper No. 268, 1991.
[33] E. Van Hunnik, B. Pots, E. Hendriksen, The formation of protective $FeCO_3$ corrosion product layers in CO_2 corrosion, in: Proceedings of CORROSION/1996, NACE International, Houston, TX, Paper No.6, 1996.
[34] S.N. Smith, Predicting corrosion in slightly sour environments, Materials Performance (August 2002) 60−64.
[35] A.K. Agrawal, C. Durr, G.H. Koch, Sulfide films and corrosion rates of AISI 1018 carbon steel in saline solutions in the presence of H_2S and CO_2 at temperatures up to 175°F, in: CORROSION 2004, Paper 04383, 2004, p. 4.
[36] J.S. Smart III, A review of erosion corrosion in oil and gas production, in: CORROSION 1990, Paper No,10, 1990, p. 10/9.
[37] American Petroleum Institute, Recommended Practice for Design and Installation for Offshore Production Platform Piping Systems. API Recommended Practice 14E (API-RP-14E, fifth ed., October 1991. Reaffirmed January 2013.
[38] DNVGL Recommended Practice O501, Managing sand production and erosion, August 2015 ed.
[39] C.N. Emiliani, K. Lejon (Statoil), M. Linden, J. Engene, O. Kvernvold (DNV), C. Packman (Roxar), D. Clarke (Cormon), T. Haugsdal (ClampOn), Improved sand management strategy: testing of sand monitors under controlled conditions, Paper SPE 146679-PP, Presented at the SPE Annual Technical Conference, October 2011, 2011.
[40] B. McLaury, TUSMP Executive Summary of Progress, May 2016. http://www.tusmp.utulsa.edu/.
[41] V. R. Ponnagandla, Tulsa University Sand Management Projects (TUSMP), Presentation on Acoustic Sand Monitoring Presented at the May 2016 Advisory Board Meeting.
[42] M.A.O. Alum, C. Nworah, A. Omolegbe, A Review of Erosion−Corrosion Monitoring and Inspection Techniques for Amenam High Pressure (HP) Header, SPE-172360−MS, Prepares for presentation at the SPE Nigeria Annual International Conference and Exhibition held in Lagos, Nigeria, August 2014, 2014.
[43] http://www.clampon.com/products/subsea/corrosion-erosion-monitor-2/.
[44] www.teledyneoilandgas.com.
[45] www.sensorlink.no.
[46] F. Al-Mutahar, Erosion−Corrosion for Carbon Steel in Sweet Production with Sand: Modeling and Experiments, 2012.
[47] Sand Production Pipe Saver (SPPS) 5.2 User Guide, October 2016.
[48] ISO 13703:2000 Petroleum and Natural Gas Industries − Design and Installation of Piping Systems on Offshore Production Platforms, International Organization for Standardization.
[49] EEMUA Publication No. 194, Guidelines for Materials Selection and Corrosion Control for Subsea Oil and Gas Production Equipment, third ed., Engineering Equipment and Materials Users Association, March 2012.
[50] API Recommended Practice 17A, Design and Operation of Subsea Production Systems − General Requirements and Recommendations, fourth ed., American Petroleum Institute, January 2006 reaffirmed April 2011.
[51] API Recommended Practice 17B, Recommended Practice for Flexible Pipe, fifth ed., American Petroleum Institute, May 2014.
[52] Prepared by TÜV NEL Limited for the UK Health and Safety Executive, Research Report 115, Erosion in Elbows in Hydrocarbon Production Systems: Review Document, 2003.

Under-deposit corrosion

15

Bruce Brown [1] *and Jeremy Moloney* [2]
[1]Ohio University, Athens, OH, United States; [2]Nalco Champion, An Ecolab Company, Sugar Land, TX, United States

15.1 Introduction

Produced fluids from many oil and gas wells have been known to carry silt, sand, and solids from the geologic reservoir, which can be left behind as deposits along the interior of a production or transmission pipeline. These deposits become a diffusion barrier between the produced fluids and the interior pipe wall, which results in the water chemistry near the steel surface to differ from that of the bulk fluids. Observations from laboratory studies and field cases have shown that these deposits influence corrosion mechanisms and lead to a localized corrosion called under-deposit corrosion (UDC). Often found at low-flow areas inside pipelines, UDC is a very aggressive form of corrosion that occurs when suspended solids and precipitated phases are given the opportunity to settle to the bottom of the pipeline. The three general categories of deposits include inorganic deposits, such as sand, clay, and corrosion products; organic deposits, such as asphaltenes and wax; and "schmoo," which is a mixture of organic and inorganic deposits [1].

Depending upon the environmental attributes and the type of deposits, different corrosion mechanisms can be applied to explain UDC. The main observation from laboratory studies [2–7] has been the large increase in electrical potential difference that occurs between a metal electrode under a sand deposit and a bare metal electrode, both in the same solution, when an inhibitor was added. The bare metal electrode would increase to a more positive potential because of the reduction in both anodic and cathodic reactions, whereas the potential of the UDC electrode might not be affected at all as a result of the sand acting as a diffusion barrier toward the corrosion inhibitor. When these two metal electrodes were connected together, the UDC electrode experienced a strong anodic polarization and, thus, galvanic corrosion. Other laboratory studies that focused on a single UDC electrode [8–14] found that the influence of a deposit on corrosion and mitigation mechanisms was to create a mass transfer barrier that limited the transfer of species (ions, inhibitors, and biocides) to and from the metal surface. Experiments have also shown deposits to provide additional surface area, which causes parasitic adsorption of inhibitors and biocides, and in turn their effectiveness is reduced. The review of research observations provided in this chapter on UDC contains information on the effect of deposits on the surface area for localized corrosion, types of deposit materials, experimental methodologies, mitigation methods for UDC, and gaps in the current knowledge that require future research.

Trends in Oil and Gas Corrosion Research and Technologies. http://dx.doi.org/10.1016/B978-0-08-101105-8.00015-2

15.2 UDC mechanisms related to the deposit

Solids are often carried by the fluid flow from the reservoir and can accumulate in an operating pipeline to become a deposit when the energy of the flow is not high enough to keep them suspended or moving. These deposits are understood to contain a mixture of water, hydrocarbons, microorganisms, and inorganic compounds along with corrosion products and scales, which, of course, differ from field to field and almost certainly differ down the same pipeline as water chemistry conditions change with temperature and pressure. It is also understood that the corrosion mechanisms are influenced by whether the deposit is inert or conductive. In this section, some of the components that make up the deposits and how each will influence corrosion, along with a calculation of the cathode to anode area ratio that can be developed in relation to the depth of the deposit, are reviewed.

15.2.1 Inert deposits

Most commercial oil and gas reservoirs occur in sedimentary rock deposits because of their characteristic permeability and porosity. Sedimentary rocks form in the Earth's crust through a sequence of physical, chemical, and biological processes. Common sedimentary minerals include silicates, carbonates, clay, and iron. Silicates and carbonates make up most of the rock-forming minerals and are considered insulators with electrical resistivity greater than 10^9 ohm·m. Sand, silt, and clay are classified by grain size and composition. Sand ranges in diameter from 2 to 0.063 mm, whereas silt ranges in diameter from 0.063 to 0.002 mm, and clay is defined as less than 0.002 mm in diameter. Both sand and silt are mainly composed of SiO_2-rich particles, whereas clay is composed mainly of aluminosilicates with a sheet structure [15]. Although some reservoirs have an inherent problem with the production of solids, high rates of production from a reservoir or a stimulation treatment to increase production from an existing well may also cause the migration of formation sand, silt, and clay through the production string into the pipeline.

The presence of non-conductive or inert deposits, such as sand, silt, and certain scales, on the pipe wall can act as a diffusion barrier to limit the mass transfer of corrosive species, inhibitors, biocides, or other oilfield chemicals from the bulk solution to the metal surface. When this is the only mechanism involved in corrosion, this diffusion barrier generally retards the corrosion under the body of the inert bed. To prove this mechanism, Huang et al. [8] tested clean inert solid deposits with different particle sizes (SiO_2 powder, glass beads, and sand) to determine the effect of the deposited solids on the fundamental mechanisms of CO_2 corrosion. The specially designed metal specimen holder used in that study is shown in Fig. 15.1. The three layers of the holder were used to (1) isolate the electrical connections from the solution, (2) support a removable metal specimen so only the top of the specimen was exposed to the environment, and (3) define the thickness of the sand bed. Using this type of specimen holder to generate a reproducible 5-mm depth for each inert solid deposit, a linear relationship between the deposit porosity and the average CO_2 corrosion rate of an X65 steel in 24-h experiments was obtained (Fig. 15.2).

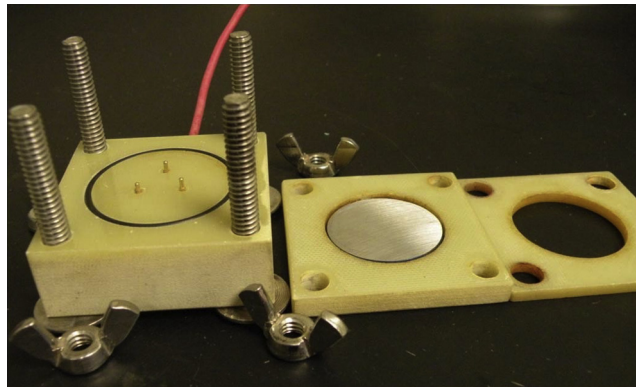

Figure 15.1 Specimen holder: (a) base, with three gold contacts to connect the steel specimen and wire for electrochemical measurements; (b) steel specimen holder; (c) sand holder, machined to the desired depth of the sand deposit [16].

This linear relationship between the deposit porosity and corrosion rate [16] was an indication that both anodic and cathodic reactions were significantly retarded underneath the deposited inert solids. As ferrous ions are released from the metal surface under a deposit, their concentration is much greater near the metal surface because of the slow flux through the low porosity of the sand bed to the bulk solution. The increase in ferrous ion concentration increases the pH and saturation value near the metal

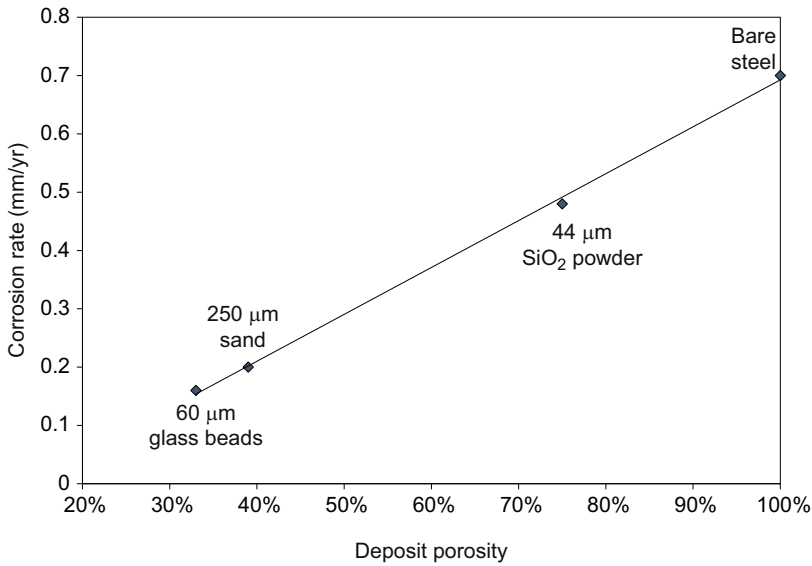

Figure 15.2 Deposit porosity and CO_2 corrosion rate relationship (pH 5, 25°C (77°F), 1 bar (14.5 psi) pCO_2, deposit depth 5 mm, 24 h) [8].

surface, leading to near surface precipitation. This was proved by Huang et al. [8], who found that the pH under the deposit was consistently near pH 6 independent of temperature (25 and 80°C or 77 and 176°F, respectively), type of deposit (SiO_2, sand), and bulk solution pH (pH 4, 5, and 6). When an inert deposit was used to fully cover the steel specimen, these types of deposits were not found to cause localized corrosion but to have consistently low CO_2 corrosion rates under the deposits for all the conditions tested. As the corrosion products within the inert deposit increase with time, corrosion was limited by blocking sites on the surface where metal loss or cathodic reactions might occur. The sand bed literally starved the reaction of the fuel that it needs to continue.

15.2.2 Conductive deposits

Iron sulfides are probably the most encountered semiconductive deposit types in oil and gas production and transmission pipelines. Numerous iron sulfides can exist, the nature of which is dependent on the environment and operating parameters. Rickard and Luther [17] provide a comprehensive review of the chemistry of iron sulfides, including their semiconductive properties. A semiconductor is a crystalline or amorphous solid with an electrical resistance (ER) much larger than metals, but with lower resistance than an insulator, that increases in electrical conductivity with an increase in temperature. Electrical resistivity is the inverse of the material's electrical conductivity. Electrical resistivity has the greatest variation of any materials' physical property from metals as low as 10^{-7} ohm·m to insulators at approximately 10^{20} ohm·m, where semiconductors range from having insulator properties (10^{6} ohm·m) to being conductive (10^{-5} ohm·m). Iron sulfides, such as pyrrhotite and pyrite, have been measured to have a resistivity between 10^{-5} and 1 ohm·m, which is in the higher range of conductive properties for a semiconductor [18,19].

Research on the effect of iron sulfides on corrosion of mild steel has shown their influence on anodic and cathodic reactions [20,21] and their influence on accelerating corrosion [11,22]. In a UDC study on X65 steel, Menendez et al. [11] used five different types of iron sulfide deposits obtained from various sources, which were characterized with respect to their particle size, crystalline structure, and surface composition using particle size analysis, X-ray diffraction, and X-ray photoelectron spectroscopy. Corrosion studies were conducted at 65°C with partial pressures of 370 bar (5.4 ksi) pH_2S and 710 bar (10.3 ksi) pCO_2. In 100-h autoclave corrosion testing, mass loss specimens fully covered with one of the specific iron sulfide deposits show that the mackinawite-type deposit facilitated the most corrosion. X65 specimens covered with two synthesized batches of mackinawite had general corrosion rates of up to 4 mm/year, whereas those covered with mackinawite synthesized with excess Na_2S exhibited the highest general corrosion rate of 6 mm/year. However, specimens covered with two commercially acquired iron sulfide powders only had general corrosion rates of 0.2 mm/year. When specimens in an autoclave were exposed to similar conditions with 48,500 ppm Fe^{2+} in solution to induce mackinawite precipitation over 168 h, the general corrosion rate was only 0.6 mm/year, but pitting corrosion ranging from 300 to 500 μm in depth (greater than 2500 mm/year) proved that the

precipitated mackinawite facilitated localized attack. The localized corrosion morphology produced in the mackinawite precipitation experiments was considered to have good agreement with UDC attack observed in the field. Jing et al. [22] also found localized corrosion was initiated once a sufficient amount of mackinawite corrosion product had formed and was transformed into greigite and/or pyrrhotite. The initiation of localized corrosion was thought to be due to the galvanic effect exaggerated by the differences in electrical conductivity of the different iron sulfides.

One specific study on iron sulfide UDC focused on evaluating the galvanic corrosion through the use of a specialized probe with an actual field sludge deposit in a CO_2/H_2S environment. Alanazi et al. [9] conducted weight loss and electrochemical corrosion tests using a coupled multielectrode array system (CMAS) that contained 25 flush-mounted carbon steel rods (UNS G10180) with an active surface area of 0.45 cm^2 and a 1.5-cm-thick sludge deposit. Analysis of the sludge deposit shows that it was made up of 85 wt% $CaCO_3$, 8 wt% pyrite, and 3 wt% mackinawite with smaller amounts of other inert species. The CMAS was coupled to a carbon steel rod (UNS G10180) with an approximate surface area of 26 cm^2, which was in the bulk solution. The gas mixture used was 0.1 mol% H_2S and 0.39 mol% CO_2, with the balance of gas being nitrogen at a total pressure of 1 bar (14.5 psi) and temperature of 48°C (118°F). Electrochemical and galvanic corrosion testing conducted with the CMAS measured average galvanic corrosion rates of 30 mm/year underneath the sludge deposit when coupled with the electrode not under the deposit. Under the same environmental conditions, the 2.54-cm-diameter weight loss specimens without deposit had general corrosion rates less than 1 mm/year over a 24-h experiment time. The mackinawite in the field sludge was believed to be the cause of the very high localized corrosion rates observed for the multielectrodes. This was expected because the mackinawite is conductive, but the weight loss specimens were also a reminder that the high localized corrosion required a large cathode external to the deposit to drive the high corrosion rates.

15.2.3 Effect of deposit on surface area in inhibited pipelines

In a pipeline, sand and solids tend to collect along the bottom of the cylindrical surface as a result of gravity, leaving a much greater metal surface area within the pipeline that is not under the sand bed. For example, an inhibited water injection line with a full pipe flow containing a sand bed with a depth that is 1% of the pipe diameter can have almost 15 times more cathodic area from the pipe walls than the anodic area under the sand bed. Fig. 15.3 shows the relationship between the depth of an inert sand bed (% depth ratio) in a pipeline and the ratio between the surface area of the pipeline above and below a deposit (ratio of cathode area to anode area) in an inhibited full-pipe flow.

Many laboratory experiments have been designed to evaluate an inhibitor's performance in the presence of an inert sand deposit. These experiments have been designed to study the effectiveness of an inhibitor through a sand bed and have used cathode to anode area ratios of 4:1 or smaller. From Fig. 15.3, it can be seen that a 10% sand bed depth ratio (i.e., 1 cm sand depth in a 10.1-cm-diameter pipeline) is almost equivalent to a 4:1 cathode to anode ratio in an inhibited pipeline.

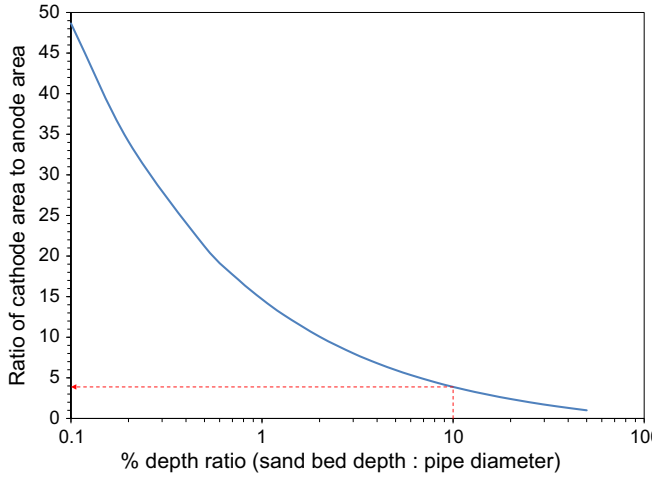

Figure 15.3 Ratio of cathode to anode based on sand depth.

15.3 Research methodologies

There are many different methods that have been used to study UDC in controlled laboratory conditions. Testing methods used by various researchers have been developed based on postulates for UDC mechanisms from failure analysis and laboratory studies, so research in this area has varied widely. Studies have focused on the mechanisms of solid deposition, the chemical makeup of the solid deposit, mechanisms of diffusion through the solid deposit, and the galvanic effect, which can be caused by the presence of both a solid deposit and the ever necessary corrosion inhibitor. The fact that UDC is a form of localized corrosion is even viewed differently by different researchers. If there is a higher general corrosion rate under the entire deposit as compared with the remaining pipe walls in an inhibited system, then the localized corrosion area of metal loss is under the entire sand bed. But most of the discussion in the literature has focused on finding deeper pitting corrosion that occurs within the area underneath the sand bed. Experiments to uncover corrosion mechanisms related to UDC have looked at the lack of inhibitor reaching the metal surface under the deposit, the corrosion experienced by a single metal specimen under the sand deposit, and the effect of galvanic corrosion when using multiple metal specimens in the same experiment (one metal specimen with a deposit coupled to another metal specimen without a deposit in the same solution).

As with any research topic, UDC has been studied with many different viewpoints because of the various possible compositions of the deposit and the method in which it was deposited. In experiments related to diffusion through solids, many have suggested parasitic consumption of inhibitor on the large surface area of the sand particles as the reason for loss of inhibition and the occurrence of localized corrosion [4,13,14,23]. In experiments using electrochemical measurements of coupled metal

specimen to characterize the UDC phenomena, it was understood that the presence of certain inhibitors in association with the characteristics of the deposit would induce a galvanic cell with the anodic part being the small area under the sand bed and the cathodic part being the much larger surface area of the surrounding pipeline [3–7,9,13,16,23]. In experiments using an uncoupled metal specimen to understand the role of the deposit material in UDC, it was understood that the depth of the deposit mainly creates a diffusion barrier that should cause widespread corrosion underneath an inert sand bed, but small areas of localized corrosion were found that required more explanation [16,24]. This led to experiments with single sand grains spread out on a single corrosion specimen in the presence of a corrosion inhibitor, which created a methodology for repeatable pit initiation in the presence of a corrosion inhibitor [24,25]. It also changed the viewpoint that parasitic consumption of the inhibitor was the main cause of the observed isolated localized corrosion under a deposit. The link between the coupled metal specimen experiments with only one specimen under a deposit and the single specimen with a partial sand coverage is the galvanic effect that occurred in the presence of an inhibitor. This shows the real need to understand how the mechanisms related to this galvanic effect could be influenced by the inhibitors used to mitigate UDC.

The examples of test methodologies in the following discussion are representative of what is found in the literature. Most techniques have been developed by one set of researchers and slightly tweaked by others to learn something new or to relate to their individual project goal. The one procedure in common with all techniques is that they all involve time for precorrosion before the inhibitor is added.

15.3.1 Parasitic loss of the inhibitor to the solid deposit

Because most inhibitors are surfactants, the first assumption is that an increased surface area caused by the addition of sand will cause a parasitic loss of the inhibitor to the liquid/solid interface. Two types of experiments have been conducted without the sand or deposit material coming into contact with the corroding sample to determine if parasitic loss is a factor for the specific inhibitor being used.

A basic bubble test method [12] has been used to assess if the presence of solids affects the efficiency of the tested inhibitor(s). The sand did not come in contact with the metal being tested but was dropped into the glass cell with the metal to increase the surface area for inhibitor adsorption. An experiment with the sand present in the glass cell would be compared with an experiment with the same exact environmental conditions without the sand. If a higher corrosion rate occurred repeatedly when sand was present in the glass cell, then parasitic loss of the inhibitor was attributed for the difference.

The second method was to use a two-stage test involving column adsorption and then a corrosion inhibition test [13,14]. These experiments used a prescreening column to determine the adsorption and penetration of each corrosion inhibitor on a solid (ideal or field specimen), then used the same inhibitor in a separate corrosion experiment. The corrosion experiment was carried out under selected test conditions using an electrochemically measured specimen with a deposited solid and an electrochemical probe

with no deposit for comparison. Good correlation was observed between low adsorption in the column tests and acceptable performance in the corrosion experiments.

15.3.2 Experiments on coupled specimen

The galvanic effect for coupled specimen, observed in UDC experiments for two metal specimens in the same solution with one under the deposit, has shown this mechanism to be the dominant driving force for localized UDC. The two methodologies shown in the following sections greatly increase the difficulty level for experimental preparations and procedures but have been used to monitor localized corrosion during an experiment through the use of an external potentiostat or zero resistance ammeter (ZRA).

15.3.2.1 Inert deposit test methods

Many researchers have found that there is a large difference in the electrode potential between a sand-covered mild steel specimen and a noncovered mild steel specimen when both are exposed to a corrosion inhibitor. When these two specimens are coupled together, using similar anode to cathode surface area ratios that might exist in an inhibited pipeline, the galvanic current between them leads to localized corrosion under the deposit.

The sand deposit test method [4] has been used to investigate environments where sand or mineral scale deposition was possible. These experiments were conducted in a 3-L glass cell with a test apparatus designed so that prepared sand could easily be added during the experiment on top of the API 5L X65 specimens. Three metal specimens were molded into a flat epoxy square, such that the two 1 cm^2 surface area specimens were next to each other and parallel to the one large 4 cm^2 surface area specimen. The square epoxy mold was mounted in the test apparatus at approximately 45 degrees angle so that the bottom two specimens would be covered by about 5 mm sand after a 2-h precorrosion. Only one of the small specimens was galvanically coupled to the non-sand-covered specimen creating a 4:1 cathode to anode surface area ratio when inhibitor was present. This design provided direct proof of the effect of sand on inhibitor performance and the effect of inhibitor on UDC. The key observation in studies with this apparatus proved the effect of inhibitor addition on the galvanic couple between a sand-covered specimen and a bare specimen that would polarize the sand-covered specimen anodically, leading to localized attack.

Testing by Pedersen et al. [2] found an increase in the open circuit potential (OCP) of an individual bulk solution specimen without sand as compared with the OCP of an individual specimen underneath a 5-mm sand deposit. Their experiments used two specimens fully covered in sand (FS1 and FS2), each of 1 cm^2 surface area, along with one specimen with no sand (NS) of 4 cm^2 in area. When NS and FS1 were coupled together, the coupled potential would be closer to the OCP for NS because of the 4:1 cathode to anode ratio. The change in OCP for FS1 was believed to be the driving force for galvanic corrosion. This experimental technique provided an

evaluation methodology for determining the effectiveness of specific inhibitors toward localized corrosion inhibition in UDC and should be considered beneficial for inhibitor comparison studies. For this methodology, factors identified during inhibitor testing on UDC conditions that increase the susceptibility to localized corrosion would include the degree of anodic polarization of a single specimen, the effect of underdosage of the inhibitor, the effect of degradation of the inhibitor with time at higher temperatures, and the effect of corrosion product layer formation. In these studies [2], testing of two inhibitors under similar conditions proved that inhibitor chemistry played a role in the mitigation efficiency of UDC, with an imidazoline salt showing better efficiency than an alkyl amino acid.

A series of experiments by Barker et al. [3], utilizing the electrode configuration in Fig. 15.4, considered the influence of inhibitor components, which included imidazoline, phosphate ester, sodium thiosulfate, and 2-mercaptoethanol, with results indicating the two sulfur-containing compounds had the highest mitigation efficiencies toward UDC general corrosion. Each inhibitor component chemical was tested at 45 ppm, equivalent to a 150-ppm inhibitor package with 30% active chemical. A test duration of 20 h was used for the comparison but was not considered long enough to develop localized corrosion on the individual 1 cm^2 surface area specimens underneath the sand bed. The phosphate ester inhibitor had the highest mitigation efficiency on the bulk solution specimen in the presence of sand, whereas it had the lowest mitigation efficiency on UDC; this led to the conclusion that consumption of inhibitor by an excessive sand surface area may not be the initiator for localized corrosion and other factors may be responsible. For each inhibitor component, it was found that the deposition of sand retarded both anodic and cathodic reactions at the steel surface. With the addition of most of the inhibitors, the galvanic current between the UDC electrode and the sand-free electrode was observed to favor anodic dissolution under the deposit. The sodium thiosulfate and the 2-mercaptoethanol were found to decrease the general UDC rates to less than 0.1 mm/year at bulk solution concentrations as low as 5 ppm.

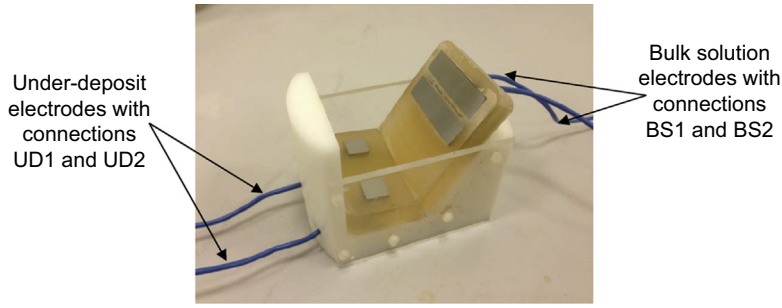

Figure 15.4 Specimen holder having under-deposit working electrodes with a 1 cm^2 area and bulk solution working electrodes with a 4 cm^2 surface area [3].

15.3.2.2 Coupled multielectrode array

A coupled multielectrode array (CMAS) test or wire beam electrode (WBE) method [5–7,10] uses multiple small-diameter wires or pins flush mounted in an inert material that are coupled together externally from the test environment so that the electrode array can be tested as one piece of metal or monitored individually for galvanic corrosion and/or localized corrosion. The cited work have used either a 24-electrode array [5,6,10] or a 100-electrode array [7].

As shown in Fig. 15.5, the 24-electrode array was designed using a polyethyl ethyl ketone (PEEK) casing around the electrodes, which was fitted into a polytetrafluoroethylene cup that would hold 10 mm of an inert deposit. Analysis of the multielectrode array was performed by progressive polishing of the PEEK holder containing the electrodes to physically determine the depth of corrosion that occurred to the nearest 20 μm. Experiments using this device [6] confirmed the addition of an inhibitor polarized a non-sand-covered electrode to a more noble potential with respect to a sand-covered electrode, which accelerated the corrosion rate under the sand deposit. In most of their experiments with industrial inhibitors relevant to oilfield applications, this galvanic corrosion would continue in excess of 30 days.

Hinds and Turnbull [10] used a 24-pin multielectrode probe under two different CO_2/H_2S partial pressure ratios of 5:3 (1.67 bar or 24 psi pCO_2 with 1 bar or 14.5 psi pH_2S) and 100:1 (2 bar or 29 psi pCO_2 with 0.02 bar or 0.29 psi pH_2S) with a 1-cm sand bed with particles of 0.1–0.3 mm diameter in a 10-L autoclave. The precorrosion step was conducted in a CO_2-purged solution by applying an anodic current of 1273 A/m^2 to individual 1-mm-diameter electrodes (UNS G10180) for a defined time before the addition of H_2S to corrode sets of pins to a specific depth (eight at 1 mm, eight at 0.1 mm, and eight uncorroded). Because of this, there was no uninhibited baseline corrosion rate for comparison. After precorrosion, all 24 pins were galvanically coupled to an external carbon steel rod (UNS G10180) with an

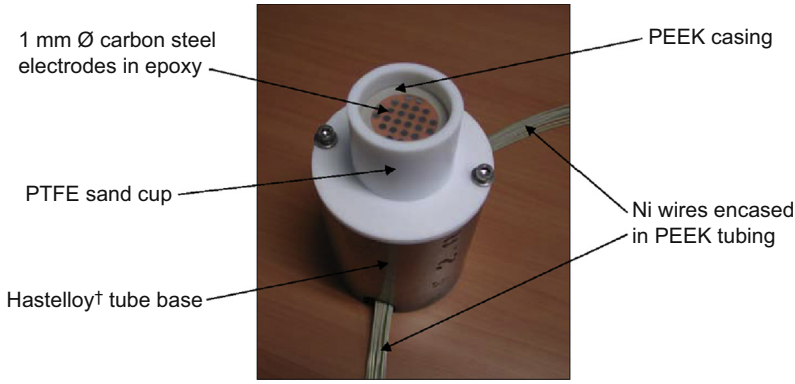

Figure 15.5 Coupled multielectrode array [6]. *PEEK*, polyethyl ethyl ketone; *PTFE*, polytetrafluoroethylene; †, trade name.

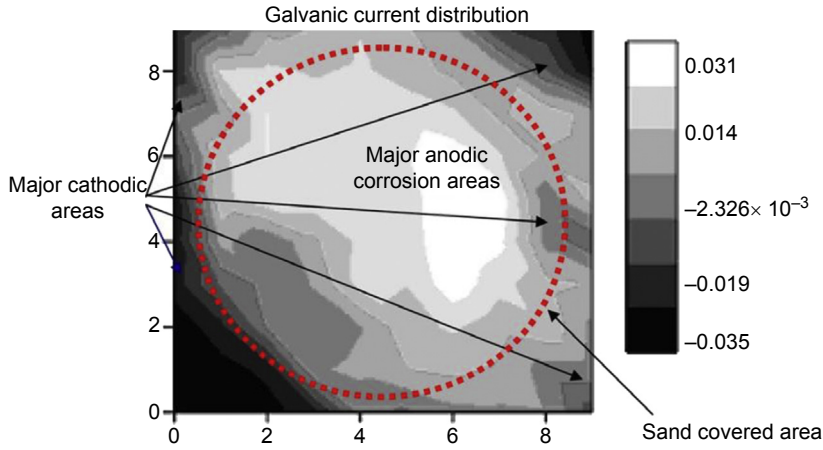

Figure 15.6 Galvanic current distribution map measured using a wire beam electrode exposed to CO_2 under-deposit corrosion conditions with imidazoline-type inhibitor present [7].

approximate surface area of 32 cm^2, which was in the bulk solution, and inhibitor was added. The CO_2/H_2S gas mix was then added and galvanic corrosion rates were monitored until the corrosion rate on most pins was less than 0.1 mm/year. They found that the amount of time for the inhibitor to provide protection through the sand bed was related to the amount of precorrosion as the non-precorroded pins were inhibited within 2 days, the 0.1-mm-depth precorroded pins were inhibited within 4 days, and the 1-mm precorroded pins took 4 days to achieve the desired corrosion rate.

As shown in Fig. 15.6, the 100-electrode WBE array [7] was used to directly measure the galvanic current distribution under the deposit. This typical map was collected in a CO_2-purged solution at 25°C (77°F) after 10 ppm imidazoline inhibitor was added. Notice that the anode areas are located within the ring under the sand deposit, whereas the cathode areas are mainly located where no sand was present. The maximum anodic current measured ranged from 0.022 to 0.034 mA/cm^2 in the central areas of the deposit.

15.3.3 Experiments on an individual specimen

Experiments using a single corroding specimen under a deposit are focused on the deposit's direct effect on the basic corrosion mechanisms associated with the deposit and/or the inhibitors' ability to diffuse through the deposit or under the individual sand grains to the metal surface. From the literature, as well as the research previously reviewed in this chapter, it appears as though there is a general consensus that a stagnant deposit acts as a diffusion barrier that slows down the transfer of corrosive species, inhibitors, and/or biocides to the metal surface while also slowing down the transport of corrosion products away from the metal surface. There is also strong evidence that the mechanism of galvanic corrosion occurs between deposit covered and

noncovered areas in the presence of specific inhibitors, even when the metal surface has a partial or minimal coverage by an inert deposit.

15.3.3.1 Full coverage deposit

A lot of experimentation has been carried out using a single specimen underneath a deposit to access the effect of the deposit on corrosion and corrosion mitigation. This type of testing should be completed as a first step to develop the foundation of information used to understand more complex corrosion mechanisms or could be used in more complex systems to gain insight on specific issues. The first example helps to build the foundation of information through repeatable experiments in a cup-style specimen holder to provide a consistent sand bed depth for electrochemical or weight loss studies in an autoclave. The second example used specially designed equipment to experimentally compare the in situ inhibited corrosion rate for a specimen with an iron sulfide corrosion product layer with a similar specimen with a deposit of iron sulfide deposited as a precipitate from the bulk solution to understand the effect of each on corrosion mitigation. The third example delivers a broader scope of the more foundational information by changing the environmental parameters of temperature, sand thickness, and inhibitor dosage to understand the effect of each on UDC and the mitigation of UDC. The different test methods discussed later show an increase in the desire to provide experimental methodologies to uncover corrosion mechanisms related to UDC.

The UDC autoclave method [13] is an extension of a regular inhibitor autoclave test with a special specimen holder that had a 1-cm raised edge to hold nonconductive solids on top of a concentric ring−type three electrode and a regular three-finger linear polarization resistance (LPR) probe to measure general corrosion. After the precorrosion step without the solid deposit, the specimens were removed from the autoclave, rinsed with ethanol, and quickly dried with nitrogen gas. The cup was filled with deoxygenated prepared sand and the autoclave put back together for the remainder of the experiment. Reported tests included four inhibitors plus a blank test with no inhibitor and no deposit. Test times ranged from 6 to 30 days, with most at 25 days. It was suggested that an inhibitor must provide good mitigation efficiency for a non-deposit-covered specimen before it should be tested with a deposit, but that does not always mean the inhibitor will perform well with a sand deposit present. If H_2S and/or iron sulfide deposits are present, then the electrochemical portion cannot be used but can be exchanged for a weight loss specimen (weight loss and microscopic examination for pitting). To overcome this limitation and facilitate electrochemical monitoring under FeS, a setup and approach for monitoring the corrosion rate under iron sulfide deposits has been proposed [26]. In this methodology, the UDC working electrode containing the FeS and the reference and counterelectrodes were separated to avoid bridging problems. It was highlighted that close attention needs to be paid to optimizing the potential scan rate of the LPR measurement to overcome shortcomings in overestimating the corrosion rate, which was attributed to the large interfacial capacitance induced by the presence of the iron sulfide. This optimized approach showed that the electrochemical corrosion rates measured under FeS deposits correlated quite well to the volume loss corrosion rates.

An iron sulfide test method for inhibited systems [27] was developed to perform ER, LPR, and weight loss in an H_2S/CO_2 environment where the FeS deposit could be developed by injection of ferrous chloride or by in situ corrosion of the specimen. This experimental setup was designed to assess the effect of the iron sulfide deposit (mackinawite) on H_2S/CO_2 corrosion and corrosion mitigation on a square ER probe in experiments that could include the use of a hydrocarbon phase. Results found that a carbon steel with an in situ precipitated iron sulfide deposit had around four times higher corrosion rate than the carbon steel probe suspended in the same inhibited solution.

In addition to the physical methodologies used in testing UDC, the environmental parameters also need focused research. In one study designed at assessing such factors [23], multiple experiments designed to determine the critical parameters that affect galvanic corrosion and the effect of inhibition on UDC were conducted. The experiments within the investigation covered temperatures from 25 to 70°C (77−158°F), sand thickness from 1 to 10 mm, and inhibitor dosage from 50 to 200 ppm using a 1-L glass cell with a CO_2 sparged 10 wt% NaCl solution. The apparatus (Fig. 15.7) was based on a typical bubble cell arrangement using a cylindrical UNS G10180 working electrode in solution (solution electrode) along with a saturated silver−silver chloride reference electrode (REF) and a stainless steel UNS S31600 counterelectrode (AUX). For under-deposit measurement, a UNS G10180 working electrode was flush mounted in epoxy with a glass tube to ensure a reproducible sand thickness (UDC electrode) and was coupled to the solution electrode to create a specimen area ratio of 17:1

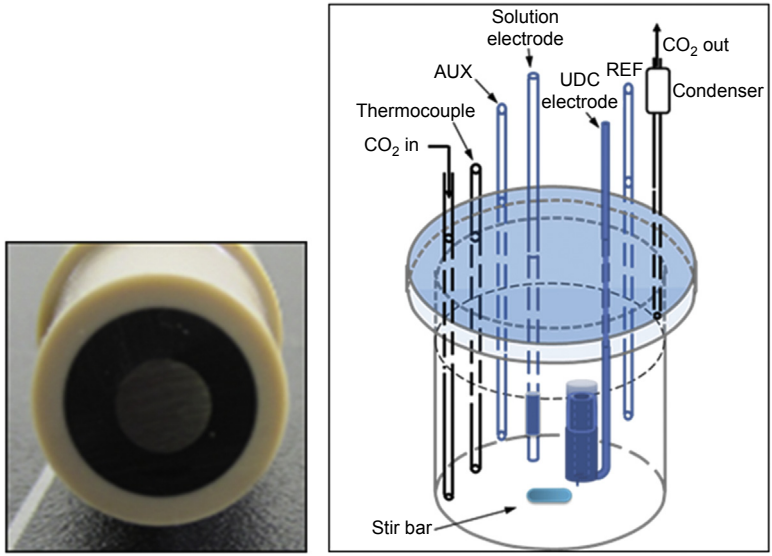

Figure 15.7 (a) Metal electrode sealed in polyethyl ethyl ketone sleeve with epoxy. (b) Under-deposit corrosion (UDC) testing setup [23].

(solution electrode: UDC electrode). The four-electrode system was coupled via a ZRA to observe the galvanic corrosion taking place.

The six major conclusions from this study shown in the following list agree with all experimental results previously reviewed while giving insights on having a thicker sand deposit, an elevated temperature, or a higher concentration of inhibitor.

1. With no inhibitor present, the solution electrode acted as the anode while the sand-covered electrode acted as the cathode.
2. Addition of inhibitor quickly reduced the corrosion rate of the solution electrode, whereas the UDC electrode experienced a strong anodic polarization.
3. As a result of this galvanic coupling, the UDC rate dramatically increased and was measured as high as 17.3 mm/year.
4. A thicker sand deposit was observed to slow the diffusion of inhibitor to the metal surface underneath, which resulted in a higher galvanic current density peak and an ultimately higher corrosion rate under the sand.
5. An increase in the inhibitor concentration also increased the galvanic current over a short period of time, but the higher concentrations did penetrate the sand bed and caused a decay in UDC.
6. Although an increase in temperature caused the solution electrode corrosion rate to increase by 150%, the UDC corrosion rate increased only by 40%.

15.3.3.2 Partial coverage deposit

In tests with a single specimen under a deposit, Huang et al. [24] reviewed the performance of an imidazoline-type inhibitor to understand mechanisms related to localized corrosion. The specimen holder (Fig. 15.1) was placed in a 2-L glass cell (Fig. 15.8) with deaerated brine for precorrosion, before the inert deposit would be transferred from a previously deaerated solution to the area on top of the specimen sand holder. These experiments were conducted over a period of 2−4 days.

They reported that general depletion of the surfactant inhibitor by adsorption on the silica sand surface and slow diffusion through the porous sand layer were not considered critical factors leading to localized corrosion, but proposed a new mechanism that the cause for localized corrosion was related to the inability of the corrosion inhibitor to protect the steel surface in the crevices immediately underneath each sand particle. By testing a single metal specimen with partial sand coverage, it was observed that the lack of inhibition under a single sand particle leads to the formation of a galvanic cell where the small area under the sand particle became anodic while the larger inhibited area around the particle was the cathode. In comparison with the previous surface area ratios discussed, an individual 250-μm sand particle only required a 1-mm-diameter area around it to have a 15:1 cathode to anode area ratio.

The partial coverage sand bed methodology developed by Huang et al. [24] was used as a repeatable procedure in the experimental comparison of mono- to di-nonylphenol phosphate ester (PE) ratios by Brown et al. [25]. This series of experiments was the first formal attempt to observe the effects of specific chemical components of an inhibitor package on UDC. In experiments lasting 28 days, nonylphenol PEs were tested at varying mono- to di-PE ratios of 90:10, 70:30, and

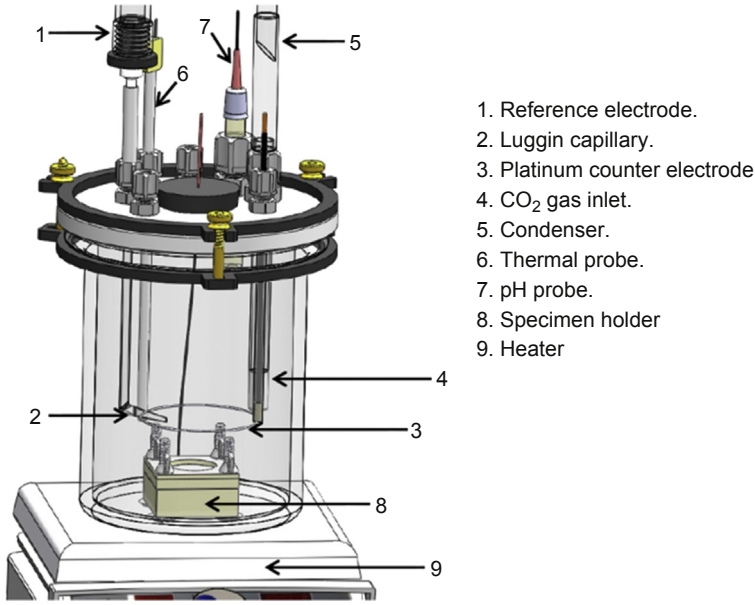

Figure 15.8 Three-electrode glass cell set up for single under-deposit corrosion specimen [16].

50:50. Using an X65 pipeline material partially covered with 250-μm-diameter silica sand particles and exposed to a CO_2 sparged brine at 1 bar (14.5 psi) total pressure and 70°C (158°F), multiple measurement techniques employing electrochemistry, weight loss, and profilometry were used for the comparison. It was found that the presence of 2-mercaptoethanol assisted the nonylphenol PE inhibitors and no localized corrosion was observed. Without the mercaptoethanol, the depth of localized corrosion observed increased with a decrease in the amount of mono-nonylphenol PE in the inhibitor package. This also provided confirmation for the theory of crevice corrosion under each sand particle being the main driving force for localized corrosion.

Multiple small grains of sand or "partial sand coverage" experiments [16] used a few grains of sand on a single metal specimen, which was monitored electrochemically from 25 to 40 days and then analyzed by weight loss and profilometry. The test began with a 2-h precorrosion of the metal specimen, followed by the addition of a few grains of 750-μm sand particles, which had been stored in deoxygenated brine to the 7.9 cm^2 steel surface area. After 24 h the inhibitor was added and the experiment monitored for the remainder of the test time. These experiments showed the inability of a generic imidazoline-type inhibitor to protect the surface directly underneath each sand particle as pit penetration rates of 2.2−3.5 mm/year were found for weight loss specimens having a uniform inhibited corrosion rate of less than 0.1 mm/year. In this type of experiment, the inhibitor can be added before the sand or the sand particles can be moved during the experiment to observe how the inhibitor works with partially stable or moving deposits.

15.4 Mitigation of UDC

The goal of the experimental methods used by various researchers has been to investigate the mechanisms of UDC, which, in some instances, was used to assist in the determination of the most effectual approach for minimizing the threat of pipeline failures. Many strategies have been reviewed with the goal to eliminate UDC by the most cost-effective means available. Most discussions on the topic of UDC mitigation tend to focus on the chemicals used in controlling corrosion as it is understood that the addition of some types of inhibitors creates galvanic corrosion for the area under the deposit. It should also be recognized that these solids can accumulate in pipelines and in turn can cause increased pressure drops as well as enhanced localized corrosion. Removal of the deposits or defining parameters of pipeline operations to limit their formation along with the addition of chemical inhibition by a predefined inhibitor seems to be the most used option to mitigate the attack from UDC. However, the true goal of diminishing or mitigating the probability for UDC may be achieved by other means in the design phase before installation and beginning operations of the pipeline. As with any process or procedure, the easiest and most efficient method should be explored first. The following list provides some approaches for achieving a cost-effective means for minimizing UDC in both the design phase and the operating phase of a pipeline operation.

Mitigation methods for minimizing UDC [12]:

1. In the Design Phase
   - **a.** Design for high flow rates by selecting optimum equipment size.
   - **b.** Minimize stagnant locations.
   - **c.** Install pigging facilities where stagnant locations cannot be avoided.
   - **d.** Use of corrosion-resistant alloys (CRAs) (selection of a proper CRA depends upon many factors and can increase cost).
   - **e.** Use of internal coatings (currently not considered a technique by itself for long-term corrosion protection because of the probability of holidays, delamination, or deterioration; there are also application difficulties for coating existing pipelines with many current coating technologies, although advances are being made in this area).
2. During the Operating Phase
   - **a.** Mechanical removal of debris by pigging (brush pigging with a batch inhibitor treatment).
   - **b.** Chemical treatment with appropriate corrosion inhibitor chemistry and dosage determined through laboratory testing and field trials. Corrosion inhibitors may be added as slugs of concentrated chemicals or through continuous application while other "cleaning" chemicals and surfactants may be used to suspend particles in the liquid phase along with increasing the velocity of produced fluids to aid in transporting the loose solid debris.

In most instances, because the larger capital expenditures for the use of CRAs and coatings may make them less likely to be used, engineers must rely on the two main mitigation strategies during operations: mechanical removal and/or chemical treatments. The following sections provide more information on these topics.

15.4.1 Mechanical removal of deposits (minimum velocities, pigging)

Mechanical removal of deposits starts with designing for higher flow rates in the operating pipeline. A correlation proposed by Salama to predict sand settling conditions can also be used as a valid approximation for velocities to define sand removal [28].

$$V_m = \left(\frac{V_{sl}}{V_m}\right)^{0.53} d^{0.17} \nu^{0.09} \left(\frac{\Delta\rho}{\rho_f}\right)^{0.55} D^{0.47} \tag{15.1}$$

V_m, minimum mixture flow velocity to avoid sand settling, m/s; V_{sl}/V_m, the ratio between the liquid superficial liquid velocity and the mixture velocity at the sand settling conditions (for single phase, this ratio = 1); d, particle diameter, m; D, pipe diameter, m; $\Delta\rho$, density difference between particles and the fluid mixture density, kg/m^3; ρ_f, fluid mixture density, kg/m^3; ν, fluid mixture kinematic viscosity, m^2/s.

As the mixture velocity is increased, the critical velocity to begin moving the sand from the sand bed to create a scouring flow or moving dunes is a more complicated process than the reverse process to create the sand bed [28].

For small amounts of sand accumulated in the pipeline, removal can be done by increasing the flow rate or by pigging. Computational fluid dynamics have been used to model the effect of near-wall velocity at the pipe floor on solids deposition to understand the influence of flow and pipeline geometry to aid in this decision [29,30]. For larger amounts of accumulated sand in an operating pipeline, removal by pigging can create hazards by having an excessive buildup of sand ahead of the pig, which could possibly plug the pipeline or damage the process facility by the sudden arrival of a large quantity of sand [28].

15.4.2 Chemical treatment for deposits

The presence of a good performing corrosion inhibitor in a water wet pipeline typically reduces the general corrosion rate by a large amount by adsorption processes at the metal surface. This low corrosion rate is related to a reduction in the anodic and/or cathodic reactions by an effect from the corrosion inhibitor active species on the corroding metal surface. As shown by Dominguez et al. [31], a positive shift in OCP is observed because the corrosion process is under mixed (charge transfer/mass transfer) control and an inhibitor affects only the charge transfer reactions (anodic and cathodic) but not the mass transfer of species to the metal surface. This positive shift in the OCP of a working electrode in a three-electrode system related to the addition of an inhibitor in solution has been observed by others under different environments with different inhibitors [25,32].

When a stagnant deposit is present in an inhibited pipeline, it can be the cause for galvanic corrosion. The deposit acts as a diffusion barrier with a low porosity and high tortuosity for the path from the bulk solution to the pipe wall under the stagnant deposit. This stagnant deposit does not reduce the anodic and cathodic reactions as much as

a good performing inhibitor, but may impede some corrosion inhibitors from reaching the pipe wall. Therefore the smaller area under the deposit does not experience the same effect caused by the reduction in anodic and cathodic reactions as on the larger pipe wall. In laboratory experiments where these areas can be separated, a large potential difference has been observed between the inhibited metal surface in the bulk solution (more positive, cathode) and the noninhibited metal surface under a deposit (more negative, anode). Because a pipeline is one continuous piece of highly conductive metal, there can only be one potential within the general vicinity that is controlled by the larger cathode surface area. The overall potential of the metal adjusts to a mixed potential between the anodic and cathodic reaction-driven potentials, which would be more similar to the cathode potential because of its much larger surface area. The smaller area underneath the deposit compensates for this difference by the transfer of electrons to the cathode. This galvanic corrosion increases dissolution of ferrous ions from the metal surface underneath the deposit to cause high rates of localized corrosion and pitting underneath the deposit as described by the mechanisms discussed and reviewed earlier.

To achieve maximum coverage to the internal pipe wall, added chemicals must be able to diffuse through the deposit to the metal substrate or the deposit must be removed to expose the bare metal surface. Testing has found that 2-mercaptoethanol can assist in mitigating some UDC as it is believed the small size of the molecule (in comparison with other actives such as imidazolines and quaternary ammonium compounds) assists it to penetrate and diffuse more easily through thicker layers and smaller crevices between the sand and the metal of the pipe wall. Some inhibitor package formulations have been developed to aid in the removal of oily sludge-type deposits but rely on flow to maintain a moving slurry of deposit materials in the liquid rather than accumulating along the bottom of the pipe. The aim of these approaches is to keep the pipe wall as clean as possible, which, in turn, allows the maximum amount of inhibitor to adsorb onto the metal surface to not only reduce the overall general corrosion rate but, perhaps more importantly, to minimize the probability of localized corrosion.

When solids, such as sand, clays, corrosion products, and biomass, collect at the bottom of a pipeline, they can become bound together with oil and are known as “schmoo” [33]. This type of deposit is known to create a physical barrier and becomes an ideal environment to grow bacteria leading to microbiologically induced corrosion (MIC). Schmoo was shown to retard the mass transfer of species and corrosion inhibitors to the pipe wall, which aids in the initiation of localized corrosion. Horsup et al. [34] reviewed multiple types of base inhibitor chemicals and tested multiple inhibitor packages on the problem of schmoo removal. They were able to determine two primary mechanisms of emulsification and roll up for the removal of schmoo from laboratory test pipelines and field evaluations, developing a chemical package that was shown to increase flow in a water injection line within 6 weeks after initial dosage. This is a good example of using laboratory testing to better understand the mechanisms of the problem situation and then in turn to utilize this understanding to develop field mitigation solutions. Although it is acknowledged that biofilms (dead or living) can also result in UDC attack, microbiological activity involving this form of UDC has been omitted from consideration in this chapter (see Chapter 8 for MIC).

15.5 Gaps in current research and areas for future study

The use of all components present in UDC field conditions (e.g., sand, iron sulfide, clays, microorganisms, asphaltenes, waxes, hydrocarbon sludges) for a single testing program presents too many variables to be effective and their presence should be limited, or added progressively, in experimental studies to minimize errors in interpretation of results. The focus should be on determining which mechanisms to study under well-controlled conditions that relate to the complex conditions found in the field. Crolet [35] summed up the behavior of corrosion deposits by stating that the conditions of formation, protective properties, and sensitivities to external parameters are extremely different for each case, so that the possible configurations and various working hypotheses to model UDC are too numerous. This infers that studies will still need to be conducted on a case-by-case basis, taking into account the physical characteristics of the deposit (formation, composition, depth, age, etc.), corrosion-related mechanisms (diffusion, precipitation, MIC, etc.), and the associated solution chemistry (water, oil, pH, salt content, etc.) in each case. Much research has been done on these three topics, with numerous companies developing methodologies on how to provide mitigation to their specific problems encountered in the field.

Although various models are available for estimating general corrosion as well as various forms of localized corrosion such as top-of-the-line corrosion, there appears to be limited activity in modeling UDC, which should be a focus for future research. The accumulation of the UDC knowledge base, shared throughout the corrosion community, may be developed not only into a mechanistic model to help predict the extent of UDC, but also as a means to derive mitigation solutions to a much larger base of operators. Furthermore, the knowledge base developed may also aid in the development of future inhibitor formulations and packages that might address the issues found related to the physical characteristics of specific deposits, the corrosion mechanisms, and the solution chemistry in each field.

Continued research needs to be conducted with different surfactant molecules to determine which attributes are valuable to address UDC. Larger inhibitor molecules might be expected to show characteristics of steric hindrance around the small crevices under a sand particle. In the same way that synergistic effects have been seen between molecules in controlling general corrosion, the identification of synergistic combinations of inhibitors for UDC and localized corrosion alleviation would also be advantageous. Such research focus may include studies on the molecular level (atomic force microscopy, molecular modeling, etc.) to better determine and identify types and mixtures of inhibitor molecules tailored for UDC mitigation.

References

[1] J. Vera, D. Daniels, M. Achour, Under deposit corrosion (UDC) in the oil and gas industry: a review of mechanisms, testing and mitigation, Paper no. 1379, in: CORROSION/2012, NACE, Houston, TX, 2012.

[2] A. Pedersen, K. Bilkova, E. Gulbrandsen, R. Nyborg, Testing of CO_2 corrosion inhibitor performance under sand deposits, in: Eurocorr 2007, European Federation of Corrosion, London, U.K., 2007.
[3] R. Barker, B. Pickles, A. Neville, General corrosion of X65 steel under silica sand deposits in CO_2-saturated environments in the presence of corrosion inhibitor components, Paper no. 4215, in: CORROSION/2014, NACE, Houston, TX, 2014.
[4] A. Pedersen, K. Bilkova, E. Gulbrandsen, J. Kvarekvål, CO_2 corrosion inhibitor performance in the presence of solids: test method development, Paper no. 08632, in: CORROSION/2008, NACE, Houston, TX, 2008.
[5] G. Hinds, P. Cooling, S. Zhou, A. Turnbull, Under deposit test method for assessing performance of corrosion inhibitors, in: EUROCORR 2008, 2008. Paper 1254.
[6] G. Hinds, A. Turnbull, Novel multi-electrode test method for evaluating inhibition of under deposit corrosion − Part 1: sweet conditions, Corrosion Journal 66 (4) (April 2010) 046001-1−046001-10.
[7] Y.-J. Tan, Y. Fwu, K. Bhardwaj, Mapping electrochemical evaluation of under-deposit corrosion and its inhibition using the wire beam electrode method, Corrosion Science 53 (2011) 1254−1261.
[8] J. Huang, B. Brown, X. Jiang, B. Kinsella, S. Nesic, Internal CO_2 corrosion of mild steel pipelines under inert solid deposits, Paper no. 379, in: CORROSION/2010, NACE, Houston, TX, 2010.
[9] N.M. Alanazi, A.M. El-Sherik, A.H. Rasheed, S.H. Amar, M.R. Dossary, M.N. Alneemai, Corrosion of pipeline steel X-60 under field-collected sludge deposit in a simulated sour environment, Corrosion Journal 71 (3) (March 2015) 301−315.
[10] G. Hinds, A. Turnbull, Novel multi-electrode test method for evaluating inhibition of under deposit corrosion—Part 2: sour conditions, Corrosion Journal 66 (5) (May 2010) 056002-1−056002-6.
[11] C.M. Menendez, V. Jovancicevic, S. Ramachandran, M. Morton, D. Stegmann, Assessment of corrosion under iron sulfide deposits and CO_2/H_2S conditions, Corrosion Journal. ISSN: 0010-9312 69 (2) (February 2013) 145−156.
[12] NACE Publication 61114, Underdeposit Corrosion (UDC) Testing and Mitigation Methods in the Oil and Gas Industry, February 2014. NACE Item no. 24253.
[13] J.A.M. de Reus, E.L.J.A. Hendriksen, M.E. Wilms, Y.N. Al-Habsi, W.H. Durnie, M.A. Gough, Test methodologies and field verification of corrosion inhibitors to address under deposit corrosion in oil and gas production systems, Paper no. 05288, in: CORROSION/2005, NACE, Houston, TX, 2005.
[14] W.H. Durnie, M.A. Gough, J.A.M. de Reus, Development of corrosion inhibitors to address under deposit corrosion in oil and gas production systems, Paper no. 05290, in: CORROSION/2005, NACE, Houston, TX, 2005.
[15] J.H. Schön, Physical Properties of Rocks, Handbook of Petroleum Exploration and Production, Elsevier, 2011, ISBN 978-0-444-53796-6.
[16] J. Huang, Mechanistic Study of Under Deposit Corrosion of Mild Steel in Aqueous Carbon Dioxide Solution, Ohio University, 2013. Electronic Dissertation Retrieved from: https://etd.ohiolink.edu/.
[17] D. Rickard, G.W. Luther III, Chemistry of iron sulfides, Chemical Reviews 107 (2007) 514−562.
[18] C.I. Pearce, A.D. Pattrick, D.J. Vaughan, Electrical and magnetic properties of sulfides, Reviews in Mineralogy and Chemistry 61 (2006) 127−180.
[19] W.M. Telford, L.P. Geldart, R.E. Sheriff, Applied Geophysics, second ed., 1998, pp. 283−292.

[20] Y. Zheng, J. Ning, B. Brown, S. Nešić, Investigation of cathodic reaction mechanisms of H_2S corrosion using a passive SS304 rotating cylinder electrode, Corrosion Journal 72 (12) (2016) 1519−1525.
[21] P. Bai, Y. Liang, S. Zheng, C. Chen, Effect of amorphous FeS semiconductor on the corrosion behavior of pipe steel in H_2S-containing environments, I and EC Research: Industrial and Engineering Chemistry Research 55 (41) (2016) 10932−10940, http://dx.doi.org/10.1021/acs.iecr.6b03000.
[22] J. Ning, Y. Zheng, B. Brown, D. Young, S. Nesic, The role of iron sulfide polymorphism in localized H_2S corrosion of mild steel, Corrosion 73 (2) (2017) 155−168.
[23] Y. Zhang, J. Moloney, S. Mancuso, Understanding factors affecting corrosion inhibitor performance in under-deposit testing with sand, Paper no. 2575, in: CORROSION/2013, NACE, Houston, TX, 2013.
[24] J. Huang, B. Brown, S. Nesic, Localized corrosion of mild steel under silica deposits in inhibited CO_2 solutions, Paper no. 2144, in: CORROSION/2013, NACE, Houston, TX, 2013.
[25] B. Brown, A. Saleh, J. Moloney, Comparison of mono- to diphosphate ester ratio in inhibitor formulations for mitigation of under deposit corrosion, Corrosion Journal 71 (12) (December 2015) 1500−1510.
[26] Y. Zhang, J. Moloney, Electrochemical corrosion rate measurement under iron sulfide deposit, Corrosion Journal 72 (2016) 704.
[27] M. Achour, J. Kolts, P. Humble, R. Hudgins, Experimental evaluation of corrosion inhibitor performance in presence of iron sulfide in CO_2/H_2S environment, Paper no. 344, in: CORROSION/2008, NACE, Houston, TX, 2008.
[28] M.M. Salama, Influence of sand production on design and operations of piping systems, Paper no. 80, in: CORROSION/2000, NACE, Houston, TX, 2000.
[29] X. Landry, A. Runstedtler, S. Papvinasam, T. Place, Computational fluid dynamics study of solids deposition in heavy oil transmission pipeline, Corrosion Journal 68 (10) (October 2012) 904−913.
[30] A. Runstedtler, P. Boisvert, T. Place, Parametric modeling studies for sediment deposition as sites for under-deposit corrosion in oil transmission pipelines, Corrosion Journal 71 (6) (June 2015) 726−734.
[31] J.M. Dominguez Olivo, B. Brown, S. Nesic, Modeling corrosion mechanisms in the presence of quaternary ammonium chloride and imidazoline corrosion inhibitors, Paper no. C2016−7406, in: CORROSION/2016, NACE, Houston, TX, 2016.
[32] J. Moloney, W. Mok, C. Menendez, In situ assessment of pitting corrosion and its inhibition using a localized corrosion monitoring technique, Corrosion Journal 66 (2010) 065003-1−065003-18.
[33] W.M. Bohon, D.J. Blumer, A.F. Chan, K.T. Ly. NACE 1998, Paper 00073.
[34] D.I. Horsup, T.S. Dunstan, J.H. Clint, A break-through corrosion inhibitor technology for heavily fouled systems, Paper no. 07690, in: CORROSION/2007, NACE, Houston, TX, 2007.
[35] J.L. Crolet, Mechanisms of uniform corrosion under corrosion deposits, Journal of Material Science 28 (1993) 2589−2606.

Top-of-the-line corrosion

16

Marc Singer
Ohio University, Athens, OH, United States

16.1 Overview of the current understanding/knowledge

Although it was first identified in the 1990s, top of the line corrosion (TLC) has only recently been recognized as an issue for the oil and gas industry. Initially regarded as a laboratory curiosity, it is now considered a major concern for pipeline integrity and is taken into account in the design of any new gas field development. Significant effort has been invested toward elucidating its governing mechanism and developing prediction and mitigation tools.

TLC is a phenomenon encountered in the transportation of wet gas, where temperature differences between the pipelines and the surroundings lead to corrosion issues. Condensation of saturated vapors present in the unprocessed gas stream collects on the internal surface of the cold pipe wall. The condensed phase is made not only of hydrocarbons but also water, which forms a thin film and/or droplets of liquid. The condensed water phase can be, at least initially, very corrosive to typical pipeline steel, because it contains dissolved acid gases (e.g., carbon dioxide and hydrogen sulfide) and organic acids. The corrosion mechanism encountered in this scenario is not different from what can be expected in the bulk liquid phase, but it holds important specificities that make its mitigation difficult and the occurrence of localized corrosion likely.

TLC mechanisms involve four main engineering processes, which can interact in a complex way:

- **Fluid mechanics**: TLC can only occur in a specific flow regime where the liquid and gas phases are clearly stratified.
- **Heat and mass transfer**: The condensation of water vapor on cold pipe wall and the transport of corrosive species to the liquid film are controlling the extent of corrosion.
- **Chemistry**: As for most corrosion phenomena, the chemical composition of the electrolyte is key in determining both the corrosion kinetics and the likelihood of corrosion product formation.
- **Electrochemistry**: The corrosion process is inherently driven by well-known electrochemical reactions.

16.1.1 TLC mechanisms

16.1.1.1 Flow regime

Flow regime determination is an important clue as to whether or not TLC may become an issue. Three major three-phase flow regimes are commonly encountered in horizontal oil and gas pipelines:

- **Stratified flow**: Segregation of the gas and liquid phases, usually at low gas and liquid flow rates

Trends in Oil and Gas Corrosion Research and Technologies. http://dx.doi.org/10.1016/B978-0-08-101105-8.00016-4

- **Intermittent flow**: Formation of slugs or plugs at high liquid flow rates as the crests of the waves intermittently reach the top of the pipe
- **Annular flow**: The bulk liquid phase is partly atomized at high gas flow rate, leading to transport and deposition of droplets to the whole circumference of the pipe

The flow regime transition lines between stratified and intermittent or annular flow are obtained following the well-known wave-mixing mechanism developed by Milne—Thomson [1] and, later, Taitel [2]. Only one of these flow regimes, stratified flow, will lead strictly to TLC, as annular and intermittent flow implies wetting of entire pipe surface with bulk liquid phase.

If the flow regime is not stratified, the bulk liquid phase is likely to wet all parts of the pipe surface, even intermittently. Coupled with the use of corrosion inhibitor, effective protection against corrosion is needed. However, TLC is encountered exclusively when noncondensable gas (light hydrocarbons, CO_2, etc.) and saturated water vapor are produced together with little or no liquid hydrocarbons. In this condition, the three-phase flow is stratified, meaning that standard corrosion inhibitors dissolved in the bulk liquid phase will not be effective in mitigating corrosion at locations where the pipe surface is not wetted, i.e., on the sides and top of the pipe.

16.1.1.2 Condensation process

Once the flow regime is established to be stratified, the next step is to determine the extent of water vapor condensation. Water vapor comes from the presence of liquid water, together with hydrocarbons, in the reservoir. It can be assumed that the water vapor, along with most of the hydrocarbon vapors (except the lighter end), is saturated in the gas phase. The fluid's pressure inevitably decreases as the fluids are produced through the tubing and flow lines. The temperature also decreases along the pipe due to heat exchange with the outside environment and to a lesser degree due to Joule—Thomson effects.

The rate of water condensation is mainly dependent on the gradient of temperature between the transported fluid and the outside environment. It is also very sensitive to any pipeline characteristics that may affect the rate of heat transfer, such as thermal insulation, concrete coating or pipe burial ratio, as well as the nature of the outside environment (soil, air, sea, or river).

Once formed, the droplets can behave differently depending on the magnitude of drag force caused by the gas flow and the nature of the steel surface. The droplets, initially small, grow to reach a critical size and either fall to the bottom of the line due to gravity forces, which is typical of low gas velocity, or slide along the pipe at higher gas velocity. A thin, liquid film typically remains on the surface, and the renewal of the droplets is governed by the rate of condensation.

16.1.1.3 Condensed water chemistry

The condensed water chemistry logically determines the corrosivity of the environment and the eventual formation of corrosion product layer. It is, therefore, essential

to have a good understanding of the basic principles of the $H_2O/CO_2/H_2S$ system as they pertain to condensed water.

The water phase present in any given oil and gas pipeline can come from either the well formation itself (formation water) or the condensation of water vapor. On the one hand, formation water typically contains elevated amounts of salts such as chloride, sodium, and calcium ions. Acid gases dissolve in the formation water and determine its pH, which is usually higher than 5.5−6.5 due to the buffering effect of high content of bicarbonate. On the other hand, there is no salt in the condensed water. This makes the pH of freshly condensed water very acidic, as will be discussed further.

The different chemical reactions involved in the H_2O/CO_2 system are well established and can be found summarized in Chapter 7. Among the organic acids often present in produced fluids, the most common and abundant are acetic acid, propionic, and formic acids [3,4], which are all weak acids.

The presence of H_2S in a growing number of fields considerably complicates the situation, especially in terms of corrosion product and electrochemical reactions [5]. Both CO_2 and H_2S dissolve in water and decrease the pH to a comparable extent at similar partial pressure. This is because compared to CO_2 gas, H_2S gas is about three times more soluble in water but has a constant acidity of about four times lower than for carbonic acid. Depending on the field, contents of CO_2, H_2S, and organic acid range from 0.1 to 10 mol%, 5 to 5000 ppm, and 0 to 5000 ppm, respectively. Typical operating pressure and temperature also range from 30 to 200 bars (435−2900 psi) and from 5 to 100°C (41 to 212°F), respectively. Under these conditions, the pH of any droplets of freshly condensed water can be expected to vary between 3 and 4.5 [6]. However, this is only the starting value of the pH, as it will rapidly change due to the release of iron ions in solution through the corrosion process occurring on the steel surface. This process will eventually lead to conditions that are favorable for the precipitation of corrosion products, a process also dependent on the rate of renewal of the condensation rate.

Two main types of corrosion products can form in $CO_2/H_2S/H_2O/Fe^{2+}$ systems, namely iron carbonate ($FeCO_3$) and iron sulfides (Fe_xS_y). Because no oxygen is present in the produced fluids, iron oxides are ignored.

The iron carbonate precipitation reaction is written as follows:

$$Fe^{2+}_{(aq)} + CO_3^{2-}{}_{(aq)} \rightleftharpoons FeCO_{3(s)}$$

Thermodynamically, precipitation occurs once the saturation level $S_{FeCO_3} = \frac{[Fe^{2+}]\left[CO_3^{2-}\right]}{K_{sp,FeCO_3}}$ is above one. However, the rate of precipitation is strongly dependent on temperature and the degree of supersaturation. Sun [7] suggested expressions for the equilibrium constant $K_{sp,FeCO3}$ and the $FeCO_3$ precipitation rates. Organic acids have also been reported to affect the corrosion product layer characteristics [8−10]. In general, iron carbonate layers provide effective protection against CO_2 corrosion, especially at high temperature, as long as their integrity is not challenged by sudden changes in chemistry, mechanical damage, or changes in operating conditions.

For iron sulfide formation, although the chemical reactions describing sulfide chemistry are well known [7], the pathways for iron sulfide layer formation are still debated [11–13]. The latest developments in the mechanism of FeS (mackinawite) formation involve a rapid formation of a thin layer by "direct" reaction, where the Fe atom does not leave the metal microstructure and reacts directly with the adsorbed H_2S, followed by a more standard precipitation reaction. As for $FeCO_3$, precipitation of iron sulfides only occurs if the saturation level is above unity.

By direct reaction	$Fe_{(s)} + H_2S_{(ad)} \rightarrow FeS_{(s)} + H_{2(g)}$
By precipitation	$Fe^{2+}_{(aq)} + HS^{-}_{(aq)} \overset{K_{sp,mck}}{\longleftrightarrow} FeS_{(s)} + H^{+}_{(aq)}$

The uncertainty related to the expressions for the equilibrium constants involved in H_2S aqueous chemistry is much more acute than with CO_2 aqueous chemistry [7]. In addition, several types and polymorphs of iron sulfides can be encountered, presenting different characteristics and providing varying levels of resistance to corrosion. The work by Smith [14] presents the most common forms of iron sulfides reported in the industry: mackinawite, pyrrhotite, cubic FeS, and pyrite. They are described briefly below:

- Mackinawite is a metastable form of FeS that forms quickly and is always present on the metal surface.
- Pyrrhotite ($Fe_{1-x}S$) is a more thermodynamically stable form of iron sulfide but suffers from relatively slower kinetics of formation. It has also been reported to form from the transformation of mackinawite.
- Cubic FeS is a metastable form of iron sulfide. Its formation is mitigated by the presence of foreign ions such as chloride ions. Condensed water environments are, therefore, more favorable.
- The most stable form of iron sulfide is pyrite, which is often associated with high H_2S partial pressure.

16.1.1.4 Corrosion process

The main corrosion mechanisms of mild steel in sour and sweet environments are reasonably well understood [15–25] and can naturally be applied directly to condensing environments. This is presented in detail in Chapters 6 and 7, respectively. However, the TLC environment holds some degree of specificity, especially as it pertains to corrosion product formation. The next sections present a comprehensive review of the current state of understanding related to CO_2 and H_2S systems, which are treated separately due to their fundamental differences.

CO_2 top of the line corrosion mechanisms

Research work related to TLC mechanisms in CO_2 environments started in the early nineties with the first systematic studies performed in small-scale setups [26,27] and large-scale flow loops [28–32].

The first stage of TLC involves the wetting of the steel surface by freshly condensed, and consequently quite "aggressive", water. Initially, the uniform corrosion rate is high but decreases with time to relatively low average values due to the release of ferrous ions in solution and the consequent increase in pH. At a certain point, depending on the system temperature, saturation of $FeCO_3$ is reached and precipitation of the corrosion product layer occurs. $FeCO_3$ layers can initially reach a relatively high level of protectiveness leading to a decrease of the rate of release of ferrous ions. However, as this process takes place, the concentration of ferrous ions diminishes as new, freshly condensed water, free of iron ions, continues to dilute the existing electrolyte. The $FeCO_3$ saturation level decreases and eventually leads to the dissolution of the existing corrosion product layer and the exposition of bare steel surface. A steady state eventually occurs when the concentration of ferrous ions and the pH reach a stable value corresponding to a saturation level of $FeCO_3$ approaching unity (or higher, depending on the temperature). The addition of ferrous ions due to steel dissolution is balanced by their dilution in the electrolyte through condensed water renewal. This also means that the rate of top of the line corrosion cannot be zero as long as the rate of water condensation is not zero. As the continuous source of fresh and acidic condensed water affects the chemistry of the solution (pH, $FeCO_3$ saturation level), the protectiveness of the $FeCO_3$ layer is constantly challenged. Very high water condensation rates can theoretically prevent the formation of corrosion products altogether and lead to high uniform corrosion. Very low condensation rates favor the formation of a relatively protective $FeCO_3$ layer, leading to a low, but nonnull, corrosion rate.

The acidity of the environment naturally affects this phenomenon. The higher the partial pressure of CO_2 or organic acid concentrations is, the higher the initial corrosion rate will be. Weak acids also act as pH buffers and require higher content of ferrous ions in solution to reach $FeCO_3$ saturation. The kinetics of $FeCO_3$ precipitation also depend strongly on temperature. Lower gas temperatures ($<40°C$, $104°F$) typically do not favor $FeCO_3$ precipitation, and the corrosion remains uniform with time with a low rate. TLC issues, especially localized corrosion, are often experienced at higher temperatures (above $70°C$, $158°F$) with a more rapid formation of the $FeCO_3$ layer.

The constant undermining of the integrity and protectiveness of the corrosion product layer leads to the initiation and propagation of localized corrosion at the top of the line. As mentioned earlier, the first few days of exposure to dewing conditions do not often yield representative corrosion rates, as the corrosion product layer needs time to form. Once this initial stage has passed, small breakdowns generally form on the surface of the $FeCO_3$ layer. They often display specific characteristics, with a top layer comprised of tightly packed crystals of $FeCO_3$ and a macroscopically amorphous phase, identified as Fe_3C, present inside these breakdowns (Fig. 16.1).

A cross-section analysis of the specimen reveals that the location of the breakdown relates clearly to the occurrence of localized attack and that the localized features involve a much wider area than the size of the layer breakdown implies. A thick $FeCO_3$ layer covers the sides of the "pit," whereas the bottom of the feature is flat-bottomed and partially covered with iron carbide. The feature is, in general, relatively empty, which is typical of a mesa-type localized attack. The localized features grow in depth but also laterally, underneath the already formed surface $FeCO_3$ layer (Figs. 16.2 and 16.3).

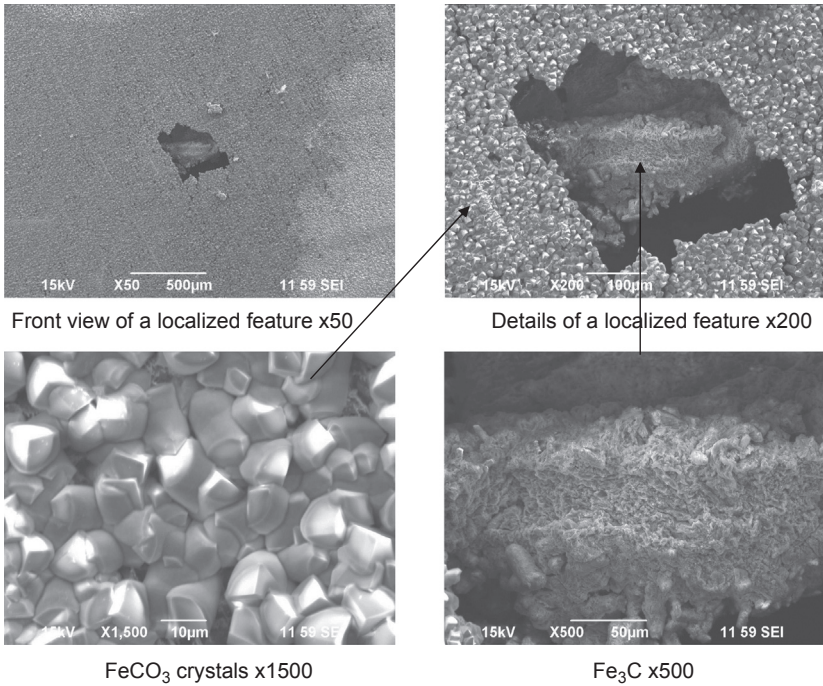

Figure 16.1 Corrosion product layer and associated breakdowns [45].

Undermining and consequent collapse of large portions of the $FeCO_3$ layer can clearly be seen. However, the localized features do not remain "active" throughout the exposure to the corrosive environment. If they become deep enough, the local chemistry within narrow localized features may favor the formation of a protective corrosion product layer. Because the flux of iron dissolution needs to be sustained, another location on the steel surface would become active and experience localized corrosion.

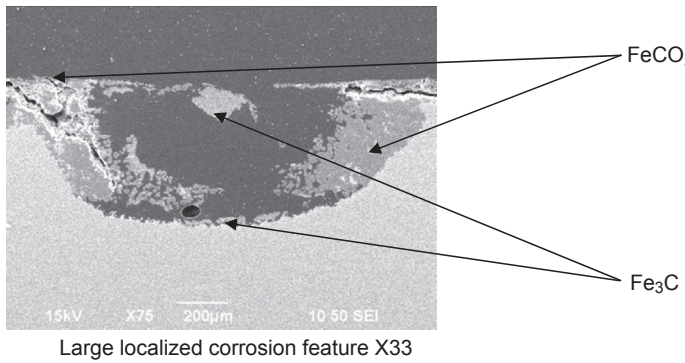

Figure 16.2 Cross section analysis − Morphology of large localized features [45].

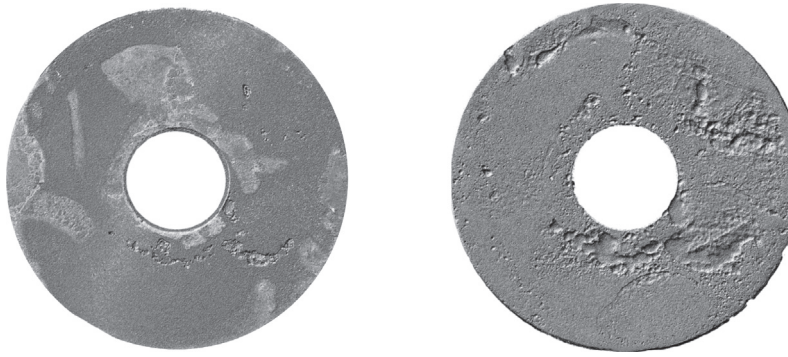

Figure 16.3 Localized corrosion features growth underneath $FeCO_3$ layer. T = 70°C (158°F), WL X65, WCR = 1 mL/m^2 s, exposure time = 21 days [45].

Depending on the water condensation rate and the corrosivity of the environment, the localized corrosion rates can be very high, often reaching 5−10 mm/year (Fig. 16.4). It is important to stress that this high rate is not driven by galvanic coupling between the corrosion product covered surface and the exposed localized corrosion features. It is rather driven by the specific chemistry of the condensed water and the effort to maintain the level of $FeCO_3$ saturation. Nevertheless, galvanic corrosion cannot be completely ruled out, especially in the early stages of pit formation. However, the localized corrosion rates at the top of the line are very similar to bare metal corrosion rates and do not require the use of galvanic coupling argument. The extent of the localized corrosion rate is consequently dependent on the concentration of organic acid specifically, and on the overall corrosivity of the electrolyte in general. The complex interaction of environmental parameters should preclude the use of restrictive threshold values, often utilized throughout the industry as engineering guidelines. Instead, a solid understanding of the mechanisms should always go hand in hand with practical field experience.

A fairly large amount of experimental work has been done on sweet TLC using a number of test setups especially designed for dewing conditions simulation [34]. A parametric study was performed by Zhang [31] and Singer [32] in 4″ID flow loops, looking at the effect of the most influencing parameters on which the severity of the corrosion attack, namely the condensation rate, the gas temperature, the gas flow rate, the CO_2 partial pressure, and the presence of organic acid. These sets of experiments, as well as other studies done through a wide array of experimental setups [27−30,33,34], have helped greatly in building the current state of understanding on TLC mechanisms in CO_2 dominated environments. Here the term "CO_2 dominated" is used to describe an environment that leads to the formation of metal carbonate corrosion products, as opposed to metal sulfide.

The influence of mono-ethylene-glycol (MEG) or pH control was also investigated [35−42]. MEG is typically used to prevent hydrate formation, mainly by decreasing

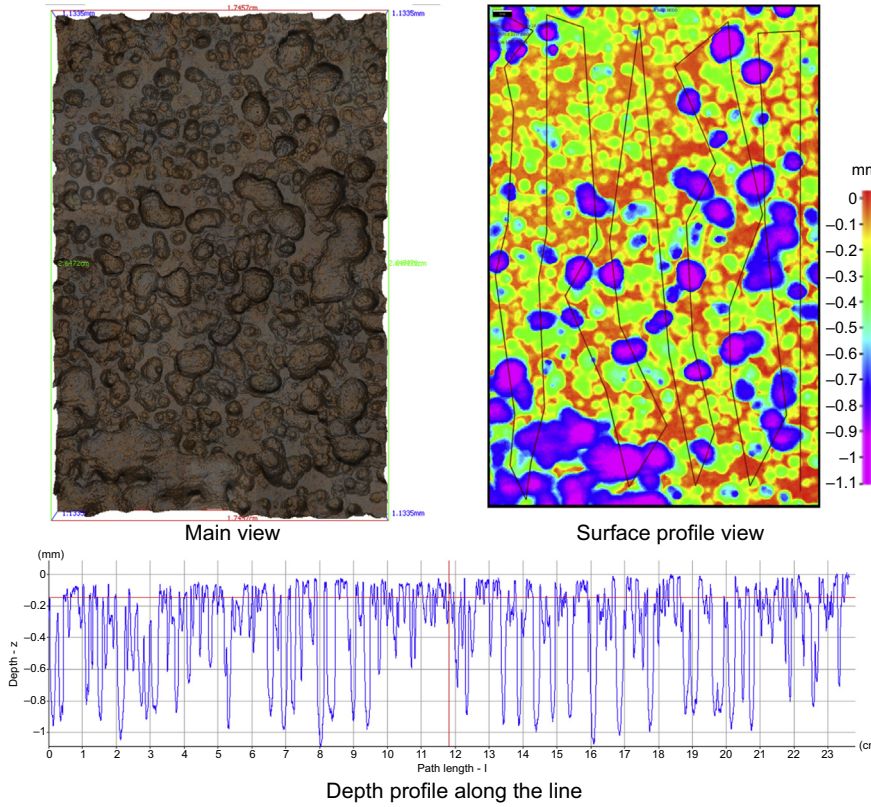

Figure 16.4 Surface profile analysis. T = 65°C (149°F), API 5L X65, WCR = 0.8−1 mL/m^2 s, pCO_2 = 2 bars (29 psi), exposure time = 21 days [45].

the water vapor pressure. MEG consequently has a direct effect on TLC by decreasing the water condensation rate. The effect is only significant when large concentrations of MEG are used (above 50 wt%). The presence of MEG also decreases the CO_2 corrosion rate, but it is debated how much can actually condense together with water because the MEG vapor pressure is much lower. pH control is also a very common method used to control the bottom of the line corrosion rate by injecting a base in the bulk aqueous phase. The bulk pH, however, has little influence on the acidity of the condensed water because it is mainly defined by the CO_2 content. Nevertheless, this method can be used to limit the concentration of undissociated acetic acid present in the bulk liquid phase, as it is pH dependent. This, in turn, limits the concentration of organic acids available for evaporation and, consequently, in the condensed water.

The possible role of hydrocarbon condensate [43] was also investigated in small-scale setup. This topic is an important aspect of TLC mechanism since it is expected that, in the field, light hydrocarbons (heptane, hexane, etc.) can co-condense at a rate 5−10 times higher than water. The experimental study showed that the presence of hydrocarbon influences the surface wetting characteristics and

segregated water droplets. However, the hydrophilicity of the steel surface seemed to guarantee water wetting on some parts of the exposed steel, and the resulting corrosion rates were similar to hydrocarbon-free systems.

The occurrence and characterization of localized corrosion have been somewhat less investigated, mostly due to the inherent complexity of the experimental procedure [44–46]. Amri [47,48] completed a comprehensive study looking at the influence of organic acid on localized corrosion propagation and developed a conceptual model of pit growth and annihilation. The authors mentioned that their findings could be applied to TLC and explain corrosion stabilization often observed in field environments [49].

H_2S top of the line corrosion mechanisms

The mechanisms of H_2S TLC are not as well investigated as their CO_2 counterparts. This is also true as it pertains to "standard" sweet or sour corrosion [50]. The controlling parameters appear to be different, but these differences are mostly due to the inherent characteristics of each type of corrosion, especially with regard to the types of corrosion products that can form.

In general, sour TLC is not as severe in terms of corrosion rate as sweet TLC. The presence of H_2S, even small amounts [51–55], often leads to a rapid and significant reduction of the CO_2 corrosion rate due to the prompt formation of a very thin mackinawite layer in the steel surface [54–56]. Depending on the conditions, different types of FeS can be formed (mackinawite, cubic FeS, and troilite) some being more thermodynamically stable or more protective than others. Experimental studies often showed the presence of two distinct layers: a thin and dense inner layer and a porous and thick outer layer [57]. As in sweet environments, the severity of TLC is directly linked to the properties of the corrosion product layers. Determining whether FeS or $FeCO_3$ precipitates is, therefore, of prime importance for TLC predictions. This is, however, quite difficult to predict [53,58,59].

Overall, sour TLC is still caused by the condensation of water vapor, but the effect of common controlling parameters is different compared to sweet systems. Only uniform corrosion is experienced in most cases, and higher rates are expected at lower gas temperatures [60,61], although these rates remain fairly low and relatively constant over time. As a result, the water condensation rate generally has little effect on the corrosion attack. The gas temperature thus becomes the key factor, as it directly affects the type and protectiveness of the formed iron sulfide. Being much less soluble than $FeCO_3$, the different types of FeS that can be encountered are stable at a pH typically encountered in condensing conditions. Therefore, the constant renewal of the condensed water does not undermine the protectiveness of the formed layer, whereas the presence of acetic acid seems to trigger the occurrence of localized corrosion in the form of small pits [55,61,62], though the penetration rate is similar to the general corrosion rate.

Even if the partial pressure reaches several bars [57], the H_2S content does not seem to have a strong effect on TLC rates as long as the integrity of the FeS layer is not challenged and that the surface is fully covered. However, more recent work investigating the presence of trace amounts of H_2S shows that even these trace amounts seem to trigger the occurrence of localized corrosion with rates approaching several mm/year [63].

16.2 Review of field experience in sweet and sour environments

Valuable information has also been published related to actual TLC field cases. Most of the well-documented cases are related to sweet fields. The first report of a CO_2-dominated TLC case was made by Gunaltun [64] regarding an onshore pipeline in Indonesia (CO_2 content of 4.7 mol%, total pressure of 90 bars (1305 psi), inlet temperature of 80°C (176°F)). This case is of particular importance because it underlines the effect of water condensation and identifies this as the main controlling parameter. In-line inspection (ILI) indicated that three locations along the flowline experienced extensive internal corrosion on the upper side of the pipe. These locations correlated strongly with zones where the pipe was crossing a river delta, being alternately buried and in contact with the flowing water. The resulting change in local heat transfer, and consequently water condensation rate, was identified as the main driving force of corrosion. The data collected enabled the identification of a critical condensation rate, below which TLC was considered to be manageable. This threshold value was set initially at 0.25 mL/m^2/s but was later reduced to 0.025 mL/m^2/s in case organic acid was present in the brine in large concentrations (above 2500 ppm) [65]. This threshold value was presented as a helpful design tool [66], but care should be taken when using it under different field conditions.

A large network of offshore pipelines off the coast of Thailand [67–72] has offered a new and very well-documented set of information containing both operating conditions and inspection data. Considering that the inlet fluid temperature could reach 90°C (194°F), very high water condensation rates occurred at the beginning of the lines, which were only partially buried. Severe TLC, with features as deep as 30%–60% of the original wall thickness, was detected in the first 500 m of the line, leading to potential derating of the pipe or replacement of entire sections. The severity of the corrosion attack decreased as the fluid temperature and the water condensation slowly decreased.

The notion of "cold spot" corrosion was introduced [71] to describe a case where the thermal insulation or coating is locally damaged, leading to a high rate of condensation. This was defined as the "worst case" TLC scenario, difficult to predict and ultimately leading to pipeline failure.

Consecutive ILI results showing no progress in localized corrosion features over time [43] seem to indicate that TLC stabilized after an initial high rate of metal loss. However, the same decrease in the severity of the corrosion attack could also be related in some cases to the overall decrease of the aggressiveness of the environment as the field ages. This point remains quite important as it could impact the design of the pipeline.

Sour TLC does not appear to be a common issue [73,74]. Only a few well-documented sour TLC field failures have been described in the literature [57,75–79]. In all cases, the flow regime was stratified with relatively low fluid velocities, and the temperature was always below 50°C. Under these conditions, the water condensation rate is not expected to be very high. Nevertheless, TLC features and pipe leakage were identified. It is, however, important to mention that methanol injection

was often used in these cases and that possible associated ingress of oxygen could have been determined to be a contributing factor with the formation of elemental sulfur.

16.3 Knowledge gaps

Although many significant improvements have been made in the understanding of corrosion mechanisms, especially in sweet TLC, some crucial aspects are still not well defined, especially in terms of corrosion assessment and management. This section aims at highlighting these concerns.

16.3.1 Gaps in the understanding

16.3.1.1 Localized corrosion and TLC stabilization

Sweet TLC is thought to be a "uniform" localized corrosion phenomenon instead of a purely pitting-dominated process. The localized aspect is explained by the fact that the corrosion attack is restricted to the top of the pipe, whereas the "uniform" qualification of the attack is supported by the large size of the features and the extent of the corrosion rate, which never surpasses the "layer free" rate.

In this sense, the penetration rate is driven by the corrosivity of the environment and the water condensation rate and is not particularly affected by any galvanic coupling between bare steel and layer-covered areas of the steel surface. Consequently, if a given pipeline is subject to TLC, metal loss is expected to occur continuously over the production life, assuming that the operating conditions do not change dramatically and that no successful mitigation method is implemented.

However, some evidence collected through multiple, consecutive in-line inspections seem to indicate that the TLC rate, although initially high, decreases with time and eventually stabilizes a fairly low value. This is indicated by the observation that TLC features do not appear to progress in depth after a certain time. If correct, this behavior would have strong implications for the design of new pipelines because added corrosion allowance would represent a relatively simple and efficient TLC management method. As mentioned earlier, some experimental work has been performed to explain how the conditions at the bottom of a pit become less corrosive as localized corrosion progresses [47,48]. This could explain why some TLC localized features may cease to progress in depth after a period of time.

However, the constant renewal of the condensed water dictates that a corresponding Fe^{2+} release must be maintained at the same time. Existing TLC features may then grow in width rather than in depth, and new features may be initiated. This would explain the wide and open characteristics of typical TLC features. However, once these pits become wide enough, the mass transfer limitations associated with TLC stabilization do not hold anymore.

Consequently, actual stabilization of TLC features, i.e., significant slowing of the wall thickness loss rate over time, cannot be fully explained theoretically. Validation of this phenomenon with actual field data is also challenging, as the lack of accuracy of

most ILI results leaves a lot of room for interpretation [43,65,67], especially when the variation of production conditions is taken into account. The experimental validation of TLC stabilization is also problematic, as it would require a very long testing time.

16.3.1.2 Hydrocarbon/water co-condensation

In real field conditions, the rate of hydrocarbon condensation is expected to be at least an order of magnitude higher than the rate of water condensation. In this environment, issues related to water wetting of the pipe become extremely relevant.

Most of the experimental work performed so far completely ignores the presence of light hydrocarbons, and only one study has been performed looking at the effect of hexane and decane [80,81]. The results of this study confirmed the tendency of liquid water to wet the steel surface in the presence of light liquid hydrocarbons. This is also validated by field experience showing that corrosion actually occurs in co-condensation environments.

However, the experimental data also highlighted that, although areas of the steel wetted by water did corrode at expected rates, areas wetted by hydrocarbon did not. The alternation of wetting conditions over time and their effect on overall corrosion severity has not been well characterized until now. Again, pipelines do corrode due to TLC, so there is no doubt liquid water eventually finds a way to wet the steel surface. The extent of the corrosion attack may not be fully understood, and therefore corrosion prediction by existing TLC models that do not take the presence of hydrocarbons into account may lack accuracy [70].

16.3.1.3 Sour TLC

The underlying mechanisms of sour corrosion and sour TLC are obviously identical. Beyond the specificity of a condensing scenario, both types of corrosion share the same fundamental chemical and electrochemical reactions and the same overall corrosion product characteristics. They also suffer from the same uncertainties related to the overall corrosion mechanisms and, more specifically, to the kinetics of corrosion reactions, the kinetics of corrosion products formation and transformation, and initiation and propagation of localized corrosion. In this sense, sour TLC inevitably lags behind the slow progress of sour corrosion understanding [82–85]. It also suffers from a relative lack of interest when compared to its sweet counterpart as actual field cases of sour TLC are relatively rare and not usually well documented.

In general, sour TLC seems to occur at low temperature, when the corrosion product layer is less protective. However, field experience is neither coherent nor conclusive on this aspect, as sour TLC does not systematically happen whenever the fluid temperature falls below a certain critical value. Also, no strong correlation could be found between the water condensation rate and the extent of corrosion. The influence of operating parameters on the characteristics and protectiveness of formed corrosion products is definitely key in determining the extent of uniform corrosion and the occurrence of localized corrosion. By itself, this topic is vast and complex.

As it pertains to TLC, most of the reported cases involve the injection of hydrate preventers such as methanol and monoethylene glycol (MEG) [75–77]. The chemistry of $H_2O/H_2S/CO_2$/MeOH or MEG systems and the associated formation thiols or dithiols [86] deserves further investigation. In addition, the effect of potential ingress of oxygen and the formation of elemental sulfur could also be key in understanding the underlying mechanism behind reported sour TLC pipe failure.

Overall, severe sour TLC is a rare event compared to sweet TLC [74]. The reasons behind this have not been fully elucidated. The low solubility of FeS corrosion product layers in water and their high protectiveness against corrosion must play a key role in the understanding of sour TLC.

16.3.2 Uncertainty related to mitigation principles and applications

Effective mitigation of TLC is a difficult process, as most commonly used methods, such as continuous injection of inhibitors, do not guarantee any protection at the top of the line, especially if the flow regime is stratified. To be successful, TLC inhibition requires that the inhibitor contact the steel surface on the entire inner pipe circumference.

Periodic batch treatment can ensure proper TLC mitigation but the selection of the correct application frequency is quite a challenge as well. The key to address this issue is to determine the inhibitor persistency. This can be done by performing laboratory testing in simulated field conditions or by conducting frequent ILI runs. However, the implementation of this method is costly in terms of both direct cost and production loss.

16.3.2.1 Volatile inhibition

Continuous injection of inhibitor is often the preferred solution for operators due to the low cost and relative ease of application. Typical surfactants included in inhibitor packages are long chain molecules that are effective in developing strong bonds with the metal surface and insulating it from the surrounding bulk water phase. However, these molecules are not typically volatile and are not present at the top part of the pipe unless they are physically transported there via droplet transport or nonstratified flow.

The search for inhibitors that retain sufficient inhibitive properties (usually held by long chain molecules) and present superior volatility (more common for smaller molecules) is of strong interest for the industry. However, this search has so far proven elusive, and only limited success has been achieved in the development and use of volatile corrosion inhibitor (VCI) in the field [87]. VCI is not a new concept. It is commonly used in the packaging industry, and attempts have been made, although only recently, to expand its domain of validity to multiphase flow systems [88–91]. Most current VCIs are made of complex mixtures of imidazoline salts and light amines. Their inhibition effectiveness obviously depends on their chemical structure,

the characteristics of the metal surface, the operating conditions, and the environments they are exposed too.

In order to select effective molecules, a "trial and error" approach is still much more common than a systematic theoretical approach. Fundamental investigations of the type of adsorption (either physical or chemical) and of the adsorption/desorption kinetics are not often performed, which greatly limits the validity domain of this type of mitigation method and, more importantly, the confidence that operators may have in the VCIs effectiveness in specific environments.

As pertains to TLC, recent efforts have been made in this direction [92], looking at the adsorption mechanism of amines (used as single components rather than part of a package). The low TLC inhibition reported and the lack of filming properties of the molecules tested highlight the gap in understanding between fundamental mechanism and field application. In addition, the influence of the steel surface characteristics (roughness, scale, presence of oxide or other corrosion product layers) on the efficiency of the volatile inhibitors has not been studied at all.

16.3.2.2 Foam matrix

The use of a foam matrix as an alternative to batch treatment has been proposed to physically transport the inhibitor to all parts of a pipeline potentially suffering from TLC. The main advantage of this method is that its application would not require any significant reduction in production rates, as is the case for batch treatment. The foam matrix concept relies on injected inhibitor liquids being carried with the foam slug along the line with the gas flow. The foam carrier would provide homogeneous delivery of the inhibitor through the pipe, which would then form a protective film all over the internal pipeline surface.

A "proof of concept" validation of this novel TLC mitigation method was successfully conducted in a small-scale laboratory setup consisting of a foaming cell and a corrosion cell used to simulate intermittent contact between the foam and the steel surface [93]. The TLC rate was reduced effectively by periodic treatment using the foam containing a tall oil fatty acid (TOFA)/diethylenetriamine (DETA) imidazoline corrosion inhibitor. Further validation was performed in a large scale flow loop to enable a more realistic simulation of the corrosive environments as well as the flow conditions typically encountered in the field [94]. Similar results were obtained, but the inhibition persistency was estimated between 3 and 20 h, depending on the inhibitor selected.

Although the use of a foam matrix to transport corrosion inhibitor to the top of the line appears to be a very promising technique, several challenges still need to be overcome before considering deployment in the field environment. Chemical compatibility with liquid hydrocarbons needs to be investigated, as the integrity of the foam matrix is likely to be strongly affected. Optimization of the type and concentration of corrosion inhibitor also needs to be addressed. Finally, considering an application in the field, the properties of the selected foaming agent need to be carefully studied in order to ensure that the foam matrix forms and remains as a plug for the first few hundred meters of line but disintegrates further along the line, thus avoiding issues with processing facilities.

16.3.2.3 Droplet transport

The atomization of liquid droplets can represent an effective means of transporting inhibitor through the vapor phase and combat TLC. Ensuring that droplets of inhibited fluids do reach the top of the pipe requires the correct sets of gas and liquid velocities, fluids density, and pipe geometry. Droplet deposition by itself may also not be enough to inhibit TLC, as it will have to "compete" against the water and hydrocarbon condensation rate, which would dilute the inhibitor concentration. Defining the onset of droplet deposition depending on operating parameters would constitute a useful tool that could help in the design and operation of wet gas pipelines. Recent efforts have been made to improve prediction of droplet transport in pipelines [95] and to link it to TLC mitigation applications [96].

16.3.3 TLC prediction

Compared to other types of corrosion, efforts to model and predict TLC have been relatively successful, especially in sweet environments. This is due to the simpler chemistry of condensed water, which leaves less room for assumptions both in terms of modeling and field data collection. An extensive effort to develop methodology for comparison between field data and model prediction has been undertaken, raising the operator confidence in using TLC prediction software for failure analysis and design. However, a number of uncertainties still remain, as models are just a representation of the current state in the understanding of mechanisms. The description of the modeling approaches developed for TLC is presented in Chapter 29.

16.4 Discussion on the corrosion trends to close gaps

Since much progress in the understanding of mechanisms has been achieved, the focus of new developments in the area of TLC is driven mostly by the need to improve and validate methods to predict and effectively mitigate corrosion. TLC prediction is covered in Chapter 29, and this section focuses on mitigation methods. On the laboratory side, there is a strong interest and need in developing standard methodology for corrosion testing and inhibitor evaluation in condensing conditions. On the field operation side, a number of TLC mitigation options that have been proposed to ensure that pipeline integrity still requires optimization.

16.4.1 Development of testing methodology for TLC assessment

16.4.1.1 Laboratory testing setups

Over the past 20 years or so, many experimental setups have been proposed to study corrosion under dewing conditions [97]. Typical CO_2 TLC setups involve low-pressure glassware under stagnant or low flow conditions [6,27,80], high pressure

autoclave systems [26,34,98], and large scale flow loops [30,32,99]. Sour TLC has also been investigated using similar setups, although the use of cracking resistant alloys is often required [57,61,100].

Each system holds its own set of advantages and drawbacks, but it is recognized that the proper simulation of the condensing conditions (i.e., condensation rate and surface wetting) is key in developing accurate and representative experimental system. It is also important to recognize that specific field conditions cannot entirely be reproduced in any laboratory setup. However, the desired outcome of most experimental study does not require exact reproduction of field conditions. If the study focuses on mechanisms, a simplified setup is often pursued where single operating parameters can be investigated separately. High-pressure and flow loop setups tend to reproduce field operating conditions more accurately but are also far more difficult to control. Proper interpretation of the results is always necessary in order to understand how experimental data and trends can be extended to field conditions. Consequently, the multitude of laboratory systems used to characterize TLC can become cumbersome in terms of interpretation of results obtained using different methods. This is especially true when it comes to validation of VCIs.

16.4.1.2 Toward a standard for volatile inhibition evaluation

Several experimental setups have been developed with the sole objective of evaluating the performance of VCIs [88,91,92,101,102]. The measured inhibition efficiency has enormous importance on the selection of inhibitors for field application and on the management of inhibition programs. It is important, therefore, that the experimental method influences the outcome of the test as little as possible. Standardization is an effective method to ensure that all tests are run following the same methodology and that the results can be compared. However, the adopted standard must be relevant and represent accurately the problem at hand. The only existing standard for VCI testing was developed for the packaging industry [103] and is not practical when it comes to TLC studies.

16.4.2 Design of multiphase pipelines

Most of the underlying mechanisms related to CO_2-dominated TLC have been elucidated in laboratory environment and are backed to some degree by extensive field experience. However, design of new pipelines still relies on the operator's in-house knowledge and on a set of guidelines specific to each company. Gunaltun presented a comprehensive review of the best TLC management practices [49] and stated that "there are still questions about the availability of sufficient know how, adequate specification and standards, and reliable prediction, corrosion control and monitoring systems." This section presents a summary of these technical "best practices". It is also important to stress that this summary applies to sweet environments, as sour TLC remains a rare event.

16.4.2.1 CRA, cladded pipe, and internal coating

The most obvious way to combat internal corrosion in general and TLC in particular is by using corrosion resistant alloy (CRA), cladded pipe, or internal coating. If applied to the entire length of the pipe, this option can also be the most expensive and is, therefore, seldom applicable. However, cladded pipe would be used along the first few hundred meters of pipe where the fluid is the hottest and when high water condensation rate and TLC rates are expected. The cladded section is purposely not thermally insulated in order to ensure maximum heat exchange and rapid decrease in the fluid temperature. The length of the cladded section is determined using flow assurance and TLC prediction models to ascertain the temperature, water condensation rate, and TLC rate profiles. Several corrosion concerns exist at the CRA/CS (carbon steel) transition. First, care must be taken to avoid galvanic coupling. Second, issues related to the so-called "hungry water" could also appear as rivulets of condensed water, coming from the cladded section and transitioning to the CS section, and are free of corrosion products and so very corrosive [104]. This condition is not TLC per se but is a direct consequence of the condensation of water in the cladded section. It is also difficult to mitigate without clever design of the CRA/CS.

16.4.2.2 Corrosion allowance

If the use of CRA is not an option, enough corrosion allowance needs to be considered during the design phase. Gunaltun proposed a minimum corrosion allowance of 10−12 mm for the warmest sections of the pipeline (above 50°C, 122°F), which can be reduced to 6−8 mm for colder sections [49]. The use of proper heat insulation could also reduce these values accordingly. These specifications are made based on field experience and also counting on TLC stabilization, which is "also the most controversial aspect in the TLC mechanism" [49]. Rather than using fixed corrosion allowance derived from a limited number of field cases, another approach is to use available TLC prediction models in order to calculate the expected metal loss during the operating life of the field.

16.4.2.3 Thermal insulation and pipe burial

The application of thermal insulation (typically polyurethane elastomers or polypropylene) can be used to reduce the water condensation rate. Full pipe burial is even more effective in ensuring low heat exchange with the outside environment. These methods, if applied well, can reduce the TLC rate considerably, but the fluids flowing inside the pipe can remain hot all along the insulated section, prohibiting any interruption in thermal insulation or pipe burial that could lead to cold spots. It is important to stress that partial pipe burial yields no benefit in terms of TLC. In addition, antiexternal corrosion coating such as three layer polypropylene (3LPP) and concrete weight coating cannot be considered effective thermal insulation as they are either too thin (3LPP) or have too high a thermal conductivity (concrete). The proper U-value of thermal insulation can be determined using fluid flow and TLC simulations.

16.4.2.4 Corrosion inhibition via chemical means

Chemical inhibition of TLC can be achieved, at least partially, with pH control, MEG injection, or volatile corrosion inhibition.

pH control involves the use of a nonvolatile base, most often methyl diethanolamine (MDEA), to neutralize organic acids present in the bulk aqueous phase. These acids dissociate into their ionic conjugate base and cannot evaporate anymore. However, this has no effect on standard CO_2 TLC as the acid gas content in the condensed water is not affected by the pH of the bulk liquid solution. Care must be taken to select the proper base dosage for this method, which only has practical applications at low produced water flow rate because scaling issues must also be avoided.

Similarly, the use of MEG can be used in wet gas lines to decrease the water condensation rate. As mentioned earlier, the presence of MEG in the condensed water in any substantial amount is doubtful in typical operating conditions. A significant effect is seen at MEG content above 70 wt% which, again, limits its application to systems with low water flow rates. The proper MEG injection flow rates are selected using flow assurance tools and TLC prediction models.

The use of VCI is probably the inhibition technique generating the most interest today due to its ease of application and its relatively low cost compared to other traditional techniques. However, evaluation of the efficiency of VCIs in laboratory and field environments has rarely exceeded 70%. The key challenge is to develop the right molecules or package of molecules "light" enough to evaporate and capable of high corrosion inhibition efficiency. Other requirements must also be taken into account, such as solubility in the hydrocarbon and water phases, compatibility with other chemicals used in oil and gas production, environmental friendliness, and health and safety. Once these challenges are overcome, VCI continuous injection could become the most practical and cost-effective TLC control system.

Finally, most current gas fields with high TLC risk operate with periodic batch treatment: a plug of fluid containing high inhibitor content is periodically pushed through the pipeline system between two pigs. A similar method involves the use of a specially designed spraying device [43]. This technique does not require the use of VCI, as it directly provides a means for the inhibitor to reach the top of the line. The line obviously has to be pig-able and the batch treatment must be carefully calibrated by evaluating the inhibitor persistency, because the inhibitor film will tend to desorb from the metal surface between two batch treatments, as pure condensed water continuously condenses.

16.4.2.5 Monitoring (corrosion probe and intelligent pigging)

Monitoring is a very important aspect of any corrosion management plan. As pertains to TLC, a number of tools exist to monitor corrosion in the field but the search for an accurate and practical tool has proven to be elusive. Common ILIs involve monitoring devices mounted on "smart" inspection pigs. Although pigging does not require a complete halt in production, it still involves slow down and consequent loss of revenue. Magnetic flux leakage (MFL) and ultrasonic testing (UT) are the two main

techniques currently used [43,65,69]. MFL detects pipeline defects through magnetization of the ferrous metal, and UT is based on measuring the ultrasonic signal propagated through the pipe wall.

Newer and possibly more appropriate monitoring methods are also available. Among them, field signature method (FSM) is very promising for TLC applications. FSM is a stationary and current-based method of internal corrosion monitoring. If positioned optimally, it could prove quite useful for TLC.

Other, much less expensive methods involve the use of electrical resistance or weight loss probes installed at specific locations in order to monitor the corrosion. The probes are cooled artificially to simulate condensing conditions. As with FSM, the relevance of the results is highly dependent on the location of the measurements [87]. Comparatively, the use of electric-chemical probes such as linear polarization resistance can be problematic in condensing environments due to the low conductivity of the electrolyte.

16.5 Conclusions

More than 40 years after it was first encountered, TLC remains a serious asset integrity concern for many oil and gas producers. The understanding of the mechanisms involved in TLC has improved tremendously, especially in CO_2-dominated conditions, and operators now have access to a set of tools and methods to effectively manage TLC risks in wet gas pipelines. However, the effects of several factors, such as the presence of H_2S, on TLC are still not fully understood. More importantly, more work is needed to develop a cost-effective technique to mitigate TLC using corrosion inhibitors. Sharing of field experience and strong collaboration between research and operation remain critical to any progress in this area.

References

[1] L.M. Mine-Thomson, Theoretical Hydrodynamics, MacMillan Co., New York, 1960.
[2] Y. Taitel, A.E. Dukler, A model for predicting flow regime transitions in horizontal and near horizontal gas-liquid flow, AIChE Journal 22 (1) (1976) 47−55.
[3] J.A. Dougherty, A review of the effect of organic acids on CO_2 corrosion, in: Proc. Corrosion, Houston, TX, 2004. Paper. 4376.
[4] D. Hinkson, G. Peck, Field assessment and verification of organic acid speciation for corrosion risk assessment, in: Proc. Corrosion, San Antonio, TX, 2010. Paper. 10100.
[5] M. Bonis, M. Girgis, K. Goerz, R. MacDonald, Weight loss corrosion with H_2S: using past operations for designing future facilities, in: Proc. Corrosion, Houston, TX, 2006. Paper. 6122.
[6] D. Hinkson, Z. Zhang, M. Singer, S. Nesic, Chemical composition and corrosiveness of the condensate in top-of-the-line corrosion, Corrosion 66 (4) (April 2010) 045001−045001-8.
[7] W. Sun, Kinetics of Iron Carbonate and Iron Sulfide Scale Formation in CO2/H2S Corrosion (Ph.D. dissertation), Ohio University, Chemical and Bio-molecular Engineering Department, 2006.

[8] J.L. Crolet, N. Thevenot, A. Dugstad, Role of free acetic acid on the CO_2 corrosion of steel, in: Proc. Corrosion, Houston, TX, 1999. Paper. 24.
[9] A. Dugstad, The importance of $FeCO_3$ supersaturation on the CO_2 corrosion of carbon steel, in: Proc. Corrosion, Houston, TX, 1992. Paper. 14.
[10] O. Nafday, S. Nesic, Iron carbonate film scale formation and CO_2 corrosion the presence of acetic acid, in: Proc. Corrosion, Houston, TX, 2005. Paper. 5295.
[11] W. Sun, S. Nesic, D. Young, R. Woollam, Equilibrium expressions related to the solubility of the sour corrosion product mackinawite, Industrial and Engineering Chemistry Research 47 (2008) 1738−1742.
[12] D. Rickard, G.W. Luther, Chemistry of iron sulfides, Chemistry Reviews 107 (2007) 514−562.
[13] J. Vera, S. Kapusta, N. Hackerman, Localized corrosion of iron in alkaline sulfide solutions. Iron sulfide formation and the breakdown of passivity, Journal of the Electrochemical Society 133 (3) (1986) 461.
[14] S. Smith, J.L. Pacheco, Prediction of corrosion in slightly sour environments, in: Proc. Corrosion, Houston, TX, 2002. Paper. 2241.
[15] C. De Waard, U. Lotz, Prediction of CO_2 corrosion of carbon steel, in: Proc. Corrosion, Houston, TX, 1993. Paper. 69.
[16] M. Matos, C. Canhoto, M. Bento, M. Geraldo, Simultaneous evaluation of the dissociated and undissociated acid concentrations by square wave voltammetry using microelectrodes, Journal of Electro-analytical Chemistry 647 (2010) 144−149.
[17] B. Hedges, L. McVeigh, The role of acetate in CO_2 corrosion: the double whammy, in: Proc. Corrosion, Houston, TX, 1999. Paper. 21.
[18] Y. Garsany, D. Pletcher, B. Hedges, The role of acetate in CO_2 corrosion of carbon steel: has the chemistry been forgotten?, in: Proc. Corrosion, Denver, CO, 2002. Paper. 2273.
[19] T. Tran, B. Brown, S. Nesic, B. Tribollet, Investigation of the mechanism for acetic acid corrosion of midl steel, in: Proc. Corrosion, Orlando, FL, 2013. Paper. 2487.
[20] E. Remita, B. Tribollet, E. Sutter, V. Vivier, F. Ropital, J. Kittel, Hydrogen evolution in aqueous solutions containing dissolved CO_2: quantitative contribution of the buffering effect, Corrosion Science 50 (2008) 1433−1440.
[21] Y. Zheng, B. Brown, S. Nesic, Electrochemical study and modeling of H2S corrosion of mild steel, in: Proc. Corrosion, Orlando, FL, 2013. Paper. 2406.
[22] Y. Sun, K. George, S. Nesic, The effect of Cl^- and acetic acid on localized CO_2 corrosion in wet gas flow, in: Proc. Corrosion, Houston, TX, 2003. Paper. 3327.
[23] S. Nesic, J. Postlethwaite, S. Olsen, An electrochemical model for prediction of corrosion of mild steel in aqueous carbon dioxide solutions, Corrosion 52 (4) (1996) 280−294.
[24] N. Nordsveen, S. Nesic, R. Nyborg, A. Stangeland, A mechanistic model for carbon dioxide corrosion of mild steel in the presence of protective iron carbonate films − Part 1: theory and verification, Corrosion 59 (5) (2003) 443−456.
[25] K. George, S. Nesic, C. de Ward, Electrochemical investigation and modeling of carbon dioxide corrosion on carbon steel in the presence of acetic acid, in: Proc. Corrosion, Houston, TX, 2004. Paper. 4379.
[26] S. Olsen, A. Dugstad, Corrosion under dewing conditions, in: Proc. Corrosion, Houston, TX, 1991. Paper. 472.
[27] B.F.M. Pots, E.L.J.A. Hendriksen, CO_2 corrosion under scaling conditions − the special case of top-of-the-line corrosion in wet gas pipelines, in: Proc. Corrosion, Houston, TX, 2000. Paper. 31.
[28] F. Vitse, Y. Gunaltun, D. Larrey de Torreben, P. Duchet-Suchaux, Mechanistic model for the prediction of top-of-the-line corrosion risk, in: Proc. Corrosion, Houston, TX, 2003. Paper. 3633.

[29] F. Vitse, K. Alam, Y. Gunaltun, D. Larrey de Torreben, P. Duchet-Suchaux, Semi-empirical model for prediction of the top-of-the-line corrosion risk, in: Proc. Corrosion, Houston, TX, 2002. Paper. 2245.
[30] F. Vitse, Experimental and Theoretical Study of the Phenomena of Corrosion by Carbon Dioxide under Dewing Conditions at the Top of a Horizontal Pipeline in Presence of a Non-condensable Gas (Ph.D. dissertation), Russ College of Eng., Dept. of Chem. Eng., Ohio Univ., Athens, OH, 2002.
[31] Z. Zhang, D. Hinkson, M. Singer, H. Wang, S. Nesic, A mechanistic model for top of the line corrosion, Corrosion 63 (11) (Nov. 2007) 1051−1062.
[32] M. Singer, D. Hinkson, Z. Zhang, H. Wang, S. Nesic, CO_2 top of the line corrosion in presence of acetic acid − a parametric study, in: Proc. Corrosion, Atlanta, GA, 2009. Paper. 9292.
[33] J.L. Crolet, M. Bonis, The role of acetate ions in CO_2 corrosion of carbon steel, in: Proc. Corrosion, Houston, TX, 1983. Paper. 160.
[34] A. Rotimi, R.A. Ojifinni, C. Li, A parametric study of sweet top of the line corrosion in wet gas pipelines, in: Proc. Corrosion, Houston, TX, 2011. Paper. 11331.
[35] M. Singer, S. Nesic, Y. Gunaltun, Top of the line corrosion in presence of acetic acid and carbon dioxide, in: Proc. Corrosion, Houston, TX, 2004. Paper. 4377.
[36] B. Brown, A. Schubert, The design and development of a large-scale multiphase flow loop for the study of corrosion in sour gas environments, in: Proc. Corrosion, Houston, TX, 2002. Paper. 02502.
[37] ASTM G1-03, Standard Practice for Preparing, Cleaning and Evaluating Corrosion Test Specimens, ASTM, Philadelphia, PA, 2009, pp. 17−23.
[38] C. Mendez, M. Singer, A. Camacho, S. Hernandez, S. Nesic, Effect of acetic acid, pH and MEG on CO_2 top of the line corrosion, in: Proc. Corrosion, Houston, TX, 2005. Paper. 5278.
[39] R. Nyborg, A. Dugstad, Top of the line corrosion and water condensation rates in wet gas pipelines, in: Proc. Corrosion, Nashville, TN, 2007. Paper. 7555.
[40] T. Andersen, A.M.K. Halvorsen, A. Valle, G. Kojen, The influence of condensation rate and acetic acid concentration on TOL corrosion in multiphase pipelines, in: Proc. Corrosion, Nashville, TN, 2007. Paper. 7312.
[41] S. Guo, F. Farelas, M. Singer, Effect of monoethylene glycol on sweet top of the line corrosion, in: Proc. Corrosion, Vancouver, CA, 2016. Paper. 7891.
[42] T. Pojtanabuntoeng, M. Salasi, R. Gubner, The influence of mono ethylene glycol (MEG) on CO_2 corrosion of carbon steel at elevated temperatures (80 to 120°C), in: Proc. Corrosion, San Antonio, TX, 2014. Paper. 4176.
[43] M. Thammachart, Y. Gunaltun, S. Punpruk, The use of inspection results for the evaluation of batch treatment efficiency and the remaining life of the pipelines subjected to top of line corrosion, in: Proc. Corrosion, New Orleans, LA, 2008. Paper. 8471.
[44] P. Okafor, S. Nesic, Effect of acetic acid CO_2 corrosion of carbon steel in vapor-water two-phase horizontal flow, Chemical Engineering Communications 194 (2007) 141−157.
[45] M. Singer, Study and Modeling of the Localized Nature of Top of the Line Corrosion (Ph.D. dissertation), Russ College of Eng., Dept. of Chem. Eng., Ohio Univ., Athens, OH, 2013.
[46] M. Singer, D. Hinkson, Z. Zhang, H. Wang, S. Nesic, CO_2 top-of-the-line corrosion in presence of acetic acid: a parametric study, Corrosion 69 (7) (July 2013) 719−735.
[47] J. Amri, E. Gulbrandsen, R.P. Nogueira, The effect of acetic acid on the pit propagation in CO_2 corrosion of carbon steel, Electrochemistry Communications 10 (2008) 200−203.
[48] J. Amri, E. Gulbrandsen, R.P. Nogueira, Effect of acetic acid on propagation and stifling of localized attacks in CO_2 corrosion of carbon steel, in: Proc. Corrosion, Atlanta, GA, 2009. Paper. 9284.

[49] Y. Gunaltun, Design of multiphase offshore pipelines with high risk of sweet top of the line corrosion, in: Proc. Corrosion, Orlando, FL, 2013. Paper. 2290.
[50] S. Smith, M. Joosten, Corrosion of carbon steel by H_2S in CO_2 containing environments, in: Proc. Corrosion, Houston. TX, 2006. Paper. 6115.
[51] A. Valdes, R. Case, M. Ramirez, A. Ruiz, The effect of small amounts of H_2S on CO_2 corrosion of carbon steel, in: Proc. Corrosion, Houston, TX, 1998. Paper. 22.
[52] J. Kvarekval, The influence of small amounts of H_2S on CO_2 corrosion of iron and carbon steel, in: Proc. Eurocorr, Trondheim, Norway, 1997.
[53] B. Brown, K.L. Lee, S. Nesic, Corrosion in multiphase flow containing small amounts of H_2S, in: Proc. Corrosion, Houston, TX, 2003. Paper. 3341.
[54] B. Brown, S. Reddy Parakala, S. Nesic, CO_2 corrosion in presence of trace amounts of H_2S, in: Proc. Corrosion, Houston, TX, 2004. Paper. 4736.
[55] A. Camacho, M. Singer, B. Brown, S. Nesic, Top of the line corrosion in H_2S/CO_2 environments, in: Proc. Corrosion, New Orleans, LA, 2008. Paper. 8470.
[56] W. Sun, S. Nesic, A mechanistic model for uniform hydrogen sulfide/carbon dioxide corrosion of mild steel, Corrosion 65 (5) (2009) 291−307.
[57] M. Singer, Top of the line corrosion in sour environments − study of the controlling parameters, in: Proc. International Corrosion Congress, Perth, 2011. Paper. 80.
[58] B. Pots, R. John, I. Rippon, Improvements on de-Waard Milliams corrosion prediction and applications to corrosion management, in: Proc. Corrosion, Houston, TX, 2002. Paper. 2235.
[59] S. Smith, Discussion of the history and relevance of the CO_2/H_2S ratio, in: Proc. Corrosion, Houston, TX, 2011. Paper. 11065.
[60] R. Nyborg, A. Dugstad, T. Martin, Top of line corrosion with high CO_2 and traces of H_2S, in: Proc. Corrosion, Atlanta, GA, 2009. Paper. 9283.
[61] D. Pugh, S. Asher, J. Cai, W. Sisak, J. Pacheco, F. Ibrahim, E. Wright, Top-of-line corrosion mechanisms for sour wet gas pipelines, in: Proc. Corrosion, Atlanta, GA, 2009. Paper. 9285.
[62] A. Camacho, CO_2 Top of the Line Corrosion in Presence of H_2S (Master's thesis), Ohio University, Chemical and Bio-molecular Engineering Department, 2006.
[63] N. Yaakob, Top of the Line Corrosion in CO_2/H_2S Environments (Ph.D. dissertation), Russ College of Eng., Dept. of Chem. Eng., Ohio Univ., Athens, OH, 2015.
[64] Y. Gunaltun, D. Supriyataman, A. Jumakludin, Top of the line corrosion in multiphase gas line. A case history, in: Proc. Corrosion, Houston, TX, 1999. Paper no. 36.
[65] Y. Gunaltun, R. Piccardino, D. Vinazza, Interpretation of MFL and UT inspection results in case of top of line corrosion, in: Proc. Corrosion, Houston, TX, 2006. Paper. 6170.
[66] G. Bouriot, Top of line corrosion cases at Total E&P Netherlands, in: Proc. 2nd TOL Corrosion Conference, Bangkok, 2009.
[67] J.R. Piccardino, M. Stuvik, Y. Gunaltun, T. Pornthep, Internal inspection of wet gas line subject to top of line corrosion, in: Proc. Corrosion, Houston, TX, 2004. Paper. 4354.
[68] Y. Gunaltun, L. Payne, A new technique for the control of top of line corrosion: TLCC-PIG, in: Proc. Corrosion, Houston, TX, 2003. Paper. 3344.
[69] U. Kaewpradap, M. Singer, S. Nesic, S. Punpruk, Top of the line corrosion − comparison of model predictions with field data, in: Proc. Corrosion, New Orleans, LA, 2012. Paper no. 1449.
[70] U. Kaewpradap, Validation of Top of the Line Corrosion Prediction Model Using Laboratory and Field Measurements (Master's thesis), Ohio University, Chemical and Bio-molecular Engineering Department, 2012.

[71] Y. Gunaltun, S. Punpruk, M. Thammachart, T. Pornthep, Worst-case TLC: cold spot corrosion, in: Proc. Corrosion, San Antonio, TX, 2010. Paper. 10097.
[72] Y. Gunaltun, M. Thammachart, M. Singer, S. Nesic, S. Punpruk, U. Kaewpradap, Progress in the prediction of top of the line corrosion and challenges to predict corrosion rates measured in gas pipeline, in: Proc. Corrosion, San Antonio, TX, 2010. Paper. 10093.
[73] Y. Gunaltun, D. Larrey, Correlation of cases of top of the line corrosion with calculated water condensation rates, in: Proc. Corrosion, Houston, TX, 2000. Paper. 71.
[74] M. Bonis, Form sweet to sour TLC: what's different?, in: Proc. 2nd TOL Corrosion Conference, Bangkok, 2009.
[75] R. Paillassa, M. Dieumegard, M. Estevoyer, Corrosion control in the gathering system at Lacq sour gas field, in: Proc. 2nd Intl. Congress of Metallic Corrosion NACE, New York, 1963, pp. 410−417.
[76] D.F. Ho-Chung-Qui, A.I. Williamson, P. Eng, Corrosion experiences and inhibition practices in wet sour gathering systems, in: Proc. Corrosion, San Fransisco, CA, 1987. Paper. 46.
[77] N.N. Bich, K.E. Szklarz, Crossfield corrosion experience, in: Proc. Corrosion, Saint Louis, IL, 1988. Paper. 196.
[78] M. Edwards, B. Cramer, Top of the line corrosion −diagnostic, root cause analysis and treatment, in: Proc. Corrosion, Houston, TX, 2000. Paper. 72.
[79] M. Joosten, D. Owens, A. Hobbins, H. Sun, M. Achour, D. Lanktree, Top-of-line corrosion − a field failure, in: Proc. EuroCorr, Moscow, Russia, 2010. Paper. 9524.
[80] T. Pojtanabuntoeng, M. Singer, S. Nesic, Water/Hydrocarbon co-condensation and the influence on top-of-the-line corrosion, in: Proc. Corrosion, Houston, TX, 2011. Paper. 11330.
[81] T. Pojtanabuntoeng, M. Singer, S. Nesic, Top-of-the-line corrosion in the presence of hydrocarbon co-condensation in flowing condition, in: Proc. Corrosion, New Orleans, LA, 2012. Paper. 1534.
[82] G. Siegmund, G. Schmitt, B. Sadlowsky, Corrosivity of methanolic systems in wet sour gas production, in: Proc. Corrosion, Houston, TX, 2000. Paper. 00163.
[83] J. Kvarekval, A. Dugstad, Pitting corrosion in CO_2/H_2S-containing glycol solutions under flowing conditions, in: Proc. Corrosion, Houston, TX, 2000. Paper. 05631.
[84] L. Morello, N. Park, Review: the effect of methanol on the corrosion of carbon steel in sweet or sour environments, in: NACE Northern Area Western Conference, 2010.
[85] R. Watts, A. Tatarov, F. Gareau, R. Leon, Sour gas pipeline failure due to the interaction of methanol with produced water, in: NACE Northern Area Western Conference, 2010.
[86] A.V. Mashkina, A.N. Khairulina, Catalytic reactions of n-propanol and n-butanol with hydrogen sulfide, Kinetics and Catalysis 43 (2002) 733−739.
[87] S. Punpruk, M. Thammachart, Y. Gunaltun, Field testing of volatile corrosion inhibitors and batch treatment efficiency by cooled probe, in: Proc. Corrosion, San Antonio, TX, 2010. Paper. 10096.
[88] Y. Gunaltun, T.E. Pou, M. Singer, C. Duret, S. Espitalier, Laboratory testing of volatile corrosion inhibitors, in: Proc. Corrosion, San Antonio, TX, 2010. Paper. 10095.
[89] R.L. Matin, Inhibition of vapor phase corrosion in gas pipelines, in: Proc. Corrosion, Houston, TX, 1997. Paper. 97337.
[90] R.L. Martin, Control of top-of-line corrosion in a sour gas gathering pipeline with corrosion inhibitors, in: Proc. Corrosion, Houston, TX, 2009. Paper. 9288.
[91] M. Shen, A. Furman, R. Kharshan, T. Whited, Development of corrosion inhibitors for prevention of top of the line corrosion (TLC), in: Proc. Corrosion, Orlando, FL, 2013. Paper. 2509.

[92] Z. Belarbi, F. Farelas, M. Singer, S. Nesic, Role of amine in the mitigation of CO_2 top of the line corrosion, in: Proc. Corrosion, Vancouver, Canada, 2016. Paper. 07274.
[93] M. Achour, D. Blumer, T. Baugh, C. Lane, P.H. Humble, J. Waters, J. Wilcher, R. Hudgins, A novel method to mitigate top of the line corrosion in wet gas pipelines: Part I—proof of concept, in: Proc. Corrosion, Houston, TX, 2010. Paper. 11332.
[94] I. Jevremovic, V. Miskovic-Stankivic, M. Achour, M. Singer, S. Nesic, Evaluation of a novel Top of the Line Corrosion (TLC) mitigation method in a large scale flow loop, in: Proc. Corrosion, Orlando, FL, 2013. Paper. 2321.
[95] K. Gawas, Studies in Low-liquid Loading in Gas/oil/water Three Phase Flow in Horizontal and Near-horizontal Pipes (Ph.D. dissertation), Petroleum Eng., The University of Tulsa, Tulsa, OK, 2013.
[96] Z. Zhang, A Study of Top of the Line Corrosion under Dropwise Condensation (Ph.D. dissertation), Russ College of Eng., Dept. of Chem. Eng., Ohio Univ., Athens, OH, 2008.
[97] M. Singer, C. Li, M. Achour, A. Jenkins, S. Hernandez, Top of the line corrosion − Part 1: review of the mechanism and laboratory experience, in: Proc. Corrosion, San Antonio, CA, 2014. Paper. 4055.
[98] L. Zhang, J. Yang, M. Lu, Effect of pressure on wet H_2S/CO_2 corrosion of pipeline steel, in: Proc. Corrosion, Atlanta, GA, 2009. Paper. 9565.
[99] A.M.K. Halvorsen, T. Andersen, E. Halvorsen, G. Kojen, J. Skar, The relationship between internal corrosion control method, scale formation, and MEG handling of a multiphase carbon steel carrying wet gas with CO_2 and acetic acid, in: Proc. Corrosion, Nashville, TN, 2007. Paper. 7313.
[100] M. Singer, A. Camacho, B. Brown, S. Nesic, Sour top of the line corrosion in the presence of acetic acid, in: Proc. Corrosion, San Antonio, TX, 2010. Paper. 10101.
[101] M.C. Oehler, S.I. Bailey, R. Gubner, Comparison of top of the line corrosion test methods for generic volatile inhibitor compounds, in: Proc. 3rd TOL Corrosion Conference, Bangkok, 2012.
[102] V. Jovancicevic, S. Ramachandran, K. Cattanach, I. Ahmed, TLC control by volatile corrosion inhibitors in sweet gas systems, in: Proc. 3rd TOL Corrosion Conference, Bangkok, 2012.
[103] NACE Standard TM0208-2008, Laboratory Test to Evaluate the Vapor-Inhibiting Ability of Volatile Vorrosion Inhibitor Materials for Temporary Protection of Ferrous Metal Surfaces, NACE International, Houston, TX, Item No. 21253.
[104] B.F.M. Pots, T. Bos, R. Henkes, Evaluation of CRA requirements to control top of line corrosion at warm gas pipeline tie-in, in: Proc. 3rd TOL Corrosion Conference, Bangkok, 2012.

Corrosion under insulation

17

Neil Wilds
Sherwin-Williams, Bolton, United Kingdom

17.1 Introduction

Corrosion under insulation (CUI) is one of the costliest problems facing the oil and gas industry today. According to many corrosion engineers, problems such as major equipment stoppages unexpected maintenance costs stemming from CUI result in more unplanned downtime than all other causes. In the 1950s there were reports of incidences of CUI, but it was not until the 1980s that there was an increased effort to mitigate CUI. Today it is a widespread problem in the oil and gas industry counting for as much as 80% of all pipe maintenance costs. As an example a study carried out between 1999 and 2001 detailed the direct cost of corrosion in the United States was estimated to be $276 billion dollars a year, i.e., about 3% of the gross domestic product. $121 billion dollars was spent on preventing corrosion, and 88.3% was spent on organic coatings. How many of these figures were exclusively related to upstream and transmission sectors was not quantified but is expected to be substantial. The use of coatings under insulation as part of a thermal insulation system has been shown to be a good solution to mitigate CUI. A very aggressive corrosive environment can occur under the insulation, but the installed insulation will hide the onset of corrosion, and the damage might not be discovered until serious event occurs, potentially causing injury or even a fatality. Because inspection or nondestructive onstream examination is difficult and almost as costly as in situ repainting of the pipes in the field, very high demands are set for the coatings.

In oil and gas production, areas such as steel piping, storage tanks, container vessels, and other *process* equipment are all subject to a variety of temperature fluctuations. Thermal insulation installed onto the pipe or vessel mitigates these effects. However, the occurrence of seams and gaps, inadequate system design or incorrect installation, damages resulting from poor maintenance practices, or other discontinuities in the insulation system makes them susceptible to ingress of water and contaminants. Sources of water can include rainfall, cooling tower drift, steam discharge, wash downs, and, because insulation is not vapor tight, condensation. Once wet, the insulation system's weather barriers and sealants trap the water inside, so the insulation remains moist for extended periods of time creating a very aggressive corrosive environment.

Typical types of insulation may be calcium silicate, expanded perlite, man-made mineral fibers, cellular glass, organic foams, or ceramic fiber. Depending on the type of insulation employed, this will vary in its water retention, permeability, and wettability characteristics. The real issue is that the insulation and cladding hides

Trends in Oil and Gas Corrosion Research and Technologies. http://dx.doi.org/10.1016/B978-0-08-101105-8.00017-6

the protective coating system that is protecting the steel substrate. Inspection ports, which provide less than 1% visibility to the metal surface, are not likely to be representative of the whole asset. Removal of insulation is usually a last resort because of cost and is typically performed only on a 15−20 year cycle. Therefore with no full removal of the thermal insulation for metal surface inspection, over time the coating system that was intended to protect the asset against corrosion can prematurely fail. It is therefore often likely for a maintenance engineer to come along, and during removal of insulation, to complete a minor repair job and likely to unearth a degree of corrosion that represents a bigger problem.

CUI not only affects carbon steel (CS) but also has a damaging effect on austenitic and duplex stainless steel (SS) substrates. In CS, CUI occurs in piping or equipment with a skin temperature in the range of −4 to 150°C (25−302°F) [1], where the metal is exposed to moisture over a period of time under any kind of insulation. The rate of corrosion varies with the specific contaminants in the moisture and the temperature of the steel surface. Waterborne chlorides and sulfates concentrate on the CS surface as the water evaporates.

In austenitic and duplex SSs, a phenomenon called external stress corrosion cracking (ESCC) occurs, but the temperature threshold is higher—between 50 and 150°C (120−302°F) [1]. For ESCC to develop, sufficient tensile stress (residual or applied) must be present. Here again, waterborne chlorides concentrate on the SS hot surfaces as water evaporates.

17.2 Examples of CUI failures

The first case [2] was a failure of an ethylene vapor line as shown in Fig. 17.1(a)−(c). The original engineering specifications of the plant reported that the line was operating at −24°C (−12°F). During inspection surveys, this was considered as high risk. However, after investigation, it became apparent that this operating temperature was only

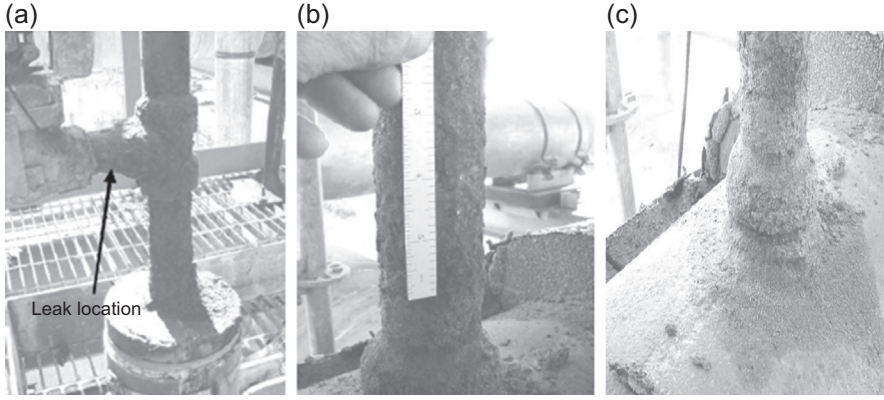

Figure 17.1 (a) Location of the leak, (b) corrosion of the vent line at 14″ branch connection, (c) corrosion of the vent line at 14″ branch connection.

correct when the pressure control valve was open and flowing. The normal operation of the valve was to be in the closed position, creating a stagnant leg with no flow. Therefore in reality the typical temperature of the line was only slightly below ambient. On removing the insulation at the location of the leak, it was found that the corrosion extended beyond the area of the leak and traveled further down the pipe back to a 14-inch line. On further inspection and removal of insulation the CUI issues were found to be more prevalent.

The second example (Fig. 17.2) was a storage tank that contained hot asphalt. During a heavy storm, its cladding and insulation were blown away, revealing extensive corrosion that had not been anticipated because no external evidence had been observed. There were areas of very significant metal loss after only 14 years—likely requiring a total replacement of the tank.

The third example is shown in Fig. 17.3 illustrating a pipe coated with inorganic zinc (IOZ)−rich primer that had been under insulation running at less than 93°C (200°F). The worst part of the corrosion was found in temperatures between 71 and 82°C (160−180°F). The key issue in this case was the incorrect specification of IOZ silicate for use in this temperature range under insulation.

The images in Fig. 17.4 show other typical examples that have been seen in oil and gas facilities during inspections. In all cases the corrosion was found at a late stage and had progressed to a point that in one case resulted in shut down and replacement of the steel.

17.3 Current understanding and industry knowledge

17.3.1 Mechanism of corrosion under insulation

CUI of CS is essentially an electrochemical reaction that consists of an oxidation reaction and a reduction reaction. Most metals and alloys prefer the ionic state rather

Figure 17.2 Corrosion under insulation on Naptha tank.

Figure 17.3 Corrosion under insulation on inorganic zinc pipe section.

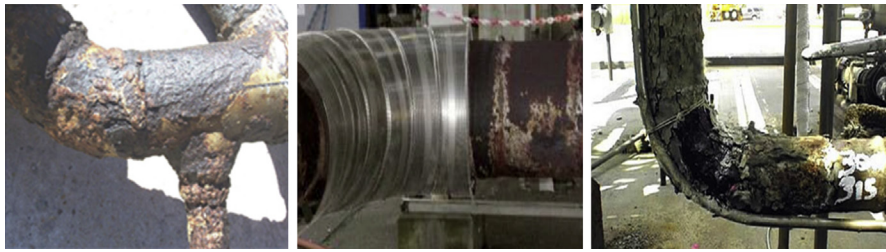

Figure 17.4 Further examples of corrosion under insulation. These photos are very typical of what is found on daily basis.

than remain in an elemental state. An oxidation reaction is where the metal atoms give up electrons and enter an ionic state. The site at which an oxidation reaction occurs is the anode. The two common iron oxidation reactions are

$$Fe = Fe^{2+} + 2e^{-} \quad \text{and} \quad Fe = Fe^{3+} + 3e^{-}$$

The electrons are then transferred and become part of another chemical species as part of a reduction reaction. When the steel surface is in contact with water containing dissolved oxygen and the presence of the free electrons, this results in the reduction reaction:

$$O_2 + H_2O + 4e^{-} = 4OH^{-}$$

The site at which the reduction reaction occurs is the cathode. The OH^{-} anions react with the Fe^{2+} and Fe^{3+} to form $Fe(OH)_2$ and $Fe(OH)_3$, respectively. The final reaction is the reformation of the H_2O and the precipitation of the Fe_2O_3 oxide. The total chemical reaction is

$$4Fe + 6H_2O + 3O_2 = 4Fe(OH)_3 = 6H_2O + 2Fe_2O_3 \text{ (precipitation)}$$

CS that is insulated corrodes because of being in contact with aerated water. The role of insulation provides a crevice that retains the water and corrosive media, the material may wick (i.e., absorbs or transports moisture via capillary action) and absorb water, and the material may contribute contaminants that increase or accelerate the corrosion rate. The primary water sources are infiltration from external sources and condensation. Contaminants in water can increase the conductivity of the water environment.

It's a common knowledge among experienced corrosion engineers dealing with CUI that dry insulation systems simply do not exist, and there is no such thing as 100% waterproof insulation throughout the life of the installed insulation. It is also a myth that at elevated service temperatures, that moisture could never get trapped within the insulation system. This leads to the fact that in many piping systems, no coating other than a basic inorganic shop primer was ever applied. The truth is that the primary function of jacketing is weatherproofing and not vapor barrier. Depending on service temperature and ambient conditions, condensation within the insulation system may not be avoidable and therefore needs to be addressed in the design/engineering phase. However, it is common that water enters into the insulation system through failed or broken cladding/jacketing. This is primarily caused by:

- Foot traffic on the cladding/jacketing itself
- Inadequate design
- Incorrect installation
- An insufficient maintenance strategy

When containing hot or cold fluid in a tank, pipe, or other equipment, insulation will be important to avoid heat loss or condensation. These, together with the requirement for protection against potential health, safety, and environment issues, are the main reasons to insulate. However, because of the temperature difference between the insulation and the steel, condensation may occur. This is a potential root cause of CUI. If there is water present, depending on temperature cycling and chemical composition of the water phase, it may develop a very aggressive corrosive environment at the steel surface. The most destructive CUI temperature range for CS is from 60 to 120°C (140−248°F), as the water evaporates at higher temperatures. However, in a closed system, corrosion may occur also at higher temperatures as the vapor may be hindered to escape the insulation by the jacketing. The vapor may condense at the inside of the jacketing and maintains the moist environment. In addition, studies by SigbjØrnsen [3] has shown that the presence of water in insulation even at temperatures in excess of the usual range for CUI occurrence can suppress the temperature of the steel to well within the range of CUI. Therefore areas that were previously left out of risk-based inspection because they had "too high temperature" could indeed be actually corroding due to CUI.

Fig. 17.5 shows the corrosion rate as a function of temperature in an open and a closed system [1]. The closed system shows similar corrosion rate as is measured for CUI. It is observed that although the corrosion rate decreases at higher temperatures for the open system, it increases for the closed system, which is also the case for CUI.

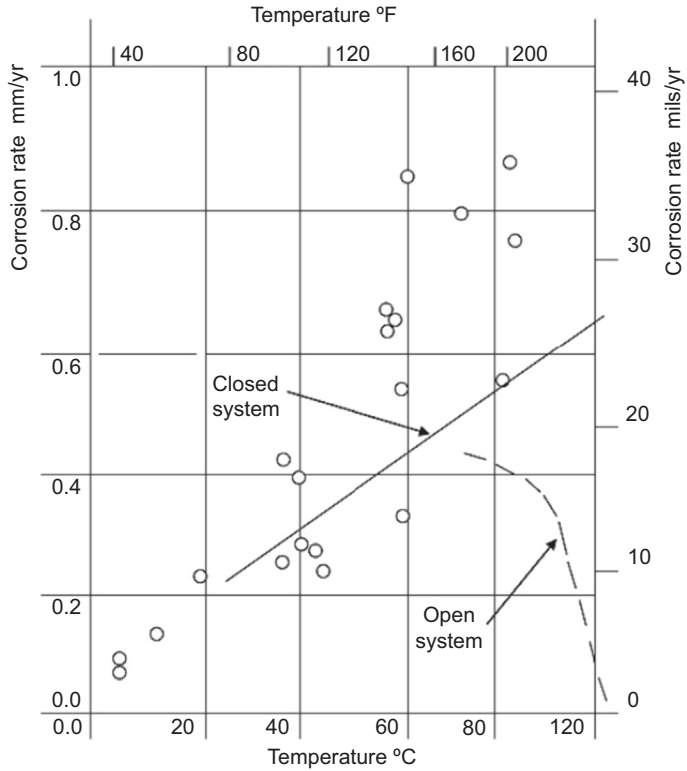

Figure 17.5 Corrosion rate of steel in water at different temperatures, open and closed systems. The plotted *circles* represent field values measured for corrosion under insulation [4].

17.3.2 Insulation solutions

Fig. 17.6 illustrates a typical cross section of an insulated pipe. The choice of insulation does not only affect the ability to maintain the temperature but also the corrosion rate. Typical types of insulation used today are calcium silicate, expanded pearlite, man-made mineral fibers, cellular glass, and organic foams, and ceramic fibers are common insulation materials used by the industry. Some types of insulation, such as phenolic foam and polyurethane foam, contain halides such as chlorides and bromide ions that can dissolve when the insulation is subjected to constant wetting. This will result in a decrease in the pH of the trapped water, which will result in an acceleration of the corrosion rate of the insulated steel. Across the range of insulation types there are also large differences in the wicking properties. For example, calcium silicate, a very popular choice of insulation, may absorb water up to 400% of its own weight, whereas another such as cellular glass (foam-glass) is a nonwicking insulation that will not absorb water, provided that the insulation cell structure is still intact. To add to this, wet calcium silicate has a pH of 9−10, which will create an adverse corrosive environment for coatings such as alkyds and IOZ. Therefore it is critical to

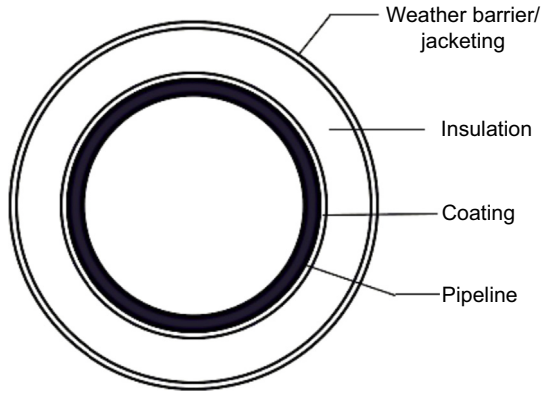

Figure 17.6 Typical cross section of an insulated pipe.

understand that when choosing insulation for austenitic and duplex SSs, the chloride content should be carefully considered because of the susceptibility to chloride-induced stress corrosion cracking.

Insulation materials can be roughly subdivided into permeable (open celled) and impermeable (closed cell) materials. For insulation requirements below ambient conditions, where surface condensation or icing is possible, closed-cell materials such as PUR/PIR foam or cellular glass are often chosen. On the other side of the spectrum for hot systems, mineral wool or expanded perlite are commonly employed.

Another added complication on the choice of insulation to use is the geographical location or for historical reasons. For example, Europe commonly uses mineral wool for hot insulation but in the United States, calcium silicate, perlite, or cellular glass are more common. In specifications, it is a common practice not to refer to product names. Therefore, many insulation specifications refer to general technical requirements such as:

- Water absorption (ASTM C610 or ASTM C612)
- Leachable chloride content (ASTM C871 or ASTM C795)
- Hydrophobicity
- Compressive strength
- Dimensional stability

17.3.3 Insulation jacketing/cladding

In all conventional insulation systems the first line of defense against the environment is the protective jacketing or cladding. This is not only used as a waterproofing system to protect from the ingress of moisture but also protects the insulation system against mechanical damage, chemical attack, and fire damage. Jacketing can come under two basic categories:

1. Metallic jacketing
2. Nonmetallic jacketing

17.3.3.1 Metallic jacketing

Metallic jacketing is predominately formed from thin sheets of 304 SS, aluminum, or galvanized steel with the internal surface coated with a moisture-resistant coating to mitigate corrosion of the jacketing. The advantages of using metallic jacketing are long service life and ease of installation. However, the disadvantages are key to the CUI issues we face today in the respect that they are difficult to seal and are easily damaged from foot traffic often from maintenance and repair operations.

17.3.3.2 Nonmetallic jacketing

Nonmetallic jacketing is generally produced from materials such as thermoplastic materials or fiber-reinforced plastics. They can be used in two forms. Preformed jacketing is usually found in sheet form and, together with the recommended adhesives, can provide water tight seals that are much more resistant to damage by foot traffic than the metallic jacketing. Formed in place jacketing is glass fiber−reinforced epoxy or polyester, which is applied to the outside of the insulation and in the case of the polyester formed into the required geometry before being cured rapidly with UV light.

17.3.4 Coatings solutions

Protective coatings under insulation are effectively used to prevent the contact between the water that has infiltrated through the insulation system and the steel and hence, mitigating corrosion. However, all types of coatings will not have an indefinite lifetime, and there are several limitations to the conditions under which they should be used. In the selection of a coating to protect against CUI, various questions are usually required to be answered:

1. What is the operating temperature?
2. What is the surface preparation?
3. What is the application method?

The most commonly used coating systems for mitigation CUI are the 2-component phenolic epoxies and novolac epoxies. However, process temperatures are increasing, and where 150°C (302°F) was used before, 205°C (401°F) might be used today. This imposes tougher performance requirements for the coatings, and new chemistries for high-temperature coatings were therefore needed to be developed.

Industry guidance, provided by the trade association NACE, holds that immersion-grade protective coatings are the best defense against CUI in both insulated CSs and austenitic and duplex SS. CUI is treated as an immersion condition because of the trapped water under the insulation. Coatings and linings formulated for immersion service are ideal for CUI because the contaminants that pass through the insulation along with the water create an aggressive operating environment. Coating systems incorporated into NACE Standard SP0198-2016 [1] have a track record of success and include 2-component epoxy aluminum or mastics, epoxy phenolics or epoxy novolacs, metalizing or thermal spray coatings, thin film silicones, and organic/inorganic hybrids. A crucial consideration when determining the appropriate protective coating system to

use under insulation is the expected service temperature of the equipment or piping, especially when intermittent thermal cycling is present. The coatings on the market are engineered to work at various temperature ranges because one size does not fit all. The most common systems are phenolic epoxies, for temperatures of −45 to 150°C (−50 to 302°F) and novolac epoxies, for temperatures of −45 to 205°C (−50 to 401°F). Additionally, coatings that can be categorized as inert multipolymeric matrix (IMM) or inorganic copolymer (IC) have shown a temperature range from −45 to 650°C (−50 to 1200°F). Modern facilities are running at temperatures as high as 205°C (400°F), where 150°C (302°F) was more standard previously. And although most equipment does not run at the high end of the temperature design, spikes can occur for various reasons and must be taken into account when specifying the appropriate coating system. Coatings suitable for use in oil and gas environments must demonstrate superior resistance to wet/dry cycling. In fact, product testing can involve as many as 30 cycles, 30 days in total duration at 450°C (842°F) dry, and cooling to 23°C (74°F) wet [4], to certify results where rusting, blistering, and coating disbondment do not occur. These coating systems can be used as tank linings as well, so they are immersion grade by their nature. One of the most useful resources within the NACE SP0198-2016 standard itself are the coatings tables, which outline, for given coating system temperature ranges, the recommended surface preparation, surface profile, and categories of prime and finish coats. Table 17.1 "Typical Protective Coating

Table 17.1 Typical protective coating systems for austenitic and duplex stainless steels under thermal insulation [1]

System	Temperature range	Generic first coat	Generic second coat
SS-1	−45 to 60°C (−50 to 140°F)	High build epoxy	N/A
SS-2	−45 to 150°C (−50 to 302°F)	Epoxy phenolic	Epoxy phenolic
SS-3	−45 to 205°C (−50 to 401°F)	Epoxy novolac	Epoxy novolac
SS-4	−45 to 540°C (−50 to 1000°F)	Air-dried silicone or modified silicone	Air-dried silicone or modified silicone
SS-5	−45 to 650°C (−50 to 1200°F)	Inert multipolymeric matrix coating or inorganic copolymer	Inert multipolymeric matrix coating or inorganic copolymer
SS-6	−45 to 595°C (−50 to 1100°F)	Thermal spray Al	Optional sealer
SS-7	−45 to 540°C (−50 to 1000°F)	Aluminum foil	N/A

Adapted from SP0198-2016.

Systems for Austenitic and Duplex Stainless Steels Under Thermal Insulation," and Table 17.2 "Typical Protective Coating Systems for Carbon Steels Under Thermal Insulation and Fireproofing," are both adapted from NACE SP0198-2016 standard. Table 17.2 includes the addition of new protective coating system technologies and

Table 17.2 Typical protective coating systems for carbon steels under thermal insulation [1]

System	Temperature range	Generic first coat	Generic second coat
CS-1	−45 to 60°C (−50 to 140°F)	High build epoxy	N/A
CS-2 (shop application only)	−45 to 60°C (−50 to 140°F)	N/A	Fusion-bonded epoxy
CS-3	−45 to 150°C (−50 to 302°F)	Epoxy phenolic	Epoxy phenolic
CS-4	−45 to 205°C (−50 to 401°F)	Epoxy novolac or silicone hybrid	Epoxy novolac or silicone hybrid
CS-5	−45 to 595°C (−50 to 1100°F)	Thermal spray Al	Optional sealer
CS-6	−45 to 650°C (−50 to 1200°F)	Inert multipolymeric matrix coating or inorganic copolymer	Inert multipolymeric matrix coating or inorganic copolymer
CS-7	60°C (140°F) maximum	Thin film petrolatum or petroleum wax primer	Petrolatum or petroleum wax tape
CS-8 inorganic zinc shop-primed pipe	−45 to 400°C (−50 to 750°F)	N/A	Typically coatings from system CS-3/4/6
CS-9 under fireproofing	Ambient	Epoxy or epoxy phenolic	Epoxy or epoxy phenolic
CS-10 galvanized steel under fireproofing	Ambient	Epoxy or epoxy phenolic	Epoxy or epoxy phenolic

Adapted from SP0198-2016.

elimination of outdated ones, the addition of metallic coating systems, and a modification of the recommendation for new bulk piping that is primed with an IOZ-rich coating. This standard has just been reaffirmed and reissued in 2016. Although it is common in the oil and gas industry to use a shop-applied IOZ coating as a primer on new CS piping because it dries quickly and is cost-effective, IOZ provides inadequate corrosion resistance in closed, sometimes wet, environments. At temperatures greater than 60°C (140°F), the zinc may undergo a galvanic reversal where the zinc becomes cathodic to the CS. Shop-primed pipe will be finish-coated at the job site depending on the service conditions needed.

The standard recommends top coating the IOZ to extend its service life, and that it is not be used by itself under thermal insulation in service temperatures up to 175°C (347°F) for long-term or cyclic service. In cases where pipe is previously primed with an IOZ coating, it should be top coated to extend its life. The CS coatings table in the NACE document should be referenced, and the coating manufacturer should be consulted for the generic coating, dry film thickness (DFT), and service temperature limits.

17.3.4.1 Epoxies

Conventional epoxies have been used for many years in the form of aluminum pigment filled or "mastic" formulations. These were generally high-solids materials, i.e., >80% volume solids and performed adequately up to temperatures of 120−150°C (248−302°F). To this date many specifications still use conventional epoxies as part of the solution to combating CUI. However, as previously mentioned, the push to higher process temperatures has seen the demise of these types of coatings. They have been replaced by either the phenolic or novolac epoxies for temperatures up to 205°C (401°F) or by modern organic/inorganic hybrids for higher temperatures.

17.3.4.2 Metallic coatings

Thermally sprayed aluminum (TSA) is a very common metallic coating used for CUI. TSA has a maximum operating temperature of 595°C (1103°F), and it has no limit to the surface temperature when it is applied, as it is arc or flame applied. SSPC-SP10, near-white blast cleaning, is needed as surface preparation. The application and surface preparation are crucial for the corrosion-resistant properties of the TSA, but when correctly applied, it has demonstrated a lifetime of 20 years with no maintenance. In rural areas it will not function as a sacrificial anode, but in marine environments containing chlorides it will have this effect.

A protective layer of Al_2O_3 is formed at the surface and slows down the corrosion rate. However, TSA has a porosity of 5%−15%, and therefore sealer paints are often applied as a final coat, because the porous surface forms a good base for the paint.

Zinc has a thinner passive film area in a chloride-containing environment and will therefore often be an active layer, which implies higher corrosion rate. When using zinc as protection against corrosion, the film will thus corrode away after much shorter time than the TSA coating. Also it has been found that for temperatures

higher than approximately 60°C (140°F), the corrosion potential for zinc increases more than that for iron. There is no reversal in the standard electrochemical potential between zinc and iron, but in closed-circuit conditions, corrosion products will form at the zinc surface but not on the iron surface, and the corrosion potential for the zinc will become greater than for the iron. This implies that zinc will transform from sacrificial anode to cathode with respect to the CS substrate [5]. However, this is dependent of the presence of dissolved oxygen, temperature, and the composition of the water. This should be taken into account when using zinc for cathodic protection. For an insulated surface, NACE SP0198-2016 stipulates that zinc should not be used at temperatures 50−175°C (120−347°F). The maximum DFT of many zinc silicates is 75 μm (3 mils), which is not sufficient for protection against CUI. The extremely harsh corrosion conditions observed under insulation will accelerate the corrosion rate of zinc. If steel is primed with an IOZ-rich material the coating should be top coated to extend the service life.

17.3.4.3 Epoxy phenolics/novolacs

Epoxy phenolic coatings are known to perform well beneath insulation but have a limited temperature resistance to around 205°C (401°F). On CUI pipe testing [4] the epoxy phenolic coating performed well at the lower temperature end of the pipe; however, the portion that was subjected to temperatures above 230°C (446°F) showed the coating degrading, flaking off, and allowing corrosion to take place. This correlates exactly with the performance that is seen of epoxy phenolics in the field. They provide good long-term protection against CUI up to 205°C (401°F) but are destroyed when subjected to high-temperature cycling, subsequently allowing corrosion to take place. Some phenolic epoxies are also used, and the coating tested has a higher maximum operating temperature of 230°C (446°F). At these higher temperatures, typically, the coating will become brittle and crack. Phenolic epoxies normally have a narrow DFT range, and it must not exceed 300 μm (12 mils) to avoid cracking. Typically, two coats of 100 μm (4 mils) each are used. The application temperature should not be less than 3°C (37°F), and temperatures lower than 10°C (50°F) result in longer curing times.

17.3.4.4 Aluminum silicones

Silicone-based coatings are formed when inorganic silicone pigments are added to a coating. They have high operation temperature limit and high resistance against moisture and weathering. However, they are somewhat expensive and will not withstand acids and alkalis. Several types of silicone-based coatings have been developed. IOZ silicate coating can endure temperatures up to 400°C (752°F), but because of unsatisfactory long-term corrosion resistance it is not used for CUI. Also the thermal cycling and shock properties of these early silicon-based coatings are poor.

Aluminum silicone coatings are another commonly used elevated temperature technology and are generally applied in two or three thin coats of 25 μm (1 mil) each.

Industry has learned that these coatings do not provide adequate protection against CUI because of their thin films and limited barrier protection, despite being able to withstand temperatures up to 540°C (1004°F).

17.3.4.5 Organic/inorganic hybrids

The first of these types of coatings were introduced in the mid-1990s and were plagued with issues of film microcracking and hence did not live up to their original performance aspirations. These types of products are no longer present and have been replaced with more robust coating systems. The next-generation inorganic/organic hybrid CUI coatings have been developed and are in use since the turn of the century and were dominated by two chemistry types:

- TMIC/IC, titanium modified inorganic copolymer/inorganic copolymer
- IMM, inert multipolymeric matrix

These types of products are now used in CUI operations across the full CUI temperature range and beyond. The chemistry used allows cryogenic usage as well as temperatures in excess of 600°C (1112°F) in the case of the IMM coatings. The first generation of IMM coating materials provided an improved solution for CUI, but a few limitations were spotted. Prolonged dry time to handle and poor sprayability (overspray) have been the main drawbacks in terms of application features. Poor mechanical resistance (softness, poor flexibility, and poor impact resistance) is the other key drawback, making shop-painted steel prone to damage during transportation from shop and at erection on site.

A second generation of IMM coating has been developed, and it has been used in the field since 2012. This second-generation IMM overcomes the drawbacks of the earlier generation.

17.3.4.6 Insulation coatings

An alternative coating solution to mitigate CUI is to install spray-applied, nonclad thermal isolative coatings that provide a monolithic barrier to water, chemicals, UV rays, and heat transfer. Such sprayable insulative coatings (SIC) provide personnel burn protection, thermal insulation for energy conservation, and protection from radiant solar heating. Coatings companies have worked to develop multipurpose insulative acrylic coating engineered to optimize thermal properties. These products enable dangerously hot systems such as piping and ductwork to stay cool to the touch, preventing burns and protecting the safety of personnel. They can be applied directly to ambient or hot surfaces offering facility operators the chance to reduce downtime by keeping systems online during coating. Such coatings are suitable for any industry where conventional insulation and cladding are required. To date, this type of technology does not cover the full range of operative temperatures and insulation needs, as the cladding approach does. But it is already able to replace cladding systems in a number of scenarios, as a viable option for providing insulation while effectively removing the source of the CUI phenomena.

Table 17.3 A generic snapshot of the technology and a list of the utilization scenarios for SIC

Snapshot	• Industrial WB acrylic resin with engineered ceramic microspheres • Low thermal conductivity (0.097 W/m × K) • Lightweight due to high air content • Expected service life of 10−20 years with recommended primers and topcoat	
Uses	Replacement for conventional insulation and cladding Personnel protection coating Hot or cold process insulation Control radiant heating of storage containers	Service temperature range (all applications) from −51°C (−60°F) to 177°C (351°F)

Table 17.3 provides a generic snapshot of this technology and lists the range of utilization scenarios that SIC can cover today, at current stage of development of the technology, using waterborne acrylic resins with ceramic microspheres.

Formulated from waterborne acrylic resins with ceramic and glass microspheres that minimize energy transfer through the film because of its high air content, these coatings adhere to the underlying primer and prevent water or moist air from corroding the steel.

The air content is so high in these coatings that the specific weight of the liquid paint typically ranging from 0.6 to 0.7 Kg/L, with an important fraction of that weight evaporating out during the drying process.

17.4 Vapor-phase corrosion inhibitors

Vapor-phase corrosion inhibitors (VCIs) are completely different alternative protection method to that of coatings. A VCI is a volatile chemical compound that forms a stable bond at the interface of the metal, preventing penetration of corrosive species to metal surfaces. These inhibitors are easy to apply and can be used to protect a selection of metal types used in various corrosive environments. VCIs work through a series of chemical characteristics:

- Stable metal passivation
- Strong surface adsorption properties
- Excellent surface wetting properties
- Thermally stable to 176°C (349°F)

When applied usually by injection into the insulating jacket either through a gravity feed system or a portable injection pump, they form a clear, dry, hydrophobic film of approximately 6 μm (0.24 mils).

17.5 Nondestructive inspection techniques to prevent CUI failures

The real issues with CUI is the fact that the only 100% certain way of knowing that there is no problem on pipes and vessels is to completely remove the insulation system. This is not the approach that corrosion engineers/end users wish to adopt because it is also the most expensive way of inspection. This created a challenge for researchers to provide techniques that eliminate the need to completely dismantle insulation systems for inspection. The techniques are required to be nondestructive (NDE) technologies and portable to be used on site. These techniques can be used along with conventional techniques to provide economical, comprehensive CUI inspection of piping networks. Some of the proven NDE techniques are as follows:

- Neutron backscatter
- Infrared (IR) thermography
- Guided wave ultrasonic technology (UT)
- Profile radiography
- Computed radiography (CR)
- Pulsed eddy current (PEC) testing

Out of these methods, profile radiography and guided wave UT are accepted in API 581 [6] as alternatives to insulation removal for inspection.

17.5.1 Neutron backscatter technique

It is effective in scanning large areas of pipe to determine wet/saturated insulation in a short period of time. It uses a radioactive source that emits high-energy (fast) neutrons into desired location of insulation. The high-energy neutrons travel through the insulation and collide with light elements such as hydrogen transforming into low-energy neutrons. A sensitive detector designed to detect low-energy neutrons is used to identify the "wet insulation" by measuring the count of low-energy neutrons. The count is proportional to the amount of water in the insulation and therefore could potentially signify a potential for CUI. This technique is a quick and accurate way to identify potential areas where CUI could occur. It is very portable and, in some cases, will negate the need for scaffolding. However, it does require a radiation source with the associated health and safety issues, and it will not directly detect CUI.

17.5.2 Infrared thermography

IR thermography can be effectively used to identify wet insulation in pipelines and is much more effective than traditional moisture density gauges in addition to being a much faster technique. An added benefit is that pipelines can be scanned with this technique from a distance, negating the need for costly and time-consuming construction of scaffolding. Inspections can be carried out on either heat-traced or nontraced insulated pipelines. The technique is dependent on the fact that wet insulation retains heat longer than dry insulation, and therefore carrying out the inspection after sunset or

when the pipelines are shaded will allow the inspector to distinguish between hot wet lines and cooler dry lines. Because the temperature between wet insulation and dry insulation is not large, it is recommended as best practice to use a small temperature span to increase the sensitivity of the technique.

17.5.3 Long-range ultrasonic testing

The use of guided waves in long-range ultrasonic testing (LRUT) to scan pipelines is particularly useful for the inspection of pipelines that are otherwise inaccessible for inspection. The ultrasonic waves are transmitted into the pipe wall from a loop of equally spaced ultrasound probes supported by a collar wrapped around the pipe. Once traveling along the pipe the ultrasonic waves are reflected by discontinuities such as girth welds, branches in pipeline circuit, and, more importantly, reductions in wall thickness. These reductions in wall thickness are associated with areas of corrosion, and once detected they can be analyzed via computer software.

LRUT can typically scan a length of straight pipeline up to a maximum 120 m. However, this will be reduced dependent on the type of insulation on the pipeline and the complications on the line such as supports, connections, and bends. Even so, LRUT is considered one of the most effective tools in identifying CUI in pipelines where removal of insulation is difficult.

The interpretation of LRUT can be complicated in comparison to the aforementioned IR technique and therefore is best used with trained specialists. However, it is recognized as one of the most reliable techniques to carry out the inspection of insulated pipelines in hard-to-access or inaccessible locations, especially lengths of pipeline passing under inaccessible culverts, buried piping, and at road crossings.

17.5.4 Profile radiography

Profile radiography is a technique that allows the internal wall thickness reduction of small diameter 8″pipelines to be inspected. For this reason it can also be used to find CUI as long as the source to film distance is sufficient to assess the entire line diameter in one measurement. When the pipeline diameter is more than 8″ then multiple measurements will be required to cover the full pipe diameter. The obvious disadvantage of this type of technique is the requirement of a radioactive source and the associated health and safety issues.

17.5.5 Computed radiography

This technique uses equipment similar to that used by conventional radiography except that in place of a film to create the image, an imaging plate is used. To fully exploit this technique for the detection of CUI under insulation, effective segregation of the target area is required to remove interference from pipe supports and the like. The images produced and data obtained from inspection is stored digitally, and hence the data can be accessed quickly to aid increased inspection efficiency.

17.5.6 Pulsed eddy current

The PEC has been a popular choice for inspection for a number of years and uses the principle of eddy currents. It consists of a probe that contains a transmitter and receiver. The transmitter is basically a coil to produce eddy currents in a conductor, typically a metallic substrate, i.e., pipeline or vessel. This method is a noncontact electromagnetic method for the determination of average wall thickness. The system works via a probe coil generating a magnetic field, which is used to magnetize the target substrate. This generates eddy currents in the pipe wall and thus diffuses inwards. If there are anomalies detected the eddy pulse is stopped, causing a sudden fall in the applied magnetic field. This is picked up by the PEC receiver probe. The thicker the pipe wall thickness, the longer it takes for the eddy currents to bounce back from the back wall of the metal. Using this data then, corrosion can be calculated as a percentage reduction in pipe wall thickness. This technique is not restricted by insulation material and can be used in situ up to operating temperature in excess of 450°C (842°F). The downside of this technique is its sensitivity. Compared with the radiographic technique it is relatively low because of the footprint of the test and therefore is predominantly used for wall loss measurements rather that the pitting corrosion caused by isolated CUI.

17.6 Knowledge gaps and future trends

Although the problem of CUI has been documented for decades, there are still numerous avenues of research remaining, to further prevent the effects of CUI. The key areas of research to fill the knowledge gaps in the oil and gas industry can be split into three categories.

17.6.1 Development of new CUI coating technologies

At present, as previously mentioned, there are numerous coatings for the mitigation of CUI, but all have their particular advantages and disadvantages. There are some key coating properties that all coating suppliers are trying to improve to further enhance coatings performance:

- Mechanical properties both before installation and in-service
- Temperature resistance both isothermal and cyclic
- Substrate tolerance
- Ease of application, one component versus two components
- Corrosion performance
- HT immersion resistance

It is not enough to focus on one of the aforementioned properties, but the coating supplier needs to address as many of them as possible to advance the coating performance. Developments in IMM have been achieved from the initial formulas and have gone a long way to address the issues mentioned. There have also been recent developments in increasing the temperature resistance of epoxy chemistry to beyond previous limits as referenced in NACE SP0198-2016 [1] of 205°C (401°F), reaching up to 250°C

(482°F) in some cases. However, as with all new developments that change the boundaries of known performance, long-term data is not available, and therefore these epoxy new based coatings need to be proven before they should be widely specified.

17.6.2 Development of new test methods

The knowledge of how coatings perform in the CUI environment is still not fully understood. This means that the ability to predict the performance of a coating in the field compared to accelerated laboratory test data is still not at a high level of confidence. As previously mentioned, there are multiple committees, standards, and JIPs by various groups, but until now there is no sight of agreement on a test or test methods.

The key issue facing the test method developers is to reproduce the extent of failure seen in CUI, which means that severe pitting within the most destructive CUI temperature range for CS (60 to 120°C (140−248°F)). However, this has to be reproduced in weeks or months, and not years, and has to include all the elements of the insulation system i.e., insulation and jacketing. One of the key issues in previous years has been the ability of the coating manufacturers to access trial areas in oil and gas facilities, which has been difficult. The importance of this type of correlating data has now been recognized with some major oil and gas producers who have now actively carried out research in CUI testing.

The key influencing group at present is NACE Task Group 516 (TG516), which has been set up to assess all currently published CUI test methods and to develop a new standard for the prequalification of coatings for use under insulation and consistently is attended by over 30 worldwide technical professionals to discuss new test methods. A committee for the TG has been formed, comprising coatings suppliers, testing companies, and end users to finalize this as a testing protocol to approve coatings for use under insulation.

17.6.3 New insulation developments

The development of insulation coatings is being concentrated into two main routes

- Higher temperature resistance
- Ability to apply higher film build in less coats

Current technologies for atmospheric liquid insulation are hampered by their chemistries. Generally, technology available today is based on either waterborne acrylic technology that has temperature limitations to 177°C (350°F) or epoxy syntactic materials with temperature limitations of 200°F (392°F). In the cases of the waterborne acrylic and the epoxy the temperature resistances come from the binder resin. The waterborne acrylic also has issues with the need for multiple coats at 300−500 μm (12−20 mils) and because they are waterborne, the epoxy can be applied at >5000 μm (200 mils) per coat. New potential technologies to try to alleviate the issue are based on solvent-borne or solvent-free materials, using silicon or polysiloxane technologies, which have been shown for many years to have better thermal stability.

Significant advances in insulation technology have been observed in the materials added to binder systems to impart thermal insulation performance. Traditional glass or

polymer beads in insulation formulations have been replaced with materials such as aerogels, nanogels, and hollow oxides.

However, even with significant progress, no material has yet solved both high-temperature resistance and high build requirements.

Appendices

Standards committees/forums

There are various active NACE committees that share knowledge and experience in the industry. These are very well attended by all types of professionals:

a. Major oil companies
b. Engineering procurement and construction companies (EPCs)
c. Coating suppliers
d. Coatings test companies
e. Academics

The current committees are listed below.

NACE TEG 351X—Advances in Coatings Under Insulation (CUI) Technologies

Assignment: Discussion of the development of recommended test procedures for qualification of coatings used under insulation service.

NACE TEG 399X—Evaluation, Testing and Specifying Coatings Materials for Elevated Temperatures for Insulated and Uninsulated Service

Assignment: Exchange information, create task group for state-of-the-art report followed by formation of a task group to write a standard practice, and sponsor symposium.

NACE TG 325—CUI: Reaffirmation of NACE SP0198 (formerly RP0198), "The Control of Corrosion Under Thermal Insulation and Fireproofing Materials—A Systems Approach"

Assignment: To reaffirm NACE SP0198 (formerly RP0198).

NACE TG516—Standard Practice for Evaluating Protective Coatings for Use Under Insulation

Assignment: To write a standard practice for testing coatings for CUI prevention.

International Organization for Standardization, ISO

The formation of ISO committee to look at the development of a test method for prequalification of coatings for CUI is a relatively new development and is again attended by the same industry professional as for NACE, indeed some of the same experts.

European Federation of Corrosion, EFC

The European Federation of Corrosion, EFC, Working parties WP13 and WP15 have worked to provide guidelines on managing CUI together with a number of major European refining, petrochemical, and offshore companies. The guidelines within this document are intended for

use on all plants and installations that contain insulated vessels, piping, and equipment. The guidelines cover a risk-based inspection methodology for CUI and inspection techniques (including nondestructive evaluation methods) and recommend best practice for mitigating CUI, including design of plant and equipment, coatings and the use of thermal spray techniques, types of insulation, cladding/jacketing materials, and protection guards. These are available in the "Corrosion Under Insulation (CUI) Guidelines (EFC55)" [7].

Test methods for prequalification of test methods

Although there is no dedicated standard to prequalify CUI coatings, there has been a lot of effort from various sources in trying to simulate the type of failure on a laboratory scale. It is fundamental to understand that this is not an easy task, and this is why today we still do not have one test, or a series of tests, which is fully endorsed by all interested parties. Some of the most reported test methods are given below in brief.

- ASTM G189—Laboratory Simulation of Corrosion under Insulation [8]
  This guide covers the simulation of CUI, including both general and localized attack, on insulated specimens cut from pipe sections exposed to a corrosive environment usually at elevated temperatures. It describes a CUI exposure apparatus, preparation of specimens, simulation procedures for isothermal or cyclic temperature, or both, and wet/dry conditions, which are parameters that need to be monitored during the simulation and the classification of simulation type.
- ASTM D2485—Evaluation of coatings for elevated temperature service [9]
  This test method covers the evaluation of the heat-resistant properties of coatings designed to protect steel surfaces exposed to elevated temperatures during their service life. Two test methods are described as follows:
  - Method A—Interior Service Coatings
  - Method B—Exterior Service Coatings
- K. Haraldsen, Statoil Test Method 2010 [10]
  The test cell consisted of test spools of coated CS tube sections flanged together in open containers. The containers are filled with seawater and then drained immediately after the spools were fully submerged, taking in the order of 20 min to complete. The spools were heated internally via steam to 140°C (284°F). The cycle was carried out three times per week. After testing to varying periods of time the coated spools were evaluated for rusting, blistering, and cracking.
- CUI Cyclic Corrosion Pipe Test (CCCPT) [4]
  A coated pipe is insulated with calcium silicate, sealed with aluminum foil, and placed on a hot plate at a temperature of 450°C (842°F) with the top of the pipe measured at approximately 60°C (140°F). The system is cycled 30 times with 8 h of heating followed by 16 h of natural cooling. Before and after each heating cycle the insulation is wetted with 1 L of 1% NaCl solution. The coatings are evaluated for rusting, blistering, and cracking.
- HTC Cell [11]
  The heart of the HTC environmental test is the heat exchanger, cell, and chamber. The coated cell is a carbon or SS $4'' \times 4''$ square pipe section 24 in. long with a $^1/_4$ in. wall thickness. The cell is placed horizontally in the chamber in a closed-loop system. Hot oil from a heat exchanger is circulated through the cell, and the temperature is controlled from ambient to 250°C (482°F). No insulation is used for this test allowing the flexibility for immersion testing, and the test media can be modified on agreement of the end user. The bottom portion

of the cell is under continuous immersion for the duration of the wet cycle. The test protocol is set for alternating wet and dry 4-h cycles. The vertical surface is scribed to the substrate to asses undercut corrosion evaluation.

- CUI Simulation test [12].

  This test method is intended to test a coating that has been designed to prevent corrosion under thermal insulation.

  The coatings under test are applied to steel panels in duplicate ($3'' \times 6''$ panels are recommended) to both sides of the panels. The edges of the panels are sealed, and the panels are allowed to cure for 7 days at ambient conditions or heat cure according to manufactures recommendation. The coated panels along with an uncoated panel are placed between pieces of insulation, mineral wool, or calcium silicate, which have been cut to fit a stainless steel pan. The pan is then covered with aluminum foil and placed in an oven maintained at 350°F (177°F) for 7 days. After 7 days, remove the pans from the 177°C (350°F) oven, saturate the insulation with tap water, and reseal, maintaining saturation during the entire 7-day period. Place the pans into an oven maintained at 66°C (150°F) for 7 days. After testing, the coated panels are evaluated for rusting, blistering, and cracking.

References

[1] Standard Recommended Practice: The Control of Corrosion under Thermal Insulation and Fireproofing Materials − A Systems Approach, NACE Standard SP0198-2016.
[2] Corrosion under Insulation − Donna Fruge Principal Production Engineer Westlake chemical Corporation.
[3] K. Sigbjørnsen, Corrosion Protection under Thermal Insulation, NTNU, Trondheim, 2013.
[4] M. Halliday, Development & testing of new generation high temperature corrosion resistant coatings, in: NACE 2005, 2005. Paper No. 05020.
[5] E.G. Haney, The zinc-steel potential reversal in cathodic protection, in: CORROSION/81, NACE, Houston,TX, 1981. Paper No. 216.
[6] API RP 581, Risk Based Inspection Methodology, third ed., April 1, 2016.
[7] S. Winnik, European Federation of Corrosion Publications Number 55: Corrosion-under-Insulation (CUI) Guidelines, Woodhead Publishing Limited, Cambridge, England, 2008.
[8] ASTM Standard G189-07, Standard Guide for Laboratory Simulation of Corrosion under Insulation, ASTM International, West Conshohocken, PA, 2007.
[9] ASTM Standard D2485-91 (Reapproved 2007), Standard Test Methods for Evaluating Coatings for High Temperature Service, ASTM International, West Conshohocken, PA, 2007.
[10] K. Haraldsen, Corrosion under insulation − testing of protective systems at high temperatures, in: NACE 2010, 2010, 51300-10022-SG.
[11] D. Betzig, Qualification testing of high temperature coatings, in: NACE − Bring on the Heat, 2013.
[12] J. Azevedo, T. Hanratty, R. Knecht, New generation CUI protective coating technology, in: 16th Middle East Corrosion Conference, 2016.

Corrosion and scale at high pressure high temperature

18

Paula Guraieb [1] *and Qiwei Wang* [2]
[1]Tomson Technologies, Houston, TX, United States; [2]Saudi Aramco, Dhahran, Saudi Aramco

18.1 Introduction

Corrosion and scale are two major production chemistry issues in oil and gas production systems. These two phenomena occur simultaneously at equipment surface and they are interlaced processes. Field observations have shown that scale deposits can either act as a physical barrier to protect the underlying metal from corrosion or induce localized corrosion, while corrosion product can facilitate the scale formation by serving as the heterogeneous sites for scale nucleation or contributing directly to heavy deposition as a major component. Also, dissolved iron released from corrosion and corrosion product particles can sequestrate scale inhibitor and reduce the effectiveness of the scale treatment program. Corrosion and scale are generally studied independently and the potential impact of scale formation is usually not considered in the corrosion studies. The importance of the interplay between corrosion and scale could become too significant to be ignored in high pressure high temperature (HPHT) environments.

Effective corrosion control is an integral part for the safe and efficient hydrocarbon recovery operation, in particular, to productions from unconventional resources including deep and ultradeep water. The encountered production conditions in these resources can experience temperatures over 200°C (392°F), pressures over 1379 bar (20,000 psig), total dissolved solids (TDS) in excess of 300,000 mg/L in produced water, and likely considerable amounts of carbon dioxide and hydrogen sulfide. Such harsh environments make production from these reservoirs challenging partially due to escalated corrosion risks. Unanticipated corrosion can damage production systems quickly. If corrosion were to break through tubing in an offshore well and expose the casing and cement to the extreme high pressures and temperatures of the formation, the economic damage could be enormous and the environmental impact is disastrous.

Development of a robust corrosion management plan starts with risk assessment using model prediction or laboratory testing. Current prediction models are able to predict the worst case corrosion in a simple solution. When a complex matrix or protective scale is introduced, these models fail to predict representative corrosion rates [1]. Preliminary work by Huang et al. [2] has shown that scaling tendencies have a large effect on the corrosion product formed and therefore on the corrosion rate. There is a clear need for corrosion studies that incorporate the effect of water composition and the presence of scale to improve the prediction results. It is also important that data collection experiments simulate the field conditions as closely as possible, and that the

Trends in Oil and Gas Corrosion Research and Technologies. http://dx.doi.org/10.1016/B978-0-08-101105-8.00018-8

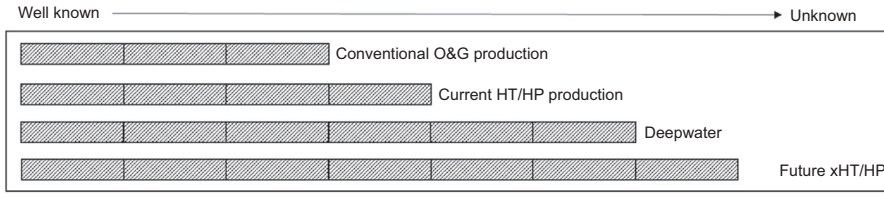

0	5,000	10,000	15000	20,000	25,000	+	Pressure (psi)
0	100	200	300	400	500	+	Temperature (°F)
0	100	200	250	400	400	+	TDS (mg/L *1000)

Figure 18.1 Illustration of current knowledge for scale and corrosion at various temperature and pressure conditions.

results are modeled to enhance the predictive ability. Finally, even less is known about the rate of scale formation and corrosion, the stability and the effect of scale and corrosion inhibitors, as well as the interaction between scale and corrosion at these extreme pressures, temperatures, and flow rates conditions.

Extensive efforts have been devoted by the oil and gas industry in understanding corrosion, scale, and fluid properties, generally up to about 150°C (302°F) and 482 bar (7000 psig) to 689 bar (10,000 psig), with limited work being done at higher temperatures and pressures. Fig. 18.1 illustrates the temperature and pressure limits of current knowledge on corrosion and scale processes. Literature data, even for calcite ($CaCO_3$) scale for which a significant amount of data is known, vary from the predicted value for solubility at high pressure high temperature (HPHT) conditions. Data used by predictive models for some species do not take into account the pressure dependence of critical equilibrium constants [3]. This alone can cause a variation of plus or minus 0.5−1.0 in logarithmic units in saturation index (SI), or a factor of 3−10 times in supersaturation. Similarly, for modeling of the gas/oil/salt−water mix the literature is mostly related to these lower pressure and temperature conditions. It is known that many of the accepted theoretical frameworks, such as Peng−Robinson-like equation of state models and Pitzer theory [4,5] are reaching their limits of the expected applications. Moreover, new corrosion and scale processes could become important in HPHT environments.

In this chapter, we summarize some new developments in corrosion and scale studies pertaining to HPHT oil and gas production systems. In the first part, we present the corrosion studies using brines with different scaling tendencies at 200°C (392°F) and 250°C (482°F). Test results demonstrate the importance of scale formation on corrosion. Pitting corrosion is developed with the formation of scale deposits on mild steel surface. Then, we examine the solubility results on iron-containing scale (siderite, iron sulfide, and magnetite) at temperature up to 250°C (482°F) and pressure up to 1655 bar (24,000 psig). We also provide a summary on recent work of inhibitor evaluations at 100°C (212°F) and 250°C (482°F). Finally, we discuss the cyclic polarization results on pitting resistance of alloys at high temperature and high TDS brine. It is hoped that this chapter will not only serve as a useful summary of recent works, but also clearly illustrate the many areas where further research is needed.

18.2 Corrosion in different scaling tendency brines

Existing corrosion models are sufficient in predicting corrosion rates in controlled laboratory testing conditions. Unidentified conditions not included in the development of the models such as mixed brine compositions cause large variations in the predicted corrosion and scale values. The corrosion prediction accuracy is limited by both the accuracy of the input data and the accuracy of the model itself [6]. Therefore, it is important to study the conditions observed in the oilfield and incorporate those observations and results into valid corrosion models.

Corrosion tests reported in the literature often use simple brine to study corrosion rate on metals and alloys. In a real field scenario with complex brine compositions, scale formation may coexist with corrosion. For example, at downhole conditions it can generally be assumed that equilibrium is reached and there should be no effect of scaling on the corrosion process, at least at the very bottom of the well. As temperature and pressure drop in rising tubing, scale formation usually occurs simultaneously with corrosion processes and may have a significant effect on corrosion rate. Nucleation and growth of scale species such as calcium carbonate may have an effect on the formation and growth of passive layers of corrosion products and on the corrosion rate. The effects of mineral scaling and deposition on corrosion are not well understood, especially at HPHT conditions.

This section shows the effect of scale formation on corrosion process at high temperatures, using calcite as an example. The test brine was selected from the United States Geological Survey (USGS) database for deepwater wells in the Gulf of Mexico. There are about 11,000 data points in the USGS database. The average concentration was 2198 mg/L calcium, 695 mg/L bicarbonate alkalinity, and 39,007 mg/L chloride. The test brine used in this study was based on the data point of USGS #14821 (Table 18.1).

Test brine solution was saturated with CO_2 and the pH was adjusted to 5.0 with deoxygenated $NaHCO_3$ solution (1 M) [7]. The test brine was in equilibrium with

Table 18.1 Summary of brine composition

Dissolved ions (mg/L)	USGS (average)	USGS #14821	Test brine
Na^+	22,115	59,200	46,200
K^+	32	235	195
Mg^{2+}	360	972	960
Ca^{2+}	2,198	3,272	2,400
Sr^{2+}	112	128	88
Ba^{2+}	52	109	55
HCO_3^-	695	206	305
Cl^-	39,007	78,020	78,377

USGS, United States Geological Survey.

respect to calcite at 200°C (392°F), and calcite scale formation was expected based on scaling tendency calculations by ScaleSoftPitzer model [8]. A carbon steel coupon (C-1018) was immersed in the test solution for 20 days at 200°C (392°F) in a Hastelloy C-276 autoclave. Fig. 18.2 shows the coupon at the end of experiment. There was no severe corrosion observed on the coupon surface.

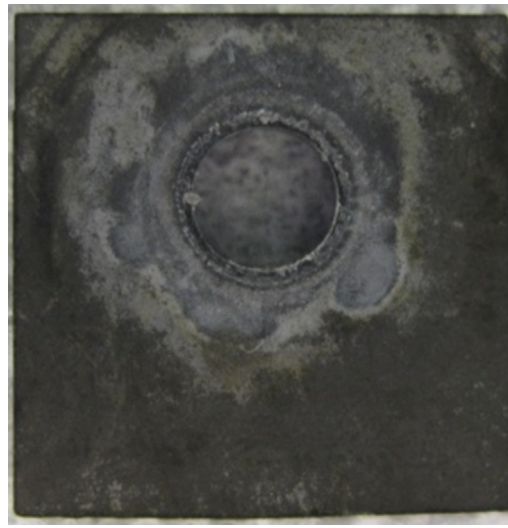

Figure 18.2 Picture of coupon after 20 days in test solution at 200°C (392°F).

The surface scale was analyzed by scanning electron microscopy (SEM) and X-ray diffraction (XRD) techniques. Fig. 18.3(a) and (b) shows that this scale consisted of siderite ($FeCO_3$) and ankerite ($Ca(Fe,Mg,Mn)(CO_3)_2$). Neither calcite nor magnetite (Fe_3O_4) precipitates were detected on the steel surface. It should be noted that ankerite, as a mixed Ca and Mg scale species, would not be formed if a simple NaCl brine solution was used.

The coupon surface was cleaned using Clark's solution for corrosion rate determination and localized corrosion was analyzed using vertical scanning interferometry (VSI). The uniform corrosion rate was found to be 0.14 ± 0.02 mm/year, while no localized corrosion was found, as shown by VSI analysis (Fig. 18.4). The corrosion rate obtained by both weight loss and VSI analyses was in good agreement. We can conclude from the corrosion rate results that corrosion of carbon steel C-1018 is low when water is at equilibrium with calcite.

A similar corrosion test was performed with the same brine at 250°C (482°F). The test brine became supersaturated with calcite at this temperature due to the inverse solubility behavior of calcite. Scaling tendency calculation showed that test brine had a calcite SI of 1.15. The C-1018 coupon was heavily corroded after only 7 days (Fig. 18.5) of exposure, corrosion rate could not be measured because the scale that formed was hard and not removable using the NACE procedure. The SEM image (Fig. 18.6) shows that a porous layer was formed on the steel surface, and the shapes

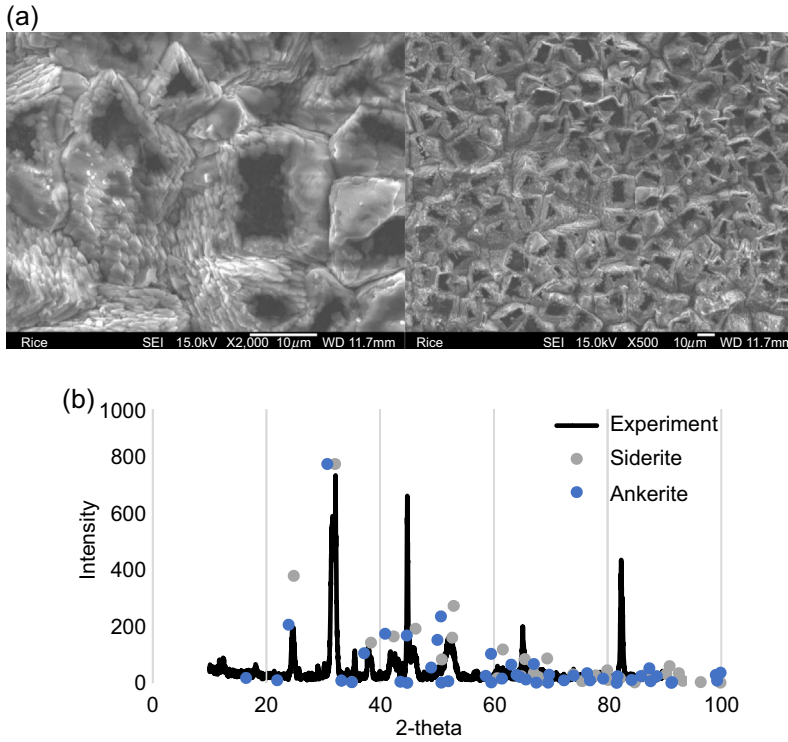

Figure 18.3 Scanning electron microscopy (a) and X-ray diffraction analysis (b) of the coupon surface after the test at 200°C (392°F) in brine equilibrium to calcite.

of the crystals were irregular and heterogeneous. The result was very different from the calcite equilibrium scenario shown in Fig. 18.3, however, little is known about the protective properties of ankerite for corrosion. The XRD spectrum showed that scale was a mixture of calcite, ankerite, and magnetite. The corrosion was significant in the rising tubing scenario compared to the downhole conditions.

Additional test was conducted at 250°C (482°F) in a simple NaCl (2 M) brine solution, which contained no dissolved calcium. This test brine was undersaturated with respect to calcite (SI < 0). The test results were similar to the calcite equilibrium scenario at 200°C (392°F) (see Table 18.2). No localized pitting was observed and magnetite was detected on the coupon surface. These results indicated that the severe corrosion in the calcite-supersaturated brine was caused by scale deposition, rather than test temperature. Ankerite, which was formed in the complex analog brine, was not detected in this simple NaCl solution.

The different results suggest that scale can cause corrosion and also alter the corrosion product film formation. The accelerated corrosion with calcite is probably due to formation of an incomplete calcite film on the steel, thereby focusing corrosion on the unprotected anodic regions.

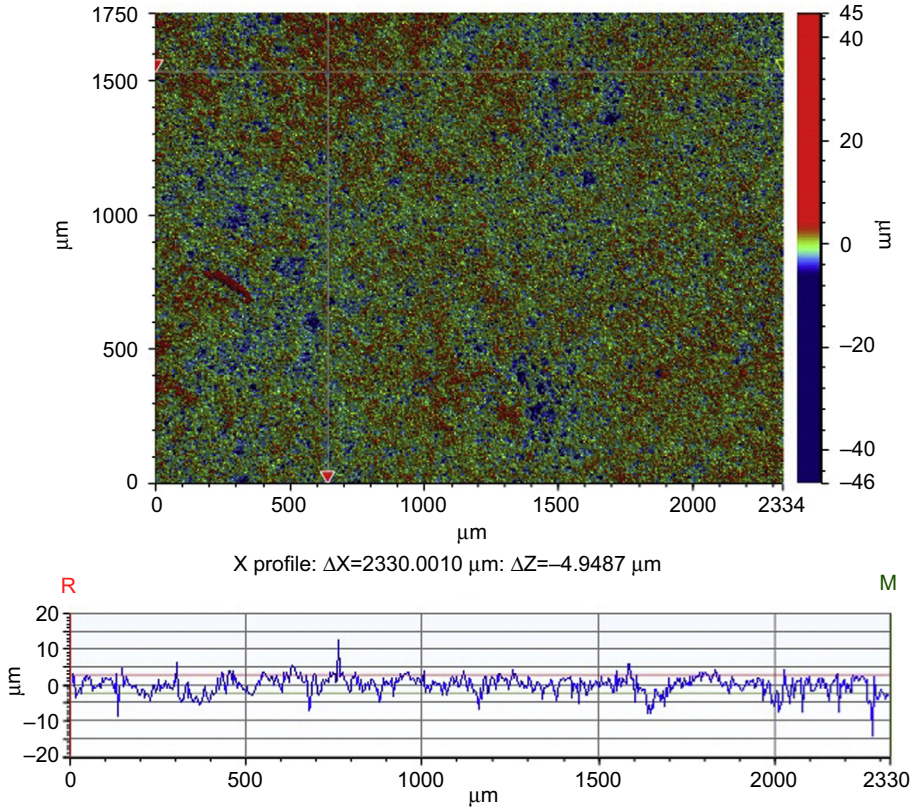

Figure 18.4 Vertical scanning interferometry image of coupon surface showing no localized corrosion in brine equilibrium to calcite and Y profile showing no pits.

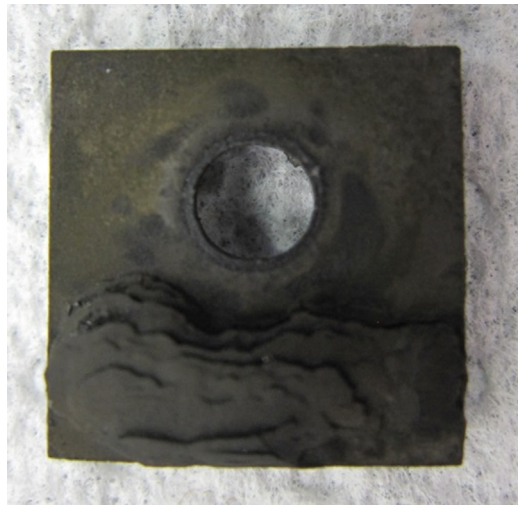

Figure 18.5 Picture of heavily corroded coupon after 7 days at 250°C (482°F) in solution supersaturated to calcite.

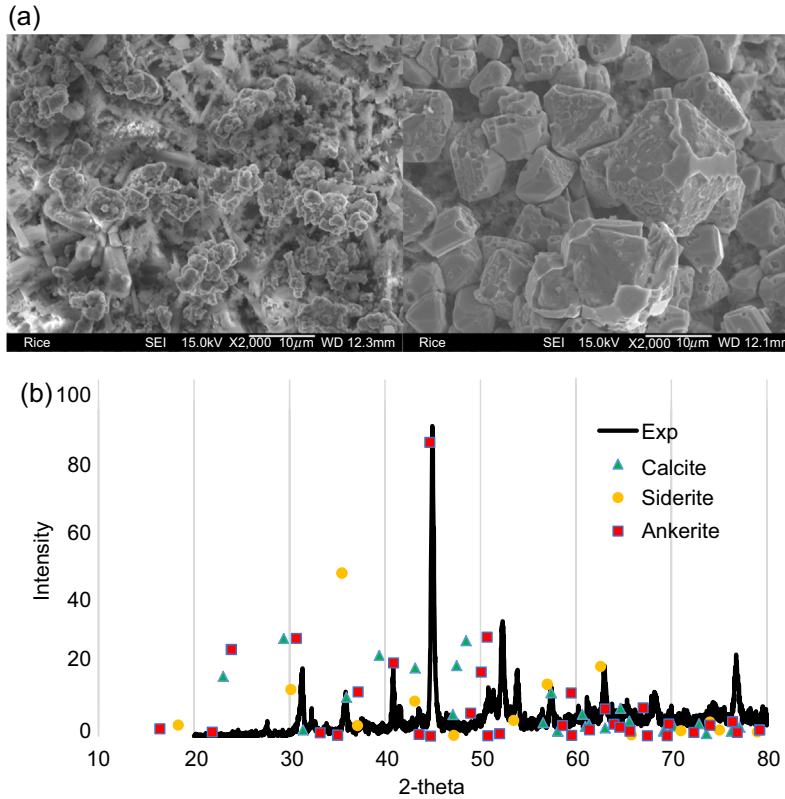

Figure 18.6 (a) Scanning electron microscopy morphology of scale and (b) X-ray diffraction composition of scale and corrosion product formed at 250°C (482°F) in solution supersaturated to calcite.

Table 18.2 Summary of corrosion testing results in brines with different calcite scaling tendencies

	Brine equilibrium to calcite (SI = 0)	Brine supersaturated to calcite (SI > 1)	2 M NaCl solution (SI < 0)
Corrosion rate (mm/y)	0.14	Severe	0.10
Localized corrosion	No	Yes	No

SI, saturation index.

These results demonstrate the importance to study corrosion and scale together. Also, the accurate representation of the field conditions using complex analog brine composition, strictly anoxic conditions has resulted in unexpected results. There are clear differences in corrosion severity in brines with different scaling tendencies. To our knowledge, this is the only such realistic systematic data at high temperature conditions in the literature. There is a need for more experimental works at realistic field conditions that accurately represent the production systems.

18.3 Solubility of iron-containing scales

Iron-containing minerals, such as such as siderite, iron sulfides, and iron oxides, are often observed on metal surface in the form of either thin layer or thick-scale deposits. A dense and uniform layer can act as a physical barrier to protect the underlying steel parts, but heavy scale negatively affects operation efficiency and system productivity [8]. For example, siderite scale deposition was considered as one of major mechanisms for the oil production decline in the Prudhoe Bay field [9]. Iron sulfide and iron oxide scales on production tubing and liner have interfered with downhole surveillance, limited well intervention, and reduced productivity in some high temperature sour gas wells [10,11].

The source of the iron for these iron-containing minerals could be generated from corrosion reaction or supplied by the produced water. Iron is commonly found in a variety of rock and soil minerals as in ferrous (Fe^{2+}) and ferric (Fe^{3+}) states. The dissolution of naturally formed minerals may contribute to the high iron concentration in the reservoir formation water. If the rate of produced water is 1000 bbl/day and the total Fe concentration is 50 mg/L in produced water, then approximately 33 Kg of siderite or 30 Kg of iron hydroxide ($Fe(OH)_3$) could potentially form each day. The total Fe concentration at downhole conditions under a strictly anoxic environment could be larger than the value measured at the surface.

Compared to the common sulfate and carbonate scales, much less is known about the thermodynamics and kinetics of these iron-containing scales. In this section, we present the new solubility studies on siderite, iron sulfide, and magnetite at HPHT conditions. Knowledge of mineral solubility behavior is necessary for the reliable prediction of corrosion risk and scale severity.

18.3.1 Siderite

Siderite is a common corrosion product in sweet systems at intermediate temperatures 60−150°C or (140−302°F), respectively, forming a passive layer to protect the metal surface and prevent further corrosion [12]. Accurate solubility constants for siderite will benefit not only the understanding of $FeCO_3$ scale formation, but also the transformation processes of passive layers for corrosion studies.

Although the solubility of siderite has been studied at different temperatures, ionic strength, electrolytes, and CO_2 partial pressures [13−19], most of the experimental

work has been conducted below 100°C (212°F) [13−19]. Limited research on the effect of high temperature, high pressure, and high ionic strength has been performed until recently. Recent works have extended the siderite solubility (K_{sp}) measurements to high temperature, up to 250°C (482°F) and high pressure, up to 1655 bar (24,000 psig). Test results showed that the predicted solubility values were in good agreement with the measured values at 150°C (302°F) and lower pressures $\leq$ 689 bar ($\leq$10,000 psig), with differences less than 0.1 in pK_{sp}. At high temperature of 150°C (302°F) and 250°C (482°F) and high pressure, $\geq$1379 bar ($\geq$20,000 psig) the predicted pK_{sp} values varied from 0.22 to 0.41 from these measured values. Experimental details and results can be found in Yan et al. [20].

Work to expand knowledge of siderite species solubility and phase transitions at HPHT and realistic field compositions is needed. Preliminary work shows fundamental differences between the predicted and the observed solubility and phases.

18.3.2 Iron sulfide

Formation of iron sulfide (FeS) precipitates in gas and oil production systems can reduce flow, plug safety valves, and downhole equipment, reduce or accelerate corrosion, and reduce oil quality. Once FeS scale is formed in wellbore or on production tubing, it can become impractical to remove chemically and could cost large amounts of money and long production downtime to clean the system mechanically [10,21]. Accurate prediction of FeS formation at reservoir conditions has great benefit for scale control and flow assurance. Also, iron sulfide formation can be either beneficial or detrimental to corrosion control, related to the integrity of the attached layer. Although of high importance, there is little understanding on its formation and transformation and the influence of operation parameters, e.g., temperature, pressure, oil−gas−brine composition, chemical additives, etc., on its thickness and physical and chemical properties.

Much of the knowledge on FeS chemistry was gained by studies in aqueous systems related to marine sediments at low temperatures [22,23]. The phase stability, precipitation kinetics, reaction pathway, or inhibition of iron sulfides largely remain unknown at oilfield conditions. This is mainly due to the complex FeS chemistry and difficulties in experimental works. Solubility of amorphous FeS_m or mackinawite, was investigated at ambient condition from 3 to 10 pH and with various concentrations of H_2S gas in both synthetic and natural waters [24,25]. In these cases, the solubility product of iron sulfide was presented in terms of iron and bisulfide ions, HS^-, because the concentration of the S^{2-} ion is insignificant in solution and the uncertainty of the secondary equilibrium constant of H_2S (K_2) is considerable. At 25°C (77°F) and 1 atm (1 bar) the K_2 value has been reported to be 10^{-12}−10^{-19} and no one has been able to establish a true value [26,27]. The activity of iron changes linearly with respect to pH at various H_2S gas concentrations.

In a recent work in one of the author's lab, FeS solubility was measured up to 250°C (482 °F) at 1654 bar (24,000 psig) in 1 M NaCl brine using troilite. Experimental results are shown in Table 18.3 and experimental details can be found in Yan et al. [28].

Table 18.3 Predicted and experimental FeS solubility values in 1 M experiments

Temperature °C (°F)	Pressure (psi)	pK_{sp} from prediction model	pK_{sp} from experimental results
100 (212)	5,000	3.56	1.82
100 (212)	15,000	3.28	1.58
100 (212)	24,000	3.06	1.32
175 (347)	5,000	4.34	3.08
175 (347)	15,000	4.08	2.43
175 (347)	24,000	3.83	2.31
250 (482)	5,000	5.45	4.93
250 (482)	15,000	5.16	4.29
250 (482)	24,000	4.96	3.87

These results also suggest that more experimental work is needed to constrain the solubility values.

Observations suggested that pyrrhotite was more stable than troilite at the test conditions. This was in agreement to the previous observations in corrosion studies. Troilite has been viewed as low temperature and stoichiometric pyrrhotite [29,30].

18.3.3 Magnetite

Magnetite appears to be the main deposit on oil and gas production systems under high temperature conditions >150°C (302°F) and anoxic conditions, especially on carbon steels [31,32]. Even though various models have been developed to predict Fe_3O_4 solubility, predictions made from these models are only applicable below 100°C (212°F) at low pressure and in low TDS brine [33]. Limited research on the effect of high pressure and salinity on solubility of magnetite has been conducted.

Measuring the magnetite solubility has proven to be more difficult than that of other oxides, such as NiO, due to the reductive dissolution of magnetite from Fe(III) to Fe(II) [32]. Thus the reduction potential of the entire system plays an important role in magnetite solubility. In more complicated synthetic brines with high ionic strength, the reduction−oxidation (redox) potential, which controls the dissolved iron concentration in the produced saltwater may cause large differences in the observed solubility.

Magnetite solubility experiments were conducted to determine the K_{sp} value at different temperatures and pressures. The results vary from the ones reported in the literature. For example, at room temperature and 345 bar (5000 psig) the total dissolved iron concentration is 0.068 mg/L, which is about six times lower than the literature reported total Fe concentration (0.44 mg/L). The effects of various reaction parameters on magnetite solubility were also studied and detailed results can be found

in Yan et al. [34]. A change in pH or E_h has a much greater effect on magnetite solubility than pressure and temperature in this preliminary investigation.

18.4 Scale inhibition at high temperatures

The common approach to prevent scale formation is to apply threshold scale inhibitors by squeeze treatment or continuous injection. Scale formation can be effectively controlled with only a few milligrams per liter of scale inhibitors, which is significantly lower than the concentration needed to sequester or chelate the divalent metal ions. Prevention of scale deposition is important not only for well productivity, but also for corrosion control. A thin-scale layer might not affect the pipe carrying capacity, but can accelerate corrosion reaction, as discussed early in this chapter.

The performance of scale inhibitor can be influenced by many factors, such as temperature, water composition, pH, saturation state, suspended solids, dissolved oxygen level, other treatment chemicals, etc. Among these, temperature is the most determining factor. Thermal stability of inhibitor product at high temperatures is a significant concern. Products may experience phase separation, solid formation, and the decomposition of active inhibition ingredient. Therefore, study of thermal stability of these inhibitors under simulated lab conditions is vital to determine how much of these inhibitors will degrade, and what inhibitor dosage should be used to protect the well.

A trace amount of dissolved oxygen, even as low as 10 parts per billion (ppb), will significantly affect experimental results. Because the equivalent weight of one electron of oxygen is only 8 g/equiv and that of iron (II → III) is 55.85 g/equiv, 10 ppb of dissolved oxygen will oxidize about 70 ppb of Fe(II), which will produce about 134 ppb of $Fe(OH)_{3,colloid}$: these oxidized colloids in the brine are known to be very surface active, to adsorb inhibitors, and to impact nucleation and crystal growth. Dissolved oxygen can also have a large effect on siderite nucleation and surface properties, which may lead to different solubility results and corrosion protective layer formation as discussed earlier in this chapter. Dissolved oxygen could also cause the degradation of inhibitor chemicals and even react directly with polymeric inhibitors under high temperature and pressure.

The scale inhibitor performance at high temperatures was studied recently by Tomson [7] and Yan et al. [35]. Various scale inhibitors, such as polyvinyl sulfonate (PVS), maleic acid copolymer (MAC), sulfonated polycarboxylic acid (SPCA), polyacrylic acid (PAA), carboxymethyl inulin (CMI), and phosphinopolycarboxylic acid and bis-hexamethylene triamine-penta(methylene phosphonic) acid (BHPMP), were evaluated at 180°C (356°F) and 250°C (482°F) for inhibition of several scaling minerals including barite, calcite, celestite, hemihydrate, and anhydrite. At 180°C PVS and MAC showed better performance than the other inhibitors for barite inhibition. BHPMP appeared to lose its inhibition ability after 70 min of temperature exposure for all scales. PAA showed poor performance for all tested scales under these conditions. At 250°C (482°F) MAC had slightly better performance than the other inhibitors

for barite inhibition. PVS had slightly better performance than other inhibitors for celestite inhibition. All of the tested inhibitors had similar performance for calcium bearing scales.

Inhibition of iron-containing scales remains a challenge. Existing scale inhibitors, developed for $BaSO_4$ and $CaCO_3$ scales, have been proven not effective in prevention of iron carbonate and iron sulfide formation. A possible explanation is due to the formation of Fe-inhibitor pseudoscale, whose solubility is much lower than the Ca−inhibitor complex. Also, the scale inhibitors might adsorb onto the steel and colloid particles and thereby not be available in solution for inhibition. Yean et al. [36] showed that sodium citrate could inhibit siderite nucleation in the simple brine solution, but the citrate inhibition efficiency is very temperature sensitive and may not be effective at 65°C (149°F) and above.

Recently, we studied the nucleation kinetics of siderite and its inhibition 100°C (212°F) and 250°C (482°F) using the dynamic tube blocking apparatus. The scale inhibitors studied were SPCA, PVS, CMI, MAC, and sodium citrate. Test results showed that at 100°C (212°F) the SPCA and PVS inhibitors not very effective, whereas the green inhibitor CMI at 10 mg/L showed better inhibition against siderite nucleation than the others. At 250°C (482°F), 1−10 mg/L SPCA will keep 80% of total injected Fe in solution for at least 2 h. 10 mg/L PVS and MAC will not prevent decrease of Fe concentration in solution. When the SPCA concentration was increased to 50 and 316 mg/L, dramatic decreases of Fe concentration occurred, indicating the formation of Fe-SPCA pseudoscale. Overdoses of scale inhibitor in iron rich wells may cause formation damage, not only due to the pseudoscale formation, but also due to the formation of barite or calcite as a result of the decrease of effective inhibitor concentration.

In general, scale inhibition remains a challenge for complex brines and in HPHT environments. There is an urgent need for inhibitors that can prevent the precipitation of iron-containing solids, such as siderite, magnetite, pyrite, and other iron sulfides. Thermal degradation, formation of cation inhibitor precipitates, and cation-assisted adsorption hinder the performance of common scale inhibitors.

18.5 Pitting corrosion potential at high temperatures

Localized corrosion in the form of pits and crevices in corrosion resistant alloys (CRAs) is one of the biggest challenges for material selection for applications in the oil and gas industry. Unlike general corrosion, which is a slow process, pitting corrosion may start and propagate very quickly leading to significant damage [37]. Monitoring for pitting corrosion requires frequent inspections over time since no corrosion may occur for a long time followed by aggressive pitting.

Pitting resistance equivalent number (PREN) has been used to describe the susceptibility of steel types to pitting or crevice corrosion [38−40]. PREN can be calculated from the alloy composition. For example, for nickel-based alloys:

$$\mathrm{PREN_{Ni}} = \%\mathrm{Cr} + 1.5(\%\mathrm{Mo} + \%\mathrm{W} + \%\mathrm{Nb})$$

PREN can be a good tool to estimate the pitting resistance of certain alloys. PREN values greater than 32−40 are often specified. From this first estimation, SS 2507 (UNS S32750) should have the best pitting resistance among the five alloys, whereas SS 316L should have the worst (Fig. 18.7). At extreme temperature, pressure, and TDS conditions often encountered in deep reservoirs, the use of PREN as the criteria for evaluation of the localized corrosion resistance of alloys may not be reliable, as will be shown below.

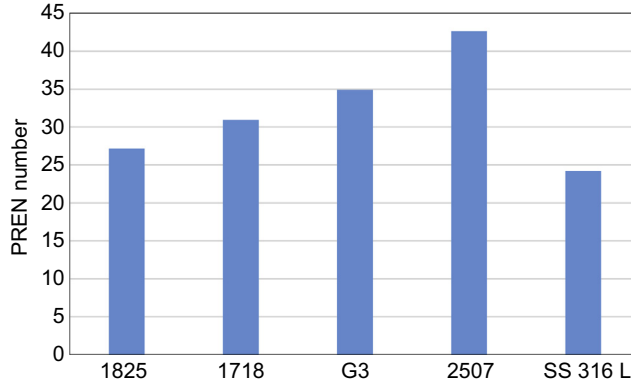

Figure 18.7 Comparison of PREN for different alloys.

Electrochemical techniques such as polarization have been used in the laboratory to evaluate the localized corrosion susceptibility of CRAs at relatively low temperature <100°C (212°F) and salinity levels (<500 mg/L) [41−49]. Very little work has been done at temperatures over 200°C (392°F). Recent work shows reliable test equipment and procedures using electrochemical measurements to experimentally study the corrosion of alloys at extreme temperature and salinity conditions [50]. With the cyclic polarization technique, features such as the critical potential related to localized corrosion of CRAs, at conditions close to actual production in deepwater reservoirs can be determined, and the pitting susceptibility of different alloys can be evaluated directly.

The methodology and procedures for using an electrochemical technique, specifically cyclic polarization, to evaluate pitting tendency of CRAs at extreme temperature and salinity conditions was modified from the NACE/ASTM standard G61 [51]. With this new method, cyclic polarization measurements can be conducted successfully at extreme temperatures up to 250°C (482°F) and extreme TDS up to 180,000 mg/L conditions with five different alloys, including stainless steel and Inconel alloy. From the cyclic polarization, characteristic potentials such as corrosion potential, i.e., open circuit potential (OCP), pitting potential, and repassivation potential (sometimes called protection potential [44]) of each alloy were identified at different temperature and salinity conditions. The repassivation potential can be defined in different ways. It can be defined as the potential at which the anodic forward and reverse scan intersects. It can also be defined as the potential at which the current density reaches its lowest readable value on the reverse portion of the

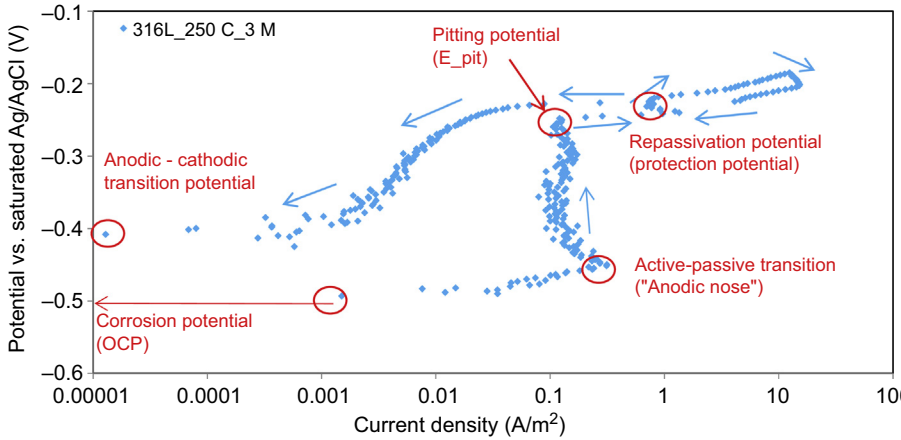

Figure 18.8 Cyclic polarization scan for SS 316L after it was immersed in a 3 M NaCl solution with 0.05 M, dissolved CO_2 at 250°C (482°F) for 20 h.

polarization scans [52]. In this study, the former definition was chosen for all the cyclic scan analyses.

As outlined in NACE/ASTM standard G6 [51], in cyclic polarization scanning, the potential is scanned from OCP and the current is monitored until a sustained/sharp increase; above that of the passive current is obtained. The scan then returns from a set value back to OCP. Reliable determination of the characteristic potentials such as pitting potential, repassivation potential for each scan has big challenges but can potentially provide insights for the pitting evaluation of the CRAs at conditions close to deepwater production.

Fig. 18.8 shows the cyclic polarization curve for SS 316L (UNS S31603) after immersion for 20 h in a 3 M NaCl solution with 0.05 M dissolved CO_2 at 250°C (482°F). Several features can be obtained from the polarization scan. It can be seen that 316L (UNS S31603) had an OCP of −0.495 V at this 250°C (482°F) condition. During the cyclic polarization process, it went through active corrosion first, where the corrosion current density increased with increasing potential, until it reached a point, labeled "active−passive transition". From this point onward, the steel became passive, as indicated by no change in corrosion current with increasing potential. The polarization was continued until the potential reached −0.257 V, after which the corrosion current increased abruptly again, indicating the breakdown or dissolution of the passivation. The forward polarization continued until the 10 mA/cm^2 limit was reached, where the polarization started going backward toward OCP. During the backward scan at the end, the potential where the forward and backward polarization curves meet is called repassivation potential. The value of the repassivation potential and its value toward the OCP also comprises the characteristic features used to evaluate the localized corrosion resistance of the material [39]. The repassivation potential does not necessarily appear in every polarization curve, it depends on the material properties and experimental conditions. At the end of the polarization, it can also be

observed that the final potential did not return to the original OCP, but stabilized at a potential more positive than the original OCP. This indicates that the steel went through an anodic−cathodic transition process. The whole cyclic polarization curve shows positive hysteresis, which indicates the good pitting resistance of 316L (UNS S31603) at these test conditions.

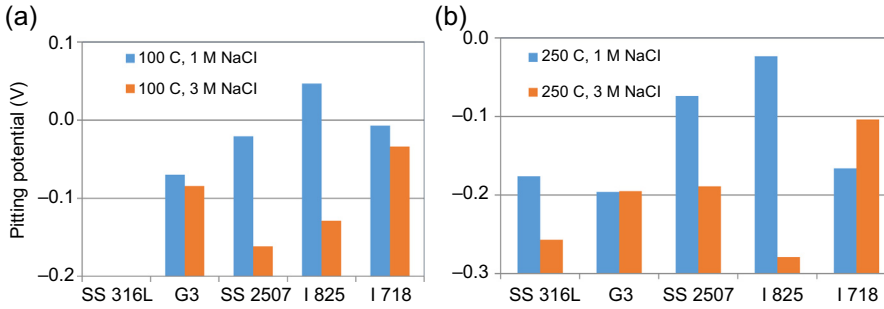

Figure 18.9 Comparison of pitting potential of different alloys at (a) 100°C (212°F) and (b) 250°C (482°F) at different salt concentrations.

Experiments were conducted with all five selected alloys at different test conditions, following the same procedure as described above. Not all of the alloys showed all of the features in their cyclic polarization curves. Fig. 18.9(a) and (b) is the pitting potential of the five alloys obtained at 100°C (212 °F) and 250°C (482°F) with two different salt concentrations. It can be seen that in a higher salt concentration, the pitting potential was more negative than in the lower salt concentration solution for most alloys. For SS 316L (UNS S31603), no passivation region was observed on the cyclic polarization curve at both salt concentrations studied. The polarization showed active corrosion during the entire forward scan.

From cyclic polarization, the tendency of pitting corrosion of each alloy can be evaluated. Cyclic polarization measurement is able to tell if pitting is possible, however, it cannot tell when and where it will occur. Corrosion tests at different exposure times are needed to estimate the appearance of pitting and also steel surface analysis, such as VSI is required to verify the pitting rate and locations. A 3-week exposure experiment was performed with I-825 (UNS N08825) at conditions used for cyclic polarization. Fig. 18.10 shows the image of the test coupon scanned by a white light interferometry after the 3-week experiment. The use of white light interferometry was found to be very powerful for both localized and uniform corrosion analysis of CRAs [53]. The uniform corrosion rate of the coupons from this experiment was 0.004 ± 0.001 mm/year, calculated from both the weight loss method and white light interferometry analysis. The uniform corrosion rate is equivalent to a 0.20 ± 0.01 μm thickness of the metal loss. As shown in Fig. 18.10, pits were found on the steel surface as large as 37 μm deep. It is clearly shown that uniform corrosion is not an issue for CRA I-825 (UNS N08825), but localized pitting corrosion is very significant at the test conditions discussed here, and may require batch-to-batch testing of CRAs.

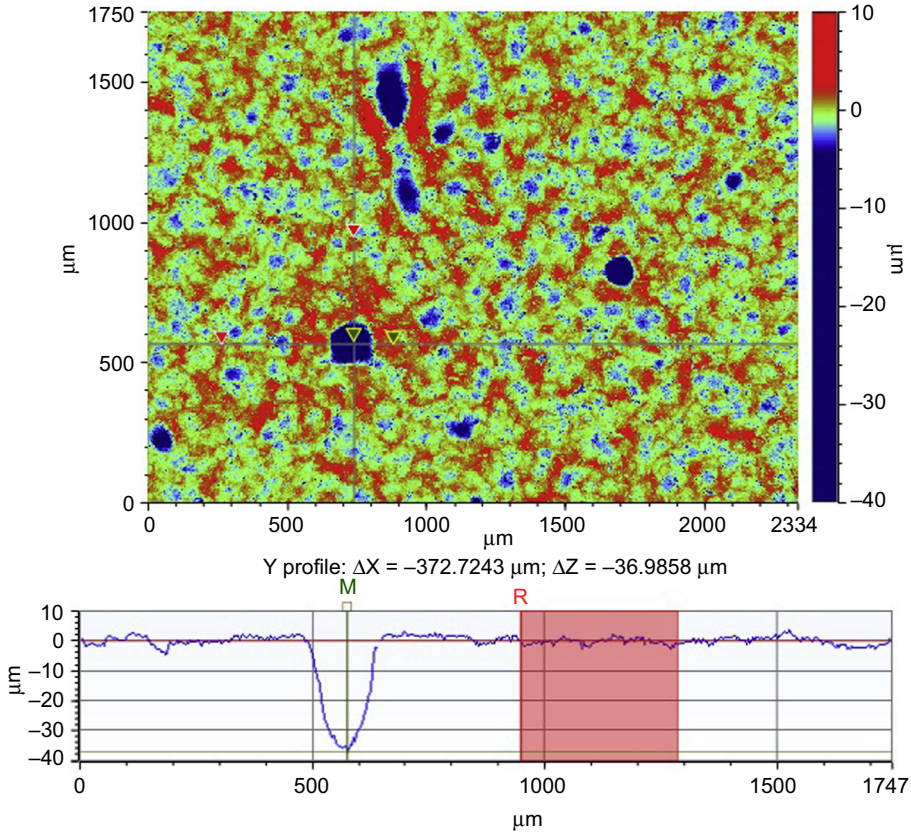

Figure 18.10 Two dimensional and Y-profile graphs of I-825 surface showing localized pitting corrosion after a 3-week exposure to a 3 M NaCl solution saturated with 0.05 M dissolved CO_2 at 250°C (482°F).

As mentioned before, the difference between pitting potential and OCP is important to characterize an alloy in terms of localized corrosion. The difference between pitting potential and the OCP is denoted in this work as "pitting driving force", ΔE_{pit}. The larger the ΔE_{pit}, the harder (or more force required) to break down or dissolve the passive film that forms on the steel surface; therefore, the better the material's resistance is to pitting. Fig. 18.11(a) and (b) shows the values of ΔE_{pit} for all alloys at 100 and 250°C (212 and 482°F). All of the alloys showed larger ΔE_{pit} at lower salt concentration at 250°C (482°F). For G3 (UNS N06985) and I-825 (UNS N08825), at 3 M NaCl condition, the ΔE_{pit} was not affected by temperature. The passivation driving force at a lower salt concentration was about 100 mV lower than that at 250°C (482°F). The results indicate that the passivation of G3 (UNS N06985) and I-825 (UNS N08825) at 250°C (482°F) is more stable, since it required more potential to break down or dissolve the passive films.

It may be proposed that an alloy will have good localized corrosion resistance if its repassivation potential is more anodic (noble) than its corrosion potential, i.e., OCP

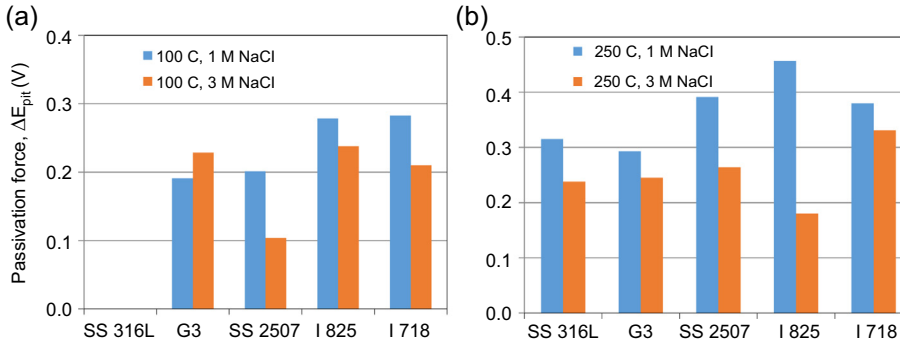

Figure 18.11 Comparison of "passivation force" (potential difference between pitting and OCP), ΔE_{pit}, of different alloys at (a) 100°C (212°F) and (b) 250°C (482°F) at different salt concentrations.

[52]. Also, although the repassivation potential values themselves are important, their relative values to the corrosion potential (OCP) are even more important. The difference of the repassivation potential and the OCP is denoted as ΔE_{rep}. A larger ΔE_{rep} means it is easier to repassivate during the reverse polarization; therefore, the material can better resist pitting.

During the polarization measurements, it was found that in some cases a secondary passivation was observed. For example, it is very likely that in the case of I-825 (UNS N08825), a nickel-based alloy with 22% chromium, at less noble (positive) potential ranges during the forward polarization, Cr(III)-oxide will be formed first. In the presence of strongly oxidizing conditions, this Cr(III)-oxide passive film transitions into the Cr(VI) oxidation region, where the soluble species Cr(VI) species are thermodynamically favored [54]. For cyclic polarization, there are various criteria to take into account when determining what the best alloy would be at the conditions studied. A summary of pitting resistance ranking, depending on the category used for the alloys evaluated in this work, is shown in Table 18.4.

Table 18.4 Summary of best alloy for pitting resistance at various conditions based on different evaluation criteria

Criteria	250°C 1 M NaCl	250°C 3 M NaCl	100°C 1 M NaCl	100°C 3 M NaCl
Passivation driving force	I 825	I 718	I 718	I 825
Repassivation potential vs. pitting potential	G3	SS 2507	I 718	SS 2507
Hysteresis	G3 & I 718	SS 2507 & SS316L	G3 & SS2507 & I 825	G3 & SS 2507
PREN	SS 2507			

PREN, pitting resistance equivalent number.

It can be seen that each criterion needs to be considered for overall evaluation of material using cyclic polarization. PREN number does not consider the experimental conditions in the calculation; therefore, the results are the same for all cases. More experimental work is needed to evaluate the materials and create a model to incorporate all the evaluation criteria.

18.6 Current knowledge gaps and future research trends

As mentioned throughout this chapter, a lot is still unknown in the area of corrosion and scale, especially at extreme temperature and pressure conditions. Corrosion and scale are two processes that happen simultaneously in production tubing, however, the effects of mineral scaling and deposition on corrosion and vice versa are not well understood, especially at HPHT conditions. As shown throughout this chapter, more experimental work needs to be performed at reservoir conditions with complex brine compositions, high temperature, high pressure, and strictly anoxic conditions. Both corrosion and scale research should be performed under these realistic conditions and study the effects of one on the other.

The knowledge gap in scale formation and corrosion protective scales is especially large for iron species, siderite, iron sulfide, and magnetite to mention a few. Work to expand knowledge of iron species solubility and phase transitions at HPHT and realistic field compositions is needed to better understand scale and corrosion processes and develop an effective prediction and prevention strategy. One specific area of uncertainty is the solubility values for these iron species at different conditions, more research is needed to obtain a general agreement on the solubility constant for iron species at temperature, pressure and anoxic conditions.

Additional data and methods are needed to classify materials performance in the working environment. More data is needed to validate the new proposed cyclic polarization method to determine the pitting tendency of steel materials and obtain more information about the performance of CRAs in the working environment. An alternative to the PREN number has been proposed and more research is needed to build a knowledge database.

18.7 Conclusions

Scale formation and water composition can have a significant impact on the corrosion rate and treatment program. It is important to incorporate the water chemistry and scaling tendencies into corrosion prediction and well design strategies. Experiments performed need to closely resemble the field conditions of water composition, strictly anoxic ($<<1$ ppb O_2) environment, temperature, and pressure, for results to be reliable, to simulate the corrosion and scaling reactions at the water−metal interface.

Solubility of scale species is a key parameter for scale risk assessment and also should be incorporated in corrosion prediction. There is very limited knowledge

on the solubility behaviors of iron-containing scales at elevated temperatures and pressures, partially due to oxygen contamination and difficulties to control redox potential. Industry should focus on more effort to determine the solubility of iron-containing scales at HPHT range. Meanwhile, current scale inhibitors are not effective to control iron-containing scales, especially in complex brine at high temperature. New inhibition chemistry and innovative mitigation strategies should be explored.

Material selection for HPHT application should be based on tests that mimic the field conditions, instead of PREN number. Cyclic polarization can be a powerful tool to evaluate the pitting resistance performance of alloys under extreme conditions of salinity and temperature. Several areas of knowledge gaps and current future research trends have been identified.

References

[1] R. Nyborg, Overview of CO_2 corrosion models for wells and pipelines, in: CORROSION 2002, Nace International, 2002.
[2] G31−72, A., Standard Practice for Laboratory Immersion Corrosion Testing of Metals, ASTM International, West Conshohocken PA, 2004.
[3] Y.K. Kharaka, et al., SOLMINEQ. 88: A Computer Program for Geochemical Modeling of Water-Rock Interactions, in: US geological Survey Water-Resources Investigation Report, vol. 88, 1988, p. 4227.
[4] K.S. Pitzer, Thermodynamics of electrolytes. I. Theoretical basis and general equations, The Journal of Physical Chemistry 77 (2) (1973) 268−277.
[5] K.S. Pitzer, J.C. Peiper, R.H. Busey, Thermodynamic properties of aqueous sodium chloride solutions, Journal of Physical and Chemical Reference Data 13 (1) (1984) 1−102.
[6] J. Kolts, P. Singh, M.W. Joosten, An engineering approach to corrosion/erosion prediction, in: CORROSION 2006, NACE International, 2006.
[7] R.C. Tomson, C. Yan, P. Guraieb, RPSEA Phase 2 Final Technical Report, 2015.
[8] A. Kan, M. Tomson, Scale prediction for oil and gas production, SPE Journal 17 (02) (2012) 362−378.
[9] B. Kriel, C. Lacey, R. Lane, The performance of scale inhibitors in the inhibition of iron carbonate scale, in: SPE Formation Damage Control Symposium, Society of Petroleum Engineers, 1994.
[10] J. Leal, et al., A Systematic Approach to Remove Iron Sulphide Scale: A Case History, SPE paper 105607, 2007, pp. 11−14.
[11] Q. Wang, et al., Iron sulfide scale dissolvers: how effective are they? in: SPE Saudi Arabia Section Technical Symposium and Exhibition, Society of Petroleum Engineers, 2013.
[12] W. Sun, S. Nesic, S. Papavinasam, Kinetics of iron sulfide and mixed iron sulfide/carbonate scale precipitation in CO_2/H_2S corrosion, in: CORROSION 2006, 2006 paper (6644).
[13] P.C. Singer, W. Stumm, The solubility of ferrous iron in carbonate-bearing waters, Journal (American Water Works Association) (1970) 198−202.
[14] R.D. Braun, Solubility of iron (II) carbonate at temperatures between 30 and 80, Talanta 38 (2) (1991) 205−211.

[15] J. Bruno, P. Wersin, W. Stumm, On the influence of carbonate in mineral dissolution: II. The solubility of $FeCO_3$(s) at 25 C and 1 atm total pressure, Geochimica et Cosmochimica Acta 56 (3) (1992) 1149−1155.
[16] J. Greenberg, M. Tomson, Precipitation and dissolution kinetics and equilibria of aqueous ferrous carbonate vs temperature, Applied Geochemistry 7 (2) (1992) 185−190.
[17] D.L. Jensen, et al., The solubility of rhodochrosite ($MnCO_3$) and siderite ($FeCO_3$) in anaerobic aquatic environments, Applied Geochemistry 17 (4) (2002) 503−511.
[18] P. Bénézeth, J. Dandurand, J. Harrichoury, Solubility product of siderite ($FeCO_3$) as a function of temperature (25−250 C), Chemical Geology 265 (1) (2009) 3−12.
[19] S. Golubev, et al., Siderite dissolution kinetics in acidic aqueous solutions from 25 to 100 C and 0 to 50 atm pCO_2, Chemical Geology 265 (1) (2009) 13−19.
[20] C. Yan, et al., Study of siderite solubility under extreme high temperature and pressure in 1 M NaCl solution, in: CORROSION 2015, NACE International, 2015.
[21] J.A.L. Jauregui, et al., Novel mechanical scale clean-out approach to remove iron sulphide scale from tubulars in vertical high pressure and temperature deep gas producers: A case history, in: EUROPEC/EAGE Conference and Exhibition, Society of Petroleum Engineers, 2009.
[22] L.G. Benning, R.T. Wilkin, H. Barnes, Reaction pathways in the Fe−S system below 100 C, Chemical Geology 167 (1) (2000) 25−51.
[23] D. Rickard, G.W. Luther, Chemistry of iron sulfides, Chemical Reviews 107 (2) (2007) 514−562.
[24] J.F. Pankow, J.J. Morgan, Dissolution of tetragonal ferrous sulfide (mackinawite) in anoxic aqueous systems. 2. Implications for the cycling of iron, sulfur, and trace metals, Environmental Science and Technology 14 (2) (1980) 183−186.
[25] W. Davison, The solubility of iron sulphides in synthetic and natural waters at ambient temperature, Aquatic Sciences 53 (4) (1991) 309−329.
[26] Q. Wang, et al., Iron sulfide and removal in scale formation sour gas wells, in: SPE International Oilfield Scale Conference and Exhibition, Society of Petroleum Engineers, 2016.
[27] R.J. Myers, The new low value for the second dissociation constant for H_2S: its history, its best value, and its impact on the teaching of sulfide equilibria, Journal of Chemical Education 63 (8) (1986) 687.
[28] C. Yan, P. Guraieb, R.C. Tomson, Solubility study of iron sulfide FeS under extremely high temperature pressure in strictly anoxic, various ionic strength solutions, in: SPE International Oilfield Scale Conference and Exhibition, Society of Petroleum Engineers, 2016.
[29] A. Wikjord, et al., Corrosion and deposition during the exposure of carbon steel to hydrogen sulphide-water solutions, Corrosion Science 20 (5) (1980) 651−671.
[30] A. Cervantes-Tobón, et al., Effect of corrosion products formed and flow rate over the surface of steels API 5L X-52 and X-70 on the rate of corrosion in brine added with kerosene and H_2S, International Journal of Electrochemical Science 9 (2014) 2254−2265.
[31] P.R. Tremaine, J.C. LeBlanc, The solubility of magnetite and the hydrolysis and oxidation of Fe^{2+} in water to 300 C, Journal of Solution Chemistry 9 (6) (1980) 415−442.
[32] S. Ziemniak, M. Jones, K. Combs, Magnetite solubility and phase stability in alkaline media at elevated temperatures, Journal of Solution Chemistry 24 (9) (1995) 837−877.
[33] F. Sweeton, C. Baes, The solubility of magnetite and hydrolysis of ferrous ion in aqueous solutions at elevated temperatures, The Journal of Chemical Thermodynamics 2 (4) (1970) 479−500.

[34] C. Yan, et al., Solubility study of magnetite under extreme high pressure and high temperature, in: Offshore Technology Conference, Offshore Technology Conference, 2014.
[35] C. Yan, et al., Systematic study of barite nucleation and inhibition with various polymeric scale inhibitors by novel laser apparatus, SPE Journal (2014).
[36] S. Yean, et al., Ferrous carbonate nucleation and inhibition, in: SPE International Oilfield Scale Conference, Society of Petroleum Engineers, 2008.
[37] R. Heidersbach, Metallurgy and Corrosion Control in Oil and Gas Production, vol. 14, John Wiley & Sons, 2010.
[38] Designation, A., Standard Test Methods for Pitting and Crevice Corrosion Resistance of Stainless Steels and Related Alloys by Use of Ferric Chloride Solution, ASTM International, 2009.
[39] M. Rao, Pitting corrosion of sheets of a nickel-base superalloy, Materials and Corrosion 60 (1) (2009) 49−52.
[40] R.W. Revie, H.H. Uhlig, Uhlig's Corrosion Handbook, vol. 51, John Wiley & Sons, 2011.
[41] G. Hinds, et al., Novel method for determination of pitting susceptibility in aggressive environments at elevated temperature and pressure, Corrosion Science 85 (2014) 33−41.
[42] A. Anderko, N. Sridhar, D. Dunn, A general model for the repassivation potential as a function of multiple aqueous solution species, Corrosion Science 46 (7) (2004) 1583−1612.
[43] D. Han, et al., Influence of the microstructure and alloying element on the polarization behaviour within the crevice of UNS S32304 duplex stainless steel, Corrosion Science 53 (11) (2011) 3796−3804.
[44] L. Machuca, S. Bailey, R. Gubner, Systematic study of the corrosion properties of selected high-resistance alloys in natural seawater, Corrosion Science 64 (2012) 8−16.
[45] A. Malik, et al., The effect of dominant alloy additions on the corrosion behavior of some conventional and high alloy stainless steels in seawater, Corrosion Science 37 (10) (1995) 1521−1535.
[46] M. Montemor, et al., Chemical composition and electronic structure of the oxide films formed on 316L stainless steel and nickel based alloys in high temperature aqueous environments, Corrosion Science 42 (9) (2000) 1635−1650.
[47] G. Mori, D. Bauernfeind, Pitting and crevice corrosion of superaustenitic stainless steels, Materials and Corrosion 55 (3) (2004) 164−173.
[48] A. Pardo, et al., Pitting corrosion behaviour of austenitic stainless steels with Cu and Sn additions, Corrosion Science 49 (2) (2007) 510−525.
[49] G. Song, Transpassivation of Fe−Cr−Ni stainless steels, Corrosion Science 47 (8) (2005) 1953−1987.
[50] H. Sontheimer, W. Kolle, V.L. Snoeyink, Siderite model of the formation of corrosion-resistant scales, Journal of the American Water Works Association 73 (11) (1981) 572−579.
[51] G61, A., Standard Test Method for Conducting Cyclic Potentiodynamic Polarization Measurements for Localized Corrosion Susceptibility of Iron-, Nickel-, or Cobalt-Based Alloys, 2009.
[52] D.C. Silverman, Tutorial on Cyclic Potentiodynamic Polarization Technique, NACE International, Houston, TX, United States, 1998.
[53] E.Q. Contreras, et al., Optical measurement of uniform and localized corrosion of C1018, SS 410, and Inconel 825 alloys using white light interferometry, Corrosion Science 87 (2014) 383−391.
[54] R.W. Revie, Corrosion and Corrosion Control, John Wiley & Sons, 2008.

PART IV

Advancements in testing and monitoring technologies

Corrosion inhibitors—advancements in testing

19

Sunder Ramachandran
Baker Hughes, Sugar Land, TX, United States

19.1 Introduction

Corrosion inhibitors are oil field chemicals used at small concentrations (usually less than 1000 ppm) that reduce the corrosiveness of the fluid and environment for the material. The corrosion inhibitors most commonly used in oil and gas production and transmission environments are imidazolines, amides, amines, phosphate esters, carboxylic acids and their derivatives, and sulfur-containing organic molecules. In this chapter, advances in testing as they relate to the use of corrosion inhibitors in oil and gas production systems and transmission lines will be presented.

The purpose of testing corrosion inhibitors is to identify the best performing corrosion inhibitor for a given application and ensure that the chemical is compatible with the system, especially the separation system where corrosion inhibitors can sometimes cause emulsions, making it difficult to separate oil and water [1]. Selection of a corrosion inhibitor requires assessment of the production and transmission systems, compatibility with system materials and fluids, use of simple screening tests and for important projects, and corrosion testing that mimics the most difficult system conditions [1]. Qualification of corrosion inhibitors for a given production and transmission system requires the determination of the worst case conditions for the material and inhibitor and the design of test conditions that best simulate these conditions [2,3]. Typical information needed to be collected for corrosion inhibitor selection is provided in Table 19.1.

Multiphase flow simulations are used to determine the corrosive gases, the temperature and pressure, the composition and ratios of brine and liquid hydrocarbon, and the flow regime of the system. Determination of the flow regime alerts one about how the pipe wall may be contacted by different phases. In stratified flow at low velocity for oil and water flow, the bottom of the pipe will be wetted by water and the top by hydrocarbon. As velocity increases, oil droplets form in the aqueous phase, whereas water droplets are present in the hydrocarbon phase. In the three-phase flow involving gas, when a system is in the slug flow regime it can experience intermittent periods of high wall shear stress. It is also useful to know when liquid droplets are elutriated in the gas phase. Results from such simulations help in designing appropriate corrosion test procedures [2,3]. Field conditions differ from laboratory conditions so it is important to assess the physical properties that need to be replicated. It is always important to

Trends in Oil and Gas Corrosion Research and Technologies. http://dx.doi.org/10.1016/B978-0-08-101105-8.00019-X

Table 19.1 Information needed to be collected for corrosion inhibitor selection

Information needed	Use of information
Piping and instrumentation diagram	This information helps us understand the system to identify flow regimes and phases present. This information is used to identify places where corrosion inhibitor is needed
Production rates of gas, oil, and produced water	This is used to locate regions of water wetting, high and low velocities, and identify different flow regimes in the system
Composition of gases	The composition of gases quantifies the amount of corrosive gases in the system, such as carbon dioxide, hydrogen sulfide, and oxygen
Composition of brine	The composition of brine helps find scaling regions in the system. It is important to analyze the brine for organic acids as high concentrations of organic acids can indicate that the system is more corrosive
Temperatures and pressures in the system	This helps us identify corrosive regions in the system where concentrations of carbonic acid and aqueous hydrogen sulfide are high and conditions where corrosion inhibitor selection requires attention
Composition of hydrocarbon phase	It is best to obtain a sample of field condensate where H_2S and sulfur are present as the condensate has a role in causing pitting corrosion
Metallurgy of tubing and piping	It is useful to have tubing and piping samples especially for sour corrosion as certain metallurgies are more amenable for pitting corrosion

test corrosion inhibitors for ancillary properties such as compatibility with production and transported fluids and compatibility with materials used in the production and transmission environments. This is especially true for deep water and arctic systems.

This chapter will confine itself to advances in the testing of corrosion inhibitors. The advances occur in testing products at high shear stresses, testing inhibitors with sand, corrosion inhibitor testing for mitigating pitting corrosion, corrosion inhibitor testing under conditions of under deposits, and testing of corrosion inhibitors for top-of-the-line conditions.

19.2 Corrosion inhibitor testing to prevent corrosion in multiphase flow with high shear

Ideally, corrosion inhibitors should be tested under the most realistic conditions. A review of corrosion laboratory testing with inhibitors indicated that the parameters that were the most challenging for successful corrosion inhibition in mild steel systems

experiencing corrosion by carbon dioxide are temperature, shear stress, total dissolved solids in brine, and predicted corrosion rate in the system [4]. Normal oil and gas production conditions occur in the absence of oxygen. Therefore, it is extremely important for inhibitor selection to test at appropriate conditions (e.g., ensuring no oxygen ingress in the test apparatus). High-shear flow apparatus may see evidence of oxygen contamination [5]. It is important during corrosion inhibitor testing that the fluids are kept at oxygen levels below 40 ppb [5].

Internal corrosion failures of a 10-inch production pipeline at Wytch farm in 1997 led to an analysis that carbon dioxide corrosion of mild steel is severe in slug flow conditions with high Froude number [7]. The system at Wytch farm did not have corrosion inhibitor [6]. In some studies, corrosion inhibition of pipelines in slug flow has been believed to be difficult at high Froude number owing to different hydrodynamic factors such as bubble collapse and high shear stresses [7]. In offshore deep water production, there is concern in protecting the deep offshore catenary riser [8]. The catenary is the natural shape that the piping follows as it moves upward from the sea floor to the platform. Blank corrosion rates vary with inclination rates [8]. Risers often introduce conditions that make it easy to experience severe slugging in the system. In one study it was found that the most difficult system to treat with corrosion inhibitor was at an inclination of 45° and high velocity [8]. Corrosion inhibition testing under multiphase flow conditions is difficult, expensive, and limited to a small number of facilities. There are several examples of corrosion inhibition testing under multiphase flow conditions [8−11].

It was found in some studies that corrosion inhibitors that exhibited strong performance in high-shear single-phase test apparatus such as single-phase flow loops [9], rotating cylinder electrode apparatus [10,11], and rotating cage apparatus [12] correlated well with performance in challenging multiphase field conditions. In other tests, rotating cylinder electrode corrosion tests did not mimic pipe flow [13].

The corrosion tests using a rotating cage have been used to select corrosion inhibitors in a challenging 45−60 mol% carbon dioxide field where mesa-type severe corrosion was experienced without the correct inhibitor [14,15]. In one study it was suggested that the rotating cage be judged as the top-ranking method to choose inhibitors in pipeline systems [16]. Rotating cage corrosion tests often mimic the most corrosive parts of a field. Often inhibitor performance at high rotation rates is consistent with excellent performance in field conditions.

Jet impingement devices have also been used to simulate environments where carbon dioxide corrosion of mild steel occurs with high shear stresses [17]. The jet impingement device and the rotating cage apparatus have been used for corrosion inhibitors in challenging deep water locations where the system was expected to experience slug flow [18]. Localized corrosion was observed in studies of carbon dioxide corrosion of mild steel with inhibitors using an innovative method of localized corrosion monitoring (LCM) using an electrochemical technique [19].

Thin flow cells have been used to study corrosion inhibition in acidic environments [20] and mild steel corrosion at high temperatures, high carbon dioxide concentrations, and high velocities [21]. Thin flow cells allow one to use linear polarization as the measurement technique and allow for in situ visualization of corrosion.

Features of the different corrosion test apparatus used to test corrosion inhibitors for high-shear applications are provided in Table 19.2.

Table 19.2 Comparison of different high-shear corrosion test apparatus

Test method	Advantages	Disadvantages
Multiphase flow loop	Corrosion measurements are made in a representative flow regime where real-time electrochemical measurements of corrosion rate can be made	The units are expensive to operate and hard to clean from inhibitor contamination
Single-phase flow loop	Performance at high velocities in this flow loop has correlated well with performance in multiphase flow in several instances. The shear stress and mass transfer in the single-phase flow loop are easy to calculate and real-time electrochemical measurements of corrosion rate can be made in the apparatus	This is less expensive than a multiphase flow loop but hard to clean from inhibitor contamination
Rotating cylinder electrode apparatus	This apparatus is less expensive to test and easy to clean from inhibitor contamination. The shear stress and mass transfer in this apparatus are easy to calculate. Real-time electrochemical measurements of corrosion rate at high temperatures and pressures are possible	Performance at high rotation rates in some studies correlate well with performance in multiphase flow loops but in other studies the correlation was not found
Rotating cage apparatus	The apparatus is used to test corrosion inhibitors that work in challenging systems. It is easy to clean and is relatively inexpensive to test corrosion inhibitors	The shear stress and mass transfer in the system are hard to calculate. Currently no real-time electrochemical measurements can be made with the apparatus just weight loss experiments are available
Jet impingement test	This apparatus is used to test corrosion inhibitors that work in challenging systems. It is easy to clean after inhibitor testing. The test is relatively inexpensive. The shear stress and mass transfer in the system are easy to calculate	This test is difficult to operate for systems with high oil cut
High-temperature thin flow cell	This apparatus is used to test corrosion inhibitors in challenging flow conditions. The shear stress and mass transfer in system are easy to calculate	At present no published studies are available on the use of this apparatus to compare inhibitors

Correlating inhibitor performance obtained in the different tests to each other and to field performance is difficult. Correlation between tests requires an understanding of boundary layer effects in turbulent flow testing [22−24]. In rotating cylinder electrode experiments one has well-developed hydrodynamic and concentration profiles at the boundary layer. Flow loops have well-developed hydrodynamic profiles but do not have well-developed concentration profiles. The jet impingement's hydrodynamic and concentration boundary layers vary with position so one tries to use a thin concentric electrode. Rotating cage and multiphase flow loop tests in slug flow do not have well-defined boundary layers so the corrosion rates are expected to be most severe in these conditions. One attempt to correlate corrosion inhibitor performance in laboratory tests to field performance is provided in reference [12].

In this section, state-of-the art performance testing of corrosion inhibitors to inhibit corrosion in conditions of high shear in a multiphase flow regime system has been discussed. In all systems that will face high shear conditions in multiphase flow, it is important to have the corrosion inhibitor tested in conditions that experience high shear. The accumulated experience in the oil field is to choose more difficult corrosion inhibitor tests in a laboratory testing protocol to avoid possible field failures. Very often the field life exceeds the field design life and water cuts in mature fields are normally higher than expected.

19.3 Corrosion inhibition testing in systems experiencing erosion corrosion

The presence of sand in carbon dioxide systems introduces erosive effects in corroding systems. In scale-forming conditions, corrosion tests without sand can lead to low corrosion rates. The presence of sand in these conditions can increase the corrosion rate because of partial removal of scale by sand impingement [25,26]. In the laboratory experiments, it is important to measure the shape and particle diameter of the sand [26]. Most producing gas wells produce some amount of sand. Corrosion inhibitor studies with sand in carbon dioxide environments have been conducted in flow loops [26,27], rotating cylinder electrode tests [28], jet impingement tests [29,30], and rotating cages [31]. In studies with carbon dioxide, sand, and inhibitor, it is important to distinguish the effects of corrosion, erosion, synergistic effects of corrosion and erosion, and assessment of inhibition [32]. For this reason it is useful to conduct studies that allow for the simultaneous use of electrochemical probes and metal loss with a material capable of corrosion and erosion and metal loss from a probe that does not corrode but may erode [33]. It is ideal to be able to experimentally measure electrochemistry, weight loss, or electrical resistance (ER) on a corrosive material and weight loss or ER on a noncorrosive material at the same conditions to be able to distinguish the effects of corrosion, erosion, and synergistic corrosion and erosion. A new apparatus to measure erosion corrosion was designed with three plugged test cells arranged in-line with one another that could use an ER probe with carbon steel to measure erosion corrosion, an ER probe with stainless steel to measure erosion, or a linear polarization probe to

measure corrosion without effects due to erosion [33]. The test cells were designed so that probes could be interchanged to check if there is variance in measurement due to a change in location [33]. Design of experiments has been used to investigate the effects of sand loading, corrosion inhibitor, and velocity [34]. Currently, it is state of the art to use flow loops or jet impingement devices to test inhibitors in carbon dioxide systems with sand. Often the effects of sand are ignored in the design of corrosion inhibitor for wells and pipelines. This is unfortunate as low amounts of sand are always present in oil and gas producing environments. In scaling conditions, the need to have corrosion inhibitor is most probably due to the low amount of sand in the operating environment, which was not considered during laboratory evaluation of inhibitors for such systems.

19.4 Pitting corrosion

Localized corrosion is the most common mode of failure [35]. In corrosion due to carbon dioxide, pitting propagates whenever the pH at the bottom of the pit is lower than at the top of the pit [36]. An increase in acetate concentrations decreases the pH at the bottom of the pit [36]. Pitting corrosion in carbon dioxide systems is a strong function of temperature, salt content, in situ pH, and acetate concentration [36]. The pitting corrosion of X65 pipeline steel by carbon dioxide has been studied using a high-speed camera to monitor the corrosion rate of the specimens and pitting initiation and growth [37]. Pitting corrosion in carbon dioxide systems has been observed in a system with a sand-covered steel specimen utilizing microchemical techniques, such as localized electrochemical impedance spectroscopy (LEIS) and scanning electrode vibrating electrode technique [38]. The pitting process was visualized as a function of time using LEIS [38].

Pitting corrosion is most often seen in sour systems. Severe pitting is seen in experiments with hydrogen sulfide and carbon dioxide with glycol [39]. This is in contrast with what is seen with pH-stabilized glycol in carbon dioxide environments. Increases in salt concentration accelerate pitting in H_2S/CO_2 systems [40]. Sulfur is also used to accelerate pitting in sour systems [41]. Precorrosion of a carbon steel coupon initially in a carbon dioxide environment with subsequent introduction of the coupon in a sour environment causes pitting in H_2S/CO_2 environments [42,43]. Studies of pitting corrosion require the statistical analysis of pit depth, size, and distribution using an automated high-resolution vertical scanning interferometer. In inhibitor testing it is important to establish a blank rate where one can reproduce pitting corrosion several times. It is important to have the results of several coupons exposed to similar conditions as pitting is a stochastic phenomenon. It is useful to plot the pit depth for each pit with each coupon and compare different conditions [43]. Inhibitor studies must also be performed for several coupons in similar conditions [43]. Effective studies of the inhibition of pitting corrosion will involve the statistical analysis of pit depth, size, and distribution. Optical profilometric techniques are important in this assessment [44].

Electrochemical techniques for localized corrosion motoring (LCM) have been used in several studies [38,43,45]. These techniques have the promise of allowing the nondestructive monitoring of pitting corrosion. The LCM technique was shown to provide in

situ quantitative information on pitting event for experiments relevant to important sour corrosion systems [45]. Other electrochemical techniques used for localized corrosion measurements are electrochemical noise analysis and wire beam electrode methods [46].

There exist a few studies where pitting corrosion tests are incorporated into corrosion inhibitor evaluation. One example is the examination of a corrosion inhibitor to prevent pitting corrosion in 7-day tests at 49°C (120°F) in a rotating cage with a 90 vol% brine and 10 vol% hydrocarbon system for CO_2 corrosion [47]. In this example, optical profilometric techniques were used to examine corrosion coupons from corrosion tests with statistical analysis of pit depth, size, and distribution for five corrosion inhibitor formulations [47]. In another study on corrosion inhibition of systems in a CO_2/H_2S system, four corrosion inhibitor formulations are studied in small autoclave and wheel bomb tests where the coupons were examined using optical profilometric techniques and the results compared using statistical analysis [48]. In this study, the LCM method was also used to establish inhibitor performance [48]. It was seen that experimental runs where no pitting was found on the coupons correlated to runs where no potential transients were found with LCM [48].

Owing to the difficulty of creating pitting corrosion, and the need to have several experiments, studies evaluating corrosion inhibitors for pitting corrosion are limited. Better experimental methods are necessary for more rational optimization of corrosion inhibitors in carbon dioxide systems and safer and cost-effective methods for producing sour oil.

19.5 Under-deposit corrosion

Methodologies to test corrosion inhibitor performance with sand and carbon dioxide have involved characterization of the sand, assessment of the adsorption of inhibitor by the sand, and corrosion testing with a bed of sand [49]. General corrosion of mild steel in carbon dioxide systems has been observed to decrease in kettle experiments with sand [50]. Pitting corrosion in oil pipeline systems is due to under-deposit corrosion [51]. Pitting corrosion in a carbon dioxide system with a layer of sand was seen in studies that used LEIS [38]. Multiarray sensors have been used to detect under-deposit and microbially influenced corrosion [52]. Inhibitor performance in carbon dioxide systems with deposited sand was studied using a coupled multielectrode array [53]. Some tests involve galvanic coupling that anodically polarize the electrode. This may not be representative of field conditions [46].

It is well known that stagnant conditions in sour environment create conditions conducive for severe pitting corrosion. A review of over 125 sour gas field cases covering 45 reservoirs found that, in most cases, corrosion occurred at the bottom of the well associated with the buildup of a thick iron sulfide deposit [54]. Experiments with different forms of iron sulfide showed that under-deposit pitting corrosion was most severe with synthesized iron sulfide that is carefully prepared and introduced in the corrosion experiment to exclude oxygen [55]. The finding explains localized corrosion observed in sour gas systems where iron sulfide is deposited [55]. The effect of FeS deposit was investigated with sand and it was found that the highest penetration

rates occurred in systems where FeS concentrations are high in the presence of brines with high chloride levels [56]. Corrosion testing with inhibitors was performed in a system with two sparged beakers with two working electrodes of the same dimensions, made from UNS G1080 [57]. In one sparged beaker, the working electrode was covered with a freshly formed FeS surface [57]. The two electrodes were connected by a salt bridge [57]. Great care was taken to keep the system free of oxygen [57]. Inhibitors were introduced in one cell or the other or in both [57]. Measurements were made of the galvanic corrosion rates when both electrodes are connected to each other as well [57]. Measurements were also made of the general corrosion rate of the UNS G1080 electrode. Best results in reducing the galvanic current occurred when inhibitors were introduced on both electrodes [57]. This indicates that it is important to ensure that the corrosion inhibitor reaches both iron sulfide covered regions and bare regions in a given system. One method that can be used to test transport of the corrosion inhibitor through a bed of deposits is liquid chromatography to analyze the inhibitor [49].

In mature fields, under-deposit corrosion is among the most common modes of failure. In areas where pigs can be used, they can be used to clean the pipeline. There are many systems that cannot be cleaned using a pig. To defer abandonment, chemical methods to clean or treat the low-volume pipelines are needed. When inhibitors are used, the corrosion inhibitor should be tested in an apparatus that mimics the effect of having metal under iron sulfide−covered region and parts of the surface without deposit [57]. It is also useful to assess the ability of the inhibitor to transfer through a solid bed [49].

19.6 Top-of-the-line corrosion inhibitor testing

The corrosion of the internal surfaces of gas pipelines is a complicated electrochemical process [58]. The importance of top-of-the-line corrosion (TLC) has been highlighted by observation of significant TLC in a multiphase gathering line in Indonesia [59]. Corrosion of the internal metal surface of the gas pipeline is caused by the presence of moisture, CO_2, O_2, and/or other contaminants [60,61]. TLC of pipelines has been demonstrated to be caused by water condensation [62,63]. In one instance it was found that TLC occurred in pipe sections where the condensation rate was above 0.15−0.25 mL/(m^2s) [64]. The water condensation rate in gas pipelines depend on the heat and mass transfer in the gas phase [65]. Oxygen entering through the gas pipeline has been shown to be a significant source of corrosion problems [66]. Acetic acid is also an important contributor to TLC; in some studies increasing the acetic acid concentration has doubled the corrosion rate at low condensation rates [67].

Testing for TLC requires an apparatus that allows for significant condensation on the surface. Significant work has been conducted in an experimental flow loop especially designed to measure TLC [68]. This flow loop has a section cooled by copper coils. Samples of condensed liquid and pH measurement can be made in the

test section. Weight loss coupons are used to measure corrosion rate in this flow loop [68]. The flow loop has been used to study the effects of H_2S and acetic acid on TLC [69]. Flow loop testing is always difficult to perform, so there is an attraction for studies with simpler and easier to use apparatus. In another paper, steel coupons are rotated above the corrosive liquid in an autoclave kept at a warm temperature while the coupons are internally cooled to create conditions of condensation [70].

Inhibitor testing for top-of-the-line conditions needs to replicate rates of condensation. As rates of condensation increase, the performance of inhibitors decrease. It is also important for a volatile corrosion inhibitor to have a low minimum effective concentration as it is difficult to condense sufficient corrosion inhibitor necessary for inhibition. One autoclave apparatus used to test TLC inhibitors involved placing a U-shaped mild steel tubing inside a pressure reaction vessel with liquid below the U-tube in a corrosive environment at the appropriate temperature and pressure [71]. Inhibited coolant is circulated inside the U-tube to create conditions for condensation [71]. In this test, it was found that one film persistent batch corrosion inhibitor showed a significant reduction in film persistency as the condensation rate increased [71]. Another test that has been used for TLC inhibitor tests has been a test modified from the Federal standard MIL-STD 3010B, Method 4031 [72,73]. This test is a simple test that does not measure the rate of condensation. The test also does not have the ability to vary the rate of condensation. Quartz crystal microbalances have been used to measure small weight changes in iron films. This method has been used to investigate the effects of relative humidity, temperature of gas and the metal surface, and oxygen and carbon dioxide on corrosion in sales gas conditions with condensation [74]. The change of frequency in the system provides a sensitive method of measuring weight loss. Careful experimentation using both gold-coated quartz microbalances and iron-coated quartz microbalances allow for the calculation of water condensation rate and corrosion product layer formation. The method was used to develop a corrosion inhibitor and assess its performance as a batch inhibitor to prevent black powder formation [75]. Four inhibitors were assessed with this method with significant differences in performance. The method was also used to assess the performance of three volatile amines and a new TLC inhibitor [76]. It was found in this work that the volatile amines had little effect on TLC in contrast with excellent inhibition by a proprietary corrosion inhibitor [76]. The effect of the inhibitors on water condensation was quantified. Morpholine and the proprietary corrosion inhibitor reduced water condensation. The method quantified very small weight changes that occurred with inhibitor adsorption to iron by the different inhibitors [76]. The proprietary corrosion inhibitor adsorbed on the iron-coated quartz microbalance significantly more than the volatile amines [76].

The requirements for corrosion inhibitor testing at the top of the line require control of the condensation rate in the apparatus and assessment of how inhibitor may change condensation rates. Methods that do not have the ability to monitor the effect of water condensation rate on corrosion inhibitor performance are not desirable as the condensation rate has a great influence on TLC and the ability to inhibit corrosion under top-of-the-line conditions.

19.7 Summary and conclusions

In this chapter, advances in corrosion inhibitor testing were reviewed. Appropriate corrosion inhibitor selection occurs when sufficient analysis of the production and transmission systems is performed to understand the regions with greatest risk for corrosion. Often high-risk areas of corrosion are in places where slug flow occurs and places where high shear stresses are present. Corrosion inhibitor selection for these systems should incorporate relevant corrosion inhibitor tests under high-shear conditions. Sand is present in small amounts in gas systems. The small amount of sand can destroy protective iron carbonate scales. There have been several new studies to test the effectiveness of corrosion inhibitors in a corrosive environment with sand. Pitting corrosion is the most common cause of internal corrosion failures in the oil and gas industry. Pitting corrosion tests require time to generate the pit. As pitting is stochastic, several tests are needed. Each coupon needs to be examined. Advances in corrosion testing have resulted in methodologies to generate pits, methods of microscopically scanning coupons, and innovative electrochemistry. In low-velocity lines deposition of solids occur. Innovative electrochemical methods can capture pitting corrosion in sand systems. In sour conditions, some iron sulfides can conduct electricity, causing accelerated corrosion. It is important in corrosion experiments with iron sulfide to exclude oxygen. Top-of-the-line corrosion occurs in gas systems with high rates of water condensation. Apparatus that simulate these conditions have been developed to select corrosion inhibitors for this system. Advances will continue in the field of corrosion testing as operators experience more demanding conditions and try to minimize their capital and operating costs.

References

[1] S.D. Kapusta, Corrosion inhibitors testing and selection for E&P: a user's perspective, in: CORROSION 1999, NACE International, Houston, Texas, 1999. Paper No. 16.
[2] B. Chambers, S. Huizinga, M. Yunovich, W.D. Grimes, R. French, Laboratory simulation of oil and gas field conditions, important phase behavior considerations and approaches, in: CORROSION 2014, NACE International, Houston, Texas, 2014. Paper No. 4285.
[3] S. Ramachandran, K. Bartrip, S. Mancuso, P. Hammonds, Important considerations for corrosion inhibitors in the laboratory and in the prediction of field performance, in: CORROSION 2008, NACE International, Houston, Texas, 2008. Paper No. 08627.
[4] A. Crossland, R. Woolam, J. Palmer, G. John, S. Turgoose, J. Vera, Corrosion inhibitor efficiency limits and key factors, in NACE international, in: CORROSION 2011, NACE International, Houston, Texas, 2011. Paper No. 11062.
[5] E. Gulbrandsen, J. Kvarekal, H. Miland, Effect of oxygen contamination on inhibition studies in carbon dioxide corrosion, Corrosion 61 (11) (2005) 1086−1097.
[6] D. Paisley, N. Barrett, O. Wilson, Pipeline failure: the roles played by corrosion, flow and metallurgy, in: CORROSION 1999, NACE International, Houston, Texas, 1999. Paper No. 18.

[7] H. Wang, H. Wang, H. Shi, C. Kang, P. Jepson, Why corrosion inhibitors do not perform well in some multiphase conditions: a mechanistic study in NACE international, in: CORROSION 2002, NACE International, Houston, Texas, 2002. Paper No. 02276.
[8] C. Kang, J. Rhodes, K. Tummala, A.A.O. Magalhae, The selection of corrosion inhibitors under oil/water/gas flow conditions in deep offshore catenary risers, in: CORROSION 2013, NACE International, Houston, Texas, 2013. Paper No. 2595.
[9] M. Swidzinski, B. Fu, A. Taggart, W.P. Jepson, Corrosion inhibition of wet gas pipelines under high gas and liquid velocities, in: CORROSION 2000, NACE International, Houston, Texas, 2000. Paper No. 70.
[10] Y. Chen, H.J. Chen, W.P. Jepson, Effects of multiphase flow on corrosion inhibition, in: CORROSION 1999, NACE International, Houston, Texas, 1999. Paper No. 12.
[11] H.J. Chen, W.P. Jepson, Inhibition of slug front corrosion in multiphase flow conditions, in: CORROSION 1998, NACE International, Houston, Texas, 1998. Paper No. 55.
[12] S. Ramachandran, V. Jovancicevic, Y.S. Ahn, Using reaction engineering to compare corrosion inhibitor performance in laboratory and field experiments, in: CORROSION 2001, NACE International, Houston, Texas, 2001. Paper No. 01027.
[13] E.J. Wright, K.D. Efird, J.A. Boros, T.G. Hailey, Rotating cylinder electrode (RCE) simulation of corrosion in sweet production, in: CORROSION 2008, NACE International, Houston, Texas, 2008. Paper No. 08629.
[14] R.H. Hausler, T.G. Martin, D.W. Stegmann, M.B. Ward, Development of a corrosion inhibition model I. laboratory studies, in: CORROSION 1999, NACE International, Houston, Texas, 1999. Paper No. 2.
[15] T.G. Martin, M.T. Cox, R.H. Hausler, R.J. Dartez, P. Pratt, J.C. Roberts, Development of a corrosion inhibition model II. verification of model by continuous rate measurements under flow conditions with a novel downhole tool, in: CORROSION 1999, NACE International, Houston, Texas, 1999. Paper No. 3.
[16] S. Papavinasam, R. Winston Revie, M. Attard, A. Demoz, J.C. Donini, K. Michaelian, Rotating cage — top ranked methodology for inhibitor evaluation and qualification for pipeline applications, in: CORROSION 2001, NACE International, Houston, Texas, 2001. Paper No. 01061.
[17] K.D. Efird, Jet impingement testing for flow accelerated corrosion, in: CORROSION 2000, NACE International, Houston, Texas, 2000. Paper No. 00052.
[18] L.A. Skogsberg, B.P. Miglin, S. Ramachandran, K.A. Bartrip, Establishment of corrosion inhibitor performance in deepwater conditions, in: CORROSION 2001, NACE International, Houston, Texas, 2001. Paper No. 01005.
[19] C.M. Menendez, V. Jovancicevic, W.Y. Mok, Quantitative analysis of localized corrosion in the prescence of corrosion inhibitors, in: CORROSION 2007, NACE International, Houston, Texas, 2007. Paper No. 07619.
[20] M. Sanchez, N. Hernandez, G. Gonzales, Designing and building an electrochemical cell to measure corrosion rate in flow lines, in: CORROSION 1999, 1999. Paper No. 217.
[21] A. Mohammed Nor, M.F. Suhor, M.F. Mohamed, M. Singer, S. Nesic, Corrosion of carbon steel in high CO_2 containing environments- the effect of high flow rates, in: CORROSION 2012, NACE International, Houston, Texas, 2012. Paper No. 1683.
[22] S. Turgoose, J.L. Dawson, J.W. Palmer, T. Rizk, Boundary layer effects in turbulent flow testing, in: CORROSION 95, NACE International, Houston, Texas, 1995. Paper No. 112.

[23] K.G. Jordan, P.R. Rhodes, Corrosion of carbon steel by CO_2 solutions: the role of fluid flow, in: CORROSION 95, NACE International, Houston, Texas, 1995. Paper No. 125.
[24] G. Liu, D.A. Tree, M.S. High, Relationships between rotating disk corrosion measurements and corrosion in pipe flow, Corrosion 50 (8) (1994) 584−593.
[25] J.R. Shadley, S.A. Shirazi, E. Dayalan, E.F. Rybicki, Using an inhibitor to combat erosion-corrosion in carbon steel piping - how much does it help? OTC 8195, in: Presentation at the 28th Annual Offshore Technology Conference Held in Houston, Texas, 5−9 May 1996, 1996.
[26] M. Tandon, J.R. Shadley, E.F. Rybicki, K.P. Roberts, S. Ramachandran, V. Jovancicevic, Flow loop studies of erosion-corrosion in CO_2 environments with sand, in: CORROSION 2006, NACE International, Houston, Texas, 2006. Paper No. 06597.
[27] J. Addis, B. Brown, S. Nesic, Erosion-corrosion in disturbed liquid/particle flow, in: CORROSION 2008, NACE International, Houston, Texas, 2008. Paper No. 08572.
[28] A. Neville, C. Wang, S. Ramachandran, V. Jovancicevic, Erosion-corrosion mitigation using chemicals, in: CORROSION 2003, NACE International, Houston, Texas, 2003. Paper No. 03319.
[29] C. Wang, A. Neville, S. Ramachandran, V. Jovancicevic, Understanding the action of inhibitors in mitigating erosion corrosion in impinging flows, in: CORROSION 2004, NACE International, Houston, Texas, 2004. Paper 04658.
[30] G. Mori, T. Vogl, J. Haberl, W. Havlik, T. Schoberl, Erosion corrosion and synergistic effects under high velocity multiphase conditions, in: CORROSION 2010, NACE International, Houston, Texas, 2010. Paper No. 10382.
[31] S. Ramachandran, M.B. Ward, K.A. Bartrip, V. Jovancicevic, Inhibition of the effects of particle impingement, in: CORROSION 2002, NACE International, Houston, Texas, 2002. Paper No. 02498.
[32] A. Neville, C. Wang, Study of the effect of inhibitor on erosion-corrosion in CO_2 − saturated sands, SPE 114081, in: Presented at 2008 SPE International Oilfield Corrosion Conference, Aberdeen, UK, 27 May 2008, 2008.
[33] A. Hall, M.W. Keller, K.P. Roberts, S.A. Shirazi, E.V. Iski, E.F. Rybicki, J.R. Shadley, A 3-cell flow loop test facility for the simultaneous evaluation of erosion, corrosion and erosion-corrosion, in: CORROSION 2015, NACE International, Houston, Texas, 2015. Paper No. 6035.
[34] K.A. Zawai, X. Hu, A. Neville, R. Roshan, A. Crossland, J. Martin, Predicting the performance of API-5L-X65 in CO_2 erosion-corrosion environments using design of experiments, in: CORROSION 2011, NACE International, Houston, Texas, 2011. Paper No. 11240.
[35] S. Papavinasam, A. Doiron, J. Li, D.Y. Park, P. Liu, Sour and sweet corrosion of carbon steel: general or pitting or localized or all of the above?, in: CORROSION 2010, NACE International, Houston, Texas, 2010. Paper No. 10332.
[36] J.D. Garber, K. Knierim, V.B. Patil, J. Herbert, Role of acetates on pitting corrosion in a CO_2 system, in: CORROSION 2010, NACE International, Houston, Texas, 2010. Paper No.10185.
[37] X. Hue, I.M. Ismail, A. Neville, Investigation of pitting corrosion and inhibition in sweet conditions, in: CORROSION 2013, NACE International, Houston Texas, 2013. Paper No. 2361.
[38] H. Xue, F.Y. Cheng, Z. Zhu, N. Tajallipour, P.J. Teevens, Internal pitting corrosion of X80 pipeline steel under deposited sand bed in CO_2 - saturated solutions, in: CORROSION 2011, NACE International, Houston, Texas, 2011. Paper No. 11264.

[39] J. Kvarekval, A. Dugstad, Pitting corrosion in CO_2/H_2S containing glycol solutions under flowing conditions, in: CORROSION 2005, 2005. Paper No. 05631.
[40] W. Sun, C. Li, S. Ling, R.V. Reddy, J.L. Pacheco, M. Asmann, G. Wilken, R.J. Franco, Laboratory study of sour/localized pitting corrosion, in: CORROSION 2011, NACE International, Houston, Texas, 2011. Paper No. 11080.
[41] M.R. Gregg, J. Lerbscher, Inhibitor developments providing mitigating benefits against pitting corrosion to carbon steel constructed assets used to process wet sulfur contaminated sour gas production, in: CORROSION 2005, NACE International, Houston, Texas, 2005. Paper No. 05627.
[42] C.M. Menendez, J. Jardine, W.Y. Mok, S. Ramachandran, V. Jovancicevic, A. Bhattacharya, New sour gas corrosion inhibitor compatible with kinetic hydrate inhibitor, IPTC17440, in: Paper Prepared for Presentation at the International Petroleum Technology Conference Held in Doha, Qatar, 20−22 January 2014, 2014.
[43] S. Stewart, C. Menendez, V. Jovancicevic, J. Moloney, Corrosion inhibitor evaluation approach for highly sour service conditions, in: CORROSION 2009, NACE International, Houston, Texas, 2009. Paper No. 9360.
[44] C.M. Menendez, Application of optical profilometric techniques to corrosion monitoring, in: CORROSION 2013, NACE International, Houston, Texas, 2013. Paper No. 2506.
[45] J.J. Moloney, W.Y. Mok, C.M. Menendez, The in-situ assessment of pitting corrosion and its inhibition using LCM, in: CORROSION 2010, NACE International, Houston, Texas, 2010. Paper No. 10156.
[46] Y. Tan, Y. Fwu, K. Bhardwaj, S. Bailey, R. Gubner, Review of critical issues in carbon dioxide corrosion testing and monitoring techniques, in: CORROSION 2010, NACE International, Houston, Texas, 2010. Paper No. 10155.
[47] S. Ramachandran, C. Menendez, M. Whitesides, P. Rodgers, P. Grawunder, R. Ponnapati, V. Jovancicevic, Broad shear-range corrosion inhibitor development for oil and gas facilities at cold temperatures, in: CORROSION 2014, NACE International, Houston, Texas, 2014. Paper No. 4315.
[48] S. Stewart, V. Jovancicevic, C. Menendez, J. Moloney, W. Wamburi, Evaluation of a new sour gas corrosion inhibitor for field applications, in: CORROSION 2010, NACE International, Houston, Texas, 2010. Paper No. 10274.
[49] J.A.M. de Reus, E.L.J.A. Hendriksen, M.E. Wilms, Y.N. Al-Habsi, W.H. Durnie, M.A. Gough, Test methodologies and field verification of corrosion inhibitors to address under deposit corrosion in oil and gas production systems, in: CORROSION 2005, NACE International, Houston, Texas, 2005. Paper No. 05288.
[50] J. Huang, B. Brown, Y.S. Choi, S. Nesic, Prediction of uniform CO_2 corrosion of mild steel under inert solid deposits, in: CORROSION 2011, NACE International, Houston, Texas, 2011. Paper No. 11260.
[51] V.V. Nikam, C. Iane, J. Fox, Electrochemical testing to investigate the role of solids in corrosion of an oil pipeline, in: CORROSION 2011, NACE International, Houston, Texas, 2011. Paper No. C2012−0001157.
[52] M.H. Dorsey, D.R. Demarco, B.J. Saldana, G.A. Fisher, L. Yang, N. Sridhar, Laboratory evaluation of a multi-array sensor for detection of under-deposit corrosion and/or microbially influenced corrosion, in: CORROSION 2005, NACE International, Houston, Texas, 2005. Paper No. 05371.
[53] A. Turnbull, G. Hinds, P. Cooling, S. Zhou, A multi-electrode approach to evaluating inhibition of under-deposit corrosion in CO_2 environments, in: CORROSION 2009, NACE International, Houston, Texas, 2009. Paper No. 09445.

[54] M. Bonis, Weight loss corrosion with H_2S: from facts to leading parameters and mechanisms, in: CORROSION 2009, NACE International, Houston Texas, 2009. Paper No. 09564.
[55] C.M. Menendez, V. Jovancicevic, S. Ramachandran, M. Morton, D. Stegmann, New method for assessing corrosion under iron sulfide deposits and CO_2/H_2S conditions, in: CORROSION 2011, NACE International, Houston, Texas, 2011. Paper No. 11265.
[56] J. Kvarekval, G. Svenningsen, Effect of iron sulfide deposits on sour corrosion of carbon steel, in: CORROSION 2016, NACE International, Houston, Texas, 2016. Paper No. 7313.
[57] Z. Liu, T. Jackson, P. Kearns, Mechanistic studies of sour under-deposit corrosion in the presence of chemical inhibition, in: CORROSION 2015, NACE International, Houston, Texas, 2015.
[58] R. Baldwin, "Black Powder" in the Gas Industry, Gas Machinery Research Council, 1997. Report No. TA 97−4.
[59] Y.M. Gunaltun, D. Supriyatam, J. Achmad, Top of the line corrosion in multiphase gas lines. A case history, in: CORROSION 1999, NACE International, Houston Texas, 1999. Paper No. 36.
[60] A. Kale, B.H. Sridhar, C.J. Waldhart, A probabilistic model for internal corrosion of gas pipelines, in: International Pipeline Conference 2004. Calgary, Alberta, Canada, 2004.
[61] R. Nyborg, Controlling internal corrosion in oil and gas pipelines, The Oil and Gas Review (2) (2005).
[62] S. Olsen, A. Dugstad, Corrosion under dewing conditions, in: CORROSION 1991, NACE International, Houston Texas, 1991. Paper No. 472.
[63] R. Nyborg, Top of the line corrosion and distribution in a large wet gas pipeline, in: CORROSION 1993, NACE International, Houston Texas, 1993. Paper No. 77.
[64] Y. Gunaltun, A. Belghazi, Control of top of the line corrosion by chemical treatment, in: CORROSION 2001, NACE International, Houston, Texas, 2001. Paper No. 01033.
[65] F. Vitse, S. Nesic, Y. Gunaltun, D.L. de Torreben, P. Duchet-Suchaux, Mechanistic model for the prediction of top of the line corrosion risk, Corrosion 59 (12) (2003) 1075−1084.
[66] N. Sridhar, D.S. Dunn, A.M. Anderko, M.M. Lencka, H.U. Schutt, Effects of water and gas composition on the internal corrosion of gas pipelines - modeling and experimental studies, Corrosion 57 (3) (2001) 221−235.
[67] M. Singer, S. Nesic, Y. Gunaltun, Top of the line corrosion in presence of acetic acid and carbon dioxide, in: CORROSION 2004, NACE International, Houston, Texas, 2004. Paper No. 04377.
[68] Z. Belarbi, F. Farelas, M. Singer, S. Nesic, Role of amine in the mitigation of CO_2 top of the line corrosion, in: CORROSION 2016, NACE International, Houston, Texas, 2016. Paper No. 7274.
[69] M. Singer, A. Camacho, B. Brown, S. Nesic, Sour top of the line corrosion in the presence of acetic acid, in: CORROSION 2010, NACE International, Houston, Texas, 2010. Paper No. 10100.
[70] H. Qin, L. Xu, W. Chang, M. Lu, L. Zhang, Top of the line corrosion under low temperature and high condensation rates, in: CORROSION 2011, NACE International, Houston, Texas, 2011. Paper No. 11328.
[71] D. John, L. Capelli, B. Kinsella, S. Bailey, Top of the line corrosion control by chemical treatment, in: CORROSION 2009, NACE International, Houston, Texas, 2009. Paper No. 09286.

[72] M. Sheng, A. Furman, R. Karshan, T. Whited, Development of corrosion inhibitors for prevention of top of the line corrosion (TLC), in: CORROSION 2013, NACE International, Houston, Texas, 2013. Paper No. 2509.
[73] Department of Defense, Test Method Standard, MIL-STD-3010B, 2008.
[74] K. Cattanach, S. Ramachandran, V. Jovancicevic, A. Sherik, New methodology for monitoring corrosion under sales gas conditions using the quartz crystal microbalance, in: CORROSION 2011, NACE International, Houston, Texas, 2011. Paper No. 11085.
[75] K. Cattanach, V. Jovancicevic, S. Ramachandran, A. Sherik, Development of new corrosion inhibitor to prevent black powder formation using quartz crystal microbalance technique, in: CORROSION 2011, NACE International, Houston, Texas, 2011. Paper No. 11093.
[76] S. Ramachandran, V. Jovancicevic, P. Rodgers, I. Ahmed, M. Al-Waranbi, A new top of the line corrosion inhibitor to mitigate carbon dioxide corrosion in wet gas system, in: CORROSION 2013, NACE International, Houston, Texas, 2013. Paper No. 2274.

Advances in monitoring technologies for corrosion inhibitor performance

20

Sunder Ramachandran
Baker Hughes, Sugar Land, TX, United States

20.1 Introduction

Monitoring of corrosion and phenomena related to corrosion allow the proper use and optimization of corrosion inhibitors in oil and gas production and transmission lines. Corrosion monitoring is important in any facility to ensure asset integrity. Risk assessment for corrosion is needed to set monitoring objectives. Risk assessment involves a number of tools from multiphase flow assessment, water chemistry assessment, metallurgy assessment and knowledge of operating pressures, and pipeline thickness. The objectives of any monitoring program can vary depending on local regulations, location of the pipeline, asset integrity conditions, frequency of inspection, and corrosion inhibition optimization. The location of monitoring devices is selected carefully using corrosion modeling in places of greatest corrosion risk. There have been a great number of advances in corrosion rate measurement technologies in different operating systems. Ideally monitoring and inspection should augment each other. Inspection methods are briefly reviewed in this chapter. Monitoring is important for economic and safe oil and gas transmission as it allows one to optimize the dosage of corrosion inhibitors while minimizing the corrosion of the wells or pipelines. When corrosion inhibitors are involved, it is important to monitor the concentration of corrosion inhibitors that are used. This requires measurement of the amount of chemical that is pumped as well as the measurement of oil and water production rates. For best use, monitoring data should be kept in a format that is easily accessible and provided in a manner that ensures timely response to corrosive threats and feedback for continual improvement. This will be discussed in the last section of the chapter.

20.2 Risk assessment

Corrosion risk assessment is important for developing a monitoring program. The initial part of risk assessment is data collection. At the beginning of the development of the field, data is acquired from appraisal wells. The collection of critical data for materials and corrosion risk assessment has been carefully considered and assessed [1]. Methods for dry gas internal corrosion direct assessment are collected in NACE International Standard SP0206-2016 [2]. NACE SP-0110-2010 provides a methodology for

Trends in Oil and Gas Corrosion Research and Technologies. http://dx.doi.org/10.1016/B978-0-08-101105-8.00020-6

assessment of internal corrosion of wet gas pipelines [3]. This process includes four steps of preassessment, indirect inspection, detailed examination, and postassessment [3]. Typical data needed for risk assessment are presented in Table 20.1.

Multiphase flow modeling is used to determine temperature, pressure, flow regime, velocity, and liquid holdup in the pipeline or well [4,5]. Brine composition with acid gas composition, temperature, and pressure determine the pH of the system, which can be used with corrosion models to assess possible corrosion rates in the system. There are a variety of corrosion models that are used in risk assessment [4,5]. SP0110-2010 has been used to implement an internal corrosion monitoring program on a high-pressure gas pipeline in Kuwait [5]. Corrosion and flow modeling have been used to determine the effects of water cut, flow rate, flow regime, gas oil ratio, hydrogen sulfide, and bicarbonate contents on corrosion in production tubulars, flow lines,

Table 20.1 Typical data needed for risk assessment

Piping and tubing lengths and elevations
Metallurgy of tubing and piping
Hydrostatic test information
In-line inspection data
Leaks/failures history
Operating history
History of process upsets
Type of dehydration process (in case of gas transmission lines)
Internal coatings
Location of sampling points, temperature and pressure gauges and valves
Production rates of gas, oil, and produced water
Composition of corrosive gases (H_2S, CO_2, and possibly O_2)
Composition of brine
Composition of hydrocarbon phase
Water cut
Temperatures and pressures
Flow regimes
Microbial populations and numbers
Corrosion product composition
Corrosion inhibitor treatment
Biocide treatment
Hydrate prevention treatment

and trunk lines [6]. The influence of weld heat affected zones is important in incorporating the risk assessment [7]. Methods of failure analysis are incorporated in risk assessment of risers and pipelines [8].

Risk assessment is performed using a qualitative risk matrix based on consequence severity and event frequency [8,9]. Operating conditions and operating environments need to be considered in risk assessment [10].

The most important regions to monitor are locations where the corrosion risk is high and the consequences of failure are significant [10,11]. Corrosion risk assessment can be linked to risk-based inspection using a methodology that quantifies the risk [11]. In many instances, the information needed for risk assessment is incomplete. In this instance, corrosion risk methodologies have been developed that incorporate existing data with an in-house expert system [12]. Offshore sour gas pipeline systems have used comprehensive corrosion risk assessment to select a cost-effective and safe corrosion management system [13].

20.3 Monitoring objectives

Risk assessment is needed to develop monitoring objectives. Ideally change management needs to be incorporated in the corrosion management program [14]. Frequent monitoring can substantially reduce risks in operating an oil and gas production or transmission lines. Corrosion monitoring tools need to be integrated in the operation practice to increase efficiency. Monitoring aids compliance with governmental regulations [15]. It is important to understand the regulation and assess what measurements can be used to comply with regulations [15]. Another monitoring objective is to ensure high life expectancy of equipment with minimal operating costs [15,16]. All information obtained from monitoring needs to be organized to generate a quick response to mitigate corrosion for unfavorable operating conditions and schedule inspections optimally [16], preventing unplanned shutdown of production operations [17]. Possible corrosion monitoring objectives are compiled in Table 20.2 [15−18].

Table 20.2 Typical corrosion monitoring system objectives

Safe operation
Risk reduction
Compliance with governmental regulations
High life expectancy of equipment
Minimized operating costs
Reduction in unplanned maintenance
Optimal inspection planning
Reduction in deferred production

20.4 Monitoring device locations

The choice of location is among the most important decisions to make in a corrosion monitoring program [19]. It is difficult to choose a monitoring location that actually experiences the worst corrosion in the system [20]. The reason that this happens is that often times operating conditions differ from the anticipated design conditions.

Often a large number of wells are connected to a production gathering line. Some wells lose production and are shut in. This leads to some extremely low velocity pipelines connected to the rest of the pipeline network. These low velocity pipelines can collect water and are good choices for monitoring corrosion [16]. Leak and failure history is one factor in determining monitoring device location [21]. Multiphase flow modeling with corrosion modeling is used to prioritize corrosion online monitoring locations [4,22]. Low lying locations, high shear stress locations, areas with periodic high shear rates and liquid hold ups, and regions of frequent slugging were chosen as monitoring locations in one study [22]. It is sometimes inconvenient to place probes at locations where corrosion is most severe [23]. Computational fluid dynamics models have helped with probe placement [24]. One way of ensuring that correct locations are chosen for corrosion monitoring is to commission relevant corrosion modeling studies and choose the locations using feedback from the study as well as from corrosion professionals who have managed oil and gas systems with similar characteristics. If the characteristics are new for the operating company it may be helpful to seek guidance from professionals who have experience with similar systems in service or consulting companies.

20.5 Monitoring corrosion in field applications

Methods to monitor corrosion rates in oil and gas production and transmission systems can be classified as methods that measure a variable directly caused by corrosion and erosion (direct method) and methods that record other variables that influence corrosion (indirect methods) [25]. Direct techniques involve probes that are directly placed in the system (intrusive methods) or probes placed outside the system (nonintrusive methods) [25]. Indirect methods such as hydrogen monitoring or dissolved oxygen monitoring involve probes that measure these parameters associated with corrosion as they change in the system (online). Offline indirect measurements such as dissolved iron in water are conducted on samples or deposits after they are taken out of the system (offline) [25]. Intrusive direct methods can be divided into those methods that measure a physical property or those that make an electrochemical measurement.

The physical methods for direct intrusive monitoring are listed in Table 20.3 with the description of the method [25].

Mass loss coupons are commonly used in oil field applications. They are commonly used on both in-line and side stream locations. They allow the detection of general and pitting corrosion [19]. A standard practice document guides the preparation, installation, and interpretation of these coupons in oil field operations [26]. Properly placed

Table 20.3 Physical methods for direct intrusive monitoring

Method	Description
Mass loss coupon	Placement of metal similar to pipe material in the system for a given duration of time
Electrical resistance	Placement of wire made of metal similar to pipe material and measurement of its resistance
Visual inspection	Visual inspection of metal using boroscope or video camera

coupons in sour gathering lines and sour oil transmission pipelines can be used to simulate the worst case corrosivity of a given pipe [27]. Examination of coupons using optical profilometric techniques has been used to evaluate pitting corrosion when two different inhibitors were used [28,29].

Electrical resistance probes measure the loss of metal by measuring electrical resistance [30]. Accurate measurement of electrical resistance is needed to measure corrosion rates. The choice of a sensitive electrical resistance probe will lead one to choose a probe with less probe life. Electrical resistance probes are ideal in systems with oil as the oil will not interfere with the measurement method. Enhanced electrical resistance monitoring has allowed some fields to have a continuous improvement process for corrosion inhibitor evaluation and development [31]. Electrical resistance monitoring has been used to monitor corrosion rates and verify corrosion inhibitor effectiveness in downhole CO_2 flood conditions [32].

Electrochemical methods for direct intrusive monitoring can be divided into methods that use direct current and those that use alternating current. The methods are listed in Table 20.4 [25].

Different electrochemical methods that use direct current are polarization resistance, electrochemical noise (EN), probes with dissimilar electrodes, single electrode arrays, coupled multielectrode arrays, and potentiodynamic and galvanodynamic polarization methods [25].

Linear polarization methods are the most commonly used electrochemical technique in oil and gas production and transmission systems [25,33]. Generally accepted procedures and practices for electrochemical techniques for field corrosion monitoring used in oil and gas environments have been recently reviewed [34]. In a study that compared several methods in a sour oil and gas production environment, the linear polarization resistance (LPR) method has been found to correspond well to general corrosion rate measurements obtained by other methods [27]. LPR methods require electrically conductive media to work [25,34]. A bypass loop can be constructed at the wellhead to ensure that the probe is placed in aqueous media [35]. The basis of polarization resistance method has been thoroughly reviewed with discussion of the most common errors that invalidate results [36]. The

Table 20.4 Electrochemical methods for direct intrusive monitoring

Method	Current	Description
Linear polarization resistance (LPR)	Direct	Working electrode perturbed from corrosion potential. At small perturbations current is linear to the perturbed voltage. This allows determination of corrosion rates.
Electrochemical noise	Direct	Two identical working electrodes coupled using a zero resistance ammeter (ZRA). Fluctuations in corrosion potential are measured with the fluctuations in the current between the two identical electrodes. These fluctuations are related to corrosion rate and pitting corrosion.
Galvanic probes	Direct	Dissimilar electrodes are connected to each other using a ZRA. The current is measured. This gives the galvanically coupled current.
Coupled multiarray electrode sensors (CMAS)	Direct	Several electrodes are coupled to each other using a ZRA. The electrode material could be similar or dissimilar. The current between the electrodes is measured. This technique provides uniform and pitting corrosion rates.
Potentiodynamic/ galvanodynamic polarization methods	Direct	The potential or current is systematically varied on a probe and the changes in current or potential are measured.
Electrochemical impedance spectroscopy	Alternating	Alternating sinusoidal voltages of different frequencies are applied on an electrode and the alternative current is measured. Often impedance is measured as a function of frequency and this is analyzed to assess pitting corrosion rates.
Harmonic distortion analysis	Alternating	Alternating sinusoidal voltage of a low frequency is applied on a three electrode system. The current is measured and analyzed for harmonic on the applied low frequency. The harmonics are interpreted in a way to obtain Tafel slopes.

effectiveness of linear polarization probes, electrical resistance probes, and metal loss coupons in process streams that included wet crude oil, effluent water, and brackish water has been assessed [37]. In this study, it was found that mass loss coupons were effective in monitoring both general corrosion rates and pitting corrosion [37].

Electrical resistance probes provided a rapid assessment of general corrosion rates in crude and effluent systems [37]. LPR methods in this study were found to be ineffective in crude and oily water systems with fairly high water cuts [37].

EN methods are used in a more limited way in the oil and gas industry [25,33]. In a study comparing different monitoring methods in sour systems, EN method was found to be extremely reliable [27]. The method is limited due to the difficulties of interpreting the data [27]. For any electrochemical technique, it is important that the probe be placed in the aqueous phase. Due to the speed in evaluating the possibility of pitting corrosion EN method has been used to make important decisions on corrosion mitigation strategy [38]. The interpretation of EN data is complex [39] and offers the promise of identification of specific features of different types of corrosion [40].

Conditions conducive for galvanic corrosion commonly occur in oilfield environments [41]. Galvanic probes are used to assess corrosion and the effect of inhibitor to prevent this corrosion in field conditions [41]. Galvanic probes can be used to detect oxygen ingress and pH excursions [42]. Use of coupled multielectrode arrays in different systems has been reviewed [43]. Use of single electrode arrays and potentiodynamic and galvanodynamic polarization methods are other direct electrochemical methods used in the industry [25].

Direct intrusive electrochemical methods that use alternative current are electrochemical impedance spectroscopy and harmonic distortion analysis [25]. It was found in sour systems that accurate corrosion rates could be determined using LPR with the Stern−Geary constant obtained from harmonic distortion analysis [43a]. Field tests using electrochemical impedance spectroscopy for field monitoring are available in the literature [44]. Multielectrode array impedance analyzers capable for direct current electrochemistry and electrochemical impedance spectroscopy have been developed [45].

Nonintrusive direct techniques to monitor metal loss in oil and gas systems include use of ultrasound, magnetic flux leakage, eddy current measurements, radiographic field mapping, and electrical field mapping [25]. In subsea operations, due to the difficulty of accessing the installation and repairing the system, expensive corrosion monitoring systems are used [46]. Guided ultrasonic lamb waves have been used to monitor erosion/corrosion on subsea pipelines in the Gulf of Mexico [46]. The use of ultrasound testing at fixed locations has become a popular method for both inspection and monitoring [24,47]. Ultrasonic measurements at fixed locations have enabled the early detection of wet gas corrosion, corrosion inhibition optimization and offshore gas production maximization of a sand producing well [48]. Ultrasonic corrosion monitoring methods have become more precise [49]. Monitoring of corrosion using eddy current measurements has been proposed [50]. Pulsed eddy current corrosion monitoring has been used in refinery applications [51].

Hydrogen flux measurement is another means for measuring corrosion in oilfield applications. Hydrogen permeation monitors have been successfully used to monitor the effectiveness of an inhibition program in a sour gas transmission system [52]. The technique has been used to determine the reduction in hydrogen flux that occurs when corrosion inhibitors are used for rod pumped wells in sour environments [53].

20.6 Field application monitoring of phenomena associated with corrosion

Corrosion monitoring is improved when ancillary phenomena associated with corrosion are monitored. Some ancillary phenomena associated with corrosion are listed in Table 20.5 [25].

The design of deep water corrosion monitoring requires several measurements of temperature, pressure, electric conductance, oxygen, pH, density, composition of chemical components, corrosion measurements, deposition, and flow [54]. It is important in any system to know the water composition of the producing system. This is obtained by regularly collecting water samples, preserving the samples appropriately, and analyzing the water samples for metal ions. In systems where the fluids do not contain dissolved sulfides or dissolved oxygen, measurement of iron concentration in the fluid can act as a reliable measure for corrosion [55]. The method is applicable for systems experiencing carbon dioxide corrosion and standard practice regarding preparation, analysis methods, and interpretation are provided in the literature [55]. Recently, there has been research in developing an automated real-time produced water composition device for scale risk prediction and prevention [56]. Portable field monitors that utilize a side stream of fluid have been developed that contain a high pressure sampling vessel, a heated high pressure corrosion probe, and an ambient pH/oxygen probe [57,58]. The device measures corrosion at the

Table 20.5 Ancillary phenomenon associated with corrosion

Phenomenon	Need
Temperature	Temperature can change corrosion and corrosion inhibitor performance
Pressure	Pressure can change flow regime, corrosion, and corrosion inhibitor performance
Dissolved oxygen	Dissolved oxygen will increase corrosion. Many oilfield corrosion inhibitors are not designed for oxygen
pH	Lower pH will increase corrosion. Oilfield production corrosion inhibitors are not meant for pH below 4
Iron concentration	Can be used to estimate general corrosion
Corrosion Inhibitor concentration	Used to determine corrosion inhibitor availability
Bacterial concentration	Used to assess potential for microbial corrosion
Carbon dioxide concentration	Assessment of corrosion due to carbon dioxide
Sand concentration	Erosion corrosion

side stream and dissolved oxygen or ambient pH online [58]. The device enables the offline analysis of the water composition and bacterial activity [58]. The device has been used to diagnose corrosion in oil field systems in Europe [58], Africa [58], Asia [58], and the Middle East [59].

For systems that use corrosion inhibitors, it is important that the corrosion inhibitor be present in the system. As an example, daily corrosion inhibitor residuals are measured along with continuous corrosion inhibitor rate monitoring and continuous corrosion inhibitor tank level monitoring for an important wet sour gas system [59]. Corrosion inhibitor availability has been an important means to control corrosion in wet flow lines at Prudhoe Bay [60]. Different operators have different approaches regarding corrosion inhibitor availability [61]. Managing corrosion inhibitor availability requires a record of inhibitor availability achieved in the system, understanding the events that decrease corrosion inhibitor availability, and a process in place to increase corrosion inhibitor availability [62]. The maintenance of corrosion inhibitor availability requires chemical injection system reliability and feedback-based control of dosage [63].

In certain instances, the composition of gas can change especially with oil production using carbon dioxide as a means of enhanced oil recovery. The presence of higher concentrations of carbon dioxide in producing wells in certain instances can create conditions for serious corrosion [64]. Monitoring changes in the gas composition is important. New developments in downhole optical spectroscopy have enabled the downhole measurement of gas composition [65].

The collection of data such as production rates of oil, water, and gas, pressure and temperature are important to help ascertain conditions in the system. This information should be used to calculate flow velocities and flow regimes. Changes in temperature, pressure, flow velocities, and flow regimes can change the type and concentration of corrosion inhibitor needed to optimally protect the system.

Acoustic sensors are being used to monitor leaks and vortex-induced vibrations on arctic pipeline spans [66]. Acoustic sand monitoring is used frequently to select optimum choke sizes to have the highest gas production rates with a minimum amount of sand [67,68]. Deposit collection and analysis are important in preventing blockage of equipment by scale [69] and corrosion product [70].

20.7 System inspection

System inspection is performed on oil and gas production and transmission lines. Inspection is carried out to identify defects in a pipeline so they may be repaired or monitored, operate safely, reduce risk exposure and cost, extend life of the pipeline, prioritize maintenance, and comply with regulations [71]. Magnetic flux leakage, ultrasonic wall measurements, ultrasonic crack detection, transverse magnetic flux leakage, caliper, and pipe deformation tools are often used in these inspections [71]. Ultrasonic in-line inspection tools are used to inspect large and long crude oil pipelines [72]. A recent electromagnetic casing−corrosion evaluation tool provides total metal

thickness, tubular internal diameter, and defect imaging inside single and multiple casings [73]. This method uses an electrochemical field to induce eddy currents in the pipe [73,74]. Electrical field signature mapping has been used to detect weld root corrosion [75]. Inspection measurements serve as an infrequent monitor for facilities. The inspection covers a large area and this is important as often some corrosion mechanism can be overlooked at the design stage. Correctly conducted inspections will ensure that such mistakes do not prove to be costly. Different strategies can be devised to make inspection strategies both effective and cost efficient [76]. Currently, most oil and gas production systems utilize risk-based methods to prioritize inspection [19]. Inspection methods compromise visual testing, radiographic testing, ultrasonic testing, magnetic particle testing, penetrant testing, and eddy current testing [19]. Corrosion monitoring provides an early indication for problems areas that may need more frequent inspection [19]. Ensuring that corrosion rates are kept below 2 mils per year at all monitoring locations allowed a facility to reduce the anticipated increase of yearly inspections as facilities ages [19]. In a properly designed asset integrity program, corrosion results are obtained from monitoring locations and inspection results should be compared. If necessary, the monitoring locations can be changed to reflect worst case inspection results. Equipment portability has made it convenient to use previously difficult to use equipment such as radiographic testing more frequently [24]. Remotely controlled drones carry cameras to inspect hard to access facilities [24]. Some low-cost inspection equipment such as drones with infrared cameras allows in-service inspection resulting in a decrease in equipment downtime [24]. Electromagnetic transducers allow inspection through coatings [24].

20.8 Monitoring for corrosion inhibitor optimization

Monitoring for corrosion inhibitor optimization requires one to have the ability to measure low corrosion rates. It is also ideal to have probes capable for measuring pitting corrosion. These may be weight loss coupons or EN or coupled multiarray electrode sensors. An electrochemical corrosion technique that utilized harmonic distortion analysis to determine Tafel slopes, and LPR was used to optimize corrosion inhibitor in a water injection system [77]. In systems containing oil, electrical resistance probes are often used. There is a tradeoff in electrical resistance probes between probe life and the smallest corrosion rate that can measured with the probe. Electrical resistance probes have been developed to be sensitive and allow corrosion inhibitor optimization [78]. Enhanced electrical resistance monitoring has been used to reduce the time of field evaluation of corrosion inhibitor for three-phase production pipelines where there is continuous field testing to measure and compare corrosion inhibitor performance [31]. Models incorporating both adsorption and partitioning in different phases of the line have been used to evaluate corrosion inhibitor performance in three phase flow lines [79]. Corrosive conditions vary with temperature, flow regime, water, and gas composition. In a program that is optimizing its corrosion dosage, these conditions need to be recorded to ensure that a comparison is made under similar conditions. Often this is difficult to do, as pressures and production decline with time.

20.9 Corrosion management and data organization

The fundamental aim of corrosion management is to improve safe operations and extend asset life. Corrosion management is essential to optimize corrosion control costs and reduce complexity [80]. This is achieved by organizing and storing information so that the organization can collectively reduce corrosion. An integrated corrosion management system consists of a corrosion control scheme, risk based inspection, corrosion risk assessment, and operation risk assessment [81]. A recommended practice for pipeline corrosion management has been compiled that covers risers, transportation pipelines, and trunklines for liquids, gases, and multiphase fluids, flowlines and gathering lines, manifolds, catenary/dynamic risers, pig launchers and receivers, flexible pipelines, and injection lines [82]. One part of the recommended practice is to store a full pipeline register that contains all basic data necessary to implement a corrosion management program [82]. Computerized corrosion management systems help store and organize information [83]. The corrosion management policy and the risk-based inspection process need to be part of the computerized system so that it provides warnings and alarms to responsible personnel when corrosion rates are high [83]. Computerization allows a rapid summary of overall conditions critical for asset integrity [83]. Implementation of corrosion management has been associated with the steady decrease in corrosion failures in offshore and onshore pipelines [84]. Probabilistic assessment is used to estimate the probability of failure with time [84]. It has been estimated that a corrosion management system has saved an oil company $3 million per annum in Nigeria [85]. Implementation of a corrosion management system in Oman led to a capital cost savings of $16 million and rapid assessment of the implications of a rupture caused by internal corrosion [86]. Integrated corrosion management systems have helped operators of gas gathering projects in Australia to optimize resources used for inspection and maintenance and decrease inspection work scope [87]. Installation of such a system saved a Western Canadian gas processing unit between $300,000 and $3 million by decreasing corrosion rates so that a vessel that may have required replacement in 3.3 years could operate such that replacement would be needed in 36 years [88]. Web-enabled corrosion management systems allow for easy access and easy input for all relevant personnel to the corrosion management system [89]. Best practices in the oil and gas industry utilize corrosion management systems with appropriate corrosion inhibition and corrosion monitoring. The use of this best practice allows one to economically and safely produce and transport oil and gas.

20.10 Summary and conclusions

In this chapter, corrosion monitoring to achieve safe and cost effective operation using corrosion inhibitors was discussed. Risk assessment needs to be conducted on the production and transmission system. Data need to be collected. Flow and corrosion

modeling should be performed on the process. A qualitative risk matrix should be created for the facility. Monitoring objectives need to be clearly stated. Monitoring locations should be chosen based on monitoring objectives and risk assessment. There are many methods to monitor corrosion in field applications. The methods are reviewed in this chapter. The methods that are commonly used are mass loss coupons and electrical resistance probes. Phenomena associated with corrosion should also be monitored. Water composition analysis, corrosion residuals, chemical injection rates, oil and water production rates, and sand production are commonly monitored in different oil and gas production and transmission facilities. Monitoring and inspection need to be augmented. Monitoring can be used to plan and schedule facility inspections. Inspection results need to be examined to corroborate the placement of monitoring devices. Different inspection methods were reviewed in the chapter. Monitoring to optimize corrosion inhibitor applications require the use of sensitive electrical resistance probes. Ideally, inhibitor evaluations need to be made under similar conditions. Data organization to collect and organize monitoring and inspection data in a manner to achieve quick and correct response to prevent corrosion failures and use correct inhibitor dosages is needed for safe and efficient operation. Corrosion management systems decrease operating costs and increase safety and asset life expectancy.

References

[1] P. Koul, H. Wang, C.A. Haarseth, Appraisal well data collection requirements for materials & corrosion risk assessment, concept selection and improved asset integrity, in: Twenty-fourth (2014) International Ocean and Polar Engineering Conference, Busan Korea, 15−20 June 2014, International Society of Offshore and Polar Engineers, 2014.

[2] NACE International, Internal Corrosion Direct Assessment Methodology for Pipelines Carrying Normally Dry Natural Gas (DG-ICDA), NACE Standard SP0206−2016, NACE International, Houston, Texas, 2016.

[3] NACE International, Wet Gas Internal Corrosion Direct Assessment Methodology for Pipelines, SP0110−2010, NACE International, Houston, Texas, 2010.

[4] P.O. Gartland, J.E. Salmonsen, A pipeline integrity management strategy based on multiphase fluid flow and corrosion modeling, Paper No. 622, in: CORROSION 1999, NACE International, Houston, Texas, 1999.

[5] A.R. Al-Shamari, S. Al-Sulaiman, A.W. Al-Mithin, J. Amer, S. Prakash, Pipeline integrity management through internal corrosion monitoring, Paper No. 3834, in: CORROSION 2014, NACE International, Houston, Texas, 2014.

[6] A.N. Moosavi, G. John, Use of corrosion & flow modeling for corrosion assessment of an oil & gas field, Paper No. 02253, in: CORROSION 2002, NACE International, Houston, Texas, 2002.

[7] I.A. Chaves, R.E. Melchers, Probabilistic risk assessment of welded offshore steel pipelines, in: Proceedings of the Twenty-third (2013) International Ocean and Polar Engineering Conference, Anchorage Alaska, June 30−July 5 2013, International Society of Offshore and Polar Engineers, 2013.

[8] P. Carr, Riser and pipeline corrosion risk assessment, in: OTC-24946-MS, Offshore Technology Conference Asia, Kuala Lumpur, March 2014, 2014.
[9] H. Duhon, J. Cronin, Risk assessment in HAZOP's, in: SPE 173544-MS Prepared for Presentation at SPE E&P Health, Safety and Environmental Conference Held in Denver, Colorado 16−18 March 2015, 2015.
[10] E. Oguski, S. McKenny, Indexing model for pipeline risk assessment and corrosion management, Paper No. 3781, in: CORROSION 2014, NACE International, Houston, Texas, 2014.
[11] M.J. Pursell, C. Selman, M.F. Nielsen, Corrosion risk assessment for sweet oil and gas corrosion-practical experience, Paper No. 9, in: CORROSION 1999, NACE International, Houston, 1999.
[12] S. Hodges, K. Spicer, R. Barson, G. John, K. Oliver, E. Tipton, High level corrosion risk assessment methodology for oil & gas systems, Paper No. 10367, in: CORROSION 2010, NACE International, Houston, Texas, 2010.
[13] I.J. Rippon, Corrosion management for an offshore sour gas pipeline system, Paper No. 05638, in: CORROSION 2005, NACE International, Houston, 2005.
[14] M. Lochmann, L. Denver, T. Berger, S.M. Stenseth, An objective indicator of change, in: SPE-173451, Paper Prepared for Presentation at the SPE Digital Energy Conference and Exhibition, the Woodlands, Texas, USA 3−5 March 2015, 2015.
[15] T. Pickthall, M. Rivera, M. McConnell, R. Vezis, Corrosion monitoring equipment, a review of application and techniques, Paper No. 11280, in: CORROSION 2011, NACE International, Houston, Texas, 2011.
[16] M.J.J. Simon Thomas, S. Terpstra, Corrosion monitoring in oil and gas production, Paper No. 03431, in: CORROSION 2003, NACE International, Houston, Texas, 2003.
[17] A.N. Moosavi, Corrosion monitoring in Abu Dhabi oilfields, in: SPE 37789 Paper Presented at the 1997 Middle East Oil Show Held in Bahrain 15−18 March 1997, 1997.
[18] M.M. Al-Arada, F.H. Al-Refai, S. Joshi, S. Patil, Effective corrosion management for enhancing mechanical integrity, Paper No.5908, in: CORROSION 2015, NACE International, Houston, Texas, 2015.
[19] B. Hedges, K. Sprague, T. Bieri, H.J. Chen, A review of monitoring and inspection techniques for CO_2 & H_2S corrosion in oil & gas production facilities: location, location, location!, Paper No. 6120, in: CORROSION 2006, NACE International, Houston, 2006.
[20] M.J.J. Simon Thomas, Corrosion inhibitor selection − feedback from the field, Paper No. 00056, in: CORROSION 2000, NACE International, Houston, Texas, 2000.
[21] L.A. Bensman, C. Byrnes, Use of an internal corrosion threat assessment to identify locations to conduct an integrity assessment, Paper No. 09148, in: CORROSION 2009, NACE International, Houston, Texas, 2009.
[22] L. Barton, D. Sadana, R. Ladwa, P. Birkinshaw, J. Soltis, Assessment of Pipeline Internal Corrosion of Challenging Pipelines through the Integration of Flow Modeling and Corrosion Risk Assessments, Paper presented in Multiphase 10, BHR Group, 2016.
[23] I.G. Winning, E. Belhimer, Practical aspects of field monitoring for corrosion, Paper No. 06411, in: CORROSION 2006, NACE International, Houston, Texas, 2006.
[24] B. Hedges, S. Papavinasam, T. Knox, K. Spraugue, Monitoring and inspection techniques for corrosion in oil and gas production, Paper No. 5505, in: CORROSION 2015, NACE International, Houston, Texas, 2015.
[25] NACE International, Techniques for Monitoring Corrosion and Related Parameters in Field Applications, Technical Committee Report 3T199, NACE International, Houston, Texas, 2012.

[26] NACE International, Preparation, Installation, Analysis and Interpretation of Corrosion Coupons in Oilfield Operations, Standard Practice, SP0775−2103, NACE International, Houston, Texas, 2013.
[27] S. Papavinasam, R.W. Revie, M. Attard, A. Demoz, K. Michael, Comparison of technique for monitoring corrosion inhibitors in oil and gas pipelines, Corrosion vol. 59 (12) (2015) 1096−1107.
[28] C.M. Menendez, Application of optical profilometric techniques to corrosion monitoring, Paper No. 2506, in: CORROSION 2013, NACE International, Houston, Texas, 2013.
[29] S. Ramachandran, V. Jovancicevic, G. Williams, K. Smith, C. McAfee, Development of a new high shear corrosion inhibitor with beneficial water quality attributes, Paper No. 10375, in: CORROSION 2010, NACE International, Houston, Texas, 2010.
[30] B.B. Brier, R.W. Bowman, G. Rose, A.J. Perkins, Corrosion monitoring in sour gas producing systems principles, practice and field experiences, in: SPE 18233, Paper Presented for 83rd Annual Technical Conference and Exhibition of the Society of Petroleum Engineers, 2−5 October 1988, 1988.
[31] T.H. Bieri, D. Horsup, M. Reading, R.C. Woolam, Corrosion inhibitor screening using rapid response corrosion monitoring, Paper No. 06692, in: CORROSION 2006, NACE International, Houston, Texas, 2006.
[32] T.G. Martin, M.T. Cox, R.H. Hausler, R.J. Dartez, P. Pratt, J.C. Roberts, Development of a corrosion inhibitor model II. Verification of model by continuous rate measurements under flowing conditions with a novel downhole tool, Paper No. 3, in: CORROSION 1999, NACE International, Houston, Texas, 1999.
[33] S. Papavinasam, A. Dorion, R.W. Revie, Industry survey on techniques to monitor internal corrosion, Materials Performance vol. 51 (2) (2012) 34.
[34] NACE International, Field Monitoring of Corrosion Rates in Oil and Gas Production Environments Using Electrochemical Techniques, Publication 31014, NACE International, Houston, Texas, November 2014.
[35] L.S. Shehorn, Corrosion monitoring on rod-pumped wells using linear polarization probes, in: SPE 9363, Paper Presented at the 55th Fall Technical Conference and Exhibition of the SPE Held in Dallas, Texas 21−24 September 1980, 1980.
[36] J.R. Scully, Polarization resistance method for determination of instantaneous corrosion rates, Corrosion vol. 56 (2) (2000) 199−217.
[37] A. Jurragh, S. Al-Sulaiman, A.R. Al-Shamari, B. Lenka, M. Islam, S. Prakash, Evaluation of the effectiveness of online corrosion monitoring utilizing ER/LPR probes and coupons within hydrocarbon systems, Paper No. 3934, in: CORROSION 2004, NACE International, Houston, 2004.
[38] S. Oliphant, S. Barr, H. Zaki, Use of electrochemical noise to monitor pipelines in oilfield applications, Paper No. 6424, in: CORROSION 2006, NACE International, Houston, Texas, 2006.
[39] A. Aballe, A. Bautista, U. Bertocci, F. Huet, Measurement of the noise resistance for corrosion applications, Corrosion vol. 57 (1) (2001) 35−42.
[40] R.A. Cottis, Interpretation of electrochemical noise data, Corrosion vol. 57 (3) (2001) 265−285.
[41] R.L. Martin, Corrosion consequences and inhibition of galvanic couples in petroleum production equipment, Corrosion vol. 51 (6) (1995) 482−488.
[42] J. Lerbscher, W. Wamburi, J. Bojes, Galvanic probes: a versatile monitoring technique to detect oxygen ingress, pH excursions, and other events in laboratory studies, Paper No. 1198, in: CORROSION 2012, NACE International, Houston, Texas, 2012.

[43] L. Yang, N. Sridhar, Coupled multielectrode array systems for real-time corrosion monitoring – a review, Paper No. 6681, in: CORROSION 2006, NACE International, Houston, Texas, 2006;
[43a] R.D. Kane, D.A. Eden, Electrochemical monitoring of corrosion in sour systems: fact and fiction of electrode bridging, fouling and other horror stories, Paper No. 05638, in: CORROSION 2005, NACE International, 2005.
[44] P.R. Roberge, V.S. Sastri, On-line corrosion monitoring with electrochemical impedance spectroscopy, Corrosion vol. 50 (10) (1994) 744–754.
[45] K.R. Cooper, M. Smith, J.R. Scully, N.D. Budiansky, Development of a multielectrode array impedance analyser for corrosion science and sensors, Paper No. 6674, in: CORROSION 2006, NACE International, Houston, Texas, 2006.
[46] Journal of Petroleum Technology, Young technology showcase: subsea corrosion/erosion monitoring, Journal of Petroleum Technology (December 2012) 40–45.
[47] S.R. Williams, A new non-invasive corrosion monitoring system, Paper No.260, in: CORROSION 1997, NACE International, Houston, Texas, 1997.
[48] G. Wallace, T. Champlin, Online asset integrity management and operational optimization through online integrity management, in: OTC-26895-MS Paper Prepared for Presentation at the Offshore Technology Conference Held in Houston, Texas, USA, 2–5 May 2016, 2016.
[49] A. Gajdacsi, F. Cegla, Nanometre precision ultrasonic corrosion monitoring, Paper No. 5664, in: CORROSION 2015, NACE International, Houston, Texas, 2015.
[50] O. Stawicki, T. Beuker, R. Ahlbrink, B. Brown, Monitoring of top of the line corrosion with eddy current combined with magnetic flux method, Paper No. 10094, in: CORROSION 2010, NACE International, Houston, 2010.
[51] P.C.N. Crouzen, I.J. Munns, W. Verstijnen, R.C. Hulsey, Application of pulsed eddy current corrosion monitoring in refineries and oil production facilities, Paper 06312, in: CORROSION 2006, NACE International, Houston, Texas, 2006.
[52] R.D. Tems, A.L. Lewis, A.I. Abdulhadi, Field and laboratoy measurements with hydrogen permeation devices, Paper No 02345, in: CORROSION 2002, NACE International, Houston, Texas, 2002.
[53] R.L. Martin, Inhibition of hydrogen permeation in steels corroding in sour fluids, Corrosion vol. 49 (8) (1993) 694–701.
[54] D.C. Eden, K.A. Esaklul, Deepwater corrosion monitoring: challenges and progress, Paper No. 4153, in: CORROSION 2004, NACE International, Houston, Texas, 2004.
[55] NACE International, Monitoring Corrosion in Oil and Gas Production with Iron Counts, NACE Standard Practice SP0192-2012, NACE International, Houston, Texas, 2012.
[56] N. Ghorbani, C. Yan, R.C. Tomson, D. Abdallah, A. Ben Aouda, N.M. Odeh, T.A. Al Daghar, An automated real-time produced water composition device for scale risk prediction, in: SPE-183158, Abu Dhabi International Petroleum Exhibition & Conference, UAE 7–10 November 2016, 2016.
[57] M.J.J. Simon Thomas, B.F.M. Pots, E.L.J.A. Hendriksen, Field corrosivity measurements—an essential component of the corrosion control process, in: CORRORION 2001, 2001.
[58] J.A.M. de Reus, E.L.J.A. Hendriksen, M.J.J. Simon-Thomas, Field corrosivity toolbox to optimize corrosion control, Paper No. 03315, in: CORROSION 2003, NACE International, 2003.
[59] E. Daher, N. Laycock, J.A.M. de Reus, E. Hendricksen, High availability corrosion inhibition and online monitoring for wet sour gas pipelines, in: IPTC-18282, International Petroleum Conference, Doha Qatar, 6–9 December 2015, 2015.

[60] B. Hedges, D. Paisley, R. Woolam, The corrosion inhibitor availability model, Paper No. 34, in: CORROSION 2000, NACE International, Houston, Texas, 2000.
[61] J. Marsh, T. Teh, Conflicting views: CO_2 corrosion models, corrosion inhibitor availbility philosophies and the effect on subsea systems and pipeline design, in: SPE 109209, Offshore Europe 2007, Aberdeen, Scotland, UK, 4−7 September 2007, 2007.
[62] I.J. Rippon, Corrosion control system availability management for reduced cost and extended life, Paper No. 03313, in: CORROSION 2003, NACE International, Houston, Texas, 2003.
[63] A. Crossland, J. Vera, A. Fox, S. Webster, G. Hickey, Developing a high reliability approach to corrosion inhibitor injection systems, Paper No. 10324, in: CORROSION 2010, NACE International, Houston, Texas, 2010.
[64] R.H. Hausler, T.G. Martin, D.W. Stegmann, M.B. Ward, Development of a corrosion inhibition model I. Laboratory studies, Paper No 2, in: CORROSION 1999, NACE International, 1999.
[65] K. Indo, K. Hsu, J. Pop, Estimation of fluid composition from downhole optical spectroscopy, in: SPE Jl, December 2015, pp. 1326−1338.
[66] P. Thodi, F. Khan, S. Imtiaz, Arctic pipeline integrity management using real-time condition monitoring, in: OTC-27322, Arctic Technology Conference St. Johns, Newfoundland and Labradour, 24−26 October 2016, 2016.
[67] F.L. Fariyibi, J.O. Umurhohwo, S.G. Olson, K.C. Scott, Acoustic sand monitor trials in the offshore CVX-NMA: results and lessons learned, in: SPE-88899, 28th Annual SPE International Technical Conference and Exhibition, 2−4 August 2004, 2004.
[68] A. Gupta, D. Kamat, N. Borhan, B. Madon, Z. Ahmad, Getting the best out of online acoustic sand monitoring system: a practical method for quantitative interpretation, in: International Petroleum Conference 2016, Bangkok, Thailand, 14−16 November, 2016.
[69] F.A. Hartog, G. Jonkers, A.P. Schmidt, R.D. Schuiling, Lead deposits in Dutch natural gas systems, SPE Production and Facilities (May 2002) 122−128.
[70] M.J. Guinee, E.W. Lamza, Cost effective methods to maintain gas production by the reduction of fouling in centrifugal compressors, in: SPE-30400, Offshore European Conference, 5−8 September 1995, Aberdeen, UK, 1995.
[71] S. Waker, G. Rosca, M. Hyton, In-line inspection tool selection, Paper 04168, in: CORROSION 2004, NACE International, Houston, Texas, 2004.
[72] M. Kondo, M. Kobayashi, M. Kurashima, Ultrasonic corrosion inspection of crude oil pipeline, Paper No. 525, in: CORROSION 1999, NACE International, Houston, Texas, 1999.
[73] T.M. Brill, J.L. Calvez, C. Demichel, E. Nichols, F.Z. Bermudez, Quantitative corrosion assessment with an EM casing inspection tool, in: SPE 149069, Saudi Arabian Technical Symposium & Exhibition, Al-khobar, Saudi Arabia, 15−18 May, 2011, 2011.
[74] T.M. Brill, J.L. Calvez, C. Demichel, E. Nichols, F.Z. Bermudez, Electromagnetic casing inspection tool for corrosion evaluation, in: IPTC 14865, International Petroleum Technology Conference, Bangkok, Thailand, 7−9 February, 2012, 2012.
[75] R. Johnsen, B.E. Bjorsen, D. Morton, D. Parr, B. Ridd, Weld root corrosion monitoring with a new electrical field signature mapping inspection tool, Paper No. 00096, in: CORROSION 2000, NACE International, Houston, Texas, 2000.
[76] P.M. Conder, K.I. McDonald, M. Stone, Inspection strategy: making pipework inspection both effective and cost efficient, in: SPE-179918, SPE International Oilfield Corrosion Conference and Exhibition, Aberdeen, Scotland, UK 9−10 May 2016, 2016.
[77] D.C. Eden, D.A. Eden, I.G. Winning, D. Fell, On-line, real-time optimization of corrosion inhibitors in the field, Paper No. 06321, in: CORROSION 2006, NACE International, Houston, Texas, 2006.

[78] B. Ridd, T.J. Blakset, D. Queen, Field trials for corrosion inhibitor selection and optimisation using a new generation of electrical resistance probes, Paper No. 78, in: CORROSION 1998, NACE International, Houston, Texas, 1998.
[79] H.J. Chen, G. Kouba, S. Lee, Optimizing corrosion inhibitor injection rate in flow lines, Paper No. 03626, in: CORROSION 2003, NACE International, Houston, Texas, 2003.
[80] R.B. Eckert, G.H. Koch, Improving corrosion control efficiencies using corrosion management principles, in: SPE-179945, SPE International Conference and Exhibition, 9−10 May 2016, 2016.
[81] P. Stokes, D. Sadana, L. Jones, Corrosion management-it's all gone holistic, in: SPE-169599, SPE International Oilfield Corrosion Conference and Exhibition, 12−13 May 2014, 2014.
[82] B. Kermani, T. Chevrot, Pipeline corrosion management; a compendium, Paper No. 3723, in: CORROSION 2014, NACE International, Houston, Texas, 2014.
[83] D.G. John, P. Attwood, A.N. Rothwell, Advances in integrated database systems for corrosion management of oil & gas production, Paper No. 249, in: CORROSION 1999, NACE International, Houston, Texas, 1999.
[84] J. Dawson, J. Race, S. Peet, R. Krishnamurthy, Pipeline corrosion management, Paper No. 01627, in: CORROSION 2001, NACE International, Houston, Texas, 2001.
[85] S. Okata, S. Ogbulie, T. George, How corrosion management system enhances pipeline integrity in oil and gas exploration and production company in the Niger Delta of Nigeria, Paper No. 03165, in: CORROSION 2003, 2003.
[86] P.A. Attwood, K.K. Bool, K. Van Gelder, Cost benefits derived from the implementation of a corrosion management system, in: SPE 36184, 7th Abu Dhabi International Exhibition and Conference, 13−16 October 1996, 1996.
[87] M.F. Nielsen, S. Bingham, Increasing availability − the benefits of introducing an integrated corrosion management system, SPE 50076, in: SPE Asia Pacific Oil & Gas Conference and Exhibition, Perth Australia, 12−14 October 1998, 1998.
[88] N. McGarry, A. Perkins, Improved asset management of a gas processing facility by an automated corrosion management system, Paper No. 01319, in: CORROSION 2001, NACE International, Houston, Texas, 2001.
[89] E.C. Dangleben, R.W. Dively, D.T. Greenfield, Web-enabled corrosion control management systems, Paper No. 04064, in: CORROSION 2004, NACE International, Houston, Texas, 2004.

Advances in testing and monitoring of biocides in oil and gas

21

Cameron Campbell
Kemira Chemical Inc., Houston, TX, United States

21.1 Current biocide practices for mitigating microbial problems

Microorganisms have been identified in oil and gas systems for almost 100 years [1], and today we know that they can and typically do cause problems in every facet of the oil and gas industry that lead to extremely costly microbial-related problems. In consideration of simply microbial influenced corrosion (MIC), the National Association of Corrosion Engineers has estimated that MIC costs the US oil and gas production industry approximately $1.372 billion a year, and MIC is estimated to account for as much as or more than 40%− 50% of all internal corrosion. Other problems that microorganisms may cause in the oil and gas industry are reservoir souring. Numerous papers have been published over the last 35 years extensively discussing the capability of sulfate-reducing bacteria (SRB) to sour reservoirs [2,3], plugging of the rock porosity leading to loss of production [4] or formation damage, emulsion formation with oil interfering with oil/water separation [5], and decreased flow-line and pipeline efficiencies. It would seem logical and convenient at this point to prevent or significantly limit the amount or type of bacteria that are in these oil and gas systems. However, it is not that simple. Microorganisms that are found in the oil and gas industry have two sources. The bacteria can be indigenous to the reservoir [6], or they can be introduced to the reservoir, process trains, tanks, and pipelines through the numerous operations that these systems endure from drilling, fracturing, stimulation, tertiary recovery, hydrotest, water bottoms for cathodic protection in tanks, etc.

Current biocide application practices for the oil and gas industry are very simple. The practices follow very closely the presence of oxygen as a primary decider for the category of biocide to use, which is then followed by the second decider for the biocide itself and the concentration to be applied. Theoretically, there are many factors that should influence the selection of a biocide to be used as well as the concentration and the application of the chemistry. However, the selection of the biocide, concentration, and application after establishing the category of chemistry, is typically status quo. The status quo is typically what chemistry is offered by the service company, what an operator is typically used to using, and one of the largest factors, cost. What should be driven by scientific data is actually more influenced by political and

Trends in Oil and Gas Corrosion Research and Technologies. http://dx.doi.org/10.1016/B978-0-08-101105-8.00021-8

preferential choices. Interestingly, through the review of numerous literature articles, the percentage of microbial problems in the oil and gas industry is continuing to increase, yet very little to no changes to biocides and their application are being implemented throughout the industry. With microbial problems rapidly accelerating within the oil and gas industry, and the lack of distinct improvements or optimization programs in the use and application of biocides, it is no wonder there appears to be a direct relationship. The standard biocide treatments of bimonthly, monthly, and quarterly will have absolutely no effect on the overall microbial populations within the system after a few hours following the biocide treatment. Standard continuous biocide treatments typically result in a failed mitigation approach as well. The standard biweekly batch treatment has shown some signs of microbial mitigation, but only when the right biocide was selected. These standard treatments are the status quo in the industry and have been so for an exceedingly long time considering bacteria were seen in oil and gas systems back in the 1920s, essentially over 100 years. It is the belief of some experts that these treatments have not changed because testing and monitoring programs have not evolved historically and have typically been insufficient to provide the data necessary to make the proper decisions, or to provide the testing data to even select the proper biocide in the very first step.

There is no one biocide that will work in all oil and gas systems. This must be realized in the industry to truly begin to advance even testing and monitoring technologies. As stated previously, biocides are the most common mitigation tool; thus it may be assumed that the biocide(s) are not mitigating the problems for which the standard application(s) were designed. Often, these same biocides are shown to control microbial-associated problems quite well in a laboratory situation following established industry practices, but do not perform well in the field. In both situations, the same standard monitoring is used, and that is typically bacterial growth media. Treatment efficacy is usually scored by monitoring changes in the population density of planktonic cells, determined by conducting a dilution series and calculating bacterial density using the Most Probable Number (MPN) approach or even more typically, a single serial dilution series. Therefore a common assumption must be made, that is, all SRB or acid-producing bacteria (APB), typical oil field bacteria as many believe, will respond similarly to chemical treatments and thus the specific identity of any SRB or APB is not important. This is almost certainly a gross simplification. By analogy, different bacterial species have intrinsically different responses to antibiotics, and thus there is no value in testing the effectiveness of antibiotic treatment on any organism other than the specific strain whose control is required. Various molecular tools, such as quantitative polymerase chain reaction (qPCR), microarrays, and high-throughput DNA sequencing technologies, have been introduced to more accurately dissect bacterial populations of relevance to the oil field. These advanced techniques have revealed that there is a larger microbial consortium that may be involved in MIC. This information is extremely important to enhance and develop a greater understanding of the resulting MIC corrosion mechanism, by understanding what bacteria are present and more directly what impact they have on the observed corrosion. However, currently, these techniques have not differentiated, or identified, a truly successful

mitigation program to address MIC. In addition, these are almost entirely limited to laboratory studies and are not widely used for field monitoring of treatment efficacy.

Another issue is that biocide efficacy tests focus on planktonic cells, whereas the organisms actually responsible for any given microbial problem are often growing in a biofilm. Planktonic and biofilm populations may have markedly different responses to chemical treatments. Much of this may be due to the structure of the biofilm. For example, the exopolysaccharide (EPS) matrix produced by biofilm organisms may exclude and/or influence the penetration of antimicrobial agents. Furthermore, bacteria in a biofilm may not be rapidly growing and thus can escape short-term chemical exposures. Poor penetration into, and reduced mass transport of the biocide chemicals within, the biofilm results in significantly less concentration of active biocide at the base of the biofilm where the problem actually exists.

Finally, environments have a profound effect on biocide efficacy. Typically, there are only two major concerns for the systems for applying biocides, and they are compatibility with the system such that the biocide chemistries do not damage the integrity of the system and the chemistries must be compatible with other chemistries and waters within the system. Numerous problems from foaming to emulsion formation and nullifying effects can occur. Interestingly, some biocides are sold trying to leverage their ability on extraneous reactions such as scale removal or sulfide removal. Ironically, when these chemistries have these cross-reactions, there is a significant decrease in the biocide efficacy, which is never discussed. This decrease in biocide efficacy will most likely result in microbial cell injury rather than death or have no biocidal efficacy at all. Injury is generally regarded as the sublethal physiological and/or structural consequence(s) that the microorganisms can repair and recover from very quickly.

Ultimately, there should be a significant pause before selecting and applying biocides to an oil and gas system to mitigate microbial problems. One must consider the advances in testing to understand and select the right biocide. Further consideration must be implemented to understand the advances in monitoring techniques and which techniques are going to best demonstrate the ability of a biocide to mitigate the problem. Finally, there should be consideration for advances in understanding biocide efficacy versus injury as well as our advances in understanding of biofilms and bacterial populations. Numerous steps should be implemented to drive new and advanced selection criteria, and as already eluded to in this discussion, advancements in testing and monitoring technologies will advance our understanding and ability to select and apply biocides such that a more effective and optimized mitigation strategy can be implemented.

21.2 Biocides mode of action, limitations, and advancements

21.2.1 Mode of action

To mitigate this microbial contamination through the majority of petroleum systems, many rely on the application of antimicrobials, biocides, to kill the bacteria present,

thus trying to eliminate microorganisms from these systems. There are a number of biocides on the market to be used for such purposes and they fall into two basic classifications. These classifications of biocides are inorganic, oxidizing, or organic, nonoxidizing. Inorganic or oxidizing biocides are biocides that kill bacteria by oxidizing protein groups within the cell, outside the cell, or in the cell wall or membrane itself, resulting in the loss of normal enzyme activity necessary for respiration and cell metabolism or disruption of the cell membrane itself. Examples of these biocides are chlorine, hypochlorous acid, bromine, chlorine dioxide, monochloramines, and peracetic acid. Organic biocides or nonoxidizing biocides describe special chemical agents that function by mechanisms other than oxidation, including interference with cell metabolism, structure, and DNA translation. Examples of these biocides are glutaraldehyde, tetra-kis-hydroxy-phosphonium sulfate (THPS), dazomet, 2,2-dibromo-3-nitrilopropionamide (DBNPA), quaternary ammonium compounds (Quats), and isothiazolines. There are two distinct systems within the oil and gas industry that require two different categories of biocides. The primary assumption within the oil and gas industry is that the majority of the systems are anaerobic, devoid of the presence of oxygen. However, this assumption is only plausible within the reservoir through the production train. Oxygen can be found in upstream water process systems, such as water injection systems, fracturing systems, hydrotest waters, and possibly tanks. The application of these two primary groups of biocides follows the division of the two very distinct systems within the oil and gas industry. Oxidizing biocides are used primarily when there is the presence of oxygen and nonoxidizing biocides are used through systems that are primarily anoxic, or devoid of oxygen. Nonoxidizing biocides are used primarily in anaerobic systems such as down hole within the reservoir downstream of deaeration equipment, production systems, and pipelines.

Inorganic biocides are considered to be nondiscriminatory, fast acting, and more corrosive. These biocides will typically oxidize organic molecules, which comprise the cell wall and cell membrane. By oxidizing the organic molecules associated with the cell wall and membrane, these biocides effectively destroy the cell for which the bacteria cannot be repaired. This oxidation is relatively quick, on the order of several minutes, but the true rate of kill is dependent on the concentration, pH, and organic load within the system.

Organic antimicrobial chemistries are considered to be more specific in their mode of action, longer acting, and considerably less corrosive than inorganics in situ. These organic antimicrobial chemistries up to recently were all grouped together as biocides. However, with advanced testing and monitoring, it became apparent that there were a couple of "biocides" that were actually preservatives. Therefore organic antimicrobial chemistries are subdivided into biocides and preservatives. Some examples of biocides are glutaraldehyde, DBNPA, THPS, and Quats. Biocides can be effective from 30 min to 6 h, and each has different target molecules whether it be cross-linking of exposed amine groups on exposed proteins, oxidation of cell walls, disruption of metabolic proteins, and membrane-active agents targeting predominantly the cytoplasmic membrane. Preservatives chemistries are typically very slow acting but with long-term control. These chemistries are dazomet, 4,4-dimethyloxazolidine (DMO) and 3,3′-methylenebis[5-methyloxazolidine] (MBO). The rate of biocidal efficacy is not

much of a concern for these chemistries as it is on the order of days, but rather how long the half-life of the chemistry is in relation to the water chemistry.

21.2.2 Limitation of biocides

In the oil and gas industry, oxidizing biocides have some very specific limitations. As the entire oil and gas industry comprises organic molecules, oil, these biocides can only be used in pure water systems or when there is oil carryover as a cleaning chemistry for the water quality. The pH of these waters has a profound effect on the free available molecule for biocidal action whether it is bromine, chlorine, or hypochlorous acid. Fig. 21.1 shows the percent active HOCl in relation to pH.

Therefore at a pH of 7 with a projection of 5 ppm of free available chlorine, only 50% active is truly available for biocidal activity, 2.5 ppm. Finally, as inorganic biocides react with anything organic, either organics or dissolved organics would react with the inorganic biocides, decreasing the overall concentration of the biocides, resulting in a decreased biocidal rate and efficacy.

Glutaraldehyde is a household name in the oil and gas industry. This biocide at one point has been used ubiquitously in every application possible in the industry. However, this does not suggest that it is the best biocide for the industry. Technically, glutaraldehyde is one of the most limited nonoxidizing biocides. The pH of many production systems may be 7 or lower. Glutaraldehyde efficacy, similar to that of chorine but opposite, is significantly limited by pH [7], as illustrated in Table 21.1.

Furthermore, there have been reports that glut can cross-react with polymers, even though it is nonionic (Excerpt from Dow's Gas and Oil Biocide Selection Guide). Finally, temperature and ammonium ions will reduce the efficacy of glutaraldehyde [8].

THPS is probably the next most popular biocide used in the oil and gas industry. This biocide is not used as diversely as glut, but it is used in many applications. However, as advances in testing and monitoring grow, a number of limitations for THPS are being revealed. Historically, THPS has been shown to be an effective biocide, an effective iron chelator, and an effective iron sulfide scale remover. Many researchers tested this biocide in the laboratory and saw that it was very

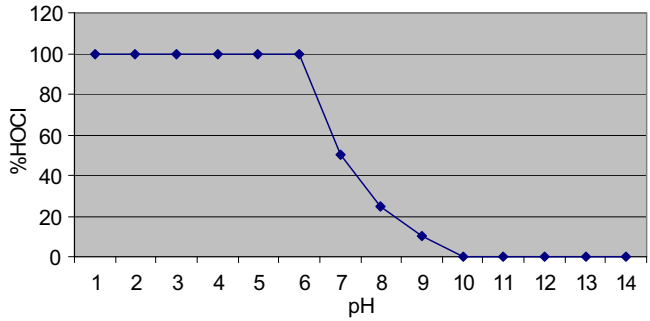

Figure 21.1 Relative percent active HOCl in relation to pH.

Table 21.1 Glutaraldehyde rate of kill versus pH

	pH 5.0	pH 6.5	pH 7.5	pH 8.0	pH 8.5
Time (hours)	**Microbial population (cfu/mL)**	**Microbial population (cfu/mL)**	**Microbial population (cfu/mL)**	**Microbial population (cfu/mL)**	**Microbial population (cfu/mL)**
0	10.5 E^7	10.5 E^7	10.4 E^7	10.4 E^7	10.3 E^7
1	10.5 E^7	10.5 E^7			0
1.5	10.5 E^7	10.4 E^7		0	
2	10.5 E^7	10.3 E^7	0		
3	10.5 E^7	10.5 E^6			
4	10.4 E^7	10 E^5			
4.5	10.3 E^7	0			
8	10 E^7				
10	10.7 E^6				
12	10.4 E^6				
14	10.8 E^5				
16	10 E^5				
18	10.4 E^4				
20	10 E^3				
22	0				

effective. However, applications in the field in certain systems revealed that it was not as effective as in the laboratory [9]. Campbell et al. [10] demonstrated that in the presence of ammonium ions, THPS would react with sulfide scales and soluble iron, significantly limiting the chemistry's biocide efficacy. This biocide is not, however, impacted by temperature.

DBNPA is a fairly popular biocide in the oil and gas industry. Interestingly, this biocide works very similarly as the oxidizing biocide bromine, but is not affected by pH as the oxidizing chemistry. However, this chemistry is significantly reactive to the presence of any sulfur molecules present in the system. Considering that many oil and gas systems have sulfur present, this should not be used as often as it is.

DMO and MBO are some of the more common preservatives used in the industry. However, these compounds are dependent on degradation to form formaldehyde. Aldehyde-based chemistries, such as glutaraldehyde, are dependent on the pH of the water and other chemistries to have a high level of efficacy.

Dazomet is a preservative that is used in numerous applications in the oil industry. This chemistry is not as compatible as others in relation to the presence of other

chemistries because of its alkaline nature as a neat chemistry. However, a very minimal separation of application between chemistries will minimize and prevent this cross-reaction. This chemistry will achieve a significant kill over a couple of days; however, it has demonstrated a prolonged control over a system in excess of 200 days with a single application.

21.2.3 Biocide advancements

As stated earlier, it is a gross simplification to assume that all bacteria will respond similarly to chemical treatments. In complement to this, biocide activity varies greatly between different types of microorganisms and it might also differ between different strains of the same species [11]. Therefore it does not seem plausible to simply select a biocide and apply it to a system. As different biocides have the potential to cross-react with components in the water or other chemistries, it is now strongly suggested that a complete water analysis is done through the system to find and understand these cross-reactions. Furthermore, in many oil and gas systems, there are combination systems. All of this dictates that advanced treatment systems are needed to fully mitigate systems with microbial problems. Two such advanced treatments are utilization of a pulse treatment method rather than batch and utilization of a dual biocide treatment system.

Finally, nanotechnology is the latest advancement in biocide technology that is just beginning to evolve. Over the past 15 years with significant legislation by the government, very strict governess is being placed on biocides because of their impact on the environment. Therefore the costs to design, test, evaluate, and register biocides may exceed $30 million. Therefore even the major corporations are searching for new ideas utilizing old biocides. It is conceivable that reducing the particle size or increasing the antimicrobial concentration to the levels applied in industrial systems [12–14] will increase the antimicrobial effects. Results obtained demonstrate that this novel biofilm control strategy may have potential public health, environmental, and economic benefits by effectively limiting the levels of biocides used in cleaning and disinfection practices [15].

21.3 Advanced testing revealing biofilms structure and microbial cell injury theory

Reports of corrosion failures in oil transportation pipelines implicating bacterial activity (in particular the activity of SRB) continue to appear in the literature and documented case histories [16]. This demonstrates that potentially many systems that are mitigating the risk of MIC with the use of biocides are still experiencing failures, suggesting that the biocide(s) are not mitigating the problems for which the application was designed. This, however, should come as no surprise, considering that within the petroleum industry, the majority of monitoring for bacteria to establish an MIC

risk is accomplished by enumerating bacteria from a planktonic sample. Therefore biocide efficacy testing is typically performed on these planktonic bacteria.

In relation to MIC, planktonic bacteria are not the problem; it is the sessile bacteria that pose a direct risk of MIC to a metal substratum. Understanding biocide efficacy against sessile bacteria, bacterial biofilms, cannot be accomplished by performing biocide efficacy studies against planktonic bacteria. Because growth rate is known to be a primary modulator of antimicrobial action and the recalcitrance of stationary phase cells (within biofilms), these controls (planktonic controls) are not only inappropriate but also misleading [17]. This not only demonstrates that planktonic biocide kill studies cannot be used to understand biocide efficacy against sessile bacteria but also suggests that there are several factors that directly impact biocide efficacy against bacteria within a biofilm, which begins to explain why planktonic kill studies are inappropriate. In addition to a reduced bacterial growth rate [17,18], and stationary phase of bacteria within biofilms, biofilms may provide a potent neutralization effect on compounds [19], influence gene expression and regulatory systems, initiating different phenotypes between planktonic and biofilm cells [20], and impose mass transfer limitations of nutrient and waste products [21], and, most importantly, biocides and antimicrobials. The EPS matrix, a component of biofilms, may exclude and/or influence the penetration of antimicrobial agents [22,23]. Exclusion of the impact of slow growth rate which has an attenuation on biocide efficacy; mass transport of the biocide chemistry within the biofilm poses the greatest limitation on biocide efficacy.

Factors that influence biocide efficacy against sessile bacteria are now being revealed. However, as stated previously, a number of these factors are a direct result of mass transport. Studies have been performed to understand the transport of biocides, nutrients, oxygen, etc. within biofilms. These studies have revealed that even with the presence of channels and pores within biofilms, the dominant transport mechanism is diffusion; thus decreasing gradients as measured from the bulk fluid/biofilm interface to the biofilm/substratum interface is established [24]. Brown and Gilbert [25] specifically stated that diffusion limitation by the glycocalyx together with localized high densities of cells creates gradients across the biofilm. Moreover, pores contribute to mass transfer only locally, and under low flow rates pores do not contribute considerably to global mass transfer [21]. Therefore as mass transfer is not significant within sessile bacterial populations, a diffusion gradient of nutrients and other chemistries including biocides is established as the transport through the biofilm. As stated previously, this phenomenon is further compounded by exclusion and/or reaction of the chemistry with the EPS. Ultimately, the concentration of the chemistry, and specifically in reference to this work, biocides concentration at the substratum/biofilm interface, will be considerably reduced from concentrations that are found in the bulk solution possibly approaching sublethal concentrations of antimicrobials at the substratum/biofilm interface.

The concept of bacterial injury has been widely used and is presently used to describe a temporary state in which an organism is unable to reproduce but still maintains limited metabolic capabilities [26]. Injury is generally regarded as the sublethal physiological and/or structural consequence(s) resulting from exposure to stressors,

such as suboptimal concentrations of disinfectants within aquatic environments [27]. Biofilms are resistant to biocidal treatments. With the potentiality that bacterial cell injury may be a result of biocide applications to mitigate MIC within the petroleum industry, current biocide treatment regimens to understand biocide efficacy in relation to "kill" versus "injury" have been evaluated. Campbell et al. [28] demonstrated that microbial injury is a real possibility to explain the rapid recovery of a biofilm following a biocide treatment. All biocide efficacy studies were performed utilizing a dynamic flow-cell system to mimic flowing systems as illustrated in Fig. 21.2. These dynamic flow cells were not recirculating loops where the biocide would either remain constant or would have to be physically removed but were once a dynamic flow-through system on a laboratory scale mimicking a pipeline or flow-line system. They observed an almost virtual recovery of the viable SRB within the biofilm on the biostuds within the flow cells after only 48 h. The doubling time of the viable SRB within the system was calculated utilizing the following growth rate equation [28]:

$$\mu = (\log_{10}N - \log_{10}N_0) \times 2.303/(t - t_0) \tag{21.1}$$

and the doubling time (dt) was determined according to the equation:

$$dt = t/g \tag{21.2}$$

where t = total time of the log phase of growth and g = the number of generations

$$g = (\log_{10}N - \log_{10}N_0)/\log_{10}2 \tag{21.3}$$

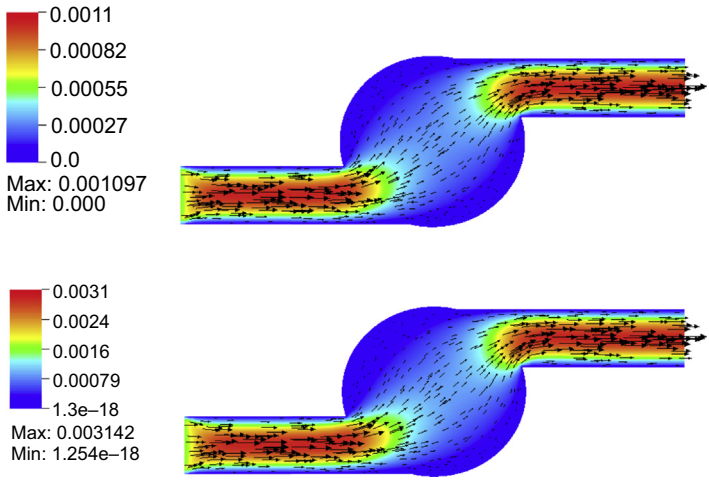

Figure 21.2 Midplane of flow cell with contours of velocity (m/s) magnitude and black velocity vectors (vector size proportional to magnitude) for the 2-mL/min case (top) and the 0.7-mL/min case (bottom). Because of the low volumetric flow rate, the flow is almost direct from the inlet to the outlet.

The growth rate for general heterotrophic bacteria (GHB), APB, and SRB following the glutaraldehyde treatment is 2.6, 2.6, and 2.4 h, respectively. For the THPS treatment, the growth rate for GHB, APB, and SRB is 2.2, 1.8, and 2.4 h, respectively. The reported approximate doubling time for SRB, in a consortium of viable bacterial population, will be over 20 h. However, in the most ideal conditions such as a pure culture, *Desulfovibrio vulgaris* has a reported doubling time of 3−5 h, and this was dependent on the energy source availability, H_2, and the appropriate carbon, acetate [29]. As these growth rates are not even close to well-documented and reported growth rates, it must be assumed that these growth rates represent not growth, but injured bacteria recovering that are still present within the natural system. Furthermore, biofilm cells will exist in a slow-growing state and in different metabolic states, making them less susceptible to antimicrobial chemicals [30,31]. These studies and the published literature confirm the presence of microbial cell injury theory in the oil and gas industry, and therefore current assumptions of biocide efficacy must be challenged. Further data could be obtained by implementing advanced monitoring techniques to demonstrate the presence of injured but viable bacteria.

21.4 Advanced monitoring techniques

Where there is water, there are microorganisms. Throughout the oil and gas industry, there is a significant amount of water from within the reservoirs, to stimulations programs and water bottoms in tanks; therefore there are numerous areas that have microorganisms that may cause problems. The real question is which of these microorganisms cause problems and which of these microorganisms actually help the system. Molecular methods are the tools that can provide the data necessary to differentiate these microorganisms, as well as understand the ecosystem as a whole for better biocide treatments. The key to these techniques lies with interpreting the data. However, the first step of understanding the data and what the data mean is paramount before we can understand the system. This is difficult because there are a number of advanced monitoring techniques that are being employed in the oil and gas industry to better understand those microorganisms that are present in the various oil and gas systems and the problems that they cause. There is also hope that these techniques will be able to reveal or assist in designing more effective biocide programs. One of the difficulties of monitoring with conventional methods such as using bacterial enumeration bottles is that only a small fraction of the microorganisms in a sample can grow under laboratory conditions on predefined growth media [32,33]. Therefore high bacterial numbers derived from cultivation-based techniques such as the MPN technique do not necessarily correlate to high SRB numbers causing MIC in a system, and conversely, viable SRB that cannot be cultivated will result in false-negative SRB counts, even though the noncultivated SRB might still be involved in MIC [34]. To further this discussion, it must be noted that the use of the terms “SRB” and “APB” are phenotypic, rather than genotypic, classification, and unrelated groups of bacteria are capable of acid production or sulfate reduction. In many cases, the focus is on

SRBs, yet the relative abundance and importance of sulfate-, sulfur-, and thiosulfate-reducing bacteria in generating H_2S in the oil field is unknown. Outside the fact that cultivation-based methods can only detect <10% of the total population, understanding the cosmopolitan population of bacteria in wells, pipelines, and storage and their influence on corrosion in the oil and gas industry is paramount and needs to happen.

Advancements in monitoring are providing incredible insights into oil and gas systems. Most of these techniques are culture-independent techniques, and thus do not require growing microorganism. Therefore, the insights that are being provided by advanced monitoring about the plethora of microorganisms within the system will provide a significant amount of information to increase our understanding of the ecosystem and the cosmopolitan populations within oil and gas systems. However, there are several considerations that must be made before implementing these techniques. Although the 16s rDNA approach, combined with other molecular techniques (fingerprinting methods, real-time qPCR), has a great potential for the analyses of oil field samples, there are many potential pitfalls when applying this method [35]. Currently, there are a large number of operators that have been applying these techniques. Consideration is needed for the significant volume of information that will be generated from these techniques as well as whom or what truly has the ability to accurately differentiate the large volume of data and interpret the results such that the data can be effectively applied to mitigating MIC, reservoir souring, etc. Second, as all these techniques rely on extraction of genetic information, extraction of the genetic material from oil field samples still requires significant efforts and further optimization. Furthermore, inadequate coverage of the selected PCR primers may not allow certain sequences to be discriminated compared with others [35]. Finally, different cloning efficiencies for 16s rDNA gene fragments from different organisms cannot be ruled out [35]. The following is a discussion about advanced techniques that are being implemented in the industry to better understand the bacteria involved in MIC.

21.4.1 Genetic hybridization methods

There are two fundamentally distinct techniques used in the oil and gas industry, although they are not prevalent at present with the application of PCR-related techniques. These hybridization techniques are fluorescent in situ hybridization (FISH) and microarray. FISH utilizes hybridization of rRNA targeted oligonucleotide probes that allow for the quantitative determination of mixed bacteria populations of a complex community in situ. These probes can be used for domain, division, genus, species, and subspecies specificity, but it is essential that the hybridization and wash solutions are adjusted for the specificity. However, to employ the FISH technique, an understanding of the organism present within the system is necessary; therefore these probes are designed and made against known organisms. Fig. 21.3 is an image of a noncorroding biofilm that was cryosectioned and the FISH technique was employed to understand the spatial distribution of bacteria present within the noncorroding biofilm [36].

Microarrays, another hybridization technique, can screen environmental samples for hundreds of bacteria at a time and give information on the presence or absence of a particular organism, but is not quantitative like FISH. Microarrays can be used

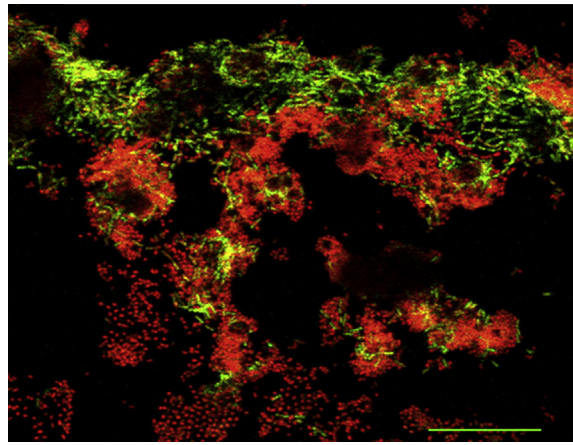

Figure 21.3 Fluorescent in situ hybridization image utilizing Oregon green with a propidium iodide counterstain. Scale bar is equivalent to 10 μm. *Leptothrix discophora* is represented as green, and when in contact with 316L stainless steel can potentially drive pitting corrosion [36].

to screen samples to obtain indications of the presence of certain microorganisms. This information can then be used in other methods (e.g., PCR-based methods) to quantify the results [35]. This technique has the ability to resolve phylogenetic relationships among the bacteria in oil and gas systems [37]; it provides poor resolution at the species level [38] and insufficient sequence information for determining the positive signal when a short oligonucleotide probe is used [35]. However, very powerful information can be obtained utilizing microarrays as demonstrated by Lee et al. [39]. They studied sublethal doses of biocides and showed that bacteria will not become immune to biocides, but rather will exhibit a defense by detecting what the cell requires to defend itself by making new proteins and new cell components and even the decision to leave a biofilm. Ultimately, this technique is still very important when evaluating genetic expression, but is giving way to PCR-based and fingerprinting methods in the oil and gas industry.

21.4.2 Fingerprinting methods

Fingerprinting techniques can provide the ability to fingerprint systems. Therefore a comparison can be made between a system that is not experiencing any microbial-related problems and a system that is experiencing microbial problems. This comparison between these two systems can then highlight the differences and further investigation into the differences can be made by potentially sequencing the problematic organism(s). Several methods are used for fingerprinting: denaturing gradient gel electrophoresis (DGGE), temperature gradient gel electrophoresis, terminal restriction fragment length polymorphism, and single-strand conformation polymorphism [35].

DGGE has been applied for over 10 years in the oil and gas industry. This method uses a constant heat and increasing concentration of denaturing chemicals that cause

the DNA to unwind or melt. At the point that the DNA molecule melts, it stops traveling in the gel matrix and creates a band when stained. The position at which the DNA melts depends on the quantitative content of the G-C (guanine−cytosine) bonds versus the A-T (adenine−thymine) bonds. Any variation of the DNA sequences within these domains will result in different melting concentrations of the gel matrix. Therefore a different cosmopolitan population within an oil and gas system can be compared with that within another and the bands, or fingerprints, can be compared. One of the significant strengths of this technique is that the different fingerprints or the bands can then be excised and sequenced. Therefore the DGGE technique can be combined with sequencing or PCR techniques to provide a more powerful evaluation technique to understand the microbiology within oil and gas systems.

21.4.3 PCR-based methods

PCR consists of cycles of constant heating, which melts the genetic double strand, and cooling, which allows for the enzymatic replication of the DNA. Primers are short DNA fragments containing sequences complementary to the target region along with a DNA polymerase, and these are used to initiate the replication process. As PCR progresses, the DNA generated is itself used as a template for replication. DNA polymerase is prone to error, however, which in turn causes mutation in the PCR fragments that are made. In addition, the specificity of the PCR fragments can mutate to the template DNA, due to nonspecific binding of primers. Thus there must be correction factors and screening to be able to remove inconsistent data or chimeras that are not valid. Nonetheless, this is a very powerful technique that is the backbone to numerous techniques, such as cloning, sequencing, quantitation, and fingerprinting. In the oil and gas industry, metagenomic sequencing, more specifically, pyrosequencing, which targets functional genome rather than the whole genome, and qPCR are applied extensively.

Pyrosequencing was used in conjunction with the gene clone libraries approach to study bacterial community in aqueous and oil phases of water-flooded petroleum reservoirs. However, pyrosequencing allowed the detection of more rare bacterial species than the clone library method [40]. Wang et al. further state that the research suggested that simultaneous analysis of DNA extracted from both aqueous and oil phases can facilitate a better understanding of the bacterial communities in water-flooded petroleum reservoirs. Pyrosequencing was used to study MIC and the authors concluded that identification of sulfur-oxidizing bacteria (SOB) and sulfate-reducing bacteria (SRB) indicates that sulfur is prevalent in the system, which indicates that MIC may be involved in the environment and that the application of this molecular method facilitated the collection of this information [41]. Furthermore, qPCR helps to further our understanding of the community structure and provides a quantification of the community structure. qPCR has even demonstrated that there was a dramatic change to the microbial community composition after the pipeline sample was inoculated to the growth media [42]. Ultimately, qPCR can be a functional gene-based analysis that can be successfully applied to the study of oil and gas systems to reveal the distribution, abundance, and functional interactions of the bacteria within the systems.

21.4.4 Flow cytometry

Flow cytometry is a laser-based technology that is used to count and sort cells, by suspending cells in a stream of fluid and passing them by an electronic detection apparatus. This method can allow for multiparametric analysis of up to thousands of particles per second, such as physical properties, chemical properties, fluorescence, and possibly morphology. This method can very accurately count cells within a system. Despite advances in molecular methods, oil field biocide efficacy testing still relies heavily on classical methodologies, such as serial dilution, which have disadvantages, such as the inability to culture all genera of Bacteria and Archaea and the amount of time needed to draw conclusions from results [43]. Thus bacterial enumeration is still very much important in monitoring programs throughout the oil and gas industry. An advanced technique such as flow cytometry can provide enumeration of bacteria very quickly and reliably while potentially providing more information about the viability or viable state of the microorganisms within the system. The ability of flow cytometry to detect and count individual cells together with its capacity to indicate specific physiologic states beyond alive or dead makes this technology particularly useful for studies with complex microbial populations, such as those encountered in the oil field [43].

21.5 Optimization

With the development and implementation of new testing such as true dynamic flow-through systems for biocide efficacy, as well as the implementation of advanced monitoring techniques, steps are being taken to better understand how to apply biocides and how to optimize treatments, as well as to explore alternative treatments. To discuss new biocide applications, alternative antimicrobial treatments, and optimizations separately is very difficult as optimization requires implementing the right applications as well as the right biocide, which may require alternative antimicrobial treatments. However, to be able to successfully implement an optimization program, each step must be fully understood: the selection of the right antimicrobial treatment, the right application, and the right monitoring technique.

21.5.1 Biocides, preservatives, and alternative antimicrobials

With the advancements in our understanding of the microbiology in oil and gas systems, testing, and monitoring, antimicrobial chemicals have progressed from simply biocides to involve preservatives and alternative treatments, such as nanotechnology, bacteriophages, and quorum sensing chemistries. Common biocides as discussed earlier, glutaraldehyde, THPS, and DBNPA, have been used extensively throughout the industry for well over half a century. Yet even with the application of these biocides, microbial problems continue to increase. Therefore it is now necessary to understand other types of treatments that, although are not the proverbial household name,

may actually provide a significant improved level of microbial control. Preservative biocides were introduced into the oil and gas industry approximately 10−15 years ago; however, they were quickly dispatched as they were not seen to work because the monitoring techniques did not actually successfully lend to the proper evaluations. These chemistries do not kill in the typically 2−6 h, but rather require days to achieve the control that is considered significant.

With the advancements in testing as well as our understanding of microbial cell injury, proper evaluations of preservative chemistries can now be accomplished. Biocide efficacy evaluations comparing a single treatment of glutaraldehyde with a single treatment of a preservative chemistry revealed that glutaraldehyde had a much more rapid reduction of viable SRBs, but only the preservative chemistry, dazomet, was able to maintain undetectable viable SRB after 28 days (Fig. 21.4) [44]. For example, drilling muds are contaminated with microorganisms and these microorganisms are known to degrade polymers, cellulose, lignosulfonates, and guar in drilling systems, which can lead to microbial contamination of the reservoir [45−47]. Long-term preservation utilizing a preservative biocide can be applied to drilling muds to preserve these muds both within the reservoir and in the storage.

Nanotechnology is defined as the engineering and utilization of materials, structures, devices, and systems at the atomic, molecular, and macromolecular scale, which have a nanoscale dimension roughly between 1 and 100 nm and frequently exhibit novel and significantly changed physical, chemical, and biological proprieties and functions resulting from their small structures [48,49]. Several engineered and natural nanomaterials have shown strong antimicrobial properties. Nanoparticles present other advantages such as high reactivity, unique interactions with biological systems, small size, and a large surface to volume ratio optimized for mass loading

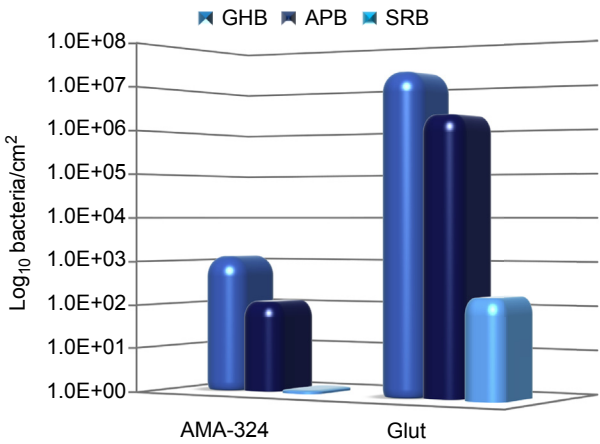

Figure 21.4 AMA-324 and glutaraldehyde against formation of sessile bacteria in synthetic frac water, pH 9.0, after 28 days with 1.0×10^6 bacteria/mL challenges at day 7 and day 14. No additional biocide treatment. *APB*, acid-producing bacteria; *GHB*, general heterotrophic bacteria; *SRB*, sulfate-reducing bacteria.

and carrying of antimicrobials [50,51]. Antimicrobials can be loaded into nanoparticles or physical encapsulations by adsorption or chemical conjugation and this can present several advantages such as significantly improved antimicrobial in contrast to the free product [52,53]. A commercially available antimicrobial chemical, FennoCide TR44, which is a nanopackaged biocide, was demonstrated to destroy biofilms at lower total amounts of active substance than by standard biocide products on the market, such that a higher proportion of added biocidal substances will reach the machine surfaces and be able to combat the microbial film effectively where it tends to grow.

The development of biocides is changing from chemical to biocidal utilizing viruses. This is unique as chemical biocides are nonspecific and can be very toxic to virtually all life forms. The new biocides, viruses, can be developed for specific organisms down to even a species level, and they would be host specific, thus not toxic to other life forms. These new viruses are known as bacteriophages. More specifically, the phages that are being targeted for application are bacteriolytic phages. These phages infect a bacterial cell and take over the genetic replication machinery, resulting in numerous copies of the new phages and lysis of the host cell. Upon lysis of the host cell, the cell is no longer viable. Phages are the abundant and diverse natural viral predators of bacteria and are composed of protein and DNA [54–57]. Although this technology is still under development and will be so for some time before commercial application, the use of phages for commercial applications is already a viable industry. Commercial phage products are available in the United States for controlling plant pathogenic bacteria on tomatoes and peppers as well as *E. coli* O157:H7 levels on slaughterhouse cattle [58]. These results are very promising. However, the development of effective phage products will ultimately depend on identifying or developing phage with expanded host ranges.

Finally, biocompetitive exclusion chemistries such as nitrates or nitrites are an important consideration. These chemistries are truly not new within the oil and gas industry, and have been around for 20+ years for water injection systems. However, what is new is the creative new application that these chemistries are being used for. These chemistries are not antimicrobial or biocidal, but they have the potential to significantly curtail SRB activity that leads to reservoir souring and corrosion. Essentially, nitrate works by the following methods: (1) It introduces competition for carbon. (2) It competes for the binding site of sulfate on SRB, not allowing sulfate to bind and be internalized for reduction. (3) The reduction of nitrate to nitrite increases the redox potential, shutting down SRB activity. (4) It stimulates the activity of NRSOB (nitrate reducing sulfur oxidizing bacteria) to utilize sulfide as an energy source, decreasing the amount of sulfide in a sour system. (5) It provides a better energy source for some SRBs that can utilize nitrate as an energy source, thus reducing the amount of sulfide produced. Nitrite is thought to work the same; however, it does not provide the first step of mitigation of SRB activity. In water floods, there are numerous reports that have documented the success of these treatments and the potential to remediate a sour reservoir. However, the conclusions as to the benefits that nitrite may provide to mitigate a sour reservoir are limited. Nonetheless, initial testing and measurements of nitrate treatments to mitigate corrosion are being performed with a level of success.

21.5.2 Chemical applications

Throughout the oil and gas industry, the applications of biocides have been nothing but extraordinarily consistent. These applications are biweekly, weekly, monthly, quarterly, and/or yearly. Sadly, these are applications that have been implemented but with no scientific data supporting them. What current data have shown is that these standard treatment applications are not working and quite possibly microbial problems are increasing because of their inadequacy. Every one of the above-mentioned treatments should never be considered for applications in any system except weekly and biweekly. This is because the doubling times of most bacteria is on the order of hours, and furthermore, biofilms can begin to form within minutes of microorganisms introduction to a system. Therefore any biocide treatment longer than weekly will have no significant impact on the mitigation of microbial activity and/or viable bacterial numbers, and thus there will be no significant mitigation of microbial problems within a system.

In consideration of preservatives, alternative antimicrobial treatments, and biocompetitive treatments, there can be no preprescribed treatment regimen in the industry as seen for the last 80 years. New and progressive steps must be taken to establish and discover new application programs for the oil and gas industry. For example, preservative biocides can stay within a system for a much longer period of time and thus retreatment will not be as necessary as required with a biocide. There is already discussion for biocide nanotechnology to significantly reduce the amount of biocide required as this technology can deliver a much higher dose per surface area of the microbial as compared with a traditional bulk solution treatment with the same biocide. Finally, in discussion of phage technology, one treatment of the appropriate phage may be all that is required for a definitive reduction in viable problematic bacteria as phages use the host microbial cell to propagate thousands of new viruses that can then continue the infection.

21.5.3 Monitoring and optimization

Successful mitigation of microbial problems within the oil and gas industry utilizing biocides begins with the selection of the appropriate mitigation chemistry whether it be a biocide or preservative. Second, optimization of the selected treatments in relation to costs and efficacy must be achieved. Therefore biocide efficacy testing must implement and follow rules accordingly to select a chemistry and its application that can be used in the field for optimized control over microbial problems. These rules are as follows:

1. *Replica Testing:* The selected chemistry(ies) must be tested appropriately in a system that mimics the real-world system, such as flowing test for pipelines, process trains, and water injection system; reactor testing with associated residence times for tanks; up-flow sand column testing for reservoir souring evaluations.
2. *Chemistry Leveraging:* Biocides, preservatives, biocompetitive chemicals and possibly phage treatments all have advantages and disadvantages. When designing antimicrobial treatments, consideration of leveraging advantages together in separated treatments such as a dual biocide treatment may be far more effective and overall more cost-effective.

3. *Targeted Approach:* The test must be more designed to target the problem of interest directly. If the problem is reservoir souring, then a minimal data set must include the production of sulfide. If the problem is MIC, then a minimal data set must include pitting corrosion analysis.
4. *Injury Versus Growth Considerations:* Bacteria are most vulnerable to chemical treatments when they are growing or recovering from injury. Therefore consideration of these vulnerabilities and when they exist in the system is needed before testing to establish and evaluate the application protocol.
5. *Monitoring Application:* Finally, the basic monitoring performed on the laboratory tests must be able to be applied to field evaluations and optimizations such that data can be compared.

A combination of replica testing and targeted approach utilizing reactors and Robbins devises can be very beneficial in understanding the proper chemical to use and application within a system. Therefore multiple systems can be evaluated simultaneously with more accuracy. Dickinson et al. [59] demonstrated this combination testing to evaluate the efficacy of a biocide and a preservative for mitigating MIC for a tank farm, but at a laboratory scale (Fig. 21.5).

The corrosion rate was significantly decreased in the flow line with the dazomet preservative biocide (Fig. 21.6). Furthermore, the testing revealed that treating the tanks with the preservative rather than trying to treat the tank and the transfer flow lines separately with biocides could protect the overall system. This evaluation was the first of its kind to demonstrate the capabilities of a preservative chemistry in the oil and gas industry. Therefore performing biocide efficacy testing focusing on the microbial problem such as corrosion rather than focusing on the kill efficacy can be done.

Certain operations within the oil and gas industry may require the ability of multiple biocides and therefore the implementation of chemistry leveraging. Hydrofracturing is a prime example of chemistry leveraging due to the operation of the process.

Hydrofracturing has an upstream system that is full of oxygen and has a very short residence time, thus oxidizing biocides would be the chemistry of choice for this

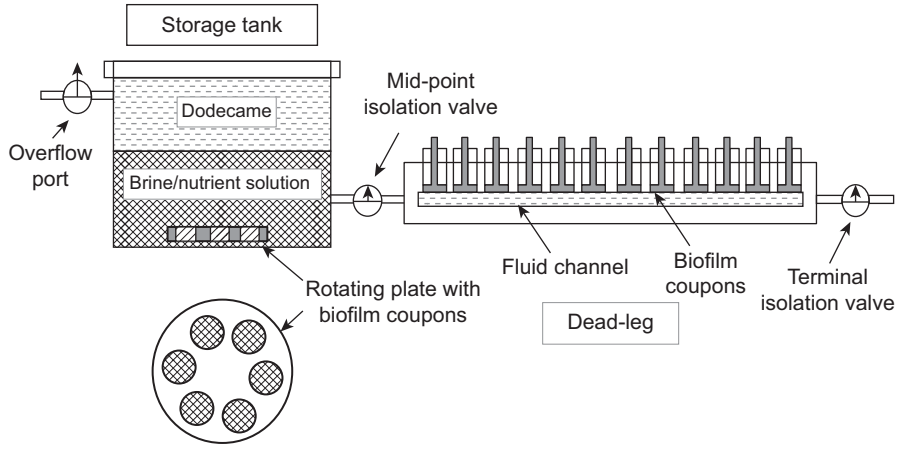

Figure 21.5 Design of laboratory tank farm to evaluate MIC on flow lines utilizing tank reactors and Robbins device [59].

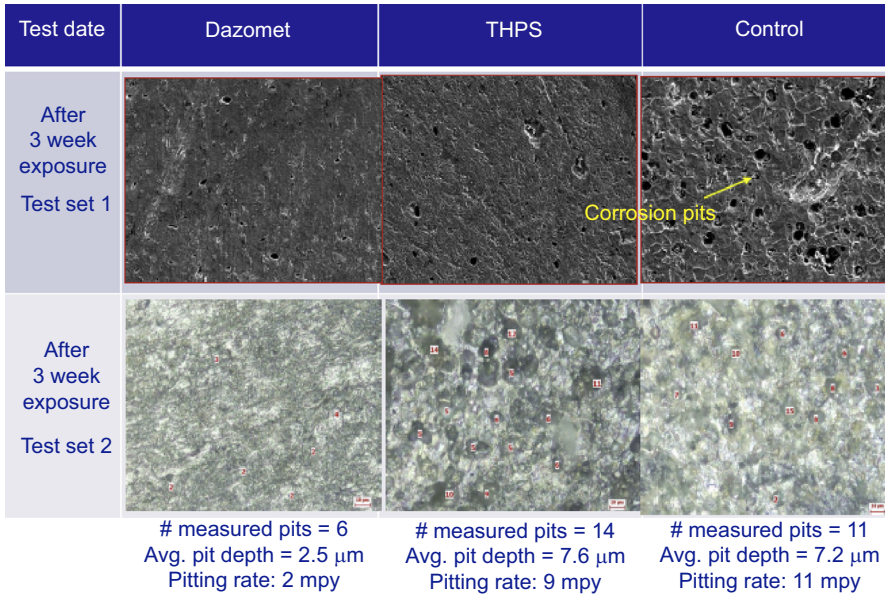

Figure 21.6 Scanning electron microscopy images of mild steel coupons that were within a flow-line laboratory scale model evaluating biocide efficacy for mitigating microbial influenced corrosion (MIC) damage. The preservative dazomet chemistry performed the best in preventing MIC damage [59].

system. However, downstream from here in the reservoir there is significant organic material; therefore oxidizing biocides will not work for full control. In the reservoir, inorganic biocides and/or preservatives would be the most effective. Campbell and Johnson [44] demonstrated that a dual biocide treatment system significantly brought the system under control and continued to reduce the viable bacteria over the course of 6 months as compared with other biocide treatments.

21.6 Summary

Advancements in testing and monitoring technologies have only recently been happening, yet in so many incidences, biocide applications are essentially the same as to what they were 30–40+ years ago. Utilizing only a handful of biocides with only a few effective applications has led to a significant increase in microbial-related problems in the oil and gas industry. Advancements in our understanding of the ecology of systems and how this influences microorganisms are leading to more and more advancements in testing and monitoring. The testing and evaluations of biocides are increasing our understanding of how chemistries truly control microbial populations. Furthermore, the advancements in monitoring have led to the identification of some bacteriophages that could in the future be a significant step toward controlling microbial problems. However, many of the monitoring advancements are at best

only revealing the complexity of these oil and gas systems and simply only providing insight into the complex system. Nonetheless, this is always the first step, and it is required to truly advance the science, knowledge, and eventually the ability to mitigate or even prevent problems.

Biocides themselves have not advanced much in the last 20−30 years as the costs behind them from development to registration are in many cases pushing $10 million. Therefore the advancements with testing and monitoring give us the ability to utilize the old chemistries in new ways that are far more functional and effective than we previously thought possible. Knowing the limitations of these chemistries because of advanced testing is leading to the development of new technologies such as nanopackaging of biocides or nanobiocides themselves. Although the majority of biocide evaluations for field applications are done against planktonic bacteria, advanced testing has revealed the specific need to evaluate chemistries against a specific environment as well as against sessile bacteria. There is no specific way to extrapolate planktonic kill data to be effective against sessile bacteria, or more specifically to sessile bacterial populations in virtually infinite different environments.

Finally, with advancements in testing and monitoring, a better understanding of microbial cell injury is being achieved, and thus a better understanding of biocide applications and a reuse of preservatives chemistries in the industry. Data are being revealed that demonstrate it is more important to preserve a system than achieve a quick kill due to microbial cell injury. With advanced testing, preservative chemistries have shown a capacity to control downstream systems utilizing upstream equipment, either by themselves or in conjunction with fast-acting biocides that can actually show an extended control in previously contaminated systems with very high microbial contaminates.

Through the discussion in this chapter, it is apparent that there is a significant push to bring new monitoring technologies into the oil and gas industry. However, these technologies are subject to a plethora of different interpretation possibilities as the data are not truly defined. Therefore it is important to utilize the data in a manner that will be beneficial to mitigating microbial problems. Optimization in the oil and gas industry is to achieve the most effective solution in relation to the best cost advantage. Optimization does not mean definitive control at all cost; it means an acceptable level of control at an acceptable level of cost. Therefore with the consideration of biocides, it is necessary to implement a set of rules to achieve the optimization desired. These rules are (1) Replica Testing; (2) Chemistry Leveraging; (3) Targeted Approach; (4) Injury Versus Growth Considerations; and (5) Monitoring Application. Optimization of systems is the sole reason that drives the advancement of testing and monitoring.

References

[1] E. Bastin, et al., The presence of sulphate reducing bacteria in oil field waters, Science 63 (1618) (1926) 21−24.

[2] D.J. Ligthelm, R.B. de Boer, J.F. Brint, W.M. Schulte, Reservoir Souring: An Analytical Model for H_2S Generation and Transportation in an Oil Reservoir Owing to Bacterial Activity, Society of Petroleum Engineers, Aberdeen, UK, 1991. Offshore Europe, September.

[3] B. Eden, P. Laycock, M. Fielder, Oilfield Reservoir Souring, HSE Books, 1993. Health and Safety Executive: Offshore Technology Report.
[4] M. Enzien, B. Yin, D. Love, M. Harless, E. Corrin, Improved microbial control programs for hydraulic fracturing fluids used during unconventional shale-gas exploration and production, in: SPE International Symposium on Oilfield Chemistry, The Woodlands, TX, 2011.
[5] L. Dorobantu, A.K.C. Yeung, J.M. Foght, M.R. Gray, Stabilization of oil-water emulsions by hydrophobic bacteria, Applied and Environmental Microbiology 70 (10) (2004) 6333−6336.
[6] M. Magot, Indigenous microbial communities in oil fields, in: B. Ollivier, M. Magot (Eds.), Petroleum Microbiology, ASM Press, Washington, DC, 2005, pp. 21−34.
[7] L. Grab, D. Emerich, S. Baron, N. Smolik, Glutaraldehyde: a new slimicide for papermaking, in: TAPPI Proceedings, 1990 Papermakers Conference, 1990, pp. 309−323.
[8] H. McGinley, M. Enzien, G. Jenneman, J. Harris, Studies on the chemical stability of glutaraldehyde in produced water, in: SPE International Symposium on Oilfield Chemistry, The Woodlands, TX, 2011.
[9] J. Wilmon, THPS Degradation in the Long-Term Preservation of Sub-Sea Flow-Lines and Risers, NACE International, Houston Texas, 2010. Paper 10402.
[10] C. Campbell, A. Cooper, Managing Microbial Influenced Problems in the Petroleum Industry by Understanding Biocide Functionality: Type, Application, and Limitation, AWT Convention, San Diego, CA, 2016.
[11] J.Y. Maillard, Bacterial target sites for biocide action, Journal of Applied Microbiology Symposium Supplement 92 (2002) 16S−27S.
[12] S.R. Block, Disinfection, Sterilization and Preservation, third ed., Leg & Feblgerpp, Philadelphia, 1983, pp. 309−329.
[13] J.W. McCoy, The Chemical Treatment of Cooling Water, second ed., Chemical Publishing Co., New York, 1983.
[14] G.L. Baker, R.J. Christensen, Composition Useful as Corrosion Inhibitor, Anti-Scalant and Continuous Biocide for Water Cooling Towers and Method of Use, US Patent no. 4710983, 1988.
[15] C. Ferreira, A.M. Pereira, L.F. Melo, M. Simoes, Advances in industrial biofilm control with micro-nanotechnology, in: Current Research, Technology and Education Topics in Applied Microbiology and Microbial Biotechnology, Formatex, 2010, pp. 845−854.
[16] S. Maxwell, S. Campbell, Monitoring the Mitigation of MIC Risk in Pipelines, in: Paper 06662. NACE Corrosion 2006, March 2006, San Diego, USA, 2006.
[17] M.R.W. Brown, P. Gilbert, Sensitivity of biofilms to antimicrobial agents, Journal of Applied Bacteriology Symposium Supplement 74 (1993) 87S−97S.
[18] P.A. Suci, J.D. Vrany, M.W. Mittelman, Investigation of interactions between antimicrobial agents and bacterial biofilms using attenuated total reflection Fourier transform infrared spectroscopy, Biomaterials 19 (1998) 327−339.
[19] X. Xu, P.S. Stewart, X. Chen, Transport limitation of chlorine disinfection of *Pseudomonas aeruginosa* entrapped in alginate beads, Biotechnology and Bioengineering 49 (1996) 93−100.
[20] C. Campanac, L. Pineau, A. Payard, G. Baziard-Mouysset, C. Roques, Interactions between biocide cationic agents and bacterial biofilms, Antimicrobial Agents and Chemotherapy 46 (5) (2002) 1469−1474.
[21] M.C.M. Van Loosdrecht, J.J. Heijnen, H. Eberl, J. Kreft, C. Picioreanu, Mathematical modeling of biofilm structures, Antonie van Leeuwenhoek 81 (2002) 245−256.
[22] R.O. Darouiche, A. Dhir, A.J. Miller, G.C. Landon, Raad II., D.M. Musher, Vancomycin penetration into biofilm covering infected prostheses and effect on bacteria, Journal of Infectious Disease 170 (3) (1994) 720−723.

[23] W.W. Nichols, Biofilms, antibiotics and penetration, Review of Medical Microbiology 2 (1991) 177−181.
[24] S. Campbell, G.G. Geesey, Z. Lewandowski, G. Jackson, Influence of the distribution of the manganese-oxidizing bacterium, *Leptothrix discophora*, on ennoblement of type 316L stainless steel, Corrosion 60 (7) (2004) 670−680.
[25] M.R.W. Brown, D.G. Allison, P. Gilbert, Resistance of bacterial biofilms to antibiotics: a growth-rate related effect, Journal of Antimicrobial Chemotherapy 22 (1988) 777−783.
[26] S.K. Zaske, W.S. Dockins, G.A. McFeters, Cell envelope damage in *Escherichia coli* caused by short-term stress in water, Applied and Environmental Microbiology 40 (2) (1980) 386−390.
[27] G.A. McFeters, M.W. LeChevallier, Chemical disinfection and injury of bacteria in water, in: R.R. Colwell, D.J. Grimes (Eds.), Non-culturable Microorganisms in Environment, ASM Press, Washington, DC., 2000, pp. 255−275.
[28] C. Campbell, A. Duggleby, A. Johnson, Conventional application of biocides may lead to bacterial cell injury rather than bacterial kill within a biofilm, in: NACE International Corrosion, Houston TX, 2011. Paper 11234.
[29] A. Brandis, R. Thauer, Growth of *Desulfovibrio* species on hydrogen and sulphate as sole energy source, Journal of General Microbiology 126 (1981) 249−252.
[30] J.W. Costerton, P.S. Stewart, E.P. Greenberg, Bacterial biofilms: a common cause of persistent infections, Science 284 (5418) (1999) 1318−1322.
[31] P. Gilbert, D.G. Allison, A.J. Mcbain, Biofilms in vitro and in vivo: do singular mechanisms imply cross-resistance? Symposium Series (Society for Applied Microbiology) 31 (2002) 98S−110S.
[32] R. Amann, W. Ludwig, K.H. Schleifer, Phylogenetic identification and in situ detection of individual microbial cells without cultivation, Microbiological Reviews 59 (1995) 143−169.
[33] M. Davies, P.J.B. Scott, Oilfield Water Technology, NACE − National Association of Corrosion Engineers, 2006, p. 249.
[34] J. Larsen, K. Rasmussen, K. Sorensen, T. Lundgaard, T. Skovhus, Consortia of MIC bacteria and Archaea causing pitting corrosion in topside oil production facilities, in: NACE Conference and Expo, 2010. No. 10252.
[35] H. Hoffmann, C. Devine, S. Maxwell, Application of molecular microbiology techniques as tools for monitoring oil field bacteria, in: NACE International Conference and Expo, 2007. No. 7508.
[36] Campbell, C. Influence of the Distribution of the Manganese Oxidizing Bacterium, *Leptothrix discophora*, on Ennoblement of 316L Stainless Steel (thesis), Montana State University − Center for Biofilm Engineeering, 2003.
[37] J. Small, D.R. Call, F.J. Brockman, T.M. Straub, D.P. Chandler, Applied and Environmental Microbiology 67 (2001) 4708.
[38] I. Dahllof, Current Opinion in Biotechnology 13 (2002) 213.
[39] M.H.P. Lee, S.M. Caffrey, J.K. Voordouw, G. Voordouw, Effects of biocides on gene expression in the sulfate-reducing bacterium *Desulfovibrio vulgaris* Hildenborough, Applied Microbial and Cell Physiology 87 (2010) 1109−1118.
[40] L.Y. Wang, W.J. Ke, X.B. Sun, J.F. Liu, J.D. Gu, B.Z. Mu, Comparison of bacterial community in aqueous and oil phases of water-flooded petroleum reservoirs using pyrosequencing and clone library approaches, Applied Microbiology and Biotechnology 98 (9) (2014) 4209−4221.
[41] J. Mand, T. Jack, G. Voordouw, H. Hofmann, Use of molecular methods (pyrosequencing) for evaluating MIC potential in water systems for oil production in the North Sea, in: SPE International Oilfield Corrosion Conference and Exhibition, 2014. No. 169638.

[42] X. Zhu, J. Kilbane, A. Ayuala, H. Modi, Application of quantitative, real-time PCR in monitoring microbiologically influenced corrosion (MIC) in gas pipeline, in: Corrosion Conference, Houston TX, 2005. No. 5493.
[43] T. Tidwell, R. De Paula, M.Y. Smadi, V. Keasler, Flow cytometry as a tool for oilfield biocide efficacy testing and monitoring, International Biodeterioration and Biodegradation 98 (2015) 26−34.
[44] C. Campbell, A. Johnson, Dual Biocide Application for Optimization of Microbial Control in Hydrofracture Fluids: Leveraging Biocide Strengths, AWT Convention, Memphis, TN, 2015.
[45] G.R. Gray, H.C.H. Darley, W.F. Rogers, Composition and Properties of Oil Well Drilling Fluids, Gulf Publishing Co., Houston TX, 1980.
[46] F. Baldi, et al., Dissolution of barium from barite in sewage sludges and cultures of *Desulfovibrio desulfuricans*, Applied and Environmental Microbiology 62 (1996) 2398−2404.
[47] L. Pereyra, S. Hiibel, M. Prieto Requelme, K. Reardon, A. Pruden, Detection and quantification of functional genes of cellulose-degrading, fermentative, and sulfate-reducing bacteria and methanogenic archaea, Applied and Environmental Microbiology 76 (2010) 2192−2202.
[48] M.C. Roco, Nanotechnology: convergence with modern biology and medicine, Current Opinion in Biotechnology 14 (3) (2003) 337−346.
[49] J. Theron, J.A. Walker, T.E. Cloete, Nanotechnology and water treatment: applications and emerging opportunities, Critical Reviews in Microbiology 34 (1) (2008) 43−69.
[50] E. Weir, A. Lawlor, A. Wheland, F. Regan, The use of nanoparticles in anti-microbial materials and their characterization, Analyst 133 (7) (2008) 835−845.
[51] E.N. Taylor, T.J. Webster, The use of superparamagnetic nanoparticles for prosthetic biofilm prevention, International Journal Nanomedicine 4 (2009) 145−152.
[52] L. Zhang, F.X. Gu, J.M. Chan, A.Z. Wang, R.S. Langer, O.C. Farokhzad, Nanoparticles in medicine: therapeutic applications and developments, Clinical Pharmacology and Therapeutics 83 (5) (2008) 761−769.
[53] L. Zhang, D. Pornpattananangkul, C.M.J. Hu, C.M. Huang, Development of nanoparticles for antimicrobial drug delivery, Current Medicinal Chemistry 17 (6) (2010) 585−594.
[54] A.M. Kropinski, Phage therapy − everything old is new again, Canadian Journal of Infectious Disease and Medical Microbiology 17 (5) (2006) 297−306.
[55] L. Zhang, P. De Schryver, B. De Gusseme, W. De Muynck, N. Boon, W. Verstraete, Chemical and biological technologies for hydrogen sulfide emission control in sewer systems: a review, Water Research 42 (1−2) (2008) 1−12.
[56] J.A. Thomas, J.A. Soddell, D.I. Kurtboke, Fighting foam with phages? Water Science and Technology 46 (1−2) (2002) 511−518.
[57] L. Goodridge, T. Abedon Stephen, Bacteriophage biocontrol and bioprocessing: application of phage therapy to industry. Feature Article, 254, 2003.
[58] R.L. Calendar, The Bacteriophages, second ed., Oxford University Press, New York, 2006.
[59] W. Dickinson, S. Campbell, V. Turk, Tank reactor studies of biocide performance and mitigation of dead-leg corrosion, in: NACE International Corrosion, Salt Lake City, UT, 2012.

Further reading

[1] J. Larsen, T. Skovhus, T. Thomsen, Bacterial diversity study applying novel molecular methods on Halfdan produced waters, in: NACE Corrosion San Diego, 2006 paper 06668.

Molecular microbiology techniques

22

Xiangyang Zhu and Mohammed A. Al-Moniee
Saudi Aramco, Dhahran, Saudi Arabia

22.1 Introduction

Petroleum is a complex mixture of hydrocarbons and other organic compounds. Hydrocarbon-metabolizing microorganisms are widely distributed in oil reservoirs and related downstream operation processes. Approaches to characterizing and understanding microbial diversity and community function can be broadly divided into culture-dependent and culture-independent methods. Traditional culture-dependent methods are based on differential morphological, metabolic, and physiological traits [1]. These include isolation and cultivation of microorganisms on selective media and the assessment based on colony morphology, color or culture turbidity, media color change. Traditional culture techniques have yielded valuable information about microbial interactions with hydrocarbons in the environment; however, there are many weaknesses associated with culture-dependent approaches. The most significant is that only a small fraction (0.1%−10%) of indigenous species can be cultured from environmental samples [2−4]. Therefore, culture-dependent approaches may severely underestimate the biocomplexity and misrepresent the true composition of microbial communities in the original environment [5,6].

Many culture-independent molecular microbiology techniques have been developed in the past decades. Molecular techniques have revolutionized microbial ecological studies in microbial characterization and enumeration in an environmental system. These methods are based on direct extraction of nucleic acids from natural samples, thus overcoming the difficulties associated with the laboratory cultivation of microorganisms and providing more detailed and comprehensive representation of an environment's microbial diversity and insight into gene functions [7,8].

Most molecular techniques are driven by polymerase chain reaction (PCR), which amplifies specific gene sequences from target microorganisms. 16S ribosomal RNA (rRNA) gene is the most important gene in microbial ecology research in determining the phylogenetic diversity of prokaryotes. 16S rRNA gene has highly conserved, variable, and hypervariable regions [9]. PCR primers targeting the conserved regions amplify the 16S rRNA genes from almost all bacterial and archaeal species, and the primers targeting the variable and hypervariable regions amplify the 16S rRNA gene from a small selection of closely related microorganisms at genus or species levels [10,11]. Although 16S rRNA genes have been used for characterization of phylogenetic diversity, functional genes have also been targeted to study the metabolic processes in a given environment [12]. For instance, sulfate reduction process, which

Trends in Oil and Gas Corrosion Research and Technologies. http://dx.doi.org/10.1016/B978-0-08-101105-8.00022-X

converts sulfate to hydrogen sulfide, is of great economic importance to oil industry. A function gene that encodes dissimilatory sulfite reductase (DSR) has been widely used as PCR primer target to characterize and monitor the phylogenetically diverse sulfate reducers present in oil industry systems.

Development and implementation of molecular microbiology techniques have benefited the oil industry in many areas such as reservoir souring and mitigation, microbial corrosion monitoring and diagnosis, oil recovery and upgrading, and oil pollution and bioremediation. The following sections describe molecular microbiology techniques widely used in oil and gas industry. The advantages and limitations of each technique are outlined and the applications in petroleum industry are illustrated with some case studies.

22.2 Molecular microbiology techniques

22.2.1 DAPI, cell viability staining, and fluorescent in situ hybridization

The 4′,6-diamidino-2-phenylindole (DAPI) is a cell permeable, blue fluorescent dye that binds to double-stranded DNA (dsDNA) and thereby detects all intact microorganisms (both living and inactive). DAPI method can be used to quantify total cell number in almost any type of liquid samples such as injection water, produced water, utility water, and fuel samples [13,14]. The stained cells are counted directly under an epifluorescence microscope. DAPI can also be used to fluorescently label cells for analysis in multicolor flow cytometry experiments because its blue fluorescence stands out in vivid contrast to green, yellow, or red fluorescent probes of other structures. However, if it is desired to know the cell viability, for instance, before and after a biocide treatment, cell viability staining is a better method to monitor the general bacteria population.

Cell viability staining uses two-color fluorescent dyes targeting the nucleic acids in live or dead cells based on whether or not the cytoplasmic membrane of the cell is intact. A green-fluorescent nucleic acid dye (e.g., SYTO-9) is cell membrane penetrative and stains both live and dead bacteria with intact and damaged cell membranes, whereas a red-fluorescent nucleic acid dye (e.g., propidium iodide) only penetrates damaged cell membranes and stains dead bacteria. With an appropriate mixture of two dyes, bacteria with intact cell membranes stain fluorescent green, whereas bacteria with damaged cell membranes stain fluorescent red. The stained cells can be directly counted using fluorescence microscope or flow cytometer for high-throughput analysis or detected by fluorescence microplate reader. However, it may be difficult to differentiate between dead cells and nonliving matter in natural samples stained for viability. Another limitation, which is also true for DAPI staining, is that cell viability staining cannot differentiate among microbial species and thus cannot measure species diversity.

Fluorescent in situ hybridization (FISH) is a more robust technique if both the number and activity of microbial population in an environmental sample are of interest and if species diversity in the sample is also of interest. In a FISH technique, a probe is

designed to target a specific gene sequence of interest and labeled with a fluorescent dye. FISH technique can detect and quantify the whole population of active prokaryotes by designing the probe to target the highly conserved regions of 16S rRNA genes. FISH technique can also detect and quantify a specific group of microorganisms or an individual species by designing the probes to target the variable and hypervariable regions of 16S rRNA genes. When the fluorescence-labeled gene probe enters the cells and hybridizes with the complementary target sequence, the target cells fluoresce and can be visualized under the fluorescence microscope. Using different fluorophores, more than one group of microorganisms can be studied at a time. With confocal microscopy, the spatial distribution of microbial communities in a biofilm can also be studied [15].

In petroleum industry, DAPI, cell viability staining, and FISH have been used as rapid analytical methods to detect and monitor the various microorganisms (bacteria, archaea, fungi) in pipelines, fuel storage, and transport system, and water system (injection water, cooling water, produced water, and drinking water) [16,17], evaluating biocide treatment, fuel degradation, and microbiologically influenced corrosion (MIC) risk. However, these techniques are not suitable for samples in which cells form aggregates, are attached to substrates, or embedded in a solid matrix (e.g., scale, biofilm, and sediment) as individual cells cannot be differentiated in the mass. Finally, cells at high density may be difficult to quantify, necessitating a dilution of the sample.

22.2.2 PCR, quantitative PCR, and quantitative reverse transcription PCR

PCR is the technique most commonly used to selectively amplify a particular gene or set of genes of individual species, groups of related species, or even all microorganisms in the environment. When targeting 16S rRNA gene, PCR primers can be designed to amplify the gene from a small group of related microorganisms or can be universal and amplify nearly all bacterial and archaeal species [10,11]. PCR primers can also be designed to target various functional genes present in an environment, providing an indication of the biological processes in the environment [12].

22.2.2.1 PCR

In conventional PCR, minute amount of DNA in the original samples is amplified through many (25−45) amplification cycles using a thermocycler. In general, each amplification cycle consists of three steps: (1) denaturation step where the template dsDNA is denatured to single-stranded DNA (ssDNA) at temperature of 94−95°C (194−203°F); (2) annealing step where the forward and reserve PCR primers anneal to each complimentary strand of the ssDNA at the temperature around 55°C (133°F) (the optimal annealing temperature depends on primer length and composition); and (3) elongation step where the *Taq* DNA polymerase catalyzes the extension of the annealed primers along the sequences of ssDNA, generally at the temperature of 72°C (162°F), to produce two dsDNA molecules. It is also common at the end of

amplification cycles, a single temperature step (often 5−10 min at 68−72°C or 154−162°F) is added to promote the complete synthesis of all PCR products. Once the PCR is complete, the thermal cycler is set to 4°C (39°F) to maintain product integrity until the PCR tubes are removed from the machine.

After the completion of cyclic reaction, the PCR products can be visualized on an agarose gel after gel electrophoresis and staining with a dye such as ethidium bromide. The detection of the band with the expected size is often used as an indicator for positive identification of a gene or microbial species of interest. However, the intensity of the band is not necessarily proportional to the amount of DNA in the original sample. Therefore, the major drawback of conventional PCR is that the PCR products can only be visualized at the end of amplification and are only semiquantitative at best [18].

PCR products can be used in many post-PCR fingerprinting techniques to estimate the microbial diversity and determine the microbial identity (e.g., cloning and sequencing).

22.2.2.2 Quantitative PCR and propidium monoazide-quantitative PCR

Unlike conventional PCR where the PCR amplicons are visualized at the end of the reaction cycles by staining and gel electrophoresis, PCR amplicons in quantative PCR (qPCR) can be visualized at each amplification cycle as amplification progresses using fluorescent reporter molecules such as SYBR Green dye. The quantification of fluorescent intensity of PCR products takes place at the exponential stage of PCR amplification, where the fluorescent intensity is in direct proportion to the amount of DNA present in the initial sample.

qPCR has been adapted to provide rapid and more accurate data concerning the quantity of various types of microorganisms present in gas and oil industry samples. Domain-specific primer and probe sets have been developed for qPCR assays to detect and quantify the total bacteria and archaea in the environmental samples by targeting 16S rRNA genes. Similarly primer and probe have also been developed to detect and quantify a subgroup of bacteria and archaea populations, such as sulfate-reducing bacteria (SRB), denitrifiers, and methanogens by targeting the function genes *dsrAB* [19,20], *nirS* [21,22], and *mcrA* [23,24], respectively. These genes encode enzymes that play crucial roles in the metabolic pathways of sulfate reduction, denitrification, and methanogenesis, respectively, and thus constitute highly specific targets to allow a more precise quantification of these types of microbes than can be achieved using microbial growth tests. qPCR offers a dynamic detection range of six orders of magnitude or more [25], does not need post-PCR manipulation such as gel electrophoresis, and has the capability of high-throughput analysis. In addition, qPCR also works for any type of samples including dry and old samples without live bacteria, a great advantage over the conventional growth method.

Propidium monoazide (PMA) is a photoreactive dye with a high affinity for DNA. The dye intercalates into dsDNA and forms a covalent linkage upon exposure to intense visible light, resulting in chemically modified DNA, which cannot be amplified by PCR or qPCR [26,27]. Because PMA dye is cell membrane impermeable, only

dead bacterial cells with compromised cell membranes are susceptible to DNA modification. Therefore, if a sample is treated with PMA dye, the isolated DNA from the treated sample cannot be detected by qPCR. Therefore, unlike qPCR, PMA-qPCR only detects and quantifies target DNA sequences from live microorganisms.

22.2.2.3 RT-qPCR

RT-qPCR is a variation of conventional qPCR, whereby messenger RNA (mRNA) is first transcribed into its complementary DNA (cDNA) using reverse transcriptase, the resulting cDNA is then amplified and quantified by qPCR using primers specific to a defined sequences of the gene of interest [18]. Conventional qPCR detects DNA present in actively metabolizing cells as well as in inactive and dead cells. In contrast, mRNA is only produced by actively metabolizing cells in order for a cell to manufacture a specific protein. By targeting mRNA, RT-qPCR has the advantage that only actively metabolizing cells are detected, providing a more reliable measure of microbial activity in environmental samples. RT-qPCR can also be used to monitor the activity of microbial processes such as sulfate reduction, methanogenesis, and nitrate reduction by targeting mRNA produced by specific functional genes.

mRNA is very unstable, which typically persists in an environmental sample for no more than a few minutes following collection [28]. Additionally, the mRNA half-life varies for different environments, microorganisms, and by function and nutritional status of the cell [28,29]. For this reason, samples must be preserved within minutes, if not seconds, of collection. The golden standard of sample preservation is to immediately freeze the samples in liquid nitrogen to prevent enzymatic RNA degradation. Although this may be possible when working in a laboratory, it is not feasible or practical in field sampling of environmental samples [30]. Finally, detection and quantification of mRNA are highly dependent both on expression levels of the target gene and on mRNA extraction protocols [31]. Consequently, assays targeting different loci or involving different mRNA extraction protocols will perform differently [32]. mRNA instability and challenges in sampling, sample preservation, and mRNA extraction make the application of RT-qPCR challenging in oil and gas industry.

22.2.3 Flow cytometry

Flow cytometry is a laser-based technology that provides rapid analysis of multiple characteristics of single cells from heterogeneous populations [33], without dependency on microbial culture techniques. A flow cytometer has been described as automated fluorescence microscope, capable of analyzing several thousands of cells per second, as they flow in a liquid stream and are presented in a single file in front of a focused light beam. As cells pass through the excitation light source, light is scattered and fluorescence is emitted as light. Light scattering is directly related to structural and morphological cell features, whereas fluorescence emission occurs if the cells are attached to a fluorescent probe or stained with a fluorescent dye [34]. Light scattering and fluorescence emission data can be used to examine a variety of biochemical,

biophysical, and molecular aspects of individual cells [35]. Moreover, a specialized flow cytometry, called fluorescence activated cell sorting, is capable of physically separating cells and sorting cells into different containers based on the specific light scattering and fluorescent characteristics of each cell.

Flow cytometry has been used for total bacteria count, live and dead bacteria differentiation, and studying cell interactions in complex structures such as bacterial biofilms [36]. Oligonucleotide probes, designed for specific nucleic acid sequences in cells and labeled with fluorescent dyes, have been used for detection and quantification of specific groups of microorganisms with flow cytometer. In microorganisms, the most common target of oligonucleotide probes is 16S rRNA, as several thousand ribosomes normally present in each cell provide built-in amplification. 16S rRNA probes are also useful for the classification of mixed populations containing unculturable species in a sample.

Flow cytometry provides a high-throughput capability for qualitatively and quantitatively examining bacteria populations, and their viability and functionality in various industrial bioprocesses [37]. Applications of flow cytometry in oil and gas industry include detecting and monitoring microbial activities in various water systems (seawater, produced water, utility water, cooling water) and storage tanks (crude oil, refined fuel products), and biocide performance screening and evaluation.

22.2.4 Microarray

Characterization of microbial community is traditionally achieved by 16S rRNA gene-based clone libraries and sequencing. However, this approach fails to detect large portions of the community, perhaps missing up to half of the biodiversity [38], and construction of large libraries are required to detect the majority of microbial diversity in the sample. When the identification of specific microbial species in a particular system is not necessary or critical, microarray technology can be used to evaluate metabolic processes or monitor gene products that are implicated in the specific activity of interest (e.g., sulfate reduction).

Microarray technology was originally developed by combining FISH technology and DNA blot technology into a smaller and compact package [39]. Thousands of specific DNA sequences known as probes can be fixed on to a glass slide, targeting either 16S rRNA genes or functional genes [40]. DNA or cDNA prepared from the samples are labeled with a fluorescent dye and hybridized to the target probes on the slide based on complimentary base pairing. The fluorescence signals from the hybridization are quantified using a fluorescence scanner, providing semiquantitative information on environmental samples. For instance, the PhyloChip is a phylogenetic oligonucleotide array, containing 500,000 16S rRNA gene probes, was designed to study bacterial population dynamics during uranium reduction and reoxidation and shown to be reliable and more reproducible than clone libraries [41]. The GeoChip, a functional gene array, was designed to monitor biogeochemical, ecological, and environmental processes such as carbon fluxes, sulfate reduction, metal reduction, and many other microbially catalyzed activities [40].

Microarray technology can screen a large number of complex DNA mixtures for known sequences or analyze RNA samples for gene expression profile; however, this technology is complicated and requires special skills and expensive equipment. To minimize the cost and simplify data analysis, microarray can be tailored to a specific industry or process. If the intent is to monitor a specific process such as MIC in oil and gas industry, an array can be designed to only contain probes for genes or microorganisms implicated in MIC. Such a compact and targeted array will only have to include less than 100 probe spots, but still offer substantial industry-specific information about the microbial status of a particular system [39]. In petroleum industry, an MIC array, containing probes targeting key genes of metabolic pathways in corrosion-related microorganisms, can serve as a useful and low-cost tool for the semiquantitative detection of major corrosion-related microorganisms in a single experiment.

Detection of sequences on an array can vary depending on the stringency of hybridization conditions, microarray data from different labs, or different experiments need to be carefully analyzed with regard to the interpretation of hybridization specificity and should be validated with more specific and quantitative methods such as qPCR [39].

22.2.5 Clone library and sequencing

The majority of microorganisms in the subsurface environment particularly those involved in heavy oil degradation, reservoir souring, or biofouling remain largely uncharacterized [42]. Identifying the microbial community structure and determining how community diversity are affected by geochemical and biological conditions are the first step to understand the microbiology in an oilfield system. This can be easily accomplished by using PCR amplification of 16S rRNA gene, construction of clone library, and sequencing of clones.

There are many different cloning vectors and techniques used in library preparation. In general, the cloning process comprises three steps. First, the DNA fragments of interest are amplified from the sample using PCR amplification with primers designed to target a specific gene (e.g., 16S rRNA gene). Second, after the amplified DNA fragments are purified, each fragment is then inserted into a cloning vector using a ligation reaction. Third, the pool of recombinant DNA molecules is transferred into a population of bacteria or yeast (i.e., competent cells) with a heat shock procedure. As a result, each competent cell contains on an average one construct (vector + insert). As the competent cells are grown in culture, the DNA molecules contained within them are copied and propagated (thus, "cloned"). Plasmid DNA including vector and insert sequences is then isolated and subject to sequencing determination. The retrieved sequence from each clone can be submitted to sequence database such as GenBank to determine the identity of microorganisms in the sample.

PCR and clone library of 16S rRNA gene have been used to characterize microbial communities in oilfield systems. Archaeal and bacteria clone libraries can be generated from total DNA collected from oilfield system such as formation water. The direct sequencing of clones and phylogenetic analysis of sequences will reveal the

predominant archaea and bacteria species in petroleum reservoirs, their functions, and interactions. Mesophilic and thermophilic sulfate reducers, methanogens, mesophilic and thermophilic fermentative bacteria, and iron-reducing bacteria have been found in oilfield systems through cloning and direct sequencing [8,43]. These microorganisms have profound economic impact on oil production and operations such as formation damage, reservoir souring, microbial corrosion, water injectivity, crude oil decomposition, and methane production.

22.2.6 Metagenomics

Many culture-independent methodologies are capable of assessing microbial diversity but these tools cannot identify all the microorganisms or functions in a high-throughput manner [44]. Amplification-based methods such as PCR and qPCR, and hybridization-based methods such as FISH and microarrays, can only identify known organisms or genes for which probes can be designed and always miss unknown genes. The advances in sequencing technology and decreases in sequencing cost make it possible to sequence the total DNA extracted from environmental samples, overcoming many of the limitations of other techniques used in community analysis [45].

There are two major approaches for sequencing an environmental sample (metagenomics) using the total extracted DNA or an enriched portion of the total extracted DNA. Sequencing of total DNA (random shotgun sequencing) provides sequence information of whole microbial community as well as all the functional genes present in an environmental sample. However, due to the complexity of most of environmental samples, this technique is expensive and requires a lot of computing and bioinformatics resources. In the last decade, several next-generation sequencing (NGS) technologies have been developed for metagenomics study in environmental samples. A portion of the DNA is amplified with PCR primers targeting phylogenetic markers (e.g., 16S rRNA gene) or functional genes (e.g., DSR gene) and then the targeted amplicons are sequenced. Compared to random shotgun sequencing, targeted amplicon sequencing requires less genetic materials from a sample, fewer sequencing runs, and simpler bioinformatics analysis.

22.2.6.1 Random shotgun sequencing

Characterizing the phylogenetic diversity of microbial community with 16S rRNA gene sequencing is only the first step to properly manage any ecosystems where the microbial community exists. Sequencing the total DNA can provide the sequences of all the genes in the environment, including the functional genes, which elucidate ongoing activities (i.e., genes and gene expression) in the environment.

Random shotgun sequencing is a Sanger-based technique and often used for sequencing large genomes. In shotgun sequencing, DNA is sheared into random small segments, which are sequenced using the chain termination method (or "Sanger

sequencing") to obtain reads. Several rounds of fragmentation and sequencing are required to obtain multiple overlapping reads for the target DNA.

The original DNA sequence is reconstructed from the reads using the sequence assembly software. First, sequences are processed to eliminate short and noisy reads. The quality overlapping reads are then collected into longer composite sequences known as contigs [46], on which gene calls and functional annotation are made. Finally, contigs are grouped into related phylogeny, and community composition profiling and functional analysis can then be performed to highlight functional activities with metabolic and ecological significance [44,47].

Random shotgun sequencing generates an impressive amount of information but it is a much more expensive and difficult approach than NGS on targeted amplicons. In many cases, knowing the metabolic pathways present in an environment is often more important than determining the species indigenous to the environment. For instance, the presence of sulfate-reducing genes in an oil and gas industry system plays an important role in microbial corrosion.

22.2.6.2 Next-generation sequencing

Although shotgun sequencing was the most advanced technique for whole-genome sequencing from about 1995 to 2005, the high demand for low-cost sequencing has driven the development of high-throughput NGS technologies. These technologies produce shorter reads (25−500 bp) but many hundreds of thousands or millions of reads in a relatively short time (on the order of a day) [48]. This results in high coverage, but the assembly process is much more computationally expensive. These technologies are vastly superior to Sanger-based shotgun sequencing due to the high volume of data and the relatively short time it takes to sequence a whole genome. The major disadvantage is that the accuracies are usually lower, although this is compensated for by the high coverage [49].

Among three major NGS platforms (Roche 454 pyrosequencing platform, Solexa/Illumina platform, and ABI's SOLiD platform), 454 pyrosequencing produces the longest read lengths (400−700 bp), but lower throughput. Longer read lengths improve basic local alignment search tool (BLAST) homology searches and assembly of long contigs. The longer reads also make phylogenic linkage of genes with their host organisms easier and improve species identification from 16S RNA sequence tags [50]. The latest 454 pyrosequencing platform can generate 900 Mb in a 20-h run. The gigabases of sequencing data will be assigned to an operational taxonomic unit (OTU) based on sequence similarity and OTUs are blasted against 16S rRNA database to identify the OTU's phylum, genus, or even species. The sequences can also be subjected to community analysis including estimation of species richness, population evenness, and diversity across communities [51].

Next-generation sequencing technique requires a relative amount of starting material, which is an advantage for applications in hydrocarbon environments where samples may be difficult to obtain or oil saturated and difficult to process. The methodology provides the identity of the microbial community members in the sample, their relative abundance and functions, and their interactions with an environment's physical and chemical parameters.

22.2.7 Sensor for microbial detection

Water injection into reservoir is a common practice in oil industry to maintain reservoir pressure and oil production. Microbial activity in water injection systems causes a variety of problems such as microbial corrosion, biofouling, injectivity loss, and reservoir plugging [52]. In the oil industry, the microbial number and activity are traditionally monitored with conventional growth methods that require manual sampling and handling. In a large injection system, an online and real-time sensor, capable of providing continuous monitoring of microbial activity, will help operators take prompt microbial control actions and ensure the continued high quality of injection water.

Sensors have several advantageous analytical features, such as selectivity, sensitivity, and rapidity to help measure dominant microorganisms in specific industrial system and thus make the necessary remedial actions to control them. They have potential for miniaturization and automation to use in the field in situ applications. Because Clark and Lyons [53] developed the first biosensor in 1962, the field of biosensors has greatly expanded. DNA-based sensing technology has been introduced in the construction of sensors for online and real-time detection and monitoring of microorganisms in the seawater injection system [54].

Staining of cells with DNA binding fluorescence dyes such as SYBR Green has been studied extensively as a sensing mechanism for microbial detection and monitoring. SYBR Green dye is very sensitive to dsDNA, yielding high signal intensity with a low background noise [55] and it is also tolerant to high-salinity seawater system and high-temperature environment [56]. SYBR Green-based staining method, followed by quantification of fluorescence signals, has been optimized and developed into an automated online sensor for microbial monitoring in the injection seawater system (salinity 5.5%, temperature from 5 to 53°C or 41 to 127°F) with a detection limit of 2×10^3/mL [57]. For detection and monitoring of specific species or group of microorganisms in various industry systems, FISH-based fluorescence staining with a specific oligonucleotide probe can be used for sensor design and construction.

22.2.8 Advantages and limitations

All molecular microbiology techniques discussed earlier have advantages and limitations when applied to address the microbiological challenges in petroleum industry [58,59], which are summarized in Table 22.1. Specifically, Table 22.2 compared a common conventional culture-dependent method, the most probable number (MPN) method, with a molecular microbiology technique qPCR, for detection and quantification of various microorganisms important to oil and gas industry. qPCR is a much better technology than MPN by targeting the 16S rRNA gene or functional genes essential for the metabolism of corrosion-causing microorganisms. qPCR can be used to analyze any type of samples (liquid, biofilms, or solid samples), including dried solid samples, which only contain dead microorganisms.

Generally, more than one molecular microbiology techniques are required to understand a particular problem in an oil industry system and develop a mitigation strategy

Table 22.1 Advantages and limitations of molecular microbiology techniques

Techniques	Advantages	Limitations
DAPI	Enumerate living and inactive microorganisms	Only applicable for liquid samples. Not suitable for solid samples such as scale, biofilm, or sediment
Cell viability staining	Allow differentiation of live, dead, and damaged microorganisms	Only applicable for liquid samples. Not suitable for solid samples such as scale, biofilm, or sediment
FISH	Allow species identification and quantification, and the observation of spatial distribution of microorganisms	Only applicable for liquid samples. Not suitable for solid samples such as scale, biofilm, or sediment
PCR	Detection of specific genes or microorganisms. Suitable for any type of samples	Semiquantitative; activity cannot be inferred from presence of genes alone. Cannot differentiate live and dead cells
qPCR	Rapid detection and quantification of specific genes. Suitable for any type of samples	Activity cannot be inferred from presence of genes alone. Cannot differentiate live and dead cells
PMA-qPCR	Rapid detection and quantification of specific genes only from viable microorganisms	PMA treatment efficiency varies in different type of samples, especially in complex environmental samples
RT-qPCR	Quantitative detection of microbial activity. Treatment effects on total cell function can be monitored	mRNA unstable. Cell activity may be skewed by short half-life and varied decay rate of mRNA, and mRNA extraction protocols
Flow cytometry	Allow species identification and quantification. Allow examination of bacteria populations, viability, and functionality	Analyzed cells must be in suspension; not easy to observe and measure individual cell behavior. Data analyses complicated
Microarray	Detect genes with function of interest; mRNA detection can reveal information about gene expression	Only determine species with probe on array. Activity cannot be inferred from presence of genes alone. Nonquantitative. Results difficult to compare among different labs or experiments

Continued

Table 22.1 Continued

Techniques	Advantages	Limitations
Clone library and sequencing	Identify the predominant microbial species in environmental samples, their functions, and interactions	Only detect a small portion of microbial community, and underestimate the biodiversity. Construction of large library is labor intensive and time consuming
Random shotgun sequencing	Analyze all phylogenetic markers and functional genes for a comprehensive profile of metabolic processes	Requires large amount of DNA; bioinformatics analysis are complicated and expensive
Next-generation sequencing	Identify a targeted phylogenetic or functional group of microbial community in environmental samples	Sequencing accuracies are usually lower. Bioinformatics analysis are complicated, and expensive
Sensor for microbial detection	Allow rapid and continuous monitoring of microbes of interest; fast response time	Need to improve the detection limit, sensitivity, and selectivity

FISH, fluorescence in situ hybridization; *mRNA*, messenger RNA; *PCR*, polymerase chain reaction; *PMA-qPCR*, propidium monoazide qPCR; *qPCR*, quantitative PCR; *RT-qPCR*, reverse transcription quantitative polymerase chain reaction;

Table 22.2 Comparison of quantitative PCR (qPCR) and most probable number (MPN) test

	qPCR	MPN test
Mechanism	Detect and quantify specific genes of target microbes	Grow in selective medium, score positive/negative growth based on indicators (color, turbidity, etc.), and enumerate statistically
Quantitative?	Yes	Semiquantitative
Time to obtain result	A few hours per microbial type	1−4 weeks
Sample type	Any types	Only if bacteria are still alive
Liquid	Yes	Yes, if fresh
Solid	Yes	Yes, if fresh, moist, and light color
Biofilm	Yes	Yes, if fresh and moist
Dry	Yes	No
Old	Yes	No
Colored	Yes	No
Sampling procedure	Simple and same for both aerobic and anaerobic microbes	Difficult to achieve anaerobic condition in the field for anaerobic microbes
Microbial target		
Bacteria	Yes	Yes
Archaea	Yes	Very difficult
Sulfate-reducing bacteria (SRB)	Yes	Yes
Sulfate-reducing archaea (SRA)	Yes	Very difficult
Acid-producing bacteria (APB)	Yes	Yes
Iron-oxidizing bacteria (IOB)	Yes	Very difficult
Methanogens	Yes	Very difficult

accordingly. The applications of molecular microbiology techniques in petroleum industry are illustrated in the next section.

22.3 Applications of molecular microbiology techniques in oil industry

In petroleum industry, microorganisms have been used to improve oil production, oil upgrading, and biogenic methane production from unrecoverable hydrocarbon resources [60,61]. However, it has to be realized that some microorganisms have detrimental effects in petroleum industry such as microbial corrosion, reservoir souring and plugging, and reduced injectivity of seawater injection wells. Characterization of the microbial communities and their activities present in petroleum industry is a critical first step if we intend to manage the resources properly. For instance, characterization of natural microbial communities impacted by petroleum hydrocarbons provides insights of long-term effects of petroleum pollution [62], helps develop and evaluate waste remediation approaches [63], and controls deleterious microbial activities during petroleum production [64].

22.3.1 Reservoir souring and mitigation

The injection of seawater to maintain reservoir pressure during oil production is a common practice in the oil industry. The huge amount of sulfate introduced via injection seawater, together with rich organics present in hydrocarbon, promotes the active growth of sulfate-reducing prokaryotes (SRPs) (i.e., SRB and SRA) in the reservoir, pipelines, and surface facilities [65,66]. SRPs produce H_2S, which has profound economic consequence to the oil industry, one of the major problems being reservoir souring.

Molecular techniques have been used to study reservoir souring and efficacy of nitrate treatment. In a study of two high-temperature oil reservoirs in the North Sea, a suite of molecular techniques were successfully used to assess the effect of nitrate addition in reservoir souring control [18,67,68]. DAPI staining technique was used to determine the total bacterial counts in produced waters. FISH technique was used to determine the viable bacteria and viable SRB using probes targeting various regions of 16S rRNA gene. qPCR assays were used to quantify the abundance of bacteria, archaea, and sulfate reducers, which form a major fraction of the prokaryotic communities in both reservoirs. RT-qPCR was used to determine the SRB activities in produced waters by measuring mRNA for the *dsrA* gene responsible for sulfate reduction in SRB. The results showed a reverse relationship between nitrate concentration and mRNA transcripts for the *dsrA* gene and the latter is positively related to the quantity of H_2S production from the well. In terms of H_2S production, the SRB activity determined by RT-qPCR analysis of *dsrA* mRNA transcripts is a better prediction parameter than viable SRB counts determined by FISH technique, as under nitrate treatment some SRB can be still viable or active but not producing H_2S (i.e., sulfate reduction is switched to nitrate reduction).

In the same study, clone libraries for bacterial and archaeal 16S rRNA gene were constructed to assess the microbial community structure, diversity, and species richness in oil reservoirs. Clone libraries for functional gene *dsrAB* were also constructed to gain a more detailed picture of the sulfate-reducing community and confirm the results obtained from the 16S rRNA-based approach. The study found that the nitrate treatment primarily affected the SRA number and activity in the reservoir but had only a minor effect on the abundance of SRB. The results indicated that the importance of SRA in the development of souring in high-temperature reservoirs.

22.3.2 MIC diagnosis and monitoring

MIC is an electrochemical process influenced by the presence or activities of microorganisms [69]. Microbial activities alter the rates and types of electrochemical reactions on a metal surface and produce a broad range of outcomes such as pitting, crevice corrosion, under-deposit corrosion, and selective dealloying, in addition to enhanced galvanic and erosion corrosion [70].

Microbial corrosion is a significant problem affecting the oil and gas and other industries. It degrades the integrity, safety, and reliability of pipeline operations and other systems. The mere presence of given classes of organisms associated with MIC (e.g., SRB) does not indicate that MIC is occurring. Neither does showing that the presence of a given type of microorganisms establishes a cause-and-effect relationship between the bacteria and metal dissolution [71]. Cost-effective MIC management requires the early detection of MIC problems, which can only be achieved by routine monitoring of the physical, chemical, and biological characteristics of pipeline systems.

MIC is rarely associated to one single mechanism or one single species of microorganism. In addition to SRP, many microorganisms occurring in natural environment are also considered corrosion-causing microbes, including methanogens, sulfur-oxidizing bacteria (SOB), acid-producing bacteria (APB), iron-oxidizing bacteria (IOB), iron-reducing bacteria (IRB), and manganese-oxidizing bacteria [72]. Each of these physiological groups of microorganisms may contain hundreds of individual species. Each group of bacteria or an individual species of bacteria alone can cause metal corrosion; however, MIC in a natural environment is always caused by microbial communities containing many different types of microbes [73].

MIC is traditionally diagnosed by visual observations of pits, the enumeration of SRB with cultivation-based method, and detection of corrosion products (e.g., FeS, pyrite). Microbiological diagnosis based on SRB enumeration is often misleading. SRB is just one of the key microbial group that causes metal corrosion. In addition, enumeration based on cultivation (e.g., MPN) often significantly underestimates the number of SRB in the sample. To date, culture-independent molecular techniques (e.g., qPCR) have been widely used for monitoring microbial numbers and activities in both water and solid samples from oil and gas industry for the problems related to MIC. The application of molecular techniques allows for improved MIC monitoring and optimization of mitigation strategies (e.g., biocide treatments, pigging operations and material selection) in oilfields and operation systems. qPCR

techniques are illustrated below for fast and accurate detection and quantification of corrosive microorganisms typically found in oil and gas industries by targeting 16S rRNA genes or function genes essential to the metabolism of corrosion-causing microbes.

22.3.2.1 MIC diagnosis

Table 22.3 illustrated the qPCR application for accurate and quick diagnosis of MIC in corroded pipe or metal pieces. Traditional growth method does not work for this type of samples because the samples are collected and stored under atmospheric conditions for various periods of time and the samples generally contain no live microorganisms due to storage and dryness. However, culture-independent qPCR assays, targeting 16S rRNA genes or other function genes, can easily detect and quantify corrosion-causing microbes in the corrosion samples. Various microorganisms (APB, SRB, SRA, IOB, and methanogens) were identified as major contributors to the corrosion of metal samples [74].

22.3.2.2 MIC monitoring

Planktonic bacteria are often the focus of MIC monitoring because system fluids are generally easier to sample than metal surface. However, the environmental conditions at biofilm and metal surface interfaces are often radically different from the bulk medium in terms of pH, dissolved oxygen, and other organic and inorganic species. MIC monitoring or risk assessment based on the results of planktonic microorganisms can sometimes be misleading, at least to some extent [75]. Table 22.4 compared the qPCR results of various microbes detected in the liquid samples and solid samples collected from the same system [74]. The number of microbes detected in the solids (#/g) was 100−10,000 times higher than the number in the liquid samples (#/mL). More importantly, some corrosion-related microbes such as methanogens were not even detected in the liquid samples. Compared to planktonic bacteria, monitoring of sessile bacteria is more relevant to microbial corrosion, though the sampling of sessile bacteria is likely to be more challenging, requiring pipeline excavation or accommodations of system design to allow for regular sampling during operation. NACE Standard TM0194-2004 provides the guidelines for the assessment of sessile bacteria in oilfield and gas systems [76].

Considering the difficulties of sampling sessile bacteria, it is advised to collect the solid samples whenever a pipe is scraped, and analyze for corrosion-related microorganisms. The results can be used as part of pipeline integrity program in the field operation to assess the corrosion risk. Due to the nature of scraping solids (toxicity, inhibitory substance, texture, color, salinity), most scraping samples are not appropriate for traditional cultivation methods. In addition, the exposure of scraping sample to oxygen during sampling kills anaerobic bacteria such as SRB and makes these types of bacteria (often corrosive) not detectable or being underestimated with traditional cultivation method. DNA-based molecular techniques are better suited for detection

Table 22.3 MIC diagnosis of corroded samples using quantitative PCR (qPCR) technique

Sample	Sample description	Thickness (in.)	Corrosion description	Major microbes	Number (#/g solids)
1	P110 grade API casing	3/8	Sig. corr. w/pitting	APB	3.9E + 06
2	Flange, carry hot water treated with nitrite	1/16	Thru-wall pit	IOB	7.0E + 05
3	Stainless steel flange (marine environment)	1	Sig. corr. w/pitting	APB	1.5E + 05
4	Drill pipe, submerged in a water-based drilling fluid	5/16	Sig. corr. w/pitting	APB	9.8E + 06
5	Aircraft water tank (AISI 321), 14 months in service		Severe corrosion	APB	1.6E + 06
				IOB	8.4E + 05
				SRB	5.6E + 04
				Bacteria	1.2E + 10
6	Solid deposits from corrosion pit			SRA	3.4E + 05
				IOB	1.0E + 04
				APB	9.3E + 03
				Bacteria	4.1E + 09
7	Pipe scale			SRB	3.3E + 07
				Methanogens	5.2E + 09
				Bacteria	1.6E + 10
8	Scale from a check valve			SRB	1.5E + 05
				APB	2.5E + 05
				Bacteria	1.6E + 08

APB, acid-producing bacteria; *IOB*, iron-oxidizing bacteria; *IRB*, iron-reducing bacteria; *MIC*, microbiologically influenced corrosion; *SOB*, sulfur-oxidizing bacteria;

Table 22.4 Monitoring of microorganisms in water systems using quantitative PCR (qPCR) technique

Sample pair	Sources	Major microbes	Number	
1	Brine well	SRB	5.2E + 02	/mL brine
		Bacteria	3.4E + 06	
	Brine pipe scrapings	SRB	9.1E + 06	/g solids
		Bacteria	6.5E + 10	
2	Water treatment plant	SRB	7.6E + 04	/mL water
	Water treatment plant pipe deposits	SRB	2.0E + 08	/g solids
		Methanogens	1.9E + 09	
		Bacteria	1.4E + 10	
3	Water injection point	SRB	4.0E + 05	/mL water
		Bacteria	5.2E + 08	
	Water injection point deposits	SRB	5.9E + 07	/g solids
		Methanogens	6.0E + 09	
		Bacteria	3.9E + 10	
4	Water treatment plant 4″ valve	SRB	5.2E + 04	/mL water
		Methanogens	4.9E + 07	
		Bacteria	2.3E + 08	
	Water treatment plant 4″ valve deposits	SRB	5.0E + 07	/g solids
		Methanogens	3.6E + 09	
		Bacteria	3.8E + 10	

SRB, sulfate-reducing bacteria.

and quantification of microbes in the scraping solids. Table 22.5 showed the major corrosion-related microorganisms detected with qPCR techniques in scraping samples collected from various pipeline systems [74].

22.4 Summary

Many culture-independent molecular microbiology techniques have been introduced into oil and gas industry in the past decade. These nucleic acids-based techniques overcome the difficulties associated with the laboratory cultivation of microorganisms, provide a direct analysis of samples and assessment of gene function, and enhance our ability to investigate the dynamics of microbial communities in petroleum ecosystems. The chapter describes molecular microbiology techniques widely used in oil and gas

Table 22.5 Monitoring of microorganisms in scraping solids using quantitative PCR (qPCR) technique

Sample ID	Source	Major microbes	Number (#/g solids)
1	Black powder from pigging operation	SRB	9.1E + 05
		Bacteria	1.3E + 09
2	Oil production pipe pig solids	SRB	9.8E + 04
		Methanogens	1.3E + 09
		Bacteria	6.1E + 08
3	Pig solids from crude dehydration plant	SRB	4.0E + 04
		SRA	3.1E + 07
		Bacteria	1.7E + 08
4	Soft water line scrapings	SRB	7.8E + 06
		Bacteria	2.1E + 09
5	Produced water pipe deposits	SRB	1.3E + 08
		Methanogens	1.6E + 09
		Bacteria	1.6E + 10
6	Waste water line pig solids	SRA	3.4E + 07
		Bacteria	1.4E + 05
7	Water injection well deposits	SRB	8.9E + 06
		SRA	1.2E + 08
		Bacteria	1.9E + 08

SRA, sulfate-reducing archaea; *SRB*, sulfate-reducing bacteria.

industry and the advantages and limitations of each technique. As a result, in the practical applications to address oil field issues, it is often necessary to use several molecular techniques to fully understand a particular problem in an oil industry system, assess the microbial risks, determine the mitigation strategy, and evaluate the treatment effectiveness.

References

[1] D.H. Pope, R.M. Pope, Guide for the Monitoring and Treatment of Microbiologically Influenced Corrosion in the Natural Gas Industry, GRI report GRI-96/0488, Gas Research Institute, 1998.

[2] R.I. Amann, W. Ludwig, K.H. Schleifer, Phylogenetic identification and in situ detection of individual microbial cells without cultivation, Microbiological Reviews 59 (1995) 143−169.
[3] B.L. Maidak, J.R. Cole, T.G. Lilburn, C.T. Parker II, P.R. Saxman, J.M. Stredwick, G.M. Garrity, B.L. Li, G.J. Olsen, S. Pramanik, T.M. Schmidt, J.M. Tiedje, The RDP (ribosome database project) continues, Nucleic Acids Research 28 (2000) 173−174.
[4] W.A. Williams, J.H. Lobos, W.E. Cheetham, A phylogenetic analysis of aerobic polychlorinated biphenyl-degrading bacteria, International Journal of Systematic Bacteriology 47 (1997) 207−210.
[5] C. Whitby, T.L. Skovhus, Chapter 1: introduction, in applied microbiology and molecular biology in oilfield systems, in: T.L. Skovhus (Ed.), Proceedings from the International Symposium on Applied Microbiology and Molecular Biology in Oil Systems (ISMOS-2), Springer, London, New York, 2009.
[6] X.Y. Zhu, A. Ayala, H. Modi, J.J. Kilbane II, Application of quantitative, real-time PCR in monitoring microbiologically-influenced corrosion (MIC) in gas pipelines, in: NACE International Annual Conference, Corrosion/2005, Houston, TX, Paper #05493, 2005.
[7] J.G. Leahy, R.R. Colwell, Microbial degradation of hydrocarbons in the environment, Microbiological Reviews 54 (1990) 305−315.
[8] M. Magot, B. Ollivier, B.K.C. Patel, Microbiology of petroleum reservoirs, Antonie van Leeuwenhoek 77 (2000) 103−116.
[9] C.R. Woese, Bacterial evolution, Microbiological Reviews 51 (1987) 221−271.
[10] G.C. Baker, J.J. Smith, D.A.J. Cowan, Review and re-analysis of domain-specific 16S primers, Journal of Microbiological Methods 55 (2003) 541−555.
[11] S.E. Morales, W.E. Holben, Empirical testing of 16S rRNA gene PCR primer pairs reveals variance in target specificity and efficacy not suggested by in silico analysis, Applied and Environmental Microbiology 75 (2009) 2677−2683.
[12] V. Kunin, A. Copeland, A. Lapidus, K. Mavromatis, P. Hugenholtz, A bioinformatician's guide to metagenomics, Microbiology and Molecular Biology Reviews 72 (2008) 557−578.
[13] J. Larsen, T.L. Skovhus, M. Agerbek, T.R. Thomsen, P.H. Nielsen, Bacterial diversity study applying novel molecular methods on Halfdan produced waters, in: NACE International Annual Conference, Corrosion/2006, Houston, TX, Paper #06668, 2006.
[14] J. Larsen, S. Zwolle, B.V. Kjellerup, B. Frolund, J.L. Nielsen, P.H. Nielsen, Identification of bacteria causing souring and biocorrosion in the Halfdan field by application of new molecular techniques, in: NACE International Annual Conference, Corrosion/2005, Houston, TX, Paper #05629, 2005.
[15] J. Bayani, J.A. Squire, Chapter 22. Fluorescence in situ hybridization (FISH), in: K.M. Yamada (Ed.), Current Protocols in Cell Biology, Maryland, Bethesda, 2004.
[16] K. Helmi, F. Barthod, G. Meheut, A. Henry, F. Poty, F. Laurent, N. Charni-Ben-Tabassi, Methods for microbiological quality assessment in drinking water: a comparative study, Journal of Water and Health 13 (2015) 34−41.
[17] L. Holmkvist, J. Ostergaard, T.L. Skovhus, Chapter 7: using fluorescence in situ hybridisation (FISH): microscopic techniques for enumeration of troublesome microorganisms in oil and fuel samples, in: T.L. Skovhus (Ed.), Proceedings from the International Symposium on Applied Microbiology and Molecular Biology in Oil Systems (ISMOS-2), Springer, London, New York, 2009.
[18] A. Price, L.A. Alvarez, C. Whitby, J. Larsen, Chapter 9: how many microorganisms are present? Quantitative reverse transcription PCR (qRT-PCR), in: T.L. Skovhus (Ed.), Proceedings from the International Symposium on Applied Microbiology and Molecular Biology in Oil Systems (ISMOS-2), Springer, London, New York, 2009.

[19] A. Dhillon, A. Teske, J. Dillon, D.A. Stahl, M.L. Sogin, Molecular characterization of sulfate-reducing bacteria in the Guaymas Basin, Applied and Environmental Microbiology 69 (2003) 2765−2772.
[20] M. Wagner, A.J. Roger, J.L. Flax, G.A. Brusseau, D.A. Stahl, Phylogeny of dissimilatory sulfite reductases supports an early origin of sulfate respiration, Journal of Bacteriology 180 (1998) 2975−2982.
[21] G. Braker, H.L. Ayala-del-Rio, A.H. Devol, A. Fesefeldt, J.M. Tiedje, Community structure of denitrifiers, bacteria, and archaea along redox gradients in Pacific Northwest marine sediments by terminal restriction fragment length polymorphism analysis of amplified nitrite reductase (nirS) and 16S rRNA genes, Applied and Environmental Microbiology 67 (2001) 1893−1901.
[22] G. Braker, A. Fesefeldt, K.-P. Witzel, Development of PCR primer systems for amplification of nitrite reductase genes (nirK and nirS) to detect denitrifying bacteria in environmental samples, Applied and Environmental Microbiology 64 (1998) 3769−3775.
[23] T. Lueders, M.W. Friedrich, Evaluation of PCR amplification bias by terminal restriction fragment length polymorphism analysis of small-subunit rRNA and mcrA genes by using defined template mixtures of methanogenic pure cultures and soil DNA extracts, Applied and Environmental Microbiology 69 (2003) 320−326.
[24] P.E. Luton, J.M. Wayne, R.J. Sharp, P.W. Riley, The mcrA gene as an alternative to 16S rRNA in the phylogenetic analysis of methanogen populations in landfill, Microbiology 148 (2002) 3521−3530.
[25] X.Y. Zhu, H. Modi, A. Ayala, J.J. Kilbane II, Rapid detection and quantification of microbes related to microbiologically influenced corrosion using quantitative polymerase chain reaction, Corrosion 62 (2006) 950−955.
[26] A. Nocker, P. Sossa-Fernandez, M.D. Burr, A.K. Camper, Use of propidium monoazide for live/dead distinction in microbial ecology, Applied and Environmental Microbiology 73 (2007) 5111−5117.
[27] B. Taskin, A.G. Gozen, M. Duran, Selective quantification of viable *Escherichia coli* bacteria in biosolids by quantitative PCR with propidium monoazide modification, Applied and Environmental Microbiology 77 (2011) 4329−4335.
[28] M.P. Deutscher, Degradation of RNA in bacteria: comparison of mRNA and stable RNA, Nucleic Acids Research 34 (2006) 659−666.
[29] D.W. Selinger, R.M. Saxena, K.J. Cheung, G.M. Church, C. Rosenow, Global RNA half-life analysis in *Escherichia coli* reveals positional patterns of transcript degradation, Genome Research 13 (2003).
[30] E.B. Hollister, J.P. Brooks, T.J. Gentry, Bioinformation and omic approaches for characterization of environmental microorganisms, in: I.L. Pepper, C.P. Gerba, T.J. Gentry (Eds.), Environmental Microbiology, Academic Press, CA, USA, 2015.
[31] T.D. Schmittgen, Real-time quantitative PCR, Methods 25 (2001) 383−385.
[32] A. Chimento, S.O. Cacciola, M. Garbelotto, Detection of mRNA by reverse-transcription PCR as an indicator of viability in *Phytophthora ramorum*, Forest Pathology 42 (2012) 14−21.
[33] D.A. Veal, D. Deere, B. Ferrari, J. Piper, P.V. Attfield, Fluorescence staining and flow cytometry for monitoring microbial cells, Journal of Immunological Methods 243 (2000) 191−210.
[34] List of Available Fluorophores and Dyes. http://www.thefcn.org/flow-fluorochromes.
[35] M. Rahman, Introduction to Flow Cytometry, AbD Serotec, 2006, pp. 1−33.

[36] V. Ambriz-Avina, J.A. Contreras-Garduno, M. Pedraza-Reyes, Applications of flow cytometry to characterize bacterial physiological responses, BioMed Research International 2014 (2014) 461941.
[37] M. Diaz, M. Herrero, L.A. Garcia, C. Quiros, Application of flow cytometry to industrial microbial bioprocesses, Biochemical Engineering Journal 48 (2010) 385−407.
[38] S. Hong, J. Bunge, C. Leslin, S. Jeon, S.S. Epstein, Polymerase chain reaction primers miss half of rRNA microbial diversity, The ISME Journal 3 (2009) 1365−1373.
[39] B.E.L. Morris, Chapter 11: microarrays, in: T.L. Skovhus (Ed.), Proceedings from the International Symposium on Applied Microbiology and Molecular Biology in Oil Systems (ISMOS-2), Springer, London, New York, 2009.
[40] Z. He, T.J. Gentry, C.W. Schadt, L. Wu, J. Liebich, S.C. Chong, Z. Huang, W. Wu, B. Gu, P. Jardine, C. Criddle, J. Zhou, GeoChip: a comprehensive microarray for investigating biogeochemical, ecological and environmental processes, The ISME Journal 1 (2007) 67−77.
[41] E.L. Brodie, T.Z. Desantis, D.C. Joyner, S.M. Baek, J.T. Larsen, G.L. Andersen, T.C. Hazen, P.M. Richardson, D.J. Herman, T.K. Tokunaga, J.M. Wan, M.K. Firestone, Application of a high-density oligonucleotide microarray approach to study bacterial population dynamics during uranium reduction and reoxidation, Applied and Environmental Microbiology 72 (2006) 6288−6298.
[42] J. Handelsman, Metagenomics: application of genomics to uncultured microorganisms, Microbiology and Molecular Biology Reviews 68 (2004) 669−685.
[43] N.M. Shestakova, V.S. Ivoilov, T.P. Tourova, S.S. Belyaev, A.B. Poltaraus, T.N. Nazina, Chapter 6: application of clone libraries: syntrophic acetate degradation to methane in a high-temperature petroleum reservoir − culture-based and 16S rRNA genes characterization, in: T.L. Skovhus (Ed.), Proceedings from the International Symposium on Applied Microbiology and Molecular Biology in Oil Systems (ISMOS-2), Springer, London, New York, 2009.
[44] S.M. Caffrey, Chapter 8: which microbial communities are present? Sequence-based metagenomics, in applied microbiology and molecular biology in oilfield systems, in: T.L. Skovhus (Ed.), Proceedings from the International Symposium on Applied Microbiology and Molecular Biology in Oil Systems (ISMOS-2), Springer, London, New York, 2009.
[45] D. MacLean, J.D. Jones, D.J. Studholme, Application of 'next-generation' sequencing technologies to microbial genetics, Nature Reviews. Microbiology 7 (2009) 287−296.
[46] R. Staden, A strategy of DNA sequencing employing computer programs, Nucleic Acids Research 6 (1979) 2601−2610.
[47] S.G. Tringe, C. von Mering, A. Kobayashi, A.A. Salamov, K. Chen, H.W. Chang, M. Podar, J.M. Short, E.J. Mathur, J.C. Detter, P. Bork, P. Hugenholtz, E.M. Rubin, Comparative metagenomics of microbial communities, Science 308 (2005) 554−557.
[48] V.V. Karl, S.A. Dames, J.D. Durtschi, Next generation sequencing: from basic research to diagnostics, Clinical Chemistry 55 (2009) 41−47.
[49] M.L. Metzker, Sequencing technologies − the next generation, Nature Reviews Genetics 11 (2010) 31−46.
[50] K.E. Wommack, J. Bhavsar, J. Ravel, Metagenomics: read length matters, Applied and Environmental Microbiology 74 (2008) 1453−1463.
[51] B.J. Bohannan, J. Hughes, New approaches to analyzing microbial biodiversity data, Current Opinion in Microbiology 6 (2003) 282−287.

[52] M.A. Moniee, S. Juhler, K. Sorensen, F.N. Abeedi, T. Lundgaard, P.F. Sanders, A review of Saudi Aramco's water flooding system and methods for monitoring microbial activity, in: 15th Middle East Corrosion Conference, Bahrain, 2014.
[53] L.C. Clark, C. Lyons, Electrode systems for continuous monitoring cardiovascular surgery, Annals of the New York Academy of Sciences 102 (1962) 29−45.
[54] M.A. Moniee, X.Y. Zhu, L. Tang, F.I. Nuwaiser, N.V. Voigt, P.F. Sanders, F.N. Abeedi, H.H. Habboubi, Validation of autonomous microbe sensor prototype for monitoring of microorganisms in injection seawater systems, Journal of Sensor Technology 6 (2016) 80−100.
[55] A.I. Dragan, R. Pavlovic, J.B. McGivney, J.R. Casas-Finet, E.S. Bishop, R.J. Strouse, M.A. Schenerman, C.D. Geddes, SYBR green I: fluorescence properties and interaction with DNA, Journal of Fluorescence 22 (2012) 1189−1199.
[56] A. Shibata, Y. Goto, H. Saito, T. Kikuchi, T. Toda, S. Taguchi, Comparison of SYBR green I and SYBR gold stains for enumerating bacteria and viruses by epifluorescence microscopy, Aquatic Microbial Ecology 43 (2006) 223−231.
[57] M.A. Moniee, X.Y. Zhu, L. Tang, S. Juhler, F.I. Nuwaiser, P.F. Sanders, F.N. Abeedi, Optimization of DNA staining technology for development of autonomous microbe sensor for injection seawater systems, Journal of Sensor Technology 6 (2016) 27−45.
[58] S.M. Caffrey, Chapter 3: application of molecular microbiological methods to the oil industry to analyse DNA, RNA and proteins, in applied microbiology and molecular biology in oilfield systems, in: T.L. Skovhus (Ed.), Proceedings from the International Symposium on Applied Microbiology and Molecular Biology in Oil Systems (ISMOS-2), Springer, London, New York, 2009.
[59] J.D. Van Hamme, A. Singh, O.P. Ward, Recent advances in petroleum microbiology, Microbiology and Molecular Biology Reviews 63 (2003) 503−549.
[60] N.D. Gray, A. Sherry, S.R. Larter, M. Erdmann, J. Leyris, T. Liengen, J. Beeder, I.M. Head, Biogenic methane production in formation waters from a large gas field in the North Sea, Extremophiles 13 (2009) 511−519.
[61] B. Ollivier, M. Magot, Petroleum Microbiology, ASM Press, , Washington, D.C., 2005.
[62] J.E. Lindstrom, R.P. Barry, J.F. Braddock, Long-term effects on microbial communities after a subarctic oil spill, Soil Biology and Biochemistry 31 (1999) 1677−1689.
[63] J.O. Ka, Z. Yu, W.W. Mohn, Monitoring the size and metabolic activity of the bacterial community during biostimulation of fuel-contaminated soil with competitive PCR and RT-PCR, Microbial Ecology 42 (2001) 267−273.
[64] R.E. Eckford, P.M. Fedorak, Planktonic nitrate-reducing bacteria and sulfate-reducing bacteria in some western Canadian oil field waters, Journal of Industrial Microbiology and Biotechnology 29 (2002) 83−92.
[65] A. Gittel, K.B. Sorensen, T.L. Skovhus, K. Ingvorsen, A. Schramm, Prokaryotic community structure and sulfate reducer activity in water from high-temperature oil reservoirs with and without nitrate treatment, Applied and Environmental Microbiology 75 (2009) 7086−7096.
[66] E. Sunde, T. Torsvik, Microbial control of hydrogen sulfide production in oil reservoirs, in: M. Magot (Ed.), Petroleum Microbiology, ASM Press, Washington DC, 2005, pp. 201−213.
[67] A. Gittel, Chapter 12: monitoring and preventing reservoir souring using molecular microbiological methods (MMM), in: T.L. Skovhus (Ed.), Proceedings from the International Symposium on Applied Microbiology and Molecular Biology in Oil Systems (ISMOS-2), Springer, London, New York, 2009.

[68] J. Larsen, T.L. Skovhus, Chapter 13: the effect of nitrate injection in oil reservoirs − experience with nitrate injection in the Halfdan oilfield, in: T.L. Skovhus (Ed.), Proceedings from the International Symposium on Applied Microbiology and Molecular Biology in Oil Systems (ISMOS-2), Springer, London, New York, 2009.
[69] D.H. Pope, R.M. Pope, Microbiologically influenced corrosion in fire protection sprinkler systems, in: J.G. Stoecker II (Ed.), A Practical Manual on Microbiologically Influenced Corrosion, NACE International, Houston, TX, 2001, pp. 5.1−5.7.
[70] NACE, Detection, Testing, and Evaluation of Microbiologically Influenced Corrosion (MIC) on External Surfaces of Buried Pipelines, NACE Standard TM0106−2006, 2006.
[71] J. Horn, D. Jones, Microbiologically influenced corrosion: perspectives and approaches, in: C.J. Hurst, R.L. Crawford, G.R. Knudsen, M.J. McInerney, L.D. Stetzenbach (Eds.), Manual of Environmental Microbiology, ASM Press, Washington, DC, 2002, pp. 1072−1083.
[72] J. Larsen, K.B. Sorensen, B. Hojris, T.L. Skovhus, Significance of troublesome sulfate-reducing prokaryotes (SRP) in oil field systems, in: NACE International Annual Conference, Corrosion/2009, Houston, TX, Paper #09389, 2009.
[73] B. Little, P. Wager, F. Mansfeld, Microbiologically influenced corrosion of metals and alloys, International Materials Reviews 36 (1991) 253−272.
[74] X.Y. Zhu, Application of quantitative PCR in monitoring MIC-related microorganisms in oil and gas industry, in: 14th Middle East Corrosion Conference & Exhibition, Bahrain, 2012.
[75] T.P. Zintel, G.J. Licina, T.R. Jack, Techniques for MIC monitoring, in: J.G. Stoecker II (Ed.), A Practical Manual on Microbiologically Influenced Corrosion, NACE International, Houston, TX, 2001, pp. 10.11−10.19.
[76] NACE, Field Monitoring of Bacterial Growth in Oilfield and Gas Systems, NACE Standard TM0194−2004, 2004.

PART V

Advancements in corrosion mitigation

Biocides overview and applications in petroleum microbiology

23

Victor Keasler[1], *Renato M. De Paula*[1], *Glen Nilsen*[1], *Ludger Grunwald*[2] *and Timothy J. Tidwell*[1]

[1]NALCO Champion, an Ecolab Co., Sugar Land, TX, United States; [2]Ecolab Deutschland GmbH, Monheim am Rhein, Deutschland

23.1 Oil and gas operational challenges directly influenced by microbes

The presence of microorganisms is usually widespread in oil and gas production systems, frequently posing challenges to the integrity of pipelines and vessels. The most common problems elicited by microbial contamination include fouling of membranes, vessels, and pipes; production of biogenic H_2S; and microbiologically influenced corrosion (MIC). Despite advances in metallurgy, engineering, and chemistry, MIC continues to be a widespread problem in many industries and represents a serious challenge to the oil and gas industry. MIC costs hundreds of millions of US dollars to the petroleum industry every year [1], including loss in production, replacement of pipelines, vessels, and environmental cleanup as the result of spills due to pipeline failures. A recent estimate of the cost of MIC to the oil/gas production was between $485B and $1.5T annually.

MIC is the process in which microorganisms increase the rates of corrosion by producing metabolic by-products that react with iron from the metal [2]. Current knowledge indicates that MIC is not caused by a single family of organisms but rather by the action of different organisms within the microbial population. MIC is a localized process that initiates by the formation of a nodule, followed by pit beneath the nodule. Within these nodules, numerous microorganisms exist in a biofilm. Each of these organisms performs different functions within the community [3].

Despite numerous reports in the literature about the involvement of other microorganisms in the MIC process, the oil industry still regards sulfate-reducing bacteria (SRB) as the major culprits in the process [4]. Nonetheless, this concept has been significantly expanded to encompass organisms that metabolize different sources of sulfur species, such as thiosulfate and polysulfides [5,6]. These reports, resulting from data mining from thousands of oilfield samples, have helped to identify the prevalence of sulfur species−reducing microbes in different regions around the globe and indicated their role in MIC where sulfate is limited. Additionally, the role of other microorganisms in MIC has been further investigated in the recent years. For example, methanogenic Archaea produce methane as a metabolic by-product in anoxic

Trends in Oil and Gas Corrosion Research and Technologies. http://dx.doi.org/10.1016/B978-0-08-101105-8.00023-1

conditions using CO_2 as main electron acceptor. This process, when localized on a metal surface, can lead to increased rates of metal corrosion. Methanogens are common Archaea in oil production systems despite being rarely detected by traditional culturing techniques [7]. Moreover, other types of bacteria such as acid-producing bacteria and metal-oxidizing bacteria can also play an important role in the MIC process.

In the last few decades, great efforts have been made toward understanding the mechanisms underlying microbial corrosion under laboratory conditions. On the other hand, on-site monitoring in field environments has proved to be challenging to allow the correct assessment of microbial corrosion. MIC occurs only when the microbes responsible for the process accumulate on a metal surface, creating biofilms. Nonetheless, testing in metal surfaces in the field is difficult, disruptive, and requires more planning and personnel. Because of that, assessment of MIC in the field is primarily done by testing fluids samples and extrapolating the results to indicate potential biofilm occurrence. However, this is a fundamentally flawed approach, because rarely the microbial populations in the fluids and in the biofilm will match in terms of composition and numbers. Moreover, the locations where fluids samples are collected are not always the locations where biofilm buildup will occur. Biofilm formation is likely in locations of slow or stagnant flow, under deposits and points of the system where water cuts are higher.

Another common problem caused by microorganisms is reservoir souring [8]. This occurs because of the proliferation of sulfur species—reducing microbes in the formation, due to injection of water during secondary recovery to maintain the pressure of the reservoir. Although this problem is particularly troublesome in offshore facilities where sulfate-rich seawater is injected, reservoir souring also occurs in onshore fields where produced water is mixed with fresh water before injection. Because of the ubiquity of microbes capable of reducing sulfur species, reservoir souring can be a chronic problem once these organisms are injected underground. Management of microbial populations in the reservoir is often difficult, and the results can be inconsistent with the current technologies (e.g., nitrate injections) [9]. The production of fluids and gases containing H_2S can lead to severe corrosion due to H_2S stress cracking and health, safety, and environment issues, particularly in assets that were not engineered to operate under sour conditions. Therefore, inhibition of sulfide production by microorganisms is an important task to prevent further corrosive conditions in addition to their contribution to directly degrading surfaces and causing MIC.

Biofouling is also a common problem in oilfield operations, particularly in injection wells used for disposal of produced water or for secondary recovery of hydrocarbons. Large volumes of water contaminated with slime-forming bacteria can lead to aggressive production and accumulation of exopolymeric substances, resulting in plugging of the reservoir, injection lines, and consequent decrease in injection rates. This is often reflected in higher energy costs to push the fluids into the reservoir [10].

23.2 Overview of biocides

Biocides are chemicals intended to disinfect, sterilize, and kill microorganisms. The extent of microbial kill is highly dependent on the duration of contact with the target

microbes and the dosage of the chemical that is applied. In low dosages, most biocides will elicit a biostatic effect, in which microbial growth is prevented, but no sterilization is achieved. Once the chemical is removed from the system, the bacteria will continue to grow again. Moreover, at doses lower than those required to elicit a biostatic effect, some biocides can even become a source of nutrition and therefore encourage growth.

In oilfield operations, biocides can be injected either continuously or periodically in batches. The latter is often the most common procedure. Although a substantial number of biocide products exist in the market, most of these products are composed of only few basic active molecules at varying concentrations. The biocides may be single active molecules or blends of a few different molecules aiming to achieve better performance by taking advantage of synergistic effects.

The biocides in the oilfield can also be divided based on the mechanism of action. In general terms, nonoxidizing biocides act on the cell membrane and cell wall of the microbes, whereas oxidizing biocides act through oxidative reactions with cellular components.

23.2.1 Nonoxidizing biocides

Among the nonoxidizing chemistries, the most common biocidal molecules are glutaraldehyde, Tetrakis hydroxymethyl phosphonium sulfate (THPS), quaternary ammonium compounds (quats), and 2, 2-dibromo-3-nitrilopropionamide (DBNPA). Other chemistries that have been used in less extent are 2-bromo-2-nitropropane-1,3-diol (bronopol), acrolein, and several molecules belonging to the family of preservatives. Although the majority of these chemistries possess the ability to act as broad spectrum antimicrobials, different microbial susceptibilities to each product have been described [11]. Moreover, the efficiency of most biocides is heavily impacted by water chemistry, temperature, salinity, oxygen content, and incompatibility with other production chemistries.

23.2.1.1 Glutaraldehyde

Glutaraldehyde is an aldehyde organic compound that has a particular high affinity for proteins, reacting specifically with amine, amide, and thiol groups. Because of this property, glutaraldehyde can be a fixative in laboratory procedures. Glutaraldehyde is more expensive but less toxic than formaldehyde, and it is broadly used in countries where regulatory restrictions prevent the use of formaldehyde [12]. Glutaraldehyde is usually applied successfully in the field and commonly shows a broad range of microbial kill. It is highly water soluble, partitioning more than 80% in the water phase. From a thermal stability standpoint, glutaraldehyde loses efficacy in temperature above 50°C (122°F), but this loss seems to be highly dependent on pH and water chemistry [13]. Although glutaraldehyde works well with most other production chemicals such as scale and corrosion inhibitors and fracturing chemical packages, some incompatibilities are well known. Common compounds that can interfere with glutaraldehyde are primary amines, ammonia, and bisulfite-based oxygen scavengers [14]. However, changes in field application (e.g., staggering applications or injection in different locations in the system) can be done to mitigate potential compatibilities problems.

Nonetheless, studies have shown limited efficiency of glutaraldehyde to penetrate and control organisms in biofilms [15].

23.2.1.2 Tetrakis hydroxymethyl phosphonium sulfate

THPS is a broadly used biocide in oilfields, mostly because of its ability to control microorganisms and chelate iron from iron sulfide deposits. It is a broad-spectrum biocide and seems to exhibit a dual mechanism of controlling SRB, by targeting specific amino acids on the cellular membrane and by shutting off the sulfidogenic reduction pathway. For this reason, THPS is often selected for treatment with system having high contamination with SRBs. Contrary to glutaraldehyde, THPS shows higher thermal stability 160°C (320°F) but displays similar incompatibility issues with ammonium bisulfite oxygen scavengers [16] and limitations to penetrate biofilms. Incompatibilities with certain friction reducers also limit the use of THPS in hydraulic fracturing operations. Additionally, high concentrations of THPS can lead to severe corrosion, especially in conditions of low buffering capacity of the water [17].

23.2.1.3 2, 2-Dibromo-3-nitrilopropionamide

DBNPA is a bromine-based chemistry that provides a quick speed of kill. Although not considered an oxidizing biocide, DBNPA acts similarly as many halogen-based antimicrobials. On use, the product is rapidly broken down into several by-products, including ammonia, bromide ions, dibromoacetonitrile, and dibromoacetic acid. DBNPA is widely used in seawater injection systems, particularly for cleaning of membranes (e.g., sulfate removing and reverse osmosis membranes) [18]. It is also important to note that DBNPA reacts with H_2S and may not be the optimal biocide choice for systems where H_2S is present and may result in less efficacy of the product as a biocide.

23.2.1.4 Quaternary ammonium compounds

Quats are common components of biocides and corrosion inhibitors because of their surfactant properties. These are positively charged nitrogen ions with alkyl or aryl groups. Quats are widely used as disinfectants and surfactants agents in many industries. As a biocide in oilfield applications, quats provide persistent microbial control and enhanced ability to solubilize biofilms. They are usually used in combination with other biocides (such as glutaraldehyde and THPS) to provide enhanced control of biomass. However, because of their filming properties, quats may not be the first choice in high TSS waters or system with high levels of mineral deposit. Additionally, the surfactant characteristic of quaternary ammonium compounds may disrupt oil and water separation through emulsification, and they can cause enhanced foaming.

23.2.1.5 Preservatives

Preservatives belong to a class of antimicrobials that are designed to provide slow acting microbial control for extended periods of time. These compounds are usually

used in industrial goods to extend shelf life and prevent spoilage. Contrary to other commonly used biocides that act in a matter of hours, the efficiency of preservatives are measured in days or even weeks [19]. Depending on the concentration, a biostatic rather than a biocidal effect is achieved, which can create problems in regards to microbial rebound. The majority of the preservatives used in oilfield applications are formaldehyde releasers, in which slow hydrolysis of the molecule results in the release of antimicrobial formaldehyde. Among these chemistries, 4, 4-dimethyloxazolidine (DMO), tris (hydroxymethyl)nitromethane (THNM), 1-(3-chloroallyl)-3,5,7-triaza-1-azoniaadamantane chloride (CTAC), and 3,3′-methylenebis[5-methyloxazolidine] (MBO) are the most common. The efficiency of these compounds depends on the rates of hydrolysis and release of formaldehyde, which can be heavily affected by the water chemistry. Frequently, preservatives are applied in combination with other biocides (either oxidizing or nonoxidizing) to provide a combination of quick kill and long-term preservation.

23.2.2 Oxidizing biocides

23.2.2.1 Chlorine dioxide

Chlorine dioxide is a noncharged chlorine compound that is produced as gas and saturated in water. Chlorine dioxide is about 10 times more soluble in water than hypochlorite. As such, it is widely used as a bleaching agent and is a potent antimicrobial chemistry. However, solubility decreases dramatically with an increase in temperature, and chlorine dioxide can decompose extremely violently when separated from diluting substances. Gas-phase concentrations of ClO_2 above 30 volume percent can lead to violent explosions leading to release of chlorine and oxygen. Because of that, the preparation methods for chlorine dioxide must take all aspects of safety into consideration. Usually, methods that involve the production of chlorine dioxide solutions bypassing the gas phase are preferred. Because of safety concerns, chlorine dioxide has not been widely used in oilfields in the past, but improvements in how it is generated have opened its use in hydraulic fracturing applications in the past few years.

As an oxidizer, chlorine dioxide is very selective, not as reactive as ozone and chlorine, and preferentially oxidizes sulfur, amines, and some other reactive organic substances. As such, the use of chlorine dioxide has proven advantageous for improvement of water quality and water recycling. However, as with most oxidizing chemistries, chlorine dioxide is consumed almost instantaneously, leaving no residuals for extended microbial control. Thus, treatment of hydraulic fluids with ClO_2 controls only microbes on the surface, but it is not adequate to control indigenous organisms in the reservoir.

23.2.2.2 Hypochlorite

Hypochlorite (bleach) is the least expensive oxidizing chemistry for use in the oilfield. Hypochlorite is unstable in its pure form and is normally handled as an aqueous solution. It is widely used in water treatment as an antimicrobial and water-cleaning agent.

Compared with other oxidizing chemistries, hypochlorite has a stronger oxidative potential than chlorine dioxide, but it is a weaker oxidizer when compared to ozone. Because it is a stronger oxidizer than chlorine dioxide, hypochlorite tends to be consumed even faster, particularly if the water contains high levels of reduced compounds. Moreover, treatment of waters containing high levels of organics can lead to the generation of organochlorine compounds such as mono-, di-, tri-, and tetrachloromethane, which are known carcinogens [20]. Many applications using bleach have been banned in Europe, although its use is still widely used in North America and other countries.

23.2.2.3 Peracetic acid

Peracids or peroxyacids are formed through the equilibrium reaction between hydrogen peroxide and a short chain organic acid. Peracids are only stable in certain concentrations of the reacting components, and its activity can be varied by addition of different ratios of hydrogen peroxide and organic acid. Peracetic acid is formed by reaction of hydrogen peroxide and acetic acid. Peracetic acid was first registered as an antimicrobial in the United States in 1985, and since then, its use has increased in different applications. Applications include agriculture, food processing facilities, hospitals, and industrial water plants. Recently, peracetic acid has been used in oilfields as an alternative to bleach and chlorine dioxide [21].

When peracetic acid dissolves in water, it disintegrates into hydrogen peroxide and acetic acid, which will be converted into water, oxygen, and carbon dioxide. The degradation by-products of peracetic acid are nontoxic and can easily dissolve in water. Although the levels of organic content will have some impact on the action of peracetic acid, pH and temperature will significantly impact its action. Peracetic acid has a redox potential higher than chlorine dioxide but lower than ozone, thus it is a less specific oxidizer than chlorine dioxide. As a result, peracetic acid will oxidize a broader range of targets than ClO_2. Because of this, peracetic acid has been successfully utilized in hydraulic fracturing applications to disinfect the fluids before fracking. Unlike ClO_2, peracetic acid does not need onsite generation and provides a safer alternative for immediate water treatment on the fly and for conditioning of water in storage tanks and ponds in between fracking stages. Additionally, peracetic acid has been used in oilfield production system as a cleaner to maintain the system free of deposits and increase the efficiency of wells and water disposal systems.

23.3 Biocide application

After a biocide is selected, the next question explored is whether it should be dosed continuously or in a batch/slug application. In general, most oilfield biocide treatments are performed in a batch/slug application. This is due to several reasons, such as the cost of continuous treatment over a very large fluid volume as well as the fact that sterility is not necessary to minimize microbial risks in oilfield applications. Another option for continuous treatment would be to use the biocide at a low dose level to act in a

more biostatic (instead of biocidal) mechanism. However, there are mounting data to suggest that oilfield microbes are able to modify their cellular structures to become less susceptible to biocides over time [22,23]. Based on the aforementioned reasons, the most common biocide application is a batch treatment where the biocide is added to the bulk fluid phase for a predetermined period of time (often in the range of 2−8 h) and at a predetermined frequency (weekly, biweekly, etc.). Some systems have effectively used 2 biocides, where one is added at a low dose continuously while the other is used at a much higher dosage (10−100x higher concentration) in a weekly/bi-weekly/monthly batch application. The concept is that the high-dosage biocide will kill microbes and remove biofilm, whereas the low-dosage product will either prevent attachment of new microbes to the surface or minimize the regrowth of biofilm between treatments [24,25]. Although biocides are often utilized as a single means of microbial control, it should be noted that a best-in-class treatment program most often includes both a chemical (biocide) and mechanical (pigging) component. The implementation of pigging will enhance the biocides ability to penetrate into and kill the biofilm. To maximize this effect, biocides are often added immediately following the pig for a period of 2−8 h.

It is critical that the biocide dosage is carefully selected to ensure that the microbial population is controlled in a manner that minimizes risk against corrosion, biotic hydrogen sulfide production, and/or biofouling. To achieve this, biocide dosage should be selected based on performance in a biofilm (sessile) assay as opposed to a planktonic kill test. It is well established that microbes within biofilms can be 500−5000 times harder to kill than the same microbes in planktonic form [26]. At the time of publication of this book, there is not a set standard that is used throughout the industry for testing biocide efficacy against biofilm. There are papers in the literature that use a recirculating flow loop, whereas others use glass bioreactors (often referred to as CDC biofilm reactors) that allow for a once through biofilm growth system [27,28]. Irrespective of the method used, there are several parameters that are key to ensure that the method is representative of oilfield biofilms. First, the test must be reproducible and the biofilm growth consistent on all coupons used in the testing. This is challenging because biofilms by nature are not expected to be uniform. In addition, most oilfield biofilms should be grown in an anaerobic environment to mimic the actual system and support the growth of anaerobic microbes such as SRB and Archaea. Finally, the biofilms should be allowed to grow to a mature state, because immature biofilms are much more susceptible to biocides. We have found that 4−6 weeks is the average amount of time required to cultivate a mature biofilm (unpublished data). This is in stark contrast to the methods described for fast-growing organisms such as *Pseudomonas aeruginosa*, where the growth phase is usually only 48 h before testing is initiated.

Biocide dosage determined in a lab or field kill study is the minimum dosage that should be present at the end of the system where the biocide is no longer required. Often, the dosage identified through a kill study is the product dosage used at the injection point, which is unlikely to be present in the same abundance at the end of the system. For example, if 500 ppm of product A is injected at the separator, it is very likely that only 100−200 ppm of the product will still be present after oil and water separation is complete, and the water stream is injected for disposal, discharged, or

recycled. In this case, the injection dosage would need to be increased sufficiently to ensure that 500 ppm was still present at the end of the system. Biocides vary greatly in their persistence through a system based on factors such as reaction with other materials in the system, partitioning, and degradation. Residual monitoring will be critical in these circumstances to confirm the amount of biocide remaining at the end of the system after a treatment is performed.

Treatment frequency is dependent on the performance of the product as well as the regrowth of the biomass in the system. Because every system is different, there is no set standard for how often a biocide treatment should be performed. The best means by which the treatment frequency can be predicted is through the sessile/biofilm kill study described earlier. These tests can be used to evaluate the regrowth kinetics of the biofilm. In most cases, treatment frequency is no more than twice per week and no less than once every other week. However, there are always exceptions and treatment frequency should be based on the key performance indicators (KPIs) of the system such as corrosion rate, biotic hydrogen sulfide production, or biofilm/slime buildup, which result in fouling.

Like treatment frequency, treatment duration is dependent on the system and can be evaluated through laboratory testing. As an example, we tested a biocide at the same concentration but with different contact times using flow cytometry (Fig. 23.1). In this figure, the movement of the pixels (which represents individual microbes) from the lower left quadrant to the upper right quadrant shows membrane damage and depolarization, resulting in microbial kill. In the untreated sample, the population is very healthy with 96% viable cells. During the first 15 min of contact with the biocide, a small population (approximately 7%) was immediately killed and is the most susceptible to the treatment. After 1 h, approximately one half of the population had shifted from viable to either depolarized or membrane damaged and depolarized and by 2 h that number had increased to nearly 90%. However, this study showed that leaving the biocide in contact with the microbes for an additional 2 h (4 h total) only increased the kill by an additional 2%, suggesting that the biocide achieved its maximal performance by the 2-h time point. Consistent with the results shown in Fig. 23.1, we have performed testing in the field, which demonstrates limited additional kill on biocide treatments that are extended longer than 8 h (data not published). The correlation between biocide dosage and the optimal contact time is field, chemistry, and dosage specific.

Once a biocide has been selected and the frequency, duration, and dosage have been identified, the final step is to determine where in the system the biocide should be applied. This step should not be overlooked as treatment location can have a major impact on product performance. Location for the biocide injection is generally selected based on availability or convenience, but this is rarely the best place to inject the product. To make a proper treatment location selection, one must first understand where the microbial problem is coming from. If it is coming from the reservoir or a producing well, then the optimal treatment location is down the back side of the well, squeezed into the formation, or delivered at the wellhead. On the other hand, if the problem is coming from a drain or sump that is reinoculating microbes into other parts of the system, then the treatment needs to be delivered at that location. When possible, it is a best practice for the biocide to be introduced upstream of where the microbes are entering

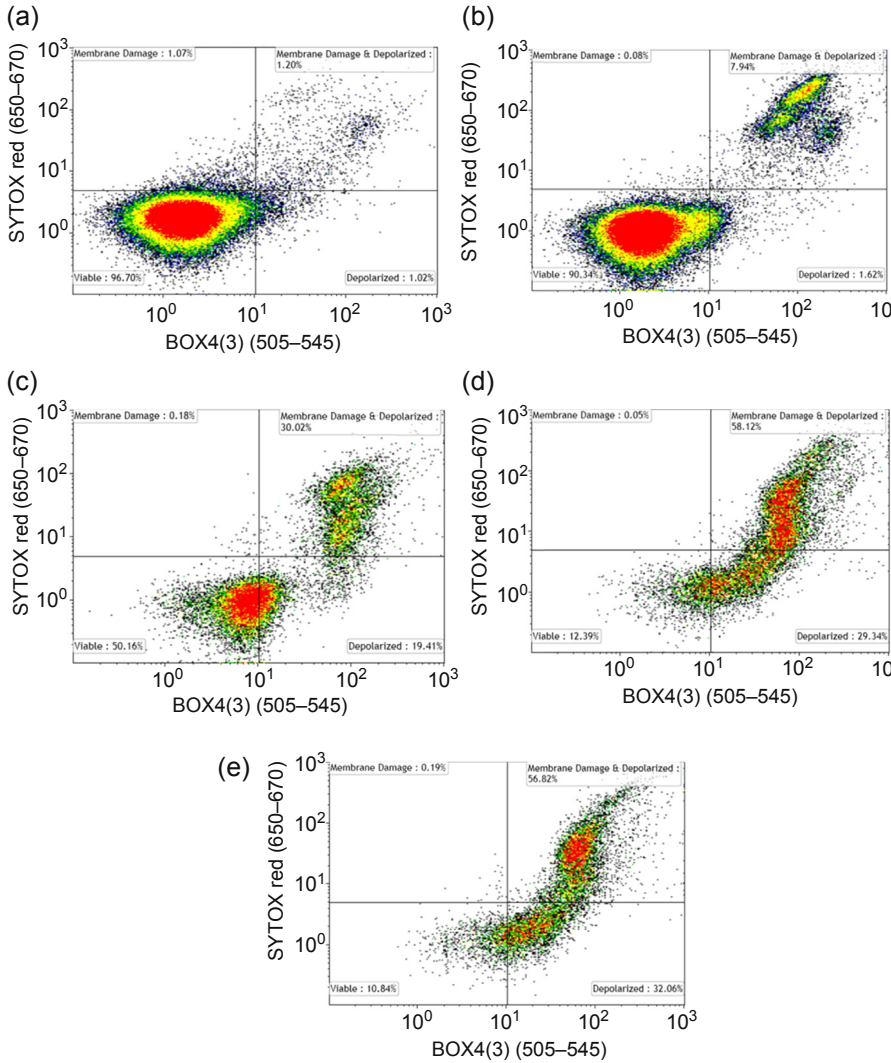

Figure 23.1 Flow cytometry showing biocide performance over time. (a) Untreated microbial population; (b) Microbes after 15-min biocide exposure; (c) Microbes after 1 h biocide exposure; (d) Microbes after 2-h biocide exposure; (e) Microbes after 4-h biocide exposure.

the system. In many cases this may not be possible—such as when the microbes are coming from the formation or the producing well. When coming from a producing well, microbes are often in a dormant stage because the temperature, pressure, or nutrients are limiting their growth. It is critical to gain control before the environmental pressures change and the microbes move into an active state.

Microbes most often follow the water phase of the system, and treatment needs to be effective in the water phase. Treatment into an oil- or multiphase system can result

in some or all of the biocide partitioning to the oil phase, and product efficacy could be significantly reduced. Even if the product does partition to the water phase, sufficient retention time must be available for the product to move to the water phase. Treatment at a wellhead or separator may mean that only half the biocide concentration (or less) is still present in the produced water downstream. Biocide residual will need to be monitored to ensure that the chemistry is actually following the same path as the microbes to minimize risk. If significant biocide residual is lost during separation, a second biocide injection point may be required in the water phase of the system (such as at a Free Water Knockout, WEMCO, produced water pipeline, or water disposal well).

A routine monitoring program is critical to understand the efficacy of the biocide in use and to determine if any optimization is required. A biocide monitoring program generally consists of three separate steps, each of which will be discussed below:

- Monitoring of the system KPIs
- Monitoring of the biocide residual in the system
- Monitoring of the microbial population

Monitoring the system KPIs provides the greatest detail into the actual performance of the biocide program. If the treatment that has been implemented does not meet the identified KPIs, then the program is not successful. That may mean that the biocide itself or the treatment duration, frequency, or location of treatment needs to be changed. The two most common KPIs that are measured in a biocide program are the corrosion rate and/or the amount of H_2S that is produced in the system. There are numerous means to measure corrosion rate, but the most common ones associated with a biocide program involve monitoring corrosion rate from a coupon that is placed in the system or using an electrochemical probe. In addition to monitoring corrosion rate or H_2S production, other KPIs could include heat transfer efficiency of equipment, injection rate/pressure, and sulfide levels, among others.

A second means by which biocide programs are commonly monitored involves residual biocide in the system. Most of the commonly used biocides in oil and gas can be easily monitored in the field using a simple test such as a titration. Although this may not provide the most accurate answer, it often provides insight that is ± 10 ppm. This resolution is generally sufficient to understand whether the biocide is making it through the system and still providing a biocidal dosage at the final point where the treatment still needs to be effective. It is important to note that biocide residual tests can be misleading if interferences occur. For example, a field residual test for a quaternary amine will also likely detect the presence of a corrosion inhibitor, making the residual number appear higher than it actually is.

Finally, a comprehensive monitoring program should also evaluate the microbial population. This could involve enumeration of microbes or speciation of the population. There are numerous methods for microbial detection, several of which are outlined here. It should be noted that best-in-class microbial monitoring programs often use at least 2 different methods for enumeration and/or speciation. In addition, it is critical that the microbial monitoring program can detect all microbes present in a given system. Historically, culture-dependent methods have been employed for microbial enumeration and metabolic classification (SRBs, IRBs, etc.). Numerous publications

in recent years have demonstrated that culture-dependent methods, despite their historical usage, often miss greater than 90% of the microbial population present. This finding is due to the diversity of microbes present in the oilfield and highlights the need for culture-independent methods of monitoring [29,30]. Research work has shown that greater than 1400 bacteria and Archaeal genera have been documented in oilfield systems [30]. Common culture-independent methods of microbial monitoring include quantification of adenosine triphosphate (ATP) and DNA-based methods such as quantitative polymerase chain reaction (qPCR) and DNA sequencing. Based on the methods that are used, it is possible that it will include testing performed in the field with rapid results and laboratory-based testing performed on a less frequent basis (quarterly/biannually) to provide a more robust data set. This type of monitoring program was proposed as a best practice for the industry [31].

In summary, the combination of monitoring system KPIs, biocide residual, and microbial populations provides a strong foundation for driving continuous improvement of a biocide program.

23.4 Regulatory impact on biocide usage

The regulation of biocides (microbiocides) in the oil and gas industry varies across the world. Individual country level requirements may range from minimal to very expensive and highly complex registration schemes. The oil and gas industry continues to see increasing regulatory and registration requirements of biocides. A few examples of established programs include Canada, Mexico, Ghana, United States, and European Union (EU). The following will provide a brief overview of the requirements and complexity of two of the more robust and established programs [Federal Insecticide, Fungicide, and Rodenticide Act (FIFRA) in the United States and the Biocide Product Regulation in the European Union].

It is strongly encouraged that the reader reference C.F.R 40 Parts 150−189, Protection of the Environment for a more detailed explanation of FIFRA law. In the oil and gas industry, products to control bacteria are often termed “biocides.” FIFRA uses the term “pesticides” to describe biocide products, and this term will be used in the explanation of oilfield biocide regulation in the following passages.

23.4.1 United States

Biocides used in oil and gas operations are regulated under FIFRA. FIFRA was first enacted by the United States Congress in 1947 under the jurisdiction of the United States Department of Agriculture (USDA). FIFRA was brought into the “newly formed” Environmental Protection Agency (EPA) in 1970. Subsequent major revisions and amendments to the Act occurred in 1972, 1988, 1996, and 2012. The law required that all pesticides be registered before distribution or sale and required warnings on the labels and instructions for their safe use. The current requirements can be found in the US Code of Federal Regulations as 40 CFR Parts 150−189.

23.4.1.1 Definition of a pesticide

It is important to understand that pesticides in the United States are not defined by the inherent characteristics of a product but rather by the intent in which the product is used. The intent and how the law identifies a pesticide are both critical components necessary for a company to determine whether or not a product must be registered with the EPA. FIFRA defines the term "pesticide" as:

- any substance or mixture of substances intended for preventing, destroying, repelling, or mitigating any pest;
- any substance or mixture of substances intended for use as a plant regulator, defoliant, or desiccant; and
- any nitrogen stabilizer

Intent is set forth by 40 C.F.R section §152.15, and the EPA considers a product to be for biocidal purposes and requires EPA registration if:

- The person who distributes or sells the substance claims, states, or implies (by labeling or otherwise):
  - That the substance (either by itself or in combination with any other substance) can or should be used as a pesticide; or
  - That the substance consists of or contains an active ingredient and that it can be used to manufacture a pesticide; or

The substance consists of or contains one or more active ingredients and has no significant commercially valuable use as distributed or sold other than (1) use for pesticidal purpose (by itself or in combination with any other substance), (2) use for manufacture of a pesticide; or

The person who distributes or sells the substance has actual or constructive knowledge that the substance will be used, or is intended to be used, for pesticidal purpose.

It is also important to consider that devices (versus chemical substances) may also be subject to FIFRA regulation and require EPA registration. Examples of devices regulated by the EPA may include certain ultraviolet (UV) light systems, ozone generators, water filters, and air filters (except those containing substances that are pesticides).

23.4.1.2 Types of biocide product registrations

EPA-registered biocides fall into two main categories.

Primary registrations: Primary registrations are registrations in which the registering company "owns" the registration. They would be responsible for providing all necessary toxicity data to support the registration and would maintain the registration at the federal level. This type of registration involves working directly with the EPA. The requirements of this registration are discussed below.

Supplemental (distributor) registrations: These registrations allow one entity "piggybacks" off another entities primary registration. As a distributor of the primary registration, the secondary registration holder would be able to rebrand the product and have their own labels, but the registration would be maintained at the federal level by the primary registrant holder. The primary registrant holder works directly with the distributor to ensure the distributed product is in compliance with FIFRA.

23.4.1.3 Primary registrations

When submitting an application for a primary registration, the applicant must provide the following information.

23.4.1.4 Confidential statement of formula

This document defines the ingredients and establishes sources of those ingredients and the certified limits for each component. Ingredients are either disclosed as "active ingredients" or "inert ingredients."

Typical examples of active ingredients may include glutaraldehyde, THPS, and several quaternary ammonium compounds.

Typical examples of inert ingredients may include water, solvents, and winterization agents.

23.4.1.5 Label

Registered biocides must bear a label, of which requirements are described in detail in 40 C.F.R Part 156—labeling requirements for pesticides and devices. In general, 40 C.F.R. §156.10 specifies that labeling contain the following:

- Product name and the name and address of the producer, registrant, or person for whom produced
- The net contents
- The product registration number and production establishment number
- An ingredient statement
- Warning or precautionary statements
- Environmental and physical/chemical hazard statement
- Directions for use

23.4.1.6 Data requirements

An application for registration must address the following data requirements to allow an EPA review:

- Product Chemistry
  - Typically, physical and chemical information
- Manufacturing process/procedure
- Toxicology and environmental information to address
  - Acute and chronic health effects
  - Environmental effects
  - Environmental fate

23.4.1.7 Specific types of registrations

New Chemical Registration: These are registrations in which the active ingredient is not registered with the EPA. Because there is no database on the molecule or experience with its use as a pesticide, this type of registration takes the longest period of time

and comes with a considerable cost because significant toxicity data would need to be generated as part of the submission package. The EPA review time for New Chemical Registrations is 540 days.

New Use Registrations: New Use Registrations are registrations in which the active ingredients are registered for a different application, and the active is registered under FIFRA. In this instance, toxicity data and experience with the chemistry are known to the EPA, which facilitates the evaluation for use in the new application; however, additional data may be required. The EPA review time for New Use Registrations is 270 days.

Me-too Registrations: Me-too Registrations are registrations in which a product being registered is identical or substantially similar to a biocide product that is already registered under FIFRA for the same use or "the pesticide and its proposed use differ only in ways that would not significantly increase the risk of unreasonable adverse effects on the environment." The EPA review time for Me-too Registrations is 90 days.

23.4.1.8 State registrations

Once a biocide product is registered at the federal level, it must be registered at the state level before the product can be sold. State registrations vary in complexity and time to register. Generally, California and New York registrations are considered to be the most complex and longest timeline. The remaining states vary from a few weeks to a few months, depending on the state.

23.4.1.9 Enforcement

Under FIFRA, it is "unlawful for any person to 'offer for sale' any pesticide if it is unregistered, or if claims made for it as part of its distribution or sale differ substantially from any claim made for it as part of the statement required in connection with its registration under FIFRA section 3." Statements of enforcement policies and interpretations are discussed in detail in 40 C.F.R. Part 168—Statements of enforcement policies and interpretations. FIFRA is enforced under the EPA's Office of Enforcement and Compliance Assurance (OECA).

23.4.2 European Union

Energy service processors more and more may recognize visible changes to products used for their end-use applications. It may be that the product formulation has been modified, or the product is not available anymore, the label text, or even the product name has changed. Many of these changes are being driven by the Biocidal Product Regulation, which aims for the harmonization of biocidal products (BPs) in the European market. Manufacturers and formulators of biocides in the EU need to undergo a complex, long-lasting but also cost-intensive registration process.

Even though this is an advantage for the environment and the harmonization of biocides in Europe, it could also delay the introduction of new innovative biocides to the European market. It is expected that not every supplier of biocides will be able to support every active substance (AS) in the future. The market harmonization is already in full process.

23.4.2.1 EU regulatory framework

The Biocidal Product Regulation (EU) 528/2012(BPR) aims for the harmonization of biocide products in the European market and the protection of humans, animals, and the environment. This regulation and the former Directive 98/8 (EC) (BPD) addressed to the Member States of the EU and countries of the European Economic Area (Iceland, Norway, and Liechtenstein). The Swiss legislation is equivalent to that of the EU.

23.4.2.2 What is a biocidal product?

A BP is defined as any substance or mixture, in the form in which it is supplied to the user, consisting of, containing, or generating one or more ASs, with the intention of destroying, deterring, rendering harmless, preventing the action of, or otherwise exerting a controlling effect on, any harmful organism by any means other than mere physical or mechanical action.

Based on that definition we could consider a BP as follows:

- A product containing one or more ASs
- A product intended to be used for biocidal applications

23.4.2.3 What is an active substance?

An AS is defined as a substance or microorganism including a virus or a fungus having general or specific action on or against harmful organisms.

Examples include peracetic acid or glutaraldehyde.

23.4.2.4 How does the BPR work?

The BPD/BPR implementation process is focused on existing ASs and BPs containing one or more existing ASs. An "existing active substance" means an AS placed on the market before May 14, 2000 in biocidal applications.

The BPR defines 22 general biocidal uses called product types (PT), which cover all product applications. The most common biocidal applications in the energy service industry are covered under the following:

Product-type 11: Preservatives for liquid-cooling and processing systems

Products used for the preservation of water or other liquids used in cooling and processing systems by the control of harmful organisms such as microbes, algae, and mussels.

Product-type 12: Slimicides

Products used for the prevention or control of slime growth on materials, equipment, and structures, used in industrial processes, e.g., on wood and paper pulp and porous sand strata in oil extraction.

The evaluation of active substances for specific applications

1. Identification of existing biocidal ASs

Each manufacturer has informed the Commission about existing ASs placed on the market for use in BPs.

2. Notification of ASs

   Those manufacturers who identified an AS informed the Commission about the application (PTs) of the AS and committed to submit an active dossier according to BPD/BPR requirements.

3. Submission of AS dossier

   Manufacturers submitted ASs dossiers to a Member State, which will evaluate the dossier and provide an opinion about the approval of the respective AS. The Biocidal Product Committee (BPC) of the European Chemical Agency (ECHA) decides based on that Member State's opinion (Evaluating member states).

The evaluation of biocide products containing approved active substances

4. Submission of a biocide product dossier for Authorization

   One Member State will evaluate the product information and will decide about the authorization for its use in that Member State.

   After authorization from the first Member State or in parallel to evaluation, the manufacturer of the BP may apply for authorization of the same product in other Member States via mutual recognition process (MRP). The Concerned Member States will then evaluate the dossier in a shortened procedure.

   Alternatively the agency (ECHA) can facilitate the authorization process for all member state in a centralized procedure, the so called union authorization.

   The BPR implementation process limits the use of ASs and also their use for specific applications. Consequently the number and diversity of BPs on the European market is reduced. To meet the aims of the BPR, an exhaustive evaluation of biocide actives and biocide products is required based on the data provided by industry; this inevitably leads to a significant investment to maintain existing products on the market.

   The BPR ensures the continued safe use of BPs in the European market. Manufacturers of BPs are committed to provide quality products that meet high standards of human and environmental safety, support the end user daily, and contribute to the wellbeing of society.

   Before the BPD/BPR came about, biocide products were regulated individually by national country legislation, which have now been adjusted because of the local transposition of the BPD.

   Currently the regulating measures still differ from country to country, although the aim is to have a harmonized European market. Each Member State requires specific information to introduce biocide products on to the market.

   In the future, after the evaluation of the biocide actives, the assessment of the biocide products should follow harmonized rules. The BPR transition period is a process that impacts existing biocide actives and biocide products in local markets.

   For new BPs containing new biocide ASs, an authorization following the BPR requirements is necessary before the product can be placed on the market. For this reason the introduction of new innovative biocide products containing new biocide ASs will take up to 5 years time.

23.4.2.5 Biocides—clear instructions for safe use

The BPR requires manufacturers to provide specific information to ensure the safe use of products. The product label is used as communication tool for that purpose.

- Identity and concentration of ASs
- Authorization number
- Type of preparation (liquid, granules, solid, etc.)

- Authorized product use
- Direction for use and dose rate
- Interval the product should be used and necessary timing to take effect
- Ventilation, transport, and storage requirements
- Batch number and expiry date

Until the BPR rules are fully active for all products of the energy service industry, biocidal manufacturers need to invest to have this regulation implemented. Energy service processors need to review their safety management systems on a regular basis. In general, the Biocidal Product legislation is a chance to have well documented and safer biocides for users.

23.5 Next-generation biocide development

Historically, antimicrobial compounds (AKA biocides) with broad spectrum efficacy against microbes have been used in the oil and gas industry. However, there are numerous other methods that have been, or are currently, under evaluation as next-generation microbial control methods. The list here is not exhaustive but is meant to highlight some of the most prominent and/or promising methods of microbial control. Although each of these methods has very exciting advantages, they also have significant risks or disadvantages that must be overcome before the method will begin to see broad acceptance in the oil and gas industry.

The first alternative method can be referred to as probiotics for oilfield systems. This method is built on the hypothesis that there are such things as "good" and "bad" microbes within the oilfield and that "good" microbes can be effectively controlled and utilized to overcome the negative consequences of "bad" microbes. The classical use of this philosophy relates to the injection of nitrate as a food source for nitrate-reducing bacteria (NRB) and the ability of the NRB to outcompete the SRBs in water injection systems. A scan of the literature over the past 10 years shows mixed results of this treatment, where some describe biotic hydrogen sulfide control and others describe challenges, especially as assets age [32,33]. The use of nitrate in water injection systems has been widespread, and the available papers in the literature highlight its use in West Africa and the North Sea in particular. However, there is a significant concern in the industry that purposefully growing large amounts of NRBs within a reservoir could lead to fouling of the near wellbore area and or plugging of the formation. Although there has not been much data presented publically on this topic, numerous examples have been observed by operators where continuous nitrate injection leads to increased injection pressure that is only reduced upon batch treatment with a biocide, which is likely breaking up the NRB-based biofilm that is causing the pressure increase. An example of this phenomenon where an oil and gas operator was continuously injecting calcium nitrate is shown Fig. 23.2. As shown in the figure, injection pressure steadily rises over a period of 3−4 days and then immediately falls upon batch biocide treatment.

Another concern with nitrate treatment is the growing evidence that even NRBs might have negative consequences in terms of accelerating microbial corrosion

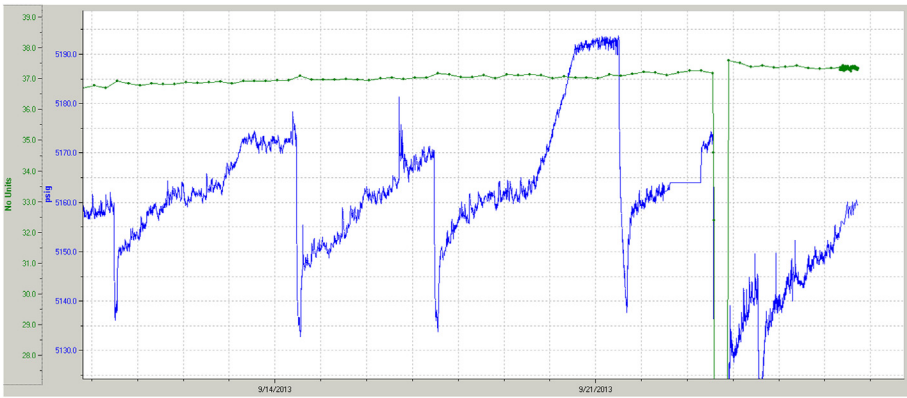

Figure 23.2 Data from a production system showing pressure build in a water injection well that subsequently decreases after a batch biocide treatment, suggesting that nitrate-reducing bacteria growth is causing biofouling/formation plugging in the near wellbore area.

(MIC). This is likely due to the incomplete reduction of nitrate to nitrite. In recent years, there have been several papers published showing a mechanism by which NRBs can increase the pitting corrosion rate, which calls into question whether competitive exclusion based on the growth of NRBs is really a viable method for control of "bad" microbes [34,35]. There is still a significant amount of work required to fully understand any potential risk of using NRB growth as a medium to control SRBs, but the data gathered to date suggest that this method should be used cautiously, and proper monitoring should be put in place to understand any fouling and/or corrosion risks that arise. The ability to develop and/or identify a microbe that provides control of high-risk microbes such as SRBs while not causing fouling or corrosion would be of significant interest to the oil and gas industry.

With increasing global regulations and pressure to use "green" chemistries, there have been numerous developments of equipment that can be used as an alternative to traditional biocides. The most commonly used equipment involves microbial removal through filtration, microbial control through nutrient depletion, microbial inactivation/kill through UV treatment, or microbial inactivation/kill through sonication or cavitation. Each of these methods will be described briefly below.

Membrane systems are most commonly observed in offshore water injection systems with membranes providing coarse filtration of the raw seawater and further downstream a fine filtration for the water that is to be injected into the formation. Of particular interest for this discussion are the sulfate-removal packages (SRUs) that are often used offshore in large water injection systems. Although these systems are a large capital expense at the start-up of an asset and require significant deck space, they provide several benefits that can be very valuable to the operator. First, they are able to remove approximately 99% of the sulfate from seawater, minimizing the risk of barium sulfate scaling in the reservoir. This is often the main intention of the SRU systems because seawater can have up to 3000 ppm of sulfate in it. However,

there is an added benefit of these systems in microbial control. The SRU systems work through size exclusion as they remove sulfate from the system for injection. Although the sulfate is not completely removed, it is often reduced to 15−30 ppm, which significantly impacts the amount of hydrogen sulfide that could be generated by SRBs in the reservoir. In addition, the size exclusion removes a large number of the microbes as they are taken out of the system in the reject water and never injected downhole. This phenomenon was observed in a paper published by Keasler et al. [36], where they showed a 90% reduction in microbes downstream of the SRU compared with upstream. Although there does seem to be value in using an SRU system for microbial reduction and to minimize biotic souring risk in the reservoir, several challenges exist as well. One major challenge is around cost. This includes both the large up-front capital investment as well as the cost of maintenance for the equipment, which will be an evergreen expense for the operator and includes membrane replacement. In addition, any downtime for the membrane system means that unfiltered seawater is likely to be diverted around the SRU and directly into the formation. This scenario results in large amounts of sulfate being introduced into the reservoir as well as larger microbe numbers. Finally, as with any equipment offering that is described in this chapter, there is no additional downstream microbial control that is gained through this treatment. For example, even if the water is sterilized on the surface, there are likely microbes already downhole that are not impacted by the SRU system and must be considered in the risk profile.

A second equipment offering that has gained momentum in the oil and gas industry, particular in US onshore unconventional applications, is the use of UV light for inactivation or kill of microbes. For this application, water is passed through a system where it is exposed to UV light for a particular period of time, which results in UV-induced damage to the microbial cell's DNA. This damage will either lead to death or, at a minimum, likely prevent the microbe from efficiently multiplying downstream of the treatment. Similar to the SRU system, there are concerns around capital costs, repair, and maintenance, as well as any microbes that are already present downstream of the UV system that is not controlled because no residual product/material is present. In addition, the ability of a UV-based system to be effective against microbes is directly proportional to the clarity of the water. As the water moves from clear to black (through the presence of iron sulfide, etc.), the performance of the UV system is directly impacted. To this end, UV treatment should only be used in systems with relatively "clean" water to maximize performance.

One final equipment offering described here is the use of cavitation, or vibrations, to injure and/or kill microbial cells. Similar to UV treatment, this method is most prevalent in US onshore unconventional applications for treating water that is to be used in fracturing applications. The advantages and disadvantages of this method are very similar to those described earlier for both SRUs and UV treatment. The lack of chemical use can be seen as "green," but must be balanced against the capital costs and equipment upkeep and repair, which can be significant. In addition, there is no carry over of the benefits to provide downstream microbial control through the presence of some type of residual material in the treated fluid. This section was not an exhaustive list of mechanical methods for microbial control but was meant to highlight

to the reader the general advantages and disadvantages of using mechanical methods for microbial control in oil and gas applications.

Delivery of a product to the source of the problem can be a huge challenge, especially for treating microbes in a reservoir. There is much debate in the industry as to whether a biocide added on the topsides of an operation and injected downhole can traverse through an entire reservoir or if it is consumed in the near wellbore area. To address this challenge, there are investigators working on coating and triggers that would allow the biocide to remain inactive until it is deep into the reservoir. These triggers can be based on environmental parameters such as salinity, temperature, pH, or pressure, among others. A commercially viable example of a technology with a trigger that is activated in the reservoir is BrightWater, which was developed in the mid-2000s for enhanced oil recovery. This molecule expands to many times its original size in the reservoir, blocking high permeability areas and increasing the sweep efficiency of a waterflood. It is also possible to encapsulate biocides inside a coating or nanoparticle that would slowly release over time. This has successfully been done through the development of solid biocide products (sticks, blocks, pucks, etc.) but is still under investigation for small particles that could be injected into a reservoir.

Although many biocides function by providing broad spectrum kill, there is growing interest in targeting specific microbes to reduce risk. This area of study has grown significantly as DNA sequencing and speciation has become more common place in the oil and gas industry, leading to specific information on which microbes (at the genus or species level) are most commonly present and could be potentially targeted to minimize risk. One technology area in particular that has been researched is the use of bacteriophage as a means to control microbial growth and proliferation. Bacteriophages are viruses that infect (and potentially kill) specific microorganisms. Significant work has been performed by Dr. Elizabeth Summer and others to identify bacteriophages that are specific to SRBs most commonly found in oil and gas systems [37]. Their work has confirmed the existence of these phages as well as the ability of the phages to reduce SRB numbers through phage addition in laboratory experiments. Follow-up work that has been presented at conferences has shown the ability of phage treatment to reduce SRB levels by up to 6–9 logs. The major advantage of phage treatment is the ability to specifically target the organism(s) of interest and leave any other microbes virtually untouched. In addition, phage infection and replication within the microbes of interest means that with each round of infection and lysis the phage titer increases in the bulk fluid phase until the microbes of interest are killed, at which point the phage quantity quickly drops to very low levels. Although there is much excitement about the potential use of phage, there are also concerns about efficacy because of the wide diversity of microbes in oil and gas systems and the potential need to have a different phage cocktail for each and every oilfield around the globe. This could make phage projects extremely complex as the user attempts to develop just the right cocktail to control microbial risk in their system.

Another alternative to traditional biocides that is currently being investigated by the oil and gas industry is the use of enzymes for microbial control. Enzymes have been successfully utilized in numerous commercial applications such as stickies removal in the pulp and paper industry, removal of protein stains in laundry, and production of

certain foods such as cheese, just to name a few. However, there has been limited usage of enzymes in oil and gas applications, particularly for control of microbes. The application of enzymes for microbial control, particularly in controlling biofilm growth, seems very plausible, given the fact that enzymes can target a number of components that often make up a biofilm matrix such as carbohydrates and proteins. A paper published by Harmon et al. [38] showed the potential impact of enzymes in biofilm control. The results presented in the paper suggest that several different enzyme classes are capable of biofilm removal, and the author also shows a slight benefit of adding enzymes along with traditional biocides to boost performance efficacy [38]. There is still a significant amount of work that needs to be done in this area, such as enzyme performance in a 3-phase system, the impact of high temperature and/or pressure, and the other components present in produced water that could negatively affect the enzyme performance. If those challenges can be understood and successfully addressed, enzymes could be a novel means by which to provide biofilm control in the oil and gas industry.

As we look to the future of biofilm control, the question always arises about the impact that a better understanding of quorum sensing will have. This phenomenon is characterized by the indirect mechanism of environmental sensing through small molecules that are secreted and/or detected by microbes within an environment [39–41]. It has been shown that numerous behaviors of microbes are under the control of quorum sensing including biofilm formation [42,43]. The work conducted to date in the area of quorum sensing has been able to identify compounds with antivirulence activity, which could play an important role in the growing crisis around antibiotic resistance (reviewed in Ref. [44]). Although quorum sensing is an area that has been studied for years and continues to show breakthroughs, we are nowhere near a commercial quorum-sensing solution for oil and gas applications. This is an area that should continuously be observed for new discoveries that may shed light on how quorum sensing could be used for biofilm control and risk management in the oil and gas industry.

23.6 Conclusions

In summary, this chapter is meant to leave the reader with a better understanding of biocides. It reviewed the problems caused by microbes (such as corrosion, fouling, and H_2S production) and discussed the commonly used chemical biocides in the oil and gas industry. The chapter highlighted different biocidal actives, the advantages and disadvantages of each, and the types of applications where they are most commonly used. This chapter also reviewed best-in-class methods for biocide application and monitoring.

One of the most challenging aspects of biocides are the complex regulations that govern their usage on a global basis. Not only are the regulations complex, but they differ significantly from one country to the next. In this chapter, we briefly reviewed the regulatory landscape for biocide usage in the United States and Europe, which are two of the more challenging regulatory environments. Finally, this chapter concluded

by discussing novel technologies that have recently emerged or are in development. The industry recognizes that although regulatory landscape complicates the introduction of new biocides, it is imperative that new technologies are brought to market to provide improved performance and reduce treatment cost.

References

[1] J.W. Costerton, J. Boivin, Biofilms and biocorrosion, in: H.-C. Flemming, Geesey (Eds.), Biofouling and Biocorrosion in Industrial Water Systems, Springer, Berlin, Heidelberg, 1991, pp. 195−204.
[2] H.A. Videla, L.K. Herrera, Microbiologically influenced corrosion: looking to the future, International Microbiology 8 (3) (2005) 169−180.
[3] R.B. Eckert, H.C. Aldrich, C.A. Edwards, B.A. Cookingham, Microscopic differentiation of internal corrosion initiation mechanisms in a natural gas gathering systems, in: CORROSION 2003, NACE, San Diego, CA, 2003. Paper no. 03544.
[4] R. Cord-Ruwisch, W. Kleinitz, F. Widdel, Sulfate-reducing bacteria and their activities in oil production, Journal of Petroleum Technology 39 (1) (1987).
[5] B. Geissler, R.M. De Paula, C. Keller-Schultz, J. Lilley, V.V. Keasler, Data mining to prevent microbiologically influenced corrosion? in: NACE Corrosion 2014, 2014. Paper 4080.
[6] B. Geissler, C. Keller-Schultz, J. Lilley, V.V. Keasler, Don't just blame the SRBs and APBs for MIC, in: NACE Corrosion 2015, 2015. Paper 6083.
[7] J. Larsen, et al., Consortia of MIC bacteria and archaea causing pitting corrosion in top side oil production facilities, in: CORROSION/2010, NACE, Houston, TX, 2010. Paper no. 10252.
[8] E. Bastin, F. Greer, C. Merritt, G. Moulton, The presence of sulphate reducing bacteria in oil field waters, Science 63 (1926) 21−24.
[9] J. Beeder, T.R. Andersen, T. Liengen, K. Dronen, T. Torsvik, Corrosion as a side effect during nitrate treatment of produced water and aquifer water injection, in: Corrosion/2007, NACE International, Nashville, TN, 2007. Paper no. C2007-07512.
[10] J.C. Shaw, N.C. Bramhill, C. Wardlaw, J.W. Costerton, Bacterial fouling in a model core system, Applied and Environmental Microbiology (1985) 693−701.
[11] T.S. Whitham, P.D. Gilbert, Evaluation of a model biofilm for the ranking of biocide performance against sulphate-reducing bacteria, Journal of Applied Microbiology 75 (1993) 529−535.
[12] H.W. Sun, R.J. Feigal, H.H. Messer, Cytotoxicity of glutaraldehyde and formaldehyde in relation to time of exposure and concentration, Pediatric Dentistry 12 (5) (1990) 303−307.
[13] H.R. McGinley, M.V. Enzien, G. Jenneman, J. Harris, Studies on the Chemical Stability of Glutaraldehyde in Produced Water, 2011. SPE paper 141449.
[14] S.L. Jordan, M.R. Russo, R.L. Blessing, A.B. Theis, Inactivation of glutaraldehyde by reaction with sodium bisulfite, Journal of Toxicology and Environmental Health 47 (3) (1993) 299−309.
[15] P.S. Stewart, L. Grab, J.A. Diemer, Analysis of biocide transport limitation in an artificial biofilm system, Journal of Applied Microbiology 85 (1998) 495−500.
[16] J. Moore, V.V. Keasler, B. Bennett, Compatibility of Tetrakis(hydroxymethyl) phosphonium sulfate (Thps) and ammonium bisulfite (ABS), in: NACE Corrosion Paper 10407, 2010.

[17] V.V. Keasler, B. Bennett, B. Bromage, R.J. Franco, D. Defevre, J. Shafer, B. Moninuola, Bacterial characterization and biocide qualification for full wellstream crude oil pipelines, in: NACE International Paper # 10250, 2010.
[18] U. Bertheas, K. Majamaa, A. Arzu, R. Pahnke, Use of DBNPA to control biofouling in RO membranes, Desalination and Water Treatment 3 (2009) 1−3.
[19] R.M. De Paula, V.V. Keasler, T.J. Tidwell, Evaluation of preservative chemistries to control microbial activity during well completion, in: NACE Corrosion 2015 Paper 6069, 2015.
[20] M. Obadasi, Halogenated volatile organic compounds from the use of chlorine-bleach-containing household products, Environmental Science and Technology 42 (5) (2008) 1445−1451.
[21] R.M. De Paula, V.V. Keasler, J. Li, D. McSherry, R. Staub, Development of peracetic acid (PAA) as an environmentally safe biocide for water treatment during hydraulic fracturing applications, in: SPE Conference for Oilfield Chemistry, 2013. Paper 164088.
[22] S. Oh, M. Tandukar, S. Pavlostathis, P. Chain, K. Konstantinidis, Microbial community adaptation to quaternary ammonium biocides as revealed by metagenomics, Environmental Microbiology 15 (10) (2013) 2850−2864.
[23] A.D. Russell, Antibiotic and biocide resistance in bacteria: introduction, Journal of Applied Microbiology Symposium Supplement 92 (2002) 1S−3S.
[24] R. De Paula, V. Keasler, B. Bennett, C. Keller, R.C. Adams, Z. Vaksman, H. Kaplan, Optimization of a microbial control program in an aging Gulf of Mexico asset to minimize the risk of corrosion, in: NACE International Paper #1195, 2012.
[25] J. Penkala, T. Salma, E. Burger, E. Bastos, N. Shioya, M. Oliveira Penna, C. Azevedo Andrade, A Cost Effective Treatment to Mitigate Biogenic H_2S on a FPSO, 2004. NACE International paper #04751.
[26] J.W. Costerton, B. Ellis, K. Lam, F. Johnson, A.E. Khoury, Mechanisms of electrical enhancement of efficacy of antibiotics in killing biofilm bacteria, Antimicrobial Agents and Chemotherapy 38 (12) (1994) 2803−2809.
[27] V.V. Keasler, B. Bennett, H. McGinley, Analysis of bacterial kill versus corrosion from use of common oilfield biocides, in: Proceedings of the 8th International Pipeline Conference IPC 2010, 2010.
[28] T. Tidwell, R. De Paula, G. Nilsen, V. Keasler, Visualization and quantification of biofilm removal for the mitigation of MIC, in: NACE International Paper #6081, 2015.
[29] J. Larsen, T. Skovhus, A. Saunders, B. Hojris, M. Agerbaek, Molecular identification of MIC bacteria from scale and produced water: similarities and differences, in: NACE International Paper #08652, 2008.
[30] B. Geissler, A. Jones, V. Keasler, Prevalence and distribution of sulfide generating microbes in the oil and gas industry, in: NACE International Paper #7569, 2016.
[31] B. Lomans, R. De Paula, B. Geissler, C. Kjijvenhoven, N. Tsesmetzis, Proposal of improved biomonitoring standard for purpose of microbiologically influenced corrosion risk assessment, in: SPE International Paper #179919-MS, 2016.
[32] A. Mitchell, H. Anfindsen, A. Bruras Harvik, B. Hustad, A review of reservoir souring for three North Sea fields, in: NACE International Paper #10248, 2010.
[33] C. Kuijvenhoven, A. Bostock, D. Chappell, J.C. Niorot, A. Khan, Use of nitrate to mitigate reservoir souring in Bonga deepwater development offshore Nigeria, in: SPE International Paper #92795, 2005.
[34] T. Gu, D. Xu, Why are some microbes corrosive and some not?, in: NACE International Paper #2336, 2013.

[35] W. Fu, Y. Li, D. Xu, T. Gu, Comparing two different types of anaerobic copper biocorrosion by sulfate- and nitrate-reducing bacteria, Materials Performance 53 (6) (2014) 66−70.
[36] V. Keasler, B. Bennett, C. Keller, C. Kuijvenhoven, T. Mahon, S. James, Multi-faceted approach for optimizing a microbial control program, in: SPE International Paper #154645, 2012.
[37] L. Summer, M. Liu, N. Summer, J. Gill, C. Janes, R. Young, Phage of sulfate reducing bacteria isolated from high saline environment, in: NACE International Paper #11222, 2011.
[38] A. Harmon, A. Reese, K. Crippen, A. Darzins, Development of an enzyme-based approach to control the formation of microbiologically influenced corrosion (MIC)-Associated biofilms, in: NACE International Paper #7346, 2016.
[39] W.C. Fuqua, S.C. Winans, E.P. Greenberg, Quorum sensing in bacteria: the LuxR-LuxI family of cell density-responsive transcriptional regulators, Journal of Bacteriology 176 (1994) 269−275.
[40] C.M. Waters, B.L. Bassler, Quorum sensing: cell-to-cell communication in bacteria, Annual Review of Cell and Developmental Biology 21 (2005) 319−346.
[41] P. Williams, K. Winzer, W.C. Chan, M. Cámara, Look who's talking: communication and quorum sensing in the bacterial world, Philosophical Transactions of the Royal Society B 362 (2007) 1119−1134.
[42] S.P. Diggle, S.A. Crusz, M. Cámara, Quorum sensing, Current Biology 17 (2007) R907−R910.
[43] D.G. Davies, M.R. Parsek, J.P. Pearson, B.H. Iglewski, J.W. Costerton, E.P. Greenberg, The involvement of cell-to-cell signals in the development of a bacterial biofilm, Science 280 (1998) 295−298.
[44] R. Popat, D.M. Cornforth, L. McNally, S.P. Brown, Collective sensing and collective responses in quorum-sensing bacteria, Journal of the Royal Society Interface 12 (2015), 20140882.

Pipeline coatings

24

Todd Byrnes
Saudi Aramco, Dhahran, Saudi Arabia

24.1 Introduction

It is hoped by the end of this chapter that the reader will leave with some understanding of what coatings are available and the salient points about how they function. In addition, current trends in coating research and the key factors driving these efforts will be illustrated. Practical implementation of new technologies is the key focus, rather than an in-depth analysis of the science.

When people talk about pipeline coatings, they think of them primarily as a barrier to aqueous corrosion. While that is a major role, coatings do so much more than just "block moisture." Some other functions include the following:

- Separating the pipeline from corrosive chemicals, gases, and microbiologically influenced corrosion (MIC).
- Reducing the amount of cathodic protection current required for corrosion mitigation.
- Protecting piping against Corrosion Under Insulation (CUI).
- Reflection of thermal radiation and insulation of the pipe contents from heat loss or heat gain.
- Reducing the friction between the liquid media and the pipe wall.
- Resisting abrasion and impact during transportation and burial.
- Controlling pipe buoyancy in offshore applications.
- Reducing or preventing deposit buildup, thus boosting production rates.
- Passive fire protection (generally cementitious or intumescent coatings).

For example, it is widely perceived that internal pipeline coatings are there for corrosion prevention—but they are just as useful as "flow coats." That is to reduce the friction between the viscous crude and the internal pipe wall. This allows more throughput and hence greater production rates.

However, the two functions cannot be simply interchanged. A flow coat can be effective from 40 μm (1.5 mils). That is, just enough to cover the "hills and valleys" of the steel surface roughness. But to operate as a meaningful corrosion barrier, it needs a minimum of about 125 μm (5 mils)! In addition to fulfilling such tasks, coatings also have to exhibit *economy, functionality, and practicality*.

Economy means that the product itself must be inexpensive, and there must be a practical pathway for its cheap application to the pipe (spray, brush, wrapping, fusing, etc.).

Functionality simply means that the product must withstand exposure to atmospheric, buried or immersion conditions, extremes of temperature, soil currents, soil stresses, microorganisms, pressure, aggressive chemicals, and so forth.

Practicality refers to the fact that the product must resist ultraviolet (UV) exposure and mechanical damage during storage and transportation, withstand mechanical

Trends in Oil and Gas Corrosion Research and Technologies. http://dx.doi.org/10.1016/B978-0-08-101105-8.00024-3

operations (bending, hydro-testing) in the field, and must be sufficiently abrasion and impact resistant to survive the rigors of burial or thrust-boring activities.

This chapter only addresses tubular oil and gas gathering or flow lines, trunk lines, and transmission lines. This discussion does not cover plastic-coated pipes, drill pipes, risers, heat exchanger tubing, coatings under insulation etc, because their requirements and protection mechanisms are outside the scope of this chapter.

24.2 Older technologies

As can be seen in Fig. 24.1, the first real external coatings were bituminous or tar based, which had the virtues of being sticky, water repellent, and available. Nevertheless, they were cheap and effective and up until 1978, coal tar enamel and cement mortar were the only two coatings listed in the American Water Works Association (AWWA) standards!

The products in this section can still be commonly found, but their performance has been, to some extent, superseded by newer products with superior characteristics [1]. This is usually higher performance, better environmental compliance, easier and safer handling, less demanding surface preparation, and so forth.

24.2.1 Coal tar enamel

Coal tar enamel (CTE) is a polymer-based coating produced from the plasticization of coal tar pitch, coal, and distillates. Inert fillers are added to provide the desired properties of the system. The coal tar pitch, which forms the basis for the enamel, consists of polynuclear aromatic hydrocarbons and heterocyclic compounds. Over the years, this coating has been used in conjunction with a primer, a fiber glass or mineral felt reinforcement, and an outer wrap [3]. A typical pipe specification is AWWA C203. For more detail on any standard referenced throughout this chapter, please refer to Table 24.1.

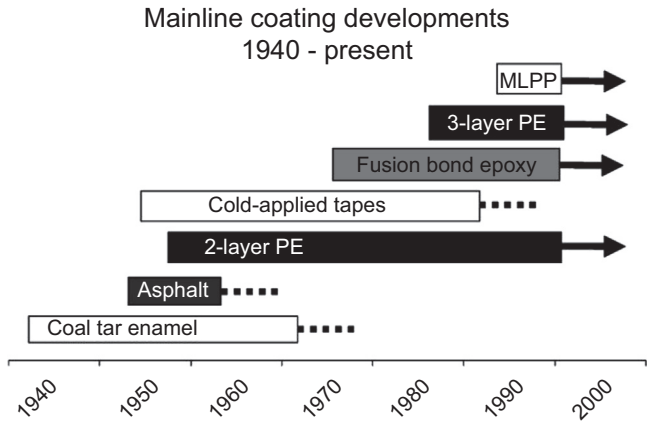

Figure 24.1 Evolution of pipe mainline coatings [2].

Table 24.1 Summary of common external pipe and joint coating standards

Standard	Title
AWWA C203	Coal-tar protective coatings and linings for steel water pipes
AWWA C210	Liquid-epoxy coating systems for the interior and exterior of steel water pipelines
AWWA C214	Tape coating system for the exterior of steel water pipelines
AWWA C217	Petrolatum and petroleum wax tape coatings for the exterior of connections and fittings for steel water pipelines
AWWA C225	Fused polyolefin coating systems for the exterior of steel water pipelines
API RP 5L9	External fusion-bonded epoxy coating of line pipe
BS EN 10300	Steel tubes and fittings for onshore and offshore pipelines. Bitumen hot applied materials for external coating
BS EN 12068	External organic coatings for the corrosion protection of buried or immersed steel pipelines used in conjunction with cathodic protection—tapes and shrinkable materials
CSA Z245.20	Plant-applied external fusion-bonded epoxy coating for steel pipe
CSA Z245.21	Plant-applied external PE coating for pipe
CSA Z245.22	Plant-applied external polyurethane foam insulation coating for steel pipe
CSA Z245.30	Field-applied external coatings for steel pipeline systems
ISO 21809-1	Petroleum and natural gas industries—External coatings for buried or submerged pipelines used in pipeline transportation systems—Part 1: Polyolefin coatings (3-layer PE and 3-layer PP)
ISO 21809-2	Petroleum and natural gas industries—External coatings for buried or submerged pipelines used in pipeline transportation systems—Part 2: Single layer fusion-bonded epoxy coatings
ISO 21809-3	Petroleum and natural gas industries—External coatings for buried or submerged pipelines used in pipeline transportation systems—Part 3: Field joint coatings
ISO 21809-4	Petroleum and natural gas industries—External coatings for buried or submerged pipelines used in pipeline transportation systems—Part 4: Polyethylene coatings (two-layer PE)
ISO 21809-5	Petroleum and natural gas industries—External coatings for buried or submerged pipelines used in pipeline transportation systems—Part 5: External concrete coatings
NACE SP0394	Application, performance, and quality control of plant-applied single layer fusion-bonded epoxy external pipe coating

The introduction of glass fiber inner wraps and the application of outer wraps onto the coating surface improved the mechanical strength of the system and provided extra protection against soil stresses and impact damage during handling and installation.

CTE coatings have very good electrical insulation and low water permeation properties that resist bacterial attack and the solvent action of petroleum oils. Coal tar is particularly durable and used for low-maintenance items. For example, the lock gates of the Panama Canal have used CTE for decades [4]. CTE is still used under Concrete Weight Coatings (CWCs) for offshore use. However, CTE has carcinogenic properties, and many countries have now banned its use.

24.2.2 Asphalt

Asphalt is a by-product of the oil refining process, but can also occur naturally. A common specification is BS-EN-10300. Asphalt's electrical resistivity and resistance to water permeation tends to drop with time compared with those of coal tar, but it is one of the cheapest coatings on the market [5].

Although it looks and behaves in a similar fashion, it is chemically distinct from coal tar. Bituminous is sometimes used to refer to both CTE and asphalt, which causes some confusion.

24.2.3 Dielectric tapes/wraps

A typical tape system comprises a liquid primer applied on the steel, followed by one or more layers of two-ply tape. Two-ply tape is usually made from polyethylene (PE) or polyvinyl chloride (PVC) with an adhesive layer of butyl rubber on one side. The backing tape and the adhesive are the "two plies" in the description.

Butyl rubber is sticky and adhesive with good resistance to oxygen (compare with tire bladders, which are mostly butyl rubber). PE and PVC have excellent water resistance and are strong dielectrics (i.e.; highly insulating). AWWA C214 is a well-known specification for tape coatings.

Robust adhesive backed outer wrap(s) are commonly used over the inner wrap(s) for mechanical protection. Variations exist where the cold adhesive is replaced by "hot-melt" adhesives as covered under AWWA C225, or the inner wrap has adhesive placed on both sides (3-ply tape) as discussed in BS-EN-12068.

While in principle it sounds like an ideal solution, tapes historically have received some "bad press." This is due to their susceptibility to soil stresses (which can wrinkle the tape) and the shielding properties of the PE/PVC. The dielectric (insulating) properties that frustrate corrosion currents unfortunately also block protective cathodic protection (CP) current. This, however, is only an issue if the tape disbonds. If CP current is prevented from reaching the disbonded areas and water is present, then corrosion can progress unchecked.

Three-ply or so-called "self-amalgamating" tapes are said to offer better performance over two-ply tapes. This is because with adhesive on one side only, there will always be a defined interface along which moisture can travel. Because butyl

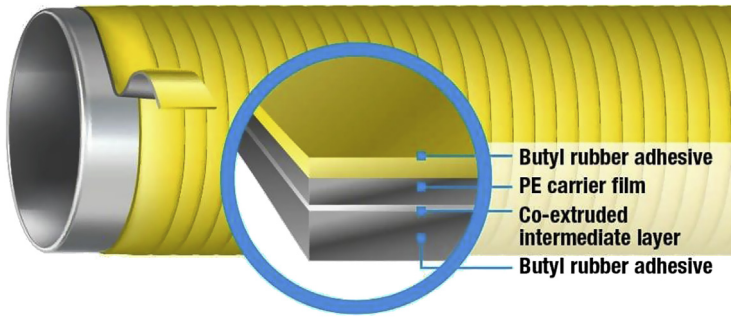

Figure 24.2 Three-ply (i.e.; double-sided adhesive) pipeline tape [7].

rubber is more like a viscoelastic than a solid, placing it on both sides (see Fig. 24.2) means the adhesives will merge, wherever it contacts itself and any interface will gradually disappear [6].

24.3 Current technologies

24.3.1 Fusion-bonded epoxy

Fusion-bonded epoxy (FBE) is also referred to as powder coating. The first commercial powder marketed in 1959 was 3M's Scotchkote 101. To demonstrate the FBE pipe coating's toughness to skeptical contractors familiar with coal tar coatings, 3M representatives would "beat the coating off a coal tar enamel-coated pipe, with a piece of pipe coated with Scotchkote 101. The coal tar enamel flew off while the Scotchkote coating remained intact" [8].

FBE is plant applied by the electrostatic application of micron-sized thermosetting powders onto heated steel (see Fig. 24.3). The FBE powders melt and flow between 180 and 250°C (356−482°F) and form a smooth, glossy film typically 300−600 μm (12−24 mils) thick on the steel surface.

As the cross-linking reactions proceed, the film gels and ultimately cures. The whole process can take place in under a minute. Internal FBE coatings usually make use of a primer, generally phenolic. FBE sees wide application to mainline pipe, girth welds (GWs), valves, etc.

The most important property of FBE and indeed all polymers is the glass transition temperature (Tg). This is the temperature at which the polymer transitions from a hard rigid state to a soft plastic material. Near the Tg, permeation of moisture and gases becomes easier.

Before the year 2000, most FBE only had a Tg of about 100°C (212°F) and were thus limited to operating temperatures of 60°C (140°F) [10]. Operating too close to the Tg risks water absorption, which can decrease the Tg. However, operating temperatures greater than 150°C (302°F) are now possible.

FBE is applied relatively thin compared to other coatings, which means it is possible for some moisture to reach the steel-FBE interface. This allows for the conduction of

Figure 24.3 Fusion-bonded epoxy powder application onto heated pipe [9].

sufficient CP current to protect the underlying steel. Very few failures due to cathodic shielding are known from FBE. Repair is usually achieved by liquid epoxies or FBE melt sticks. Common specifications include CSA Z245.20, ISO 21809-2, API RP 5L9, and NACE SP0394.

24.3.2 Dual-layer coatings

Sometimes, two layers coatings are specified (e.g.; Dual Layer FBE). The secondary layer may be for abrasion resistance, a friction surface for CWCs, a thermal or impact barrier, a UV barrier for increased corrosion resistance, and so on. The second layer need not necessarily be the same as the first layer and could be polyurethane, polyester, or some other coating.

24.3.3 Polyolefin

PE and polypropylene (PP) are both examples of polyolefins (POs). POs are specified almost as often as FBE for the protection of steel pipe.

PE is impermeable to water but has poor gouge resistance. PP has superior resistance to impact, indentation, abrasion and soil stress, excellent chemical resistance, and low water vapor transmission. PP is also resistant to higher operating temperatures than PE.

CSA Z245.21 is one of the more widely used specifications. Repair is by melt sticks or repair patches. There are instances where it can be used on GWs, but heat shrink sleeves (HSSs) are more typical. It is not practical for valves.

24.3.4 Two layer—2LPO

POs are nonpolar and do not bond well to steel. Therefore either a mastic or PE-copolymer adhesive is used to generate adhesion between the PO and steel (the

PO and the adhesive are the 2 layers in a 2LPO system). Mastic-based adhesives, although being relatively inexpensive, provide good cathodic disbondment (CD) resistance.

However, they have low shear and peel strength values and are restricted to low-temperature applications. Products based on copolymers have very good adhesion and shear resistance but generally poor CD resistance. CD is measured as the growth of a circular holiday made on an immersed coating subject to an electrical potential. The bigger the hole grows, the lower the resistance. A common specification for 2LPO is ISO 21809-4.

24.3.5 Three layer—3LPO

A three-layer system consists of the PO, a copolymer adhesive layer and an FBE layer against the steel as a primer (hence 3 layer). All three layers are applied sequentially onto a prepared pipe as can be seen in Fig. 24.4.

The FBE has excellent adhesion to steel and is an excellent corrosion barrier, whereas the PO has excellent mechanical and impact properties. The copolymer has polar functional groups grafted onto a PE or PP backbone, usually through reaction with free radical initiators and maleic anhydride [12]. The resultant polymer therefore has affinity with both the polar FBE and the nonpolar PO [13].

The PO itself is applied hot—either by coextrusion or by side-extrusion (wrapping) as shown in Fig. 24.5. Usually the FBE, adhesive, and PO are applied within seconds of each other, before completion of the cross-linking process to ensure the best interlayer adhesion. A common 3LPO specification is ISO 21809-1.

Part of the limitation on the operating temperature of FBE is environmental moisture and mechanical impact at or near the Tg. However, because the PO jacket is a tough and very effective moisture barrier, 3LPE and 3LPP can sometimes be used at temperatures at or above the Tg of the FBE primer. This is tempered, however, by the reality that significant stresses are present in the PO coating that may damage the primer layer if the Tg of the FBE is on par with the operating condition.

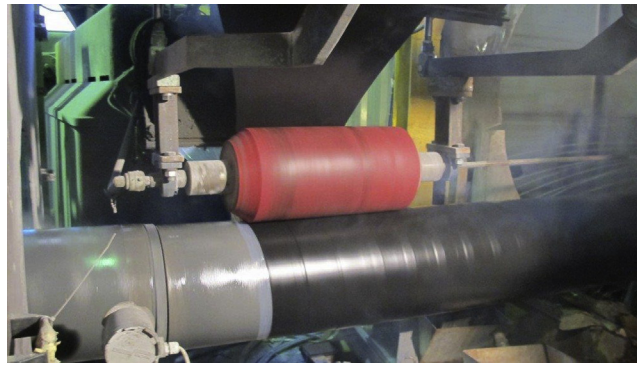

Figure 24.4 3LPE coating in-line application process [11].

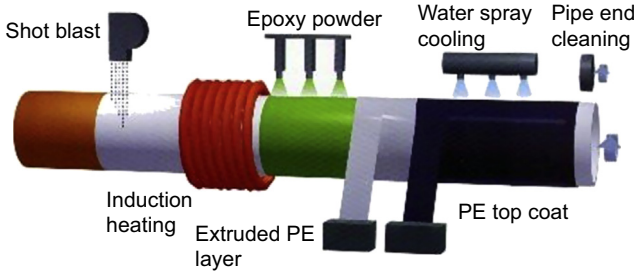

Figure 24.5 3LPE inline coating process [14].

24.3.6 Liquid coatings

Liquid coatings can be applied by spray, brush, or roller. A typical standard is AWWA C210. Although the volumes of liquid coatings used for mainline pipes are small compared with FBE and 2LPO/3LPO, there are definite applications, for example, repairing other coatings, short coating runs, GWs, valves, spools, tanks, vessels, specialized environments (wear, chemical, UV), etc. where liquid coatings are indispensable.

Typically liquid paints tend to be epoxies, but almost any coating can be utilized to protect pipe surfaces. Polyurethanes have been used for external UV protection, abrasion coatings, and GWs. Even inorganic zinc has been used as an external coating for the Morgan−Whyalla above groundwater pipeline in South Australia, which has delivered outstanding service since 1944 [15].

For aggressive media, specialty formulations such as Epoxy Novalac are used to combat low pH, high temperatures, and aggressive solvents. Baked phenolics are occasionally used for the internals of tube heat exchangers because of their high chemical and heat resistance up to 200°C (392°F).

24.3.7 Tapes and wraps

24.3.7.1 Viscoelastic wraps

Viscoelastics are novel materials based on polyisobutene−the same material used in chewing gum. They adhere to almost any surface, flow under pressure, and are insensitive to surface preparation. In addition, they are highly moisture repellent, immune to polar solvents and bacteria, and can be applied at very low temperatures. The material is normally sold as a roll or tape with an internal mesh layer for support and a release film. But it is also sold as a profiling putty or even an injectable liquid.

This system is occasionally described as being “CP compatible”; however, this is misleading. CP compatible is generally understood to mean that CP current will pass through a coating, and disbondment will not increase the risk of corrosion. In reality, viscoelastic systems are rarely used without a rigid outer wrap (usually PVC) to provide rigidity and impact protection to the whole system. PVC or PE will not pass CP current.

Therefore more accurate descriptions are "CD resistant" and "CP cooperative." This is because in the event of a penetration the material will flow around and out of the hole, effectively healing the puncture. That is, the outer wrap is wound sufficiently tightly that the viscoelastic is placed under compression. In other words, CD values of zero or even *negative* values are possible!

The second point is that the material is so sticky that it tends to fail cohesively, rather than by disbondment (adhesively). This should be apparent from Fig. 24.6. That is significant quantities of material will always adhere to the steel, which means that no additional CP current will be required.

Field data suggest that this material has excellent corrosion resistance [17]. A relevant specification is CSA Z245.30. Viscoelastics can be used as maintenance coatings, for mainline pipes, GWs, valves, flanges, and other complicated shapes.

24.3.7.2 Wax tapes

Wax systems generally use a primer against the steel followed by a microcrystalline wax-impregnated carrier mesh. AWWA C217 is a typical specification. This product makes use of the water-repellent properties of wax to exclude water from the steel surface. An outer wrap is often required for mechanical protection. Wax tapes can dry out and crack, and like all tapes, there is some possibility of damage due to soil stresses. They are not commonly specified for mainline pipe or GWs, but they do have good utility for valves, flanges, and other similarly complicated shapes because of their ability to conform to such surfaces.

24.3.7.3 "Cathodic protection-compatible" tapes

To retain the convenience of tape mounted systems, some manufacturers have dispensed with dielectric backings in favor of woven geotextile meshes or fabrics backed with rubber-modified bituminous adhesive.

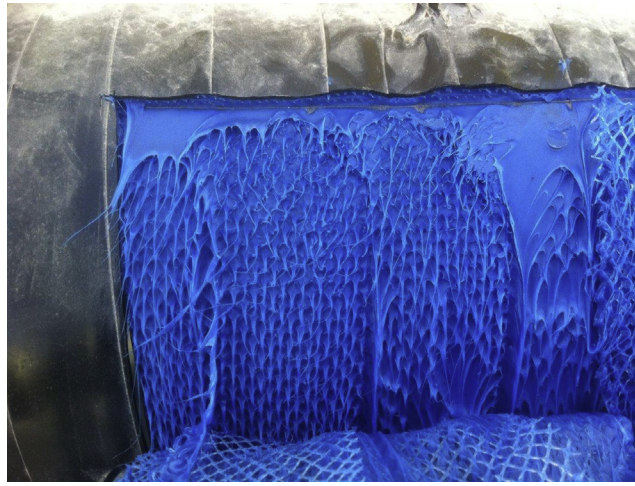

Figure 24.6 Viscoelastic with expanded carrier mesh and outer wrap [16].

The geotextile is for shear and impact protection. The open weave of the tape is meant to allow electrolyte (hence current) to access the surface of the tape, whereas the adhesive adheres tenaciously to the steel, providing the corrosion protection [18]. These products are not common, and the number of manufacturers is limited.

24.3.8 Abrasion-resistant overlays

There is a distinction between pipe that is buried in rocky ground where impact resistance is desirable; and pipes that are thrust-bored where abrasion resistance is mandatory [19]. Both need tough, gouge-resistant coatings, and abrasion-resistant overlay (ARO) is the blanket term used for both scenarios. AROs usually take the form of a secondary coating over a primary corrosion barrier layer.

For alluvial soils, polyolefinic coatings or polyurethane might be quite satisfactory. For rockier soils, dual layer epoxies with superior hardness and gouge resistance are needed. For severe soil conditions or horizontal directionally drilled applications, composite wraps employing fiber (glass) reinforcement or polymer concrete (a mixture of concrete and epoxy) present a particularly hard wearing surface.

24.3.9 Concrete

Concrete is not a material that springs to mind as a corrosion coating; however, the passivating action on iron and the self-healing properties of concrete actually make it a very good solution for protection of steel. For example, an underground pipe lined with cement mortar lining (CML) and externally coated with concrete was constructed in 1855 in St. John, New Brunswick, Canada. This pipeline was inspected in 1963 and still found to be in reasonable condition [20]. Indeed mortar lining is still routinely used for water transmission purposes. Incidentally, the mortar itself is occasionally protected with an organic coating to minimize leaching and calcification of the conduit.

In the context of the petrochemical industry, cement is used but mainly for buoyancy control on subsea pipelines, namely as Concrete Weight Coatings (CWC). ISO 21809-5 is a common specification. Because concrete is permeable to chloride ions and chloride depassivates steel, FBE (or CTE) is used as the corrosion barrier against steel for offshore piping, with the concrete placed over the top. Concrete is also occasionally used as an ARO as described in the previous section.

24.3.10 Summary

Several standards that were referenced throughout this chapter are compiled in Table 24.1. They are good references for those interested in the different coating types.

Only the most commonly used coating materials were covered, but many others are possible. For example polychloroprene, ethylene propylene diene monomer, and so on. The coatings discussed in the previous sections are summarized below in Table 24.2, which also includes the maximum operating temperatures and benefits and disadvantages of each method.

Table 24.2 Summary of modern external pipe coating technologies [21]

Coating	"Maximum" temperature	Benefit	Disadvantage
FBE	90°C (194°F)	• FBE is more flexible than other coatings, meaning pipes can be bent *after* coating in the field. • Excellent adhesion to steel. • Is able to pass cathodic protection (CP) current eliminating CP shielding. • Cures instantly.	• Not as mechanically robust as 3LPE. • Pipe must be heated.
2LPE	60°C (140°F)	• Cheap effective coating.	• Low temperature resistance.
3LPE	90°C (194°F)	• Damage tolerant, water impermeable coating. • Respectable temperature resistance.	• Susceptible to cathodic shielding.
3LPP	140°C (284°F)		
Liquid epoxy	~150°C (302°F)	• Tends to be a wider range of chemistries available to suit different roles (e.g.; epoxy, polyurethane, etc.). • Usual for field repairs.	• Pipe generally bent before coating. • Cure is sensitive to temperature and humidity. • Very long cure times.
Viscoelastic	80°C (176°F)	• Excellent corrosion resistance. • Excellent cathodic disbondment resistance. • Self-healing properties. • High tolerance to underprepared surfaces.	• Maintenance problematic. • Limited temperature.

24.4 Field joint coatings

Field joint (FJ)—also referred to as GW coatings—are listed here in a separate section from the mainline coatings covered in Sections 24.2 and 24.3, because they represent a number of different challenges. These include the following:

- Ensuring adhesion between the mainline (parent) and FJ coating.
- Maintaining quality in joint surface preparation and coating application, because such coatings are usually applied in the field.
- The need to execute the joint quickly. For offshore applications, the FJ and coating must be completed in minutes, as the cost of the pipe-laying barge is measured in thousands of dollars per day. The same applies to thrust-bored pipes, where the pipe string cannot be jacked until the preceding pipe GW and coating is completed.
- Practical issues such as availability of equipment and skilled personnel.

The history of FJ coating development is shown in Fig. 24.7. FBE powder or liquid paints (e.g.; epoxies) are commonly used for the FJ of FBE mainline pipe. For PO mainline pipes, there are a number of options. Tape wraps were traditionally employed as they were cheap, effective, and simple to use, but have fallen from favor because of a number of historical failures. Similar failures have also been experienced under HSS.

In Table 24.3 are summarized the most common current external FJ coatings, including a description, benefits, and drawbacks. The code in the first column (labeled "Type") is the same code to be found in Table 1 of ISO 21809-3, which is a more comprehensive list of FJ coatings. This is to allow the reader to easily cross-reference between our table and the ISO 21809-3 table.

Most of the methods detailed are already familiar to the reader. New developments in FJ coating technology are discussed in later sections. A good source of information regarding the field performance of GW coatings is the Gas Research Institute report; "Field Applied Pipeline Coatings" [22].

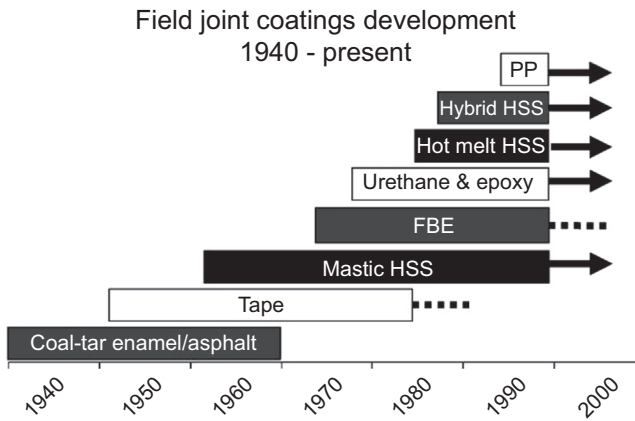

Figure 24.7 Evolution of field joint coatings [2]. *FBE*, fusion-bonded epoxy; *HSS*, heat shrink sleeve; *PP*, polypropylene.

Table 24.3 Summary of common current external field joint coatings

Type	Coating	Description and benefits	Drawbacks
1A	Bituminous	Hot applied bituminous tapes	Older method, not commonly employed.
1C	Wax tapes	A blend of microcrystalline wax-saturated synthetic fabric in tape form. Conforms to item shape. Can have good temperature resistance.	Relatively soft.
1D	Dielectric tapes	Usually a PVC or PE backed tape employing a butyl rubber adhesive or fusible bituminous backing. Simple to apply and good short term performance.	Liable to soil stress, loss of adhesion, substrate disbondment, and cathodic protection (CP) shielding effects.
1Ea	Viscoelastic	Excellent corrosion resistance.	Maintenance problematic.
		Excellent cathodic disbondment resistance.	Low temperature resistance.
		Self-healing properties.	
2A	PE-based heat shrink sleeve (HSS)	Applied onto steel with a mastic or hot melt backed HSS. Used for 2LPE mainline coatings.	Same as 2B, 2C.
2B	PE/ polypropylene (PP) HSS for 3LPE mainline coatings	Steel is first primed with epoxy [e.g.; fusion-bonded epoxy (FBE)]. A copolymer adhesive backed HSS is employed. Quick and compatible with most mainline coatings.	Some incidents of delamination due to soil stress, etc.
2C			Susceptible to cathodic shielding and pitting corrosion.
3A 3B	FBE. Single or dual Layer	Compatible with mainline pipes using FBE as the primary corrosion protection barrier. Compatible with CP protection.	Requires induction heating power supply.

Continued

Table 24.3 Continued

Type	Coating	Description and benefits	Drawbacks
4A 4B	Liquid Paint Epoxy or polyurethane	Tends to be a wider range of chemistries available to suit different roles. Does not need specialized equipment.	Takes time to cure usually.
5A 5D	Thermally sprayed PE/PP (3LPO)	Epoxy primer is required. Highly compatible with polyolefin mainline pipe.	Not commonly used.
5B 5E	Hot spiral wound polyolefin (PO) (3LPO)	A heated tape of PO is wound around the girth weld (GW) after application of the FBE and adhesive.	Properties similar to parent coating.
5C	Injection-molded PP (3LPP)	The GW is coated with FBE and then copolymer adhesive. A mold is placed around the GW and liquid PP is injected into the cavity.	Fast system for offshore use.

24.4.1 Heat shrink sleeves

An HSS is a radiation cross-linked PO sheet with usually some form of adhesive backing. For application to bare steel, either a mastic or hot melt adhesive would be employed. For application to FBE (or liquid) epoxy primed pipe, a copolymer adhesive backing is preferred. In both cases, the sheet is wrapped around the GW and the free ends joined by means of a closure strip.

The sleeve is then heated. The polymer chains "shrink" and the internal diameter (ID) of the wrap shrinks until it is tightly clamped onto the GW. Fig. 24.8 is an example of a sleeved GW. A successful application is usually signaled by the absence of wrinkles in the sleeve and the uniform extrusion of the adhesive from out of the open end(s) of the sleeve.

However on occasion the heating is uneven, or soil stress deforms the shrink. This can generate a path for moisture to enter. Because the wrap is a strong dielectric, cathodic protection is unable to combat corrosion underneath the film. HSSs are still popular, but CP shielding and pitting failures can be the result if the specification or application is poorly executed.

Figure 24.8 Heat shrink sleeve [23].

24.5 Challenges and drivers

Improvements in pipeline coating technologies are influenced by four main drivers: Economics, Legislation, Innovation, and Efficiency.

Economics means the cost associated with the construction (capital cost) and ongoing maintenance of a coated pipeline. These can be broken down into the following:

- *Material Costs*: the costs of the paints and abrasives used.
- *Labor Costs*: associated with mobilization, surface preparation, coating application, stand-by time etc. Upfront material and labor costs can be lumped together under the term CAPEX (capital expenditure).
- *Maintenance Costs*: associated with maintaining the coating to a reasonable condition. The frequency of maintenance depends on the quality of the original specification and products used, skill of the applicator, and so on. These costs are sometimes described as OPEX (operating expenses).

Improvement in any one of these areas translates into a financial or performance windfall for the asset owner.

Legislation alludes to the greater scrutiny that operators are subjected to, thanks to a greater public awareness of the environmental and safety consequences posed by "uncontrolled hydrocarbon releases." The Santa Barbara incident in May 2015, where a 24" pipeline failed and released 2934 barrels of heavy crude oil (500 of which went into the Pacific Ocean), is a recent example [24]. This even impacts testing protocols, because the best way to avoid failures is to ensure that the standards are truly representative of operating conditions.

Innovation implies advancements in technology that facilitate new opportunities previously considered unfeasible. For example; FBE coatings beyond 150°C (302°F) will allow exploitation of oil reservoirs inaccessible to "older" technologies,

which translates into greater national economic output. Some other examples of immediate industry challenges would be the following:

- Internal coatings resistant to methanol and monoethylene glycol or MEG (used for hydrate prevention) at temperatures above 60°C (140°F).
- Successful application of FBE onto high strength steel at temperatures, without adversely impacting the metallurgical properties of the pipe.
- External coatings for subsea piping below 2000 m (6560 ft.). That is, lower profile, lower weight, better insulating coatings, resistant to higher pressures.
- Internal coatings for sour gas service (>5 mol% H_2S, >8 mol% CO_2) with service temperatures higher than 95°C (203°F).
- More rapidly applied or cured GW coatings (powder, liquid or wraps) for offshore or thrust-boring applications.
- More resistant and flexible ARO coatings.
- Improvement in PO chemistries and elimination of the adhesive layer in 3LPO applications (direct application of PO onto FBE).
- External coatings with improved adhesion and lower CD values.
- Improved standard testing methodologies that better reflect and predict real-life environments.

Other challenges include the growing use of biofuels (e.g., ethanol), which tend to have more moisture absorption and MIC problems. Carbon sequestration means coatings that will have to resist 100% CO_2. Oil sands and shale oil are very viscous, abrasive, and tend to be transported at elevated temperatures. As exploration delves into the Arctic, permafrost and ultra-low temperatures present issues for application and operation of coated lines.

Efficiency relates to any technological advance that will decrease running costs (or boost production) under a fixed set of operating conditions. An example would be the use of a smoother ID coating to increase production rates on an existing line.

24.6 Incremental technologies

The term "incremental" in the section title refers to the fact that most progress revolves around steadily improving the properties of coatings that are already functioning in a particular role. So what are the properties of interest for pipeline coatings and how are they being improved?

24.6.1 Improved heat and pressure resistance

Before we start, the important property of the Tg should be defined. Each polymer has a different Tg value, and it represents a point where the intermolecular forces that render the polymer chains relatively immobile with respect to one another are overcome by the thermally activated motion of those chains.

Therefore as the temperature is increased, a transition from a rigid to a rubbery state is observed. This is particularly important for coatings as the rate of diffusion of water,

anions, cations, and oxygen accelerates at temperatures beyond the Tg [25]. The further the operating temperature is *below* the Tg, the more inelastic the behavior. This can cause issues with pipe bending and so on. The Tg can be influenced by altering the base chemistry, the functional groups, chain lengths, degree of cross-linking, and crystallinity of the polymer.

The current maximum temperature limit for commercial FBE is around 125°C (257°F). While higher Tg epoxies can already be realized by using highly functionalized resin systems to increase the cross-link density, this negatively impacts the *flexibility* of the material. Therefore most efforts have been aimed at increasing the stiffness of the polymeric backbone. Operating temperatures above 150°C (302°F) are seen as attainable.

An example is OUDRATherm HPC 6510, which DOW claims can deliver a Tg of 160°C (320°F) [26]. AXALTA says that has developed a product with a Tg of 180°C (356°F) and good resistance to high levels of H_2S and CO_2 [27]. These performances are a large improvement on current products.

Of course, research is not only limited to epoxies and many other systems including polyetherimides, bismaleimides, polycyanurates, vinyl esters, fluorinated compounds, and so forth are under investigation [28].

24.6.2 Low application temperature fusion-bonded epoxy

To achieve optimal performance, current FBE products require application temperatures in excess of 230°C (446°F) for single layer systems and 200°C (392°F) for three-layer systems. The introduction of high-strength steels such as X80, X100, and X120 for use in pipeline construction has presented a challenge to the industry in terms of the availability of suitable coating systems.

High-strength steels (particularly grades X100 and greater) cannot withstand preheat temperatures in excess of 200°C (392°F). Exposure to the high heat required when coating with a typical FBE product results in the degradation of some of the key properties of these high strength steels. Low application temperature (LAT) chemistries that can be applied under 180°C (356°F) are under development [29].

One project in Alberta Canada, applied a LAT primer onto 36″ X-120 steel, followed by a high-performance composite coating system (HPCC) 3LPE type coating with good results [30]. LAT products are also useful for offshore GW coatings, where the shorter heating times mean more production and hence greater cost savings.

24.6.3 High-performance composite coating system

An HPCC system is a monolithic, all powder, multicomponent coating system consisting of an FBE base coat, a tie layer containing a chemically modified PE adhesive, and a medium-density PE outer coat. All three components of the composite coating are applied as powders, using an electrostatic powder—coating process.

The tie layer is a blend of adhesive and FBE with a gradation of FBE concentration. Thus there is no sharp and well-defined interface between the tie layer and the FBE

base coat, nor with the PE outer coat. The adhesive and PE are similar to each other and intermingle easily to disperse any interface.

The coats are therefore strongly interlocked and behave as a single-layer coating system without the risk of delamination. Delamination has been a performance issue with some three-layer PE coatings, especially under cyclic conditions. Being a single layer coating and thinner, the HPCC will have less internal stress development when subjected to large temperature changes.

24.6.4 Improved chemical resistance

Of the world's remaining conventional gas reserves to be produced, approximately 40%—representing over 2600 trillion cubic feet (tcf)—are sour. Among these sour reserves, more than 350 tcf contain H_2S in excess of 10 mol%, and almost 700 tcf contain over 10 mol% CO_2 [31]. For example the Kashagan Field in the Caspian Sea has 15 mol% H_2S and 4 mol% CO_2.

Acid gases such as H_2S and CO_2 are highly corrosive, and new resin chemistries are required to deal with them. As existing wells age, seawater is often injected to boost reservoir pressures. However, this increases the water-cut of the produced oil and introduces oxygen, chlorides, and bacteria with corresponding negative impacts on downstream pipelines.

A 2008 United States Geological Survey (USGS) report estimated that 90 billion barrels of undiscovered, technically recoverable oil, 1670 trillion cubic feet of technically recoverable natural gas, and 44 billion barrels of technically recoverable natural gas liquids are contained north of the Arctic Circle. Of this figure—which represents 13% of the expected undiscovered oil in the world—84% is expected to occur offshore [32].

But with lower temperatures comes a greater likelihood of methane hydrate formation, which can build up and plug a pipeline. The common solution thereto is with methanol or MEG injection. However, these chemicals are highly aggressive to organic coatings.

Many firms are working on products to meet all of the challenges mentioned. One such example is ethylene-chlorotrifluoroethylene (ECTFE) powder coatings, which can withstand very high concentrations of chemicals up to 150°C (302°F) but can still be applied using conventional powder application methods [33]. Fluorinated coatings are already in common use for offshore and subsea fasteners.

24.6.5 Improved flow properties

The use of internal flow coatings has many beneficial effects: control over corrosion during storage and operation, improved flow and production rates, and reduced fouling and fuel (pumping) costs [34]. The degree of drag imposed by the coating onto the media depends on the physical smoothness of the coating and/or the physio-chemical affinity between the coating and the media.

One manufacturer produces a flow coat that provides a pipe surface that is over 50% smoother, with surface roughness reduced to 1−4 μm (0.04−0.15 mil). Compare this

with 20−35 μm (0.78−1.37 mil) for bare steel, or 10−15 μm (0.4−0.6 mils) for solvent-based coatings. The term IPC (Internal Plastic Coating) is sometimes used for flow coats. See also Section 24.7.4 on hydrophobic coatings.

24.6.6 Improved abrasion resistance

For coated pipes buried in rocky ground or pipes installed by thrust boring, resistance to abrasion, impact, and gouging are essential. The same applies to pipes installed by microtunneling, pipe jacking, or horizontal directional drilling. Currently the chief means of protection is with dual layer FBE coatings. Work is being done on even tougher FBE coatings, but polyurethane—a highly wear resistant material—is also sometimes specified.

For particularly severe conditions, laminate wraps using glass or carbon fiber in thermoset resins are gradually being adopted. The main problem with ARO type coatings—and that includes the GWs—is that there is a strong time pressure to apply and cure them, because the pipe string is usually laid as soon as the GW or ARO layer is ready.

24.6.7 Improved mechanical properties

Improved mechanical properties such as flexibility (resistance to cracking) are particularly desirable in liquid coatings subject to bending. Products such as FBE already tend to have good flexibility ($\geq$3 degrees/PD). This is important because pipes are often bent in the field to accommodate changes in terrain. Some concrete jacketing products even claim to have some capacity for bending.

24.6.8 Improved insulation

As offshore exploration pushes into deeper waters, more effective insulation is required to prevent cooling of the product. As the temperature drops, the viscosity of the fluid and the risk of hydrate formation rise. Hydrates, also known as methane clathrates, can solidify and block a flowline.

The immense subsea pressures mean that the external insulation must be *incompressible* and prevent migration of water to the steel interface. It turns out that PP is an ideal candidate. PP can be foamed to various densities. It can be filled with glass (up to 25%) to form "syntactic polypropylene." Or it can be used as a solid coating. As the density of the PP increases, so does the incompressibility, but at the expense of the insulation factor.

So ubiquitous is this PP insulation technology, that new designations have been developed to communicate the concept within the industry. For example, **5LPP** is similar to 3LPP, but with an added thick layer of PP insulation, finished off with an outer shield layer as demonstrated in Fig. 24.9. Sometimes an additional insulating/shield layer is added, forming **7LPP**. Even more layers can be added, giving rise to what is known as "multilayer coatings."

Treatment of GWs in such pipes is difficult. If HSSs are used, insulation must be first formed in place using temporary molds or preformed sections cut to fit. Only

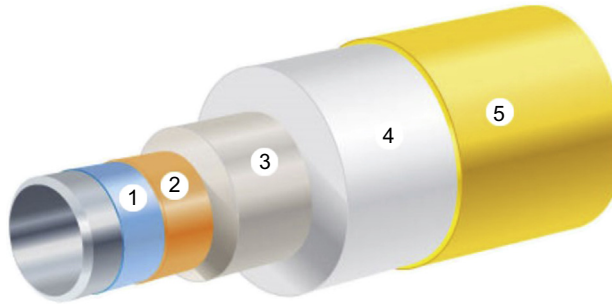

1. Fusion bonded epoxy 2. Adhesive 3. Solid PP 4. TDF 5. Outer shield

Figure 24.9 5LPP insulated pipe [35].

then can the HSS be installed at the FJ and shrunk. If the outer GW jacket is rigid, it must be installed first and joined to the parent material by mastic adhesive or fusion welding. Then the foam can be injected or foamed in place using the jacket as a mold. CSA Z245.22 is a useful reference for further discussion of this technology.

24.6.9 Advances in preparation and application

If a coating engineer had a wish list, it might include coatings tolerant of marginal surface preparation, insensitive to surface contamination (salts, oxidation, humidity) and applicable by unskilled labor. Other items on the list might include the ability to reliably blast and coat smaller diameter pipe (using robotic techniques), improved inspection possibilities (again via robotic techniques), less environmentally damaging products (reduced waste, lower VOC's), and so forth. These are all areas of active investigation.

24.6.10 3LPO field joint coatings

One of the limitations of 3LPO coating is that the application of the FBE primer, the copolymer adhesive layer and the final PO topcoat are applied within seconds of each other to ensure that sufficient unreacted functional groups are available to react and develop decent interfacial adhesion between each layer. This can be problematic for FJs.

A new product which combines the adhesive and the PO components together is based on a semi-interpenetrating network (IPN) of linear POs and a cross-linkable monomeric epoxy [36]. The term "protective network coatings (PNCs)" is used interchangeably with IPN.

An example is Scotchkote's PNC1011. This is sold as tape in 16″−28″ wide rolls of 1 mm (40 mil) thick film. It can be applied directly to a gelled or cured FBE primer by machine in under 6 minutes. Multiple layers can be applied up to 3 mm total. It bonds equally well to itself, the FBE, and the PO parent coating. The benefit of such products is that the adhesive application step is eliminated and processing times are speeded up considerably.

Other providers offer a complete GW coating system where a machine applies the FBE powder coat, followed by a hot melt PE. The PE is modified with active functional groups so that an intermediate adhesive layer is not required to ensure bonding to the FBE [37].

24.6.11 Advances in testing and standards

There are many shortcomings in existing test standards. For example, older weathering tests had poor correlation to actual field results. For CUI coatings, there are no international standards. Accurate testing is particularly critical in an era where coating (i.e.; pipe) failures can attract heavy fines and intense scrutiny.

Coatings subject to cathodic protection are at risk of CD. This is because where there are breaks in the coating, alkaline conditions are generated, which may degrade the ability of the coating to adhere to the steel. New products that are tolerant of much higher CP current densities are being produced.

Most of the existing standard CD test methods were originally designed for onshore pipeline applications with service temperatures $\leq$95°C (203°F). Limited CD data are available for testing temperatures higher than 95°C (203°F). There is also some debate about the best place to measure the test temperature in the experimental set-up, because this will obviously affect the results.

That existing standards or their modifications are suitable for the needs of subsea/deep-water pipeline applications needs to be investigated with the proliferation of new higher temperature and often much thicker coating systems [38].

24.7 "Breakout" technologies

"Breakout" refers to innovations and products that are not familiar to average coating engineer and represent a significant departure from current practice. Many of the new developments revolve around an explosion of research into smart coatings, surface engineering, and nanotechnology.

24.7.1 Self-healing coatings

"Smart" coatings—especially ones that automatically react to repair or limit corrosion in the event of damage—are nothing new. The use of zinc to cathodically protect galvanized steel was first recorded in 1742 by Melouin [39]. Chromate conversion coatings have been used for the last century to passivate nonferrous alloys. The leaching behavior of chromate allows it to repassivate exposed metal in the presence of sufficient moisture.

Chrome-free self-passivating coatings have been developed, such as Chemically Bonded Phosphate Ceramics (CBPC) that show 10,000 hours resistance under ASTM B117 testing [40]. CBPC takes the well-known passivating effect of phosphates on iron but complements it with a secondary ceramic layer, which acts as a

reservoir for phosphate to maintain the passivated layer. As might be anticipated, this coating exhibits unique heat, flame, abrasion and chemical resistance, and good thermal and electrical insulating behavior. It requires little surface preparation and can be returned to service an hour after application.

Next imagine a coating that cracks or is scratched, exposing millions of imbedded pores. Now imagine that in half the pores is a liquid resin, and in the other half is a liquid catalyst. Or maybe all the pores are resin filled, with polymerization triggered by moisture or oxygen from the environment or by electrochemical reactions associated with corrosion [41].

For example, anodic (corroding) sites are associated with increasing acidity, whereas the cathodic areas are associated with alkalinity. Whatever the mechanism, these newly liberated materials flow or react and protect the damaged area. The active agents could be added as *immiscible* submicron-sized droplets, which would be evenly dispersed in the parent coating during the mixing process. Or they could be "prepackaged" in micron-sized inert shells.

Another variation is that otherwise-soluble inhibitors could be held in nanostructures formed by sol−gel chemistry for release as a result of chemical or mechanical stress from the environment.

Inherently conducting polymers (ICPs) such as polyaniline (PANI) are believed to anodically protect steel by maintaining the steel potential in the passive region. Or by becoming itself (the ICP) polarized through galvanic coupling to the base metal substrate at defects in the coating such that the ICP releases an inhibiting anion. Both cathodic reduction of the conducting polymer and ion exchange with cathodically generated OH^-, or both, can lead to the release of the anion dopant. When the anion dopant is a corrosion inhibitor, damage-responsive corrosion protection occurs [42].

24.7.2 Self-inspecting coatings

Self-inspecting or self-monitoring is a loose term applied to coatings, which do more than just passively fail. That is, they are able to signal distress or loss of performance to the asset owner. Some examples already familiar to the engineer are bleaching (due to chemicals or excessive potentials), the use of multilayered coatings of different colors (useful as wear indicators as each successive layer is exposed), pH-sensitive coatings (that change color, courtesy of the addition of pH-sensitive indicator), and so on. However, these are all visual effects.

Coatings possess many more interesting properties such as capacitance, impedance, resistance, etc. These in turn are affected by temperature, strain, interfacial reactions (at the steel surface), and so on. On macroscopic levels, these influences are moderated by thinning, cracking, and swelling of the coating film. Therefore changes in base properties can be indicative of macroscopic damage.

Such changes can be detected by sensors internal or external to the pipe. A miniature sensor has been developed, which is attached to the internal pipe wall and is hidden underneath an internal polyurethane lining. External piezoelectric devices communicate with the internal sensor through the pipe wall ultrasonically. The internal sensors in turn feed back the information regarding thinning of the polyurethane lining. This is useful

in slurry pipelines where there are high rates of wear [43]. Another example is the incorporation of Fiber Optic Bragg gratings into external coatings for measuring strain and other properties [44].

24.7.3 Nanotechnology

Nanotechnology, in the context of paint, normally relates to the addition of nanosized additions with a view to achieve certain outcomes. By way of analogy, lamellar Micaceous Iron Oxide pigment has been added to paint since the 1900s because of its barrier effect to the diffusion of moisture and oxygen [45]. In the 1970s glass and aluminum flake was added for a similar reason.

While nanotechnology can manifest itself in a variety of applications, the onus will be to try to concentrate here on solutions that are firmly on the nanoscale. A good example is the partial replacement of zinc in zinc-rich coatings with carbon nanotubes. The reason why the zinc loading is traditionally so high is to ensure particle-to-particle (i.e.; electrical) contact. If the protective current could be "short-circuited" through the coating to where it is needed (areas of exposed steel) by carbon nanotubes instead, this would represent a significant weight and cost savings to the coating purchaser.

It turns out that nanotube impregnated coatings also have a raft of other unexpected benefits. For example; the nanotubes also work like composite fibers, adding strength and crack resistance to the coatings [46].

Another example is built-in controlled-release corrosion inhibitors (CRCIs). That is, the CRCI is encapsulated in a micron-sized ceramic shell or absorbed inside the internal cavities of a porous sphere—ready to passivate the steel whenever a "free surface" is exposed. For example, when the overlying coating is gouged or penetrated. Porous particles, unlike ceramic shells, allow the paint to withstand vigorous mixing [47].

24.7.4 Hydrophobic coatings

Hydrophobic surfaces have immense potential for corrosion "repellent" surfaces, biofouling reduction, drag minimization, and microbial-resistant surfaces. Water is a very destructive element. It is the electrolyte for most corrosion processes and can permeate protective coatings, resulting in osmotic blistering, lowering of the Tg, and so on.

Hydrophobic coatings operate on the relatively simple assumption, that if one can eliminate water before it has a chance to permeate the coating, then one should be able to greatly extend the service life of the coating. A number of products are already on the market and do indeed have some impressive water-repelling properties.

ACULON is a commercial coating used for superhydrophobicity and oleophobicity and also antifouling applications. Superhydrophobicity can be realized by materials such as polysiloxanes, fluoroalkylsilanes, or fluoropolymers; or by lowering the surface energy by using densely packed and vertically aligned carbon nanotubes or polyacrylonitrile (PAN) nanofibers.

Other techniques include self-assembled monolayers of phosphonates, organometallics, and so forth. Hydrofoe by LotusLeaf Coatings uses microtexturing nanotechnology to mimic the bumps on lotus leaves, which lowers the surface energy to generate water repellency.

24.7.5 Antifouling coatings

Fouling refers to the deposition on internal pipe walls of biological organisms (e.g.; zebra mussels) or marine flora, scale buildup (e.g.; carbonates in hard water systems), hydrocarbon deposits such as waxes in oil lines or in the case of subsea gas lines—methane hydrates.

Combating fouling requires injection of antibiological agents, water-treatment chemicals, insulation systems, and deicing agents, depending on the cause. Apart from being expensive, chemicals can sometimes damage the coating and more often than not, are an inefficient means of control. Surface treatments or coating modification that could prevent these deposits in the first place would be more efficient and could avoid continuous injection and monitoring.

Hydrophobic coatings have already been given as an example. Smith et al. have developed a functionalized coating with reduced hydrate adhesion to internal pipe surfaces [48], whereas Subramanyam discovered that nanotextured surfaces filled with a lubricating liquid effectively prevent scale adhesion [49].

24.7.6 Microbiologically influenced corrosion-resistant coatings

Various active and passive compounds can be imbedded into a coating, which are destructive to the attachment and replication of certain microbiological organisms, known to attack coatings or the pipe itself. For example, sulfate-reducing bacteria generate acid conditions, which will cause metal loss.

Some coatings exploit surface effects such as surface tension to prevent the attachment of microorganisms, whereas others incorporate antimicrobial agents into the paints in the form of fillers or encapsulated chemicals. Graphene has been identified as being effective against MIC attack [50].

Other coatings incorporating silver and copper colloids have been promoted. Silanes like the AEGIS antimicrobial coating use polysiloxane to destroy microbial cells. Effective antimicrobial surface coatings can be based on an anti-adhesive principle that prevents bacteria from adhering, or on bactericidal strategies where organisms are killed either before or after contact is made with the surface. Many strategies, however, implement a multifunctional approach that incorporates all of these mechanisms.

For anti-adhesive strategies the use of polymer chains or hydrogels is preferred. Bacterial destruction can be achieved using antimicrobial peptides, antibiotics, chitosan or enzymes directly bound, tethered through spacer-molecules or encased in biodegradable matrices, nanoparticles, and quaternary ammonium compounds.

24.7.7 Nonmetallic solutions

Because this is out of the scope of the chapter, only a cursory examination of this topic will be made. Alternatives to coated steel pipe have existed now for several decades. RTR (reinforced thermosetting resin) pipe uses thermosetting resins and is therefore somewhat rigid. It is used for large diameter pipes such as desalination transmission lines.

Unlike the familiar PE and PVC piping, reinforced thermoplastic pipe (RTP)—also known as flexible composite pipe—is available with pressure ratings from 300 to 1500 psig (2.1−10.3 MPa) and is chiefly supplied in internal diameters from 2" to 5" (50−125 mm). RTP is simply a thermoplastic like HDPE with internal reinforcement (e.g.; braided PET). It is spoolable and flexible. An example use might be offshore risers.

Whatever the case, the absence of steel means the absence of corrosion. While *external* polyolefinic coatings are nothing new, drawn polymeric pipe *liners* for new and existing pipes are seeing wider application as the lining technology improves. Thick inert liners such as HDPE and polytetrafluoroethylene (PTFE) offer particularly good chemical resistance and are used for drain lines, acid lines, etc.

While such a discussion may be somewhat removed from the coating sphere, it is still important to understand that as the nonmetallic technology improves, coated steel pipe will be pushed out of more and more applications.

24.7.8 Encapsulant materials

Considerable effort has been directed at protecting line pipe and FJs—but mechanical connections such as flanges, valves and well heads often suffer the worst corrosion, thanks to their complex three-dimensional geometries. The reason behind this is that protective coatings have a hard time maintaining a minimum coating thickness on sharp edges (thanks to surface tension effects), whereas tapes and wraps struggle to conform to sharp changes in section.

Such equipment usually requires far more inspection and maintenance, which is almost an impossibility for semi-permanent solutions such as tapes and wraps. Even coatings are not ideal as protection usually takes the form of a single continuous film. Bolted joints cannot be disassembled without breaking this film, and reinstatement of the coating in the field is much more difficult than in the shop.

Mechanical protection techniques such as Band Protectors and Bolt Caps have been the traditional solution, but limitations in all the discussed methods have driven the development of *total Encapsulation systems*. Encapsulants are basically thick build elastomeric polymers, deliberately engineered to have no adhesion to the substrate. This is to enable rapid removal, rapid inspection, and rapid resealing of the encapsulated equipment.

That is the polymer can be cut, stretched, peeled away, and resealed in minutes. The "lack of adhesion" is usually achieved by incorporating a corrosion inhibitor somewhere in the system. This has the side benefit that protection is available to the equipment should the encapsulation be penetrated. All the mentioned points can be observed in Fig. 24.10. The thickness of the encapsulation is typically very high to maintain structural integrity and to act as a diffusion barrier to moisture, salt, and oxygen.

Some commercial products are brush applied and are built up in layers of 2−3 mm. For these products, peeling from the substrate is achieved by application of an initial primer layer of corrosion inhibitor, except at the free ends where adhesion is required to prevent water ingress. The benefits of this system are ease of application and repair in the field coupled with higher flexibility. The limitation is temperature resistance of 60°C (140°F).

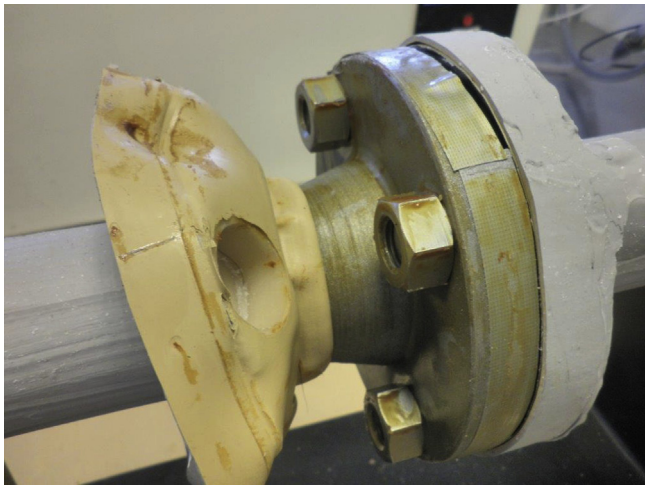

Figure 24.10 Brush applied, flexible, peelable encapsulation [51].

Other products use fusible thermoplastics (usually cellulosic), which are melted on-site and "spray" applied. Typical application temperatures are 165°C (329°F). They can be built to almost any thickness. The product acts as a jacket that can be cut and peeled away to allow rapid inspection and resealed again using a smaller melt device. Decohesion from the substrate is achieved by imbedding the corrosion inhibitor (usually an oil) into the product itself.

This product however, suffers from a lack of adhesion to the pipe at the free ends thanks to the corrosion inhibitor. The polymer is typically less flexible than the brush product and application, and repair can be more complicated. However, ASTM B-117 salt spray resistance values exceeding 11,000 hours are not uncommon.

24.7.9 "Green" coatings

The move to 100% solids coatings has been driven by the desire to eliminate harmful solvent emissions (VOC's) on environmental and Occupational Health and Safety grounds. The success of this can be seen in the widespread usage of FBE and 100% solids coatings.

Similar concerns plus the nonrenewable nature of petrochemical-based coating raw materials and precursors have encouraged the development of plant-based resins, monomers, and reactants. Some products such as RILSAN-PA11 by ARKEMA, based on the Castor Oil Plant, have been around for 60 years. Continuing research has led to many substitutions like a Bisphenol-A free coating based on acetoacetyl-modified soybean oil [52].

24.8 Conclusion

The earliest recorded use of pipe to transport hydrocarbons dates back to the Chinese in 1000 CE, where bamboo piping was used to transport natural gas used in the heating of

brine. However, it was not until the advent of steel pipes in the 1900s that the first concerted pipeline coatings emerged.

The first coating c.1920 was probably coal tar or asphalt, poured directly onto steel pipe in the trench, and smeared on with a mitt and/or rag. Within the space of 100 years, coatings have been developed which can operate up to 150°C (302°F) in quite severe conditions. However, the number of emerging technologies suggests an explosion of innovation in the coming decades.

This is not only important to the exploitation of the world's current resources, but is instrumental in meeting the challenges of the next century like pipelines for carbon sequestration and biofuel transport.

Those interested in learning more about *current* coatings are referred to the excellent publication "Onshore Pipelines: The Road to Success" by the International Pipe Line & Offshore Contractors Association (IPLOCA) for more information [53].

References

[1] IPLOCA, The Road to Success, third ed., IPLOCA, September 2013.
[2] D. Tailor, Field Joint Developments and Compatibility Considerations, ResearchGate, October 2003.
[3] Journal of Protective Coatings and Linings, Protecting and Maintaining Transmission Pipeline, Technology Publishing Company, Pittsburgh, 2012.
[4] Coal tar enamel, PCI International (May 31, 2001). http://www.pcimag.com/articles/85670-coal-tar-enamel.
[5] K. Andre, The use of coal tar enamel for lining and wrapping pipes, The Civil Engineer 9 (1) (January 1967) 1−8.
[6] T. Rehberg, M. Schad, Corrosion protective coating technology for transit pipelines in europe, in: 3R International, February 2010.
[7] DENSOLEN®-AS40 Plus, [Online]. Available: http://www.denso.de/en/products/product/densolen-pebutyl-tapes-and-mastics/densolen-corrosion-prevention-tape-three-ply/densolen-as40-plus/.
[8] J. Dickerson, Fifty Years of EPON Resins: A History of the Epoxy Resin Business.
[9] Seamless Carbon Steel Pipe, [Online]. Available: http://www.seamlesscarbonsteelpipe.com/Content/ue/net/upload1/Other/98544/636132576075038176590 1925.png.
[10] S. Guan, A.J. Kehr, High-temperature cathodic disbondment testing: review and survey—Part 1, Materials Performance 54 (2) (February 2015).
[11] International Supplies − Oil and Gas, [Online]. Available: http://isog.al/references/3-layer-polyethylene-coating-line-pipe/.
[12] V. Russell, K. Leong, Polymer coatings for oilfield chemicals, in: A.E. Hughes, J. Mol, M.L. Zheludkevich, R.G. Buchheit (Eds.), Active Protective Coatings: New-Generation Coatings for Metals, Springer, Netherland, 2016, pp. 385−428.
[13] S. Guan, Advanced two layer polyethylene coating technology for pipeline protection, in: International Corrosion Control Conference, Sydney, Australia, 2007.
[14] 3LPE Pipe Coating Process, [Online]. Available: http://www.prdcompany.com/wp-content/uploads/2016/03/PRD-3-Layer-PE-Coating.jpg.
[15] R.A. Francis, Sixty Years of Inorganic Zinc Coatings: History, Chemistry, Properties, Applications and Alternatives, Australasian Corrosion Association, 1999.

[16] VISCOWRAP-HT, [Online]. Available: http://www.viscotaq.com/en/products/corrosion-prevention/viscowrap-ht.html.
[17] J. Doddema, The use of visco-elastic self-healing pipeline coating, in: NACE CORROSION 2010, San Antonio, Texas, 14−18 March 2010, 2010.
[18] R. Norsworthy, Fail safe tape system used in connection with cathodic protection, Materials Performance 43 (6) (June 2004) 34−38.
[19] A. Williamson, J. Jameson, Design and coating selection considerations for successful completion of a horizontal directionally drilled (HDD) crossing, in: CORROSION 2000, Orlando, Florida, 26−31 March 2000, March 2000.
[20] American Water Works Association, External Corrosion Introduction to Chemistry and Control − Manual 27, third ed., AWWA, 2014.
[21] R. Buchanan, W. Hodgins, High temperature pipeline coatings − field joint challenges in remote construction, in: BHR 16th International Conference on Pipeline Protection, Paphos, Cyprus, 2−4 November 2005, 2005.
[22] Gas Technology Institute, GRI-05/0179-Field Applied Pipeline Coatings, Gas Technology Institute, Des Plaines, IL.
[23] Dirax − Welded joint heat shrink sleeve, [Online]. Available: http://www.samm.com/en/product/163/dirax-welded-joint-heat-shrink-sleeve-for-directional-drilling.html.
[24] Failure Investigation Report, Plains Pipeline, LP, Line 901 Crude Oil Release, PHMSA, Santa Barbara County, California, May 19, 2016.
[25] M. Batallas, P. Singh, Evaluation of anticorrosion coatings for high temperature service, in: CORROSION 2008, New Orleans, Louisiana, 2008.
[26] J. Weernink, Opportunities for growth, PCE International 5 (3) (September 2013) 64.
[27] D. Traylor, High Tg Internal Pipe Coating System, Coatings World, December 9, 2016.
[28] J.A. Kehr, M. Smith, S. Attaguile, New technology helps develop coatings for high-operating temperature, in: CORROSION 2008, New Orleans, LA, USA, 2008.
[29] J. Pratt, M. Mallozzi, Development of a low application temperature FBE, in: CORROSION 2009, Atlanta, Georgia, 2009.
[30] S. Edmondson, D. Wong, R. Steele, Low application temperature graded structure polyolefin coating system based on a next generation FBE for strain-based design pipelines using high strength steel, in: Integrity Management, Calgary, Alberta, Canada, September 25−29 2006, 2006.
[31] F. Lallemand, J. Magne-Drisch, S. Gonnard, G. Perdu, L. Normand, C. Weiss, Extending the Treatment of Highly Sour Gases: Part 1, Digital Refining PTQ, Q4, 2013.
[32] K.J. Bird, Circum-Arctic Resource Appraisal: Estimates of Undiscovered Oil and Gas North of the Arctic Circle, United States Geological Survey, 2008.
[33] SOLVAY ECTFE Pipe Lining Coatings, [Online]. Available: http://www.solvay.com/en/markets-and-products/markets/energy-and-environment/specialty-polymers-for-oil-and-gas.html.
[34] M. McDonnell, Liquid applied internal flow coatings for oil transmission lines, in: 1st. Pipeline Technology Conference, Hanover, 2006.
[35] Thermotite® TDF, [Online]. Available: http://www.brederoshaw.com/solutions/offshore/thermotite.html.
[36] M. Mallozzi, M. Perez, A new 3LPP offshore filed joint coating, in: CORROSION 2010, San Antonio, Texas, 2010.
[37] T. Stark, Wehocoat-Borcoat field joint coating technology for PE onshore application, in: 6th Pipeline Technology Conference, Hannover, 7th April 2011, 2011.
[38] S. Guan, A. Kehr, High temperature cathodic disbondment testing for pipeline coatings, in: CORROSION 2014, San Antonio Texas, 2014.

[39] History of galvanizing, [Online]. Available: http://www.galvanizing.org.uk/hot-dip-galvanizing/history-of-galvanizing/.
[40] K. Larsen, Chemically bonded phosphate ceramics provide corrosion protection for storage tanks, NACE Materials Performance − Tank Corrosion Control (Suppl.) (May 2016) 3.
[41] W. Li, L. Calle, P. Hintze, J. Curran, Smart coating for corrosion indication and prevention: recent progress, in: CORROSION 2009, Atlanta, Georgia, 22−26 March 2009, 2009.
[42] M. Kendig, Past, present and future 'smart' protective coatings, in: Advanced Research and Development of Coatings for Corrosion Protection: Offshore Oil and Gas Operation Facilities, Marine Pipeline and Ship Structures, Biloxi, Mississippi, April 14−16 2004, 2004.
[43] M. Magerstädt, Pipeline monitoring by intelligent high performance elastomer coatings, in: 11th Pipeline Technology Conference, Berlin, 2016.
[44] X. Liang, Y. Huang, S. Galedari, F. Azarmi, Pipeline corrosion assessment using embedded fiber Bragg grating sensors, in: SPIE Proceedings: Sensors and Smart Structures Technologies for Civil, Mechanical, and Aerospace Systems, 9435, 2015.
[45] E. Carter, Polymer Paint Colour Journal 4 (1983) 234.
[46] A. Stewart, D. Hunter, S. Hoenig, W. Hoenig, Novel technology enables industrial coatings to perform at new and longer-lasting levels, PCI International (November 1, 2016). http://www.pcimag.com/articles/102657-novel-technology-enables-industrial-coatings-to-perform-at-new-and-longer-lasting-levels.
[47] A. Noble-Judge, C. Barbé, Controlled-release corrosion inhibitors, PCI Magazine (October 1, 2016). http://www.pcimag.com/articles/102554-controlled-release-corrosion-inhibitors.
[48] J. Smith, A. Meuler, H. Bralower, R. Venkatesan, S. Subramanian, R. Cohen, G. McKinley, K. Varanasi, Hydrate-phobic surfaces: fundamental studies in clathrate hydrate adhesion reduction, Physical Chemistry Chemical Physics (14 (17), March 2012, 6013).
[49] S. Subramanyam, G. Azimi, K. Varanasi, Designing lubricant-impregnated textured surfaces to resist scale formation, Advanced Materials Interfaces (1 (2), January 20, 2014), 1300068. http://scholar.google.com/citations?view_op=view_citation&hl=en&user=3QJc-YQAAAAJ&citation_for_view=3QJc-YQAAAAJ:d1gkVwhDpl0C.
[50] A. Krishnamurthy, R. Mukherjee, V. Gadhamshetty, B. Natarajan, O. Eksik, A. Shojaee, D. Lucca, W. Ren, H. Cheng, H. Koratka, Superiority of Graphene over Polymer Coatings for Prevention of Microbially Induced Corrosion, Scientific Reports, September 09, 2015.
[51] The flange protection challenge, [Online]. Available: http://pecm.co.uk/the-flange-protection-challenge/.
[52] R. Lalgudi, R. Cain, M. Perry, B. Vijayendran, B. McGraw, High-solids reactive oligomers derived from soybean oil, PCI International (May 1, 2016). http://www.pcimag.com/articles/101988-high-solids-reactive-oligomers-derived-from-soybean-oil.
[53] IPLOCA, Onshore Pipelines: The Road to Success, third ed., International Pipeline & Offshore Contractors Association, September 2013.

Advancements in Cathodic Protection of offshore structures

25

Jim Britton and Matthew L. Taylor
Deepwater Corrosion Services Inc., Houston, TX, United States

25.1 Introduction—how have things changed?

Corrosion control of assets installed below the waterline and exposed to seawater or saturated seabed environments is the subject of this section. We will not address internal corrosion or downhole corrosion that is addressed in separate chapters in this book. First, therefore, we should revisit the basics of CP (cathodic protection) in seawater: How does it work? How do we measure it? Worthy of mention is the fact that high-performance coatings are often employed synergistically with CP in these environments; because coatings are covered in Chapter 24 we will focus here on the CP part.

Before CP in seawater can be fully understood, it is necessary to understand how steel corrodes in seawater. For corrosion to occur three things must be present: (1) two dissimilar metals, (2) an electrolyte that is seawater in this case, and (3) a metallic conducting path between the dissimilar metals.

The two dissimilar metals could be two different alloys such as steel and aluminum, or more likely will be macroscopic or microscopic differences on the surface of a piece of steel. These differences could be caused by many things, such as welds, mill scale, surface inclusions mechanical impact (cold worked areas), etc. So in this case, we will consider freely corroding steel that is nonuniform. If the above three conditions are present, the following reaction takes place at the more active sites on the steel surface (two iron ions plus four free electrons):

$$2Fe \rightarrow 2Fe^{2+} + 4e^{-}$$

The free electrons move through the metallic path to the less active sites where the following reaction occurs (dissolved oxygen is converted to oxygen ion by combining with the four free electrons—which then combines with water to form hydroxyl ions).

$$O_2 + 4e^{-} + 2H_2O \rightarrow 4OH^{-}$$

These ions then recombine at the active metal surface sites yielding the iron corrosion product ferrous hydroxide.

$$2Fe + O_2 + H_2O \rightarrow 2Fe(OH)_2$$

This reaction is commonly described as current flow through the water from the anode (active site) to the cathode (less active site). The corrosion thus occurs at the active site.

Trends in Oil and Gas Corrosion Research and Technologies. http://dx.doi.org/10.1016/B978-0-08-101105-8.00025-5

CP prevents this type of corrosion by converting all the active (anodic) sites on the metal surface into passive (cathodic) sites by supplying the free electrons from an alternate source. This commonly takes the form of galvanic or sacrificial anodes that are made from materials that are more active than the active sites on the steel surface [usually alloys of zinc (Zn) or aluminum (Al)]. They are called sacrificial anodes because they corrode preferentially to the steel, thus sacrificing themselves. In the case of the most common sacrificial material, (aluminum), the reaction at the aluminum anode surface is (4 aluminum ions plus 12 free electrons).

$$4Al \rightarrow 4Al^{3+} + 12e^{-}$$

At the steel surface, the reaction is (oxygen converted to oxygen ions which convert with water to form hydroxyl ions) as follows:

$$4O_2 + 12e^{-} + 6H_2O \rightarrow 12OH^{-}$$

Provided that the free electrons arrive at the cathode (steel) surface faster than the oxygen arrives, corrosion is arrested (Fig. 25.1).

There are some cases where sacrificial anodes are not desirable, usually because the mass required would be prohibitive. In these cases, there is an optional way to provide the current (electrons) required to arrest the corrosion. This alternate method is referred

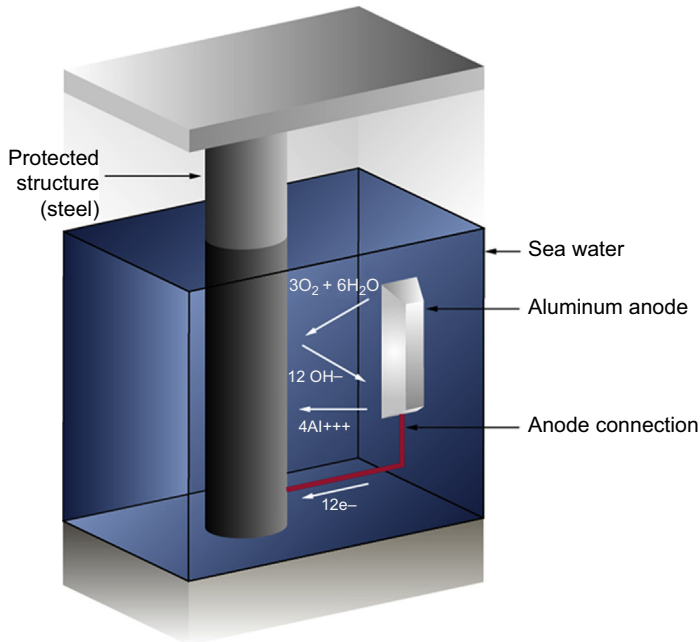

Figure 25.1 Sacrificial anode cathodic protection system in seawater.

to as ICCP (impressed current cathodic protection). These systems utilize nonconsumable anode materials that are fed with the DC current from a topside power source. In this case, the free electrons are generated by the oxidation of the chloride ions in the seawater.

$$2Cl \rightarrow Cl_2 + 2e^-$$

The reaction at the cathode (steel) is the same as with the sacrificial anodes (Fig. 25.2).

How do we tell that we have enough CP to arrest the corrosion? We do this by measuring the change in the surface electrical potential of the steel cathode. Because of the arrival of excess free electrons, the steel to seawater surface potential will shift in the negative direction as more CP (free electrons) are supplied. This surface potential change can be read against a reference electrode immersed in the seawater adjacent to the structure under test. History has shown that if sufficient current is supplied to shift the potential to (−) 0.800 V as compared to a silver/silver chloride (Ag/AgCl) reference electrode the corrosion is arrested. Due to the benefits of surface deposits that precipitate onto the steel surface with applied CP, designers try to achieve a potential of between −0.950 and −1.000 V vs. Ag/AgCl. These surface deposits are called calcareous deposits and they serve to limit oxygen diffusion to the surface, hence reducing the amount of CP current required to maintain the potential.

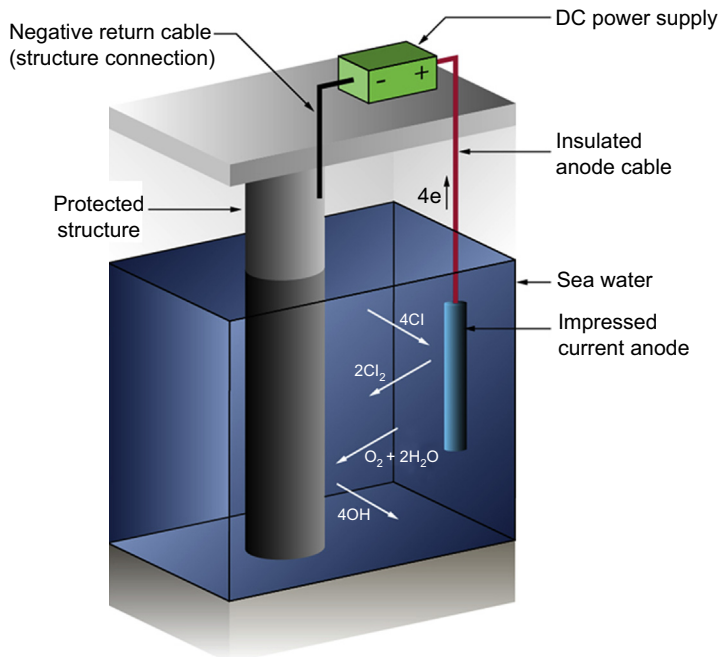

Figure 25.2 Impressed current cathodic protection system in seawater.

25.1.1 Evolution of applied offshore CP

To understand fully how offshore CP technology and methodology has developed over the years, we must look to how the offshore industry has evolved over the years. The major shift in focus has been the exploration and production of oil and gas in ever greater water depths, and in generally harsher offshore environments. This has necessitated a major change in the hardware used to drill wells and then produce them.

In the early days, we had drilling/production platforms made from carbon steel, mostly fixed to the seabed with steel piles and steel pipelines running between the platforms and back to shore-based facilities. Water depths were typically less than 300 m. Mainly divers performed inspection and repair work subsea and ROVs (remotely operated vehicles) were used in the deeper areas. The steel platform structures, mainly left uncoated below the splash zone, were protected mainly with large sacrificial anodes welded all over the structure. Pipelines had either mastic enamel or fusion bonded epoxy coatings and bracelet sacrificial anodes attached every dozen joints or so. Anodes were either zinc or aluminum alloys. Systems were designed to provide a life of 20−25 years normally.

With transitions into deeper waters, it was necessary to look to alternate ways of producing the fields, the depth and economics precluded the use of fixed platform systems with large truss-type jacket structures. So we saw a transition through slender tower type structures eventually to floating production systems (FPS) like TLPs (tension leg platforms) and moored semisubmersible platforms. Already we were seeing a shift in strategy, we now had to deal with high-strength steel tendons and weight limitations on floaters resulted in greater use of coatings to reduce anode mass. We also had to deal with colder waters that caused us to revisit the design criteria for CP and the composition of anode alloys that would work reliably in the deeper colder water. We also saw the introduction of flexible risers and complex permanent mooring systems with chains ropes and anchor systems. This soon evolved into subsea wellhead structures and flowlines connected to complex manifold structures. These wells were often great distances from the host floating production structure. This phase saw the introduction of many new materials, duplex and super duplex stainless steels, titanium alloys, very high strength high hardness steels. New types of coating for fasteners were introduced. Pipe coatings started to evolve into multilayer systems to provide superior protection and complex thermal insulation systems were introduced to aid with flow assurance. Pipeline installation techniques evolved which often precluded anode installation on land. Smaller reservoirs were made commercial by the evolution of FPSOs (floating production storage and offloading), these are often converted oil tankers connected to complex turret and swivel systems with internal tanks converted to handle produced fluids often at elevated temperatures. This added a complication by bringing the marine (shipping) industry into the upstream oil and gas business. The many changes in CP technology that are followed will be addressed in the later sections of this chapter. The increasing water depths, now often in excess of 3000 m, would not have been possible without parallel improvements in ROV technology. Everything subsea just about had to be ROV compatible. So we saw new developments in inspection and monitoring to accommodate this requirement. The next step

is to use AUVs (autonomous underwater vehicles) to do much of the work of the ROV, which will reduce costs by freeing up the surface support vessel. So new corrosion control inspection technologies must anticipate the transition from ROV to AUV and be compatible.

The latest challenge to the offshore CP industry has been the growth in offshore wind energy. These wind farms often comprise around 100 structures. These are usually located quite close to shore and very often close to river estuaries where the wind resource is typically optimal for turbine deployment. New challenges of providing CP to the foundations of these structures arise from the very high water currents, variable salinity, abrasive flow caused by entrained silts, and difficult structure geometries.

25.2 Offshore pipelines

25.2.1 History—how was it done?

Offshore pipelines have historically been protected with pipe coatings supplemented with CP. The CP was typically provided with preinstalled sacrificial anodes in the form of circumferential bracelets spaced at between 500 and 1000 feet. In order to prevent the subsea pipelines from floating off bottom, concrete weight coatings were added to many of these pipelines.

The early offshore pipe coatings were mainly mastic or coat tar enamels applied at thicknesses of between $^1/_4''$ and $^1/_2''$ (6−12 mm). Field joints were applied on the lay barge and were usually manually applied versions of the same materials. In the late 1970s, thinner fusion-bonded epoxy powder coatings made an appearance that these coatings would be factory applied usually at a thickness of 250−500 μm. At around the same time, the development of heat shrinkable plastic sleeves provided the solution for the field joints.

Early anodes were poured from a zinc alloy, these anodes provided reliable protection but they had a low galvanic efficiency. Early aluminum anodes were alloys of aluminum, zinc, and mercury. These anodes proved to be unreliable in saline mud service so the pipeliners are stuck with the zinc. It was in the late 1970s, when the indium-activated aluminum anode began to be used; this alloy performed very well in saline mud and was lighter and more efficient, so from the early 1980s most operators were specifying the Al−Zn−In alloys.

25.2.2 New design guidelines

25.2.2.1 Improved coatings

As the offshore industry moves into ever deeper waters, pipeline design is changing to accommodate the new pipe-lay techniques as well as we are seeing significant changes in pipe coating technology. Now the single and double coat FBS-coating systems are being replaced with three- and five-layer systems to give better thermal and mechanical properties. In many cases, very thick (up to 100 mm) thermally insulated coatings are

being applied for flow assurance reasons. These coatings provide a very high level of efficiency such that the only areas where CP is really required is at the field joints and on the end termination structures. This has caused a revision in the design guidelines for coating breakdown factors and the way in which CP is designed and applied. When an operator invests in a coating system that can cost close to $1000/m, it is not smart to start poking holes in the coating to provide attachment for anode bracelets.

25.2.2.2 Anode sleds and attenuation modeling

Because the coatings are now so efficient 99.95% or better, the amount of backup CP required is minimal. Also the wall thickness of the pipes used in deep water is heavier. These two factors mean that CP can be "thrown" much further along the pipeline than on a conventional pipeline. So the new design codes allow for the anodes to be located off the pipeline and "attenuation" calculations can be used to estimate the distance that can be protected from an anode sled, or alone on an end termination sled. So now we see new pipelines being installed with anode sleds connected with clamps (Fig. 25.3) and sleds can be spaced tens of kilometers apart and the pipeline is well protected. These attenuation formulae can conveniently be computed by modern multiphysics finite element analysis software to give a graphic output. The CP designs on these pipelines are really only looking at the field joints.

25.2.3 Inspection and monitoring

As the pipelines age and approach the end of their design life, the need to be able to accurately assess the condition of the coating and CP system becomes more urgent. As expected, a lot of work has been completed to optimize how pipelines are inspected.

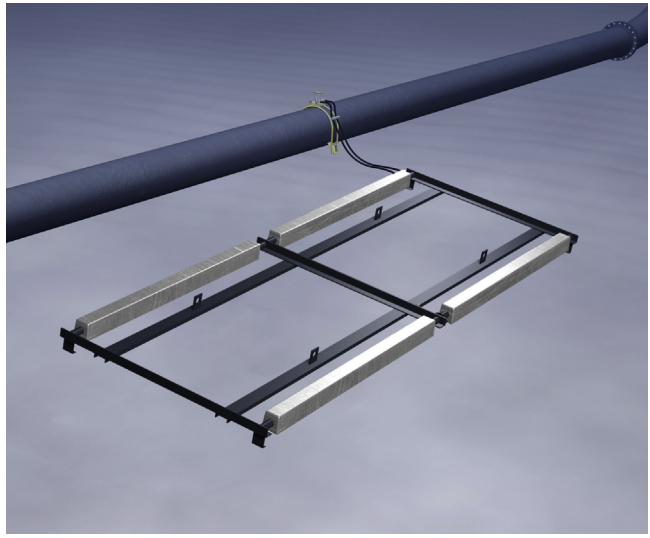

Figure 25.3 Pipeline anode sled attached with clamp.

In the very early days before the 1980s, offshore pipelines were inspected using various methods such as towed electrode or trailing wire surveys that were a carryover from onshore survey techniques. These methods were of little use because of various factors [1]. The early 1980s saw the introduction of ROV-based survey methods. The "three electrode method" became the system of choice because of its accuracy and the ability to combine the CP survey with other survey elements such as visual and positional. The three-electrode survey was used pretty much exclusively until quite recently when budget constraints and limitations of the method to deal with buried offshore pipelines became apparent.

Offshore pipeline integrity managers have relied on in-line (smart pig) surveys for many years. These surveys are basically looking at pipe wall thickness changes and the development of crack anomalies, techniques such as magnetic flux leakage, and ultrasonic measurements are common. A few years ago, a tool was developed [2], which could measure the electrical voltage drop along a section of the pipeline by making electrical contact at two spaced points on the pipe wall. In essence, the direct current flowing in the pipe wall is being measured. The principle source of these currents is the CP system, where it becomes possible for the first time to measure the effectiveness of CP on the outside of the pipeline from the inside. Of course, there are some drawbacks to this technology that was originally designed for onshore pipelines that are normally protected with widely spaced ICCP systems. The system is only really effective offshore when the pipeline is protected with periodically spaced anode sleds. This normally means that the line has had a life extension system installed. Other limitations are erratic performance in gas pipelines and other restrictions that limit pigging.

Modern approaches look toward more intelligent fixed points for monitoring and trending. This involves the installation of the equivalent of an onshore "test station". When retrofitted to pipelines at intervals, it is possible to measure unambiguous data at a few widely spaced points and use the aforementioned attenuation predictors to fill in the gaps. These test stations can utilize portable ROV or diver transported CP probes (Fig. 25.4) or they can include fixed sensors that can measure and convey data via a number of different methods.

Of particular interest to the industry is the rapidly improving capabilities of AUVs. Free swimming vehicles with no surface support vessel can slash the costs of pipeline and subsea inspection. At present, they are not capable of remote intervention tasks but have a good visual capabilities. Solar powered measurement systems offer one way to use such vehicles to obtain CP survey data as shown in Fig. 25.5.

25.2.4 Life extension

The worlds in situ pipeline network are aging and many thousands of kilometers of pipeline are currently operating beyond their original design life. The actual life requirement of many key offshore pipelines will likely approach 100 years, this requires that external corrosion control systems are maintained.

Repair or refurbishment of coatings on offshore pipelines is not really practical, so the job falls to the CP systems.

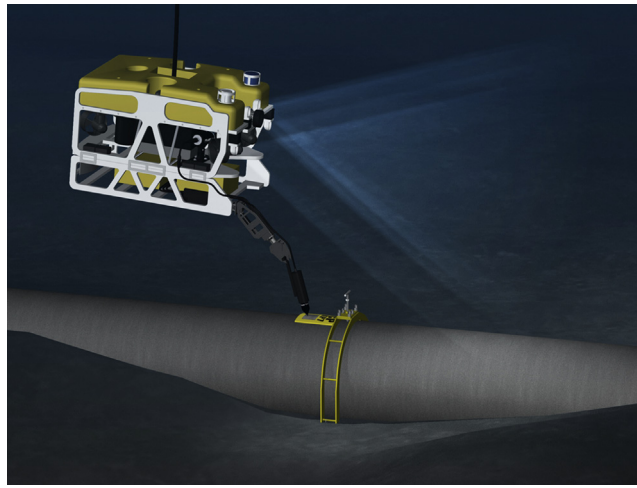

Figure 25.4 Remotely operated vehicles with mounted cathodic protection probe stabbing an offshore test station.

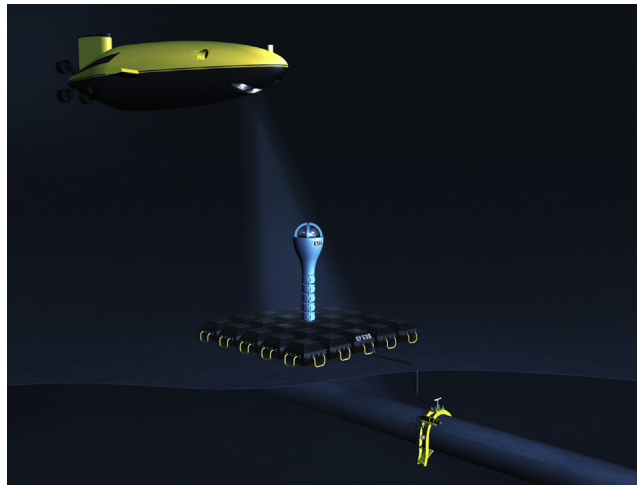

Figure 25.5 Solar powered test station with autonomous underwater vehicle.

There have been a number of innovations designed to facilitate cost-effective life extension of offshore pipeline CP systems. The key focus has been on assessing the condition of the pipeline and then optimizing the spacing between replacement CP anode devices. Obviously, the greater the distance between interventions, the lower the cost of the retrofit project.

Key recent hardware innovations have been the development of clamping systems that can provide the required electromechanical connection safely to a live pipeline

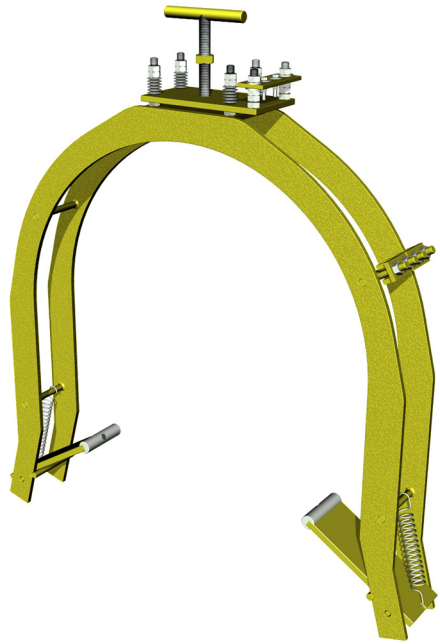

Figure 25.6 Retrofitted clamp system.

(Fig. 25.6) and a range of anode systems that provide high reliability and simple installation. Modeling tools have also improved dramatically and are available in off the shelf multiphysics packages from a number of vendors.

What has been learned from early retrofit projects is that pipe coatings have performed very well. So well that the current design codes predictions of coating degradation look ridiculously conservative. This conservatism is fine for design purposes but not for cases where life extension is needed, in these cases we need to know actual condition. Where design codes would predict a coating breakdown of 75% on a 30-year-old pipeline, we are measuring values typically well below 5%.

25.3 Fixed structures—platforms and monopiles

25.3.1 History—how was it done?

The early structures offshore were often provided with impressed current CP systems. The problem was that they were generally not engineered to very high standards and failed frequently mainly due to cable failures. This caused the industry to shift toward sacrificial anodes that, although more costly initially, were much more reliable in the longer term. This left a lasting negative impression of impressed current systems that is only recently being laid to rest.

Early sacrificial anodes were mainly zinc, but as the industry grew, the development of aluminum-based alloys showed improved efficiency with significant weight savings. The castings were typically formed onto core materials with structural shapes such as angles, tees, and channels that could be directly welded to the structures. These irregular shapes caused many problems in the castings; irregular cooling led to cracking that resulted in large sections of the anode materials falling away from the support cores after a few years of operation. So the industry moved to pipe core inserts which solved this problem. As subsea inspection procedures developed, the anodes were frequently problematic in snagging diver hoses or ROV umbilicals, so more modern designs utilize pipe cores designed to prevent snagging (Fig. 25.7).

Early aluminum alloys used mercury or tin as activator elements. The mercury was particularly successful yielding a very high galvanic efficiency and a good working potential. However, in the late 1980s, the material was passed over due to environmental concerns and indium was substituted as an alternate. Al−In−Zn anode alloys are still the standard alloys used today in seawater CP.

In the early days, there was a division in the industry regarding the need and benefits of coating the subsea parts of the structures. Some did and some did not. The capital cost of the coating generally proved to be uneconomic compared to adding more anodes and leaving the majority of the structure uncoated. So this philosophy, largely dominated and large platform structures were usually left bare steel. The benefits of coating can be seen in a recent comparison between two similar large North Sea structures that required a life extension after around 35 years in service. The coated

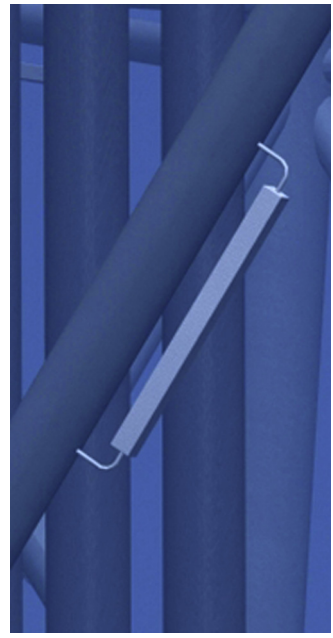

Figure 25.7 Platform anode with core design to prevent snagging.

structure had a current requirement of <1000 Amp to retrofit, while the similarly sized bare structure required 7500 Amp. A true life cycle cost comparison has not yet been completed, however.

As offshore exploration and production moved into more global areas, it quickly became apparent that CP design criteria needed to take into account the varying met-ocean conditions around the globe. The North Sea, for example, could not be designed to the same standards as the Gulf of Mexico. So the first recommended design codes were produced initially by NACE and then by other certification bodies such as DNV and ISO. These design guidelines are constantly under review as offshore energy moves into new frontiers.

As water depths increased, platform design changed to try and reduce the vast amounts of steel required for a platform jacket in 1000 feet plus. So we started to see more slender guyed towers and compliant tower structures. These presented challenges as they were both weight sensitive and had some critical areas that were hydrogen embrittlement sensitive. In order to reduce weight coatings we used in some areas and the use of thermal sprayed aluminum became popular with some operators.

Offshore wind turbine foundations came along fairly recently and have presented more challenges. Large diameter monopile structures were most prevalent in the early wind farms. CP systems were mainly located on the transition pieces that sit on top of the main foundation pile. There were problems with these systems both sacrificial and impressed current because the monopiles were left bare, their high strength did not allow direct anode attachment, and many systems did not provide adequate protection to the mud line and below. Newer designs are using more coatings to overcome this issue.

25.3.2 Inspection and monitoring

Monitoring CP performance on fixed structures is generally easily achieved with a simple drop cell survey. A reference electrode is dropped through the water adjacent to the structure and is connected to a topside voltmeter that is grounded to the structure topside. This allows the potential to be measured at various locations around the structure. The accuracy of these surveys is somewhat compromised because of the distance between the structure and the reference electrode, readings tend to be somewhat optimistic.

Accuracy can be improved if the reference electrode is transported by a diver or an ROV. This allows the measurements to be taken close to the structure and in critical areas such as complex joint nodes. Many maintenance campaigns use the drop cell survey annually supplemented by a diver or ROV survey every 5 years.

As remote communications improve and the cost of putting personnel offshore increases, there is a trend toward the use of fixed CP monitoring systems. These systems generally locate a few instruments at strategic and representative locations on the structure. Sensors are hard wired to surface data acquisition systems. The advantage of having fixed repeatable sensors is obvious; data are available continuously and can be trended to make time based predictions. Also the instruments can measure both

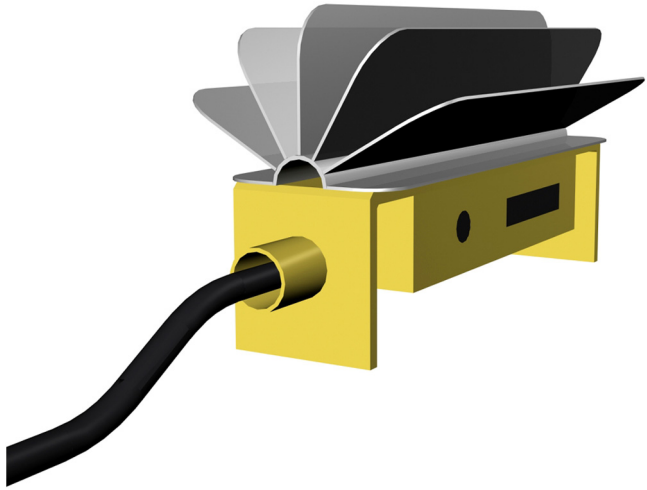

Figure 25.8 Polarization monitor measures potential and current density.

potential and current density (Fig. 25.8). These polarization monitors provide the corrosion engineer with the data required to analyze present and future CP system performance.

25.3.3 Life extension

Many large structures are being operated well beyond the original design life. Thus retrofitted CP systems are frequently required to replace the depleted original systems. This activity is becoming more frequent and some of the projects are very large.

When the operator has determined that a life extension is required and for how long, the next major task is to determine the capacity of the retrofitted system in amperes. This is a critical step that is often miscalculated. The available design codes and guidelines do not address design of retrofitted systems so offer no help. This lack of info often results in the new build guidelines being applied. This results in extremely conservative current requirement estimates that can drive the cost up dramatically. In reality, we only need to provide enough current to maintain protection through the desired life extension period; this can be achieved using a small fraction of the current densities required to polarize a newly installed structure. It is prudent to consult with an expert through this phase of the project. There have been many attempts to use predictive models to assist in this process, the actual results and benefits of this have been dubious on life extension projects; this is due to a lack of understanding of the in situ condition of the structure that is critical input into these models.

Early life extension and retrofit systems were attempts to essentially replace the original system by clamping new sacrificial anodes to the structure. The only real innovation was to attach two at a time rather than as singles (Fig. 25.9). This persisted for many years, then the concept of using anodes as free standing arrays tied back to the

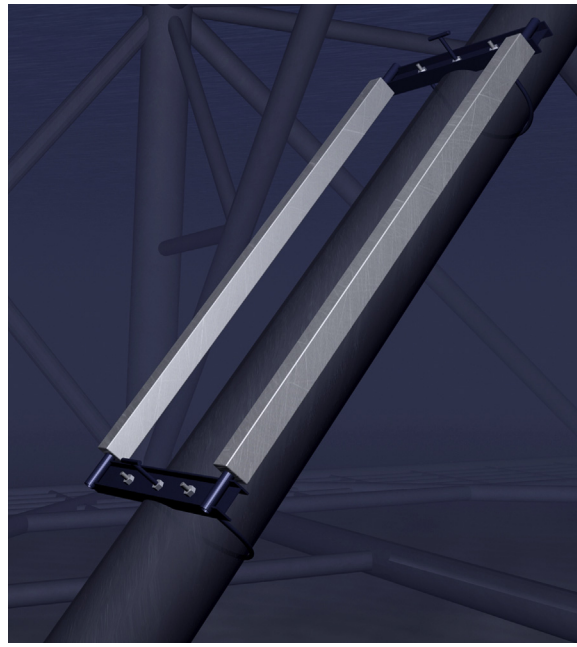

Figure 25.9 Dual clamp on anode.

structure with clamps offered significant improvements in installation efficiency (Fig. 25.10), allowing the job to be completed with divers or ROV's and overall improved the process. As offshore maintenance is moving toward an integrated IMR (inspection, maintenance, and repair) format, where the operator contracts offshore resources on a 5-year basis, the use of short-life extension strategies is

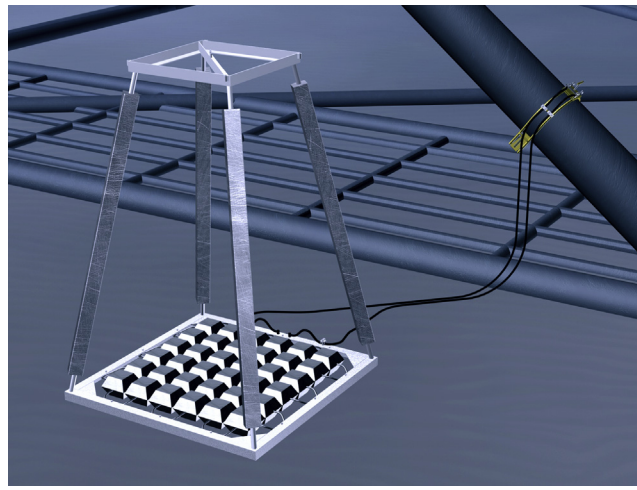

Figure 25.10 Anode pod structure attached with clamps allows remotely operated vehicle installation.

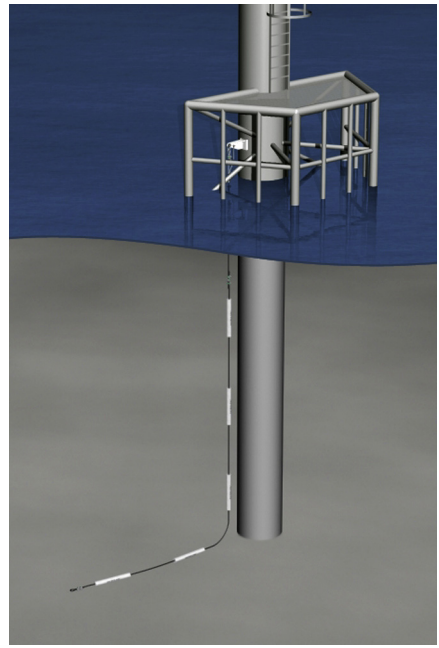

Figure 25.11 Short-life anodes strings.

growing in popularity. These are short-life CP retrofits designed around a simple anode string configuration that can be installed with a light inspection spread offshore. They are relatively inexpensive but only provide a 5- to 6-year life (Fig. 25.11).

Impressed current versus sacrificial becomes an economic decision that favors impressed current as the current requirements escalate. A small platform with a current requirement of 250 Amp requiring a 20-year life extension would require approximately 22 tons (20 ton) of aluminum anodes. This could be achieved with the installation of 15 anode pods which would be a 1- or 2-day job. This would more than likely be the preferred solution. If on the other hand, we had a large platform with a current requirement of 7500 Amp for a 20-year life we would require around 660 tons (600 tons) of anode material. Or over 450 anode pods, this clearly is not a viable retrofit option. As an alternate, we could use just 8 × 950 Amp rated ICCP anodes, a cost savings of millions of dollars. Impressed current anode systems have developed considerably over the last decade and now offer a reliable option for high-capacity offshore life extension projects (Fig. 25.12).

25.4 Floating production systems

25.4.1 History—how was it done?

FPS offers the operator a cost-effective solution for deep water and marginal yield developments where a fixed structure is not possible. So over the last 25 years we

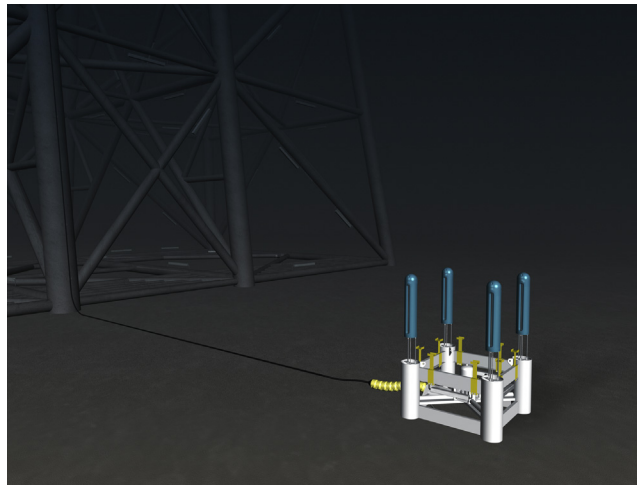

Figure 25.12 High capacity impressed current anode system.

have seen significant technological advances in the FPS design. From a corrosion control standpoint, these structures offer a number of new challenges and a new set of design regulations and guidelines. These structures are floating hulls and thus are subject to a combination of maritime and offshore engineering rules and codes.

It is this maritime influence that sees a greater use of subsea coatings and impressed current systems as original equipment. This is particularly true on FPSO, which are often oil tanker conversions. This has caused many problems in the industry and has led to many offshore system repairs and replacements.

The main problems arise from the fact that ocean going ships are required to enter a dry dock every 2.5−5 years. During these dry docks, repairs are made to the coating and CP (usually ICCP) systems. Thus the systems in common use are designed to fulfill this relatively short-life requirement. An FPSO is not brought to dry docks and may stay on station for 20 years or more. This is why many systems fail in service and have to be replaced.

Other problems arise by combining ICCP and Sacrificial Anode Cathodic Protection (SACP) systems. The normal ship ICCP systems are all potentially controlled, that is, they sense protective levels on the hull and ramp the system output up or down to maintain the level within a preset range.

There are areas on these structures that are routinely fitted with sacrificial anodes, usually because of concerns that the ICCP will not reach them. These include thruster tunnels, sea chests, and annular spaces inside turrets. The problem is that these anodes are able to protect the well-coated hull to such a level that the ICCP systems never energize, thus the sacrificial anodes are consumed prematurely. This can be problematic because the anodes are by definition hard to replace in these inaccessible areas. Newer purpose build FPS systems are choosing to go with entirely sacrificial systems to alleviate these issues.

These FPS systems also introduce many internal compartments, sea water ballast tanks, produced water tanks, and permanent ballast (soft) tanks. These systems must

be cathodically protected, but system designers must be aware of the potential for hydrogen gas accumulation, elevated temperatures, or significant pH changes in static tanks. Many internal spaces are protected with zinc rather than aluminum anodes to alleviate some of these issues; it is a good idea to consider the placement of permanent reference electrodes in such spaces as access can be difficult after commissioning.

25.4.2 New developments

Floaters have thrown some new challenges to CP designers. Riser technology has seen radical changes, steel catenary risers, top tensioned risers, free standing risers are all new ways to deal with transporting product in deep water. Some of these designs are dynamic or buoyant and thus there are concerns with weight and fatigue, high-strength steels are common, and the risk of hydrogen-induced cracking is elevated. These systems also call on flexible piping systems for flowlines and umbilical; these systems often combine exotic metallic alloys with elastomeric materials. Coatings are used extensively and CP designs must be tailored to fit the service condition of the equipment, taking into account hydrodynamic effects, hydrogen charging from CP, and current distribution under monolithic buoyancy modules. These problems have been solved using long line attenuation modeling to keep anodes off of dynamic sections. Thin-film thermal spray coatings coatings are used to reduce current demand in confined spaces such as under buoyancy modules or nonmetallic Vortex Induced Vibration (VIV) strake systems. And the development of low potential anode alloys and diode-controlled anode systems both used to control cathode potentials below the levels where hydrogen charging can occur.

Mooring systems are a feature that is unique to these systems. Chain, wire rope, synthetic rope, and various metallic connection elements can provide a number of "hot spots" that are difficult to protect and places to locate anodes are few. It is advisable to build in corrosion allowance to these systems and locate as many anodes as possible on connectors and other hardware to attempt to offset the inevitable current drain to the chain sections.

25.4.3 Inspection and monitoring

Floating systems are normally subject to periodic underwater inspection in lieu of dry docking inspections. This will include a CP assessment scope utilizing portable survey instruments deployed on an ROV. However, these floaters can benefit greatly from fixed CP monitoring systems, sensors can be located in critical areas such as tanks, on risers, and mooring systems and inside tight annular spaces associated with turrets or moon pools.

25.4.4 Life extension

As previously indicated, there are frequent problems with CP systems on FPS so retrofitted repairs are not uncommon. In situ replacement of sacrificial anodes can be accomplished but would normally be a very tedious and time-consuming exercise

with high associated costs. For this reason, most successful system replacements have been impressed currently with the exception of system for internal spaces, which are normally retrofitted with sacrificial anodes.

FPS systems are either moored with a spread mooring system or tendons or they are connected to a turret system that allows the hull to freely "weathervane" 360° around the mooring. In the former case, impressed current systems have been deployed to the seabed and fed power through a dynamically deployed cable connected to a topside transformer rectifier system. These systems have the advantage of providing excellent current distribution to the hull and associated attachments and are quick and easy to install. Most projects are completed in just a few days offshore. This approach works very well for spread moored FPSOs and SPAR-type structures. It is possible to use this approach on turret moored FPSOs also; however, the main power feed cable must deploy through the turret. In these cases, it is normally required to locate the power supply system within the turret to avoid passing all the current through the electrical slip rings in the swivel system.

On TLPs, the hall can be protected as previously described; however, a second sacrificial system many be required to handle the tendon foundation structures and the lower half of the tendons themselves.

When designing retrofit CP systems for this type of installation, predictive computer models can be useful to check on current distribution and look for possible interference sites. Boundary element models or finite element analysis can be used, providing that valid electrochemical polarization data are used as input.

25.5 Subsea production systems

25.5.1 History—how was it done?

The development of subsea production systems really started to gain momentum from the mid-1980s. Technological developments in subsea equipment have made deep water and ultradeep water exploration and production a reality. These subsea systems can be extremely complex, combining subsea Christmas trees, flowlines, manifolds, pipeline connection skids, and more recently subsea separation and process skids. From a corrosion control perspective this means a lot of mixed materials, a wide range of operating temperatures, coated and uncoated systems, and many mechanical connections and joints. All these systems normally provided by a number of different suppliers. The challenge is to make all the corrosion control systems compatible; this has not been very well accomplished to date and as a result many early in situ repairs and anode supplements are required. The major recurring problems that we have seen on these types of systems are as follows:

Electrical continuity issues. All the bolted connections, coated fasteners, and heavy epoxy-based coating systems used can result in some components being isolated from the CP system. This can be very difficult to correct when the system is sitting in 3000 m of seawater. The solution is to provide multiredundant continuity paths with jumper cables between components. Use coated fasteners carefully and if the coating

is dielectric, provide methods to endure continuity such as serrated (star) washers under nuts. Most importantly, check continuity with a milliohm meter between all components and the part of the structure where the anodes are located. These checks should be conducted as part of system integration testing, and as factory acceptance, but should also be rechecked immediately prior to load out offshore as road transportation vibration can cause problems.

Mismatched anodes. Sacrificial anodes are the only viable alternative to cathodically protect these assets. However, when designing sacrificial anode systems, there are a few basic rules, which must be followed, but which are routinely ignored by many operators on subsea systems.

Cardinal rule is not to mix anodes of different cross-sections on a common structure. A fact that is commonly overlooked by system designers is that when a flowline is connected to a subsea tree there is no electrical isolation between the two elements, so by default they become a "common structure". Small cross-section bracelet type anodes are usually connected to the flowline and bulky block anodes are attached to the tree structure or end connection skid. The anodes (being merely unintelligent castings) do not realize that they are supposed to only protect the element to which they are attached. They rather follow the basic laws of physics and all deliver protective current basically in accordance with ohms law. If the anodes are all of the same basic chemistry, this means that the smaller cross-section anodes will deplete first, rather than them all depleting through the design life as intended by the designers.

Rule number 2 is to ensure that all anodes are of the same chemistry. This is very difficult to achieve in reality if different foundries, in different countries, produce the anodes. The chemical composition range may be to a common specification but foundry practice, anode size, and rate of cooling can produce anodes that exhibit a range of driving voltages. Obviously, anodes with a higher driving voltage will take on a disproportionate amount of the CP task, leaving others virtually untouched.

Another rule is to distribute anodes evenly across the structure; this is important for several reasons. The main reason is to ensure adequate current distribution. Second, it is not good to crowd anodes as they will interfere with one another reducing current output and causing uneven consumption that can lead to significant efficiency reduction.

Location of anodes should also consider the proximity of elements that are possibly susceptible to hydrogen embrittlement, such as cold bends in duplex stainless steel control tubing. It is common for anode corrosion products to remain and build up on the anodes in deep water because there is no current to disperse them. Significant build-up of these products may be detrimental if allowed to build into a dense packed mass and engulf uncoated materials.

25.5.2 New developments

Recent developments to attempt to alleviate some of the problems have actually evolved from systems that were designed to fix the problems in the first place. As the first systems started to need repair, usually because of premature anode consumption, the methods used involved connecting free-standing anode structures to the subsea equipment with an ROV installable clamping systems. As a number of these projects were executed, it

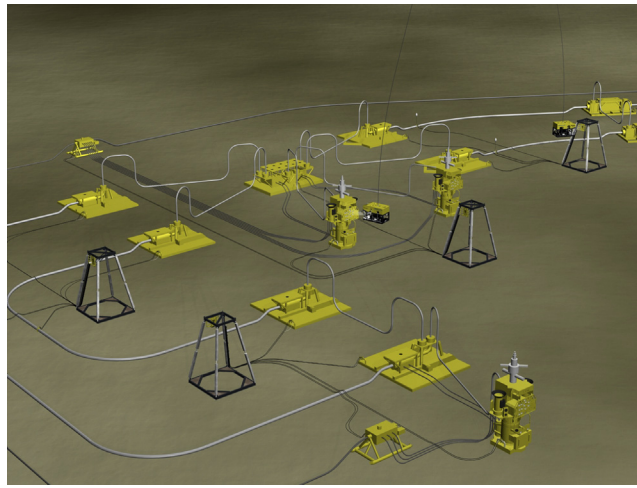

Figure 25.13 Decoupled anode sleds are the future of deepwater cathode protection system.

became apparent that these fixes were quite easy to install. The method solved all of the aforementioned problems while providing a number of additional benefits.

The decoupling of the CP current source from the actual structures solves all the problems of anodes shapes and chemistry while giving the opportunity to centralize monitoring of the CP system (Fig. 25.13). The semiremote location of the anodes also provides superior current distribution and allows for more control over the potentials that can exist on the subsea equipment.

Having a centralized CP source allows a number of subsea equipment items to be protected from the central location, and the current returning from each element can be monitored along with the potential. This provides invaluable data to CP designers as well as providing a significant reduction in subsea inspection time. Again the use of solar powered subsea voltage readouts eliminates the need for ROV interfaced monitoring equipment and will allow AUVs to be used in the future.

Flow assurance is a critical issue on these deep water fields. It is being addressed in a number of ways using chemicals. But also the ability to keep the produced oil hot is a major challenge. The latter is being achieved either with electrically heated flowlines [3]. Or by the use of thick thermally insulating pipeline coatings, often up to 100 mm thick. The thick coatings obviously preclude the use of conventional bracelet anodes because they would cause a local heat sink and would poke a hole through a very expensive coating, apart from the fact that a 100 mm thick coating should provide close to 100% coverage, thus reducing CP current requirements to infinitesimally low levels. It is only the field joints that should be considered for coating imperfections. Indeed, recent updates in CP design guidelines have kept pace and allow separate coating efficiencies to be applied to factory-applied coatings and field joints. CP designs now move to anodes located on sleds or on end connection structures[1].

[1] Pipeline End Termination Structure or Pipeline End Manifold Structure

Potential attenuation models show that tens of kilometers of pipelines can be protected from anodes located on the end termination skids. This methodology is the way to protect all pipelines subsea, again pioneered in deep water. The elimination of the pipeline bracelet anode makes sound engineering and economic sense, maintains the pipe coating intact thus reducing CP requirements, improves pipe lay efficiency by not having to deal with bracelet anodes offshore, and improves CP efficiency by installing fewer anodes on greater spacing.

25.6 Conclusions

As the offshore oil and gas industry moves into deeper waters and as more of the existing infrastructure begins to reach 50 years of age, new methods will be required to manage the corrosion issues. A key area of improvement will be expanded to the use of intelligent monitoring devices that can be remotely interrogated to provide the asset integrity manager with the critical information required to keep the installations safe and profitable. Also, new corrosion control inspection technologies must anticipate the transition from ROV to AUV and be compatible.

References

[1] G.H. Backhouse, R.J. Holt, Fundamental errors in subsea pipeline cathodic protection survey techniques, in: UK Corrosion 1984—Proceedings of the Conference, vol. 2, 1984, pp. 77—92.
[2] D. Janda, Innovative inspection, World Pipelines (August 2010).
[3] R. Roth, Direct Electrical Heating of Flowlines - A Guide to Uses and Benefits, Presented at the OTC Brasil, 2011.

New steels and corrosion-resistant alloys

26

Richard Hill [1] *and Aquiles L. Perez* [2]
[1]Microalloying International, Houston, TX, United States; [2]Universal Pegasus International, Houston, TX, United States

26.1 History and development

Iron production started as early as 2000 BC, while carbon steel production emerged around 1870 as the main player in the industrial era. Carbon steel has been and continues to be the "workhorse" for upstream oil and gas projects. However, carbon steel tends to corrode rapidly in the presence of aggressive operating conditions. Corrosion inhibitors have been used to reduce the time rate of corrosion of carbon steel; however, inhibitors add additional operating costs and can be unreliable under certain conditions. The use of corrosion-resistant alloy (CRA) as an alternative to using carbon steel with corrosion inhibition was initiated by the Dutch operating company NAM between 1975 and 1980 by installing seven flow lines internally clad with 316 L stainless steel and four duplex stainless steel lines (total length 13.3 km). Two of the duplex lines were the first offshore CRA flow lines.

The first duplex lines were manufactured using alloy 3RE60 (18% chromium). Shortly thereafter, a 22% chromium alloy was introduced. Starting in 1981 and over a period of 13 years, Mobil Exploration and Production installed more than 28 km of 13% chromium martensitic stainless steel. In 1990, the higher strength 25% chromium alloy was introduced (known as super duplex).

In parallel to the use of solid CRA pipe materials, the use of carbon steel pipe with CRA clad (mechanically lined or metallurgically bonded) has developed. Initially, 316L stainless steel was selected as the preferred clad material. From 1986 onward, alloy 825 and more recently alloy 625 have been the preferred clad alloys for extreme service conditions [1].

Developments in carbon manganese and high-strength low-alloy steels have focused more on improved manufacturing processes known as "clean steel technology." Included are improvements in the control of steel melting, secondary refining, and continuous casting technologies. The development of CRAs has been driven more toward a "fine-tuning" of the chemical composition, thereby resulting in enhanced material properties. Fig. 26.1 illustrates the evolution of CRA alloy used in the oil and gas flow industry.

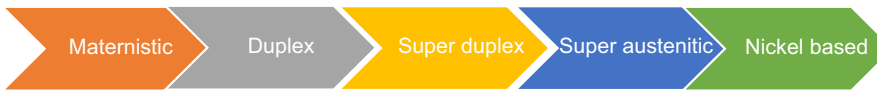

Figure 26.1 Corrosion-resistant alloy flow line used in the oil and gas industry.

Trends in Oil and Gas Corrosion Research and Technologies. http://dx.doi.org/10.1016/B978-0-08-101105-8.00026-7

Extreme operating conditions and more aggressive produced fluids have driven the evolution of CRA materials. As an example, one of the most common CRA material used in upstream oil and gas is 12% chromium alloy, which is a high-strength martensitic stainless steel with wide acceptance among many operators. However, failures related to hydrogen stress cracking, sulfide stress cracking, and chloride stress corrosion cracking (SCC) limit the application of this alloy. As such, the use of duplex and super duplex stainless steels has become a more viable alternative when considering the use of a solid CRA material for flow line applications. The use of nickel base alloys for solid flow lines has been used on a limited basis but is difficult to weld under field conditions and is not cost effective.

Clad pipes and components use carbon steel materials (for instance, API 5L X65 for pipes or ASTM A182, F22 and ASTM A694 F65 for forging bodies) either mechanically or metallurgically bonded with CRA material. The selection of the "clad material" depends on the production fluids and operating conditions. The material selection can include austenitic stainless steels such as 316 L, super austenitics such as 904L, or nickel-based alloys such as 625 or 825. Currently, nickel-based alloys such as 625 are the most commonly used for clad pipes and weld inlay. The main advantage of using a clad material is the combining of the strength of the substrate material with the corrosion resistance of the cladding.

26.2 Material selection process

Material selection starts with determining the requirements needed to safeguard against internal and external environments. Key factors taken into account for internal corrosion are the following:

- Production conditions
  - Oil, gas, gas condensate
  - Gas−oil ratio (GOR)
  - Temperature and pressure
  - Flow rate
  - Water cut
- Production composition
  - Acid gas content (Mole percentage of CO_2 and H_2S)
  - Elemental sulfur
- Produce or condensed water composition
  - Chlorides content
  - Bicarbonates content
  - Acetic acid content
- Other considerations
- Microbial activity

In assessing quantitative corrosion rates and cumulative damage, these factors are used as input data for numerous corrosion models. For example, programs designed to predict CO_2 corrosion rates such as Norskok M-506 [2] were based on a de Waard corrosion model. Recent corrosion prediction tools such as ECE 5.3 [3] have also incorporated the ability to assess the influence of H_2S, organic acids, and the presence

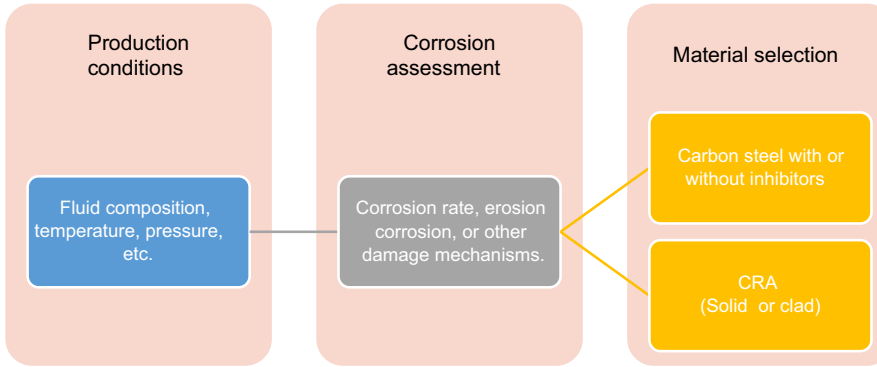

Figure 26.2 Decision diagram for material selection. *CRA*, corrosion-resistant alloy.

of high chlorides. The results from these programs provide estimated corrosion rates (both in the form of uniform CO_2 corrosion as well as pitting corrosion rates in mm/year), which then can be used to determine if carbon steel, carbon steel with chemical inhibition, or CRAs should be used. For CRAs, other considerations include the susceptibility of these materials to sulfide stress cracking, chloride stress cracking, and hydrogen embrittlement. NACE MR0175/ISO 15156 [4] part 3 provides guidance for the use CRA material in specific environmental conditions, which included partial pressure of H_2S, temperature, and chloride content. A proposed decision diagram for material selection is shown in Fig. 26.2.

Material selection charts have been developed by a number of suppliers that incorporate critical service considerations (acid gas content, temperature, chlorides, elemental sulfur, etc.). An example of material selection chart that has been developed for Old Country Tubular Goods (OCTG) is shown in Fig. 26.3 [5].

26.3 Advances in carbon and high-strength low-alloy steels

As discussed in the previous sections, the use of carbon steel is based on the corrosivity of the system. Depending on the predicted corrosion rates for CO_2 and H_2S pitting and the life of the project, the use of carbon steel and high strength alloys with and without chemical inhibitors can be considered. For sour service applications, MR0175/ISO 1556 [5] Part 2 addresses the general guidelines for hardness control to avoid sulfide stress cracking and provides acceptance criteria for hydrogen induced stepwise cracking.

Regardless of the product form (pipes, forgings, etc.), clean steel technology has had the biggest impact on improving the resistance of carbon and low-alloy steels to hydrogen damage. Clean steel technology refers to the use of improved manufacturing technology to produce steels with reduced impurities, improved reliability, and a more homogeneous metallurgical structure. To ensure steel cleanliness and homogeneity, comparative analyses are used to address inclusion type, morphology, distribution, and elemental segregation.

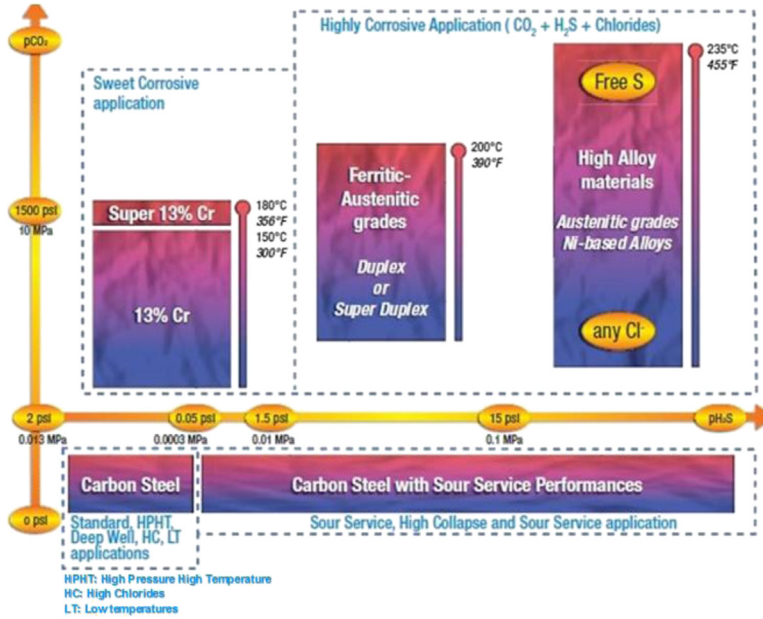

Figure 26.3 Vallourec and Mannesmann—tubing selection guide, Vallourec and Mannesman—CRA OCTG selection guide [5]. *CRA*, corrosion-resistant alloy.

An example of the relationship of the impurity levels such as sulfur content and hydrogen induced cracking resistance is illustrated in Fig. 26.4.

Finally, fabrication considerations have to consider sulfide stress cracking resistance. MR0175/IS015156 [5] Part 2 addresses hardness control in carbon and low-alloy steels.

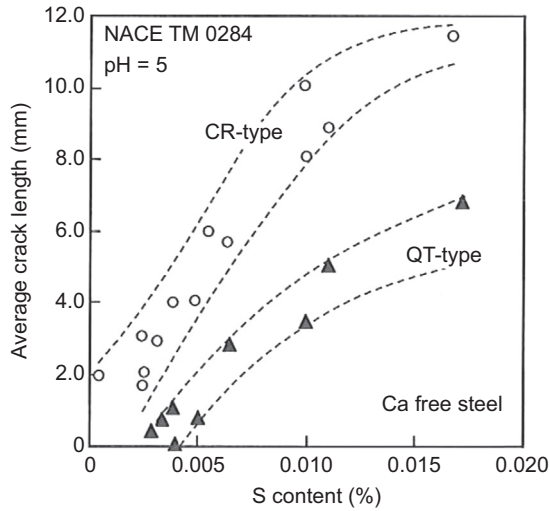

Figure 26.4 Effect of sulfur content on hydrogen induced cracking [6].

26.4 Corrosion-resistant alloys for critical service conditions

When carbon steel materials are not a viable option because of the aggressiveness of production conditions, CRA materials either in solid or clad form are used. While CRA materials protect against CO_2 corrosion, recent advances have focused on reducing the susceptibility to other corrosion mechanisms such as sulfide stress cracking, hydrogen embrittlement, and chloride SCC. The "fine-tuning" of these alloys involves modifying the chemical composition while maintaining ranges prescribed in various specifications. Modifications include increasing the percentage and presence of enhancing elements such as molybdenum, tungsten, cobalt, etc., while maintaining cleanliness and the absence of detrimental microstructures (sigma phase, chi phases, etc.).

26.4.1 Martensitic stainless steels

Martensitic stainless steels can provide resistance to CO_2 corrosion while providing good mechanical and toughness properties. The evolution of martensitic stainless steels is grounded in improving their resistance to sulfide stress cracking and chloride SCC. New materials called super martensitic (also known as weldable 12%Cr, 13%Cr, etc.) have high strength, typically 80 ksi (551 MPa) or above, very good corrosion resistance in brines containing carbon dioxide (CO_2), and rely on molybdenum added in the level 1%−3% in some grades to improve resistance to fluids containing H_2S. The new super martensitics are considered an attractive alternative to duplex stainless steel [6]. However, the susceptibility of super 13% Cr to cracking at high temperature and high chlorides in the presence of an H_2S partial pressure higher than 0.11 psia has to be considered [7]. A new super 17% Cr alloy (martensitic/ferritic) provides enhanced corrosion resistance up to 200°C (392°F), whereas under similar conditions Super 13% Cr steels suffer both SCC and high corrosion rates [8]. Table 26.1 summarizes typical chemical composition and applications of martensitic stainless steels.

26.4.2 Duplex stainless steel

When martensitic steels cannot be used, the use of duplex and super duplex steels comes into play. Typical duplex and super duplex steel materials used for upstream applications are UNS S32205 and UNS S32750. For less aggressive production environments, some lean duplex materials have been used. Fabrication of duplex and super duplex stainless steels require special consideration in the developing of welding procedures or other thermomechanical processes (such as hot induction bending) to ensure the mechanical and toughness properties, and the corrosion resistance is not compromised. ASTM G48 Method A (ferric chloride test) is used to determine the susceptibility of pitting (especially after welding), whereas ASTM A923 is used for detecting detrimental intermetallic phases. Table 26.2 summarizes the grades and limitations of duplex and super duplex stainless steels.

Table 26.1 Chemical compositions (% by weight) and characteristics of Martensitic stainless steel used on the upstream oil and gas industry

Designation	Type	UNS	Cr%	C%	Mn%	Ni%	Mb%	Other (%)	Remarks
410	Martensitic	S41000	13.5	0.15	1.00	–	–	P% 0.04, S% 0.03, Si% 1.0	Low cost, general purpose, heat-treatable stainless steel. Used widely where corrosion is not severe
410S	Martensitic	S41008	12.6	0.08	0.65	0.55	0.55	P% 0.03, S% 0.01, Si% 0.5	Lower carbon than type 410, offers improved weldability but lower hardenability. Type 410S is a general purpose corrosion and heat-resisting chromium steel recommended for corrosion-resisting applications.
425	Super martensitic	S41425	13.3	0.02	0.76	5.00	1.68	Cu% 0.040, Si% 0.30	High strength, acceptable stress corrosion cracking (SCC) performance under mild sour conditions [7]
427	Super martensitic	S41427	12.0	0.023	0.33	5.36	1.92	Cu% 0.050, Si% 0.22	High strength, acceptable SCC performance under mild sour conditions up to 150°C (302°F) [7]
Super 17 Cr	Super martensitic	S17400	17.0	0.03	0.50	5.00	2.5	Si% 0.05	High strength, acceptable SCC performance under mild sour conditions [8] up to 200°C (392°F)

Table 26.2 Chemical compositions (% by weight) and characteristics of duplex stainless materials used in the upstream oil and gas industry

UNS	Type	Cr%	Ni%	Mo%	N	Mn%	Other (%)	Remarks
S32101	Lean	21.5	1.5	0.3	0.22	5	–	Good resistance to localized and uniform corrosion, as well as stress corrosion cracking, used in flanges and valves
S31803/ S32205	Standard	22	5.7	3.1	0.17	–	–	Typical duplex stainless steel used in subsea applications such as flow lines, tubing, flanges, fittings, and valves.
S32750	Super	25	7	4	0.27	–	–	A molybdenum-containing duplex stainless steel with higher contents of chromium, nickel, and nitrogen. It combines increased strength with improved corrosion resistance. Used in seawater systems, umbilical tubing, flow lines, flanges, fittings, and valves.
S32760	Super	25	7	3.2	0.25	–	W% 0.7, Cu% 0.7	Used as an alternative to S32750 where enhanced corrosion resistance is required.
S32520/ S32550	Super	25	6.5	3.5	0.25	–	Cu% 1.5	Also an alternative to S32750 where higher strength and corrosion resistance is required.
S32707	Hyper	27	6.5	4.8	0.4	<1.5	Co% 1.0	Specifically designed for raw seawater heat exchanger applications.

26.4.3 Super austenitic stainless steel

Because of their low strength, typically austenitic materials are not used in solid form for pressure-containing equipment in oil and gas industry. To overcome this issue, the evolution of austenitic materials has yielded to super austenitic materials. Super austenitic alloys provide additional strengthen—as well as superior chloride pitting, crevice, and SCC resistance to the type-300 austenitic stainless steel. Super austenites use additional alloys to enhance their properties. Higher percentages of molybdenum (>6 wt%) improve resistance to pitting and crevice corrosion in aqueous chloride–containing environments. Nitrogen addition enhances metallurgical stability, improves pitting and crevice corrosion resistance, and increases strength. Furthermore, higher nickel content ensures a higher resistance against SCC.

Table 26.3 summarizes the grades and limitations of super austenitic stainless steels.

Caution should be used during fabrication, ensuring that welding procedures that follow the guidelines of the alloy producer are developed. Selection of consumables and welding parameters is essential to prevent the formation of detrimental intermetallic phases.

26.4.4 Nickel-based alloys

As the operating conditions and the produced fluids become more aggressive, nickel-based alloys are in the forefront. The advances focused on the modification of their constituent elements. In formulated combinations, these elements result in materials that provide excellent resistance to general corrosion, localized corrosion, pitting and crevice corrosion in the presence of acid gas compositions, chlorides, and elevated temperatures. These alloys also provide resistance to microbial corrosion (MIC) and environmental assistant cracking (sulfide stress cracking, chloride SCC, etc.). The benefits of each constituent element in nickel-based alloys are summarized in Fig. 26.5 [9].

Table 26.4 summarizes the grades and limitations that the nickel-based the alloys most commonly used in upstream oil and gas:

Fabrication of nickel-based alloys is extremely critical, and all welding procedures must follow the recommended guidelines of the product supplier. Deleterious intermetallic phases (chi, Laves, and sigma) and precipitates can result in the loss of strength, toughness, and corrosion resistance. A typical test preformed to determine the susceptibility of based material and weld metal to corrosion damage is ASTM G28 Method A. Also, for high-pressure/high-temperature applications ASTM G78 is used to evaluate the susceptibility to crevice corrosion of iron-base and nickel-base stainless alloys in seawater.

26.5 CLAD CRA materials

The evolution of carbon steel materials clad with CRA has developed in parallel with the evolution of solid CRA materials. Clad products combine the strength of carbon steel with the corrosion resistance of CRAs, providing a material cost benefit but requiring a more labor intense fabrication process.

Table 26.3 Chemical compositions (% by weight) and characteristics of super austenitic stainless steel used in the upstream oil and gas industry

Designation	UNS	Ni%	Cr%	Mo%	Fe%	Cu%	Other (%)	Remarks
904L	N08904	23–28	19–23	4–5	Bal.	1–2	C 0.02, Mn 2, Si 1	Added with copper to improve its resistance to strong reducing acids, such as sulfuric acid. The steel is also resistant to stress corrosion cracking and crevice corrosion
6MO	N08367	17.5–18.50	19.5–20.5	6–6.5	Bal.	0.5–1	C 0.02, Mn 2, Si 1	High resistance to chloride pitting, crevice corrosion and stress corrosion cracking
254 SMO	S31254	18	20	6.1	Bal.	0.7	C 0.02, Mn 1, Si 0.08	Good impact strength both at room temperature and at cryogenic temperatures. Not recommended for high temperatures (above 600°C). Higher general corrosion and pitting resistance than 904L
Alloy 24	S34565	16–18	23–25	4–5	Bal.	–	C 0.03, Mn 5–7, Si 1.00	Used in seawater systems, high resistance to localized corrosion such as pitting and crevice corrosion, good weldability
654 SMO	S32654	21–23	24–25	7–8	Bal.	0.3–0.6	C 0.02, Mn 2–4	High strength and toughness, enhanced resistance to chloride pitting and crevice corrosion

Figure 26.5 Benefits of constituent elements in nickel-based alloys [9].

Clad products are produced either using a metallurgical bond (weld overlay, roll bonding, coextruded, etc.) or mechanical bond (inserted liner). Typically, metallurgically bonded clad products are used on small sections of flow lines as well as equipment (valve, connectors, etc.), whereas mechanical cladding is used for longer flow lines.

Table 26.5 summarizes typical austenitic clad materials used in combination with carbon steel.

Other CRAs used for metallurgical and mechanical clad applications are 904 L, alloy 625, alloy 825. These alloys are used in production conditions with increased H_2S, temperature, and chloride content.

26.6 Authors comments

The continue development of oil and gas reserves under more aggressive conditions such as high pressure, high temperature, higher acid gas composition, and increased exposure to workover and stimulation fluids will require improved CRAs. Likewise,

Table 26.4 Chemical compositions (% by weight) and characteristics of the nickel-based alloys used in the upstream oil and gas industry [9]

Designation	UNS	Ni%	Cr%	Mo%	Fe%	Cu%	Other (%)	Remarks
INCONEL alloys 625 and 625LCF	N06625 N06626	61.0	21.5	9.0	2.5		Ti% 0.4, Nb% 3–4, Mn% 0.5	For optimum resistance to mechanical and thermal fatigue up to 1200°F (650°C). Typically used for weld overlay and cladding.
INCONEL alloy 718	N07718	54.0	18.0	3.0	18.5		Nb% 5.0, Ti% 1.0	Age-hardenable alloy combining strength up to 1300°F (700°C) with corrosion resistance and weldability.
INCOLOY alloy 825	N08825	42.0	21.5	3.0	28.0	2.0	Ti% 0.6–1, C% 0.05, Mn% 1.0, Si% 0.5	A Ni-Fe-Cr-Mo Ti-stabilized alloy with excellent resistance to sulfuric and phosphoric acids. Resistant to reducing and oxidizing acids, pitting, stress corrosion cracking and intergranular corrosion.
INCOLOY alloy 925	N09925	44.0	21.0	3.0	28.0	1.8	Ti% 2, Al% 0.3	Comparable with that of INCOLOY alloy 825 but with higher strength obtainable by age hardening. Used in the oil, gas, and marine industries for applications calling for high strength and resistance to general corrosion and pitting.

Continued

Table 26.4 Continued

Designation	UNS	Ni%	Cr%	Mo%	Fe%	Cu%	Other (%)	Remarks
INCOLOY alloy 945	N09945	55.0	23.0	4.0	Bal	3	Si% 0.5, Ti% 2.5, Al% 0.7	Resistance to sulfide stress corrosion cracking (SCC) and SCC in H_2S environments, used in oil and gas components for downhole and surface gas well including subsea valves.
AF955	N09955	57.8	21.8	5.87	8.19		Nb% 4.74, Ti% 0.85, Co% 0.12, Al% 0.46	Microstructure in compliance with new requirements of API 6ACRA, corrosion resistance up to NACE Level VII, low susceptibility to hydrogen embrittlement [10].
INCOLOY alloy 028	N08028	32.0	27.0	3.5		1.0	Mn% 2.0	Austenitic stainless steel used for downhole tubing in oil and gas extraction operations.
INCOLOY alloy 25-6MO	N08926	25.0	20.0	6.5	47.0	0.9	N% 0.20	A 6% molybdenum, nitrogen-bearing super austenitic stainless steel resistant to pitting and crevice corrosion in fluids containing chlorides and other halides.

Table 26.5 Chemical compositions (% by weight) and characteristics of austenitic materials used in the upstream oil and gas industry

Designation	UNS	Type	Ni%	Cr%	Mo%	Fe%	Cu%	Other (%)	Remarks
316 L	S31603	Austenitic	10–14	16–18	2–3	Ba	N/A	C% 0.03, Mn% 2.00, Si% 0.75	Good option for mild chloride environments. Resistance to CO_2 corrosion in mild sour environments.
317 L	S31703	Austenitic	11–15	18–20	3–4	Ba	N/A	C% 0.03, Mn% 2.00, Si% 1.00	Increased resistance to mild chlorides and improved strength over 316L.

the formulations of the chemicals used for corrosion control in carbon and low-alloy steels will need to take higher temperatures and resistance to high-velocity flow rates into consideration.

The evolution of corrosion models used for predicting uniform and pitting corrosion associated with production fluids containing acid gases will continue as features such as produced water composition and other environmental species are integrated into the programs. Note that the programs, until now, do not account for microbial-induced corrosion. The interaction of MIC with other corrosion mechanisms may play a role that is still to be determined.

References

[1] L. Smith, Intetech Ltd (Consultant to NiDI), M. Celant, Pipe Team, Belgian Welding Institute, Paper 017, Belgium − Brussels, October 3-4 2002.

[2] NORSOK M-506 CO2 Corrosion Rate Calculation Model on Public Enquiry Standard.No., https://www.standard.no/en/nyheter/nyhetsarkiv/petroleum/2016/norsok-m-506−co2-corrosion-rate-calculation-model-on-public-enquiry/#.V7R_RjUZNMM.

[3] Intetech, Electronic Corrosion Engineer® version 5.3 (ECE5) Corrosion Program, Recent Results Enhance ECE5 Corrosion Model. http://www.intetech.com/resources/features/89-recent-results-enhance-ece-5-corrosion-model.

[4] ANSI/NACE MR0175/ISO 15156. Petroleum and natural gas industries—materials for use in H2S-containing environments in oil and gas production.

[5] Vallourec, Mannesmann - Tubing Selection Guide, Vallourec and Mannesmann - CRA OCTG selection Guide, Vallourec and Mannesmann CRA OCTG Selection Guide, 2010. http://www.vallourec.com/OCTG/EN/Documents/VAM%20OCTG%20Product%20guide.pdf.

[6] N. Ishikawa, Design of steels for large diameter sour service pipelines, in: R.W. Revie (Ed.), Oil and Gas Pipelines, John Wiley & Sons, Inc, 2015, pp. 225−232.

[7] R. Morana, P.I. Nice, J.W. Martin, L. Smith, Updated application limits for 13Cr super martensitic steel bar-stock materials, in: Paper No. 7382 NACE Corrosion 2016 Conference and Expo, 2016.

[8] Nippon Steel & Sumitomo Metal, New Super Martensitic − Ferritic Stainless Steel has been Developed for HPHT Applications, January 5, 2012, http://www.tubular.nssmc.com/news/details/new-super-martensitic-ferritic-stainless-steel-has-been-developed-for-hpht-applications.

[9] Special Metals, High-Performance Alloys for Resistance to Aqueous Corrosion. http://www.parrinst.com/wp-content/uploads/downloads/2011/07/Parr_Inconel-Incoloy-Monel-Nickel-Corrosion-Info.pdf.

[10] L. Foroni, C. Malara, R. Montani, S. Gregory, UNS N09955 corrosion cracking resistance, NACE Paper No. 7355, in: NACE Corrosion 2016 Conference and Expo, 2016.

Nonmetallics applications in oil and gas production (pipes, liners, rehabilitations)

27

Khlefa A. Esaklul[1] *and Jim Mason*[2]
[1]Occidental Oil and Gas Corporation, Houston, TX, United States; [2]Mason Materials Development LLC, Wyomissing, PA, United States

27.1 Introduction

Nonmetallic materials, designated here as polymers and composites, have played a major role in the control of corrosion and related damage mechanisms in the oil and gas production for over 50 years. This evolved from the inherent resistance of nonmetallic materials to the corrosive conditions that exist in oil and gas production. Natural oil and gas deposits occur in reservoirs underground, which accumulate at different depths driven mainly by the decomposition of living matter and the changes that have occurred in planet earth. These natural and geological changes led to the formation of oil and gas deposits that are being harvested today to meet the continuously increasing energy demands. The formation of oil and gas deposits can generate high pressures and temperatures in the reservoir in addition to deleterious gases such as CO_2 and H_2S, which are acid-forming gases that can cause corrosion. The decaying matter can also produce naturally occurring organic compounds that can contribute to corrosion, such as organic acids or inorganic compounds that can break down and form acid gases such sulfates, sulfides, and carbonates once they come in contact with water. Other corrosion-inducing organisms such as bacteria may exist in formations and can flourish once added nutrients become available. Such is the case of acid-producing and sulfate-reducing bacteria.

As the oil is produced, the reservoir conditions change, leading to pressure decline and encroachment of surrounding fluids, typically water (as oil and water coexist), leading to an increase in water production. In gas production, a drop in pressure and temperature can lead to water vapor condensation (wet gas) and dropout of water in production tubing or flow lines and pipelines.

As the demand for energy increased, the industry extended exploration for oil and gas into many frontiers (offshore, deepwater, arctic, etc.) and increased the recovery efficiency of oil deposits through use of many different enhanced oil recovery techniques: gas lift, water injection, steam injection, CO_2 injection, polymer injection, and air injection. All of these techniques are inherently corrosive if not effectively controlled. They add to the corrosivity of the produced fluids through an increase in the water to oil ratio (water cut), drop in pH, presence of oxygen, contamination (nutrient for bacteria), and increase in pressure and temperature.

Trends in Oil and Gas Corrosion Research and Technologies. http://dx.doi.org/10.1016/B978-0-08-101105-8.00027-9

The inherent corrosion resistance of nonmetallics made them the obvious choice to manage aging assets, decline in production, control of corrosion of producing fluids, and the demand for increased safety and asset integrity. The use of nonmetallics in oil and gas production operations emerged with time and had to overcome several hurdles to become accepted as a viable and reliable solution to mitigate corrosion. Time was required to develop expertise in the design, fabrication, and installation to gain acceptance by codes and regulatory bodies.

Nonmetallics also offer, in addition to the corrosion resistance, the advantages of lower weight compared with the traditionally used metals in offshore developments and continue to be of considerable interest as the demand for lighter materials increase with the developments of deepwater assets.

Like metals, nonmetallic materials have limitations. Temperature resistance and mechanical properties are the main limitations. But chemical degradation, limitations on inspection, and impact of aging must also be addressed in the engineering assessment of the application.

27.2 Nonmetallic materials in use in oil and gas production

Many nonmetallic materials are in use in oil and gas production in both onshore and offshore applications [1,2]. Although there are many materials proposed by suppliers, just a few materials account for the vast majority of installed product, with high-density polyethylene (HDPE) making up the largest fraction of that population. The reasons are mostly related to long history of use, cost, and availability. Composite materials are also in common use for pipelines, seal components, and repair technologies [3]. The applications are not limited to pipe and tubing. Nonmetallic valves have been used with success [4].

HDPE is very frequently used [5–9]. It is defined as having a density of 0.93–0.97 g/cm^3. Higher density is caused by higher crystallinity, which brings benefits of greater stiffness (strength) over a broader temperature range and lower gas permeation rates. Modern grades of HDPE designed for use as pipes and other pressure-rated applications are designated as PE100 in the International Standards Organization (ISO) system and PE 4710 in the American Society for Testing and Materials (ASTM) system. They are not necessarily interchangeable, but they can be joined together by conventional means and both materials have good properties as pipe and pipe liners. Certain grades of HDPE, known as PE-RT Type II, have been designed for long-term use as pipe or tubing, with water temperatures in the range of 70°C (122°F) and a 50-year design life [10]. Cross-linked polyethylene (PEX) is a form of polyethylene in which the polymer chains have covalent bonds between adjacent chains to form a network. This network increases the temperature at which the material can be used, but at the expense of limitations on joining technologies. Among low-cost thermoplastic polymers polyethylene materials have the highest temperature range in water because water does not attack the polymer. Hydrocarbons tend to swell

and soften all polyethylene materials, leading to loss in strength and increase in gas permeation rates resulting in much lower temperature ratings in hydrocarbon service.

Polyamides (PA or nylons) are a group of polymers with an amide linkage between monomer units and are used in conditions where HDPE is not suitable [11,12]. The amide linkage is generated by reaction of a carboxylic acid and an amine. In forming the bond, a water molecule is generated. This reaction is reversible in a process known as hydrolysis, in which a water molecule attacks the amide bond and is consumed, regenerating the carboxylic acid and amine. The hydrolysis process is accelerated by high-temperature and low-pH (acidic) conditions. This aging mechanism makes it necessary for the designer to consider the operating chemistry and temperature conditions to determine the upper use temperature for a given design life. Several types of nylon are available. Each type ages by hydrolysis at a unique rate determined by the polymer type. In upstream oil and gas PA11 and PA12 have the widest use, longest history, and longest lifetime. PA6 and PA6.6 are lower cost and have lower lifetimes.

Polyphenylene sulfide (PPS) is a thermoplastic material with outstanding chemical and permeation resistance. It is suitable for application in oil and gas production up to 150°C (302°F) [13]. It's main disadvantage is the difficulty in processing, making it a high-cost option.

Polyvinylidene fluoride (PVDF) is a thermoplastic material with high resistance to most oil and gas produced and injected fluid environments and has an upper temperature limit of 130°C (266°F) [14]. It has limited resistance to strong amines, concentrated acids, and sodium hydroxide, and is typically recommended for use in pH range < 8.5.

Polyvinyl chloride (PVC) is a thermoplastic material with moderate strength and chemical resistance available in rigid and flexible forms based on the level of plasticizers used. Other additives are used to enhance the properties of the polymer. In general, it has good resistance to many chemicals, particularly acids, but is less resistant to solvents, leading to swelling and loss in strength, and in some solvents significant degradation.

Poly-ether-ether-ketone (PEEK) is a thermoplastic polymer with very high chemical resistance, high strength, dimensional stability, and stiffness. It has wider continuous use temperature, up to 170°C (338°F), with resistance to hydrolysis in steam, water, and seawater. PEEK is available in various forms to produce any type of engineering components from tubular shapes to seals and couplings. Its major disadvantage is high cost.

Polyketones (PK) is another group of polymers that have similar chemical resistance to polyamides and are less costly but susceptible to hydrolysis in the same way as polyamides. Their oil and gas history is very limited [15].

Fiber-reinforced plastic (FRP) or glass-reinforced epoxy (GRE) composite materials are made of glass fiber reinforcement impregnated with thermoset resins [16,17]. They are used for internal liners and pressure pipes. Depending on the application, the fiber reinforcement is typically made of either continuous or discontinuous glass fibers, with E-glass being the most common. Other glass fiber types, such as ECR-, C-, AR-, and S-glasses, are used mainly to meet chemical/corrosion resistance.

The fibers are woven or wound in certain patterns and angles to meet the axial and hoop strength requirements of the application. The thermoset resins provide the chemical resistance and thermal stability as determined by their glass transition temperature (Tg). Polyester, vinyl ester, epoxy-based vinyl ester, epoxy, phenolic, and modified acrylic resins are used. In addition, other additives, such as catalysts, hardeners, and fillers, are used to enhance processing and properties. The selection of the resin and the interior liner determines the corrosion resistance and temperature stability of the product. Similarly, the exterior layer determines the suitability of the product application and may include additives such as ultraviolet (UV) stabilizers. The type of resin and hardener determines the chemical resistance and maximum temperature of the FRP component. Water and aromatic hydrocarbons are the most damaging to FRP. To resist this effect, amine-cured epoxy has been used with aromatic amine−cured resins, providing the highest usable temperature of 130°C (266°F), compared with aliphatic amine−cured resins at 115°C (239°F), whereas anhydride curing resins have a maximum temperature in water of 80°C (176°F). Vinyl ester and epoxy resins are immune to attack by the main hydrocarbon components of crude oil and acid gases CO_2 and H_2S, making them suitable for oil and gas production applications. However, epoxy resins are affected by hydrolysis and are not suitable for use in steam applications [5].

Considerable experience has been gained with the use of these materials in both onshore and offshore oil and gas production applications that resulted in improvements in the products, engineering design, installation, and introduction of new improved materials [18−29]. Studies have shown that these materials are cost-effective, particularly when evaluated based on life cycle cost [1,30−33].

27.2.1 Mechanical properties

The key mechanical properties of nonmetallics used as pressure pipes and liners are a consequence of their chemical structure and the end use conditions. Mechanical properties are strongly influenced by temperature and absorbed fluids. Often the absorbed fluids reduce the strength of the polymer by acting as a plasticizer. For example, light hydrocarbons dissolve in polyethylene, causing a reduction in tensile modulus compared with the unexposed material, depending on the temperature and hydrocarbon mix. Lighter and aromatic hydrocarbons are more aggressive than heavier, aliphatic hydrocarbons. Fig. 27.1 shows the effects of temperature and diesel on a typical HDPE pipe grade that was immersed in diesel at 80°C (176°F) until full saturation before tensile testing at the indicated temperature. Different grades likely display somewhat different effects of temperature and hydrocarbon absorption. The material supplier should be able to supply information specific to their material. In stress-bearing applications this must be considered for all materials. These effects are always considered by competent designers during the engineering assessment for the application.

Nonmetallic materials have a more complex mechanical behavior than metals. Like metals, nonmetallic materials exhibit the common properties of tensile elongation, yield, and ultimate tensile strength. These values are strongly influenced by temperature. In addition, nearly all of the nonmetallic materials used in oil and gas corrosion management applications display stress regression over long time periods, meaning

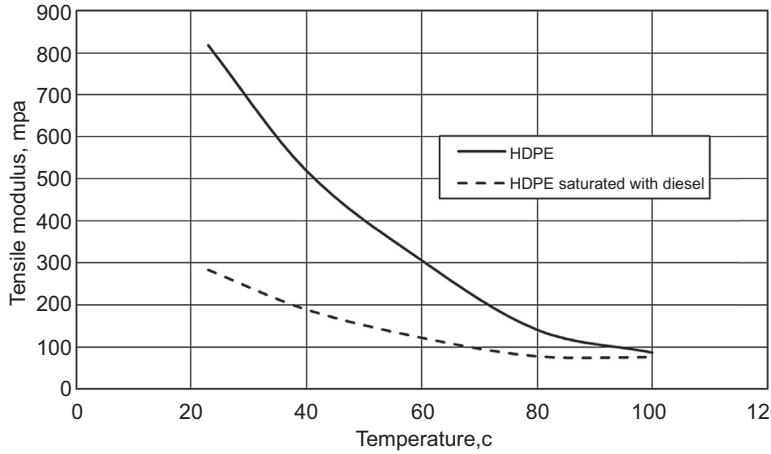

Figure 27.1 Increasing temperature and absorbed hydrocarbons decrease the tensile modulus of high-density polyethylene (HDPE).

that over time, and under load, the strength decreases. Mechanical strength measured over short time periods (seconds to minutes) is higher than the long-term strength of the material. The slope of the regression is usually fairly flat, and small differences in applied stress can have large effects on product lifetime (see Fig. 27.2).

In the case of thermosetting fiber-reinforced materials, stress regression is caused mostly by progressive failure of the reinforcement fibers. As a single fiber fails, the load is safely redistributed to the many remaining fibers in the structure, reducing the overall strength of the structure. Eventually enough fibers are broken that the average stress per fiber is too high and the pipe will fail. The progression to failure can be quite fast once the process starts.

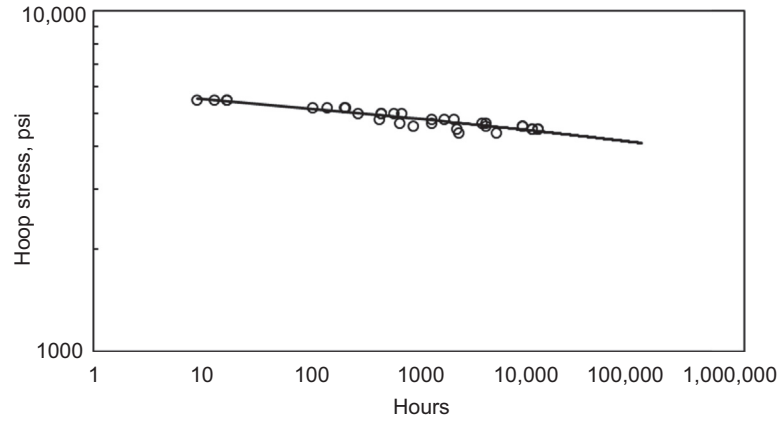

Figure 27.2 An example of long-term stress regression of plastic pipe. Data points represent failures (ruptures) at the indicated time and hoop stress. The slope and vertical position of the line depends on the polymer type and grade being tested.

For unreinforced thermoplastic materials the structure is held together by entanglement of the many polymer chains that comprise the solid phase. Under load they slowly disentangle, leading to eventual ductile failure. In some cases (such as for polyethylenes), there is another mechanical failure mechanism called slow crack growth that eventually results in a brittle failure while under load. For thermoplastic pressure piping like HDPE pipe, both of these mechanisms must be considered because the polymer is under hoop stress. The most frequently referenced standards to determine the long-term pressure capacity of nonmetallic piping require that the materials are tested for transition to the brittle regime.

The long-term hoop strength (pressure capability) is governed by stress regression over the design life of the pipe. Most international standards for determining the long-term strength of nonmetallic pipe require measuring the strength over at least four logarithmic decades of time to at least 10,000 h. The log-log regression fit line is then extrapolated to 100,000 h to determine the long-term strength. The long-term stress rating is established after application of a suitable design factor to the long-term strength. This method is used to establish the pressure rating of monowall plastic pipe, FRP and GRE pipes, and nonmetallic fiber-reinforced thermoplastic pipe (RTP). The long-term ratings for a single material pipe such as polyethylene pipe is usually a hydrostatic design basis (HDB) using ASTM standards or a minimum required strength (MRS) using ISO standards. For composite material pipes a pressure design basis (PDB) is the usual rating method.

Materials with HDB, PDB, or MRS listings in PPI TR-4, published by the Plastics Pipe Institute, have been judged as suitable in pressure piping applications with 20- or 50-year stress regression behavior validated by testing using well-established test methods from ASTM International and ISO [34—37]. Depending on the location and regulatory requirements, a listing in TR-4 may not be necessary for a resin or pipe product to be qualified. Independent auditing bodies may also attest to the completeness and quality of the test results obtained by any of the three listed long-term stress testing methods.

27.2.2 Chemical resistance of important polymers in oil and gas

Because of their chemical makeup polymeric materials are subject to a variety of types of chemical attack [38]. There are two main categories: softening and chemical degradation. Softening is the loss of stiffness (modulus) when chemicals from the environment are absorbed into the bulk. Softening is usually accompanied by swelling as the invading chemicals fill the available free volume of the bulk and interfere with attractions between the polymer molecules, enabling further volume expansion. Chemical degradation is the breakage of chemical bonds in the polymer chain. Bond breakage shortens the polymer chains and, eventually, reduces the ductility of the polymer to zero. Chemical degradation can happen at the same time as softening and swelling, which usually accelerate the process by making the attacking chemicals more available and providing an enhanced opportunity for the broken bond ends to move away from each other, reducing any chance that the reaction will be reversed in an equilibrium-driven process.

The principle of "like dissolves like" applies to chemical resistance. Produced hydrocarbons are similar in chemical structure to polyolefins such as polyethylene and polypropylene. For this reason, hydrocarbons are readily absorbed by polyolefins. Polyolefins do not absorb significant quantities of water.

27.2.2.1 High-density polyethylene

Low-molar-mass hydrocarbons dissolve in HDPE with the result that the polymer swells and the modulus decreases. Shell Canada reported [39] the properties of a particular grade of HDPE after exposure to an aromatic natural gas condensate. Table 27.1 contains data from their paper and illustrates the impact of that exposure environment on the properties of that particular grade of HDPE [39].

It is clear from these measurements that there are useful properties at 60°C (140°F) for this particular HDPE grade. The authors reported that the maximum swell was about 6% and the maximum weight gain was about 10%. This is consistent with known properties of HDPE exposed to liquid hydrocarbons. The authors conclude that HDPE is suitable for use up to at least 40°C (104°F) in hydrocarbons, and possibly up to 60°C (140°F) in well-controlled, fully understood applications. Since this work was reported, resin manufacturers have made improvements in HDPE materials and new grades of HDPE have been developed that have improved modulus values. Designers are encouraged to get updated mechanical property data on the grade being used.

27.2.2.2 Permeation effects in HDPE

The permeation rate of hydrocarbon liquids and gases through a polymer is a function of the temperature, partial pressure differential, solubility of the permeant in the polymer, and diffusion rate of the permeant through the polymer bulk.

Gas permeation proceeds until the partial pressure of the gas is equal on both sides of the polymer. In the case of a solid-wall free-standing pressure pipe (e.g., polyethylene

Table 27.1 Property retention of HDPE after exposure to condensate [39]

Material property	23°C (73.4°F)		40°C (104°F)		60°C (140°F)	
	Unexposed	At equilibrium	Un-exposed	At equilibrium	Un-exposed	At equilibrium
Young's modulus MPa	394	205	254	181	141	162
Yield stress MPa	21.3	18.3	17.1	17.9	11.6	17.1
Yield elongation %	19.7	34.0	24.8	37.3	54.1	48.1

pipe for distribution of natural gas to homes), gas permeation will reach a constant, steady state rate. If that pipe is encased in an impermeable shell, as is the case of a HDPE corrosion barrier liner pipe within a steel host pipe, permeation will proceed until the pressure is the same on both sides of the liner pipe wall.

Liquid hydrocarbons are soluble in polyethylene. They will dissolve into the HDPE and diffuse to the other side of the pipe where they will exit the bulk and remain on the exterior surface of the liner unless they evaporate into the environment. When the exterior of the liner is coated with a thin monolayer of liquid hydrocarbons, the concentration gradient (equivalent to the partial pressure differential for gases) flattens and permeation effectively stops for a given temperature. In this case the hydrocarbons usually also have a softening and swelling effect. Swelling increases permeation rate. If the pipe is transporting a mixture of gas and liquid (e.g., produced gas and gas condensate) the swelling caused by the condensate will increase the permeation rate of the gas.

27.2.2.3 Polyethylene in water applications

HDPE pipe has a long history of successful use in water applications at moderate temperatures. PEX and PE-RT pipes have been used in pressurized hot water systems operating at temperatures up to about 80°C (176°F) with a proper pipe design.

New-generation HDPE materials, such as PE 4710, have been used as corrosion barrier liners in structurally sound steel pipes for up to 9 years at 90°C (194°F) in Canadian produced water systems, according to one major liner Installation Company. The time frame is not based on knowledge of failures at 9 years, but rather that they started installing HDPE liners in this service type about 9 years ago. In water the chief concern is loss of tensile modulus with the increased temperature. Modulus is directly related to liner collapse pressure, leading designers to use thicker liners at high temperatures, typically DR17-20 instead of the more conventional DR 30-40 designs. Fig. 27.1 shows that for HDPE without absorbed hydrocarbons the tensile modulus declines from about 800 MPa to about 150 MPa at 80°C (176°F). Although in water systems liner collapse due to differential gas pressure across the liner wall is unlikely, the combination of softening and thermal expansion at operating pressures far above the installation temperature can cause buckling because the liner is constrained by the steel host pipe, and buckling is the most likely stress relief mechanism.

27.2.2.4 Polyamides—PA6, PA6.6, PA11, and PA12

As the chemical structure of the polymer deviates from hydrocarbon-like (nonpolar) to a more polar structure, the ability of hydrocarbons to swell and soften the polymer is reduced, but the amount of water absorbed increases compared with polyolefins. For this reason, polyamides (nylons) are highly resistant to swelling by hydrocarbons but they absorb water, which causes swelling of the polymer. Polyamides 11 and 12 absorb up to 2% by weight of water and swell about the same amount. Nylons 6 and 6.6 absorb as much as 9% by weight but swell less than that with water absorption.

Nylons are subject to hydrolysis as the principal degradation mechanism. PA11 and PA12 have been thoroughly investigated as part of their qualification as pressure barriers in American Petroleum Institute (API) 17J-compliant offshore flexible pipes [40]. The hydrolysis behavior of PA11 is well documented in API 17 TR2 [41]. The hydrolysis behavior of PA12 is very similar. PA6 and PA66 have significantly faster rates of hydrolysis compared with PA11 and PA12. The reason is that PA6 and PA66 have many more amide linkages for attack by water, making a successful attack much more likely.

27.2.2.5 Effects of water on polyamides

Water is one of the reaction products of making polyamides, and the polymerization reaction is reversible under the right conditions. Hydrolysis, the reverse reaction, is the principal aging mechanism. In this reaction, water reacts with the amide bonds in the polymer to reform the acid and amine end groups, thus reducing the molecular weight of the polymer. If enough hydrolysis reactions happen, the molecular weight will be reduced to the point that the polymer becomes brittle and eventually will dissolve. This reaction has been extensively studied for PA11 and PA12, but little has been published on the hydrolysis of PA6 and PA6.6 in the solid state.

Hydrolysis of PA6 and PA6.6

El-Mazry et al. published a comprehensive aging model for PA6.6 [42]. When using the available published PA11 data, the model predicts the same lifetime as the API 17 TR2 model, providing validation to the new approach for PA6.6. Fig. 27.3 shows the time to embrittlement for PA6.6 calculated using the El-Mazry model. The times shown in Fig. 27.3 are probably a worst case scenario for PA6.6 in pure water. The work was done with thin films, and this makes water abundantly available to all the

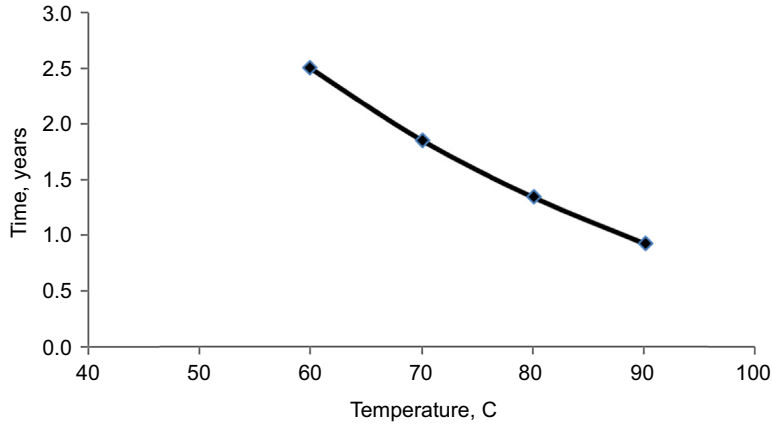

Figure 27.3 Time to embrittlement for PA6.6 calculated using the model of El-Mazry et al. [42]

amide bonds in the bulk. Thicker sections like pipe walls would take much longer to saturate and there would be a gradient of degradation from the wet surface to the relatively dry interior until full saturation is achieved. Nevertheless, it makes sense to limit PA6 and PA6.6 use temperatures to 40°C (104°F) and below. If the pH of the fluid is acidic, the rates will accelerate significantly because acids are potent catalysts for hydrolysis.

Hydrolysis of PA11 and PA12

As with PA6 and PA6.6 water can react with the polymer causing loss of molecular weight, resulting in embrittlement. The phenomenon has been extensively studied for these materials. Because of their critical importance as pressure barrier and external sheath materials in offshore flexible risers and flow lines compliant with API Spec 17J, offshore operators worked with subject matter experts in a Joint Industry Project to develop a technical report that thoroughly describes the hydrolysis behavior of PA11, including an aging model. The report, eventually issued as API 17TR2 concludes that, for PA11, there is a minimum molecular weight for retention of ductility and describes the relationship between time, temperature, and pH to reach that lower bound molecular weight. The general rule based on the API 17TR2 model and current offshore flexible pipe industry practice is that for nonacidic pH values the temperature limit is 67°C (153°F) for a 20-year lifetime. If the pH is acidic, the lifetime gets shorter for the same temperature, so to get the 20-year lifetime it is essential to reduce the temperature.

Since the API model for PA11 was published, extensive work has been done on PA12 and the aging behavior in hydrolytic conditions has been published [43]. PA12 has similar hydrolysis kinetics to PA11, and the results indicate the API 17TR2 model is more conservative for PA12. Another interesting observation is that PA12 samples fully saturated with hydrocarbon liquids have a slower rate of hydrolytic degradation than identical coupons exposed only to water. The authors conclude that the absorbed hydrocarbons increase the bulk hydrophobicity, decreasing the water absorption and transport rate in the polymer bulk, with the result that the availability of water to react with amide linkages is reduced, compared with the water exposure only case. It is reasonable to assume that the same effect would be observed in PA11.

Fig. 27.4 shows the hydrolytic degradation rate for PA12. This plot represents the results of a lifetime study in which end of life was defined as a reduction of tensile elongation at break to 10% engineering strain [44]. This end-of-life criterion may not be applicable to all applications and the reader is advised to consult the material manufacturer for more application-specific information. The rate of hydrolytic degradation is not the same for all polyamides. Comparing Fig. 27.4 for PA12 with Fig. 27.3 for PA6.6 one can see that the rate for PA12 is significantly slower than for PA6.6. At 60°C (140°F) the anticipated lifetime for PA6.6 is about 2.5 years, compared with over 20 years for PA12. Generally speaking, aliphatic polyamides with more methylene units between the amide linkages have slower hydrolytic degradation rates than polyamides with fewer methylene units between amide linkages.

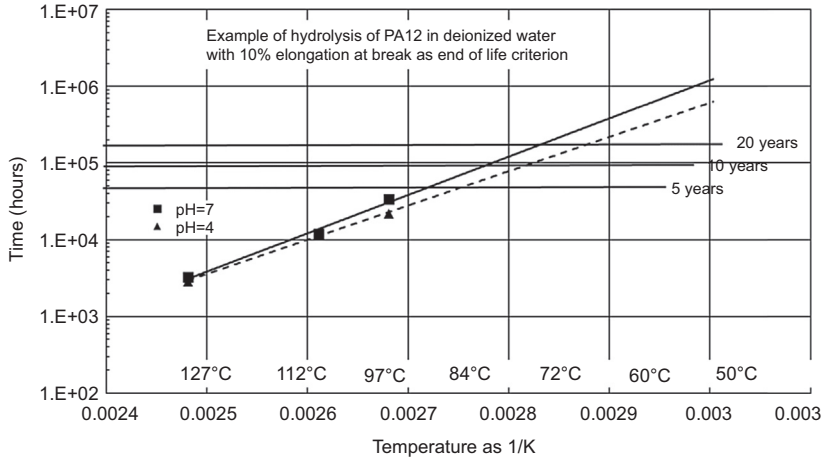

Figure 27.4 Hydrolytic degradation rate of PA12.

27.2.2.6 Effect of hydrocarbons on nylons

PA6 and PA6.6 materials are resistant to hydrocarbons such as natural gas condensate and diesel fuel up to about 90°C (194°F). Some swelling is likely. If the formulation is described as "super tough," the effect will be larger because of the impact modifiers in the formulation. The impact modifiers are elastomers that are finely dispersed in the PA bulk. These elastomers will swell when exposed to hydrocarbons. However, these materials are regularly used in automotive hydrocarbon exposure applications with proper part designs. Mechanical stiffness will be less, but the change will be much less than in a polyethylene (PE) material in the same service.

PA11 and PA12 are not significantly affected by produced hydrocarbon fluids and most fuels. In plasticized grades, the plasticizer may slowly exchange with pipeline contents hydrocarbons with the result that the mechanical properties and dimensions of the polymer remain stable as one plasticizer exchanges for another.

27.2.2.7 Effect of alcohols on nylons

Alcohols, especially methanol, are capable of swelling polyamides. If the polyamide formulation contains plasticizers or other small-molecule additives in quantities of more than a few percent by weight, methanol is able to extract the small molecules quickly at mild temperatures. Methanol works significantly faster than ethanol or propanol, mostly because of the difference in molecular size. Methanol, being smaller, moves into the polymer faster to extract and replace the additive. It is also much more soluble in the polymer than most additives and will soften and swell the polymer significantly, much like light hydrocarbon effects on HDPE. The result is that the polymer contains the alcohol instead of the additive. The problem with this is that, unlike additives, the alcohol is easily removed. So, for example, if a nylon-lined wet-gas gathering line is treated with methanol to break or prevent hydrates, then is shut in, and the

methanol is allowed to stay in the pipeline for more than a few hours, some additives will exchange for methanol. Then when the methanol is swept out of the system by more wet gas the methanol will eventually return to the flow stream (driven by a concentration gradient) and the polymer liner will get stiffer and shrink because the additives that comprised a significant fraction of its weight are gone. If methanol is added continuously or frequently in large quantities over a long enough period of time the material could swell and soften, possibly causing a premature failure. Methanol should be avoided except as the solvent in periodic inhibitor treatments with short-term, transient exposure. Ethanol is much less of a problem.

27.2.2.8 Effect of inorganic chemicals on nylons

Mineral acids, such as hydrochloric, sulfuric, and nitric acids, should generally be avoided. Transient exposure like in a flow back from an acidizing job may be well tolerated as long as the exposure time is short (hours, not days) and the temperature is low. Each nylon type has a different sensitivity to acids and a subject matter expert should be consulted if exposure to mineral acids is anticipated.

Alkaline solutions such as those found in completion fluids are less aggressive than acids and are well tolerated for long times at temperatures of about 40°C (104°F) and lower. This general statement may not be relevant because completion fluids are subject to temperatures much higher than 40°C. Each case should be examined individually by a subject matter expert to determine compatibility.

Both materials have limited resistance to bromides. Bromides are often a significant component in completion brines and choke and kill fluids.

27.2.2.9 Permeation of nylons by gases

There are little useful published data regarding the permeation of oil-field gases through PA6 and PA6.6. Because of the important role of HDPE, PA11, and PA12 in offshore flexible pipe pressure barriers they are well characterized with a large body of published data. Permeability coefficients have been established by various researchers. Table 27.2 summarizes permeability coefficients measured under conditions relevant to upstream applications [45].

PA12 values are in the same order of magnitude as PA11. The permeability coefficients were measured near the upper use temperatures of the materials.

PVDF, PPS, PEEK, and PVC do not absorb much water because, in addition to their very different chemical structure, they are highly crystalline and the crystalline phase is not penetrated by water. But they are not without their own chemical resistance vulnerabilities in the right circumstances.

27.2.2.10 Polyvinylidene fluoride

Effect of hydrocarbons on PVDF

Petroleum environments are well tolerated by PVDF and its copolymers. The grades developed for offshore flexible pipe pressure barriers have been extensively tested in hydrocarbon environments intended to simulate upstream conditions. Volume changes

Table 27.2 Permeability of PA11 and HDPE [45]

Gas species	Measurement pressure/ temperature	Permeability of HDPE cm^3 (at standard temperature and pressure)/cm s bar	Measurement pressure/ temperature	Permeability of PA11 cm^3 (at standard temperature and pressure)/cm s bar
CH_4	100 bar/60°C (1450 psi/ 140°F)	5.0×10^{-8}	100 bar/80°C (1450 psi/ 176°F)	1.1×10^{-8}
CO_2	40 bar/60°C (580 psi/ 140°F)	16×10^{-8}	40 bar/80°C (580 psi/ 176°F)	7.5×10^{-8}
H_2S	20 bar/80°C (290 psi/ 176°F)	18×10^{-8}	40 bar/80°C (580 psi/ 176°F)	42×10^{-8}

HDPE, high-density polyethylene.

are on the order of -1% exposed to diesel at 150°C (302°F). This reflects an exchange of plasticizer for hydrocarbons in the bulk.

PVDF and its copolymers are highly resistant to attack by acids. Bases can be a problem. Alkaline conditions catalyze a decomposition that imparts color and eventually brittleness. Highly alkaline completion fluids would be a problem for continuous exposure, but transient exposure should not pose a large risk.

Highly polar solvents, such as dimethyl sulfoxide, dimethyl formamide, and *n*-methyl-2-pyrrolidone, dissolve PVDF at ambient temperatures. These are not normally transported by pipeline and are unlikely to present a hazard to pipe. They may be present in small concentrations as a carrier solvent for some types of corrosion inhibitor or other well treatment chemical, but in that form are unlikely to present a threat to structural integrity, although over time, depending on temperature and pH, it could affect the pressure capabilities of free-standing PVDF pipe.

Aging mechanisms of PVDF

In normal upstream oil and gas use as a barrier polymer for fluid transport PVDF and its copolymers do not exhibit any chemical reactions that result in a predictable rate of properties loss over time. Instead, experience for PVDF in offshore flexible pipes is that plasticizer loss accompanied by volume shrinkage and loss of ductility is the biggest threat [46]. Material manufacturers have reformulated their offerings to retain ductility and volume in conditions that would result in extraction of plasticizer.

27.2.2.11 Polyphenylene sulfide

PPS is highly resistant to severe chemical environments. It has no known solvents up to about 200°C (392°F). PPS is generally inert to the oil and gas environment and

reactions of PPS with water, hydrocarbons, and gases are not observed. However, grades proposed for pipeline service are formulated to improve flexibility and low temperature impact strength. The additives that can change over time, affecting flexibility, yield stress, and elongation, and impact toughness during service. Although these characteristics may change, the PPS matrix material retains integrity.

27.2.2.12 Poly-ether-ether-ketone

PEEK is a high-melting-temperature engineering resin that is also very highly crystalline. It is highly resistant to hydrocarbons and water at temperatures below about 250°C (482°F) and has high stiffness up to nearly 300°C (572°F) in air. At higher temperatures and in the presence of aqueous salts and completion fluids PEEK degrades to unacceptable levels quickly [47].

27.3 Applicable standards

There are numerous standards that apply to nonmetallic oil-field pipes. Table 27.3 lists the key standards for pipe and liner products. The high-level product standards apply to the finished, ready-to-install pipe for pressure piping products or to the fully installed liner for liner products. API and ASTM have standards that cover common pressure piping products for use in oil and gas applications. By referencing them, these standards include material standards and test method standards that must be complied with for the product to comply with the high-level product standard.

27.4 Qualifications

Fabricated articles such as pipe, fittings, and structural components are built and tested to industry standards to qualify them for the intended service. The standards are developed by consensus of subject matter experts and are cited in purchasing specifications. Table 27.4 is not intended to be an exhaustive list, but rather to serve as a guide to the most commonly applied qualification standards.

27.5 Nonmetallic materials application in oil and gas production

Generally, it can be stated that nonmetallic materials have been used or are being qualified for use in practically all equipment in oil and gas production. These applications include:

- Downhole tubing liners (FRP and HDPE, PE-RT, PPS, PEEK)
- Tubing and casing (FRP)
- Flow lines and gathering lines (solid: FRP, HDPE) (liners in steel or RTP: FRP, HDPE, PA, PEX, PE-RT, PPS, PVDF)

Table 27.3 Standards that apply to nonmetallic materials and structures in oil and gas applications

Application	Publisher	Designation	Title
Polyethylene line pipe	API	API 15LE	Specification for polyethylene line pipe
	ASTM	ASTM F2619	Standard specification for high-density polyethylene line pipe
Reinforced thermoplastic pipe	API	API 15S	Spoolable reinforced line pipe, second edition
Fiberglass line pipe	API	API 15HR	High-pressure fiberglass line pipe
		API 15LR	Low-pressure fiberglass line pipe and fittings
	ASTM	ASTM D3517	Standard specification for fiberglass (glass-fiber-reinforced thermosetting-resin) pressure pipe
Thermoplastic liners for oil-field pipelines	NACE	NACE RP0304	Design, installation, and operation of thermoplastic liners for oil-field pipelines
Fiberglass lined steel	API	API RP 15CLT	Recommended practice for composite lined steel tubular goods
Thermoplastic materials	ISO	ISO 23936-1	Petroleum, petrochemical, and natural gas industries—nonmetallic materials in contact with media related to oil and gas production—Part 1: thermoplastics
Thermosetting materials	ISO	ISO 23936-3 in development	Petroleum, petrochemical, and natural gas industries—nonmetallic materials in contact with media related to oil and gas production—Part 3: thermosets
Composite materials	ISO	ISO 23936-4 in development	Petroleum, petrochemical, and natural gas industries—nonmetallic materials in contact with media related to oil and gas production—Part 4: fiber-reinforced composites

Table 27.4 List of commonly cited qualification standards for nonmetallic structures used in oil and gas exploration, production

Application	Standard for qualification	Notes
Plastic pressure pipe	PPI TR3 ISO 9080 API 15LE ASTM F2807	Each of these standards contains requirements for determining the long-term hydrostatic strength of plastic pipe. Some have additional requirements
Reinforced thermoplastic pipe (RTP)	API 15S, second edition, 2016	This standard specification covers all spoolable reinforced thermoplastic line pipes. It includes requirements for qualification, determination of operating pressure, end fittings, quality, and documentation
Thermoplastic liners for steel pipe	NACE RP-0304, second edition 2016	This recommended practice was updated in 2016 and provides guidance for design, installation, and operation of thermoplastic liner for oil-field pipelines
Composite coiled tubing, jumpers	API 17Z (in development)	As of late 2016 this standard is still in development, but good progress is being made
Composite risers and tensioners	DNV-RP-F202	This is a comprehensive engineering design standard
Unbonded offshore flexible pipe	API 17J API 17B API 17TR2	17J is a standard specification and 17B is a recommended practice that serves as a companion document to 17J. API 17TR2 addresses hydrolytic aging of PA11, which is used extensively in offshore flexibles as the pressure barrier, wear tapes, and outer sheath
Fiber-reinforced plastic (FRP) piping and components	ASTM D2992 API 15HR API 15LR	ASTM D2992 is the standard method to determine the long-term hydrostatic strength of fiberglass pipe. API 15 HR and LR are, respectively, standard specifications for high-pressure and low-pressure fiberglass line pipes
FRP lined tubing	API 15CLT	Recommended practice for composite-lined steel tubular goods

Table 27.4 Continued

Application	Standard for qualification	Notes
FRP vessels and tanks	API 12P	Specification for fiberglass-reinforced plastic tanks—fourth edition 2016
	BS 4994	Design and construction of vessels and tanks in reinforced plastics, 1987 BSI, UK
	ASME RTP-1	Reinforced thermoset plastic corrosion-resistant equipment
	ASME Section X	Fiber-reinforced plastic pressure vessels

- Injection lines (solid: FRP, HDPE) (liners in steel or RTP: FRP, HDPE, PA, PEX, PE-RT, PPS, PVDF)
- Tanks and vessels (FRP, HDPE, PA, PVDF)
- Fire mains and piping (FRP)
- Cooling water (FRP)
- Produced water piping (FRP, HDPE)
- Coil tubing
- Seawater and water disposal systems
- Flexible pipe reinforcement
- Composite risers and riser components (tensioners)
- Jumpers
- Choke and kill lines
- Structural components (grating, ladders, handrails, helidecks, fire and blast walls, machinery foundation, derricks, living quarters, etc.)
- Others (cable trays, cable ladders, survival crafts, escape systems, buoys, etc.)
- Floating platform tendons
- Umbilicals
- Composite repair for maintenance and rehabilitation (pipe and vessel repairs)
- Spoolable composite tubing

27.6 Major applications of nonmetallic materials in oil and gas

27.6.1 Solid wall nonmetallic pipe

Solid wall plastic pipe is commonly used in low-pressure gathering networks and fuel gas distribution networks [48]. It is also used in siphon strings (velocity strings) and injection capillaries. Hydraulic control umbilicals and injection umbilicals also use solid wall plastic pipe or tubing. Polyethylenes, including HDPE, PE-RT, and PEX are the most commonly used materials, but in specialty applications PA11 and PA12 are in wide use.

27.6.1.1 Polyethylene pipe

HDPE is the basic engineering polymer grade of polyethylene. There are grades of HDPE with material designation codes including PE4710 and PE100 that are designed to be pressure piping materials and have long-term hydrostatic strength characteristics established by the manufacturer and usually verified by a third party certifying body. These grades and others have found broad use in oil and gas as pressure pipes and liners. Heavy wall HDPE pressure pipes are widely used for gathering lines at low pressures. As HDPE absorbs light hydrocarbons and becomes softer (lower Young's modulus and creep modulus), it is typically necessary to derate the nominal pressure capacity of HDPE pipes transporting more than 1 mol% hydrocarbons by 50%.

27.6.1.2 PE-RT pipe

Certain grades of HDPE, known as PE-RT, have been designed for long-term use in under-floor radiant heating applications with water temperatures in the range of 70°C (158°F) with a 50-year design life. PE-RT has been available and in common use since before 2006 when the first ISO standard describing the long-term hydrostatic performance (ISO 24033:2006) was published describing PE-RT Type I. Type II was introduced before 2009, the date of the most recent revision, ISO 24033:2009 [49]. Both standard versions include long-term strength reference curves that define the minimum acceptable high-temperature long-term hydrostatic strength requirements.

Type II grades have been designed to eliminate Stage 2 failure (brittle failure) during long-term hydrostatic stress applications. These PE materials are different from ordinary HDPE materials in that they incorporate at highly regular intervals a linear 6- to 10-carbon side chain along the backbone chain. These side chains are able to incorporate into adjacent crystalline lamellae and act as physical cross-links. This internal reinforcement significantly increases resistance to slow crack growth and inhibits transition to Stage 2 failure. Cross-linking is a traditional method to improve the thermal range of plastic materials, but more standard chemical cross-linking renders the material unsuitable for fabrication operations using melt processing techniques, like butt fusion, which are important for fabrication of piping systems and especially critical for liner technology.

Commercial PE-RT raw materials are required to show conformity with the ISO 24033 standard reference curves by submitting pipes for a year-long hydrostatic pressure testing in an accredited laboratory. PE-RT Type II is formulated with highly robust and extraction-resistant antioxidant additives that suppress Stage 3 (thermooxidative) failure for much longer times than older generation materials.

PE-RT is still polyethylene, so it suffers from many of the same disadvantages as HDPE: swelling and loss of strength with hydrocarbon absorption, low modulus at 100°C (212°F), and essentially the same permeability to gases as HDPE. Using this material at high temperatures will require knowledge of the Young's modulus,

swelling in the service environment, and permeability to the expected gases at the design conditions.

27.6.1.3 PEX pipe

PEX has been used for a long time in radiant heating applications. Of the three types, PEX-b, also known as silane cross-linked, is the most likely candidate for pressure pipe and liners because cross-linking happens at some time after extrusion with exposure to hot water. Once extruded, PEX-b starts to cross-link at a rate that is determined by the catalyst concentration and type, availability of water, and temperature. In hot, humid, storage, and transport conditions PEX-b begins to cross-link before joining. Some suppliers claim they have formulations that resist premature cross-linking. PEX-a, which is cross-linked in the extruder at the pipe plant using peroxides cannot be joined using conventional butt fusion, so mechanical or electrofusion couplers must be used. To minimize joints in the field coiled pipe made from both material types is available in diameters of about 8 in. (200 mm) and smaller. The principal barrier to larger diameter coiled pipe is the size of the coil, which tends to become very large for large-diameter pipe, exceeding limits on modes of transportation to the job site.

It is interesting to note that some reported long-term testing of PEX shows inferior slow crack growth resistance when compared with the PE-RT data [50]. PPI TR-4 contains HDB listings for some specific PEX compounds at 200°F (93°C). These grades are subsequently derated in mechanical end couplings because of this known susceptibility to stress cracking, particularly in hot chlorinated potable water. Some data suggest transition to Stage 2 behavior at lower temperatures than for other grades.

27.6.1.4 PA11 and PA12 pipe

The unplasticized grades of PA11 and PA12 have been fully qualified to transport natural gas at twice the pressure of HDPE gas pipes. Both materials are listed in PPI TR-4/2016 with a HDB at 23°C (73°F) and 217 bar (3150 psi), which is twice the HDB of HDPE at the same temperature. They also have HDB ratings that are significantly higher than HDPE at elevated temperatures. These materials are not softened by hydrocarbons to the same extent as HDPE, but some small swelling is observed in aromatics. The effects on long-term hydrostatic strength have not been established.

27.6.1.5 FRP/GRE pipe

FRP/GRE pipe is composed of a thermosetting resin reinforced by fibers. FRP is fiber-reinforced polymer. GRE is glass-reinforced epoxy. FRP and GRE are usually considered interchangeable names for the same product. FRP/GRE is widely used in oil and gas production, with produced water, utilities, and fire water systems being the primary applications [51]. Other applications include flow lines for oil production and chemical handling [52]. Use of FRP/GRE in offshore applications provides both the required corrosion resistance and the weight saving, and offers such a significant

cost advantage that today most fire water systems for offshore platforms are made of FRP/GRE.

Applications in downhole have been limited to FRP/GRE where it has been used for casing and tubing, particularly in shallow wells where the stresses are low and threaded couplings can withstand the load. The type of FRP/GRE reinforcement as well both inner layer and outer layer resins are selected for the required chemical resistance and temperature stability because produced fluids could come in contact with both the inner diameter (ID) and outer diameter of the tubing and the ID of the casing. The limited application in downhole tubulars is a result of the pressure rating limitation, limited temperature range, and low abrasion resistance in sucker rod lift wells or where wire lines are frequently used.

Choices for resins are driven by the operating conditions and environments, with amine epoxy cured offering the widest operating temperature and chemical resistance ranges. FRP/GRE can be affected by UV and applications with continuous exposure to sun light require the use of UV-stabilized resins for the exterior layer.

The reinforcement is the key structural component of GRE/FRP, carrying all of the hoop, axial, and other loads through the design life of the product. Reinforcement fibers may be continuous or discontinuous, woven textile or filament-wound. The helical winding angle affects the performance, cost, flexibility, and dynamic fatigue tolerance of the pipe. There is no standard reinforcement material and many different types are in use: continuous or discontinuous glass fibers, different classes ECR, C, AR, or S (woven or filament-wound) variants; all the reinforcement types display stress regression behavior.

The thermoset resins determine the other properties. The resin on the inner layer determines the chemical resistance and the thermal stability. The resin for the outer layer serves to protect the reinforcement from damage caused by outside mechanical forces such as abrasion and low impact, from radiation damage caused by UV light from the sun, and from chemical attack by components of the soil in which the FRP/GRE may be buried. It also serves as the carrier of a print line identifying the product lot number, manufacturer, nominal diameter, pressure rating, and other pertinent information.

The challenges in the use of FRP/GRE are the lack of ways to determine the degradation or the damage in the pipe as there are no nondestructive evaluation (NDE) techniques that can show damage, and the only means for ensuring the integrity of the pipe is through visual inspection, hydrotesting, or destructive testing of removed sections.

27.6.2 Reinforced thermoplastic pipe

RTP consists of a plastic pipe (the liner) around which is wrapped at least two layers of reinforcement: one with a left-handed helical configuration and the other right handed. This sequence may be repeated, but always with an even number of helical wraps, to maintain balance under pressure. The reinforcement is covered by another polymeric layer, the cover or jacket. This is very similar to the construction of hydraulic hoses. Each of these layers relies on the others for the RTP to properly function for the design

life. These products may be designed and manufactured in compliance with API 15S (see Table 27.3).

The liner is required to contain the internal fluids, but does not offer any contribution to the hoop strength of the structure. It must retain its barrier properties for the design life of the RTP product. The liner usually, but not always, serves as the mandrel around which the reinforcement is wrapped. There are many polymer materials that can serve as a liner. Most RTP liners are made from commodity materials, such as HDPE [53]. At least one supplier offers multiayer liners in which the liner is manufactured such that there is a high-performance engineering polymer in contact with the fluids and adhered to a commodity backing pipe that provides the structural characteristics to the liner [54]. Solid wall PA12 liners are available for applications requiring superior resistance to gas and liquid permeation [55].

The reinforcement is the key structural component of RTP, carrying all of the hoop, axial, and other loads through the design life of the product. Reinforcement type affects cost, weight, flexibility, and dynamic fatigue tolerance of the RTP product. There is no standard reinforcement material and many different types are in use: aramid fiber, dry glass fiber, thermoset impregnated glass fiber, steel strips, and steel wires. Except for the steel variants, all the reinforcement types display stress regression behavior.

The cover serves to protect the reinforcement from damage caused by outside mechanical forces such as abrasion and moderate impact, from radiation damage caused by UV light from the sun, and from chemical attack by components of the soil in which the RTP may be buried. It also serves as the carrier of a print line identifying the product lot number, manufacturer, nominal diameter, pressure rating, and other pertinent information. HDPE is the most common cover material.

The end fitting or coupler is another key component of the RTP system. It allows the connection of the RTP to the pipeline system, through flanges on piping, tees, elbows, and valves. The end fitting must remain leak-tight for the service life of the RTP and may be required to sustain high axial loads during installation and possibly operation. Most end fittings are mechanical devices made of steel or corrosion-resistant alloys. Some incorporate o-rings and/or other elastomeric sealing elements. Some designs use electrofusion technology to join the liner so that no metal is exposed to the pipeline contents. Each RTP manufacturer designs their end fittings. They are not interchangeable between manufacturers.

27.6.3 Liners

Liners are nonstructural corrosion barrier plastic pipes that are inserted into a structural host pipe. The liner acts as a barrier to shield the host pipe from the corrosive fluids and to interrupt the corrosion−erosion cycle that is responsible for wall loss. Liners usually perform this function with exceptional reliability, but rare exceptions have been described in the literature. One review discusses the details of material selection, design, and operation [56]. NACE International has published a recommended practice on the subject [57]. The Plastic Pipe Institute maintains a detailed guidance document on the subject that addresses polyethylene liners for mostly municipal and industrial applications but the general principals apply in many oil and gas applications [8]. Liners are

used in RTP as the fluid barrier, in structurally sound steel pipe as a corrosion barrier, and in jointed downhole production tubulars to prevent corrosion and wear.

27.6.3.1 As used in pipelines

Thermoplastic liners have almost exclusively been polyethylene based, predominantly PE80, PE100, PE4710, and PE3408 materials with much more limited use of PEX and PE-RT. PE80, PE100, PE4710, and PE3408 are well-established pipe grade materials that have been very well characterized for pipe applications and widely employed as liners. They are typically limited to around 60°C (140°F). PEX was introduced to raise that temperature limit. PE-RT Type II materials raise the limit to 80°C (176°F) and do not have the processing and butt fusion limitations associated with PEX.

It is widely claimed that PEX and PE-RT liners have been used up to, and in some case in excess of, 90°C (194°F) in oil-field water service. But at this time there are no published reports to support the claim. While it is possible that 90°C (194°F) is the design temperature, not the operating temperature, it is likely that there are some polyethylene liners operating in the 80−85°C (176−185°F) range in oil-field water service.

As the operating temperature goes above 60°C (140°F), failure rates of PE liners appear to become significant. There are several reports of failure rates of up to 5% in older systems using older grades of polyethylene and with an uncertain design history [48]. In gas service, radial collapse due to gas permeation through the liner and buildup of pressure within the annulus is major failure mechanism.

Liner failures are usually discovered long before there can be significant damage to the host pipe. When a failure is detected, the line must be shut in and emptied of fluids and the liner replaced. Even this cost, including lost production, repeated every 5−10 years, can be competitive with more expensive chemical inhibition programs.

PA11 and PA12 have been used for higher temperature service, especially for multiphase pipelines where all polyethylene liners have a short lifetime due to swelling and softening from hydrocarbon absorption [44,58]. Both materials are resistant to swelling and softening in hydrocarbons and maintain good properties well beyond the limits of HDPE. Both materials are susceptible to swelling and softening by methanol but can easily tolerate the normal amounts of methanol used in injection fluids.

PVDF has been proposed for conditions beyond the PA11 and PA12 range, with offshore pipelines as the most viable application because of the cost [14]. Moving away from commodity polyethylene materials to more specialized polymers brings with it a significant cost increase, for example, compared with HDPE, a cost factor of $\times 5$ for nylon materials and $\times 10$ or more for fluoropolymers and high-grade resins is not unusual. In some applications, this may mean that other, metallurgical, options become attractive. Operators should expect that high-performance engineering polymer liners will be expensive compared with HDPE, because of not only increased materials costs but also the development costs incurred during qualification for first use in a given, usually high-risk, service.

27.6.3.2 As used in downhole tubulars

Thermoplastic liners have been used in jointed production tubing since the early 1990s. Polyethylene is the most frequently used material. The liner provides resistance to internal corrosion caused by produced fluids and guards against tubing wear, a well-known failure mechanism in rod and progressive cavity pumped production systems [59]. Other materials, including PPS and PEEK, have been introduced for higher temperature and more severe service applications [60].

27.6.3.3 As shop-lined piping and fittings

Lined pipe bends, fittings, tees, reducers, and elbows are produced in all types of materials used in the lining of metallic pipe at all sizes. However, all are shop applied and require flange connection. Fabricated pipe spools with multiple bends can be lined. Lining of pipe elbows, tees, reducers, and fittings is well-established technology and has been in use for several decades, particularly in the chemical process industry.

27.6.3.4 As FRP composite and nonbonded thermoplastic liners

FRP/GRE has been widely used as corrosion-resistant, low-cost liners for tubing [61]. FRP/GRE-lined tubulars are typically made of FRP/GRE liner with a grout occupying the space between the lining and the metal tubular ID. FRP/GRE-lined tubulars have been in use for over 50 years in water injection, oil and gas production, water disposal, and acid gas injection. They are available for wide range of operating temperatures, up to 177°C (350°F). FRP/GRE liners offer another advantage in cases where they are used to rehabilitate corroded tubulars, which offers further cost advantage over corrosion resistant alloy (CRA) materials. Earlier problems with the coupling sealing rings were experienced mainly because of improper selection of material that led to degradation of the rings or lack of proper installation that led to squeezing and protrusion of the ring, reducing the drift.

FRP/GRE liners have a flow velocity limitation of 10 m/s (33 ft/s) mainly as a result of lack of data at higher velocities [62]. Also, FRP/GRE liners are prone to mechanical damage during well intervention, particularly from sharp tools or wire lines. To prevent such damage, the speed of the wire line is controlled and use of nonsharp tools is required.

Similarly, HDPE and nylon with their various grades have been used as nonbonded for downhole tubulars [63]. Their application mirrors the use in piping systems with the primary limitation on temperature and chemical degradation by produced fluids. Their application is also limited to environments where gas permeation through the liner is limited. Because tubulars use threaded connections it is not possible to vent off any permeated annulus gases.

Solid thermoplastic liners also offer added lubricity and have shown improvement in wear in sucker rod applications.

Other materials, PPS, PK, and PEEK, have been considered but have not been used because of cost. Certain grades are being evaluated as a replacement for CRA materials.

27.7 Rehabilitation

Nonmetallic materials are frequently used in rehabilitation projects, especially for pipelines. In this context rehabilitation is defined as intervention in an operating system component for the purpose of arresting structural degradation and/or repairing structural damage so that the system can be returned to full operational status without replacement of the rehabilitated component. A common example is the insertion of a plastic liner into a steel pipeline that has been determined to be at risk of pressure derating unless wall loss due to corrosion is stopped. There are three classes of pipe rehabilitation: structural, semistructural, and nonstructural.

Structural rehabilitation restores the pressure capacity of a pipeline that has been compromised by wall loss. These products are designed to be fully pressure containing and do not require any strength contribution of the host pipe. These are usually composite products consisting of three layers: a plastic liner, a continuous helically wound reinforcement layer, and a plastic cover. RTP products are often used for structural rehabilitation. These solutions are used in offshore and onshore projects. API 15S defines the qualification requirements for this product type. There are numerous suppliers around the world. Nearly all RTP products compliant with API 15S have nominal diameters of 8 in. or less. A notable exception is Smart Pipe, which is available in diameters up to at least 16 in., is manufactured on the job site, and has the option of including fiber optic sensors along the length of the pipe [64]. These sensors can detect and reveal the location of temperature changes and mechanical stresses along the pipeline. This and other RTP products can be pulled into an existing pipeline to provide a pressure-rated "liner" that effectively replaces the function of the steel host pipe, but without the potential for corrosion.

A semistructural rehabilitation uses a liner that has not been rated to the host pipe operating pressure and cannot fully perform the strength function of the host pipe, but because of a specific set of conditions the liner is able to restore the pipe to full operating pressure. Semistructural liners are used when a defect in the host pipe, usually a small hole, must be repaired. Properly designed thermoplastic and composite liners can bridge small holes for long periods of time, effectively restoring the pressure capacity of a pipeline. This works because the stresses on the liner at the steel pipe defect are far below the long-term strength of the liner in the service conditions, but unless there is assurance that the defect (hole) will not grow in size after the liner is inserted, the liner should not be assumed to be capable of bridging the hole indefinitely. Liner design for hole bridging requires comprehensive understanding of the complete stress tensor of the liner at the defect site and is a specialty that is properly left to subject matter experts.

Nonstructural liners act as corrosion barriers to protect structurally sound steel pipes from internal corrosion and have been discussed in the Liners section. In the rehabilitation role, an inserted liner separates the pipeline contents from the steel host pipe ID, effectively breaking the corrosion−erosion cycle that is a major cause of wall loss, and cuts off the supply of corrosive fluids and bacterial nutrients, which is the leading cause of localized corrosion.

27.8 Limitations

There are dozens of polymers and composite structures proposed for use in oil and gas. The limitations of these materials are mostly related to chemical resistance and the combined effects of chemical attack and mechanical stress. The chemical resistance characteristics from polymer to polymer can be enormous. Resistance to oil-field fluids can vary from extremely resistant to almost nonresistant, depending on temperature and fluid mix. Different classes of nonmetallics have different aging mechanisms and kinetics. Most find a few applications in which they are very good but perform poorly in others.

The lack of long-term performance data inhibits routine adoption of most materials. Long term means at least 20 years in the projected service environment. Because it is rare to have 20 years of aging data available, materials suppliers have used classical chemical kinetics to develop long-term, lower temperature, aging rate estimates based on very high-temperature, short-term testing (Eyring models). All of these models involve assumptions about the chemical or physical aging mechanism. If the assumptions are wrong, then so is the model. Validation of a model requires rigorous control of sample preparation, exposure conditions, testing methods, and data analysis. There are no standard methods from ASTM, API, ISO, and other standardization bodies for developing these models, making it harder for a nonexpert to determine whether a model has been properly developed and its results can be believed.

Nonmetallic materials have elastic, plastic, and viscous mechanical responses to applied stresses. The extent to which one or two of these responses dominates the total mechanical response limits the application range of the material. Absorbed chemicals can change these response levels, resulting in a different profile of mechanical properties. And mechanical stresses combined with chemical and/or UV exposure can limit the useful range of a material.

NDE technologies for nonmetallics lag behind those for metals. This makes in-service inspection for integrity verification difficult or impossible. For nonmetallics stress regression is the usual long-term mode of mechanical failure and it is not possible at this time to inspect for progress along this curve. Chemical degradation and aging are the usual chemical modes of failure. Measuring this requires chemical analysis and there are few nondestructive methods suitable for the field, and they rarely penetrate the surface of the specimen more than a few micrometers.

Repairing nonmetallic materials can be done in some applications. Plastic pipe wall damage can be repaired using electrofusion saddles over the site, and full encirclement sleeves have been used to reinforce larger damaged areas of both thermoplastics and fiberglass pipe. Composites such as RTP cannot be repaired without cutting out the damaged section, although minor damage to the cover can be repaired using the same types of tapes used to cover bare steel at weld zones.

27.9 Typical failures

Failures of nonmetallic equipment in oil and gas production can occur as a result of multiple causes, with chemical compatibility due to softening, crazing, or permeation

leading to collapse and improper selection of materials being the dominant factors. Other failure mechanisms such as mechanical damage, UV degradation, creep, fatigue, and environmental assisted damage can occur but are not as common. The type of failure mechanism varies with the type of application and operating conditions. Failures in FRP piping and vessels typically occur during construction mainly during hydrotesting, with failures mainly in the joints and fittings. The primary cause for these failures are due to defective installations and overloading of materials due to improper design such as lack of accounting for water hammer and bending stresses. Mechanical damage and chemical degradation are the most common causes of failures that occur during operation. Mechanical damage can occur without leaving any indication or sign and can be missed by inspection, making it difficult to verify the integrity of components. Examples of some of these common failures are presented in the following sections.

27.9.1 Downhole

Failures in downhole applications have been mainly in liners, with liner collapse in HDPE liners as the most common. This can happen for a number of reasons, including mechanical damage done to the pipe by sucker rod strings, overheating, over torqueing, and CO_2 and/or H_2S permeation effects from the produced fluids. If the pipe collapses, the ID is greatly reduced and can even cause the rods to get stuck. Example of collapsed lines is shown in Fig. 27.5.

In cases of FRP-lined tubulars, mechanical damage is generally the most common but fatigue of the liner can occur if there are voids in the grouting. An example of this type of failure is a liner in water/CO_2 injection FRP-lined tubing that failed after nearly 8 years in service. Cracks in the liner developed in an area where there were voids in the grouting. Failure of the liner led to corrosion of the steel tubing that led to burst as shown in Fig. 27.6, which shows the breaking of the fibers in the liner.

Figure 27.5 Example of collapsed liner in reinforced thermoplastic pipe line.

Figure 27.6 Example of failed fiber-reinforced plastic liner in downhole tubing.

27.9.2 RTP line failures

Like any product if operating conditions are not well specified and construction practices are not adhered to, RTP lines can fail. Examples of the type of failures experienced with RTP applications are listed.

A 3.5″ 103 bar (1500 psi) 82°C (180°F) RTP line with HDPE liner used for gas production flow line operating at 51 bar (745 psi) and 39°C (102°F) with flow rate of 6.2 MMSCF (million standard cubic feet) failed due to excessive loading at the connection Fig. 27.7.

A 3″ 52 bar (750 psi) 121°C (250°F) RTP line with PPS liner used for oil and gas production flow line operating at 8 bar (120 psi) and 94°C (195°F). The produced fluids had high CO_2 (47 mol%), 5 ppm H_2S, and 97 vol% water cut with very low-salinity produced water. The line failed after 2 years because of cracking that has been caused by crazing of the PPS liner due to high CO_2, high temperature, and manufacturing anomalies acting as stress concentrations. The cracking in the liner shown in Fig. 27.8 led to leak of the produced fluids, which came in contact with the nylon reinforcing fibers causing them to become brittle and crack due to hydrolysis by water and CO_2 at high temperature.

A 3.5″ 103 bar (1500 psi) 82°C (180°F) RTP line with HDPE liner operating at 76 bar (1100 psi) and 52°C (126°F) with production rate of 5.8 MMSCFD (million

Figure 27.7 Example of failure of reinforced thermoplastic pipe line due to excessive loading at couplings.

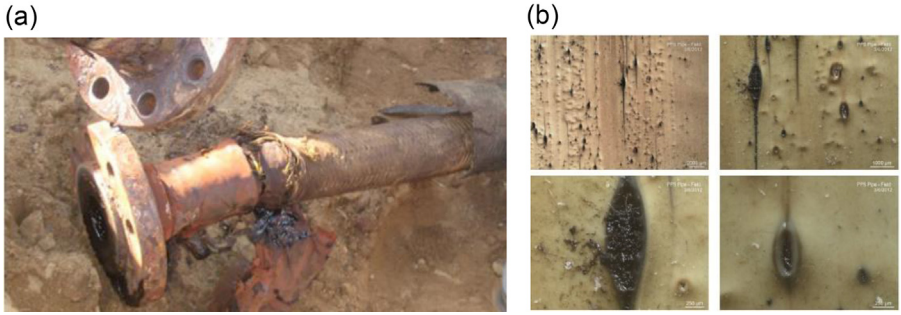

Figure 27.8 Reinforced thermoplastic pipe line failure showing failure of liner, reinforcement fibers, and outer jacket (a) and blistering and cracking of the liner with the axial markings are manufacturing anomalies (b).

Figure 27.9 Failure due to rock damage on reinforced thermoplastic pipe line.

standard cubic feet per day) failed after a month in operation. The analysis showed that the failure was as a result of rock impact as shown in Fig. 27.9.

A 4″ RTP line with HDPE liner in gas service operating at 83 bar (1200 psi) and 80°F failed in service. The line was unburied and unconstrained. The line failed after over a year in service as a result of uncontrolled movement resulting in kinking (Fig. 27.10).

A 3.5″ 83 bar (1500 psi) 82°C (180°F) RTP line operating at 76−90 bar (1100−1300 psi) and 79°C (175°F) in continuous service, failed after several months in service. The failure was attributed to exceeding operating limits of the liner (Fig. 27.11).

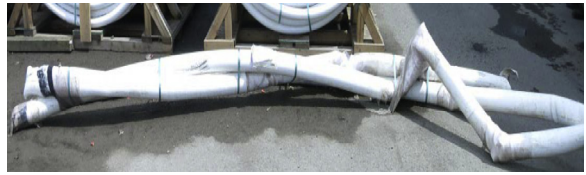

Figure 27.10 Example of reinforced thermoplastic pipe line failure due to kinking.

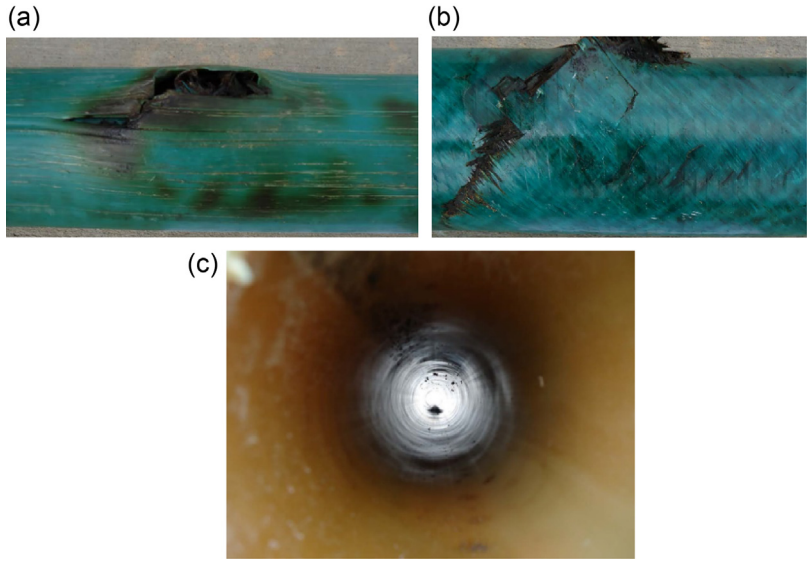

Figure 27.11 Typical failure of reinforced thermoplastic pipe line due to exceeding operating limit. Note discoloration and degradation of the liner in (c).

A 3.5″ 103 bar (1500 psi) 60°C (140°F) RTP line operating at 90 bar (1300 psi) initially, with gradual drop to 52 bar (750 psi) and 41°C (105°F), failed after nearly 12 months in service. Several failures had occurred but over 90% of the lines were still in operation. Different failure patterns were observed: liner collapse, jig saw tooth failure, laminate cracking, and spiral cracking. Sections from the failed pipe when tested showed suppressed mechanical and chemical properties. In some cases the liner suffered significant discoloration and collapse (Fig. 27.12). The analysis showed the degradation in properties was likely a result of chemical attack and/or fatigue due to severe cycling. Neither case could be substantiated from operating data, raising question on the quality of the liners of the failed lines. The failure was likely a result of

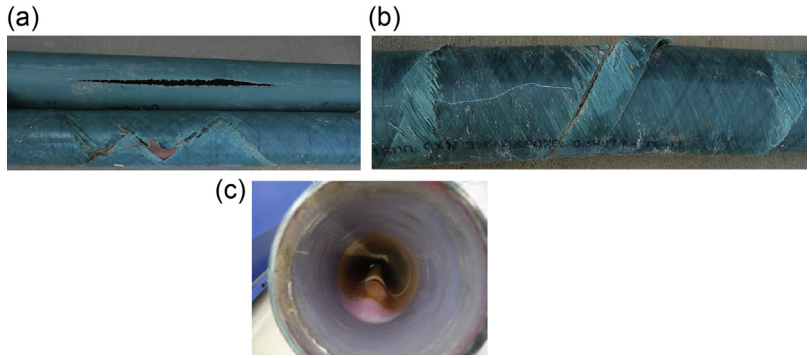

Figure 27.12 Failure of reinforced thermoplastic pipe line that initiated as liner collapse shown in (c).

exceeding operating limits of the installed liner and exposure to pressure cycling and sudden depressurization.

27.10 Future trends in development of nonmetallics

As experience with nonmetallic materials accumulates, the deficiencies in the incumbent material technologies become clear. New polymer developments usually result in very expensive materials with better high-temperature behavior or enhanced chemical resistance. Yet the fitness for service test methods lag new polymer development. Material failures can be attributed to a large variety of causes, including chemical attack, short- and long-term mechanical overloading, pressure cycling, and radiation (UV) damage. Most experts identify chemical resistance as a key area in which further development is needed. Standard test methods to assess chemical resistance in oil and gas applications are in development at ISO and there is active discussion of how to develop an accelerated lifetime test for a wider variety of thermoplastics and thermosets, as has been done for PA11 and PA12 in API 17TR2. Eventually it will be necessary to include mechanical loading at the same time as chemical exposure. Anecdotal evidence points to that combination as more damaging than either factor alone.

The effect of flow rate and erosion due to solids has limited the use of nonmetallic materials to flow velocity of 10 m/s (33 ft/s) in solid-free systems mainly as a result of lack of experimental data and models.

Beyond new materials is the development of new structures taking advantage of the benefits of combinations of materials, both new and existing. Composites fall into this category. It is not difficult to identify materials with desired characteristics, but the manufacturing technologies needed to realize complex structures are in constant evolution. Simply placing the materials together in the right orientation is not necessarily sufficient to a successful application. It is often necessary to treat the surface of one component with a chemical that makes possible good adhesion to the other component. This is not always straightforward and is the subject of ongoing research.

Finally, one important challenge in the use of nonmetallics is the difficulty of inspection using NDE methods. Because nonmetallics are not magnetic conventional pipeline wall inspection tools and weld inspection tools are rendered useless. NDE methods are the subject of academic and commercial research, although few developments have been widely applied.

27.11 Summary

Nonmetallic components have been in use for nearly 50 years and have proven as a viable product for compacting corrosion, weight saving, and cost-effectiveness and have established good track record in various applications. The use of these materials requires in-depth knowledge of the limitation and compatibility with operating environments. Failures have occurred where wrong materials were selected, operating limits were exceeded, and exposure to damaging environment and failure to adhere

to construction practices have occurred. Lack of data on many of the new materials and limited field application will slow the expansion of use of these materials. Several new materials and product lines offer further extension to the use of these materials as they become widely accepted, more cost-effective, and readily available. Nonmetallic products will continue to play a role in exploitation of oil and gas resources and other energy sectors.

References

[1] S. Berge, T. Glomsaker, Robust Material Selection in the Offshore Industry − Flexible Risers, Report MT70 A040408, Norwegian Marine Technology Research Institute, 2004.
[2] S. Papavinasam, Corrosion Control in the Oil and Gas Industry, Elsevier Publisher, 2015.
[3] D. Dawson, Composites extend service of corrosion-prone oil and gas steel subsea pipelines, Composite World (August 2015) 50−55.
[4] V. Savino, B.M. Al-Jarallah, A.K. Al-Dossary, The utilization of nonmetallic valves in oil producing facilities, Paper No. 31-NM-06, in: 14th Middle East Corrosion Conference, 2013.
[5] A.G. Gibson, J.M. Linden, D. Elder, K.H. Leong, Non-metallic pipe systems for use in oil and gas, Plastics, Rubber and Composites 40 (10) (2011) 465−480.
[6] J. Wolodko, B. Fotty, T. Perrars, Application of Non-metallic materials in oil sands operations, in: Paper No. 7298 NACE International Corrosion Conference, 2016.
[7] A. Comeau, Y. Bar, Significant reduction of corrosion induced pipe failures in oil sands/SAGD facilities using PE-Xa materials, Paper No. 7890, in: NACE International Corrosion Conference, 2016.
[8] Pipeline Rehabilitation by Slipping with PE Pipe, Plastic Pipe Institute, pp. 397−420 (Chapter 11).
[9] B. Dalmolen, S.J. Picken, I.W. Sengers, Comparative study of polyethylene based resins for flexible oil and gas pipeline applications for use at higher temperature, Paper No. 14044, in: 15th Middle East Corrosion Conference, 2014.
[10] ISO 24033:2009, Polyethylene of Raised Temperature Resistance (PE-RT) Pipes − Effect of Time and Temperature on the Expected Strength.
[11] J.F. Mason, Pipe liners for corrosive high temperature oil and gas production applications, in: Paper No. 80 NACE International Corrosion Conference, 1997.
[12] A.M. Berry, Installation of polyamide-11 liners for sour service using loose fit technology, Paper No. 00781, in: NACE International Corrosion Conference, 2000.
[13] H. Ramathal, T. Baus, D. Raudies, Linear PPS for use in high temperature oil and gas sour/acid fluid handling, Paper No. 6, in: Oilfield Engineering with Polymers, Smithers RAPRA, 2006.
[14] N. Messina, M. Colladon, P. Fossati, C. Meynet, Internal lining of carbon steel flowlines with plastic liner based on a fluorinated polymer: introduction of the concept and evidences on CAPEX and OPEX reductions, in: Offshore Technology Conference Brasil Paper no. OTC-26150-MS, 2015.
[15] C.J. Kau, L. Vanderschuren, Polyketone polymers: a new liner material for corrosion control in the oil and gas industry, Paper No. 787, in: NACE International Corrosion Conference, 2000.
[16] Research Report 039, The Cost Effective Use of Fiber Reinforced Composites Offshore, UK Health and Safety Executives, 2003.

[17] S.P. Turnipseed, Fiber glass pipe effective for offshore water handling, Oil and Gas Journal (1995).
[18] Y. Yuan, J. Goodson, Advanced composite downhole applications and HPHT environmental challenges, Paper No. 04616, in: NACE International Corrosion Conference, 2004.
[19] D. McCauley, S. Linnemann, The first ETFE lined dual-laminate equipment: a case study after 13 years of service, Paper No. 05520, in: NACE International Corrosion Conference, 2005.
[20] D.L. Keeler, Thermoplastic dual laminate applications the good and the bad, Paper No. 03611, in: NACE International Corrosion Conference, 2003.
[21] K. Morland, B. Weller, The use of reinforced thermoplastic pipe (RTP) in liquid hydrocarbon transfer: an Australian case study, paper 14213, in: 15th Middle East Corrosion Conference, 2014.
[22] G.R. Ruschau, Novel polymers for applications as liners, Paper No. 00780, in: NACE International Corrosion Conference, 2000.
[23] A.S. Al-Omari, M.S. Mehdi, A.F. Al-Marri, J. Schell, Revolutionary non-metallic liners to rehabilitate the aged/corroded carbon steel water injection laterals, Paper No. 3756, in: NACE International Corrosion Conference, 2014.
[24] K.E. Szklarz, J.J. Baron, Learning from thermoplastic liner failures in sour gas pipeline services and replacement liner design and installation, Paper No. 04702, in: NACE International Corrosion Conference, 2004.
[25] J.F. Mason, J.D. Alkire, Effect of rapid decompression condition on liner materials, Paper No. 00782, in: NACE International Corrosion Conference, 2000.
[26] J. Taylor, S. Groves, B. Melve, S. Frost, Effective annular venting of thermoplastic liners for added value and benefits, Paper No. 00784, in: NACE International Corrosion Conference, 2000.
[27] B. Bulleri, A. Ticci, M. Genoni, J. Sutherland, Engineering thermoplastic-liners, Paper No. 04705, in: NACE International Corrosion Conference, 2004.
[28] G. Hopkins, B. Linneman, Case studies of dual-laminate FRP in service environments, Paper No. 04607, in: NACE International Corrosion Conference, 2004.
[29] J.L. Bustillos, W.F. Holtzclaw, Built in accordance with ASME RTP-1, what does this really mean?, Paper No. 00538, in: NACE International Corrosion Conference, 2000.
[30] R. Smallwood, Life cycle maintenance consideration of non-metallic process equipment compared to metallic equipment, Paper No. 06223, in: NACE International Corrosion Conference, 2006.
[31] E. Lyons, Engineered thermoplastic solutions: advantages of dual laminate piping systems, Paper No. 04610, in: NACE International Corrosion Conference, 2004.
[32] E. Lyons, Case history of dual laminate system life cycle cost analysis vs. metallic piping, Paper No. 07539, in: NACE International Corrosion Conference, 2007.
[33] A. Vaidya, K. Spoo, Performance and cost comparison of stainless-steel and E-CR-FRP composites in corrosive environments, Paper No. 3910, in: NACE International Corrosion Conference, 2014.
[34] Plastics Pipe Institute Technical Report TR-4, PPI Listing of Hydrostatic Design Basis (HDB), Hydrostatic Design Stress (HDS), Strength Design Basis (SDB), Pressure Design Basis (PDB) and Minimum Required Strength (MRS) Ratings for Thermoplastic Piping Materials or Pipe, Plastics Pipe Institute, Irving, TX, USA, 2016.
[35] ASTM D2837, Standard Test Method for Obtaining Hydrostatic Design Basis for Thermoplastic Pipe Materials or Pressure Design Basis for Thermoplastic Pipe Products, ASTM International, West Conshohocken, PA, USA.

[36] ASTM D2992, Standard Practice for Obtaining Hydrostatic or Pressure Design Basis for "Fiberglass" (Glass-Fiber-Reinforced Thermosetting-Resin) Pipe and Fittings, ASTM International, West Conshohocken, PA, USA.
[37] ISO 9080, Plastics Piping and Ducting Systems − Determination of the Long Term Hydrostatic Strength of Thermoplastics Materials in Pipe form by Extrapolation.
[38] G.R. Ruschau, Consideration for polymers in enhanced oil recovery operations, Paper No. 86, in: NACE International Corrosion Conference, 1997.
[39] J.J. Baron, K.E. Szklarz, L.C. MacLeod, Non-metallic liners for gas/condensate pipelines, in: NACE Corrosion 2000 Conference Paper 00783, 2000.
[40] API Specification 17J, Specification for Unbonded Flexible Pipe, fourth ed., American Petroleum Institute, Washington DC, 2014.
[41] API Technical Report 17TR2, The Ageing of PA-11 in Flexible Pipes, first ed., American Petroleum Institute, Washington, DC, USA, June 2003.
[42] C. El-Mazry, O. Correc, X. Colin, A new kinetic model for predicting polyamide 6-6 hydrolysis and its mechanical embrittlement, Polymer Degradation and Stability 97 (2012) 1049−1059.
[43] J. Berger, J. Franosch, C. Schuett, A. Dowe, The ageing of offshore polyamides under services conditions in subsea applications, Paper OTC-22613-PP, in: Offshore Technology Conference Brasil, Offshore Technology Conference, 2011.
[44] J. Mason, A. Ponda, D. Demicoli, M. Stanley, Case study: engineered polyamide 12 (PA12) pipeline liner for management of sour gas corrosion at elevated temperatures, in: NACE Corrosion Conference 2017, Paper 9592.
[45] B. Flaconneche, M.H. Kopffer, J. Martin, C. Taravel-Condat, High pressure permeation of gases in semicrystalline polymers: measurement method and experimental data, in: Oilfield Engineering with Polymers, RAPRA Technology Limited, 2001.
[46] B. Melve, Principles for life time estimation of PVDF pressure barriers in high temperature flexible pipes based on fracture mechanics, in: Proceedings of 20th International Conference on Offshore Mechanics and Arctic Engineering, Paper MAT-3575, June 3−8, 2001, Rio de Janeiro, Brazil, 2001.
[47] J. Ren, Y. Yuan, D. Gerrard, Performance gaps of polyetheretherketone (PEEK) in ultra-HP/HT oil and gas applications, in: Proceedings of ANTEC 2014, Society of Plastics Engineers, Newtown, CT, USA, 2014.
[48] H.J.M. Jansen, N.I.S. Al-Behlani, H.A.H. Qamshoey, Application of non-metallic line pipe materials to reduce life cycle cost of upstream oil & gas gathering production facilities, Paper No. 05527, in: NACE International Corrosion Conference, 2005.
[49] ISO 24033:2009, Polyethylene of Raised Temperature Resistance (PE-RT) Pipes — Effect of Time and Temperature on the Expected Strength, International Standards Organization, 2009.
[50] S. Dreckötter, H. Hammar, Prolonged ISO 9080 testing revealing the full capabilities of PE-X, in: Proceedings of the 17th Plastic Pipes Conference PPXVII Sept 22−24, 2014, Chicago, USA, 2014.
[51] S. Beckwith, M. Greenwood, Don't Overlook Composite FRP Pipe, Chemical Engineering, May 2006, pp. 42−47.
[52] Y. Yin, Making the transition from metals to FRP − case history, Paper No. 05508, in: NACE International Corrosion Conference, 2005.
[53] A. Parvez, A. Sakr, M. Yates, B. Weller, Suitability of reinforced thermoplastic pipe in crude oil containing aromatic solvents and additionally alkaline liquids for enhanced oil recovery, in: Gas & Oil Expo & Conference North America, 2011. GOXC11−102.
[54] Polyflow Thermoflex pipe, http://www.polyflowglobal.com/product/why-thermoflex/.

[55] Soluforce™ High Pressure Piping Systems Catalog, November 2011, p. 17. Pipelife Nederland BV.
[56] J. Mason, Thermoplastic liners for oilfield pipelines, in: R.W. Revie (Ed.), Oil and Gas Pipelines: Integrity and Safety Handbook, first ed., John Wiley & Sons, Inc., 2015, pp. 447−455 (Chapter 31).
[57] Design, installation, and operation of thermoplastic liners for oilfield pipelines, in: NACE Standard RP0304-2016, NACE International, Houston, TX, 2016.
[58] J. Mason, Pipe liner material wears well in tests of field specimens, Oil and Gas Journal 97 (October 18, 1999) 76−81.
[59] D. Duttlinger, Poly lined tubing is cost effective option to reduce downhole failures, in: The American Oil and Gas Reporter, November 2001.
[60] www.WesternFalcon.com.
[61] A.Y. Asiri, M.A. Parvez, Q.J. Sharif, S.I. Al-Turki, G. Radhakrishnan, Composite lined carbon steel tubular for downhole production applications, Saudi Aramco Journal of Technology (Summer 2014).
[62] DNV RP O501 Erosive Wear in Piping Systems, 4.2−2011. Det Norske Veritas.
[63] R.H. Davis, The versatility of internal thermoplastic tubular liners in mitigating downhole corrosion and wear, Paper No. 03148, in: NACE International Corrosion Conference, 2003.
[64] K. Bethel, et al., The development and validation of a high strength, self monitoring, composite tight fit liner for offshore pipelines and risers, in: Fourth International Conference on Composite Materials for Offshore Operations. Houston, TX, October 4-6, 2005.

PART VI

Advancements in modeling and prediction

Pitting corrosion

28

Sankara Papavinasam
CorrMagnet Consulting Inc., Ottawa, ON, Canada

28.1 Introduction

Internal pitting corrosion is a significant factor in the degradation of pipelines and assets used in the oil and gas industry. Both carbon steel and corrosion-resistant alloys (CRAs) can undergo pitting corrosion. The susceptibility of metals to pitting corrosion and pitting corrosion rate (PCR) depend on the metallurgy of the metal and the environment in which it is operating.

Carbon and low-alloy steels are extensively used in the oil and gas and other industries. At least 80% of all components in the oil and gas industry are made from carbon steels because they are inexpensive, readily available, and easily fabricated. Every efforts, including changes to processes, are made to use carbon steels. When carbon and low-alloy steels cannot withstand operating conditions, CRAs are used. Localized corrosion, in the form of isolated pits on both the internal and external surfaces, continues to cause failures of carbon steel pipes, pipelines, and other process equipment [1]. Although the resistance of CRAs to pitting corrosion is far higher than that of carbon steel, they are also susceptible to pitting corrosion.

Modeling pitting corrosion of carbon steel and CRAs is necessary because it will help to estimate the remaining service life of an asset, type, and extent of mitigation (e.g., corrosion inhibitors, biocides, or alternative materials) as well as the frequency of monitoring, inspection, and maintenance.

This chapter describes various principles that can be used to model pitting corrosion and predict pitting corrosion rate.

28.2 Theories of pitting corrosion

If the corrosion proceeds uniformly over the entire surface then the metal becomes thinner uniformly. This happens when the percentage area of anode and cathode is 50% on the entire structure and for the entire duration of service. Uniform or general corrosion represents loss of metal on a tonnage basis, but this type of corrosion is not of concern in the oil and gas industry because it seldom occurs. In a way this type of corrosion is the most desirable corrosion type because the probable life can be predicted accurately. Most common corrosion mechanisms are localized, i.e., corrosion is limited to specific areas or parts of a structure resulting in unexpected or premature

Trends in Oil and Gas Corrosion Research and Technologies. http://dx.doi.org/10.1016/B978-0-08-101105-8.00028-0

failures. Many factors alone or in combination with one another make uniform corrosion become localized corrosion. These factors include variations of:

Metallurgy	The grains and grain boundaries are at different energy levels, facilitating localization of corrosion. In addition to metallographic inhomogeneities, impurities, oxides, inclusions, mill scale, orientation of grains, dislocation arrays, microstructure, precipitated phases, localized stresses, scratches, and nicks facilitate localized corrosion.
Corrosion potential	Corrosion potential is not uniform across the entire surface.
Surface layers	If the product of a corrosion reaction dissolves in the environment, the corrosion continues to take place uniformly. Beyond certain duration, because of solution saturation, some products may deposit back on the surface. If the deposition occurs uniformly, then the surface is fully covered, and no corrosion reaction takes place. This seldom occurs. The surface layers are formed discontinuously and at various thicknesses at various locations of the structure.
Extraneous materials	When extraneous materials such as sand, clay particles deposit on the surface, they facilitate nonuniform corrosion.
Dissolved salts	The presence of dissolved salts may alter the corrosion environments locally.
Velocity	The effect of velocity is complex and depends on the characteristics of the metal and the environments to which it is exposed. If the velocity of the flow across the entire surface is constant, then general corrosion takes place, but velocity varies across the surface facilitating localization.
Temperature	Temperature facilitates diffusion and convection. In general an increase in temperature increases the corrosion rate. If there is a temperature gradient along the pipeline, then localized corrosion conditions prevail.

The theories of localized pitting corrosion may be broadly classified into classical and nonclassical.

28.2.1 Classical

The pitting corrosion of CRAs can be explained by classical theory. According to that theory, the process of pitting corrosion takes place in three stages [2]:

1. Formation of a passive film or surface layers on the metal surface
2. Initiation of pits at localized regions on the metal surface where films or surface layers break down.
3. Pit propagation

Passive films generally form as a bilayer, with a compact layer adjacent to the metal and an outer layer comprising a precipitated phase that may incorporate anions

and/or cations from the solution. Passivity is still observed in the absence of the outer precipitated phase; hence, passivity is attributed to the compact inner layer. The precipitated outer layer may often be unstable. Although these layers can have a dramatic effect on film properties, they have not been systematically investigated.

There is much current debate concerning the initiation of pitting corrosion. One approach puts an emphasis on the inherent microscopic defects on the metal surface: inclusions, grain boundaries, scratches, etc. (a priori), whereas the other acknowledges that a nonuniformity on the metal surface and its development to visible dimensions occur after a passive metal is placed in a corrosive medium (a posteriori). The priori approach assumes that heterogeneities are present on the passive metal, whereas the posteriori approach assumes an induced heterogeneity at the interface between a passive metal and corrosive media. In connection with a posteriori assumptions, the significance of stochastic or fluctuation processes have been stressed as the initial step of pitting. Experimental pit initiation results show significantly more scatter than those for other types of corrosion, although the origin of this scatter is still open to discussion. Both the stochastic and deterministic approaches have value and are not mutually exclusive.

The final stage during pitting corrosion is the formation of stable and continuously propagating pits. This happens when the pits become sufficiently large and conditions and processes taking place are closely related to those occurring in crevice corrosion.

28.2.2 Nonclassical

Localized pitting corrosion of carbon steel may be explained by nonclassical pitting corrosion theory. According to this theory, the primary passive layer that has traditionally been associated with pitting corrosion of CRAs (classical theory) is not present and surface layers are formed because of corrosion of carbon steel in a given environment. These surface layers may be considered as the precipitated outer layers as defined in the classical pitting corrosion mechanism.

1. The metal will undergo uniform corrosion until the surface layer is formed.
2. As surface layer(s) form the corrosion rate decreases.
3. If the surface layers completely and permanently cover the surface, the metal underneath will be fully protected and corrosion rate will be low. A compact surface layer can decrease the corrosion rate to as low as 4 mpy or 0.1 mm/y.
4. If the surface layers are destroyed or removed, accelerated corrosion will take place, and the rate will reach rate found in Step 1 (this process may also be known as pit initiation) and as additional surface layer(s) form, the corrosion rate will decrease and reach rate found in Step 3 (this process may be known as repassivation or reformation of surface layer).
5. The process of pit initiation and repassivation will take place alternatively until the pit reaches a critical depth at which time repassivation process does not take place at the tip of the pit. At this point the pit will continue to grow (pit propagation phase). The rate of pit propagation may exceed the rate found in Step 3.

Thus in the presence of surface layers the corrosion rates will have several values: rate before surface layer formation, rate during the formation of surface layer, steady-state corrosion rate in the presence of surface layer, rate when the surface layers are destroyed, and pit propagation rate.

When carbon steel is exposed to oil and gas operating environment it will undergo uniform corrosion for short duration (for about 12 h) before surface layers are formed. Under the operating conditions of oil and gas industry, three types of surface layers can form on carbon steel: iron carbonate, iron sulfide, and iron oxide in the presence of carbon dioxide, hydrogen sulfide, and oxygen, respectively. When the surface layers form on the carbon steel, the corrosion rate decreases. The kinetics of FeS formation is higher than that of $FeCO_3$ formation. Furthermore, addition of corrosion inhibitors and/or presence of oil layer on the metal surface may reinforce the surface layer.

The types, morphology, and kinetics of layer formation depend on several operating variables, including flow rates and compositions of oil, gas, brine, and solids, partial pressures of acid gases, total pressure, temperature, microbial activities, and duration of operation. The types and morphology determine the susceptibility of carbon steel to localized pitting corrosion.

- Compact, adherent, and uniform surface layer protects carbon steel surface from pitting corrosion.
- Noncompact, loosely adherent, and nonuniform surface layers increase susceptibility of carbon steel for pitting corrosion.

28.3 Models for predicting pitting corrosion rates

Field operators are not only interested in the probability of pitting corrosion but also in the rate of pitting corrosion, i.e., kinetics. Almost all (kinetic) models developed for predicting pitting corrosion of carbon steel in the oil and gas industry are based on nonclassical theory and those developed for CRAs are based on classical theory. Furthermore, depending on the data and techniques used, the kinetic models to predict PCR may further be classified into those based on corrosion science, electrochemical science, and corrosion engineering principles.

28.3.1 Corrosion science

The corrosion science approach to developing models that predict pitting corrosion involves the following steps:

- The factors influencing corrosion are assumed.
- Short-term laboratory tests are carried out to determine the extent of the influence of these parameters on general corrosion rates.
- A theoretical explanation (based on corrosion kinetics and/or thermodynamics) is developed.
- The influences of various parameters are integrated.

Several corrosion science models are available, and only one prominent model is discussed below. Many other corrosion science models either corroborate this model or provide slight improvement to this model.

The model developed by de Waard and Milliams is the most frequently referenced model used to evaluate internal corrosion [3–5]. The first version of this model was

published in 1975, and it has since been revised several times. However, it should be noted that this model was specifically developed for general corrosion. It cannot be applied to predict localized pitting corrosion.

Corrosion rates were determined in the laboratory using polished cylindrical X-52 carbon steel specimens in a 0.1 wt% NaCl solution, saturated with carbon dioxide (CO_2) and oxygen-free nitrogen. The corrosion rate was monitored using the linear polarization resistance technique. Experiments were also performed in an autoclave for 7 days, and mass losses were determined.

Some of the electrodes, particularly at temperatures above 60°C (140°F), became covered with a black layer, while the corrosion rate decreased. In a stagnant environment, this effect was observed even at 40°C (104°F). To account for the changes in CO_2 solubility and the dissociation constant, the pH was measured as a function of temperature at 1 bar (14.5 psi) CO_2 partial pressure.

At a constant pH level, the effect of temperature on corrosion rate is characterized by an activation energy of 10.7 kcal/mole. Based on these simple experiments, it was concluded that the uniform corrosion rate of carbon steel as a function of CO_2 partial pressure and temperature could be predicted, provided that surface layer formation does not occur. Both the de Waard−Milliams equation and the nomogram that was subsequently developed have gained wide acceptance. Additionally, correctional factors were introduced to account for the effects of total pressure, scaling, and hydrocarbons.

In the earlier versions of the model, there was no significant consideration of the effects of liquid flow velocity on the CO_2 corrosion rate. The corrosion reaction was assumed to be activation controlled, although the observed corrosion rates were, in some cases, about twice the rate predicted. Therefore, a semiempirical equation was developed to describe and predict the effect of the flow rate.

In 1995, the effect of carbides on the CO_2 corrosion rate was addressed, with a stipulation that the modification proposed (which would account for differences between various low-alloy steels) should be regarded as tentative and that it would only apply under conditions where protective films do not form.

Both DeWaard and Milliam models and several of their derivatives are useful in establishing the general corrosion rate (in Step 1 of the nonclassical theory) and in understanding the types of surface layers formed (in Step 2). Because of the short-term laboratory tests and non-evaluation of corrosion rates after surface layer formation, the corrosion science models do not provide rates in the presence of surface layers; frequency of pit initiation and repassivation and their kinetics; and pit propagation rates.

28.3.2 Electrochemical models

The electrochemical models mostly follow the classical PCR theory. Several models are available, but only a few are described here to illustrate how electrochemists model pitting corrosion.

Macdonald [6] developed a point-defect model for the steady-state properties of passive films that form on metals and alloys in aqueous environments. The model predicts that the steady-state thickness of the barrier film and the log of the steady-state

current vary linearly with applied voltage. The Macdonald model is used to calculate steady-state thickness (Lss) of surface layers [6]:

$$\mathrm{Lss} = \frac{1}{\varepsilon}\left[1 - \alpha - \frac{\alpha\alpha_d(\delta - \chi)}{2}\right]V - \frac{1}{2K}\left[n - \frac{2\beta\gamma}{2.303}\right]\ln C_{\mathrm{H}^+} + \frac{1}{2K}\ln\left[\frac{4KD_oC_o^L}{\chi^k K_{s^o}}\right] \quad (28.1)$$

where

$$\gamma = F/RT \quad (28.2)$$

$$K = \varepsilon\gamma \quad (28.3)$$

where Lss represents steady-state surface layer thickness; ε, electric field strength; α, constant depending on electric potential drop across film−solution interface; α_d, transfer coefficient; δ, constant depending on passive film nature; χ, stoichiometry of film; β, constant depending on potential drop across the film−solution interface; γ, activity coefficient; K, Macdonald constant; V, potential; n, kinetic order of primary film dissolution; C_{H^+}, hydrogen ion concentration; D_o, diffusion coefficient; C_o, concentration of chloride ions; L, thickness of passive film; and K_{s^o}, reaction rate constant.

In Eq. (28.1), the dependencies of the surface layer thickness on the applied voltage and hydrogen ion concentration (or pH) are separated into the first and second terms on the right-hand side, respectively. The third term on the right-hand side of Eq. (28.1) reflects the kinetics of dissolution of the barrier film at the film−solution interface as well as the transport properties of oxygen vacancies in the film.

Macdonald [7] further developed a deterministic model to describe the surface layer breakdown and pit nucleation. According to the model, the breakdown potential,

$$V_c = \frac{4.606RT}{c^{aF}}\log\left(\frac{J_m}{J^o u^{-c/2}}\right) - \frac{2.303RT}{aF}\log(a_x) \quad (28.4)$$

where V_c represents breakdown potential; R, gas constant; T, temperature; α, depends on the electrical potential drop across the film−solution interface; F, Faraday constant; J_m, vacancy flux in metal phase; J^o and u, Macdonald constants as defined in Eqs. (28.5) and (28.6), respectively; χ, stoichiometry of the film; a_x, thermodynamic activity of the aggressive anion (e.g., Cl^-) in the solution, and

$$J^o = \chi KD[N_v/\Omega]^{1+\chi/2}\exp\left(-\Delta G_s^o/RT\right) \quad (28.5)$$

$$u = \left(\frac{N_v}{\Omega}\right)\exp\left[\frac{\Delta G_{A-1}^o - \beta F\mathrm{pH} - F\phi_{f/s}^o}{RT}\right] \quad (28.6)$$

$$K = F\varepsilon/RT \tag{28.7}$$

$$\phi_{f/s} = \alpha V + \beta \mathrm{pH} + \phi^o_{f/s} \tag{28.8}$$

where D, diffusivity of cation vacancies; N_v, Avogadro's number (6.023×10^{23}); Ω, electric field strength within the film; ΔG^o_s, thermodynamic free energy; $\phi^o_{f/s}$, Gibbs energy for Cl^- absorption; and ϕ_{fls}, Gibbs energy for cation vacancy formation.

By combining Eq. (28.4) through Eq. (28.8), an expression for the induction time has been derived

$$t_{\mathrm{ind}} = \xi' \left[\exp\left(\frac{\chi \alpha F \Delta V}{2RT} \right) - 1 \right]^{-1} + \tau \tag{28.9}$$

where t_{ind}, induction time for pit nucleation; ξ', defined in Eq. (28.10); ΔV, defined in Eq. (28.11); and τ, Macdonald constant.

It is assumed that beyond the induction time the probability of at least one stable pit is formed.

$$\xi' = \xi / J^{o_{u-\chi/2}} (a_x)^{\chi/2} \exp\left(\frac{\chi \alpha F V_c}{2RT} \right) \tag{28.10}$$

$$\Delta V = V - V_c \tag{28.11}$$

where ξ, Macdonald constant; ΔV, change in potential; V_c, breakdown (critical) potential; and V, applied potential.

Several electrochemical models are available to predict kinetics of pit growth rate. However, these five models are described here to illustrate the complexity of electrochemical pit growth models.

Tester [8] developed a model to distinguish between two distinct phases of pit growth in nickel and stainless steel in concentrated chloride solutions. According to this model in the early period of dissolution, the electrode surface is flush with the surface of the cavity, and a semiinfinite approach has been used to model the diffusion process that causes the electrolyte concentration to increase at the metal surface. After the initial period of saturation of the dissolving cation species at the metal-solution interface, a quasi−steady-state period of diffusion control commences.

The time-dependent depletion of corrosive species can be obtained from this model. From the depletion rate, the pit growth rate is determined. Pit growth is controlled by diffusion with a concentration-driving force ($C_s - C_b$).

$$l = \frac{n\mathbf{F}D(C_s - C_b)}{i} \tag{28.12}$$

The parameters are defined in Table 28.1, and i_o, current density, is given by:

$$i^{-2} = i_o^{-2} + \frac{2Mt}{n^2\mathbf{F}^2 d_M D(C_s - C_B)} \tag{28.13}$$

Table 28.1 Parameters and their values used in pit growth models

Description	Units	Symbol	Tester	Beck	Ateya	Ben Rais	Galvele
Current	A	I	0.001			Eq. (28.17)	
Ionic concentration at the pit tip	Mole/m^3	C_b	0			0	
Current density	A/m^2	i	Eq. (28.12)		0.001		0.001
Pit radius	M	R	0.005	0.005		0.005	
Valency	No units	n	2				
Saturation concentration	Mole/m^3	C_s	8.00E−06	8.00E−06		8.00E−06	
Ionic diffusion coefficient	m^2/s	D	1.29E−9	1.29E−9		1.29E−9	
Bulk Fe^{2+} ions concentration	Mole/m^3	C_1					3.27
Bulk H^+ ion concentration	Mole/m^3	C_{H^+}, C_5			3.16		3.16
Diffusion coefficient (Fe^{2+})	m^2/s	D_1					1.29E−9
Diffusion coefficient (H^+)	m^2/s	D_{H^+}			1.29E−9		
Diffusion coefficient (OH^-)	m^2/s	D_4					1.29E−9
Diffusion coefficient ($Me(OH)_2$)	m^2/s	D_6					1.29E−9
Faraday constant	A·s/mole	F	96,500		96,500	96,500	96,500
Molecular weight	kg/mole	M	0.05585	0.05585		0.05585	

Table 28.1 Continued

Description	Units	Symbol	Tester	Beck	Ateya	Ben Rais	Galvele
Metal density	Kg/m^3	d_M	7870	7870			
Pit diameter	M	d		0.01	0.01	0.01	
Pit area	m^2	A_p		7.85E−05		7.85E−05	
Local current density	A/m^2	i_o			520		
pH	No units	pH			5.5		5.5
Ionic product of water	$Mole^2/L^2$	K_w					1E−14
Time of maximum current	S	t_{max}				20	
Current density at maximum time	A/m^2	i_{max}				0.001	
Beta 1 (Fe^{2+})	L/mole	β_1					3.16E+04
Beta 2 (Fe^{2+})	$L^2/mole^2$	β_2					2.51E+07
Time	S	t	6.31E+07	6.31E+07	6.31E+07	6.31E+07	6.31E+07
Pit depth	M	l	Eq. (28.12)	Eq. (28.14)	Eq. (28.15)	Eq. (28.18)	Eq. (28.19)

Beck [9] assumed that the geometry and migration effects exert opposite and nearly equal influences on the dissolution rate and that they cancel out one another. Under these conditions, the depth of a hemispherical pit, l, at time t, is given by:

$$l = \left[r^2 + \frac{2DC_sM}{d_m} t \right]^{1/2} \tag{28.14}$$

The parameters are defined in Table 28.1.

Ateya and Pickering [10] proposed a model for the combined effect of ohmic, mass transfer, and concentration polarizations on current, concentration, and potential profiles inside a pit or crack in iron, nickel, and copper. The Ateya model assumes that negative potentials are maintained within the pits so that cathodic reactions occur only at the outer surface. The geometry of the pit is such that the depth of the pit is greater than its width. A geometric characteristic value, X, is defined. It is assumed that mass transfer in the electrolyte within the pit takes place by molecular diffusion and ionic migration. The electrolyte considered is a simple acid, which completely dissociates to produce ions. According to the model, the pit depth, l, is given by:

$$l = -\left(\ln \left[\frac{i}{2 \cdot i_o} \right] \right) \cdot X \tag{28.15}$$

where X, the characteristic length, is defined by Eq. (28.16):

$$X = (D \cdot C_b F d / i_o)^{1/2} \tag{28.16}$$

The parameters are defined in Table 28.1.

Ben Rais [11] obtained an analytical solution to calculate the current delivered as a function of time for aluminum undergoing pitting corrosion, based on the following assumptions:

- Diffusion and migration effects are calculated assuming the solution is very dilute.
- Saturation at the bottom of the pit is considered without taking into account the effects of supersaturation, pH variation, and ionic strength.
- Metal hydrolysis can be neglected.

The model has been primarily developed to describe the pit growth in aluminum. According to the model, the current at any time during pit growth is given by:

$$I = \frac{6FA_p}{t_{\max}} \sqrt{\frac{(2C_s - C_b)D}{M}} \left[t^{1/2} - (t - t_{\max})^{1/2} \right] \tag{28.17}$$

From the current, pit depth is calculated using Faraday's law as:

$$l = t \cdot \frac{I}{A_p} \cdot \frac{0.5M}{F} \cdot d_M^{-1} \tag{28.18}$$

The parameters are defined in Table 28.1.

Galvele [12] analyzed the transport processes for pitting of iron and other metals and found that surface layer breakdown could be associated with a depletion of OH^- ligands at the metal−solution interface. Assuming only the first step of cation hydrolysis, important pH changes are shown to be possible during the initial stages of pitting. Pit growth rate can be calculated based on full hydrolysis. The ion concentration profiles inside a pit on a metal (e.g., iron) giving bivalent metal ions, with only soluble species being produced, were calculated by accounting for all chemical species. According to the model, the pit depth, l, is given by:

$$l = \frac{2 \cdot F \cdot C_1 \left\{ D_1 + \frac{D_4 \cdot \beta_1 \cdot K_W}{C_5} + \frac{D_6 \cdot \beta_2 \cdot K_w^2}{C_5^2} \right\}}{i} \tag{28.19}$$

The parameters are defined in Table 28.1.

The applicability of this model to predict the pit's length is somehow difficult because it needs the value of the concentration of Fe^{2+} (C_1) within the pit. This value is virtually impossible to measure experimentally. An incorrect assumption of C_1 results in a poor estimation of the length of the pit.

The classical pitting corrosion growth models based on electrochemical principles may be used to predict pit growth rate of within constrains of input data used in the models. However, the number of scientific parameters required to use electrochemical models and unavailability of many of them make it difficult to use electrochemical models in the oil and industry operating conditions.

28.4 Corrosion engineering models

Corrosion engineering models to predict internal pitting corrosion of oil and gas pipelines are based on nonclassical theory of pitting corrosion. According to these models the internal pitting corrosion of carbon steel in the oil and gas industry operating conditions occurs in four stages (Fig. 28.1):

1. The low- or no-corrosion stage when the internal surface of the pipeline is covered by hydrocarbons, i.e., oil-wet conditions,
2. Formation of surface layers on the steel surface due to corrosion reactions once the surface is covered with water, i.e., water-wet conditions,
3. Initiation of pits at localized regions on the steel surface when surface-layer breakdown occurs, and
4. Pit propagation and eventual penetration of the pipe wall.

Although some corrosion engineering models address one or two stages of internal pitting corrosion of carbon steels, only one model [13−16] integrating all four stages is described in this section.

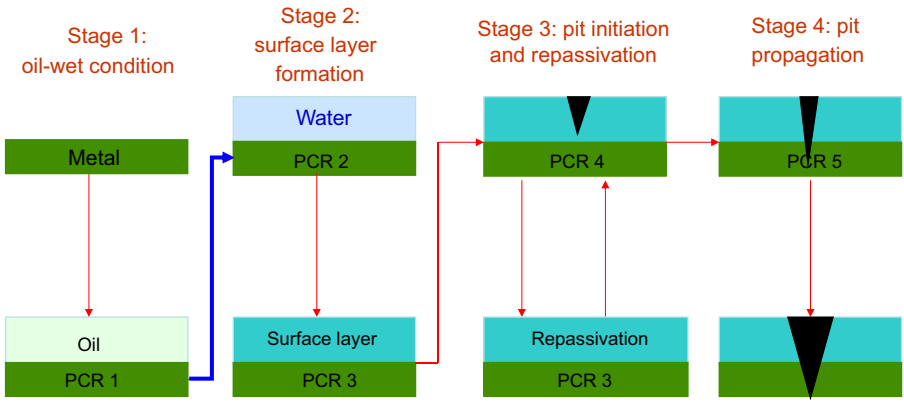

Figure 28.1 Stages of pitting corrosion according to the corrosion engineering model (Papavinasam model).

28.4.1 Stage 1

Oil and gas industry infrastructures do not suffer from corrosion if the surface is wetted and covered with oil or any hydrocarbon. But during operation, water may enter the system. Water enters into a pipeline from various sources:

- A new pipeline, after construction, is hydrotested to ensure its integrity. If the pipe is not dried properly after hydrotesting, water may accumulate at low-lying regions.
- In a production pipeline, water enters from the formation well. Initially the volume of formation water being transported in the pipeline is low, but as production continues the amount of water transported increases.
- Water content of a gas production pipeline depends on the moisture content of the gas. Below dew point, the water condenses out from the gas and accumulates at low-lying regions.
- Transmission pipelines in principle should not carry more than 0.5 vol% of water. Over years of operation, however, water accumulates in low-lying regions of the pipeline.

Whatever the source of water in pipelines, whenever it comes in contact with the surface of pipeline material (typically carbon steel) the surface becomes susceptible to corrosion. Hydrocarbons play an important role in determining whether the water will come in contact with the surface and in determining the corrosivity of the water.

Because of their nonionic nature, hydrocarbons cannot dissolve in ionic water. However, at low concentrations of water, hydrocarbons can form emulsion with the water. The type of emulsion and its stability depend on the type of hydrocarbon, the ionic content of the water, as well as the pressure, temperature, and flow rate.

There are two kinds of emulsions: oil-in-water (o/w) and water-in-oil (w/o). In a w/o emulsion, oil (hydrocarbon) is the continuous phase; therefore, w/o has low conductivity and is noncorrosive. In an o/w emulsion, water is the continuous phase. Therefore o/w has high conductivity and is corrosive. In an operating pipeline, initially the amount of water carried is lower and the amount of oil carried is higher, and the water content progressively increases. The percentage of water at which w/o converts to o/w is known as the emulsion inversion point.

The presence of free water, or of o/w emulsion, does not necessarily lead to corrosion. Under this condition, wettability of the hydrocarbon on the carbon steel determines corrosivity. Based on the wettability, oil can be classified into three categories [13]:

- **Oil-wet surface**: The oil has a strong affinity to be in contact with carbon steel. Oil-wet surfaces physically isolate the pipe from the corrosive environment, and under such conditions, corrosion does not occur.
- **Water-wet surface**: The oil does not have an affinity to be in contact with carbon steel; in fact the oil may not be in contact with the carbon steel at all, even when it is the only phase. A water-wet surface (in the presence of oil) is highly susceptible to corrosion.
- **Mixed-wet surface**: The oil does not have any preference to be in contact with carbon steel. The oil may be in contact with the carbon steel surface as long as there is no competing phase present.

In the presence of free water or o/w emulsion, and on a water-wet surface, hydrocarbon can influence the incidence of corrosion in the water phase. If the hydrocarbon contains water-soluble corrosion inhibitors, it could either prevent (preventive hydrocarbon) or decrease (inhibitory hydrocarbon) corrosion. On the other hand, if the hydrocarbon contains water-soluble corrosive substances, it could increase the corrosion rate (corrosive hydrocarbon). If the hydrocarbon does not contain any water-soluble substances, or substances that could adsorb on steel, it will not have any influence on the corrosivity of brine (neutral hydrocarbon).

The factor responsible for one property may or may not influence other properties. For this reason, all three properties (emulsion, wettability, and corrosivity) are required, and based on them the influence of hydrocarbons can be predicted (Fig. 28.2).

In stage 1, the PCR will be low, i.e., PCR 1 in Fig. 28.1, as long as the oil is wet and is protecting the surface.

28.4.2 Stage 2: surface layers

Once the surface becomes water-wet, corrosion takes place leading to formation of surface layers. Under the oil and gas operating conditions iron sulfide (FeS), iron carbonate ($FeCO_3$), iron oxides (FeO, Fe_2O_3, Fe_3O_4), biofilms, and any combination of them can form. Both composition of the surface layers and morphology of their formation are important. The composition and stability of the layers depend on various factors, including temperature, brine composition, oil composition, steel composition, pressure, velocity, microbes, corrosion inhibitors, and biocides [14].

In stage 2, the corrosion rate will be high at the beginning, i.e., PCR 2 in Fig. 28.1, and as more and more protective layers are formed, it will progressively decrease. When the surface layer formation reaches the steady state the PCR will be low, i.e., PCR 3 in Fig. 28.1.

28.4.3 Pit initiation

On a surface layer—protected surface, pits can be randomly initiated. In a study, experiments have been carried out in a high-temperature, high-pressure rotating cylinder

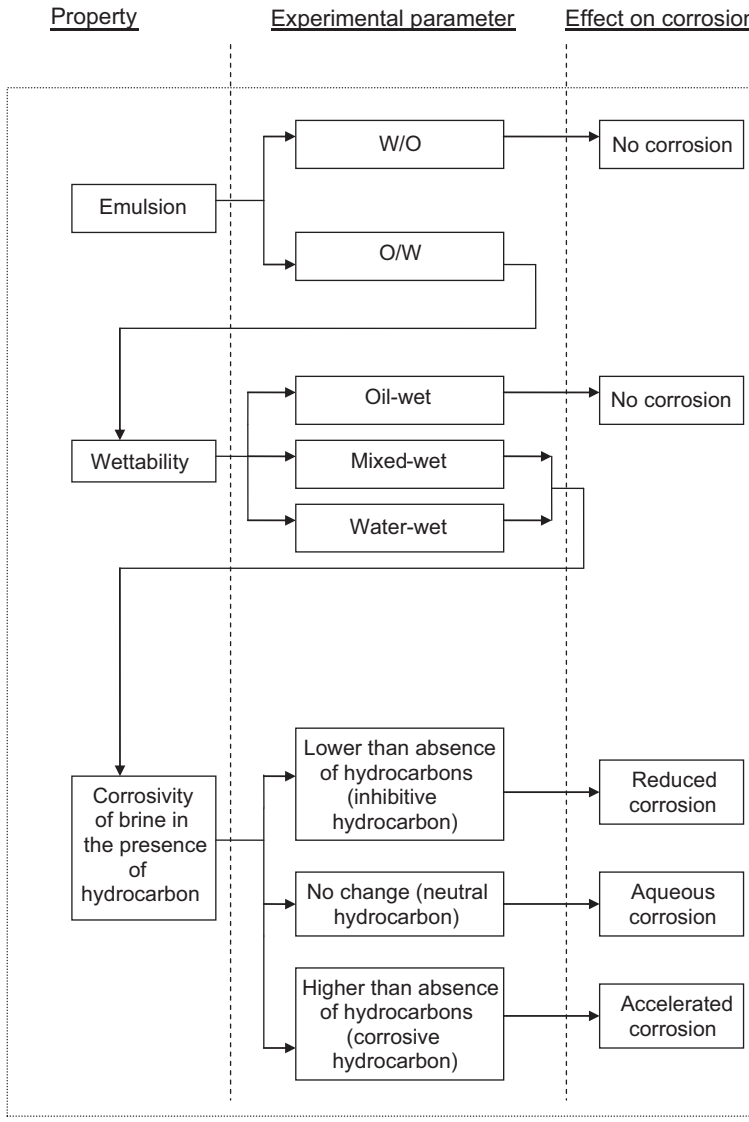

Figure 28.2 Predicting influence of hydrocarbons on internal corrosion of pipelines. Adopted from ASTM G205.

electrode (HTHPRCE) apparatus under 40 conditions to cover the spectrum of conditions found in oil and gas production pipelines in Western Canada [15]. Each experiment was conducted over a period of 100 h. During the experiments, the electrodes were monitored using electrochemical noise technique. After the experiments, the surfaces of the samples were analyzed using a scanning electron microscope (SEM). Potentiodynamic polarization (PP) experiments were also conducted under the same 40 conditions.

Based on the electrochemical noise, SEM, and PP data, it was found that the probability of the initiation of pitting corrosion:

- increased with increase in flow rate, temperature, and chloride ion concentration and
- decreased with increase in oil wettability, H_2S partial pressure, CO_2 partial pressure, total pressure, bicarbonate concentration, and sulfate concentration.

The variation in the probability of initiation of pitting corrosion depends on the type of surface layers formed. Depending on the type of surface layer characteristics, the PCR can be high, i.e., PCR 4 in Fig. 28.1, may be higher than PCR 2.

28.4.4 Pit propagation

When the pits become sufficiently deep, they continue to grow until failure occurs; sometimes the growth rate will accelerate (autocatalytic process), i.e., PCR 5 in Fig. 28.1 can be higher than PCR 4. The depth of a corrosion pit depends on the pit growth rate and the timing of its initiation. Based on experiments conducted in six operating oil and gas production pipelines over a period of 4 years, internal pit growth rates under realistic operating conditions have been determined [16]. The study concluded the following:

- Pit growths in both horizontal and vertical pipelines were similar when the compositions of surface layers were the same.
- When compact layer of single species was formed, the surface was protected from pitting corrosion and that FeS-covered surfaces were less susceptible to pitting corrosion than $FeCO_3$-covered surfaces.
- The pit growth rate increased when the surface layers of multiple species were formed. Sudden changes in the operating conditions appeared to facilitate formation of layers of multiple species, leading to higher pit growth rate.
- In the absence of surface layers, the pit growth rate decreased but not eliminated, because even materials not adherent on to the surface might create uneven distribution of anodic and cathodic areas.

According to the corrosion engineering model described in this chapter, operational parameters required to predict PCR s are (1) production rate of oil, (2) production rate of water, (3) production rate of gas, and (4) production rate of solid, (5) total pressure, (6) partial pressure of CO_2, (7) partial pressure of H_2S, (8) temperature, and (9) concentration of chloride ion, (10) concentration of sulfate ion, and (11) concentration of chloride ion. Each one of the operational parameters individually can alter the PCRs. The ultimate rate at which the pits will propagate depends on the combined effect of all of the operational parameters. Although the individual effect of each of the parameters can be predicted deterministically, determining the combined effect of these variables needs application of statistical principles. Several methods have been used to predict the probability of long-term PCRs based on short-term experiments. In all these approaches, one commonality is the acceptance that the driving force for the pitting corrosion is a “distributed parameter”; the different approaches vary on how “driving force” and “pattern of distribution” are treated.

It is assumed that each operational variable produces an individual pit growth rate (resulting in 11 different PCRs) and that pit growth rate as a result of the variables not considered (e.g., acetic acid effect) is the mean value of these 11 pit growth rates. The 12th parameter does not have any effect on the predicted PCR; it does, however, increase the uncertainty of the prediction. The actual pit growth rate taking place in the oil and gas pipeline is the "distributed function," which is the mean value of the 12 pit growth rates and the uncertainty is expressed as standard deviation. The resultant pit growth rate is the rate at which the pits will start to grow in the localized anodic region where the surface layers are removed. It should be noted that except for one operational variable (i.e., water), removal or control of other variables, does not prevent pit growth although it does change the pit growth rate. The absence of water prevents pitting corrosion regardless of the effect of other variables. In the model described in the chapter, the uncertainty is expressed as standard deviation.

Pits will not continue to grow at the same rate at which they start growing, for various reasons including partial reformation of the surface layers, local solution saturation, change of corrosion potential, and local increase of pH at these locations. As a result, the pit growth rate diminishes parabolically as a function of time.

Thus based on laboratory experiments conducted under pipeline operating conditions and assumptions made on the probabilistic nature of the pitting corrosion, the PCR of oil and gas pipelines can be calculated using Eq. (28.20):

$$\begin{aligned}\text{Pitting Corrosion Rate (mpy)} = \{[\textstyle\sum(-0.33\theta + 55) + (0.51W + 12.13)\\ + (0.19W_{ss} + 64) + (50 + 25R_{solid}) + (0.57T + 20) + (-0.081P_{total} + 88)\\ + (-0.54P_{H_2S} + 67) + (-0.013C_{sulfate} + 57) + (-0.63P_{CO_2} + 74)\\ + (-0.014C_{bicarbonate} + 81) + (0.0007C_{chloride} + 9.2)\\ + (C.R._{general})]/12\}\end{aligned} \tag{28.20}$$

where θ is the contact angle of oil in a water environment; W is (water production rate/water + oil production rates × 100); W_{ss} is wall shear stress; R_{solid} is equal to 1 if the pipeline has solids or 0 if the pipeline does not have solids pipe; T is temperature in degrees celsius; P_{total} is total pressure in psi; P_{H_2S} is partial pressure H_2S in psi; P_{CO_2} is partial pressure of CO_2 in psi; $C_{sulfate}$ is sulfate concentration in ppm; $C_{bicarbonate}$ is bicarbonate concentration in ppm; $C_{chloride}$ is chloride concentration in ppm; $C.R._{general}$ is the average pit growth rates in oil, water, flow, solid, temperature, total pressure, partial pressure of H_2S, partial pressure of CO_2, and chloride; and t is a constant depending on the time.

In developing this model, the following assumptions have been made:

- The type of carbon steel used will not effect of the PCR.
- The volume and type of solid production is assumed to be irrelevant.
- CO_2 and H_2S concentrations are not zero.
- Unless the actual emulsion type is determined, the emulsion is oil-in-water.

Within the constraints of the assumptions made and the range of conditions in which the experiments were conducted, Eq. (28.20) can be used to predict the internal pitting corrosion of sour and sweet carbon steel pipelines.

It should also be pointed out that the elements that drive the PCRs of oil and gas pipelines are the statistical functions and hence the predicted PCR is probabilistic in nature. The incidence error in the prediction was determined using the standard deviations of Eq. (28.20). The driving forces could also be distributed other statistical tools [17,18].

While Eq. (28.20) provides the trend in the variation of PCR when only one variable is changed, under operating conditions of the oil and gas production, some or all variables coexist and coinfluence the localized PCRs. The ultimate rates at which the pits would propagate depend on interactions between any or all of the variables. The interactions can be independent, synergistic, or antagonistic.

- Independent: Presence of other variables does not affect the localized pitting corrosion caused by a particular variable. The model described in this chapter, considers that the variables are independent to one another.
- Synergistic: Presence of other variables mutually increases the localized pitting corrosion caused by each one of them. The net result is that the corrosion rate will be higher than the corrosion rate calculated from the average of corrosion rates due to individual variable. This is also known as autocatalytic effect.
- Antagonistic: Presence of other variables mutually decreases the localized pitting corrosion caused by each one of them. The net result is that the corrosion rate will be lower than the corrosion rate calculated from the average of corrosion rates due to individual variable [19–21].

The predominant types of bacteria associated with microbiologically influenced corrosion (MIC) are sulfate-reducing bacteria, sulfur oxidizing bacteria, iron oxidizing/reducing bacteria, manganese-oxidizing bacteria, acid-producing bacteria, and slime formers. These organisms coexist within a biofilm matrix on metal surfaces, functioning as a consortium, in a complex and coordinated manner. The various mechanisms of MIC reflect the variety of physiological activities carried out by these different types of microorganisms when they coexist in biofilms. Despite decades of study on MIC, how many species of microorganisms contribute to corrosion are still not known with certainty, and researchers continue to report on the formation of biofilms by an ever-widening range of microbial species.

Frequently, an engineer may be required to make an appraisal of the MIC threat with limited information on the corrosion history and with little or no historic microbiological test data. In such cases, a preliminary analysis of the system operating conditions may be sufficient to exclude the MIC threat when these conditions are not compatible for the survival of sessile bacteria/biofilm. With this approach, a qualitative risk score model has been developed. Table 28.2 presents the score according to the MIC model. The PCR_{MIC} (PCR_{MIC} in mpy or PCR_{MIC} in mm/y depending on units used in Eq. 28.20) including the influence of MIC is then calculated using Eq. (28.21) [22–24]:

$$PCR_{MIC} = PCR \times \left(\frac{MIC\_Risk\_Score}{50}\right) \tag{28.21}$$

where PCR is the corrosion rate due to non-MIC activities (as calculated using Eq. 28.20) and MIC_Risk_Score is the MIC factor, calculated using Table 28.2.

Table 28.2 Risk scores for microbiologically influenced corrosion (MIC)

Influence of parameter	Range of parameter	Unit of parameter	MIC risk score[a]	Remarks
Temperature	Less than −10	°C	0	
	−10–15		1	
	15–45		7–10	
	45–70		7–4	
	70–120		4–1	
	Above 120		0	
Pressure	Greater than 20	P_{CO_2}/P_{H_2S}[b]	10	Only if gas contains H_2S greater than 10 mol/kmol (1%) by volume.
	Less than 20		2	
Flow rate	Above 3	m/s	1	
	2–3		2–12	
	1–2		12–18	
	0–1		18–20	
pH	Less than 1		0	
	1–4		5	
	4–9		10	
	9–14		1	
	Above 14		0	

Table 28.2 Continued

Influence of parameter	Range of parameter	Unit of parameter	MIC risk score[a]	Remarks
Langelier saturation index (LSI)	Less than −6		10	
	−6−−1		10−5	MIC tendency decreases as the LSI value increases in the negative direction because the tendency of non-MIC increases.
	−1−1		0	
	1−8		1−8	MIC tendency increases as the LSI value increases as more scales are formed.
	Greater than 8		8	
Total suspended solids (TSS)	Present		10	If the flow rate is between 0 and 3 m/s.
	Present		0	If the flow rate is above 3 m/s.
	Absent		0	
Total dissolved solids	Less than 15,000	ppm	1	
	15,000−150,000		1−10	
	Greater than 150,000		10	
Redox potential (Eh)	Less than −15	mV	1	
	−15 to +150		1−10	
	Greater than 150		10	
Sulfur content	Present		10	
	Absent		1	

[a]Summation of all MIC factors. The maximum value is 100.
[b]Partial pressure ratio.

Table 28.3 Variation of pitting corrosion rate as a function of flow regimes

Flow regime type	PCR_{MIC} modification
Slug flow	No change
Plug flow	$PCR_{MIC} \times 0.98$
Bubble flow	$PCR_{MIC} \times 0.96$
Dispersed flow	$PCR_{MIC} \times 0.94$
Oscillatory flow	$PCR_{MIC} \times 0.92$
Annular flow	$PCR_{MIC} \times 0.90$
Churn flow	$PCR_{MIC} \times 0.88$
Wave flow	$PCR_{MIC} \times 0.86$
Stratified flow	$PCR_{MIC} \times 0.84$

PCR, pitting corrosion rate; *MIC*, microbiologically influenced corrosion.

When applying internal localized pitting corrosion model to a real operating environment, the dynamic aspects of the operating conditions must be taken into account. There are several variables to consider to account for the dynamic nature of field operation. However, four important variables are flow velocity, flow regime, operating boundaries, and time. The following sections describe how the four variables are treated in this model.

Depending on the pressure, temperature, pipe diameter, and elevation profile, the flow velocity varies. Flow velocity determines where water accumulates. Detailed procedures to determine flow velocities and to calculate locations where water may accumulate are available elsewhere [1].

Flow patterns of multiphase (transporting simultaneously oil, water, gas, and solid) pipelines are commonly known as flow regimes. The flow regimes depend on the diameter of the pipe, orientation of the pipe, the flow rates in the pipe, and fluid properties. Description of types of flow regimes and their characteristics are beyond the scope of this chapter but are available elsewhere [1]. Based on evaluation of several field data, general guidelines on the influence of flow regimes on corrosion have been established (Table 28.3). PCR_{MIC} determined by Eq. (28.21) is corrected with factors presented in Table 28.3 to account for flow regime to obtain PCR_{mean} (in mpy or in mm/y depending on unit used in Eq. 28.20).

Pits will not continue to grow at a constant rate for various reasons. To account for this effect the average pitting corrosion rate, $PCR_{(average)}$ (in mpy or mm/y depending on unit used in Eq. 28.21) from PCR_{mean} is calculated using Eq. (28.22):

$$PCR_{(average)} = \frac{\frac{PCR_{mean}}{1} + \frac{PCR_{mean}}{2} + \frac{PCR_{mean}}{3} + \cdots\cdots + \frac{PCR_{mean}}{t}}{T} \tag{28.22}$$

where "*T*" is the total number of years between the start date and current date, *t* is the number of times the PCR_{mean} should be calculated. For example, the system that is operating for 5 years, the value of *T* is 5, and the PCR_{mean} calculation should be carried out five times, i.e., in year 1, 2, 3, 4, and 5 (*t*).

The PCR calculated using Eq. (28.22) is valid only if the production conditions are constant over the years. If the production conditions change for a particular year the value of "*t*" is set to unity for that year, and the "*t*" values for subsequent years increase

Table 28.4 Boundaries to determine if the production conditions change or not

Parameter	Boundaries
Temperature, °C	$X \leq 25$
	$25 < X \leq 50$
	$X > 50$
Pressure, psi (kPa)	$X \leq 100$ (689)
	100 (689) $< X \leq 500$ (3447)
	$X > 500$ (3447)
H_2S, psi (kPa)	$X \leq 2.5$ (17.24)
	2.5 (17.24) $< X \leq 10$ (69)
	10 (69) $< X \leq 50$ (345)
	$X > 50$ (345)
CO_2, psi (kPa)	$X \leq 2.5$ (17.24)
	2.5 (17.24) $< X \leq 10$ (69)
	10 (69) $< X \leq 30$ (207)
	30 (207) $< X \leq 100$ (689)
	$X > 100$ (689)
SO_4^{2-} (ppm)	$X \leq 750$
	$750 < X \leq 1000$
	$1000 < X \leq 1500$
	$1500 < X \leq 2500$
	$X > 2500$
HCO_3^- (ppm)	$X \leq 500$
	$500 < X \leq 1000$
	$1000 < X \leq 2000$
	$2000 < X \leq 4000$
	$X > 4000$

Continued

Table 28.4 Continued

Parameter	Boundaries
Cl^- (ppm)	$X \leq 10{,}000$
	$10{,}000 < X \leq 20{,}000$
	$20{,}000 < X \leq 40{,}000$
	$40{,}000 < X \leq 60{,}000$
	$60{,}000 < X \leq 80{,}000$
	$80{,}000 < X \leq 100{,}000$
	$100{,}000 < X \leq 120{,}000$
	$X > 120{,}000$

as per Eq. (28.22). Table 28.4 provides the boundary conditions to determine if the production conditions change or not. For a system with PCR_{mean} of 10 mpy (0.25 mm/y) operating within the boundary (See Table 28.4), the $PCR_{average}$ over 5 years will be about 4 mpy (0.1 mm/y). For a system with same PCR_{mean} of 10 mpy (0.25 mm/y) but with operating conditions changing beyond the boundary conditions (see Table 28.4) in the third year, the $PCR_{average}$ over 5 years will be about 7 mpy (0.18 mm/y). For a system with same PCR_{mean} of 10 mpy (0.25 mm/y) but with operating conditions changing beyond the boundary conditions (see Table 28.4) every year, the $PCR_{average}$ over 5 years will be 10 mpy (0.25 mm/y).

Table 28.5 Validation of localized pitting corrosion model

Field[a]	pH_2S, psi (kPa)[b]	pCO_2, psi (kPa)	Predicted PCR, mpy (mm/y)[b]	Field maximum PCR, mpy (mm/y)[b]	References
1	0.2 (1)	320 (2206)	20 (0.45)	18 (0.45)	[16]
2	2 (14)	4 (28)	13 (0.33)	2 (0.05)	[16]
3	2 (14)	4 (28)	16 (0.40)	2 (0.05)	[16]
4	2 (14)	4 (28)	31 (0.78)	27 (0.68)	[16]
5	0.2 (1)	2 (14)	16 (0.40)	11 (0.28)	[16]
6	0.2 (1)	0.1 (1)	16 (0.40)	17 (0.43)	[16]
7	60 (414)	6 (41)	47 (1.18)	48 (1.20)	[20,21]
8	0 (0)	21 (145)	0.7 (0.02)	0.1 (0.00)	[22]
9	0 (0)	20 (138)	1.2 (0.03)	0.1 (0.00)	[23]
10	0 (0)	21 (145)	0.5 (0.01)	0.1 (0.00)	[24]

[a]Validation of the model for another 17 fields have previously been presented [1].
[b]See original papers for other operating conditions and for pitting corrosion rate distributions.

Table 28.6 Boundary for using the model (applicable to carbon steel only)

Experimental parameter	Minimum condition	Maximum condition	Units
Solid	No solids present	Solids are present	n.a
Temperature	5	65	°C
Total pressure	0	750 (5171)	Psi (kPa)
H_2S partial pressure	0	50 (345)	Psi (kPa)
CO_2 partial pressure	0	100 (689)	Psi (kPa)
Bicarbonate concentration	0	4000	Ppm
Sulfate concentration	0	2500	Ppm
Chloride concentration	0	120000	Ppm
Flow	0	5	m/s

The prediction from the internal localized pitting corrosion model has been validated using data collected from 27 fields. Table 28.5 presents a comparison of localized PCRs predicted by the model and field maximum pitting corrosion rates. The validation data presented in Table 28.5 are only values at the time the data were collected. Any changes in the operating conditions will influence the predicted PCR.

The model presented in this chapter is validated only under certain conditions, and hence should only be used within the conditions. Table 28.6 provides the boundary conditions for this model.

28.5 Selection of pitting corrosion model

Before using a specific internal localized pitting corrosion model, the suitability of it for a given field must be established. Selection of appropriate flow and corrosion models is a key step in predicting the internal corrosion.

The user must determine if the selected model considers all parameters causing corrosion under the operating conditions. For example, if the operating condition is sour (i.e., presence of H_2S), only those models including the effect of H_2S must be considered. Furthermore, if the model shouldconsider appropriate mechanism of corrosion. For example, corrosion rates determined from general corrosion models have no relevance to localized pitting corrosion. Recently published NACE technical report provides guidelines to select appropriate flow and corrosion models [25].

28.6 Use of models

The primary function of modeling is to predict the types of corrosion a given material will suffer from, in a given environment and to estimate the rate at which the material would corrode in that given environment. Models also help to identify locations where

corrosion may take place. Models thus help the corrosion professionals to establish material of construction, corrosion allowance (i.e., material wall thickness to account of loss due to corrosion), and to decide if corrosion mitigation strategies are required. The model should be used in conjunction with other integrity management activities including monitoring, maintenance, and management.

28.7 Status of pitting corrosion models

Corrosion science models provide insight on the initial stages of pitting corrosion; however, the focus has been more on short-term laboratory tests and only on determining corrosion rates in stage 2 (See Fig. 28.1) before formation of surface layers. Many laboratory test results published have scattered corrosion rates. To build the confidence in these models, round robin tests must be conducted to establish "repeatability" and "reproducibility" of test results. Repeatability is defined as the test results obtained by the same person conducting the same test several times (typically 3 or 4 times) using same apparatus and same test procedure. Reproducibility is defined as the test results obtained by the several persons conducting the same test several times (typically 3 to 4 times) using similar apparatus and same procedure. Test results from at least six persons are compiled to determine "reproducibility."

Electrochemical science models provide insight and theoretical explanation to various stages of pitting corrosion including passive layer formation, pit initiation, pit repassivation, pit growth, and autocatalytic process leading to accelerated pit growth rate. However, several scientific parameters (in some cases up to 150 parameters) are required to use these models. Several of these parameters are difficult to obtain for the oil and gas industry operating conditions. Until these issues are resolved the use of electrochemical pitting corrosion models for the oil and gas industry will be limited.

Corrosion engineering models are developed based on field experience and on inputs that are readily available for field operators. However, many details of the models are not publicly available. From the limited amounts of information published, it appears that these models do not address all stages of pitting corrosion. In the one publicly disclosed corrosion engineering model (see Section 28.4), a balance is established between corrosion science developed based on laboratory tests and corrosion engineering developed based on field tests and field data analysis. As more and more field operators use and validate this corrosion engineering model the confidence of using it will increase. Such exercise will also help to fine-tune the "synergistic" and "antagonistic" interactions between PCR accelerators and decelerators.

28.8 New trends in modeling of pitting corrosion

With the advent of computers, modern computer power, and web-based technologies, the computing power has increased over the past two decades. This advancement has enabled several groups to develop models and software products. However, the corrosion rates used in many of the models and software products have been based on

general corrosion rates, which are in turn based on short-term laboratory tests. As explained in Section 28.4, the PCRs of carbon steel may vary as a function of time and a function of operating conditions. None of the corrosion science models at this stage can account for the time-dependent variation of PCRs.

On the other extreme, certain corrosion engineering models use some random numbers to correlate general corrosion rate to PCR, in spite of many published results indicating that there is no correlation between general corrosion rates and localized PCRs [26].

Both these shortcuts methods (short-term data from laboratory tests alone and usage of random factors to convert general corrosion rates to localized PCRs) have not only been unsuccessful in predicting localized PCRs but also are scientifically invalid. For instance, these approaches do not and cannot explain fundamental characteristics of localized pitting corrosion, i.e., failures occur through teeny tiny pit, whereas the surrounding area around the pit is in pristine condition.

Because of the short comings, more and more field operators are convinced that collection and analysis of field data (operating conditions, data from monitoring and inspection, and failure analysis) appropriately provide invaluable information on localized pitting corrosion of carbon steel and enable development of strategies to control it. Collection and retention of field date are also increasingly being required by regulatory agencies and standards-making organizations.

Several methods are being used to generate localized PCRs based on field operating conditions, including corrosion engineering models, statistical analysis methods (especially extreme value statistics such as Weibull and Gumbel distribution analysis), fuzzy logic, and artificial neural network. Among them, use of reliable corrosion engineering model (such as described in Section 28.4) and statistical analysis methods have been successful in recent years. Other methods, although showing promise in the academic circles, have not been used in the industry for localized PCR of carbon steel.

References

[1] S. Papavinasam, Corrosion Control in the Oil and Gas Industry, 1,020 pages, Gulf Professional Publication, October 2013, ISBN 978-0-1239-7022-0 (Imprint of Elsevier).
[2] S. Papavinasam, A. Doiron, J. Li, D.Y. Park, P. Liu, Sour and sweet corrosion of carbon steel: general or pitting or localized or all of the above? in: NACE Corrosion Conference Paper #14054, 2010.
[3] C. de Waard, D.E. Milliams, Carbonic acid corrosion of steel, Corrosion 31 (5) (May 1975) 177−181. NACE.
[4] C. de Waard, U. Lotz, Prediction of CO_2 corrosion of carbon steel, in: NACE CORROSION 93, Paper #69, Houston, Texas, 1993.
[5] C. de Waard, U. Lotz, A. Dugstad, Influence of liquid flow velocity on CO_2 corrosion: a semi-empirical model, in: NACE CORROSION 95, Paper #128, Houston, Texas, 1995.
[6] D.D. Macdonald, M.U. MacDonald, Theory of steady-state passive films, Journal of the Electrochemical Society 137 (1990) 2395.
[7] D.D. Macdonald, M.U. MacDonald, Distribution functions for the breakdown of passive films, Electrochimica Acta 31 (1986) 1079.
[8] J.W. Tester, H.S. Issac, Journal of the Electrochemical Society 122 (1975) 1438.

[9] T.R. Beck, R.C. Alkire, Occurrence of salt films during initiation and growth of corrosion pits, Journal of the Electrochemical Society 126 (1979) 1662.
[10] B.G. Ateya, H.W. Pickering, Journal of the Electrochemical Society 122 (1975) 1018.
[11] A. Ben Rais, J.C. Sohm, Corrosion Science 25 (1985) 1047.
[12] J.M. Galvele, Journal of the Electrochemical Society 123 (1976) 464.
[13] S. Papavinasam, A. Doiron, T. Panneerselvam, R.W. Revie, Effect of hydrocarbons on the internal corrosion of oil and gas pipelines, Corrosion 63 (7) (2007) 704−712.
[14] S. Papavinasam, A. Doiron, R.W. Revie, Effect of surface layers on the initiation of internal pitting corrosion in oil and gas pipelines, Corrosion 65 (10) (2009) 663−673.
[15] A. Demoz, S. Papavinasam, O. Omotoso, K. Michaelian, R.W. Revie, Effect of field operational variables on internal pitting corrosion of oil and gas pipelines, Corrosion 65 (11) (2009) 741−747.
[16] S. Papavinasam, A. Doiron, R.W. Revie, Model to predict internal pitting corrosion of oil and gas pipelines, Corrosion 66 (3) (2010) 35006 (11 pages).
[17] S. Papavinasam, A. Doiron, T. Panneerselvam, Integration of localized internal pitting corrosion and flow models, in: CORROSION 2012, Paper #23794, NACE International, Houston, TX, 2012.
[18] S. Papavinasam, R.W. Revie, W. Friesen, A. Doiron, T. Panneerselvam, Review of models to predict internal pitting corrosion of oil and gas pipelines, Corrosion Reviews 24 (3−4) (2006) 173−230.
[19] S. Papavinasam, Sour localized pitting corrosion model of carbon steel: a status update, in: CORROSION 2016, Paper 7250, NACE International, Houston, TX, 2016.
[20] S. Papavinasam, A. Doiron, V. Sizov, R.W. Revie, A model to predict internal pitting corrosion of oil and gas pipelines (Part 1), Oil and Gas Journal 105 (44) (November 26, 2007) 68−73.
[21] S. Papavinasam, A. Doiron, V. Sizov, R.W. Revie, A model to predict internal pitting corrosion of oil and gas pipelines (Part 2), Oil and Gas Journal 105 (45) (December 2007) 62−67.
[22] R. Sooknah, S. Papavinasam, R.W. Revie, Validation of a predictive model for microbiologically influenced corrosion, in: NACE 2008, Paper 8503, Houston, Texas, 2008.
[23] T. Haile, S. Papavinasam, T. Zintel, Validation of corrosion models using field data obtained from oil and gas production pipelines, in: CORROSION 2013, Paper #2170, NACE International, Houston, Texas, 2013.
[24] A.D. Turris, M.D. Romero, S. Papavinasam, R. Lastra, Effect of SRB, CO_2, crude oil, and chemical treatment on the corrosiveness of synthetic produced water, in: CORROSION 2013, Paper #2213, NACE International, Houston, Texas, 2013.
[25] NACE Publication 21410, Selection of Pipeline Flow and Internal Corrosion Models, NACE International, Houston, TX.
[26] R.E. Ricker, Analysis of Pipeline Steel Corrosion Data from NBS (NIST) Studies Conducted between 1922−1940 and Relevance to Pipeline Management, National Institute of Standards and Technology, Gaithersburg, MD 20899, May 2, 2007. NISTIR 7415.

Top-of-the-line corrosion

29

Marc Singer
Ohio University, Athens, OH, United States

29.1 Review of water condensation modeling

The water condensation rate (WCR) is typically calculated by evaluating the water dropout via temperature change in a given section of pipe. However, this approach can lead to underprediction, for example in the case of cold spots, as condensation rates are averaged. A more accurate, albeit more cumbersome, approach considers local heat transfer at the top of the pipe. Both methods are presented here.

29.1.1 Water dropout approach

The most common methodology used by flow assurance software to predict WCR involves the determination of the temperature drop along a section of pipe and of the amount of water condensation from the vapor phase. A comprehensive heat loss module, considering pipeline and outside environment characteristics, is necessary to determine the temperature profile. Thermodynamic models can be used to calculate the water vapor partial pressure, which decreases along the pipe following the temperature drop. The reduction in water vapor pressure is directly used to calculate an average condensation rate considering only the upper half of the pipe area. The equation below is only valid for small sections of pipes:

$$\mathrm{WCR} = m_{\mathrm{gas}} \frac{M_{\mathrm{water}}}{M_{\mathrm{gas}}} \frac{2}{AL} \left(\frac{P_{\mathrm{vap}}^{\mathrm{in}} - P_{\mathrm{vap}}^{\mathrm{out}}}{P_{\mathrm{Total}}} \right) \tag{29.1}$$

where WCR is given in kg/m^2/s; m_{gas} is the gas mass flow rate (kg/s); M_{gas} and M_{water} are molecular weight of gas phase and water (kg/mol); $P_{\mathrm{vap}}^{\mathrm{in}}$ and $P_{\mathrm{vap}}^{\mathrm{out}}$ are vapor pressure at the inlet and outlet of the pipe section (bar); $A/2$ is half of pipe perimeter (m); and L is the pipe length of the section considered (m).

However, this method can be inaccurate in some cases because as the water vapor condenses, the bulk aqueous phase present at the bottom of the line tends to evaporate to counter the more rapid cooling of the gas phase. The water drop out does not distinguish between these two parts and only calculates an overall rate of water accumulation, i.e., the rate of water condensing from the vapor minus the rate of water evaporating from the bulk liquid. This approach can consequently underpredict the actual WCR happening locally at the top of the pipe.

Trends in Oil and Gas Corrosion Research and Technologies. http://dx.doi.org/10.1016/B978-0-08-101105-8.00029-2

29.1.2 Local water condensation approach

The calculation of local WCR is linked to the phenomenon of dropwise condensation, which has been studied extensively over the past 60 years. It can be described in terms of a four-stage scenario [1]: nucleation, growth, coalescence, and removal. The fundamentals of the mechanism and modeling of dropwise condensation have been published by Rose [2–6] over the past 30 years. As dropwise condensation is a random process, the common approach is to calculate the heat flux through a single droplet and to integrate the expression over an average distribution of drop sizes:

$$Q = \int_{r_{\min}}^{r_{\max}} q(r)N(r)dr \tag{29.2}$$

where Q is the total heat flux (W/m^2); $q(r)$ is the heat flux through an individual droplet of radius r (W/m^2); $N(r)dr$ is the number of drops per area with radius between r and $r + dr$ (m^{-2}); $r_{\max}$ and $r_{\min}$ are maximum and minimum radii of droplet (m).

Then the total heat flux includes the heat transfer due to the phase change and the presence of noncondensable gas. It has been reported that the main resistance for heat transfer comes from the presence of noncondensable gas [7–9]. The relationship between total heat flux and condensation rate can be stated in the following way [10]:

$$Q = Q_g + Q_c = h_g \times \left(T_b^g - T_i^g\right) + \mathrm{WCR} \times H_{fg} \tag{29.3}$$

where Q is the total heat flux (W/m^2); Q_g is the heat flux through the gas boundary layer (W/m^2); Q_c is the latent heat flux released by the phase change (W/m^2); h_g is the heat transfer coefficient in the gas boundary layer (W/m^2/K); $\left(T_b^g - T_i^g\right)$ is the temperature difference between bulk and vap/liq interface (K); WCR is given in kg/m^2/s; H_{fg} is the latent heat of evaporation/condensation (J/kg).

The heat transfer theory applied to dropwise condensation is well understood and has been described and applied by many authors [11–14]. The approach can be directly applied to a pipeline considering heat resistances due to the presence of noncondensable gas, the curvature of the droplet, the vapor/liquid interface, the liquid thickness and the promoter (pipe material) surface itself. The approach was described by Zhang [10] and described schematically in Fig. 29.1, assuming a semihemispherical droplet shape.

The difference in temperature between the vapor and the condensing surface can be expressed as

$$\Delta T = \Delta T_c + \Delta T_i + \Delta T_d + \Delta T_w \tag{29.4}$$

where ΔT is the total temperature difference $\left(T_i^g - T_o^w\right)$ (K); ΔT_c is the temperature drop due to droplet curvature (K); ΔT_i is the temperature drop at the vapor/liquid interface $\left(T_i^g - T_i^d\right)$ (K); ΔT_d is the temperature drop in the liquid layer $\left(T_i^d - T_i^w\right)$ (K); ΔT_w is the temperature drop in the promoter layer $\left(T_i^w - T_o^w\right)$ (K).

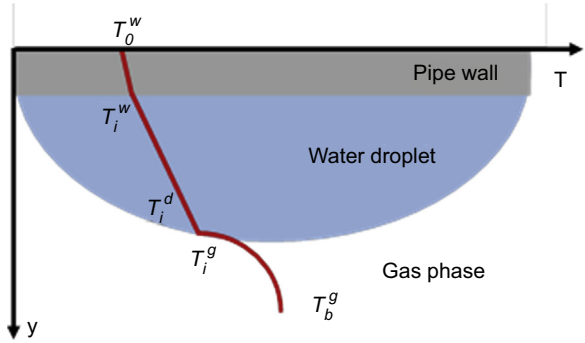

Figure 29.1 Description of the temperature gradient for a single droplet with T_o^w as the outer promoter temperature; T_i^w as the inner promoter temperature; T_i^d as the interfacial temperature in the liquid side; T_i^g as the interfacial temperature in the gas side; and T_b^g as the bulk gas temperature.
Adapted from Z. Zhang, D. Hinkson, M. Singer, H. Wang, S. Nesic, A mechanistic model for top of the line corrosion, Corrosion 63 (11) (November 2007) 1051−1062.

The temperature gradients are calculated the following way:

- Temperature drop due to droplet curvature [12]

$$\Delta T_c = \frac{2T_i^g \sigma}{H_{fg} r \rho_w} \tag{29.5}$$

where r is the radius of the droplet (m); σ is the vapor−liquid surface tension (N/m); ρ_w is the water density (kg/m^3).

- Temperature drop due to vapor/liquid interface [15]

$$\Delta T_i = \frac{q}{2\pi r^2 h_i} \tag{29.6}$$

where h_i is the heat transfer coefficient at the droplet interface (W/m^2/K).

- Temperature drop through the liquid droplet [16]

$$\Delta T_d = \frac{q \times r}{4\pi r^2 k_c} \tag{29.7}$$

where k_c is the water thermal conductivity (W/m/K).

- Temperature drop through the promoter layer [12]

$$\Delta T_w = \frac{q \times L_p}{4\pi r^2 k_p} \tag{29.8}$$

where k_p is the promoter thermal conductivity (W/m/K) and L_p is the thickness of the promoter layer (m).

Finally, the heat flux through a single droplet can be expressed by combining all of the equations given earlier:

$$q(r) = \frac{T_i^g\left(1 - \dfrac{2\sigma}{H_{fg} r \rho_w}\right) - T_o^w}{\dfrac{r}{4\pi r^2 k_c} + \dfrac{1}{2\pi r^2 h_i} + \dfrac{L_p}{4\pi r^2 k_p}} \tag{29.9}$$

where $q(r)$ is the heat flux through an individual droplet of radius r (W/m^2).

The expression of the dropsize distribution was developed by Le Fevre [17] and is commonly accepted by many authors [3,4,18,19] in the following form:

$$N(r)dr = \frac{1}{3 \times \pi \times r^2 \times r_{\max}} \times \left(\frac{r}{r_{\max}}\right)^{-\frac{2}{3}} dr \tag{29.10}$$

where $N(r)dr$ is the number of drops per area with radius between r and $r + dr$ (m^{-2}); r is the radius of the droplet (m); $r_{\max}$ is the maximum droplet radius (m).

The final equation becomes

$$h_g \times \left(T_b^g - T_i^g\right) + \mathrm{WCR} \times H_{fg} = \int_{r_{\min}}^{r_{\max}} \frac{T_i^g\left(1 - \dfrac{2\sigma}{H_{fg} r \rho_w}\right) - T_o^w}{\dfrac{r}{4\pi r^2 k_c} + \dfrac{1}{2\pi r^2 h_i} + \dfrac{L_p}{4\pi r^2 k_p}} \times \frac{1}{3\pi r^2 r_{\max}} \left(\frac{r}{r_{\max}}\right)^{-\frac{2}{3}} dr \tag{29.11}$$

The expression of the size of the smallest thermodynamically viable droplet is [11]

$$r_{\min} = \frac{2T_s\sigma}{H_{fg}\rho_w \Delta T} \tag{29.12}$$

where T_s is the aturation temperature (K).

The maximum droplet size based on a dimensional analysis is expressed as [4]

$$r_{\max} = K \times \left(\frac{\sigma}{\rho_w g}\right)^{0.5} \tag{29.13}$$

where K is the experimentally defined constant close to unity; g is the gravitational acceleration (m/s^2).

Eqs. (29.11) still contains two unknown variables, namely WCR and the interfacial temperature in the gas side T_i^g. Consequently, another equation is needed to solve the

problem. Zhang [10] added a mass balance of the water in order to calculate the condensation rate:

$$\mathrm{WCR} = \rho_g \beta_g \times \left(x_b^g - x_i^g\right) = \rho_g \beta_g \times \frac{M_w}{P_T M_g}\left(P_{\mathrm{sat}}\left(T_b^g\right) - P_{\mathrm{sat}}\left(T_i^g\right)\right) \qquad (29.14)$$

where WCR is given as kg/m^2/s; β_g is the mass transfer coefficient in the gas boundary layer (m/s); x_b^g is the mass fraction of water vapor in the bulk gas flow ($\mathrm{kg_v/kg_g}$); x_i^g is the mass fraction of water vapor at the gas-liquid interface ($\mathrm{kg_v/kg_g}$); ρ_g is the density of gas ($\mathrm{kg_g/m^3}$); M_w and M_g are the molecular weight of the water and the gas mixture (g/mol); P_T is the total pressure (Pa); P_{sat} is the saturation pressure as a function of temperature (Pa).

Zhang [10] was the first to propose a dropwise condensation approach to calculate the WCR in a TLC configuration. Since then, Pojtanabuntoeng [20,21] and, later, Gao [22] have upgraded this model to include the prediction of co-condensation of hydrocarbon and the effect of glycol on the overall condensation process, respectively.

As shown earlier, this approach calculates a local condensation rate at the 12 o'clock position of a pipeline. In contrast, the water dropout approach described in the previous section calculates an overall water accumulation rate considering the net effect between the vapor condensation and the water evaporation from the brine.

29.2 Review of existing TLC models

This section presents different attempts to model TLC and predict rates of corrosion considering either empirical and semiempirical or mechanistic approaches.

29.2.1 Empirical and semiempirical approaches

In 1991, Olsen [23] was the first to lay out the fundamental concepts of CO_2-dominated TLC modeling, which are still valid today and are at the core of most current TLC models. Olsen stated that the competition between corrosion (Fe^{2+} source) and condensation (Fe^{2+} source) controls the $FeCO_3$ saturation level and, consequently, the level of protectiveness of the corrosion product and the extent of the corrosion attack. At high temperatures $\geq$70°C (158°F) and low condensation rate, a dense and protective $FeCO_3$ is favored. At high condensation rate, the saturation in $FeCO_3$ is more difficult to obtain due to the rate of fresh water renewal. Although no proper mathematical model was proposed, this work is fundamental in many respects.

The first actual TLC prediction equation in sweet environments was proposed by DeWaard [24] who adapted his well-known correlation to a TLC scenario. DeWaard introduced a correcting factor $F_{\mathrm{Cond}} = 0.1$ in order to adapt his model to condensation conditions for condensation rates below an experimentally determined critical rate of 0.25 mL/m^2 s. This equation is still widely used today due to its simplicity but gives an

extremely conservative prediction. For instance, the presence and effect of $FeCO_3$ is completely ignored.

$$CR = F_{Cond} \times 10^{\left(5.8 - \frac{1710}{T_k} + 0.67 \times \log\left(p_{CO_2}\right)\right)} \tag{29.15}$$

where P_{CO_2} is the partial pressure of CO_2 (bar); T_k is the temperature (K); F_{Cond} is 0.1; CR is the corrosion rate (mm/year).

In 2000, Pots [25] proposed a more comprehensive attempt to mathematically represent the competition between the scale formation rate—linked to the iron dissolution—and the condensation rate. Pots developed the so-called "supersaturation model" based on the calculation of the concentration of iron at saturation under film-forming conditions. The corrosion rate CR, calculated using the formula below, is equated with the precipitation rate PR, calculated using an equation developed by Van Hunnik [26]. The concentration of Fe^{2+} present on both sides of the equations (Eqs. 29.16 and 29.17) is calculated and reinserted in the corrosion rate equation. This approach highlighted the need to develop in parallel a solid chemistry model as well as a correct evaluation of the condensation rate in order to accurately predict the corrosion rate. However, no clear guidelines on how to calculate it were provided.

$$CR = \frac{M_{Fe} \times 10^6 \times 24 \times 3600 \times 365}{\rho_{Carbonsteel}} \times \left[Fe^{2+}\right]_{supersat} \times \frac{WCR}{\rho_w} \tag{29.16}$$

where CR is the corrosion rate (mm/year); WCR is given as $g/m^2/s$; ρ_w is the water density (g/m^3); $[Fe^{2+}]_{supersat}$ is the iron concentration at $FeCO_3$ saturation (mol/L); M_{Fe} is the iron molecular weight (55.847 g/mol); $\rho_{carbonsteel}$ is the density of a typical carbon steel (CS) (7,860,000 g/m^3).

$$PR = A_p \times e^{\frac{-E_a}{RT}} \times K_{sp} \times (s-1)\left(1 - \frac{1}{s}\right) \text{ and } s = \frac{\left[Fe^{2+}\right] \times \left[CO_3{}^{2-}\right]}{K_{sp}} \tag{29.17}$$

where PR is the precipitation rate converted in $mol/m^2/s$; A_p is the constant E_a is the activation energy (KJ/mol); R is the deal gas constant (J/K/mol); T is the temperature (K); s is the $FeCO_3$ saturation; K_{sp} is the $FeCO_3$ solubility product (mol^2/m^2).

Based on the same concepts, Nyborg et al. [27] developed in 2007 a new empirical equation validated through experimental work. The expression developed by Nyborg depends on the WCR, the iron carbonate solubility and a supersaturation factor. According to the author, it is valid only for low acetic acid content (<0.001 mol/L), low to medium carbon dioxide partial pressure <3 bars (44 psi), and no H_2S. The iron carbonate solubility is represented as "solubility of iron ion" and is expressed as a function of temperature, total pressure, and CO_2 partial pressure. This calculation step requires a comprehensive water chemistry module, which can be adapted to include the effect of organic acid and glycol content [28]. Although no detail is provided on how the condensation rate is calculated, Nyborg stresses the importance of

predicting an accurate condensation rate, as it will have a much more pronounced effect on TLC than, for example, the CO_2 partial pressure.

$$\mathrm{CR} = 0.004 \times \mathrm{WCR} \times \left[\mathrm{Fe}^{2+}\right] \times (12.5 - 0.09 \times T) \tag{29.18}$$

where CR is the corrosion rate (mm/year); WCR is given as g/m^2/s; [Fe^{2+}] is the solubility of iron ions (ppm_w); T is the temperature (°C).

29.2.2 Mechanistic models

Mechanistic efforts to model TLC date back to early 2000 and focus exclusively on sweet (CO_2 dominated) environments. These mechanistic efforts usually yield vastly more accurate predictions but are much more cumbersome to implement as they typically require solutions to systems of nonlinear differential equations. Although much progress has been made in the understanding of sour TLC and sour corrosion in general, no modeling approach has been properly validated.

In 2002, Vitse [29–31] presented the first mechanistic attempt to model both condensation and corrosion processes. Vitse's condensation model assumed a continuous water film thickness mostly dependent on surface tension according to the following equation:

$$\delta = \left(\frac{\sigma}{g \times (\rho_l - \rho_g)}\right)^{0.5} \tag{29.19}$$

where g is the gravitational acceleration (m/s^2); σ is the surface tension (N/m); ρ_l and ρ_g are liquid and gas density, respectively (kg/m^3).

Considering the phase change and the heat resistance through the pipe wall and water layer, Vitse used Nusselt's theory of filmwise condensation [32,33] to develop his model. However, Vitse acknowledged that this approach was not properly suited to simulate the condensation process at the top of the line, which is dropwise [34]. Vitse then directly used the film-free electrochemical model proposed by Nesic [35] to estimate the corrosion rate. Furthermore, he conducted an Fe^{2+} flux balance in the droplet, taking into account the fluxes of Fe^{2+} created by corrosion, removed by $FeCO_3$ precipitation and transported by condensed water film convection. The $FeCO_3$ precipitation rate is calculated using the expression from Van Hunnik [26]. The role of the corrosion product layer was simplified by considering that the part of the steel surface covered by $FeCO_3$ was not corroding. The estimation of this covering factor K was done empirically, by fitting with experimental data. Under this model, an iterative process is performed until no change in the iron ion concentration is computed inside the control volume. Although still based on the fundamental mechanisms initially proposed by Olsen [23], and although not fully mechanistic, Vitse's method gave insight into how to model TLC phenomena. The equation used in the Fe^{2+} flux balance is displayed below:

$$\frac{d\left[\mathrm{Fe}^{2+}\right]}{dt} = \frac{1}{\delta} \times \left[K \times \mathrm{CR} - (1 - K) \times \mathrm{PR} - \mathrm{WCR} \times \left[\mathrm{Fe}^{2+}\right]\right] \tag{29.20}$$

where Fe^{2+} is the concentration of iron ion inside the control volume (mol/m^3); t is the time (s); CR is the corrosion rate (mol/m^3/s); PR is the precipitation rate (mol/m^3/s); WCR is given as m^3/m^2/s; δ is the liquid film thickness (m); K is the covering factor.

In 2007, Zhang et al. [10] published the first fully mechanistic approach to TLC modeling. Like Vitse's approach [29−31], the model covers the three main processes involved in top of the line corrosion (TLC) phenomena: dropwise condensation, chemistry in the condensed water, and corrosion at the steel surface. The condensation model, based on a dropwise approach valid for the 11−1 o'clock position in a pipeline, is presented in the previous section. The chemistry of the condensed liquid is established through standard chemical and thermodynamic equations [36,37]. Finally, the corrosion model is directly adapted from the mechanistic CO_2 corrosion approach developed by Nordsveen et al. [38] and Nesic et al. [39,40]. This corrosion model considers chemical reactions, transport of species, and the electrochemical reactions at the metal surface. For instance, the expression of the transport of chemical species in the liquid film and the porous corrosion product can be simplified assuming no convection (stagnant droplet):

$$\frac{\partial \varepsilon C_i}{\partial t} = D_i \frac{\partial^2 (\kappa C_i)}{\partial x^2} + \varepsilon R_i \tag{29.21}$$

where C_i is the concentration of species i (mol/L); ε is the volumetric porosity of the film, equal to 1 outside the corrosion product layer; κ is the surface permeability of the film, equal to 1 outside the corrosion product layer; D_i is the molecular diffusion of species i (m^2/s); R_i is the source or sink of species i (mol/L/s); t is the time (s); x is the spatial coordinate (m).

The porosity ε can be expressed as a function of the $FeCO_3$ precipitation rate, defined by the Van Hunnik equation [26] for $FeCO_3$ dissolution/precipitation rate:

$$\frac{\partial \varepsilon}{\partial t} = -\frac{M_{FeCO_3}}{\rho_{FeCO_3}} R_{FeCO_3} \tag{29.22}$$

where M_{FeCO_3} is the iron carbonate molecular weight (kg/mol); ρ_{FeCO_3} is the iron carbonate density (k/m^3); R_{FeCO_3} is the iron carbonate precipitation rate (mol/m^3/s).

The flux of electroactive species is calculated with the following equation:

$$N_j = -\frac{i_j}{n_j F} \tag{29.23}$$

where i_j is the current density for species j (A/m^2); n_j is the number of electrons exchanged for species j; F is the faraday number (A·s/mol); N_i is the flux of species j (mol/m^2/s).

Finally, the current density of each corrosive species can be expressed following the Tafel approximation:

$$i = \pm i_0 \cdot 10^{\pm \frac{E - E_{rev}}{b}} \tag{29.24}$$

where i_0 is the exchange current density; E_{rev} is the reversible potential; b is the tafel slope.

This system constitutes a set of nonlinear differential equations that need to be solved both in time and space. Zhang's innovation is to adapt these models to a TLC scenario. Zhang's main assumption is that the steel surface is corroding uniformly considering that, although the condensation is dropwise, every point on the metal surface has the same probability of being covered by liquid droplets. The problem can then be simplified from a three-dimensional (semihemispherical droplet) to a one-dimensional (1-D; liquid layer) problem. The validity of this 1-D assumption with respect to the occurrence of localized corrosion is discussed later in this chapter. The droplet growth is simulated by considering the increase in liquid film thickness due to the condensation process. Once the droplet reaches a calculated maximum size, the liquid film thickness is reset to its initial value, simulating a situation where the droplet either slides or falls due to gravity forces. This cycle is carried out until the corrosion process reaches a steady state. Fig. 29.2 shows how the calculation domain is structured and how the boundary conditions, at the steel surface and the liquid vapor interface, are defined.

This approach represents to date the most comprehensive attempt to model TLC as it takes into account all of the controlling parameters following a fully mechanistic methodology.

In 2011, Asher presented a comprehensive summary on best modeling practices related to sweet and sour TLC [42]. Although no specific algorithm was presented in the publication, the approach seemed to agree with Zhang's methodology, stressing the importance of the chemical, condensation, and corrosion processes and highlighting the balance between the fluxes of iron ions due to corrosion and required to form the corrosion product layer.

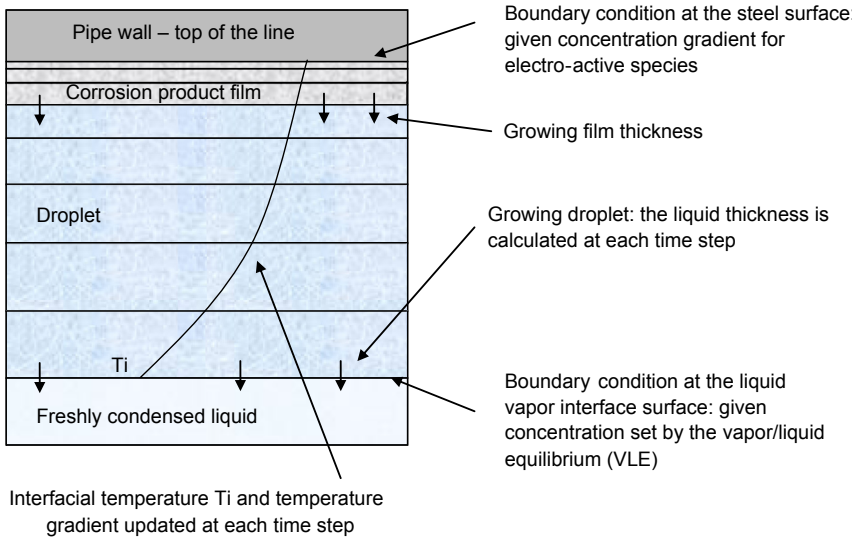

Figure 29.2 Schematic of the corrosion calculations in a growing droplet [41].

29.2.3 Prediction of localized corrosion

As mentioned in Chapter 16, sweet TLC is thought to be a "uniform" localized corrosion phenomenon instead of a purely pitting-dominated process. The "uniform" qualification of the attack is supported by the large size of the features and the extent of the corrosion rate, which never surpasses the "layer-free" rate. It is thought that the penetration rate is driven by the corrosivity of the environment and the WCR and is not particularly affected by any galvanic coupling between bare steel and layer-covered areas of the steel surface.

However, understanding and modeling how the localized corrosion features initiate, grow, and eventually coalescence in a dewing environment is of great importance. As for any type of localized corrosion in a sweet environment, a prerequisite of any local attack is a formation of a partially protective $FeCO_3$ scale. Based on an experimental study performed at the bottom of the line, Sun was able to identify a zone where localized corrosion occurrence and propagation were most likely [43]. The presence of a partially protective $FeCO_3$ was crucial, as under film-free or fully protective film conditions, no localized corrosion was observed. The scaling tendency (i.e., the ratio of precipitation and corrosion rate) was introduced to quantify the likelihood of localized corrosion occurrence. The precipitation rate was directly derived for the $FeCO_3$ saturation level in the bulk phase, which could also be used to evaluate the protectiveness of the scale.

The possibility of a galvanic affect between the bottom of the mesa attack feature (film-free) and the surrounding area covered with $FeCO_3$ was also introduced by Han [44–47]. The induced difference in potential could accelerate the corrosion rate of the exposed steel. Using a novel experimental setup artificially simulating a pit, Han could actually measure the difference in potential between the film-covered surface and the film-free site of the bottom of the pit. He could also link the localized corrosion growth with a $FeCO_3$ saturation level between 0.5 and 2, as did Sun et al. [43]. More importantly, Han stipulated that the pH of the solution trapped between the corrosion product layer and the steel was actually much higher than the pH in the bulk, leading to the formation of thin iron oxide (Fe_3O_4) film. This layer could provide an explanation for the significant increase in potential of the film-covered "passive" surface and the establishment of a galvanic cell with the active site of the pit. However, the existence of the iron oxide film has been debated as attempts by several authors to identify the oxide layer were inconclusive at best [46,48]. In addition, the mechanism cannot be applied easily to a dewing environment because the condensed water is not sufficiently conductive to "carry" the current at any significant level.

In 2008, Amri [49,50] performed similar experiments in an effort to relate pit growth and environmental conditions, especially in the presence of acetic acid. It was found that the growth of the pit was related to the depletion of the acetic acid concentration inside the pit. It was also stated that the growth should stop once the pit reaches a certain depth. Many of the observations made by the author were typical of a TLC scenario and were put forward to explain TLC stabilization. Consequently, this study constituted the first attempt to adapt the localized corrosion process to TLC.

Later, in 2013, Singer performed a comprehensive experimental study focused on the localized nature of TLC in sweet environments [41]. The author clearly identified

conditions where little to no corrosion was observed (low WCR and CO_2 content), where localized corrosion was present (moderate condensation rate, high gas temperature, and high organic acid content), and where uniform corrosion dominated (low steel temperature and high WCR). From these observations, the author developed a narrative for localized corrosion initiation and growth:

1. Initially, the steel surface corrodes uniformly and the rate of corrosion decreases with time due to the increase in solution pH (Fe^{2+} ions accumulation inside the droplet). The situation lasts as long as the droplet remains undersaturated with respect to $FeCO_3$.
2. If the $FeCO_3$ saturation level reaches one, the formation of the corrosion product layer decreases the corrosion rate even further. (Practical laboratory experience shows that supersaturation values of 5−10 are often sustainable, especially at high temperature [51].)
3. The condensation rate of fresh water being constant, the droplet eventually becomes slightly undersaturated, leading part of the layer to redissolve. The steel surface can become segregated between areas well-protected by the $FeCO_3$ layer and uncovered areas suffering from "bare steel" corrosion.
4. Uncovered areas corrode actively, whereas covered areas are protected, but the overall flux of Fe^{2+} ions due to corrosion, averaged over the entire steel surface, becomes constant in order to maintain the $FeCO_3$ saturation level. Localized TLC features are created.
5. The localized features initially propagate in depth as the immediate surroundings are covered by protective $FeCO_3$. However, the corrosion also progresses laterally, underneath the already existing $FeCO_3$ layer. The deeper features may stop progressing in depth while new damages in the corrosion product layer appear.

This narrative explains why the overall wall thickness loss rate becomes constant while localized features are present. The overall rate of iron dissolution is controlled by the corrosivity of the droplet, considering the chemistry at $FeCO_3$ saturation.

29.3 Remaining gaps in the modeling of TLC mechanisms

29.3.1 Prediction of sour TLC

Although much progress has been achieved in sweet TLC prediction, the modeling of sour corrosion remains a considerable challenge. As mentioned in Chapter 16, sour TLC is much less dependent on the WCR and seems to be controlled by the properties of the corrosion product layer. Most of the more mechanistic models have been adapted to predict sour TLC, a task made possible due to their fundamental physical structure [52]. However, comprehensive validation of these models has been difficult due to the lack of accurate field data. Occurrence of sour TLC is rare and often difficult to clearly identify. In addition, modeling of sour TLC clearly lags behind modeling of sour corrosion, and proper understanding of the effect of Fe_xS_y corrosion product layers on corrosion and pitting is lacking.

29.3.2 Modeling of TLC stabilization

Modeling approaches based on a uniform corrosion mechanism have been successfully used to predict the trend and order of magnitude of TLC, at least in sweet

environments. By itself, this observation represents a validation of this choice of overall mechanism. However, it also means that, for a fixed set of operating conditions, wall loss due to TLC is expected to occur continuously over the production life. As mentioned in Chapter 16, in-line inspections (ILIs) have shown that TLC features stop progressing in depth after some time, a phenomenon called TLC stabilization [53]. Current models cannot explain this behavior completely: although individual TLC features may very well cease to progress in depth due to geometrical considerations and mass transfer limitations, it is expected that other nearby features should "take over" or new features should appear in order to maintain the overall Fe^{2+} flux and the $FeCO_3$ saturation. Field evidence of TLC stabilization is still controversial and the phenomenon has not been comprehensively investigated in a laboratory. Consequently, the lack of widely approved explanation for TLC stabilization makes its modeling quite challenging for now.

29.3.3 Limitations in the use of TLC predictive models

Using corrosion models that have been developed in academic and research institutions and applying them to field conditions has always been a challenge. On one hand, researchers are often hesitant to use incomplete and inaccurate field data to validate their models. On the other hand, field engineers often distrust the models' ability to simulate complex field conditions, preferring to rely exclusively on field experience, as the models' validity and limitations are often misunderstood. Comprehensive and open validation of modeling performances with field experiences involving actual pipeline TLC failures is an essential step in bridging that gap. The first comprehensive effort to compare modeling predictions with TLC field data was performed by Gunaltun in 2010 [54]. The author selected 11 flow lines and determined a set of average operating conditions (temperature, pressure, CO_2 content, and flow rates) for each of them. These data were fed as input parameters for the TLC model, which was based on Zhang's approach [10]. One single TLC rate was predicted for each flow line and compared to maximum thickness loss measurements obtained through magnetic flux leakage (MFL) inspection. The comparison between the predicted TLC rates and the maximum measurable thickness losses showed a generally poor degree of agreement.

However, this effort was successful in highlighting some of the difficulties related to the development an accurate methodology for comparing model and field data. Among them, averaging decades of fluctuating operating conditions into one single set of parameters cannot be seen as an accurate representation of the production history. In addition, taking the maximum thickness loss measured from an MFL run cannot be used to represent the overall severity of the corrosion attack along a given pipeline. Too much confidence is often placed in ILI data, and the inaccuracy of the inspection tools must be accounted for, especially when comparing successive runs. In summary, efforts must be made both to ensure that the models are fed with the most accurate conditions possible and that the ILI data extracted for comparison are indeed representative of the TLC severity.

29.4 Best practices and emerging trends

As described earlier, comparison between model predictions and field data is still a difficult exercise. Often, the models are quickly blamed for their perceived ineffectiveness while too much trust is placed on notoriously inaccurate field data. In any case, the quality of the model predictions cannot be expected to be of better than the input field data.

29.4.1 Methodology for comparing field data and model prediction

In 2012, Kaewpradap developed a comprehensive methodology aimed at effectively utilizing both field data and model predictions [55–57]. The author identified several challenges and separated them into three main groups.

29.4.1.1 Issues related to the accuracy of field data

Kaewpradap listed all the field parameters needed to perform a proper simulation: history of production data, inlet pressure and temperature, gas and liquid composition. The author also highlighted the importance of topographic data, burial depth, environmental conditions, and pipeline properties. Some of these parameters can vary greatly over the course of a field's production life. Mechanistic models are very sensitive to this information, both for the calculation of the WCR and the TLC rate. As much as possible, the collection of complete and accurate field data is a definite prerequisite.

29.4.1.2 Issues related to the model predictions

The author highlighted the importance of fully understanding the meaning of predicted parameters. Most current models calculate steady-state uniform corrosion rates. The validity of using uniform corrosion models to simulate localized TLC features has been debated earlier in this section. Based on the current understanding of the mechanism, predicted steady-state corrosion rates apply to the growth of large mesa-type corrosion features but not pitting. It is also clear that current TLC models cannot be used to simulate corrosion rates at the bottom of the line, or defects at field joints, for example. Simulated corrosion rates are only valid for one set of input conditions, and calculations need to be repeated and integrated over time in order to represent the total wall thickness loss experienced over an entire production history. It is often necessary to identify production periods showing similarities and determine time-averaged input parameters over several time periods in order to balance practicality and accuracy.

29.4.1.3 Issues related to the analysis of ILI data

It is crucial to understand how the TLC feature size is actually measured, whether the ILI is performed through MFL, ultrasonic testing, or any other nondestructive testing tool. For instance, MFL, which is the most widely used technique, determines the

feature depth by converting deviation in magnetic flux using proprietary algorithms. In addition, typical accuracy is on the order of 10%−20% of the nominal wall thickness [58]. ILI data logs contain a wealth of information, most of it not directly related to TLC. These data must be filtered in order to identify large features (clusters not pitting) located at the 10−2 o'clock position and to eliminate noisy data related to field joint or girth welds.

Based on these observations, Kaewpradap proposed a multistep methodology for the comparison of model predictions and field data, considering a given pipeline [57].

Field condition analysis

Step 1: Identification of operating time periods showing similarities in term of inlet temperature and pressure, gas−liquid flow rates, and determination of a simple, time-averaged value for each operating parameter
Step 2: Calculation of WCRs and temperature profiles using a heat and mass transfer line model
Step 3: Simulations of steady-state TLC rate along the pipeline for each time period
Step 4: Calculation of cumulative wall thickness losses for the entire operating life of the field and comparison with provided MFL data

ILI data analysis

Step 1: Selection of ILI data over sections of pipe where the most severe TLC is typically encountered (start of line except riser, cold spots)
Step 2: Omission of features in the section of line where flow regime is clearly not stratified (vertical riser)
Step 3: Selection of features in the upper section of the pipe (between 10 and 2 o'clock)
Step 4: Omission of features located ±0.5 m around the weld joints
Step 6: Selection of large clusters and omission of small-size, isolated features. (Clusters are defined as large corrosion features, where width and depth is at least three times the wall thickness, following the classifications developed by the pipeline operators forum [59]).

Kaewpradap implemented this procedure to simulate several fields in the gulf of Thailand and obtained reasonably good agreement with field data [55,57]. Some discrepancies remain, as expected, especially in the prediction of the severity of the TLC attack in the first hundreds meters of line. The model, following the author's current understanding of the mechanisms, predicts the highest TLC rate at the inlet of the pipe, whereas ILI data show that the wall thickness loss typically reaches its maximum only after a few 100 m. The reason behind this behavior is not understood and requires further investigation.

29.4.2 How to use TLC prediction?

There is no question that corrosion prediction models in general should always be used in conjunction with field experience. This is also true for TLC prediction models. Recent efforts use some of these models to explain measured high thickness losses have been successful, validating this use of the tool for failure analysis.

TLC prediction software can also be used for the design of new pipelines. Examples are as follows:

- The expected operating conditions and production flow rates can be used to evaluate the TLC severity and implement the appropriate design decisions: corrosion allowance, characteristics of thickness of thermal insulation [53,60].
- Corrosion resistant alloy (CRA) and cladded pipe have been used for cooling spool pieces, where the vapor is forced to condense with no risk for the pipe material. TLC models can be used to determine the optimal length of the CRA spool piece [53].
- The transition between CRA and CS sections can also pose an elevated risk of corrosion as fresh condensed water, containing no dissolved iron ions, can travel to the CS section [53]. Although this does not constitute a pure case of TLC, existing models can be used to predict the severity of the corrosion attack. Similarly, the expected TLC rates at tie-ins can also be evaluated in a similar way.
- Expected TLC rates can be used to prioritize ILI runs on lines that are found more critical [60].
- The frequency of batch inhibition can be determined using predicted TLC rates [60], although the inhibition persistency is also a required parameter that can only be obtained through field experience or laboratory evaluation.

29.5 Conclusions

Much progress has been made over the past 20 years with regards to the understanding and modeling of TLC. Academic and research institutions have conducted carefully designed experimental studies and developed models that can accurately simulate this corrosion phenomenon. Efforts are still needed to fully represent the complexity of field environments, but TLC prediction software has been used with growing confidence by the industry, partly due to comprehensive and open validation activities.

References

[1] P. Meakin, Dropwise condensation: the droplet growth and coalescence of fluid droplets, Physica Scripta T44 (Febuary 1992) 31–41.
[2] J.W. Rose, On the mechanism of dropwise condensation, International Journal of Heat and Mass Transfer 10 (1967) 755–762.
[3] J.W. Rose, Dropwise condensation theory and experiment: a review, Journal of Power and Energy 216 (2002) 115–128.
[4] J.W. Rose, Dropwise condensation theory, International Journal of Heat and Mass Transfer 24 (1981) 191–194.
[5] J.W. Rose, On interphase matter transfer, the condensation coefficient and dropwise condensation, Proceedings of the Royal Society of London, Series A, Mathematical and Physical Sciences 411 (1841) (June 1987) 305–311.
[6] J.W. Rose, Some aspects of condensation heat transfer theory, International Communication in Heat and Mass Transfer 15 (1988) 449–473.

[7] D.W. Tanner, C.J. Potter, D. Pope, D. West, Heat transfer in dropwise condensation − Part1 & 2, International Journal of Heat and Mass Transfer 8 (1965) 419−426, 426−436.
[8] C.Y. Wang, C.J. Tu, Effect of non-condensable gas on laminar film condensation in a vertical tube, International Journal of Heat and Mass Transfer 31 (11) (1988) 2339−2345.
[9] S. Wang, Y. Utaka, Effect of non-condensable gas mass fraction on condensation heat transfer for water-ethanol vapor mixture, JSME International Journal, Series B 47 (2) (2004) 162−167.
[10] Z. Zhang, D. Hinkson, M. Singer, H. Wang, S. Nesic, A mechanistic model for top of the line corrosion, Corrosion 63 (11) (November 2007) 1051−1062.
[11] C. Graham, P. Griffith, Drop size distribution and heat transfer in dropwise condensation, International Journal of Heat and Mass Transfer 16 (1973) 337−346.
[12] M. Abu-Orabi, Modeling of heat transfer in dropwise condensation, International Journal of Heat and Mass Transfer 41 (1998) 81−87.
[13] B.M. Burnside, H.A. Hadi, Digital computer simulation of dropwise condensation from equilibrium droplet to detectable size, International Journal of Heat and Mass Transfer 42 (1999) 3137−3146.
[14] S. Verumi, K.J. Kim, An experimental and theoretical study on the concept of dropwise condensation, International Journal of Heat and Mass Transfer 49 (2006) 649−657.
[15] J.R. Maa, Drop size distribution and heat flux of dropwise condensation, The Chemical Engineering Journal 16 (1978) 171−176.
[16] N. Fatica, D.L. Katz, Dropwise condensation, Chemical Engineering Progress 45 (11) (1949) 661−674.
[17] E.J. Le Fevre, J.W. Rose, A theory of heat transfer by dropwise condensation, Proceedings of Third International Heat Transfer Conference AIChE 2 (1966) 362.
[18] J.W. Rose, L.R. Glicksman, Dropwise condensation − the distribution of drop sizes, International Journal of Heat and Mass Transfer 16 (1973) 411−425.
[19] Y.T. Wu, C.X. Yang, X.G. Yuan, Drop distribution and numerical simulation of dropwise condensation heat transfer, International Journal of Heat and Mass Transfer 44 (2001) 4455−4464.
[20] T. Pojtanabuntoeng, M. Singer, S. Nesic, Water/hydrocarbon co-condensation and the influence on top-of-the-line corrosion, in: Proc. Corrosion, Houston, TX, 2011, Paper. 11330, 2011.
[21] T. Pojtanabuntoeng, M. Singer, S. Nesic, Top-of-the-line corrosion in the presence of hydrocarbon co-condensation in flowing condition, in: Proc. Corrosion, New Orleans, LA, 2012, Paper 1534, 2012.
[22] S. Guo, F. Farelas, M. Singer, Effect of monoethylene glycol on sweet top of the line corrosion, in: Proc. Corrosion, Vancouver, CA, 2016, Paper 7891, 2016.
[23] S. Olsen, A. Dugstad, Corrosion under dewing conditions, in: Proc. Corrosion, Houston, TX, 1991, Paper. 472, 1991.
[24] C. DeWaard, U. Lotz, D.E. Milliams, Predictive model for CO_2 corrosion engineering in wet natural wet gas pipelines, Corrosion 47 (12) (1991) 976−985.
[25] B.F.M. Pots, E.L.J.A. Hendriksen, CO_2 corrosion under scaling conditions − the special case of top-of-the-line corrosion in wet gas pipelines, in: Proc. Corrosion, Houston, TX, 2000, Paper. 31, 2000.
[26] E.W.J. Van Hunnik, B.F.M. Pots, E.L.J.A. Hendriksen, The formation of protective $FeCO_3$ corrosion product layers in CO_2 corrosion, in: Proc. Corrosion, Houston, TX, 1996, Paper. 6, 1996.
[27] R. Nyborg, A. Dugstad, Top of the line corrosion and water condensation rates in wet gas pipelines, in: Proc. Corrosion, Nashville, TN, 2007, Paper. 7555, 2007.

[28] G. Svenningsen, R. Nyborg, Modeling of Top of the line corrosion with organic acid and glycol, in: Proc. Corrosion, San Antonio, TX, 2014, Paper. 4057, 2014.
[29] F. Vitse, Y. Gunaltun, D. Larrey de Torreben, P. Duchet-Suchaux, Mechanistic model for the prediction of top-of-the-line corrosion risk, in: Proc. Corrosion, Houston, TX, 2003, Paper. 3633, 2003.
[30] F. Vitse, K. Alam, Y. Gunaltun, D. Larrey de Torreben, P. Duchet-Suchaux, Semi-empirical model for prediction of the top-of-the-line corrosion risk, in: Proc. Corrosion, Houston, TX, 2002, Paper. 2245, 2002.
[31] F. Vitse, Experimental and Theoretical Study of the Phenomena of Corrosion by Carbon Dioxide Under Dewing Conditions at the Top of a Horizontal Pipeline in Presence of a Non-condensable Gas (Ph.D. dissertation), Russ College of Eng., Dept. of Chem. Eng., Ohio Univ., Athens, OH, 2002.
[32] W. Nusselt, Die oberflächenkondensation des wasserdampfes, Zeitschrift des Vereines Deutscher Ingenieure 60 (27) (1916) 541−546.
[33] W. Nusselt, Die oberflächenkondensation des wasserdampfes, Zeitschrift des Vereines Deutscher Ingenieure 60 (28) (1916) 569−575.
[34] Y. Gunaltun, D. Larrey, Correlation of cases of top of the line corrosion with calculated water condensation rates, in: Proc. Corrosion, Houston, TX, 2000, Paper. 71, 2000.
[35] S. Nesic, J. Postlethwaite, S. Olsen, An electrochemical model for prediction of corrosion of mild steel in aqueous carbon dioxide solutions, Corrosion 52 (4) (1996) 280−294.
[36] D. Hinkson, M. Singer, Z. Zhang, S. Nesic, A study of the chemical composition and corrosiveness of the condensate in top of the line corrosion, in: Proc. Corrosion, New Orleans, LA, 2008, Paper. 8466, 2008.
[37] D. Hinkson, Z. Zhang, M. Singer, S. Nesic, Chemical composition and corrosiveness of the condensate in top-of-the-line corrosion, Corrosion 66 (4) (April 2010) 045001−045001-8.
[38] N. Nordsveen, S. Nesic, R. Nyborg, A. Stangeland, A mechanistic model for carbon dioxide corrosion of mild steel in the presence of protective iron carbonate films − Part 1: theory and verification, Corrosion 59 (5) (2003) 443−456.
[39] S. Nesic, N. Nordsveen, R. Nyborg, A. Stangeland, A mechanistic model for carbon dioxide corrosion of mild steel in the presence of protective iron carbonate films − Part 2: a numerical experiment, Corrosion 59 (6) (2003) 489−497.
[40] S. Nesic, N. Nordsveen, R. Nyborg, A. Stangeland, A mechanistic model for carbon dioxide corrosion of mild steel in the presence of protective iron carbonate films − Part 3: film growth model, Corrosion 59 (7) (2003) 616−628.
[41] M. Singer, Study and Modeling of the Localized Nature of Top of the Line Corrosion (Ph.D. dissertation), Russ College of Eng., Dept. of Chem. Eng., Ohio Univ., Athens, OH, 2013.
[42] S.L. Asher, W. Sun, R.A. Ojifinni, S. Ling, C. Li, J.L. Pacheco, J.L. Nelson, Top of the line corrosion modeling in wet gas pipelines, in: Proc. 18th International Corrosion Congress, Perth, Australia, 2011, Paper. 303, 2011.
[43] Y. Sun, S. Nesic, A parametric study and modeling on localized CO_2 corrosion in horizontal wet gas flow, in: Proc. Corrosion, Houston, TX, 2004, Paper. 4380, 2001.
[44] J. Han, Y. Yang, B. Brown, S. Nesic, Electrochemical investigation of localized CO_2 corrosion on mild steel, in: Proc. Corrosion, Nashville, TN, 2007, Paper. 7323, 2007.
[45] J. Han, Y. Yang, S. Nesic, B. Brown, Role of passivation and galvanic effects in localized CO_2 corrosion of mild steel, in: Proc. Corrosion, New Orleans, LA, 2008, Paper. 8332, 2008.
[46] J. Han, Galvanic Mechanism of Localized Corrosion for Mild Steel in Carbon Dioxide Environments (Ph.D. dissertation), Russ College of Eng., Dept. of Chem. Eng., Ohio Univ., Athens, OH, 2009.

[47] J. Han, D. Young, H. Colijn, A. Tripathi, S. Nesic, Chemistry and structure of the passive film on mild steel in CO_2 corrosion environments, Industrial and Engineering Chemistry Research 48 (2009) 6296−6302.
[48] W. Li, Investigation of Pseudo-Passive Layer Formation in CO_2 Corrosion (Master's thesis), Russ College of Eng., Dept. of Chem. Eng., Ohio Univ., Athens, OH, 2011.
[49] J. Amri, E. Gulbrandsen, R.P. Nogueira, The effect of acetic acid on the pit propagation in CO_2 corrosion of carbon steel, Electrochemistry Communications, 10 (2008) 200−203.
[50] J. Amri, E. Gulbrandsen, R.P. Nogueira, Propagation and arrest of localized attacks in carbon dioxide corrosion of carbon steel in the presence of acetic acid, Corrosion 66 (3) (March 2010) 035001−035001-7.
[51] Y. Yang, Removal Mechanisms of Protective Iron Carbonate Layer in Flowing Solutions (Ph.D. dissertation), Russ College of Eng., Dept. of Chem. Eng., Ohio Univ., Athens, OH, 2012.
[52] M. Joosten, D. Owens, A. Hobbins, H. Sun, M. Achour, D. Lanktree, Top-of-line corrosion − a field failure, in: Proc. EuroCorr, Moscow, Russia, 2010, Paper. 9524, 2010.
[53] Y. Gunaltun, Design of multiphase offshore pipelines with high risk of sweet top of the line corrosion, in: Proc. Corrosion, Orlando, FL, 2013, Paper 2290, 2013.
[54] Y. Gunaltun, M. Thammachart, M. Singer, S. Nesic, S. Punpruk, U. Kaewpradap, Progress in the prediction of top of the line corrosion and challenges to predict corrosion rates measured in gas pipeline, in: Proc. Corrosion, San Antonio, TX, 2010, Paper. 10093, 2010.
[55] U. Kaewpradap, M. Singer, S. Nesic, Top of the line corrosion − comparison of model predictions with field data, in: Proc. Corrosion, Salt Lake City, UT, 2012, Paper. 1449, 2012.
[56] U. Kaewpradap, Validation of Top of the Line Corrosion Prediction Model Using Laboratory and Field Measurements (Master's thesis), Ohio University, Chemical and Bio-molecular Engineering Department, 2012.
[57] U. Kaewpradap, M. Singer, S. Nesic, S. Punpruk, Comparison of model predictions and field data − the case of top of the line corrosion, in: Proc. Corrosion, Dallas, TX, 2015, Paper. 5809, 2015.
[58] R. Hall, M. McMahon, Report on the Use of In-Line Inspection Tools for the Assessment of Pipeline Integrity, US Department of Transportation, 2002. Report No. DTRS56-96-C-0002-008.
[59] Pipeline Operators Forum (POF) document, Specifications and Requirements for Intelligent Pig Inspection of Pipelines, 2009.
[60] M. Thammachart, Corrosion mitigation for pipeline failure due to top of the line corrosion, in: Proc. 3rd TOL Corrosion Conference, Bangkok, 2012, 2012.

Modeling and prediction of stress corrosion cracking of pipeline steels

30

Weixing Chen
University of Alberta, Edmonton, AB, Canada

30.1 Introduction

The accuracy of modeling and prediction of stress corrosion cracking (SCC) of pipeline steels will largely rely on the following two key prerequisites:

1. The accuracy of modeling methodology or approaches in capturing the outcome of simulating attempts, either experimental or numerical, that are designed to simulate the field occurrence of SCC cracking of pipeline steels.
2. The true relevance of the simulative attempts to the field conditions that have caused the occurrence of SCC cracking of pipeline steels.

The trends in SCC research have always been moving in the direction of narrowing down the gaps that exist in the two aforementioned areas. As a result, this chapter is structured first to understand the field conditions pertinent to SCC crack initiation and growth. This discussion is followed by an overview of the different modeling approaches and a brief discussion of the current best practices and most recent advancements in modeling and predicting SCC of pipeline steels. From a critical analysis of the gaps between the field reality and the modeling hypotheses, the needs for future research and emerging trends in modeling SCC of pipeline steels are envisioned at end of the chapter.

30.2 Field conditions pertinent to SCC crack initiation and growth

The most common forms of SCC in pipeline steels are high-pH SCC (HpHSCC) and near-neutral pH SCC (NNpHSCC), as have been detailed in Chapter 12 in terms of their mechanisms of initiation and growth. SCC is a special form of environmentally assisted cracking that causes failures of pipeline steels when a susceptible pipeline steel surface is exposed to a corrosive environment under a constant stress usually below their yield strength.

Although the general conditions associated with SCC of pipeline steels are well defined, laboratory simulations aimed to reproduce SCC cracks, which are the basis of modeling, still remain to be improved. The following are the two most important

Trends in Oil and Gas Corrosion Research and Technologies. http://dx.doi.org/10.1016/B978-0-08-101105-8.00030-9

considerations in designing laboratory simulations to reproduce SCC cracking of pipeline steels found in the field:

1. Cracks are reproducible in terms of their macroscopic, microscopic, and metallurgical characteristics.
2. Crack growth rates are reproducible when compared with the lifetime of failures often found during field operation.

The simulations aimed to achieve the first objective are generally successful. In laboratory conditions, a blunt crack tip, wide crack crevice, and transgranular path of growth for NNpHSCC, whereas a sharp crack tip, narrow crack crevice, and intergranular growth path for HpHSCC have been observed. However, the simulations for the purpose of achieving the second objective are inadequate, in general. This deviation reflects some irrelevances of test conditions used in laboratory simulations, and the inability of the modeling approach to capture the complexity of field variables affecting crack growth rate. Nevertheless, the key to improving the prediction accuracy should start with the understanding of field operation variables that are responsible for crack initiation and growth, which will be the focus of this section.

30.2.1 Initiation and growth of high-pH stress corrosion cracking

SCC modeling is mainly for the purpose of determining the remaining lifetime for the safe operation of a pipeline. A time-dependent crack initiation and growth behavior found in the field should be determined first. Fig. 30.1 illustrates the time-dependent behavior of HpHSCC proposed by Parkins [1]. Fig. 30.1 was revised to name the stages of crack initiation and growth using a number system different from what was initially proposed by Parkins simply for the sake of consistency of fracture mechanics conventions. A brief description of each stage is given below:

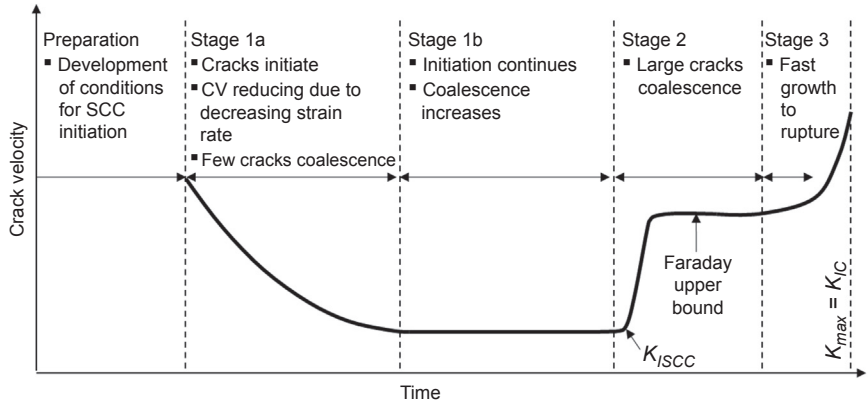

Figure 30.1 Schematic illustration of the effect of time upon stress corrosion cracking (SCC) velocity of pipeline steel exposed to carbonate–bicarbonate solution [1].

Preparation stage: This stage involves pitting and the creation of an occluded, often acidic, local environment, usually at sites of sulfide inclusions, as suggested by Parkins [1].

Stage 1a: This stage is characterized with the highest rate of crack growth and gradual reduction of crack velocity with increasing time or crack depth. It is believed that cracks are initiated by grain boundary selective dissolution, and the duration of initiation is probably greatly exaggerated in this illustration [2]. It should be noted that the early phases of cracking are unlikely to take place in situations where the crack tip−driving force can be described by the linear elastic fracture mechanics (LEFM) stress intensity factor, K (assuming Mode I loading in the current chapter). In general, significant surface or blunt notch plasticity will be involved in the early stage of crack development, which, nevertheless, can occupy a very large fraction of the total time to failure. Consequently, SCC initiation can be strongly influenced by surface roughness, cold work, initial air oxidation state, presence of surface defects and inclusions, and the applied and residual fabrication strains [1].

Stage 1b: This stage is featured with continuous initiations of small SCC cracks and their coalescence. This process takes up a large portion of the lifetime of the pipeline steel. It is believed that the process of multiple crack initiation, coalescence, and growth is essentially stochastic, and individual cracks in an ensemble of cracks are observed to grow in an irregular manner, frequently displaying dormancy (in contrast to the behavior of single isolated cracks) [2−5]. This stochastic feature arises, first, because of the presence of multiple initiation sites with differing sensitivities to initiation and orientation with respect to the principal stress. Second, interactions between the stress fields of nearby crack tips leading to crack coalescence and the phenomenon of shielding of small cracks by larger ones give rise to irregular propagation [1].

Stage 2: This stage concerns primarily the growth of a dormant crack, which can be characterized as a function of the LEFM crack tip stress intensity factor, K, and is normally relatively rapid by comparison with the preceding stages.

Stage 3: This stage has no engineering significance because rapid crack growth occurs and pipelines should be replaced prior to the occurrence of Stage 3.

For the convenience of modeling, the various stages of crack initiation and growth are reillustrated in Fig. 30.2 from a mechanistic point of view. The crack velocity, da/dt or da/dN (crack growth per fatigue cycle), is related to the range of stress intensity factor, ΔK, in the presence of cyclic stresses, or to K, in the case of crack growth by a constant stress. Both ΔK and K vary with the location of the crack tip and crack geometries. Because pipeline failures are primarily caused by the growth of cracks toward the opposite surface, it is the highest value of ΔK and K at the depth tip of a crack that is usually correlated to the crack velocity. With an increase of time, K and ΔK increase either because of the growth of an individual crack in its depth direction and/or the coalescence of small cracks in their length direction. The decrease of the crack growth rate with the increasing ΔK and/or K in Stage 1 indicates the irrelevance of crack initiation and crack growth with ΔK and/or K, because crack velocity should increase with their increase.

The lifetime of a pipeline is obviously limited by the onset of Stage 2. In Fig. 30.2, fast crack growth from a dormant state in Stage 1 starts when mechanically driven processes become predominant. Two mechanical processes are illustrated in

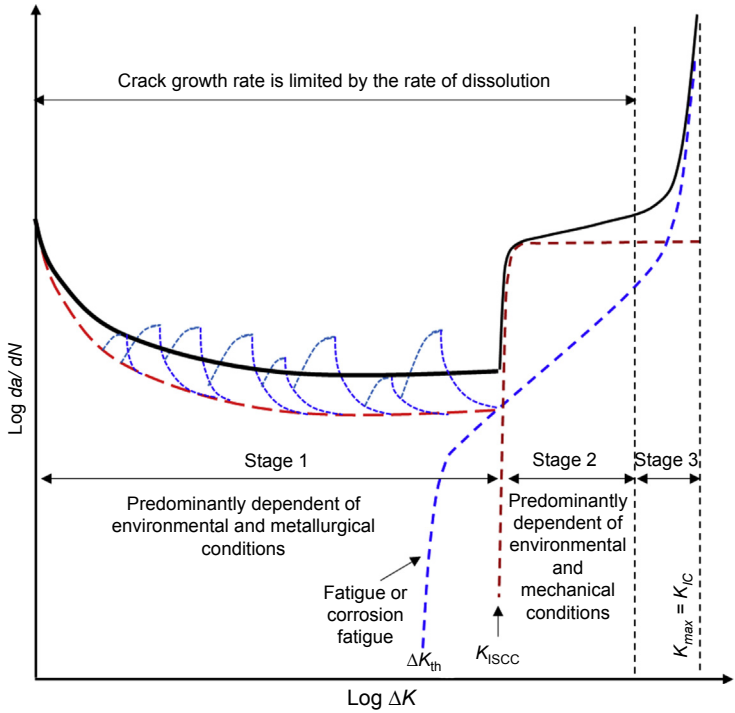

Figure 30.2 Schematic illustration of the effect of ΔK upon stress corrosion cracking velocity of pipeline steel exposed to carbonate−bicarbonate solution.

Fig. 30.2: one process of the fast growth is initiated when the maximum stress intensity factor at the crack tip exceeds K_{ISCC}, the threshold for SCC, whereas the second process of fast growth occurs when the maximum ΔK at the crack tip exceeds the fatigue threshold, ΔK_{th}. It should be noted that "maximum" here refers to the highest ΔK or K calculated at a given time for a given crack, depending on both the nature of pressure fluctuations and the crack geometries.

For the situation shown in Fig. 30.2, the fatigue threshold is lower than the SCC threshold; however, the SCC process corresponds to a much higher crack growth rate than the fatigue process. As a result, the contribution of crack growth by fatigue is negligible at the beginning of Stage 2 but becomes appreciable later in Stage 2.

The fatigue component of crack growth during a pipeline operation certainly varies with pressure fluctuations during pipeline operation. This situation will be examined later in detail. Accepting the fact that fatigue contributes to crack growth, the so-called superposition model can be used [6−8]:

$$\frac{da}{dt} = \left(\frac{da}{dt}\right)_{Stage\ 1} + \left(\frac{da}{dt}\right)_{Stage\ 2-SCC} + \frac{1}{f}\left(\frac{da}{dN}\right)_{Stage\ 2-CF} \tag{30.1}$$

where $(da/dt)_{Stage\ 1}$ is the crack growth attributed to the growth mechanisms in Stage 1 if they still exist in Stage 2; $(da/dt)_{Stage\ 2-SCC}$ is the crack growth contribution caused by SCC mechanisms; $(da/dN)_{Stage\ 2-CF}$ is the contribution of crack growth caused by fatigue or corrosion fatigue; and f is the frequency of fatigue cycle.

Eq. (30.1) can be universal for crack initiation and growth before the onset of Stage 3. From Eq. (30.1) and the illustration shown in Fig. 30.2, one can construct several crack growth scenarios representing different relative contributions of the three-crack growth terms included in Eq. (30.1). A total of six different scenarios could be generated based on Eq. (30.1) and the illustration shown in Fig. 30.2. These six scenarios are further demonstrated in Fig. 30.3 and could also be expressed by representative equations summarized in Table 30.1. Each of these six scenarios is briefly discussed below.

Model A—Pure dissolution limited, represented by Curve A: This is a situation where conditions for the onset of mechanisms of crack growth for Stage 2 are not realized before pipeline failure. Under the circumstances, SCC cracks appear shallow and can be long in their length direction; they are often termed as dormant cracks in crack colonies found on the surface of pipeline steels.

Model B—Pure fatigue or corrosion fatigue limited, represented by Curve B: Cracks can be initiated directly by mechanisms of fatigue or corrosion fatigue, and the entire life of the pipeline is also governed by mechanisms of fatigue or corrosion fatigue. Model B is most likely to occur in oil pipeline steels because of the very frequent pressure fluctuations and their large amplitude. Despite the above facts, the accumulated number of fatigue cycles are usually well below those required for the initiation of fatigue cracks because of a much lower frequency of pressure fluctuations, which will be further discussed.

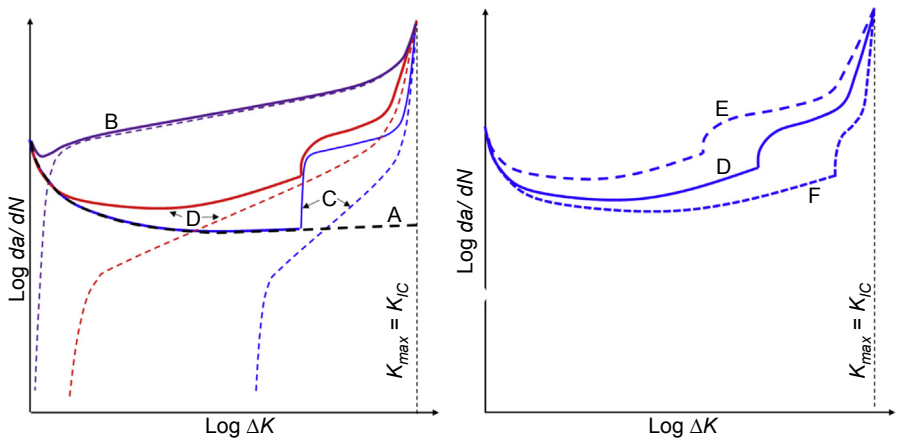

Figure 30.3 Schematic illustration of the effect of ΔK upon stress corrosion cracking velocity of pipeline steel exposed to carbonate−bicarbonate solution and the ways of superimposing the contribution to crack growth rate by different crack growth mechanisms.

Table 30.1 Crack growth rate expressions representing individual crack growth mechanisms and their combinations

Model	Description	Equations
A	Pure dissolution limited—Curve A	$\frac{da}{dt} = \left(\frac{da}{dt}\right)_{Stage\ 1\ and\ Stage\ 2}$
B	Pure fatigue or corrosion fatigue limited—Curve B	$\frac{da}{dt} = \frac{1}{f}\left(\frac{da}{dN}\right)_{F\ or\ CF}$
C	Sequential summation—Curve C	$\frac{da}{dt} = \left(\frac{da}{dt}\right)_{Stage\ 1} + \left(\frac{da}{dt}\right)_{Stage\ 2-SCC}$
D	Simple superposition—Curve D	$\frac{da}{dt} = \left(\frac{da}{dt}\right)_{Stage\ 1} + \left(\frac{da}{dt}\right)_{Stage\ 2-SCC} + \frac{1}{f}\left(\frac{da}{dN}\right)_{Stage\ 2-CF}$
E	Positively interactive superposition—Curve E	$\frac{da}{dt} = \varphi\left[\left(\frac{da}{dt}\right)_{Stage\ 1} + \left(\frac{da}{dt}\right)_{Stage\ 2-SCC} + \frac{1}{f}\left(\frac{da}{dN}\right)_{Stage\ 2-CF}\right]$, and $\varphi > 1$
F	Negatively interactive superposition—Curve F	$\frac{da}{dt} = \varphi\left[\left(\frac{da}{dt}\right)_{Stage\ 1} + \left(\frac{da}{dt}\right)_{Stage\ 2-SCC} + \frac{1}{f}\left(\frac{da}{dN}\right)_{Stage\ 2-CF}\right]$ $\varphi < 1$

Model C—Sequential summation—Curve C: This is a situation at which Stage-1 initiation and growth and Stage-2 growth occurs all by direct dissolution of iron at the crack tip. However, crack initiation and growth in Stage 1 is not mechanically driven. In Stage 2, mechanical driving forces reach to the threshold of SCC and are responsible for fracturing passivating film but do not make any direct contribution to the advancement of a crack. Model C is an idealized situation of HpHSCC where the effect of fatigue on crack growth is ignored or too small to consider.

Model D—Simple superposition—Curve D: Because the first term in the Model D equation is negligible (see Model A for explanation), usually only the last two terms are seen, forming the most common format of superposition model. For the latter two terms, mathematic operations such as summation and integration are often used to calculate crack growth rate. The summation operation includes the addition of the crack growth rate corresponding to each load cycle, as determined from a constant amplitude fatigue or corrosion fatigue test [9], to the crack growth rate of SCC. Integration is used to integrate the SCC crack growth rate under cyclic stresses [10].

Models E and F—Interactive superposition—Curves E and F: Different from model D, the crack growth rate is enhanced or reduced because of the load interaction effects, which consist of load history interactions, time- or cyclic loading frequency–dependent load interactions, and their mutual interactions, which will be discussed in detail in Section 30.2.3. In the case of $\varphi > 1$, the interactions would yield an enhanced crack growth rate (Curve E), whereas a reduction of the crack growth rate can be observed when $\varphi < 1$ (Curve F).

Fig. 30.4 is a replot of Fig. 30.3 in terms of crack growth velocity, *da/dt*, versus time. It is clear that the positively interactive superposition—Curve E—would yield the shortest time of operation. The pure fatigue or corrosion fatigue limited models—Curve B—may yield quite a long time of safe operation. This is because of the extended time for crack initiation and early crack growth by fatigue, as well as the very low loading frequency of the fatigue cycle, despite the fact that crack growth per each fatigue cycle, *da/dN*, can be high, especially during Stage-2 crack growth. As a result of low loading frequency, Curve B_2 would be a more accurate representation of the crack growth caused by the pure fatigue crack initiation and growth of pipeline steels.

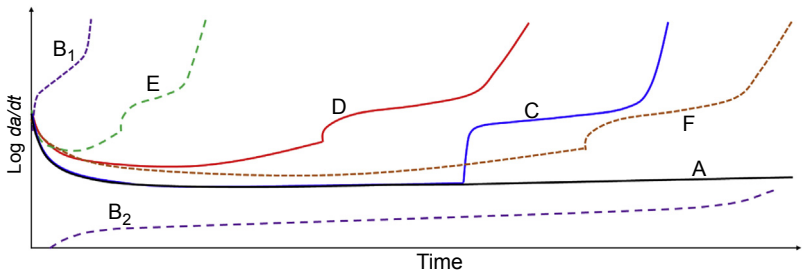

Figure 30.4 Schematic illustration of the dependence of crack growth rate, *da/dt*, on time of pipeline steel exposed to carbonate–bicarbonate solution.

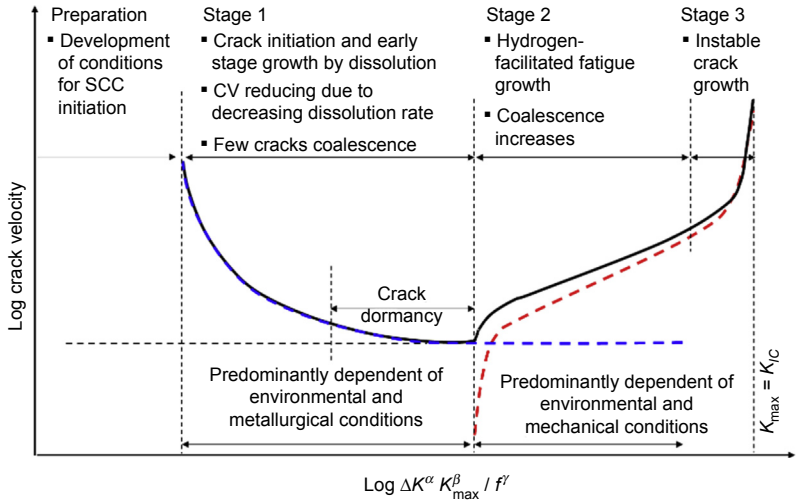

Figure 30.5 Schematic illustration of the effect of $\left(\Delta K^{\alpha} K_{\max}^{\beta} / f^{\gamma}\right)$ upon stress corrosion cracking (SCC) crack velocity of pipeline steel exposed to near-neutral pH solution.

30.2.2 Initiation and growth of near-neutral pH SCC

From extensive investigations for over 30 years since the discovery of NNpHSCC [11,12], the physical processes of crack initiation and growth have been determined, despite the fact that some details in various aspects of crack initiation and growth are yet to be understood [13]. The crack growth in Fig. 30.5, *da/dt*, is correlated to a combined factor, $\Delta K^{\alpha} K_{\max}^{\beta} / f^{\gamma}$ [14,15], where α, β, and γ are constant; f is the cyclic frequency of pressure fluctuations to be discussed in Section 30.5. Fig. 30.5 shows the latest understanding of the physical processes involved in crack initiation and growth of pipelines in near-neutral pH environments. The growth curve is a superposition of crack growth by direct dissolution of steels at localized areas on pipe surface during initiation or at the tip of a crack during crack growth (**the dissolution growth curve**), and by a process involving the interaction of fatigue and hydrogen embrittlement (**the hydrogen-facilitated fatigue growth curve**).

The dissolution growth curve is predominantly important during crack initiation and early-stage crack growth. Crack initiation results from localized corrosion at the pipe surface, leading to the formation of cracklike defects. This stage is usually dependent on coating conditions, soil environments, and steel metallurgy. The rate of dissolution reduces as crack depth increases, and many cracks stop growing when reaching a crack depth of ~1 mm. At this point, the crack enters a state of dormancy [16–18], as shown in Fig. 30.5. Stage 1 can be controlled through effective coatings and cathodic protection. A dissolution-dominant crack growth model in this stage is valid because of the following facts:

1. Mechanical driving forces are negligible primarily because of a very small stress intensity factor at the crack tip. Direct initiation of a fatigue crack from metallurgical discontinuities,

such as inclusions, often requires very aggressive fatigue conditions that are far from realistic pressure cyclic conditions found during operating oil and gas pipelines [19]. For example, crack initiation by fatigue usually required over 10^5 cycles under very low *R*-ratios (~0.4) and high maximum stresses (100% yield strength) [19]. Such an aggressive cyclic condition is not realistic in the case of pipeline operations. The worst cyclic loading conditions are usually at discharge sites of oil pipelines where the number of underload cycles, with low *R*-ratios, are well below 1000 cycles per year [20–22]. It would take more than 100 years to reach sufficient fatigue damage in order for a crack to initiate solely by fatigue.

2. Direct initiation of a crack by a hydrogen mechanism is not possible because of a very low diffusible hydrogen content in the NNpH environments. It has been determined that the amount of diffusible hydrogen in pipeline steels exposed to a NNpH environment is about an order of magnitude lower than the critical hydrogen concentration necessary for developing hydrogen-induced blistering in pipeline steels [23].
3. NNpHSCC cracks are characterized with a wide crack crevice in general [16,24,25], which is formed because of the nonpassivating nature of the NNpH environments and general corrosion occurring concurrently at the crack tip and on crack walls [26]. This corrosion scenario often turns a defect with large depth/width ratio into a pit with reduced mechanical driving forces for further growth by a cracking mechanism. This situation is sharply different from a HpHSCC scenario in which preferred corrosion along grain boundaries and passivation of a corroded surface enable the crack to maintain a high depth/width ratio with a high stress intensity factor for growth [25].

The hydrogen-facilitated fatigue growth curve shown in Fig. 30.5 can be best justified by the following experimental results, although other extensive investigations have also been performed [27–29].

1. The role of fatigue: Crack propagation has never been observed under a static loading condition in laboratory testing, even at high stress intensity factor, except during crack initiation and early stage growth associated with the mechanisms of corrosion, as discussed previously [30–34]. An active crack often ceases to grow when loading is switched to static hold [27]. In contrast, crack growth is found to grow under cyclic loading above the critical fatigue threshold. Fig. 30.6 shows a typical example of a nonpropagation scenario under static hold at two levels of maximum stress intensity factors [27]. However, crack growth is observed when cyclic loading is resumed, although immediate crack growth did not occur in an environment when the mechanical driving force applied was low, as caused by its relatively lower diffusible hydrogen generated in the system.
2. The role of hydrogen: The decisive role played by diffusible hydrogen is directly demonstrated by testing compact tension (CT) specimens with different conditions of coating coverage, as shown in Fig. 30.7 [27,28]. These specimens have the same crack geometry and mechanical conditions at the start of the tests. Only the specimen with a bare surface shows a sudden increase of crack growth rate after a period of incubation, corresponding to the generation of hydrogen at the sample surface as a result of general corrosion and the time required for achieving a state of hydrogen equilibrium throughout the specimen [27].

The hydrogen-facilitated fatigue growth curve exhibits a very low crack growth rate in the stage of crack initiation and early crack growth because of very benign mechanical driving forces. However, the curve has a growth rate significantly higher than the rate of the dissolution growth curve after crack dormancy. The crack growth by dissolution beyond crack dormancy is possible, although at very low growth rate, as assumed by

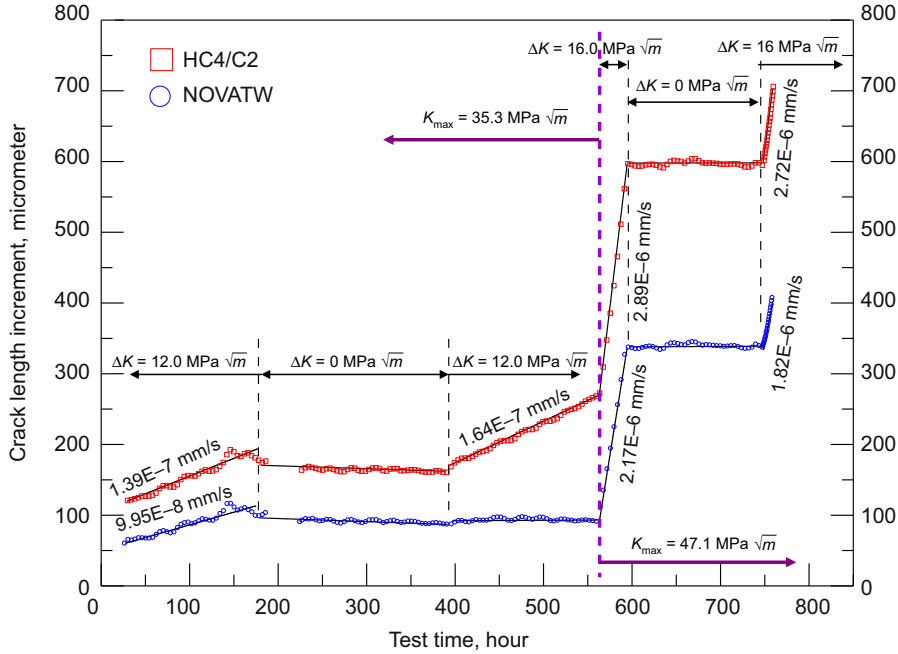

Figure 30.6 Crack length increment as a function of test time in two different near-neutral pH soil solutions [27].

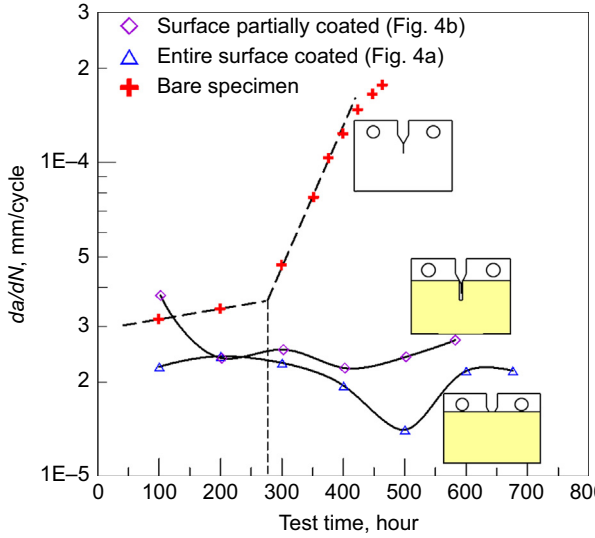

Figure 30.7 Crack growth rate as a function of test time for three specimens tested in C2. All the tests were performed at the same starting conditions at $K_{max} = 35.3$ MPa$\sqrt{m}$, K = 12.0 MPa$\sqrt{m}$, and $f = 0.005$ Hz [27].

the dissolution curve shown in Fig. 30.6. However, a near-zero crack growth rate during holding at maximum stress intensity factors in Fig. 30.6 was observed. Assuming a growth rate by dissolution of 7.7×10^{-10} mm/s [35,36], a hold at maximum stress intensity factor in Fig. 30.6 would yield a crack growth as low as 0.66 μm [27], which is too small to be resolved, even under the examination of a scanning electron microscope. The insignificant crack growth has further justified the minor contribution of crack growth by dissolution in the stage where crack growth by the hydrogen-facilitated fatigue mechanisms is predominant.

The transition from the dissolution-dominant growth to hydrogen-facilitated fatigue-dominant growth is caused by an increase of mechanical driving forces, making the Stage-2 mechanisms operate. Details of the transition are further discussed in Section 30.4 (Fig. 30.8).

30.2.3 Interactive behavior of crack initiation and growth

Interactive behavior of crack initiation and growth can be defined as enhanced or reduced crack initiation and growth caused by mutual interactions between different mechanisms concurrently present in a given cracking stage. Interactive behavior of crack initiation and growth can be categorized into the following two types:

30.2.3.1 Load history–dependent interactions

Engineering components are generally operated under variable amplitude cyclic loadings in service [20–22], although they are designed by considering the level of static stress or constant amplitude fatigue strength. When a component is subjected to variable amplitude cyclic loadings, the crack growth of the component can be retarded or accelerated through load interactions; that is, the crack growth rate at any given time may depend not only on the current loading conditions but also on the prior loading history. The fatigue life of engineering structures can be also extended or shortened.

Underload and overload are two common features of variable amplitude cyclic loadings. Any other types of variable amplitude fatigue waveforms can be obtained by combining these two fundamental forms. Underload and overload can accelerate and retard subsequent fatigue crack growth, respectively [37,38]. The obtained growth rates differ from the crack growth predicted by a linear summation of damage of constant amplitude cyclic loadings with magnitudes equal to the variable amplitude. The predicted growth rate by linear summation can be expressed by the following equation [9]:

$$\left(\frac{da}{dN}\right)_{block} = N_1\left(\frac{da}{dN}\right)_1 + N_2\left(\frac{da}{dN}\right)_2 + \cdots \tag{30.2}$$

where $(da/dN)_{total}$ is the linear summation; $(da/dN)_1$ is the constant amplitude crack growth rate at amplitude 1 and N_1 is the number of cycles in the block with amplitude

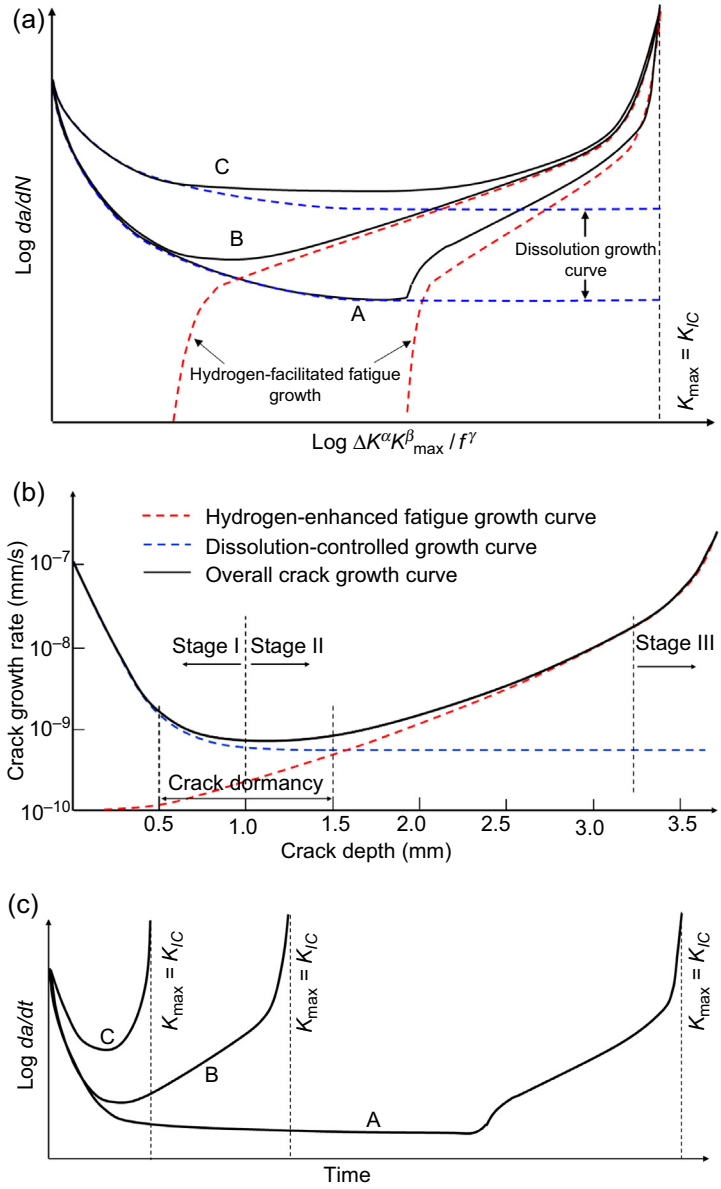

Figure 30.8 Schematic illustration of crack growth velocity of pipeline steel exposed to near-neutral pH environments: (a) *da/dN* versus $\left(\Delta K^{\alpha} K^{\beta}_{\max} / f^{\gamma}\right)$, (b) *da/dt* versus crack depth/time, (c) *da/dt* versus time.

1; and $(da/dN)_2$ is the constant amplitude crack growth rate at amplitude 2 and N_2 is the number of cycles in the block with amplitude 2.

Such variable amplitude fatigue waveforms are performed in the laboratory to simulate the crack growth in many engineering components in service, including turbine

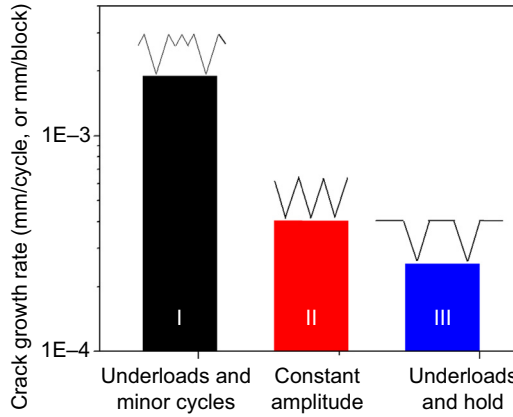

Figure 30.9 A comparison of crack growth rates of the same pipeline steel tested under different loading conditions [52].

blades [39,40], aircraft [41,42], bridges [43], and welded joints [44,45]. The predicted lifetime based on such testing results is much closer to the actual service time of the components. The materials studied under variable amplitude fatigue tests include steels [9,46,47], titanium alloys [40,48], and especially Al alloys [9,37,39,46,47,49,50] that are widely used in the aircraft industry.

A simple example of load history−dependent interactions for crack growth of pipeline steels in NNpH environments is shown in Fig. 30.9, in which the underload cycles in all three cases have an R-ratio of 0.5 and the minor cycles in Case I have $R = 0.9$ [51]. The latter was determined to be nonpropagating without the underload but obviously lead to crack growth when combined with underload cycles (Case I) and compared with the crack growth rate measured under constant amplitude loading (Case II). In contrast, the crack growth rate was reduced when the minor cycles were replaced with a hold at the maximum load (Case III). This observation reflects the fact that crack growth proceeds by corrosion fatigue, and the crack growth under constant load, a situation of SCC, can be negligible.

To assess the degree of load history interactions, the mechanical loading or pressure fluctuation conditions acting on the pipelines must be well characterized. The spectra of pressure fluctuations consist of large pressure fluctuations with relatively low *R*-ratios (minimum pressure/maximum pressure) and many smaller pressure fluctuations with high *R*-ratios called minor cycles or ripple loads [22].

Depending on the location of pipeline sections, pressure fluctuations could be further characterized into three types based on relative pressure levels of the large loading events and minor cycles. Examples are shown in Fig. 30.10 for both oil pipelines and gas pipelines [22,52].

Type I—underload pressure fluctuations: Type-I pressure fluctuations are often found within 30 km downstream of a compressor station on gas pipelines or a pump station on oil pipelines. The maximum pressure of Type-I fluctuations is often controlled to be at or close to the design limit, allowing fluctuations only to a level

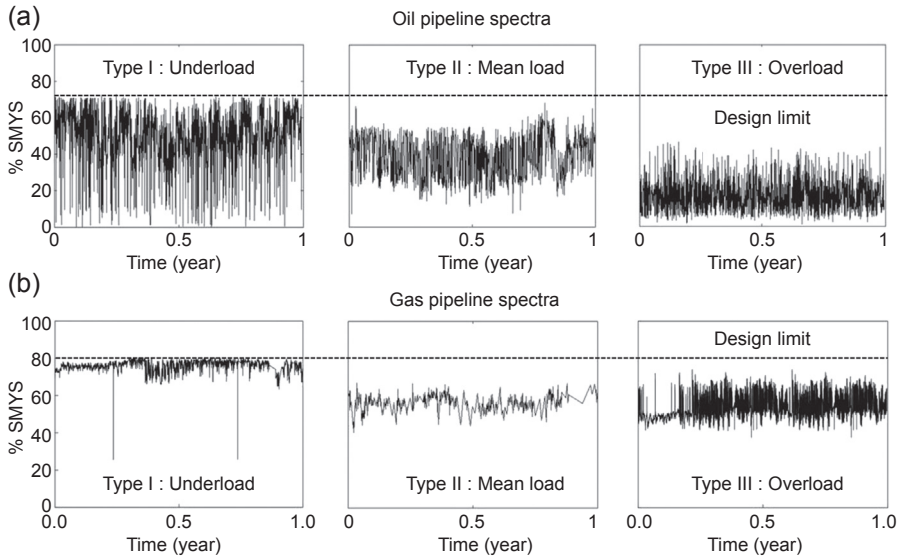

Figure 30.10 Three types of pressure fluctuations: (a) oil pipelines, (b) gas pipelines [22].

lower than the design limit. The spectrum consists of so-called underload cycles, which are large cycles with low *R*-ratios (min pressure/max pressure) and minor/ripple load cycles with very high *R*-ratios. Underload cycles in oil pipelines often have lower *R*-ratios, higher number of occurrences, and a faster rate of pressure changes (Fig. 30.10(a)) than the underload cycles in gas pipelines (Fig. 30.10(b)). Ripple load cycles are a main feature of gas pipelines.

Type II—mean load pressure fluctuations: Type-II pressure fluctuations are typically observed further down from compressor and pump stations. In the case of the Type-II pressure fluctuations, the mean pressure is lower than Type-I pressure fluctuations, and pressure spikes with a pressure level above the mean pressure but below the design limit are frequently seen. The mean pressure is still not low enough to eliminate the underload fluctuations typically seen in the case of Type-I pressure fluctuations.

Type III—overload pressure fluctuations: Type-III pressure fluctuations typically exist at, or close to, a suction site, where pressure spikes occurring above the mean pressure, also referred to as overload cycles, become predominant while the occurrence of underload cycles is minimized.

Because of the relatively high maximum pressure and large amplitudes of pressure fluctuations, Type-I pressure fluctuations have been further analyzed [22]. Typical characteristics in gas and oil pipelines are compared in Table 30.2. Oil pipelines are featured with higher frequency of underload cycles when compared to gas pipelines. The rate of loading is slightly different from the rate of unloading in the underload cycles. However, the range of loading/unloading frequency is very different between oil pipelines and gas pipelines. Both the unloading and loading frequencies in oil pipelines vary over a wide range from 10^{-6} to $\sim 10^{-1}$ Hz, whereas they are very

Table 30.2 Characteristics of Type-I pressure fluctuations in gas and oil pipelines [22]

Items		Oil pipelines	Gas pipelines
Underload cycles	Typical # of underload cycles/year	537	8
	Range of unloading frequency (Hz)	$6.89 \times 10^{-6} \sim 1.0 \times 10^{-1}$	$1.30 \times 10^{-6} \sim 9.16 \times 10^{-5}$
	Range of loading frequency (Hz)	$5.11 \times 10^{-6} \sim 1.0 \times 10^{-2}$	$1.34 \times 10^{-6} \sim 5.26 \times 10^{-6}$
Minor cycles	# Of minor cycles between two adjacent underloads	0–26	0–37

low and manifest over a narrower range in gas pipelines. The number of minor cycles between two adjacent underload cycles is generally higher in gas pipelines than in oil pipelines. The crack growth is predominantly driven by more frequent and larger amplitudes of fatigue loading during oil pipeline operation, while it is driven by enhanced crack growth at lower loading frequency and stronger load interactions. The latter is due to the presence of more crack growth–contributing minor cycles under the underload-type pressure fluctuations during gas pipeline operation.

It is clear that a reasonable modeling of SCC crack growth behavior must be made with a consideration of load history interactions. The simple superposition model as listed in Table 30.1 considers only a summation of crack growth under constant fatigue loading and under constant stress. Both the idealized loading conditions do not exist in field operation. As a result, the interactive approaches as listed in Table 30.1 must be considered for SCC modeling.

30.2.3.2 Time-dependent/frequency-dependent interactions

The time-dependent interactions arise from synergistic interactions among mechanical driving forces, environmental, and metallurgical attributes to crack growth. A brief description of various time-dependent synergistic interactions is given below.

1. The rate of corrosion, the most essential time-dependent process for crack growth: Locally focused dissolution leads to the formation of cracklike features, which is a predominant process of crack initiation and early stage of crack growth for both NNpHSCC and HpHSCC. It seems also common for both the SCC types that the rate of dissolution in the crack depth direction decreases with increasing crack depth, leading to dormancy in the crack depth direction. In the case of NNpHSCC, the rate of dissolution in Stage-2 crack growth may cause a limited advance of the crack. However, dissolution can cause crack tip blunting, because of nonpassivating nature of NNpH environments, especially when cracks grow at low rates. An example of this process can be found in Ref. [53].
2. The time-dependent film formation in HpHSCC: A stronger tendency of repassivation film results in a lower crack growth rate because of a smaller duration for charge transfer during a film rupture event. Repassivation kinetics was found to depend on temperature, water

chemistry, potential, and the compositions and microstructures of steels [1,54,55]. The corrosion products formed may also cause the closure of a crack, which in turn may affect the effective mechanical driven forces for crack growth.

3. The time-dependent process of hydrogen diffusion to the crack tip: The effect of hydrogen on crack growth would be enhanced when the rate of hydrogen diffusion, as governed by law of diffusion, is synchronized with the rate of loading, as will be discussed below. The time- and temperature-dependent hydrogen segregation to the crack tip will also lead to hydrogen-enhanced localized plasticity (HELP) [56,57], which would in turn affect the stress distribution at the crack tip.
4. The time-dependent rate of loading: The rate of loading is critical for both NNpHSCC and HpHSCC. For the former, increasing the load would increase the magnitude of the triaxial tensile stresses in the plastic zone ahead of the crack tip and therefore the segregation of diffusible hydrogen to the crack tip. Maximum hydrogen effects can be achieved when the rate of loading is slow enough to allow hydrogen achieving maximum segregation to the crack tip. In the case of HpHSCC, the loading rate is directly related to the strain rate, and a matching of the loading rate with the rate of film formation would lead to the highest susceptibility to crack growth.
5. The time-dependent plastic deformation such as low-temperature creep: Low-temperature creep is caused by the motion of mobile dislocations generated from prior plastic deformation [58–62]. The advance of the crack tip causes instantaneous plastic deformation to the material at the crack tip because of the increased stress intensity factor. Plastic deformation continues with time because of a gradual exhaustion of mobile deformations generated by instantaneous plastic deformation. Maintaining a critical strain rate, especially at the grain boundaries within the plastic zone, is key to the film rupture for HpHSCC [1]. In the case of NNpHSCC, low-temperature creep is further enhanced in the presence of atomic hydrogen, which reduces the bonding strength of Fe, making the motion of mobile dislocation occur at lower critical shear stress.
6. The time-dependent morphological changes at the crack tip: The crack tip blunting, either caused by direct dissolution of materials at and around the crack tip, or by low-temperature creep or HELP, would affect the stress distribution. The highest triaxial stress would shift from the tip of a sharp crack to the region away from the crack tip as the crack tip becomes blunt. This shift of highest triaxial stress creates a process of sampling during which the highest triaxial stress sweeps a region of material within the plastic zone where the weakest links, such as grain boundaries, inclusions, or other metallurgical discontinuities, are sampled and may be fractured to form microcracks. The latter may propagate to join the main crack. Such a cracking process would not be possible if the time-dependent crack tip blunting had not occurred.

The discrepancies between the existing crack growth models based on the results of constant amplitude corrosion fatigue and those models with a consideration of load interactions resulting from variable amplitude corrosion fatigue are further summarized and illustrated in Fig. 30.11 [13]. Fig. 30.11 demonstrates that a direct application of the Paris law (see Section 30.5 for details) to the cracking of pipeline steels in a corrosive environment is not justified, which should be also true when modeling HpHSCC.

30.3 Modeling of crack initiation and growth in Stage 1

From the view of pipeline integrity management, the modeling of Stage 1 crack growth behavior is less important than the modeling of Stage 2 crack growth behavior. This

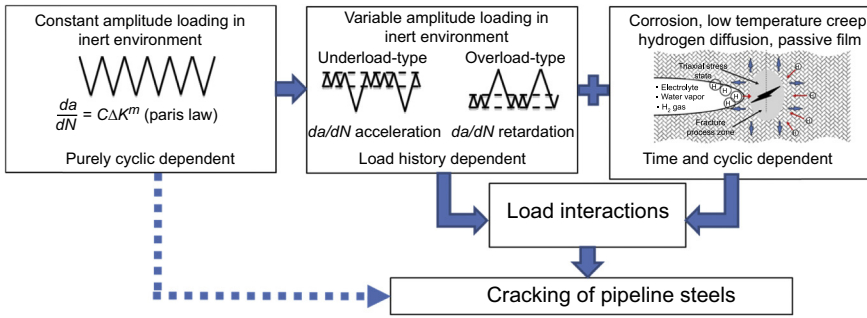

Figure 30.11 Various load interaction scenarios and their links to the cracking pipeline steels [13].

lower priority is because crack dimension in Stage 1 is small, usually around or less than 1.0 mm, which is not detectable during inline inspections, and would not cause premature failure of pipeline steels if Stage-2 mechanisms were not operative. For the reasons above, the modeling of Stage-1 cracking growth behavior has not been well studied, although initiation mechanisms of microstructurally short cracks, cracks with depths about a few grain sizes or less than 100 μm, have been reasonably studied.

30.3.1 Modeling of crack initiation and early stage crack growth of HpHSCC in Stage 1

A common feature of the Stage 1 behavior of either HpHSCC or NNpHSCC is that the rate of crack growth is highest upon the onset of the crack initiation, but decreases gradually as it propagates. The observations are not well rationalized and often conflict with explanations. For Stage 1 of HpHSCC, it was believed that crack velocity reduces because of decreasing strain rate, and further crack growth in depth is limited, but crack growth in length continues because of the coalescence of multiple small cracks in the length direction [1].

The highest strain rate at the beginning of a test was first related to low-temperature creep of pipeline steels that usually exhibit a logarithmic behavior with time because of gradual exhaustion of mobile dislocations from prior processing [1,58–62]. A low-temperature creep rate usually will become infinitely small beyond 24 h when applied stress is below or around yield strength. It should be noticed that self-sustainable creep deformation leading to ductile failure could be achieved under a constant load corresponding to a stress above yield strength but well below the tensile strength. Although the creep strain–time curve under the circumstances could be very similar to that observed when thermally activated processes of creep deformation are involved, the sustained creep strain results from a gradual increase of tensile stress from the gradual reduction of load-bearing cross-section.

Consideration has also been made to incorporate the dependence of the strain rate of pipeline steel under cyclic loading. Similar to the situation of constant load, pipeline steels would usually undergo either a cyclic softening or cyclic hardening, for which

the highest strain rate would be seen at the beginning of cyclic loading, and cyclic strain rate approaches zero with an increasing number of cycles, which should be reached before the onset of SCC initiation for pipeline steels experiencing SCC in the field. However, in laboratory simulations, the highest strain rate is seen as soon as a test starts and conditions of cracking are established, before the exhaustion of mobile dislocations for low temperature creep deformation. Strain rate at special metallurgical discontinuities, such as grain boundaries, phase interfaces, and inclusions, within the pipeline steels under a given bulk strain rate, can be very different because of strain incompatibility at metallurgical discontinuities. However, the heterogeneity of strain rate still cannot be used to rationalize the highest strain rate or a critical strain rate required at the time of crack initiation occurring in the field because the SCC initiation preparation stage may take several years. It is therefore obvious that a simple correlation of strain rate to crack initiation is not justified. It also seems true that the observation that HpHSCC cracks cease to grow in the depth direction after initiation may not be solely caused by the reduced strain rate as postulated by Parkins [1]. This is because strain rate at the crack tip should increase as a crack becomes deeper. The stress intensity factors and the corresponding strain rate at the tip of the crack should be very small during crack initiation and the early stage of crack growth.

Investigations on crack initiation in HpHSCC environments have been primarily conducted under very aggressive mechanical conditions, such as a slow strain rate test (SSRT) [63−66]. Although SSRTs are fast and relevant to some extent, they could yield a conclusion that might be inconsistent with the mechanisms found in the field. Pipeline steels are susceptible to HpHSCC initiation within some critical potential ranges, which changes with the temperature, and the stress at which the initiation of HphSCC was observed was larger than the yield stress of steel, which seems inconsistent with the fact that pipeline steels are normally operated at stresses below 80% specified minimum yield strength (SMYS). The initiation is very much surface dependent. The original surface was more susceptible to SCC initiation than the polished surface.

The investigation was further determined that for a mechanically polished surface with a deformed layer, SCC initiation involved the following [67]: Cracks in the surface oxide concentrated the anodic dissolution to such an extent that there was transgranular SCC in the deformed layer. Cracking was intergranular when it had penetrated the deformed layer. Transgranular cracks could be stopped at ferrite grain boundaries oriented perpendicular to the crack propagation direction. SCC initiation on an electropolished surface involved the following: The oxide film was cracked at many locations, but intergranular stress corrosion cracks only propagated into the steel when an oxide crack corresponded to a grain boundary. Oxide cracking away from a grain boundary is expected to be healed. The observed SCC initiation mechanism was not associated with preferential chemical attack of the ferrite grain boundaries.

The crack growth rates determined from SSRTs are usually much higher than and bear no connection to the rate of crack initiation and early-stage crack growth found in the field. It has also not been demonstrated that the rate of crack velocity was highest at the beginning of crack initiation as suggested by the bathtub model shown in Fig. 30.1.

In Stage 1, the crack becomes substantially longer because of the coalescence of multiple small cracks along the longitude of the pipeline. Although the critical geometrical conditions to achieve crack coalescence has been defined, it is not clear whether the coalescence of these small cracks is a result of the randomness of crack initiation sites or sequential events in which existing cracks created conditions to initiate new small cracks in the vicinity of an existing crack.

It can be concluded, from the above arguments, that clear mechanisms leading to HpHSCC crack initiation and their earlier stage of growth and coalescence consistent with the HpHSCC bathtub model shown in Fig. 30.1 remain to be developed. Modeling of the cracking behavior in Stage 1 would require the determination of growth rate functions with conditions realistic to those of field operations. This is an area of knowledge that is still lacking.

30.3.2 Modeling of crack initiation and early-stage crack growth of NNpHSCC in Stage 1

In the case of NNpHSCC, initiation can be caused by many different mechanisms [19,21,31,32,68–72], such as preferential dissolution at physical and metallurgical discontinuities: scratches [68], inclusions [69], grain boundaries, pearlitic colonies, banded structures [31,32,69] in the steel, corrosion along persistent slip bands induced by cyclic loading before corrosion exposure [21,31], crack initiation at stress raisers such as corrosion pits [70,71], and localized corrosion through various galvanic effects related to mill scale [72], microstructures [31,32] and residual stresses [17,18]. The initiation of the microstructurally short cracks, usually less than 100 μm, can occur under constant stress loading. The early crack growth is due to the presence of high tensile residual stresses at the pipe subsurface that add to the applied stress. However, these cracks generally go into dormancy for the following reasons:

1. The reduced rate of dissolution at the crack tip in the depth direction due to a complicated process involving the gradient of CO_2 and the variation of ionic concentrations in the system. This is believed to be a primary cause for crack dormancy [73,74].
2. The nature and the magnitude of residual stresses at and near the outer surface of pipeline steels: Because the residual stress must be self-equilibrated, the high tensile residual stresses, if present at or close to the outer surface, which is a prerequisite for crack initiation, will usually decrease toward the inner surface and even become compressive. The reduction of tensile residual stresses or the presence of compressive residual stresses reduces the overall mechanical driving force for the growth in Stage 2. In the majority of crack colonies, the overall mechanical driving forces are below the threshold for crack propagation, and cracks remain in dormancy. Therefore, the nature and the magnitude of residual stresses determine largely when a dormant crack can be reactivated [17,18,35,36].
3. The level of diffusible hydrogen [27]: It acts together with the residual stresses. The chance of the crack remaining in a dormant state will be high if the concentration of diffusible hydrogen in the material surrounding the crack tip is low.

Among the three factors listed above, the first factor is predominant, whereas the second and third factors contribute little to Stage 1 crack growth but would define the length of dormancy in Stage 1 [35,36]. Fig. 30.12 shows the length and depth

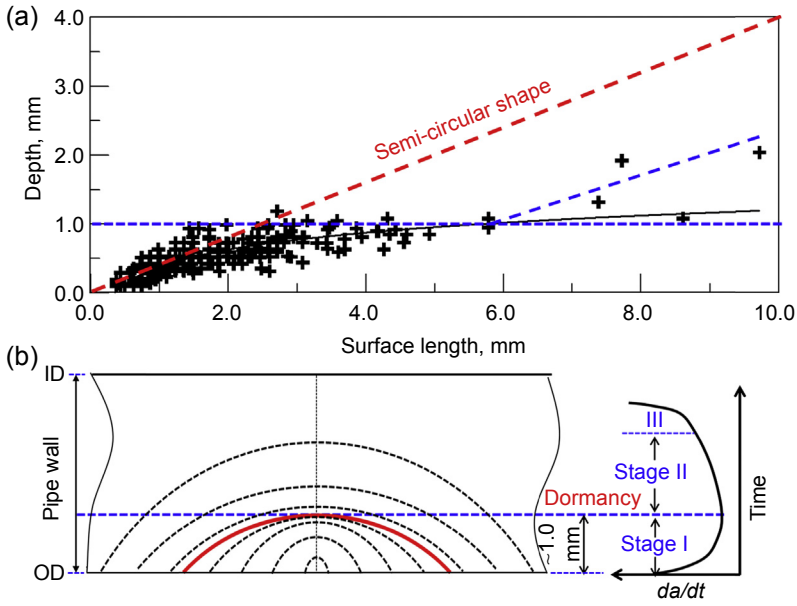

Figure 30.12 (a) Crack depth versus crack length found in the field: The horizontal *blue line* indicates the depth of cracks at which crack dormancy occurs; the inclined *blue line* indicates crack length−depth profile for growing cracks. (b) Three stages of crack initiation and growth: The *red line* demarcates between stage-I crack growth by dissolution and Stage-II crack growth by hydrogen-facilitated fatigue [13].

relationship of NNpHSCC cracks from crack colonies near the rupture site. Approximately 1% of cracks were found to have a crack depth larger than 1.0 mm. The dashed line in Fig. 30.12 represents the crack depth/length ratio of 0.5, which indicates a semicircular shape (left red dashed line in Fig. 30.12). As shown in Fig. 30.12, the crack ceases to grow or grows slowly in the depth direction when the crack depth reaches 1.0 mm, which indicates that the crack growth in the depth direction gradually decreases with an increase in crack length. This decrease of crack growth rate in the depth direction is a widely observed feature of NNpH SCC cracks, which is often referred to as crack dormancy. In general, less than 5% of cracks found in crack colonies were found to be able to grow continuously or discontinuously to a critical size, leading to rupture [53].

As a crack grows, the mechanical driving forces become higher, which should lead to an increase in crack growth rate. The increase of mechanical driving forces is obviously contrary to the observation of crack dormancy in the depth direction as shown in Fig. 30.12. Crack growth will also be governed by the principles of fracture mechanics when crack dimensions become appreciable. A semielliptical crack with its long axis parallel to the pipe surface would yield the highest stress intensity factor at the depth tip. In this case, a higher growth rate can be expected such that a semicircular shape, as illustrated in Fig. 30.12, could be formed. This evolution of crack geometries is

inconsistent with the crack profiles found from the field, because the ratio of crack length to depth is much higher than 2.0 (see Fig. 30.12). Therefore, the occurrence of dormancy should not be driven by mechanically related conditions, although such mechanical conditions could extend or shorten the length of dormancy, as will be discussed later.

The cracked oxide scale or mill scale on the pipeline surface is believed to form a galvanic couple with the steel substrate at the bottom of the cracks within the mill scale [72]. The rate of dissolution is inversely related to the pH of the solutions. Lower CO_2 levels in the environments yield higher pH of the solution in general. Much reduced corrosion was also observed at the bottom of a simulated disbonded coating with a narrow disbonding gap, as compared with the corrosion at the open mouth of the gap where the CO_2 level is highest. It has also been observed that a galvanic cell can be formed between the region with low/compressive residual stress and the region with high/tensile residual stresses.

The governing equations for crack initiation and early-stage growth have been established recently based on the crack length−depth profiles determined from characterizing cracks developed during field operation [35]. Crack depth, a, and crack length, $2c$, during Stage 1 crack initiation and growth, can be expressed as:

$$\frac{da}{dt} = \begin{cases} e^{-\frac{a}{m}} \cdot r, & a \leq 1.0 \text{ mm} \\ h, & a > 1.0 \text{ mm} \end{cases} \tag{30.3}$$

and

$$r = \frac{dc}{dt} = \text{constant}, \quad t = 0 \; and \; a = 0 \tag{30.4}$$

In the above equations, h represents the stable value of the depth crack growth rate by dissolution during Stage-1 crack growth. The value of h can be measured and determined experimentally; r is the crack growth rate by dissolution along the pipe surface, which could be regarded as a constant during crack propagation because the surface is assumed to be fully exposed to the same NNpH environment during the process of cracking; and m is a fitting parameter that could be obtained by fitting the field crack depth and length data.

The determination of constants, r, h, and m, is detailed in Ref. [35]. Fig. 30.13 shows three cases of Stage-1 crack growth with a constant h value, which was measured experimentally to be 7.69×10^{-10} mm/s in average when an X65 pipeline steel was tested in NNpH solution [35,36]. For a given h value, three different m values were selected to fit the crack depth−length profile shown in Fig. 30.13. Different values of m could be related to the different dissolution rates of soil environments, galvanic behavior, and materials resistance to dissolution. In particular, a crack depth−length profile with a high m value would correspond to a crack approaching a

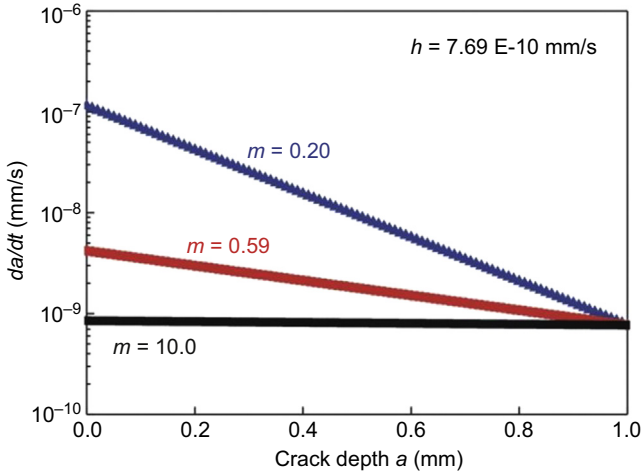

Figure 30.13 Dependence of crack growth rate as a function of crack depth for cracks with different *m*-value but the same *h*-value [35].

semicircular shape, which is not typical of NNpHSCC cracks. On the other hand, a crack depth−length profile with a low *m* value is associated with cracks having large crack length/depth ratios and is very typical of NNpHSCC cracks.

A crack growth rate at the surface, as high as 1.1×10^{-7} mm/s, has been observed during simulation of enhanced crack initiation and growth caused by the galvanic coupling or the presence of residual stresses [17,18]. In the latter case, a high average crack growth rate was obtained with an estimated value of r of 0.8×10^{-7} mm/s. Based on this average rate and assuming an a-$2c$ curve with $m = 0.2$, the value of r is estimated to be 8.3×10^{-7} mm/s. This value is even higher than the crack growth rate of 1.1×10^{-7} mm/s (the *blue curve* in Fig. 30.13).

The high dissolution rate at the surface, for example, at around 1.0×10^{-7} mm/s, forms a sharp contrast with the crack growth rate that was determined based on the dissolution rate measured by exposing a steel coupon with a polished surface directly to a near-neutral pH solution, which was determined to be 1.4×10^{-9} mm/s [14]. At the latter growth rate, it would take about 22 years for the crack to reach a depth of 1.0 mm, which is not consistent with the field observation that the life of pipeline steels with SCC is usually about 20−30 years [11,12]. On the other hand, it would take less than 2 years for a crack to reach a depth of 5 mm at a growth rate of 1.0×10^{-7} mm/s, which is also not reasonable. Therefore, a high dissolution rate at the surface but a reduced dissolution crack growth rate at the crack tip is supported.

Because of the nonpassivative nature of near-neutral environments, localized corrosion leading to the formation of cracklike/flawlike features is found to be caused by galvanic corrosion associated with grain boundaries, among ferrite−pearlite interfaces, and along banded microstructures [31,32]. In the latter case, galvanic corrosion leading to the formation of flawlike features took place parallel to the direction of applied stresses. This suggests that applied stress plays a little role during crack initiation [31].

A number of simulations of crack initiation under constant applied stresses below yield strength have also been performed [31,34]. These simulations usually lead to a flaw depth well below 100 μm, a corresponding rate of crack growth at order of 10^{-9} mm/s and decrease with the increasing time of tests. The crack growth rate of 9.6×10^{-9} mm/s, measured after a test for 110 days, is almost the same as that measured along the banded structure where the applied stress was actually parallel to the direction of crack growth. This observation strongly confirms the microstructurally sensitive process of crack initiation.

Almost all crack initiation studies were conducted using specimens with machined surfaces. The machined surfaces are usually located well below the actual pipe surface in order to make a straight specimen from curved pipes and are inside the pipe wall where banded structures are present. Microstructural bands are continuous and very susceptible to galvanic corrosion. As a result, the microcracks are primarily observed at locations where microstructural bands intercepted the machined surface. The microstructural bands are seldom found at and near pipe surface because of a much faster cooling rate during controlled rolling. Therefore, the overwhelming number of cracks found and the crack growth rate determined from these crack initiation studies can be highly unrealistic.

Despite the fact that the crack growth rates measured from laboratory simulations are somehow high, they are still too low to yield a lifetime of initiation consistent with what the field experiences. For example, the crack growth rate after an exposure of 1 year, would approach the stabilized rate of crack growth by dissolution. Based on the rate of 3.9×10^{-9} mm/s, it would require about 8 years to initiate a crack of 1.0 mm deep. This is still at the lower bound of the lifetime spent in crack initiation, considering the fact that pipeline steels with SCC often failed in 20−30 years of operation and Stage 1 is believed to elapse for a relatively short time.

It should be pointed out that the high rate of corrosion caused by the so-called "hydrogen-facilitated dissolution" [75,76] is not justified. As stated by Lu and his coworkers [30,77], "the fact that the active dissolution is almost unaffected by the hydrogen charging and tensile stress indicates that the phenomenon of hydrogen-promoted SCC is unlikely a result of hydrogen-facilitated active dissolution."

30.4 Modeling of the transition from Stage 1 to Stage 2

A dormant crack would not cause a threat to pipeline integrity if it does not evolve into Stage-2 crack growth. It is important to define the conditions that would potentially lead to the Stage-2 crack growth. Regardless of the type of SCC cracks, Stage-2 crack growth starts when mechanical driving forces meet the critical mechanical thresholds for growth. This prerequisite can be achieved because of a continuous increase of mechanical driving forces and/or a reduction of the critical threshold for Stage-2 crack growth. Each of these must be defined.

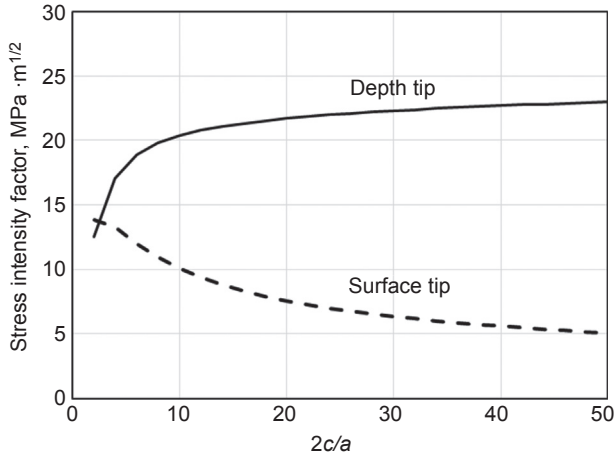

Figure 30.14 Variation of stress intensity factor at the depth tip as a function of $2c/a$. The calculations were made by assuming a crack with a fixed depth of 1.00 mm in a X-65 pipeline steel with an out-diameter of 914.2 mm, and thickness of 9.9 mm was loaded to 75% SMYS.

30.4.1 Conditions for the increase of mechanical driving forces

One of the most important features of HpHSCC in Stage 1 is the continuous formation and coalescence of multiple small cracks, which leads to an increase of crack length but limited growth in crack depth. Such a geometrical evolution of cracks would cause a continuous increase in K at the depth tip but a decrease in K at the surface tip. This is demonstrated in Fig. 30.14, in which a surface crack with a fixed depth of $a = 1$ mm but varied surface length ($2c$) in a X-65 pipeline steel with an out-diameter of 914.2 mm and thickness of 9.9 mm is loaded to 75% SMYS. It is obvious that crack coalescence in length direction is equivalent to crack growth in crack depth direction in terms of mechanical driving force. This is also applicable to NNpHSCC, for which crack growth preferentially occurs at surface tip than the depth tip in Stage 1, in addition to the increase of length/depth ratio caused by crack coalescence.

The second condition that could lead to an increase of mechanical driving forces is the presence of residual stresses [17,18,35,36]. Depending on the location on the surface and across pipe wall thickness, the residual stresses in pipeline steels could be either compressive or tensile and would vary across a pipeline steel wall in such a way that the net forces are equilibrated to zero.

Among all of the efforts made on the effect of residual stresses, a noteworthy study by Beavers et al. [78] on steel line pipes using a hole drilling technique has shown that the mean residual stress near the SCC colonies was about twice as high as in the control areas, and the difference was highly statistically significant at a 99.98% confidence level. The average residual stress for the SCC colonies was 216 MPa, with a standard deviation of 104 MPa, which gives a low bound tensile residual stress for SCC colonies of 112 MPa.

For plastically deformable materials, the residual and applied stresses can be added together directly until the yield strength is reached. For an X65 pipeline steel operated

at 75% SMYS, the maximum tensile residual stresses that can be added would be about 110 MPa (=0.25 × 65 ksi × 7 MPa/ksi = 113 MPa). This value is surprisingly consistent with the minimum residual stresses found in SCC colonies, as indicated previously.

The steel surface with the highest tensile residual stress is much more prone to pitting formation [17]. However, NNpHSCC cracks are mostly found at surface locations with the intermediate level of tensile residual stresses [18]. This discrepancy is related to the quick transition of high tensile residual stresses at the pipe surface to low tensile or even compressive stresses at the pipe subsurface. Details on how various patterns of residual stress distribution affect crack dormancy can be found in Ref. [35].

Residual stresses in the plastic zone ahead of the crack tip can also play a role in affecting the net mechanical driving force available. As characterized in Section 30.2.3, pipelines are subjected to variable amplitude pressure fluctuations. Therefore, stresses corresponding to a loading before the current loading could condition the material within the plastic zone to have different magnitudes and/or nature of residual stresses (compressive vs. tensile), affecting the crack growth during the current and future stress cycles. A compressive stress can be achieved when prior loading stress is higher than the current cycle of loading, whereas a tensile residual stress is produced when an underload is applied. The former loading scenario can reduce crack growth and is often termed as retardation effect, whereas the latter accelerates crack growth. As a result, the presence of an underload cycle could generate a tensile residual stress at the crack tip, which adds to the applied stress and leads to an increase of mechanical driving forces.

Increased mechanical driving forces could also be caused by special abnormalities associated with the pipeline section and the pipe surface (such as bents, surfaces with mechanical damage, and bottoms of pits), additional stresses caused by soil movement, and surface activities. The pipe location with those abnormalities would be more susceptible to crack initiation and growth.

30.4.2 Conditions for the reduction of the threshold values

It has been determined that the environmental conditions at the depth tip would become in favor of crack growth as crack growth in Stage 1 continues. Crack growth in the depth direction is usually considered because it leads to direct rupture or leak of pipeline steels. Growth of crack depth tip would be possible only when mechanical driving forces reach the thresholds. The critical thresholds themselves vary with time and depend on the location of the crack or crack colonies. The critical thresholds specific to a crack or crack colony locations have been defined for NNpHSCC, as summarized below:

- The first location-specific condition is the level of diffusible hydrogen [27]. It acts together with the residual stresses. The chance of a crack to remain at the dormant state will be high if the concentration of diffusible hydrogen in the material surrounding the crack tip is low.
- The second location-specific condition would be related to the pipeline sections with respect to the distance to pump stations or compressor stations, which yield different type of pressure

fluctuations as defined in Section 30.2.3. When the underload-type of pressure fluctuations are present, the critical thresholds for the onset of Stage 2 behavior can be much reduced. This reduction of thresholds could also be explained to be a result of an increase of mechanical driving force because of the addition of tensile residual stresses at the crack tip, as discussed in the previous section.

The threshold at a given location can be also time dependent. For example, the level of diffusible hydrogen may be affected by the seasonal changes in the environments surrounding the pipe surface with SCC cracks; the time when the most severe mechanical conditions occur; the availability of cathodic protection, which may fluctuate in a way that makes a location with SCC colonies not initially protected (leading to crack initiation) but protected or overprotected (generating more diffusible hydrogen) after crack initiation; and the time when the most severe mechanical driving forces coincide with the time of maximum segregation of hydrogen to the crack tip.

In the case of HpHSCC cracking, the location-specific conditions are also related to the temperature of pipeline steels because pipeline steels become more susceptible to cracking at higher temperatures and the specific range of cathodic potential within which pipeline steel is proven to be the most susceptible to crack initiation and growth [1,54,55].

30.5 Modeling of crack growth in Stage 2

30.5.1 Modeling of the threshold for Stage-2 crack growth

It is generally believed that Stage 2 crack growth starts when a critical value of mechanical driving forces has been reached at the tip/root of a crack/flaw. In general, both the threshold conditions for cyclic loading and constant stress loading must be considered when modeling the threshold of SCC in pipeline steels.

Fatigue crack growth generally follows a "Paris Law" [79] relationship wherein the log of the rate of fatigue crack growth varies linearly with the log of the change in the applied stress intensity factor associated with a given stress (i.e., pressure) cycle. Mathematically, the Paris Law relationship is as follows:

$$\frac{da}{dN} = C(\Delta K)^n, \tag{30.5}$$

where da/dN is the crack rate in mm/cycle; C and n are constants that depend on the material and the environment. The direct use of Paris law to consider crack growth attributed to cyclic loading in high or near-neutral pH environments can be very problematic for the reasons indicated in Section 30.2.3.

Fatigue crack growth will not occur from an existing cracklike defect below a threshold of stress intensity ΔK_{th}. A conservative lower bound estimate for ΔK_{th} was determined to be 2.2 MPa$\sqrt{m}$ (2.0 $ksi\sqrt{in.}$), according to API RP 1176—Assessment and Management of Cracking in Pipelines [80]. The crack growth rate, da/dN, corresponding to this threshold was found to be at 10^{-10}–10^{-9} in/cycle. Such a crack growth

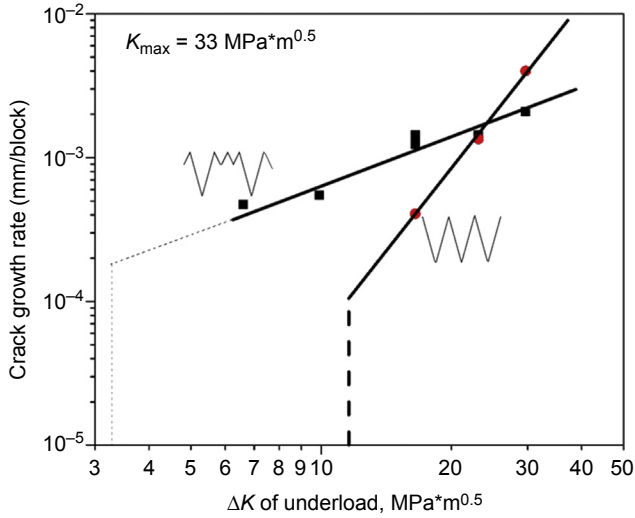

Figure 30.15 Determination of the threshold for crack growth under constant amplitude fatigue loading and variable amplitude fatigue loading (a), and the critical *R*-ratio of minor cycles for enhanced crack growth under variable amplitude fatigue loading in near-neutral pH environment (b).

rate may not have any engineering significance considering the fact that the frequency of fatigue cycles during oil and gas pipeline operation is very low, in the range of 10^{-6}–10^{-1} Hz, as listed in Table 30.2. The fatigue crack growth rate at ΔK_{th} would be at around 10^{-11}–10^{-12} mm/s assuming an intermediate level of loading frequency of 10^{-3} Hz. Under such a low crack growth rate, it would take a period of several 1000 years for a crack to grow 1 mm deep.

In contrast, the crack growth rate corresponding to the threshold determined under variable amplitude cyclic loading is found to be much higher. A direct comparison of the threshold, ΔK_{th}, is shown in Fig. 30.15 for the crack growth rate measured in a NNpH environment under both the constant amplitude fatigue loading and a variable cyclic loading consisting of one underload cycle and a number of minor cycles with a stress ratio of $R = 0.9$ [51,81,82]. The minor cycles are found to be nonpropagating if the underload cycle were not present. It is obvious that crack growth rate under variable cyclic loading is much higher than that under the constant amplitude loading for a given ΔK.

The crack growth rates shown in Fig. 30.15 were measured under constant K_{max} and loading frequency, f, from which ΔK_{th} can be determined based on the Paris law. It has been found that crack growth rate in NNpH environments can be also strongly influenced by K_{max} and f. It has been further determined that the crack growth rate under constant amplitude cyclic loading can be described by Eq. (30.6) [14,27].

$$\frac{da}{dN} = A\left(\frac{\Delta K^{\alpha} K_{max}^{\beta}}{f^{\gamma}}\right)^{n} + h \tag{30.6}$$

where A, n (=2), α (=0.67), β (=0.33), and γ (=0.033) are all constants, $\alpha + \beta = 1$, and h represents the stable value of crack growth rate in the depth by dissolution during Stage-2 crack growth. The value of h can be determined experimentally and was found to be about one order of magnitude lower than the first term in Stage-2 crack growth [35,36]. The power of the frequency was found to be a factor representing the influence of the corrosion environment on the crack growth rate. In particular, γ is related to the diffusible hydrogen in the steels, as discussed previously. $\Delta K^{\alpha} K_{\max}^{\beta} / f^{\gamma}$ is the combined factor that makes it possible to model the crack growth with all of the attributing factors included, such as crack dimension, pressure fluctuations, materials, and environments. The experimental correlation of crack growth rate with the combined factor is detailed in Ref. [14], where the combined factor was not normalized to have the unified expression in Eq. (30.6). Under the circumstances, the threshold value in terms of the combined factor was determined to be about 8000−8500 $(\mathrm{MPa}\sqrt{m})^3 / f^{0.1}$ [14].

The use of the combined factor as the crack growth threshold provides new insights of preferential growth of selected cracks. The shallow cracks after initiation with the crack tip located in the region of pipeline wall with appreciable level of tensile residual stresses would increase the value of $K_{\max}$ and therefore ΔK [$=K_{max}(1 - R)$]. For example, a crack with $a = 1.0$ mm and $2c = 10$ mm in a X-65 pipeline steel loaded to 75% SMYS would yield a combined factor of $\sim$4000 $(\mathrm{MPa}\sqrt{m})^3 / f^{0.1}$, assuming a loading frequency of 10^{-3} Hz and $R = 0.5$, which is well below the threshold of growth. The tensile residual stress could be added to the applied stress up to the actual yield strength of the material, which could be around 30% of SMYS. Under such a condition, the combined factor for the same crack under the same pressure conditions could be raised to over 9000 $(\mathrm{MPa}\sqrt{m})^3 / f^{0.1}$, which is well above the threshold of growth.

It should be noted that the crack growth threshold shown in Ref. [14] was determined using CT specimens representing crack growth behavior of a long through-thickness crack. The SCC cracks in the pipeline steels are initiated as small surface cracks, which usually have much lower thresholds than those of long cracks as the through-thickness cracks of CT specimens even under constant amplitude cyclic loading. Fig. 30.16 is a comparison of the threshold determined using CT specimens and with that of surface cracks from a full-scale test [83].

Eq. (30.6) predicts an increased crack growth rate with decreasing loading frequency. This growth rate dependence of loading frequency has been experimentally proven to be true only up to a loading frequency of 10^{-3} Hz or higher, as shown in Fig. 30.17 [82]. However, the loading frequency recorded during field operation can be much lower than 10^{-3} Hz, especially for gas transmission pipelines as shown in Table 30.2. Further tests under a loading rate lower than 10^{-3} Hz demonstrate the breakdown of Eq. (30.6). As shown in Fig. 30.23, the crack growth rate is found to decrease with decreasing f when f is lower than 10^{-3} Hz [82].

The transition of crack growth behavior at $f = 10^{-3}$ Hz is surprising but has been found to be related to the saturation of hydrogen ahead of the crack tip at the peak stress of the loading cycle [82,84]. A theoretical model has been developed to understand this crack growth behavior transition based on hydrogen effects on the crack tip

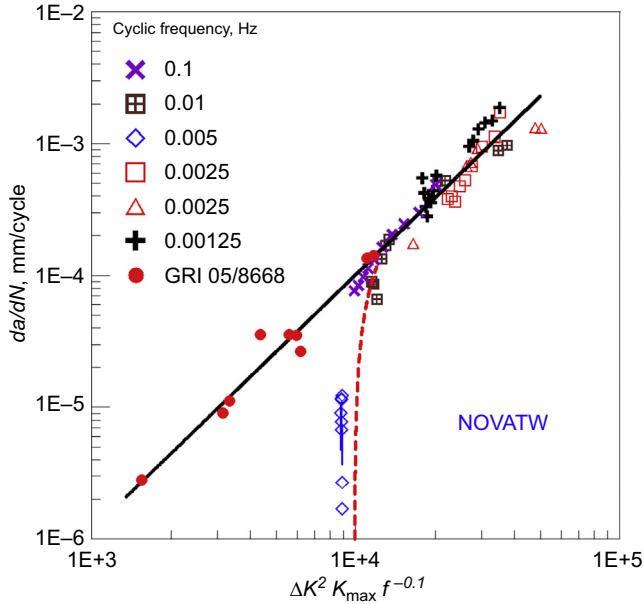

Figure 30.16 Through-thickness crack and surface crack threshold [83].

during the cyclic load condition [82,84]. The model suggests that this critical frequency depends on loading condition, temperature, mechanical properties of the steel, and hydrogen diffusivity at the crack tip. It was estimated by the authors that the critical frequency is of the order of 10^{-3} Hz, which has a very good

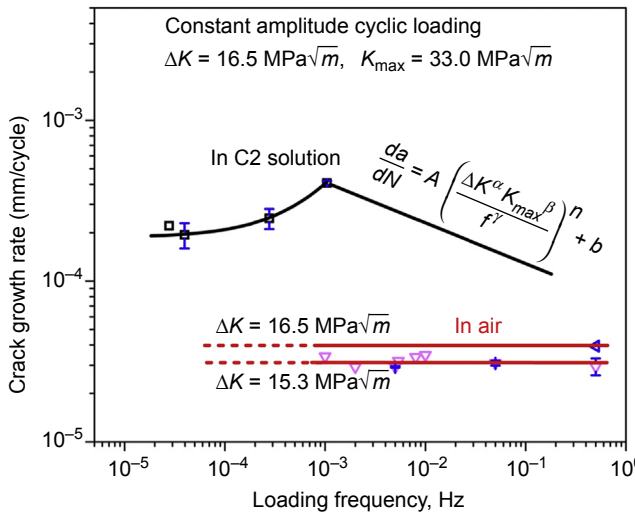

Figure 30.17 Dependence of crack growth rate on constant amplitude loading frequency in C2 solution and in air [82].

agreement with the experimental results shown in Fig. 30.17. Interestingly, similar dependence of crack growth rate on loading frequency has also been observed in an aluminum alloy charged with hydrogen. The critical frequency in the latter material was determined to be in the range from 1 Hz to 10 Hz, reflecting the much higher diffusivity of hydrogen in aluminum-based alloys [85].

The discussion above involves the threshold of crack growth for NNpHSCC. In the case of HpHSCC, multiple thresholds representing different crack growth mechanisms could be defined:

- K_{ISCC}: This is related to the minimum K required to achieve a sustainable crack growth under constant load, although it is recognized that small cracks can initiate and propagate at K levels well below K_{ISCC}, as indicated in Fig. 30.2. The magnitude of K_{ISCC} for a given crack can depend on the surrounding environmental conditions. Using precracked specimens, Parkins et al. measured a K_{ISCC} in 1N-1N carbonate−bicarbonate solution at 75°C to be 21 MPa$\sqrt{m}$ [5,86]. This threshold value is equivalent to a crack penetration of 1 mm into the pipe wall for an X60 pipe with a 1016 mm (40 in.) outer diameter, 8.12 mm (0.32 in.) wall thickness, and operating at 70% of SMYS. Table 30.3 provides the crack depths required to reach K_{ISCC} at 21 MPa$\sqrt{m}$ for several steels [87]. It is obvious that the critical depths would also vary with $2c/a$ ratios and much smaller critical depths can be expected for cracks with larger $2c/a$ ratios, according to Fig. 30.19.
- ΔK_{th}: This threshold is related to the minimum stress intensity factor ranges above which the crack growth is possible and is often calculated using Eq. (30.7) [1]

$$\frac{da}{dt} = A\dot{\varepsilon}_{ct}^{n} \tag{30.7}$$

where A and n are constant, and $\dot{\varepsilon}_{ct}$ is the crack tip strain rate, which is related to cyclic loading through the following expressions [1]:

$$\dot{\varepsilon}_{ct} = \varepsilon_o f \Delta K^2 = \varepsilon_o f (1-R)^2 K_{\max}^2 \tag{30.8}$$

Or,

$$\dot{\varepsilon}_{ct} = \varepsilon_o f (1-R)^2 \left(K_{\max}^2 - K_{ISCC}^2\right), \tag{30.9}$$

Table 30.3 Crack depth (mm) required to meet $K_{\max} = 20\,\text{MPa}\sqrt{m}$ [87]

a_{hoop}/specified minimum yield strength	Pipeline steel	X52	X60	X65	X70
72%	40″OD/0.32″w	1.2	0.95	0.85	0.75
72%	20″OD/0.24″w	1.1	0.9	0.75	0.71
50%	10″OD/0.12″w	1.1	1	0.92	0.86

where ε_o is a constant and R is the stress ratio. Because fatigue crack growth could start at a K well below K_{ISCC}, Eq. (30.9) that defines the occurrence of fatigue crack growth above K_{ISCC} is obviously not justified.

It appears that the same value of ΔK_{th} is used for both NNpHSCC and HpHSCC, which is 2.2 MPa$\sqrt{m}$(2.0 $ksi\sqrt{in.}$), according to API RP 1176—Assessment and Management of Cracking in Pipelines [80], as discussed previously. This value of threshold is smaller than those determined in air, which was found to be in the range of 3−7 MPa$\sqrt{m}$ [88].

There appear to be some conflicts between ΔK_{th} and K_{ISCC} when they are used to analyze SCC of pipeline steels under field operating conditions. The range of ΔK_{th} in air could be achieved when pressure fluctuates at $R = 0.66-0.86$ and assuming $K_{ISCC} = 21$ MPa$\sqrt{m}$. From the thresholds determined in air and in SCC environments, fatigue crack growth could occur well before the reach of K_{ISCC} because pressure fluctuates with R-ratios well below the range of 0.66−0.86, especially for oil pipelines. Under the circumstances, crack growth could be caused by fatigue loading when the following condition is met:

$$\Delta K \geq \frac{K_{\max}(\leq K_{ISCC})}{R(\leq 0.66 \sim 0.86)} \tag{30.10}$$

- **A combined threshold incorporating both $K_{\max}$ and ΔK similar to the combined factor defined in Eq. (30.6) for NNpHSCC**: The threshold in terms of a combined factor has not been determined for HpHSCC. The combined threshold for HpHSCC should also be dependent of load frequency, f, but should be related to the crack growth rate, for example, through crack tip strain rate as expressed by Eqs (30.8) and (30.9).
- **Interactive threshold defined based on a critical growth rate**: This would be related to the threshold that reflects the effect of interactive behavior as described for NNpHSCC under variable amplitude pressure fluctuations. Investigations on determining the interactive threshold in HpHSCC have not been reported. It should be noted that the value of the interactive threshold in HpHSCC can be very low but corresponds to a crack growth rate, da/dN (mm/cycle), which is still appreciably large when converted to da/dt (mm/s), even if the cyclic loading frequency is low.
- **Strain rate−based threshold for HpHSCC**: The above stress or stress intensity factor−dependent threshold is not physically meaningful for HpHSCC if one believes that the crack growth in HpHSCC environments is step-limited by the critical strain rate necessary to fracture the passivating film at the crack tip. There does not exist a direct correlation between the critical strain rate threshold and the critical mechanical driving forces, such as ΔK_{th}. It would make more sense if the critical strain rate threshold at grain boundaries can be used for HpHSCC as cracks propagate along the grain boundaries [89].

During field operation, consistent and constant mechanical conditions for crack growth as those used during laboratory simulations are not maintained. Even under a consistent and constant mechanical and environmental condition, a growing crack may periodically or repeatedly experience a process of active growth, dormancy, and reactivation for growth, especially when mechanical driving forces are low, such as in the beginning of Stage-2 crack growth [53].

It was found that there exist two thresholds above which continuous crack growth is observed [53]. The lower threshold is the minimum combined factor above which continuous growth of the crack with a sharp tip is seen, whereas the upper threshold is the critical combined factor above which continuous growth of the crack with a blunt tip takes place. Crack dormancy during Stage-2 crack growth has been shown to be either mechanically or environmentally induced. The former is related to the room temperature creep occurring at the crack tip when the crack is loaded to a combined factor below the lower threshold (nonpropagating condition). The latter is caused by the dissolution of material from the cracked surface, which leads to an increase of crack width and the crack tip radius and, therefore, a higher upper threshold for continuous crack growth. A discontinuous crack growth mechanism was found to operate when the cracks with a blunt tip were loaded to a combined factor between the lower and the upper thresholds. Crack growth takes place by repeated dormant-active growth cycles. Each cycle can advance the crack by a length comparable with the size of grains in the material. The active growth is initiated by forming microcracks at the weakest links, such as grain boundaries, inclusions, or phase interfaces, located in the fracture process zone ahead of the blunt tip, as a combined result of cyclic loading, stress concentration, and hydrogen segregation and trapping. The contribution to crack advancement by a direct dissolution of materials at the crack tip is negligible. The transition of discontinuous crack growth to continuous crack growth would occur when microcrack initiations in the facture process zones can take place simultaneously at most locations of the crack front.

30.5.2 Modeling of Stage-2 crack growth rate

In API RP 1176—Assessment and Management of Cracking in Pipelines [80], four different methods of estimating crack growth rate, briefly summarized below, were recommended.

Uniform average growth rate: This model assumes that the occurrence of SCC and SCC growth observed in the field is the second stage, which is characterized by more or less steady growth. Critical defect size is calculated using a fracture mechanics model, and the time to failure is the difference between the critical and the current flaw depth divided by that crack growth rate.

Two stage SCC and fatigue analysis: SCC occurs when the crack depth is small, then becomes primarily fatigue driven once the SCC crack depth becomes sufficiently large. The depth at which fatigue governs occurs when the incremental crack growth rate due to fatigue exceeds the average crack growth rate for SCC. The net time to failure is the time for SCC to enlarge the flaw to the point where fatigue takes over plus the time for fatigue to enlarge the flaw to failure.

Coupled SCC and fatigue analysis: Crack growth by SCC caused by time at constant stress is added to the growth by fatigue caused by stress cycles [90,91], which can be represented by Model D in Table 30.1.

Load interaction approach for near-neutral pH SCC: Pipelines are operated under variable pressure fluctuations. The models discussed above do not necessarily consider crack growth acceleration or retardation by both the stress-dependent and

the time-dependent load interactions on crack growth during variable pressure fluctuations. The load interaction approach considers both the stress history−dependent and the time-dependent load interactions on crack growth during variable pressure fluctuations as introduced in previous sections.

The interactive approach would best match the operational conditions of oil and gas pipelines. Crack growth rate could be either enhanced (positively interactive superposition—Model E in Table 30.1) or reduced (negatively interactive superposition—Model F in Table 30.1).

An example of positively interactive behavior of crack growth simulating the effect of interaction between an underload cycle and minor cycles on crack growth in NNpH environments is shown in Fig. 30.18 [82]. The top two curves are crack growth rates obtained under variable amplitude loads whereas the two lower curves were under constant amplitude loads. The former is the so-called underload minor load−type cycles, the Type-I loading scheme shown in Fig. 30.18. The underload cycles have the same amplitude and frequency as the constant amplitude loadings for the two lower curves. The minor cycle in the variable amplitude loading has an R-ratio of 0.9, which is nonpropagating if underload cycles are not present. It is clear from Fig. 30.18 that the variable loading conditions have caused crack growth at a rate about one order of magnitude higher than that determined under constant amplitude underload cycles alone. It is also seen from Fig. 30.18 that crack growth in air is insensitive to the loading frequency, whereas a strong frequency-dependent crack growth behavior is observed in the NNpH environment, depending on the rate of loading. The importance of minor cycles in crack growth exists both in air and in NNpH environments. The enhancement in the crack growth rate in air is even larger than that in the NNpH

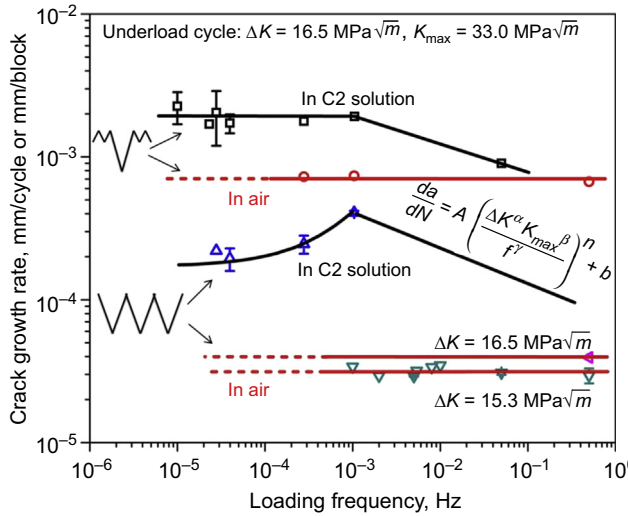

Figure 30.18 Crack growth rate under different loading frequency of underload in C2 solution [82].

environment by the presence of minor cycles. In the former case, an increase of the crack growth rate by a factor of as high as 20 is observed when the underload minor cycle−type variable amplitude fatigue loading was applied. It is about a factor of 5 in an NNpH environment (C2 solution). The observation of load interaction effects in both environments indicates that the load-interaction effects are an intrinsic behavior of ductile materials and exist in all environments.

The observation of very strong enhancement of crack growth caused by load interactions in air suggests that an interactive approach must be adopted for the crack growth rate analysis of HpHSCC as well. Although a time-dependent/frequency-dependent load interaction related to hydrogen embrittlement does not exist in HpHSCC, the crack growth could grow by a fatigue mechanism similar to that in air, in which a strong load interaction has been identified as shown in Fig. 30.18. The actual crack growth rate would be higher than the fatigue crack growth rate determined in air because of additional crack growth by direct dissolution of materials at the crack tip.

30.6 Modeling of remaining life of pipeline steels with SCC cracking

From the information provided in previous sections, an interactive approach must be adopted for the crack growth rate analysis and life prediction of pipeline steels with SCC. In this section, only the interactive approaches of remaining life modeling will be introduced. For noninteractive approaches of modeling of remaining life of both types of SCC, one can refer to previous publications [1,87]. Owing to the availability of experimental data, the interactive approach of modeling of the remaining life of pipeline steels experiencing SCC can be performed at the current time only for the pipeline sections operated with the Type-I pressure fluctuations defined in Fig. 30.10 and exposed to an NNpHSCC environment.

Based on the crack growth mechanisms being identified, Matlab codes have been written for the prediction of crack growth rates and service life of pipeline steels with the Type-I underload-minor cycle loading schemes. The governing crack growth equations for each loading event and their combined effect on crack growth can be found in Ref. [35,36]. All the governing equations were built based on the actual experimental results obtained.

Fig. 30.19 shows the results of the life prediction of a high-pressure gas pipeline with the underload-type loading spectrum. Three predicted service life curves are shown in Fig. 30.19:

1. The life curve predicted based on the crack growth rate caused by dissolution only [36]: In this prediction, the crack growth curve representing the average condition of growth profile was selected for the purpose of comparison, although the most severe failure-attributing conditions should be considered in integrity management.
2. The life curve predicted solely based on the equations governing the crack growth in Stage 2, which yields a lifetime over 1000 years because of very benign mechanical driving forces

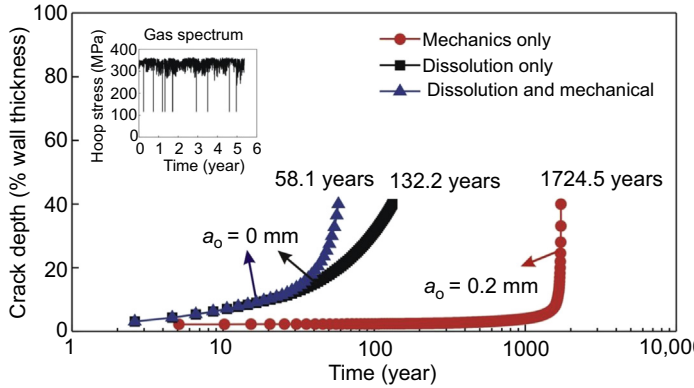

Figure 30.19 Comparison of crack growth contributed by dissolution and mechanics [35,36].

during the initial stage of crack growth. It is also seen from the life curve that crack growth driven by mechanical driving forces becomes life-limiting only when crack depth reaches about 1.0 mm. This observation further indicates the importance of initial dissolution growth in providing a bridge to the crack growth in Stage 2, without which a prolonged dormant period and longer service life can be expected.

3. The life curve predicted by incorporating Stage-1 and Stage-2 crack growth, which yields a predicted life comparable to those found in the field. It should be noted that these predictions have been made without a consideration of the bulging factor that takes into account the effect of a curved pipe surface on the calculation of K at the crack tip. The consideration of the bulging factor would yield a shorter predicted life for deeper cracks. The predicted lifetime can also be much shorter when cracks have larger $2c/a$ ratios because of the increased K at the depth tip of a crack as illustrated in Fig. 30.14.

Fig. 30.20 compares the life curve of a gas pipeline with an oil pipeline [36]. Both pipelines were operated under the Type-I pressure fluctuation scheme. The oil pipeline

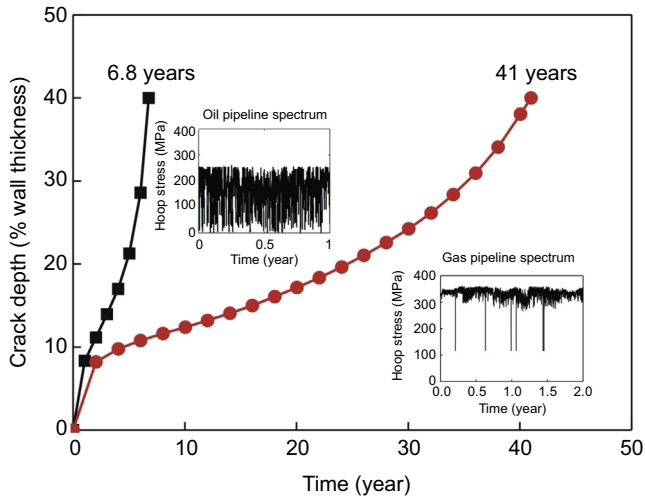

Figure 30.20 Prediction on oil and gas underload-type spectra [36].

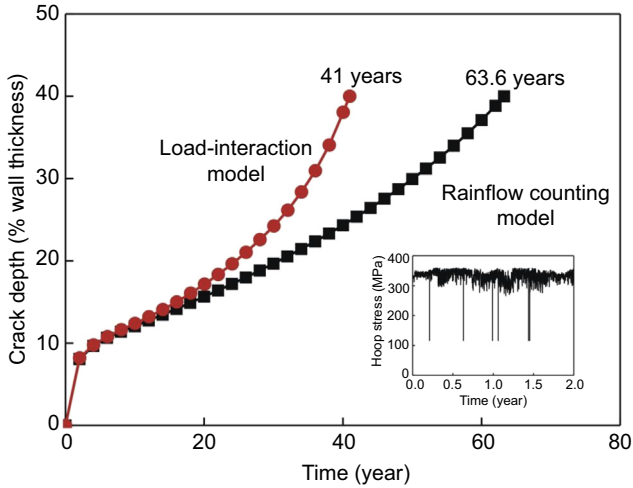

Figure 30.21 Comparison with rainflow counting method [36].

has a much shorter predicted life because of frequent underload cycles with larger stress amplitudes. The gas pipeline was operated with much fewer large-amplitude underload cycles but a higher number of minor load cycles that can also contribute to crack growth in the presence of underload cycles.

Rainflow cycle counting has been widely used to analyze fatigue crack growth in the past [92,93]. The rainflow counting is a method for counting fatigue cycles from a time history. It reduces a spectrum of varying stress into a set of simple stress reversals, and overall crack growth rate is calculated using Eq. (30.2). The results obtained from the rainflow cycle counting analysis were generally very conservative and even irrational in some cases. It is believed that the discrepancies arise from the fact that the load interaction effects could significantly enhance crack growth but are not considered in the rainflow cycle counting method.

Fig. 30.21 shows an example of the conservative lifetime estimate using the rainflow counting method, which was implemented in Matlab code, strictly following the protocol established by ASME [94]. The lifetime of the pipeline predicted by the rainflow cycle counting method yields a lifetime about 55% longer than the current method when the crack reaches to 40% of wall thickness. In this comparison, the same Stage-1 growth curve was used. The difference in predicted life proves the significant effect of the load-interaction effects on crack growth. Precision of prediction can be improved when the load interaction effects are considered.

The interactive approach is able to predict lifetimes that are comparable to the actual service life of pipeline steels with NNpHSCC developed during field operation. This level of accuracy of prediction has not been achieved by any existing models. The prediction could be made for an individual crack or for crack colonies with a range of conditions. In either case, higher accuracy can be achieved if the

input data are specific and relevant. In the majority of situations it is hard and not necessary to make predictions for each crack in a colony, but rather more practical to make a prediction for the crack with the largest dimension by inputting data representing the worst case of scenario. This could be similar for pipelines at locations with similar soil and geological conditions. After all, it is the fastest growing crack that determines when failure will occur.

It should be noted that the accuracy of prediction could be improved if the input data are specific and relevant to the cracks or crack colonies of interest. Among many input values, the most important one would be the historical data of the pressure fluctuations that must be recorded to capture all crack growth-contributing events with methodologies as suggested in Ref. [95,96].

30.7 Gaps of knowledge in stress corrosion cracking modeling

As indicated in Introduction, the trends in SCC research have been moving to the direction achieving higher accuracy in terms of developing better modeling methodology and using results from simulative attempts with improved relevance to the field conditions that have caused the occurrence of SCC cracking of pipeline steels. Despite many progresses achieved, gaps of knowledge in the area of modeling still exist, and efforts must be made to narrow down the gaps, especially in the following areas.

On the crack initiation and early-stage crack growth in Stage 1: This is a stage that is less studied and presents many contradictions. Although a number of simulations have been made in the case of NNpHSCC, they were conducted by using a mechanically polished surface where the surface of specimens intercepts with the microstructures in the middle or near-middle sections of pipe wall where localized corrosion takes place because of galvanic effect of microstructural heterogeneity, and/or using very aggressive simulations such as SSRT that bear little relevance to the Stage-1 behavior found in the field. In the case of HpHSCC, the mechanisms of crack initiation remain to be understood. For both types of SCC, experimental and/or numerical simulations have not been done to reveal the decreased rate profile, and the physical and mathematic equations governing the rate profile have not been well developed.

On crack growth behavior in Stage 2: In the case of NNpHSCC, progress has been made in the following key areas: (1) The identification of three types of pressure fluctuations and their different susceptibility to crack growth; (2) The importance of load interaction effects during variable amplitude pressure fluctuations in the prediction of crack growth rate. The latter is termed as an interactive approach for SCC modeling, which has not been sufficiently addressed in the past and should be investigated in future efforts, especially for the SCC cracking of pipelines in HpHSCC environments.

References

[1] R.N. Parkins, Strain rate effects in stress corrosion cracking, 1990 plenary lecture at corrosion/90, Corrosion 46 (3) (1990) 178−189.
[2] R.N. Parkins, Corrosion Science 29 (1989) 1019.
[3] J.T. Evans, R.N. Parkins, Acta Metallurgica 25 (1976) 511.
[4] A.J. Winter, Philosophical Magazine 31 (1975) 411.
[5] R.N. Parkins, B.S. Greenwell, Metal Science 11 (1977) 405.
[6] R.P. Wei, J.D. Landes, Materials Research and Standards 9 (1969) 25−46.
[7] X.Y. Zhang, S.B. Lambert, R. Sutherby, A. Plumtree, Corrosion 55 (1999) 297−305.
[8] J.A. Beavers, C.J. Jaske, Effects of Pressure Fluctuations on SCC Propagation, PRCI report PR-186-9706, PRCI, Houston, 2000.
[9] N.A. Fleck, Fatigue crack growth due to periodic underloads and overloads, Acta Metallurgica 33 (7) (July 1985) 1339−1354.
[10] A.J. McEvily, R.P. Wei, Fracture mechanics and corrosion fatigue, in: Corrosion Fatigue: Chemistry, Mechanics and Microsturctures, NACE International, Houston, TX, 1972, pp. 25−30.
[11] J.T. Justice, J.D. Mackenzie, Progress in the control of stress corrosion in a 914 mm O.D. gas transmission pipeline, in: 7th Biennial Joint Meeting on Line Pipe Research, American Gas Association, Washington, DC, 1988. NG-18/EPRG.
[12] J.A. Beavers, Corrosion 70 (1) (2014) 3−18.
[13] W. Chen, An overview of near-neutral pH stress corrosion cracking in pipelines and mitigation strategies for its initiation and growth, Corrosion 72 (7) (2016) 962−977.
[14] W. Chen, R.L. Sutherby, Metallurgical and Materials Transactions A 38 (2007) 1260.
[15] W. Chen, J. Zhao, J. Been, K. Chevil, G. Van Boven, S. Keane, Update of understanding of near-neutral pH SCC crack growth mechanisms and development of pipe-online software for pipeline integrity management, in: Proceedings of the 2016 11th International Pipeline Conference, IPC2016, September 26−September 30, 2016, Calgary, Alberta, Canada, 2016. IPC2016−64626.
[16] W. Chen, F. King, E.D. Vokes, Characteristics of near neutral pH stress corrosion cracks in an X-65 pipeline steel, Corrosion 58 (3) (2002) 267−275.
[17] G. Van Boven, W.X. Chen, R. Rogge, The role of residual stress in neutral pH stress corrosion cracking of pipeline steels. Part I: pitting and cracking occurrence, Acta Materialia 55 (2007) 29−42.
[18] W. Chen, G.V. Boven, R. Rogge, The role of residual stress in neutral pH stress corrosion cracking of pipeline steels. Part II: crack dormancy, Acta Materialia 55 (2007) 43−53.
[19] M. Elboujdaini, Y.Z. Wang, R.W. Revie, R.N. Parkins, M.T. Shehata, Stress corrosion crack initiation processes: pitting and microcrack coalescence, Corrosion (2000). Paper No. 00379.
[20] M.J. Wilmott, R.L. Sutherby, The role of pressure and pressure fluctuations in the growth of stress corrosion cracks in line pipe steels, in: Proc. Int. Pipeline Conference, The American Society of Mechanical Engineers, New York, NY, 1998, pp. 409−422.
[21] S. Wang, W. Chen, Pre-cyclic loading induced SCC initiation of pipeline steels in a near-neutral pH soil environment, Corrosion 58 (6) (2002) 526−534.
[22] J. Zhao, K. Chevil, M. Yu, J. Been, S. Keane, G.V. Boven, R. Kania, W. Chen, Statistical analysis on underload-type pipeline spectra, Journal of Pipeline Systems Engineering and Practice 7 (4) (1 November 2016), 04016007.

[23] W. Chen, M.L. Wilmott, T.R. Jack, Hydrogen permeation behaviour of X-70 pipeline steel in NS4 neutral pH environment, Inter Pipeline Conference 2 (2000) 953−960.
[24] B.S. Delanty, J. O'Beirne, Oil and Gas Journal 90 (24) (1992) 39.
[25] R.N. Parkins, W.K. Blanchard Jr., B.S. Delanty, Corrosion 50 (1994) 394.
[26] X. Liu, X. Mao, Scripta Metallurgica et Materialia 33 (1995) 145.
[27] W. Chen, R. Kania, R. Worthingham, G.V. Boven, Transgranular crack growth in the pipeline steels exposed to near-neutral pH soil aqueous solutions: the role of hydrogen, Acta Materialia 57 (2009) 6200−6214.
[28] Y.W. Kang, W. Chen, R. Kania, G.V. Boven, R. Worthingham, Simulation of crack growth during hydrostatic testing in near-neutral pH environment, Corrosion Science 53 (2011) 968−975.
[29] M. Yu, Crack Growth Behavior of Pipeline Steels Under Variable Pressure Fluctuations in a Near-Neutral pH Environment (Ph.D. thesis), University of Alberta, 2015.
[30] B.T. Lu, L.J. Qiao, J.L. Luo, K.W. Gao, Role of hydrogen in stress corrosion cracking of austenitic stainless steels, Philosophical Magazine 91 (2011) 208−228.
[31] W. Chen, S.H. Wang, R. Chu, F. King, T.R. Jack, R.R. Fessler, Effect of pre-cyclic loading on SCC initiation in an X-65 pipeline steel exposed to near-neutral pH soil environment, Metallurgical and Materials Transactions 34A (2003) 2601−2608.
[32] R. Chu, W. Chen, S.H. Wang, F. King, T.R. Jack, R.R. Fessler, Microstructure dependence of SCC initiation in X-65 pipeline steel exposed to a near-neutral pH soil environment, Corrosion 60 (2004) 275−283.
[33] W. Zheng, D. Bibby, J. Li, J.T. Bowker, J.A. Gianetto, R.W. Revie, G. Williams, Near-Neutral pH SCC of Two Line Pipe Steels under Quasi-Static Stressing Conditions. IPC 2006-10084.
[34] J. Kang, W. Zheng, D. Bibby, B.S. Amirkhiz, J. Li, Initiation of stress corrosion cracks in X80 and X100 pipe steels in near-neutral pH environment, Journal of Materials Engineering and Performance 25 (1) (January 2016) 227.
[35] J.X. Zhao, W. Chen, M. Yu, K. Chevil, R. Eadie, G.V. Boven, R. Kania, J. Been, S. Keane, Crack growth modelling and life prediction of pipeline steels exposed to near-neutral pH environments: dissolution crack growth and occurrence of crack dormancy in stage I, Metallurgical and Materials Transactions A 48 (4) (April 1, 2017) 1629−1640.
[36] J.X. Zhao, W. Chen, M. Yu, K. Chevil, R. Eadie, G.V. Boven, R. Kania, J. Been, S. Keane, Crack growth modeling and life prediction of pipeline steels exposed to near-neutral pH environments: stage II crack growth and overall life prediction, Metallurgical and Materials Transactions A 48 (4) (April 1, 2017) 1641−1652.
[37] M. Skorupa, Load interaction effects during fatigue crack growth under variable amplitude loading- a literature review. Part I: empirical trends, Fatigue & Fracture of Engineering Materials & Structures 21 (8) (August 1998) 987−1006.
[38] M. Skorupa, Load interaction effects during fatigue crack growth under variable amplitude loading- a literature review. Part II: qualitative explanation, Fatigue & Fracture of Engineering Materials & Structures 22 (1999) 905−926.
[39] V. Zitounis, Fatigue Crack Growth Rates Under Variable Amplitude Load Spectra Containing Tensile Underloads (Ph.D. thesis) 28, Cranfield University, October 2003.
[40] S.M. Russ, Effect of Underloads on Fatigue Crack Growth of Ti-17 (Ph.D. thesis), Georgia Institute of Technology, October 2003.
[41] K.R. Fowler, R.T. Watanabe, Development of jet transport airframe fatigue test spectra, ASTM STP 1006, in: J.M. Potter, R.T. Watanabe (Eds.), Development of Fatigue Loading Spectra, American Society for Testing and Materials, Philadelphia, 1989, pp. 36−64.

[42] R. Sunder, Contribution of individual load cycles to crack growth under aircraft spectrum loading, ASTM STP 1122, in: M.R. Mitchell, R.W. Landgraf (Eds.), Advances in Fatigue Lifetime Predictive Techniques, American Society for Testing and Materials, Philadelphia, 1992, pp. 176−190.
[43] T.L. Anderson, Fracture Mechanics, Fundermentals and Applications, third ed., Taylors & Francis Group, 2005, pp. 473−488.
[44] H. Agerskov, The Fatigue Behavior of Steel Structures Under Random Loading vols. 378−379, Key Engineering Materials, 2008, pp. 3−16.
[45] Y.-H. Zhang, S.J. Maddox, Investigation of fatigue damage to welded joints under variable amplitude loading spectra, International Journal of Fatigue 31 (2009) 138−152.
[46] C. MacDougall, T.H. Topper, The influence of variable amplitude loading on crack closure and notch fatigue behavior, International Journal of Fatigue 19 (5) (1997) 389−400.
[47] M. El-Zeghayar, T.H. Topper, F.A. Conle, J.J.F. Bonnen, Modeling crack closure and damage in variable amplitude fatigue using smooth specimen fatigue test data, International Journal of Fatigue 33 (2) (Feb. 2011) 223−231.
[48] J.C. Newman Jr., E.P. Phillips, Prediction of crack growth under variable-amplitude and spectrum loading in a titanium alloy, ASTM STP 1439, in: P.C. McKeighan, N. Ranganathan (Eds.), Fatigue Testing and Analysis Under Variable Amplitude Loading Conditions, American Society for Testing and Materials, Philadelphia, 2005, pp. 232−250.
[49] N. Ohrloff, A. Gysler, G. Lütjering, Journal DE Physique (Sept. 1987) C3−C801. Colloque C3, supplement au n°9, Tome 48.
[50] M. Krkoska, S.A. Barter, R.C. Alderliesten, P. White, R. Benedictus, Fatigue crack paths in AA2024-T3 when loaded with constant amplitude and simple underload spectra, Engineering Fracture Mechanics 77 (11) (July 2010) 1857−1865.
[51] M. Yu, W. Chen, R. Karina, G.V. Boven, J. Been, Fatigue and fracture of Engineering Materials and Structures 38 (6) (2015) 681−692.
[52] J. Zhao, W. Chen, S. Keane, J. Been, G. Van Boven, Development and validation of load-interaction based models for crack growth prediction, in: Proceedings of the 10th International Pipeline Conference, Held September 29−October 3, 2014, International Petroleum Technology Institute, Calgary, Canada, 2014.
[53] A. Egbewande, W. Chen, R. Eadie, R. Kania, G.V. Boven, R. Worthingham, J. Been, Transgranular crack growth in the pipeline steels exposed to near-neutral pH soil aqueous solutions: discontinuous crack growth mechanism, Corrosion Science 83 (2014) 343−354.
[54] J. A Beavers, C.L. Durr, B.S. Delanty, High-pH SCC: temperature and potential dependence for cracking in field environments, in: Proceedings of the 1998 3rd International Pipeline Conference, June 7−11, 1998, Calgary Alberta, ASME, New York, N.Y., 1998, p. 423.
[55] F.P. Ford, Quantitative prediction of environmentally assisted cracking, Corrosion 52 (1996) 375−395.
[56] A. Troiano, Transactions of the American Society of Metals 52 (1960) 147−157.
[57] H. Birnbaum, P. Sofronis, Materials Science and Engineering A 176 (1994) 191−202.
[58] A. Oehlert, A. Atrens, Acta Metallurgica et Materialia 42 (1994) 1493.
[59] A. Oehlert, A. Atrens, Parkings symposium on fundamental aspects of stress corrosion cracking, in: S.M. Bruemmer, et al. (Eds.), The Minerals, Metals & Materials Society, 1992, p. 255, 5.
[60] M.M. Festen, J.G. Erlings, R.A. Fransz, in: Proc. First Int'l. Conf. on Environment-induced Cracking of Metals, NACE, Houston, Oct. 2−7, 1988, p. 229.
[61] S. Wang, Y.G. Zhang, W. Chen, Room temperature creep, S-R-D. Stress-strain behavior of pipeline steels, Journal of Materials Science 36 (8) (2001) 1931−1938.

[62] S. Wang, W. Chen, Low temp. Creep deformation and its effect on yielding behavior of a line pipe steel with discontinuous yielding, Materials Science and Engineering A A301 (2001) 147−153.
[63] T.J. Barlo, Origin and validation of the 100 mV polarization criterion, in: CORROSION/2001, NACE, Houston, TX, 2001 paper no. 581.
[64] J.A. Beavers, K.C. Garrity, 100 mV polarization criterion and external SCC of underground pipelines, in: Corrosion 2001, 2001. Paper # 01592.
[65] R.N. Parkins, A review of stress corrosion cracking of high pressure gas pipelines, in: Corrosion 2000, 2000. Paper # 00363.
[66] J.A. Beavers, C.E. Jaske, SCC of underground pipelines: a history of the development of test techniques, in: Corrosion 99, 1999. Paper # 142.
[67] J.Q. Wang, A. Atrens, SCC initiation for X65 pipeline steel in the ''high'' pH carbonate/bicarbonate solution, Corrosion Science 45 (2003) 2199−2217.
[68] D. He, T.R. Jach, F. King, W.X. Chen, in: International Pipeline Conference, 2000, vol. 2, 2002, p. 997.
[69] T. Kushida, K. Nose, H. Asahi, M. Kimura, Y. Yamane, S. Endo, H. Kawano, in: Proceedings of Corrosion 2001, NACE, Houston (TX), 2001. Paper no. 01223.
[70] B.Y. Fang, R.L. Eadie, W.X. Chen, M. Elboujdaini, Corrosion Engineering, Science and Technology 44 (2009) 32−42.
[71] B.Y. Fang, R.L. Eadie, W.X. Chen, M. Elboujdaini, Corrosion Engineering Science and Technology 45 (2010) 302−312.
[72] Z. Qin, B. Demko, J. Noel, D. Shoesmith, F. King, R. Worthingham, K. Keith, Corrosion 60 (2004) 906−914.
[73] K. Chevil, A. Eslami, W. Chen, R. Eadie, R. Kania, G. Van Boven, R. Worthingham, Disbonding geometry dependent cathodic protection strategies, in: Full Paper Submitted to the 9th International Pipeline Conference (IPC2012), Sep 24−28, 2012, Calgary, Canada, 2012. IPC2012-90675.
[74] K. Chevil, W. Chen, G. Van Boven, R. Kania, J. Been, Correlating corrosion field data with experimental findings for the development of pipeline mitigation strategies, in: Proceedings of the Biennial International Pipeline Conference, IPC, IPC 2014; Calgary; Canada; Sep 29, 2014 to Oct 3, vol. 2, 2014. Code 109496.
[75] B. Gu, J. Luo, X. Mao, Corrosion 55 (1) (1999) 96−106.
[76] Y.F. Cheng, Journal of Materials Science 42 (2007) 2701−2705.
[77] B.T. Lu, J.L. Luo, P.R. Norton, H.Y. Ma, Acta Materialia 57 (2009) 41−49.
[78] J.A. Beavers, J.T. Johnson, R.L. Sutherby, Materials factors influencing the initiation of near-neutral pH SCC on underground pipelines, in: Proceedings of 3rd International Pipeline Conference, Held October 1−5, 2000, International Petroleum Technology Institute, Calgary, Canada, 2000, p. 979.
[79] P.C. Paris, F. Erdogan, A critical analysis of crack propagation laws, Journal of Basic Engineering 85 (1960) 528−534.
[80] R.P. API, 1176 − Assessment and management of cracking in pipelines, first ed., STANDARD by American Petroleum Institute, 07/01/2016.
[81] M. Yu, W. Chen, R. Kania, G. Van Boven, J. Been, Crack propagation of pipeline steel exposed to a near-neutral pH environment under variable pressure fluctuations, International Journal of Fatigue 82 (2016) 658−666.
[82] M. Yu, X. Xing, H. Zhang, J. Zhao, R. Eadie, W. Chen, J. Been, G.V. Boven, R. Kania, Corrosion fatigue crack growth behavior of pipeline steel under underload-type variable amplitude loading schemes, Acta Materialia 96 (2015) 159−169.

[83] W. Chen, R. Kania, R. Worthingham, S. Kariyawasam, Crack growth model of pipeline steels in near neutral pH soil environments, in: Proc. of the 7th International Pipeline Conf., IPC2008, Sep 29−Oct 3, 2008, Calgary, Canada, 2008, p. 10. Paper # IPC2008−64475.
[84] X. Xing, W. Chen, H. Zhang, Materials Letters 52 (2015) 86−89.
[85] Z.M. Gasem, Frequency Dependent Environmental Fatigue Crack Propagation in the 7XXX Alloy/Aqueous Chloride System (Ph.D. thesis), University of Virginia, 1999.
[86] A.K. Pilkey, S.B. Lambert, A. Plumtree, Stress corrosion cracking of X-60 line pipe steel in a carbonate-bicarbonate solution, Corrosion 51 (1994) 91−96.
[87] F. Song, B. Lu, M. Gao, M. Elboujdaini, Development of a Commercial Model to Predict Stress Corrosion Cracking Growth Rates in Operating Pipelines, U.S. Department of Transportation Pipeline Hazardous Materials Safety Administration, June 2011. Final report, DTPH 56-08-T-000001.
[88] A. Bussiba, P.P. Darcis, J.D. McColskey, C.N. McCowan, G. Kohn, R. Smith, J. Merritt, Fatigue crack growth rates in six pipeline steels, in: Proceedings of 6th International Pipeline Conference, Held September 25-29, 2006 (Calgary, Canada), 2006. Paper #: IPC2006-10320.
[89] J. Griggs, E. Gamboa, O. Lavigne, A review of modelling high pH stress corrosion cracking of high pressure gas pipelines, Materials and Corrosion 67 (3) (2016) 251−263.
[90] S.B. Lambert, J.A. Beavers, B. Delanty, R. Sutherby, A. Plumtree, in: Proceedings of 3rd International Pipeline Conference; 2000, Calgary, 2000, pp. 961−965.
[91] J.A. Beavers, Near-Neutral pH SCC: Dormancy and Re-Initiation of Stress Corrosion Cracks, GRI report #: GRI-7045, August 2004.
[92] G. Van Boven, R. Sutherby, F. King, in: Proceedings of 4th International Pipeline Conference, Sep 29−Oct 3, 2002, Calgary, Canada, 2002. IPC2002−27149.
[93] J. Schijve, Fatigue of Structures and Materials, second ed., Springer, 2009 with CD-ROM.
[94] Standard Practices for Cycle Counting in Fatigue Analysis, 2011, p. e1. ASTM, E1049−85.
[95] J. Zhao, W. Chen, M. Yu, K. Chevil, R. Eadie, R. Kania, G. Van Boven, J. Been, "Effect of pressure sampling methods on pipeline integrity analysis, Submitted to Journal of Pipeline Systems - Engineering and Practice (Jan 2016).
[96] J. Zhao, K. Chevil, W. Chen, J. Been, S. Keane, Optimized methods of recording pipeline pressure fluctuations for pipeline integrity analysis, in: Proceedings of the 2016 11th International Pipeline Conference, IPC2016, Sep 26−30, 2016, Calgary, Alberta, Canada, 2016. IPC2016-64295.

Mechanistic modeling of erosion–corrosion for carbon steel

31

Faisal Mutahhar[1], *Gusai Aithan*[1], *Erin V. Iski*[2], *Michael W. Keller*[2], *Siamack Shirazi*[2] *and Kenneth P. Roberts*[2]
[1]Saudi Aramco, Dhahran, Saudi Arabia; [2]University of Tulsa, Tulsa, OK, United States

31.1 Introduction

With advancements in erosion and corrosion research, several mechanistic models have been developed for predicting erosion or corrosion. However, until recently, none of the models were developed for predicting erosion and corrosion simultaneously. This is attributed to the complexity of the processes and the large numbers of variables involved. The development of a mechanistic model requires an in-depth understanding of the erosion–corrosion processes and their interdependencies. What increases the complexity of the process is the synergistic effect between erosion and corrosion under certain experimental conditions. One such condition is when iron carbonate scale forms on the pipe wall providing a barrier to corrosion. However, the scale begins to lose its protection as it is removed by solid particle erosion. This has the potential to accelerate metal losses through processes such as localized corrosion, i.e., pitting corrosion.

One of the first efforts toward developing an erosion–corrosion model under scale-forming conditions was developed by Shadley et al. [1–3]. The model predicts the threshold flow velocity above which iron carbonate scale is partially or totally removed. Several years later, a mechanistic model was developed by Mutahhar et al. [4] for multiphase flow under scale-forming conditions. Both models were developed at the Erosion–Corrosion Research center (E/CRC) at the University of Tulsa for CO_2 corrosion under iron carbonate scale-forming conditions in the presence of sand. Other forms of corrosion or other erodent particles were not considered at the time.

In the Mutahhar erosion–corrosion model, a three-step approach was utilized based on existing models for erosion only and corrosion only. In the first step, the erosion rate is predicted by the Sand Protection Pipe Saver (SPPS) erosion model [5,6]. In the second step, the corrosion rate is predicted by the mechanistic corrosion model called SPPS:CO_2 [7,8]. Finally, the combined erosion–corrosion rate is predicted for different scenarios based on the presence or absence of the iron carbonate scale.

In this chapter, the erosion–corrosion threshold velocity model and the erosion–corrosion prediction model, SPPS:E-C, are presented. To begin, a brief discussion is provided about the SPPS erosion model. Second, the conditions and propensity of iron carbonate scale formation under various conditions are discussed along with its

Trends in Oil and Gas Corrosion Research and Technologies. http://dx.doi.org/10.1016/B978-0-08-101105-8.00031-0

implications to erosion–corrosion. Finally, a comparison between multiphase prediction results and laboratory data for SPPS:E-C will be presented at the end of the chapter.

31.2 Erosion model (SPPS)

The SPPS erosion model and computer program were developed by the University of Tulsa E/CRC program [5,6]. The model calculates the metal penetration rate by erosion using an equation that accounts for sand properties, sand rate, fluid properties, flow rates, flow geometry, and material properties for the pipe. The metal penetration rate (h) can be calculated as follows.

$$h = F_M F_S F_P F_{r/D} \frac{W V_L^{1.73}}{D^2} \tag{31.1}$$

where h = penetration rate, m/s (can be converted to mm/year or mpy); F_M = an empirical constant that accounts for material hardness of the pipe; F_S = empirical sand sharpness factor; F_P = penetration factor for steel (based on 1″ pipe diameter), m/kg; $F_{r/D}$ = penetration factor for elbow radius; W = sand production rate, kg/s; V_L = characteristic particle impact velocity, m/s; D = ratio of pipe diameter in inches to a 1-in. pipe.

This model has been successfully employed by many of the top oil and gas producers in the world to predict the loss of metals impacted by solid particles, e.g., sand entrained in single or multiphase production conditions. Although this is the most mature model from the E/CRC, it does not take into account the effect corrosion might have on erosion and vice versa.

31.3 SPPS:CO_2 model and erosion resistance

Iron carbonate scale formation on pipe walls plays a major role in the synergy between erosion and corrosion, especially in the production of sweet crude oil, i.e., an environment rich in CO_2. When the flow conditions are right to form iron carbonate scale ($FeCO_3$), a reduction in the corrosion rate is observed as a result of the protection provided by the film. The model for predicting scale formation (SPPS:CO_2) was developed at the E/CRC as a means of determining under what production conditions scale would likely form [7,8]. However, in the presence of sand, iron carbonate scale can be removed partially or completely, which will expose the metal surface for further corrosion. In this case, the combined metal loss could be much higher than the summation of the individual losses, i.e., a synergistic result.

Iron carbonate, $FeCO_3$, can form and deposit on the surface of metals when concentrations of Fe^{2+} and CO_3^{2-} exceed the solubility product, K_{sp}. The tendency of scale formation is expressed by the saturation factor (F_{sat}) that is given by Eq. (31.2).

$$F_{sat} = \frac{\left[CO_3^{2-}\right]\left[Fe^{2+}\right]}{K_{sp}} \tag{31.2}$$

From this equation, when F_{sat} is smaller than 1, scale is less likely to form because the product of the concentrations of Fe^{2+} and CO_3^{2-} is below the saturation level. However, when F_{sat} is larger than 1, the scale is more likely to form. Larger values of F_{sat} indicate a greater likelihood for scale formation.

31.3.1 Scale characterization

The erosion resistance of iron carbonate to solid particle impingement can be partially addressed through characterization of the type of scale formed under various simulated production conditions. Specifically, thickness, porosity, and the microcrystallinity of the scale are very important for interpreting the corrosion and erosion–corrosion behaviors and can be linked to the protectiveness of the scale. It was demonstrated that different experimental conditions (temperature, flow geometry, etc.) are key factors in determining scale behavior. For example, Fig. 31.1 shows two scanning electron microscopy (SEM) images for a scale formed in channel flow at 93°C (200°F), 1.4 bar (20 psig) CO_2, and pH 6.5. The first image shows a top view of the scale surface, whereas the second image shows a cross-section of an epoxy-mounted specimen. Scale thickness was measured to be around 5 μm in this case. For scale formed in jet flow, Fig. 31.2 shows images of a scale formed at 80°C (175°F), pH 5.9, and 20 psig CO_2. The scale formed under these conditions was much thicker than the scale presented earlier. In some locations, scale thickness exceeded 50 μm.

Table 31.1 provides a summary of scale thickness measurements obtained in channel and jet flows. For channel flow, scales were formed at different temperatures (150–200°F) and almost constant pH of 6.5. With this condition, scale thickness was measured to be between 2 and 6 μm. Scale thickness increased to 8 μm when the temperature was lowered from 93°C (200°F) to 79°C (175°F). As the scale formation temperature was further lowered to 66°C (150°F), scale thickness increased up to 13 μm. The steady-state corrosion rates for these three cases were very low, between 2 and 6 mpy.

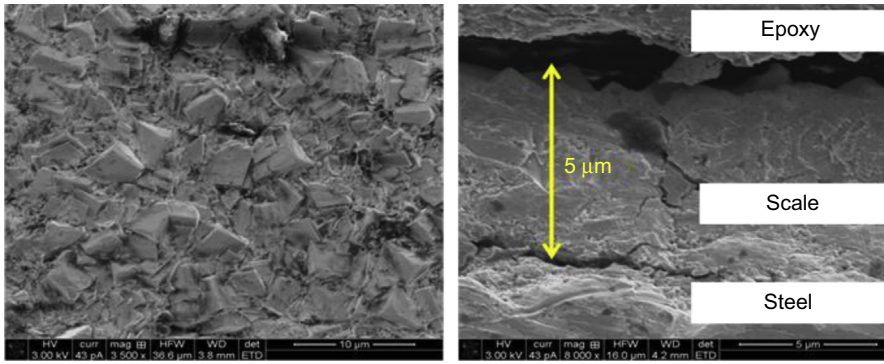

Figure 31.1 Scanning electron microscopy images [magnification 3,500× *(left)* and 8,000× *(right)*] for a scale that was formed at 93°C (200°F), pH 6.5, and 1.4 bar (20 psig) CO_2. The geometry of the specimens was in-line channel flow.

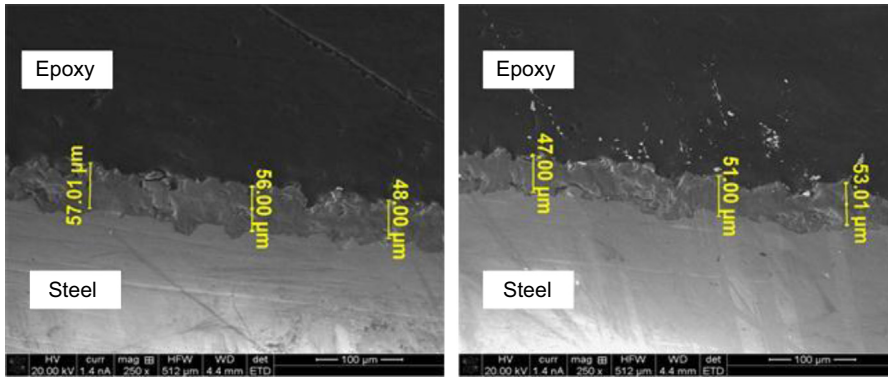

Figure 31.2 Scanning electron microscopy images (magnification 260×) for a scale formed at 93°C (200°F), pH 5.9, 1.4 bar (20 psig) CO_2, and a jet-flow geometry.

Table 31.1 $FeCO_3$ scale thickness measurements obtained by scanning electron microscopy

Case	T (°F)	pH	F_{sat} (surface)	Scale thickness (µm)	CR @ steady state (mpy)
Channel flow configuration					
1	200	6.5	256	2–5	2.5
2	200	6.3	119	3.5–5.5	6.0
3	175	6.3	176	6–8	3.0
4	150	6.1	52	10–13	3.7
Jet flow configuration					
5	190	6.5	1.8	4–10	10, 29
6	190	6.2	2.9	30–40	20
7	175	5.9	2.4	40–70	30
8	190	5.4	0.2	50–70	100

For jet flow, scales were formed at almost constant temperatures and different pH values. At a temperature of 88°C (190°F) and pH 6.5, the scale thickness was between 4 and 10 µm, almost twice the thickness of the scale formed in channel flow under similar testing conditions. Scale thickness increased significantly to between 30 and 40 µm when the pH was lowered slightly to 6.2. At pH 5.9 and temperature 79°C (175°F), scale thickness was 40–70 µm. At pH 5.4 and temperature 88°C (190°F), the scale thickness was 50–70 µm.

From these results, important observations can be made. The first observation is that the cell configuration can affect the scale thickness. Scale formed in jet flow were

much thicker and less protective, i.e., more porous than the scales formed in channel flow. This was indicated by the higher steady-state corrosion rate values. The degree of protection offered by the scale depends, in part, on scale porosity. Porous scale allows higher diffusion rates of cathodic reactants through the scale, and consequently results in higher corrosion rates. Jet flow cases were conducted at higher velocities and much higher shear stresses compared with channel flow cases. Higher velocity and higher shear stress enhance the mass transfer process and might impose mechanical damage on the scale, which results in higher corrosion rates [9].

The second observation is that lower temperature and pH values led to thicker and less protective scale formation. The effect of temperature is demonstrated by the data collected for scale formed in channel flow. For a better understanding of this effect, F_{sat} values at the metal surface were computed by SPPS:CO_2. For channel flow, F_{sat} values were computed at 1 ft/s flow velocity, 0.5 ppm Fe^{2+}, 2% by weight NaCl and specified concentrations of HCO_3^-. For jet flow, F_{sat} values at the metal surface were computed at 10 ft/s flow velocity, 0.5 ppm Fe^{2+}, 2% by weight NaCl, and specified concentrations of bicarbonate. The results showed that cases conducted with lower temperatures have lower F_{sat} values. Lowering the F_{sat} value slows the scale formation process, which generates a thicker and less protective scale. The relation between F_{sat} and temperature is not shown directly in the F_{sat} equation. However, it is indirectly included as part of the solubility product. Lower temperature increases the solubility product, K_{sp}, for iron carbonate scale, which, in turn leads to a lower saturation factor, F_{sat}.

The effect of pH on scale formation was evidenced for scale formed in jet flow. It has been previously shown that lower pH values result in higher solubility of iron carbonate, which leads to a lower precipitation rate and, consequently, lower scaling tendency [10,11]. Scale formed at lower precipitation rates has been associated with higher porosity. This observation was also reported by Chokshi et al. [12]. He reported that scale formed at pH 6.0 was less protective and showed higher scale porosity compared with that formed at pH of 6.6.

31.3.2 Scale erosion resistance

The extent of the $FeCO_3$ removal by erosion is governed by the erosion resistance of the scale. The tenacity of the scale is based on the conditions under which the scale is formed as discussed in the earlier section. For example, laboratory data presented by Al-Aithan et al. [13] showed that scale formed at (190°F, 10 ft/s, pH 6.4, 2 wt% NaCl, 1900 ppm $NaHCO_3$) erodes five times faster than bare mild steel, e.g., 1018 carbon steel. On the other hand, less erosion resistance (15 times less than that of bare steel) was observed for scale formed at lower temperatures and decreased pH (150°F, 10 ft/s, pH 6.24, 2 wt% NaCl, 1900 ppm $NaHCO_3$) as shown in Fig. 31.3. This variation in the erosion resistance is attributed to the change in the microstructure and mechanical properties of iron carbonate scale formed under these differing production conditions.

Another interesting feature is that iron carbonate scale erosion behavior in wet condition (flow loop) is quite different from the scale erosion resistance in a dry

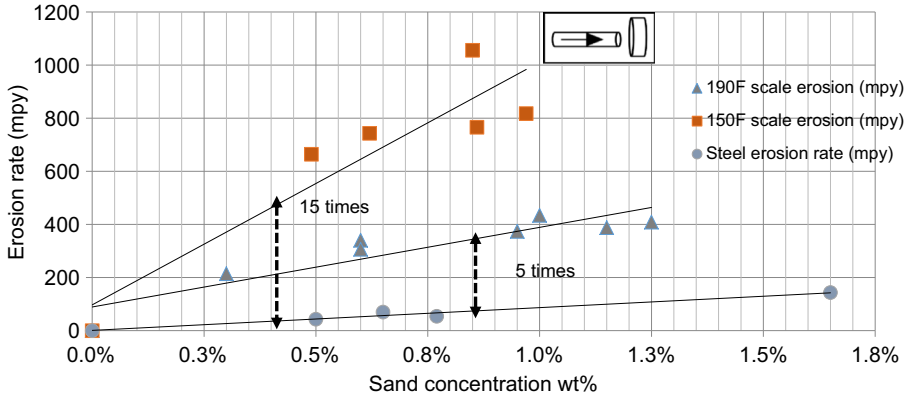

Figure 31.3 Scale erosion rates and bare G10180 mild steel erosion rate [6].

condition. Experiments showed that wetted scale has higher erosion resistances than those of dry scale as illustrated in Fig. 31.4. However, a review of erosion ratios for wetted bare steel versus dry bare steel revealed that the erosion ratio for wetted bare steel was also about an order of magnitude lower than those for dry bare steel as shown in Fig. 31.5. Erosion ratio is defined as the mass loss of material divided by mass of sand throughput given in Eq. (31.3).

$$\text{Erosion Ratio}\left(\frac{g}{g}\right) = \frac{\text{Erosion mass loss rate (g/min)}}{\text{Sand Mass throughput rate (g/min)}} \tag{31.3}$$

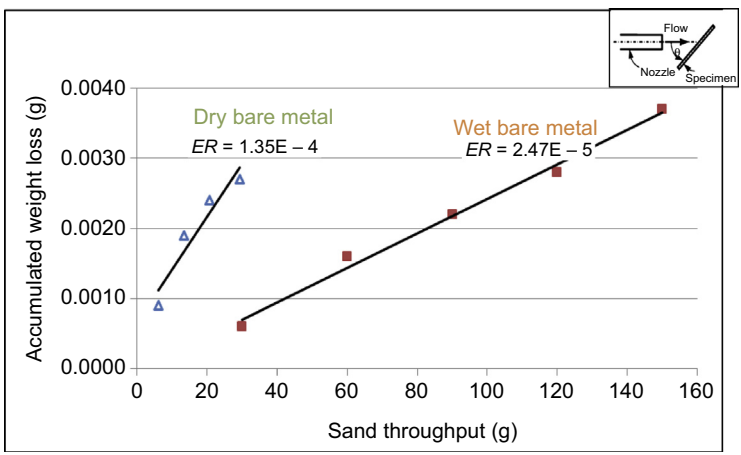

Figure 31.4 Comparison between erosion ratios for dry and wetted scale tested at $V_{gas} = 36.4$ m/s, 30-deg, 150-μm sand.

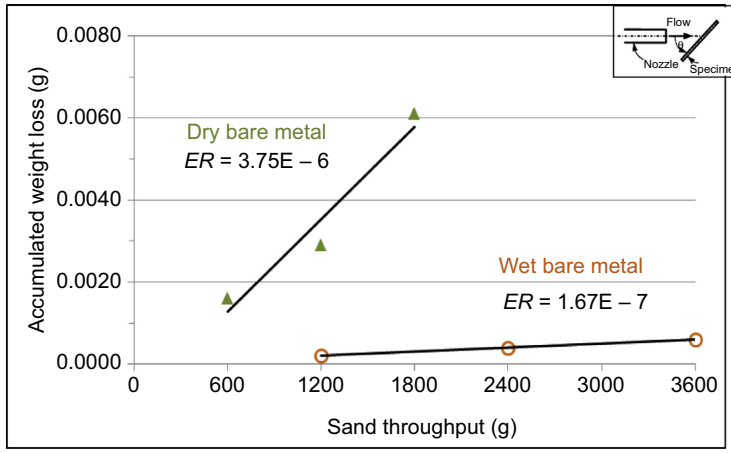

Figure 31.5 Comparison between erosion ratios for dry and wet bare metal tested at V_{gas} = 36.4 m/s, 30-deg, 150-μm sand.

31.4 Erosion–corrosion threshold velocity model

As mentioned earlier, some of the earliest modeling of erosion–corrosion was reported by Shadley et al. in a single-phase flow loop study for iron carbonate scale removal in CO_2-saturated flow with sand [1–3]. The objective of the study was to develop a procedure for identifying the threshold flow velocity above which iron carbonate scale is partially or totally removed. This procedure could be used for setting a guideline to control erosion–corrosion in production facilities. Several sets of environmental conditions were examined in flow loop studies. For each data set, the highest erosivity that a scale could tolerate before being partially or totally removed was identified. The total erosion–corrosion resistance (*ECR*) was used to develop a correlation for predicting *ECR* as a function of temperature, pH, and F_{sat}. The *ECR* correlation is given by Eq. (31.4). The *ECR* defines the iron carbonate scale resistance in an erosion–corrosion environment depending on several factors explicitly described by the equations, such as pH, temperature, and F_{sat}. Other factors impacting *ECR* are CO_2 partial pressure and flow velocity.

$$ECR\ (\text{mm/year}) = C_0 F_{sat}^{C_1} f_T f_{\text{pH}} \tag{31.4}$$

where the temperature and pH functions, f_T and f_{pH}, were given by Eqs. (31.5) and (31.6) and the empirical constants, C_0 through C_7, are shown in Table 31.2.

$$\log(f_T) = C_2 e^{C_3(T-C_4)} \tag{31.5}$$

$$\log(f_{\text{pH}}) = C_5 \tan[C_6(\text{pH} - C_7)] \tag{31.6}$$

The *ECR* correlation and SPPS program were used to predict the threshold velocity for erosion–corrosion. The threshold velocity (V_{th}) is the maximum flow velocity that

Table 31.2 Constants used in Eqs. (31.3 through 31.5)

C_0 (mm/year)	C_1	C_2	C_3	C_4	C_5	C_6	C_7
1.038E-6	1.594	0.7748	0.0504	65.56	3.629	1.560	5.650

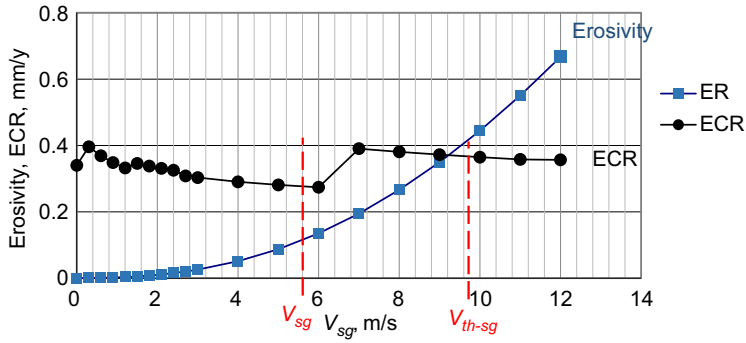

Figure 31.6 Prediction of threshold velocity for environmental and flow conditions for 3.5-in. elbow [temperature 135°F, CO_2 pressure 64.7 psia, pH 5.5, Fe^{2+} concentration 10 ppm, 30 lb/day, particle diameter of 150 μm, water rate (V_{sl}) of 1.2 m/s, and a gas rate (V_{sg}) of 5 m/s].

the scale can tolerate at a given environmental condition before being partially or totally removed. Fig. 31.6 shows a graphical illustration for predicting threshold velocity for a multiphase flow case [temperature of 57°C (135°F); 64.7 psia CO_2 pressure; pH 5.5; 10 ppm Fe^{2+}; 30 lbs/day particle rate; 150 μm sand particle diameter; water rate, V_{sl}, 1.2 m/s; gas rate, V_{sg}, 5 m/s]. The *ECR* and the erosivity (*ER*) values were computed at a range of gas superficial velocities (V_{sg}). The intersection of the *ECR* and the *ER* curves represent the threshold velocity given here in terms of gas superficial velocity ($V_{th\text{-}sg}$). For this sample case, the superficial gas velocity is smaller than the gas threshold velocity. This indicates that the *ER* of the flowing system is smaller than the *ECR*. In such cases, iron carbonate scale is assumed to be able to form throughout the piping interior. However, when operating at flow velocities above the threshold velocity, the *ER* of the flowing system exceeds the *ECR*. In these cases, scale is assumed to be prevented from adhering to piping surfaces, and pitting or uniform corrosion ensues.

31.5 Erosion–corrosion prediction mechanistic model

Mutahhar et al. [4] developed a model to predict steady-state erosion–corrosion rates. The erosion–corrosion model integrates the CO_2 corrosion model (SPPS:CO_2)and the solid particle erosion model (SPPS). The combined model (SPPS:E-C) model uses SPPS to predict the scale erosion rate in mils per year (mpy) with reference to the correlation that was developed between steel and scale erosion rate explained in Fig. 31.3. Then the model uses SPPS:CO_2 to calculate the bulk ion concentrations, mass transfer rates, bare metal corrosion rates, and other data that affect the scale formation tendency

and rate. These data are used by the erosion–corrosion model to compute the scale formation rate. The model then predicts the CO_2 corrosion rate at steady-state condition for which the scale erosion rate equals the scale deposition rate.

For conditions were the scale erosion rate is greater than the maximum scale deposition rate (occurring for bare metal conditions), the scale is considered to be completely removed, or to be prevented from accumulating, and the erosion–corrosion rate is determined to be equal to the summation of the erosion rate and bare metal corrosion rate. On other hand, when the maximum scale formation rate is greater than the rate of scale removal by erosion, the scale is considered to be maintained with only partial removal by erosion. In this case, the model will iterate to calculate the scale thickness, deposition rate, and the corrosion rate at steady-state conditions. The framework of the model is illustrated in Fig. 31.7.

The erosion–corrosion model developed by Mutahhar et al. [4] used the Yean et al. [14] precipitation rate correlation to predict the scale formation process as given in Eqs. (31.7) and (31.8).

$$\frac{d[\mathrm{Fe}]_t}{dt} = -k\left([\mathrm{Fe}]_t - [\mathrm{Fe}]_{eq}\right) \tag{31.7}$$

$$[\mathrm{Fe}]_t = [\mathrm{Fe}]_{eq} + \left([\mathrm{Fe}]_{\mathrm{o}} - [\mathrm{Fe}]_{eq}\right)e^{-kt} \tag{31.8}$$

where $[\mathrm{Fe}]_t$ is the total dissolved iron concentration (molality, m) at time t (in min), k is the nucleation reaction rate constant (in min^{-1}), $[\mathrm{Fe}]_{eq}$ is the expected total dissolved

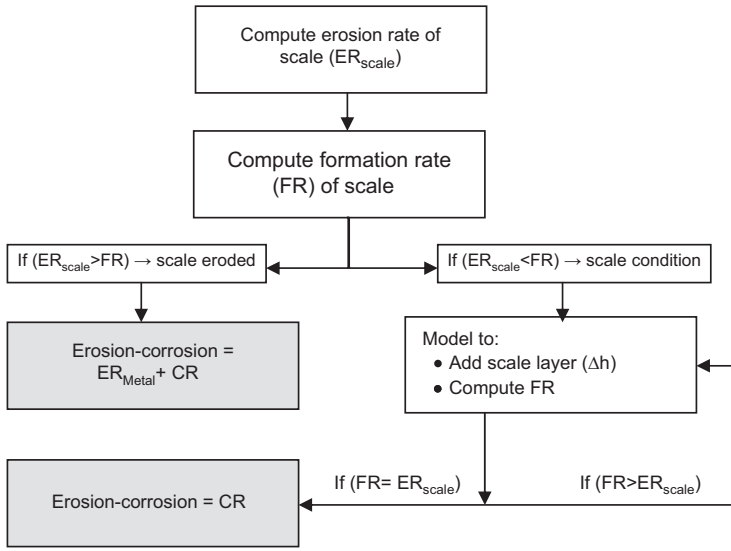

Figure 31.7 Principle of multiphase erosion–corrosion model [4].

iron concentration at equilibrium, and $[Fe]_o$ is the initial total dissolved iron concentration in solution at time $t = 0$.

$$\dot{m}\left(\frac{\text{mole } Fe^{2+}}{m^2 s}\right) = \rho_{liq} h_{bl} \frac{k}{\left[CO_3{}^{2-}\right]} \left(\left[Fe^{2+}\right]\left[CO_3{}^{2-}\right] - K_{sp}\right) \tag{31.9}$$

Eq. (31.9) is an expression of Yean's equation for calculating the scale precipitation rate in [mole/($m^2 \cdot s$)], where $\dot{m}$ is the scale deposition rate, ρ is the liquid density, h_{bl} is the diffusion boundary layer thickness, $[Fe^{2+}]$ is the iron concentration, $\left[CO_3{}^{2-}\right]$ is the carbonate concentration, K_{sp} is the solubility product, and k is the temperature-dependent reaction rate constant given by the Arrhenius equation, Eq. (31.10).

$$k_r = e^{\left(A - \frac{B}{R\,T}\right)} \tag{31.10}$$

where k_r is the kinetics constant in $(s)^{-1}$, A is a preexponential factor, and B is the activation energy for nucleation.

Using Eq. (31.10) with constants provided by Yean, the preliminary model predicted that the rate of iron carbonate scale formation was much lower than scale deposition rates that were observed in flow loop laboratory results. These results suggest that the scale deposition rates predicted by the proposed Arrhenius constants were too low. Similarly, using other values suggested by other researchers Sun, Hunnik, Johnson and Tomson (J&T), and Yean [9,15,16], iron carbonate scale formation rates did not match the experimentally measured scale deposition rate.

An attempt to understand the predictions of the different deposition rate correlations proposed by Sun, Hunnik, J&T, and Yean [9,15,16] is presented in Fig. 31.8; it shows differences in scale precipitation rates at temperature 88°C (190°F), 10 ft/s, pH 6.4, 1900 ppm $NaHCO_3$, and 5% Fe^{2+}. As it can be noted, there are huge differences between the results of the correlations developed by Sun, Hunnik, J&T, and Yean.

The rate of iron carbonate scale deposition was investigated by the measurement of the actual scale deposited onto the metal surface for different time intervals. With this, different values of Arrhenius constants were considered in this work as shown in Table 31.3. The new values showed better agreement with the experimental data

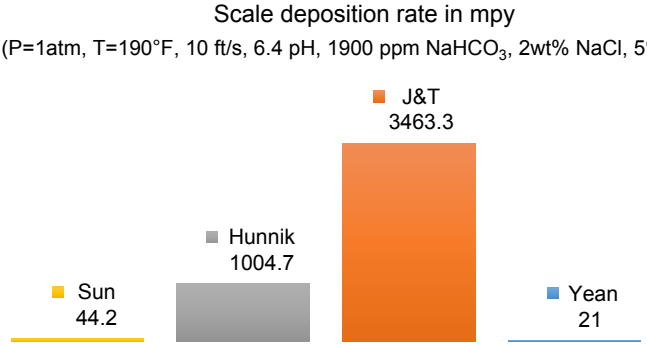

Figure 31.8 Scale deposition rate under different correlations.

Table 31.3 Arrhenius's equation constants derived for scale deposition rate

	Equation	Activation energy *B* kJ/mol	Preexponential factor *A*
1	Johnson and Tomson [15]	127.3	56.3
2	Van Hunnik [16]	119.8	52.4
3	Yean [14]	197	68
4	Sun [17]	64.85	28.2
5	E-C Model [13]	95.5	34.62

and were, therefore, used in the SPPS:E-C model [13]. The new values are close to those reported by Sun [3].

31.6 SPPS:E-C model validation

The SPPS:E-C mechanistic model was validated through various flow loop experiments [13] under different erosion–corrosion environments. Erosion–corrosion experiments were conducted in the submerged jet impingement flow loop to validate the erosion–corrosion rate prediction model.

The corrosion rates of the erosion–corrosion process, with scale fully or partially covering the metal surface, were compared with the predicted values. Fig. 31.9 shows

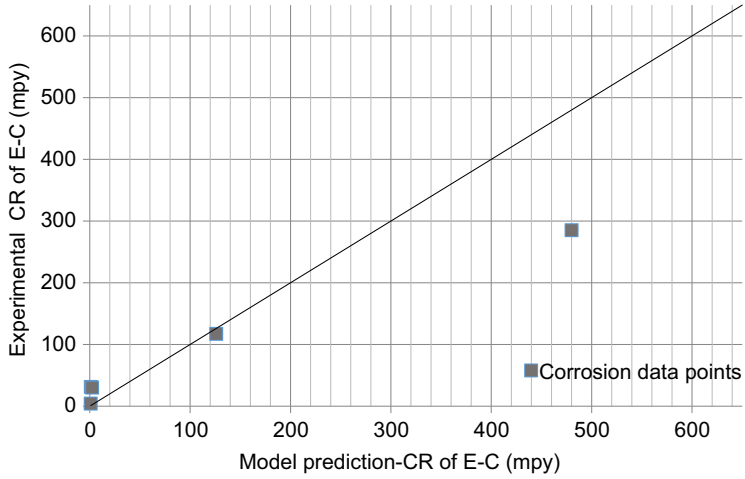

Figure 31.9 Corrosion rate comparison between model and experimental data for 190°F, 10 ft/s, pH 6.4, 2 wt% NaCl, 1900 ppm $NaHCO_3$.

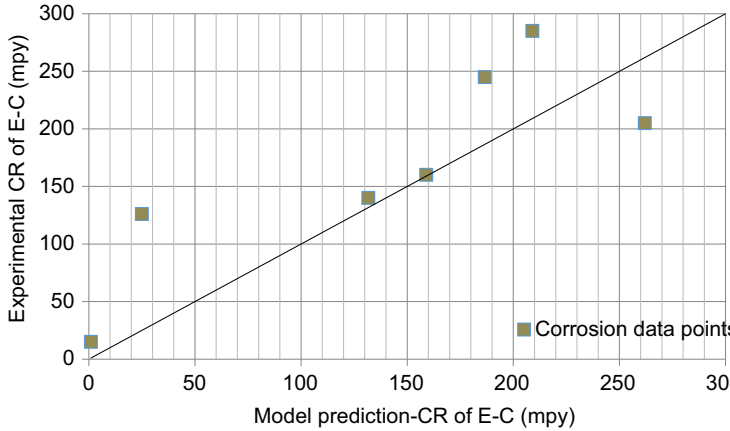

Figure 31.10 Corrosion rate comparison between model and experimental data for 150°F, 10 ft/s, pH 6.24, 2 wt% NaCl, 1900 ppm $NaHCO_3$.

the model versus experimental results at 88°C (190°F). The performance of the model at these conditions was considered acceptable.

A similar comparison between measured and predicted corrosion rates was made for the 66°C (150°F) conditions as shown in Fig. 31.10. In almost all cases at this temperature, posttest examination of the specimen showed patches of bare metal. In all cases involving bare patches, the model predicted bare metal corrosion rates (the model recognizes that scale is completely removed from a location on the pipe and calculates the bare metal corrosion rates at that location). However, in these cases, the model was not able to accurately predict the corrosion rate of the specimen as a whole as monitored by linear polarization resistance (LPR), where LPR measures the average corrosion rate for surfaces covered or not covered by scale.

31.7 Emerging trends in erosion–corrosion modeling and prediction

As illustrated in the aforementioned results, developing a mechanistic erosion–corrosion model involves accounting for the competition between the deposition rate of iron carbonate by corrosion and its removal rate from erosion. Therefore, developing erosion–corrosion models such as SPPS:E-C to be used in the oil and gas industry is ever more reliant on understanding how erosion–corrosion behaves in a variety of erosive and corrosive conditions. Although the initial data set provided insight into many factors related to the erosion–corrosion rate under select conditions, further model improvements necessitates more erosion–corrosion testing for a wider variety of production-like conditions. Parameters such as gas or solution chemistry, water cut, erodent properties and concentration, scale properties, pH, temperature, flow rates, flow geometries, and properties of the tested material must all be accounted for to effectively model erosion–corrosion. In addition, characterization of the scale types

formed under various conditions will be essential for generating data on erosion resistance, scale porosity, crystal microstructure, erosion−corrosion penetration rate, etc. Many of these data can be obtained through analytical techniques in electron microscopies, 3-D profilometry, X-ray diffraction, and a variety of electrochemical techniques. By being able to predict the scale type at a given production condition, the tenacity of the scale to resist erosion can also be predicted. Under such conditions, the production flow rate could be adjusted to stay within an operating regime that retains the protective iron carbonate scale.

Furthermore, although there has been significant success in the development of models for the prediction of erosion and corrosion for single- and multiphase flows, there still exists a significant need for development in the area of complex multiphase flows. Research has also investigated the effect of chemical inhibitor in these systems, expanding erosion−corrosion prediction capabilities that have great practical importance in many industries. The presence of sand and/or other erodent particles can have significant effects on inhibitor performance depending on the flow and chemical environments. The inclusion of inhibitor in systems that are actively forming scale and subject to erosion would greatly expand the range of environmental conditions that could be modeled by these prediction approaches.

In addition to expanding prediction capabilities to multiphase, multicomponent flows, the current models for predicting erosion and corrosion are most accurate in the steady state regime. Expanding these models to include the ability to predict erosion−corrosion behavior during transient events would lead to a more complete understanding of the impact of changing conditions in a variety of gas and oil production conditions.

31.8 Conclusion

This chapter discussed the development in the research of erosion−corrosion modeling for sweet production in the presence of sand under iron carbonate scale-forming conditions. An overview was provided for two erosion−corrosion models. The first model is one of the earliest that was developed by Shadley et al. [1−3] for predicting the threshold velocity at which iron carbonate scale is partially or totally removed. Although the model could not yet predict the erosion−corrosion penetration rate, it was useful for establishing flow velocity guidelines to control erosion−corrosion in production facilities by maintaining the presence of iron carbonate scale, and in developing the framework for a future research in modeling the complex E-C process. In this work, a correlation was developed for predicting the *ECR* of iron carbonate scale. The *ECR* correlation and SPPS program were used to predict the threshold velocity for erosion−corrosion.

In a later development, Mutahhar et al. [4] developed a model for predicting the erosion−corrosion penetration rate. The erosion−corrosion model (SPPS:E-C) integrates the CO_2 corrosion model (SPPS:CO_2) and the solid particle erosion model (SPPS) for modeling the competition between iron carbonate scale formation rate and erosion rate. Modeling the competition between scale formation and removal is very important for predicting the synergy between erosion and corrosion. SPPS-E

was used to predict the scale erosion rate in mils per year with reference to a correlation that was developed between steel and scale erosion rates. Then the model uses SPPS: CO_2 to calculate the bulk ion concentrations, mass transfer rates, bare metal corrosion rates, and other data that affect the scale formation tendency and rate. These data are used by the erosion−corrosion model to compute the scale formation rate. The model then predicts the CO_2 corrosion rate at steady-state condition for which the scale erosion rate equals the scale deposition rate. A comparison between experimental and predicted data showed acceptable performance of the model.

The SPPS erosion model utilized by both erosion−corrosion models mentioned earlier was developed by the University of Tulsa E/CRC program [5,6]. The model calculates metal penetration rate by erosion using an equation that accounts for sand properties, sand rate, fluid properties, flow rates, flow geometry, and material properties for the pipe. This model has been successfully employed by many of the top oil and gas producers in the world to predict the loss of metals impacted by solid particles, e.g., sand entrained in single or multiphase production conditions.

Understanding the formation mechanism of iron carbonate scale and its role in protecting metal surfaces from erosion and corrosion is essential for developing a mechanistic model for predicting the erosion−corrosion rate. This chapter presented experimental observations for iron carbonate scales formed at different environmental conditions. The first observation is that the flow configurations and geometries can affect the scale thickness and porosity. Scale formed in jet flow were much thicker and less protective, i.e., more porous than the scales formed in channel flow. The second observation is that lower temperature and pH values led to thicker and less protective scale formation. It was also observed that erosion resistance of iron carbonate scale depends heavily on the condition under which the scale is formed. This variation in the erosion resistance is attributed to the change in the microstructure and mechanical properties of iron carbonate scale formed under these differing production conditions.

References

[1] J. Shadley, E. Rybicki, S. Shirazi, E. Dayalan, Velocity guidlines for avoiding erosion-corrosion damage in sweet production with sand, Transactions of the ASME 120 (1998) 78−83.

[2] J. Shadley, S. Shirazi, E. Dayalan, E. Rybicki, Prediction of erosion-corrosion penetration rate in a carbon dioxide environment with sand, Corrosion 54 (12) (1998) 972−978.

[3] J. Shadley, S. Shirazi, E. Dayalan, E. Rybicki, Velocity guidelines for preventing pitting of carbon steel piping when the flowing medium contains CO_2 and sand, in: Corrosion/96, NACE International, Houston, TX, 1996.

[4] F. Mutahhar, Erosion-Corrosion for Carbon Steel in Sweet Production with Sand: Modeling and Experiments, Mechanical Engineering Department, The University of Tulsa, Tulsa, OK, 2012.

[5] S. Shirazi, B. McLaury, J. Shadley, E. Rybicki, Generation of the API RP 14E guidelines for erosive services, Journal of Petroleum Technology 47 (1995) 693−698.

[6] B. McLaury, S. Shirazi, Generalization of API RP 14E for erosive service in multiphase production, in: SPE Annual Technical Conference and Exhibition, Society of Petroleum Engineers: Houston, TX, 2: pp. 10, 1999, 1999.
[7] E. Dayalan, J. Shadley, E. Rybicki, S. Shirazi, F. De Moraes, CO_2 corrosion prediction in pipe flow under $FeCO_3$ scale-forming conditions, in: Corrosion/98, NACE International, San Diego, CA, 1998.
[8] E. Dayalan, G. Vani, J. Shadley, S. Shirazi, E. Rybicki, Modeling CO_2 corrosion of carbon steels in pipe flow, in: Corrosion/95, NACE International, Houston, TX, 1995.
[9] K. Gao, F. Yu, X. Pang, G. Zhang, L. Qiao, W. Chu, M. Lu, Mechanical properties of CO_2 corrosion product scales and their relationship to corrosion rates, Corrosion Science 50 (2008) 2796−2804.
[10] S. Nešić, S. Wang, J. Cai, Y. Xiao, Integrated CO_2 corrosion − multiphase flow model, in: Corrosion 2004, NACE International, Houston, TX, 2004.
[11] S. Nesic, G. Solvi, J. Enerhaug, Comparison of the rotating cylinder and pipe flow tests for flow-sensitive carbon dioxide corrosion, Corrosion 51 (10) (1995) 773−787.
[12] K. Chokshi, W. Sun, S. Nešić, Iron carbonate film growth and the effect of inhibition in CO_2 corrosion of mild steel, in: Corrosion 2005, NACE International, Houston, TX, 2005.
[13] G. Al-Aithan, Erosion-Corrosion Modeling for Scale Forming Conditions in CO_2 Environment (Master thesis), Mechanical Engineering Department, The University of Tulsa, Tulsa, OK, 2013.
[14] S. Yean, H. Saiari, A. Kan, M. Tomson, Ferrous carbonate nucleation and inhibition, in: SPE International Oilfield Scale Conference, Aberdeen, UK: Society of Petroleum Engineers, 2008, 2008.
[15] M. Johnson, M. Tomson, Ferrous carbonate precipitation kinetics and its impact on CO_2 corrosion, in: Corrosion/91, NACE International, Houston, TX, 1991.
[16] E. Van Hunnik, B. Pots, E. Hendriksen, The formation of protective $FeCO_3$ corrosion product layers in CO_2 corrosion, in: Corrosion/96, 1996. Houston, TX.
[17] W. Sun, S. Nešc, Kinetics of corrosion layer formation: Part 1-iron carbonate layers in carbon dioxide corrosion, Corrosion 64 (4) (2008) 336−843.

Residual life predictions—extending service life

32

Richard B. Eckert
DNV GL, Dublin, OH, United States

32.1 Introduction

Most oil and gas production, processing, and transportation assets are designed, constructed, and operated on the basis of a finite design life. The design life is based on the assumptions made in regard to various degradation mechanisms that are relevant to the asset, particularly those that are time sensitive, e.g., external and internal corrosion, fatigue, etc. During the operation of an asset, degradation mechanisms may progress at a higher or lower rate than the assumptions made to establish design life, since they are affected by many variables that are difficult to predict. If the preventive and mitigative measures applied to reduce the degradation mechanisms were highly effective, the asset may be completely fit for service at the end of its design life. Today, in fact, a large percentage of oil and gas assets are still functioning safely and reliably well beyond their original design life, although few have gone through a formalized process of qualifying and documenting asset life extension (LE). Where, as in most places in the world, LE is not governed by regulatory requirements, assets continue to be operated based largely on their operational integrity and often in consideration of the overall risk. One LE standard that can be applied to pipelines is International Organization for Standards/Technical Specification (ISO/TS) 12747: 2011 petroleum and natural gas industries, pipeline transportation systems [1]. This ISO standard is a recommended practice for pipeline LE that provides guidance in assessing the feasibility of extending the service life of a pipeline system, as defined in ISO 13623 [2], beyond its specified design life.

Norway has a well-formalized processes and standards governing asset LE, largely because LE requires approval of the Norwegian Petroleum Directorate (NPD) and the Petroleum Safety Authority (PSA). Oil and gas facilities installed on the Norwegian Continental Shelf are granted "Consents to Operate," which have a finite life based on assumptions that are the basis for the approval of the "Plans for Development" and "Plan for Installation and Operation." Use of the facilities beyond the approved Consent period in Norway requires a new application and a new Consent to Operate from the NPD and the PSA.

Extending the design life of an asset requires consideration of degradation mechanisms that affect all systems and components of the asset, including pipelines, wells, and well head equipment, subsea equipment, load bearing structures, processing systems, health and safety systems, etc., NORSOK standards are developed by the Norwegian petroleum industry, and are administered and published by Standards

Trends in Oil and Gas Corrosion Research and Technologies. http://dx.doi.org/10.1016/B978-0-08-101105-8.00032-2

Norway. Technical guidelines for different parts of Norwegian Oil and Gas assets have been developed as follows:

- Load-bearing structures; NORSOK standard N-006, assessment of structural integrity for existing offshore load-bearing structures (April 2009) [3].
- Transportation systems; NORSOK standard Y-002, Life Time Extension For Transportation Systems (December 2010) [4].
- Subsea systems; NORSOK standard U-009, LE for subsea systems (March 2011) [5].
- Drilling and wells, process topside systems, Health and Safety Executive's (HSE), and technical safety systems; Norwegian Oil and Gas Association recommended guideline for the Assessment and Documentation of Service Life Extension of Facilities No. 122 (April 2012) [6].

The design life of an asset is typically considered to be the original time period over which the asset was intended to operate based on certain assumptions. Some pipeline design standards define design life differently:

ASME B31.4:2006 [7]—Design life is a period of time used in design calculations selected for the purpose of verifying that a replaceable or permanent component is suitable for the anticipated period of service. The ASME standard's position is that design life does not pertain to the life of the pipeline system because a properly maintained and protected pipeline system can provide transportation indefinitely.
DNV-OS-F101:2014 [8]—Design life is the initially planned time period from initial installation or use until permanent decommissioning of the equipment or system. The original design life may be extended after a requalification.
ISO 13623:2009—Design life is the period for which the design basis is planned to remain valid.
NORSOK standard Y-002—Design life is a specified period for which the integrity of the system is documented in the original design with anticipated maintenance, but without requiring substantial repair.

For new facility developments, there is also an "economic design life" that drives project development decisions. The economic design life is not focused on operational integrity and is typically less than 25 years based on the financial considerations of the stakeholders, e.g., agreements with lenders, implications of tax laws, unique interests of partners, etc.

In NORSOK standard Y-002, the service life is defined as the length of time the system is intended to operate and the standard identifies a recommended process for extending service life. Therefore, in the next section of this chapter, the term "service life" will be used when referring to the extended period of time over which the asset is intended to be operated. In addition, since the focus of this book is on corrosion, threat mechanisms other than corrosion that could affect pipelines will not be discussed; however, all relevant degradation mechanisms must be considered in an actual LE project.

32.2 Methodology for extending service life

Offshore oil and gas production assets have been in service for over 50 years in some parts of the world. First oil in the North Sea was in discovered in 1969 [9], followed by

the development of Norway's extensive Ekofisk oil field, which began producing oil in 1980. In the US Gulf of Mexico, platforms were being installed in waters up to 1000 feet in depth by 1969 [10]. The US onshore pipeline infrastructure has pipelines that were installed as early as the 1930s that are still in service and some gathering systems contain piping dating back to around 1910, and probably earlier. Certainly, when operated and maintained properly such that the integrity of the asset does not decline appreciably, oil and gas assets can have a long, safe, and reliable service life. Although there are different drivers for following a formalized process for extending asset service life, the process is generally the same for onshore and offshore transportation systems. Here, the NORSOK standard Y-002 "Life Extension of Transportation Systems" will be referenced as an example of one means to proceed through the various steps used in extending service life.

Before LE becomes a consideration, an asset has gone through the design, construction, commissioning, and operational phases of life. All of these phases of asset life affect the potential for extending service life. Shortcomings in design, e.g., inadequate corrosion allowance, or construction, e.g., poorly applied external coating, will have consequences in the LE phase of asset life. Perhaps even more significant; however, is how the integrity of the asset was maintained and monitored during the operations phase through the asset integrity management system (AIMS). The core of the integrity management process usually includes system risk review and strategy; inspection and monitoring; integrity assessment; and mitigation, prevention, and repair. The process should occur continually throughout the operations phase of asset life and it should also provide data and information that will be useful in the LE process. However, even if the integrity management process was carried out completely and perfectly, this alone would not be adequate for documenting and justifying LE.

The overall purpose of applying a LE process is to demonstrate that system integrity will be acceptable to the end of the extended service life. The LE process typically includes the following steps:

- Defining the premise or basis for operation over the extended asset life and identifying potential new threats to the assets that have emerged since the original design was placed in service.
- Assessing the integrity of the asset to the extent possible to quantify the current condition, and evaluating whether the asset has been operated within the original design envelope conditions.
- Conducting a design and/or condition-based engineering reassessment of the system using information from the integrity assessment (previous step) and established LE models, industry best practices, and technology.
- Documenting and implementing the LE, if the assessment determines that the asset integrity will be acceptable for the extended service life. Implementation may be conditional, requiring new continuous or one time measures to meet the requirements for LE.

If the reassessment determined that the integrity of the asset would *not* be acceptable at the end of the new extended life, modifications could be considered together with a feasibility review. An overview of the LE process from NORSOK Y-002 is shown in Fig. 32.1. It should also be noted that the LE process may require compliance with various regulations that are applicable to operation and design of the asset.

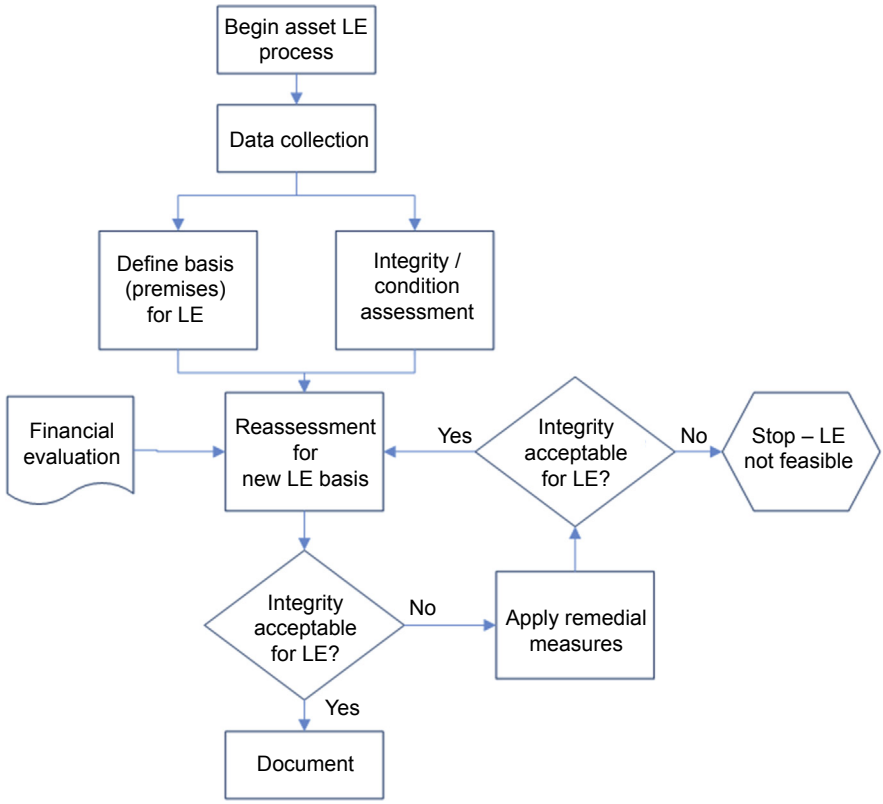

Figure 32.1 Life extension process.
After NORSOK Standard Y-002.

32.2.1 Identifying the basis for asset LE

32.2.1.1 Design life and extended design life

As mentioned previously, NORSOK standard Y-002 describes that design life is "a specified period for which the integrity of the system is documented in the original design with anticipated maintenance, but without requiring substantial repair."

The original design assumptions (premises) must be reviewed to assess whether they are still applicable for the LE period. The original premises that have been applied in the original design, fabrication, construction, operation, and repair/maintenance of the assets must first be identified.

32.2.1.2 System description

The first step in the LE process is to clearly define the system of assets to be included in the assessment. Often, LE is applied not just to a single pipeline, but to an entire production operation that may consist of everything from wells to subsea equipment to

risers and surface processing platforms. Because there are considerable complexities and multiple service types involved in offshore production, the boundary limits or battery limits must be clearly defined. In addition to crude production assets, seawater and produced water (PW) injection systems may also be included as they are an integral part of most oil and gas production operations. Appurtenances, e.g., valves, fittings, chemical injection hardware, pig traps, etc., must also be included in the description of the system for which LE is being performed. The designs of various pipeline system components are likely to be covered under different standards and potentially are constructed from differing materials that have different responses to operating conditions, in terms of corrosion threats and service life. Oil and gas production systems may have multiple owner/operators with different standards from each other, and this must also be considered when reviewing the original design basis and battery limits. Different operators may also define battery limits in different ways so it is important to establish clear interfaces in the LE review.

From a corrosion standpoint, the pressure containing components are those that are most recognizable; however, nonpressure containing components also play important roles in asset integrity and can be affected by corrosion. Structural elements, for example, are subject to external corrosion and have mitigation measures in place to control corrosion; those mitigation measures, in some cases, have a finite life, as in the case of anodes. Mooring chains are known to suffer serious corrosion in some environments and would be included in the nonpressure containing equipment that is in scope of the LE assessment. Some elements, such as flexible joints, are affected by both mechanical and corrosion degradation mechanisms that can be compounded by one another (e.g., corrosion fatigue).

32.2.1.3 Design, fabrication, and construction basis

In the design, fabrication, and construction phases of asset life, certain assumptions (premises) are identified and provide the basis for the decisions made by designers and engineers and for materials selection. In terms of corrosion, one of the most important design decisions is materials selection because this decision has a profound effect on asset life and mitigation costs over the operations phase. Corrosion resistant alloy (CRA) selection typically increases capital costs by a factor of three (or more) over carbon steel construction; however, operating costs for carbon steel can far outweigh the increased initial costs of CRA. Material selection also has a strong influence on the types of corrosion mechanisms that will be applicable and that will need to be evaluated in the LE process. Assumptions are also made in regard to the operating environment that will be encountered, in terms of flow, pressure, temperature, fluid physical properties, fluid composition, mode of operation (continuous vs. intermittent), and changes in these factors over the service life. External condition assumptions also play a role in determining the life of the asset relative to both corrosion and other threats. For subsea pipelines, assumptions are often made in terms of the potential for subsidence, ship and anchor damage, strudel scour, and other geotechnical threats that can damage the pipeline or damage the coating and lead to increased corrosion susceptibility.

During design, assumptions are also made in regard to the fabrication and construction phases of the assets. For example, for welding of heavy wall pipe, a range of acceptable preheating before welding or between welding passes is typically specified. It is generally assumed that if criteria, such as preheating, are in a welding procedure, then they are to be met during fabrication. However, if these conditions were not documented or verified by welding inspectors during the fabrication process, there is uncertainty as to whether the requirements were actually met. Deviations from the preheating standard could lead to cracking or heat affected zone hardness that is at increased risk of hydrogen cracking mechanisms or sour cracking in service. Material verification is another area where actions that occurred during fabrication and construction can have an impact on LE. If materials deviations were not caught before installation, this increases the threat of having material present in the asset that is nonconforming and potentially more susceptible to corrosion or other threats, such as mechanical failure. Therefore, it is not simply the operational phase of the asset that must be considered in LE because fabrication and construction practices may have resulted in increased potential for corrosion failure. The uncertainty around this potential can be reduced by checking fabrication and construction documentation, if available. If documentation is not available then the effect of uncertainty should be included in the LE assessment.

In many cases, the original design of the asset was likely based on standards and industry best practices that are over 20–30 years old. Older standards are likely to differ from the current applicable standards as technology and modeling have improved. Further, if the asset was built over a period of many years, different standards may have been in effect during each period of construction. Differences between the standards used for design and construction and those that are currently in use need to be considered in the LE assessment. There are likely to be gaps or different conservatism in older standards because new standards often evolve from lessons learned by industry. These differences must be reconciled when developing the new service life. Details about the types of data that are collected for the LE are discussed in Section 32.3 of this chapter.

32.2.2 Internal corrosion threats and LE

Here, an overview of internal corrosion threats common to oil and gas operations is discussed. The threats are presented in general categories of composition-related, flow-related, surface deposit-related, environmental cracking-related, and other threats. Depending upon the service type of the assets undergoing an LE process, the applicable mechanisms for that service will need to be considered along with the mitigation measures that were applied to control each threat.

32.2.2.1 Composition-related corrosion

In sweet to mildly sour conditions, internal corrosion of oil producing assets is largely a product of whether the metal surface is water wetted, which is a function of the water cut, velocity, and fluid composition. When water, or a hygroscopic deposits/film, is in contact with the metal, internal corrosion is a possible outcome. The presence of

dissolved and gaseous species determines the corrosion mechanisms and rates that will be present.

Carbon dioxide (CO_2)

CO_2 combines with the PW to form carbonic acid (H_2CO_3), which then dissociates, releasing hydrogen ions; lowering the pH of the water. The corrosivity of the water is a function of the pressure, temperature, and water chemistry, which drives the types of surface films and reaction kinetics that may occur. Generally speaking, the higher the partial pressure of CO_2, the greater the corrosivity of the water. Increasing the temperature (to a point) increases the potential corrosion rate and can lead to formation of nonprotective films that increase localized pitting. The chemistry of the PW, including alkalinity, dissolved iron level, and presence of organic acids, also has an effect on corrosivity. Preferential weld corrosion is a selective form of attack, which corrodes the weld metal in wet gas environments containing CO_2. Numerous models [11,12] exist for estimating the CO_2 corrosion rate; however, they are often conservative and are only as reliable as the data used to run the modeling. If reliable historical fluid composition data are not available, the ability to reliably apply corrosion models to LE is limited.

Hydrogen sulfide (H_2S)

H_2S may originate in the reservoir and/or be produced by the activities of sulfate-reducing prokaryotes (SRP), inclusive of both bacteria and archaea. Producing fields can start out with low H_2S levels and become sour over time with seawater injection breakthrough or due to contamination during the drilling or well work processes. In the last decade, nitrate has been injected into seawater in some fields to mitigate souring due to SRP activity; however, this has produced mixed results. In some cases, increased corrosion has been experienced. Reliable historical composition records are needed to determine when sulfide levels may have increased and the potential effects that have resulted over time.

H_2S in water forms a weak acid, which partially dissociates to form hydrogen (H^+) and bisulfide (HS^-) ions, depending on pH and other factors. The corrosion rate will depend on the levels of H_2S and CO_2 in the water. The reaction of dissolved sulfides forms iron sulfide (Fe_xS_y) on the steel surface. When this iron sulfide film is continuous, it can be protective. However, if the Fe_xS_y film is broken or is not uniform, any exposed steel becomes anodic to the film and localized corrosion can be driven by a large cathodic area of iron sulfide film. Constituents including CO_2, oxygen, and chlorides can create iron sulfide films that are nonprotective. CRAs have different susceptibilities to H_2S than carbon steels.

The presence of sulfide ion also increases the potential for hydrogen cracking mechanisms. Normally, atomic hydrogen atoms forming on the cathode of a corrosion cell combine to form molecular hydrogen. In the presence of sulfide ions, the combination of atomic hydrogen at the cathode is impeded, resulting in atomic hydrogen entering the steel. Joint NACE/ISO standard MR0175/ISO 15156 [13] is typically used to guide the selection of materials resistant to sulfide stress cracking (SSC). Oil and gas designs

typically specify that materials must be suitable for sour service, per this NACE/ISO standard.

Oxygen (O_2)

The presence of oxygen, even in small concentrations, i.e., >20 parts per billion (ppb), in water can significantly increase corrosion rates because it is a strong cathodic reactant. Oxygen is most prevalent in water injection systems where removal of oxygen from naturally oxygenated waters is ineffective. Although crude oil production and processing is typically anaerobic (oxygen free), it is possible for oxygen to enter systems through leaking seals, valves, or equipment that is open or occasionally opened to the atmosphere. Severe pitting corrosion of carbon steel can then occur.

The primary systems affected by oxygen are the SW (and PW to a lesser extent) systems, dewatering operations, and utility systems such as firewater.

32.2.2.2 Flow-related corrosion

Erosion and erosion–corrosion

Erosion and erosion–corrosion are typically associated with the presence of solids and solids plus high fluid velocities, respectively. Solids combined with high-fluid velocities in multiphase systems can accelerate CO_2 corrosion rates by removing any protective films from the metal surfaces and/or interfering with corrosion inhibitor film formation on the pipe wall surface. This threat is more acute at valves, reducers, bends, tees, and sections of straight flow lines immediately downstream of choke valves.

The erosion resistance for the commonly used stainless steels and duplex stainless steel is only nominally better than the erosion resistance of carbon steel.

Flow-assisted corrosion

High-flow velocities and turbulence usually accelerate corrosion rates due to increases of shear stresses and mass transfer of reactants to the carbon steel surface, leading to flow-assisted corrosion. In addition, the efficiency of filming inhibitors may be reduced due to shear stresses above a critical value, depending on the inhibitor type and concentration.

32.2.2.3 Surface deposit-related corrosion

Under deposit and crevice corrosion

Under deposit corrosion is related to the deposition or settling of solids on the internal surface of a pipeline or vessel. Corrosion processes, either purely electrochemical or microbiologically related, can occur under or around these deposits, leading to localized pitting and increased corrosion rates. In preventing corrosion byproducts from being removed from the corrosion sites, they contribute to the autocatalytic process of pitting development. Deposits also act as a barrier, preventing corrosion inhibitors from adsorbing onto the metal surface.

Crevices may be formed by the mechanical joining of two components, beneath fasteners, under gaskets, and under naturally formed scales. Crevices can lead to ion concentration cells or oxygen depletion within the crevice, promoting localized corrosion. The design must consider where crevices may be created and plan for corrosion control or change the joint design.

A minimum velocity is critical to prevent solids deposition, deter (to some extent) microbiological growth, and provide effective chemical transport for inhibitors, dispersants, and biocide.

Microbiologically influenced corrosion

Microbiologically influenced corrosion (MIC) is caused by the metabolic processes of certain types of bacteria, mainly sulfate-reducing bacteria and archaea (i.e., sulfate reducing prokaryotes). SRPs are predominantly anaerobic and are present in crude oil, PW, and seawater injection systems. Microorganisms can colonize metal surfaces within organic deposits and under other solids in aqueous environments (e.g., under deposits in pipelines, storage tanks and vessels, and in deaerators). Once biofilms are established, they are difficult to remove by chemical treatment alone.

SRP and many other microorganisms are typically present in production systems. Given the right conditions of temperature, reduction−oxidation ("redox") potential, and nutrient sources, SRPs produce hydrogen sulfide by the reduction of the sulfate present in many oil field brines. Other groups of microorganisms, e.g., methanogens, acetogens, iron reducers, and oxidizers, are also common to many oil production environments, which can contribute to corrosion directly or indirectly. Typically, internal corrosion is not the result of merely one type of microorganism, rather the activities and interaction within a community of microbes having a more significant effect on corrosion.

MIC can be found in water and hydrocarbon systems where solids and/or biofilms are allowed to accumulate. High-flow velocities tend to decrease the potential for solids and biofilms to accumulate, whereas low-flow velocities favor both solids deposition and increased biofilm thickness. MIC is more likely in the areas of low flow that remain untreated, under deposits, and in dead legs. In sour production systems, the combination of H_2S, bacteria, and CO_2 can lead to rapid and deep pitting. The presence of even low concentrations of dissolved oxygen in combination with a microbiologically generated iron sulfide film can result in oxidation of sulfide to elemental sulfur, resulting in the pitting attack of seawater injection piping.

32.2.2.4 Environmentally assisted cracking

Environmental cracking is defined as the brittle fracture of a normally ductile material in which the corrosive effect of the environment is a causative factor. Environmental cracking can occur with a wide variety of metals and alloys and includes the following:

- Hydrogen embrittlement
- Hydrogen-induced cracking, including stress-oriented hydrogen induced cracking
- Stress corrosion cracking
- SSC

A combination of tensile stresses (applied or residual) and a specific corrosive environment are commonly the cause of sudden cracking-type failures of metal structures. Proper design is the most important consideration to avoid environmentally assisted cracking (EAC) in conjunction with adequate material selection for the environment. Gradually increasing levels of H_2S may occur as a producing field ages. If material selection did not account for souring in the design stage, EAC is likely to become a significant problem in the future.

32.2.2.5 Other causes of internal corrosion

Acid/chemically induced corrosion

During well stimulation and acidizing operations, concentrated hydrochloric acid (HCl) or mixtures of HCl and hydrofluoric acid can be used. The main corrosion threat here is related to high concentration of hydrogen ions present at the low inherent acid pH. Acid formulations may use corrosion inhibitors developed for carbon steel or for CRAs such as 13% chromium steels. If acids are not inhibited properly, corrosion damage can result even if the acid or stimulation job is short in duration. "Spent" acid returning from a well treatment can still be extremely corrosive to carbon steel equipment downstream (separators, filters, etc.) of treatment and can also cause processing problems (e.g., emulsion formation).

Degraded glycol may contain organic acids that can be corrosive to carbon steel pipeline and piping systems. The potential for carryover of glycol should be examined when considering internal corrosion threats. In many subsea pipelines, glycol is continuously added for hydrate prevention and its influence on corrosion has been studied.

The lack of adequate transport (dispersion) of low pH corrosion inhibitor or biocide can result in accumulations that may result in locally elevated corrosion rates of carbon steel and pipeline and piping systems.

Galvanic corrosion

This mechanism is generally a result of a metal being in direct contact with a more noble metal (e.g., carbon steel with duplex stainless steel) or other conductor in the presence of an electrolyte. The rate of corrosion is a function of the difference in electrochemical potential between the dissimilar metals, temperature, resistivity of the electrolyte, and the relative surface areas of each component in contact with the electrolyte. It affects carbon steel in contact with higher-alloy steels (e.g., chrome steels) and attack is the greatest at the interface between the dissimilar materials. Generally, this threat is mitigated by the use of insulation kits at flanged connections.

Practically speaking, susceptibility to galvanic corrosion may be suspected when dissimilar conductors (e.g., metals such as carbon steel in contact with stainless steel, Inconel alloys, brass, bronze, copper) are in contact in the presence of an electrolyte (conductive fluid).

32.2.3 External corrosion threats

External corrosion mechanisms are largely dictated by the environment in which the asset or pipeline is installed. Generally, these environments can be broadly grouped

into buried, sea-floor, free exposure to seawater, near surface underwater, splash zone, atmospheric (onshore and offshore), and corrosion under insulation. Each of these broad groupings can be further divided in subgroups, for example, for atmospheric onshore, onshore marine, onshore rural, onshore industrial, and even these vary with climatic regions. Susceptibility to external corrosion is also temperature dependent. Coating life can be degraded by environmental conditions, operating conditions, and mechanical damage. Depending on operating conditions, external corrosion protection is primarily based on protective coatings and cathodic protection (CP) where applicable, in addition to maintenance of these corrosion control methods. In some cases, coating inspection and CP systems can be tested and inspected; however, for buried pipelines external corrosion at coating flaws or damage is typically only found during in-line inspection (ILI) or sometimes through close interval CP surveys.

32.2.4 Effects of operational history

32.2.4.1 Operational data

Historical operating history data are important for determining whether the asset was operated outside the design basis or integrity operating window (IOW) and for determining the types and potential severity of corrosion threats that were, or are, still present. Operating data include physical parameters and fluid composition parameters. For most data types, the following data characteristics should also be considered over the life of the asset, if data are available; average, minimum, maximum, trends over time, upset conditions, exceedance of IOWs, reliability and accuracy of data, locations where measurements are made, etc. Examples of operational data to collect to perform the LE process are listed in Table 32.1.

32.2.4.2 Inspection data

Inspection data for both external and internal corrosion assessment are collected and analyzed in the LE process to determine the extent to which corrosion threat mechanisms have affected the assets, the distribution of corrosion damage relative to potential causes of corrosion, and the current integrity as associated with these threats. Inspection data also provide insight on the performance of corrosion mitigation measures over the life of the asset, and potentially, the extent to which changes in operating conditions resulted in increased corrosion damage. For example, if ILI data from 10 years earlier show little internal corrosion and now the ILI reinspection data show significant corrosion damage, records of operating conditions, and mitigation measures can be examined from before and after the change in corrosion damage to identify potential causes. Such an analysis can provide useful information for the LE process, particularly if the underlying cause of the increased corrosion could be mitigated, e.g., increased flow rates over the extended operating life could be managed to prevent water accumulation.

Table 32.1 Examples of operating and fluid composition data used in life extension projects

Data type	Examples of data to collect
Operational data	• Volumetric flow rates • Frequency and duration of shut-ins • Frequency and duration of stratified flow (where applicable) • Operating temperatures • Operating pressures • Liquids and solids entrainment velocity vs. actual velocity • Changes to fluid sources over time • History of process upsets • Analysis of integrity operating window or operating envelope exceedance events • Cathodic protection surveys • Biocide and corrosion inhibitor injection records
Fluid composition data	• Fluid type (crude, produced water, seawater, three-phase production, gas, etc.) • Historical water cuts • CO_2 and H_2S historical levels; measurements of oxygen or dissolved oxygen • Compositional analyses of water (anions, cations, etc.) and hydrocarbon phases, as applicable • Solids analyses; volume and type of solids, compositional analysis, particle size distribution • Presence of waxes and asphaltenes • History of microbiological data; type of tests performed, sample handling and integrity, molecular microbiological results

Inspection data should be collected for all of the pipe and components included within the battery limits of the asset undergoing LE. The types of inspection data that are useful for conducting the LE process include those shown in Table 32.2.

32.2.4.3 Incidents/modifications

If repairs, pressure deratings, or other modifications to the asset have occurred as a result of corrosion, this information should be collected and considered in the technical integrity assessment. The contributing causes to the damage or failure incident can be reviewed to assess the types of corrosion mechanisms that were active during the history of the asset. The reasons for the failure of preventive or mitigative barriers that led to the corrosion damage should be evaluated, if root cause analysis (RCA) has not been performed previously. RCA can also provide insights on gaps in management systems or corporate culture (e.g., de facto standardization of deviation) that may lead to concerns about the historical management of other threats in addition to corrosion.

Table 32.2 Examples of inspection data used in life extension projects

Inspection type	Examples of data to collect
In-line inspection	• Inspection dates, tool specifications, tool technology • Corrosion features: outer diameter, inner diameter, clock position, axial location, size (length, width, depth), positional accuracy, depth/length sizing accuracy, minimum detection limits for general and localized wall loss, limitations at girth and seam welds, confidence level • Confirm locations of fittings, bends, appurtenances • Field calibration, verification digs/assessments • Growth prediction analysis reports; unity plots
Routine nondestructive testing	• Ultrasonic inspection reports for corrosion monitoring locations on topside piping and vessels • Investigation and sizing of metal loss due to corrosion • Assessments for stress corrosion cracking and other cracking mechanisms
Direct assessment	• Dig site assessments for internal corrosion direct assessment (ICDA) and external corrosion direct assessment (ECDA) of onshore pipelines including full pipe condition characterization data
Visual	• Atmospheric corrosion inspections on topsides and aboveground/facility piping and equipment • Documentation of pipe internal/external condition during repairs or maintenance • Examination of hot tap coupons

32.2.5 Technical integrity assessment

Based on the operational history, inspection, incident reports, and other data described in the previous section, the next step after data collection is to determine the current integrity/condition of the asset. The data generated from an AIMS are quite valuable for supporting the integrity assessment, particularly for the threat of internal and external corrosion. If data from the AIMS are organized, reliable, and accessible in a central database, the technical integrity assessment will be much easier than if the data are all in paper files or multitudes of spreadsheets. In a full LE exercise, all of the parts of the asset will need some type of condition assessment relative to all of the applicable threats. In addition to corrosion, for example, subsea pipelines would need to have their integrity determined relative to the threat of subsidence or free spanning.

In keeping with the theme of this book, the focus here will be on integrity assessment relative to corrosion threats. The types of corrosion threats that are applicable to the internal and external surface of a pipeline were described in Section 32.2.3 of this chapter. Corrosion threats are time dependent, meaning that they typically result in increased degradation over time. The rate of degradation can be measured by comparing the change in damage between inspection intervals or it can be estimated

based on experience in similar service or through the use of growth models. Not all corrosion threats are as straightforward as general or pitting corrosion, and there are some mechanisms (e.g., MIC) for which reliable, industry accepted growth models do not exist; only susceptibility models. Other threats related to corrosive species such as sulfide, e.g., SCC or SSC, are difficult to detect and model. Therefore, if corrosion threats such as SCC and SSC have appeared in the assets and were not considered in material selection in the original design, the ability to confidently extend service life may be greatly impaired.

Fig. 32.2 shows an overview of the condition/integrity assessment phase of the LE process. The figure shows several approaches that can be used to evaluate current condition of the asset; however, not all of the approaches shown here are accepted under LE standards, such as NORSOK Y-002. The assessment approaches are discussed in the following text.

The premises and assumptions used in developing the initial asset design essentially establish the operating limits or IOW within which the design and planned mitigative measures will maintain the condition of the asset for the initial service life. Thus, the review of operating history data, and mitigation and inspection data, is necessary to ascertain whether the asset was operated within the design window. For external corrosion, this means that CP records, surveys, inspections, repairs, and maintenance records should all be reviewed. For internal corrosion, records to be reviewed include product composition and operating history (e.g., water cut, H_2S, CO_2, temperature, pressure, flow rates, etc.), mitigation measures, including corrosion inhibitor, biocide, and scale inhibitor, injection pump runtime, solids control, and maintenance pigging. Records from any type of inspection that can detect corrosion should be reviewed,

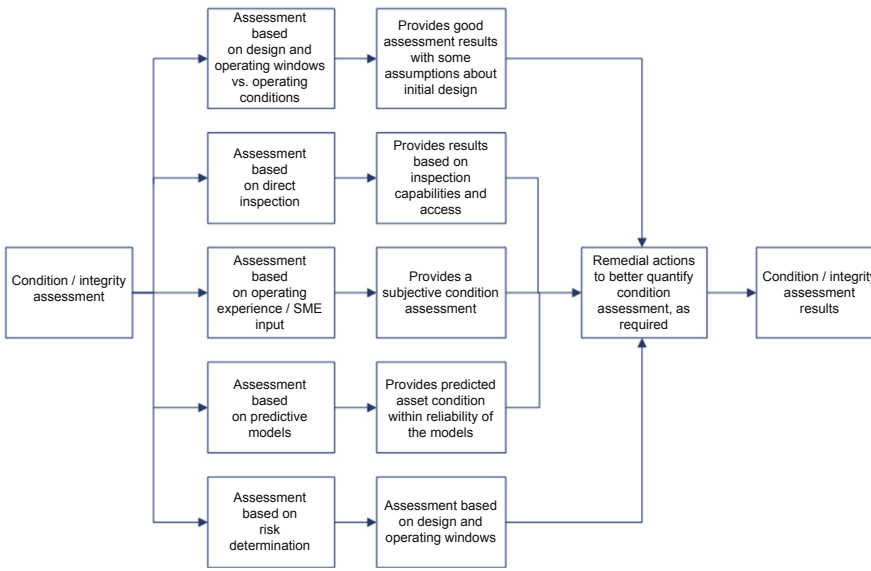

Figure 32.2 Condition/integrity assessment phase of life extension process.

including ILI, other NDE methods, visual inspection, pipe replacement, direct assessment, and service records for pipeline appurtenances. Bypasses, for example, are often dead legs and are susceptible to different corrosion threats than a flowing pipeline. If documentation demonstrates that the asset has been operated within the original design premises, this increases confidence that the asset has been maintained adequately for the initial service life, and potentially for LE.

Particularly for corrosion, it is essential that the assumptions in the initial design have not been exceeded, the models used were reliable and adequately conservative and that new threats have not emerged over time that were not considered in the original design. In the case of the latter, it may be difficult to validate extended life unless comprehensive inspection has been performed to assess damage that could have resulted from the emerged threat. Assumptions from the initial design, such as internal corrosion and erosion allowances, should be compared to present state conditions to help determine if LE is feasible.

If a pipeline is capable of ILI and high-resolution wall loss tools can be run, both internal and external condition can be assessed. The accuracy of the ILI data and confidence (or variance) in the data must be known in order to draw reasonable conclusions about the actual condition of the pipeline. Analytical and statistical calculations, such as probability of exceedance (PoE) and based on known or assumed corrosion growth rates, can be applied to evaluate the current asset condition and also later when performing the LE reassessment. Crack detection inline tools are also used; however, the ability to accurately measure and then perform engineering assessment to determine the effects of the cracks on integrity is far more complicated than modeling general wall loss due to some corrosion mechanism. Other types of inspection data besides ILI are also useful, as mentioned earlier.

Operating experience with other similar assets, possibly in the same producing field, may also be used to help ascertain the current asset condition. Usually subject matter expert (SME) input is collected and documented, and operating conditions of the two assets being compared are also carefully reviewed and documented. If the asset that is similar to the one being assessed has inspection data to support its current condition, then the comparison exercise can provide value. However, if the asset used in the comparison does not have reliable and thorough inspection data, then the comparison should not be performed. This SME approach to condition assessment may also have biases, particularly if the same personnel operate both of the assets being compared.

Predictive models and engineering assessments can sometimes be used to help support the condition assessment, particularly when at least some inspection data are available. Condition modeling can be also be simulated using a Monte Carlo approach or Bayesian [14] network approach to help improve confidence in the results of the model.

Finally, although it is not an approved approach in Y-002, a risk-based assessment can be used to examine the effects of missing data or incomplete inspection, for example, and to prioritize areas where more data should be collected to improve confidence in the condition assessment.

If the condition of the asset (relative to corrosion) cannot be sufficiently quantified, or if the operating windows have been exceeded or inadequate mitigation measures applied, these gaps should be documented and moved forward to the reassessment phase of the LE process. In the reassessment process, the opportunity to identify measures to close these gaps will be provided.

32.2.6 Reassessment process for extended service life

Once the condition assessment is completed and the initial design premises have been documented, the reassessment process essentially combines the two to determine if the intended LE is feasible. The reassessment process includes all of the activities related to analysis of the generated information (i.e., inspection and monitoring data, as well as LE premises), and establishing the integrity of the system through the full extended lifetime. The output of the reassessment process is the basis for LE that will then be used to document and implement LE for the asset, or the modifications that are needed for LE to be feasible.

Fig. 32.3 illustrates the reassessment process and the way in which it relates to the overall process that was shown in Fig. 32.1. Note that a financial evaluation is shown in Fig. 32.3 as input to the reassessment process; however, this is not a component of the Y-002 standard, but is typically performed by the asset owner in evaluating the feasibility of the LE process and the justification for modifications that may be needed later to qualify for an LE.

The reassessment process considers the current and predicted future operating conditions, the functional requirements of the asset, and the new design basis, along with

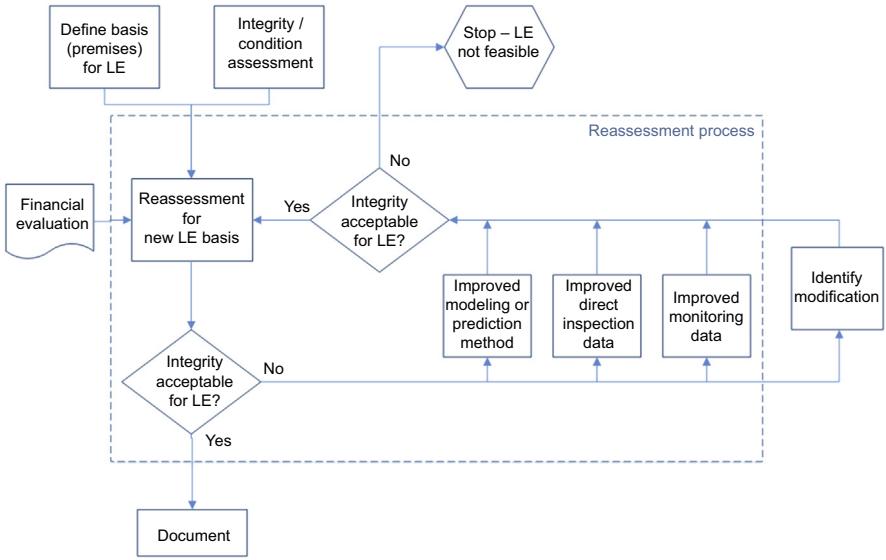

Figure 32.3 Reassessment process overview.
After NORSOK Standard Y-002.

current condition, to determine whether the life of the asset can be extended. The reassessment also needs to consider the confidence level of the available data, particularly inspection data, because no asset is likely to have 100% inspection coverage with 100% reliability. Conservative engineering assumptions must be applied to the LE to account for the lack of knowledge and confidence level of the condition assessment. Corrosion rate predictions and models will be applied in the reassessment phase to determine degradation rates and these rates are applied to assets that are already degraded to some extent, in many cases. The condition of the assets and the type of corrosion damage that is present can also affect the way in which new corrosion manifests itself. Preexisting internal pits, for example, may be difficult to clean with pigs and to reach with inhibitors or biocides, resulting in greater variability in predicted rates over the extended life of the asset. The reassessment usually benefits from the development of better degradation models than those used many years ago in the original design.

As shown in Fig. 32.3, if based on reassessment, the asset is not suitable for LE, additional steps can be taken to provide missing or incomplete information and improve confidence in the predicted results of degradation models. As mentioned, the use of improved models is one means to improve the reassessment; other means include access to improved inspection and monitoring data and technologies. For example, advances in online continuous monitoring technology that can be linked through system logic directly to the application of mitigation measures or preventing IOW excursions before they escalate can benefit the reassessment outcome.

In some cases, the only way to extend the asset life is through modifications to the asset; however, these fall outside the reassessment because the asset life cannot be extended based on the current condition of the asset. Modifications are discussed later in this section.

Finally, again in Fig. 32.3, it is shown that there are two potential outcomes of the reassessment; LE is feasible or it is not. If LE is feasible, the process moves to documentation and implementation planning. If LE is not feasible, modifications may be made or gaps filled to allow a subsequent reassessment. The financial analysis also provides information to the asset owner, not necessarily as to whether LE is possible or not, but whether it is financially viable, given corporate objectives and policies.

Overall, the reassessment process can take a design-based or condition-based approach, as discussed in the following sections. Deciding between a condition-based or design-based approach is largely a function of the available data regarding asset condition and operating conditions.

32.2.6.1 Condition based

A condition-based reassessment uses operational experience and inspection data to examine degradation mechanisms and rates and the effect they have had on asset integrity. In consideration of both historical and future planned operating conditions, the potential for extending the life of the asset can be evaluated. For corrosion threats, this means that the historical operating conditions are understood and documented well enough to characterize the corrosion mechanisms and rates, such that the

knowledge can be applied to conditions expected during the future life of the asset. Operating experience can also be applied to reduce uncertainties that were associated with initial design assumptions. For example, the fluid corrosivity may originally have been predicted to produce a general corrosion rate of 40 mils/year (mpy) for carbon steel with a mitigated rate of 5 mpy, where in practice, the mitigated corrosion rate experienced was >1 mpy.

32.2.6.2 Design based

When asset condition data are inadequate to complete an assessment, a design-based reassessment is performed using corrosion damage growth models and documented industry best practices from technical and scientific literature and recognized standards.

32.2.6.3 Acceptance standards

The LE must be performed on the basis of complying with all applicable design standards, which will vary based on where the asset is built and operated. In some jurisdictions, the government does not impose certain design standard requirements on operators; however, they expect the operator to comply with industry best practices, ISO standards, and internal company standards. Another consideration during the reassessment of extended service life is that standards are likely to have changed over a 30-year operation life, and new standards may have more or less conservatism than the original standards. If the original standards were overly conservative, the LE may be more feasible when current standards and engineering models/criteria are applied.

32.2.6.4 Modifications and mitigation

As shown in Fig. 32.3, if the reassessment determines that asset integrity will not be acceptable to extend the service life, then modifications or mitigation may be undertaken by the operator/owner to remedy the conditions that are prohibiting attainment of the desired future asset life. These modifications and mitigations occur "outside" of the asset life reassessment process, meaning that once the activities are completed and integrity is improved or threats reduced, the reassessment is conducted again to verify that there is a sound basis for the LE.

Modifications could include making repairs or replacement of certain parts of the asset to improve overall integrity. Mitigation could be accomplished through a pressure reduction in the system based on assessments of corroded carbon steel piping using standards such as Recommended Practice DNV-RP-F101 [15]. Another mitigation could be reducing the predicted internal corrosion growth rates by increasing corrosion inhibitor availability by installing backup chemical injection pumps. The reassessment process may also provide recommendations for addressing data gaps, such as lack of inspection data for certain parts of the asset.

32.2.6.5 Financial evaluation

Financial evaluation is often performed at some point during the LE evaluation process to determine the feasibility or practicality of implementing the LE. As discussed previously, the reassessment may identify modifications or mitigation measures that must be applied before the conditions for LE can be met, potentially resulting in significant costs that must be weighed against the benefits of LE for the asset.

In March 2016, NACE International released the a study called "IMPACT—the International Measures of Prevention, Application, and Economics of Corrosion Technologies" [16], which examined ways to determine the costs associated with managing corrosion as well as ways to improve corrosion management practices within various industries, including oil and gas. Some of the corrosion management financial evaluation tools discussed in the study included the following:

- Return on investment analysis
- Cost adding methodology
- Constraint optimization
- Maintenance optimization
- Life-cycle costing

Although there are numerous financial assessment tools and methods that can be applied, the main point here is that the decision to extend asset life has financial implications that will need to be considered by operators/owners who are considering asset LE.

32.2.7 Documentation and implementation

At the conclusion of the reassessment for extending asset life, the assessment is documented and recommendations are provided for implementing the LE (if feasible). The documents produced essentially become the "roadmap" to LE for the asset, if the owner/operator is willing to meet the stated requirements.

32.2.7.1 Documentation

The documentation, relative to corrosion and other threats, produced from a LE project will often include

- Documentation demonstrating the current integrity of the asset
- Recommendations for inspection, monitoring, and mitigation, going forward
- Recommended changes and modifications to the asset
- Analysis of the potential for LE
- The basis (premises) for LE

The recommended changes and modifications are likely to impact the AIMS, inspection and monitoring plans, engineering procedures and drawings, future data collection and databases, etc. The documentation should include the required time limits for taking actions and making changes.

32.2.7.2 Implementation

According to NORSOK standard Y-002, the LE project may conclude with requirements to be met by the operator of the asset during the implementation phase of LE. These requirements may be continuous or one-off measures, and they result from assumptions used in the new design basis for extending asset life.

Continuous measures could be changes to be incorporated into maintenance, inspection, and monitoring strategies; for example, or new mitigation that will be applied continuously in the future, such as high availability corrosion inhibition. Continuous measures may also be established to be applied on some regular basis (e.g., monthly, annually) over the future life of the asset. An annual internal corrosion threat assessment review is an example of a process that could be repeated throughout the period of extended asset life to ensure that new corrosion threats were not evolving as operating conditions changed.

One-off measures are activities that may be initiated immediately during the implementation or within some designated time frame. The one-off activities may be related to improvements in monitoring, inspection, or mitigation capabilities, such as establishing permanent corrosion rate monitoring locations on certain equipment to ensure that corrosion is not occurring or advancing during the extended life of the asset. One-off measures could also include replacement of certain equipment that affects pipeline integrity, e.g., pig launchers and receivers.

32.3 Needs for future work

Although there are standards (e.g., NORSOK and ISO) that elucidate the LE process, the fact is that formal LE processes are not widely employed relative to the global footprint of the oil and gas industry. Where license to operate is conditional based on formal LE, the process is applied to comply with regulations. In other cases where there are no regulations governing asset operating life, LE may be applied more or less as the operator determines necessary. In many instances, LE is based on current knowledge of asset integrity and the calculated remaining life driven by one or more degradation mechanisms. One possible problem with this approach is that all applicable degradation mechanisms may not be given adequate consideration in degradation or remaining life models. In addition, the complete condition of asset integrity can rarely be fully known, and engineering assumptions must be made regarding current condition. Many oil and gas operators also manage, or at least prioritize, integrity programs based on risk, which incorporates both consequence of failure and probability of failure (PoF), whereas the AIMS used in the operational phase of asset life primarily affects PoF. Thus the drivers for determining the acceptable level of integrity and/or risk for LE projects originate from design codes, regulatory requirements, and the reduction of risk (by reducing PoF) to some tolerable level. For this reason, the utility of formally applying the LE process varies significantly across the industry. Regardless, there are advantages to approaching LE more consistently and universally to continue to operate aging oil and gas assets safely and reliably.

A report [17] by the UK HSE Key Programme 4 (KP4), Ageing, and LE presented the results and recommendations of a study carried out between 2011 and 2013. The report examined the challenges faced by exploration and production assets on the UK's Continental Shelf; half of which were fixed platforms that were approaching or exceeding their original design life. The report examined the impact of aging and LE on the risk of major accidents and the influence of safety critical elements (SCEs) on 33 onshore and offshore assets. The HSE KP4 report found that installation age alone was not necessarily a reliable indicator of the asset condition or the likelihood of loss of primary containment. Although corrosion was one of the elements of the study, the HSE KP4 program examined a variety of topics, including the following:

- Safety management systems
- Structural integrity
- Process integrity
- Fire and explosion
- Mechanical integrity
- Electrical, control, and instrumentation
- Marine integrity
- Pipelines
- Corrosion
- Human factors

The HSE KP4 report found that in terms of documentation, SCE lists, and engineering drawings needed updating in some cases and that redundant equipment was not always identifiable onsite or on drawings. The study found that additional focus was needed on forecasting potential long-term future failure mechanisms, which is particularly relevant to internal corrosion with regards to souring that can occur later in field life. Along the same lines, the HSE KP4 report also noted that in some cases there were insufficient plans in place for managing the consequences of creeping changes. Such changes can occur over time, for example, as corrosion inhibitor chemistry changes without the awareness of the end user or due to the normalization of routine nonconformance with operating windows. Another interesting finding of the study was that the asset LE needed more attention at the component level, which can be relevant to CP equipment, corrosion inhibitor injection pumps, and so forth. Not completely surprising, the study found evidence of missing data, and insufficient data trending, which can be a significant problem when data are needed to substantiate the LE effort. Finally, the study found that there were insufficient leading key performance indicators around asset LE, which could be (or should be) used to help forecast potential future problems. A key conclusion of the HSE KP4 report was that the management of LE requires the advanced and continuing assessment of SCEs to ensure that they are fit for purpose and safe to use when required to operate longer than their anticipated service.

In terms of corrosion and LE, the most significant uncertainties in remaining life prediction originate from (1) lack of information about the effectiveness of the corrosion control measures used over the previous asset life and (2) the ability to predict

how changing production environment conditions in the LE period will affect corrosion mechanisms in the future. One lesson that operators can take away from these observations is that maintaining thorough documentation on corrosion mitigation, monitoring, and threat assessment for assets that are currently being operated will provide an improved basis for LE if the assets are required beyond their initial design life.

References

[1] ISO/TS 12747, Petroleum and Natural Gas Industries − Pipeline Transportation Systems, 2011.
[2] ISO 13623, Petroleum and Natural Gas Industries − Pipeline Transportation Systems, 2009.
[3] NORSOK Standard N-006, Assessment of Structural Integrity for Existing Offshore Load-Bearing Structures, April 2009.
[4] NORSOK Standard Y-002, Life Time Extension for Transportation Systems, December 2010.
[5] NORSOK Standard U-009, Life Extension for Subsea Systems, March 2011.
[6] Norwegian Oil and Gas Association, Recommended Guideline for the Assessment and Documentation of Service Life Extension of Facilities (No. 122), April 2012.
[7] ASME B31.4, Pipeline Transportation Systems for Liquid Hydrocarbons and Other Liquids, The American Society of Mechanical Engineers, New York, NY, 2006.
[8] DNV-OS-F101, Submarine Pipeline Systems, Det Norske Veritas AS, 2014.
[9] "The NPD's Fact-Pages − Ekofisk", Norwegian Petroleum Directorate, Retrieved from: http://factpages.npd.no/FactPages/default.aspx?nav1=field&nav2=PageView%7CAll&nav3=43778.
[10] M.D. Max, A.H. Johnson, W.P. Dillon, Economic Geology of Natural Gas Hydrate, vol. 9, Spring, 2006, p. 28.
[11] C. de Waard, U. Lotz, D.E. Milliams, Predictive model for CO_2 corrosion engineering in wet natural gas pipelines, Corrosion 47 (12) (December 1991) 976−985.
[12] B.F.M. Pots, S.D. Kapusta, Prediction of corrosion rates of the main corrosion mechanism in upstream applications, in: CORROSION 2005, NACE International, Houston, TX, March 2005 (Paper 05550).
[13] ANSI/NACE MR0175/ISO 15156, Petroleum and Natural Gas Industries—Materials for Use in H_2S-Containing Environments in Oil and Gas Production, NACE International, Houston, TX, 2015.
[14] F. Ayello, T. Alfano, D. Hill, N. Sridhar, A Bayesian network based pipeline risk management (Paper 2012-1123), in: CORROSION 2012, NACE International, March 2012.
[15] Recommended Practice DNV-RP-F101-2015, "Corroded Pipelines", Det Norske Veritas AS.
[16] G.H. Koch, N.G. Thompson, O. Moghissi, J.H. Payer, J. Varney, Impact International Measures of Prevention, Application, and Economics of Corrosion Technologies Study (Report No. OAPUS310GKOCH (AP110272)), NACE International, Houston, TX, 2016.
[17] UK HSE Key Programme 4 (KP4) Report: "Ageing and Life Extension Programme", UK Health and Safety Executive's (HSE) Energy Division, May 2014.

Nonmetallic materials—coupling of multiphysics for ageing rate prediction

33

Sebastien Didierjean and Högni Jónsson
Flowtite Technology AS, Sandefjord, Norway

33.1 Introduction

In the oil and gas industry, the environments for metallic piping can be extremely harsh and corrosion management of pipelines is a significant cost in the oil and gas industry. One solution adopted is the use of pipes made of composite materials or glass reinforced plastic (GRP) pipes. Such pipes have been installed extensively in challenging environments including desert regions in the Middle East and on offshore platforms with great success. Fig. 33.1 shows a typical application of GRP pipework in an industrial plant. Reinforced thermosetting resin (RTR) and glass reinforced epoxy (GRE) are also common denominations used in the industry for GRP pipes.

Industrial pipelines are designed for lifetime that often exceeds 20 years. GRP piping does not corrode but can age depending on the combination of loading and environmental conditions (type of chemicals in contact with the pipe wall and temperature). The corrosion of metallic pipes is included in the design of pipelines and corrosion engineers seek similar design tools for nonmetallic structures.

Figure 33.1 Application of glass reinforced plastic pipework in an industrial plant.

Trends in Oil and Gas Corrosion Research and Technologies. http://dx.doi.org/10.1016/B978-0-08-101105-8.00033-4

The aim of this chapter is to identify the most important aging modes of GRP pipes and simulate their aging rate to allow for a trustworthy prediction of GRP lifetime expectancy.

33.2 Definition of environmental conditioning

The corrosion of metals has been studied extensively compared to aging of composite materials. For GRP and polymers in general, corrosion technology used for metals must be replaced with "aging" and "chemical resistance".

33.2.1 Aging of GRP pipelines

The factors affecting the life of GRP can be divided in two categories: (1) operating conditions and (2) materials factors. By operating conditions, one can list different types of interactions the pipe has with its environment. For example,

- Temperature (internal and external to the pipe wall)
- Nature of fluids—gases in contact with the inside as well as the outside surfaces of the pipeline
- Radiations (ultraviolet light, etc.)
- Mechanical loading (fluid pressure, soil pressure, piping loads, impact during transportation, installation or in service, etc.)
- Time

Materials factors are related to the manufacturing of the GRP pipe and involve the following:

- Raw materials (type of resin, glass, rubber for gaskets, etc.)
- Built-in residual stresses
- Presence of flaws (porosities, local resin dryness, etc.)

Aging of a pipeline depends on all these factors whose effects are often coupled and therefore the lifetime prediction for such structures becomes quite complex.

In order to ease the aging analysis, it is of importance to focus on a few (if possible only one) failure mode of a pipeline. Indeed, experience shows that the pipeline operators is mostly interested in structural integrity (avoiding any pipeline burst) or liquid—gas containment (avoiding any weepage).

33.2.2 Evaluation of long-term properties in standards

Standards have been developed to account for GRP aging and establish safety factors to ensure sufficient lifetime for the product. DNV-OS-C501 [1] standard discusses the various effects on mechanical properties under the influence of temperature, moisture, and chemicals but does not give any methodology for assessment. ISO 14692 Part 2 Annex D [2] provides information on defining partial factors A_1 and A_2 to assess the effects of temperature and chemical resistance. These factors are used to account

for the change in mechanical properties of virgin materials that were measured at standard temperatures.

According to ISO 14692, if the effect of temperature alone has to be considered, A_1 can be calculated following Eq. (33.1):

$$A_1 = \frac{T - T_g}{T_{\text{qual}} - T_g} \tag{33.1}$$

where T is the required design temperature, T_g is the glass transition temperature, and T_{qual} is the temperature at which the material has been qualified.

The partial factor for chemical resistance A_2 is generated from regression analysis following ASTM D2992 [3], which consists of analyzing test results performed at elevated strains and temperatures for at least 10,000 h. The results are mostly available for water but are less well defined for other chemicals.

Testing of pipes requires significant time and effort and is very challenging especially for very harsh chemicals. The numerical multiphysics approach developed in this chapter defines a methodology that focuses mostly on the experimental characterization at raw material level, avoiding long-term testing of pipes containing dangerous substances.

33.3 Aging mechanisms and processes

In oil and gas applications, two main failure modes for GRP are considered: weepage and fiber breakage.

33.3.1 Weepage

Weepage can be defined as a minor loss of containment created by a coalescing microcrack network developing as the pipe ages. Fig. 33.2(a) and (b) shows evidence of damages in both inner and outer surface of a GRP sample.

A methodology for identification of weeping points was developed in collaboration with the laboratory Composite and Heterogeneous Material Analysis and Simulation Laboratory (COHMAS) from King Abdullah University of Science and Technology (KAUST). It is based on propagation of dye penetrant and X-ray computed tomography. Fig. 33.3 exhibits the weeping path for the same sample shown in Fig. 33.2 where the liquid (light gray stains) enters the sample in the liner area (red circles) and propagates through the pipe wall until reaching the outer surface.

See also Ref. [4], where Frost describes a model that simulates failure by weeping of GRP under various environmental loads.

33.3.2 Fiber breakage

To the contrary of weeping, fiber breakage can result in rupture of a pipeline. In most pipelines, pressure is the dominating mechanical load and continuous glass fiber is the

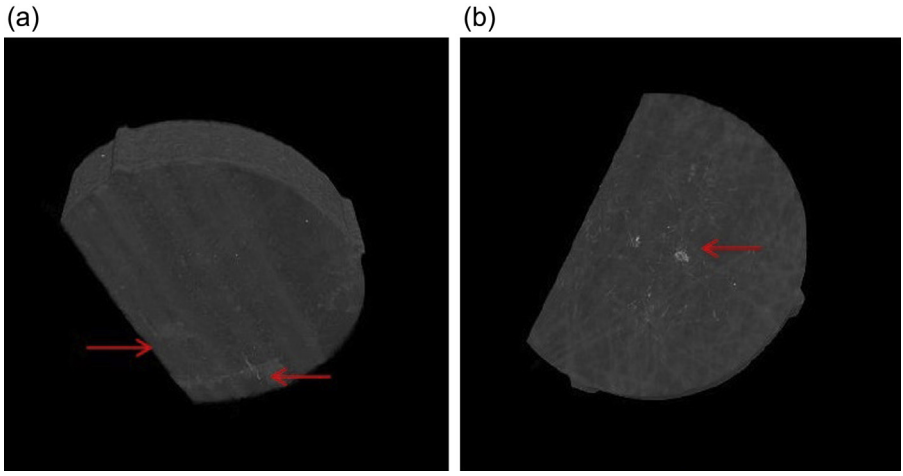

Figure 33.2 (a) Weepage on the outer surface of a glass reinforced plastic sample; (b) presence of a damage on the liner side of the same sample.

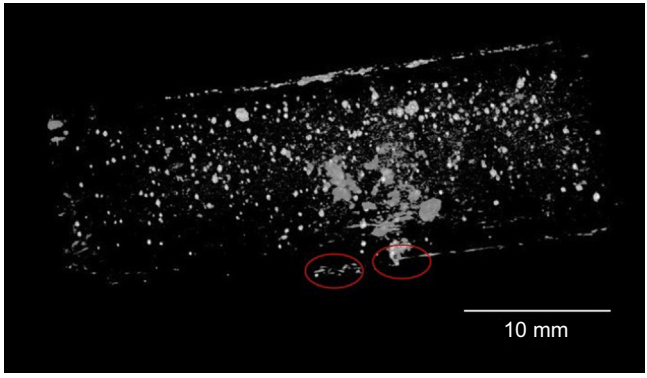

Figure 33.3 Cross-section of a weeping point by X-ray computed tomography.

material ensuring structural integrity by its natural mechanical strength and chemical resistance, when combined with the appropriate resin system.

This chapter will, from now on, focus only on fiber breakage as mode of failure. It is worth mentioning that so far weepage has not been clearly identified as a precursor to fiber breakage in particular for water application (see Section 33.5.1.2).

The aging of a GRP pipe has many stages and it is up to the user to determine which phase constitutes failure. In Fig. 33.4, Stage 1 corresponds to a fresh pipe right after manufacturing. In the case of water due to the presence of moisture in the air, the pipe enters Stage 2 almost immediately. The molecular propagation is often driven by two reversible mechanisms: diffusion and reaction following a Langmuir catch-and-release scheme. Stage 3 corresponds to the saturation level whose gradient through the pipe wall depends on the amount of the given chemical species at both extremities

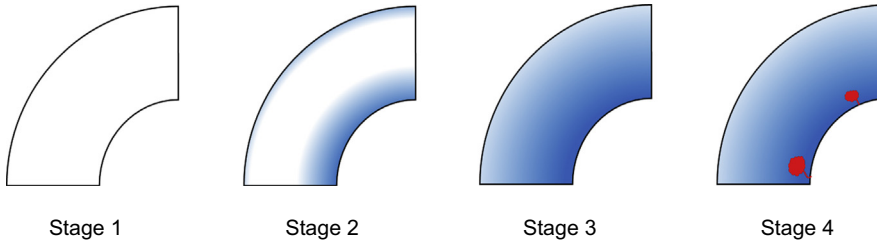

Figure 33.4 Evolution of molecular (in blue) propagation of a fluid through a pipe wall before penetration of liquid (in red).

(inner and outer surface). The time to saturation level depends mostly on the thickness of the pipe wall and on its temperature. It is generally fast when compared to the expected lifetime of the GRP pipeline (~1 year vs. 20 years of expected lifetime). Stage 4 represents the beginning of nonreversible damage caused by the penetration of the fluid in the pipe wall. This chapter concentrates mostly on stages 1−3 as Stage 4 shall in most cases be avoided for normal pipeline operation.

33.3.3 Matrix plasticization and swelling

The uptake of molecular species in the pipe wall can represent several percent of the pipe initial weight. Its presence has two major effects: it softens and swells the composite matrix. The effect of matrix plasticization on the GRP pipe is a reduction of its stiffness only to a limited extent. Frost [4] presented test results of hoop modulus after saturation in different fluid used in the oil and gas industry at elevated temperature. Apart from toluene at 110°C (230°F), the reduction in hoop modulus does not exceed 10% after 1 year of testing. Matrix swelling can be beneficial for the material as it can counteract the shrinkage generated by both the curing of the resin and thermal contraction during the cooling phase of the pipe manufacturing.

33.4 Characterization of models based on accelerated testing

In order to predict the remaining life of a GRP laminate the following parameters need to be characterized:

- The molecular concentration profile of the diffused chemical species through the wall thickness. This can be determined by knowing the rate of aging (physical and chemical) for a given set of conditions (fluid type, temperature profile, time, etc.).
- The key material properties at a given amount of aging. In the case of fiber breakage as failure mode of the laminate, the main parameter to evaluate is its stiffness as a function of the local concentration of chemical species and temperature. To a certain extent, the chemical swelling coefficients should also be measured.
- The residual life of the structure depending on the concentration of diffused chemical species in the pipe wall (and subsequent reduction in stiffness).

Expected lifetime of GRP in oil and gas industry often exceeds 20 years. Several pipelines used as cooling water or crude flowlines have their service life extended well over the initial 30 years.

The characterization of the evolution of mechanical properties over such long time periods requires the use of accelerated testing. Elevated temperatures and strains are used to speed up aging. The increase in temperature is limited by the glass transition temperature of the pipe resin, which is in some cases already close to the maximum operating temperature.

Accelerated testing is the corner stone of the whole prediction scheme as the selection of the acceleration factors must give conservative results (ensuring the overall integrity of the aged pipeline) while remaining representative of the aging conditions (for example, not entering stage 4 during accelerated testing when the pipe only sees stage 3 during its lifetime—see Fig. 33.4).

33.4.1 Accelerated chemical aging

Although there are many literature reports on the chemical resistance of GRP pipes, the studies are dominated by exposure to water rather than organic solvents and hydrocarbons. It should be noted, however, that long-term exposure to water is not necessarily a benign process. This is because substantial hydrolysis of the resin and the interface may occur.

In the case of a fully reversible diffusion process, the relationship between time and liquid mass uptake can classically be characterized using Fick's law [5]. Fick used the analogy between heat conduction and the diffusion of chemical species in isotropic solids. He defined its flux through a unit surface of normal $\overrightarrow{x}$ as shown in Eq. (33.2):

$$J_x = -D\,\frac{\delta c}{\delta x} \tag{33.2}$$

where c is the amount of chemical species (usually in mol/kg) and D is the coefficient of diffusion (in m^2/s).

For composite materials, the value of the diffusion coefficient, D, for the neat polymer needs to be modified to account for the tortuous path created by the presence of the fibers (their size, distribution, aspect ratio, orientation, etc.).

The isotropic model has been extended to anisotropic materials, with a different diffusion coefficient for each direction of anisotropy (see Ref. [5] and Eq. 33.3). ISO 62 [6] is used to assess coefficient of diffusion "through-the-thickness" of composite samples.

With time, the chemicals diffuse into the pipe wall through the surfaces and there is a concentration gradient through the thickness. The local level of concentration is assessed by solving the following partial differential Eq. (33.3):

$$\frac{\delta c}{\delta t} = D_x\frac{\delta^2 c}{\delta x^2} + D_y\frac{\delta^2 c}{\delta y^2} + D_z\frac{\delta^2 c}{\delta z^2} \tag{33.3}$$

Diffusion can be accelerated by increasing the temperature and follows the Arrhenius relationship shown in Eq. (33.4).

$$D_i = D_0 \cdot e^{-\frac{E_a}{RT}} \tag{33.4}$$

where E_a is the activation energy of the diffusion rate, R is the universal gas constant, and T is the absolute temperature of the exposure in degrees Kelvin.

Time thickness scaling allows the long-term prediction of absorption in thick laminates from thin sample measurement.

Fickian law may not always be demonstrated in composites that could experience different sorption processes. Among the reversible schemes, it is worth noting the diffusion reaction where part of the diffused molecules react with the polymer network belonging to either the composite matrix or the interface fiber/matrix.

This study only presents simulation performed with Fickian materials with water as the diffused molecule. The coefficients of diffusion have been characterized by Bodin [7].

The simulations performed in the present work have been implemented in the software Comsol Multiphysics. This software has also the option to replace the Fickian model by another capable of simulating more complex sorption processes (such as diffusion reaction, Langmuir, etc.).

Different sorption curves of hydrocarbons at elevated temperature that could be integrated in the model to perform a simulation with another fluid than water at room temperature [4] (p. 386).

33.4.2 Accelerated mechanical aging

Built-in stresses generated during the GRP manufacturing process as well as swelling strains caused by molecular diffusion of chemical species in the pipe wall should be accounted for as environmental loads and participate in the evolution of the material. Residual stresses are not yet included in the analyses performed in this study.

The swelling generated by the propagation of chemical species from the fluid counteracts the shrinkage (both chemical and thermal) that appeared during the curing of the pipe. It is then conservative to consider only swelling in the simulation. This study uses the swelling coefficients characterized in Ref. [7].

Mechanical aging is used in this section to reflect changes in the way the material distributes the external mechanical loading. The major effect is the plasticization that the matrix endures during the diffusion of the chemicals into the polymer network.

As for the parameters of water propagation, the simulations performed in this work use the data collected in Ref. [7] to account for the loss in stiffness. The reduction is applied linearly as a function of the local level of water as illustrated in Eq. (33.5):

$$E_i(c) = E_0 \cdot \left(1 - \frac{c}{M_s}\right) \tag{33.5}$$

where E_i (in GPa) is the reduced local stiffness for a given material in a given direction, E_0 (in GPa) is the modulus before aging, and M_s is the amount of chemical entities (in this case, water) at saturation (in mol/kg).

33.4.3 Accelerated long-time strength

The evolution of the material strength with time, when exposed to a constant load, is consistent with the mechanical loading experienced by a pipe in service. It is generated by the fluid pressure that remains stable during most of its operational life.

In order to assess the strength level of the material after several decades, increased stress is used as an accelerating factor. The model used to extrapolate the results obtained at high-stress levels is based on Zhurkov's theory of fracture mechanics [8]:

$$\log(t_r) = A - B \cdot \left(\frac{\sigma}{\sigma_0}\right) \tag{33.6}$$

where $\left(\frac{\sigma}{\sigma_0}\right) = F_a$ is the failure function related to the GRP failure mode (fiber breakage), t_r is the time to rupture (in s), and A and B are constants of the model.

The long-term strength of the material exposed to tap water at 23°C (73°F) was extracted from a study performed by Renaud and Greenwood [9]. The results give the time to failure of pultruded rods (made out of glass rovings and polyester, consistent with the raw materials from the simulated GRP) that were tested at different creep levels (see Fig. 33.5). The diagram shows regression analysis of both Advantex glass (which was being introduced at the time) and E-glass fibers.

This chapter focuses on traditional E-Glass that has been used in the production of GRP before Owens Corning introduced Advantex in daily production. The blue curve is then used to model the change in residual strength of the E-Glass rods with time. Zhurkov's model has been adapted to better fit the data from Ref. [9] using the following approach:

$$\log(t_r) = A - B \cdot \log\left(\frac{\sigma}{\sigma_0}\right) \tag{33.7}$$

The constants A and B from Eq. (33.7) have been identified on Fig. 33.5 (dashed line in blue) and give $A = 2.27$ s and $B = 9.04$ s for an E-glass/polyester rod immersed in tap water at 23°C (73°F).

The same approach is used in ASTM D2992 [3] and in the Comsol simulation. All results presented in this chapter have been scaled by the amount of hoop rovings in the structure. In the case of the pultruded rods, the glass content was in average 77.2 wt%.

It is worth noting that similar data for the following fluids/gas at 23°C (73°F) are also available in the Renaud-Greenwood [9] study:

- Air
- Salt water
- Deionized water
- Cement extract (pH 12.6)
- Hydrochloric acid (pH 0.1)
- Sulfuric acid (pH 0.3)

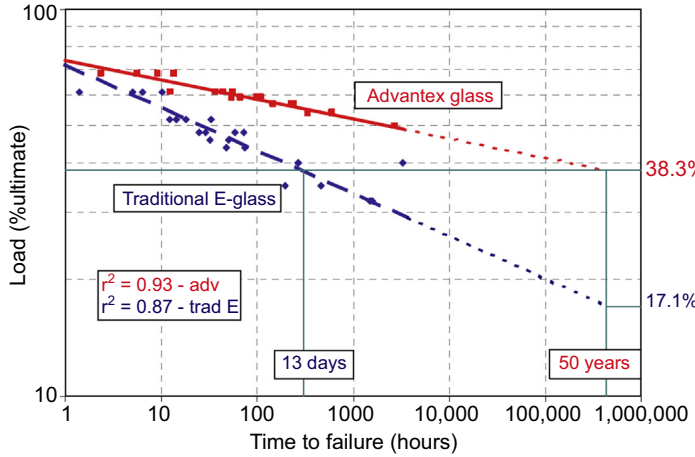

Figure 33.5 Stress-rupture of E-glass/polyester rods in tap water at 23°C (73°F). Courtesy of Owens Corning.

33.5 Validation of the prediction approach by comparison of the numerical simulations with in-service long-term data

Accelerated testing is used to evaluate the performance of glass reinforced polyester pipes. ASTM D2992 [3] and D3681 [10] are examples of accelerated tests that extrapolate short-term results (obtained after less than 10,000 h) to 50 years. They use mechanical strain level as main accelerating parameter. These methods require testing pipes at strain levels beyond their proportional limit making the linear extrapolation highly conservative.

This section is about the development of a numerical model able to predict via the coupling of multiphysics the burst pressure of aged GRP pipes based on long-term testing of raw materials. Its aim is to strengthen the link between the long-term properties of raw materials and the final product. Another objective is to reduce the accelerating factors used in long-term testing that often lead to unrealistic strain levels and damage during testing.

In order to begin the process of validation of the model, three pipes were tested to burst. One of them was taken out from a water cooling line after 15 years of service and the two others are fresh pipes that have been preconditioned at nominal pressure for 7200 h.

33.5.1 Pressure testing of GRP pipe after environmental conditioning

33.5.1.1 Burst testing of GRP pipe after 15 years of service

A GRP pipe was taken out of service after 15 years of operation as part of a cooling line in Germany. It was a continuous filament wound polyester pipe manufactured according to ISO 10639 with a 50 years design lifetime. It operated at a normal working

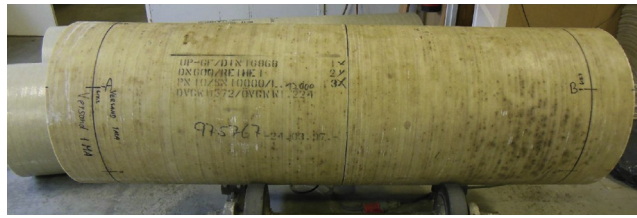

Figure 33.6 Pipe taken out after 15 years of service at 4.5 bar (65 psi).

pressure of 4.5 bar (65 psi) with a maximum temperature of 35°C (95°F). The pipe (see Fig. 33.6) had an average amount of 9.9 wt% glass hoop rovings.

In order to evaluate its remaining life, the pipe was pressure tested to burst following ISO 8521:2009, Method A [11]. The burst pressure was 69 bar (1000 psi).

Fig. 33.7 shows the pipe after burst testing. The failure mode was breakage of hoop rovings (see Fig. 33.8). It is in line with the main hypothesis of this simulation work: assuming fiber breakage as the mode of failure.

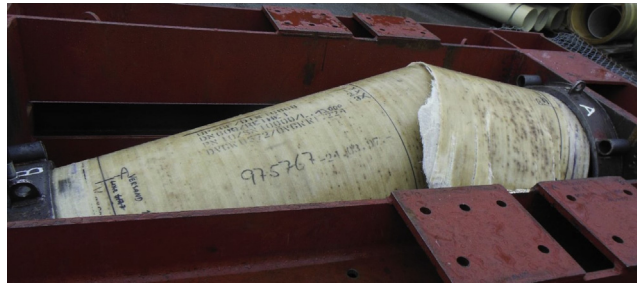

Figure 33.7 Pipe and jig after burst testing up to 69 bar (1000 psi).

Figure 33.8 Detail of the failure zone.

33.5.1.2 Burst testing of GRP pipes after 7200 h preconditioning at nominal pressure

Two pipes DN300 PN16 were preconditioned at the nominal pressure of 16 bar (232 psi) for 7200 h before pressure testing up to burst. They were continuous filament wound polyester pipes manufactured according to ISO 10639 with a 50 years design lifetime. Both pipes were selected in a way that they would present weepage at a very early stage during the preconditioning phase. The aim of this test is to evaluate the effect of weepage on fiber breakage. The hoop roving content in the pipe wall was 23.7 wt%.

After 7200 h of preconditioning, the pipes were pressure tested to burst at 81 bar (1175 psi) and 88 bar (1276 psi), respectively.

33.5.2 Numerical model

This study uses the numerical model developed by Reifsnider [12] to simulate the long-term aging of GRP pipes. The life prediction method follows the workflow shown in Fig. 33.9.

The failure function, F_a, mentioned in Fig. 33.9 corresponds to the stress of the composite layers composed of continuous glass fiber normalized by its stress allowable:

$$F_a = \frac{\sigma_\varphi}{\sigma_{\varphi,\,\max}} \tag{33.8}$$

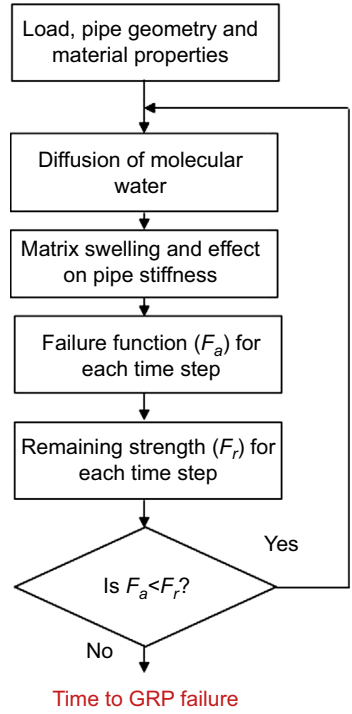

Figure 33.9 Diagram of the life prediction simulation tool.

where σ_φ is the hoop stress and $\sigma_{\varphi,\max}$ is the maximum allowable in hoop stress (730 MPa or 106 ksi for the analyzed continuous glass layer of flowtite pipes).

The remaining strength of the skins (F_r) depends on the time to rupture (t_r) of the hoop rovings (E-glass) that was identified based on the results of Fig. 33.5.

F_r is then calculated by the following relation:

$$F_r = 1 - \int_0^{\frac{t}{t_r}} (1 - F_a) j \tau^{j-1} d\tau \tag{33.9}$$

where t is time, $\tau = t/t_r$ and j is the material property.

Long-term failure occurs when the failure function (related to the applied load) meets the remaining strength or: $F_a = F_r$.

As mentioned previously, the model has been implemented in Comsol, a Multiphysics Finite Element software, capable of handling the coupling between mechanical loading, diffusion and aging of the materials.

The numerical model is axisymmetric and represents only half a pipe length (taking advantage of the plane of symmetry in the middle of the pipe cylinder), with a coupling at the end. The model does not take into account yet the action of the soil on the pipe if the pipe is buried.

33.5.3 Results of numerical analysis

33.5.3.1 Simulation of remaining strength of GRP pipe after 15 years of service

In this simulation, the model is used to evaluate the remaining strength of a DN300 pipe taken out of service after 15 years (see Section 33.5.1.1).

Fig. 33.10 shows the distribution of hoop stresses in half the pipe length after 15 years at 4.5 bar (65 psi). The graph shows the boundary conditions at only one

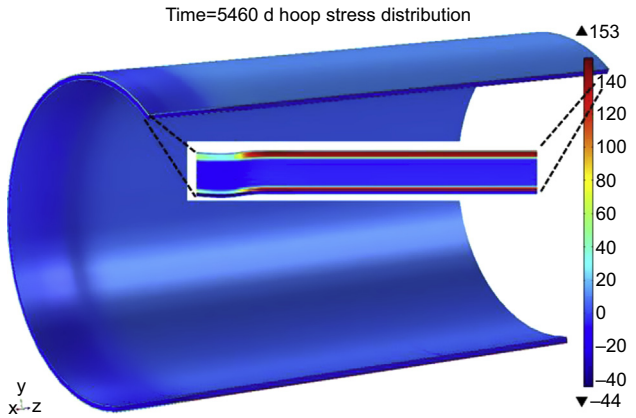

Figure 33.10 Hoop stresses (in MPa) after 15 years at 4.5 bar (65 psi) nominal pressure.

end of the 2 m pipe (on the left). The cylinder is shown with an open section to enhance the view of the displacements and stresses.

At the left end of Fig. 33.10, the simulation exhibits negative stresses in some layers due to the presence of the mechanical coupling. The highest computed stress is 153 MPa (22 kpsi) in the structural layers away from the coupling zone.

The normalized failure function, F_a, for the whole lifetime of the pipe, including the final burst test, is displayed in Fig. 33.11. The red circle in Fig. 33.11 shows the influence of water penetration and its effect on softening of the pipe with an increase of F_a. During the 15 years of service life, a stable pressure was assumed as being the only load. Also displayed in Fig. 33.11 is the remaining strength F_r based on the results from Fig. 33.5. F_a is constant for 15 years while remaining strength, F_r, decreases due to environmental effects.

Fig. 33.12 focuses on pressure testing, the last part of the simulation. In this phase, the pressure in the pipe is increased until the failure function F_a reaches the same value as the remaining strength F_r.

One can read, in Fig. 33.12, a burst pressure of 64 bar (928 psi). Even if the model does not simulate the effect of the soil for a buried pipe and does not take into account residual stresses generated during the manufacturing process, this result is in very good agreement with the burst pressure obtained by testing, 69 bar (1000 psi).

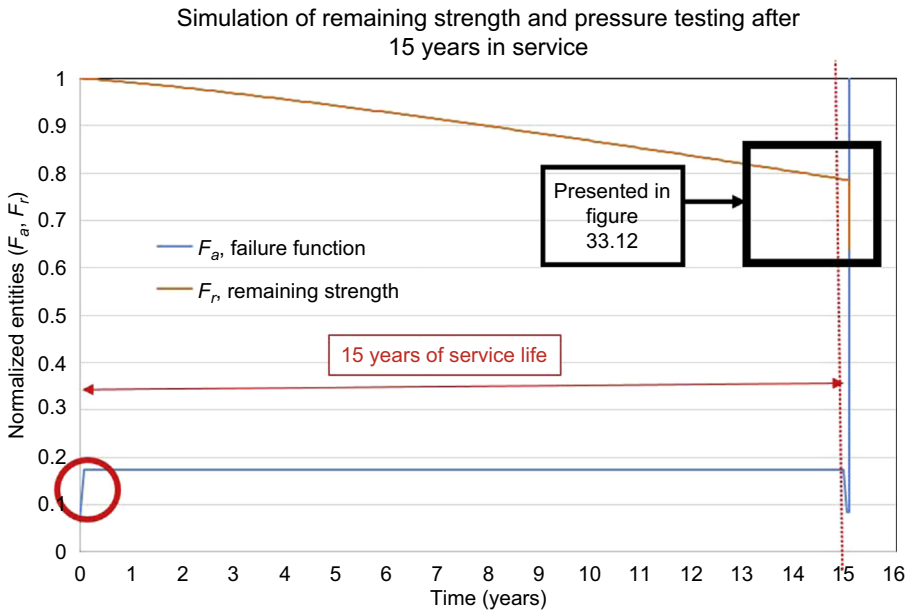

Figure 33.11 Remaining life prediction after 15 years of service. Failure function F_a and remaining strength F_r as a function of time.

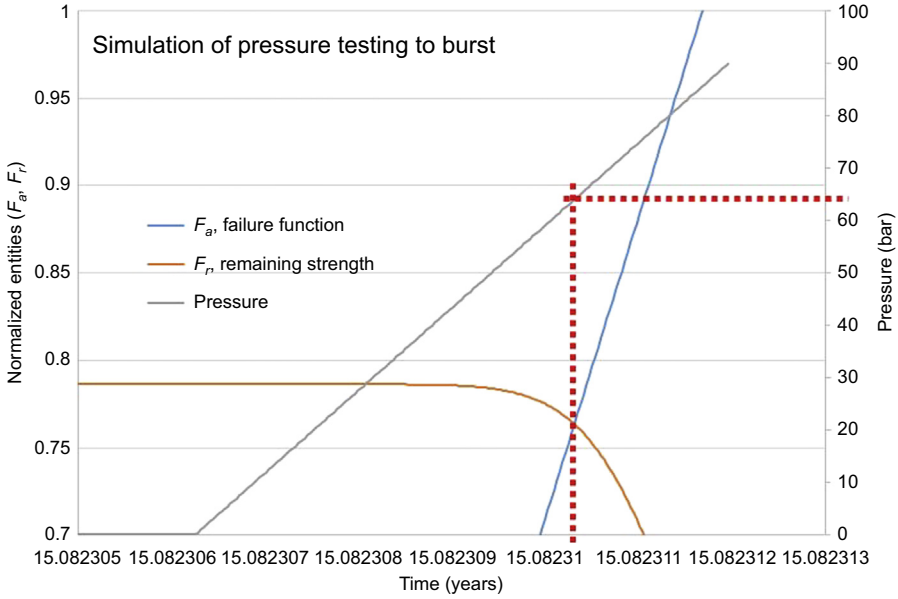

Figure 33.12 Condition assessment—pressure testing to burst.

33.5.3.2 Simulation of remaining strength of GRP pipes after 7200 h preconditioning at nominal pressure

In this simulation, the model was used to evaluate the aging of a DN300 GRP pipe after 7200 h preconditioning at nominal pressure of 16 bar (232 psi). The pipes were selected such as they would present early weepage behavior in order to evaluate its effect on fiber breakage.

Fig. 33.13 shows the simulation of remaining strength F_r along with the failure function F_a under preconditioning followed by pressure testing.

When focusing on the simulation part dealing with pressure testing to fiber breakage (see Fig. 33.14), the failure function F_a meets remaining strength F_r at a pressure close to 80 bar (1160 psi).

This result is in good agreement with the test results giving an average burst pressure of 84.5 bar (1226 psi) for two pipes after 7200 h preconditioning [(one at 81 bar (1175 psi), the other at 88 bar (1276 psi)].

This result consists in the first phase of a program dealing with the identification of the possible effect of weepage on fiber breakage. It indicates that in the case of the two pipes preconditioned at nominal pressure, early weepage was not an indicator of early burst failure.

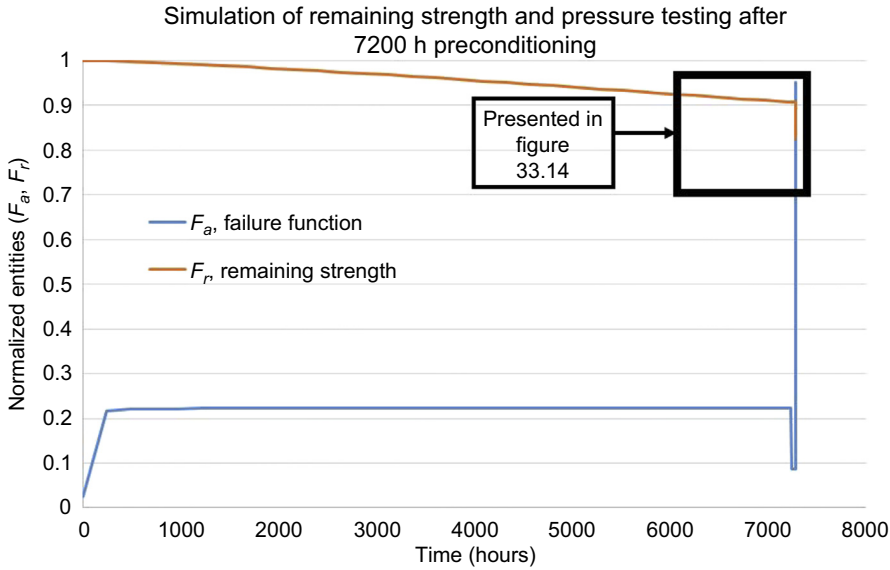

Figure 33.13 Remaining life prediction after 7200 h precondition at nominal pressure. Failure function F_a and remaining strength F_r as a function of time.

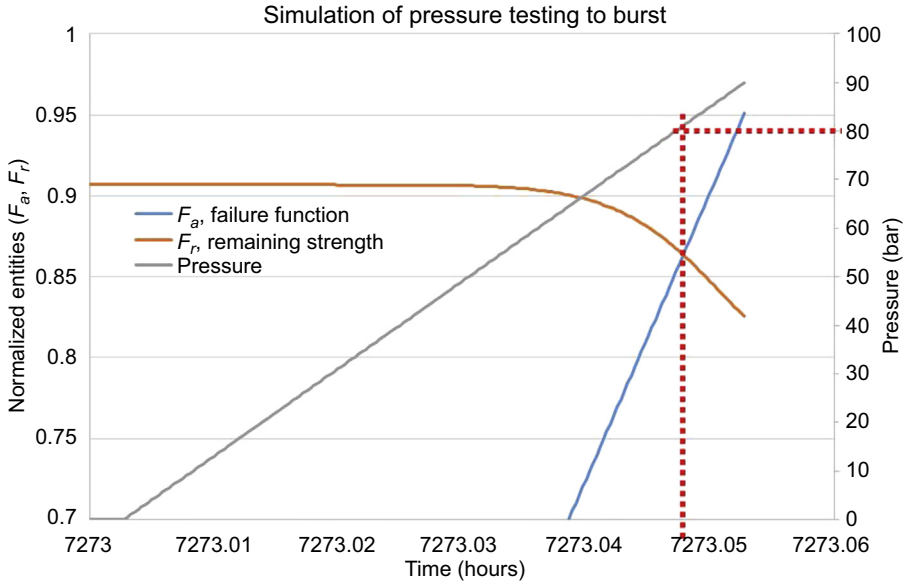

Figure 33.14 Simulation of pressure testing to burst—weeping pipes after 7200 h preconditioning at nominal pressure.

33.6 Conclusions

The environmental aging results obtained by simulation are in good agreement with accelerated tests results. It is very encouraging with respect to the capacity of the numerical model to predict life of GRP pipes based on the long-term performance of its constituents exposed to a given chemical environment.

The numerical model developed by Amiantit Technology can be seen as a tool to extrapolate the long-term properties obtained by the sole testing of raw materials to the final GRP pipe. It could be considered as the GRP counterpart of the models used for the design of metallic pipes when it comes to predicting the evolution of corrosion over time.

The study also highlights that 50 years lifetime with respect to burst failure is very conservative for the present design of tested pipes (Flowtite GRP).

The same approach has been applied on two epoxy cross-wound pipes (GRE or RTR) with the same success when comparing the performance of both pipes after 30 years in service with the multiphysics model.

This model is to be developed further to account for external environment, residual stresses as well as more testing to corroborate the simulation.

Acknowledgments

The authors are very grateful to AMIANTIT that supported the work reported in this chapter. We would like to thank the whole staff of the Flowtite Technology laboratory for their involvement in most of the mechanical testing and particularly Mrs. Grete Karlsen and Mr. Leif Richard Hotvedt.

We would also like to thank Prof. Gilles Lubineau and Mr. Hussain Al-Sinan, from the COHMAS laboratory of KAUST University, for the study performed on identification of weep points by X-Ray tomography. We thank Element that was involved in the Joint Industry Project: Pipeage, in particular, Dr. Rod Martin and Mr. Glyn Morgan.

We would also like to show our gratitude to Owens Corning and specially to Mr. Stéphane Mouret for the permission to reproduce part of their work on aging of glass fiber.

References

[1] Offshore Standards, DNV-OS-C501, Composite Components, November 2013, http://rules.dnvgl.com/docs/pdf/DNV/codes/docs/2013-11/OS-C501.pdf.

[2] ISO 14692 Part 2, Petroleum and Natural Gas Industries—Glass-Reinforced Plastics (GRP) Piping—Part 4: Fabrication, Installation and Operation, International Organization for Standardization, Geneva.

[3] ASTM D2992-12, Standard Practice for Obtaining Hydrostatic or Pressure Design Basis for “Fibreglass” (Glass-Fibre-Reinforced Thermosetting-Resin) Pipe and Fittings, ASTM International, West Conshohocken, PA, 2012.

[4] S. Frost, Ageing of composites in oil and gas applications, in: R. Martin (Ed.), Ageing of Composites, Woodhead Publishing Ltd., Cambridge, 2008.
[5] J. Crank, The Mathematics of Diffusion, second ed., Oxford University Press, Oxford, 1975.
[6] ISO 62:2008, Plastics − Determination of Water Absorption, International Organization for Standardization, Geneva.
[7] J.M. Bodin, Buried Pipe Life Prediction in Sewage Type Environments, MSc thesis, Virginia Polytechnic Institute, 1998.
[8] S.N. Zhurkov, Kinetic concept of the strength of solids, International Journal of Fracture Mechanics 1 (1965) 311−322.
[9] Renaud, Greenwood, Effect of Glass Fibres and Environments on Long-Term Durability of GFRP Composites, Owens Corning Composites http://www.efuc.org/downloads/CLR_MEG_Paper_on_Advantex_E-CR_Glass.pdfhttp://www.efuc.org/downloads/CLR_MEG_Paper_on_Advantex_E-CR_Glass.pdf.
[10] ASTM D3681-12e1, Standard Test Method for Chemical Resistance of "Fibreglass" (Glass−Fibre−Reinforced Thermosetting-Resin) Pipe in a Deflected Condition, ASTM International, West Conshohocken, PA, 2012.
[11] ISO 8521:2009, Plastics Piping Systems − Glass-Reinforced Thermosetting Plastics (GRP) Pipes − Test Methods for the Determination of the Apparent Initial Circumferential Tensile Strength, International Organization for Standardization, Geneva.
[12] S. Reifsnider, A critical element model of the residual strength and life of fatigue loaded coupons, ASTM STP 907, in: Composite Materials: Fatigue and Fracture, 1986, pp. 298−303.

Mathematical modeling of uniform CO_2 corrosion

34

Aria Kahyarian [1], *Mohsen Achour* [2] *and Srdjan Nesic* [1]
[1]Ohio University, Athens, OH, United States; [2]ConocoPhillips, Bartlesville, OK, United States

34.1 Introduction

Developing more accurate and reliable corrosion rate—predictive tools, specifically for oil and gas industry applications, has been the main objective of many research studies in last few decades. The significance of the predicted corrosion rate in defining the design life of an industrial infrastructure with all the associated health, safety, environmental, and financial concerns, has been a strong driving force for developing better understanding of the corrosion phenomena and advancements in the corrosion rate—predictive tools.

CO_2 corrosion rate—predictive models have undergone a long journey from the initial simplistic nomograms developed in the 1970s [1] to the comprehensive and elaborate mechanistic mathematical models that are now available in the open literature [2]. The progressive development of the ever more capable predictive models was a response to the industrial demands for more accurate corrosion rate predictions. The modern mechanistic models have also become a platform on which it is possible to implement the continuously advancing understandings of the underlying corrosion mechanisms of CO_2 corrosion and illustrate how all the "pieces of the puzzle" fit together to describe the overall process.

The text below is focused on the mathematical models of the CO_2 corrosion of steel (the so-called *sweet* corrosion) as the most common type of internal pipeline corrosion in the oil and gas industry. Even though CO_2 corrosion is almost always observed in transmission pipelines, it is often complicated by the presence of other corrosive species such as organic acids and hydrogen sulfide (aka *sour* corrosion). The detailed discussion of sour corrosion models is beyond the scope of the present article; however, the comprehensive modeling approach described in this chapter for the sweet corrosion can be extended to cover sour corrosion as well as organic acids with slight modifications.

The CO_2 corrosion can be defined as an undesired spontaneous conversion of the iron $Fe_{(s)}$ from steel to its chemically more stable aqueous form $\left(Fe^{2+}_{(aq)}\right)$, where the presence of CO_2 plays an accelerating role. The overall process may be expressed in term of a net redox reaction (34.1).

$$Fe_{(s)} + CO_{2(g)} + H_2O_{(l)} \rightarrow Fe^{2+}_{(aq)} + CO^{2-}_{3(aq)} + H_{2(g)} \tag{34.1}$$

The reaction above summarizes a number of chemical and electrochemical reactions that occur simultaneously, as briefly described below.

Trends in Oil and Gas Corrosion Research and Technologies. http://dx.doi.org/10.1016/B978-0-08-101105-8.00034-6

Table 34.1 Chemical equilibria of dissolved CO_2 in acidic aqueous solutions

$$CO_{2(g)} \rightleftharpoons CO_{2(aq)} \tag{34.2}$$

$$CO_{2(aq)} + H_2O_{(l)} \rightleftharpoons H_2CO_{3(aq)} \tag{34.3}$$

$$H_2CO_{3(aq)} \rightleftharpoons HCO^-_{3(aq)} + H^+_{(aq)} \tag{34.4}$$

$$HCO^-_{3(aq)} \rightleftharpoons CO^{2-}_{3(aq)} + H^+_{(aq)} \tag{34.5}$$

$$H_2O_{(l)} \rightleftharpoons OH^-_{(aq)} + H^+_{(aq)} \tag{34.6}$$

The relevant chemical reactions are the result of CO_2 dissolution in water. Although dissolved CO_2 is not a corrosive species, it leads to acidification of the aqueous solution. The dissolution of CO_2 in water is accompanied by series of homogenous chemical reactions as listed in Table 34.1, giving rise to chemical species such as H^+, H_2CO_3, HCO_3^-, which are known to be electrochemically reactive.

As a heterogeneous process, the corrosion of steel is a result of a number of spontaneous electrochemical reactions occurring simultaneously at the metal surface. Specifically, the cause of metal loss is the anodic oxidation of iron as described via "half-reaction" (34.7), which results in dissolution of solid iron into the aqueous phase and release of electrons. The produced electrons are consumed by simultaneous cathodic (reduction) reactions, keeping the process going. The cathodic "half reactions," commonly associated with CO_2 corrosion, are listed in Table 34.2. The main

Table 34.2 Electrochemical redox reactions associated with CO_2 corrosion of mild steel

Electrochemical reaction	
$Fe^{2+}_{(aq)} + 2e^- \leftarrow Fe_{(s)}$	(34.7)
$H^+_{(aq)} + e^- \rightarrow \frac{1}{2}H_{2(g)}$	(34.8)
$H_2O_{(l)} + e^- \rightarrow OH^-_{(aq)} + \frac{1}{2}H_{2(g)}$	(34.9)
$H_2CO_{3(aq)} + e^- \rightarrow HCO^-_{3(aq)} + \frac{1}{2}H_{2(g)}$	(34.10)
$HCO^-_{3(aq)} + e^- \rightarrow CO^{2-}_{3(aq)} + \frac{1}{2}H_{2(g)}$	(34.11)

electroactive (corrosive) species are H^+, H_2CO_3, HCO_3^-, and H_2O, while their relative importance debated and defined by researchers over the past few decades [3–12].

The mass transfer of species between the bulk solution and the metal surface, where the electroactive species are consumed/produced, defines the concentration of species at the metal–solution interface—the reaction site.

The corrosion rate–predictive models developed to date can be best classified depending on the mathematical description of the abovementioned fundamental thermodynamics and kinetic processes underlying the corrosion process. That includes the following:

- *empirical models* employ arbitrary mathematical expressions with no true theoretical underpinning, similar to the so-called Norsok model [13–15] or the model proposed earlier by Dugstad et al. [16]. Because of this major deficiency these models will not be further discussed in this review;
- *semiempirical models* are based on some rudimentary mechanistic considerations, such as the series of models developed by de Waard and collaborators [1,3,17–20];
- *elementary mechanistic models* that use a theoretical approach similar to what was originally introduced by Gray et al. [4,5,21,22]; and
- *comprehensive mechanistic models* similar to that introduced by Nešić et al. [2,23–25], where majority of the processes are described based on the fundamental physiochemical laws.

With the focus on more recent mechanistic models, the following sections cover a brief historical review of the key studies[1] that had a significant impact on mathematical modeling of the CO_2 corrosion. To make it easier to follow, the mathematical models are grouped into three main classes: *semiempirical*, *elementary mechanistic*, and *comprehensive mechanistic*, based on how deeply they are rooted in the theory of the corrosion process. The general idea behind each group of models, in addition to their advantages and drawbacks are discussed. Furthermore, the relevant mathematical relationships describing various physiochemical aspects of CO_2 corrosion—the building blocks used in developing mechanistic models—are compiled and the appropriate solution method for each group is briefly discussed.

34.2 Water chemistry calculations

Irrespective of the corrosion modeling approach, one of the primary steps for determining the corrosivity of an aqueous CO_2 solution is the so-called water chemistry calculation, used essentially to obtain the concentration of the chemical species involved in the corrosion process. Although aqueous CO_2 is not a corrosive species itself, its hydrated form (H_2CO_3) is a weak acid, often associated with high corrosivity of CO_2 solutions [2–4,22,26]. The term *weak acid* denotes that carbonic acid only partially dissociates in an aqueous solution (also true for the bicarbonate ion). The chemical

[1] This was not meant to be a comprehensive review in a sense that all the models that appeared in the open literature are described.

equilibria can be used to calculate the concentrations of species in an aqueous CO_2 saturated solution, as listed in Table 34.1.

Carbon dioxide dissolution equilibrium, as shown by Reaction (34.2), can be mathematically expressed through Eq. (34.12):

$$\frac{C_{CO_{2(aq)}}}{P_{CO_{2(g)}}} = K_H \tag{34.12}$$

For a binary H_2O-CO_2 system, carbon dioxide partial pressure is $P_{CO_2} = P_{tot} - P_{ws}$, where P_{ws} is the water saturation pressure calculated from Eq. (34.13) with a_i constants shown in Table 34.3 [27].

$$P_{ws} = 10\left[\frac{2C}{-B + (B^2 - 4AC)^{0.5}}\right]^4 \tag{34.13}$$

$$A = \theta^2 + a_1\theta + a_2; \quad B = a_3\theta^2 + a_4\theta + a_5; \quad C = a_6\theta^2 + a_7\theta + a_8;$$

$$\theta = T + \frac{a_9}{T - a_{10}}$$

Assuming a dilute, ideal solution, the equilibrium constant (K_H) can be expressed in terms of modified Henry's constant:

$$K_H = \frac{10^{-3}\rho_w}{(1 + K_{hyd})} e^{\left(-\ln\left(K_H^0\right) - PF + \ln\left(\varphi_{CO_2}\right)\right)} \tag{34.14}$$

where K_H is corrected for unit conversion from molality to molarity with water density ρ_w (see Table 34.4). The term $(1 + K_{hyd})$ is a correction factor that may be relevant, because in majority of CO_2 solubility studies [32,33], the measured concentration of CO_2^* is in fact the sum of concentrations of CO_2 and H_2CO_3. Then the equilibria are discussed in term of Reactions (34.15) and (34.16) with $[CO_2^*] = [CO_2] + [H_2CO_3]$, where carbonic acid is not explicitly considered.

$$CO_{2(g)} \rightleftharpoons CO^*_{2(aq)} \tag{34.15}$$

$$CO^*_{2(aq)} + H_2O_{(l)} \rightleftharpoons HCO^-_{3(aq)} + H^+_{(aq)} \tag{34.16}$$

Therefore, the equilibrium constant of Reaction (34.15) is $K_H{}^* = K_H \times (1 + K_{hyd})$.

The $K_H{}^0$ term in Eq. (34.14) is the Henry's constant of CO_2 dissolution at water saturation pressure shown via Eq. (34.17), where a_i are the constants as shown in Table 34.3 [28]:

$$\ln\left(K_H^0\right) = a_1 + a_2T + \frac{a_3}{T} + \frac{a_4}{T^2} \tag{34.17}$$

Table 34.3 a_i constants of Eqs. (34.13), (34.17), (34.19), (34.22), (34.24), (34.26)[a]

	K_H [28]	φ_{CO_2} [29]	K_{ca} [30]	K_{bi} [30]	K_w [31]	P_{ws} [27]
a_1	1.3000 $E1$	1.0000	233.51593	−151.1815	−4.098	0.1167 $E4$
a_2	−1.3341 $E-2$	4.7587 $E-3$	–	−0.0887	−3245.2	−0.7242 $E6$
a_3	−5.5898 $E2$	−3.3570 $E-6$	−11974.3835	−1362.2591	2.2362	−0.1707 $E2$
a_4	−4.2258 $E5$	–	–	–	−3.984 $E7$	0.1202 $E5$
a_5	–	−1.3179	−36.5063	27.7980	13.957	−0.3233 $E7$
a_6	–	−3.8389 $E-6$	−450.8005	−29.5145	−1262.3	0.1492 $E2$
a_7	–	–	21313.1885	1389.0154	8.5641 $E5$	−0.4823 $E4$
a_8	–	2.2815 $E-3$	67.1427	4.4196	–	0.4051 $E6$
a_9	–	–	0.0084	0.0032	–	−0.2386
a_{10}	–	–	−0.4015	−0.1644	–	0.6502 $E3$
a_{11}	–	–	−0.0012	−0.0005	–	–

[a]The a_i values are rounded to four digits after the decimal.

Table 34.4 Temperature dependence of the physiochemical properties

Parameter	Relationship	References
Water density (kg/m^3)	$\rho_w = 753.596 + 1.87748\ T - 0.003562\ T^2$	[2]
Water viscosity (cP)	$\mu = \mu_{ref} 10^{\left(\frac{1.1709\ (T_{ref}-T)-0.001827(T_{ref}-T)^2}{(T-273.15)+89.93}\right)}$ $T_{ref} = 293.15\ K,\ \mu_{ref} = 1.002\ cP$	[34]
Diffusion coefficient[a]	$D_i = D_{i,ref} \frac{T}{T_{ref}} \frac{\mu_{ref}}{\mu}$	
Molar volume of $CO_{2(aq)}$ (cm^3/mol)	$\widetilde{V_m} = 37.51 - 9.585 \times 10^{-2}\ (T - 273.15) + 8.74 \times 10^{-4}(T - 273.15)^2 - 5.044 \times 10^{-7}(T - 273.15)^3$	[35]
Saturation pressure of CO_2 (mm Hg)	$\log(P_{CO_2 S}) = 7.58828 - \frac{861.82}{(T - 273.15) + 271.883}$	[36]

[a]Reference values are listed in Table 34.7.

The *PF* term in Eq. (34.14) is the so-called Poynting correction factor (Eq. 34.18), which accounts for the change in solution volume as a result of CO_2 dissolution, where $\widetilde{V_m}$ is the partial molar volume of $CO_{2(aq)}$ (see Table 34.4), and P_{ws} is the water saturation pressure calculated via Eq. (34.13).

$$PF = \frac{\widetilde{V_m}(P - P_{ws})}{RT} \tag{34.18}$$

The fugacity coefficient of $CO_{2(g)}$, φ_{CO_2} may be calculated based on the empirical expression of Duan et al. [29], which was shown to agree well with the more complex iterative calculations of the fifth-order virial equation of state used in their earlier study [37].

$$\varphi_{CO_2} = a_1 + \left[a_2 + a_3 T + \frac{a_4}{T} + \frac{a_5}{T - 150}\right]P + \left[a_6 + a_7 T + \frac{a_8}{T}\right]P^2 \tag{34.19}$$

Eq. (34.19) is valid for pressures up to CO_2 saturation pressure (P_{CO_2S} in Table 34.4) when $T < 305$ and at $305 < T < 405$ up to $P = 75 + (T - 305) \times 1.25$, where T and P are in Kelvin and bar, respectively. The K_H values calculated based on Eq. (34.14) were found to be in a good agreement with those of Oddo and Tomson [38] and Weiss [39].

Carbon dioxide hydration equilibrium for Reaction (34.3) may be described by Eq. (34.20).

$$\frac{C_{H_2CO_{3(aq)}}}{C_{CO_{2(aq)}}} = K_{hyd} \tag{34.20}$$

The CO_2 hydration reaction and its equilibrium constant, K_{hyd}, have been discussed by a number of authors [33,40–43]. Although the reported values are not always in good agreement, the lack of temperature dependence of the equilibrium constant has been agreed upon [33,42]. In a more recent study Soli and Byrne [42] reviewed the existing literature briefly and reported $K_{hyd} = 1.18 \times 10^{-3}$ based on their own measurements.

Carbonic acid dissociation, Reaction (34.4), equilibrium is described mathematically through Eq. (34.21):

$$\frac{C_{HCO_{3(aq)}^-} C_{H_{(aq)}^+}}{C_{H_2CO_{3(aq)}}} = K_{ca} \tag{34.21}$$

The temperature–pressure dependence relationship describing K_{ca} have been developed by Li and Duan [28,30] in the form of Eq. (34.22), where the preexponential

terms are the corrections for the units and accounting for the hydration reaction, and a_1–a_{11} are constants as listed in Table 34.3.

$$K_{ca} = \left(1 + \frac{1}{K_{hyd}}\right) 10^{-3} \times \rho_w e^{\left(a1 + a2T + \frac{a3}{T} + \frac{a4}{T^2} + a5\,\ln(T) + \left(\frac{a6}{T} + \frac{a7}{T^2} + \frac{a8}{T}\ln T\right)(p - p_s) + \left(\frac{a9}{T} + \frac{a10}{T^2} + \frac{a11}{T}\ln T\right)(p - p_s)^2\right)} \tag{34.22}$$

The term P_s in Eq. (34.22) is equal to unity at $T < 373.15$ and $P_s = P_{ws}$ at higher temperatures.

Bicarbonate dissociation equilibrium, Reaction (34.5), is mathematically expressed through Eq. (34.23):

$$\frac{C_{CO^{2-}_{3(aq)}} C_{H^+_{(aq)}}}{C_{HCO^-_{3(aq)}}} = K_{bi} \tag{34.23}$$

Li and Duan [28,30] also developed a temperature–pressure dependence relationship for K_{bi}, where P_s and the preexponent terms have a similar meaning to that discussed for carbonic acid dissociation reaction, and a_1–a_{11} values are listed in Table 34.3.

$$K_{bi} = 10^{-3} \rho_w e^{\left(a1 + a2T + \frac{a3}{T} + \frac{a4}{T^2} + a5\,\ln(T) + \left(\frac{a6}{T} + \frac{a7}{T^2} + \frac{a8}{T}\ln T\right)(p - p_s) + \left(\frac{a9}{T} + \frac{a10}{T^2} + \frac{a11}{T}\ln T\right)(p - p_s)^2\right)} \tag{34.24}$$

Water dissociation reaction, shown via Reaction (34.6), is mathematically described by Eq. (34.25):

$$K_w = C_{OH^-_{(aq)}} C_{H^+_{(aq)}} \tag{34.25}$$

The values for K_w can be obtained from the formulation introduced by Marshall and Frank [31] following the form of Eq. (34.26) with a_1–a_7 coefficients listed in Table 34.3. The first term in Eq. (34.26) is also the correction for units conversion from molality to molar concentrations.

$$K_w = \left(10^{-3}\rho_w\right)^2 10^{-\left(a1 + \frac{a2}{T} + \frac{a3}{T^2} + \frac{a4}{T^3} + \left(a5 + \frac{a6}{T} + \frac{a7}{T^2}\right)\log(10^{-3}\rho_w)\right)} \tag{34.26}$$

The equilibrium concentrations of the different chemical species in the bulk solution can be obtained by solving the set of mathematical expressions presented above. In a

solution without an externally induced electric field, the concentration of ions must also satisfy the electroneutrality constraint as shown by Eq. (34.27).

$$\sum_i z_i C_i = 0 \tag{34.27}$$

Assuming an "open" system with an excess of CO_2 gas (i.e., constant $P_{CO_{2(g)}}$), the carbonic acid concentration is defined solely by the $P_{CO_{2(g)}}$, whereas the concentration of the other carbonate species is a function of the solution pH. These can be obtained by considering the electroneutrality equation along with CO_2 chemical equilibria, forming a set of six nonlinear, coupled algebraic equations. These can be solved using various methods (e.g., numerical Newton−Raphson method), to obtain the concentration of the six chemical species: $CO_{2(aq)}$, $H^+_{(aq)}$, $H_2CO_{3(aq)}$, $HCO^-_{3(aq)}$, $CO^{2-}_{3(aq)}$, and $OH^-_{(aq)}$.

The examples of such calculations are demonstrated in Fig. 34.1 through 34.3. Fig. 34.1 shows the comparison of molar fraction of the dissolved CO_2 at various CO_2 partial pressures obtained experimentally [44], with the water chemistry calculations as described earlier. The significant effect of nonideal behavior of CO_2 gas at high partial pressures on the water chemistry can be seen when comparing the calculations based on Henry's law (Eq. 34.17) and the one based on CO_2 fugacity (Eq. 34.19). These results suggest that at partial pressures above 10 bar (145 psi), a significant deviation from ideal conditions should be expected.

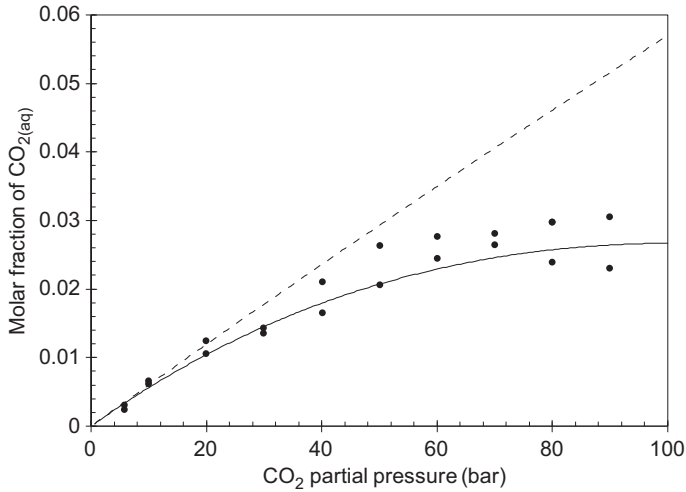

Figure 34.1 Comparison of the experimental molar fraction of dissolved CO_2 in water (*closed circles*) with calculated results based on Henry's law (*dashed line*) and nonideal gas calculations (*solid line*) at 298.15K, as a function of CO_2 partial pressure.
Experimental data taken from M.F. Mohamed, A.M. Nor, M.F. Suhor, M. Singer, Y.S. Choi, Water chemistry for corrosion prediction in high pressure CO_2 environments, in: CORROSION, 2011. Paper No. 375.

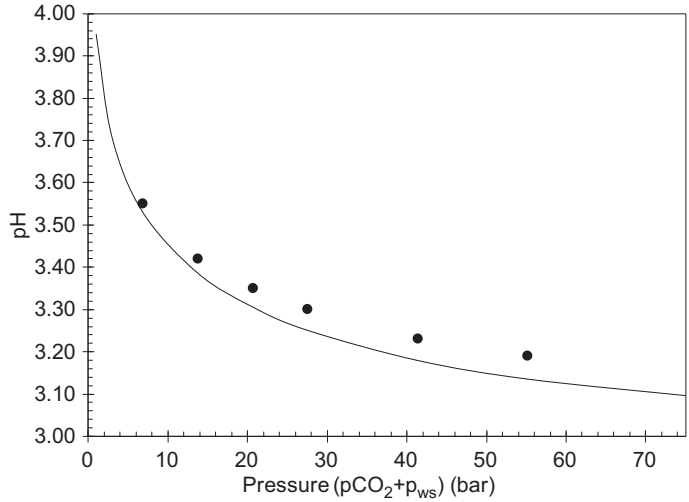

Figure 34.2 Calculated pH of water saturated with $CO_{2(g)}$ at 305.15K, as a function of total pressure (*solid line*) compared with experimental data (*closed circles*), taken from B. Meyssami, M.O. Balaban, A.A. Teixeira, Prediction of pH in model systems pressurized with carbon dioxide, Biotechnology Progress 8 (1992) 149−154, http://dx.doi.org/10.1021/bp00014a009.

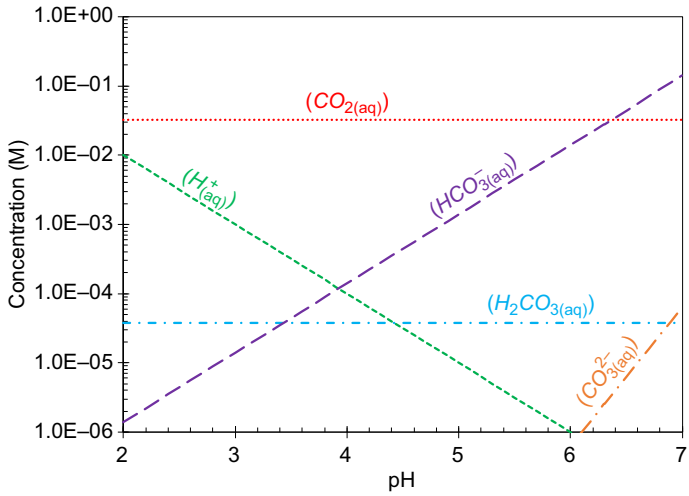

Figure 34.3 Concentration of different species in CO_2/water equilibrium at various acidic pH values and $T = 298.15$K in an open system with a 1 bar total pressure ($P_{CO_2} \simeq 0.968$ bar(14 psi)).

Fig. 34.2 shows the pH of the CO_2 saturated aqueous solutions, obtained at pressures up to 75 bar (1087 psi). These results were in good agreement with the experimental data of Meysammi et al. [45], whereas at higher pressures, some deviations were observed because of the departure from ideal solution assumption.

Similar calculations can be used to determine the chemical composition of an aqueous CO_2 saturated solution. Fig. 34.3 shows the concentration of the species involved in CO_2 equilibria under atmospheric pressure at various pH values.

However, the earlier discussion applies for a particular case where the chemical speciation is only a result of CO_2 equilibria (which is true in condensed water systems, for example). That is not always the case in industrial applications, where additional species and reactions may be present, such as those in formation water. Nevertheless, one can readily introduce the additional species, include additional equilibrium relationships as appropriate, and may perform a very similar calculation then to obtain the speciation for a more complex scenario. That may include the species such as neutral salts (e.g., sodium chloride and calcium chloride, barium sulfate), additional cations, organic acids, hydrogen sulfide, etc.

34.3 The CO_2 corrosion rate calculation

The existing mechanistic mathematical models used for calculating CO_2 corrosion rate can be classified in one of the following groups, when considering their modeling approach and the depth of mechanistic treatment of the involved physiochemical processes [9]:

- *Semiempirical models* are simple tools used to represent the experimentally obtained corrosion rate data. These models are obtained by fitting mathematical functions to a corrosion rate data set. In some cases, these functions may carry some rudimentary mechanistic meanings. These types of models are merely a mathematical reflection of a given experimental data set used to calibrate them and are restricted in validity to the experimental conditions associated with those of the data sets. That makes any extrapolated calculation dubious at best, whereas the expansion to include a wider range of influential variables may require extensive experimentation and a complete reconstruction of the model.
- *Elementary mechanistic models* are developed using the basic understanding of the electrochemical nature of the corrosion process as the basis of the calculations. The current/potential relationships are used to obtain the rate of the surface electrochemical reactions. Using a mechanistic approach, other significant processes such as mass transfer and homogenous chemical reactions may also be incorporated into the corrosion rate calculation. The mathematical relationships used to develop these models are theoretical expressions rooted in fundamental physiochemical theories. That makes these types of models more dependable for corrosion rate prediction across a broader range of environmental conditions (e.g., temperature, flow, pCO_2, pH, etc.), as well as for extrapolation. However, these types of models do resort to certain simplifications to make them easier to understand and resolve mathematically. For example, in these models each electroactive species is treated individually when it comes to mass transfer, and their possible interaction with other species through chemical reactions or electrostatic forces is disregarded.
- *Comprehensive mechanistic models* are based on a detailed description of the solution composition and reactions at the metal−solution interface, expressed through fundamental physiochemical laws. Most of the shortcomings of the elementary mechanistic models are here rectified; for example, they properly incorporate the effect of homogeneous chemical reactions into surface concentration and corrosion rate calculations, while maintaining the accurate mass and charge transfer balances. The comprehensive mathematical models enable

more accurate predictions, they are easier to extend by adding new physics, and their extrapolation capability is limited only by the validity range of the underlying fundamental physicochemical laws and not by the data used to calibrate them. However, to develop these models, a more in-depth mechanistic understanding of the various processes in CO_2 corrosion is required, these models are also more mathematically complex and more computationally demanding.

34.3.1 Semiempirical models

Generally, the semiempirical models are simple predictive tools justifiable when limited fundamental understanding is available. The basic mathematical functions used in these models may originate from rudimentary approximations of the fundamental physicochemical processes underlying the corrosion phenomena; however, the more elaborate aspects are accounted for by introducing correction factors in the model [46,47]. In most cases, these factors are best-fit functions based on limited experimental data with no theoretical significance. This lack of theoretical basis makes any combination of these empirical correction factors (required to cover more complex conditions)—dubious, to say the least. More importantly, these models cannot reliably be extrapolated outside the conditions used for their development. For the same reason these models have little flexibility needed for further extensions to account for new phenomena or new data and require recalibration of the model with the entire data set to accommodate any such extension. To date, many variations of empirical/semiempirical models that address a particular application are found [1,14,16–19,48,49].

In an attempt to focus this review on the more recent mechanistic developments in CO_2 corrosion modeling, the discussion of semiempirical models is limited to a brief review of the work by de Waard et al. because of its significance in shaping the understanding of CO_2 corrosion as we know it today. However, numerous reviews on empirical and semiempirical models are available in the literature for further reference [13,46,47,50–53].

The initial study by de Waard and Milliams in 1975 has been considered the first mechanistic attempt to describe and further, predict the CO_2 corrosion of steel [3]. Using a model developed based on simplistic charge transfer relationships, the authors proposed a catalytic mechanism for CO_2 corrosion as shown via Reactions (34.28) and (34.29). This mechanism considered carbonic acid as the dominant reduced species, whereas its concentration was buffered by the chemical equilibrium between the reaction product $\left(HCO_3^-\right)$ and hydrogen ions present in an acid solution:

$$H_2CO_{3(aq)} + e^- \rightarrow HCO_{3(aq)}^- + \frac{1}{2}H_{2(g)} \tag{34.28}$$

$$HCO_{3(aq)}^- + H_{(aq)}^+ \leftrightharpoons H_2CO_{3(aq)} \tag{34.29}$$

De Waard and Milliams proposed the following relationship for corrosion rate estimation by considering the charge balance at corrosion potential ($i_a = i_c$) and using pH dependence expressions to relate the potential to corrosion current [3]:

$$\log i_{corr} = -A\ \mathrm{pH} + B \tag{34.30}$$

The term A in Eq. (34.30) is only defined by the Tafel slopes of the cathodic and anodic reactions, whereas the term B also contains the reaction rate constants. The correlation coefficient in Eq. (34.30), A, was experimentally obtained to be 1.3. This value was used as the basis for their proposed mechanism, which gives the theoretical value of 1.25, considering 40 and 120 mV Tafel slopes for anodic and cathodic reactions, respectively. Ultimately, using a simplistic correlation between the solution pH and CO_2 partial pressure, de Waard and Milliams introduced their well-known nomogram for corrosion rate calculation as a function of CO_2 partial pressure, based on the following relationship [1]:

$$\log i_{corr} = -1/2\, A \log(pCO_2) + B' \tag{34.31}$$

The initial model developed by de Waard and Milliams did not include the effect of other electroactive species, such as hydrogen ion, bicarbonate ion, and water; the pH was assumed to only be defined by the CO_2 equilibria; and the effect of mass transfer, CO_2 hydration reaction, and other homogeneous chemical reactions associated with carbonate species was also disregarded [3]. That made the model simple but narrowed the range of its applications drastically.

In a series of studies, extending over almost two decades, the initial model of de Waard and Milliams [3] was used as the basis to add in the effect of various relevant parameters and environmental conditions [1,17–20]. The effect of pH, flow rate, nonideal solutions, protective scales, glycol, top of line corrosion, and steel microstructure are among those covered in the subsequent publications of de Waard et al. [1,17–20]. These new effects were accounted for by simply introducing additional empirical correction factors as multipliers in the original de Waard and Milliams correlation. That transformed the original mechanistic approach of de Waard and Milliams into a semiempirical model with all the disadvantages discussed earlier.

34.3.2 Elementary mechanistic models

In the context of aqueous CO_2 corrosion of steel, the deterioration is due to the electrochemical oxidation of iron as shown in Reaction (34.7), which results in dissolution of iron and release of electrons. This reaction would spontaneously progress only if the released electrons are consumed through simultaneous cathodic reactions (Reactions 34.8–34.11). The corrosion rate is therefore defined by the charge balance between cathodic and anodic reactions at the steel surface. Hence, it can be mathematically expressed by describing the current/potential response of the underlying electrochemical reactions. Based on this scenario, the corrosion rate is equal to the iron oxidation (dissolution) rate when

$$i_a = \sum_j i_{c,j}$$

As outlined in Section 34.3.1, the same expression served as the basis for the first model of de Waard and Milliams [3]; however, they only considered reduction of

carbonic acid as the main cathodic reaction and rate-controlling step. The elementary mechanistic models expanded on this to include the other relevant physiochemical processes such as additional cathodic reactions, mass transfer, and chemical reactions, in the calculation of the charge transfer rates. This gave these models a much improved ability to incorporate the more advanced understanding of CO_2 corrosion, without making them overly complicated.

34.3.2.1 Historical background

The first elementary mechanistic model for CO_2 corrosion of steel was introduced in 1989 by Gray et al. [4]. The authors developed their model with iron dissolution as the anodic reaction and hydrogen ion and carbonic acid reduction as the cathodic reactions. Their model accounted for the mass transfer at a rotating disk electrode for hydrogen ion and carbonic acid reduction. The effect of CO_2 hydration reaction was also incorporated in the charge transfer calculation of carbonic acid reduction. Gray et al. [4] adopted most of the mechanistic findings of Schmitt and Rothmann [26], while suggesting that the preceding adsorption step for CO_2 hydration reaction was unnecessary in predicting the observed polarization behavior.

Gray and coworkers expanded their experimental conditions toward higher pH values in a later publication, covering up to pH 10 [5]. The authors suggested that at a pH range of 6−10 the reduction of bicarbonate ion becomes significant, and the original model was expanded to also include the bicarbonate ion reduction. The mechanism for CO_2 corrosion of steel, as proposed by Gray et al. in these two studies [4,5], has rapidly gained general acceptance and was further developed in the following years.

In 1995 Dayalan et al. proposed a model based on equating the mass transfer and charge transfer of electroactive species at the metal surface and imposing the chemical equilibria of the carbonic acid and bicarbonate ion dissociation [54]. This set of algebraic equations was then solved to obtain the surface concentration of chemical species as well as the corrosion potential. This was an ambitious step forward, yet the model proposed by Dalayan et al. suffered from miscalculations in charge transfer rates, did not include the temperature effect, and did not account for the effect of CO_2 hydration reaction. Even with these shortcomings, this model was of significance because it provided the first insight into the surface concentration of species, which are necessary for protective iron carbonate layer formation calculations [55]. Furthermore, this study was one of the first to discuss and incorporate carbonic acid and bicarbonate ion dissociation reactions at the metal surface.

In 1996, an elementary mechanistic model was also developed by Nešić et al., mainly focused on improving the estimated electrochemical rate constants and implementation of this mechanistic approach into corrosion rate prediction for industrial applications [22]. This model was developed by considering the mass transfer, CO_2 hydration reaction, and the kinetics of the electrochemical reactions similar to that previously proposed by Gray et al. [4,5]. Hydrogen ion, carbonic acid, water, and oxygen reduction was included in the model as the possible cathodic reactions and iron dissolution as the only anodic reaction. In this model, Nešić et al. assumed that the carbonic acid reduction was only limited by the CO_2 hydration reaction, as the preceding chemical reaction step, and the

effect of mass transfer on the chemical reaction limiting current of carbonic acid reduction was ignored. Although such an assumption is reasonable for stagnant conditions, it may lead to significant errors at high solution velocities where the rate of mass transfer is comparable with the rate of the chemical reaction. This issue was addressed by Nešić et al. in a later publication where the effect of mass transfer was also included in chemical reaction limiting current calculations for turbulent flow regimes [21].

The elementary mechanistic models are now well established for calculation of internal pipeline corrosion rates. After the initial study by Gray et al. [4,5], numerous similar models have been developed and used to improve the mechanistic understanding of the corrosion process as well as the accuracy of the predicted corrosion rates [56–61]. The scope of these models was expanded to incorporate more complex scenarios such as the effect of corrosion product layer [55,62], multiphase flow [63], and the presence of other corrosive species such as oxygen, hydrogen sulfide, and organic acids [11,21,57,61,64,65].

34.3.2.2 Mathematical description

The net current density resulting from the electrochemical reactions occurring at the metal surface can be obtained by superposition of the current density from every individual reaction (i_j) as shown in Eq. (34.32).

$$i_{net} = \sum_j i_j \tag{34.32}$$

For the electrochemical reactions involved in aqueous CO_2 corrosion of steel, the current/potential relationships are given in Table 34.5. Considering the heterogeneity of the electrochemical reactions, the concentration terms appearing in these relationships represent the concentration at the metal surface, which may be different from the bulk concentrations as a result of the mass transfer limitation. Nevertheless, the effect of mass transfer on the surface concentration of electroactive species and thus the rate of electrochemical reactions can be incorporated in current density calculations through Eq. (34.33).

$$\frac{1}{i} = \frac{1}{i_{ct}} + \frac{1}{i_{lim}} \tag{34.33}$$

The term i_{ct} in Eq. (34.33) is the pure charge transfer controlled current, which is obtained from the relationships listed in Table 34.5, where the surface concentrations of electroactive species are equal to bulk concentrations at the pure charge transfer control condition. The electrochemical parameters required for charge transfer calculations are listed in Table 34.6. The i_{lim} term in Eq. (34.33) is the mass transfer limiting current as described in Eq. (34.34).

$$i_{lim} = nFk_m C^b \tag{34.34}$$

Table 34.5 Current potential relationships for the reactions listed in Table 34.2

Electrochemical reaction	Mathematical relationship for half reaction[a]
Reaction (34.7)	$i_{a,\mathrm{Fe}} = n_{\mathrm{Fe}} F k_{0_{\mathrm{Fe}}} C^{s}_{\mathrm{OH}^-} e^{\left(\frac{(2-\alpha_{\mathrm{Fe}})F\left(E_{app}-E_{0_{\mathrm{Fe}}}-\phi_s\right)}{RT}\right)}$[b]
Reaction (34.8)	$i_{c,\mathrm{H}^+} = -n_{\mathrm{H}^+} F k_{0_{\mathrm{H}^+}} C^{s}_{\mathrm{H}^+} e^{\left(\frac{-\alpha_{\mathrm{H}^+} n_{\mathrm{H}^+} F\left(E_{app}-E_{0_{\mathrm{H}^+}}-\phi_s\right)}{RT}\right)}$
Reaction (34.9)	$i_{c,\mathrm{H_2O}} = -n_{\mathrm{H_2O}} F k_{0_{\mathrm{H_2O}}} e^{\left(\frac{-\alpha_{\mathrm{H_2O}} n_{\mathrm{H_2O}} F\left(E_{app}-E_{0_{\mathrm{H_2O}}}-\phi_s\right)}{RT}\right)}$
Reaction (34.10)	$i_{c,\mathrm{H_2CO_3}} = -n_{\mathrm{H_2CO_3}} F k_{0_{\mathrm{H_2CO_3}}} C^{s}_{\mathrm{H_2CO_3}} e^{\left(\frac{-\alpha_{\mathrm{H_2CO_3}} n_{\mathrm{H_2CO_3}} F\left(E_{app}-E_{0_{\mathrm{H_2CO_3}}}-\phi_s\right)}{RT}\right)}$
Reaction (34.11)	$i_{c,\mathrm{HCO_3^-}} = -n_{\mathrm{HCO_3^-}} F k_{\mathrm{HCO_3^-}} C^{s}_{\mathrm{HCO_3^-}} e^{\left(\frac{-\alpha_{\mathrm{HCO_3^-}} n_{\mathrm{HCO_3^-}} F\left(E_{app}-E_{0_{\mathrm{HCO_3^-}}}-\phi_s\right)}{RT}\right)}$

[a] i_c and i_a denote the current density calculations for cathodic half reactions and anodic half reactions, respectively.
[b] ϕ_s is the potential in the solution at adjacent to the metal surface, which accounts for ohmic drop if applicable.

Table 34.6 Electrochemical parameters for the relationships in Table 34.5, where $k_{0_j} = k_{0_{j,ref}} e^{\left(-\frac{\Delta H_j}{R}\left(\frac{1}{T} - \frac{1}{T_{j,\,ref}}\right)\right)}$

	n_j	α_j	$E_{0,j}$ versus SHE (V)	$k_{0\ j,\ ref}$	ΔH_j (kJ/mol)	$T_{j,\ ref}$ (K)
$j = \mathrm{Fe}$	2	0.5^a	-0.447^b	$1.59 \times 10^5 \left(\frac{\mathrm{mol}}{\mathrm{s \cdot m^2 \cdot M}}\right)^a$	37.5^a	298.15^a
$j = \mathrm{H^+}$	1	0.5^a	0.000	$5.18 \times 10^{-5} \left(\frac{\mathrm{mol}}{\mathrm{s \cdot m^2 \cdot M}}\right)^a$	30^a	298.15^a
$j = \mathrm{H_2O}$	1	0.5^c	-0.8277^b	$2.70 \times 10^{-5} \left(\frac{\mathrm{mol}}{\mathrm{s \cdot m^2}}\right)^c$	30^c	293.15^c
$j = \mathrm{H_2CO_3}$	1	0.5^a	-0.381^f	$3.71 \times 10^{-2} \left(\frac{\mathrm{mol}}{\mathrm{s \cdot m^2 \cdot M}}\right)^a$	50^a	293.15^a
$j = \mathrm{HCO_3^-}$	1	0.5^d	-0.615^f	$7.37 \times 10^{-5} \left(\frac{\mathrm{mol}}{\mathrm{s \cdot m^2 \cdot M}}\right)^d$	50^e	298.15^e

Parameters obtained or recalculated from, *a*: Nordsveen et al. [2], *b*: CRC Handbook [73], *c*: Zheng et al. [11], *d*: Gray et al. [5], *e*: Han et al. [57], *f*: Linter and Burstein [74].

The mass transfer coefficients (k_m) for variety of common flow geometries are readily available in the literature. For example, the well-known Levich equation is used to calculate the mass transfer limiting current density at a rotating disk electrode as shown in Eq. (34.35) [8]:

$$i_{lim} = 0.62 \times 10^3 \, nFD^{2/3}\omega^{1/2}\nu^{-1/6}C_b \tag{34.35}$$

where C_b is the bulk molar concentration of the reactant, ω (rad/s) is angular velocity, D is the diffusion coefficient as listed in Table 34.7 for the common chemical species, and other parameters are in SI units.

For a rotating cylinder electrode, a correlation developed by Eisenberg et al. [66] (simplified as Eq. 34.36) or similar expressions [67] may be used. In Eq. (34.36) the bulk concentration of the active species, C_b, is in molar, d_{cyl} is the diameter of the cylinder electrode in meter, and other parameters have their common meaning in SI units.

$$i_{lim} = 0.0487 \times 10^3 \, nFD^{0.644}d_{cyl}^{0.4}\omega^{0.7}\nu^{-0.344}C_b \tag{34.36}$$

The mass transfer correlation in fully developed single-phase turbulent flow through straight pipes was developed by Berger and Hau [67a], where the Sherwood number (Sh) is correlated to the Reynolds number (Re) and the Schmidt number (Sc), as shown in Eq. (34.37), and the mass transfer coefficient can be obtained using $k_m = Sh \cdot D/L$.

$$Sh = 0.0165 \, Re^{0.86}Sc^{0.33} \tag{34.37}$$

$$8 \times 10^3 < Re < 2 \times 10^5, \quad 1000 < Sc < 6000$$

Table 34.7 Reference diffusion coefficients at 25°C (77°F)

Species	Diffusion coefficient in water $\times 10^9$ (m^2/s)	References
CO_2	1.92	[94]
H_2CO_3	2.00	[2]
HCO_3^-	1.185	[73]
CO_3^{2-}	0.923	[73]
H^+	9.312	[85]
OH^-	5.273	[73]
Na^+	1.334	[85]
Cl^-	2.032	[73,85]
Fe^{2+}	0.72	[85]

For many other flow regimes and geometries such as multiphase flow, U-bends, and elbows, similar correlations also exist in the literature [68–72].

In addition to the mass transfer from the bulk solution, the effect of slow CO_2 hydration reaction on the carbonic acid reduction needs to be included in calculations. In this case also, Eq. (34.33) can be used whereas the mass transfer limiting current (i_{lim}) has to be modified for simultaneous accommodation of the preceding chemical reaction through the diffusion layer. At a rotating disk electrode, the limiting current density for an electrochemical Reaction (34.39) proceeding a generic homogeneous Reaction (34.38) can be calculated via Eq. (34.40) [75]. These equations can be readily applied for the case of CO_2 corrosion with the chemical reaction being CO_2 hydration and the electrochemical reaction being carbonic acid reduction, as implemented in the models developed by Gray et al. [4,5].

$$\mathrm{Y} \rightleftharpoons \mathrm{O} \tag{34.38}$$

$$\mathrm{O} + ne^- \rightleftharpoons R \tag{34.39}$$

$$i_{lim,\mathrm{O}} = \frac{nFD\left(C_{\mathrm{O}}^b + C_{\mathrm{Y}}^b\right)}{\delta_d + \delta_r/K} \tag{34.40}$$

$$\delta_d = 1.61\, D^{1/3}\omega^{-1/2}\upsilon^{1/6} \tag{34.41}$$

$$\delta_r = \left(\frac{D}{(k_f + k_b)}\right)^{1/2} \tag{34.42}$$

The δ_d term in Eq. (34.40) is the diffusion layer thickness that can be calculated via Eq. (34.41), and δ_r is the so-called reaction layer thickness as described via Eq. (34.42).

Nešić et al. proposed a similar relationship for turbulent flow conditions such as the cases of rotating cylinder electrodes or pipeline flow, using a series of assumption suitable for the particular case of CO_2 corrosion [76]. Based on their proposed relationship, the limiting current for carbonic acid reduction can be calculated as shown in Eq. (34.43), considering both turbulent mixing and the slow hydration of CO_2.

$$i_{lim,\mathrm{H_2CO_3}} = n_{\mathrm{H_2CO_3}} F C_{\mathrm{H_2CO_3}}^b \left(D\, k_{b,hyd}\right)^{1/2} \coth\frac{\delta_d}{\delta_r} \tag{34.43}$$

$$\delta_d = D/k_m \tag{34.44}$$

$$\delta_r = \left(D/k_{b,hyd}\right)^{1/2} \tag{34.45}$$

Table 34.8 List of equations required to describe the current/potential response of each electroactive species

Reaction	Corresponding mathematical relationships
Iron oxidation	Eq. (34.7)
Hydrogen ion reduction	Eqs. (34.8), (34.33), (34.34)
Carbonic acid reduction	Eqs. (34.10), (34.33), (34.40) or Eq. (34.43)
Bicarbonate ion reduction	Eqs. (34.11), (34.33), (34.34)
Water reduction	Eq. (34.9)

Based on the discussions in this section so far, the current/potential response of the commonly accepted electrochemical reactions involved in CO_2 corrosion can be calculated. The relevant relationships to calculate the rate of each reaction are summarized in Table 34.8. For iron oxidation or water reduction reactions, no mass transfer consideration is required because of the constant concentration of the reactant, thus, the current density resulting from these reactions can be calculated via Eqs. (34.7) and (34.9) (in Table 34.5), respectively. For hydrogen ion, carbonic acid, and bicarbonate ion reduction, Eq. (34.33) should be used to account for the mass transfer and chemical reactions as required.

Using the mathematical relationships as summarized in Table 34.7, at a known electrode potential the current density from every individual reaction may be readily obtained. On the other hand, if the electrode potential is unknown, such as in the case of corrosion rate calculations, the current density/potential relationships of all the reactions can be introduced into Eq. (34.32), forming a single nonlinear algebraic equation to be solved for one unknown, the electrode potential. The corrosion potential (mixed potential) can be obtained using numerical root finding methods such as bisection or Newton−Raphson. Finally, the anodic current density calculated via Eq. (34.7) at corrosion potential yields the corrosion current. This value can be further translated to corrosion rate based on Faraday's law and proper unit conversion. For example, for corrosion current i_{corr} (A/m^2) the conversion to corrosion rate (mm/year) is

$$CR = \frac{i_{Corr}}{2F} \times \frac{Mw_{\mathrm{Fe}}}{\rho_{\mathrm{Fe}}} \times 3600 \times 24 \times 365 \tag{34.46}$$

An example of the elementary mechanistic models has been developed and published as an open source code for public users by Nešić et al. [21] called FREECORP. This model is based on the physiochemical processes discussed earlier and can be considered as an improved version of their initial study published in 1996 [22]. The model includes the effect of flow for rotating cylinder electrodes and straight pipelines, the effect of CO_2 hydration reaction, additional corrosive species such as oxygen, acetic acid, and hydrogen sulfide, and the effect of corrosion product layer.

Fig. 34.4 demonstrate a comparison of the predicted steady state voltammogram by the model developed by Nešić et al. with experimental data at pH 4 and 1 bar pCO_2 [21]. The predicted corrosion rates using the same model [21] are also compared with the experimental data in Fig. 34.5 for a wide range of solution composition and environmental conditions.

34.3.2.3 Summary

The development of the elementary mechanistic models created a platform to apply the more recent understandings of the CO_2 corrosion into corrosion rate predictions. With the mechanistic approach in the calculations, these models also provided the opportunity for investigating the individual underlying processes. The elementary mechanistic models are used to quantify the polarization behavior (usually the steady state voltammograms) of the system to obtain the physiochemical parameters involved in various underlying processes, i.e., reaction rate constants of the electrochemical reaction and their activation energies, kinetic, and thermodynamic parameters describing the homogeneous reactions, mass transfer coefficient, etc. The mechanistic nature of the model, and the parameters obtained during the model development, allows for more confident extrapolated corrosion rate calculations. For the same reason, these models have the flexibility to easily include additional corrosive species and, to some extent, new physics.

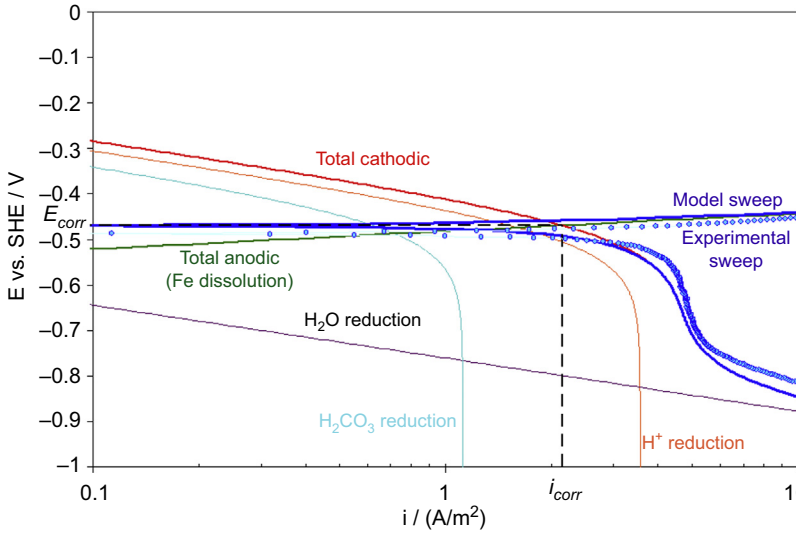

Figure 34.4 Comparison of the predicted steady state polarization behavior (*solid lines*) with the experimental data (*points*) at 20°C (68°F), 1 bar (14.5 psi) CO_2, pH 4, pipe diameter of 0.015 m, and flow velocity of 2 m/s.

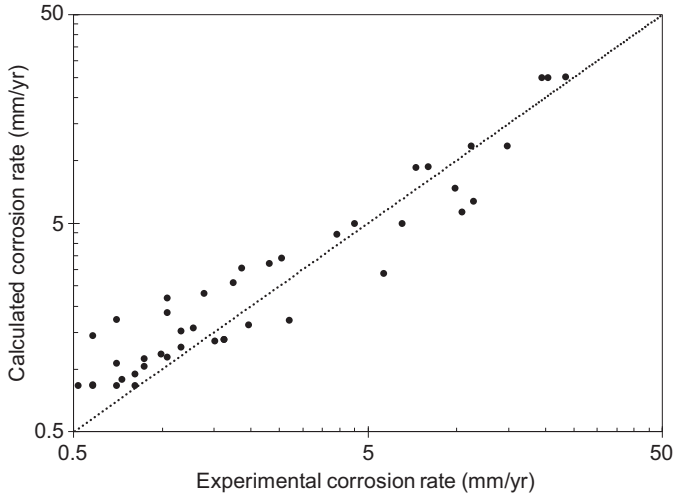

Figure 34.5 Comparison of the experimental and predicted corrosion rates at pCO_2 from 1 to 10 bar (14.5−145 psi), temperature from 20 to 60°C (68−140°F), flow velocity from stagnant to 12 m/s, pH from 4 to 6, and acetic acid concentration from 0 to 390 ppm.
Data taken from S. Nešić, H. Li, J. Huang, D. Sormaz, An open source mechanistic model for CO_2/H_2S corrosion of carbon steel, in: CORROSION, 2009. Paper No. 572.

However, the simple approach of implementation of physicochemical theory in the elementary mechanistic models discussed here suffers from one fundamentally flawed assumption. In these models it is assumed that species are transferred from the bulk fluid toward the metal surface and back independently from each other. In other words, the well-defined homogeneous chemical reactions as well as the ionic interaction (electromigration) between species inside the diffusion layer are ignored.

34.3.3 Comprehensive mechanistic models

The comprehensive mechanistic models are developed based on the fundamental physicochemical laws describing the processes involved in the corrosion phenomena. Using such a rigorous fundamental approach gives these models a great advantage in simulating elaborate, interconnected processes underlying CO_2 corrosion with its complex water chemistry, mass transfer, and electrochemical reactions. For the same reason, these models by nature have a broad range of validity across varying environmental conditions—as long as the used physiochemical laws hold true—and the flexibility to incorporate additional processes and chemical species.

The in-depth treatment of the underlying processes in these models provides a unique insight into the possible reaction pathways and the significance of individual processes, which in turn, further improves the understanding of CO_2 corrosion mechanism. For example, the significance of the buffering ability of weak acids such as carbonic acid and organic acids were not well understood until these models emerged [2,6,77].

The comprehensive mathematical models are built around the mass transfer and homogeneous chemical reactions in the solution near the metal surface; the two key elements in CO_2 corrosion. This can be expressed as the well-known Nernst–Planck equation:

$$\frac{\partial C_i}{\partial t} = -\nabla \cdot N_i + R_i$$

where N_i represents the mass transfer via molecular diffusion, electromigration, convective flow, and turbulent mixing, and the R_i includes the homogeneous chemical reactions. Using the proper boundary conditions along with the Nernst–Planck equation, as discussed in Section 34.3.3.3, the concentration distribution of the chemical species and the rate of electrochemical reactions (hence the corrosion rate) can be accurately determined.

34.3.3.1 Historical background

The first attempt to describe the CO_2 corrosion with the general approach of the comprehensive mathematical models was by Turgoose et al. in 1992 [78]. The mathematical model developed in that study accounted for the mass transfer by diffusion and convective flow as well as homogeneous chemical reactions as independent phenomena in series, rather than the simultaneous treatment as in the Nernst–Planck equation. Despite that deficiency, the authors were able to demonstrate the potential of this type of modeling in providing detailed information about the concentration distribution of chemical species in the diffusion layer. It was shown that the various corrosion mechanisms proposed previously, such as the catalytic mechanism (EC′) proposed by de Waard and Milliams [3] and Więckowski et al. [79] or the CE mechanism proposed by Schmitt and Rothmann [26], are only limited interpretations of a complex water chemistry coupled with electrochemical reactions. However, the authors ignored the charge transfer kinetics of both cathodic and anodic reactions, and the model was only used to calculate the current response at mass transfer limiting condition.

In 1995, Pots developed the first comprehensive mathematical model utilizing the Nernst–Planck equation to simultaneously account for the mass transfer and homogeneous chemical reactions at the solution near the metal surface [77]. The charge transfer rates were assumed to follow the Tafel equation as the boundary conditions at the metal/solution interface. In that study also, the corrosion under mass transfer limiting conditions was at focus and much of the details about the kinetics of the electrochemical reactions were ignored. In such conditions, Pots noted that the carbonic acid reduction at the metal surface is not necessarily required to explain the limiting current, and that its effect may be also explained through the parallel homogeneous carbonic acid dissociation followed by hydrogen ion reduction. That was one of the first reports on the significance of the buffering ability of carbonic acid (or other weak acids [8]) during the corrosion process, which was quantified by employing the comprehensive mathematical models.

The comprehensive mathematical models of CO_2 corrosion of steel were further improved in a series of publications by Nešić et al. [2,23–25,80]. Besides the use of

Nernst–Planck equation to describe the concentration profile of the chemical species in the solution, the homogeneous chemical and electrochemical reactions were treated with more details than in the previous models [77,78]. The scope of the model was further expanded by demonstrating its ability to incorporate the corrosion product layer formation and determining the porosity distribution throughout that layer. The buffering ability of carbonic acid, as reported by Pots [77], was also confirmed by Nešić et al. [2,23]. However, the authors noted that while the carbonic acid reduction reaction was not required to explain the observed limiting currents in polarization curves, this additional cathodic reaction significantly improved the corrosion rate prediction when the corrosion current was controlled by the rate of electrochemical reactions.

In a study by Remita et al., the mechanism of CO_2 corrosion was revisited using a similar modeling approach for quantitative analysis of the experimental data [6]. In that study, authors simplified the model introduced by Nešić et al. [2,23], using steady state calculation (i.e., $dC/dt = 0$ in Nernst–Planck Equation). Using their model, Remita et al. analyzed the experimental cathodic polarization curves and claimed that not only the limiting currents can be fully explained through the buffering effect of carbonic acid but also the charge transfer–controlled currents may be quantified only through the hydrogen ion reduction reaction.

The comprehensive mathematical models, with their analytical approach, have attracted many researchers in the last decades. In more recent years, similar models have been developed and used to describe various corrosion scenarios. A few examples are the studies of sour corrosion by Triobollet et al. [12,81], CO_2 corrosion under a thin water film by Remita et al. [82], pit propagation in CO_2 and acetic acid environment by Amri et al. [83], and top of the line corrosion by Zhang et al. [84].

34.3.3.2 Mathematical description

Since heterogeneous electrochemical reactions are involved in CO_2 corrosion, the concentration of the chemical species at the metal surface may deviate from those at the bulk solution. The comprehensive mathematical models are able to accurately calculate the surface concentration of chemical species based on the known concentrations at the bulk, and with simultaneous consideration of the mass transfer between the bulk and the surface along with the homogeneous chemical reactions.

The mass transfer in corroding systems, or electrochemical systems in general, occurs via three simultaneous mechanisms: *convective flow* due to the (turbulent) movement of the bulk fluid; *molecular diffusion*, as a result of the concentration gradient of the species; *electromigration* of the ions, arising from the presence of an induced or a spontaneous electric field. Hence, the flux of any given species i can be described through Eq. (34.47) [85].

$$N_i = -z_i u_i F C_i \nabla\phi - D_i \nabla C_i + v C_i \tag{34.47}$$

The concentration of each chemical species at an elementary volume of the solution can therefore be defined through its flux and by applying mass conservation. The change in concentration of species i over the time interval of Δt is defined by the

change in its flux over Δx, in addition to the rate of consumption/production of species i through homogeneous chemical reactions. This is mathematically expressed via Eq. (34.48), which is also known as the Nernst–Planck equation [85].

$$\frac{\partial C_i}{\partial t} = -\nabla \cdot N_i + R_i \tag{34.48}$$

For most practical applications, the tangential and radial components of Eqs. (34.47) and (34.48) are not of any practical significance. Furthermore, the mobility of ions can be estimated using Einstein–Smoluchowski relationship ($u_i = D_i/RT$). Therefore, for a one-dimensional semi-infinite geometry in the direction x normal to the metal surface, Eqs. (34.47) and (34.48) can be simplified to Eqs. (34.49) and (34.50), respectively.

$$N_i = -D_i \frac{\partial C_i}{\partial x} - \frac{z_i D_i F C_i}{RT} \frac{\partial \phi}{\partial x} + v_x C_i \tag{34.49}$$

$$\frac{\partial C_i}{\partial t} = -D_i \frac{\partial}{\partial x} \frac{\partial C_i}{\partial x} - \frac{\partial}{\partial x} \left(\frac{z_i D_i F C_i}{RT} \frac{\partial \phi}{\partial x} \right) + v_x \frac{\partial C_i}{\partial x} + R_i \tag{34.50}$$

The average bulk movement of the fluid in the direction normal to the surface is accounted for in the convective flow term ($v_x C$), where v_x describes the velocity profile inside the diffusion layer. Unlike the elementary mechanistic models, where all the mass transfer processes are lumped into a single parameter (mass transfer coefficient, k_m), the comprehensive mathematical models implement the velocity distribution of the fluid inside the diffusion layer. For a laminar flow regime of rotating disk electrodes, the analytical solution of the velocity profile and the diffusion layer thickness were shown as Eq. (34.51), where $a = 0.510$, and Eq. (34.52), respectively [86].

$$v_x = -a\omega \left(\frac{\omega}{\upsilon} \right)^{1/2} x^2 \tag{34.51}$$

$$\delta = \left(\frac{3 D_{lim}}{a v} \right)^{1/3} \left(\frac{\omega}{\upsilon} \right)^{-1/2} \tag{34.52}$$

However, at the conditions of interest for most corrosion applications, the dominant mass transfer mechanism in the bulk solution is in the form of turbulent mixing, which then decays as the solid wall is approached—in the diffusion boundary layer. The turbulent mixing of the fluid can be expressed as eddy diffusivity profile within the diffusion boundary layer. The mathematical relationships for eddy diffusivity of turbulent flow through straight tubes have been developed in a number of different studies [87,88]. A simple expression for eddy diffusivity (D_t) distribution and diffusion layer thickness (δ) is shown in Eqs. (34.53) and (34.54), respectively [88].

$$D_t = 0.18 \left(\frac{x}{\delta} \right)^3 \upsilon \tag{34.53}$$

$$\delta = 25\, Re^{-7/8} d \tag{34.54}$$

The eddy diffusivity (D_t) can be lumped with molecular diffusion coefficient (D_i) in Eqs. (34.49) and (34.50), to account for the turbulent mixing, whereas the convective flow term ($v_x C$) is no longer applicable.

An accurate account of the homogeneous chemical reactions involved in the complex water chemistry of CO_2 saturated solution is essential for calculating the surface concentration of the chemical species. This is of significance, because the buffering system of the solution containing weak acids such as carbonic acid, organic acids, and hydrogen sulfide may act as an additional source (or sink) for the chemical species as their surface concentrations depart from the equilibrium at the bulk solution. The effect of these homogeneous reactions is reflected in the R_i term of Eq. (34.50).

The rate of each chemical reaction j in the general form of Reaction (34.55) can be calculated as shown in Eq. (34.56).

$$\sum_{r=1}^{n_r} C_r \rightleftharpoons \sum_{p=1}^{n_p} C_p \tag{34.55}$$

$$R_j = k_{f,j} \prod_{r=1}^{n_r} C_r - k_{b,j} \prod_{p=1}^{n_p} C_p \tag{34.56}$$

With simple mathematical manipulation, the rate of production (or consumption) of every species i (R_i) for j chemical reactions shown in Table 34.1 may be expressed in a matrix format as Eq. (34.57) [2]. The kinetic rate constant of the chemical reactions can be found in Table 34.9.

$$\begin{bmatrix} R_{CO_{2(aq)}} \\ R_{H^+_{(aq)}} \\ R_{H_2CO_{3(aq)}} \\ R_{HCO^-_{3(aq)}} \\ R_{CO^{2-}_{3(aq)}} \\ R_{OH^-_{(aq)}} \end{bmatrix} = \begin{bmatrix} 1 & -1 & 0 & 0 & 0 \\ 0 & 0 & 1 & 1 & 1 \\ 0 & 1 & -1 & 0 & 0 \\ 0 & 0 & 1 & -1 & 0 \\ 0 & 0 & 0 & 1 & 0 \\ 0 & 0 & 0 & 0 & 1 \end{bmatrix} \times \begin{bmatrix} R_{dis} \\ R_{hyd} \\ R_{ca} \\ R_{bi} \\ R_w \end{bmatrix} \tag{34.57}$$

Considering the discussion so far in this section, Eq. (34.50) can be applied for each chemical species to determine its concentration distribution inside the diffusion layer. The diffusion coefficients of the chemical species and the physical properties of water can be found in Tables 34.7 and 34.4, respectively. However, for this system of equations to be complete, the electric potential appearing in the electromigration term also needs to be specified. This parameter can be characterized through an additional relationship

Table 34.9 Rate constants for reactions listed in Table 34.1 k_f denotes the reaction progress from left to right and $K = k_f/k_b$

Reactions #	Reaction rate constant	References
(34.3)	$k_{f,hyd} = e^{\left(22.66 - \frac{7799}{T}\right)}\ (1/\mathrm{s})$	[42]
(34.4)	$k_{b,ca} = 4.7 \times 10^{10}\ (1/\mathrm{M \cdot s})$	[89–91]
(34.5)	$k_{b,bi} = 5.0 \times 10^{10}\ (1/\mathrm{M \cdot s})$	[89,91][a]
(34.6)	$k_{b,w} = 1.4 \times 10^{11}\ (1/\mathrm{M \cdot s})$	[90,92]

[a]In the absence of direct measurements the value of $k_{b,bi}$ was estimated based on $k_{b,ca}$.

known as the Poisson's equation, which relates the electric potential in a medium with a uniform dielectric constant, to a given charge distribution [85]:

$$\nabla^2\phi = -\frac{F}{\varepsilon}\sum_i z_i C_i \tag{34.58}$$

Although Eq. (34.58) is a more valid theoretical description of the electric potential distribution inside the diffusion layer, a simplified expression known as the "electroneutrality" constraint (Eq. 34.59) has commonly been used as an approximation in mathematical simulation of electrochemical systems:

$$\sum_i z_i C_i = 0 \tag{34.59}$$

This simplification is based on the very large values of the proportionality constant in Poisson's equation (F/ε) [85]. With the relative dielectric constant of saline water being in the range of 60–80 for salt concentrations up to 1 M [93], this proportionality constant would be in order of 10^{14} V·m/C. Therefore, while the electroneutrality constraint is not a fundamental law of nature, it is a reasonable mathematical simplification for the electrochemical systems with moderate or high ionic conductivity where the Laplacian of the potential ($\nabla^2\phi$) is not numerically significant when considering the proportionality constant. In such conditions, the resulting error arising from this assumption is generally well below the error threshold considered for the numerical methods in use. This assumption is favored in mathematical models because it significantly simplifies the mathematical expressions and notably decreases the computational demands of the calculations.

It should be noted that, in mathematical models of electrochemical systems, it is also common to assume that the effect of electromigration on concentration distribution of electroactive species is negligibly small. This allows for the electromigration term appearing in Eq. (34.47) to be disregarded, which simplifies the calculations significantly. Bearing in mind that this assumption is only valid for the solutions with relatively high

conductivity (i.e., high ionic strength) and at low current densities, this approach may be used in many CO_2 corrosion scenarios.

34.3.3.3 Initial and boundary conditions

The solution of Eq. (34.48), as a transient partial differential equation, requires the proper initial and boundary conditions to be specified. At the initial time ($t = 0$) it can be assumed that the well-mixed solution comes into contact with the metal surface. Hence, the concentrations of chemical species throughout the diffusion layer are constant, known values, defined by the chemical equilibria of the solution as discussed in Section 34.2.

At the bulk solution ($x = \delta$) the concentration of chemical species remains unchanged at all times ($t \geq 0$). Therefore, a Dirichlet type boundary condition can be defined for the bulk solution based on the known concentration of species identical to the initial conditions.

The boundary condition at the metal/solution interface is the Neumann boundary condition of defined fluxes and includes all the electrochemical reaction rate calculations. For an electroactive chemical species, the flux at the metal/solution boundary is equal to the rate of the corresponding electrochemical reactions. For an electroactive species, i involved in j electrochemical reactions, the flux at the metal surface can be described through Eq. (34.60).

$$N_i\big|_{x=0} = -\sum_j \frac{s_{ij} i_j}{n_j F} \tag{34.60}$$

The current−potential relationships, used to calculate the rate of electrochemical reactions, can be found in Table 34.5. The negative sign in Eq. (34.60) represents a sign convention, where cathodic currents are presumed negative and anodic currents are positive. For the electrochemical reactions shown in Table 34.2, the species on the left hand side are represented with a negative stoichiometric coefficient (S_{ij}) and the ones on the right hand side, with positive numbers.

Similar to the homogeneous chemical reaction, Eq. (34.60) can be transformed into a matrix notation to include all the electroactive species:

$$\begin{bmatrix} N_{Fe^{2+}_{aq}}\big|_{x=0} \\ N_{H^{+}_{aq}}\big|_{x=0} \\ N_{H_2CO_{3,aq}}\big|_{x=0} \\ N_{HCO^{-}_{3,aq}}\big|_{x=0} \\ N_{CO^{2-}_{3,aq}}\big|_{x=0} \\ N_{OH^{-}_{aq}}\big|_{x=0} \end{bmatrix} = \begin{bmatrix} 1 & 0 & 0 & 0 & 0 \\ 0 & -1 & 0 & 0 & 0 \\ 0 & 0 & -1 & 0 & 0 \\ 0 & 0 & 1 & -1 & 0 \\ 0 & 0 & 0 & 1 & 0 \\ 0 & 0 & 0 & 0 & 1 \end{bmatrix} \times \begin{bmatrix} i_{Fe}/2F \\ i_{H^+}/F \\ i_{ca}/F \\ i_{bi}/F \\ i_w/F \end{bmatrix} \tag{34.61}$$

For nonelectroactive species the flux at the metal surface is zero:

$$N_i\big|_{x=0} = 0 \tag{34.62}$$

Eq. (34.60) and (34.62) can be applied to describe the mass transfer for all chemical species at the metal surface. The electric potential inside the solution may also be specified through the electroneutrality constraint via Eq. (34.59) (or Poisson's equation) similar to that in the governing equations.

Considering the governing equations, the initial conditions, and the boundary conditions discussed so far, this system of equations is fully specified if the potential at the metal surface (E_{app} in Table 34.5) is known so that the rate of electrochemical reactions can be calculated. That is common in case of electroanalytical measurements (e.g., potentiodynamic sweep) where electrode potential is the controlled parameter. However, in corrosion rate predictions this parameter (E_{app} = corrosion potential) is generally not known a priori. In that case, an additional relationship is required—the charge conservation at the metal surface. All the cathodic (reduction) currents are balanced by the anodic (oxidation currents), meaning that the net current resulting from all j electrochemical reactions is equal to zero (i.e., there is no need for an externally "applied" current i_{app}). The charge conservation can be mathematically expressed as Eq. (34.63).

$$i_{app} = 0 = \sum_j i_j \tag{34.63}$$

Table 34.10 summarizes all the relevant mathematical equations required to develop a comprehensive mathematical model as discussed in this section.

34.3.3.4 Numerical solution

The mathematical equations as summarized in Table 34.10 form a set of nonlinear, coupled, partial differential equations to be solved numerically. With the simple one-dimensional geometry spanning from the metal surface toward the solution, typical for uniform corrosion rate calculations, the finite difference method can be used to solve the equations. This method is commonplace in mathematical modeling of electrochemical systems [95–97] and have been discussed in detail elsewhere [85,98].

The partial differential equations are discretized using Taylor's series approximations, resulting into a set of algebraic equations. These equations can further be transformed into a matrix format for convenience. The final solution can then be obtained through various solution algorithms such as Neman's "BAND" open source code where the coefficient matrix is developed and further solved by LU decomposition method [85,98].

In the numerical solution of this set of non-linear differential equations an explicit time integration approach is sometimes preferred over the implicit methods for simplicity. However, the nonlinear expressions in the electromigration and chemical reaction terms, as well as the nonlinear boundary conditions related to electrochemical

Table 34.10 Summary of equations used in the comprehensive mathematical model

Electrode surface boundary	
$N_i = -\sum_j \frac{s_{ij} i_j}{n_j F}$	for all electro active species
$N_i = 0$	for all non-electro active species
$\sum_i z_i C_i = 0$	
$i_{app} = 0 = \sum_j i_j$	for unknown electrode potential case
Diffusion layer	
$\frac{\partial C_i}{\partial t} = -D_i \frac{\partial}{\partial x}\frac{\partial C_i}{\partial x} - \frac{\partial}{\partial x}\left(\frac{z_i D_i F C_i}{RT}\frac{\partial \phi}{\partial x}\right) + v_x \frac{\partial C_i}{\partial x} + R_i$	for all species
$\sum_i z_i C_i = 0$	
Bulk boundary and initial condition	
$C_i = C_i^b$	for all species
$\Phi = 0$	

rate calculations, are often the cause of instability of calculations when an explicit approach was used. A simple remedy is using iterations; although this approach is mathematically simple, it can be computationally demanding, because it requires a very fine spatial and temporal resolution to ascertain the convergence of the calculation.

A more robust approach is based on the use of implicit methods including Taylor series expansion for linear approximation of the nonlinear terms [2,85]. Although this approach adds more complexity to the mathematical treatment, it improves stability of the calculations and enables handling of a variety of different imposed environmental conditions during corrosion rate calculations. Furthermore, to decrease the computational errors, higher order approximations of the nonlinear terms can be used along with an iterative scheme.

Depending on the simulation goals, one may prefer either of these approaches. For example, if the purpose of the model is to predict a highly transient, short time, response of the system such as potentiodynamic sweeps, a high temporal resolution is already required to achieve a reasonable accuracy and therefore, a simple explicit scheme would be suitable. On the other hand, if the model is developed to predict long-term corrosion rates, using much larger time steps is the only feasible approach that would keep the computational time reasonable, which must be done by using implicit methods coupled with higher order approximations and iterative procedures.

An example of comprehensive mechanistic models for CO_2 corrosion of steel was developed by Nešić et al. [2,23,24]. In addition to current/potential calculation for each electrochemical reaction, these models can provide the concentration profile of the chemical species throughout the diffusion layer. Fig. 34.6 illustrates an example of such calculations at pH 6 and 1 bar (14.5 psi) CO_2 [2].

34.3.3.5 Summary

The comprehensive mathematical models reflect the state of the art in the mechanistic understanding of the uniform CO_2 corrosion. These models allow the simultaneous consideration of all the main physiochemical processes in CO_2 corrosion, with each process being described through basic theoretical laws. The comprehensive models have all the key advantages of the elementary mechanistic models and much more. The ability of these models to incorporate any number of homogeneous and surface reactions provides a strong platform for corrosion rate predictions for more realistic industrial conditions. In particular, the effect of homogeneous chemical reactions and the complex interaction of the chemical species in the solution is an essential aspect of CO_2 corrosion that remains unresolved in the elementary models, making it an exclusive feature of the comprehensive mechanistic models. Of course, there are still many knowledge gaps with respect to various aspects of CO_2 corrosion; yet these models have the necessary flexibility to include new/improved understanding of physiochemical processes as they are uncovered. With such a strong theoretical foundation, these models are well suited to serve as a basis for future developments. Challenges would include modeling for higher temperatures and pressures, prediction of localized corrosion, effect of oil/water wetting, effect of corrosion inhibitors, etc.

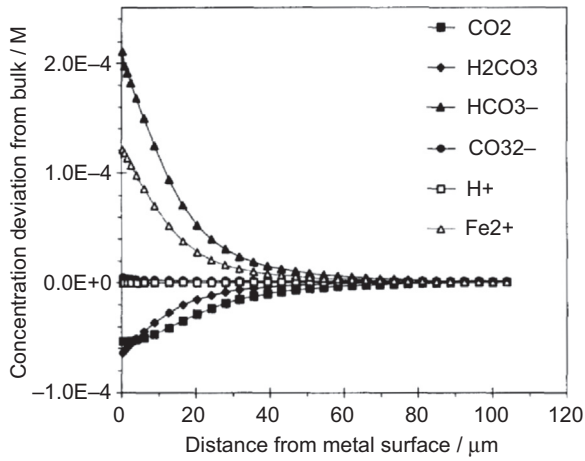

Figure 34.6 Concentration profile of electroactive species at pH 6, 1 bar CO_2 (14.5 psi), 20°C (68°F), pipe with 0.1 m diameter, and 1 m/s flow velocity.

However, the comprehensive mathematical models come with their own "price tag." These models are mathematically and computationally more demanding and are more complicated to construct. The numerical solution algorithms, computational stability, and the calculation time are among the aspects that one needs to consider when developing these types of models.

34.4 Effect of the corrosion product layer

The CO_2 corrosion is often accompanied by corrosion product layer formation at the metal surface. In the simplest case, at the conditions typical for CO_2 corrosion in transmission lines, this corrosion product layer is dominated by the iron carbonate deposit. The protectiveness, mechanical properties, and physical properties of this precipitated layer are affected by numerous parameters such as water chemistry, environmental conditions such as temperature and fluid flow, steel composition, and microstructure, etc. [99−107].

The precipitation/dissolution of iron carbonate as demonstrated through the following heterogeneous chemical equilibrium (Reaction 34.64) is mathematically described via Eq. (34.65), where K_{sp} is the iron carbonate solubility product constant [102].

$$Fe^{2+} + CO_3^{2-} \rightleftharpoons FeCO_{3(s)} \tag{34.64}$$

$$K_{sp} = C_{Fe^{2+}} C_{CO_3^{2-}} \tag{34.65}$$

If the product of the concentration of the dissolved ions exceeds the saturation limit (K_{sp}), the formation of iron carbonate precipitation is thermodynamically favored. This porous deposit may affect the corrosion rate through two main mechanisms:

- Limiting the rate of mass transfer of the chemical species toward and away from the metal surface, as a physical barrier.
- Reducing the rate of electron transfer reactions by blocking a portion of the metal surface, making them unavailable as reaction sites.

The formation of a protective iron carbonate layer in CO_2 corrosion of steel can be discussed from both a thermodynamic and a kinetic point of view [99]. A thermodynamic indicator for the precipitation process is described by the extent of departure from equilibrium Eq. (34.64), represented by "saturation value" (S_{FeCO_3}) defined as:

$$S_{FeCO_3} = \frac{C_{Fe^{2+}} C_{CO_3^{2-}}}{K_{sp}} \tag{34.66}$$

However, although a high saturation value is an indication of iron carbonate layer formation, it does not represent the protectiveness quality of the deposit. The latter is mainly determined by the properties of the iron carbonate layer, such as density,

porosity, and adherence to the metal surface, which are greatly affected by kinetics of iron carbonate precipitation [99,106]. Furthermore, the protectiveness of the corrosion product layer can be influenced by various chemical and mechanical removal processes [103,108,109].

A more representative measure for the quality of a protective iron carbonate layer would therefore have to include the kinetic aspects of the layer deposition, in addition to the thermodynamic feasibility of the layer formation. In this regard, van Hunnik et al. [99] introduced the so-called "scaling tendency" parameter—described by Eq. (34.67)—as a practical measure to assess the protectiveness and sustainability of an iron carbonate layer [99,100,110]. The authors suggest that, the formation of an iron carbonate layer does not completely stop the corrosion process, which in turn causes the existing corrosion product layer to detach from the metal surface [99,111]. This process, known as "film undermining" [25], affects the adherence, density, and porosity of the corrosion product layer and ultimately its protectiveness.

$$ST = \frac{R_{FeCO_{3(s)}}}{CR} \tag{34.67}$$

Based on the aforementioned discussion, a scaling tendency of ST $\gg$ 1 suggests that the undermining is overpowered by the rapidly forming iron carbonate precipitate, creating a dense protective layer. On the other hand, a scaling tendency of ST $\ll$ 1 represents the case where the undermining is much faster than the formation of the corrosion product layer; therefore, only a porous and nonprotective layer may be formed, even at high saturation values [25,110].

The precipitation rate of iron carbonate in Eq. (34.67) can be described by an expression in general form of Eq. (34.68) [112].

$$R_{FeCO_{3(s)}} = \frac{A}{V} f(T) g(S_{FeCO_3}) \tag{34.68}$$

where $f(T) = e^{\left(A - \frac{B}{RT}\right)}$ represents the temperature dependence of the rate constant based on Arrhenius' law with constants A and B to be determined empirically. The precipitation rate dependence on saturation value is accounted for by the $g(S_{FeCO_3})$ function that is defined by the mechanism of the precipitation/dissolution reaction. For an elementary reaction this function can be theoretically expressed as Eq. (34.69) [112].

$$g(S_{FeCO_3}) = K_{sp}(S_{FeCO_3} - 1) \tag{34.69}$$

This equation is similar to what was proposed by Sun and Nesic [113] indicating that the precipitation reaction follows a first-order reaction kinetics. Alternative forms of the function $g(S_{FeCO_3})$, such as the ones introduced by van Hunnik et al. [99] and Johnson and Tomson [107], may suggest a more complex mechanism for this reaction (Table 34.11). However, the lack of mechanistic justification of these precipitation rate equations reduces them to semiempirical expressions with all of their intrinsic limits. A summary of the expressions for precipitation rate proposed by the abovementioned references is provided in Table 34.11.

Table 34.11 Summary of the precipitation rate expressions.

Reference	$f(T)$	$g(S_{FeCO_3})$	K_{sp}
Johnson and Tomson [107]	$e^{\left(54.8-\frac{-123000}{RT}\right)}$	$K_{sp}\left({S_{FeCO_3}}^{0.5}-1\right)^2$	$e^{\left(-36.22-\frac{-30140}{RT}\right)}$
van Hunnik et al. [99]	$e^{\left(52.4-\frac{-119800}{RT}\right)}$	$K_{sp}(S_{FeCO_3}-1)\left(1-{S_{FeCO_3}}^{-1}\right)$	Not specified
Sun and Nesic [113]	$e^{\left(21.3-\frac{-64851.4}{RT}\right)}$	$K_{sp}(S_{FeCO_3}-1)$	[102]

Reprinted with permission from A. Kahyarian, M. Singer, S. Nesic, Modeling of uniform CO_2 corrosion of mild steel in gas transportation systems: a review, Journal of Natural Gas Science and Engineering 29 (2016) 530−549.

In the case of elementary mechanistic models, the effect of a protective iron carbonate layer can be accounted for by introducing an additional mass transfer resistance layer and the blocking effect of the iron carbonate deposit on the charge transfer rates. Under such circumstances, the current density is calculated using Eq. (34.33), whereas a composite mass transfer coefficient should be used when calculating the limiting current densities (Eq. 34.34), to account for the effect of corrosion product layer on the mass transfer rate of the electroactive species. The composite mass transfer coefficient for each species ($k_{comp.}$) can be obtained via Eq. (34.70).

$$\frac{1}{k_{comp.}} = \frac{1}{k_m} + \frac{1}{k_d} \tag{34.70}$$

The term k_m in Eq. (34.70) is the mass transfer coefficient inside the solution similar to that discussed in Section 34.3.2.2, whereas k_d, is the mass transfer coefficient for species i inside the porous corrosion product layer. That is essentially the diffusion through a porous medium with porosity of ε, tortuosity of τ, and the thickness of δ_l, which can be described as:

$$k_d = \frac{\varepsilon \tau D_i}{\delta_l} \tag{34.71}$$

The effect of slow carbon dioxide hydration reaction on carbonic acid limiting current density can be included in the calculations in a similar fashion as described in Section 34.3.2.2. However, the mathematical relationships, such as the one derived by Nešić et al. [76], need to be reworked with a different set of boundary conditions to accommodate for the effect of the corrosion product layer.

While this approach can be used to properly reflect the effect of corrosion product layer, the aforementioned intrinsic shortcoming of the elementary mechanistic models remains unresolved—i.e. disregarding the homogeneous chemical reactions in the diffusion layer. Additionally, although being simple to implement, this approach further requires that the thickness (δ_l) and porosity (ε) of a protective iron carbonate layer to be specified before any corrosion rate calculation (Eq. 34.71). As these parameters are usually not known, an additional empirical correlation is needed, relating the properties (protectiveness) of a protective iron carbonated layer to environmental conditions [23].

Using an approach similar to that discussed above, the comprehensive mechanistic models can also be adapted to account for the effect of a precipitated corrosion product layer. An additional mass transfer barrier can be included in these models by considering a new boundary at the corrosion product layer interface ($x = \delta_l$), with the boundary conditions based on the known flux of chemical species. To account for mass transfer through a porous media, with a porosity ε, the Nernst–Planck equation is rewritten as [2,23]:

$$\frac{\partial(\varepsilon C_i)}{\partial t} = -\nabla \cdot \left(\varepsilon^{3/2} N_i\right) + \varepsilon R_i \tag{34.72}$$

where at the $x > \delta_l$ distance away from the steel surface, where there is no iron carbonate layer, the porosity ε is equal to one. Furthermore, all electrochemical rate expressions (current densities) are modified by multiplying with surface porosity ε, to account for the surface blocking effect. Although these models benefit from accurate surface concentration calculations and account for the homogeneous chemical reactions, the distribution of porosity in the precipitating iron carbonate layer still needs to be predefined. In a simplistic approach it could be described by an empirical function in the same way as it is done for the elementary models [23].

Using a more comprehensive approach, Nešić et al. presented a model for calculation of porosity distribution in the iron carbonate layer [24,80]. The authors proposed that the porosity could be calculated using a mass balance for the solid iron carbonate precipitate as:

$$\frac{\partial \varepsilon}{\partial t} = -\frac{M_{FeCO_3}}{\rho_{FeCO_3}} R_{FeCO_3} - CR\frac{\partial \varepsilon}{\partial x} \tag{34.73}$$

where the first term is related to precipitation kinetics (Eq. 34.68) and the second (convective-like) term arises from the undermining effect as described earlier. This approach is equivalent to using the concept of scaling tendency but one that is based on local concentrations at the steel surface and in the porous iron carbonate layer, rather than bulk concentrations. With this approach, the porosity is treated as an additional variable in calculations and its distribution through the diffusion layer can be obtained by solving Eq. (34.73) simultaneously with Eq. (34.72) for all the other unknown variables (e.g., concentration of species).

Fig. 34.7 shows the comparison of the calculated results with the experimental data obtained in the study by Nešić et al. [25]. The estimated profile of corrosion product

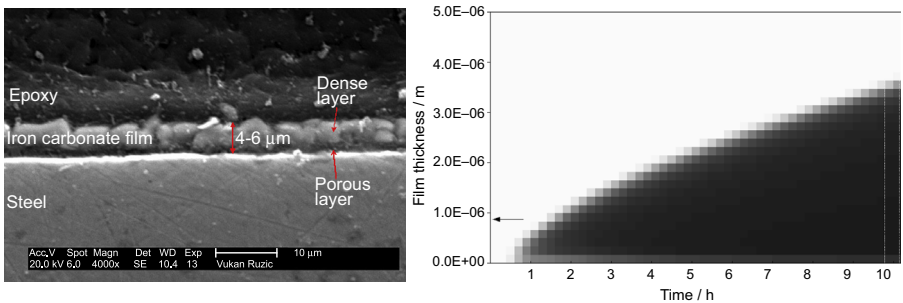

Figure 34.7 SEM image of the corrosion product layer cross section formed after 10 h at $T = 80°C$ (176°F), pH = 6.6, $P_{CO_2} = 0.54$ bar (7.8 psi), ferrous ion concentration of 250 ppm, and $v = 1$ m/s. The graph at right shows the calculated porosity profile along the film thickness of the iron carbonate layer depicted in different shades of gray in similar conditions where white corresponds to $\varepsilon = 1$ and black is $\varepsilon = 0$.

layer porosity shows good qualitative agreement with the SEM image, where a dense precipitate is found with the part closer to the metal surface appearing to be more porous. However, as discussed by the authors, the estimated corrosion product layer thickness lacks accuracy at some of the conditions, which could be due to imprecise iron carbonate deposition kinetics or a removal processes via mechanical destruction as well as chemical dissolution [103,108,109], which are not considered in that model [25].

34.5 Summary

Uniform CO_2 corrosion can now be considered a mature topic in the context of corrosion science and engineering. The understanding of the underlying physiochemical processes enables construction of mechanistic models of varying complexity, which can be successfully used to aid our understanding of the complex interplay between different parameters and to predict the corrosion rates. Furthermore, they may serve as a repository of the current knowledge on the topic, as well as a solid platform for building in new effects as they are discovered and understood.

While we have come a long way in the past few decades, plenty of challenges lie ahead. Modeling the effect of high pressure (close to and above the critical point for CO_2) and high temperature (above 100°C) is currently being addressed. Complexities arising from multiphase flow affecting water wetting in oil transportation lines and water condensation in wet gas lines are another major modeling challenge. The effect of H_2S, organic acids, nonideal solutions (due to very high concentrations of dissolved solids), scaling, underdeposit corrosion, erosion–corrosion, and corrosion inhibition are some of the new frontiers in CO_2 corrosion modeling. A number of research groups around the world are currently working on many of these issues, and as the understanding matures, it will find its way into the mechanistic CO_2 corrosion models of the future.

A special mention should be given to modeling of localized CO_2 corrosion. This is the ultimately challenging topic lying ahead of us, because there is no single cause or mechanism governing localized CO_2 corrosion. However, some progress has been made and the solid foundation built in terms of mechanistic CO_2 corrosion models will serve as a good platform for expanding these models to address localized corrosion.

Nomenclature

Symbol	Definition
A	Surface area (m^2)
C_i	Concentration of species i (M)
C_i^b	Concentration of species i at bulk (M)
C_i^s	Concentration of species i at metal surface (M)
CR	Corrosion rate (mm/year)

Continued

Symbol	Definition
D_i	Diffusion coefficient of species i (m^2/s)
$D_{i,ref}$	Diffusion coefficient of species i at reference temperature (m^2/s)
E	Electrode potential (V)
E_{0_j}	Standard potential of reaction j (V)
F	Faradays constant (C/mol)
ΔH_j	Enthalpy of reaction j (kJ/mol)
i_j	Current density of reaction j (A/m^2)
i_{corr}	Corrosion current density (A/m^2)
i_{net}	Net current density (A/m^2)
i_{ct}	Charge transfer−controlled current density (A/m^2)
i_{lim}	Limiting current density (A/m^2)
i_{app}	Applied current density (A/m^2)
K_j	Equilibrium constant of reaction j
K_{sp}	Solubility product constant (M^2)
k_{0_j}	Rate constant of electrochemical reaction j
$k_{0_{j,ref}}$	Rate constant of electrochemical reaction j at reference temperature
K_H^0	Henry's constant at water saturation pressure (M/bar)
k_m	Mass transfer coefficient in solution ($mol/s \cdot m^2 \cdot M$)
k_d	Mass transfer coefficient in porous deposit ($mol/s \cdot m^2 \cdot M$)
$k_{comp.}$	Composite mass transfer coefficient ($mol/s \cdot m^2 \cdot M$)
k_f	Forward reaction rate constant
k_b	Backward reaction rate constant
Mw_{Fe}	Molecular weight of Fe (kg/kmol)
$M_{\mathrm{FeCO_3}}$	Molecular weight of $FeCO_3$ (kg/kmol)
n_j	Number of transferred electrons in electrochemical reaction j
N_i	Flux of species i ($mol/m^2 \cdot s$)
R	Universal gas constant ($J/K \cdot mol$)
PF	Poynting correction factor
$P_{\mathrm{CO_{2(g)}}}$	Partial pressure of CO_2 (bar)
P_{tot}	Total pressure (bar)
P	Pressure (bar)

Symbol	Definition
P_{CO_2S}	Saturation pressure of CO_2 (bar)
P_{ws}	Saturation pressure of water (bar)
R_i	Reaction rate of species i (M/s)
Re	Reynolds number
S_{FeCO_3}	Saturation value
Sc	Schmitt number
Sh	Sherwood number
ST	Scaling tendency
s_{ij}	Stoichiometric coefficient of species i in reaction j
T	Temperature (K)
T_{ref}	Reference temperature (K)
t	Time (s)
u_i	Mobility of species i (m/s)
V	Volume (m^3)
$\widetilde{V_m}$	Molar partial volume of $CO_{2(aq)}$
v_x	Velocity along x axis (m/s)
x	Distance from metal surface (m)
z_i	Charge of ion i
α_j	Transfer coefficient of electrochemical reaction j
δ	Diffusion layer thickness (m)
δ_d	Diffusion layer thickness (m)
δ_r	Reaction layer thickness (m)
δ_l	Corrosion product layer thickness (m)
ε	Dielectric constant
ε	Porosity
μ	Water viscosity (kg/s·m)
μ_{ref}	Water viscosity at reference temperature (kg/s·m)
ρ_{Fe}	Density of iron (kg/m^3)
ρ_w	Density of water (kg/m^3)
ρ_{FeCO_3}	Density of iron carbonate (kg/m^3)
υ	Kinematic viscosity (m^2/s)
ϕ	Electric potential inside liquid (V)

Continued

Symbol	Definition
ϕ_s	Electric potential inside liquid at the metal surface (i.e., ohmic drop) (V)
φ_{CO_2}	Fugacity coefficient of $CO_{2(g)}$
τ	Corrosion product tortuosity
ω	Angular velocity (rad/s)

References

[1] C. de Waard, D.E. Milliams, Prediction of carbonic acid corrosion in natural gas pipelines, in: Intern. Extern. Prot. Pipes, 1975. F1-1−F1-8.

[2] M. Nordsveen, S. Nešić, R. Nyborg, A. Stangeland, A mechanistic model for carbon dioxide corrosion of mild steel in the presence of protective iron carbonate films − part 1: theory and verification, Corrosion 59 (2003) 443−456.

[3] C. de Waard, D.E. Milliams, Carbonic acid corrosion of steel, Corrosion 31 (1975) 177−181.

[4] L.G.S. Gray, B.G. Anderson, M.J. Danysh, P.R. Tremaine, Mechanisms of carbon steel corrosion in brines containing dissolved carbon dioxide at pH 4, in: CORROSION, 1989. Paper No. 464.

[5] L.G.S. Gray, B.G. Anderson, M.J. Danysh, P.R. Tremaine, Effect of pH and temperature on the mechanism of carbon steel corrosion by aqueous carbon dioxide, in: CORROSION, 1990. Paper No. 40.

[6] E. Remita, B. Tribollet, E. Sutter, V. Vivier, F. Ropital, J. Kittel, Hydrogen evolution in aqueous solutions containing dissolved CO_2: quantitative contribution of the buffering effect, Corrosion Science 50 (2008) 1433−1440.

[7] T. Tran, B. Brown, S. Nešić, Corrosion of mild steel in an aqueous CO_2 environment − basic electrochemical mechanisms revisited, in: CORROSION, 2015. Paper No. 671.

[8] A. Kahyarian, B. Brown, S. Nesic, Mechanism of cathodic reactions in acetic acid corrosion of iron and mild steel, Corrosion 72 (2016) 1539−1546.

[9] A. Kahyarian, M. Singer, S. Nesic, Modeling of uniform CO_2 corrosion of mild steel in gas transportation systems: a review, Journal of Natural Gas Science and Engineering 29 (2016) 530−549.

[10] T. Tran, B. Brown, S. Nešic, Investigation of the electrochemical mechanisms for acetic acid corrosion of mild steel, Corrosion 70 (2014) 223−229.

[11] Y. Zheng, B. Brown, S. Nešic, Electrochemical study and modeling of H_2S corrosion of mild steel, Corrosion 70 (2014) 351−365.

[12] J. Kittel, F. Ropital, F. Grosjean, E.M.M. Sutter, B. Tribollet, Corrosion mechanisms in aqueous solutions containing dissolved H_2S. Part 1: characterisation of H_2S reduction on a 316L rotating disc electrode, Corrosion Science 66 (2013) 324−329.

[13] S. Olsen, CO_2 corrosion prediction by use of the Norsok M-506 model − guidelines and limitations, in: CORROSION, 2003. Paper No. 623.

[14] S. Olsen, A.M. Halvorsen, P.G. Lunde, R. Nyborg, CO_2 corrosion prediction model − basic principles, in: CORROSION, 2005. Paper No. 551.

[15] A.M. Halvorsen, T. Sontvedt, CO_2 corrosion model for carbon steel including wall shear stress model for multiphase flow and limits for production rate to avoid mesa attack, in: CORROSION, 1999. Paper No. 42.
[16] A. Dugstad, L. Lunde, K. Videm, Parametric study of CO_2 corrosion of carbon steel, in: CORROSION, 1994. Paper No. 14.
[17] C. de Waard, U. Lotz, Prediction of CO_2 corrosion of carbon steel, in: CORROSION, 1993. Paper No. 069.
[18] C. de Waard, U. Lotz, A. Dugstad, Influence of liquid flow velocity on CO_2 corrosion: a semi-empirical model, in: CORROSION, 1995. Paper No. 128.
[19] C. de Waard, U. Lotz, D.E. Milliams, Predictive model for CO_2 corrosion engineering in wet natural gas pipelines, Corrosion 47 (1991) 976−985.
[20] C. de Waard, L.M. Smith, B.D. Craig, Influence of crude oils on well tubing corrosion rates, in: CORROSION, 2003. Paper No. 629.
[21] S. Nešić, H. Li, J. Huang, D. Sormaz, An open source mechanistic model for CO_2/H_2S corrosion of carbon steel, in: CORROSION, 2009. Paper No. 572.
[22] S. Nešić, J. Postlethwaite, S. Olsen, An electrochemical model for prediction of corrosion of mild steel in aqueous carbon dioxide solutions, Corrosion 52 (1996) 280−294.
[23] S. Nešić, M. Nordsveen, R. Nyborg, A. Stangeland, A mechanistic model for CO_2 corrosion with protective iron carbonate films, in: CORROSION, 2001. Paper No. 040.
[24] S. Nešić, J. Lee, V. Ruzic, A mechanistic model of iron carbonate film growth and the effect on CO_2 corrosion of mild steel, in: CORROSION, 2002. Paper No. 237.
[25] S. Nešić, K.L.J. Lee, A mechanistic model for carbon dioxide corrosion of mild steel in the presence of protective iron carbonate films − part 3: film growth model, Corrosion 59 (2003) 616−628.
[26] G. Schmitt, B. Rothmann, Studies on the corrosion mechanism of unalloyed steel in oxygen-free carbon dioxide solutions part I. Kinetics of the liberation of hydrogen, Werkstoffe Und Korrosion 28 (1977) 816.
[27] Revised Release on the IAPWS Industrial Formulation 1997 for the Thermodynamic Properties of Water and Steam, The International Association for the Properties of Water and Steam, Lucerne, Switzerland, August 2007.
[28] D. Li, Z. Duan, The speciation equilibrium coupling with phase equilibrium in the H_2O-CO_2-NaCl system from 0 to 250°C, from 0 to 1000 bar, and from 0 to 5 molality of NaCl, Chemical Geology 244 (2007) 730−751.
[29] Z. Duan, R. Sun, C. Zhu, I.-M. Chou, An improved model for the calculation of CO_2 solubility in aqueous solutions containing Na^+, K^+, Ca^{2+}, Mg^{2+}, Cl^-, and SO_4^{2-}, Marine Chemistry 98 (2006) 131−139.
[30] Z. Duan, D. Li, Coupled phase and aqueous species equilibrium of the $H_2O-CO_2-NaCl-CaCO_3$ system from 0 to 250°C, 1 to 1000 bar with NaCl concentrations up to saturation of halite, Geochimica et Cosmochimica Acta 72 (2008) 5128−5145.
[31] W.L. Marshall, E.U. Franck, Ion product of water substance, 0−1000°C, 1-10,000 bars New International Formulation and its background, Journal of Physical and Chemical Reference Data 10 (1983) 295−304.
[32] A.G. Dickson, C. Goyet (Eds.), DOE Handbook of Methods for the Analysis of the Various Parameters of the Carbon Dioxide System in Sea Water, second ed., 1994.
[33] D.A. Palmer, R. Van Eldik, The chemistry of metal carbonate and carbon dioxide complexes, Chemical Reviews 83 (1983) 651−731.
[34] L. Korson, W. Drost-Hansen, F.J. Millero, Viscosity of water at various temperatures, The Journal of Physical Chemistry 73 (1969) 34−39.

[35] J.E. Garcia, Density of Aqueous Solutions of CO_2, Lawrence Berkeley National Laboratory, 2001.
[36] C.L. Yaws, The Yaws Handbook of Vapor Pressure: Antoine Coefficients, second ed., 2015.
[37] Z. Duan, R. Sun, An improved model calculating CO_2 solubility in pure water and aqueous NaCl solutions from 273 to 533 K and from 0 to 2000 bar, Chemical Geology 193 (2003) 257−271.
[38] J. Oddo, M. Tomson, Simplified calculation of $CaCO_3$ saturation at high temperatures and pressures in brine solutions, Journal of Petroleum Technology 34 (1982) 1583−1590.
[39] R.F. Weiss, Carbon dioxide in water and sea water: the solubility of a non-ideal gas, Marine Chemistry 2 (1974) 203−215.
[40] T.H. Maren, L.C. Garg, The rates of hydration of carbon dioxide and dehydration of carbonic acid at 37°, Biochimica et Biophysica Acta 261 (1971) 70−76.
[41] D.M. Kern, The hydration of carbon dioxide, Journal of Chemical Education 37 (1960) 14−23.
[42] A.L. Soli, R.H. Byrne, CO_2 system hydration and dehydration kinetics and the equilibrium CO_2/H_2CO_3 ratio in aqueous NaCl solution, Marine Chemistry 78 (2002) 65−73.
[43] W. Stumm, J.J. Morgan, Aquatic Chemistry: Chemical Equilibria and Rates in Natural Waters, 1995.
[44] M.F. Mohamed, A.M. Nor, M.F. Suhor, M. Singer, Y.S. Choi, Multiphase Technology, Water chemistry for corrosion prediction in high pressure CO_2 environments, in: CORROSION, 2011. Paper No. 375.
[45] B. Meyssami, M.O. Balaban, A.A. Teixeira, Prediction of pH in model systems pressurized with carbon dioxide, Biotechnology Progress 8 (1992) 149−154.
[46] R. Nyborg, Overview of CO_2 corrosion models for models for wells and pipelines, in: CORROSION, 2002. Paper No. 233.
[47] S. Nešić, J. Postlethwaite, M. Vrhovac, CO_2 corrosion of carbon steel − from mechanistic to empirical modelling, Corrosion Reviews 15 (1997) 211−240.
[48] V.R. Jangama, S. Srinivasan, A computer model for prediction of corrosion of carbon steels, in: CORROSION, 1997. Paper No. 318.
[49] B.F.M. Pots, R.C. John, I.J. Rippon, M.J.J.S. Thomas, S.D. Kapusta, M.M. Grigs, et al., Improvements on de Waard-Milliams corrosion prediction and applications to corrosion management, in: CORROSION, 2002. Paper No. 235.
[50] R. Nyborg, P. Andersson, M. Nordsveen, Implementation of CO_2 corrosion models in a three-phase fluid flow model, in: CORROSION, 2000. Paper No. 048.
[51] S.D. Kapusta, B.F.M. Pots, I.J. Rippon, The application of corrosion prediction models to the design and operation of pipelines, in: CORROSION, 2004. Paper No. 633.
[52] S. Nešić, Key issues related to modelling of internal corrosion of oil and gas pipelines − a review, Corrosion Reviews 49 (2007) 4308−4338.
[53] R. Nyborg, Field data collection, evaluation and use for corrosivity prediction and validation of models, in: CORROSION, 2006. Paper No. 118.
[54] E. Dayalan, G. Vani, J.R. Shadley, S.A. Shirazi, E.F. Rybicki, Modeling CO_2 corrosion of carbon steels in pipe flow, in: CORROSION, 1995. Paper No. 118.
[55] E. Dayalan, F.D. de Moraes, J.R. Shadley, S.A. Shirazi, E.F. Rybicki, CO_2 corrosion prediction in pipe flow under $FeCO_3$ scale-forming conditions, in: CORROSION, 1998. Paper No. 51.
[56] J. Han, J.W. Carey, J. Zhang, Effect of sodium chloride on corrosion of mild steel in CO_2-saturated brines, Journal of Applied Electrochemistry 41 (2011) 741−749.

[57] J. Han, J. Zhang, J.W. Carey, Effect of bicarbonate on corrosion of carbon steel in CO_2 saturated brines, International Journal of Greenhouse Gas Control 5 (2011) 1680−1683.
[58] S. Rajappa, R. Zhang, M. Gopal, Modeling the diffusion effects through the iron carbonate layer in the carbon dioxide corrosion of carbon steel, in: CORROSION, 1998. Paper No. 026.
[59] M. Sundaram, V. Raman, M.S. High, D.A. Tree, J. Wagner, Deterministic modeling of corrosion in downhole environments, in: CORROSION, 1996. Paper No. 30.
[60] J. Han, J.W. Carey, J. Zhang, A coupled electrochemical-geochemical model of corrosion for mild steel in high-pressure CO_2-saline environments, International Journal of Greenhouse Gas Control 5 (2011) 777−787.
[61] Y. Zheng, J. Ning, B. Brown, S. Nesic, Electrochemical model of mild steel corrosion in a mixed H_2S/CO_2 aqueous environment, Corrosion 71 (2014) 316.
[62] A. Anderko, Simulation of $FeCO_3$/FeS scale formation using thermodynamic and electrochemical models, in: CORROSION, 2000. Paper No. 102.
[63] R. Zhang, M. Gopal, W.P. Jepson, Development of a mechanistic model for predicting corrosion rate in multiphase oil/water/gas flows, in: CORROSION, 1997. Paper No. 601.
[64] K. George, S. Nešić, C. de Waard, Electrochemical investigation and modeling of carbon dioxide corrosion of carbon steel in the presence of acetic acid, in: CORROSION, 2004. Paper No. 379.
[65] S.N. Esmaeely, B. Brown, S. Nesic, Verification of an Electrochemical Model for Aqueous Corrosion of Mild Steel for H_2S Partial Pressures up to 0.1 MPa, Corrosion 73 (2017) 144−154.
[66] M. Eisenberg, C.W. Tobias, C.R. Wilke, Ionic mass transfer and concentration polarization at rotating electrodes, Journal of the Electrochemical Society 101 (1954) 306−320.
[67] D.C. Silverman, Practical corrosion prediction using electrochemical techniques, in: Uhlig's Corros. Handb., John Wiley & Sons, Inc., 2011, pp. 1129−1166.
[67a] F.P. Berger, K.-F.F.-L. Hau, Mass transfer in turbulent pipe flow measured by the electrochemical method, International Journal of Heat and Mass Transfer 20 (11) (1977) 1185−1194.
[68] M.W.E. Coney, Erosion-Corrosion: The Calculation of Mass-transfer Coefficients, 1981.
[69] B. Poulson, Measuring and modelling mass transfer at bends in annular two phase flow, Chemical Engineering Science 46 (1991) 1069−1082.
[70] J. Wang, S.A. Shirazi, J.R. Shadley, E.F. Rybicki, E. Dayalan, A correlation for mass transfer coefficients in elbows, in: CORROSION, 1998. Paper No. 42.
[71] J. Wang, S.a Shirazi, A CFD based correlation for mass transfer coefficient in elbows, International Journal of Heat and Mass Transfer 44 (2001) 1817−1822.
[72] E.L. Cussler, Diffusion: Mass Transfer in Fluid Systems, Cambridge University Press, 1997.
[73] W.M. Haynes, CRC Handbook of Chemistry and Physics, 2009.
[74] B.R. Linter, G.T. Burstein, Reactions of pipeline steels in carbon dioxide solutions, Corrosion Science 41 (1999) 117−139.
[75] A.J. Bard, L.R. Faulkner, Electrochemical Methods : Fundamentals and Applications, John Wiley & Sons, Inc., 2001.
[76] S. Nešić, J. Postlethwaite, N. Thevenot, Superposition of diffusion and chemical reaction controlled limiting current-application to CO_2 corrosion, Journal of Corrosion Science and Engineering 1 (1995) 1−14.

[77] B.F.M. Pots, Mechanistic models for the prediction of CO_2 corrosion rates under multi-phase flow conditions, in: CORROSION, 1995. Paper No. 137.
[78] S. Turgoose, R.A. Cottis, K. Lawson, Modeling of electrode processes and surface chemistry in carbon dioxide containing solutions, in: Comput. Model. Corros., 1992, pp. 67−81. ASTM STP 1154.
[79] A. Więckowski, E. Ghali, M. Szklarczyk, J. Sobkowski, The behaviour of iron electrode in CO_2^- saturated neutral electrolyte—II. Radiotracer study and corrosion considerations, Electrochimica Acta 28 (1983) 1627−1633.
[80] S. Nešić, M. Nordsveen, R. Nyborg, A. Stangeland, A mechanistic model for carbon dioxide corrosion of mild steel in the presence of protective iron carbonate films—part 2: a numerical experiment, Corrosion 59 (2003) 489−497.
[81] B. Tribollet, J. Kittel, A. Meroufel, F. Ropital, F. Grosjean, E.M.M. Sutter, Corrosion mechanisms in aqueous solutions containing dissolved H_2S. Part 2: model of the cathodic reactions on a 316L stainless steel rotating disc electrode, Electrochimica Acta 124 (2014) 46−51.
[82] E. Remita, B. Tribollet, E. Sutter, F. Ropital, X. Longaygue, J. Kittel, et al., A kinetic model for CO_2 corrosion of steel in confined aqueous environments, Journal of the Electrochemical Society 155 (2008). C41−C45.
[83] J. Amri, E. Gulbrandsen, R.P. Nogueira, Numerical simulation of a single corrosion pit in CO_2 and acetic acid environments, Corrosion Science 52 (2010) 1728−1737.
[84] Z. Zhang, D. Hinkson, M. Singer, H. Wang, S. Nešić, A mechanistic model of top-of-the-line corrosion, Corrosion 63 (2007) 1051−1062.
[85] J. Newman, K.E. Thomas-Alyea, Electrochemical Systems, third ed., Wiley-Interscience, 2004.
[86] W.G. Cochran, The flow due to a rotating disc, Mathematical Proceedings of the Cambridge Philosophical Society 1 (1934) 365−375.
[87] S. Aravinth, Prediction of heat and mass transfer for fully developed turbulent fluid flow through tubes, International Journal of Heat and Mass Transfer 43 (2000) 1399−1408.
[88] J.T. Davies, Turbulence Phenomena, 1972, pp. 121−174.
[89] R.E. Zeebe, D. Wolf-Gladrow (Eds.), CO_2 in Seawater: Equilibrium, Kinetics, Isotopes, Elsevier, 2001.
[90] M. Eigen, Proton-transfer, acid-base catalysis, and enzymatic hydrolysis, Angewandte Chemie 3 (1964) 1−72.
[91] K.G. Schulz, U. Riebesell, B. Rost, S. Thoms, R.E. Zeebe, Determination of the rate constants for the carbon dioxide to bicarbonate inter-conversion in pH-buffered seawater systems, Marine Chemistry 100 (2006) 53−65.
[92] F.H. Stillinger, Proton transfer reactions and kinetics in water, Theoretical Chemistry, Advances and Perspectives 3 (1978) 177−234.
[93] N. Gavish, K. Promislow, Dependence of the dielectric constant of electrolyte solutions on ionic concentration: a microfield approach, Physical Review E − Statistical, Nonlinear, and Soft Matter Physics 94 (2016) 1−7.
[94] E. Cussler, Diffusion: Mass Transfer in Fluid Systems, third ed., Cambridge University Press, 2009.
[95] D. Coleman, R. White, D. Hobbs, A parallel-plate electrochemical reactor model for the destruction of nitrate and nitrite in alkaline waste solutions, Journal of the Electrochemical Society 142 (1995) 1152−1161.

[96] D. Fan, Modification of Newman's BAND(J) subroutine to multi-region systems containing interior boundaries: MBAND, Journal of the Electrochemical Society 138 (1991) 1688−1691.
[97] K.-M. Yin, T. Yeu, R.W. White, A mathematical model of electrochemical reactions coupled with homogeneous chemical reactions, Journal of the Electrochemical Society 138 (1991) 1051.
[98] J. Newman, Numerical solution of coupled, ordinary differential equations, Industrial and Engineering Chemistry Fundamentals 7 (1968) 514−517.
[99] E.W.J. van Hunnik, B.F.M. Pots, E.L.J.A. Hendriksen, The formation of protective $FeCO_3$ corrosion product layers in CO_2 corrosion, in: CORROSION, 1996. Paper No. 006.
[100] E. Gulbrandsen, Acetic acid and carbon dioxide corrosion of carbon steel covered with iron carbonate, in: CORROSION, 2007. Paper No. 322.
[101] J.-L. Crolet, N. Thevenot, A. Dugstad, Role of free acetic acid on the CO_2 corrosion of steels, in: CORROSION, 1999. Paper No. 24.
[102] W. Sun, S. Nešić, R.C. Woollam, The effect of temperature and ionic strength on iron carbonate ($FeCO_3$) solubility limit, Corrosion Science 51 (2009) 1273−1276.
[103] V. Ruzic, M. Veidt, S. Nešić, Protective iron carbonate films—part 3: simultaneous chemo-mechanical removal in single-phase aqueous flow, Corrosion 63 (2007) 758−769.
[104] M.B. Kermani, A. Morshed, Carbon dioxide corrosion in oil and gas production − a compendium, Corrosion 59 (2003) 659−683.
[105] D.H. Davies, T. Burstein, The effect of bicarbonate on the corrosion and passivation of iron, Corrosion 36 (1980) 416−422.
[106] A. Dugstad, Mechanism of protective film formation during CO_2 corrosion of carbon steel, in: CORROSION, 1998. Paper No. 31.
[107] M.L. Johnson, M.B. Tomson, Ferrous carbonate precipitation kinetics and its impact on CO_2 corrosion, in: CORROSION, 1991. Paper No. 268.
[108] V. Ruzic, M. Veidt, S. Nešsić, Protective iron carbonate films—part 2: chemical removal by dissolution in single-phase aqueous flow, Corrosion 62 (2006) 598−611.
[109] V. Ruzic, M. Veidt, S. Nešsić, Protective iron carbonate films—part 1: mechanical removal in single-phase aqueous flow, Corrosion 62 (2006) 419−432.
[110] W. Sun, S. Nesic, Basics revisited: kinetics of iron carbonate scale precipitation in CO_2 corrosion, in: CORROSION, 2006. Paper No. 365.
[111] B.F.M. Pots, E.L.J.A. Hendriksen, CO_2 corrosion under scaling conditions − the special case of top-of-line corrosion in wet gas pipelines, in: CORROSION, 2000. Paper No. 031.
[112] A.C. Lasaga, Kinetic Theory in the Earth Sciences, Princeton University Press, 1998.
[113] W. Sun, S. Nešić, Kinetics of corrosion layer formation: part 1 - iron carbonate layers in carbon dioxide corrosion, Corrosion 64 (2008) 334−346.

Abbreviations

°/PD	Degrees per pipe diameter. A measure of flexibility in pipe coatings subject to bending
3LPE	Three-layer polyethylene. Coating used for pipe
3LPP	Three-layer polypropylene. Coating used for pipe
AC	Alternating current
ACA	Australian Corrosion Association
ACS	American Chemical Society
AFM	Atomic force microscope
AGA	American Gas Association
AIM	Asset integrity management
AIMS	Asset integrity management system
ANN	Artificial neural network
APB	Acid-producing bacteria
API	American Petroleum Institute
ARO	Abrasion resistant overlay—secondary coating for protection against impact and abrasion during burial
ASD	Acoustic sand detectors
ASME	American Society of Mechanical Engineers
ASR	Acceptable sand rate
ASTM	American Society for Testing and Materials
AUV	Autonomous underwater vehicles
AWWA	American Water Works Association
bbl/day	Barrels per day
BCSR	Biocatalytic cathodic sulfate reduction
BHP	Bottom hole pressure
BHT	Bottom hole temperature
BOD	Basis of design
BS&W	Bottom sediments and water
BSI	British Standards Institute
CAPEX	Capital expenditure
CCBP	Corrosion control best practices
CCD	Corrosion control document
CCT	Critical crevice temperature
CD	Cathodic disbondment—coating delamination arising out of CP exposure
CEM	Corrosion−erosion monitor
CEPA	Canadian Energy Pipeline Association
CFD	Computational fluid dynamics—a modeling technique typically to simulate flow of fluids

CIP	Coating Inspection Program—Provided by NACE International
CIPS	Close Interval Potential Survey—a technique used to assess the performance of cathodic protection
CLR	Crack length ratio
CLSM	Confocal laser scanning microscopy
CM	Corrosion manual
CMAS	Coupled multielectrode array system
CMIC	Chemical microbiology-influenced corrosion
CML	Cement mortar lining—concrete coating for steel pipe internals
CMPs	Corrosion management plans
CMS	Corrosion management system
CO_2	Carbon dioxide, an acid forming, suffocating, heavier than air gas
CP	Cathodic protection—externally applied current for corrosion control
CPT	Critical pitting temperature
CR	Computed radiography
CR	Corrosion rate (mm/year)
CRA	Corrosion resistant alloy
CS	Carbon steel
CSA	Canadian Standards Association
CSCC	Chloride stress corrosion cracking
CTE	Coal tar epoxy enamel
CUI	Corrosion under insulation. Common external corrosion mechanism of insulated assets such as pipes, storage tanks etc.
CWC	Concrete weight coating. Used to control buoyancy of pipes
DA	Direct assessment
DC	Direct current
DCVG	Direct current voltage gradient—a technique that provides information both on the stability of cathodic protection and performance of the coating
DEG	Diethylene glycol
DFT	Dry film thickness
DLFBE	Dual layer FBE. Two layer coating, both of FBE. Popular for abrasion or UV environments
EAC	Environmentally assisted cracking
ECDA	External corrosion direct assessment
ECR	Erosion−corrosion resistance
ECTFE	Ethylene chlorotrifluoroethylene. A fluorinated polymer
EDS	Energy dispersive spectroscopy
EEMUA	Engineering Equipment and Materials Users Association
EFC	European Federation of Corrosion
EMAT	Electromagnetic acoustic transducer
EMIC	Electric microbiology-influenced corrosion
EN	Electrochemical noise
EOR	Enhanced oil recovery
EPA	Environmental Protection Agency
EPRI	Electric Power Research Institute
EPS	Extracellular polymeric substances
ERW	Electric resistance welding
ESCC	External stress corrosion cracking
ESEM	Environmental scanning electron microscope

FBE	Fusion bonded epoxy. Common coating used for line pipe
FCP	Flexible composite pipe. Thermoplastic pipe with internal reinforcement
FHWA	Federal Highway Administration
FIFRA	Federal Insecticide, Fungicide, and Rodenticide Act
FISH	Fluorescence in situ hybridization
FJ	Field joint (also girth weld). Weld connection between two pipes
FPS	Floating production systems
FPSO	Floating production storage and offloading
FRP	Fiber reinforced plastic FRP
FSM	Field signature method
FST	Flow suction tanks
GDP	Gross Domestic Product
GHB	General heterotrophic bacteria
GMAW	Gas metal arc welding
GNP	Gross National Product
GOR	Gas−oil ratio
GRE	Glass-reinforced epoxy
GRPP	Glass reinforced Plastic Pipe
GW	Girth weld (also field joint). Weld connection between two pipes
HAC	Hydrogen-assisted cracking
HAZ	Heat-affected zone of a weld in which welding heat has altered in microstructure
HDB	Hydrostatic design basis
HDD	Horizontal directional drilling—coated pipe string is drawn through a prebored hole, usually under road crossings, etc.
HDPE	High-density polyethylene (used for piping or pipelining)
HE	Hydrogen embrittlement
HELP	Hydrogen enhanced localized plasticity
HER	Hydrogen evolution reaction
HIB	Hydrogen-induced blistering
HIC	Hydrogen-induced cracking
HID	Hydrogen-induced disbonding
HPCC	High-performance composite coating. All-powder pipe coating
HpHSCC	High pH stress corrosion cracking
HPHT	High-pressure high temperature
H_2S	Hydrogen sulfide, an acid forming, toxic, corrosive gas
HSC	Hydrogen stress cracking
HSE	Health, safety and environment
HSLA	High-strength low alloy
HSS	Heat shrink sleeve—used as a girth weld protection
HTHPRCE	High-temperature, high-pressure rotating cylinder electrode
ICCP	Impressed current cathodic protection
ICDA	Internal corrosion direct assessment
ID	Internal diameter
IGSCC	Intergranular stress corrosion cracking
ILI	In-line inspection
IMM	Inert multipolymeric matrix, is a hybrid coating for CUI control
IMPACT	International measures of prevention, application, and economic of corrosion technologies—a study published by NACE International
IOB	Iron-oxidizing bacteria

IOW	Integrity operating window
IPLOCA	International Pipe Line & Offshore Contractors Association
IR	Infrared thermography
IRB	Iron-reducing bacteria
ISO	International Organization for Standardization
KPI	Key performance indicator
LAT	Low application temperature. Refers to coatings that melt at a lower than normal temperature
LCC	Life cycle costing
LE	Life extension
LEFM	Linear elastic fracture mechanics
LPR	Linear polarization resistance
LRUT	Long range ultrasonic testing
MAOP	Maximum allowable operating pressure
MEA	Monoethanolamine
MEG	Monoethylene glycol
MFL	Magnetic flux leakage
MIC	Microbiological induced corrosion—bacteria that cause metal loss
MIG	Metal inert gas
MIO	Micaceous iron oxide—used as barrier pigment in paints
MNP	Most probable number—a method of getting quantitative data of live bacteria in media
MOB	Manganese-oxidizing bacteria
MOC	Management of change
MPY	Mills per year
MYS	Minimum yield strength
NACE	National Association of Corrosion Engineers
NBS	National Bureau of Standards
NDE	Nondestructive examination
NIST	National Institute of Standards and Technology
NNpHSCC	Near-neutral pH stress corrosion cracking
NPD	Norwegian Petroleum Directorate
NRB	Nitrate-reducing bacteria
NRIM	National Research Institute for Metals
OCP	Open-circuit potential
OH&S	Occupational health and safety
OPEX	Operational expenditure
PAUT	Phased array ultrasonic testing
PCE	Pressure containing equipment
PCR	Pitting corrosion rate
PCR	Polymerase chain reaction
PDB	Pressure design basis
PDV	Present discounted value
PE	Polyethylene. Sometimes colloquially “polythene”
PEC	Pulse eddy current
PEEK	Polyethyl ethyl ketone
PIM	Pipeline integrity management
PM	Parent material
PO	Polyolefin (e.g., polyethylene, polypropylene)

PP	Polypropylene
PP	Potentiodynamic polarization
PPC	Personnel protection coating
ppm	Parts per million
PR	Precipitation rate (mol/m^2 per s)
PRCI	Pipeline Research Council International
PREN	Pitting resistance equivalent number
PSA	Petroleum Safety Authority
PTFE	Polytetrafluoroethylene (chemical-resistant polymer)
PVC	Polyvinyl chloride
PWHT	Postweld heat treatment
PWMC	Preferential weld metal corrosion
QCM	Quartz crystal microbalance
qPCR	Quantitative polymerase chain reaction
RBI	Risk-based inspection
RBMI	Risk-based maintenance and inspection
RCA	Rotating cylinder autoclave
RCE	Rotating cylinder electrode
ROI	Return on investment
ROV	Remotely operated vehicle
RPCM	Ring pair corrosion monitor
RTP	Reinforced thermoplastic pipe. Thermoplastic pipe with internal reinforcement
RTR	Reinforced thermosetting resin. Usually glass, aramid or carbon fiber in epoxy, polyester or vinyl ester matrices
SACP	Sacrificial Anode Cathodic Protection
SAGD	Steam-assisted gravitational drainage
SAW	Submerged arc welding
SCC	Stress corrosion cracking
SCCDA	Stress corrosion cracking direct assessment
SCE	Standard calomel electrode
SEM	Scanning electron microscopy
SFB	Slime-former bacteria
SHE	Standard hydrogen electrode
SIC	Sprayable insulative coatings
SMAW	Shielded metal arc welding
SMYS	Specified minimum yield strength
SOB	Sulfur-oxidizing bacteria
SOHIC	Stress oriented hydrogen-induced cracking
SPAR	A generic name for floating production facilities that comprise a vertical cylindrical buoyant hull.
SRA	Sulfate-reducing archaea
SRB	Sulfate-reducing bacteria.
SRP	Sulfate-reducing prokaryotes
SRU	Sulfate-removal package
SSC	Sulfide stress cracking
SSPC	Society for Protective Coatings Standards
SVEM	Scanning vibrating electrode microprobe
SWC	Stepwise cracking
SZC	Soft zone cracking

TDS	Total dissolved salts
Tg	Glass transition temperature—rigid to flexible transition point
TGB	Total general bacteria
THPS	Tetrakis hydroxymethyl phosphonium sulfate—it is a water treatment chemical
TIL	Thermal insulating layer
TLC	Top-of-line corrosion
TMIC/IC	Titanium-modified inorganic copolymer/inorganic copolymer, is a hybrid coating for CUI control
TSA	Thermally sprayed aluminium
TSS	Total suspended solids
UDC	Under deposit corrosion
UNS	Unified numbering system
USDA	United States Department of Agriculture
UT	Ultrasonic testing
UTS	Ultimate tensile strength
UWILD	Underwater inspection in lieu of dry docking
VCI	Volatile corrosion inhibitor
VFA	Volatile fatty acids
VHN	Vickers hardness number
VIV	Vortex Induced Vibration
VOC	Volatile organic compound—solvents used in paint manufacture
VSI	Vertical scanning interferometry
WCR	Water condensation rate (kg/m^2 per s)
WHP	Water hole pressure
WHT	Water hole temperature
WL	Weight loss
WM	Weld metal
XPS	X-ray photoelectron spectroscopy
XRCT	X-ray computed tomography
XRD	X-ray diffraction
ZRA	Zero resistance ammeter

Index

'*Note*: Page numbers followed by "f" indicate figures, "t" indicate tables.'